JAERI-M
92-028

PROCEEDINGS OF THE THIRD ASIAN SYMPOSIUM ON RESEARCH REACTOR

NOVEMBER 11~14, 1991, SUNPIA HITACHI, HITACHI-SHI, IBARAKI-KEN, JAPAN

March 1992

Department of Research Reactor

日本原子力研究所
Japan Atomic Energy Research Institute

JAERI-Mレポートは，日本原子力研究所が不定期に公刊している研究報告書です。
入手の問合わせは，日本原子力研究所技術情報部情報資料課（〒319-11茨城県那珂郡東海村）あて，お申しこしください。なお，このほかに財団法人原子力弘済会資料センター（〒319-11 茨城県那珂郡東海村日本原子力研究所内）で複写による実費頒布をおこなっております。

JAERI-M reports are issued irregularly.
Inquiries about availability of the reports should be addressed to Information Division Department of Technical Information, Japan Atomic Energy Research Institute, Tokai-mura, Naka-gun, Ibaraki-ken 319-11, Japan.

編集兼発行　日本原子力研究所
印　　刷　いばらき印刷㈱

JAERI-M 92-028

Proceedings of the Third Asian Symposium on Research Reactor November 11~14, 1991, SUNPIA HITACHI, Hitachi-shi, Ibaraki-ken, Japan

Department of Research Reactor

Tokai Research Establishment
Japan Atomic Energy Research Institute
Tokai-mura, Naka-gun, Ibaraki-ken

(Received January 31, 1992)

The upgraded new JRR-3 (JRR-3M) is in operation since November, 1990, and the MPR-30 in Indonesia is now under power ascending tests for aiming at the full power of 30MW. In addition, the KMRR in Korea is also under construction. Research reactors in the world are now in the stage of alternation of generations, and R&D works for a research reactor is thus active in Asian countries.

Under these circumstances, there is an urgent need to have an opportunity for the exchange of information and discussion concerning the current status and future plans, operation and utilization experiences, technology development and so on in nuclear research reactors. A series of the Asian Symposium on Research Reactor (ASRR) are being held in accordance with those demands. The first ASRR (ASRR-I) was held at Tokyo in 1986 and the ASRR-II was followed at Jakarta, Indonesia in 1989. The ASRR-III has been hosted by Japan Atomic Energy Research Institute (JAERI) under the cooperation with Science and Technology Agency, Japan Atomic Industrial Forum, Inc. and the Atomic Energy Society of Japan at SUNPIA HITACHI, Ibaraki-ken, Japan from November 11th to 14th, 1991.

There were more than three hundred attendances in total from not only the Asia but also over the world including 62 participants from 12 foreign countries. One special, eight invited and 72 general lectures were presented.

In this proceeding, the general lectures were stored in eleven sessions in accordance with the major and technical fields of research

reactors.

In general speaking for the ASRR-III, most of the papers presented were related to the operation of reactors and the presentations concerning the utilization of reactor were limited to Japan. This fact tells us that almost all reactors in Asian countires are utilized on the RI production, activation analysis and training at present and on the other hand, such utilizations as the beam experiments will be future items. It is also pointed out that the active contribution was done by the presentations from USA, France and Canada.

In this proceeding, the participants list and the members list of organization and planning committees are attached for the convenient use.

Keywords: Proceeding, Research Reactor, ASRR-III, Asian Symposium, Future Plan, Operation Experience, Utilization Experience, Current Status

JAERI－M 92－028

第3回研究炉に関するアジアシンポジウム報文集

1991年11月11～14日，サンピア日立，日立市

日本原子力研究所東海研究所
研究炉部

（1992年1月31日受理）

世界的に研究炉が世代交代期にある中で，我国の新JRR－3（JRR－3M)が平成2年11月から利用運転を開始し，インドネシアの MPR－30が30MWを目指して出力上昇試験中である。また韓国においては，KMRRの建設が進捗するなどアジア各国の研究炉の発展はめざましいものがある。このような状況の下で，アジアの研究者，技術者が一堂に会し，各国の研究炉の現状と将来の動向，運転・利用経験，技術開発等について情報交換を行うとともに，交流を図り相互理解を深めることを目的としてアジア研究炉シンポジウム（略称ASRR）が開催されている。第1回は東京(昭和61年)，第2回はインドネシア，ジャカルタ（平成元年）において開催され，今般第3回会議が当研究所主催，科学技術庁，日本原子力産業会議，日本原子力学会の後援によって，平成3年11月11日から4日間，日立市・サンピア日立を会場に行われた。

出席者は，アジア地域外の国々も合わせて12カ国，62名を含め 301名で，特別講演1件，招待講演8件，一般論文72件の合計81件であった。総体的にみて，研究炉の運転等に関連する発表が多く，利用面に関しては国外からの発表は少なかった。換言すれば，アジア諸国における研究炉の利用は，RI製造，放射化分析，教育訓練が中心で，ビーム実験（中性子散乱),照射利用等は今後に待つところが多いともいえる。また先進国（米国，仏，カナダ）からの積極的な発表もあった。

本報告書では，発表論文を11のセッションに分け集録している。この他に，参加者リスト，開催・運営の任にあった組織委員会，企画調整部会及び事務局名簿も加え，論文集としての利用の便を考慮した。

東海研究所：〒319－11　茨城県那珂郡東海村白方字白根2－4

Contents

目　　次

Foreword

The Third Asian Symposium on Research Reactor (ASRR-III) was held at SUNPIA HITACHI, Ibaraki-ken, Japan from November 11 to 14, 1991. This symposium was originated from an urgent need from many researchers and engineers engaged in the field of research reactors in Asian countries. It is one of the top necessity for them to have an opportunity of the information exchange and discussion of the present status and future plans, operation and utilization experiences, technology development and so on. A series of the Asian Symposium on Research Reactor (ASRR) is being held in accordance with those demands. The first ASRR was held at Tokyo in 1986 and the ASRR-II followed it at Jakarta, Indonesia in 1989.

The ASRR-III has been hosted by Japan Atomic Energy Research Institute (JAERI) under the cooperation with Science and Technology Agency, Japan Atomic Industrial Forum Inc. and the Atomic Energy Society of Japan. The total number of participants was more than three hundred. From 12 overseas countries, not only Asia but also over the world, 62 foreigners attended. One special, eight invited and 72 general lectures were presented.

The exhibition by the research reactor related companies was open through the symposium term. The technical visit to Hitachi Works, Power Reactor and Nuclear Fuel Development Corporation (PNC) and JAERI was carried out on the closing day.

The ASRR-III was successful under the strong contribution and co-operation with persons and organizations concerned. The next symposium will be expected to follow within a few years.

Opening Address

Takumi ASAOKA

Chairman, Organization Committee

Director General, Tokai Research Establishment
Japan Atomic Energy Research Institute

Distinguished Guests, Ladies and Gentlemen:

It is a great honor and pleasure for me to be able to address the opening of this Third Asian Symposium on Research Reactor. As the Chairman of the Organization Committee, I would like to welcome all of participants. I would also like to thank the members of the Organization Committee, the Planning and Management Committee and the Symposium Secretariat for their competent and energetic cooperation in making many arrangements. Thanks are also due to the Science and Technology Agency, the Atomic Energy Society of Japan and the Japan Atomic Industrial Forum for their collaboration to Symposium.

It seems that research reactors are entering a new era. The first era of research reactors started about some thirty years go. Many research reactors had been constructed over the world, and they have played essential roles in various fields of nuclear activities from education and basic research to research and development of power reactors. Although, many reactors among those first generation reactors are still working well, new reactors of second generation are expected for the second era of research reactor utilization.

As a recent trend over the world, higher performance and availability of a research reactor is in strong demand to present and future scientific and technological needs. Some of research reactors are upgraded or modified, and new reactors are planned to construct and under construction. In Asia, for instance, in Indonesia, the Multi-purpose Reactor G.A.Siwabessy is now under commissioning test and is expected to reach a maximum power level of 30 MW at the beginning of next year. In Korea, the construction of KMRR is promoted smoothly, and is expected to achieve the criticality in 1993 hopefully. In JAERI, modified JRR-3 has been operated since November 1990. Moreover, in the other Asian countries, R&D for research and test reactors are also now in progress steadily. Under these circumstances, it is significant and indispensable for our researchers and engineers to have opportunities for exchanging informations concerning present status and future plans, experiences of operation and utilization, modification and safety analyses for research reactors.

Here, during the following three days, I believe this Symposium is able to offer an attractive technical program consisting of about 80 of oral presentations including status reports by the invited speakers from 6 countries. In addition, we could have a special talk of Recent Activities of the International Group on Research Reactors and of the Advanced Neutron Source by Dr. Colin D. West of the Oak Ridge National Laboratory as guest presentation.

Now, expecting for every success, here, I declare opening the Third Asian Symposium on Research Reactors.

Thank you.

Organizing Comittee

Chairman : T.Asaoka
Members of Comittee

Y.Oka (Univ. of Tokyo)	H.Nishihara (KURRI)
T.Shibata (Kinki Univ.)	T.Sato (Musashi Inst. of Tech.)
S.Harasawa (IAER, Rikkyo Univ.)	N.Mizoo (PNC)
T.Sugawara (Toshiba Ltd.)	K.Kokubu (JAIF Inc.)
S.Matsuura (JAERI)	E.Shirai (JAERI)
O.Horiki (JAERI)	

Program Comittee (JAERI's Staff)

Chairman : S.Matsuura
Members of Comittee

A.Kohsaka	K.Kaieda	T.Hiraoka
M.Kawasaki	E.Shirai	H.Takahashi
T.Kodaira	T.Tobioka	I.Kobayashi
O.Horiki	Y.Futamura	H.Ando
Y.Ichihashi	S.Saito	N.Ogino
N.Itoh	H.Ichikawa	

Secretariat

E.Shirai
Director, Department of Research Reactor
Japan Atomic Energy Research Institute
Tokai-mura, Naka-gun, Ibaraki-ken, 319-11
Telephone 0292-82-5318
Fax 0292-82-5258

O.Horiki	T.Nemoto	H.Ando	H.Itoh	S.Suzuki
T.Kodaira	H.Shitomi	K.Shimizu	H.Ichikawa	N.Ogino
Y.Izumi	K.Okumura			

Third Asian Symposium on Research Reactor
November 11 1991 SUNPIA HITACHI, HITACHI, JAPAN

1. Recent Activities of the International Group on Research Reactors (IGORR) and of the Advanced Neutron Source (ANS)

C. D. West

Oak Ridge National Laboratory
P.O. Box 2009, FEDC Building
Oak Ridge, Tennessee 37831-8218, USA

ABSTRACT

The International Group on Research Reactors (IGORR) was formed in 1990 to facilitate the sharing of knowledge and experience among those institutions and individuals who are actively working to design, build, and promote new research reactors or to make significant upgrades to existing facilities.

The Advanced Neutron Source Project expects to complete conceptual design in mid-1992. In the present design concept, the neutron source is a heavy-water-cooled, moderated, and reflected reactor of about 350 MW(f) power.

INTERNATIONAL GROUP ON RESEARCH REACTORS

About 10 research and test reactors have been commissioned in the last decade or so, and almost as many major upgrades of existing facilities are underway or have been completed. In addition, at least four major new research reactors are in the construction or design phase (Table 1). During this period new technologies (e.g., silicide fuels), new regulations, and new scientific opportunities have emerged and have influenced reactor and facility design.

During this period, there was no organized forum devoted entirely to the exchange of information and the sharing of lessons-learned among the various groups involved in research reactor design, construction, and upgrade projects around the world. Informal discussions resulted in widespread agreement that such a forum would serve a useful purpose, and, accordingly, a proposal to form one was submitted to several leading

organizations known to be involved in research reactor projects. Essentially all agreed to join in the formation of an International Group on Research Reactors and nominated a senior staff member to serve on its international organizing committee.

The committee organized the first meeting of IGORR, which was hosted by the Advanced Neutron Source (ANS) Project of Oak Ridge National Laboratory. The meeting dates and a specific agenda were prepared in consultation with the wider research reactor community. The first IGORR meeting took place on February 28-March 2, 1990, in Knoxville, Tennessee, USA. It was very successful and well attended; more than 50 scientists and engineers from 25 organizations in 10 countries participated in 2 1/2 days of open and very informative presentations and discussions. There were two workshop sessions, one on the R&D needs of IGORR members and one on worldwide facilities, plans for various user needs, offering opportunities for more detailed interactions. Speakers were asked to provide manuscripts, and proceedings of the meeting were prepared (ref. 1).

Table 2 taken from the *Proceedings* summarizes the findings of the session on R&D needs. The final column and footnote to the table have been added recently and indicate that results are now available for sharing with the community in certain of the key research areas (refs. 2-6).

It was also agreed that a newsletter would be an appropriate way of keeping IGORR members notified of major changes or additions to the various projects in progress or being planned, and two newsletters have already been issued (Ref. 7). The newsletter is compiled from material solicited from the IGORR organizing committee and from other members.

Dr. Bernard Farnoux offered to host a second IGORR meeting, which will be held at Saclay, France, on May 18-19, 1992. The dates were chosen so that members could attend IGORR-2 and also the International Conference on Irradiation Technology on May 20-22, 1992, in Saclay that is being jointly organized by the Commissariat a l'Energie Atomique/CEN, Saclay, France and the Commission of the European Communities/JRC Institute for Advanced Materials, Petten, The Netherlands.

The ANS Project has certainly benefitted from the communications established through IGORR, and we believe that other members find the organization valuable also.

ADVANCED NEUTRON SOURCE PROJECT

The Advanced Neutron Source (ANS), a proposed new reactor-based facility for all kinds of neutron research, is currently in the conceptual design phase. Table 3 lists the

top-level technical objectives of the project, and Fig. 1 is the schedule presently proposed by the Oak Ridge National Laboratory (ORNL).

The conceptual design and the associated R&D activities are a team effort, involving national laboratories, universities, and industry; funded by the U.S. Department of Energy (DOE); and led by Oak Ridge National Laboratory. Table 4 lists the major past and present participants.

Given that the main scientific justification for the project is neutron beam research, the broad outlines of the reactor system design are easily understood: we need a small, high-power core surrounded by a large reflector so that a high-thermal neutron flux is generated outside the core where it is accessible to neutron beam tubes and to cold and hot neutron sources. Figure 2 is a computer drawing of the core and reflector tank components.

The project has devised a core design (Fig. 3) that combines the short heated length (and hence the high-power density capability) of the High Flux Isotope Reactor and the long neutronic length (and hence the high-neutronic efficiency) of the High Flux Reactor at the Institut Laue-Langevin. It is heavy-water cooled and reflected, with coolant flowing upward through the core to avoid the need for a flow reversal during the transition from forced to natural convection.

Safety considerations have played a major role in the ANS conceptual design. Probabilistic risk analyses have been used to examine proposed design features and to improve the design. As with the U.S. DOE's Advanced (Power) Reactors Program, passive safety features are employed to decrease risk (Fig. 4).

The reactor serves only as a source of neutrons for the experimenters. The design of the experimental facilities is guided by the user community through the National Steering Committee for an Advanced Neutron Source (NSCANS). Table 5 lists the major research facilities planned at the ANS. Of course, these figures may be modified somewhat as the design proceeds and in response to new scientific opportunities, but major changes are not expected.

CONCLUSION

The international research reactor community has been strengthened by the formation of an International Group on Research Reactors (IGORR). The activities of IGORR include meetings and newsletters to exchange information and to provide a mechanism for identifying common research needs and for sharing results.

The Advanced Neutron Source is planned as a major new neutron research facility in the United States. It will provide neutron beams an order of magnitude more intense than any now available, as well as isotope production and materials irradiation testing capabilities.

REFERENCES

1. "IGORR-1, Proceedings of the First Meeting of the International Group on Research Reactors," compiled by C. D. West, CONF-9002100, May 1990.

2. R. E. Pawel, G. L. Yoder, D. K. Felde, B. H. Montgomery, and M. T. McFee, "The Corrosion of 6061 Aluminum Under Heat Transfer Conditions in the ANS Corrosion Test Loop," *Oxidation of Metals* 36 (1/2), 175 (1991).

3. W. K. Sartory, "Analysis of Hydraulic Instability of ANS Involute Fuel Plates," ORNL/TM-11580, (to be published).

4. W. F. Swinson and G. T. Yahr "Dynamic Pressure Approach to Analysis of Reactor Fuel Plate Stability," *Trans. Am. Nuc. Soc.* **61**, 390, June 1990.

5. D. L. Selby, R. M. Harrington, and F. J. Peretz, "Advanced Neutron Source (ANS) Project Progress Report," ORNL-6656, February 1991.

6. G. L. Copeland (ORNL), J. L. Snelgrove (ANL), "Fuel Development for the Advanced Neutron Source," *Proceedings of the Amer. Nuc. Soc. 1990 Annual Meeting, June 10-14, 1990*, TANSAO 61 1-482 (1990).

7. "IGORR News, September 1990; IGORR News, July 1991," compiled by C. D. West.

Table 1. Some new research reactor projects

Reactor	Country	Power, MW	Status
PiK	USSR	100	In construction
KURR	S. Korea	30	In construction
FRM-II	Germany	20	Design
ANS	USA	350	Design
TRIGA	Morocco	1.5	In construction
"	USA	1.1	In construction

Table 2. R&D needs identified at IGORR-I

topics: (being planned (+) or results needed (o):)	ANS	FRM-II	MURR	BNL	Riso	JAERI	Petten	Berlin	ORPHEE	MAPLE	MIT	Status
1. Thermal-hydraulic tests and correlations	+	o	+	o		+						
2. Corrosion tests and analytical models	+	o	o								o	*
3. Multidimensional kinetic analysis for small cores	o	o								+		
4. Fuel plates fabrication	+	+										
5. Fuel plates stability	+	+	o									*
6. Fuel irradiation	+	o	+			+						*
7. Burnable poison irrad.	+	+										
8. Structural materials irradiation	+	o	+	+			+	o	+	+		
9. Neutron guides irradiation	o	o				+						
10. Cold Source materials irradiation	o	o			+			o	+			
11. Cold Source LN_2 test	+											
12. Cold Source LH_2-H_2O reaction (H or D)	o	?		+		+						
13. Instrumentation upgrading and digital control system	+		o	o			+		+			
14. Man-machine interface	o	o									+	

Comments: + results needed and own work/tests planned.
? results needed, but own tests not decided yet.
o results needed, but own work not planned.
* results obtained since the IGORR meeting.

Table 3. Mission of the Advanced Neutron Source

To design and construct the world's highest flux research reactor for neutron scattering - 5-to-10 times the flux of the best existing facilities
To provide isotope production facilities that are as good as, or better than, the High Flux Isotope Reactor (HFIR)
To provide materials irradiation facilities that are as good as, or better than, the HFIR

Table 4. Major participants in the ANS Project

Oak Ridge National Laboratory	Kyoto University
Brookhaven National Laboratory	Tohoku University
Argonne National Laboratory	Kinki University
Idaho National Engineering Laboratory	Osaka University
Babcock & Wilcox	Nagoya University
University of Tennessee	Kyushu University
University of Virginia	Japan Atomic Energy Res. Inst.
University of California	Interatom GmbH
Australian Nuclear Science & Technology Org.	

Table 5. Quantitative expression of performance goals

Neutron beams	
Peak thermal flux in reflector, $m^{-2}.s^{-1}$	$5\text{-}10x10^{19}$
Thermal/fast flux ratio	≥80
Materials irradiation	
Fast flux, $m^{-2}.s^{-1}$	$\geq 1.4x10^{19}$
Fast/thermal flux ratio	≥0.5
Transuranium production[2]	
252Cf production rate, g/y	1.5
254Es production rate, micro/yr	40

[1]To match or exceed the capabilities of the irradiation positions in the HFIR flux trap.

[2]To match or exceed production capabilities at HFIR.

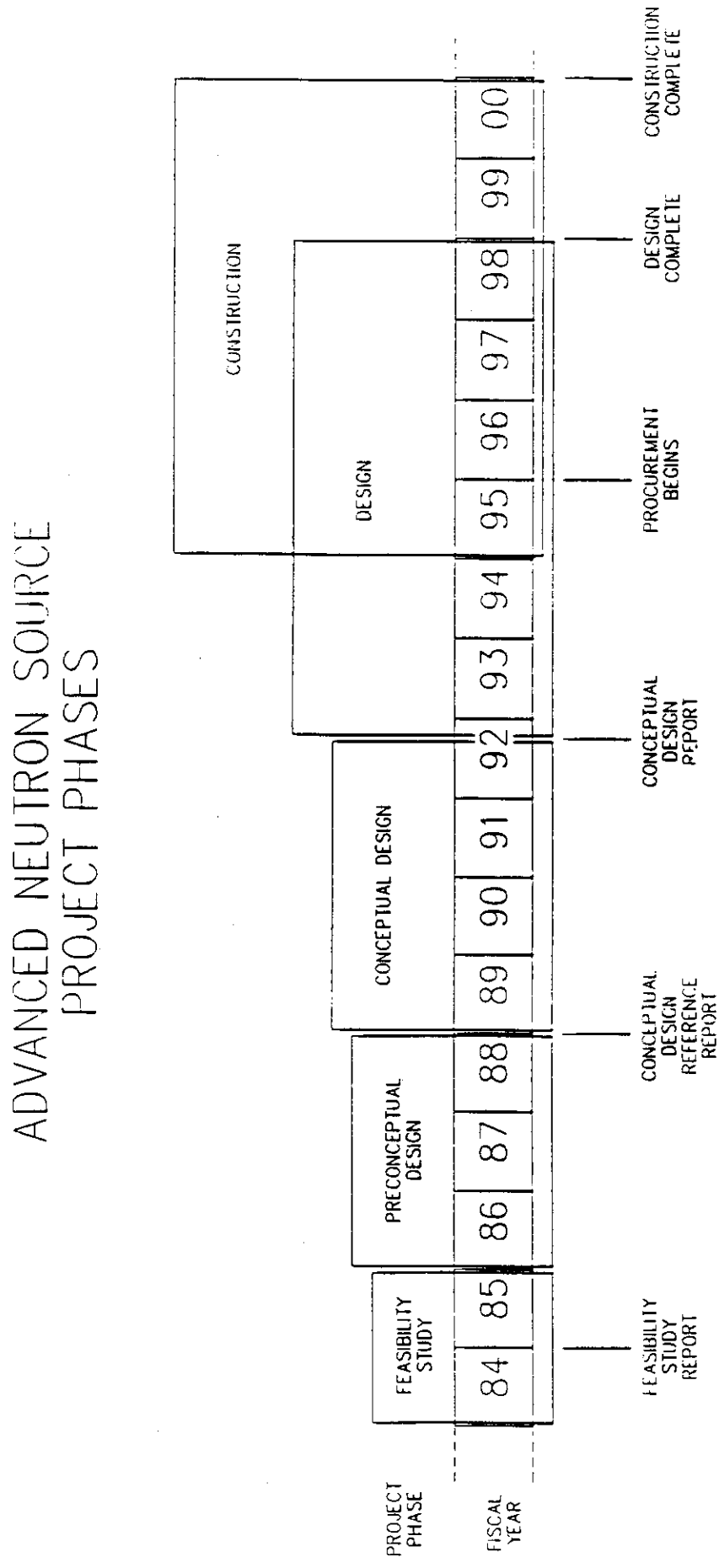
ADVANCED NEUTRON SOURCE
PROJECT PHASES
PROJECT PHASE
FISCAL YEAR
FEASIBILITY STUDY
PRECONCEPTUAL DESIGN
CONCEPTUAL DESIGN
DESIGN
CONSTRUCTION
84
85
86
87
88
89
90
91
92
93
94
95
96
97
98
99
00
FEASIBILITY STUDY REPORT
CONCEPTUAL DESIGN REFERENCE REPORT
CONCEPTUAL DESIGN REPORT
PROCUREMENT BEGINS
DESIGN COMPLETE
CONSTRUCTION COMPLETE

Figure 1

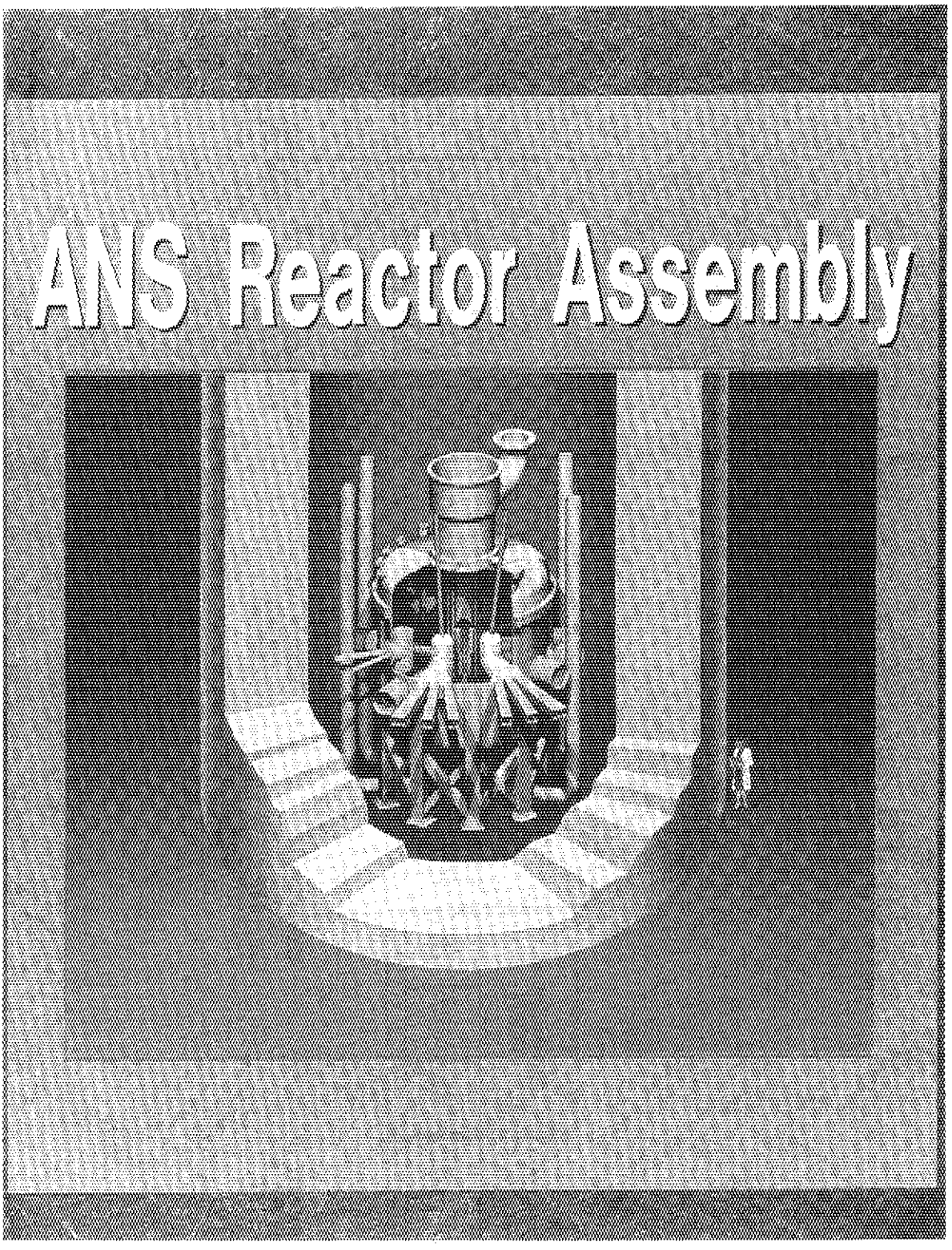

Figure 2. ANS Reflector Tank

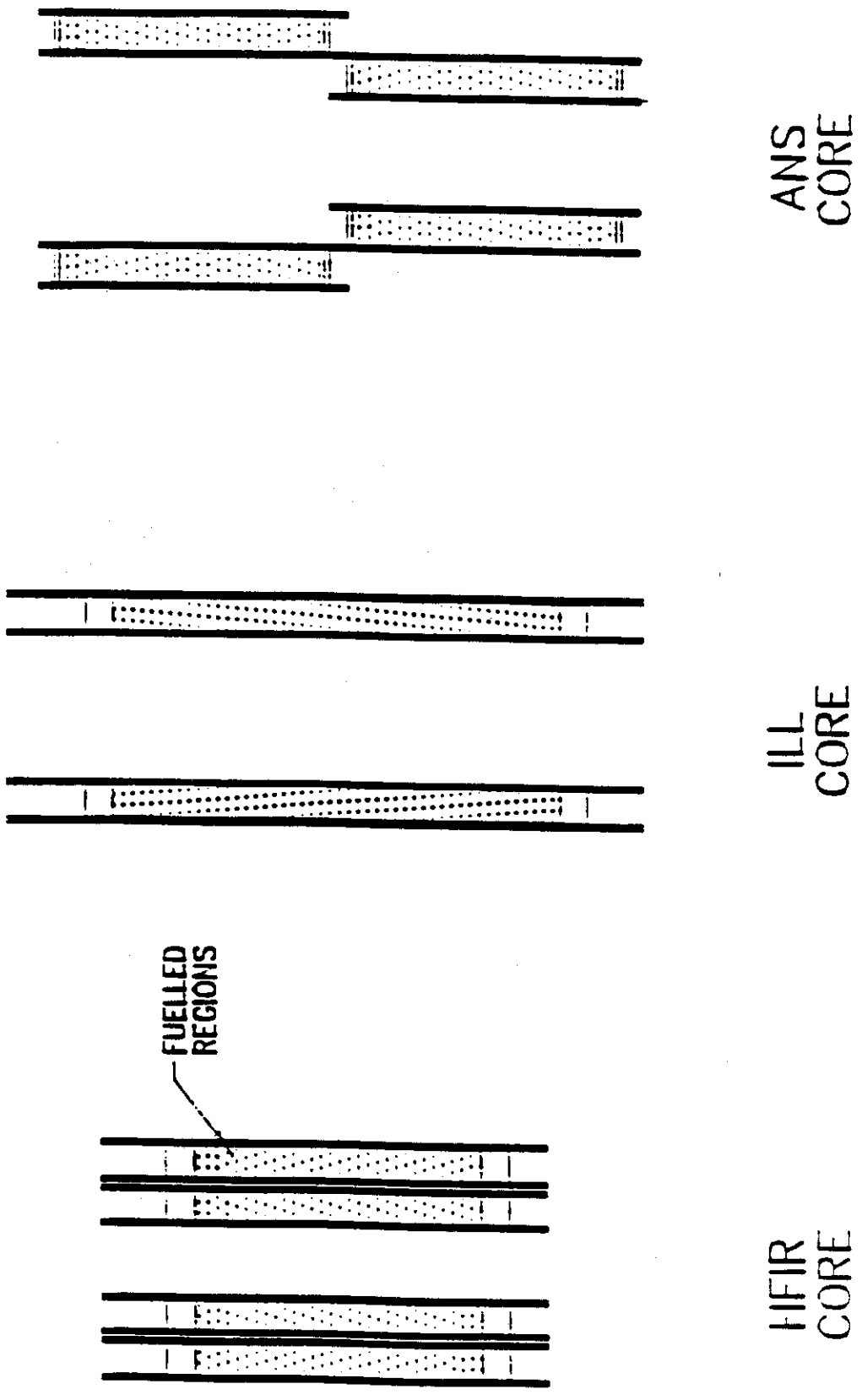

Figure 3. HFIR, ILL, and ANS Cores

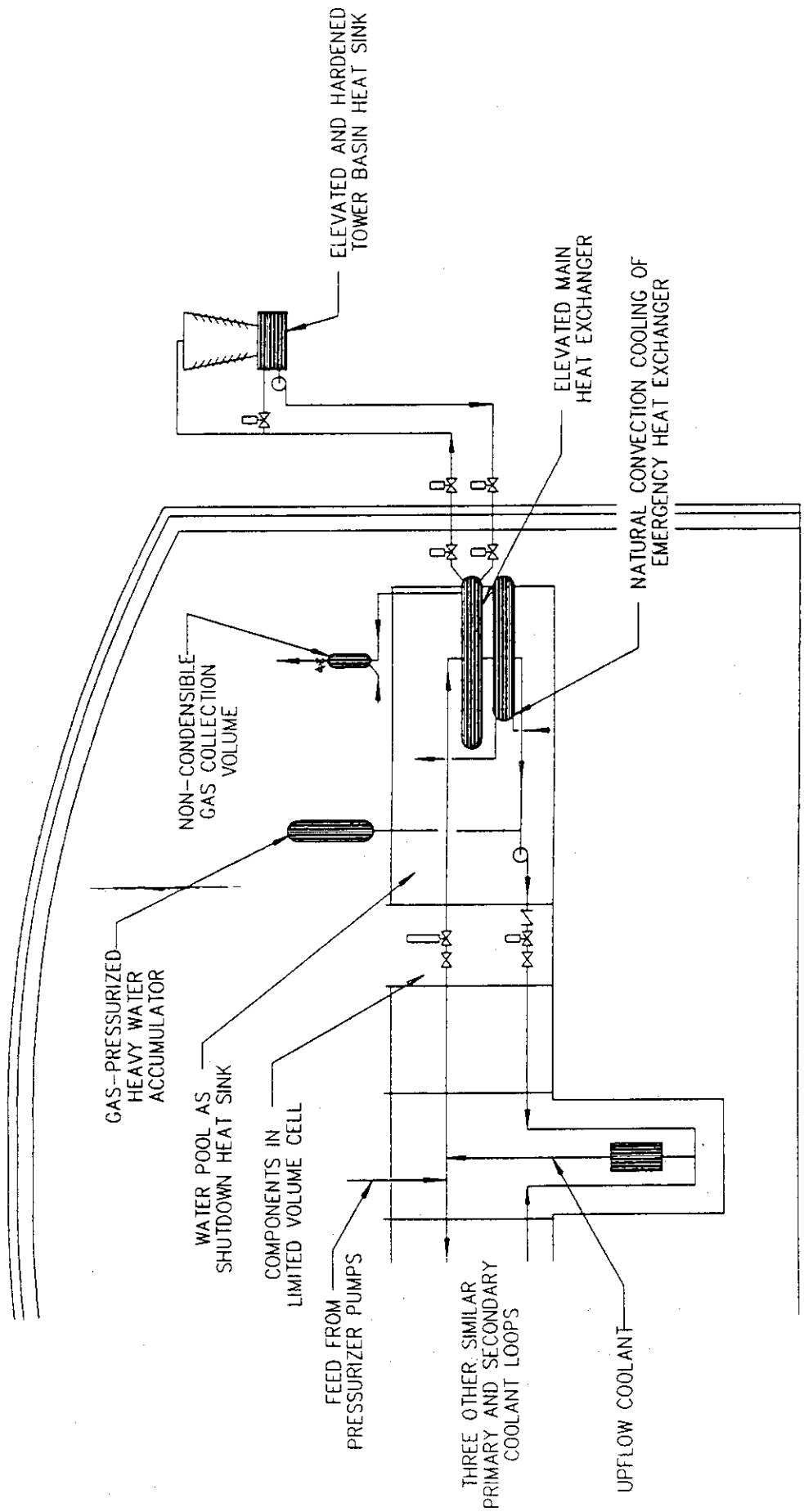
SOME PASSIVE SAFETY FEATURES OF THE
ADVANCED NEUTRON SOURCE REACTOR COOLING SYSTEM DESIGN
ELEVATED AND HARDENED TOWER BASIN HEAT SINK
ELEVATED MAIN HEAT EXCHANGER
NATURAL CONVECTION COOLING OF EMERGENCY HEAT EXCHANGER
NON-CONDENSIBLE GAS COLLECTION VOLUME
GAS-PRESSURIZED HEAVY WATER ACCUMULATOR
WATER POOL AS SHUTDOWN HEAT SINK
COMPONENTS IN LIMITED VOLUME CELL
FEED FROM PRESSURIZER PUMPS
THREE OTHER SIMILAR PRIMARY AND SECONDARY COOLANT LOOPS
UPFLOW COOLANT

Figure 4.

1. Current Status of Research Reactors

TOSHIKAZU SHIBATA, SHOJIRO MATSUURA

Research Reactor Association of Japan

ABSTRACT

The status of research reactors in Japan is reviewed briefly. The related problems are discussed.

INTRODUCTION

In 1955, research and developments of nuclear energy began in Japan. The first research reactor JRR-1 was constructed in JAERI, Tokai in 1957. In about 10 universities, departments of nuclear engineering opened and student educations started at about the same time.

The JAERI made several research reactors sequentially according to research requriements. However, each university which opened nuclear engineering department did not provide research reactors except 3 universities since opening of the department of nuclear engineering. It was supposed that the biggest reason must be difficulties to obtain the public acceptance. As the results, research reactors in Japan are less than 20 including critical facilities shown in the Table.

Research reactors in Japan have a large variety and there is no reactor of the same type except a couple of the TRIGA MarkⅡ.

Almost of the research reactors are being used for joint research among researchers under the sponcership of the Goverment of Japan.

BRIEF DESCRIPTIONS OF EACH REACTOR

JAERI

JRR-2

The JRR-2 is a CP-5 type heavy water reactor of 10MW. It reached the first criticality in 1960. The total operating time is approximately 72,000 hours, and integrated power is 640,000 MWh. In 1987, the enrichment of the fuel was changed to "medium enriched uranium." Normally, the reactor is in operation for 12 cycles of two weeks period per year.

The main utilization fields are neutron scattering, irradiation of fuels and materials, radio isotope (RI) production and so on. Recently, the reactor is being used for neutron capture therapy and related studies.

In 1990, reactor core tank and cooling system were examined for their integrity. In July, 1991, however, the main cooling pump had a trouble and it is shut down for reparing. Because of the completion of JRR-3M upgrading

RESEARCH AND TEST REACTORS IN JAPAN

Reactor	Year of Crit.	Reactor Type	Power	Flux Th.	Flux Fast
JRR-2	1960	D_2O CP-5	10,000KW	2.0E14	6.0E13
JRR-4	1965	Pool	3,500KW	3.5E13	8.7E13
JMTR	1968	H_2O Tank	50,000KW	4.0E14	4.0E14
NSRR	1975	TRIGA ACRR	300KW (Pulse 2,300MW)	1.3E12	4.0E12
JRR-3M	1990	H_2O	20,000KW		
VHTRC	1961	Graphite Crit. Assembly	10W	1.0E7	4.0E7
TCA	1962	H_2O Crit. Assembly	200W		
FCA	1967	Fast Crit. Assembly	2KW		5.0E9
UTR (KINKI UNIV.)	1960	ARGONAUT	1W	1.5E7	1.0E7
TRIGA-II (RIKKYO UNIV.)	1961	TRIGA MARK-II	100KW	3.7E11	2.0E12
MITRR (MUSASHI Inst.)	1963	TRIGA MARK-II	100KW	3.5E12	9.8E11
KUR (KYOTO UNIV.)	1964	H_2O Tank	5,000KW	6.0E13	6.5E13
YAYOI (UNIV of TOKYO)	1971	Fast	2KW		8.0E11
KUCA (KYOTO UNIV.)	1974	H_2O,Solid state Crit. Assembly	100W	1.0E8	1.0E8
TTR-1 (TOSHIBA)	1962	Pool	100KW	1.0E12	5.0E11
NCA (NAIG)	1963	H_2O Crit. Assembly	200W	1.0E9	3.0E9
JOYO (PNC)	1977	Fast Breeder Na.	100,000KW		5.1E15
MUTSU (JAERI)		Nuclear Ship	36MW		

program, the decommissioning of the reactor in near future is under consideration.

JRR-4

The JRR-4 is a pool type reactor of 3.5 MW. It went the first criticality in 1965, and total operating time is approximately 26,000 hr. The reactor was used for shielding experiments at the early stage, and now it is used for reactor operator trainning, activation analysis, RI productions and so on.

The fuel will be changed to low enriched uranium (less than 20 %) in near future.

JMTR

The JMTR (Japan Materials Testing Reactor) is a light water moderated and cooled MTR type reactor of 50 MW. The reactor went the first criticality in 1968. Total operating time is approximately 43,000 hr, and integrated power is 86,000 MWD. The reactor is operated continuously for 24 days in one cycle. Five cycles per year including refueling, overhauls, periodical inspection are usual.

The JMTR has the highest neutron flux in Japan. And the reactor has been used for irradiations of reactor materials and fuel samples, and for RI productions.

Regarding the reducing enrichment program, licensing procedures is now being progressed. In the latter half of 1993, the reactor is expected to restart the operation with low enriched uranium fuel.

NSRR

The NSRR (Nuclear Safety Research Reactor) is a principally TRIGA type reactor, and went the first criticality in 1976. Since then, fuel behaviors at reactivity initiated accident have been studied by intense pulsed irradiation. More than 2,200 pulsed operations have been done.

At the beginning, fresh fuels for light water reactor were tested. In 1989, irradiated fuel tests were started with some improvements of the experimental facilities. Also, combined and, sequential pulsed operations (with low flat top pulse and high peak pulse) were begun in the irradiations.

Some of the results of the studies have been employed as the scientific basis of the standards of reactor safety analysis by Japanese Government.

In 1990, silicide plate type fuel tests were started.

While no big troubles have been experienced since the first criticality, some irregular functions were observed in the transient control rod system. The system has been renewed in this year, and comprehensive overhauls are being done under safety point of view.

In future plans, irradiated mixed oxide fuel tests will begin in 1992, and fast reactor fuel tests are expected in the succeeding stage.

JRR-3M

The JRR-3, which was 10 MW, heavy water and slightly enriched uranium reactor, was modified and upgraded to JRR-3M.

The JRR-3M is a pool type, low enriched uranium fuel reactor of 20 MW. The old reactor was removed from the reactor building and new reactor was constructed in the same building. The construction period was 7 years from 1983 to 1990.

The reactor went critical in March, 1990, and is operating 9 cycles of 4 weeks period per year since November, 1990.

The cold neutron source and several neutron guide tubes are installed in JRR-3M. Neutron scattering experiments are main research subjects in JRR-3M and efficient activation analysis which is requested by many researchers is also available.

The JRR-3M is the newest and most powerful research reactor in Japan. Many researchers are expecting its high duty ratio of the operation and grade up of the experimental apparatus for promoting basic research in this field.

VHTRC-EX SHZ (High temperature reactor critical facility, JAERI)

The VHTRC was built in 1961 for graphite reactor experiments. The JAERI is going to construct a high temperature gas cooled test reactor(HTTR). The VHTRC is now being used for preliminary design study of the HTTR.

The power distribution, reactivity worth of control rods and burnable poison etc. are the main issues for the HTTR project.

TCA (Tank type Critical Assembly, JAERI)

The TCA is a light water moderated critical assembly. The construction was completed in 1962. Some parts of transfer cable of instrumentation were renewed in 1989, and water system is now being renewed because of aging of the parts.

The main research subjects are studies for neutronics of light water reactor and criticality of fuel handling facilities. Experiments for APWR and HCLWR core, measuring and monitoring system of criticality, reactivity supressions are involved in the subjects.

The MOX fuel experiments are expected in near future.

FCA (Fast Critical Assembly, JAERI)

The FCA was built in 1967 for fast reactor study. Since then various critical experiments of fast reactor cores have been done, with enriched uranium, plutonium fuels. Void coeffients, reaction rate, Doppler effects are main research subjects.

Metallic uranium fuel will be used in near future.

UNIVERSITY

UTR-KINKI (Kinki University)

The UTR-KINKI (University Trainning Reactor-KINKI) belongs to KINKI University, and is located in the eastern part of Osaka City area. The reactor was constructed in the university main campus and has been used for various research and student experiments.

The reactor power is 1 watt and operated daily for 5 to 6 hours. Using the ever clean and cold core because of the small power, special research works are being carried out. Main research subjects are reactor physics, radiation measurements, biological effects of low level radiation, neutron radiography and so on.

In addition to these activities, a special course for school teacher's trainning using the actual UTR is opened periodically in order to enhance their scientific knowledge and experience on nuclear reactor and general nuclear energy.

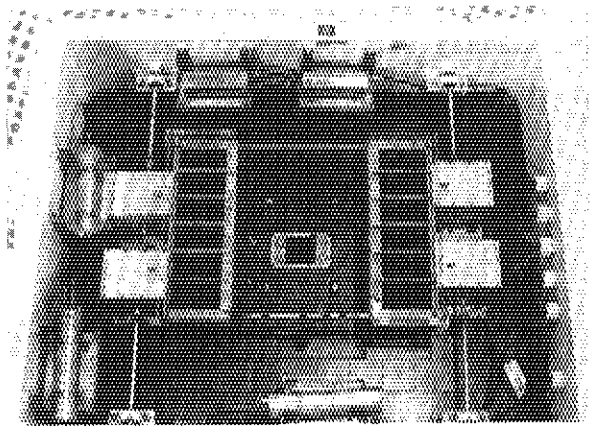

Core configuration of UTR

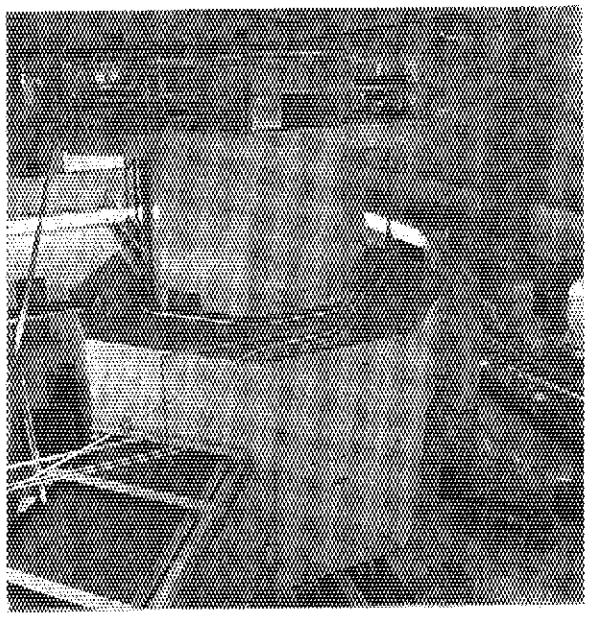

TRIGA-Ⅱ RIKKYO

TRIGA-Ⅱ RIKKYO (RIKKYO University Reactor)

In Japan, there are two 100 kW TRIGA MarkⅡ reactors of steady state operation. The Rikkyo reactor is one of them, and the other one is the Musasi Reactor.

The reactor is operating daily for 6 hours, and approximately 830 hours in the last year.

The reactor is being used in various basic research fields rather than nuclear energy field, i.e. physics, chemistry, biology, archaeology, and so on. The activation analysis is a typical experimental technique in these fields. Fission truck technique, neutron radiography are also important research fields in the RIKKYO Reactor.

MITRR MUSASHI (Musashi Reactor)

Another TRIGA MarkⅡ reactor is the Musashi Reactor which belongs to the Musashi Institute of Technology.

The distinguishing facility of the Musashi reactor is a research facility for neutron capture therapy. The medical facility is well designed and suitably equipped . Many patients have been treated by neutron capture method.

Unfortunately the reactor is now shut down because of pool water leakage which was found in December 1989. the Musashi Institute of Technology is now investigating the technical causes of the leakage and considering the future plan.

KUR (Kyoto University Reactor)

The KUR (Kyoto University Reactor) is a typical tank type light water reactor of 5MW. It went critical in 1964. The average annual operating time is approximately 2,000 hours. In 1988, small leakage of heavy water was found in the heavy water thermal neutron facility. Approximately 28 liters of heavy water and accordingly 6.8 Ci (2.5×10^{11} Bq) of tritium was leaked from the system. The reactor was shut down for more than one years for reparing the leakage.

Many experimental facilities are mounted aroud the reactor. i.e. various neutron scattering apparatus, neutron radiography facilty, low temperature irradiaition loop, on-line mass separator, heavy water thermal neutron facility, graphite thermal neutron facility, three conventional pneumatic tubes, hydraulic conveyer, slant tube etc.

In the heavy water thermal neutron facility, medical studies on neutron capture therapy is being done intensively and 17 canser patients have been treated in the past 2 years. And cold neutron source is mounted in the graphite thermal column.

The KUR is also used for student experiment.

As the future plan, the abortion of the High Flux Reactor program was decided officially in 1991. Following the decision, the Research Reactor Institute started the work to access the integrity of the KUR and to make its modernization plan.

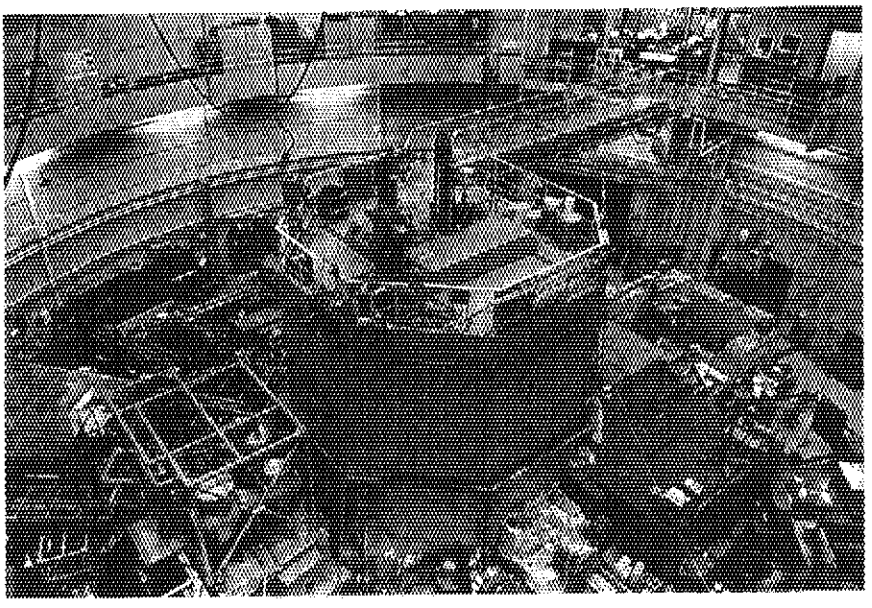

Perspective view of KUR

YAYOI (University of Tokyo)

The Yayoi is located in JAERI, Tokai area, but it belongs to the University of Tokyo. The Yayoi is a fast neutron source reactor of solid cylindrical metal core. It's power is 2KW for steady state operation, and about 1,000 MW for pulsed power operation.

Small metallic core of high enriched urauium produces extremely hard neutron spectrum. The core is movable, and the reactor can be operated in six positions according to purposes of the experiments.

The main subjects are as follows, 1) Various studies using standard fast neutron spectrum, 2) Preliminary study for neutron capture therapy using epithermal neutrons, 3) Study for fusion reactor blancket, 4) Radiation damage by fast neutrons, 5) Radiography using fast neutrons, 6) Student experiments.

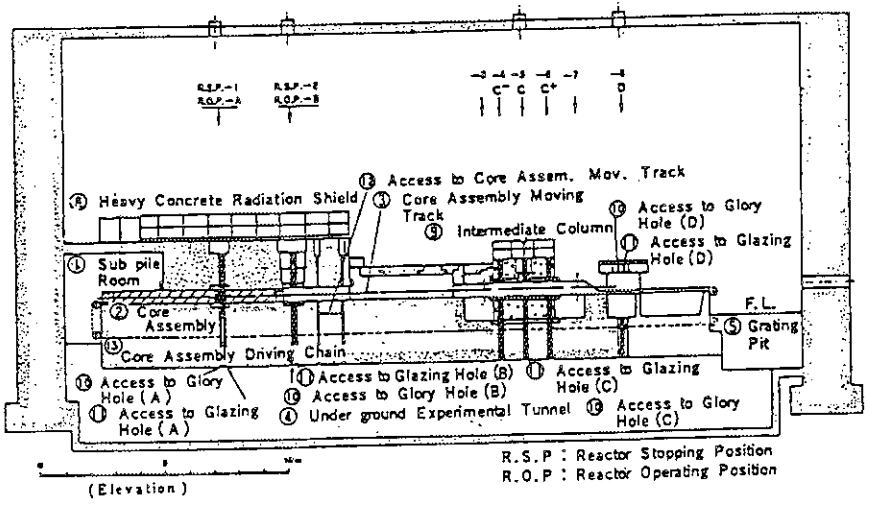

Sectional view of YAYOI

KUCA (Kyoto University Critical Assembly)

In general, critical assmbly is built for preliminary study for a certain type reactor core prior to its construction. KUCA has, however, something different objectives, that is general studies of reactor physics including new type research reactor design study, intensive education of graduate students. Recently studies on criticality safety, and tight lattice core as well as on thorium cycle have been done.

To increase the capacity and flexibility for experiments, KUCA has three core positions of which one is for light water moderated core and two are for solid state moderated cores.

The control and safety system of KUCA is so ingenious that even students of no operating experience can operate safely by themselves except core handling or special operations.

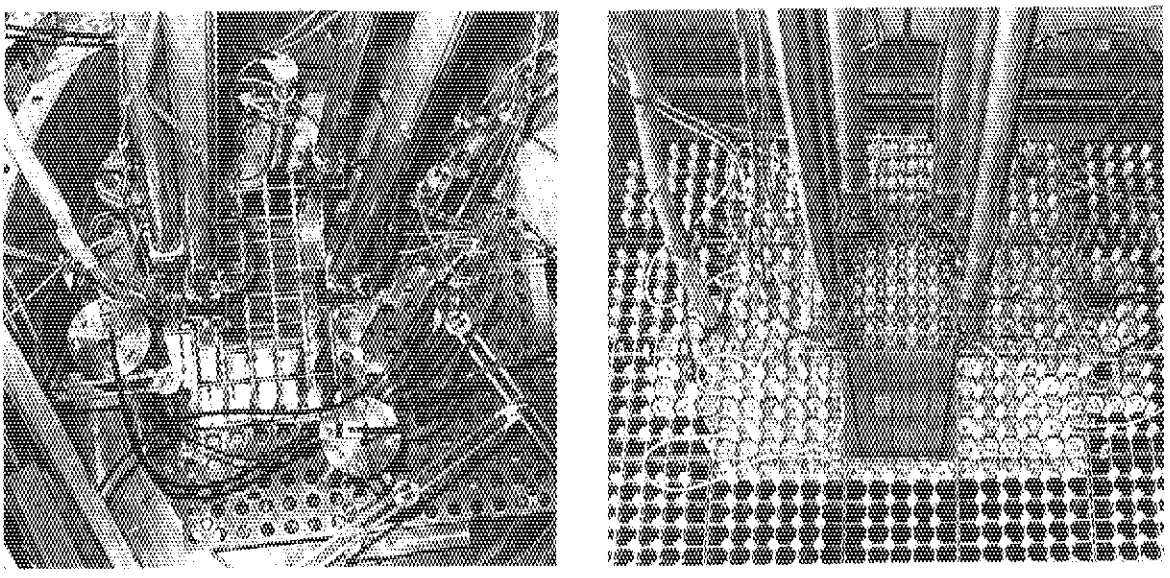

Water moderated core(left) and solid state moderator core(right) of KUCA

INDUSTRY AND OTHERS

TTR-1 (Toshiba Training Reactor-1)

TTR-1 is a swimming pool type reactor of 100 KW. The initial criticality was in 1962. The objectives of the reactor were research for reactor technology, reactor physics including studies for neutronic calculation of reactors, neutron experiments, shielding, radio isotope productions, trainings and so on.

Recently the reactor is being used mainly for studies of neutron counter and activation analysis.

The utilizations are limited within the Toshiba group companies. The reactor is operated for one or two days a week.

NCA (NAIG Critical Assmbly)

The NCA belongs to Toshiba, one of the biggest industrial company in Japan. The NCA is low enriched uranium and light water moderated type. The main subjects are experimental reactor physics, including criticality study and neutronics calculation study on light water reactors. The NCA is in operation for about 10 days a month.

Other typical reactors

In Japan noncommercial power reactors in developing and testing period are involved in the category of research and test reactors. In this category, there exists "JOYO" which is a experimental fast power reactor and "Mutsu" which is a nuclear ship. Among them, the "Mutsu" reactor was shut-down for long time because of imperfections of radiation shielding. After careful repair the reactor was restarted and raised the power in 1990. In October, 1990, the reactor reached the nominal power, 36 MW.

The "Mutsu" is now continuing sea trials. According to the official schedule, after one year sea trial, the nuclear ship "Mutsu" will retire.

CONCLUSION

At the very early stage of the R and D, power reactors were imported urgently due to energy policy in Japan. Accordingly, the importance of research reactors have been minimized in scientific, engineering and political considerations.

The priority of research in the universites moved to the other subjects than nuclear reactors, therefore training and education about nuclear reactors in the universities were not sufficient.

On the other hand, nuclear reactors, are now going into aging stages, and they have many engineering problems while many power reactors are increasing.

To increase engineers which have intension to concern the engineering problems and sufficient ability for solving these problems, education and training using real reactors might be effective and neccessary.

As the matter of fact the lack of the number of research reactor causes the lack of experience on nuclear reactor practice. The lack of practice makes persons of concern an excessive fear, and then causes a delay or mistake of judgements.

Sometimes, research reactors are considered merely as neutron sources and compared with the other neutron sources such as accelerators. Reactors, however, have other unique performances than conventional neutron source. The experience of the research reactors are very effective not only for education and training, but for engineering progress such as various improvements of reactor design, operation manuals and reactor type.

Those who have not sufficient understandings about research reactors, tend to evaluate them by apparent contributions. In this occasion, the author wishes to change their minds.

2. Status Report of Indonesian Research Reactor

BAKRI ARBIE, SUTARYO SUPADI

ABSTRACT

A general description of three Indonesian research reactor, its irradiation facilities and its future prospect are described.

Since 1965 Triga Mark II 250 KW Bandung, has been in operation and in 1972 the design powers were increased to 1000 KW. Using core grid form Triga 250 KW BATAN has designed and constructed Kartini Reactor in Yogyakarta which started its operation in 1979. Both of this Triga type reactors have served a wide spectrum of utilization such as training manpower in nuclear engineering, radiochemistry, isotope production and beam research in solid state physics.

Each of this reactor have strong cooperation with Bandung Institute of Technology at Bandung and Gajah Mada University at Yogyakarta which has a faculty of Nuclear Engineering.

Since 1976 the idea to have high flux reactor has been foreseen appropriate to Indonesian intention to prepare infrastructure for nuclear industry for both energy and non-energy related activities.

The idea come to realization with the first criticality of RSG-GAS (Multipurpose Reactor G.A. Siwabessy) in July 1987 at PUSPIPTEK Serpong area. It is expected that by early 1992 the reactor will reached its full power of 30 MW and by end 1992 its expected that iradiation facilities will be utilized in the future for nuclear scientific and engineering work.

I. INTRODUCTION

National Atomic Energy Board of Indonesia or Badan Tenaga Atom Nasional (BATAN) owned and operated three research reactors which consist of two Triga type low flux reactors and one high flux multipurpose reactor.

The first reactor, Triga Mark II reactor located at Bandung West Java, is a thermal, light water moderated and cooled, open pool type research reactor. It became critical in 1965 and operated at a power of 250 KW. The power level was upgraded, following total renewal of the core gird, cooling and instrumentation system, to 1000 KW in 1972. The reactor is initially introduced together with Bandung Institute of Technology as the first tool to gain know how in nuclear technology.

Kartini Research Reactor as a second reactor located at Yogyakarta, Middle Java, is a similar Triga type designed for operation up to 200 KW thermal power. Using Triga reactor as a reference and used component from Bandung, Batan staff had designed, and constructed Kartini reactor which obtained its criticality in 1979. The reactor utilization has been implemented by Batan together with Gajah Mada University which has a faculty of Nuclear Engineering.

Since 1976 the idea to have high flux reactor has been foreseen appropriate to Indonesian intention to prepare infrastructure for nuclear industry for both energy and non energy related activities.

Having experience gained during operation and construction of previous two reactors and its supporting facilities Batan has developed specification and objective of Centre for Nuclear Industry Development at Puspiptek area which consists of Multipurpose Research Reactor (RSG-GAS) and its affiliated facilities such as Fuel Element Production Installation (FEPI) to produce MTR type fuel element, Experimental Fuel Element Installation (EFEI) and Radio Metalurgy Installation (RMI) to gain know how on nuclear fuel for power reactor, Radio Isotope Installation (RII) to process various radioisotopes, Engineering Safety Installation (ESI) and Nuclear Mechano Electric Installation (NMEI) to obtain know how in nuclear engineering and manufacturing capability of special nuclear component and Radioactive Waste Installation (RWI) to have capability to manage and handle radioactive waste in Indonesia.

The idea come to realization with the first criticality of RSG-GAS in July 1987 and since then reactor has been in commissioning stage to reach full power of 30 MW by early 1992 and by end of 1992 it is expected that irradiation facilities at RSG-GAS have been installed and commissioned.

The role of Triga type reactor which is mainly for training, research and isotope production classified as a low flux research reactor will be used in ways that complement the RSG-GAS which has neutron fluxes exceeding 10^{14} $n/cm^2.s$.

Small research reactors in Indonesia have demonstrated its ability as the focal point for broad range of nuclear technology transfer and as the training ground for developing techniques prior to construction of much larger reactor.

Research reactors provide powerfull tool for research in nuclear physics, material science, fuel technology; analytical chemistry, nuclear safety and control instrumentation, radioisotope production for agriculture, industry medicine beside providing also the basic infrastructure for training personal for future nuclear power stations.

II. REACTORS DESCRIPTION

For discussing the status of research reactors in Indonesia, table I gives the basic features of BATAN Research Reactors.

Table I : Basic Features of Indonesian Research Reactors

	Triga Mark II	Kartini	RSG-GAS
- Reactor Type	Tank	Tank	Tank
- Date of Criticality	20 Feb. 65	25 Jan. 79	29 July 87
- Reactor Power	1000 KW	200 KW	30 MW
- Fuel Material	UZrH, 19.7% enrichment	UZrH, 19.7% enrichment	U3O8Al 19.75 % enriched
- Fuel Element	Rod	Rod	Plate
- Fuel Cladding	St. steel	Al	AlMg
- Core Size	H (55 cm) D (53.16 cm)	H (55 cm) D (45.7 cm)	H (73.8 cm) L (80.6 cm) W (76.1 cm)
- Maximum thermal neutron flux (n/cm^2sec)	10^{10}-10^{12}	10^{10}-10^{11}	3.5×10^{14}
- Moderator	light water	light water	light water
- Coolant	light water (Natural circ.)	light water (Nat. Circ)	light water (Forced Cooling)
- Control Rod	B4C	B4C	AgIndCd
- Utilization	- Training - R&D in nuc lear tech. - Radio Iso tope Pro- duction/NAA - Beam Tube Experiment	- Training - Reactor Physics Studies - NAA	- Material testing - Isotope production - Beam tube Experiment - Fuel testing - Training

Triga Reactor with a normal operating power of 1000 KW is cooled and moderated by demineralized light water circulating in a closed circuit. The cylindrical tank which houses the reactor core consist of an alumunium construction of 6 m height and 2 m in diameter.

The generated heat is dissipated in one heat exchanger to secondary coolant which than discharged the heat through cooling tower.

The operating pattern of Triga reactor depend on the need, for example to produce reactor radioisotope may be operated for 7 days continous power operation.

Inside the reactor tank the irradiation devices installed in a core position of the fuel region or of the reflector region. Rotating radioisotope production facility called Lazy Susan provide irradiation space for 80 irradiation capsule. One pneumatic tube permanently installed provides possibility for short term irradiation of samples with a very short transit time, which is necessary for studying very short lived activation products.

Kartini Reactor has similar design to Triga Mark II reactor with unique advantage is that the reactor is coupled to the natural uranium light water subcritical assembly through one of its beamport.

The basic design of both Triga Mark II and Kartini Reactor is highly inherent safe using UZrH fuel which means that mechanical or human error would not give serious risk make it suitable for training purposes.

RSG-GAS is a multipurpose reactor with a normal operating power of 30 MW termal. The reactor is cooled and moderated by demineralized light water circulating in a closed circuit.

The rectangular core arranged at 13.75 m deep tank pool. A 10x10 array of grid containing 40 fuel assemblies, 8 control fuel elements, one Central Irradiation Position, 4 Irradiation Positions, 37 beryllium reflector elements and beryllium block in L size as reflector for two sides of the core. Inside the beryllium block housed 6 beam tubes penetrating reactor tank and biological shielding at experimental hall level. The U308A1 fuel element with 19.75 enrichment consist of 21 plate for standard element and 15 plate for control element.

The generated heat is dissipated in two heat exchangers to the secondary coolant which is taken and discharged through cooling tower.

The operating pattern of RSG-GAS follows a 27 days operating period in one cycle.

III. RESEARCH AND UTILIZATION

In appropriate to nuclear application in energy and non energy field in Indonesia there seems no need to emphasize the tremendously important role of the human factor.

The two Triga type reactor have survived 26 years and 12 years of operation time. During this time period technicians, engineers and scientist have learned many activities through operation, maintenance and utilization of the reactor facilities.

Human resource development based on interdisciplinary application of low flux research reactor are set forth in table II.

Table II. Interdisciplinary applications of low flux Reaseach Reactors in Indonesia

Reactor Physics and Core Thermohydraulic
Operator and Student Training
Nuclear Instrumentation
Health Physics and Radiation Portection
Radioactive waste disposal
Activation Analysis
Hot Atom Chemistry
Neutron diffraction
Biology
Isotope Production for Medical, and Industrial
Nuclear Engineering (Process and water chemistry)
Neutron Radiography

A basic education in nuclear engineering for student of Dept. of Nuclear Engineering, University of Gajah Mada and Nuclear Specialist School of Batan was established which allowed mainly the study of handling radiation sources, the application of radiation measuring technique and shielding properties of different materials. Furthermore experiments are supplemented with the following :

- criticality experiments,
- reactivity changes due to variations of the core configuration or insertion of different material
- measurement of neutron flux
- control rod characteristics
- radiation field in the vicinity of the reactor
- reactor operation
- power calibration

Similar activities or experiment for reactor operator and supervisor allow in particular difference in depth of theoritical knowledge and number of practical training.

Other reactor utilization and experiments using low flux research reactor in neutron diffraction, chemistry, biology, reactor physics and neutron radiography has been described elsewhere (1,2,3,4).

Owing to limited availability of neutron flux, research and application in some area has been performed only to a limited extent such as beam tube experiment, radioisotope production, fuel and material testing, neutron radiography, silicon doping and neutron activation analysis.

To accomodate the increasing demands in area mentioned above multipurpose reactor with high neutron flux and its incorporated irradiation facilities were constructed and installed (5).

In the construction of such high flux reactor several consideration has been performed owing to the evolution in two specific experimental reactor area 1) technology state of art and 2) utilization program which have to be adapted (6) such as :

- need for higher neutron flux available for experiment which generally obtained by higher reactor power,
- development in reactor and its irradiation technology which should confirm with the latest safety criteria,
- development in experimental irradiation program,
- imposed utilization of Low Enriched Uranium (LEU).

Experimental facilities at RSG-GAS will be fully installed in 1992. These irradiation facilities could be specified in three different area of application i.e Fundamental Research, Applied Research and Production by Neutron Irradiation as in Table III.

Table III. Utilization Facilities at RSG-GAS

Type of activities	Facility	No	Note
Fundamental Research	1) Triple axis spectrometer (TAS) at beam tube S-4	1	Material science and solid state physics
	2) SANS and HRSANS at S-5	1	
	3) Powder Diffractometer/High Resolution powder diffractometer	1	
	4) Four Circle Diffractometer and Texture Diffractometer.	1	
Applied Research	1) Dynamic Neutron Radiography (at beam tube S-2)	1	NDT, Inspection of composition
	2) Wet Neutron Radiography (inpool)	1	Fuel/Material
	3) Power Rampt Test Facility		Fuel
	4) PWR/PHWR inpile loop (CIP)		Fuel
	5) Capsules (pin+ Cyrano)	2	Fuel/Material
	6) Pneumatic Rabbit System	1	NAA

Activities	Facility	No	Note
Production by Neutron Irradiation	1) Be Reflector irradiation hole	4	Isotope production
	2) Neutron Transmutation Doping	1	Si doping
	3) Irradiation Capsule at IP	2	Isotope production
	4) Iodine loop	1	Isotope production
	5) Hydraulic Rabbit System	4	Isotope production and NAA

Status of RSG-GAS core configuration now reached 6th core and due to the installation of inpile loop system reactor will resume operation January 1992. Starting on third core, reactor had been used to performed irradiation services such as :

- Irridium-192 (two batches production test for consumer)
- Fission product molybdenum (bi weekly)
- Silicon doping (testing, commissioning and characterization, 2 batches for Japanese Company)
- Hot start up of the NDT and TAS
- Irradiation of the fuel assemblies (domestic manufactured fuels, 2 silicide and 2 oxide fuels)
- Experiment using powder diffractometer (in cooperation with JAERI two paper have been published).

After low power and qualification test it is expected that by February 92 reactor will reached full power operation of 30 MW thermal.

IV. FUTURE PROGRAMS

Appropriate to evolution in experimental reactor technology and its utilization program there are still two main criteria has to be adapted for the reactors existing in Indonesia. Firstly to make sure that the existing reactor and its irradiation facilities should confirm with the latest safety criteria and secondly developing and optimising utilization of existing reactor facilities in accordance to the latest development.

With existing facilities in which some still need improvement the most important resource is the people who will design, implement, and evaluate experimental being performed and last but not least the people to operate and maintain the facility. All the people involve should have certain qualification which means trained and experienced engineers, scientists and technician.

Due to this fact the reactor utilization in Indonesia will be divided into 1) Fundamental Research 2) Applied Research 3) Production by Neutron Irradiation and 4) Training and Familiarization.

The reactor utilization in the future based on number of activities (%) will be expected as :

	Fundamental Research	Applied Research	Production by Neutron	Training
Triga Mark II	20	10	40	30
Kartini	30	5	5	60
RSG-GAS (design)	30	30	30	10
(1992-94)	20	10	40	30

In case of RSG-GAS because of its status as a multipurpose reactor idealy has to accomodate 3 main activities in a similar manner even though in the early period (92-94) the main activities will be production by neutron irradiation which is readily available and training/familiarization to more sophisticated equipment and need for basic know how for Fundamental and Applied Reasearch activities. Immediate activities will be reorientation and relocation of human resource in order to have optimum utilization of the reactor and furthermore for :

1. Kartini Reactor
   - to equipped reactor with additional facilities for training and fundamental research.

2. Triga Mark II
   - to renovate old part of reactor system
   - to maintain reactor as a complimentary to RSG-GAS for radioisotope production

3. RSG-GAS
   - to maintain availability of the reactor for user and experimenter in the safe manner (5 cycles/year)
   - to have the basic data of all irradiation facilities
   - to familiarize with behaviour of reactor and its irradiation facilities
   - to see the possibility of using U3Si2 as a reactor fuel

Possible utilization of research reactors in reactor operation and maintenance, irradiation services/experiments, post-irradiation experiment and technical development under an International Research program will be highly appreciated.

References :

1. Ismuntoyo, R.P.H, Operating Experience of Bandung Triga Mark II Reactor, ASRR I, Tokyo November 1986

2. M. Salman Suprawardhana, Status of Kartini Research Reactor at Yogyakarta Nuclear Research Centre ASRR II, Jakarta, May 1989

3. Syarip et al, Performance of the Subcritical Assembly Using the Radial Beamport of Kartini Triga Reactor as a Neutron Souce, ASSR II, Jakarta, May 1989

4. Arlinah Kusnowo, Personal Communication

5. B. Arbie, Supadi, Albat, Irradiation facilities at the MPR G.A Siwabessy Reactor for R & D programs. Proceeding MPR Sympossium, Grenoble, October 1987

6. J.M. Cerles, J.F. Veyrat, les developpements recents des reacteurs de recherche du CEA et leur utilisation pour des progrmmes internationaux, Proceeding MPR Symposium, Grenoble, October 1987

3. Operating Experience of TRIGA MK-II Research Reactor in Bangladesh

M.A. Mannan and Kamal Ahmed
Bangladesh Atomic Energy Commission
P.O. Box. 158, Dhaka-1000, Bangladesh

ABSTRACT

A 3 MW TRIGA MK II Research Reactor was installed in Bangladesh in 1986. The reactor is being utilized for research, training and for production of radio-isotopes. Recently two faults were detected, one in the Emergency core Cooling System and the other in the Primary Coolant Loop, which hindered the operation of the reactor partially. The faults were investigated by a team of local experts. Results of analyses of possible initiating events of the faults and the remedial steps are briefly discussed in the paper.

1. INTRODUCTION

Bangladesh Atomic Energy Commission (BAEC) installed a 3 MW pulsing type Research Reactor at its Atomic Energy Research Establishment (AERE). The reactor had achieved criticality in September 1986 and reached 3 MW steady state power with 100 LEU fuels in the later part of the same year [1]. The reactor is being used for training, research and isotope production. The Central Thimble was designed, installed and tested successfully by the BAEC personnel at a later stage in 1988 [2]. The Reactor was operated for 133 hours for a total of 195 MWh in 1990. On one occasion the reactor was operated almost continuously for 54 hours for production of Scandium-46 isotope. Such an extended operation of the reactor provided valuable experience and added to the confidence of the operation team. In the previous year (1989), the reactor was operated for 270 hours at a total of 606 MWh. The apparent under utilization of the reactor in 1990 was caused partially by two major problems that were encountered since its commissioning. These problems are described in the following paragraphs.

2.1 PROBLEM IN THE EMERGENCY CORE COOLING SYSTEM (ECCS)

The essential safety requirement of the design is that the reactor core has to be covered with water for an extended period following the loss of primary coolant. The Emergency Core Cooling

System is designed to meet this requirement. Part of the system is shown schematically in Fig. 1. The reactor core assembly includes an upper shroud containing a column of 76.2 cm of water over top of the core. In the event of a tank or beam tube rupture or break in the primary coolant line, this volume of water is available for removal of decay heat from the fuel elements, primarily by evaporation. Coolant from the ECCS must be available before this water is evaporated completely. The float level switches activate the pump of the ECCS whenever the water level reaches 4.27 m below the normal pool level. The pump and the float level switches receive independent power supply from a battery, which is kept fully charged by a charger connected to the electrical power system of the reactor building. The emergency pump can circulate water from 32,600 liter N-16 decay tank through the reactor core assembly at a rate of 3.8 liters per minute for about an hour. The valve of the emergency pump is always kept open when the reactor is in operation. A manual back-up system is also provided by connecting a reliable water tank located on the top of the building. This can be used if the emergency pump fails.

The decay tank is separated from the adjacent primary pump room by a thick layer of concrete shielding. As such, the part of the ECCS located inside the shielding was not accessible for conducting regular and routine inspection by the maintenance personnel. Aluminum pipping of the ECCS was placed in a small trench in the floor of the decay tank room.

Evidence of leakage of water from the piping of the ECCS was detected at one stage of routine inspection of the primary pump. It was also found that some cracks had developed in the aluminum piping of the ECCS.

2.1.1 POSSIBLE INITIATING EVENTS

Analysis of the reasons that might have caused the cracks indicated the following two possible initiating events:

a. The Aluminum piping was in contact with the floor. The floor sometimes gets wet and physical contact with the moist cement floor over an extended period might have caused the corrosion in the pipe.

b. There did not exist any gap between the floor and the first right angle bend of the pipe drawn from the bottom of the decay tank. The decay tank itself might have settled down slightly since its construction. As there was no room for accommodating the displacement of the decay tank, the ECCS pipe might have been subjected to severe stress.

Analysis carried out by the local team, indicated that the crack was probably caused by one of the two factors or by a combination of these two.

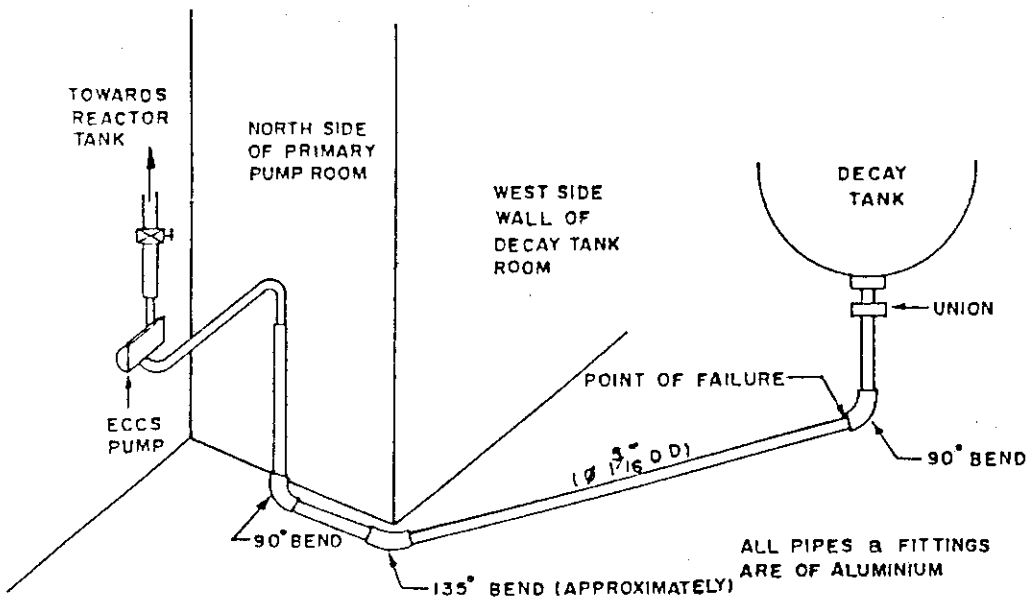

FIG. 1. ORIGINAL INSTALLATION

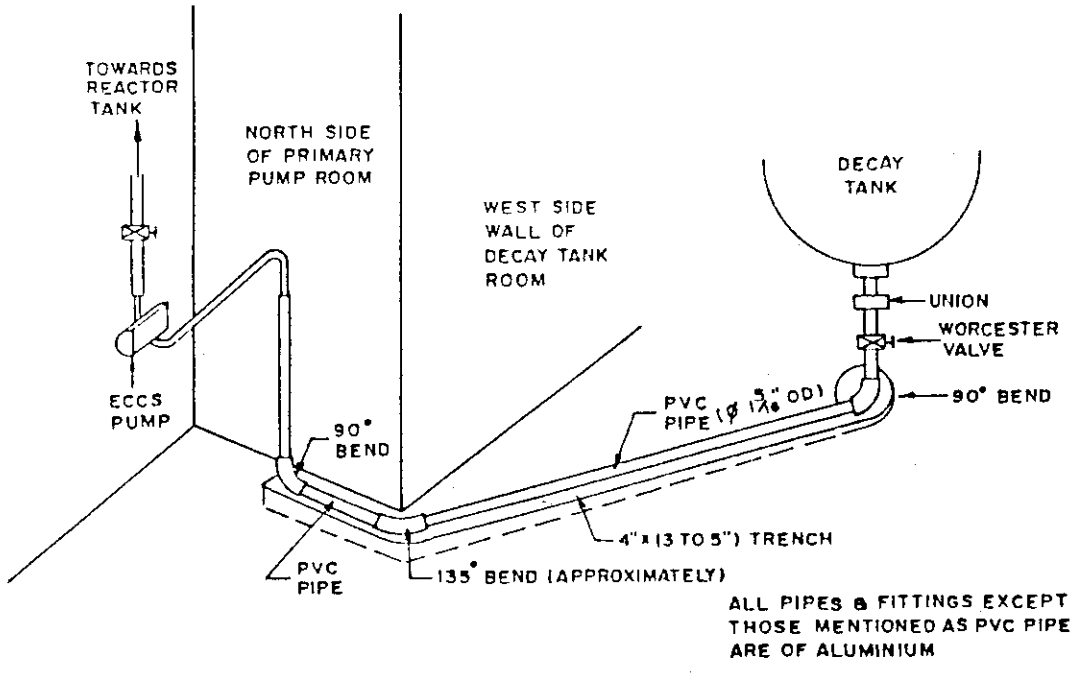

FIG. 2. MODIFIED INSTALLATION

2.1.2 REMEDIAL MEASURES

The team of local experts had opined that, the possibilities of any future corrosion must be eliminated. Since the moisture could not be eliminated altogether, PVC was recommended to replace Aluminum as the piping material. Further, a larger trench in the decay tank room was provided for housing the new pipe so as to avoid possibilities of direct contact with the cement surface. This arrangement is expected to be useful in accommodating any further settlement of the decay tank structure.

The ECCS was modified on the basis of recommendation of the local team of experts. The supplier of the reactor was also consulted in undertaking the stated modifications. The modified ECCS is given schematically in Fig. 2. It may be seen that the modified ECCS is provided with a valve in the suction side, which is designed to remain open in normal operation. This valve is designated to isolate the ECCS manually whenever required. This was deemed essential from maintenance point of view, which was not envisaged in the original design and installation.

2.2. PROBLEM IN THE PRIMARY COOLING SYSTEM

Part of the primary cooling system is shown schematically in Fig 3. The coolant enters the reactor tank through the top of the pool. The coolant is drawn by pump suction down through the reactor core lower plenum. From the lower plenum the coolant enters a 30.5 cm diameter pipe and flows through a shielded trench to the N-16 decay tank and then to the suction side of the primary pumps. Two pumps operating in parallel circulate the coolant through the heat exchanger and back to the reactor tank through 25.5 cm diameter pipe. An anti-siphon line is provided to allow air into the suction line if the water level in the tank drops below a preset point. This prevents the primary pump from pumping the core dry in the event of a break in the system down stream of the pump. This anti-siphon line is a back up to the float level switches which are intended to turn the primary pumps off. The primary flow rate of 13,250 liters per minute has to be ensured before the reactor is allowed to operate in the forced cooling mode. One Exi-check valve is provided in the discharge line of each pump. These valves are intended to prevent back flow of the coolant. Two butterfly valves are included, one in the suction side and the other in the discharge side of each pump. Normally such valves are required principally for maintenance purposes and should remain open during normal operation. But in the present case, the butterfly valve is to be kept partially closed (55%) in order to achieve the desired flow of 6625 liters per minute for each pump. Circumferential welding of one exi-check valve was found to be cracked during a routine inspection. Extensive investigation of the primary cooling system was subsequently carried out by a team of local experts. Findings of the team is outlined in the following paragraphs.

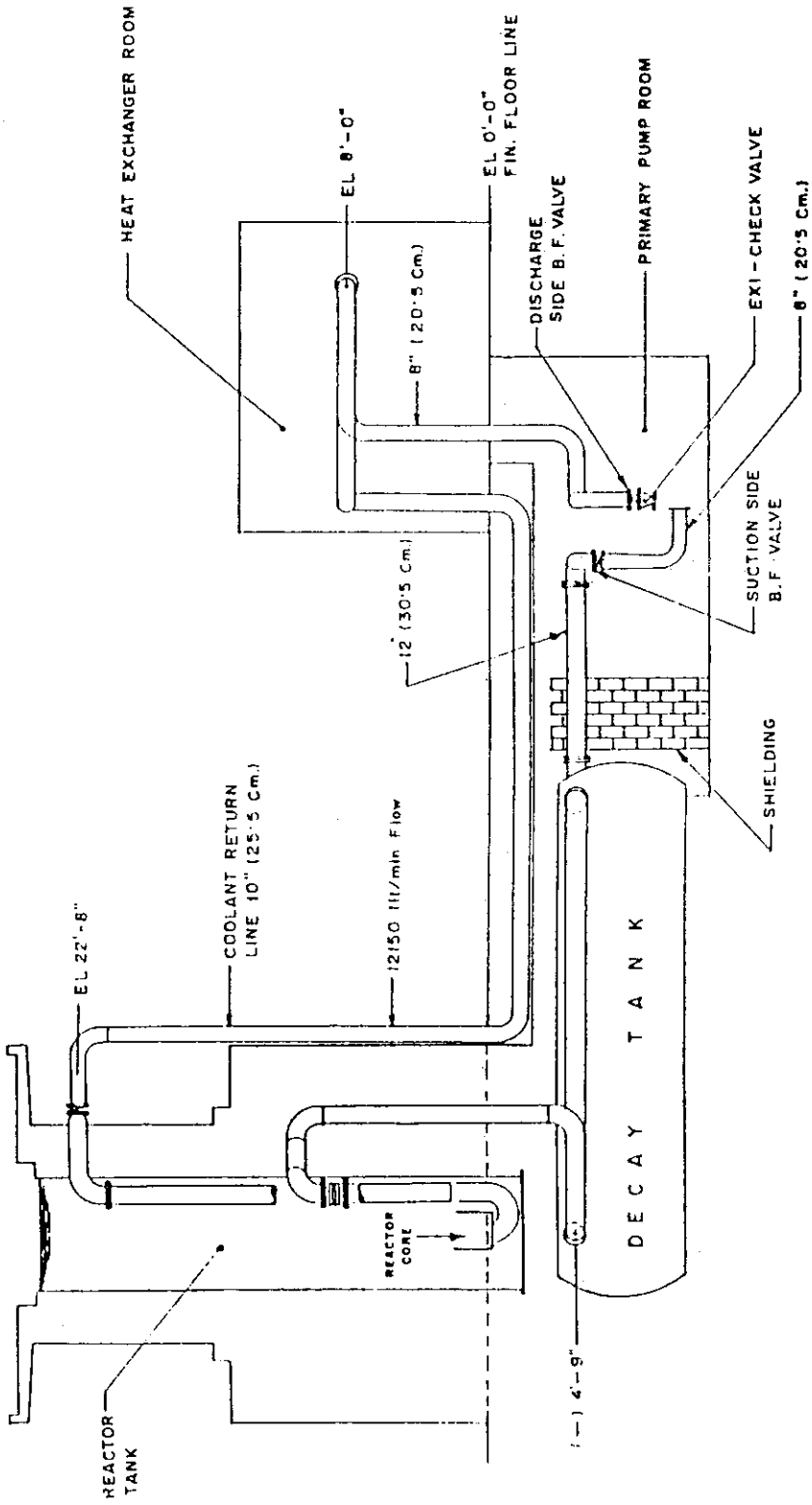

FIG. 3. PRIMARY WATER SYSTEM INSTALLATION

2.2.1. SELECTION OF PUMPS

As stated earlier 13,250 liter per minute of coolant flow has to ensured for operating the reactor in the forced cooling mode. Ideally the primary pump should be selected accordingly. A redundancy of at least one stand-by pump of 100 % capacity is required to be available for ensuring safety, reliability and also availability of the system. In the present design, however, the primary loop has two pumps each with rated output of about 12,100 liters per minute, so that either of them is not sufficient to ensure the minimum flow for the forced cooling mode. Therefore, the flow from each pump has to be regulated by closing each butterfly valve by about 55 % in order to attain the desired level of flow.

Butterfly valves are intended to isolate the system for maintenance purposes and also for minor flow regulations. But in the present case these valves are used for major flow regulations. In this process an unnecessary pressure drops are developed across the butterfly valve. Pressure drop across the butterfly valve was measured to be 0.62 bar at a head loss of 6.4 meters of water. Calculated system head with the butterfly valves fully open is approximately 18.3 meters. Allowing 20 % margin for unexpected problems, the required system head works out to be 22 meters. But at a flow of 6625 litres per minute, pump delivery head as calculated from the characteristic curve is 28.00 meters. Such a pressure drop eventually leads to some vibration in the primary loop. At the same time, the impact of water on the disk of the butterfly valves causes unwanted stresses on various weld joints close to it. These repeated stress is thought to have ultimately caused the development of crack in the circumferential welding of exi-check valve.

2.2.2 DIAMETER OF PIPE

Diameter of the pipe used in the primary line is smaller than the required size causing high coolant velocity and eventual vibration. Coolant velocities at different sections of the primary pipe are shown in Table I.

Table -I Calculated Coolant velocity at different pipe section

Pipe Diameter (cm)	Flow(lit/min)	Velocity(m/sec)
20.5	6625	3.41
25.5	13250	4.40
30.5	13250	3.00

2.2.3 T - CONNECTION TO DISCHARGE LINE

The discharge line of each pump is connected to the common 25.5 cm diameter pipe by a T-connection. During the starting of the pumps two flows have a head on collision causing sudden impulses which eventually leads to vibrations.

2.2.4. POOR PIPE SUPPORT AND INSTALLATION

Pipes close to the pumps are not well supported. Limited number of supports are provided from ceiling which can only take dead load of the pipe. During long operation supports failed which were remedied by supports from the side wall. The installation of the pumps is not satisfactory. Pumps are leveled and mounted on small pieces of iron packings which were found to be shifted slightly since installation.

2.3. REMEDIAL MEASURES

To solve the above mentioned problems, it has been decided to use small diameter (30.50) impeller so that each pump can deliver the required discharge of 6625 liters per minute thus allowing to keep the discharge valve fully open. Proper installation of pump sets and additional ground support to the pipes are planned to be provided to take care of vibration. The pipe diameter will be changed to economic diameter of 30.50 cm so as to minimize flow induced vibration. The T connection will be changed either to Y connection or a guide vane will be provided in the T junction to avoid the head on collision and thus ensure a smooth flow. Upon completion of these works the primary system integrity and safety will be increased.

3. CONCLUSION

In spite of limited facilities available, it has been possible to utilize the reactor for carrying out different R & D programmes and for production of certain types of short-lived radio-isotopes like Tc-99, I-131 as substitutes for their import for use locally. Full scale production of such isotopes would resume after completion of the under implementation Radio-isotope laboratory. On going R & D programmes like neutron scattering would be strengthen when the installation of the Triple Axis Spectrometer is completed by the end of this year. It is envisaged that based on the results of on-going research on Neutron Radiography, it will be possible to provide such services to local industries and other production related activities. Such

future uses of the reactor facilities and the stated remedial steps towards improvement of its function would be helpful in increasing its capacity utilization.

It is worthwhile to note that the TRIGA Mk II reactor of Bangladesh does not have any reference unit and that its design was evolved on the basis of experience with such rectors of 1 MW and smaller sizes. The most significant change in this context was the introduction of forced cooling mode of heat transfer. Some of the faults with the present reactor were associated with this mode of cooling. It has been possible to identify initiating events for such faults and also to suggest remedial steps fully at the initiative of the local expertise. It is expected that similar possible faults and solution to these will be considered duly in future designs of similar reactor.

It may be mentioned that the rated pulsing (2000 MW) could not be attained during commissioning of the reactor and the pulse had to be limited to 852 MW corresponding to $2 of reactivity insertion. The limitation was forced partially by overheating of certain fuel elements in proximity of the pulsing control. It is felt that such a limitation on pulsing should be investigated comprehensively, taking factors like core configuration, neutron physics, and mechanical characteristics of fuel elements into consideration. BAEC plans to undertake such a study in future.

REFERENCES

1. M.A.Mannan and Moazzem Hossain, Characteristics and facilities of a 3 MW LEU fuelled Triga Research Reactor, Proceedings of the First Asian Symposium On Research Reactor, Tokyo, November 18-21, 1986.

2. M.Hossain and M.A.Mannan, Installation of dry central thimble in the Bangladesh 3 MW TRIGA Mk-II Research Reactor, Proceeding of the Second Asian Symposium on Research Reactors, Jakarta, May 23-25,1989.

3. TRIGA MK-II Reactor Mechanical Maintenance Manual GA- A 17054, May,1984.

4. Outline of Examination Guides of Water-Cooled Research Reactors in Japan

F. YOSHINO, R. KIMURA

Reactor Regulation Division, Nuclear Safety Bureau,
Science and Technology Agency

ABSTRACT

The Nuclear Safety Commission of Japan published two examination guides of water-cooled research reactors on July 18, 1991; one is for safety design, and another is for safety evaluation. In these guides, careful consideration is taken into account on the basic safety characteristic features of research reactors in order to be reasonable regulative requirements. This paper describes the fundamental philosophy and outline of the guides.

INTRODUCTION

Since most research reactors in Japan were constructed in 1960's, some of these are recently required modification to accomodate changing needs of research and experiments or to take countermeasures for ageing of reactor facilities. In addition, high enriched fuel are being replaced with low enriched one, which requires re-evaluation for core safety. Considering these situations, the Nuclear Safety Commission decided to establish safety examination guides of research reactors and started the works at the Special Committee on Safety Standard of Reactors in January 1988.

After three and a half years deliberation, the Commission approved and published two guides; Examination Guide for Safety Design of Water-Cooled Type Research and Testing Nuclear Reactor Facilities (hereinafter to be referred as the Guide for Safety Design of Research Reactors), and Examination Guide for Safety Evaluation of Water-Cooled Type Research and Testing Nuclear Reactor Facilities (hereinafter to be referred as the Guide for Safety Evaluation of Research Reactors). The Guides are to be used as general evaluation guides for examining appropriateness of the safety design principles and safety evaluation, respectively, of a proposed research reactor facility in response to the application of installation license (including amendments).

As the fundamental policy for establishing the Guides, the following characteristic features of research reactors were taken into consideration, comparing with power reactors.

1) Diversity of reactor structure, thermal output and operational features
2) Lower coolant energy and simpler cooling system due to low coolant temperature and pressure
3) Lower thermal output and small fission product inventory

4) Larger reactivity worth of fuel assembly and higher power density in case of high output reactor
5) Short operating duration period and accessibility to the system and components for inspection and maintenance.

Concerning power reactors in Japan, guides for safety design and safety evaluation of light water nuclear power reactor facilities were established in 1970's. Revision works for the guides of power reactors had been in progress when the works for research reactors started. Accordingly, in establishing the Guides of Research Reactors, consideration were also taken into to be compatible with the guides of power reactors. Thus the Guides of Research Reactors were established with consideration of the characteristic features and accumulated experiences and knowledge on the experiments and operation of research reactors, and also based on the latest technology.

SCOPE OF THE GUIDES

The both Guides apply to the safety examination of the reactors which are used for research and/or testing, cooled by water and operated with constant power (hereinafter to be referred as research reactors). For other reactors such as pulse reactor and critical assembly, the Guides may be referred to except specific matters derived from water-cooled type or those intrinsic plant features.

CLASSIFICATION OF RESEARCH REACTORS

In the Guides, the research reactors are classified into following three groups depended on the reactor thermal output, in order to be reasonable for the requirements of the Guides.

1) Low output reactor (under 500 kW)
2) Middle output reactor (not less than 500 kW, under 10 MW)
3) High output reactor (not less than 10 MW, not higher than 50 MW)

This classification is based on the differences on the importance of decay heat removal in abnormal conditions and the amount of radioactivity release to be postulated in accident conditions. The articles of the Guide for Safety Design may apply in accordance with the importance of the safety function of the respective group. For the reactors higher than 50 MW, there may be matters which cannot be covered by the Guides. For these matters, the guides of power reactors may be referred to.

GUIDE FOR SAFETY DESIGN OF RESEARCH REACTORS

The Guide for Safety Design of Research Reactors is to be used as a general evaluation for examining the appropriateness of the safety design principles of a proposed research reactor. The Guide is mainly composed of definition of words, fifty articles and interpretation of the articles. In addition, "Fundamental Principles for Classification of Safety Function Importance of Water-Cooled Research

Reactors and Its Supplement", which are to be described in the next section, are attached in the Guide.

The articles are grouped into ten, as follows. In the parentheses, a number of articles are shown.

1) Overall Requirements(10)
2) Reactor and Reactor Shutdown System(10)
3) Reactor Cooling System(5)
4) Reactor Building and Experimental Facility(2)
5) Safety Protection System(6)
6) Control Room and Its Related Facility(4)
7) Instrumentation and Control System and Electric Power Supply System(2)
8) Fuel Handling System(3)
9) Radioactive Waste Disposal Facility(4)
10) Radiation Control(4)

Noticeable matters of this Guide are as follows.

- A concept and article on "Testing Fuel Assembly" are introduced in order to enable to carry out in-core testing on cladding failure or partial melt of fuel meat for the purpose of research and development of fuel.
- For emergency core cooling, the definition and articles on "Core Submersion Keeping System" are clarified.
- The concepts of coolant pressure boundary and containment vessel of Light Water Reactors (LWRs) are excluded because the coolant energy and radioactivity inventory of the research reactors are much lower than those of LWRs.
- Requirements for low and middle output reactors are generally lightened.

FUNDAMENTAL PRINCIPLES FOR CLASSIFICATION OF SAFETY FUNCTION IMPORTANCE

This Fundamental Principles supplements to the Guide for Safety Design to clarify the construction of the safety function importance described in the Guide. That is, safety-related buildings, systems and components are classified into the specified safety importance grades which imply respective design requirements. The constitution, definition and requirements of the fundamental principles are almost the same as those of LWRs in order that the criterion of judgement may be clarified in comparison with that of LWRs. However, consideration on special features of the research reactors appears in the examples of the classification which is attached in the Fundamental Principles.

In the first stage of the Fundamental Principles, safety-related equipment is devided into two groups; Prevention System(PS) whose loss of function may cause an abnormal condition resulting excess exposure to the public or workers, and Mitigation System(MS) whose function prevents the enlargement of abnormal conditions and mitigates the excess exposure. In the next stage, the equipment belonged to PS and MS is classified into Class 1 to Class 3, respectively, which imply the respective basic design targets to be accomplished by the established technology of design, construction and testing, and operational management, as follows.

Class 1: to assure reliability as high as reasonably achievable

Class 2: to assure high reliability
Class 3: to assure reliability equal to or higher than the general industrial facilities.

In the attached examples of the classification, most safety equipments are classified into Class 2 and Class 3 except only a part of those of high output reactors.

GUIDE FOR SAFETY EVALUATION OF RESEARCH REACTORS

The Guide for Safety Evaluation of Research Reactors is prepared as a general criterion for examining the appropriateness of safety and site evaluation of a proposed research reactor. The Guide is consisted of three parts; the text, interpretation and supplement. The text describes, for both safety and site evaluation, scope to be evaluated, selection of events to be evaluated, judgement criteria of the evaluation and features to be considered in the analysis. In the supplement, the concrete events, conditions of analysis and criteria to be applied to the respective selected events are described. The consideration on safety evaluation of critical assemblies is attached as a reference in the interpretation.

I. Safety Evaluation

In order to confirm the adequacy of safety design principles, it is necessary to evaluate abnormal conditions which are "Abnormal Transient during Operation" and "Accident". The events of Abnormal Transient during Operation include the conditions resulting from a single failure of equipments or a single operator error anticipated to occur during the reactor life time. The events of Accident include the conditions which are beyond those of Abnormal Transient during Operation, and to be postulated from the view point of safety evaluation of the reactor facility because of the possible release of radioactivity, though the frequency of those occurrences is smaller than that of Abnormal Transient during Operation. In the Guide, internal events are to be evaluated because the adequacy of countermeasures for external events due to natural phenomena or external human events are evaluated in the Guide for Safety Design.

For safety evaluation, the representative events are selected as follows.

1. Abnormal Transient during Operation
   (1) abnormal changes of reactivity or power distribution in the core
   (2) abnormal changes of heat generation or heat removal in the core
   (3) other events depended on the design features of the reactor facility

2. Accident
   (1) abnormal reactivity insertion
   (2) flowing out of reactor coolant or remarkable change of core cooling conditions
   (3) abnormal release of radioactivity to the environment
   (4) other events depended on the design features of the reactor facility

Judgement criteria for safety evaluation are as follows.

1. Abnormal Transient during Operation

In the events, the core shall not exceed the permissible design limits of fuel, and the reactor facility shall be restored to the normal operation. That is,
   (1) minimum critical heat flux shall over the permissible design limit, and
   (2) fuel cladding shall not fail mechanically.

2. Accident

In the events, the core shall not melt or not be damaged remarkably, and any secondary damages to cause other abnormal events shall not occur, thus the adequacy of the design of radioactivity barrier shall be confirmed. That is,

(1) fuel shall not generate mechanical energy in occurrence of fuel failure,
(2) core shall not be remarkably damaged, and shall maintain enough coolability, and
(3) risk of radiation exposure of the public shall not be remarkable.

Features to be considered in the analysis are mainly as follows.

(1) Initial conditions of the core shall be selected so that the result of analysis is the severerst for the judgment criterion.
(2) Safety functions to be considered in the analysis shall be of MS-1 and MS-2, and shall be assumed a single failure of each system, adding the event, of reactor shutdown, core cooling and radioactivity enclosure so that the result of analysis is the severest.
(3) Adequate time margin shall be considered for operator manual action which is necessary to mitigate the effect of the event.
(4) Adequacy of the computing programs shall be demonstrated, and the model and parameters shall be selected so that the result is severe.

II. Site Evaluation

Appropriateness of the reactor siting condition is examined based on "Examination Guide for Reactor Siting and Guideline for Interpretation in Their Application" (hereinafter to be referred as the Guide for Reactor Siting), while, for the reactor whose thermal output is less than 10 MW, this is used as a reference. The Guide for Reactor Siting requires that radiation exposure of the public in "Major Accidents" and "Hypothetical Accidents" shall be under the respective guideline.

In the Guide for Safety Evaluation, the evaluation of Major Accidents and Hypothetical Accidents are required without regard to the thermal output, and the judgement criteria are cited those of the Guide for Reactor Siting. In selecting Major Accidents, the Accidents which have the possibility of causing spread of radioactive materials are evaluated, then the maximum release of radioactive material is postulated from a technological point of view. For Hypothetycal Accidents, more release of radioactive material is postulated in the selected Major Accidents. In the analysis of Major Accidents and Hypothetical Accidents, evaluation shall be performed based on the philosophy of the Guide for Reactor Siting.

As a typical Major Accident of high and middle output reactors used plate type fuel, a coolant channel blockage accident is selected, and for reactors used rod type fuel, a fuel failure accident to occur release of fission product in the fuel gap is referred. These are resulted from study on the experienced fuel failures including overseas research reactors.

CONCLUDING REMARKS

In establishing the Guides, efforts were made on the optimization of securing safety and applying the specific features of the existing diverse research reactors. A partial nonconformity with the Guides in a proposed reactor facility is permitted if the nonconformity is based on a technological progression. Thus the Guides should be adequately revised to take in the technological progression.

5. Research Reactor Utilization in the Philippines

A.M. DELA ROSA, C.R. ALETA

Philippine Nuclear Research Institute
Diliman, Quezon City 1101
Philippines

ABSTRACT

The Philippine Research Reactor (PRR-1) has been used since 1963 for a wide spectrum of scientific activities ranging from fundamental research in nuclear physics, nuclear chemistry, and radiobiology to radioisotope production, neutron activation analysis, materials testing, and manpower development. The paper gives a brief history of the establishment of PRR-1 and its utilization. The current research programme of the Philippine Nuclear Research Institute (PNRI) using the PRR-1 is then presented. The main objective of the programme is to accelerate the application of nuclear energy for the industrialization of the country through the utilization of the PRR-1. The paper also presents the PNRI's regulatory protocol which ensures the safe operation of the PRR-1.

INTRODUCTION

The developed countries have reaped tremendous benefits from nuclear science and technology in their scientific development and industrialization programmes. In like manner, the developing countries want to have access to the benefits of nuclear science and technology.

The national nuclear institutions of these countries want the capability to participate in basic and applied research in topics that either directly affect them or are of global interest in order to contribute more to the pool of scientific knowledge. They want to master the science and the technology of nuclear power to enable them to localize such technology. They want to develop the capability to make practical use of neutrons and gamma radiation to benefit the various sectors of the community.

The PNRI aims for these capabilities, and the PRR-1 is one

of the major facilities to attain most of these objectives. The PRR-1 has played an important role in the promotion and support of nuclear R & D and manpower development in the Philippines for the past 25 years. It has served a wide spectrum of uses ranging from fundamental research in the natural sciences and engineering to radioisotope production, neutron activation analysis, materials testing, and manpower development. The paper presents a brief history of the establishment and utilization of the PRR-1, the current PNRI research program on reactor utilization and the safety aspects of PRR-1 operation.

HISTORICAL PERSPECTIVE ON RESEARCH REACTOR UTILIZATION

The Philippines entered the nuclear field in 1955 when the Philippine Government signed a bilateral agreement with the USA on the civil uses of atomic energy. Under the agreement, the USA was to provide a research reactor, and the Philippines was to provide the site and building for the facility. This initial activity was followed by the enactment of the Science Act and the creation of the Philippine Atomic Energy Commission (PAEC) in 1958. The first years of the PAEC were devoted to the training of the scientists and engineers, the development of the R & D infrastructure for basic and applied research, radioisotope production, and applications of radiation and nuclear techniques, and the establishment of the PRR-1. The Philippine Atomic Research Center, the research arm of the PAEC, was established in 1960. On the same year, the construction of the PRR-1 began. The reactor is of open-pool design, and originally used plate-type aluminum-clad fuel elements. It has a free-standing concrete pool with 6.35 mm thick aluminum liner and with walls up to 3m thick. The pool consists of a circular high power section which opens to a rectangular fuel storage section, and a rectangular low-power section. The PRR-1 achieved initial criticality in August 1963. Its rated thermal power of 1MW was reached in October 1964.

The PRR-1 fostered nuclear R & D activities and applications of radioisotopes in medicine, agriculture, and industry in the country and international cooperation among countries in Asia.

The PRR-1 served as the host reactor for the India-Philippines-IAEA Regional Project on neutron crystal spectrometry (IPA Project) from 1964-1969. International cooperation in the nuclear field in Asia and the Pacific region took place for the first time under the IPA Project (1). This was a regional research and training program the objective of which was to establish a research center on neutron diffraction in which scientists and technicians from member states of the IAEA in Asia and the Pacific could come to participate in research and training. The participants came

from Indonesia, Korea, Thailand, Taiwan, India and the Philippines. Studies in solid state physics based on elastic and inelastic scattering of neutrons were undertaken. The project became the forerunner of the IAEA Regional (RCA) Project which was implemented in 1972.

The early nuclear activities in the Philippines using the the PRR-1 include, but are not limited to, the following (2):

1. Reactor physics: physics calculations in cross sections, flux calculations and excess reactivities, reactor control system, studies of neutron spectra, initial flux and power distribution of the PRR-1.
2. Nuclear Physics: neutron diffraction studies, structure determination of alloys and crystals, orientation of magnetic moments in the lattice of magnetic substances, Mossbauer effect spectroscopy, and proton-recoil fast neutron spectrometry.
3. Nuclear and Radiochemistry: hot atom chemistry, tracer studies of chemical reactions using radioisotopes, neutron activation analysis of various samples, kinetics of chemical reactions using radioisotopes, radiolysis of organic compounds.
4. Radioisotope (RI) production: 18 radioisotopes were in routine production starting 1966, e.g. ^{198}Au colloid, ^{192}Ir needles, ^{24}Na, ^{32}P, ^{128}I, ^{131}I, ^{64}Cu, ^{35}S, ^{82}Br, ^{58}Co, ^{45}Ca, ^{51}Cr, ^{56}Mn, ^{85}Sr, ^{60}Co, ^{99m}Tc, ^{69m}Zn, ^{65}Ni. Some development work on the production of ^{99}Mo and ^{99m}Tc was undertaken. These were used for nuclear medicine, research, and training.
5. Radiolabelling of organic compounds: ^{75}Se-labelled methionine and cystine, ^{131}I-labelled L-thyroxine, human serum albumin, hippuran, and rose bengal.
6. Training of scientists, engineers and technologists in the operation and utilization of the PRR-1.

PRR-1 operation in MWH from 1964 to 1983 is shown in Fig.1. The reactor operated with essentially no modification nor major problems for almost 20 years. At the end of 1984, the reactor was shut down for modernization.

UPGRADING OF THE PRRI-1

The PRR-1 underwent upgrading to a TRIGA type reactor in 1985-1987 (3). The instrumentation and cooling system were also upgraded to allow the rated thermal power to be raised to 3MW. The TRIGA conversion start-up tests were conducted in March 1988. The reactor was successfully brought up to full rated power of 3MW.

A month after the start-up tests, the reactor developed a pool water leak. The reactor staff believes that the leak was

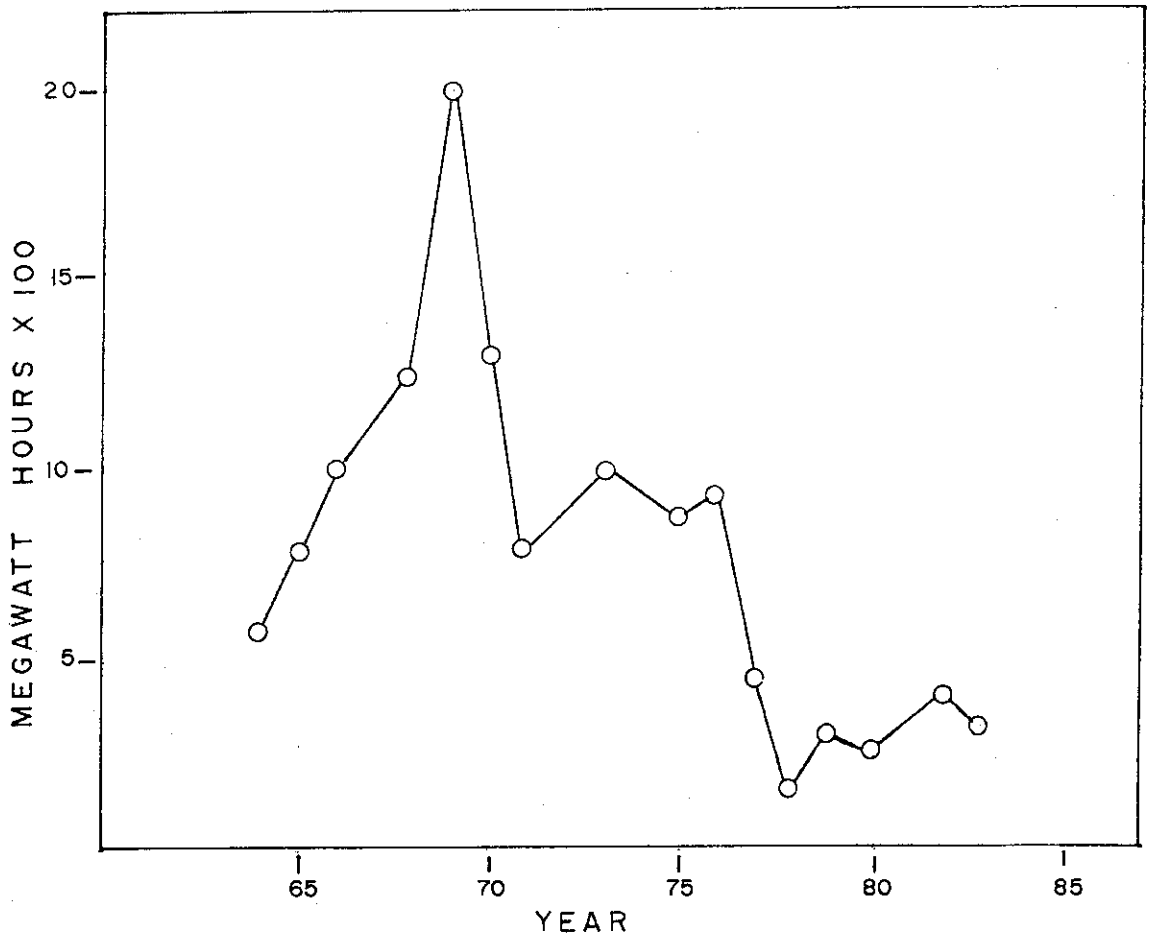

FIG.1 PRR-1 Operation (1964 - 1983)

caused by the reopening of an old leak pathway observed in 1963, most likely the thermal column joints (4).

In view of the absence of a separate fuel storage facility, the spent fuel elements and the TRIGA fuel clusters are stored in the pool during the repair work. To insure that the workers will not be unduly exposed to radiation in the work area, the fuel elements are stored in stainless steel holding tanks filled with demineralized water and placed in the low power section. To reduce the radiation dose at the side fronting the intermediate power section, 10 cm of lead consisting of 3680 kg of cast lead bricks was assembled and set in place between the low power and intermediate power sections. The lead shield rests on the pool floor. Polyethylene containers filled with demineralized water were placed side by side with the lead shield to augment the shielding. Radiation measurements have shown safe radiation levels in the pool. The high power section is now completely emptied of water, and the beam-tube ends were unbolted to allow a bigger work area near the thermal column joints. The resealing of the thermal column joints is about to be started. After the thermal column joints have been repaired, then the

pool liner will be inspected for back-side corrosion using ultrasonic techniques. The old phenolic coating will be sandblasted and a new coating will be applied. The pool area will be subjected to these steps section by section with utmost consideration of the radiation protection measures required to protect the radiation workers.

Two years were spent securing the funding for the repair work. The repair work began in January 1990, and it should be completed in mid-1992.

PNRI NUCLEAR RESEARCH PROGRAMME

The Nuclear Science and Technology Plan of the PNRI for 1989-1993 aims for maximum utilization of radiation and radioisotopes which will contribute to the national effort of transforming the Philippines into a newly industrializing country by turn of the century. The program under the Plan are presented in Table I.

Research reactor utilization is an integral component of Programs II and III. The PNRI is committed to undertake the following activities:

A. In-Core Utilization
   1. Radioisotope production
      - Irradiation of targets for I-131 and other RI
      - Production of Mo-99 for Tc-99m
      - Development of sealed sources such as check sources for nuclear instruments, industrial nucleonic sources, etc
      - Re-irradiation of Ir-192 sealed sources both for industry and nuclear medicine
      - Fabrication and design of irradiation facilities
   2. Neutron activation techniques with application in industry and environment
      - application of NAA in rare earth elements geochemistry
      - characterization of volcanic and geological regimes
      - development of activable tracers for industrial processes
      - development of regional reference materials
      - reactor-based analytical services for industry
   3. Nuclear transmutation doping (NTD)
   4. Radiation defect studies

B. Neutron Beam Utilization
   1. Neutron radiography
      - non-destructive technique for materials
      - materials research
   2. Neutron scattering

- materials research
- molecular biology research

C. Reactor Operation and Maintenance
- Operation and maintenance
- Reactor safety studies
- Environmental impact of PRR-1 operation

D. Training and Education

Table II shows the areas of application covered by the research programme. The available facilities to carry out the programme as well as the facilities being planned to be established are presented in Table III.

TABLE I. PROGRAMS UNDER THE PNRI NUCLEAR S & T PLAN

PROGRAM	OBJECTIVES
I. Radiation Protection and Nuclear Safety	The program stresses the requirements that will ensure the safety and protection of the Filipino and his environment in the use of nuclear technology.
II. Radiation Technology and Egineering	The program ensures that the demand for radioactive products such as radioisotopes, radiopharmaceuticals, radiolabelled compounds, are met locally through upgraded and improved nuclear techniques, facilities and equipment.
III. Radioisotopes and Nuclear Techniques Application	The program envisions the continued application of radioisotopes and radiation for inceased efficiency and productivity.
IV. Special Projects	The program comprises the activities which will support the previous three programs such as manpower development, and infrastructure development.

Table II : PNRI NUCLEAR PROGRAMME ON RESEARCH REACTOR UTILIZATION

ACTIVITIES	FIELD OF APPLICATION					
	MATERIALS SCIENCE	AGRI-CULTURE	MEDICINE	ENVIRON-MENT	INDUSTRY	NUCLEAR SAFETY
A. NAA	X	X	X	X	X	X
RI Production		X	X	X	X	X
NTD						
Radiation defect studies	X		X		X	X
B. Neutron radio-graphy	X		X		X	X
Neutron scattering	X	X	X	X	X	X
Molecular biology		X	X	X		
C. Reactor Safety Stydies						
Reactor Physics						X
Fuel Management						X
Environmental Impact				λ		X
D. Training and Education	X	X	X	X	X	X

Table III : PNRI FACILITIES FOR RESEARCH REACTOR UTILIZATION

Facility	Year 1991	1992	1993
1. NAA	laboratories and counting system operational	Installation of pneumatic transfer and automatic counting systems	Operational
2. ^{131}I Production	Installation of additional hot cell		Operational
3. Production of other RI			Operational
4. DNAA			Operational
5. Neutron radiography		Construction & installation	Operational
6. Neutron Transmutation Doping			Construction and installation

SAFETY ASPECTS OF PRR-1 OPERATION

The Facility Safety Committee of the PNRI is charged with the responsibility of ensuring the safe operation of its nuclear facilities including the PRR-1. The 5-member Committee which is chaired by the Head of the Nuclear Licensing, Regulations and Safeguards Division is independent from the reactor operations section. The Committee performs the following functions: a) to review and recommend to the PNRI Director approval of safety analysis report, procedures for reactor operation, experiments in the reactor and safety documentation; b) to inspect and audit the facility in order to ensure comformance to regulations; c) to review and recommend to the PNRI Director approval of experiments in the reactor, and d) to review safety-related incidents.

The Committee is guided by the following safety standards:

a) PNRI Radiological Safety Manual 1991 edition.
b) IAEA Safety Series Standards, Safety Series No. 35
c) ANSI N 18.9 - 1972 and USNRC Guide 2.1, May 1973 entitled "Shield Test Program for Evaluation of Installed Biological Shielding in Research Training Reactors"
d) ANSI N 401 - 1974 and USNRC Guide 2.4, July 1976 entitled "Review of Experiments for Research Reactors"
e) USNRC Reg. Guide 2.2 November 1973 entitled "Development of Technical Specifications for Experiments in Research Reactors"
f) ANSI/ANS 15.16 - 1982 and USNRC Reg Guide 2.6 March 1983 entitled "Emergency Planning for Research Reactors"

REFERENCES

1. Anonymous (1965). "The IPA Project: An International Research and Training Program", Annual Report, Philippine Atomic Research Center, PAEC, Quezon City, Philippines
2. Anonymous (1961- 1981), Annual Report, Philippine Atomic Energy Commission, Quezon City, Philippines.
3. Leopando, L. and G. West (1987), "International Cooperation in Converting the Philippine Research Reactor PRR-1 and the Impacts of the Upgraded Facilities", Proc. Intl. Symp. on the Utilization of Multipurpose Research Reactors and Related International Cooperation, held in Grenoble, France, 19-23 October 1987.
4. Lepando, L. (1990), "The 1988 PRR-1 Pool Leak", unpublished technical report, PNRI, Quezon City, Philippines

6. The Current Status and Future Plan of Nuclear Research Reactor in Thailand

Y. BUSAMONGKOL

Office of Atomic Energy for Peace
Bangkok 10900, THAILAND.

ABSTRACT

Thailand has involved in the field of Nuclear Research Reactor for about 30 years since the first Research Reactor TRR-1 was established in 1962. In 1975 the TRR-1 was shutdown for the first modification (TRR-1/M1) mainly with the Reactor Core by replacing the Core with TRIGA Mark III. Also the modifications were performed with the associated system i.e. Cooling, I&C and Irradiation facilities. Major utilizations of the TRR-1/M1 are NAA basic research, Radio isotope production for medical uses, and personnel training. Currently, the TRR-1/M1 is being shutdown for the second modification principally with the reactor pool and beam tubes. The shutdown has been started early this year and is expected to last by the end of 1991.

Upon the Thai's cabinet, agreement on December 27, 1989 the decision was made to relocate the reactor TRR-1/M1. The OAEP responds to this decision by considering to purchase a new reactor with about 5 MW thermal power capacity for the new center. In the meantime, the TRR-1/M1 will continue further operation for about 8-10 years until the complete establishment of the New Research Reactor in the New Nuclear Research Center by the next decade. Decommissioning of the TRR-1/M1 after then is also being planned by the OAEP staff.

1. INTRODUCTION

The current research reactor (TRR1/M1) is the modified reactor from the TRR1 (was U3O8-A1 HEU fuel). Modification was made in 1975-1977 by replacing the rectangular HEU-core with the circular/hexagonal TRIGA-mark III core. The reason for modifying was the problem of transportation of the HEU-fuel from supplier to Thailand because of the Non-proliferation Treaty policy of the IAEA member states resulting in strictly supply of the HEU fuels. Concurrently, the IAEA has encouraged and issued technical support to the member states to convert the existing research reactor from the use of HEU-fuels to the LEU-fuels. Thailand had took this opportunity by switching to the LEU-TRIGA fuels. At the beginning period the whole core was composed of LEU-8.5% (Uranium weight) fuel elements. These fuels have been gradually replaced by 20% (Uranium weight) both of them are 20%

enriched Uranium, resulting in mixed-core operation. The present status of mixed fuel of different densities (The former is Ø.51 g/cc the later is 1.3 g/cc) in this condition the power peaking of the fuel in the mixed core is concerned, thermal hydraulic calculation has been performed to ensure the peaking factor is still kept under limited value.

The major utilizations of the reactor are isotopes production for medical uses i.e. I-131, Tc-99m, P-32, neutron activation analysis for environmental research and other fields are being conducted. Some beam experiments for basic research are also performed. The reactor utilization is limited by improper of existing irradiation and experimental facilities.

In the early period of converting to TRIGA Core, these facilities were still originally designed unfit to the reactor core they have been gradually modified to meet the requirement of reactor users.

The present situation of reactor utilization is now discontinued because of the reactor has been shutdown for the reactor pool refurbishment since January 1991.

2. THE REACTOR POOL REFURBISHMENT

Aging is the problem of the TRR1/M1 since it is nearly thirty-years old, most parts and components are worn need to be repaired or replaced. The reactor pool is one of the major part of the reactor since the pool has been painted by epoxy-paint for more than 14 year ago. Some bubbles are appeared on the pool wall, surface, and on the pool floor this can be the problem of radiation contamination because the water contact directly with the concrete. Not only the pool itself but also the components attached to the pool such as piping, beam tubes, pneumatic tubes, through tubes and etc., As mentioned previously the reactor core and its irradiation and experimental facilities are not fit properly. To modify some facilities are required, taking this chance to replace these facilities by the new items is timely schedule.

3. REFURBISHMENT PLANNING

The experience from the first repainted in 1975-1977 during the time before dismantling the TRR-1 core in order to replace by TRIGA-core is very useful for planning to perform the refurbish task. Residual radiation exist in the pool and piping facilities after reactor shutdown is rather high . To reduce the radiation problem and facilitate the activities such task, working schedule had been established one year in advance, the time schedule are as follows :-

3.1 Operate the reactor in the big pool (December 1989-December 199Ø)
3.2 Shutdown the reactor (January 199Ø-January 1991)
3.3 Move fuel element from reactor core to fuel storage pool.
3.4 Pool drainage
3.5 Shielding installation
3.6 Dismantle irradiation & experimental facilities.

3.7 Sand Blasing
3.8 Installation of beam tubes, void tank
3.9 Primer painting
3.10 Epoxy Araldite coating
3.11 Fill the pool with demineralized water
3.12 Critical Assembly & refueling
3.13 Normal operation of the reactor

The procedures and activities in each step will be performed very carefully. The most important procedures is the fuel manipulation. Before manipulating the fuel elements in reactor core and transferring to the storage rack in the storage pool, storage and pool had to be provided outside the reactor building by installing the fuel rack in the existing spent fuel storage pool. The spent fuel elements of the former reactor (U3O8-Al HEU-fuel of the TRR-1 reactor) already storage since 1975. To add the TRIGA-fuel together with spent HEU-fuel is very serious consideration of the operating staff.

k-effective calculation (1,2) had been performed, first for the storage rack itself and second together with the spent HEU-fuel. The results of calculations confirmed the safe storage of the mixed fuels in the same storage pool. Due to the method utilized in calculation is rather conservative the k-effective of the total fuel is less than 0.6-0.7 (see fig. 1) this means the pool can be storaged for more additional fuels element of the TRR-1/M1 TRIGA fuels in the near future.

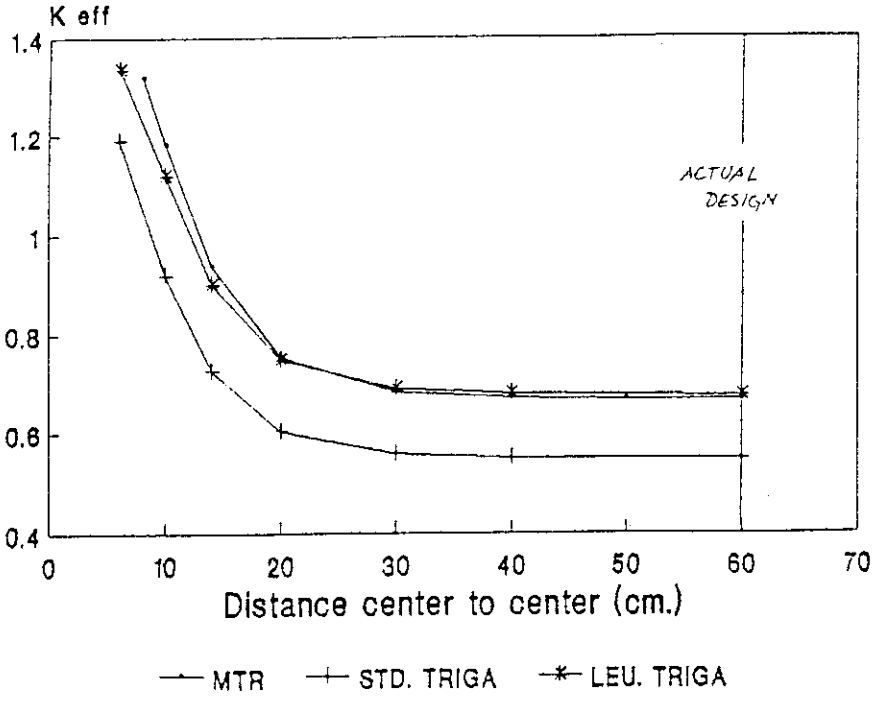

Fig.1 k-eff as a function of distance between racks for three types of fuel elements, fresh fuel.

The fuel transportation from the reactor pool to the storage had been accomplished by carrying in the specially designed transfer casks (there are two sizes one is for STD elements another is for FFCRs (Fuel Follower Control Rods) each can handle four elements, see fig.2). All of the FFCRs have to be transferred to storage pool together with fuel elements. Since these FFCRs attached with connecting rod and they are inconvenient to be carried by transfer cask. To put in transfer cask is the only way that can be done they have to be dismantled from connecting rod and special adapter have been built and attached to the end of FFCRs for easy handling.

Some of the rested components are kept in the core shroud such as Neutron Detectors, Transient Control Rod. Three instrumented fuel elements are also put in transfer cask and kept in the reactor pool.

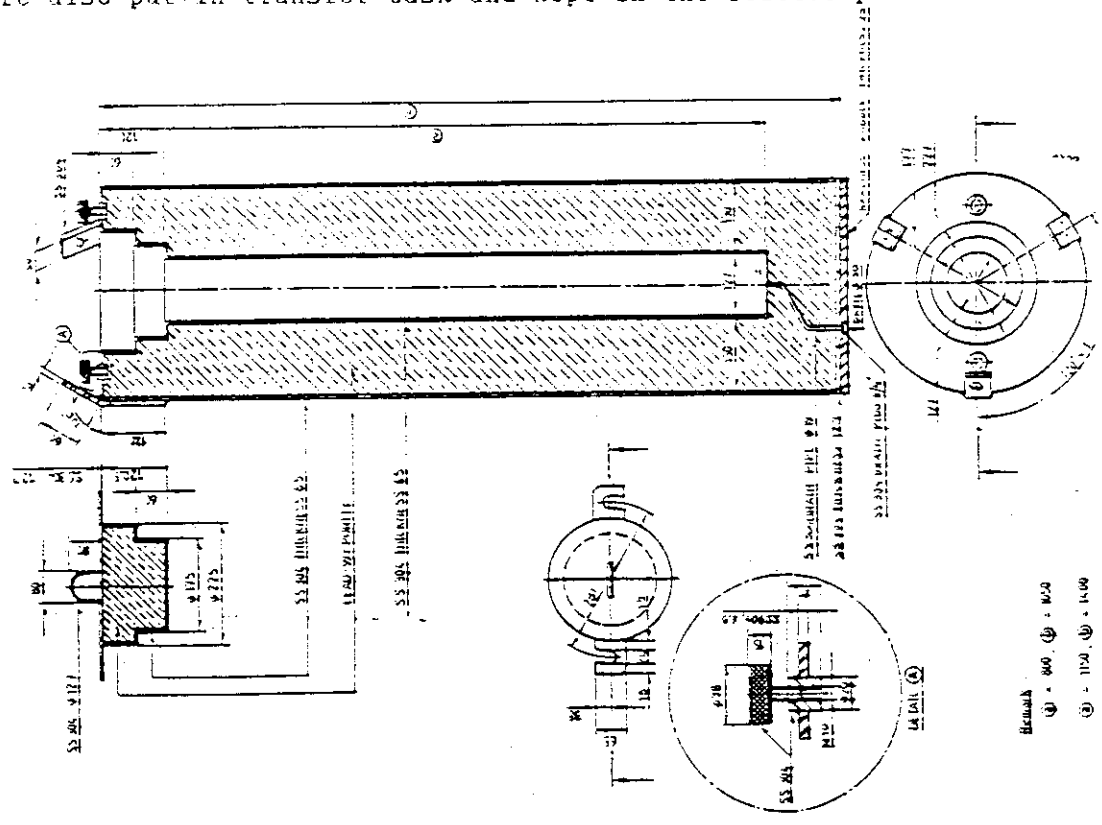

Fig.2 Transfer cask for transferring fuel elements and FFCRs

The debris of paint, sand, concrete, the old beam tubes and pneumatic tubes, etc. most of these are radioactive need to be treated as radioactive waste.

Modification of irradiation and experimental facilities are also the main objectives of the refurbishment. New void tank was redesigned. Since the void tank had been installed at the time of installing the TRIGA-core, this void tank exists between the reactor core and thermal column and it is not properly fit with the space between thermal column and reactor core. The new void tank is thinner than the old one resulting to the reactor core can move more closer to thermal column and make the core center close to the center line of beam tube and the new void tank facilitated the two irradiation tubes in each side of void tank. After finished the modification it is expected that the utilization of beam tube such as beam experiments, neutron radiography will be more effective.

4. PLANNING FOR THE ESTABLISHMENT OF THE NEW NUCLEAR RESEARCH CENTER

4.1 BACKGROUND INFORMATION

On December 27, 1989 the Thai cabinet has decided to relocate the TRR1/M1 reactor to an appropriated and safe location. The Ministry of Science Technology and Energy take this responsibility by mean of OAEP working group. In February 1990 the "Preliminary Plan" had been established. This plan consists of the procedure in relocating the reactor and associated facilities, schedule and budget.

However, the "Preliminary Plan" is in the rough estimation and expectation of the project. Studying in more deep information has been performed by OAEP staff prior to establish of the new working group and with the IAEA expert's mission upon this project, the tentative outline schedule(3) had been established to conduct the activities being performed by the OAEP staff.

The tentative outline schedule shown as below.

1. Preliminary study/Indicative budget : year 1990
2. Site selection/confirmation : year 1990-1991
3. Establishment of Project Team : year 1991
4. Project definition, Justification, Conceptual Design, Budget revision, Documentation : year 1991-1992
5. Government Review/Approval : year 1992
6. Reactor Performance Definition : year 1990-1991
7. Preparation of Reactor/Associated Plant Specifications : year 1991
8. Reactor proposals invitations, Response reviews, Clarifying discussions, Evaluations, Preferred choice, Estimated cost : year 1991-1992
9. Detailed Design of Rx, Rx Plant, Rx Buildings and Associated Equipment, Price and contract : year 1992-1993
10. Construct/install Rx, etc. : year 1993-1996
11. QA Training, Experience and Definition of Requirements : year 1991
12. Design/Implementation of Preliminary site preparation, Main service, etc. : year 1991-1993
13. Detailed Design/construction all other building, Facilities : year 1993-1996
14. Commissioning of Rx, etc. and all other major plant, Building : year 1995-1997
15. Transferal, Installation and Testing of equipment from present OAEP site : year 1997-1998

4.2 CONCEPTUAL PLAN OF THE ESTABLISHMENT OF NEW REACTOR AND ASSOCIATED FACILITIES

The OAEP steering committee had taken many considerations regarding to the relocation of the existing reactor and associated facilities. The conclusion was that, to install the new reactor at the new site is practicable, due to it is uneconomic both physical considerations and the absence further development potential to meet anticipated growth in performance demand which is expected before the new site could become operational. The time schedule (see table 1.) will take about 8-10 years before the completion of the new center. Prior to the referred time it is necessary and most important to maintain the existing reactor (TRR1/M1) in operation, this is the reason of the refurbishing the reactor as mentioned previously.

The steering committee has established the project team to work out in more detailed information related to the new Nuclear Center to state the requirements of various facilities in the new site these are the conceptual specification of the reactor, isotope production facilities, waste disposal system and etc.

The ongoing activity of this project is the site selection/confirmation. So far it is concluded that after 31 sites were proposed to the OAEP some are near or around Bangkok some are far away the nearest is 35 kilometers and the most furthest is 300 kilometers north-eastern from Bangkok, the selected site is approximately 60 kilometers form OAEP in Nakornnayok province, It took about one and a half year for site selection/confirmation the difficulties are those they against IAEA criterions, the site itself must be the government already owned, the site size, the possibility of radioisotope transportation to the users in Bangkok hospitals and the associated infrastructure.

5. DECOMMISSIONING PLAN OF THE REACTOR

The OAEP steering Committee also concerned about the existing reactor after commissioning beyond the year 2000, regarding to this concern the Decontamination & Decommissioning (D/D) team had been established in order to carry out this task. Due to the time prior to decommission the reactor & associated facilities is rather long, too soon to make a detailed plan and it contribute many factors. In the year 1990 the IAEA expert mission(4) based on discussion with the OAEP staff had made the "Conceptual Decommissioning Plan". This plan is being developed for more deep details upon information available.

6. CONCLUSIONS

The present situation of the nuclear research activities in Thailand is now interrupted especially the activities those contribute with reactor, such as radioisotope production. It is expected that these activities will continue soon when the refurbishment of the pool and beam facilities are completed by the early of next year. (1992)

For the new project as the Establishment of the Nuclear Research Center is now on progress. After the site selection/confirmation had been made, many of documentations are being prepared and evaluated by project team under the recommendations and guidances from either the IAEA experts or from Japanese expert(s) via STA-program.

The decommissioning plan of the TRR1/M1 is being considered in more details upon the availability of information.

REFERENCES

1. M. Ravnik, IAEA expert mission (THA/4/010) on "Fuel Management" November 1990.
2. Y. Busamongkol, "Criticality Calculation", OAEP Internal report, June 1991.
3. D.B. McCulloch, IAEA expert mission (THA/4/010-14) Project Coordinator "New Nuclear Research Center" November 10-December 23, 1990.
4. P.L. De, IAEA expert mission (THA/4/012) " Decommissioning of Research Reactor" February 4-February 8, 1991.

7. Assessment of RTP Cores Since Commissioning in 1982

MOHAMMAD SUHAIMI BIN KASSIM
Nuclear Energy Unit,
Ministry of Science, Technology and Environment
PUSPATI Complex, Bangi, 43000 KAJANG
MALAYSIA

ABSTRACT

Since commissioning in 1982, RTP has undergone seven different core configurations. Only the first core consisted of all standard 8.5 wt%, 20% enriched fuel. Subsequently the next six cores consisted of mixed cores of 8.5 wt% and 12 wt%. SCRAM code originally obtained from the Penn. State University was modified for use in assessing the different core configurations. The results are sufficiently enough for a good understanding of the fuel burnup during normal operation of the core, although more accurate computer codes would be required to properly manage the core fuel available.

Introduction

The PUSPATI TRIGA Research Reactor achieved its first criticality on June 28, 1982. Since this date up to September 1991, RTP has released about 334 MWDs of energy equivalent to more than 400 grams of U-235. An effective fuel management program will be required to oversee the requirements of refueling such as to optimize utilization of the fuel elements within the safety limits of operation. In the next section, the code used in fuel management will be briefly described.

Short Description of the PUSPATI TRIGA Reactor

Like all TRIGA reactors, the PUSPATI TRIGA Reactor (RTP) is an open swimming-pool type reactor, cooled and moderated by light water. Fuel used is a homogeneous mixture of uranium and zirconium hydride. The core design is cylindrical with fuel elements arranged in form of concentric rings. The vertical and horizontal cross sections of the RTP MARK II core design is depicted in Figure 1[1],[2]. Figure 2 shows the TRIGA MARK II core grid plate arrangement.

Nominal steady-state power level is 1 MW with pulsing capability of up to 1300 MW. Cooling is provided by natural circulation.

Fuel elements are in the form of rods with overall length of about 75 cm. Fuel section is 38.1 cm length and 3.64 cm diameter. Cladding material used is stainless steel.

Table 1 lists some of the parameters as relevent to the PUSPATI TRIGA Reactor.

The SCRAM Code Used

The SCRAM code, abbreviated from Study of Core Reloads Using An Analytical Model, was originally developed at the Pennsylvania State University to provide a simple but accurate TRIGA core management program for the Pennsylvania State University Breazeale Reactor (PSBR) Facility. Two main objectives of the code is to reduce the number of fuel elements required during the operational cycle and the prediction of core reactivity changes and individual fuel element burnup and fission product buildup within the constraints of the model.

Three basic criteria were followed for the model:

1. Only two types of fuel elements are to be utilized; 8.5 w/o U-Zr and 12 w/o U-Zr fuel elements.
2. The neutron flux in the core will not be allowed to changed by more than 25% for the same power.
3. It is assumed that the optimum reloading schemes place the fuel elements containing the maximum U-235 closest to the core center.

The TRIGA C-M model requires the following data:

1. A k_{eff} loss rate as a function of the megawatt days of operation
2. A set of power fractions describing power production at each location in the core.
3. A series of equations which describes the k_{eff} changes resulting from fuel changes and/or fuel burnup throughout the core.

One of the major limitations of the model is that Xenon and other fission product poisoning is not accounted for. During the development of the code, it is believed that the added accuracy, due slight alteration of the power fractions of the element in the core, is not commensurate with the effort required, since these effects will be masked by errors in fuel depletion content.

The theoretical considerations of the TRIGA Core Management Model can be found in [3] and [4].

Some of the modifications that the writer has introduced is the choice of the input filenames to start the burnup calculations. Two choices are given, namely the EOC file of the last core configuration, which does not include any fuel movements or the BOC filename which include the fuel movements. At the end of the calculations, the output filename is automatically chosen for

easy reference. The writer also expands the fuel inventory to include new fuel elements and its unique identification in the fuel storage cabinet.

Input for the RTP

The full list of the fuel inventory is necessary. The parameters needed are the fuel location, fuel identification number, fuel weight percent and initial mass of U-235.

Other input include the initial ring power fractions and initial k_{eff}. A most important data is the cycle burnup in MWdays.

The data source for the calculations is gathered from Naughton[3]. Burnup rate is input as 1.234 grammes/MWday. The burnup slope, also from Naughton, is given as −0.00016843 rho/MWday.

Scram code also allows fuel movement into, within, or/and out of the core prior to actual burnup step calculations. The program also allows adjustments to the initial ring power fractions.

Results

The output from SCRAM comprises of individual EOC U-235 fuel masses, EOC ring-average power fractions, k_{eff}, and core excess reactivities (Table 2). Table 3 lists the number of different types of fuel elements during each cycle. Table 4 enlists the U-235 mass, core reactivity and total burnup in grams at EOC.

The accuracy of these results is very dependent upon the input of the BOC ring-averaged power fractions and also k_{eff} at BOC. However, comparison with calculations from the operational data shows good agreement, as shown at the bottom of Table 4.

Discussion

The results are sufficiently enough for a good understanding of the fuel burnup during normal operation of the core, although more accurate computer codes would be required to properly manage the core fuel available. However, thermal hydraulic constraints such as flux peaking need to be properly evaluated when mixed cores are assessed.

Since the type of fuel elements utilized is limited to only 8.5 w/o and 12 w/o U-235 restricts assessment to mixed cores of such fuel elements only. Either modifications need to be done to the model or otherwise a different code have to be used.

Another area of modification to the SCRAM code should include actual calculation of the initial k_{eff} and the initial ring

power fractions as these data is not easy to be obtained.

No effort has yet been undertaken to verify the results of the above calculations.

1 References

[1] "*Preliminary Safety Analysis Report for the PUSPATI TRIGA MARK II Research Reactor*", November 1979

[2] "*Safety Analysis Report for the PUSPATI TRIGA Mark II Reactor Facility*", PPA-R5, Nuclear Energy Unit, Malaysia,August 1983.

[3] Naughton, W. F. "Core Management Program To Optimize Fuel Utilization in TRIGA Research Reactors", Ph. D. Thesis, Pennsylvania State University, Sep. 1972.

[4] Cenko, M. J. "Comparison of PSBR Operation's History with the TRIGA Core Management Model", M. Sc. Thesis, Pennsylvania State University, Dec. 1972.

[5] I. Mele "Optimization of TRIGA Reactor Operation Using Reactor Calculations". Lecture presented during *Workshop on Reactor Physics Calculations for Applications in Nuclear Technology*, Trieste, Italy, 12 Feb -16 Mar 1990.

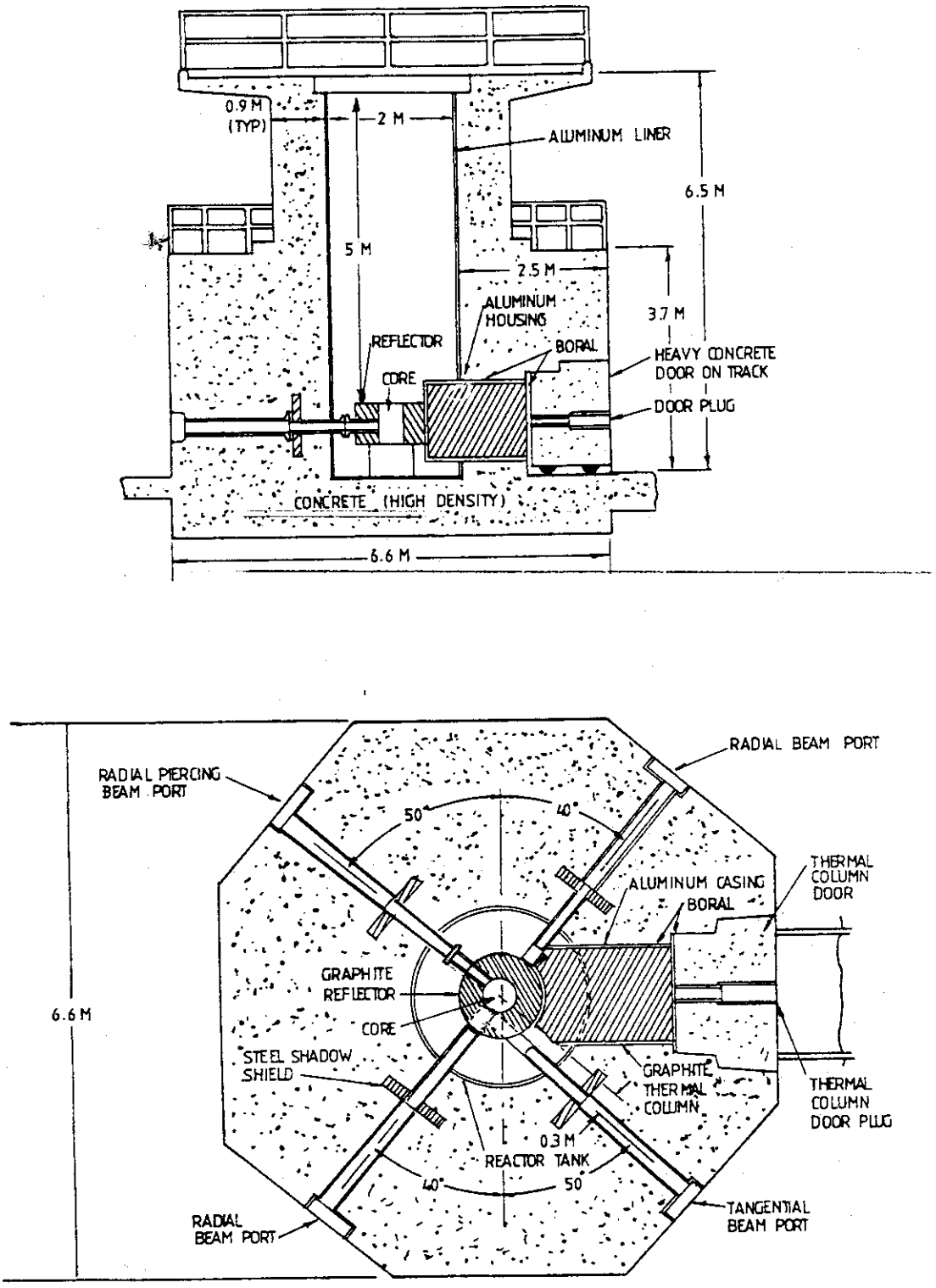

Figure 1: The vertical and horizontal cross sections of the PUSPATI TRIGA MARK II reactor.

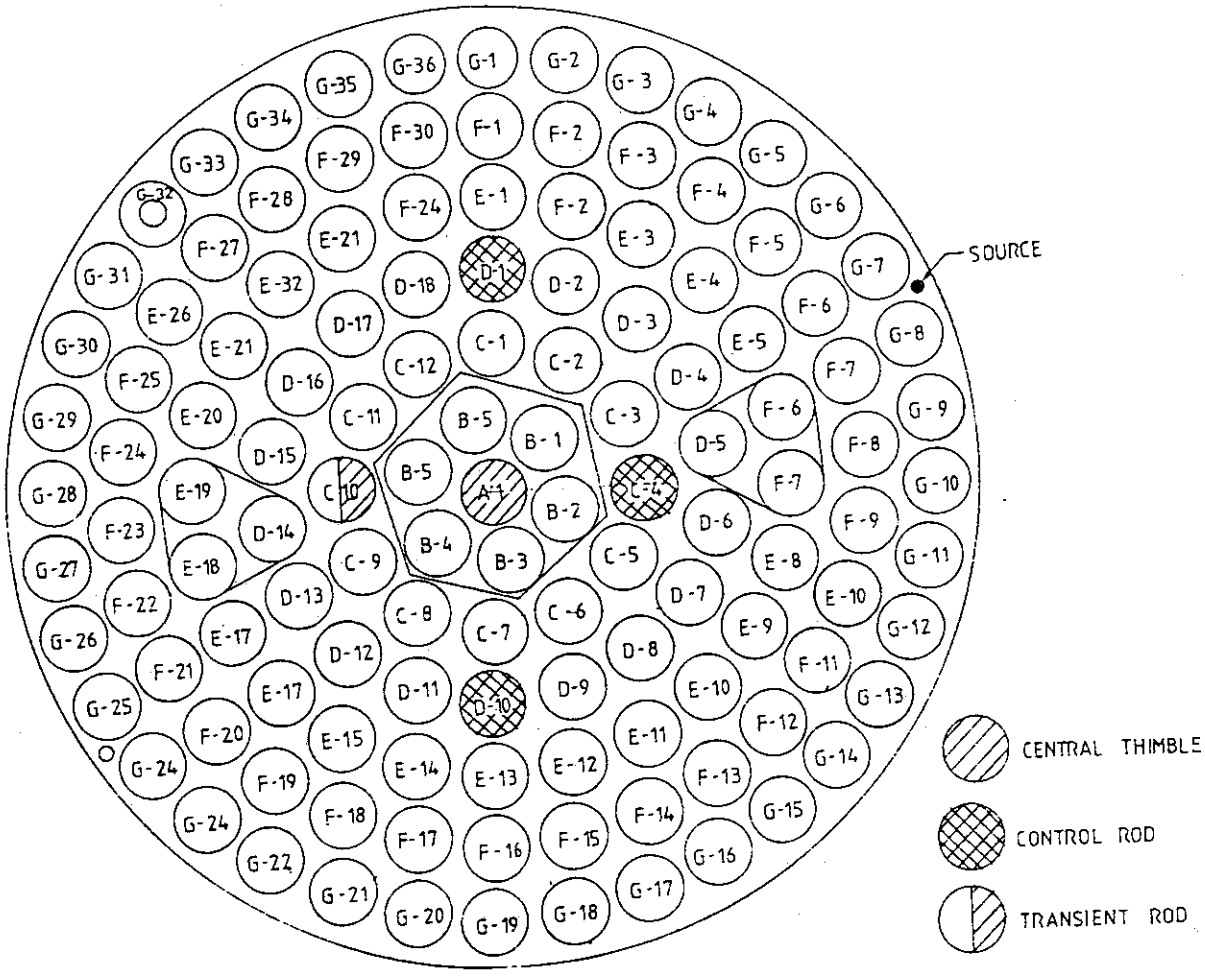

Figure 2: PUSPATI TRIGA MARK II Core Grid Plate Arrangement.

Table 1: PUSPATI TRIGA CORE NUCLEAR PARAMETERS

Ref RTP PSAR p 3-45

Cladding Material	SS-clad U-$ZrH_{1.6}$	
Cold Clean critical loading	54 elements; 2.1kg U-235	
Operational loading	86 elements; 3.2kg U-235	
l Prompt Neutron lifetime	39 μsec	
β Effective delayed neutron fraction	0.007	
α Prompt negative temperature coefficient	~ 1.0×10^{-4} δk/k°C	
T_f Average fuel temperature	23 °C	400 °C
T_w Average water temperature	23 °C	23 °C
k_∞	1.3816	1.3427
k_{eff}	1.0460	1.0085

Table 2: Power Fractions

Ring	1 BOC	1 EOC	2 BOC	2 EOC	3 BOC	3 EOC	4 BOC	4 EOC	5 BOC	5 EOC	6 BOC	6 EOC	7 BOC
B	1.900	1.872	1.902	1.873	1.902	1.887	1.847	1.818	1.818	1.809	1.808	1.782	1.782
C	1.500	1.488	1.574	1.565	1.574	1.565	1.775	1.754	1.754	1.747	1.746	1.727	1.727
D	1.000	1.000	1.002	1.002	1.002	1.001	0.979	0.977	0.977	0.976	0.976	0.973	0.973
E	0.900	0.902	0.894	0.894	0.894	0.895	0.875	0.877	0.877	0.877	0.877	0.877	0.877
F	0.700	0.704	0.706	0.709	0.706	0.709	0.647	0.653	0.653	0.655	0.654	0.659	0.659
G	0.000	0.000	0.000	0.000	0.000	0.000	0.000	0.000	0.450	0.452	0.452	0.458	0.458
k_{eff}	1.050	1.0427	1.050	1.0423	1.0533	1.0461	1.0521	1.0381	1.0490	1.0444	1.0450	1.0327	1.047
Core Excess	$6.80	$5.85	$6.80	$5.79	$7.23	$6.30	$7.07	$5.24	$6.67	$6.07	$6.15	$4.53	$6.80

Table 3: Core Configuration and Changes

Ring	1	2	3	4	5	6	7
B	6	6	2	2	2	2	1
	0	0	4	4	4	4	5
C	11	6	6	2	2	2	2
	0	5	5	9	9	9	9
D	18	18	18	18	18	18	17
	0	0	0	0	0	0	1
E	24	24	24	24	24	24	24
	0	0	0	0	0	0	0
F	27	29	29	29	29	29	28
	0	0	0	0	0	0	0
G	0	0	0	0	10	10	13
	0	0	0	0	0	0	0
Sub total	86	83	79	75	85	85	85
	0	5	9	13	13	13	15
Total Incore	86	88	88	88	98	98	100

Note: The top row lists the number of 8.5 weight-percent U-235 fuel elements while the second row lists the 12 wt% fuel elements.

Table 4: Fuel Mass in the Core

Ring	1 BOC	1 EOC	2 BOC	2 EOC	3 BOC	3 EOC	4 BOC	4 EOC	5 BOC	5 EOC	6 BOC	6 EOC	7 BOC	7 EOC
Date	820628	851231	860101	870531	870601	880531	880601	891231	900101	900531	900601	910531	910601	910930
B	229.1	222.0	222.0	214.6	290.1	283.3	283.3	270.4	270.4	266.6	266.6	256.3	285.8	284.0
C	413.1	402.8	493.0	481.9	481.9	471.5	547.5	524.7	524.7	518.1	520.9	502.6	501.8	498.4
D	671.4	660.2	660.0	648.4	648.4	637.6	637.6	617.1	617.1	611.0	611.0	594.3	609.9	606.8
E	902.9	889.4	889.4	875.6	875.6	862.8	862.8	838.3	838.3	831.1	831.1	811.0	811.1	807.3
F	1004.	992.6	1067.	1054.	1054.	1042.	1042.	1020.	1020.	1014.	1014.	996.0	961.5	958.2
G	0.0	0.0	0.0	0.0	0.0	0.0	0.0	0.0	360.8	359.3	359.3	355.0	454.2	453.1
Total	3221.	3167.	3332.	3275.	3350.	3297.	3373.	3271.	3632.	3600.	3603.	3515.	3624.	3608.
Burnup grams	53.86		57.15		53.06		102.66		31.67		87.66		16.38	
(MWD)	43.45		45.95		42.67		83.20		27.26		75.54		14.33	
Cumulative Burnup grams	53.86		111.01		164.07		266.73		298.47		386.06		402.44	
(MWD)	43.45		89.40		132.07		215.27		242.53		318.07		332.40	
Comparison with Operational Data														
Burnup grams	53.74		55.77		53.65		107.54		28.82		93.41		17.76	
Cumulative (MWD)	53.74		109.51		163.16		270.70		299.52		392.93		410.69	

8. Preliminary Analysis for the Cut-Off of All Off-Site Power Supplies at HWRR

WAN MINGZHI

China Institute of Atomic Energy

ABSTRACT

During the long period of operation(33years), though the cut－off of all off－site power supplie is a kind of accidient which occurs scarcely at HWRR, there is need to analysis such accident in order that we can assess HWRR' s safety characteristics. By means of theoretical calculation and experimental demonstation in this paper, we have proved that when the cut－off of all off－site powers occurs and there is no secondary water circulation, the residual heat can be brought by the emergency cooling system and the convection cooling of the primary loop with environment lso long as HWRR' s emergency system is in normal state.

INTRODUCTION OF HWRR

Heavy Water Reserch Reactor (HWRR) with a low－enriched uranium dioxide fuel which lies about 35 Km southeast of Beijing was built and reached critical in 1958. After 20 years safe operation, we reconstructed HWRR in 1978. Now its maximum thermal power is 15 MW, its maximum thermal neutron flux is $2.6 \times 10^{14} n/s.cm^2$. The main uses of HWRR is as following:

(1) Fundamental physics experiments such as neutron inelastic scattering and neutron diffraction study.
(2) Neutron activation analysis.
(3) Production of all kinds of isotopes.
(4) Monocrystalline silicon neutron transmutation doping.
(5) Fuel elements irradiation testing for Nuclear Power Plant.

POWER SUPPLIES OF HWRR

During normal operation, HWRR is supplied by two independent offsite power supplies, One comes from the East Station, the other comes from the West Station. HWRR is also supplied by emergency power supply which comes from a battery for aftercooling after the cut－off of all off－site power supplies accurance. It is illustrated in Fig.1.

According to incomplete statistics, during HWRR operation there were about total 54 times cut－off of single offsite power supply from 1958 to 1988 because of thund and storm, the east wire occured 22 times and the west wire occured 32 times. There have never been the cut－off of all offsite power supplies in HWRR during operation, i.e., since 1958 the cut－off of east wire and the cut－off of west wire haven't occured at the same time.

The HWRR will shutdown immediately and automatically as soon as there occurs the cut－off of any offsite power supply. The other offsite power supply and the emergency power supply will take into action for aftercooling immediatelly. The cut－off of single offsite power supply in HWRR may be included in ordinary accidents and won't bring any bad consquence to HWRR. We can take it easy. But how about the cut－off of all offsite power supplies? Is it hard－to－handle? Would it bring any bad consquence and hazard to HWRR and environment? Considering its feasibility, we should do some safety analysis and assess HWRR's safety characteristics under such adventitious accident condition.

EMERGENCY SHUTDOWN SYSTEM

There are 10 accident protections in HWRR. They are as following:

(1) Reactor power excursion
(2) Reactor fast period
(3) Failure of electron device for power protection
(4) Failure of electron device for period protection
(5) Cut－off of any HW pump power supply
(6) Cut－off of 110V DC emergency power supply
(7) Loss of core inlet pressure
(8) Loss of secondary water flowrate
(9) Fuel element rupture
(10) Hitch of cold neutron source device

During HWRR' s operation, any accident protection above can put the emergency shutdown system into effect by means of control safeguard

circuit automatically, i.e. the HWRR can be shutdown immediately (all the control rods fall to the bottom of reactor core). Each accident above should be tested periodically (once or twice a year, called Protection Safety Test). The test result and long period operation have proved that the Emergency Shutdown System has good reliability and safety.

COOLING SYSTEM AND BACKED－UP POWER SUPPLY

Cooling system is a safety－related system which includes primary coolant(heavy water) circuit and sedondary coolant(ordinary water) circuit.The normal heat rejection flow path may therefore be divided into two distinct parts: from the core to the heat exchanger via the primary circuit,and then from the heat exchanger to the cooling tower via the secondary circuit.There is no special purpose emergency cooling circuit in HWRR. The primary circuit also undertake the emergency aftercooling, only variation in pump's number and pump's revolutions per minute, i.e., during normal operation two or three pumps run in 3000 rpm.; after the cut－off of all offsite power supplies, only one of the two or three pumps run down to 1500 rpm. The primary circuit and the secondary circuit are illustrated in Fig.3 and Fig.4.

After the cut－off of all offsite power supplies accurance and reactor trp, forced circulation in the primary circuit for aftercooling is guar－anteed by means of ine HW pump in 1500 rpm. drive energized from the 110V dc battery backed supply via a GM generator and arranged to engage when HW pump run down to 50% of nominal speed. The diagram for HW pump's power supplies is illustrated in Fig.5.

Reliability analysis of the HW pumps in 1500 rpm, drive has indicated an upper probability of a single HW pump failing to engage on demand of the order of 2.0E－3 so that with two HW pumps the probability of all drives failing is 4.0E－6, with three HW pumps the probability of all drives falling is about 8.0E－9 －－two satisfactory results.

RESIDUAL HEAT REJECTION CAPACITY

The capacity of the aftercooling system is considerably in excess of

requirements and will bring core thermal parameters down very quickly. Fig.6 shows the transients of core outlet temperature (T^{out}), fuel element surface temperature (T_w), fuel element center temperature (T_c), DNBR, which are invoked immediately following a reactor trip arised from the aftercooling system are in normal state. If the HW pump could not start until 7.7 seconds from the cut－off of all offsite power supplies, the fluid temperature would exceed boiling point, such trancient would be harmful to HWRR's safety and illustrated in Fig.8 .

ANALOG EXPERIMENT

From April 6, 1990 to April 8, 1990 we did the analog experiment of the cut－off of all offsite power supplies as a schedueled shutdown. The cooling curve is illustrated in Fig.9. According to the "HWRR Operation Rules", the core temperature limitation after shutdown is as following:

Within 5 HRS, Tc < 70 ℃
From 5 HRS to 24 HRS, Tc < 80 ℃
After 24 HRS, Tc < 90 ℃

Every cooling was not done for ten minutes till the core temperature reached tc its limitation. The result indicated that the maximun colddown temperature is 62 ℃ . As the time went on, the colddown temperature would became small and small, it meant that the primary circuit only could be fully competent at the aftercooling.

The battery capacity was limited. It could maintain 22 times cooling (about 2.5 days cooling). Its discharge curve is illustrated in Fig.10 and Fig.11.

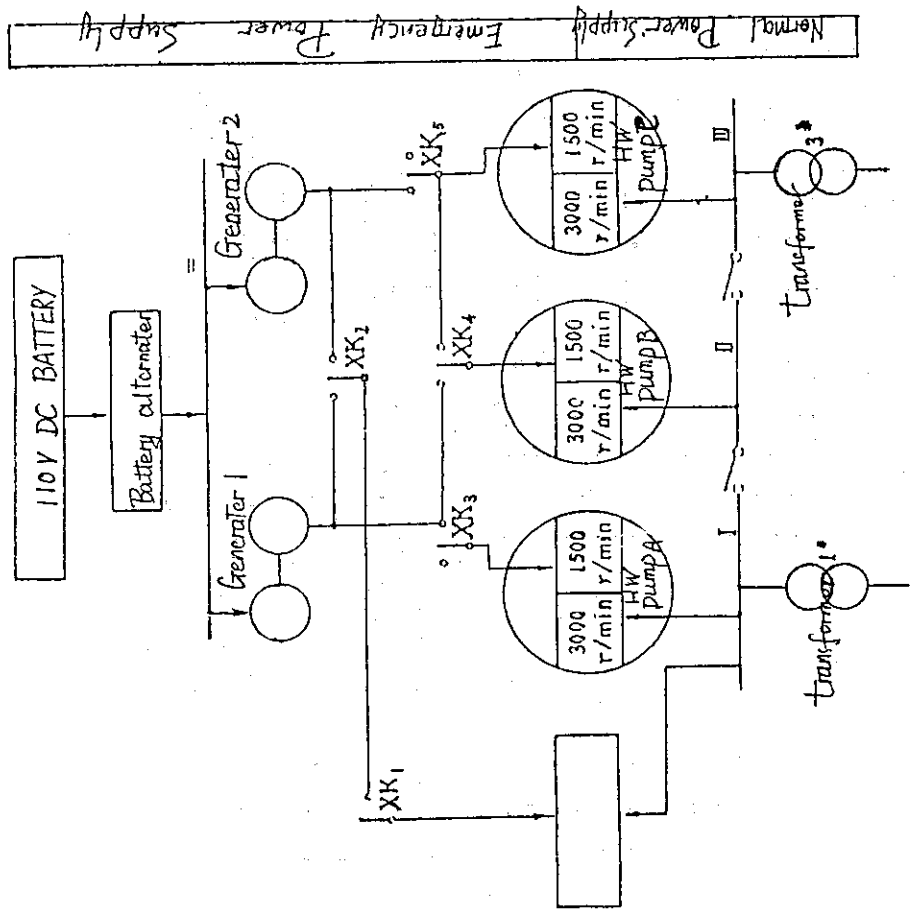

Fig. 2 Diagram for HW pumps power supplies

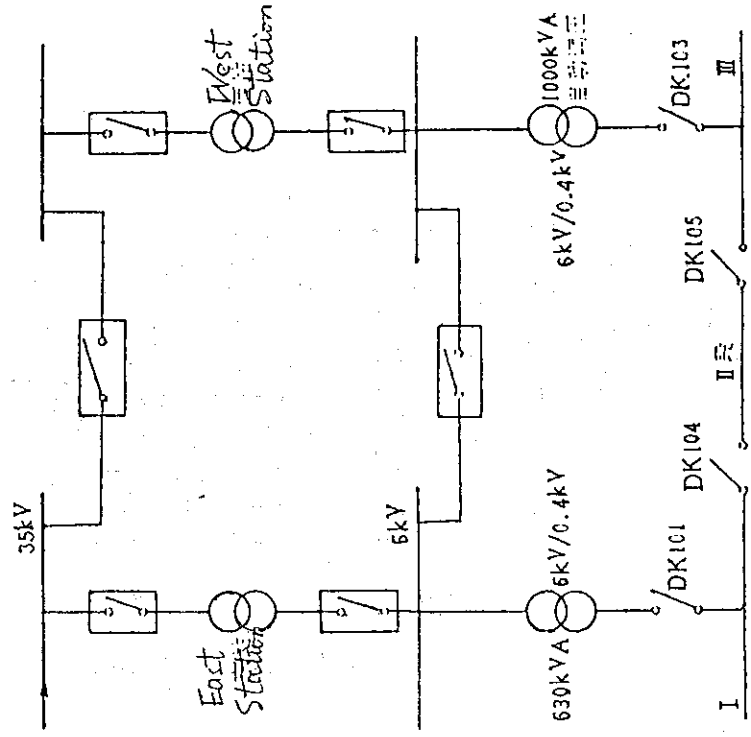

Fig. 1 Offsite power supplies for HWRR

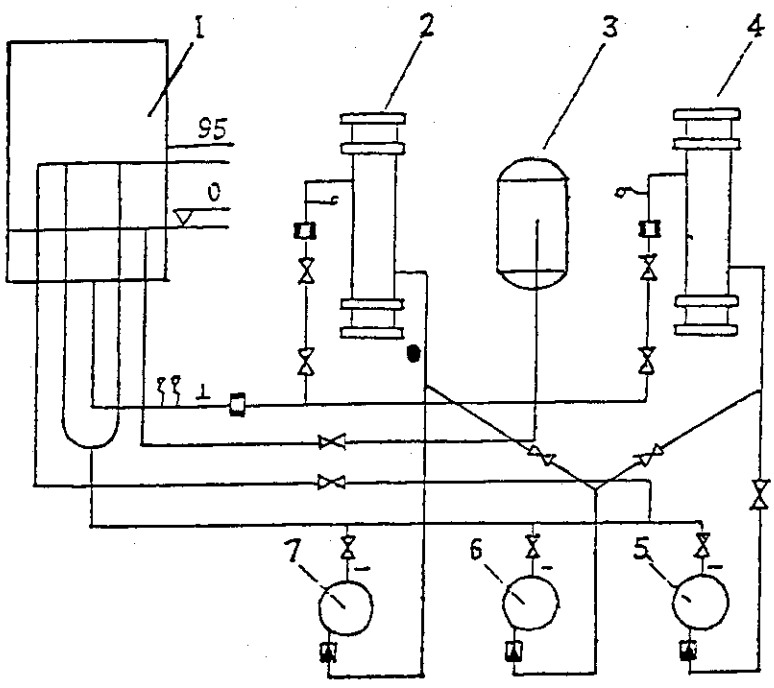

1 - cfdvrmr core　　3 - tank

2 - heat exchanger A , 4 - heat exchanger B

5 , 6 , 7---HW pump A,HW pump B,HW pump C

Fig. 3 Diagram for primary circuit

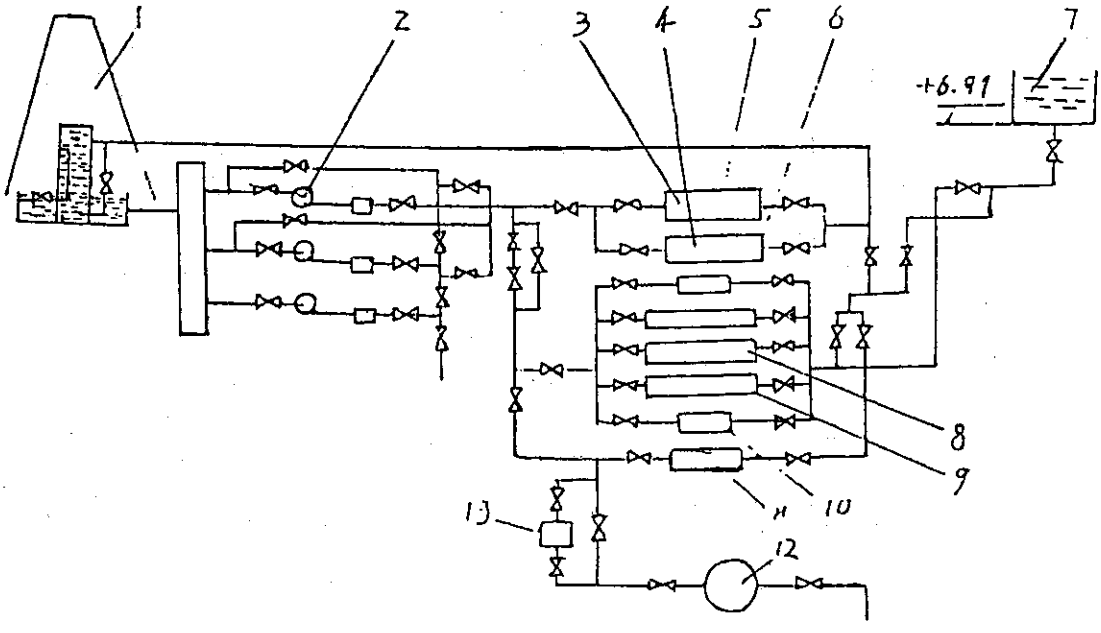

Fig. 4 Diagram for secondary circuit

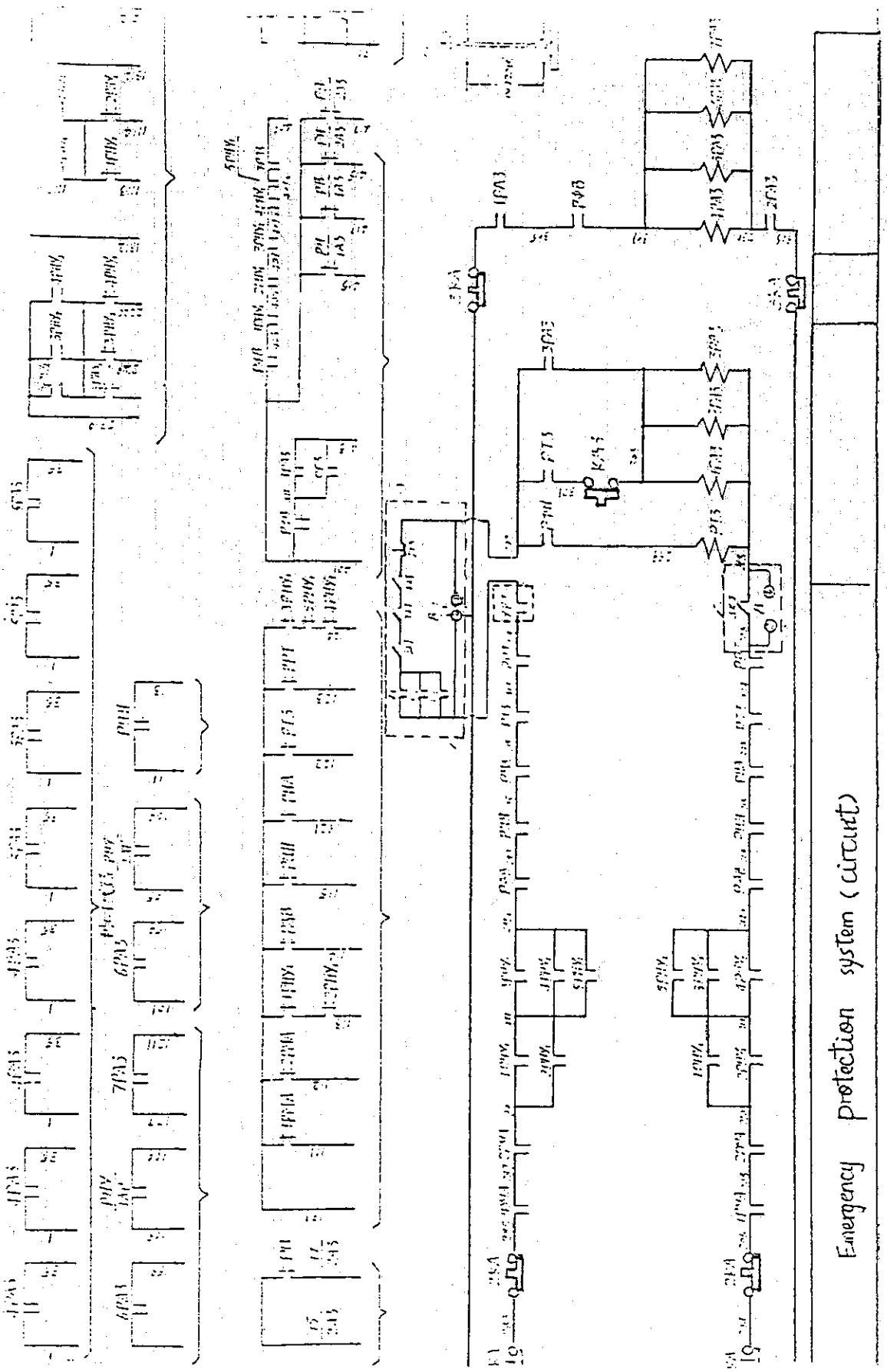

Fig.5 Part of accident protection and shutdown system for JWRR

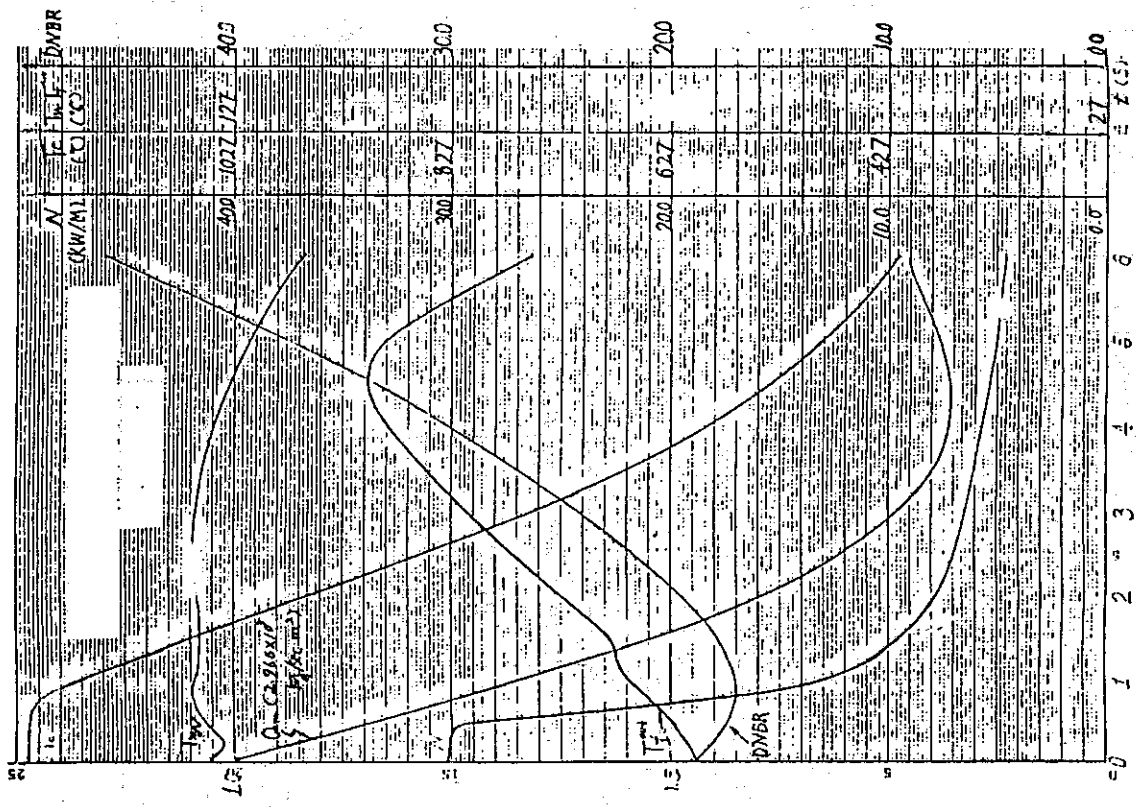

Fig. 7 Thermal parameters transients with HWRR in normal operation immediatelly following reactor shutdown (15 MW , 3 pumps)

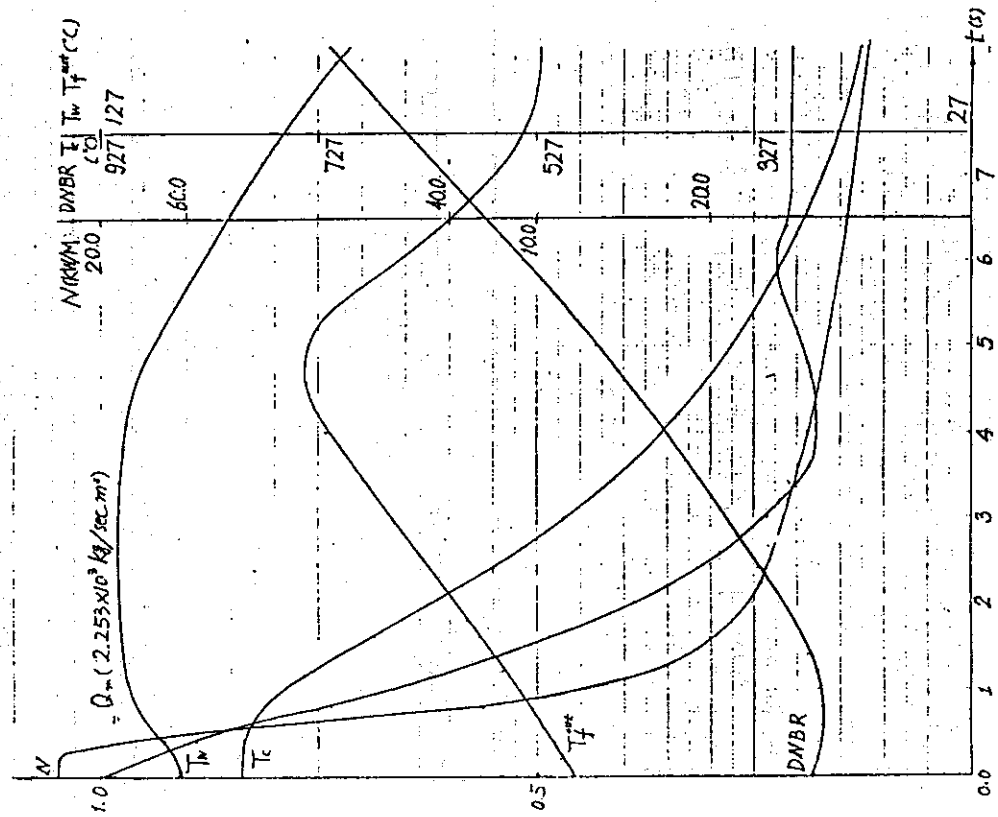

Fig. 6 Thermal parameters transients with HWRR in normal operation immediatelly following reactor shutdown (10 MW , 2 pumps)

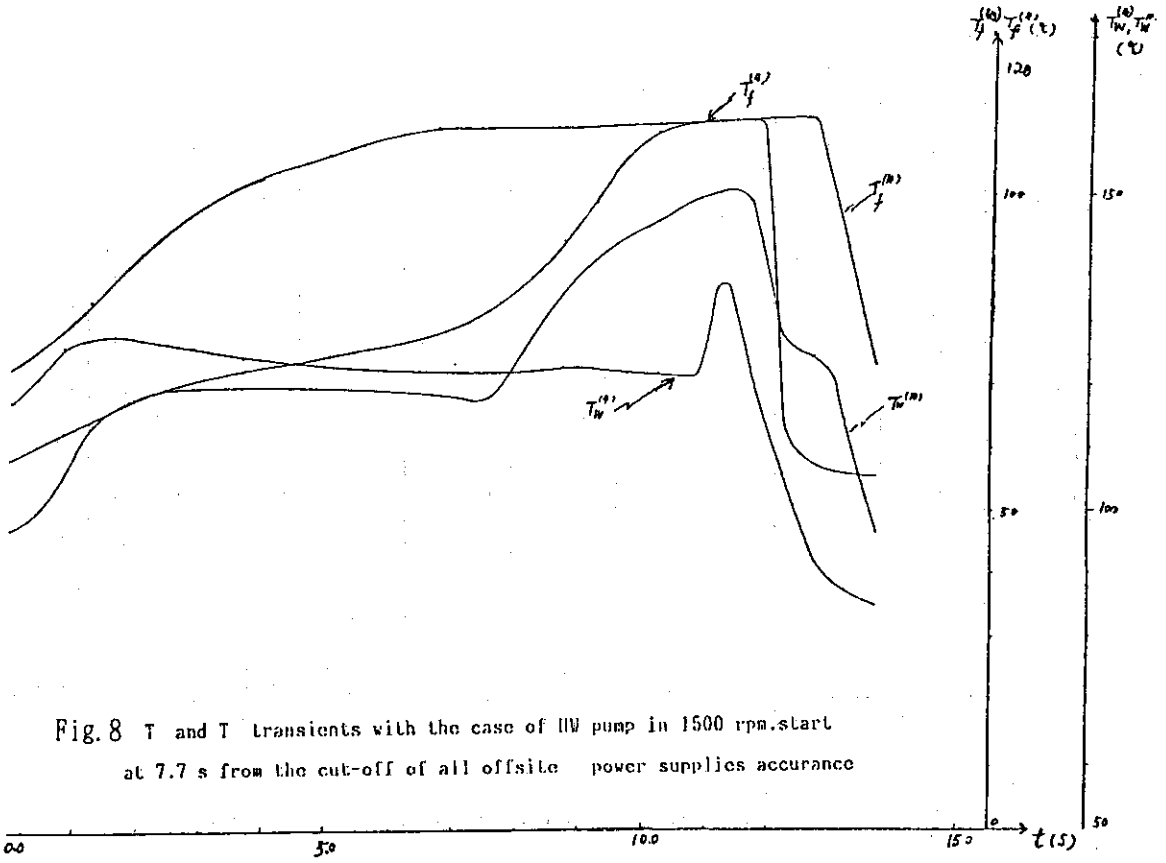

Fig. 8 T and T transients with the case of HW pump in 1500 rpm.start at 7.7 s from the cut-off of all offsite power supplies accurance

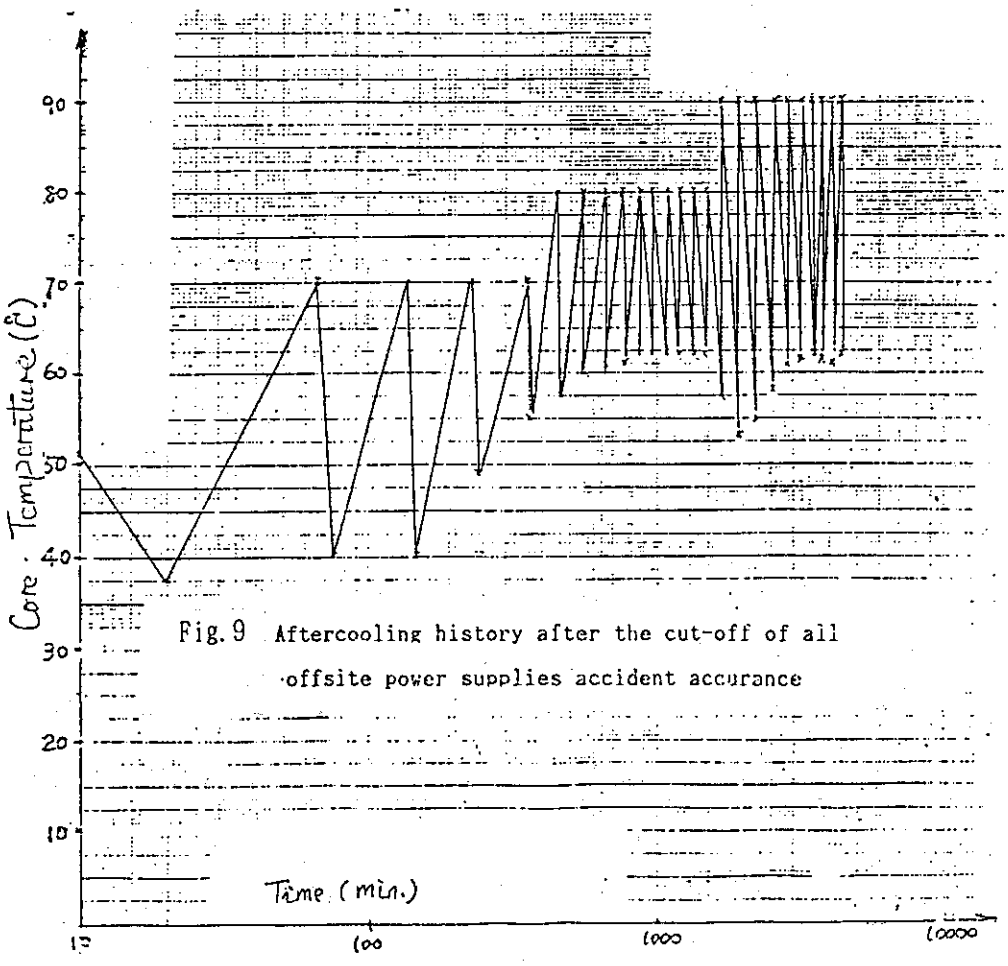

Fig. 9 Aftercooling history after the cut-off of all offsite power supplies accident accurance

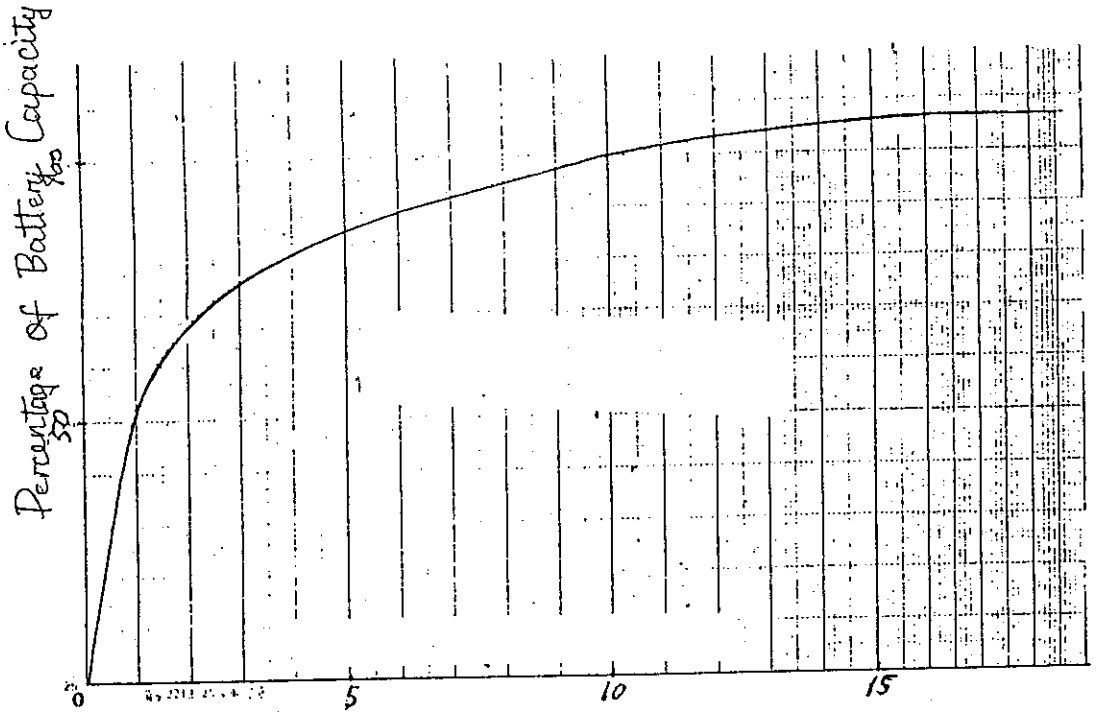

Fig. 10 GFD-1200 type of batery electricity discharge curve 1

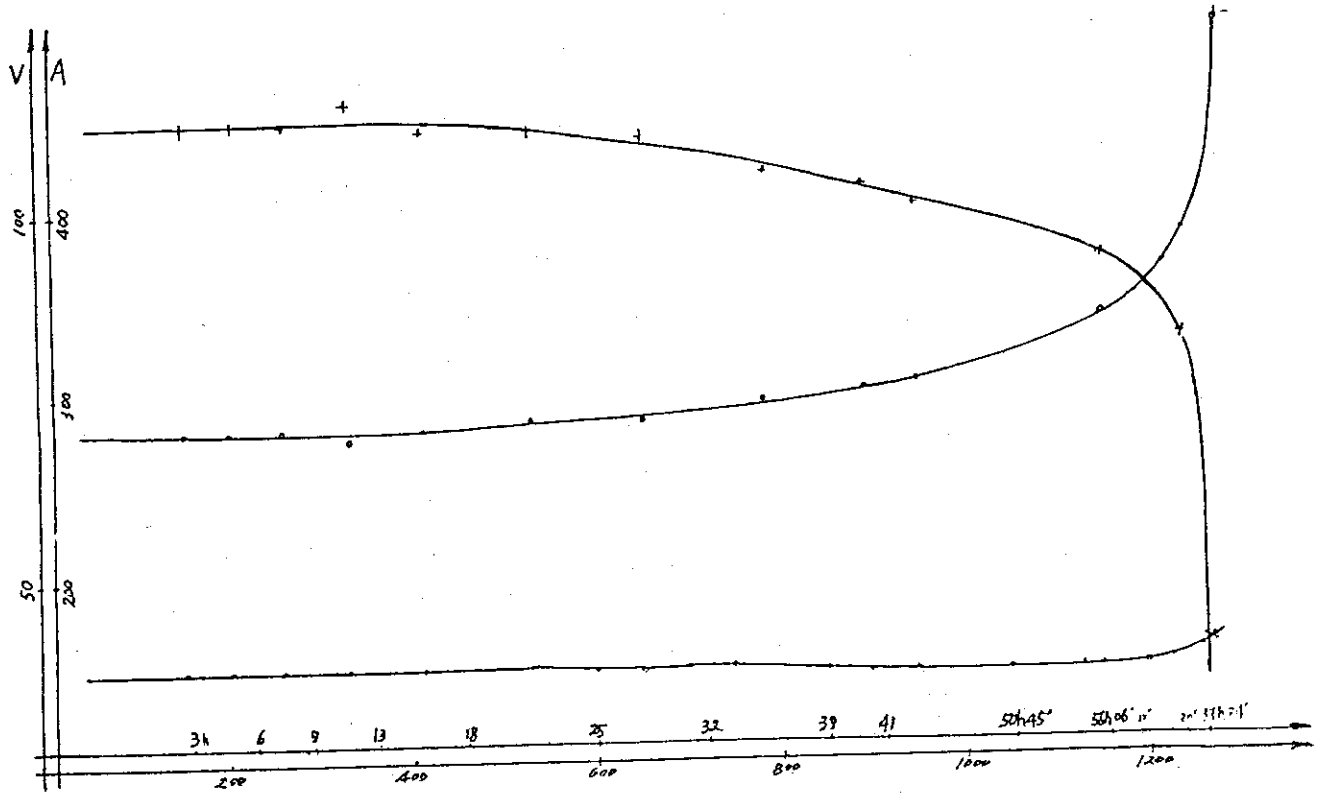

Fig. 11 GFD-1200 TYPE OF BATTERY ELECTRICITY DISCHARGE CURVE 2

APPENDIX A

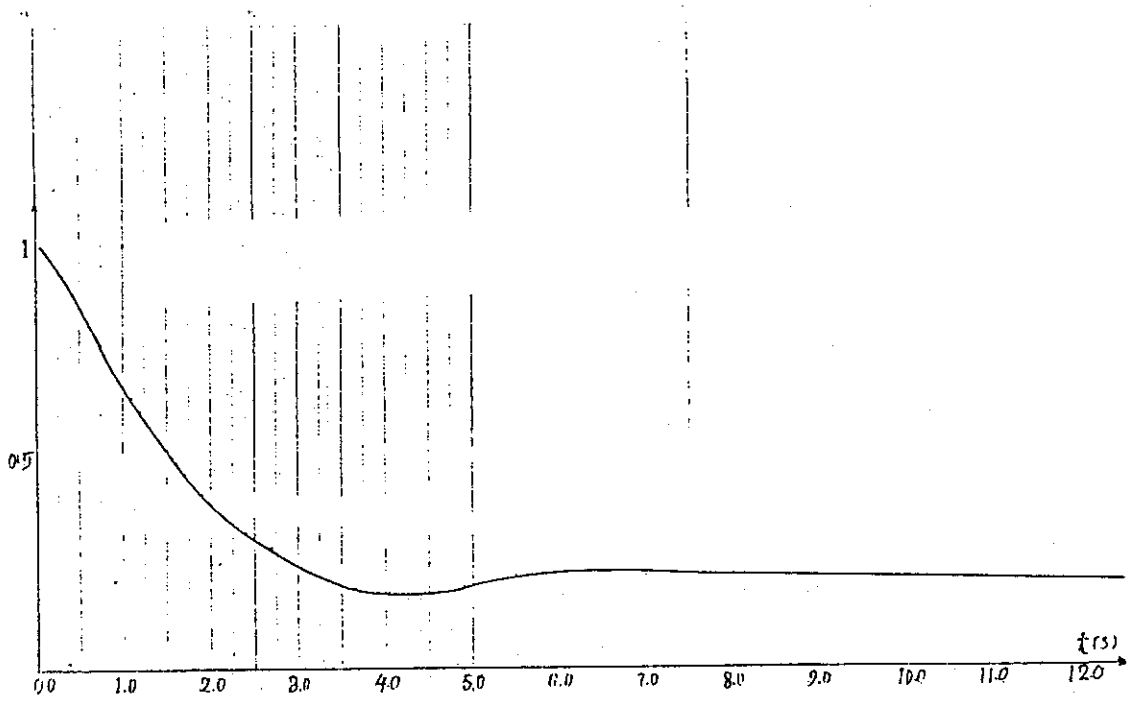

Normalized flowrate after the cut-off
of all offsite power supplies accurance

APPENDIX B

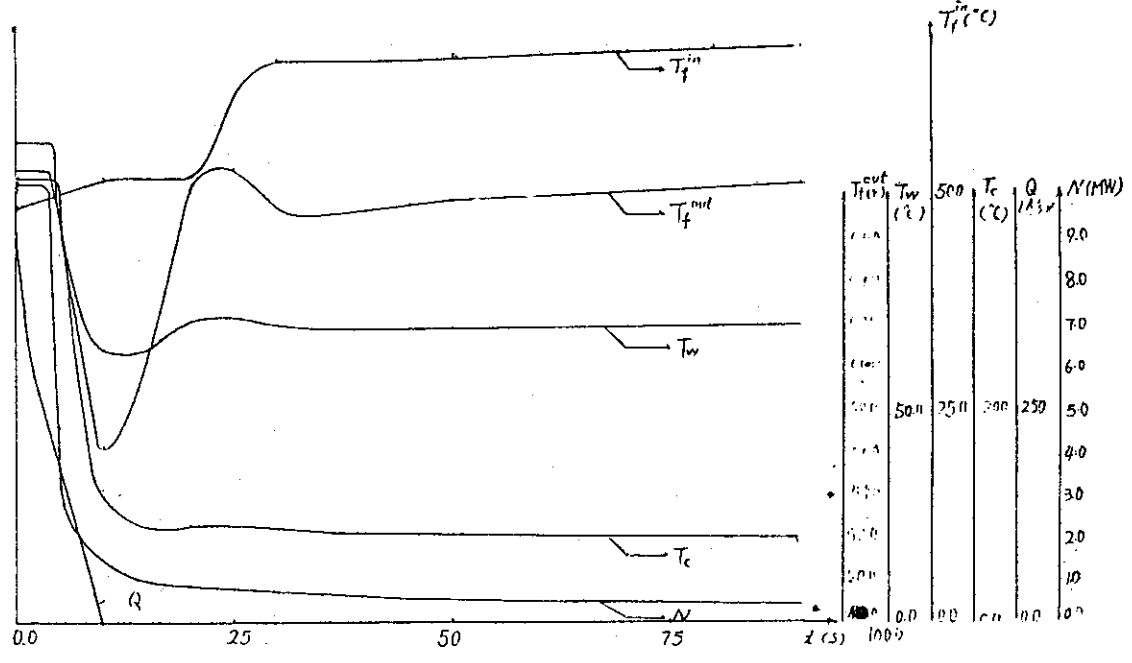

1. Completion of Reconstruction for Japan Research Reactor No.3

K. KAKEFUDA, M. TANI and M. ISSHIKI

Department of Research Reactor
Tokai Research Establishment, JAERI
Tokai-mura, Naka-gun, Ibaraki-ken 319-11, Japan

ABSTRACT

The works of the reconstruction for the Japan Research Reactor No.3(JRR-3) started in 1985 and initial criticality of the new reactor achieved in March, 1990. After commissioning test, the new JRR-3 has been operated some operational cycles since Novemmber, 1990. This paper presents outline of the removal work on the old JRR-3 and the new JRR-3.

INTRODUCTION

High quality irradiation conditions and high neutron flux condition had been required. To fulfil these requirements, it was decided that the JRR-3 should be reconstructed to be upgraded. [1]

The first domestic research reactor in Japan, JRR-3, had been operated for 21 years since its criticality in 1962. It was shut down in 1983 and had been reconstructed to be upgraded as a part of the International Reduced Enrichment for Research and Test Reactors(RERTR) program. During the reconstruction, the whole of the old core with the biological shield and all of reactor components had been removed, except the reactor building, and a new high performance multi-purpose reactor had been constructed at the same place. Figure 1 shows the construction schdule of upgraded JRR-3.

The new JRR-3 was achieved to the criticality in March 1990. That is upgraded to a 20MW(th) light water moderated and cooled, beryllium and heavy water reflected, pool type research reactor using 20% low enriched UAlx-Al(LEU) plate type fuel. That is equipped with various kinds of experimental facilities for irradiation and beam experiments including a cold neutron source.

The new JRR-3 has been operated some operational cycles since Novemmber, 1990. One operational cycle consists of 4 weeks for operation and 1 week for shutdown work.

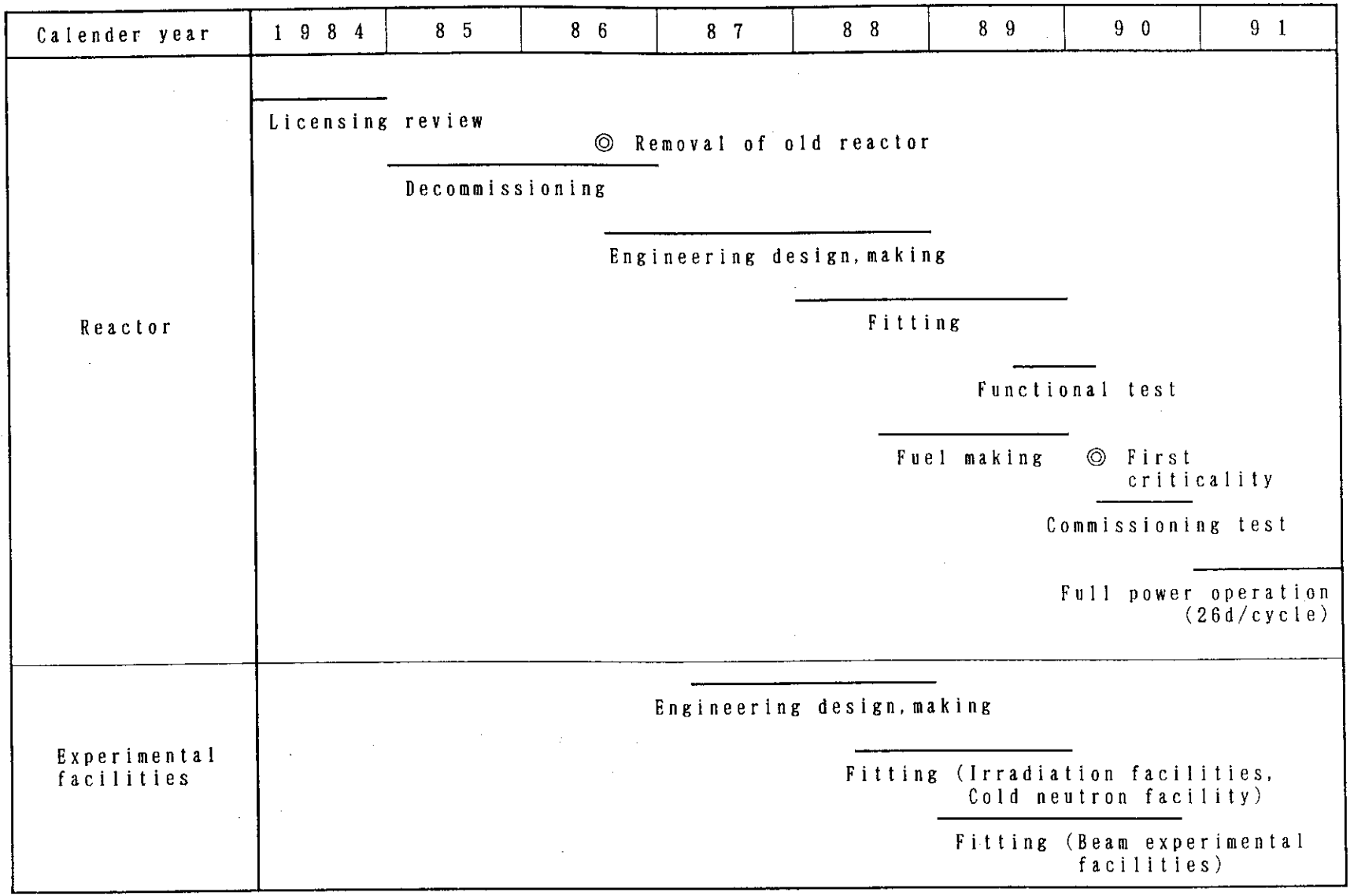

Figure 1 Construction schedule of upgraded JRR-3

REMOVAL WORK ON THE OLD REACTOR

The main body of the reactor was removed by the one-piece-removal method. The procedure is illustrated in Figure 2. The main body consists of the core tank, graphite reflector, thermal shield tank and biological shield and is about 2200 tons in total weight.

First, the main body was separated, with all components contained in the biological shield, from the concrete in the reactor room by means of continuous core boring, and was lifted up using a hanging frame and center hole jacks. Next, it was transferred horizontally out of the reactor room through a temporary opening in the wall of the reactor building. Finally, it was housed in the large scale waste storage room constructed under the experiment building near the reactor room. This main body will be kept permanently under close observation.

The reasons why this method was adopted are as follows; First, the spread of radio-active materials can be avoided. Second, this method could be carried out with established techniques. Third, the cost and time required for this method were acceptable for this project.

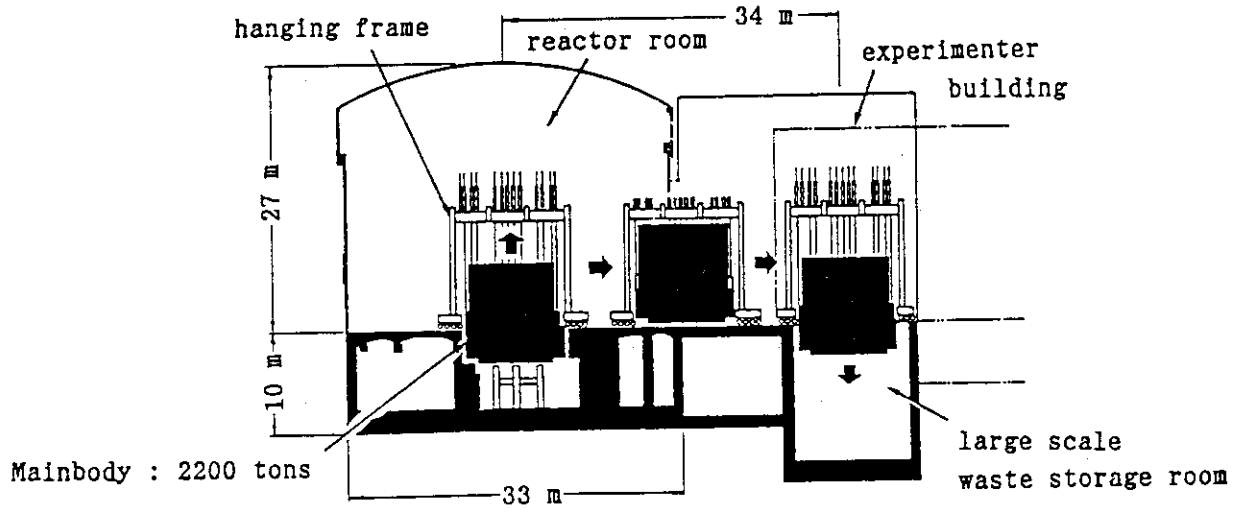

Figure 2 Outline of One-piece Removal Method

OUTLINE OF THE UPGRADED JRR-3

Figure 3 shows the reactor components of the JRR-3. The JRR-3 is upgraded to a 20MW(th), multi-purpose, light water moderated and cooled pool type reactor. The depth of the pool is about 8 m. The core components consists of the core, heavy water tank, plenum and structual components. The core is submerged in the pool.

The core is compact and cylindrical in shape, 0.6 m in diameter and 0.75 m in hight. It is composed of 26 standard fuel elements, 6 control rod elements, 5 irradiation elements and 12 pieces of beryllium reflector. Each control rod element consists of neutron absorber, box shape hafnium, and follower fuel element connected with the absorber. They are driven through the core by CRDM installed beneath the core.

Beryllium reflectors are installed between the fuel region and the inner wall of the heavy water reflector tank.

The heavy water reflector tank is a double cylindrical type aluminium vessel, with hight of 1.6 m and outer diameter of 2 m. Nine vertical irradiation thimbles, nine horizontal beam tubes and cold neutron source facility are installed in this tank. Horizontal beam tubes are arranged tangentially to the core in order to reduce fast neutron and gamma-ray fluxes. The aluminum alloy is chosen for the core components to reduce neutron absorption and radiation dose under the maintenance work.

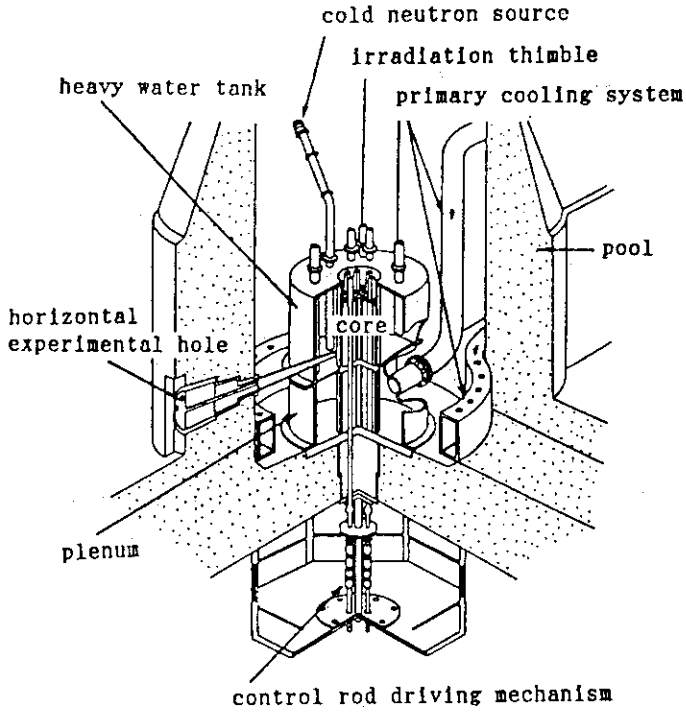

Figure 3 Reactor Components

A flow diagram of the cooling system is shown in Figure 4. The flow of primary coolant is downward through the core for the purpose of reduction of the radiation dose cause of ^{16}N which is produced by the (n,p) reaction in ^{16}O, and a ^{16}N decay tank is installed in the primary cooling system. The coolant flow rate in normal operation is 2400 m^3/hr.

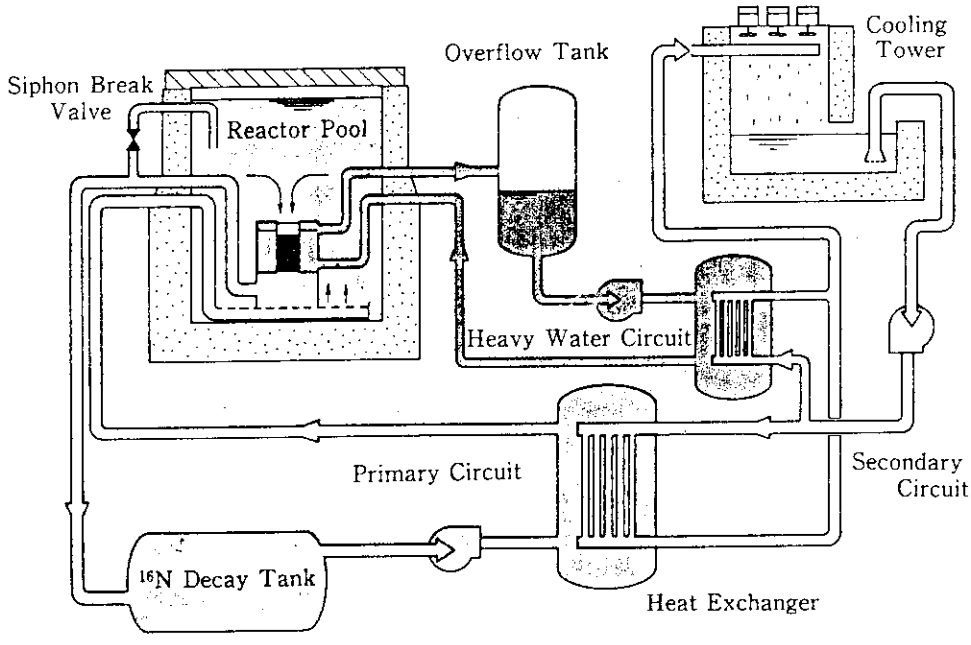

Figure 4 Flow Diagram of the Cooling System

The cross section of a standard fuel element is shown in Figure 5. The fuel element is MTR type, with 19.75 wt% enriched UAlx-Al dispersion fuel and the uranium density of fuel core is 2.2 g/cc. Low enriched uranium fuel is chosen because of the general international availability and acceptance of 20 % or less enriched fuel.

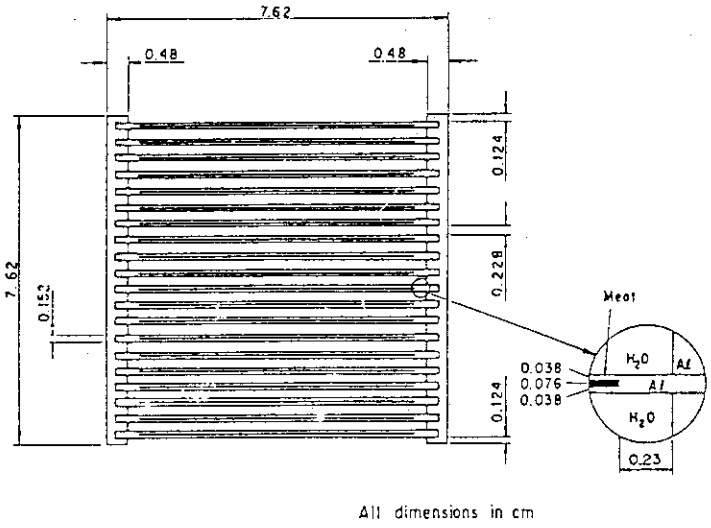

Figure 5 Cross Section of the Standard Fuel Element

EXPERINENTAL FACILITIES

The JRR-3 has some irradiation facilities. In the these facilities, specimens are inserted into the region of the core or heavy water reflector for the purpose of irradiation tests on neuclear reactor fuels and materials, radioisotope production and activation analysis.

The beam experimental tubes lead neutrons from the core to the experimental equipment for neutron scattering experiment and neutron radiography. Nine horizontal beam tubes(1G to 7R, 8T, 9C) are arranged tangentially to the core, as shown in Figure 6, to reduce fast neutrons and gamma rays in the thermal neutron beam. The beam tube 8T and 9C are followed by neutron guide tubes. Neutron guide tubes lead neutrons with high transfer efficiency to the beam hall in the experimenter building. 9c is provided for experiments where cold neutrons are used. 8T is provided for experiments where thermal neutrons are used. The neutron guide tubes are divided into three beams in 9C and into two beams in 8T. The arrangement of the neutron guide tubes is shown in Figure 7.

The cold neutron source moderate thermal neutrons by means of liquid hydrogen at 20K, and supply cold neutrons with wavelength of about 0.4 nm and an energy of about 5 meV.

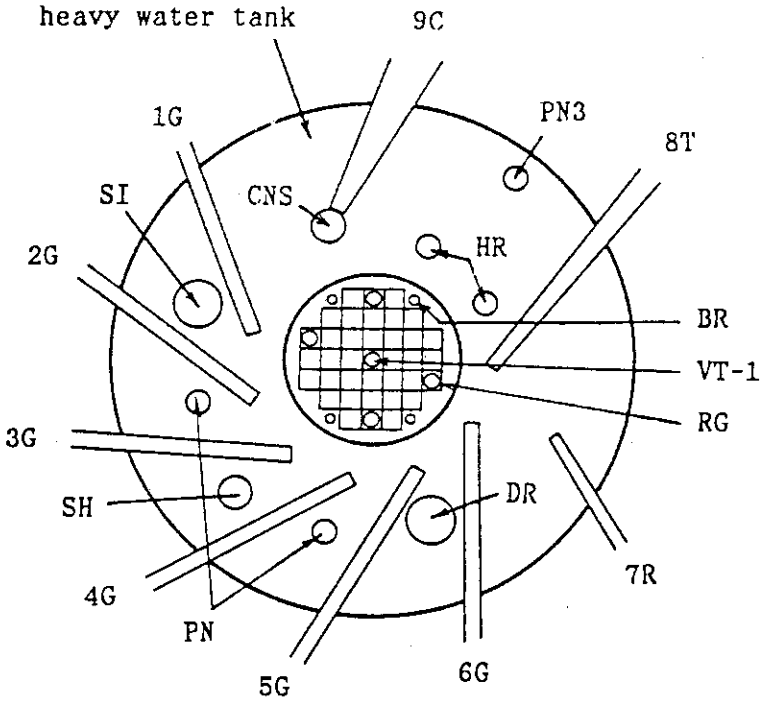

Figure 6 Arrangement of the Experimental Holes

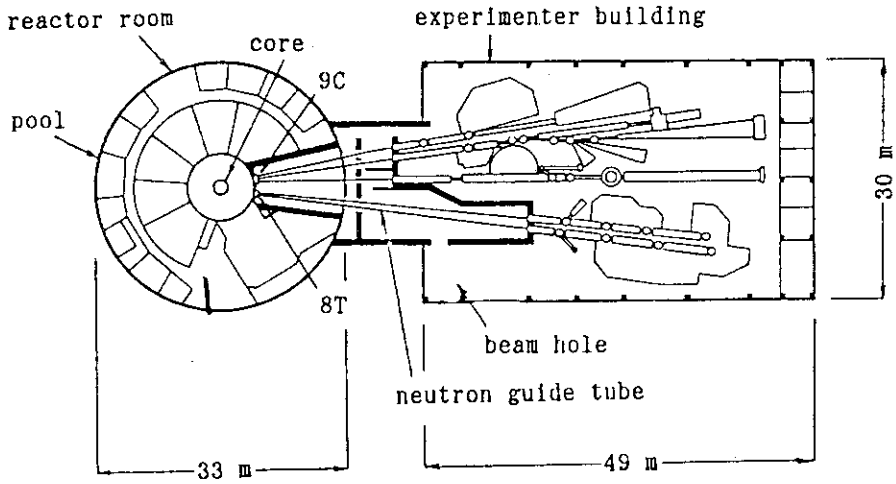

Figure 7 Arrangement of the neutron guide tubes

COMMISSIONING TESTS

A commissioning tests started in March 1990, succeeding the completion of functional tests of all reactor systems. These tests consists of three phase. [2]

In the first phase, primary coolant flow distribution of the core was measured at non-nuclear stage. The first fuel element was loaded to the core on March 15, and the first criticality of upgraded JRR-3 was acheived on March 22. In this phase, core nuclear characteristics, such as excess reactivity, control rod worth, shut down margin, reactivity coefficients, neutron flux distributions, etc. have been measured mainly at zero-power.

The second phase was the power-up test phase in which reactor power was raised step by step, and reached the maximum designed power level, 20MW, on August 22. In this phase, measurement of thermal power, neutron flux monitor calibration, examination of automatical reactor control system, check of radiation shielding, etc. have been performed.

In the final phase, reactor was continuously operated at 20MW for 100 hours, in order to examine the stability of all the reactor system.

OPERATION AND REFUELING

Figure 8 shows the operation schedule. The upgraded JRR-3 has been operated some operational cycles since Novemmber, 1990. The JRR-3 is planed 8 or 9 opertational cycles in a year. One opertational cycle consists of 4 weeks for operation and 1 week for shutdown work. During each operational cycle, reactivity is measured after the refueling at the low power of the reactor in the shutdown week. Next Monday, the reactor power is increased step by step to 20 MW, checking the cooling system, and kept at 20MW.

Figure 9 shows the core batch. The core is divided into five batches. The fuel elements with the highest burnup in each batch are removed and new fuel elements are loaded instead of them after the each operation in order to make the power distribution as flat as possible. In the shutdown period, five or six fuel elements are refueled, so that fuel elements of nearly 2 cores will be necessary for one year reactor operation.

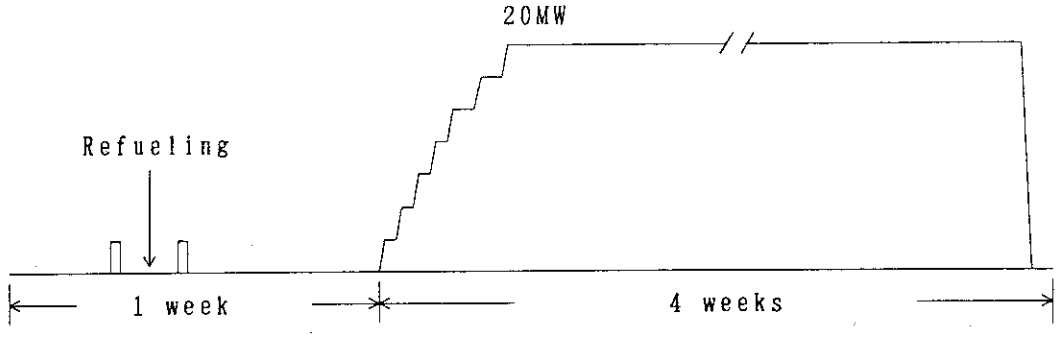

Figure 8 Operation Schedule

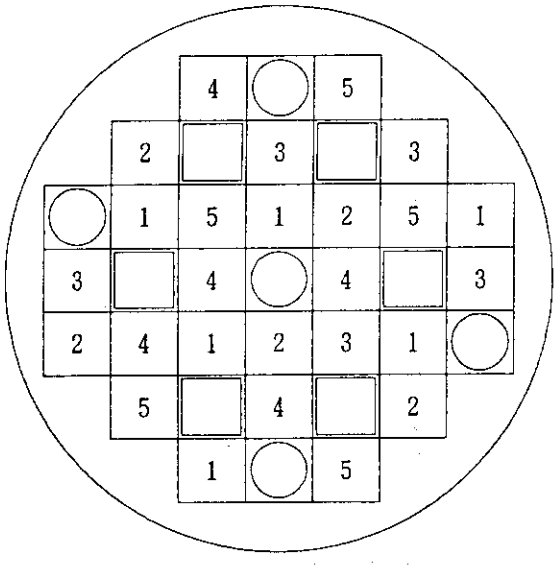

Figure 9 Core Batch

REFERENCES

[1] N.ONISI, et al.,"Reconstruction Program of Japan Research Reactor -3(JRR-3) ," Int. Syp. on the Utilization of of Multi-Purpose Research Reactors and Related Int. Co-operation, IAEA-SM-300/002(1987).

[2] H.ICHIKAWA, et al.,"Commissioning Test of Low Enriched UAlx-Al Fuel Core on Upgraded JRR-3," Int.Meeting on Reduced Enrichment for Research and Test Reactors(RERTR), ANL,1990

2. The Operational Experience of the Experimental Fast Reactor "JOYO"

T. AOYAMA, K. KINJO, N. MIZOO and F. ASAKURA

Oarai Engineering Center
Power Reactor and Nuclear Fuel Development Corporation
4002, Narita, Oarai, Ibaraki-ken, 311-13 JAPAN

ABSTRACT

The experimental fast reactor JOYO achieved initial criticality in April, 1977, as the first liquid metal fast reactor in Japan. JOYO achieved the maximum design output of 100MWt in 1983 and has been operated as a fuels and materials irradiation test facility. Recent major achievements, including decay heat removal tests of natural convection, irradiation tests with instrumented test assemblies, upgrade of fuel failure detection system and installation of fission product traps, and a power-to-melt fuel test, are described in this paper.

INTRODUCTION

JOYO is an experimental fast reactor which uses plutonium-uranium mixed oxide fuel. Preliminary design studies followed by R&D of sodium technology began in 1964 and the site construction started in January 1970. JOYO attained initial criticality in April, 1977 with a breeder core (Mark-I core). The reactor initially operated at 50MWt and then 75MWt. These Mark-I operations (50 and 75MWt) were completed at the end of 1981, with a natural convection test from 75MWt. During the Mark-I operations, the reactor experienced total 260 start-ups, conducting tests on reactor physics, reactor dynamics, power ascent and transient behaviors. The maximum pin-averaged burn-up level of the Mark-I driver fuels was 40,500MWd/t, while the design limit was 42,000MWd/t.

In 1982, the Mark-I core was converted to the Mark-II irradiation bed core for testing fuels and materials. The main core parameters and operational experience data are listed on Table 1 and Table 2. The main features of the Mark-II driver fuel were as follows ; (1) increase of Pu enrichment, (2) decrease of fuel pin diameter with increasing pin number, (3) shortening the height of the core zone and (4) replacement of the axial and radial blanket by stainless steel reflectors. The following improvements of irradiation characteristics were attained by the above modifications : (1) increased neutron flux, (2) increased power density, and (3) enlarged fast neutron zone.

The Mark-II core has been operated at 100MWt rated power. The complete operation history of JOYO is illustrated in Fig. 1. 23 rated power operation cycles at 100MWt were carried out by June 1991. The period of each duty cycle was first 45 days, and later extended to 70 days. Consequently, the maximum pin-averaged burn-up of the Mark-II driver fuel reached 71,000MWd/t, while its design limit increased to 75,000MWd/t.

Some major experiences on reactor operation and test results of fuels irradiation are described in this paper, including future modification program in order to gain higher irradiation capacity.

Table 1 Main Core Parameters of JOYO

Items \ Core(Fuel)		Mark-I		Mark-II	Mark-III
		First	Second		
Reactor Output	MWt	50	75	100	140
Primary Coolant Flow Rate	t/h	2,200	2,200	2,200	2,690
Reactor Outlet Temperature	°C	370	370	370	350
Reactor Outlet Temperature	°C	435	470	500	500
Core Stack Length	cm	60	60	55	50
Core Volume (max.)	ℓ	294	304	250	235
Linear Heat Rate (max.)	W/cm	210	320	400	444
Fuel Pin Diameter	mm	6.3	6.3	5.5	5.5
$PuO_2/(PuO_2+UO_2)$	w/o	18	18	~30	~30
^{235}U Enrichment	w/o	23	23	~12 (J1) ~18 (J2)	~12 (Inner Core) ~20 (Outer Core)
Neutron Flux (max.)	$n/cm^2 \cdot sec$	2.1×10^{15}	3.0×10^{15}	4.2×10^{15}	5.5×10^{15}
Neutron Flux (Core av.)	$n/cm^2 \cdot sec$	1.2×10^{15}	1.9×10^{15}	3.1×10^{15}	4.1×10^{15}
Max.Excess Reactivity	%Δk/k	~4.5	~4.5	~5.5	T.B.D.
Control Rod Worth	%Δk/k	Safety Rod ~5.6 Regulating Rod ~2.8	Safety Rod ~5.6 Regulating Rod ~2.8	~9	T.B.D
Max.Burn-up (pin av.)	MWd/t	25,000	42,000	75,000	90,000
Operation Cycle		45days Operation 15days Outage	45days Operation 15days Outage	70days Operation 23days Outage	T.B.D.

Table 2 JOYO Operational Experience Data (As of May, 1991)

Accumulated Reactor Operation Time	45,072 hrs
Accumulated Heat Generation	3,627,701 MW•h
Fuel Irradiation Maximum Fuel Burn-up Achieved (Driver Fuel) Number of Irradiated Fuel Subassemblies	 71,000 MWd/t (Fuel Pin Average) 412 (Including UNIS)
Number of Start-ups	441 (Including Critical Test)
Number of Annual Inspections	8

PLANT DESCRIPTION

JOYO is a sodium cooled fast reactor with two primary sodium loops, two secondary loops, and an auxiliary system. The auxiliary system consisting of primary and secondary loops is used for decay heat removal in case the main cooling systems are not available. A flow sheet of the cooling system is shown in Fig. 2.

Approximately 200 tons of sodium are used for the JOYO cooling systems. The sodium enters the core at 370°C at a flow rate of about 1100 t/h/loop, and exits the reactor vessel at 500°C in the 100MWt condition. The maximum outlet temperature of fuel subassembly is about 550°C. An intermediate heat exchanger (IHX) separates radioactive sodium in the primary system from non-radioactive sodium in the secondary system. Secondary sodium loops transport the reactor heat from the IHXs to the air-cooled dump heat exchangers (DHXs).

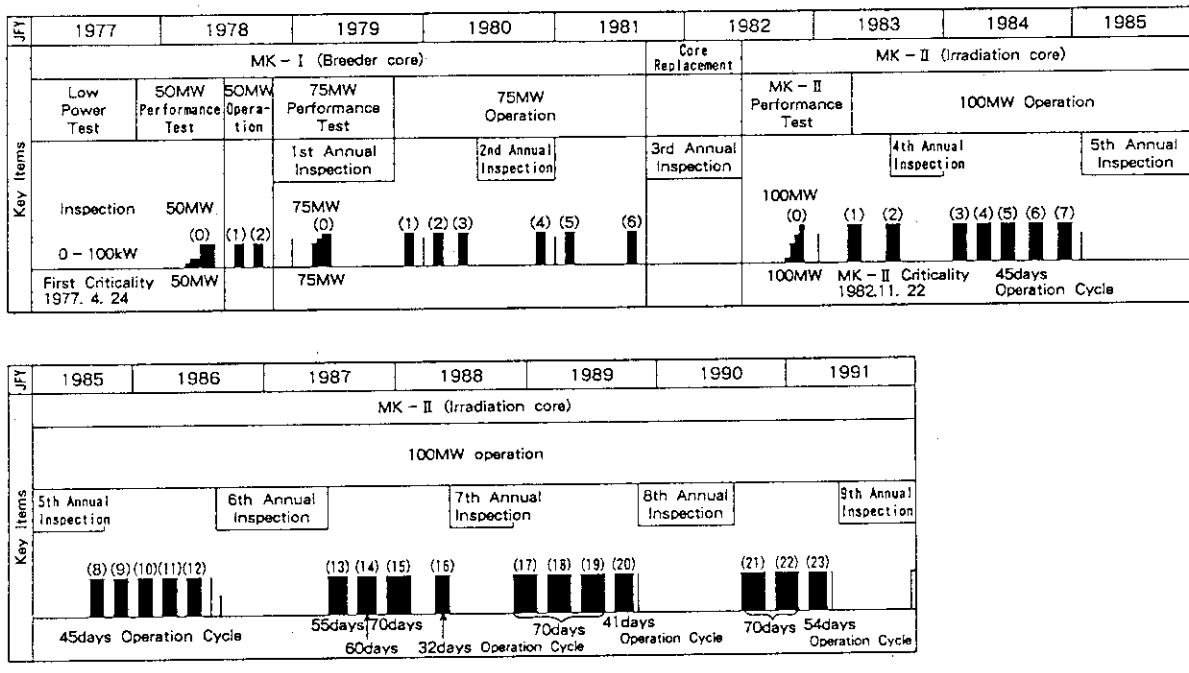

Fig. 1 Operating History of Experimental Fast Reactor JOYO

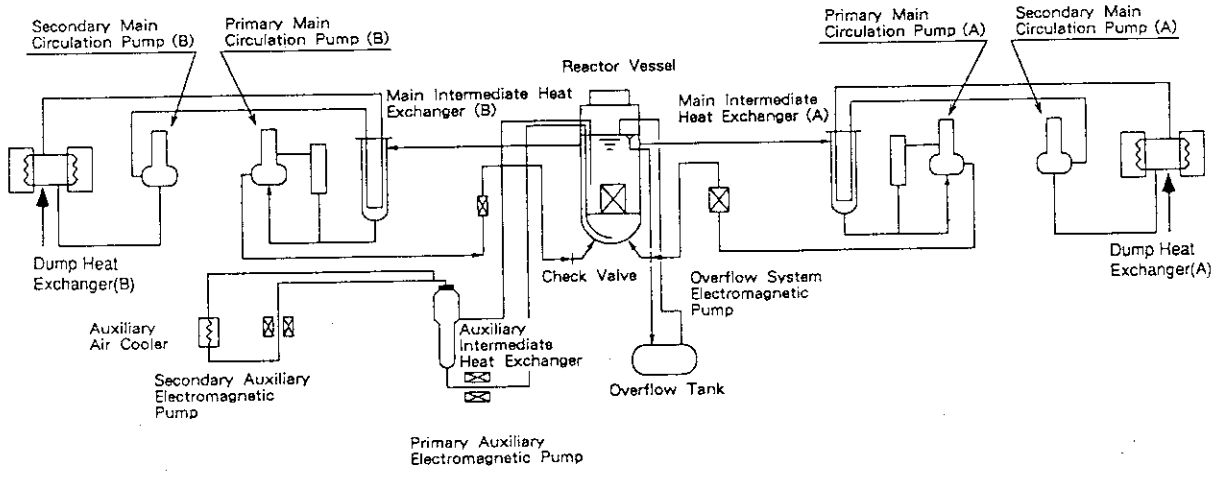

Fig. 2 Reactor Cooling System

DECAY HEAT REMOVAL TEST OF NATURAL CONVECTION

The inherent safety of fast breeder reactors (FBRs) can be demonstrated by proving the natural convection capability and through establishing analytical techniques based on experiments. A series of natural convection tests was performed from 1981 to 1986 in JOYO. A natural convection test from 100MWt, which is the most critical situation for the reactor, was carried out at the end of 12th cycle of the Mark-II core.

The test was initiated by tripping primary and secondary sodium pumps manually without pony motor operation, and the reactor was shut down simultaneously by tripping the pumps; moreover, the blowers of the DHXs were stopped immediately with the reactor scram signal.

Fig. 3 shows the outlet temperature of a central driver fuel subassembly which undergoes the severest temperature transition during the tests, together with primary coolant flow rate variations. The peak temperature reached 519°C due to coolant flow rate reductions. This peak is, however, largely below the initial temperature of 548°C. Consequently, it is shown that temperature increase will never cause any safety-related problems, such as fuel cladding failure.

The post analysis results with a plant wide dynamics code are in excellent agreement with the experimental data as shown in Fig. 3. The experimental result is also applied to the assessment of natural convection characteristics in the MONJU reactor.

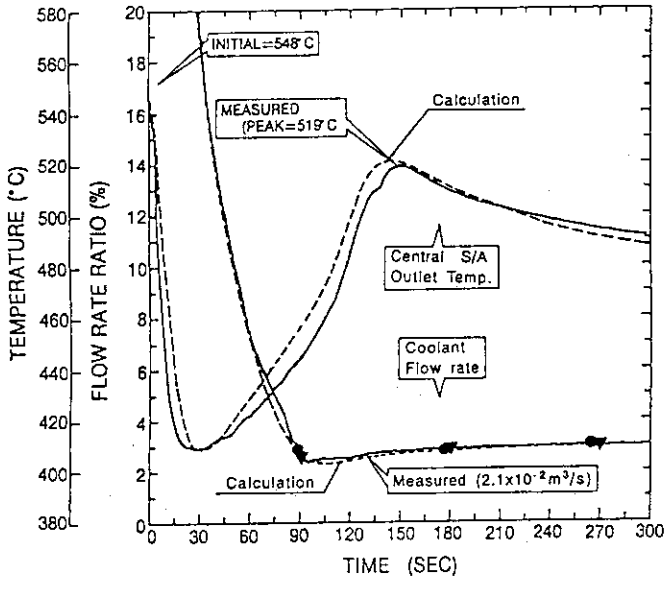

Fig. 3 Test Results and Analysis of Natural Convection Test

IRRADIATION TESTS WITH UNIS AND INTA

One of the important role of JOYO is the irradiation tests for developing fuels and materials for FBRs. Thus, JOYO provides some instrumented test assembly, as well as various uninstrumented irradiation subassemblies (UNISs).

Three types of UNIS have been used for fuels irradiations in JOYO, as shown in Fig. 4. Type A subassembly is used for irradiations in the condition of higher linear heat rate with less reactivity loss. Type B subassembly is composed of six compartments of which temperatures and sodium flow rates are controllable. The structure of type B subassembly allows easy dismantling and assembling. Type C subassembly was developed for bundle irradiation. The maximum pin-averaged burn-up of UNISs reached about 105,000 MWd/t.

Instrumented test assemblies (INTAs) have been developed to monitor the behavior of fuels and materials during irradiation. The signals from the INTA are sent to a data acquisition system through the boundary of the reactor. These are available for the post analysis code system. The first instrumented test assembly (INTA-1) was loaded into the core from 8th cycle through 12th cycle (for cumulative 225 days). The fuel center temperature was in good agreement with calculated data as shown in Fig. 5. To monitor temperatures of materials, e.g. boron carbide (B_4C) pellets, the second instrumented assembly (INTA-S) was irradiated from 13th cycle through 23rd cycle in 1991. The third instrumented assembly (INTA-2) will be irradiated during a short period for monitoring of fuel behavior at initial stage of irradiation in September, 1991.

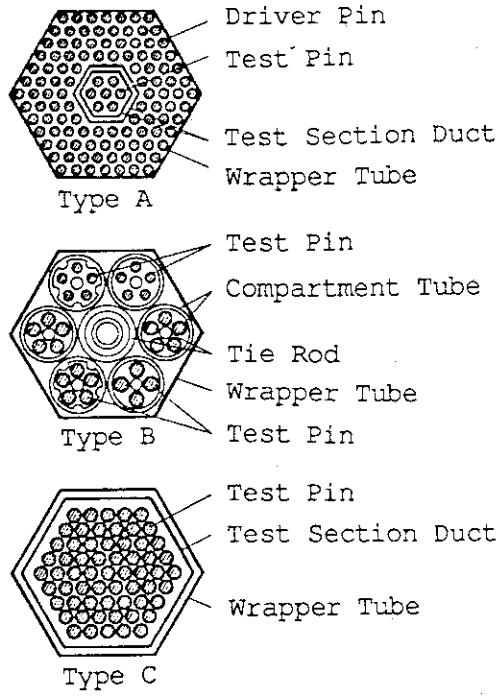

Fig. 4 Uninstrumented Irradiation Subassembly (UNIS)

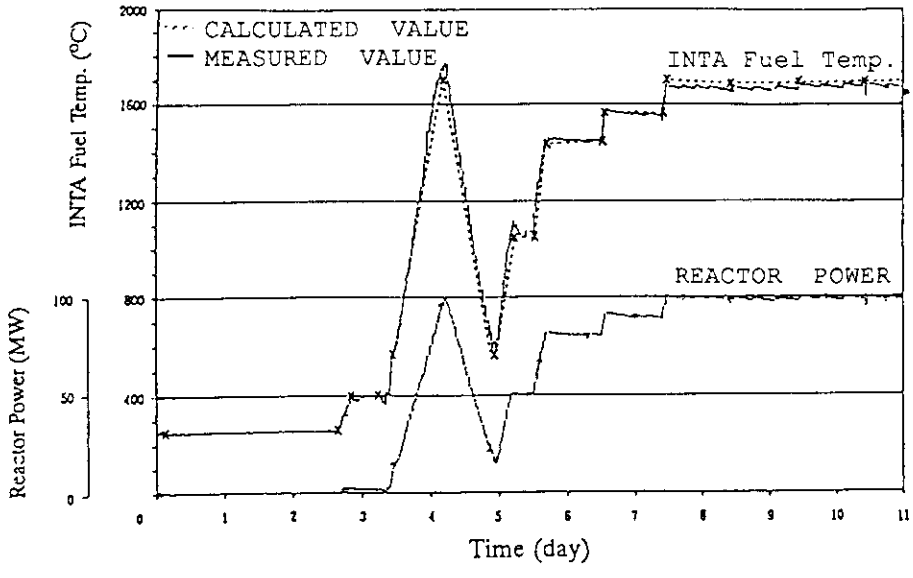

Fig. 5 Measurement of Fuel Center Temperature of INTA

UPGRADE OF FFD SYSTEM AND INSTALLATION OF FP TRAPS

The fuel failure detection (FFD) and the failed fuel detection and location (FFDL) are important for LMFBR plants to achieve a high availability and to secure the operational reliability. On the other hand, fission product (FP) traps are important for LMFBR plants on safety reasons, especially for conducting safe Run-beyond-Cladding-Breach (RBCB) tests.

FFD system of JOYO consists of both delayed neutron monitoring systems (DNMs) and a cover gas precipitating system (CG). The schematic diagram of JOYO FFD system is illustrated in Fig. 6. Two DNMs are located adjacent to each piping of primary cooling loops for detecting the delayed neutrons emitted from their precursors released into the coolant sodium. CG detects fission product of ^{88}Rb i.e., beta decay of ^{88}Kr released into the cover gas argon.

Run-to-Cladding Breach (RTCB) test is planned in JOYO. RTCB test is expected to contribute to improving the performance of FBR fuels. The results will be useful for the consideration of the increase in the fuel life. As part of the preparation work for this test, the FFD system has been upgraded, FP traps have been installed and a series of simulated fuel failure tests has been conducted.

An on-line gamma-ray monitor (OLGM) has been developed and installed in JOYO, which is shown in Fig. 6, as one of the upgrading procedures of the FFD system. OLGM is composed of charcoal bed which is made to adsorb the isotopes of krypton and xenon selectively, and a Ge(Li) detector. The special feature of this system is to be able to identify the amounts of the isotopes contained in the cover gas by gamma-ray spectrum analysis.

On the other hand, two types of FP traps have been installed in JOYO. One is a cesium trap which is installed in primary coolant purification system to trap cesium released from failed fuels during the RBCB test of the reactor. An open-pore, foam-like glassy carbon which is consisted of thin struts (Reticulated Vitreous Carbon) is used as a material for collecting cesium, and the capacity of this trap is designed to be 7.4×10^{12}Bq. The other is a cover gas clean-up system (CGCS) to trap and store the noble fission gas released from failed fuels at RTCB test or during the RBCB test. Although it is intended that only one failed fuel pin will be in the core at any time during RTCB and, possibly, RBCB tests, CGCS is designed to handle the activity released from up to twelve failed fuel test pins.

An in-pile simulation test was carried out at the end of 7th cycle using two identically slit fuel pins in order to verify the performance of the FFDL system with sodium sipping method. The slit is 1.0mm in length and 0.1mm in width, and perforated on the fuel cladding at gas plenum position.

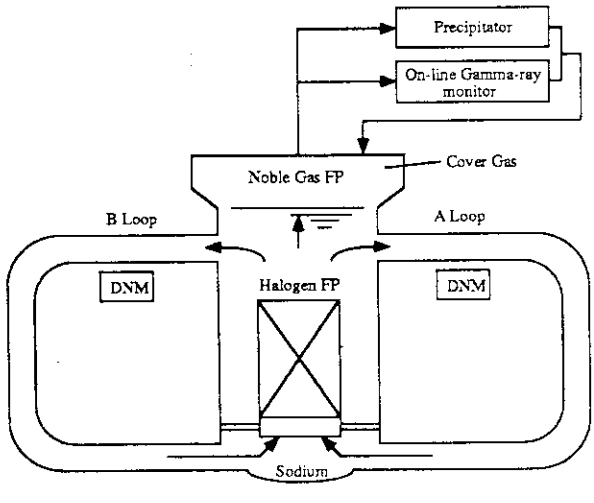

Fig. 6 Schematic Diagram of FFD

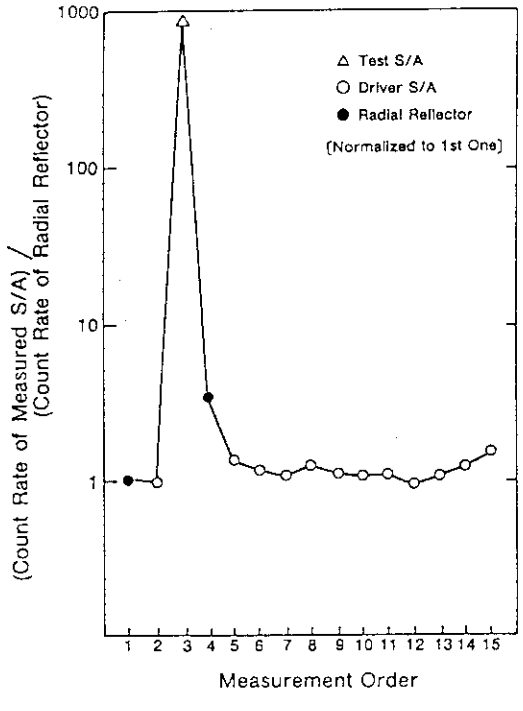

Fig. 7 Count Rate Ratio of ^{133}Xe γ-ray

In the FFDL operation, a signal level of the test subassembly was several hundreds times of the background which was measured for other core subassemblies (see Fig. 7). Thus, FFDL system was confirmed to have capability to identify the failed fuel with defect at gas plenum position. Further tests of FFDL system for pins with slit at fuel column position are planned.

A fission-product source was irradiated at the end of 15th cycle. The test results show that : (1) both of CG and DNMs were successfully calibrated, (2) major constants for the cover gas and the delayed neutron activity models were determined to confirm validity of computer codes, and (3) availability of failed fuel location by the flux tilting and the triangulation methods were demonstrated to optimize the FFDL system for demonstration plants, particularly the flux tilting method using OLGM was found out to be very useful.

POWER TO MELT TEST

A power-to-Melt (PTM) test was conducted at the end of 23rd cycle. The purpose of this test was to evaluate the effects of fuel-cladding gap size, fuel pellet density and O/M on the thermal performance of a fuel pin and on the linear heat rate required to cause incipient melting in unirradiated fuel.

The specification of the first test fuel pins is described in Table 3. Test fuel pins were loaded in the center channel of the core using special subassembly of which structure is similar to type B of UNIS.

The power history of the test is shown in Fig. 8. Reactor power was held about one hour at 60MW, then ramped up at 0.4MW/min to a level of 95MW, of which rate is higher than that of normal start-up, so as not to produce fuel structural change due to irradiation. After ten minutes at 95MW, the reactor power was decreased.

The test subassembly was then transferred from the core and disassembled for examination at fuel monitoring facility (FMF) which is located adjacent to JOYO. Examination of the ceramographic sections in the as-polished condition was completed in August, 1991, which indicated the amount of fuel melting at the axial positions of peak power. Post irradiation examination results will be used to verify the fuel pin performance analysis code. The second test is scheduled to be conducted in June 1992. Results of PTM tests are expected to contribute to the consideration of the increase in the fuel power density.

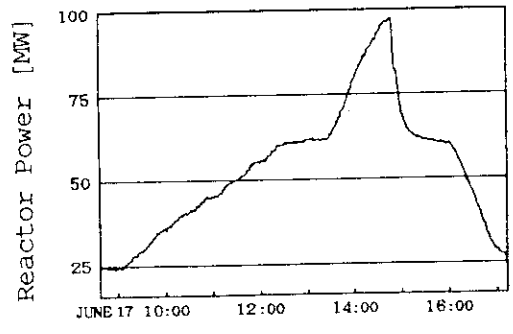

Fig. 8 Reactor Power History in Power-to-Melt Test

Table 3 Specification of Power-to-Melt Test Fuel Pins

Pin No.	Pellet Diameter (mm)	Pellet Density (% T. D.)	O/M	Maximun Linear Heat Rate (W/cm)
1	6.50	90.7	1.96	~600
2	6.45	90.7	1.96	~590
3	6.45	90.9	1.96	~590
4	6.46	94.3	1.96	~610

FUTURE PROGRAM

For the commercialization of FBRs, the development of high performance fuels and materials are required. From this point of view, the JOYO modification program (Mark-III program) is planned to provide greater irradiation capability. The main core parameters of the Mark-III are shown in Table 1.

Modification on reactor core, such as number of fuel subassemblies, and re-evaluation of maximum allowable linear heat rate improves the fast neutron flux by about 30%. In addition, expansion of the core and shift of two control rods from 3rd row to 5th row of the core increases the capacity of irradiation rigs or test fuel subassemblies. As the result of the core modification, JOYO is expected to increase its thermal rating from 100MWt to 140MWt. For the increase of thermal rating, it is required to exchange the IHXs and the DHXs.

The improvement of plant availability can be achieved by reduction of refueling time, annual inspection period, and by development of handy irradiation equipment. As the result, the average plant availability factor of the Mark-III is expected to improve from 40% to 60%.

To increase the flexibility of irradiation tests performed in JOYO, advanced irradiation equipments (material testing rig with temperature control, in-sodium connector, etc.) are under development.

CONCLUDING REMARKS

(1) Through a series of natural convection tests performed in JOYO and their analysis, it was proved that decay heat could be safely removed by natural convection and an analysis technique was established for evaluating such behavior.
(2) Instrumented test assemblies have been developed to monitor behavior of fuels and materials during irradiation. The fuel center temperatures were in good agreement with calculated values.
(3) As part of the preparation work for the Run-to-Cladding-Breach test, the FFD system has been upgraded, FP traps have been installed and a series of simulated fuel failure tests has been conducted.
(4) A power-to-melt test using fresh fuel has been conducted to verify the fuel pin performance analysis code. An analysis result will be expected to reduce the design margin in the thermal calculation.

REFERENCES

(1) N. MIZOO, "Operational Experience of Experimental Fast Reactor JOYO", Second Asian Seminar on Research Reactors, Jakarta, Indonesia, May 1989.
(2) T. AOYAMA, Y. ARII, Y. YAMASHITA, T. IKEGAMI and N. MIZOO, "Core Management Experience of the Experimental Fast Reactor JOYO", BNES International Conference on Fast Reactor Core and Fuel Structural Behavior, P.299, Inverness, U. K. , June 1990.
(3) M. SAWADA, H. ARIKAWA and N. MIZOO, "Experiment and Analysis on Natural Convection Characteristics in the Experimental Fast Reactor JOYO", Nuclear Engineering and Design, Vol.120, P.341 (1990)
(4) S. NOMOTO, et al., "Operational Experience from the "JOYO" Fast Breeder Reactor", Trans. Am. Nucl. Soc., Vol.38, P.608 (1981)

3. A Dedicated Program for the Extended Longevity of Research and Training Reactors

GARY W. CARRIVEAU

General Atomics
P O Box 85608
San Diego, California 92186
USA

ABSTRACT

In the past 49 years, over 555 research and training reactors have been in operation, with approximately 325 currently in service. The age distribution of operating research reactors shows that the average age is about 24 years; about 74% are 20 years old or older and about 33% are 30 years old or older. This group of reactors represents a very large investment in capital expense with replacement costs in 1990's prices much higher than when they were originally constructed. Furthermore, decommissioning costs may be much greater than the original investments. General Atomics has been directly involved for the better part of the nearly fifty year history of research and training reactors. This paper will describe a General Atomics program illustrating a dedicated commitment to the full service support of extended and improved use for all types of research and training reactors.

"The ultimate use of technology is to take what you have and make something more, rather than invent a new piece of equipment"

Anon.

Since December 1942, over 555 research and training reactors have been in operation. According to statistics compiled by the International Atomic Energy Agency, there are approximately 325 research and training reactors currently in service. In the past 20 years, over 180 reactors have been shutdown compared to 130 that have been commissioned. Recent data show that there are 9 reactors currently under construction and 14 in the planning stage.

This total of currently operating reactors includes a wide variety of designs, covering a range of power and research capabilities, located virtually around the world. Although there are some high geographical concentrations of research facilities, no continent is without a training and research reactor of some type.

The uses of these reactors have evolved over the years. Primary uses now include (but are not restricted to):

1. Fundamental research in nuclear and reactor physics

2. Studies of the physical properties of materials

3. Training of nuclear engineers, reactor operators, and reactor operations personnel

4. Production of radio-isotopes for a variety of uses including nuclear medicine

5. Analytical techniques such as instrumental neutron activation analysis

6. Non-destructive evaluation and testing

7. Modification of materials

The age distribution of the research and training reactors in operation shows that the average is about 24 years. Figure 1 illustrates this distribution; note that it is skewed, with about 74% being 20 years or older and about 33% being 30 years or older.

This group of reactors represents a very large investment in capital expense. Of course, replacement costs today would be much higher than when the facilities were originally constructed. Furthermore, the costs of decommissioning may be much larger than the original investment. For example, the cost of a typical new 500 kW TRIGA Mark I reactor (excluding the building) would be approximately $3 million. Compare this with the estimated costs of decommissioning and removal of the same type of reactor at between $6 million and $10 million.

These financial observations alone should lead one to ensure that these versatile and important facilities are kept up to date and fully operational for as long as possible. Although the original engineering may not have specifically considered research and training reactor life times of greater than 30 years, current technology can provide for this and even longer active service life.

General Atomics has been directly involved with research and training reactors for the better part of the nearly 50 year history. The original TRIGA Mark I reactor is now over 32 years old and remains in daily operation, still using much of its original fuel. It has been designated as a Nuclear Historical Site by the American Nuclear Society. The TRIGA reactor was General Atomics first commercial product and examples from the TRIGA family of reactors are found world-wide.

General Atomics continues to supply the TRIGA family of reactors, being the only remaining United States supplier of research and training reactors, and one of only a few suppliers remaining world-wide. Based upon this long standing interest, General Atomics has established a program dedicated to the support of extended longevity of training and research reactors. There have been a great number of training and research reactor manufacturers over the years. Many of these have ceased to remain in the reactor business. Many others have dropped out of the research and training reactor field to concentrate on commercial power reactors. This has left many reactor operators without support from their original supplier. Because of this, the General Atomics Longevity Extension Program support is extended to all types of research, training, and testing reactors located around the world.

The Longevity Extension Program includes the following areas of attention:

(a) New digital and analog instrumentation and control systems.

(b) Improved and upgraded nuclear monitoring and control channels, including both analog and digital instruments.

(c) Reactor facility testing, repair, and upgrade services including:
pool or tank integrity
cooling systems
water purification systems.

(d) Fuel element testing and replacement and core replacement and conversions.

(e) Control rod drive testing, rebuilding, and replacement.

(f) Control and monitoring system evaluation, calibration, and repair service.

(g) Training services, including reactor operations, maintenance, instrumentation calibration and repair.

(h) Development and training in expanded or new reactor uses such as neutron radiography and autoradiography, radioisotope production, nuclear medicine including boron neutron capture therapy, instrumental neutron activation analysis, and the modification of material properties.

Space in this paper does not allow a detailed description of each area of interest, however, it is felt that one specific area bears special interest. This is the research and training reactor tank and pool integrity testing effort, an integral part of the General Atomics Longevity Extension Program.

Based on many years of experience, General Atomics can provide critical information about the state of health of the reactor tank or pool and how to avoid leak related problems. Furthermore, valuable information can be provided to assist in the repair of leaking tanks and pools. This dedicated service includes both a full testing capability **and** remediation assistance for **all** research and training reactors.

A survey of research and training reactor facilities has shown that at least ten facilities have reported pool or tank leaks in the past few years. In some instances, the leaks resulted only in an untimely interruption of services; in other cases, the problems resulted in a complete shutdown. Sometimes small leaks have been allowed to continue without successful or even attempted repair and have become more severe with time.

Using modern ultrasonic techniques, General Atomics originally developed the testing methods to thoroughly investigate tanks where leaks had already occurred as an aid in developing repair procedures. As an extension of this valuable service, the program further evolved so that the tests could be used to assess the integrity or state of health of a non-leaking tank. These results could then be used to determine if remedial actions should be required before leaks occurred, mitigating problems associated with costly damage, clean up, or shut-down.

Based on recent state-of-the-art inspection techniques, unseen potential problems brought about by dangerous thinning or cracking of tank material have been shown to exist. This valuable information is now available to the reactor operator even though actual leaks are not

visually apparent. State-of-the-art ultrasonic techniques were specifically chosen to measure the integrity of the tank liner. In the past, it had been fairly common to inspect the tank liner visually, using binoculars or other optical devices, in an attempt to detect faults through observable cracks, corrosion, or discoloration. This method is still sometimes employed with results critically limited because most potential leaks cannot be visually observed. Using optical methods, problems were normally identified only after the tank integrity had been compromised and a failure and leak ensued.

Integrity inspection can be accomplished without making significant physical changes to the reactor. For example, water does not have to be removed from the reactor tank. In fact, the water is used as an ultrasonic couplant during the tests. The reactor must be shutdown, however, so that the radiation field does not unnecessarily damage the ultrasonic transducers.

In a typical inspection, nearly all of the tank area is inspected. There may be some difficulty introduced by core locations, beam tubes, or other tank penetrations, or by obstacles such as fuel storage racks placed along the tank wall or bottom. By moving obstacles out the way and through the use of special transducer manipulators, nearly 100% of the tank area can be tested. Through the use of a variety of different ultrasonic transducers, special areas indicating potential faults or features can be critically mapped in greater detail.

The time required for physical tests at the reactor site is quite dependant on the size, shape and configuration of the reactor tank or pool. For purposes of estimating, a typical TRIGA Mark I tank (nominally 2-meters in diameter and 7-meters deep) would require approximately three days for inspection and data taking, following one day for pre-inspection, set-up and planning. Additional time would be required to write a report certifying the state of health of the tank.

General Atomics has performed a number of inspections, both on TRIGA and non-TRIGA tanks and would be most happy to provide details upon request.

The author wishes to acknowledge and thank Mr. R. G. Muranaka for providing statistical information on research and training reactors.

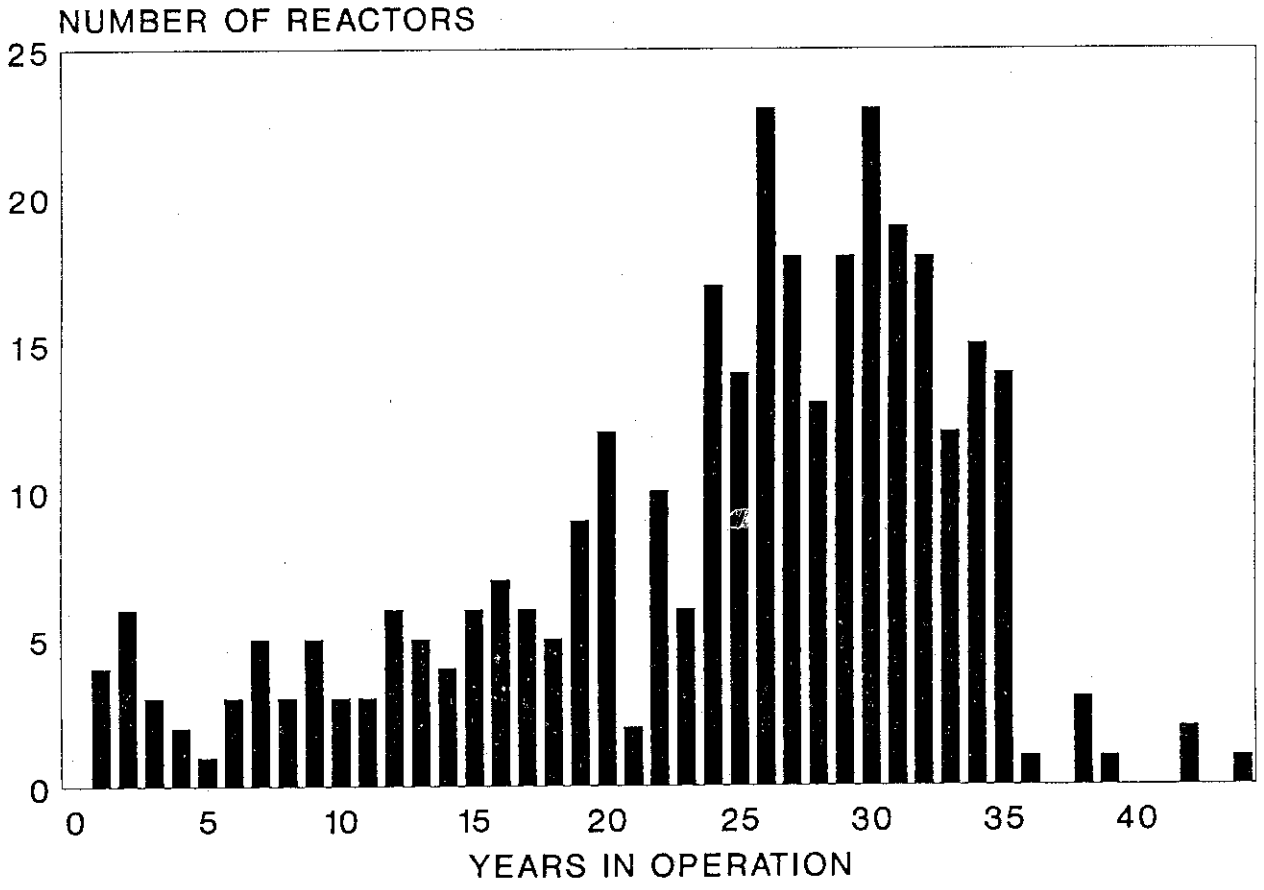

Figure 1 Age distribution of operating research and training reactors.

4. Current Status of HTTR Project at JAERI

SHINZO SAITO, YUKIO SUDO, TOSHIYUKI TANAKA, OSAMU BABA

Department of HTTR Project
Oarai Research Establishment, JAERI
Oarai-machi, Higashi-ibaraki-gun, Ibaraki-ken, 311-13, Japan

ABSTRACT

The HTTR is a high temperature gas cooled test reactor with thermal output of 30 MW, outlet coolant temperatures of 850°C at rated operation and 950°C at high temperature test operation and primary coolant pressure of 4 MPa. The HTTR consists of a reactor pressure vessel with a prismatic core in it, a primary cooling loop with an intermediate helium-helium heat exchanger and a pressurized water cooler in parallel, an auxiliary cooling system, a reactor vessel cooling system and related components. The HTTR is utilized for establishing and upgrading the technology bases for advanced HTGRs including irradiation tests for fuels and materials, safety demonstration tests for HTGRs and nuclear heat application and for carrying out various kinds of innovative basic researches on high temperature technologies.

Since 1969, the JAERI has carried out research and development works on block type fuel, high temperature materials, high temperature in-core instrumentations, high temperature components, reactor physics, heat transfer and fluid dynamics, plate-out of fission products etc., in order to construct the HTTR which can supply high temperature coolant of 950°C to the outside of the pressure vessel for the nuclear heat application, for the first time in the world. In November 1990, the installation permit was issued by the Government through about 20 month safety review by the Science and Technology Agency and Nuclear Safety Commission. The construction of the HTTR facility was initiated on the site in the Oarai Research Establishment, JAERI in March 1991. The excavation of ground is now finished at the HTTR site.

It will take about six years for the completion of the HTTR facility and the first criticality will be attained in 1996.

INTRODUCTION

The high temperature gas cooled reactor (HTGR) is one of the most promising reactors with high thermal efficiency and inherent safety and the Japan Atomic Energy Research Institute (JAERI) has carried out the research and development on HTGRs for more than 20 years. In June 1987, the Japan Atomic Energy Commission issued the revision of the Long-Term Program for Development and Utilization of Nuclear Energy, recommending that Japan should proceed with the development of more advanced new technologies for the future, in parallel with the existing nuclear systems. It also emphasized that HTGR is one of the most promising reactors with high efficiency and inherent safety, therefore it should be explored for the broad use of nuclear energy, not only for power

generation. Then, the construction of the High Temperature Engineering Test Reactor (HTTR) was decided instead of an experimental HTGR. The HTTR aims at establishing and upgrading the technology basis necessary for an HTGR, serving at the same time as a potential tool for new and innovative basic researches and demonstrating nuclear heat utilization of HTGR.

The JAERI submitted the safety analysis report of the HTTR to the Science and Technology Agency (STA) for the safety review by the Government in February 1989. After about two years' safety review, the JAERI obtained the installation permit in November 1990. The construction of the HTTR was officially initiated in March 1991.

This paper presents the major features of HTTR design and current status of the HTTR construction as well as the operation and test plans scheduled in the HTTR.

MAJOR FEATURES OF HTTR DESIGN

Major objectives of the HTTR are to establish basic technologies for advanced HTGRs in future, to utilize the HTTR for conducting researches in innovative high-temperature technologies and to demonstrate direct nuclear heat utilization of HTGR, by achieving the coolant temperature as high as 950°C at the outlet of reactor vessel for the first time in the world.

The facility arrangement of the HTTR is shown in Fig. 1 and a cutaway view of the HTTR reactor building is illustrated in Fig. 2.

The HTTR consists of a core of 30 MWt, a main cooling circuit, an auxiliary cooling circuit and related systems. The reactor pressure vessel is 13.2m high and 5.5m in diameter and contains the core, graphite reflectors, core support structure and radial restraining devices. Major specification of the HTTR is shown in Table 1 and a cutaway view of reactor vessel is shown in Fig 3.

Core : The reactor core is graphite-moderated, helium gas-cooled and hexagonal fuel elements are used. The active core consists of 30 fuel columns and 7 control rod columns, each column of 5 blocks (2.9 m high). Reactivity is controlled by control rods, which are individually supported by the mechanisms located in stand-pipes connected to the hemispherical top head of the reactor vessel and are inserted into the channels in the active core and replaceable reflector regions. The reactor core is cooled by helium gas of 395°C at the reactor inlet, which flows downward through the core. The maximum fuel temperature is approximately 1500°C under the high temperature test operation condition with the reactor outlet coolant temperature of 950°C. Figure 4 shows the horizontal cross-section of the core with the irradiation regions for fuels and materials. Table 2 shows major characteristics of core neutronics and thermohydraulics.

Fuel elements : A fuel element assembly with 36 cm wide across the flats and 58cm in length is made up of fuel rods and a hexagonal graphite block as illustrated in Fig. 5. The fuel consists of TRISO coated particles of low enriched uranium oxide whose average enrichment is about 6% and the kernel diameter is 0.6 mm. The particles are dispersed in the graphite matrix and sintered to form a fuel compact. These compacts are contained in a sleeve to form a fuel rod. The fuel rods of 3.4cm in diameter are contained within vertical holes of a graphite block. Helium gas flows through a gap between a vertical hole and a fuel rod to remove heat generated in the core. Graphite material used for fuel rod sleeves and fuel blocks is IG-110, which has characteristics superior to the previous graphite materials.

Cooling systems : The reactor cooling systems are composed of a main cooling system (MCS), an auxiliary cooling system (ACS) and two reactor vessel cooling systems (VCSs). The reactor cooling system is schematically shown in Fig. 6. The MCS is separated into two lines outside the reactor vessel. The heated helium gas is cooled in a He/He intermediate heat exchanger (IHX) in one line and in a pressurized water cooler (PWC) in the other line. The heat is finally removed by an air cooler, while another PWC provided after the IHX in the first line. When the first line with heat transfer capacity of 10 MW is operated, the second line, which has heat transfer capacity of 30MW, is operated at 20MW. Co-axial double wall pipings, which separate a pressure-resistant function from the heat-resistant function, are used in the MCS and the ACS for transferring helium gas, adopting Hastelloy XR as the material of the liner of the inner piping which directly contact with the coolant as high as 950°C. A schematic of co-axial double wall piping is illustrated in Fig. 7.

The IHX is utilized to connect the heat utilization system to the HTTR to demonstrate its availability in near future. A cutaway view of IHX is shown in Fig. 8. Hastelloy XR is used for the material of heat transfer tubes which contact with the helium of 950°C. The ACS consists of an auxiliary heat exchanger, auxiliary gas circulators and an air cooler. The heat transfer capacity of the ACS is about 3.5 MW and the components are similar to those of the MCS. The VCSs are so designed as to cool by radiation the reactor vessel including the core in such accidental conditions as the loss of forced core cooling. Each VCS has heat removal capacity of 100% to cool the reactor vessel and the core in emergency.

Core neutronics and thermohydraulics : In order to achieve high reactor outlet coolant temperature with assuring fuel intactness, it is important to keep the maximum fuel temperature as low as possible. To minimize the maximum fuel temperature, the fuel and burnable poison zonings were determined. A pattern selected for fuel zoning of enrichment is shown in Fig. 9. Preferable fuel temperature distributions have been obtained as shown also in Fig. 9.

Reducing the core pressure drop is effective to reduce the core bypass flow and it has been achieved by increasing the total number of coolant channels in a fuel block. The dimensions of the fuel channel have been determined by optimizing the heat transfer characteristics and the core pressure drop to obtain the maximum fuel temperatures as low as possible through burnup. As a result of these optimizations in the fields of thermohydraulics, a directly effective core flow rate as high as 88% of total flow has been achieved.

As the results of above-described design considerations, the maximum fuel temperatures evaluated with consideration of various uncertainty factors are limited below about 1500°C under the 950°C operation condition. The engineering uncertainties considered are systematic uncertainties for total power, power distribution, total flow rate, flow distribution and core inlet temperature. Random uncertainties are also considered for manufacturing tolerances, material properties of graphite and so on.

PRESENT STATUS OF HTTR CONSTRUCTION

Table 3 illustrates the overall schedule of HTTR construction. In February 1989 the JAERI submitted the safety analysis report of the HTTR to the Government immediately after the budgetary approval by the Government. The safety review was performed by the STA at the first step, hearing the opinions of the Technical Advisory Committee on Reactor Safety. In December 1989, the STA concluded that the safety design was satisfactory in the draft report on

its safety examination of the HTTR design and consequently, the STA inquired the opinions of the Nuclear Safety Commission (NSC). The Committee on Examination of Nuclear Reactor Safety under the NSC actually reviewed the safety of the HTTR as the second step of the safety review. The installation permit was issued in November 1990 by the Government. The JAERI, then, submitted the construction plan of the HTTR to the STA, which was the first part of five in total into which the whole reactor facility was divided, covering the reactor building and containment vessel which are the first to be built. The approval was issued in January 1991.

The excavation of ground was officially started in March 1991 to be completed in the end of July 1991 and the examination of supporting foundation was performed by the STA in the middle of August, 1991. Photo 1 shows the view of the excavated area of reactor building at the HTTR site as of June 1991. The construction of concrete base-matt will be initiated in the late fall of this year. The manufacturing of containment vessel is being proceeded in the factories, and it will be transported to the Oarai site, JAERI in the middle of 1992.

The construction plan of the second part of the HTTR facility, which covers reactor core, core support structures and some components of reactor cooling system, was submitted to the STA in June 1991 and the approval to the construction was issued in September 1991. Other reactor equipments are being designed for fabrication on the industrial side.

It will take about six years for the completion of the HTTR facility. The first criticality will be attained in FY 1996. Full power operation will be achieved in 1997 through one year for performance and power up tests.

OPERATION AND TEST PLANS OF HTTR

The aims of the HTTR are, as already described, to utilize it for establishing and upgrading the technology bases necessary for advanced HTGRs including the nuclear heat application and to provide it at the same time as a potential tool for new and innovative high temperature basic researches. To meet these objectives, the program of operations and tests after the achievement of the first criticality is planned as shown in Table 4.

(1) Establishment of technology basis on HTGRs

Following R&D items will be performed through the operation of the HTTR.

a)Confirmation of the nuclear and thermal-hydraulic characteristics through the criticality test, start-up test and normal operation.

b)Confirmation of the plant dynamics and plant control characteristics of parallel loading system of the IHX and the PWC.

c)Confirmation of the overall performances of the high temperature material and high temperature components such as gas circulators, valves, pipings, etc.

d)Evaluation of the FP release behavior such as FP release from fuel, FP plate out, shielding performance, etc.

e)Accomplishment of the long-term continuous operation and accumulation of experience of the plant operation and maintenance through the operation, maintenance and repair.

(2) Upgrading present HTGR technologies

a)Advanced fuels: As for coated particle fuel, it is important to improve FP retaining capability of fuel with high power density and high burn up under long term high temperature operation. By the irradiation experiments strength and chemical stability are to be clarified and demonstrated.

b)Advanced materials: As for graphite materials and graphite/carbon composites used for fuel elements and reflectors, their higher strength and dimensional stability at high temperature and under high fluence are of importance. Irradiation experiments on several types of graphite materials using the HTTR are to be conducted to obtain chemical and physical properties, strength, corrosion properties, etc. As for heat resistant materials, material and structural tests are to be conducted in the HTTR. Irradiation test regions for fuel, material and so on in the HTTR core are shown in Fig. 4.

c)Nuclear process heat application: It is important and necessary to establish high temperature nuclear heat process application technology through the R&D. Recently, the greenhouse effect and climate change on the earth has become real concerns internationally. Since the contribution of fossil fuels and felling of wood are the major source of CO_2, the utilization of nuclear heat should help to solve the problems as an potential alternative of energy source. As for hydrogen production, steam reforming of methane, high temperature electrolysis of steam and the thermo-chemical Iodine-Sulfur(IS) process have been studied as the candidates of nuclear heat application system for the HTTR in the JAERI. Pilot plant tests of heat utilization system is, first, to be conducted and then, the verification test by supplying high temperature heat of about 900°C is to be performance by connecting the system to the HTTR through the IHX in future.

d)Safety demonstration tests: In order to confirm the unique and inherent safety of the HTGRs, two kinds of safety demonstration tests are planned in the HTTR. One is a test in which a pair of control rods are withdrawn continuously at a constant low speed during a test and the other is a test in which partial loss of forced coolant flow occurs during a test.

(3) Innovative basic researches on high temperature technologies

a) Tests on continuous recovery of released tritium for fusion reactor are to be conducted by irradiating tritium breeding targets, Li_2O, $LiAlO_2$ and etc., at high temperature.

b) Basic researches on thermal decomposition of plastics, pitch tar, etc. under irradiation are to be carried out.

c) Various basic researches on high temperature technologies such as high temperature irradiation tests of large sized specimens with installed instruments, are to be carried out, using the HTTR, which has irradiation regions of 10 to 30 cm in diameter, at temperature from 400 to 1100°C.

CONCLUDING REMARKS

The HTTR is a first HTGR in Japan, which has various aims and operational modes, while at the same time it can provide coolant with very high temperature up to 950°C at the outlet of the reactor vessel and it can be utilized to the nuclear process heat application at the outside of reactor vessel for the first time in the world. The JAERI has carefully established the design concept and safety design principles of the HTTR, reflecting the results of R&D works on HTGR technology and experiences of LWR designing and operation. The JAERI will endeavor than ever to promote the HTTR project and operate the HTTR with various kinds of tests, for establishing and upgrading the HTGR technology bases and conducting the innovative basic researches on high temperature technologies under broad international cooperation.

Table 1 Major Specification of HTTR

Thermal power	30 MW
Core diameter	2.3 m
Core height	2.9 m
Average power density	2.5 W/cm^3
Fuel loading	off-load, 1 batch
Outlet coolant temp.	850°C (rated operation) 950°C (high temp. operation)
Inlet coolant temp.	395°C
Fuel	Low enriched UO_2
Fuel element type	Pin-in-block
Direction of coolant flow	Downward flow
Number of fuel block	30 column x 5 layers = 150
Number of main cooling system	1
Heat removal	IHX and PWC (parallel loaded)
Primary coolant press.	4 MPa
Containment type	Steel containment

Table 2 Major Features of Nucleonics and Thermal-hydraulics

Nuclear		
Excess reactivity	15 %Δk	
Uranium enrichment	3 - 10 wt%	
Average	6 wt%	
Fuel burn-up (average)	22 GWd/t	
Reactivity coefficients		
Fuel temperature coefficient	$-(1.5 \text{ to } 4.6)\times10^{-5}$Δk/k/°C	
Moderator temperature coefficient	$(-17.1 \text{ to } 0.99)\times10^{-5}$Δk/k/°C	
Power coefficient	$-(2.4 \text{ to } 4.0)\times10^{-5}$Δk/k/MW	
Power peaking factor		
Radial	1.1	
Axial	1.7	
Prompt neutron lifetime	0.67 - 0.70ms	
Effective delayed neutron fraction	0.0047 - 0.0065	
Thermal-hydraulic data	850°C operation	950°C operation
Total coolant flow rate	12.4kg/s	10.2kg/s
Effective core coolant flow rate	88%	88%
Maximum fuel temperature	1420°C	1492°C
Core pressure drop	8.8kPa	6.5kPa

Table 3 Construction Schedule of HTTR

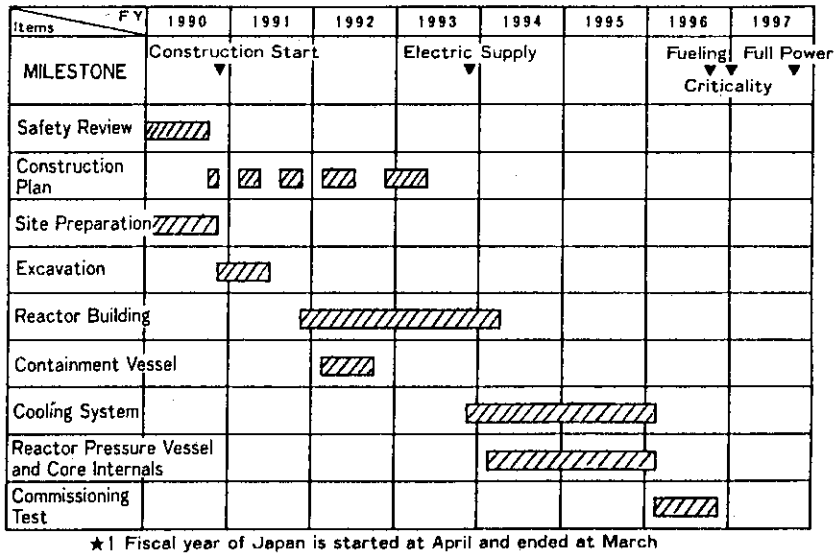

★1 Fiscal year of Japan is started at April and ended at March

Table 4 Operation and Test Plan in HTTR

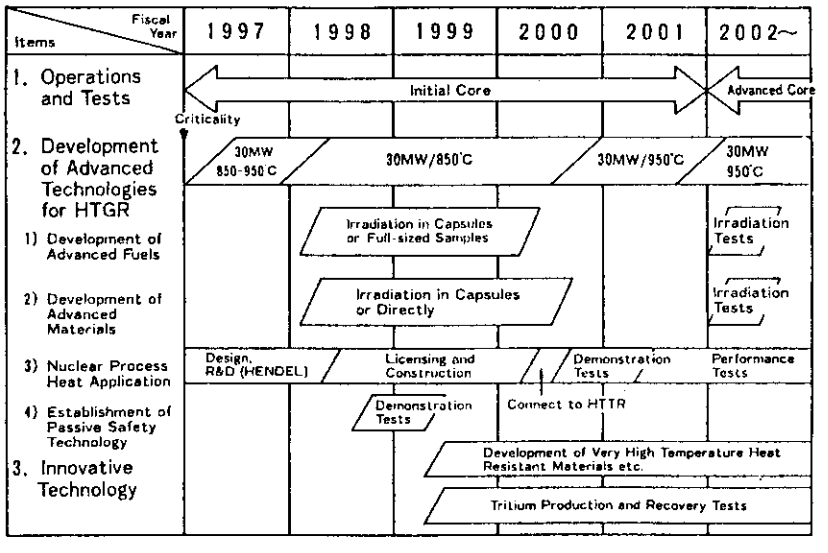

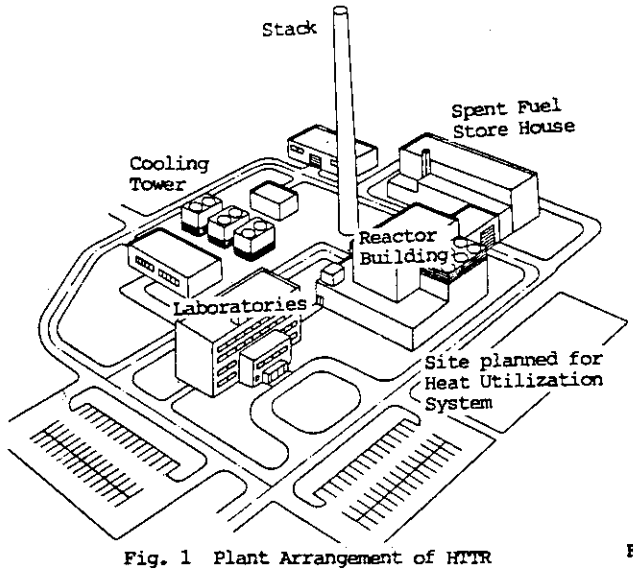

Fig. 1 Plant Arrangement of HTTR

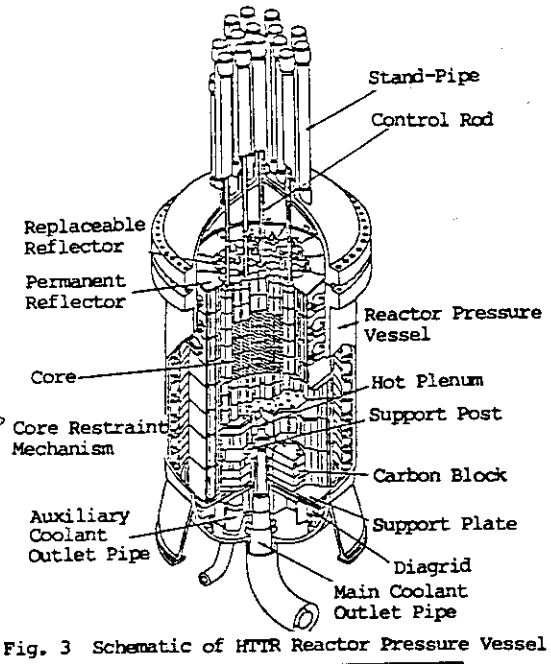

Fig. 3 Schematic of HTTR Reactor Pressure Vessel

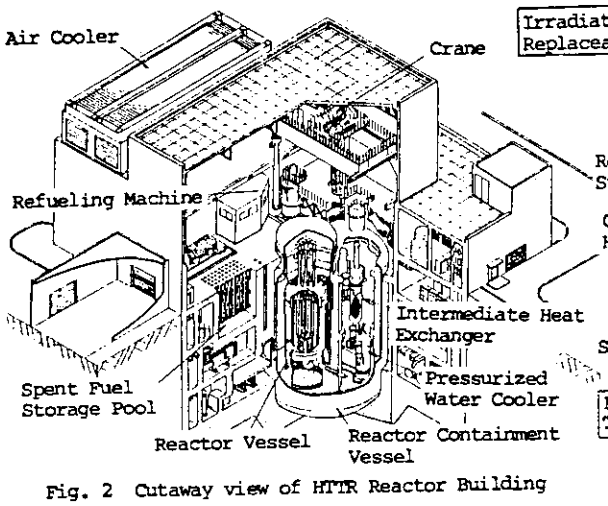

Fig. 2 Cutaway view of HTTR Reactor Building

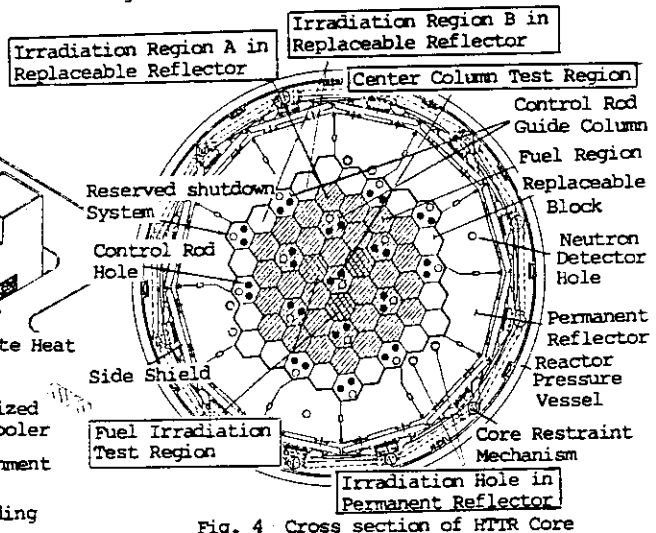

Fig. 4 Cross section of HTTR Core and Irradiation Regions

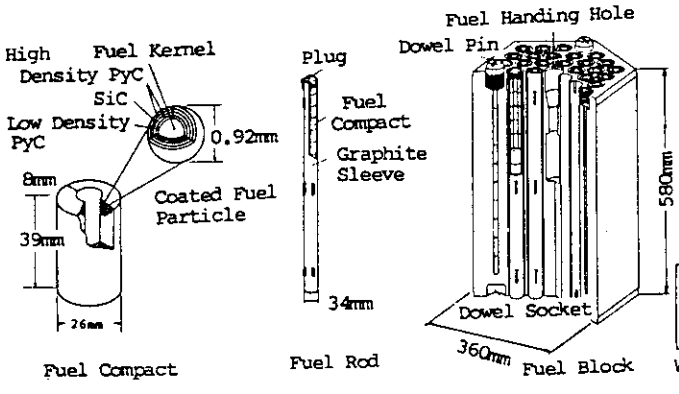

Fig. 5 Pin-in-Block Type Fuel in HTTR

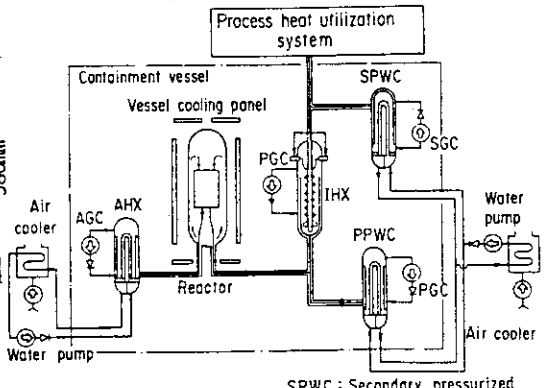

IHX : Intermediate heat exchanger
PPWC : Primary pressurized water cooler
PGC : Primary gas circulator
SPWC : Secondary pressurized water cooler
SGC : Secondary gas circulator
AHX : Auxiliary heat exchanger
AGC : Auxiliary gas circulator

Fig. 6 Schematic of HTTR Cooling Systems

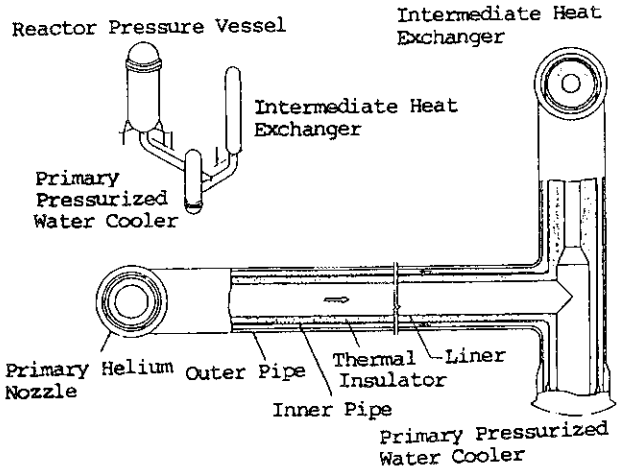

Fig. 7 Schematic of Co-axial Double-wall Piping

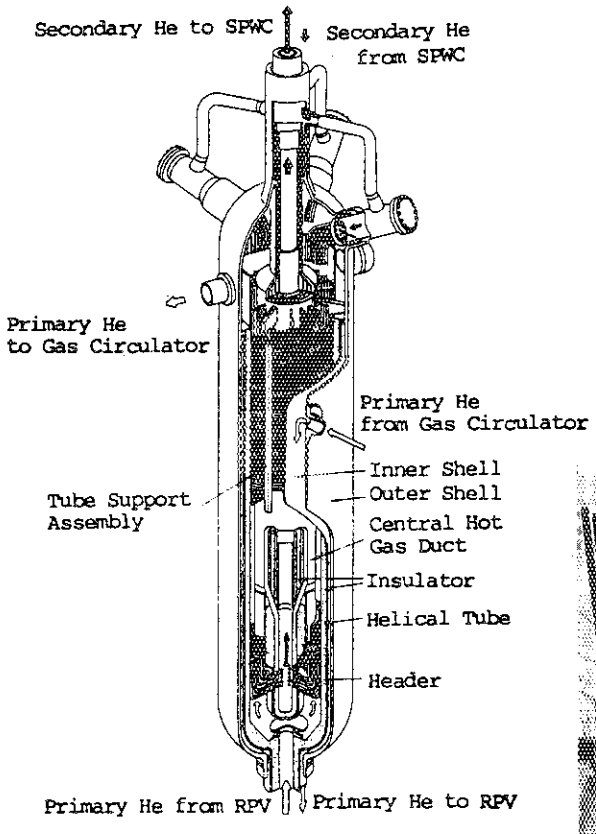

Fig. 8 Schematic of IHX

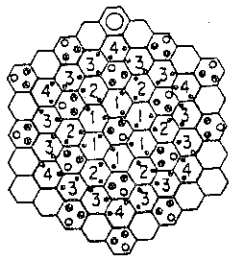

(Unit:wt%)

Radial zone / Layer	1	2	3	4
1	6.7	7.9	9.4	9.9
2	5.2	6.3	7.2	7.9
3	4.3	5.2	5.9	6.3
4	3.4	3.9	4.3	4.8
5	3.4	3.9	4.3	4.8

: Fuel Region
N: Zone Number
•: Burnable Poison
: Replaceable Reflector
: CR Guide Column
•: Control Rod
○: Reserved Shutdown System

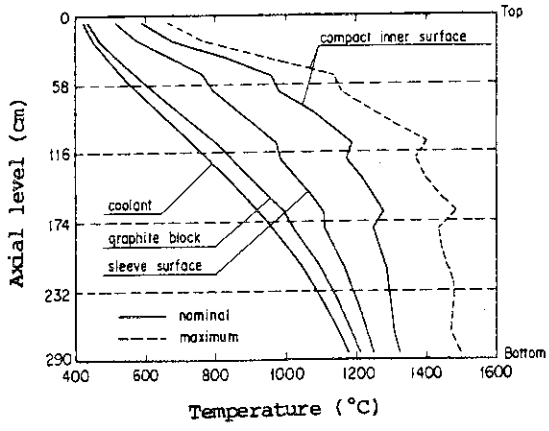

Fig. 9 Core Arrangement of Fuel Enrichment and Axial Temperature Distribution

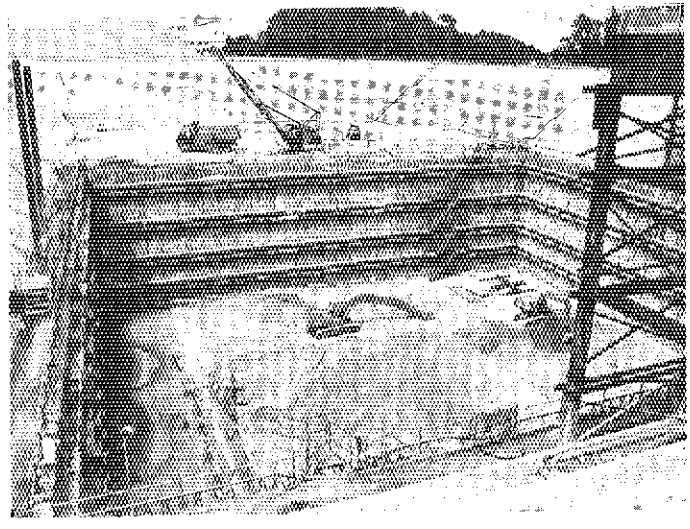

Photo 1 View of Excavation at HTTR Site

5. Researches at the University of Tokyo Fast Neutron Source Reactor, YAYOI

S. Koshizuka, Y. Oka, I. Saito, N. Aizawa, N. Sasuga, T. Sukegawa,
K. Okamura, T. Terakado, Y. Mabuchi and T. Nakagawa

Nuclear Engineering Research Laboratory
Faculty of Engineering
The University of Tokyo
2-22 Shirane, Shirakata, Tokai-mura, Naka-gun, Ibaraki 319-11, Japan

ABSTRACT

The fast neutron source reactor YAYOI was critical in 1971 at the Nuclear Engineering Research Laboratory, the Faculty of Engineering, the University of Tokyo (UTNL). The core is fueled with the enriched uranium surrounded by the depleted uranium. YAYOI is the first fast reactor in Japan. Many types of studies have been carried out by the researchers of the University of Tokyo in these 20 years. It also contributed to the Japan's national project of developing fast breeder reactors. The reactor is opened to the visiting researchers from universities and research institutes. YAYOI has also been utilized for education of undergraduate and graduate students of the Department of Nuclear Engineering of the University of Tokyo. The present paper briefly summerizes past and present researches.

1. INTRODUCTION

YAYOI is the first fast reactor built in Japan. Various unique researches can be performed using fast neutrons from YOYOI. It is called as fast neutron source reactor. The choice of this type of the reactor was made by the following reasons,

(1) new type reactor in Japan
(2) the reactor to meet the R&D needs of the development of the fast breeder reactors which are prompted as the national project
(3) small reactor to be managed by the university

There are only four fast neutron source reactors in the world (Table 1). Three of them are managed by national laboratories and operated for relatively focused objectives: AFSR for the calibration of the detectors, HARMONIE for the experiments of fast neutron shielding, TAPIRO for the shielding experiments and

Table 1 Characteristics of fast neutron source reactors

	AFSR	HARMONIE	TAPIRO	YAYOI
Country	U.S.A.	France	Italy	Japan
Location	Idaho Falls INEL	Cadarache CEA	Casaccia ENEL	Tokai-mura Univ. of Tokyo
Thermal Output	1kW	2kW	5kW	2kW
Fuel	E.U.	E.U.	E.U.	E.U.
Blanket	D.U.	N.U.	None	D.U.
Reflector	None	S.S.	Copper	Lead
Cooling	Forced Air	Forced Air	Forced He	Forced Air
Maximum Flux	5.7×10^{11}	1×10^{12}	3×10^{12}	8×10^{11}
Core Movement	None	Vertical	None	Horizontal
Date of Critical	1960	1965	1969	1971

irradiation of mice. On the other hand YAYOI was constructed to meet the needs of the variety of researches and it is called as a general-purpose fast neutron source reactor.

YAYOI is fueled with enriched uranium which is surrounded by depleted uranium blanket. The fuel is located in the square lead reflector (Fig.1). Including the heavy concrete shield blocks and a control rod system, the dimensions of the core assembly are 0.5m×0.6m×7.3m. The assembly can be moved horizontally along the moveing track and operated at six positions as shown in Fig.2: Two in the heavy concrete shield (A and B), three in the intermediate neutron column (C^-, C and C^+), and one without shielding (D). The position is chosen by the objective of the research. The intermediate neutron column is fabricated by a hexagonal 130tons of lead and intermediate neutrons are effectively generated using the scattering with lead. When the reactor is operated either at C or D position, the concrete walls of the reactor building shield the radiation. Neutrons can be also generated by a target, which is situated in the intermediate neutron column and bombarded by 35MeV electron beam from LINAC. The time-of-flight pipe (T.O.F.P.) is also equipped through the reactor building wall.

YAYOI has many experimental beam holes more than 40. This amplify the capability of YAYOI. For example, Glory hole is located in the central core fuel. The fast neutrons generated in YAYOI accompany with very few γ-rays. This property is unique and useful compared with other thermal reactors.

2. RESEARCH AT YAYOI

YAYOI has been used by researchers and graduate students of the University of Tokyo. It is also opened to the researchers of other universities and institutes. The following studies are carried out.

(1) Fast neutron shielding

YAYOI has been used to study fast neutron shielding as HARMONIE does in France. To date more than 10 kinds of studies have been carried out. In the first stage, YAYOI was used for the development of fast breeder reactor shields in Japan. A mock-up experiment of the neutron source of JOYO and the experiment of the grid plate shields of fast breeder reactors were carried out. The former proved that the satisfactory number of neutrons reach the start-up detector through the graphite pedestal. The latter contributed to the design of shielding blocks below the fuel assemblies to prevent the neutron damage to the core support structure of the prototype fast breeder reactors [1]. Furthermore fundamental studies of fast neutron shielding have been carried out, benchmark experiments of the fast neutron penetration through the iron and sodium blocks [2], fast neutron streaming through a cavity, duct and slit [3], and the experiments of the neutron transmission through the depleted and natural uranium slabs.

Neutron skyshine was measured by releasing fast neutrons through the experimental hole of the roof [4]. Simulation experiments using liquid air are also measured. They are the benchmark data of the neutron skyshine. Experiments for the verification of the albedo method were performed in serpentinite concrete in relation to the shield improvement of the nuclear ship MUTSU [5].

The experimental data obtained were also used for the development and verification of analytical and numerical methods of neutron transport theory. These studies have contributed to not only the neutron shielding but also the development of the fusion neutronics.

(2) Development of neutron standard fields

The neutron spectra were measured in the holes and columns of YAYOI. The typical spectra of fast neutron and intermediate neutron were obtained in the Glory hole and the lead column, respectively. Neutron standard fields are used for the calibration of detectors and the irradiation purpose [6]. The neutron fields of YAYOI are nominated as the standard not only in Japan but in the world. Very recently a fluence monitor of MONJU has been calibrated in YAYOI by the request of PNC.

(3) Pulsed operation

YAYOI was operated with a pulse mode though it was not designed for the so-called fast pulsed reactor. The reactivity above the prompt critical was inserted and the power successfully reached to 1000MW (500,000 times larger than the rated power of the steady operation, 2kW). The pulse width was only 100μs due to the fast fission chains. Various experiences concerning the fast pulse reactor were obtained and an inherent safety property of YAYOI was demonstrated [7]. This operation was used for verification of the operation of the criticality detector of the reprocessing plant in Japan.

(4) Measurement of decay heat of the fast fission products

Decay heat is important to the reactor safety because it is a main heat source after the reactor shutdown. The experimental data were inaccurate especially by the fast fission products. A series of accurate measurement was performed using YAYOI [8,9]. The results were contributed to improve the nuclear data library of the fission products composed by Nuclear Data Center of Japan.

(5) Irradiation for medical and biological purposes

When neutrons are irradiated after the boron compound is selectively absorbed by tumor cells, the cells are selectively destroyed by α-particles released by the neutron capture reaction because the range of α-particle is similar to the cell size. It is called as boron neutron capture therapy and considered to be superior to other radiotherapies which also destroy the tumor cells including normal ones. Since the kerma factor of the wet tissue becomes minimum around 30eV, epithermal neutron irradiation is superior to thermal neutron therapy by decreasing the surface dose and increasing the penetration distance. It was studied to generate many epithermal neutrons using YAYOI [10]. But it was turned out that the power 2kW was too small for the practical use. From the design study, a 5MW reactor enable us to realize the epithermal neutron therapy [11]. The irradiation field of YAYOI was used for fundamental studies using dogs and mice. Irradiation effects of various energy neutrons are being investigated using blood.

(6) In-situ tritium recovery experiment from fusion blanket breeding materials

Tritium recovery mechanism from the breeding materials such as Li_2O is important to establish the fuel cycle of fusion reactors. The experimental study was pioneered with YAYOI. Release process and recovery mechanism of tritium generated by the neutron irradiation have been studied in detail under high temperature simulating the environment of the fusion reactor blanket. To date diffusivity and surface reaction rate of tritium were obtained in solid materials: Li_2O, $LiAlO_2$, etc [12]. Presently liquid breeder materials, e.g. Li-Pb alloy, is studied.

(7) Water chemistry by fast neutron

Water chemistry in the nuclear reactors is relevant to the problems of the radioactive clad accumulation and stress corrosion cracking. Therefore it is important to obtain the threshold values of radiolysis products in the high temperature coolant. Fast neutron has larger LET than γ-ray and plays a more important role in the core. The irradiation in YAYOI are providing the essential data for the purpose [13].

(8) Fast neutron irradiation effect to various materials

Organic materials, semiconductors, metals and ion crystals have been irradiated. For example, the polymers have different threshold energy of cross-linkings of the molecules. Fundamental and application studies, e.g. development of radiation resistant materials or chemical dosimeters, are carried out. Recently high temperature superconductor materials are irradiated to improve its performance.

(9) Fast neutron radiography

Fast neutron radiography is useful for inspecting thick materials than other non-destructive testings using X-ray and thermal neutrons. It is also available to inspect composite materials made of heavy and light elements. However the R&D of fast neutron radiography is far behind that of thermal neutron. The fast neutron

radiography are being studied at YAYOI [14]. Higher resolution image is pursued now.

(10) Development of new radiation measurement methods

Scintillation optical fibers, in which scintillator is used as the core material, are examined in YAYOI to detect multiple informations (energy, radiation type, location and time) simultaneously. A neutron measurement system using nuclear excitation laser has been also studied. A wide range measurement system based on the multi-level counting method and a position-sensitive detector are also developed.

We have three types of joint research projects open to other universities and research institutes, on-pile researches using YAYOI described above, off-pile researches not using YAYOI, and YAYOI workshops. The workshops are held 1 or 2 days for various research topics. The off-pile research subjects cover the development of new numerical methods, new concepts of reactors, magneto-mechanics etc.

Another major characteristic of YAYOI is that the experiments can be cooperated with other facilities situated in UTNL, an electron linear accelerator (the shortest electron pulse in the world can be generated), the accelerators for the heavy irradiation of materials, and the neutron generator and a tritium experiment facility in the blanket engineering research facility building.

3. EDUCATIONAL ACTIVITIES

New generation researchers and engineers should be brought up for the future development of the nuclear engineering. These 20 years many graduate and undergraduate students of the University of Tokyo carried out their researches using YAYOI and other facilities in UTNL; approximately total 140 students have belonged to UTNL. Including those who belonged to the Department of Nuclear Engineering, 250 - 300 students studied in UTNL for their graduate and master theses.

4. CONCLUSIONS

YOYOI has the unique characteristics, pure fast neutrons with low γ-ray contamination and good accessibility to the irradiation fields. We are now planning to develop a new area of fast neutron science and technology establishing a well-controlled irradiation facility and high performance measurement devices.

REFERENCES

[1] Y. Oka et al., Nucl. Technol. **31**, 12 (1976)

[2] Y. Oka et al., Nucl. Sci. Eng. **73**, 259 (1980)

[3] H. Hashikura et al., Nucl. Sci. Eng. **84**, 337 (1983)

[4] N. Nakazawa and A. Sekiguchi, IPCR Symp. on Several Topics of Environmental Neutrons (1980)

[5] T. Kosako et al., J. Faculty of Eng., Univ. of Tokyo (B) **34**, 409 (1977)

[6] A. Sekiguchi et al., Consultant's Meeting on Integral Cross Section Measurements in Standard Neutron Fields (1976)

[7] H. Wakabayashi et al., Proc. US/Japan Seminar on Fast Pulse Reactors (1976)

[8] M. Akiyama et al., J. Atom. Energ. Soc. Japan **24**, 709 (1982)

[9] M. Akiyama et al., J. Atom. Energ. Soc. Japan **24**, 803 (1982)

[10] S. An et al., Nucl. Technol. **48**, 204 (1980)

[11] Y. Oka, I. Yanagisawa and S. An, Nucl. Technol. **55**, 642 (1981)

[12] S. Tanaka et al., Fusion Technol. **19**, 1018 (1991)

[13] Y. Katsumura et al., Proc. JAF Int. Conf. on Water Chemistry, 575 (1991)

[14] K. Yoshii et al., J. Atom. Energ. Soc. Japan **32**, 611 (1990)

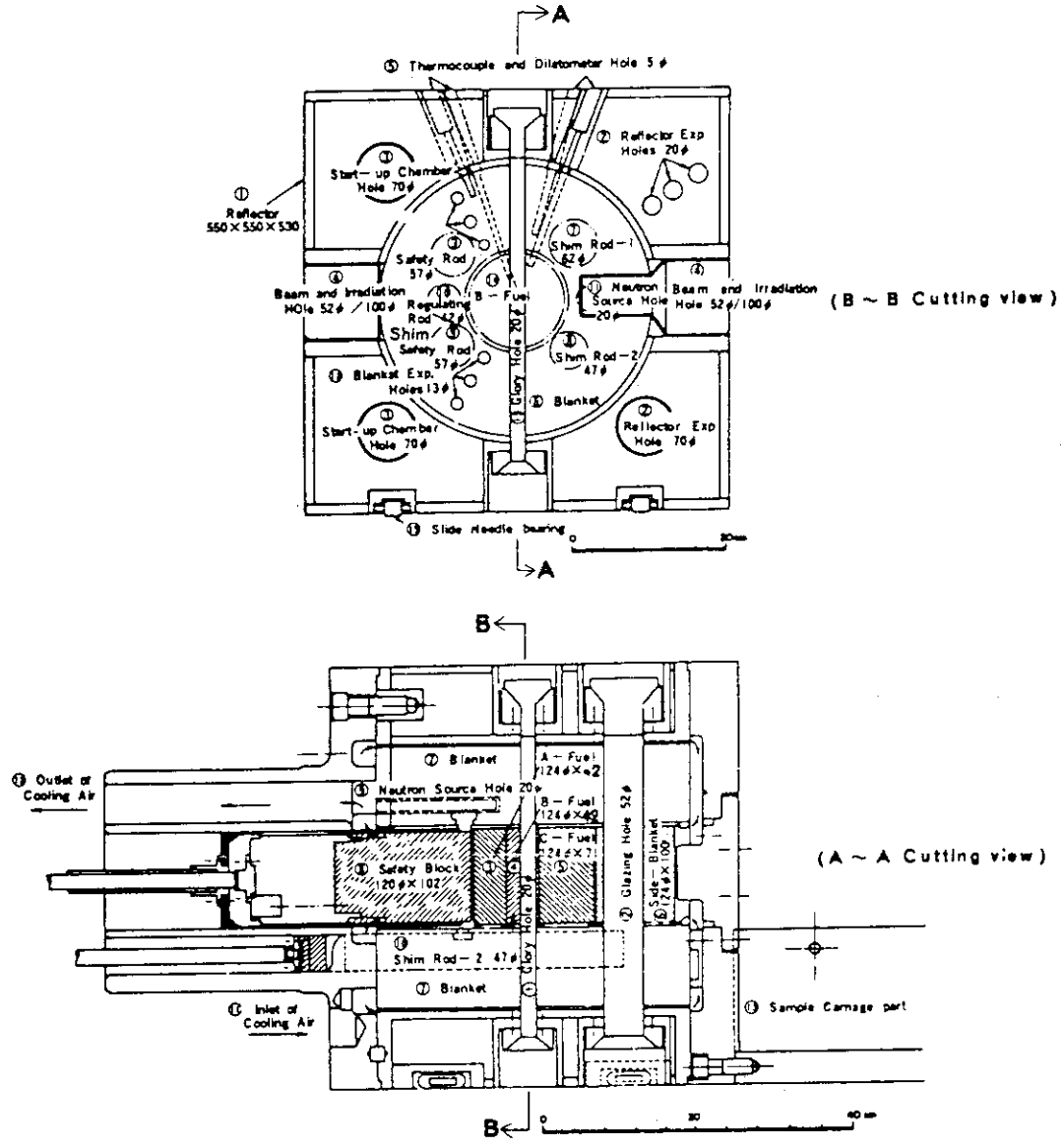

Fig.1 Core assembly of YAYOI

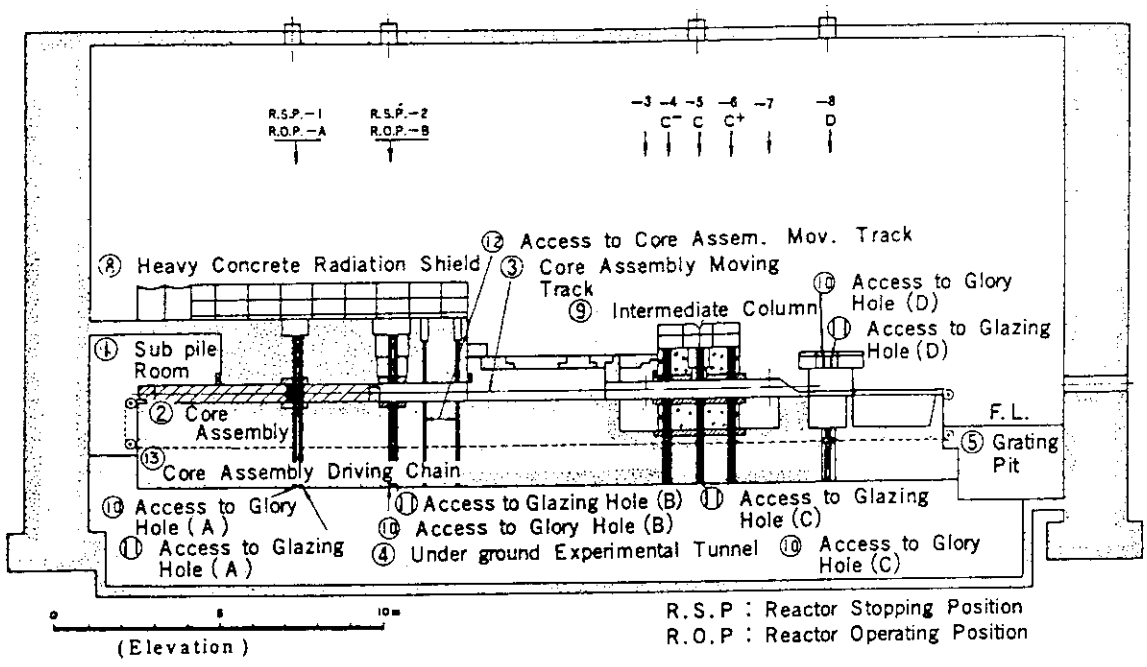

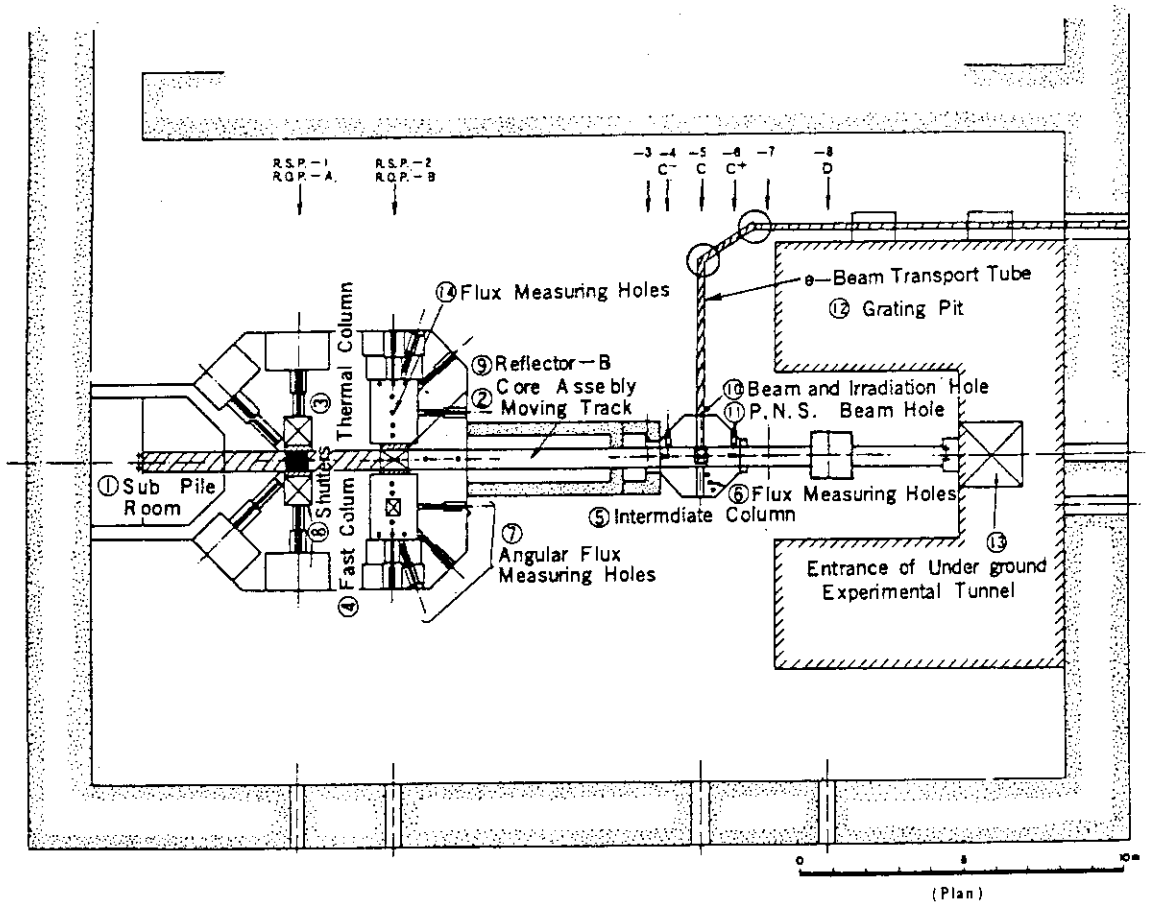

Fig.2 Layout of YAYOI

6. Operation Program of MPR-30 GA Siwabessy

I.Kuntoro, S.Kuntjoro, K.S.Ontowiryo

Center for Multipurpose Reactor, BATAN
Puspiptek, Serpong, Tangerang 15310, Indonesia

ABSTRACT

Operation program of the MPR-30 GA Siwabessy (MPR-GAS) for its transition cores to achieve the typical working core (TWC) with nominal power of 30 MW has been set-up by using 2-dimensional diffusion code, IAFUEL. Operation planning comprising nuclear commissioning, routine operation and the operation experience are also presented.

The commissioning results show that the reactor performance until the sixth core meet the designed calculation.

INTRODUCTION

The MPR-GAS is the first research reactor using low enriched uranium (LEU) MTR fuel element. Nowadays, it is under commissioning of power ascent stages succeeding its first criticality achievement on July 27, 1987. The reactor was designed to produce 30 MW power and average neutron flux of 2.0 E+14 neutron/(cm^2.s).

The operating (typical working) core is designed to have nuclear parameter as shown in table 1 with core configuration as illustrated in figure 1. It has 7 different burn-up level with 8% difference as required to run the reactor over a cycle. At the end of cycle (EOC), 7 or 8 of 56 % burn-up level will be discharged and replaced by the new ones.

The problem to set the operation program during commissioning period is how to conduct the operation safely to produce fuel elements in 7 group burn-up levels of 0, 8, 16, 24, 32, 40, and 48 %, starting with all 48 fresh fuel elements. This in-core fuel management problem was solved by means of 2-dimensional, 4 group of neutron energy-diffusion code so called IAFUEL with its flow diagram as illustrated in figure 2.

The implementation of the program have been started since its first criticality and by now is reaching the beginning of the sixth core (full core) operation test. The nominal power of 30 MW is expected to be reached in the beginning of 1992.

FE/CE/BE : Fuel/Control/Beryllium
XXX.X : BU BOC
YYY.Y : BU EOC

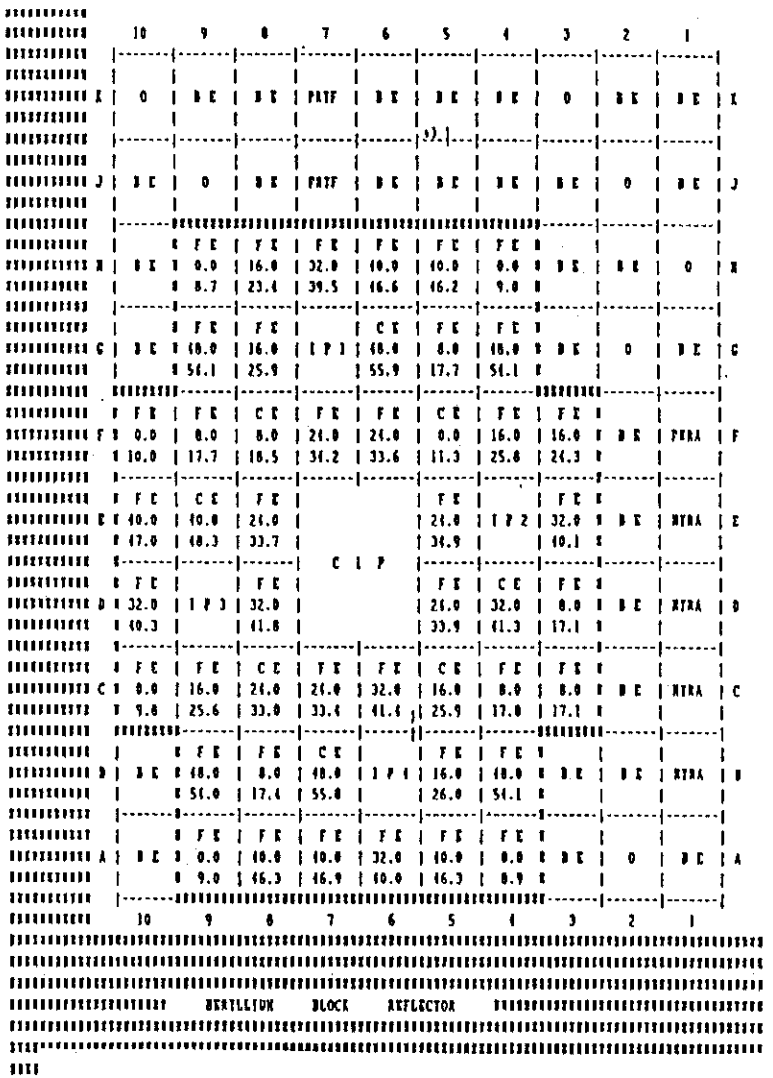

Figure 1. : Design TWC of MPR-GAS

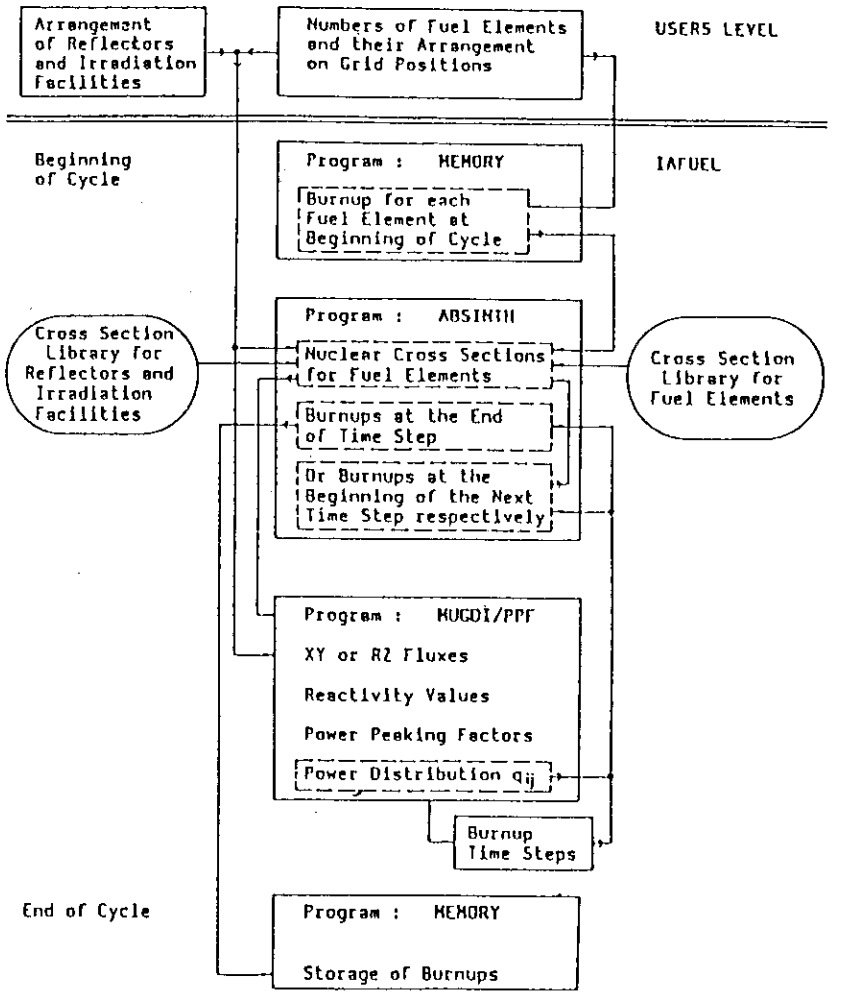

Figure 2. : IAFUEL flow scheme

Table 1. : The design nuclear parameter of MPR-GAS

No.	parameter	value
1.	Nominal power, MW	30
2.	Number of fuel element	40
3.	Number of control element	8
4.	Number of absorber	8
5.	Cycle duration, full power day	25
6.	Ave. burn-up at BOC, %	23.3
7.	Ave. burn-up at EOC, %	31.3
8.	Ave. burn-up of discharge FE,%	53.7
9.	Excess reactivity BOC, %	9.2
10.	Control rod worth, %	- 14.5
11.	Shut-down reactivity, %	- 5.3
12.	Shut-down reactivity, 1 stuck rod, %	- 3.2

OPERATION PROGRAM

Operation phases of MPR-GAS is described by figure 3. The non-nuclear and start-up stages have been conducted successfully and completed in August 1987. The rest is power ascent stage until the TWC or operating core is achieved. This paper describes mainly, the strategy of fuel management in reaching the operating core.

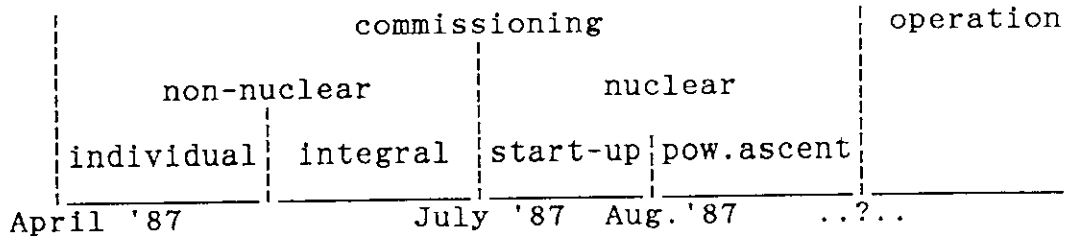

Figure 3. : Operation phase of MPR-GAS

In order to be able to provide fuel elements in several burn-up levels for the designed TWC, the reactor will be operated in several cores starting with the smallest core-I arranging a number of fresh fuel elements over a certain period of time in the operating cycle. The core size is then gradually increased by adding some fuel elements per cycle until the full-core of 48 elements are loaded (see figure 4). By arranging the core configuration each cycle with the help of IAFUEL code, operation program for the transition core was generated and presented in table 2 and figure 5, by taking into considerations :

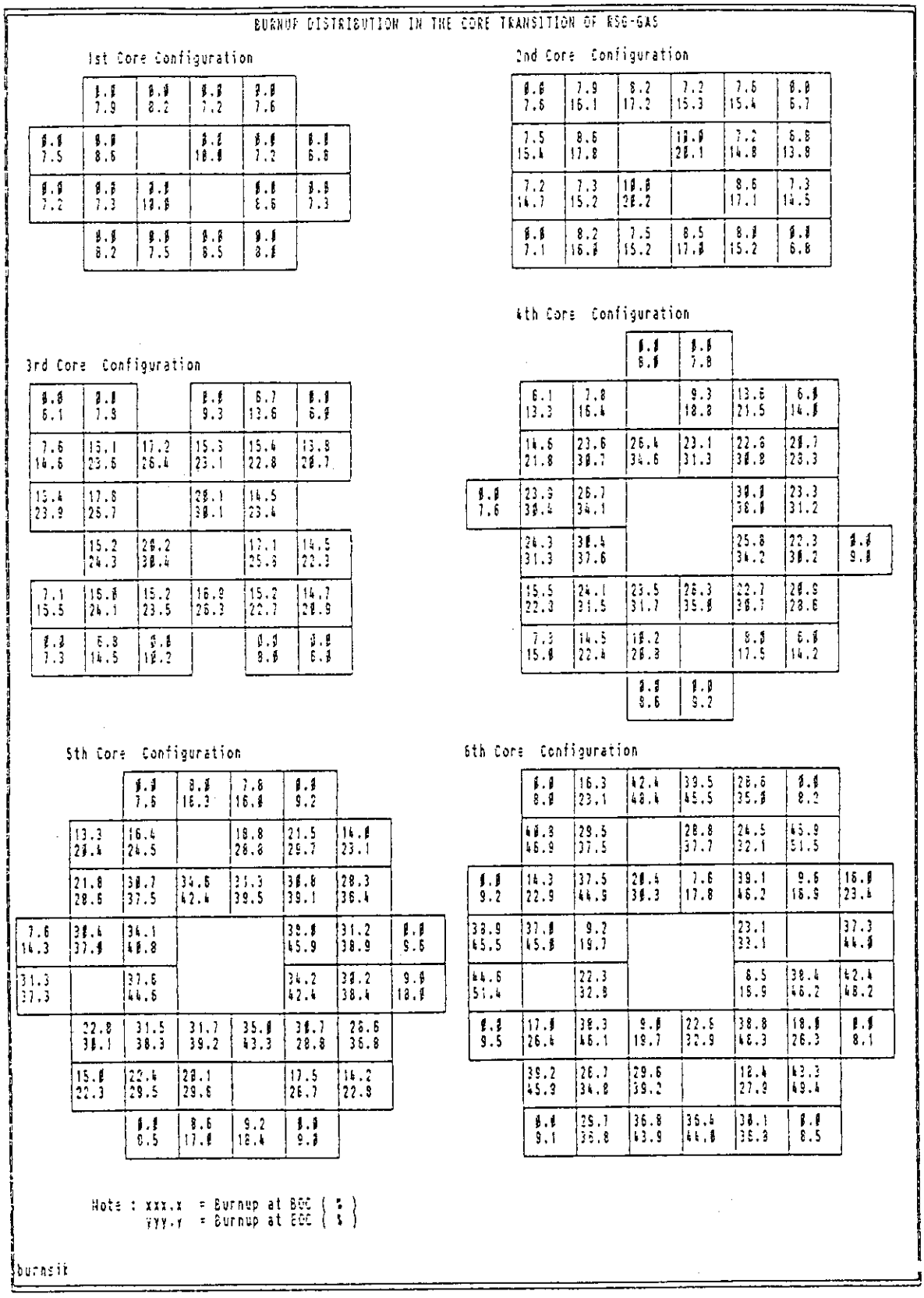

Figure 4. : Design transition core configuration

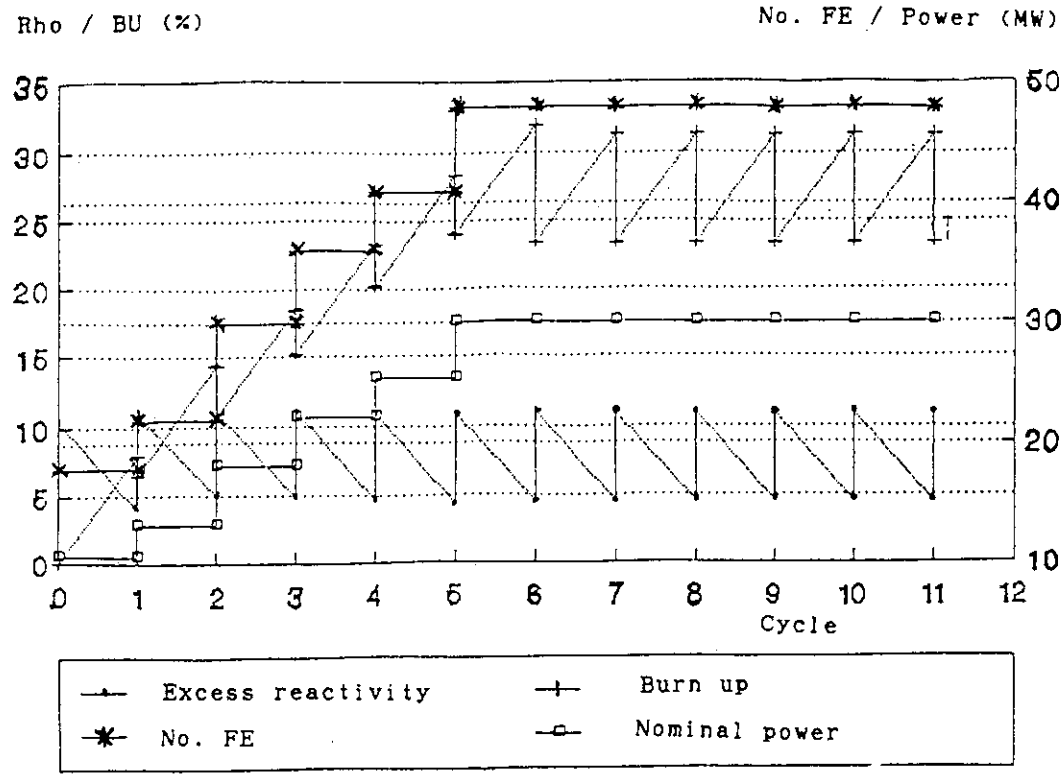

Figure 5. : Transition core operation program

Table 2. : TRANSITION CORE DESIGN OF MPR-GA.SIWABESSY

	CORE 1		CORE 2		CORE 3		CORE 4		CORE 5		CORE 6		CORE 7		CORE 8		TWC	
Burnup step	BOC	EOC	BOC	EOC	BOC	EOC	BOC	EOC	BOC	EOC	BOC	EOC	BOC	EOC	BOC	EOC	BOC	EOC
FE/CE 64 %																0/1		
56 %														6/3	0/1	4/0		4/2
48 %												12/6	6/3	4/0	4/0	6/2	4/2	6/1
40 %										12/6	12/6	4/0	4/0	6/2	6/2	6/0	6/1	6/1
32 %								12/6	12/6	4/0	4/0	6/2	6/2	6/0	6/0	5/0	6/1	6/1
24 %						12/6	12/6	4/0	4/0	6/2	6/2	6/0	6/0	5/0	5/0	7/0	6/1	6/1
16 %				12/6	12/6	4/0	4/0	6/2	6/2	5/0	6/0	5/0	5/0	7/0	7/0	6/3	6/1	6/1
8 %		12/6	12/6	4/0	4/0	6/2	6/2	6/0	6/0	5/0	5/0	7/0	7/0	6/3	6/3	6/2	6/1	6/1
0 %	12/6	0/0	4/0	0/0	6/2	0/0	6/0	0/0	5/0	0/0	7/0	0/0	6/3	0/0	6/2	0/0	6/1	0/0
Total	12/6	12/6	16/6	16/0	22/8	22/8	28/8	28/8	33/8	33/8	40/8	40/8	40/8	40/8	40/8	40/8	40/8	40/8
Power (MW)	10.68		13.31		18.19		22.13		25.41		30		30		30		30	
BU time (h)	504		572		578		583		590		600		600		600		600	
Average Burnup	0.00	8.00	8.42	14.42	10.56	18.55	15.25	23.25	20.25	28.25	23.93	31.93	23.33	31.33	23.33	31.33	23.33	31.33
Keff BOC XE free	1.11679		1.12226		1.12384		1.12310		1.12416		1.12258		1.12350		1.12459		1.12375	
EOC XE equ	1.04172		1.05327		1.05090		1.05064		1.04911		1.04548		1.04615		1.04752		1.04686	
PPF	1.26	1.24	1.29	1.27	1.30	1.27	1.23	1.21	1.24	1.23	1.30	1.27	1.29	1.28	1.28	1.29	1.28	1.26

coretran

- constant power density of 175 kW/l
- sufficient shut-down margin reactivity (> 0.5% at 1 rod stuck)
- flat power distribution, with power peaking factor < 1.6
- producing around 8 % averaged burn-up per cycle.

According to the above program, full core with nominal power of 30 MW will be reached at the sixth core and the TWC is expected to start with ninth core. TWC is operating core with an order fuel loading pattern. In each cycle, operating parameters should be measured and analyzed. The data are then used to verify the next program.

OPERATION PATTERN

Principally, MPR-GAS is operated in 3 stages per cycle, namely:

1. Beginning stage : core unloading; critical experiment; operating core formation, instrumentation setting, low power test, flux neutron measurement, flow adjustment, power calibration and power level test.
2. Operating stage : power operation for utilization.
3. End stage : low power test, neutron flux measurement and reactor systems inspection.

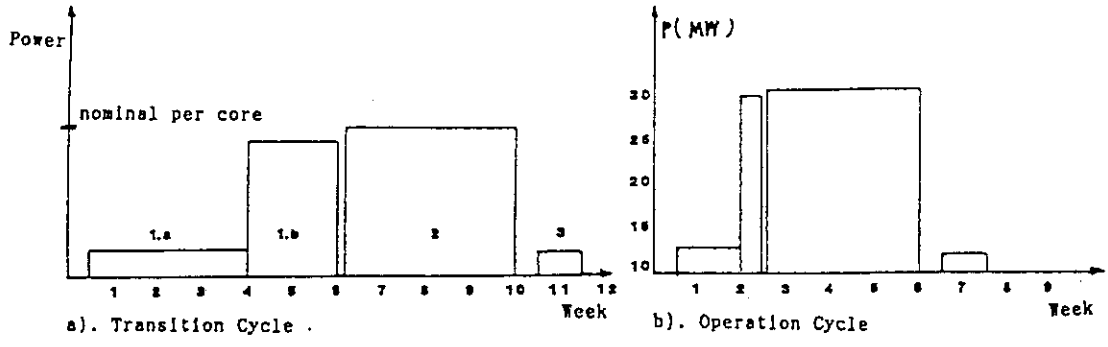

Note: 1. Beginning period
a. low power test
b. high power test
2. Operation period
3. End period

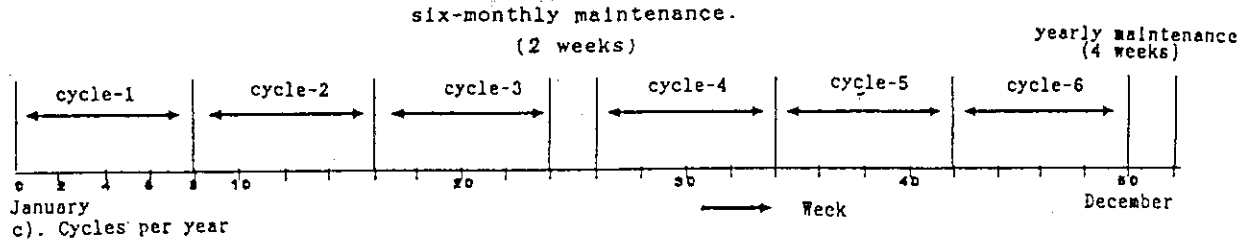

Figure 6.: Operation pattern of MPR-GAS

At the commissioning phases, the time period of a cycle is predicted to be about 12 weeks, due to many parameters should be measured for characterizing the core. On the other hand, for routine operation in which the operating parameters are known, it takes about 8 weeks by cancelling some measurements and tests.

For the whole year, besides inspection at the end of the cycle, it is required to carry-out six-monthly (2 weeks) and yearly (4 weeks) maintenance. Under these conditions, MPR-GAS can be operated 3 cycles (cores) per year during commissioning and 6 cycles per year for the routine operations (- 3500 effective ours) as illustrated by figure 6.

IMPLEMENTATION OF THE PROGRAM AND PRESENT STATUS

The commissioning results of the transition cores I - VI can be shown in table 3 and figure 7. By comparing table 2 and 3, it can be summarized that the fuel element group with the desired burn-up levels were fulfilled and the other parameters are in good agreement to the calculated ones.

Table 3. : REAL TRANSITION CORE OF MPR-GAS

	CORE 1		CORE 2		CORE 3		CORE 4		CORE 5		CORE 6	
Burnup step	BOC	EOC	BOC	EOC	BOC	EOC	BOC	EOC	BOC	EOC	BOC	EOC
FE/CE 64 %												12/6
56 %										12/6	12/6	4/0
48 %								12/6	12/6	4/0	4/0	6/2
40 %						12/6	12/6	4/0	4/0	6/2	6/2	6/0
32 %				12/6	12/6	4/0	4/0	6/2	6/2	5/0	6/0	5/0
24 %		12/6	12/6	4/0	4/0	6/2	6/2	6/0	6/0	5/0	5/0	7/0
16 %	12/6	0/0	4/0	0/0	6/2	0/0	6/0	0/0	5/0	0/0	7/0	0/0
8 %												
0 %												
Total	12/6	12/6	16/6	16/0	22/8	22/8	28/8	28/8	33/8	33/8	40/8	40/8
Power (MW)	10.68		13.31		18.19		22.13		25.41		30	
BU time (h)	558.19		567.64		601.75		583		616		...	
Average Burnup	0.00	7.43	6.08	14.14	10.37	19.50	15.53	23.46	20.61	29.43	23.92	
Keff BOC XE free	1.10132		1.10827		1.10266		1.11483		1.12277		1.12842	
EOC XE equ	1.04172		1.05327		1.05090		1.05102		1.08234			
PPF Max.	1.24	1.23	1.26	1.25	1.29	1.26	1.20	1.18	1.24	1.23	1.29	

realcore

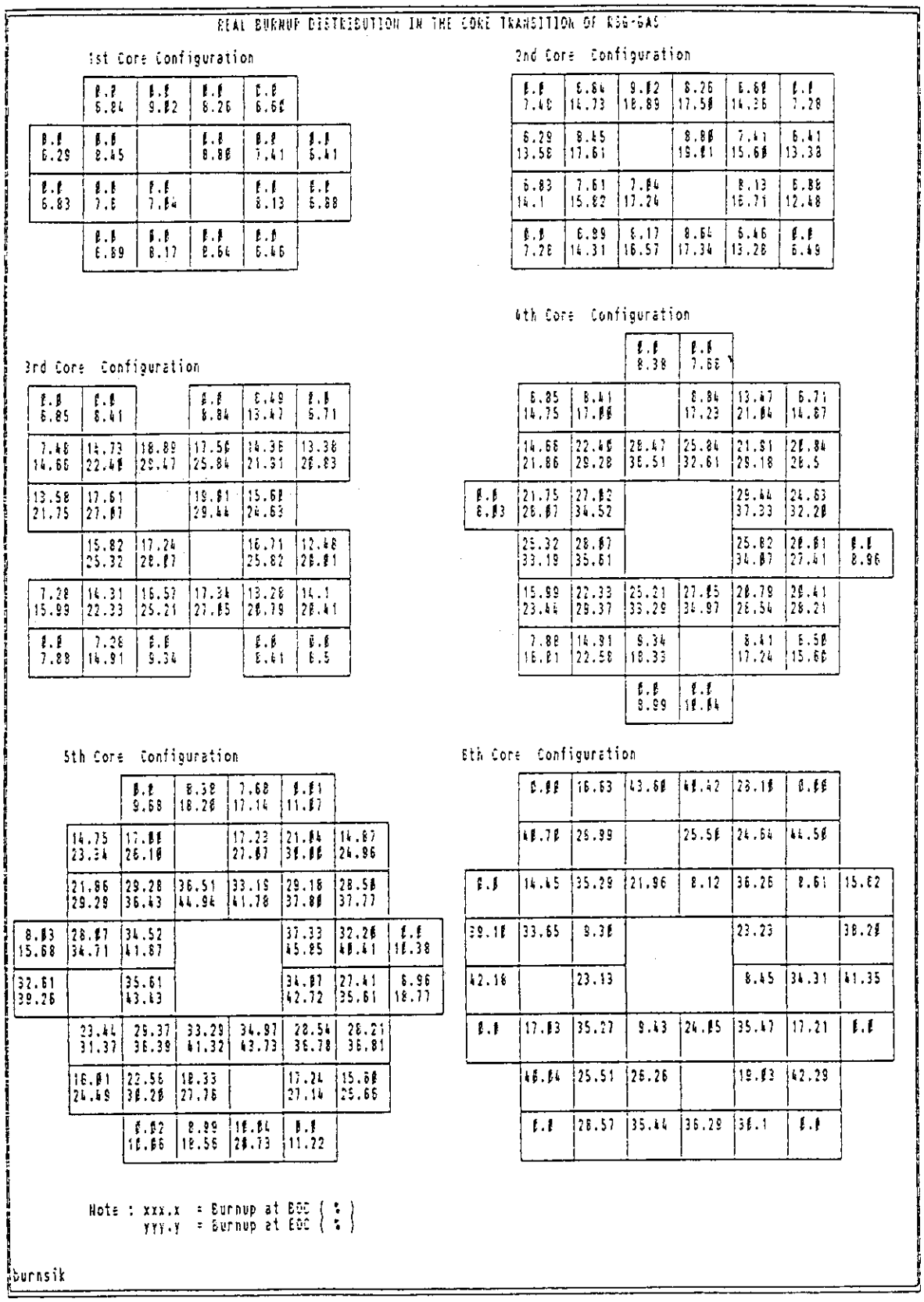

Figure 7. : Real transition core configuration

It is, however, far behind the schedule from the time point of view, since during time period of August 1987 to July 1991, only 5 transition cores operation could be conducted which means about 10 month per cycle. The delay was coming out due to some reasons such as :

- supporting ring modification of the beam tubes no S-5,
- one power channel modification,
- operation disturbances,
- installation of experiment facilities either in-pool or at the beam tubes,
- utilization requirements during operation stages.

Since September 21, 1991, again, core VI commissioning should be terminated at low power test stage, since the reactor pool should be emptified for installation of In-pile Loop facility and neutron guide at S-5, for 4 months. Hence, it is expected that core-VI of 30 MW-operation will be completed by the end of March 1992.

REFERENCES

1. Safety Analysis Report MPR-30 GA Siwabessy, Rev. 7, Batan, Indonesia, September, 1989.
2. M. Wickert, Muller, "IAFUEL Operating Manual", Interatom, 1986.

7. The Reduced Enrichment Program for JRR-4

M.TAKAYANAGI

Tokai Research Establishment
Japan Atomic Energy Research Institute
Tokai-mura,Naka-gun,Ibaraki-ken,JAPAN

ABSTRACT

Japan Research Reactor No.4(JRR-4) with the rated power of 3.5MW, swimming pool type research reactor, 93% enriched uranium ETR-type fuel used, light water moderated and cooled.

The first criticality reached on 28th January , 1965. The reactor has operated for about 26 years. However, it was planed to the reduced enrichment of the fuels to low enrichment according to the International Reduced Enrichment for Research and Test Reactors(RERTR) program.

This paper describes the program for conversion of the enrichment of fuel from 93% to less than 20%.

INTRODUCTION

JRR-4 is a swimming pool type research reactor, 93% enriched uranium ETR-type fuels used, light water moderated and cooled. It was initially constructed to pursue mainly shielding experiments for nuclear ship"Mutu". Today, it is widely utilized for many researches and experiments, such as irradiation on reactor fuels and materials, radioisotope production, silicon doping, and reactor operation training for Nuclear Engineering School students.

The first criticality of JRR-4 reached on 28th January, 1965. The reactor was started to operate with max. thermal power of 2.5MW from April 1966. The maximum power of JRR-4 was increased to 3.5MW in october 1976. The reactor has been operated satisfactorily for about 26 years since the first criticality.

The reduced enrichment program for JRR-4 is planed to respond to the RERTR program, "Examination Guide For Safty Design of Water-Cooled Type Research and Testing Nuclear Reactor Facilities" and "Examination Guide For Safty Evaluation of Water-Cooled Type Research and Testing Nuclear Reactor Facilities".

The principal concepts of the modification for JRR-4 are summarized as follows.

1) The fuels are to be converted the enrichment from HEU (93% enriched uranium) to LEU(bellow 20% enriched uranium) fuels.
2) Experimental utilization facilities should be complied with user's requirements with respect to the biological-medical neutron irradiation facility.

REDUCED ENRICHMENT OF JRR-4 FUEL

THe reduced enrichment of fuels in JRR-4 should satisfy the requirements shown in the following.

1) THe core configuration should not be changed.
2) The enrichment of the fuels should be less than 20%, so called "low enrichment".
3) The neutron flux should be higher than the present flux at the utilization positions.

At the first stage of investigation, the uranium siliside plate fuels which have the same shape and dimension have been evaluated by calculations on neutronics and thermohydraulic behavior. On the other hand, the guide both "Examination Guide For Safety Design of Water-Cooled Type Research and Testing Nuclear Reactor Facilities" and "Examination Guide For Safety Evaluation of Water-Cooled Type Research and Testing Nuclear Reactor Facilities" published in July 1991 suggest the unnecessary of evaluation on design based event of flow blockage at cooling channel when U-ZrH fuels are applied. In this case, the event of fission products release from the fuels during the operation can not be applied to evaluate for the middle out put research reactor such as JRR-4 with 3.5MW of thermal out-put.

This may bring the simplification of emergency exhaust systems. The calculation on U-ZrH fuel core has also carried out. THe result of the calculation on the both of siliside fuel core and U-ZrH fuel core are shown in Fig.1.

And it should be necessary to confirm that the U-ZrH fuel keep the enough stability for the reactor operation. For this purpose, we evaluate the thermohydraulic behavior and make clear irradiation behavior.

UTILIZATION FACILITY

JRR-4 is characterized by its capability of operating at low, intermediate, high power and of doing power-up and shut-down every day to meet experimental requirements, that is different from large research reactors operating continuously at high power.

At present, the reactor operation is carried out basically during the daytime for 7 hours a day, 4 days a week, 43 weeks a year.

The service of joint use in JRR-4 was approved in January 1974 and joint use for outside users were initiated at the same time.

Furthermore, the reactor maximum power increased from 2.5MW to 3.5 MW in November 1976.

As mentioned above, JRR-4 makes use of its characteristics of research reactor with high performance, purporting and extending equipments, to meet utilizations which are not available in large reactor operating at constant power.

THe reduced enrichment program for JRR-4 fuels is proceeded basically to keep its characteristic mentioned above. Furthermore, JRR-4 which was expanded its utilization facility and JRR-3 are requested cooperative supplement each other after the retirement of JRR-2 which is scheduled in the near future.

Therefore, JRR-4 should be expanded on its present facilities like follows.

(a) Biological and Medical Irradiation Facility

JRR-4 Lid tank which is utilized as a pure thermal neutron field will modified as a biological and medical irradiation facility. The facility will consist of the horizontal beam tube which supplies thermal neutron flux of $2x10^9$ (n/cm^2s), the irradiation room and the medical operation room which is offered to the surgical medical operation on patients before and after irradiation respectively.

(b) Large Bore Irradiation Facility

The L-pipe which is the largest bore in existence will be replace to the other place increased the higher flux of about 50% than the present state.

The large bore irradiation facility is newly settled for the current multifarious request of users and production of Si semi-conductor.

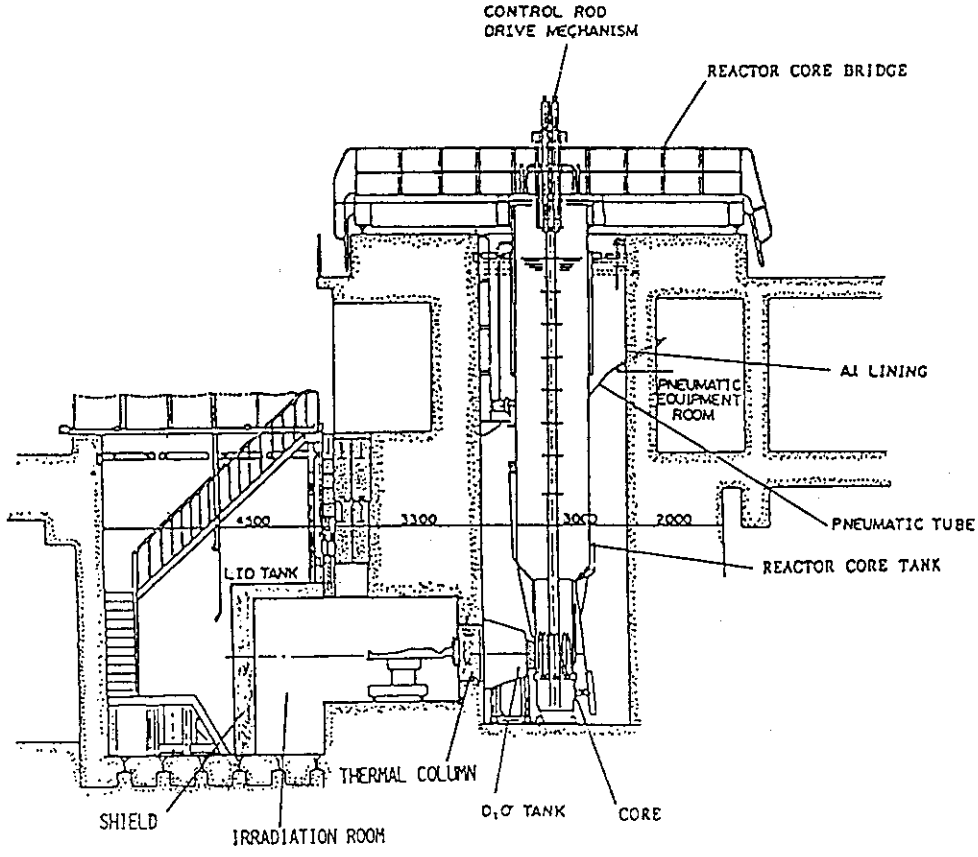

(c) Activation Analysis Equipment

Irradiation for activation analysis is most popular in the utilization of JRR-4.

According to user's needs, "Very Short-lived nulide analysis equipment" having high-speed sending device is developed and installed in JRR-4.

RENEWAL OF REACTOR FACILITIES

JRR-4 has been operated for about 26 years, and some works of reactor facilities are necessary for keeping it on at this time.

Those works will belong the modification program of reactor building, which are renewal of primary cooling system, nuclear and process instrumentations and control rods drive mechanisms will be carry out with works of core conversion and upgrading of utilization facility for the same time.

If JRR-4 didn't has the program described this paper , those works should be done at using probably different term respectively.

According to this reason, JRR-4 resting term of operation can be shorted for the term of each work which consume for the application of safety review and other works mentioned on this chapter, and it will make also early restart of JRR-4 for users.

JRR-4 should be checked as classified a middle out put reactor both "Examination Guide For Safty Design of Water-Cooled Type Research and Testing Nuclear Reactor Facilities" and "Examination Guide For Safty Evaluation of Water-Cooled Type Research and Testing Nuclear Reactor Facilities" published in July 1991 on "Design basis accident",. "Separation and Redundancy" for safety device, and so on.

Schedule of the reduce enrichment program of fuel etc. is shown bellow.

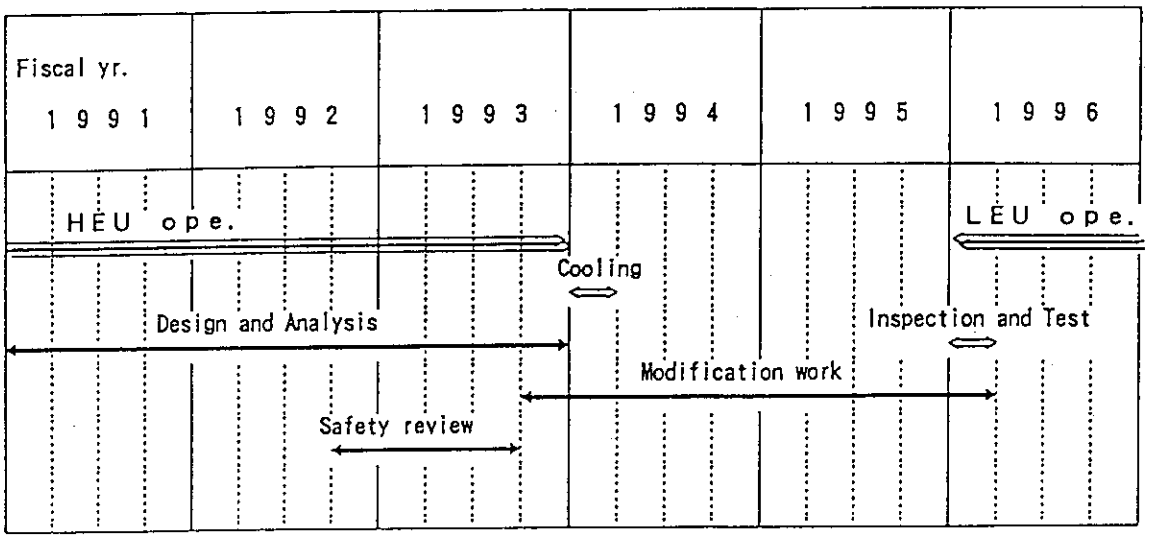

CONCLUSIONS

The modification of JRR-4 will be carry out not only core conversion from HEU to LEU,but also upgrading of the utilization facility and renewal of the reactor facilities, responded to "The Guide for Safty Design of Research Reactors" and "Guide for Safety Evaluation of Research Reactors".

Thus JRR-4 provided with many safty equipments of the most up-to date model can be compiled with user's requirement after that.

ACKNOWLEDGMENTS

The following are gratefully acknowledged for their contributions; the staffs of Department of Research Reactor of JAERI, and the members of JRR-4 modification team.

REFERENCES

1. K.KANDA, H.NISHIHARA, "Status of Reduced Enrichment Program for Research Reactors in Japan",in Proceeding of the 13th RERTR Meeting, Newport, Rhode Island, U.S.A., (Sep.1990)
2. U. S. NRC, "Safety Evaluation Report Related to the Evaluation of Low-Enriched Uranium Silicide-Aluminum Dispersion Fuel for Use in Non-Power Reactors", NUREG-1313, (Jul. 1988)
3. "Research Reactor Core Conversion from the Use of Highly Enriched Uranium to the Use of Low Enriched Uranium Fuels", Guide Book, IAEA-TECDOC-324, IAEA, Vienna 1985

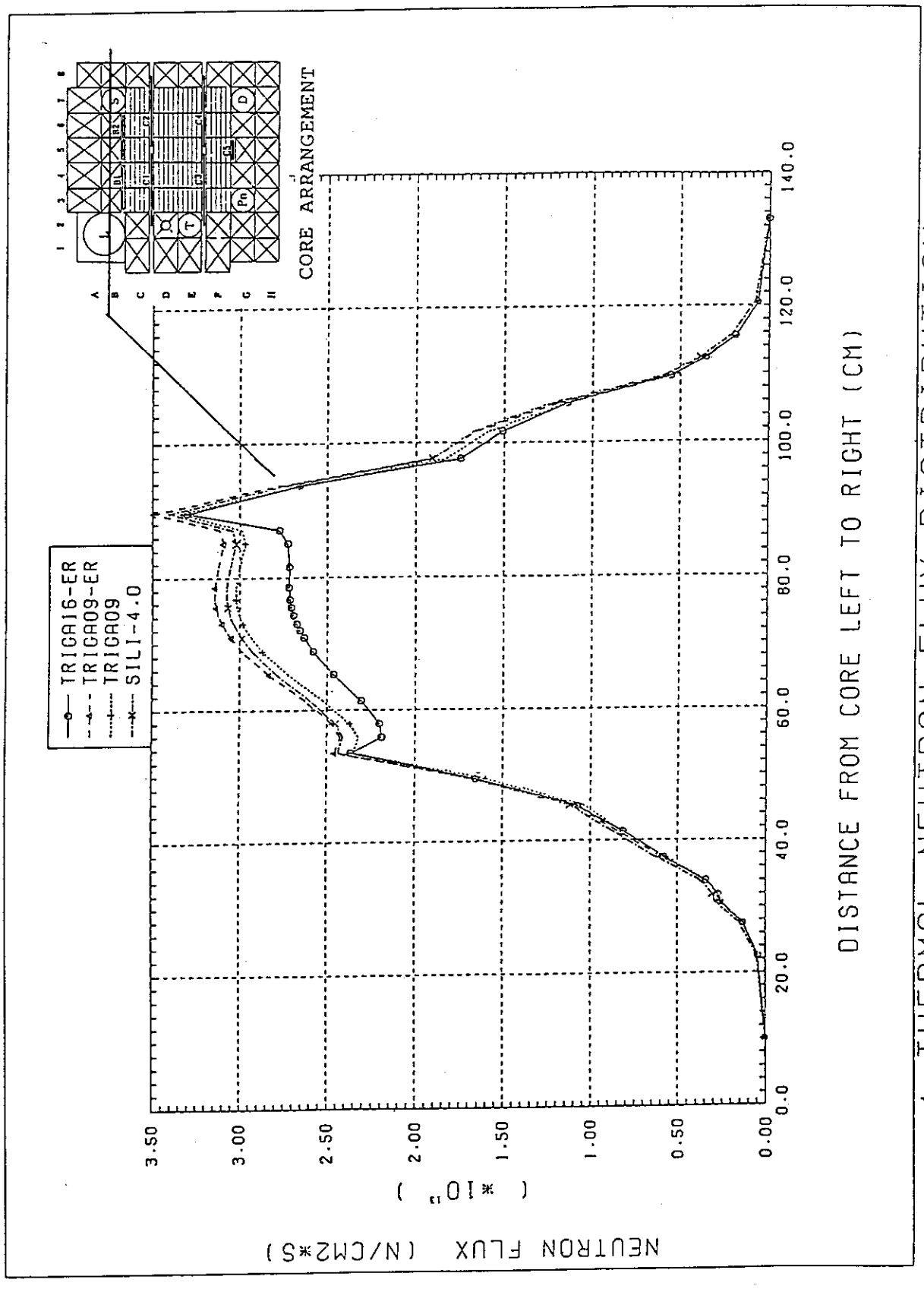

Fig.1 THERMAL NEUTRON FLUX DISTRIBUTION

8. The Experimental Study and Operation Features of the 5MW Heating Reactor

Wang Dazhong Zhang Dafang Dong Duo
Lin Jiagui Su Qingshan

Institute of Nuclear Energy Technology
Tsinghua University
P.O.Box 1021 Beijing 102201, China

Abstract

The 5MW experimental Heating Reactor (EHR-5) was developed by Institute of Nuclear Energy Technology (INET) Tsinghua Unwersity.

The EHR-5 is a integrated, light water vessel type reactor cooled by natural circulation with self-pressurized performace. The construction of the EHR-5 began in March 1986, and its initial criticality reached on November 3, 1989 and full power operation on December 16, 1989. Until now, the EHR-5 has been successfully operated for two heating seasons.

Some important experimental studies were carried out during the commissioning and operation period. The results obtained from these experiments show that the EHR-5 has excellent features of responding perfectly to all transient, and higher degree of inherent safety.

DESCRIBTION OF THE EHR-5[1]

The EHR-5 is a integreted, vessel type light water reactor cooled by natural circulation with self-pressurized performance. Fig.1 shows the reactor structure with dual vessel.

The reactor vessel is designed on operating pressure of 1.5 Mpa (a). The core is located at bottom and four primary heat exchangers are arranged on the periphery in the upper part of the vessel.On the top in the vessel there is a cavity for self-pressurized.

The contaiment is designed to surround closely to the reactor vessel and can stand high pressure.

There is a long riser on the top of the core to enhance natural circulation. and the control rod position sensors are also placed there.

There are 16 fuel assemblies and 13 control rods in the core as shown in Fig.2.

Two kinds of assemblies are used, one consists of 96 fuel elements and another consists of 35 fuel elements. The fuel element with zircaloy-4 clading has an active length of 690mm and a diameter of 10mm. The nuclear fuel is uranium dioxide with 3% enrechment.

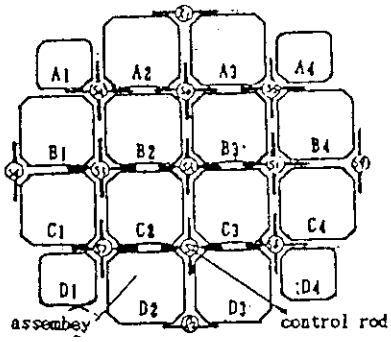

Fig.2 Cross section of EHR—5 core

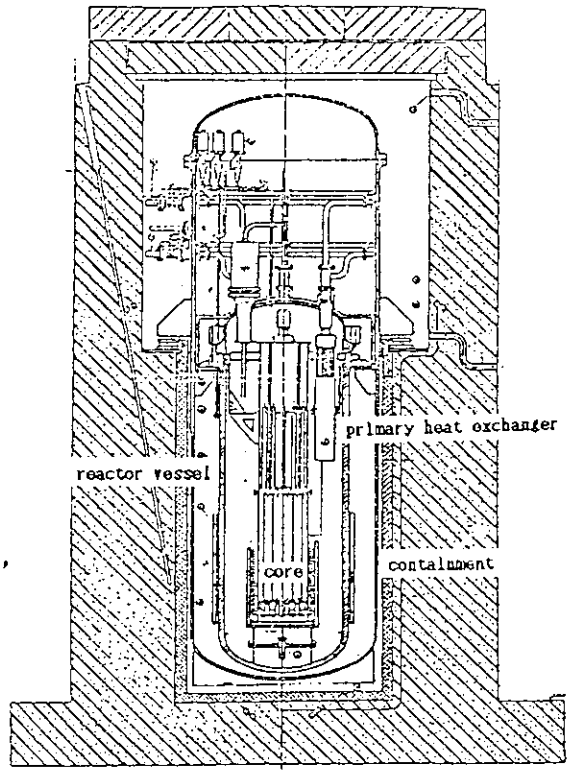

Fig.1 The reactor structure with dual vessel

The reactivity is controlled bya combination of fixed burnable poison, movable absorb rods and the negative reactivity coefficient which isgiven in table 1. There are 4 fuel rods containing burnable poison of 1.5% Gd_2O_3 in the core. The movable absorb rod is made of boron carbite with metal-clading thathave the shape of the cruciform.

Table 1. Various Reactivily coefficient

term	unit	value
fuel temperature coefficient	mk／℃	−0.0162
moderator temperature coefficent	mk／℃	−0.37 (1)
void coefficient	mk／1%	−2.20
pressure coefficient	mk／bar	+0.35 (2)

(1) messured value
(2) estimated value

The control rod drive is a new type of hydraulic driving system which consist of a actuating loop outside the containment, and step cylinder in the core and control unit. The control rods can be dropped into the core by gravity when reactor shutdown is needed.

A reserve reactor shut down system is provided by injection system of borate solution that can be injected into the core in the event of ATWS.

The cooling system of EHR-5 is composed of three circuits - the primary circuit housed in the reactor vessel, a intermediate circuit and heating grid. The intermediate circuit between the primary circuit and heating grid can keep the heating grid free of radioactivity, its operating pressure is higher than primary circuit. The cooling system is shown in Fig.3. Heat genarated in the

core is transfered to heating grid through both the primary heat exchangers and intermediate heat exchangers.

The residual heat removal system is connected to the intermediate circuit.

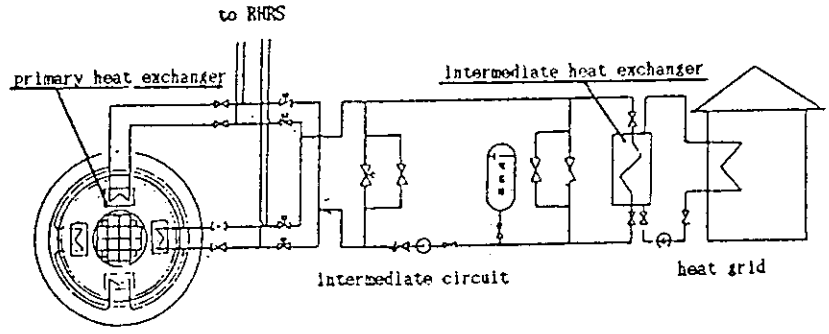

Fig.3 The cooling system of EHR－5

The operation parameters at power of 5MW is given in table 2.

Table 2. Operation parameters at 5MW

thermal power	MW	5
pressure of primary circuit	MPa	1.5
core outlet temperature	℃	186
core inlet temperature	℃	151
Intermediate circuit		
pressure	MPa	1.7
flow rate	t／hr	95
outlet temperature	℃	143
inlet temperature	℃	100
flow rate of Heating grid	t／hr	154
supply water temperature	℃	82
return water temperatare	℃	56

THE OPERATION CHARACTERISTICS OF EHR-5[2]

Above the liquid level in reactor vessel there is a cavity for self-pressurization. The operation pressure in the vessel is formed by both partial pressure of inert gas and steam that corresponds to the outlet temperature of the core. The partial pressure of gas can keep the coolant subcooling at the core outlet. This operation mode is called as pressurized water operation mode. Following experimental studies are carried out at this mode.

1. The Regulation Test of Coolant Water Level and Gas Partial Pressure of Primary Circuit

Both supplement gas and coolant into reactor vessel are significant for reactor operation. The experimental results are shown in Fig.4 and Fig.5.

As result of supplement of gas into the vessel, the primary circuit pressure was increased. The reactor power increased with increase in pressure and came to a peak, after that, it begins to decrease by coolant temperature increasing and finally reached at a new stable state.

In this process of supplement gas into vessel, the power peak inereased about in 5.7%, the core inlet and outlet temperature rised 1.1℃ and 1. 4℃ respectively.

The variation of reactor power indicate, there is certain void content in the core at operation condition. Pressure coefficient was estimated by the change of coolant temperature at the new stable state.

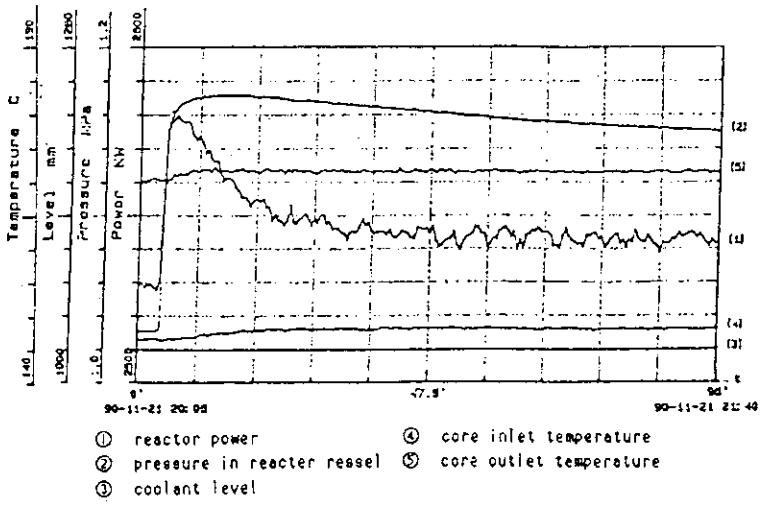

Fig.4 Gas supplement into reactor vessel

Water supplied into the primary circuit via purification system is reheated and enters to the downcomer and then into the core.

The volume above the liquid level of reactor vessel decreases due to the level rising, so that the pressure increases. The core inlet temperature has a slight decrease. Owing to mentioned reasons the reactor power increases.

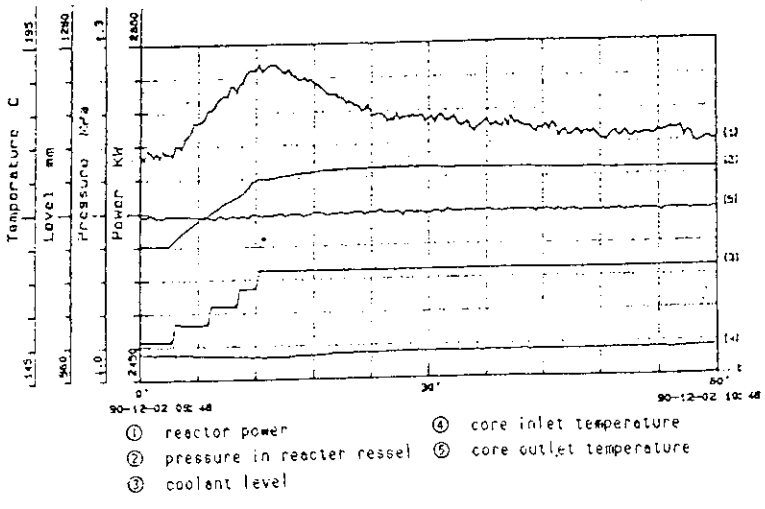

Fig.5 Coolant water supplement into reactor vessel

Although the speed and quantity in supplement water and gas into reactor vessel have some difference. the system parameters have some changes with the same way

2. Self-stability Feature

The Self-stability of EHR-5 is a inherent safety capability that can bring itself to a new stable state safely under the reactivity inserted.

This experiment has been carried out with introducing reactivity of 2mk by a control rod withdrawing two steps.

In this case, reactor power increased rapidly due to introducing a large reactivity and reached at a maximum relative value of 1.18 in 100 seconds. then began to decrease, and reached to a new stable value of 1.08 in 30 minuts.

The core inlet and outlet temperature add an increment of 3.8℃ and 4.2℃

respectively. The primary system pressure adds in an increment of 0.102MPa.
These experimental results are illustrated in Fig.6.

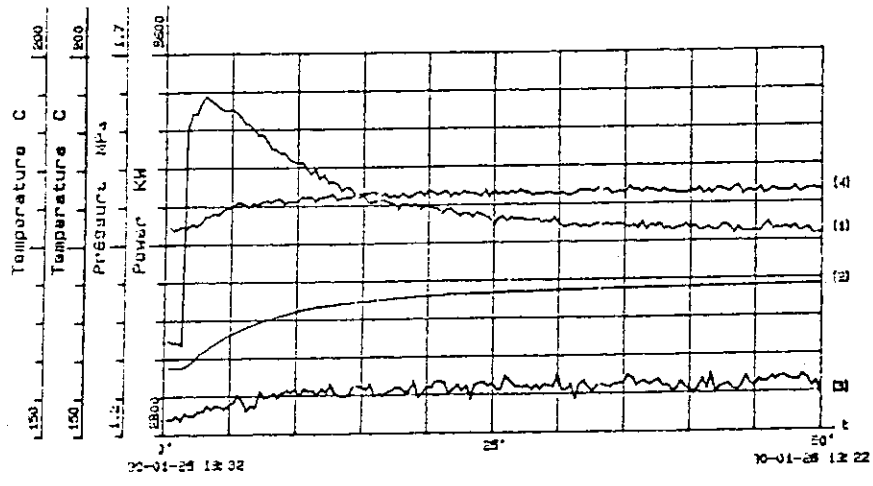

Fig.6 The transient of inserting reactivity of 2mk

3. Self-regulation Feature

Self-regulation of EHR-5 is the capability that can make the reator power to follow the change of the heating load.

Under the normal operation condition, the flow rate in intermediate circuit is always kept constant. By means of adjusting its bypass flow rate, the flow rate passing through the intermediate heat exchanger can be varied, and hence the heating load is also changed. In this experiment the flow rate was changed from 8t／hr to 35t／hr and then recoveried to 8t／hr. Fig. 7 shows the experimental result.

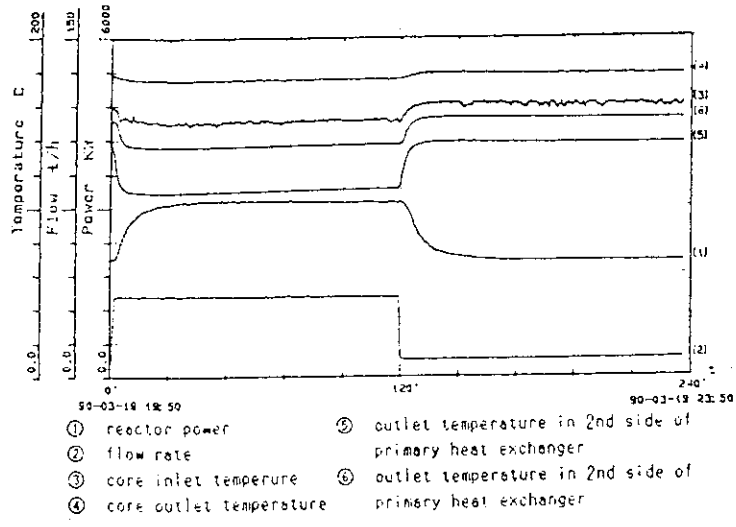

Fig.7 The feature of self-regulation at EHR—5

The inlet temperature in the secondary side of the primary heat exchanger changed rapidly no more than 10 seceonds as the flow rate changed, and then the core inlet temperature started to vary at about 60 seconds. The reactor power started to vary at 90 seconds and came to a new stable state in 30 minuts. The temperature coefficienf of moderator plays main role in this process.

The results have shown that the reactor power can follow large load changes properly based on its self-regulation capacity without any operator action.

THE OPERATION SAFETY OF EHR-5

The inherent safety is based on natural laws to garentee the reactor safety. The most important things are that the reactor has a passive capability to shutdown and to remove residual heat.

1. Residual Heat Removal System

The residual heat removal system (RHRS) is composed of three natural circulation loops, i.e. the first is the loop between primary heat exchanger of intermediate loop side and the vapourizer in RHRS, the second is the vapour-condensation circulation between the vessel side of vapourizer and air-cooler, and the third is the circulation between the air-cooler and the ultimate heat sink-atmosphere. The RHRS is shown in Fig.8.

Some important experiments have been completed in commissioning[3] and operation stage. The results obtained from these experiment are as follows:

(1) The first circulation can be set up at normal or abnormal condition.

(2) The condition to set up the second circulation is to discharge the air in the vessel side of vapourizer at its high temperatare.

(3) The reactor can be brought to cold shutdown state by the RHRS.

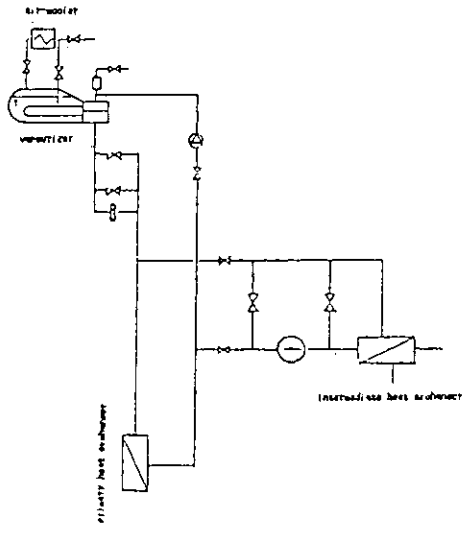

Fig.8 The residual heat removal system

2. The Experiment of ATWS

The loss of main heat sink-ATWS experiment has been conducted under 40% of power level. The experimental result is shown in Fig.9.

In this transient, the reactor power automatically and safely decreased from 2MW to about 0.2MW which is a new stable state in about 30 minuts. At the stable state, the core inlet and oulet temperatures added in increment of 20.4℃ and 4.7℃ respectively, the liquid level in reactor vessel increased an addion of 50mm, and the

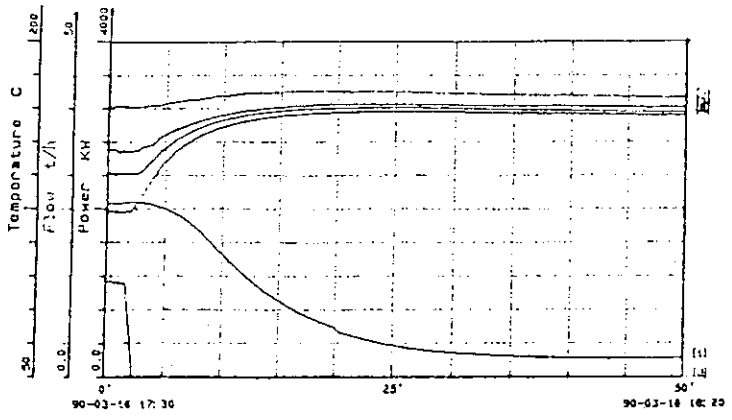

Fig.9 The transient of loss main heat sink without shutdown

primary system pressure rised an increment of 0.233MPa. All of these parameters changed smoothly in this transient.

CONCLUSION

All of these experiments proved that EHR-5 has excellent operation and safety features which are presented as follows:

EHR-5 is regarded as a ability of responding perfectly to all trasients without any operator action.

EHR-5 has a capabilify to shutdown passively and to remove decay heat on natural circulation.

The reator structure of EHR-5 can keep the core covered with water under any design basis accidents.

As mentioned descussion indicates, that EHR-5 is a new type of reactor with higher degree of inherent safety. It would be as more safe, clean and economic energy source for district heating.

REFERENCES

1. "Finall Safety Analysis report of EHR-5" INET Document March, 1988.
2. Zhang Dafang, et al. "Experimental Report on the Operational Characteristics of the EHR-5" INET Document, April, 1990.
3. Zhang Dafang, et al. "The Experimental study for Residual Heat Removal System in EHR-5" Nuclear power Engineering Vol.12, NO.2, Apr. 1991.

9. Higher Power TRIGA Research Reactors

J. T. Ganley, G. B. West, W. L. Whittemore

General Atomics
San Diego, California, U.S.A.

ABSTRACT

The 65 TRIGA reactors and reactors refueled with TRIGA fuel have had a wide range of power levels (10 kW to 14 MW). Many of the higher power reactors ($P \geq 1$ MW) have benefitted from use of long lived TRIGA LEU fuel. All the well recognized TRIGA safety features are retained. For improved reactor performance the standard square fuel cluster can be redesigned to provide a hexagonal array with improved utilization of cooling water. The result can be higher power densities and hence higher neutron fluxes for the same reactor power. TRIGA research reactors with 5 to 10 MW power levels and higher power densities can provide in-core thermal neutron fluxes in excess of 3×10^{14} n/cm^2.s and reflector neutron fluxes available for beamports in excess of 10^{14} n/cm^2.s.

INTRODUCTION

The uranium zirconium hydride (U-ZrH$_x$) fuel is the fundamental feature of the TRIGA family of reactors that accounts for its widely recognized safety, good performance, economy of operation, and its acceptance worldwide. Of the 65 TRIGA reactors or TRIGA fueled reactors, several are located in hospitals or hospital complexes and in buildings that house university classrooms. These examples are a tribute to the high degree of safety of the operating TRIGA reactor. In the early days, the majority of the TRIGA reactors had power levels in the range from 10 to 250 kW, many with pulsing capability. An additional number had power levels up to 1 MW. By the late 1970s, 7 TRIGA reactors with power levels up to 2.0 MW had been installed. A reduction in the rate of worldwide construction of new research reactors set in during the mid 1970s but construction of occasional research reactors has continued until the present.

Starting in the early 1980s and even before, an interest developed in the larger power TRIGA reactors. The 14-MW Romanian research and test reactor was commissioned during the interval October 1979 to March 1980. In 1986 and 1988 3.0 MW TRIGA reactors were installed in Dhaka, Bangladesh and Quezon City, Philippines. Under construction at present are two new TRIGA reactors at the University of Texas and in Rabat, Morocco as well as an upgrade from 1.0 to 3.0 MW at Taipei, Taiwan.

Table 1 illustrates the recent TRIGA reactors with power levels above 1 MW including those presently (1991) under construction or conversion.

TABLE 1
RECENT HIGHER POWER TRIGA REACTORS

Date	Power (MW)	Site
under construction	1.5	Rabat, Morocco
under construction	1.1*	University of Texas
under conversion	3.0	Taipei, Taiwan
1986	3.0*	Dhaka, Bangladesh
1988	3.0*	Quezon City,Philippines
1979	14.0	Pitesti, Romania

*with pulsing capability

PERFORMANCE OF HIGHER POWER TRIGA REACTORS

The excellent performance of the half-inch diameter TRIGA fuel during the ten-year operational history of the Romanian reactor and the high burnup tests of TRIGA LEU fuel at Oak Ridge under the RERTR program provide the basis for higher power and higher power density operation of TRIGA reactors. A 5 MW reactor with these LEU TRIGA fuel elements arranged in a hexagonal pitch can provide high thermal fluxes ($\sim 10^{14}$ n/cm^2.s) for beam ports and in-core irradiation. The same core can also provide fast neutron (>0.1 MeV) and thermal neutron fluxes of $>10^{14}$ n/cm^2.s for sample irradiations.

The performance of the higher power TRIGA reactors with their consequent need for longer core life has been facilitated by the early development of TRIGA LEU fuel. The development of higher uranium loaded TRIGA fuel with low enriched uranium (TRIGA-LEU fuel) started in 1978 (1). It is characterized as higher loaded fuel because the standard, basic TRIGA U-ZrH_x fuel has always utilized low enriched uranium and contains 8.5 wt-% U with an enrichment of 19.7 - 19.9%. The higher loaded TRIGA LEU fuels contain either 20, 30, or 45 wt-% U each with the above enrichment. An important aspect of the TRIGA-LEU fuel is the fact that the presently manufactured highest loaded fuel with 45 wt-% U has a uranium volume fraction of only about 20%. This compares with about 50 vol-% uranium in the present LEU silicide fuels which is near the manufacturing limit.

General Atomics was a participant in the RERTR program since its inception (1). It tested the above mentioned range of fuel loadings (20, 30 and 45 wt-% U) in the ORR to burnup values reaching about 65% averaged over the entire fuel rod. A number of tests on LEU fuel were also conducted in the TRIGA Mark F reactor in San Diego. Sales of TRIGA-LEU fuel began in 1979 and the first deliveries were made in 1980. Table 2 presents a summary of TRIGA-LEU fuel usage to date.

Operating Performance. The 3 MW TRIGA reactor in Bangladesh with its LEU fuel (20 wt-% - 20% enriched, erbium burnable poison) is an example of a higher power TRIGA Mark II reactor (2, 3). Measurements of neutron flux in the central water-filled thimble have given values of 1.07 x 10^{14} n/cm^2.s (thermal) and 2.51 x 10^{13} n/cm^2.s (epithermal). As another example, the Philippines research reactor was converted to TRIGA LEU fuel and upgraded to 3 MW using four-rod fuel clusters of 20-20 LEU TRIGA fuel. Both of these 3 MW reactors have pulsing capability. An example of a still higher power research and test

TABLE 2
OPERATIONS WITH TRIGA LEU FUEL

Location	Reactor (LEU start date)		Wt-% Enrichment
San Diego	Mark F (1978) testing	1/2-inch	45-20
		1-1/2-inch	20-20
			45-20
	Mark F (1989) reload		30-20
Oak Ridge	ORR (1979) testing		20-20
			30-20
			45-20
Taiwan	MTR Conversion (began stepwise 1977) Full TRIGA Core 1987		20-20
Thailand	MTR Conversion (1980) Reload		20-20
Yugoslavia	TRIGA Mark II (1983) Reload		20-20
Malaysia	TRIGA Mark II (1982) Reload		20-20
Philippines	MTR Conversion (1986) Full Core		20-20
Bangladesh	TRIGA Mark II (1986) Full Core		20-20
Romania	14 MW Reload Fuel Available to replace HEU fuel stepwise		45-20

reactor is the 14 MW TRIGA reactor (licensed for 16.5 MW) installed in Pitesti, Romania. The multipurpose nature of this installation is indicated by the following:

- six in-core test locations [3 large (17.5 x 17.5 cm^2) and 3 small (8.75 x 8.75 cm^2)]
- two horizontal beamports (tangential, radial)
- large beam room
- Numerous irradiation facilities in beryllium reflector blocks
- 14 MW power level
- Annular Core Pulsing Reactor with its large central pulsed fuel test facility and two horizontal beamports located in same reactor tank

The 14 MW Romanian reactor was specifically designed to test in-core fuel assemblies and loops. The core was designed to produce specified fluxes in the several in-core locations with experiments in place. The core configuration is therefore not optimum for the production of maximum in-core and leakage fluxes. Nevertheless, it may be of interest to report the fluxes predicted for the core configuration but without experiments. The fast flux ($E>9$ keV) in an air-filled central experimental region is calculated to be 1.63×10^{14} n/cm^2.s. The corresponding thermal flux ($E<0.4$ eV) in the water-filled, central experimental region is calculated to be 2.75×10^{14} n/cm^2.s. The measured thermal flux was 2.65×10^{14} n/cm^2.s.

HIGHER POWER DENSITY REACTOR CORES

The design to reach the higher power densities, especially for neutron beam experiments with research reactors, is straightforward: use a compact core with limited or no in-core voids or experiments and a fuel array that provides for optimal cooling. Designs for such higher power density TRIGA cores have been based on the 0.543-inch (13.8 mm) and 0.359-inch (9.14 mm) diameter TRIGA LEU fuel rods. Starting with the design using the 0.543-inch diameter TRIGA-LEU fuel rods in a 16-rod square array, we have improved the design by use of a triangular pitch for the fuel rods. While a hexagonal array of 7 or 19 fuel rods is possible, the latter is probably to be preferred because of the reduced number of fuel clusters to be handled.

In designing for the higher power densities (hence higher neutron fluxes), the power level is relatively unspecified. For example, a 5 MW reactor with a large core will have a lower power density whereas a much smaller core operating at the same 5 MW will have a substantially increased power density. For the designs using TRIGA-LEU fuels, the limit in increased power densities will be set by the maximum allowable operating fuel temperatures and not primarily by the reactor power.

Several concepts for higher power densities have been evaluated based on the above ideas. In one case for a 2 MW research reactor which had typically 20 plate-type fuel clusters, the proposed core would be nine 16-rod TRIGA LEU fuel clusters (45 wt-%, 20% enriched, erbium) with the remainder of the core positions filled with beryllium reflector elements. The core lifetime would be greater than 1110 MWD. At 2 MW, the peak thermal neutron flux between the beryllium and the location of the beamports would be 2.9 x 10^{13}n/cm^2.s.

For the higher power TRIGA reactors (P $\geq$5 MW) and increased power densities, we have compared the performance parameters of the standard water reflected 10 MW TRIGA reactor using a square array of 16-rod TRIGA LEU fuel (6) with those predicted for a hexagonal array of the same (13.8 mm rod diam.) fuel with a beryllium reflector. Table 3 presents these data. Two hexagonal configurations of fuel rods were considered, one that retained the same basic water volume fraction in the fuel cell and one that retained the same minimum spacing from the square array (e.g. 0.101 inches or 0.26 mm). At the same 10 MW power level, the major difference in core configuration is the reduced core size (30 x 16 rods versus 16 x 19 rods). For the compact HEX cluster the increased peak fuel temperature (750°C) is still within the acceptable operating limit. As can be seen, the fast neutron flux (E >0.1 MeV) is substantially increased (2.1 x 10^{14} versus 1.4 x 10^{14} n/cm^2.s) as is the thermal neutron flux in the reflector (1.7 x 10^{14} versus 1.0 x 10^{14} n/cm^2.s). The thermal flux leaking into the beamports is correspondingly improved but was not calculated directly in this study although it should be similar to that in the reflector region. The in-core thermal flux in water filled locations depends on the core location and size. The values in Table 3 are for somewhat different condiitons but indicate that a compact HEX array core will provide a peak thermal flux of more than 3 x 10^{14} n/cm^2.s at a power level of 10 MW. Also included in Table 3 are data for the smaller diameter fuel rod (9.1 mm) as used in a 25 MW research reactor. Although calculations have not as yet been made to evaluate the improvements to be expected through the use of a 19-rod hexagonal fuel array with this smaller diameter fuel, it is expected that this approach for fueling a 10 MW TRIGA reactor can increase the power density still further than that in the 25 MW reactor because the smaller fuel diameter will result in better cooling and reduced peak fuel temperature compared to the 13.8 mm diameter fuel rod diameter.

Although the calculations and comparisons were mainly for a 10 MW TRIGA core, it may be noted that designs are possible to maintain similar power densities (hence neutron fluxes)

at lower power levels at, for example, 5 MW. The exact reactor power level will also depend on other requirements such as desired number and size of in-core irradiation locations.

TABLE 3

Comparison of Higher Power Density TRIGA
LEU Fuel Performances at 10 MW
(smaller diameter fuel performance at 25 MW shown for comparison)

Parameter	16-rod square cluster	19-rod HEX cluster	19-rod HEX compact cluster	36-rod square cluster
Power (MW)	10	10	10	25
Fuel Diam. (mm)	13.8	13.8	13.8	9.1
(U-ZrH/water) ratio	0.856	1.01	1.41	0.794
Minimum rod spacing (in.)	0.101	0.149	0.101	0.080
Cluster dimensions (mm) (flat to flat)	75.7 x 79.6	80.37	74.97	72.14 x 72.14
Clusters	30	16	16	40
Reflector	H_20	Be	Be	Be
$\hat{T}_{fuel}$ (°C)	640	750	750	708
$\hat{\phi}$ (>0.1 MeV)(n/cm^2.s)	1.4x10^{14}	1.7x10^{14}	2.1x10^{14}	2.0x10^{14}
$\hat{\phi}_{th}$ in Reflector	1 x 10^{14}	1.5x10^{14}	1.7x10^{14}	1.2x10^{14}
$\hat{\phi}_{th}$ in central H_20 trap	3 x 10^{14}	2.9x10^{14}	~3.6x10^{14}	4.3x10^{14}

CONCLUSION

The extremely safe TRIGA fuel, including the more recent TRIGA LEU fuel, offers a wide range of possible reactor configurations. A long core life is assured through the use of a burnable poison in the TRIGA LEU fuel. In those instances where large neutron fluxes are desired but relatively low power levels are also desired, the 19-rod hexagonal array of small diameter fuel rods offers exciting possibilities. The small diameter fuel rods have provided extremely long and trouble-free operation in the Romanian 14 MW TRIGA reactor.

REFERENCES

1. G. B. West and R. H. Chesworth, "Update on World-Wide Use of TRIGA-LEU Fuel Including Loss of Flow Tests," RERTR Annual Meeting, Rhode Island, September 1990.

2. M. A. Mannan, M. Hossain, "Characteristics and Facilities of a 3 MW LEU FUELED TRIGA Reactor," Proc. ASRR-I, November 1986, p. 82-93.

3. M. A. Mannan, M. Hossain, and W. Whittemore, "Facilities and Utilization of the Bangladesh Multipurpose 3 MW TRIGA Reactors", Proc. on Multipurpose Research Reactors, IAEA Symp. Grenoble, October 1987, p 339-347.

4. W. L. Whittemore, "Startup Testing of Romania Dual-Core Test Reactor," Seventh Biennial U.S. TRIGA Users' Conference, GA Document TOC-12, March 1980, p 4-30 to 4-37.
5. M. Ciocanescu, et:al., "10 Years of Operating Experience at Steady State Reactor in Romania", Eleventh European TRIGA Users Conference, GA Document TOC-22, p 1-61 to 1-71.

6. "10 MW TRIGA-LEU Fuel and Reactor Design Description", GA Document UZR-14 (Rev), October 1979.

10. Application of Digital Process Controller for Automatic Pulse Operation in the NSRR

K.ISHIJIMA(*), T.UEDE(**), M.SAIGO(**)

(*) Department of Fuel Safety Research
Tokai Research Establishment, JAERI
Tokai-mura, Naka-gun, Ibaraki-ken 319-11, Japan
(**) Nuclear Engineering Department
Nuclear Power Division, Fuji Electric Co., Ltd.
Tanabeshinden 1-1, Kawasaki-ku, Kawasaki-shi 210, Japan

ABSTRACT

The NSRR at JAERI is a modified TRIGA Reactor. It was built for investigating reactor fuel behavior under reactivity initiated accident (RIA) conditions. Recently, there has been a need to improve the flexibility of pulsing operations in the NSRR to cover a wide range of accidental situations, including RIA events at elevated power levels, and various abnormal power transients. To satisfy this need, we developed a new reactor control system which allows us to perform "Shaped Pulse Operation: SP" and "Combined Pulse Operation: CP". Quick, accurate and complicated manipulation of control rods was required to realize these operations. Therefore we installed a new reactor control system, which we call an automatic pulse control system. This control system is composed of digital processing controllers and other digital equipments, and is fully automated and highly accurate.

INTRODUCTION

The Nuclear Safety Research Reactor (NSRR) at the Japan Atomic Energy Research Institute (JAERI) is a modified TRIGA-ACPR (Annular Core Pulse Reactor). It was built to investigate reactor fuel behavior under reactivity-initiated accident (RIA) conditions, and went to the initial criticality on May 1975. The NSRR is open pool type water cooled reactor and its reactor core is mounted on the bottom of an open pool 3.6m wide 4.5m long and 9m deep. The reactor core contains 149 driver fuel rods, 8 control rods with fuel-followers (2 safety rods and 6 regulating rods) and 3 transient rods with air-followers.

The NSRR was capable of performing pulsing operations with a reactivity insertion of up to $4.7 (licensed limit). Such pulsing operations were realized by withdrawing 3 transient rods pneumatically. The maximum peak reactor power of 21,000MW (the licensed limit is 23,000MW) and the maximum burst energy of 117MWs (the licensed limit is 130MWs) were

attained when a reactivity of $4.67 was inserted. This type of pulsing operation can simulate an RIA event only from nearly zero power. We call this operation "Natural Pulse: NP". The NSRR could also operate in a steady state (SS) mode of up to 300kW.

Recently there has been a need to improve flexibility of pulsing operations in the NSRR to cover a wide range of accidental situations, including RIA events at elevated power levels, and various abnormal power transients. To satisfy this need, we developed a new reactor control system for the NSRR, including the modification of nuclear instrumentation and control-rod drive mechanisms. The new control system allows us to perform "Shaped Pulse Operation: SP" and "Combined Pulse Operation: CP".

As illustrated in Table 1, SP is a power transient of from a few seconds to a few minutes long of up to 10MW produced by fast movement of the 6 regulating rods. CP is a combined SP and NP power transient produced by fast movement of the 6 regulating rods and quick withdrawal of the 3 transient rods. Reactivity insertion with transient rods during CP operation is limited to $4 and burst energy during SP and CP operation is limited to 110MW.

Table 1 NSRR Operation Modes and Reactor Power Characteristics

Operation Modes	Reactor Power Behavior		Research Items
1. Steady State Operation	Steady State	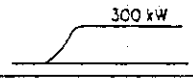	Fuel Relocation
2. Natural Pulse Operation	Pulse from Zero Power	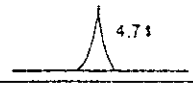	Fuel Behavior in an RIA from Cold Start-up Molten Fuel-Coolant Interaction
3. Shaped Pulse Operation	Power Decrease from High Power	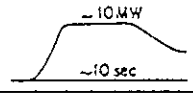	Fuel Relocation and Coolability
	Power Increase from High Power	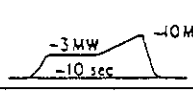	Fuel Behavior during Power Ramping
4. Combined Pulse Operation	Pulse From High Power	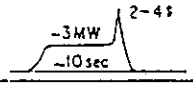	Fuel Behavior in an RIA from Rated Power
	Pulse from Zero Power / High Runout Power	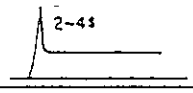	Debris Coolability

MODIFICATION OF REACTOR CONTROL SYSTEM

To realize SP and CP operations, it is necessary to overcome the large and prompt negative temperature feedback which is unique feature of the TRIGA type reactor. Quick, accurate and complicated manipulation of the control rods is required to overcome such feedback. SP and CP operations are too dangerous to perform manually. Therefore, we developed a fully automated and computerized reactor control system. We call this control system an automatic pulse control system. Fig. 1 shows the modified reactor control system for the NSRR, including this fully automated and computerized control system.

Reactor control equipment and safety circuits are installed in a reactor operation console and a reactor control auxiliary panel. The console and panel are located in the control room.

The reactor operation console is equipped with indicators, recorders and lighting displays necessary for monitoring reactor operating conditions. Several switches necessary for control rod drive, operation mode changing, manual scram, automatic operation starting, etc. are also located on the reactor operation console. All equipment necessary for normal operation is on the reactor operation console, so that reactor operations can be conducted by only one operator.

AUTOMATIC PULSE CONTROL SYSTEM

The automatic pulse control system automatically controls reactor power during SP and CP operations. The system has the following functions.

- During SP and CP operations, bank driving of the control rods is performed according to operation data : distances of control rod movement or reactor power as a function of time.
- During CP operation, the rapid withdrawal of transient rods is performed with operation data : timing of withdrawal.

Important requirements conditions for the automatic pulse control system are that all calculations must be performed at high speeds (sampling cycle of less than 10ms) and that control rod movement must be highly accurate (accuracy of position control to within 0.1%), to realize power pattern operation intervals of several to several tens of seconds.

To satisfy the accuracy requirements of automatic pulse operation, we adopted the following two control methods. In one control method, called "open loop control"(OL), the regulating rods move according to a position demand signal from the computer without any feedback as a function of time. In another control method, called "closed loop control" (CL), the computer sends a reactor power demand signal as a function of time. Movement of the regulating rods is controlled with reactor power feedback. A power regulating circuit in the CL loop is capable of calculating PID gain digitally and giving a feed-forward gain proportional to reactor power demand. We can use any combination of OL and CL in sequence in SP and CP operations. Timing of control method changeover and initiation of transient rod withdrawal during CP operations are also controlled by the computer.

Fig. 2 shows a block diagram of the automatic pulse control system. One of the unique features of this control system is the introduction of digital control equipment. All of the reactor operation data are supplied to the computer in the control demand release circuit with a floppy disk. No manipulation of the control rods by an operator is necessary during SP or CP operations.

The control demand release circuit calculates and sends reactor power, rod drive speed and transient rod withdrawal signals in accordance with the operation data. The control demand release circuit is a PMS-200, which is a computerized process controller developed by Fuji Electric. The PMS-200

has a CRT-display unit and a floppy disk input-output unit. The process control programs and display programs are run in parallel. We can set several sampling speeds for the control program according to the control speed. The minimum sampling cycle is 10ms, which allows the high speed control required for NSRR pulse operation. Data from the control demand release circuit to the power regulating circuit are sent by a dedicated data way called a MC-BUS. The data refresh cycle of this data way is also 10ms. Operation data input by floppy disk are confirmed on the CRT. The control demand data necessary during pulse operation are calculated with input data and stored before beginning on-line operation. During on-line operation the control demand release circuit sends only necessary control demand data and, so makes possible high speed control.

The power regulating circuit works like a PID controller in case of normal feedback control. We use not only a normal PID calculation but also additional compensation with reactor power demand called feed-forward control. This circuit needs high speed processing too, that is, a sampling time of 10ms. To satisfy this requirement we use a computerized process controller called the HDC-100 developed by Fuji Electric. Reactor power demand data are sent from the control demand release circuit through a MC-BUS and compared with real reactor power data. PID calculations are made with the difference of reactor power demand and real reactor power.

The stepping motor control circuit was developed especially for the NSRR. This circuit sends pulse signals to the stepping motor drive circuit according to speed demand signals from the control demand release circuit or the power regulating circuit. Fig. 3 shows a block diagram of this circuit. A smooth, high-speed startup (startup to maximum 2500pps within 10ms), as well as highly accurate speed control, are realized with this circuit.

SOFTWARE PROGRAM FOR CONTROL DEMAND RELEASE CIRCUIT AND POWER REGULATING CIRCUIT

There are two categories of control demand release circuit programs: initial processing programs and automatic operation programs. An initial processing program works before beginning on-line operations. And an automatic operation program works during real time on-line operations.

An initial processing program performs the following. (Complicated calculations that require a long processing time are basically made in this program.)

Calculations of OL data ;
- Bank rod drive distances.
- Bank rod drive speed.
- Pulse numbers required to speed up or slow down.
- Other calculations.

Calculations of CL data ;
- Changing rate of reactor power for each control step.
- Other calculations.

Confirmation of data acceptability ;
- Bank rod drive speed for OL.

- Control rod position.
- Duration of operation.
- Number of control steps.
- Other confirmations.

The automatic operation program directs the progress of operations and confirms operating conditions during automatic pulse operation. The program consists of

- Control operating steps.
- OL processing.
- CL processing.
- Processing of control method change from OL to CL.
- Processing of control method change from CL to OL.
- Transient rod withdrawal signal production.
- Processing to finish automatic pulse operation.

There are no complicated calculations in this program. It sends control demand data calculated with the initial processing program.

The power regulating circuit basically performs only control data calculations during CL operations in order to realize a high-speed sampling cycle. The reactor power demand signal comes from the control demand release circuit through a MC-BUS in real time and the real reactor power comes from the nuclear instrumentation system for the calculation.

OPERATING PROCEDURE OF AUTOMATIC PULSE OPERATION

Fig. 4 shows the overall flow of operation. A SP or CP operation is directed and automatically performed by the computer in the automatic pulse control system based on the data stored on a floppy disk.

Fig. 5 shows an example of operation procedure obtained with a combination of OL, CL, transient rod withdrawal and automatic control rods insertion.

In this example, the reactor was first operated in a steady state and then changed over to combined pulse operation. When the start button is pushed, automatic pulse operation starts and regulation rods are withdrawn up to the prescribed position within the prescribed time. The reactor power then begins to rise. When the reactor power reaches the prescribed power P_1, the CL starts automatically and keeps reactor power at demand power levels until time t_1. At time t_1 reactor power is raised rapidly to high power P_2 until time t_2 with CL.(The maximum rise rate is from 1MW to 10MW within 2 seconds.) The high power P_2 is maintained until the time t_3 with CL, and the transient rods are withdrawn at time t_3 according to the withdrawal signal from the control demand release circuit. If reactor protection interlocks are activated, transient rod withdrawal is prevented and reactor is stopped by the automatic control rod insertion circuit. When a certain interval passes after transient rod withdrawal, the regulating rods are entirely inserted according to the operation schedule. When reactor power reaches a low level, the operation mode is shifted to steady state operation and the reactor is shut down.

The duration of the automatic operation is limited by the integrated reactor power and fuel temperature rise, so that almost all automatic pulse operations must be limited to from several to several tens of seconds. The control of this sort of complicated operation cannot be conducted by hand and, so, fully automatic operation is required.

EXAMPLES OF SP AND CP OPERATIONS

Fig. 6 illustrates a typical SP operation (shift from constant high power operation to steady state operation). In this case, reactivity of ¢80 is inserted within 1 second using OL of the regulating rods. They are kept in position for 13 seconds to wait for the increase of reactor power to about 1MW. Then the control method is changed from OL to CL to keep reactor power exactly at 1MW for 3 seconds. The CL method allows reactor power to be increased from 1MW to 9MW within 2 seconds and reactor power to be kept at 9MW for 5 seconds. The control method is then changed again from CL to OL to insert regulating rods to the 200 unit level to decrease reactor power quickly to shift from SP to steady state operation.

A typical example of CP operation is shown in Fig. 7. In this case, the high power level of 3MW is maintained for 5 seconds according to almost the same procedure shown in Fig. 6. The control method is then changed from CL to pulse operation to withdraw transient rods pneumatically. Maximum reactor power reached about 2,000MW when a reactivity of $2 was inserted in this operation.

As shown in these examples, the SP and CP operations newly developed for the NSRR have very stable characteristics. Especially, overshoots of reactor power with the CL method were always less than 3% of the desired power level even when the power increase rate of 4.5MW/s (from 1MW to 10MW for 2 seconds) was tried. These stable characteristics are due to the properties of TRIGA reactors, which have a large and negative prompt temperature feedback, and the design of the automatic pulse control system, which takes the characteristics of the NSRR into account.

SUMMARY

New reactor control systems for NSRR have been designed to simulate various types of power transients. They have been used to simulate LWR abnormal power transients to confirm the safety of LWR fuel, and to simulate FBR overpower transients to confirm the safety of FBR fuel. A new test program to study fuel behavior with slow power transients and RIA events at high power levels has been started using SP and CP operations.

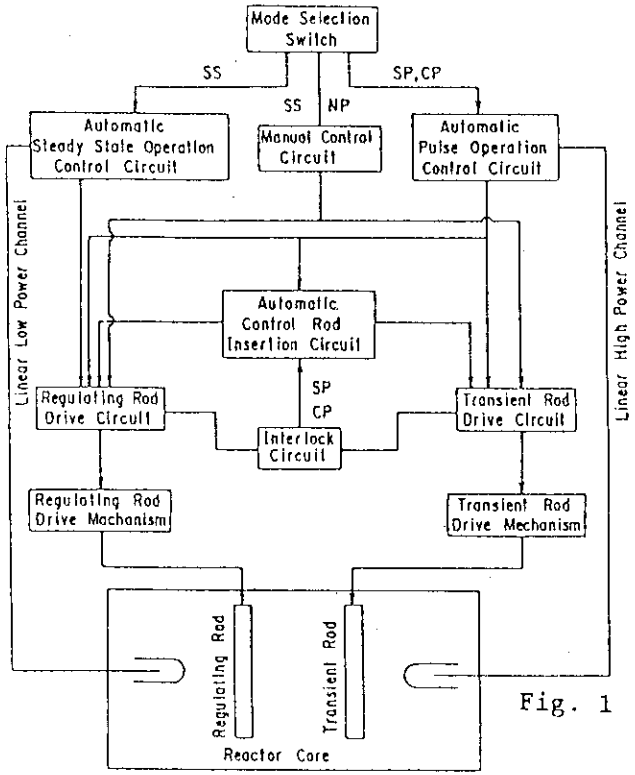

Fig. 1 Modified Reactor Control System of the NSRR

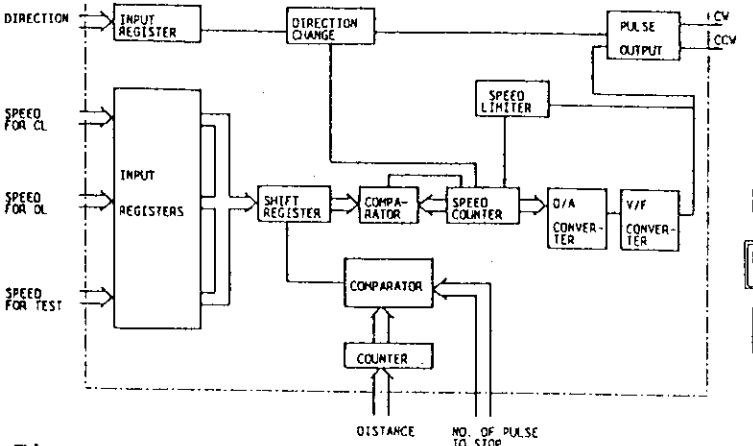

Fig. 3 Block Diagram of Steeping Motor Control Circuit

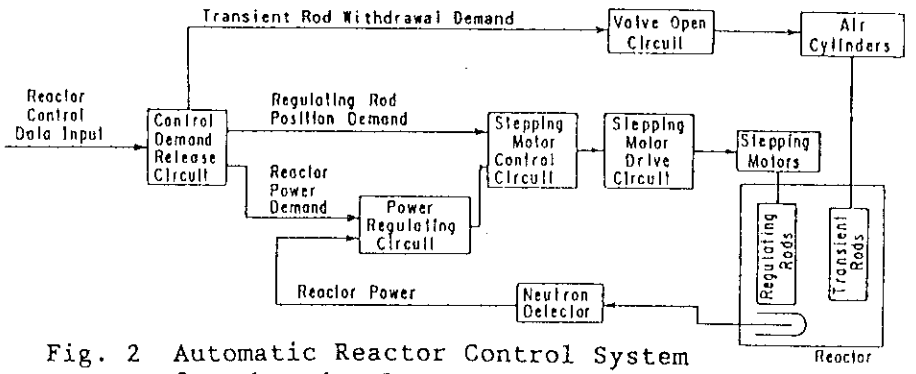

Fig. 2 Automatic Reactor Control System for Shaped Pulse Combined Pulse Operation

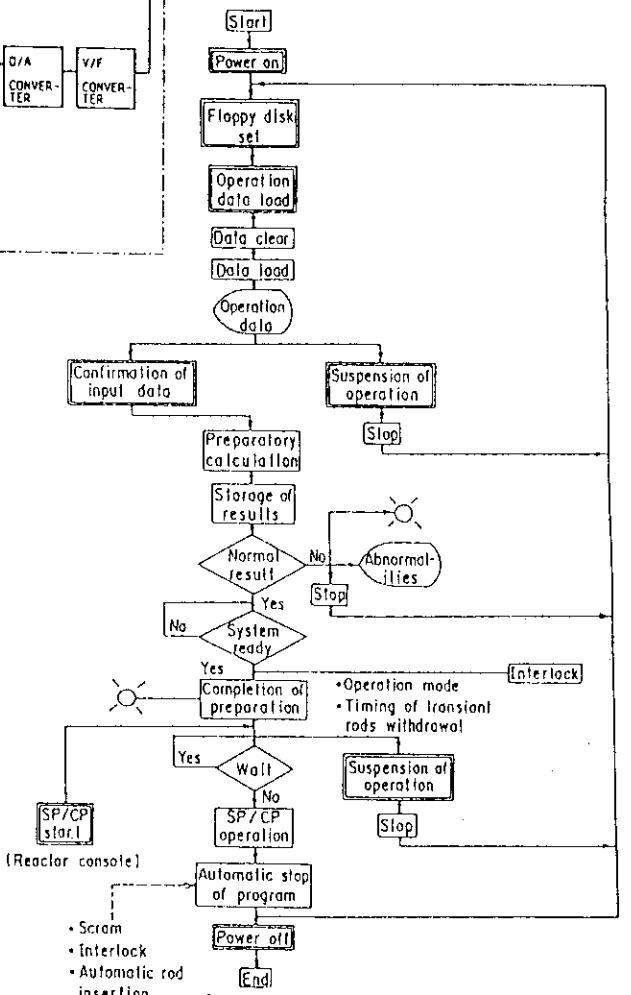

Fig. 4 Operation Sequence of SP and CP

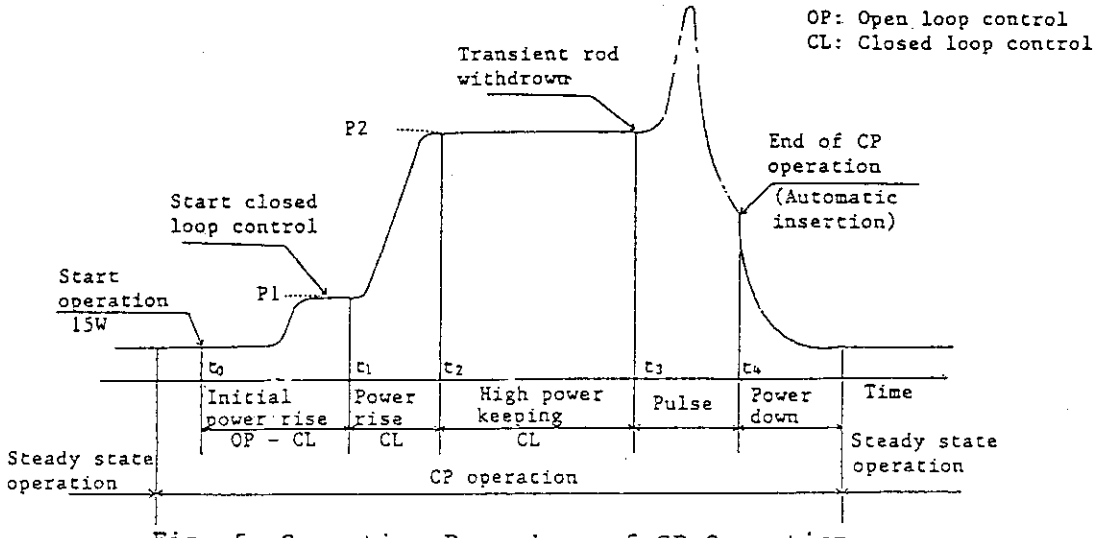

Fig. 5 Operating Procedure of CP Operation

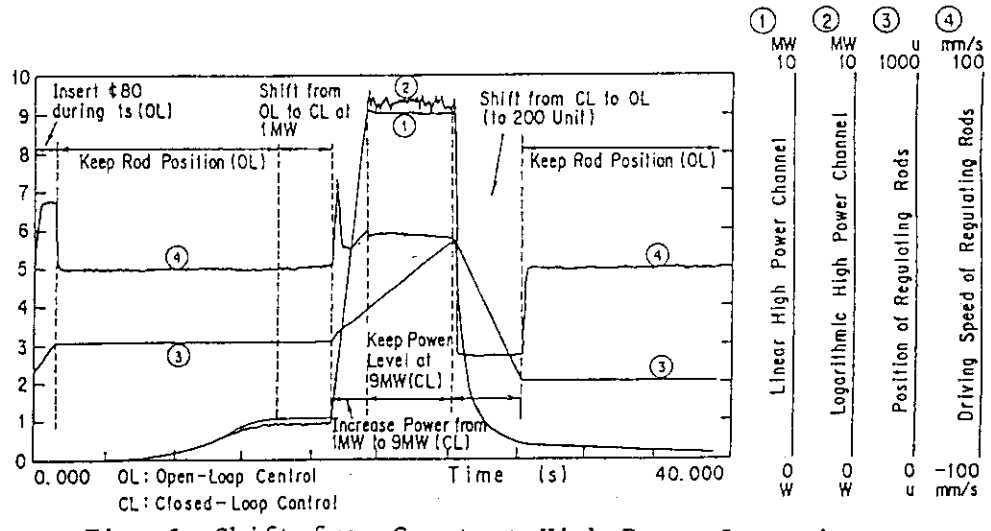

Fig. 6 Shift from Constant High Power Operation in SP Mode to Steady State Mode

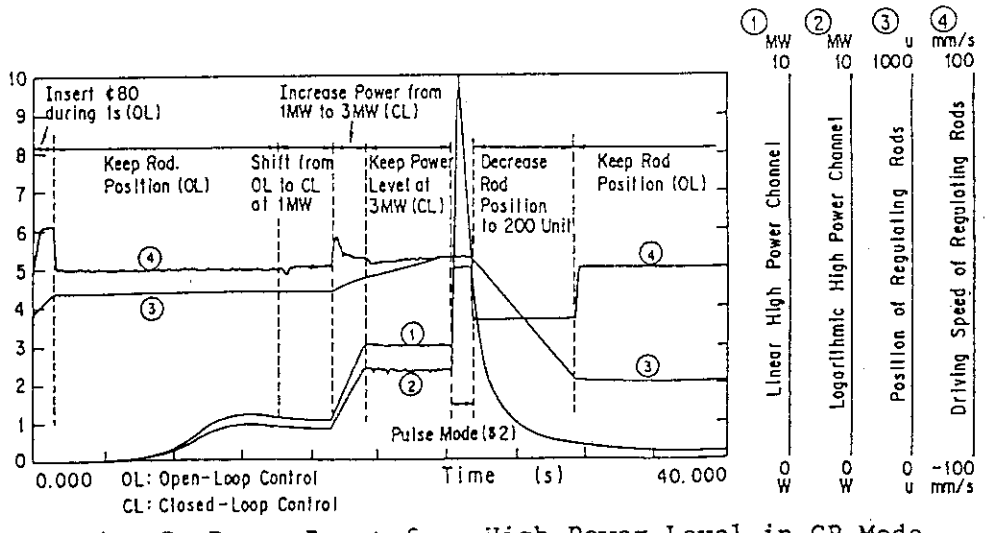

Fig. 7 Power Burst from High Power Level in CP Mode

11. Modified Pulsing Characteristics of the NSRR

S. KATANISHI, K. ISHIJIMA, S. YACHI, S. OTOMO,
O. HORIKI and T. FUJISHIRO

Department of Fuel Safety Research
Tokai Research Establishment, JAERI
Tokai-mura, Naka-gun, Ibaraki-ken 319-11, Japan

ABSTRACT

Nuclear Safety Research Reactor in Japan Atomic Energy Research Institute is a TRIGA-ACPR(Annular Core Pulse Reactor) which is able to generate very sharp pulse power with the maximum of 23GW and steady state power with the maximum of 300kW. Many test fuel rods were irradiated in NSRR to study fuel behavior under Reactivity Initiated Accident conditions. However, the simulated power burst in the past tests was initiated from essentially zero power due to the limited capability of NSRR.

The reactor control system of NSRR has been modified to extend the capability of the pulse operation and two new operation modes have become applicable. One is the shaped pulse operation mode which produces a controlled high power transient, and another is the combined pulse operation mode which is a combination of a high power transient and a sharp pulse power generation. In this article, characteristics of the shaped pulse operation is presented.

NSRR is to be operated under the limitations of the maximum integral power of 110MWs, the maximum core fuel temperature of 900 ℃, the maximum regulating rod speed of 75mm/s and the maximum regulating rod position of 850units. Through a number of test operations, characteristics of the shaped pulse mode under these limitations were obtained. The stability and capability of the various power shapes were certified. The maximum regulating rod position as a function of the integral reactor power and the limit of the operational ability in the shaped pulse mode were clarified.

INTRODUCTION

Nuclear Safety Research Reactor (NSRR) in Japan Atomic Energy Research Institute (JAERI) is an annular core pulse reactor to investigate the fuel behavior under reactivity initiated accident condition. This reactor generates very sharp pulse power with the maximum of 23GW by rapid reactivity insertion with the maximum of 4.7$[1], and has capability to simulate a power burst in the reactivity accident of the power reactor. The control system of NSRR was modified to extend the operation ability to simulate the accident and the abnormal transient of the power reactor, such as the transient at power, reactivity initiated accident at power, decay heat of the fuel of the reactor core, and so on. Before the modification, all the tests had been conducted under the pulse power operation by rapid reactivity insertion in which the power burst was generated from essentially zero power[2].

A number of test operations were conducted to clarify the modified pulsing characteristics and the capability of the experiment to simulate abnormal transient. The objectives of these test operations were focused on the stability, the maximum capability of the operation and the irradiation characteristics with test fuel rods.

SPECIFICATION OF NSRR

NSRR is a swimming pool type, annular core reactor, as shown in Figure 1. The reactor core is placed at the bottom of the water pool whose depth is approximately 9m. It has a large experimental cavity in the core center where an experimental capsule with test fuel rods is fixed and irradiated.

There are three kinds of control rods in NSRR, 6 regulating rods, 3 transient rods and 2 safety rods. The regulating rods are driven by electric motors to control the reactor power level at the steady state operation. The transient rods are withdrawn rapidly by the injection of compressed air into the rod drive cylinder and the reactivity for the pulse power generation is inserted according to the initial position of the transient rods. The control rods is driven between the lowest position (100 unit) and highest position (900 unit) and the stroke is 380mm which is divided into 800 units. The reactor fuel in NSRR is made of 20% enriched Uranium-Zirconium hydride. Since contained hydrogen in the fuel is moderator which is easy to be heated by nuclear fission, this reactor has a large temperature coefficient of negative feedback reactivity and the reactor power decrease spontaneously after the rapid power generation by withdrawal of the transient rods. The specification of NSRR is listed in Table 1.

The test fuel rod is placed in the inside of the experimental capsule which is fixed at the core center, and the heat generated in the test fuel rod during irradiation is approximately proportional to the heat generated in the reactor core. Transient heat up of the core fuel of the power reactors under reactivity initiated accident conditions is simulated by the pulse irradiation of the test fuel rod in NSRR.

MODIFICATION OF THE OPERATION SYSTEM

All of the operation modes and typical power shape of each operation mode at the modified NSRR are listed in Table 2. The shaped pulse operation mode and the combined pulse operation mode have become applicable by the modification[3]. The shaped pulse operation mode is to produce a controlled high power transient, such as constant high power operation, power increase and power decrease from high power, using the regulating rods driven by the open or closed loop control system. The combined pulse operation mode is to produce a combination of the controlled high power transient and a sharp pulse power, using the regulating rods and the transient rods. In the combined pulse operation mode, the power burst in reactivity initiated accident at power and the high run-out power following the power burst can be simulated. In the shaped and combined pulse mode, demands for the time sequence of regulating rod position and reactor power shape should be input to the computer and the reactor is operated automatically.

NSRR is to be operated under the limitation for the safety reason, and the most important items are,

(1) the maximum integral reactor power of 110MWs,

(2) the maximum core fuel temperature of 900 ℃,

(3) the maximum regulating rod speed of 75mm/s, and
(4) the maximum regulating rod position of 850unit

PULSING CHARACTERISTICS

The stability and the maximum capability of the operation under limitation mentioned above were investigated through the test operations.

Figure 2 shows time histories of the reactor power and regulating rod position during one of the constant high power operations. The regulating rods were withdrawn for 1 second according to the rod position demanded as a function of time in "open loop" control, as shown in the figure, and the reactivity of 0.8$ was inserted. After the reactor power rose to 1MW, the control system was changed automatically into the "closed loop" system with feedback of measured reactor power and the regulating rods were withdrawn according to the deviation of measured power to the demanded power. During the closed loop control, the reactor power was increased and was kept at 9MW for 5 seconds. During the closed loop control, the the deviation of the reactor power from the demanded power was less than 3% of the demanded power. This shows good operation ability at the shaped pulse operation mode.

The time histories of the reactor power and the regulating rod position in some test operations with various power shape are shown in Fig.3. As shown in this figure, power decrease from high power and power increase from high power were successfully done under the limitation which was mentioned above.

The overshoot of the reactor power after fast power increase at the various operation are summarized in Fig.4. Overshoot is less than 3% of the rated power in every case, even in the fastest power increase operation from 1MW to 10MW for 2 seconds. These results shows that the various kinds of operation became available and they were conducted stably.

Figure 5 shows the relation between integral reactor power and the maximum regulating rod position at various operations in the shaped pulse mode. Upper and lower limit of regulating rod position and upper limit of integral reactor power are shown in this figure as broken lines. Reactor operation must be conducted under the limitation. The maximum regulating rod position depends on the integral reactor power and it is independent on the power shape. In case of the operation without experimental capsule, the regulating rod position may have sufficient operable margin from the limit even in the operation with 110MWs which is the upper limit of integral reactor power. However, in case of the operation with the NSRR standard experimental capsule of which reactivity worth is -2.3 dollars in the cavity of the reactor core, the regulating rod position reaches upper limit of 850unit when integral reactor power is 80MWs and it still has a sufficient margin of 30MWs in integral reactor power. This is caused by the negative reactivity worth of the experimental capsule. Compared with the operation without experimental capsule, the initial regulating rod position should be higher to compensate the negative reactivity of the capsule at the initial criticality and during the following operation. The operation is limited by the regulating rod position in case with the experimental capsule, while it is limited by the integral reactor power at the operation without capsule. This figure shows the effect of the experimental capsule and the maximum capability of the operation.

The fuel temperature of the reactor core was also measured in these test operations, and the maximum temperature was less than 900 °C in every case.

IRRADIATION CHARACTERISTICS WITH THE TEST FUEL ROD

Irradiation tests using test fuel rods were conducted in the shaped pulse operation mode to clarify the ability of the simulation test of abnormal transient of power reactors.

Figure 6 shows the schematic of the test fuel rod and the experimental capsule in the test to measure the fuel center temperature. As shown in this figure, the test fuel rod was a shortened PWR size fuel rod with cladding tube of Zircaloy-4 and ten 20% enriched Uranium-dioxide pellets. Active length was 10cm. A tungsten rhenium thermocouple to measure the pellet center temperature was fixed at a center hole of five pellets in upper part and three platinum-platinum rhodium thermocouples were attached at the surface of the cladding tube. The test fuel rod was fixed at the center of the experimental capsule and was surrounded by stagnant water under room temperature and atmospheric pressure condition. The test fuel rod within the capsule was irradiated in the shaped pulse operation.

The reactor power shape and time histories of fuel rod temperatures in this test are shown in Fig.7. After the initial power up to 1MW, the reactor power was increased to 3MW and this power level was kept constant for 5 seconds. When the reactor power was 3MW, the linear heat rate of the test fuel rod was approximately 45kW/m which was equivalent to the maximum linear heat rate of the power reactors. After keeping the power at 3MW, the reactor power was increased up to 9MW in 10 seconds and the test was terminated. The pellet center temperature increased beyond 2000 ℃ when reactor power reached 9MW. This result shows that the abnormal transient condition of the power reactor is able to be simulated in irradiation test by the shaped pulse operation of the NSRR. The maximum cladding surface temperature was approximately 100 ℃ and no DNB (Departure from Nucleate Boiling) occurred in this test.

Through these irradiation tests, the ability of the test to simulate the abnormal power transient was certified.

CONCLUSIONS

Test operations were conducted to investigate the characteristics of the shaped pulse mode and the capability of irradiation test to study the fuel behavior under abnormal transient conditions.

(1) The capability of operation in the shaped pulse mode with various power shape was certified.
(2) It was shown that reactor power is controlled stably by modified automatic control system.
(3) The maximum capability of the operation was clarified by the relation between the maximum regulating rod position and the integral reactor power at various power shape.
(4) The capability of irradiation test to simulate the fuel behavior under the abnormal transient of the power reactors was certified.

ACKNOWLEDGEMENTS

The authors wish to thank the collaboration in the test operations conducts by colleagues in NSRR Operation Division, Japan Atomic Energy Research Institute.

REFERENCES

[1] S. Saito, et al., Measurement and Evaluation on Pulsing Characteristics and Experimental Capability of NSRR, J. Nucl. Sci. Technol., 14(1977)226-238
[2] M. Ishikawa and S. Shiozawa , A Study of Fuel Behavior under Reactivity Initiated Accident Conditions - Review, J. Nucl. Mater., 95(1980)1-30
[3] K. Ishijima, et at., The Upgrade of Pulsing Capability of the NSRR with Special Regard for the Safety of Operation, Proc. Internat. Topic. Meeting on The Safety, Status and Future of Non-Commercial Reactors and Irradiation Facilities, Boise, USA, 1990, pp412-419.

Table 2 NSRR operation modes and reactor power characteristics

Operation Modes	Reactor Power Behavior		Research Items
1. Steady State Operation	Steady State	300kW	· Fuel Relocation
2. Natural Pulse Operation	Pulse from Zero Power	4.7$	· Fuel Behavior in an RIA from Cold Start-up · Molten Fuel-Coolant Interaction
3. Shaped Pulse Operation	Power Decrease from High Power	~10MW, ~10sec	· Fuel Relocation and Coolability
	Power Increase from High Power	~3MW, ~10MW, ~10sec	· Fuel Behavior during Power Ramping
4. Combined Pulse Operation	Pulse From High Power	2~4$, ~3MW, ~10sec	· Fuel Behavior in an RIA from Rated Power
	Pulse from Zero Power/High Runout Power	2~4$	· Debris Coolability

Tabel 1 Specifications of NSRR

Type	Swimming pool, annular core, steady and pulse power reactor	
Power	Steady power 300kW Pulse power 23GW (peak value)	
Core	Effective height Ca. 38cm Equivalent diameter Ca. 63cm Moderator ZrH and H_2O Reflector Graphite and Water	
Fuel rod	Type 12wt% U-ZrH Enrichment 20wt% Shape Cylindrical rod 3.56cm OD. Clad material 304SS Number 157 rods	
Control rod	Safety rod Regulating rod Transient rod	2 6 3
Pool	Width Length Depth	3.6m 4.5m 9m

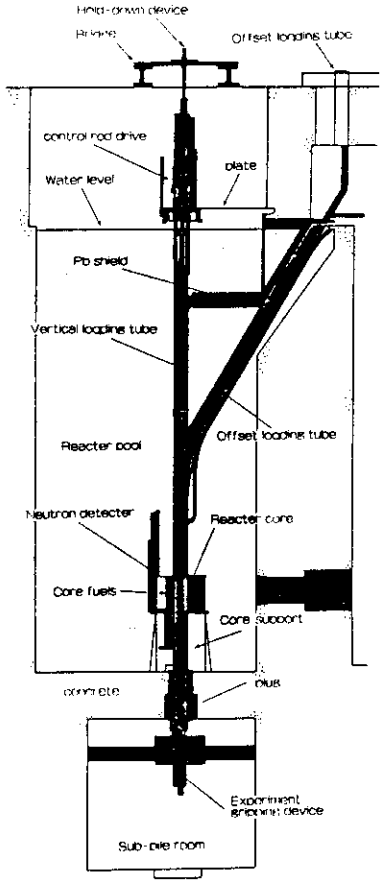

Fig.1 Schematic drawing of NSRR

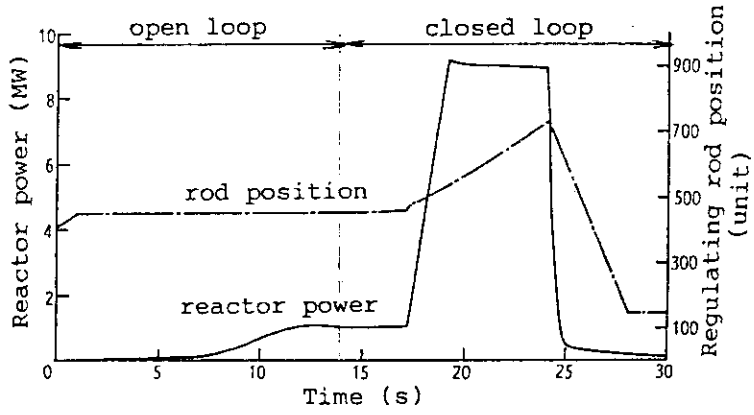

Fig.2 Reactor power shape and time history of regulating rod position at high power operation in shaped pulse mode

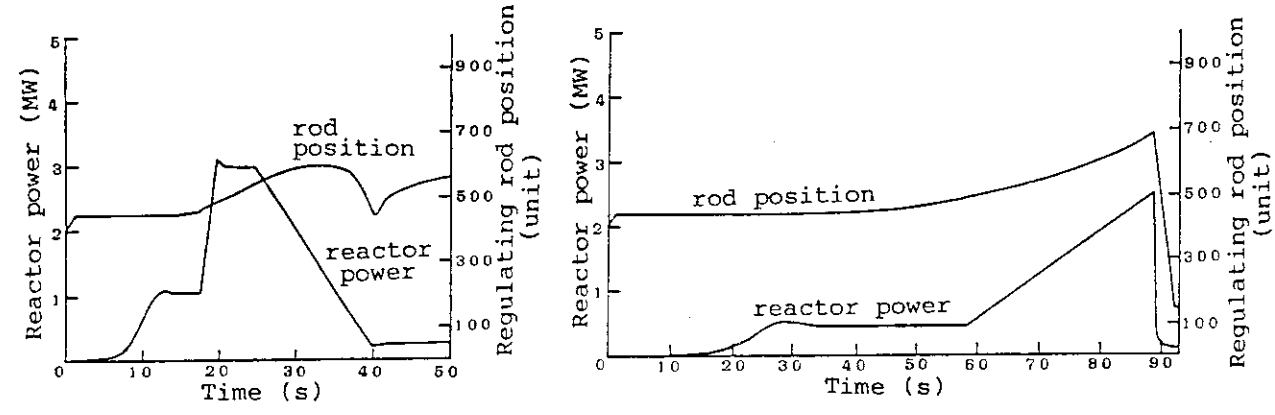

(a) Power decrease from high power　　(b) Power increase from high power

Fig.3 Reactor power shape and time history of regulating rod at various operation in shaped pulse mode

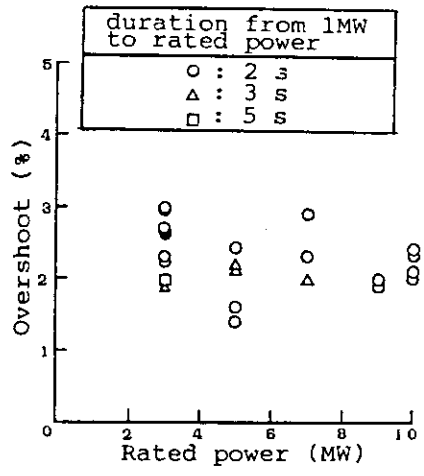

Fig.4 Overshoot after fast power increase at various power shape

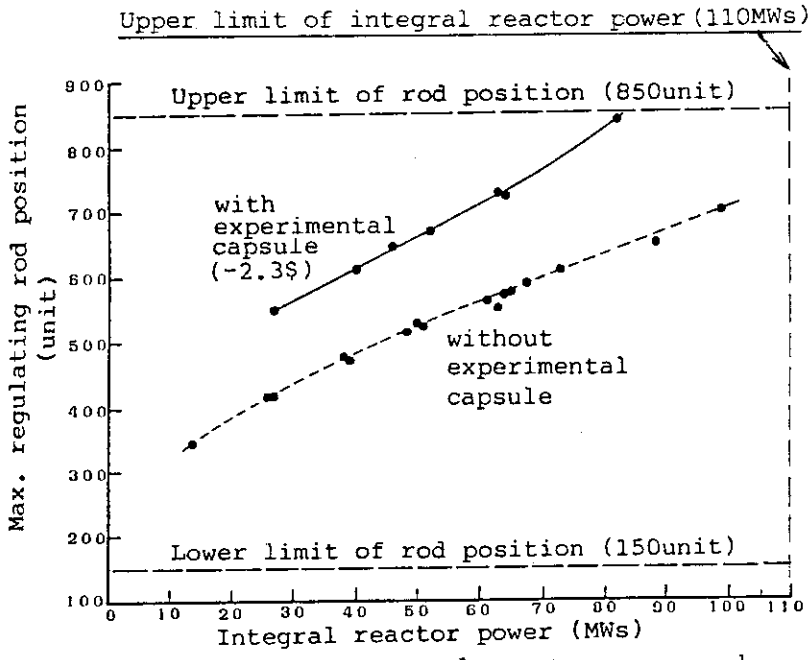

Fig.5 Relation between integral reactor power and maximum regulating rod position at various power shape in shaped pulse mode

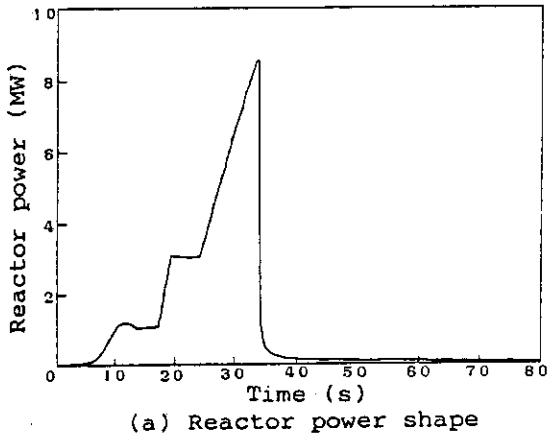

(a) Reactor power shape

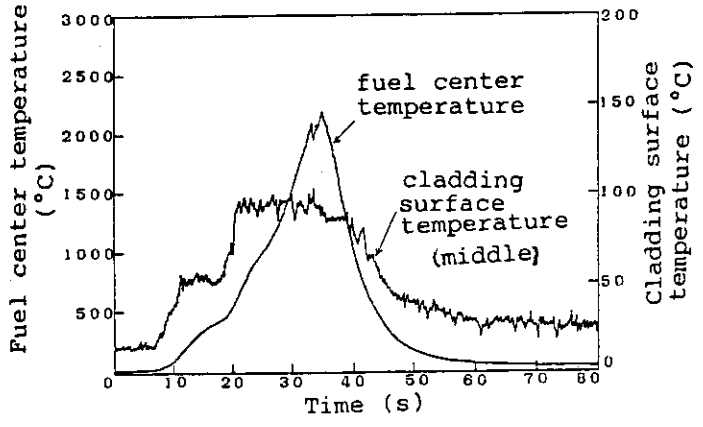

(b) Temperature behavior of test fuel rod

Fig.7 Reactor power shape and temperature of test fuel rod in irradiation test

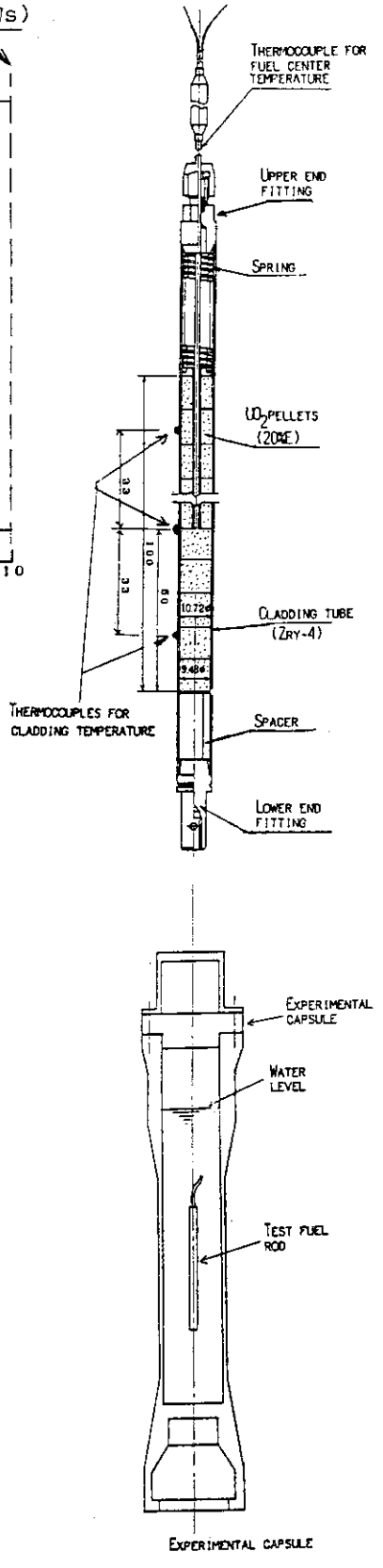

Fig.6 Schematic drawing of test fuel rod and experimental capsule

12. Study on Shadowing Effect Caused by Transient Rods at NSRR

T. NAKAMURA, S. YACHI and K. ISHIJIMA
Department of Fuel Safety Research
Tokai Research Establishment, JAERI
Tokai-mura, Naka-gun, Ibaraki-ken 319-11, Japan

ABSTRACT

Irregularly inserted three control rods created so called shadowing effects on some of the neutronic instruments at the Nuclear Safety Research Reactor (NSRR). During operations at the reactor power of up to 10 MW, the three control rods called transient rods, could be fully or partly inserted into the NSRR core. Reactor power monitors located outside of the core at the direction of deeply inserted transient rods indicated lower power in such operations. Power profiles of the reactor and neutron fluxes at power monitor locations were calculated with a three dimensional neutron diffusion code, CITATION. The calculation indicated that the real reactor power could be smaller than the measured maximum power by as much as 30 % in such operations. The calculated neutron fluxes well described the changes in the apparent power monitor indications as a function of the transient rod position.

INTRODUCTION

The NSRR is equiped with two sets of operational control rods, i.e. regulating rods and transient rods. The regulating rods are used for relatively slower operations, such as for steady state operations (<300kW) and for shaped pulse operations(<10MW). The transient rods are used for very quick pulse operations at half widths of mili-seconds.

Combinational operations with the two sets of the control rods are conducted in so called combined pulse mode. Three transient rods can be irregularly inserted into the core, while the reactor power is controlled below 10 MW by bank operations of six regulating rods. A quick pulse power, by total withdrawals of the 3 transient rods out of the core, follows the high power operation. The magnitude of the pulse power is adjusted by the initial positions of the 3 transient rods. Only one of the transient rod position can be finely adjustable, while the other two can be fully inserted or fully withdrawn. Thus, the positions of the 3 transient rods can be all different during the high power operation in the combined pulse mode. This irregularly positioned transient rods create a non-uniform power profile in the NSRR, and variety of shadowing effects on the neutronic instruments (reactor power monitors) located outside of the core at directions of the transient rods. In other words, indications of the other power monitors vary depending on the transient rod patterns, while the reactor is operated at a constant power.

Descriptions on the NSRR configuration and its operational methods are

presented, followed by operation results showing the shadowing effects. Whole core neutronic calculations with neutron diffusion code, CITATION, were performed. The calculations were conducted with three dimensional triangular and hexagonal geometries of the core. The calculated neutron flux at the reactor power monitor locations showed good agreements with the measured indications of the monitors. Real reactor powers at various operations were estimated by the calculations. The calculation indicated some other important perspectives on conducting experiment in the combined pulse mode. These results will also discussed in the following sections.

NSRR FACILITY

NSRR Configuration

The NSRR is a modified TRIGA - Annular Core Pulse Reactor Exclusively designed to perform irradiation tests simulating Reactivity Initiated Accidents of commercial power reactors. The NSRR has an experimental cavity of 22 cm in diameter at the center of the core, in which short sized test fuel rods contained in a test capsule are pulse irradiated. The core structure is located in a 9 m deep open pool, as is shown in Fig. 1, and is cooled by natural circulation of the pool water.

The core configuration of the NSRR is illustrated in Fig. 2. The core contains 149 driver fuel elements, 6 fuel follower regulating rods and 2 fuel follower safety rods, making 157 driver fuel elements in total. In addition, three transient rods with air filled followers are used to insert reactivities for pulse operations. The transient rods are driven pneumatically, while the regulating and safety rods are electrically operated.

A total of 8 neutron detectors serves as reactor power monitors in the NSRR. The monitors cover the reactor power from 0.03 mW to 30,000 MW, consisting of 4 groups, namely steady state operation monitors (channels A and B), high power operation monitors (channels E and F), pulse operation monitors (channels D1 and D2) and safety monitors (channels C1 and C2). Those power monitors were consisted of fission chambers and compensated ionization chambers.

The eight power monitors are placed outside of the NSRR core in a circular positions at a radius of 592.8 mm, while the core radius is about 310 mm. The monitors are located in groups behind the three transient rods, as are shown in Fig. 2. Channels E, C1 and D1 are located behind the transient rod A (Tr. A), initial position of which is fully adjustable by an electric motor. Channels D2 and C2 are located behind the transient rod B (Tr. B). Channels B, A and F are located behind the transient rod C (Tr. C). The initial positions of Tr. B and Tr. C can only be fully inserted to the core (100 unit, down) or fully withdrawn (900 unit, up). The positions of all the control rods, regulating rods, transient rods and safety rods, of the NSRR are presented in units, which divide 381 mm of the core height into 800 units, starting at 100 (down) and ending at 900 units (up).

Operational Modes

The NSRR has been operated in four modes, as are illustrated in Fig. 3, since a modification of the operating system was completed in fiscal year 1988. Steady state operation of a power of up to 300 kW is controlled by adjusting a bank of the regulating rod positions and is monitored by channels A and B for operational purpose and by C1 and C2 for safety purpose. High power operations at powers up to 10 MW in the shaped pulse

mode and the combined pulse mode are achieved by rather quick operations of the bank of the regulating rods up to a maximum speed of 75 mm/s. Reactor powers in these operation modes are monitored by channels E and F, in addition to the channels C1 and C2. The reactor energy release is limited below 110 MWs in this shaped and combined pulse modes.

Very sharp pulses of half widths of mili-seconds from 0 and rated powers are realized by pneumatic withdrawals of the 3 transient rods in the natural pulse mode and in the combined pulse mode, respectively. The maximum reactivity insertion of $ 4.7 from 0 power is allowed to produce a peak reactor power of 23,000 MW and reactor energy release of 130 MWs for the pulsing operations. The pulsing power is safely controlled by an enhanced neutron spectrum hardening effect in addition to the Doppler effect in the NSRR. Reactor powers in the pulse operations are monitored by channels D1 and D2.

The NSRR is usually operated to have only regulating rods uniformly inserted and the other control rods full up, while the reactor is operated at a certain power except in the combined pulse operations. Figure 4 illustrates positions of regulating rods and transient rods in the natural pulse mode, in the shaped pulse mode and in the combined pulse mode. In a combined pulse operation as is shown in Fig. 3, a sharp pulse power follows a rated power of up to 10 MW. Control rod patterns during the operation are shown in Figs. 4C and 4D, for the high power operation section and the following pulse power operation section, respectively. The transient rods A, B and C position 650, 100 and 900 units, respectively, during the high power operation, expecting a pulse of $ 2.0. This irregular transient rod position creates varying shadowing effects on the power monitors located behind each of the transient rods.

OPERATION RESULTS

A set of steady state operations simulating combined pulse operations were conducted with various transient rod patterns. In other words, the NSRR was operated changing Tr. A position gradually, while the reactor power indicated by the channel B was kept constant. Reactor power indications by the other monitors were recorded through the operations. A clear sign of the shadowing effect of Tr. A is seen in the indications of power monitors located behind the rod, such as channels E and C1. The indications of the two power monitors decreases by as much as 35 %, when the Tr. A was down, as is shown in Fig. 5.

The change in power profile and subsequent changes in power peaking factors by the irregularly positioned transient rods were predicted prior to the operations. However, the shadowing effects on the power monitors were not evaluated. Thus, maximum indications of the power monitors were kept below the power limit for the safety purpose during the operations.

Numbers of operations in the combined pulse operation mode were conducted with 4 transient rod patterns. Indicated powers of the various monitors showed the shadowing effects basically identical to those observed in the simulating steady state operations. These results will be discussed later in accordance with the results of steady state operations and the calculations.

CALCULATION

Method

Full core neutronic calculations were performed in three dimensional geometries using a vectorized version[1] of a neutron diffusion code, CITATION[2]. The NSRR core consists of 157 fuel elements (including 8 fuel follower control rods) and three transient rods arranged in a hexagonal pattern at a pitch of 41.7 mm, surrounding the experimental cavity of about 220 mm in diameter, as is shown in Fig. 2. Each of the fuel elements and control rods were modeled as a hexagonal unit cell of 27.1 mm in each side length. Each unit cell was divided into 6 regular triangles. The full core neutronic calculations were conducted with the triangular geometries consisting of 7566 triangles X 52 axial nodes. The NSRR core and surrounding water including power monitor locations within a radius of about 850 mm and a height of about 1600 mm was modeled. The modeled core configuration is illustrated in Fig. 6. In addition to the detailed calculations in the triangular geometries, scoping calculations were performed in hexagonal geometries taking the unit cell as a hexagonal mesh.

Nine group constants (4 groups for fast neutrons and 5 groups for thermal neutrons) were condensed from a public microscopic cross section library of SRAC code system[3], which consists of 107 groups of cross section data based on JENDL-2 and ENDF/B-IV libraries. A one dimensional Sn code, ANISN, was used to condense group constants in zones located in radial or axial directions from the driver fuel zone, as is shown in Fig. 6.

Results

Results of triangular geometry calculations are presented in this section. Scoping calculation results in the hexagonal geometries are presented in the next section in accordance with the measured results.

A calculated power profile of the NSRR, with a Tr. A position of 100 units (down) and the rest of control rods positions up, is shown in Fig. 7. A locally depressed power distribution is clearly seen in the profile. The thermal neutron profile is almost identical to the power profile in the core region. The depressed neutron flux at the direction of the deeply inserted transient rod affects the indications of the reactor power monitors located at the direction. Calculated neutron fluxes at the power monitor locations with various transient rod positions are illustrated in Fig. 8. The neutron fluxes are relative values taking the value with all the transient rods up as the unity (1.0), while the reactor power is assumed to be 1.0 in all the calculations. The figure indicates that the reactor monitors will indicate about 25 % higher or lower powers depending on the transient rod positions, even the real reactor power is kept constant.

Thermal neutron fluxes at the center of the experimental cavity are summarized in Table 1. The neutron flux is constant within a deviation of 0.4 % as long as the reactor power is kept constant even when the transient rods are positioned irregularly. In addition, the azimuthal thermal flux distributions in the central cavity region in a diameter of 80 mm are found to be very flat within a deviation of 0.3 % in all the conditions. Thus, it is concluded that the irregularly positioned transient rods will not cause any azimuthally uneven power depositions in the test fuel rods irradiated in the experimental cavity in the NSRR experiments. Calculation results will be reported in detail in ref.(4).

DISCUSSION

All the calculations shown in the former section were conducted assuming a constant reactor power, even the transient rod patterns were different in all the cases. However, in the real operations, the real reactor powers were not known. The operations were conducted keeping a power monitor indications constant, e.g. in the steady state operations channel B output was kept constant. So, Calculated results were normalized by the thermal neutron fluxes at the channel B location and were compared with the measured power monitor outputs in Fig. 9. The calculated power monitor outputs, especially of the triangular geometries, showed good agreements with those measured at the three locations, suggesting that the simulation calculations were successful. Scoping calculations in the hexagonal geometries showed the tendency very well, however they underestimated the shadowing effect by as much as about 10 %.

Outputs of C1 channel measured in the combined pulse operations are shown in Fig. 10, as well as the calculated values normalized by the neutron flux at the channel F location. The calculated results showed a good agreement with the measured outputs with four transient rod patterns.

A set of correction factors are estimated and are shown in Fig. 11 to obtain the real reactor powers in the steady state operations from the channel B output, based on the triangular geometry calculation results. The estimated relative reactor powers at various transient rod patterns are shown in the figure, when the channel B indicates reactor power of 1.0. When the transient rods A and B are down and C is up, the real reactor power is estimated smaller than the channel B indication by about 20 %. On the other hand, the real reactor power will be 16 % higher than the channel B indication, when Tr. B and C are down and Tr. A is up. Still the channel C1 is estimated to indicate about 50 % higher reactor power than the channel B does, as is shown in Fig. 9. In this way, the real reactor powers are estimated to be always smaller than the highest indications of the reactor power monitors by as much as about 30 %.

Another set of correction factors are similarly estimated and are shown in Fig. 12 to obtain the real reactor powers from measured channel F outputs in the combined pulse operations.

Because the thermal neutron fluxes at the center of the experimental cavity are calculated to be independent to the transient rod positions, the real reactor power could be measured by using an additional power monitor locating at the center. Calculation results would be confirmed further by this measurements.

CONCLUSIONS

Some combined pulse operations and simulating operations of the NSRR, having the transient rods irregularly positioned, demonstrated variety of shadowing effects of the transient rods on the reactor power monitors. The full core neutronic calculations showed a good capability in predicting the shadowing effects. The calculations gave us a useful perspectives in conducting irradiation experiments using the combined pulse operations. Following findings were obtained through this study.

(1) Real reactor powers, while the transient rods were irregularly positioned, were estimated using the calculation results. The estimated real

reactor powers were always smaller than the maximum indications of the power monitors by as much as 30 %. Thus, the current operating method of the NSRR, in which the maximum power indication is kept below the operational limit, is judged to have extra safety margins in terms of reactor power.

(2) The real reactor power could also be experimentally evaluated by measuring the neutron fluxes at the center of the experimental cavity, where the fluxes were calculated to be independent to the transient rod positions and to be proportional to the real reactor power.

(3) In the NSRR experiments in which test fuel rods contained in a experimental capsule were irradiated at the center of the core, coupling factors between the test fuel rod power and the NSRR power were calculated to be proportional to the real reactor power, even when the transient rods were irregularly positioned. Azimuthal power distributions in the test fuel rods were calculated to be practically even in all the operations with various transient rod positions.

ACKNOWLEDGEMENT

The operations of the NSRR were conducted by staff members of NSRR Operation Division of Department of Fuel Safety Research, headed by Mr. Horiki. The authors would like to acknowledge them. They are grateful to Mr. Hosoyamada of Cube System Co. for running the neutronic codes. Suggestion and useful discussions from members of Reactivity Initiated Accident Laboratory, headed by Dr. Fujishiro are also acknowledged.

REFERENCES

(1) Nonomiya, I. et al. : Vectorization of Nuclear Codes 88-1 - SRAC, CITATION, TWOTRAN-II, COREBN, CITATION-FBR -, JAERI-M 89-030, (in Japanese),(1989).

(2) Fowler, T. B. et al. : Nuclear Reactor Core Analysis Code : CITATION, ORNL- TM-2496 Rev. 2, (1971).

(3) Tsuchihashi, K. et al. : Revised SRAC Code System, JAERI 1302, (1986).

(4) Nakamura, T. et al. : Analysis of Shadowing Effect Produced by Irregularly Positioned Transient Rods During Combined Pulse Operation in NSRR, JAERI-M 91-185 (in Japanese)

Table 1 Relative thermal neutron flux at the experimental cavity center

TA Position (Unit)	TB:Up TC:Up	TB:Down TC:Up	TB:Down TC:Down
900	1.000	1.000	1.004
500	1.004		
100	1.004	1.004	

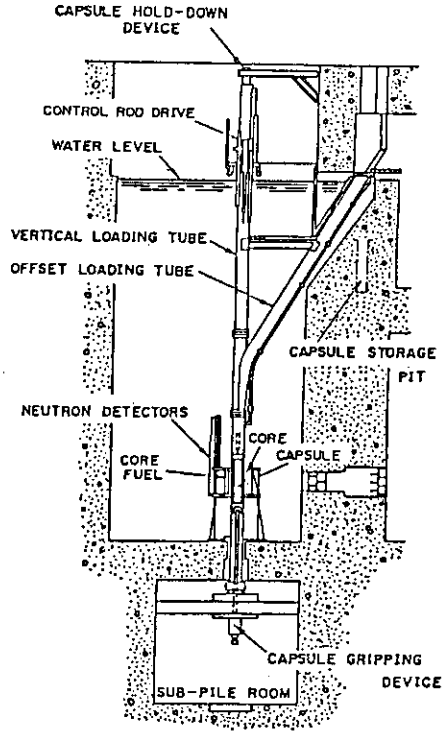

Fig. 1 NSRR core structure arrangement.

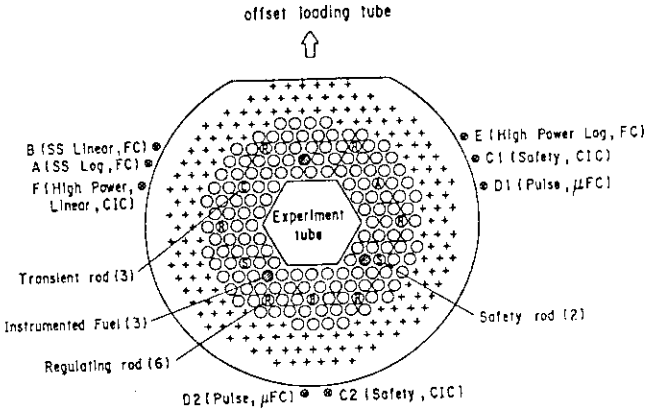

Fig. 2 NSRR rod arrangement.

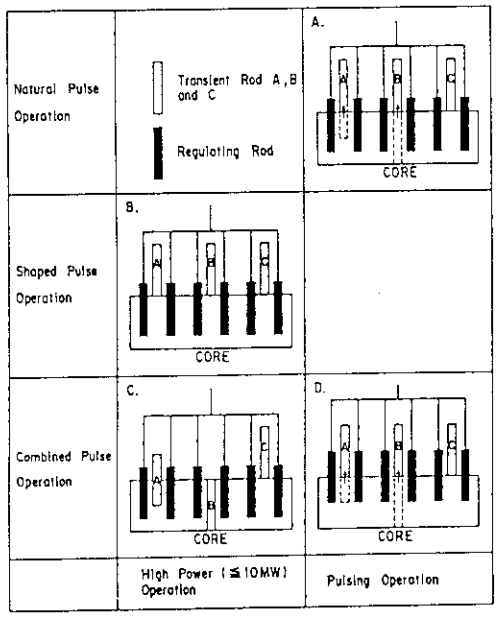

Fig. 4 Control rod positions in various NSRR operation modes.

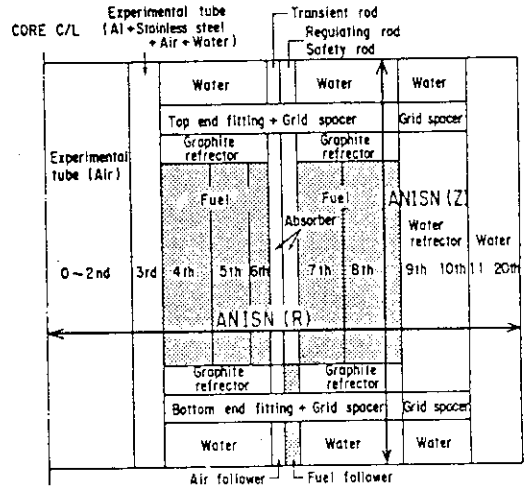

Fig. 6 Calculational geometries for full core analysis.

Operation Modes	Operational Limits and Exampls of Power History	Reseach Items
Steady State Operation	Reactor Power, 300kW, Time	Decay Heat Simulation etc.
Natural Pulse Operation	Reactor Power, 23,000MW, Energy Release 130MW·s, Time	Cold Start-up RIA
Shaped Pulse Operation	Reactor Power, 10MW, Energy Release 110MW·s, Time	Fuel Relocation Coolability
	Reactor Power, Energy Release 110MW·s, 10MW, Time	Power Ramping
Combined Pulse Operation	Reactor Power, 23,000MW, 10MW, Energy Release 110MW·s, Time	RIA from Rated Power
	Reactor Power, 23,000MW, Energy Release 10MW 110MW·s, Time	High Runout Power

Fig. 3 Operation modes of NSRR.

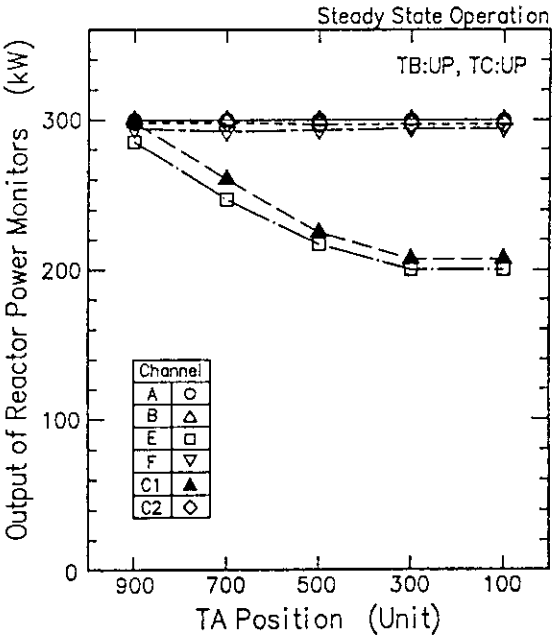

Fig. 5 Measured reactor power monitor outputs in simulating operations.

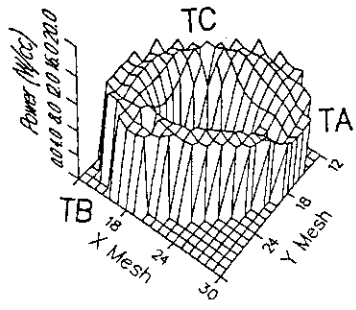

Fig. 7 Power profile of NSRR with Tr. A down and Tr. B/C up.

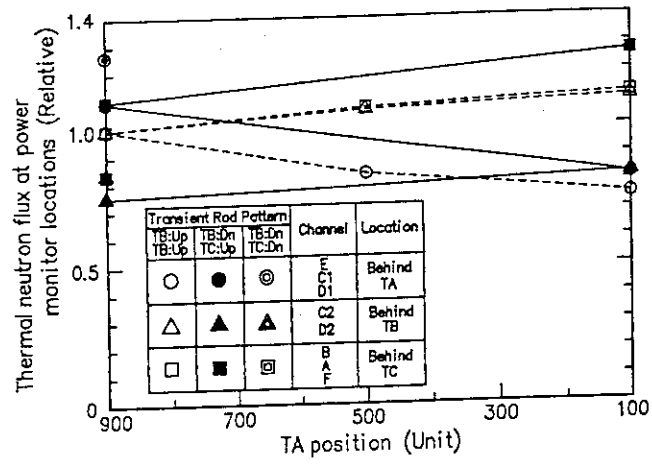

Fig. 8 Calculated neutron flux changes at power monitor locations as a function of Tr. A position.

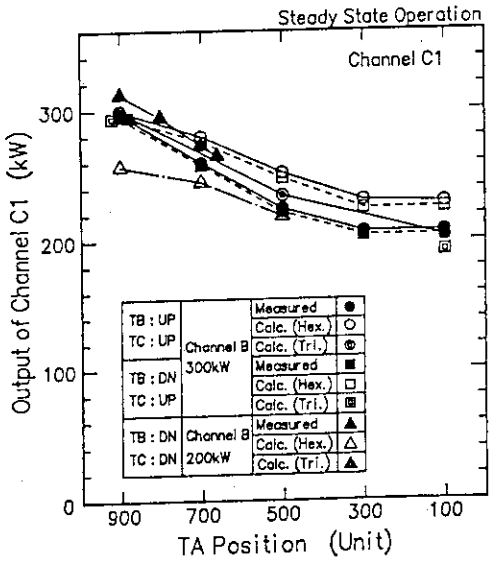

Fig. 9 Comparison of channel C1 output measured and calculated.

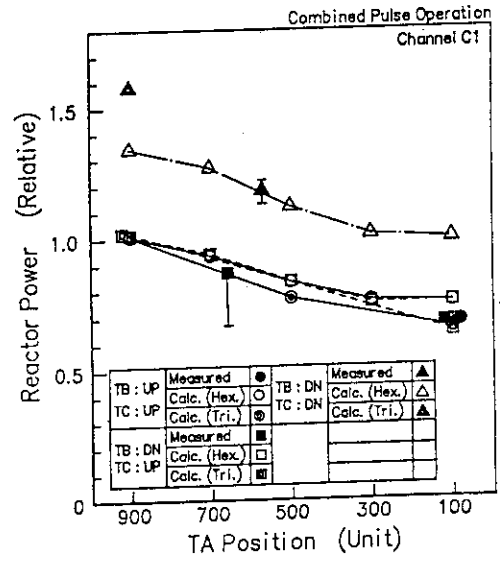

Fig. 10 Comparison of channel C1 output measured and calculated.

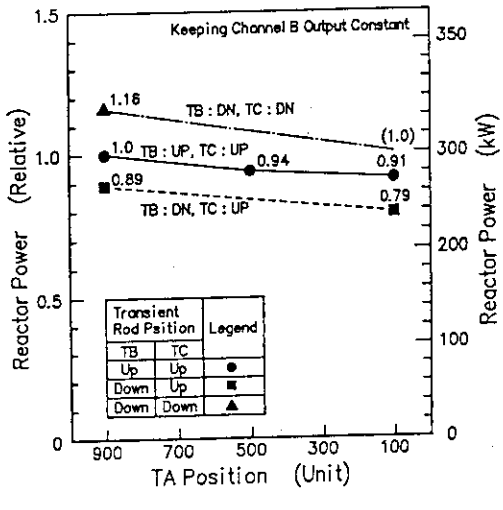

Fig. 11 Calculated reactor power correction factor for channel B.

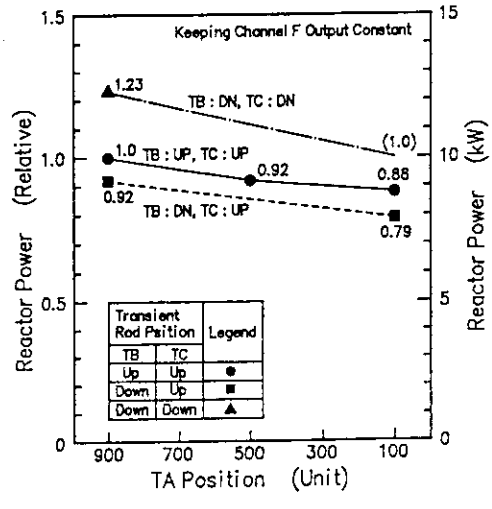

Fig. 12 Calculated reactor power correction factor for channel F.

13. Calculational and Experimental Experience on Core Management of Experimental Fast Reactor "JOYO"

A. Yoshida, Y. Arii, A. Shono, S. Suzuki, and K.Kinjo

O-arai Engineering Center,
Power Reactor and Nuclear Fuel Development Corporation,
4002 Narita, O-arai-machi, Ibaraki-ken, 311-13 JAPAN

ABSTRACT

For the core management of JOYO Mark-II, many core characteristics have been calculated with the core management code system"MAGI", and measurements have also been carried out at each duty operation cycle. From the evaluation of these results, the characteristics of core parameters such as criticality, reactivity coefficients, and control rod worth can be predicted accurately as followings; •excess reactivity : ±0.1%Δk/k, •outlet temperature of subassembly : ±10°C, •fuel burn-up : ±5%, •control rod worth : ±5%. As a result, we can not only get steady operation of JOYO but also perform various irradiation tests with satisfied conditions. This paper presents experience obtained until now through twenty three duty cycle operations of Mark-II core in JOYO.

1.INTRODUCTION

The experimental fast reactor JOYO was initially made critical in April 1977, as the first liquid metal cooled fast reactor in Japan. Following this, a breeder core named Mark-I core was operated for several duty cycles and was replaced by a Mark-II core after the mission of the Mark-I core. The Mark-II core, which is an irradiation test bed, achieved initial criticality in November 1982 and started 100MW rated power operation in March 1983. Since then, twenty three duty cycles have already been carried out successfully until September 1991. The comparison of core configuration of Mark-I and Mark-II are shown in Fig.1, and their main core parameters are listed in Table1.

From the viewpoint of safe and steady operation of the reactor, it is essential to predict the core characteristics accurately before operation. In JOYO, a core management code system "MAGI" was developed and has been employed for pre- and post-analyses of neutronics and thermal-hydraulics of JOYO Mark-II core. The key core characteristics calculated by MAGI for each cycle are represented by excess reactivity, control rod worths, reactor shut down margin, linear heat rate, fuel temperature, cladding temperature, etc. The irradiation conditions such as neutron exposure rate and fuel burn-up are also predicted for fuel/material irradiation tests, which are most important mission of Mark-II core. These analytical results have been compared with measured values in order to make the core management system more accurate and reliable.

2. OUTLINE OF CORE MANAGEMENT OF JOYO

The main activities of core management of JOYO are 1) making the refueling plan, 2) predicting reactor parameters, and 3) evaluating them by taking into account on-line operational data and the precise irradiation history of each assembly(S/A), i.e. fuels,

control rods and reflectors. Throughout these activities, following design criteria should be considered from the viewpoint of safe and steady operation;

- o Excess reactivity at 100°C less than 5.5%Δk/k.
- o Control rod total worth more than 9%Δk/k.
- o Shut down margin under condition with one rod stuck.
- o Linear heat rate less than 400W/cm
- o Fuel temperature less than 2650°C
- o Cladding temperature less than 650°C
- o Fuel burn-up(pin average) less than 75,000MWd/t

These criteria are applied to the core management.

3. CORE MANAGEMENT CALCULATION

The core management of JOYO has been performed mainly by the core management code system "MAGI" developed by PNC and also by the three dimensional diffusion theory calculation code "CITATION"[1].

MAGI is the code system that calculates criticality, power distribution(including gamma heating), burn-up of fuels, perturbation of reactivity coefficients, core flow distribution and thermal hydraulics of individual S/As.

Figure 2 shows the basic input / output system diagram of MAGI. The parts of neutronic calculations of MAGI use the calculation code HONEYCOMB-II that has been developed by Japan Atomic Energy Research Institute(JAERI), and flux synthesis method and flux perturbation method are applied. Thermal hydraulics calculations use the reactor coolant flow distribution calculation code "SMART".

Three-dimensional hexagonal-Z(Hex-Z) calculation is employed in a standard method of calculation. On X-Y plane, one node has the same cross section as one S/A, i.e. S/A pitch is 8.15cm. The calculation is made for 331 nodes including all S/As(313) from the core center to the reflectors in the outermost 10th row. In the axial direction, the calculation is made for 140cm height region that includes fuel, insulator pellets and axial reflectors(stainless steel). The region is divided into 20 nodes, with especially the fuel region of 55cm height divided into 11 nodes(ΔZ=5.0cm). Thus the total number of spatial nodes are 6620.

The multi-group cross sections, mainly based on JAERI FAST SET VersionII(JFS-2)[2], of 25 groups structure of Abagyan type for neutrons and 7 groups structure for gamma-rays are prepared. First, flux distributions are calculated for two-dimensional RZ model using multi-group cross sections. Next, the multi-group cross sections are collapsed to broad-group cross sections of 7 groups for neutrons and 3 groups for gamma-rays using the spectra mentioned above. The flow chart for evaluating broad-group cross sections is shown in Fig.3. In addition, to increase reliability, the bias factor (C/E) that has been evaluated with the analyses of the core performance tests at the MK-II initial core is considered in MAGI .

After this series of calculations of reactor parameters, the information obtained for each spatial node is edited and recorded in unit of S/A to be utilized as an initial data at a run of next duty cycle.

The calculation of control rod(C/R) worth is carried out at each duty cycle according to the precise compositions of fuel S/As calculated by MAGI, because the C/R worths differ from each other in every duty cycle by the effects of core burn-up and loading of Uninstrumented irradiation subassemblies(UNISs), which have less fuel inventory than driver fuels. The C/R worth is evaluated as the difference in the calculated effective multiplication factor (k_{eff}) between the core with all C/R withdrawn and the one with

certain C/R inserted in certain position. In order to calculate C/R worths of all C/R at several positions, runs should be carried out for several cases that C/R patterns are different from each other. The diffusion calculation code CITATION is used for the C/R worth calculations instead of MAGI because of its short CPU time. The conditions of the standard calculation by CITATION is principally the same as that of MAGI, i.e. 7 neutron energy groups, three-dimensional Hex-Z (same sizes of spatial nodes) diffusion model is employed.

4. CALCULATION AND/OR MEASUREMENT ON CORE PARAMETERS

In order to perform the irradiation tests more effectively by extending the period of one cycle operation from 45 days to 70 days, modified fuel S/A named J2 fuel was replaced with conventional J1 fuel. To get higher reactivity, the ^{235}U enrichment of J2 fuel is increased from 12% to 18%. The replacement began from 13th duty cycle gradually, and now, at 23rd duty cycle, replacement is 90% complete. The core management of JOYO has been conducted placing an emphasis on the loading effect of J2 fuel. Following is the summary of experimental experiences of core management obtained from the core characteristics tests carried out at each duty cycle and post irradiation examinations(PIEs) until now[3].

4-1 Excess reactivity

Excess reactivity is evaluated from k_{eff} value calculated by MAGI. The refueling plan is made by taking account of the calculated excess reactivity by considering bias factor(C-E) of one cycle before. To complete the one cycle operation for 70 days long and with 100MW thermal output, about 11 fresh fuel S/A should be refueled .Fig 4 shows the comparison of measured and calculated excess reactivities of MK-II duty cycles. By using the bias method, the excess reactivity after refueling can be predicted within an error of 0.1%Δk/k even at the J1 to J2 fuel transition core. It means that the accuracy of prediction is enough high to enable us to optimize the number of refueling S/As.

4-2 Reactivity coefficients

Figure 5 shows the change of measured isothermal temperature reactivity coefficient. Considering the measurement error, isothermal temperature reactivity coefficient is almost constant throughout the cycles and has no relationship with core burn-up and the number of J2 fuels.

Figure 6 shows the relation between measured power reactivity coefficient(average value between 0 and 100MW) and the core average burn-up. It seems that power reactivity coefficient increases with increasing core average burn-up.

Figure 7 shows the relation between measured burn-up reactivity coefficient and the core average burn-up. It seems that the burn-up reactivity coefficient also depends slightly on the core average burn-up.

4-3 Coolant temperature at S/A outlet

In MAGI, the coolant temperature at each S/A outlet is evaluated from the power distribution obtained from nuclear calculation and S/A coolant flow rate obtained from core flow distribution calculation. The coolant temperature at each S/A outlet is also measured with the thermocouple located at the bottom of Upper Core Structure(UCS) during operation. Table 2 shows the comparison of calculated and measured coolant outlet temperatures. The calculated coolant outlet temperatures at core center(1st row) and at the boundary of fuel region and reflector region(5th row) are in good agreement with the measured values, but some difference was observed for the S/A which is loaded at the neighbor of C/R (3rd row). On the whole, it seems that the change of outlet temperature by the effect of burn-up is well predicted by MAGI

In JOYO, to avoid fuel failures caused by anomalous temperature rise, the alarm is set for the temperature rise that exceeds the predicted value by 10°C.

4-4 Fuel burn-up

The burn-up of each fuel S/A is calculated by MAGI by taking into account the effective integrated thermal output. Figure 8 shows the comparison of calculated burn-up and the evaluated one from the results of PIE. The calculated burn-up of the fuel S/A showed good agreement with PIE data within 5%.

4-5 Control rod worth

The measurements of C/R worths have been carried out by using both period method and source multiplication method at the beginning of each duty cycle. The effective delayed neutron yield (β) and the decay constants (λ) are calculated by MAGI with using the Tomlinson data by accounting for the neutron flux distribution. These are used for solving the in-hour equation to evaluate the data obtained by period method . Figure 9 shows the comparison of calculated C/R worth and those measured by Period method. The difference between calculation and measurement by the former method are about 2%,and those by the later are 5%. It is considered that the differences derive mainly from the loading effect of UNISs adjacent to a C/R.

5. CONCLUSION

The core management code system MAGI has been developed for the JOYO Mark-II core, and has been verified and improved by measured results. From experience of core management of JOYO, MAGI predicts core characteristics accurately even at the transition state of the core replacement by fuel S/As which have different specifications.

By evaluating the measured results of core characteristics such as reactivity coefficients and control rod worth, the relations between these characteristics and the core burn-up or the core configuration have been made clear as followings; •excess reactivity : ±0.1%Δk/k, •outlet temperature of subassembly : ±10°C, •fuel burn-up : ±5%, •control rod worth : ±5%. This means that the detailed irradiation tests conditions can be predicted with high accuracy and reliability.

Finally the experience obtained through the core management of JOYO enables not only the safe and steady operation but also the accurate and reliable irradiation for fuels and materials development.

REFERENCE

1) H. Takano, et al., "JAERI Fast Reactor Group Constants Set Version II", JAERI 1255, November 1977
2) D.R. Vondy, and G.W. Cunningham, "Nuclear Reactor Core Analysis Code: CITATION", ORNL-TM-2496,Rev.22, July,1971
3) T. Aoyama, et al., "Core Experience of the Experimental Fast Reactor JOYO", BENS International Conference on Fast Reactor Core and Fuel Structural Behavior, P.299, Inverness, U.K., June 1990.

Table 1 Main core parameters of JOYO

Items \ Core (Fuel)		MK-I First	MK-I Second	MK-II
Reactor Output	MWt	50	75	100
Primary Coolant Flow Rate	t/h	2,200	2,200	2,200
Reactor Inlet Temperature	°C	370	370	370
Reactor Outlet Temperature	°C	435	470	500
Core Stack Length	cm	60	60	55
Core Volume (max.)	ℓ	294	304	250
Linear Heat Rate (max.)	W/cm	210	320	400
Fuel Pin Diameter	mm	6.3	6.3	5.5
$PuO_2/(PuO_2+UO_2)$	w/o	18	18	~30
^{235}U Enrichment	w/o	23	23	~12(J1) ~18(J2)
Neutron Flux (max.)	$n/cm^2 \cdot sec$	2.1×10^{15}	3.0×10^{15}	4.2×10^{15}
Neutron Flux (Core av.)	$n/cm^2 \cdot sec$	1.2×10^{15}	1.9×10^{15}	3.1×10^{15}
Max. Excess Reactivity	%Δk/k	~4.5	~4.5	~5.5
Control Rod Worth	%Δk/k	Safety Rod ~5.6 Regurating Rod ~2.8	Safety Rod ~5.6 Regurating Rod ~2.8	~9
Max. Burn-up(pin av.)	MWd/t	25,000	42,000	75,000
Operation Cycle		45 days Operation 15 days Outage	45 days Operation 15 days Outage	70 days Operation 23 days Outage

Table 2 The comparison of calculated and measured coolant outlet temperatures at S/A outlet

Items \ CYCLE		17	18	19	20
1st ROW	Calc.(℃)*	573	566	570	566
	Muas.(℃)	574	563	574	569
	Burn-up(MWd/t)	14,000	28,000	14,000	22,000
	S/A ID	PFD332		PFD341	
3rd ROW	Calc.(℃)*	545	540	532	529
	Muas.(℃)	541	533	529	524
	Burn-up(MWd/t)	16,000	26,000	36,000	41,000
	S/A ID	PFD328			
5th ROW	Calc.(℃)*	522	520	514	510
	Muas.(℃)	524	519	513	509
	Burn-up(MWd/t)	36,000	43,000	49,000	53,000
	S/A ID	PFD311			

* Calculated Value by MAGI

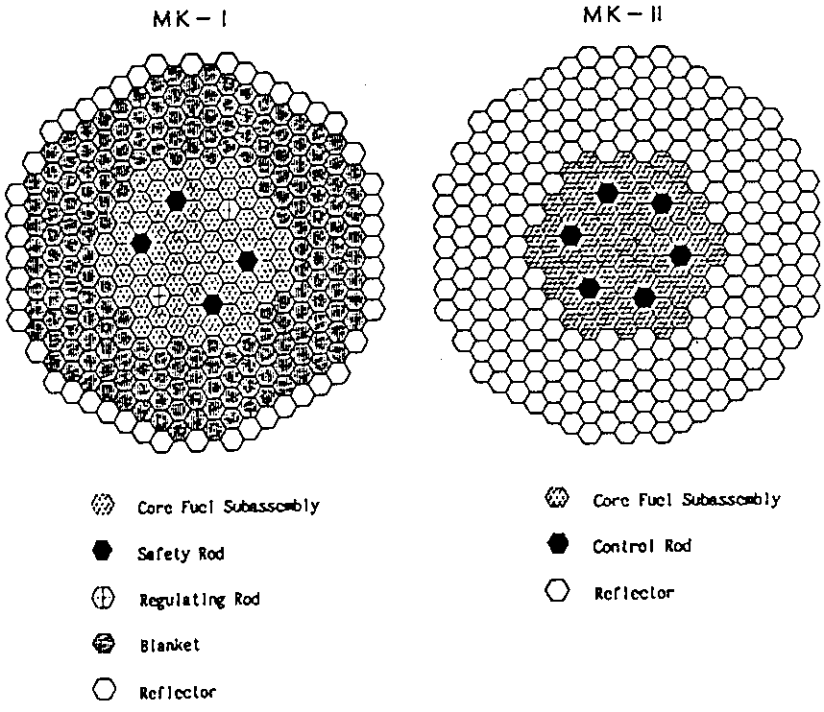

Fig.1 The comparison of core configuration of Mark-I and Mark-II

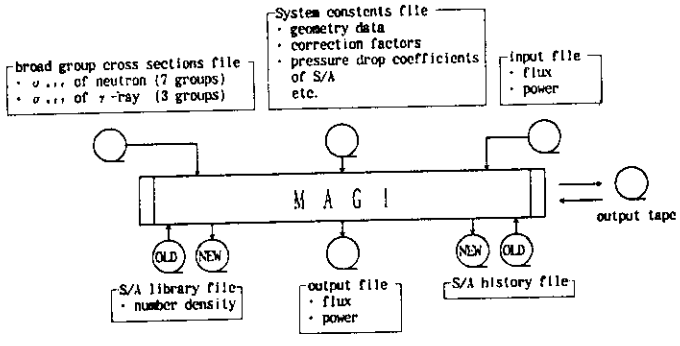

Fig.2 The basic input/output system diagram of MAGI system.

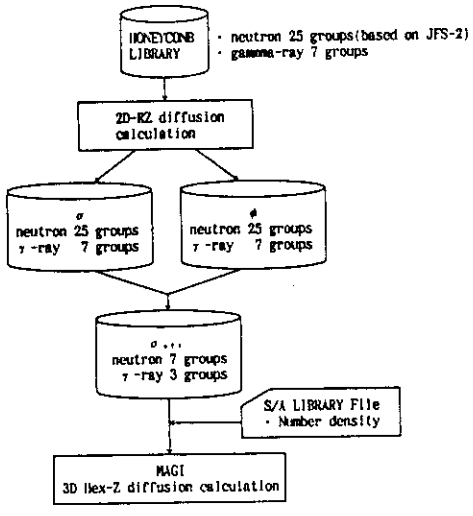

Fig.3. The flow chart for evaluating broad-group cross sections

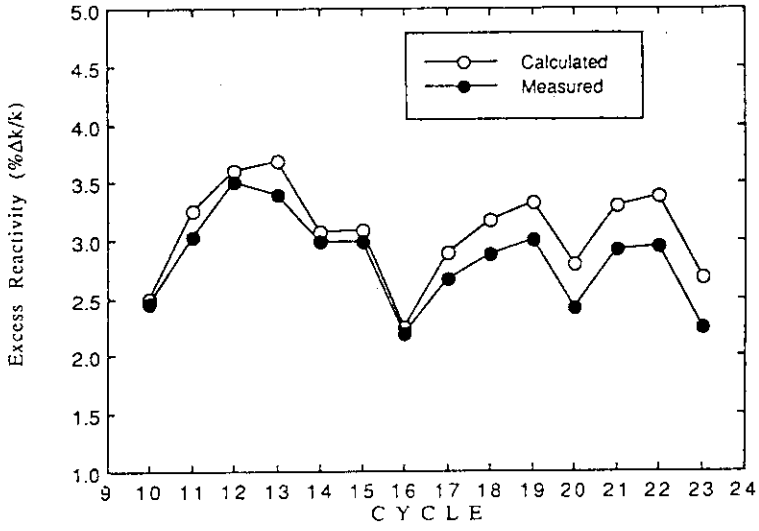

Fig 4 The excess reactivities from the 10th duty cycle to 23rd duty cycle.

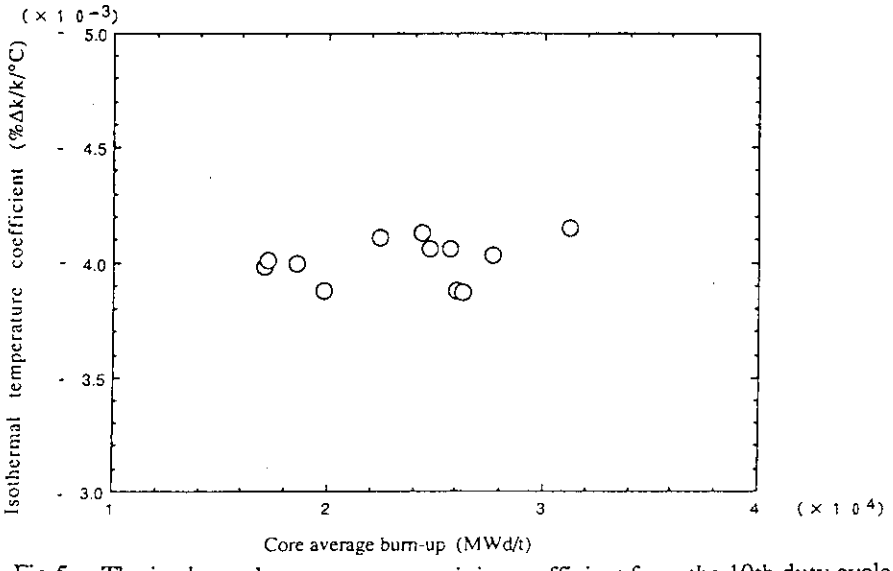

Fig.5 The isothermal temperature reactivity coefficient from the 10th duty cycle to 23rd duty cycle.

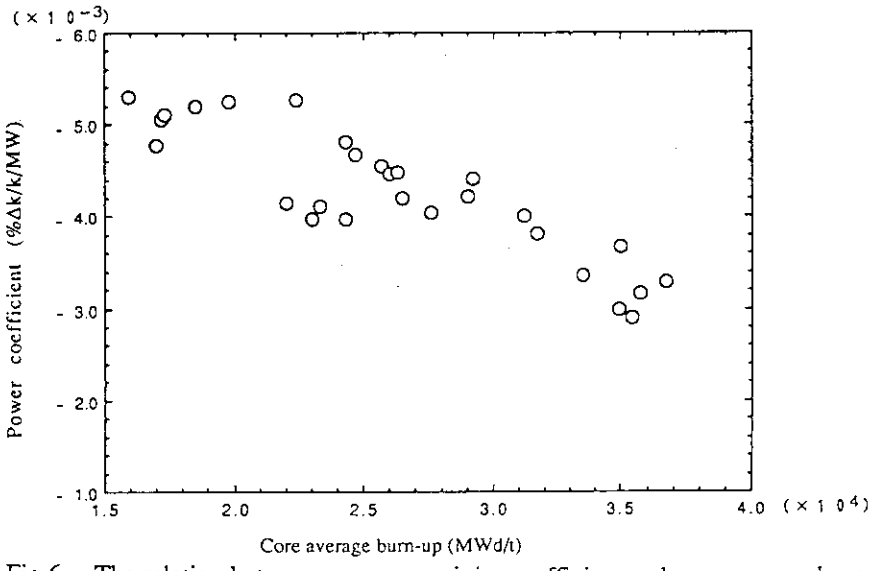

Fig.6 The relation between power reactivity coefficient and core average burn-up

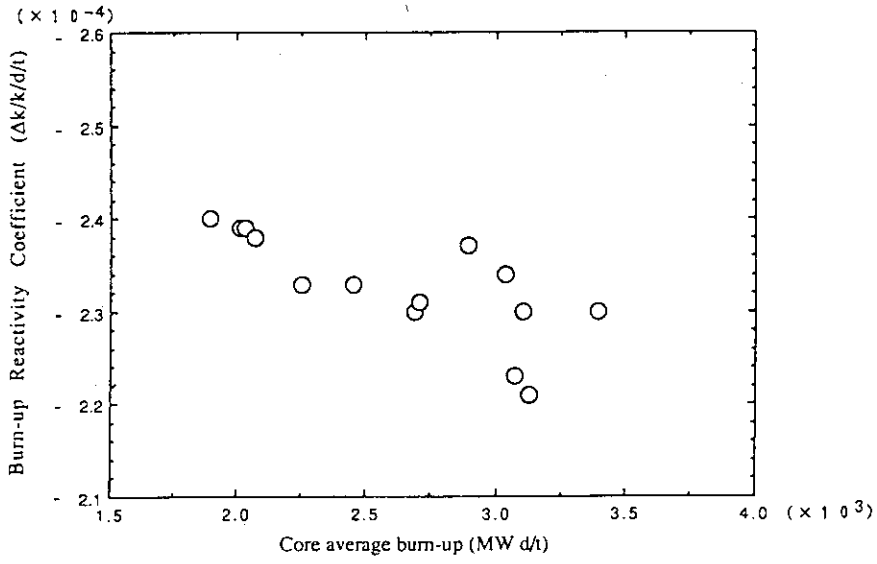

Fig.7 The relation between burn-up reactivity coefficient and core average burn-up

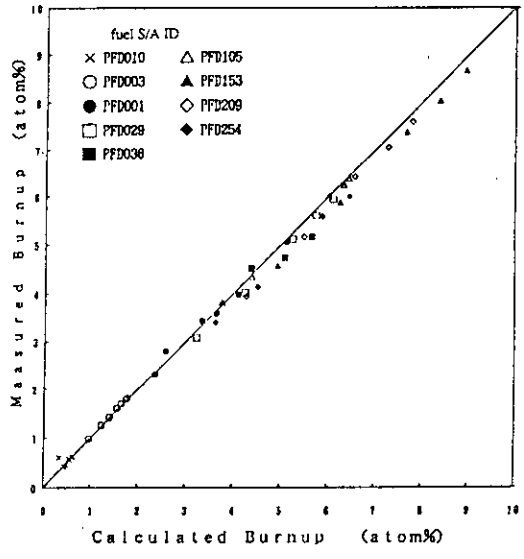

Fig.8 The corelation of burn-up between measured and calculated values

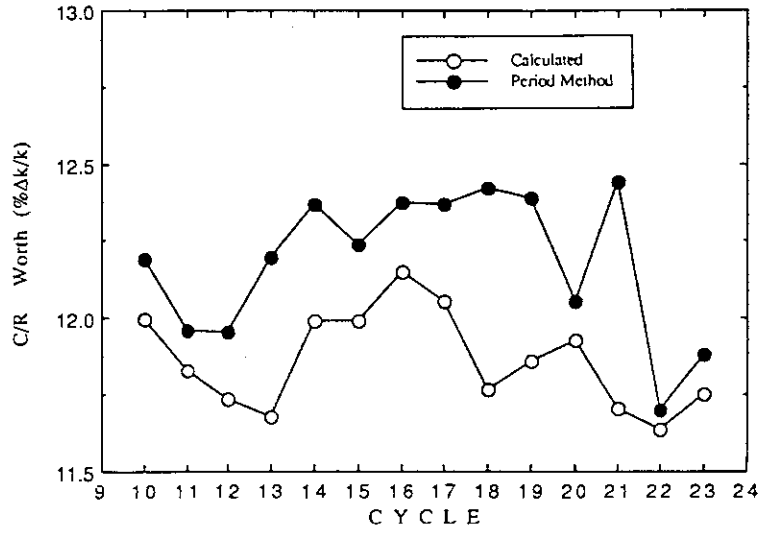

Fig 9 The comparison of calculated C/R worth and those measured by Period method from the 10th duty cycle to the 23rd duty cycle.

14. Core Management Method Considering Time-Dependent Xenon Distribution for High Flux Reactors

Akinobu NAKAJIMA, Hidemasa KATO and Kanji KATO
Energy Research Laboratory, Hitachi Ltd.,
Akinori TAGISHI
Hitachi Works, Hitachi Ltd.
and
Kazuhiko SOYAMA
Tokai Research Establishment,
Japan Atomic Energy Research Institute

ABSTRACT

In high flux research reactors, the flux and the power distribution are significantly affected by the transient xenon distribution. For supporting such operation as quick start-up or daily operation including large power level change, a practical core management method considering three-dimensional and time-dependent xenon distribution has been developed with sufficient accuracy and acceptable calculation time, and applied to reactor operation plan for upgraded Japan Research Reactor-3.

1.INTRODUCTION

To date, a number of useful core management programs[1-2] have been developed, mostly based on the steady state approximation to the xenon concentration. Some programs[3-5] considering spatial xenon dynamics have emerged, for quick start-up or load following operation in power reactors. However, improved methods are still needed to simulate accurate xenon behavior on account of the calculation time.

Particularly, the increasing need for higher flux densities on research reactors has required precise representations of time-dependent spatial xenon distribution in order to predict accurate power distribution.

The purpose of this paper is to demonstrate a core management method[6] which employs a three-dimensional and time-dependent xenon model, compared with the results of application to upgraded Japan Research Reactor-3[7-9] (upgraded JRR-3).

2.METHOD

2.1 CALCULATION MODEL FOR XENON NUMBER DENSITIES

In previous method, the xenon number density of space $\vec{r}$ and time $t+\Delta t$; $N(\vec{r},t+\Delta t)$ is calculated by numerically integrating differential equation on

the xenon number density, using the power density of space $\vec{r}$ and time t ; $P(\vec{r},t)$ and the power density of space $\vec{r}$ and time $t+\Delta t$; $P(\vec{r},t+\Delta t)$.

A disadvantage of this model is to require a large computation time on convergence for obtaining $P(\vec{r},t+\Delta t)$ in core performance prediction of the research reactor, which requires a large number of energy groups.

One of the usefull assumption which may successfully deal with a program is that the shape of power distribution does not change during a small time step interval for computing increase of xenon number density. This is called constant shape assumption (CSA), here. According to this assumption, the increase of xenon number density of space $\vec{r}$ and time $t+\Delta t$; $\Delta N(\vec{r},t+\Delta t)$ can be obtained from the power distribution of space $\vec{r}$ and time t ; $P(\vec{r},t)$ and the changing rate of the total reactor power, which is known from the operating plan. After $\Delta N(\vec{r},t+\Delta t)$ is obtained, the power distribution of space $\vec{r}$ and time $t+\Delta t$; $P(\vec{r},t+\Delta t)$ is calculated by iterations needed to achieve convergence of the power distribution.

Furthermore, in order to reduce the calculation time, an analytical solution has been used instead of a numerical integration in a previous method. This is called analytical solution technique (AST). This can bring an advantage of capability to select an effective large time interval Δt considering changing rates of xenon number density. Because of the reason mentioned above, the new model has adopted both the CSA and the AST in the developed core management program.

2.2 CORE MANAGEMANT PROGRAM

Figure 1 shows the core management program based on a three-dimensional, three-group diffusion model, which includes the new xenon model.
The program except the xenon model are basically simillar to the program[10] developed for the heavy water reactor "FUGEN", which is based on two-group diffusion model.

The features of the program are concentrated on the full core simulation for both the core and reflector region in which many irradiation facilities are installed.The program adopts the number of meshes in X-Y-Z co-ordinates:44×40×36, in which the number of meshes in the core region is 34×30×19. This means that 70% of the total number of meshes is used for simulating unsymmetrical out of core region accurately, since the experimental facilities in the reflector region bring a large influence for the flux distributions and the

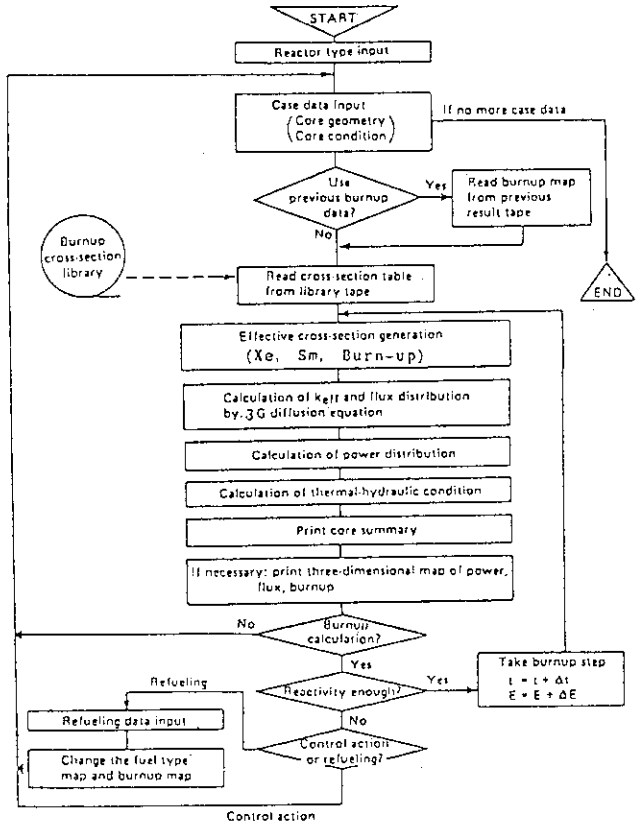

Fig.1 Flow chart of the calculation.

reactivity worths of the control rods.

Nuclear group constants are prepared by LWR-WIMS code[11] in this study.

3.RESULTS AND DISCUSSION

3.1 VERIFICATION

This program was verified by using the core performance test data of the upgraded JRR-3 as below.

(1) 20MW 100hr continuous operation (Experiment 1)
(2) 10~15MW daily operation (Experiment 2)
(3) Flux distributions measurement by Au-foil (Experiment 3)

The horizontal cross cection of the reactor is shown in Fig.2. The reactor is light water-cooled and moderated, of pool type. The maximum thermal neutron flux is approximately 2×10^{14}(n/cm^2·sec) and the full thermal power is 20MW. Many irradiation facilities are installed in the reactor. The standard fuels consist of 20 sheets of U-Al alloy fuel plate using U^{235} enrichment of approximately 20w/o. The control rods are made of hafnium with follower fuel. The core height is 750mm.

Figure 3 shows comparison between the calculated and measured reactivity, which mainly depend on the change of xenon concentration in the experiment 1. Here, the reactivity zero corresponds to critical state in the cold clean core. When the reactor starts up, the xenon reactivity increases and the saturated reactivity is approximately 5%Δk/k. After the reactor shuts down, the reactivity increases to the maximum of approximately 13.4%Δk/k. The calculated reactivity, which mainly depends on the change of xenon concentration, agrees with the measured reactivity within ±0.3%Δk/k.

Figure 4 shows the calculated and measured effective neutron multiplication factor. In the calculation, measured control rods positions were used, which were obtained in the Experiment 2. The calculated effective neutron multiplication factor agrees with the measurement within ±0.4%Δk/k. By the control rod calibration by the positive period method, the differential reactivity worth of a control rod is approximately 0.01%Δk/k/mm near the center of the core height. In ordinary operation of the reactor, the critical approach of the reactor is achieved by using symmetrical two control rods, and the height of both control rods is maintained approximately to be the same height. The caclulation error of effective neutron multiplication factor of ±0.4%Δk/k corresponds to the control rod stroke of ±20mm. The calculation time (CPU time) is 20 sec per burnup step using HITAC S-820 super computer (1.5GFLOPS). Approximately 25 steps are usually enough to make a plan of a reload cycle (4 weeks) operation. And, 15 steps are usually enough for a re-start-up plan. Namely, the total CPU time of about 500sec and 300sec are required for a cycle operation and a re-start-up plan, respectively.

Usually, reseach reactors have out-core neutron power monitors, and have not in-core monitors. Thefore, the overall power peaking factor is neccesary to be obtained only from the calculation by core management program. The calculated overall power peaking factor is not able to be directly compared with the measured data. Figure 5 shows a typical example of the calculated and the measured thermal neutron flux for axial direction in the standard fuel, located in the position A, which has the maximum overall power peaking factor. In the thermal neutron flux measurement, the height of all control rods (R,S and Sa) are the same of 260mm. The calculated flux agrees with the

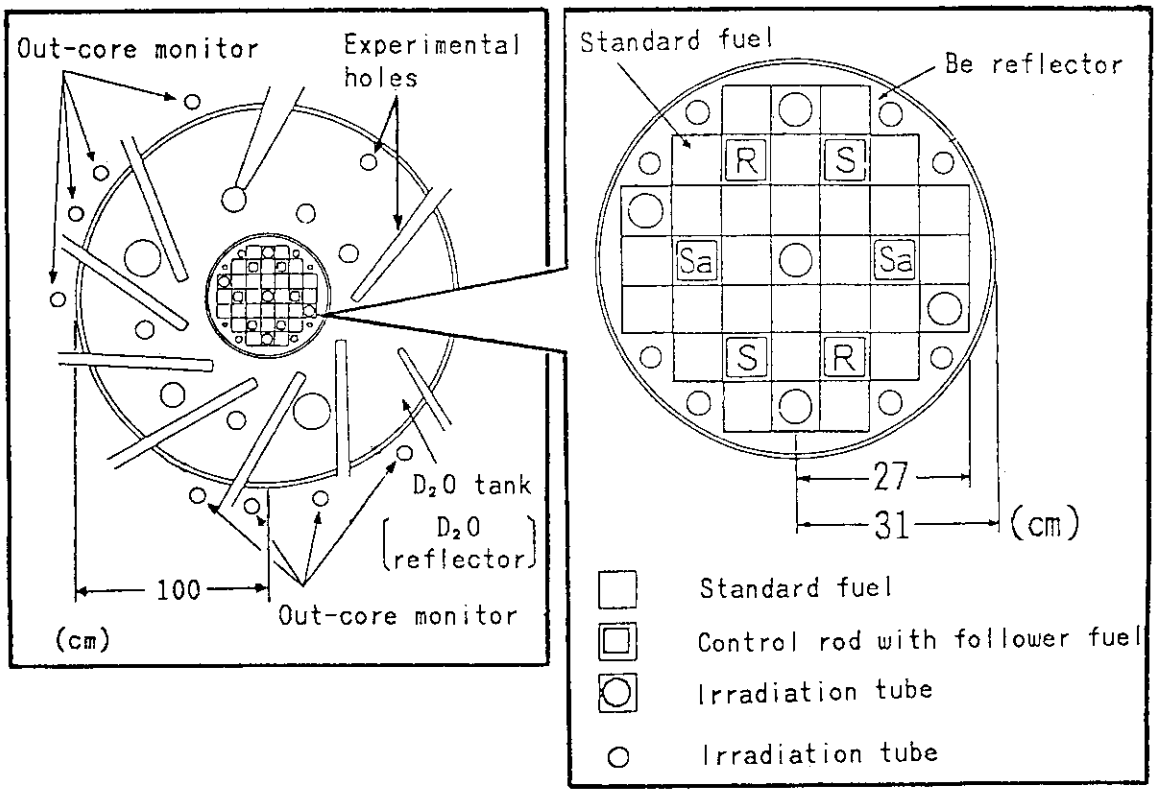

Fig.2 Horizontal cross section of upgraded JRR-3.

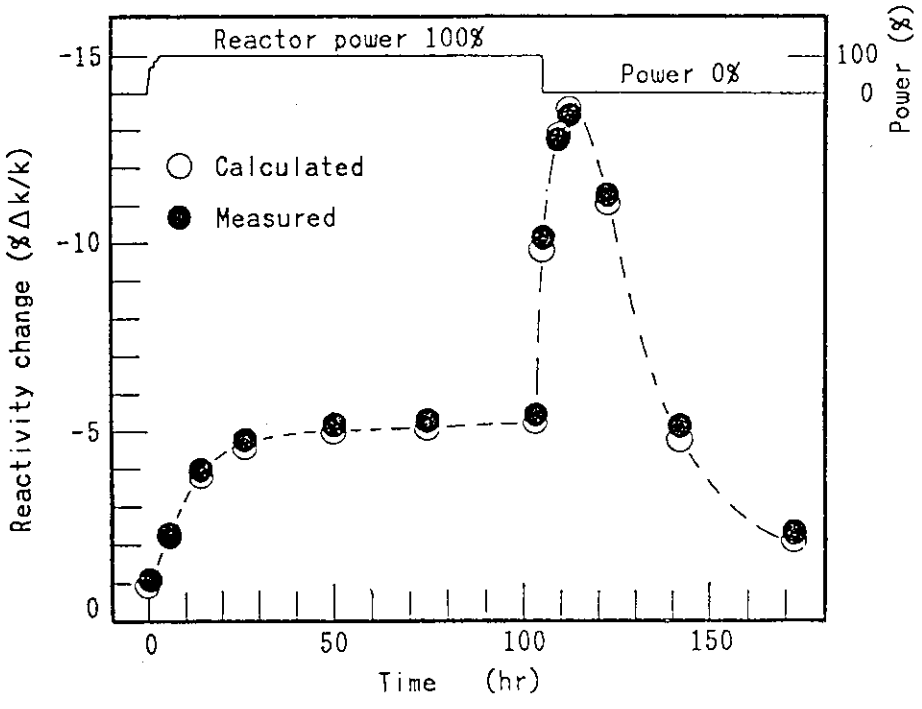

Fig.3 Calculated and measured Xe reactivity change mainly depending on the xenon concentration.

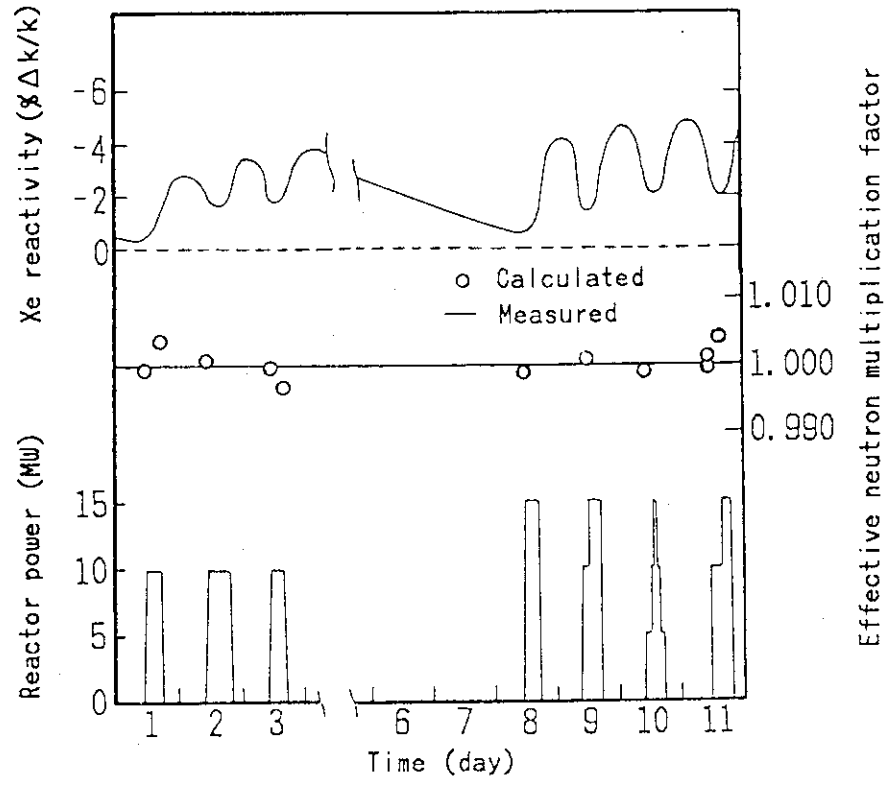

Fig.4 A typical example of the calculated and measured effective neutron multiplication factor in 10~15MW daily operation.

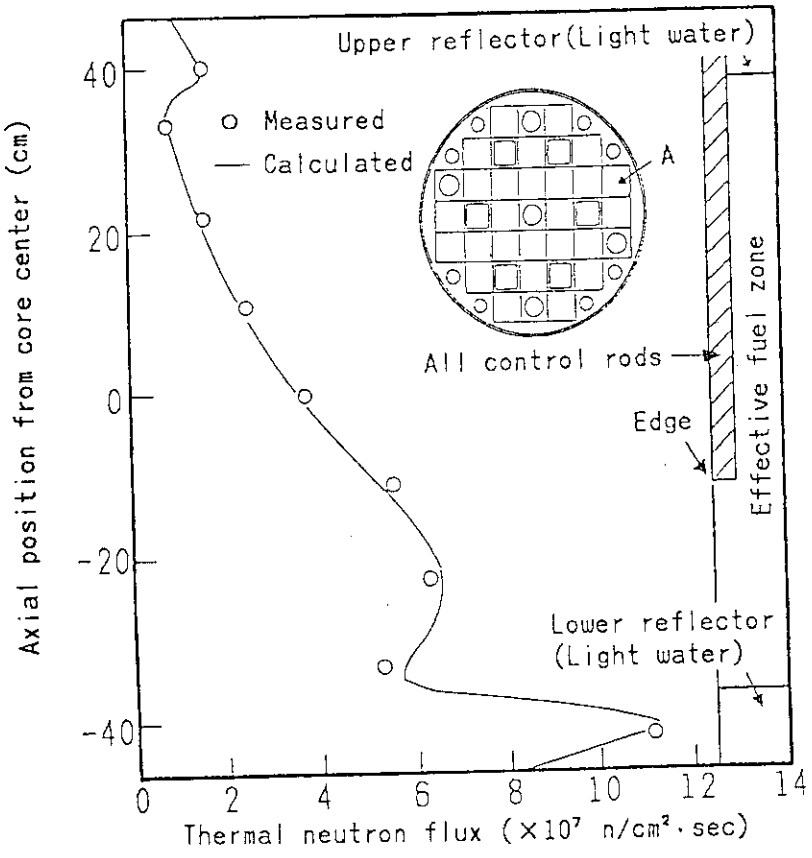

Fig.5 A typical example of the calculated and measured axial thermal neutron flux distribution in the hottest fuel.

measurement over the whole core in the rms error of 5%. This calculation error is smaller than the design margin of overall power peaking factor (20%).

3.2 APPLICATIONS

In research reactors, the reactor power is usually measured by the following two ways. One is obtained from neutron flux monitors (flux power), and the other is obtained from the measurement of coolant flow rates and coolant temperature differences (thermal power). When a control rod near the neutron detectors moves, the two kinds of reactor power has usually different values. The height of inserted control rods positions distinctively changes, when xenon concentration increases or decreases in high flux research reactors, such as upgraded JRR-3.

Therefore, we searched for the control rod pattterns which meet the restriction of overall power peaking factor and agreement of two measured reactor powers, using the program[12].

Figure 6 shows a typical example of the calculated and measured reactor powers and control rods positions in full power daily operation. On the start -up of the second day, at the beginning, the two control rods (Sa) are withdrawn up to 580mm to require the restriction of overall power peaking factor. The other four control rods (R,S) are withdrawn to attain the critical state, keeping the each rod to the same height. When the reactor power begins to be increased, the four conrtol rods are inserted because xenon concentration decreases by neutron absorption. After the control rods (R,S) are inserted in the position of the first day (190mm), the two control rods (Sa) are used to operate the reactor power. Through operation, the four control rods (R,S), near the neutron flux detctors, are operated to make the change of control rod heights to be small. This control rod pattern causes good agreement of two kinds of reactor powers, as shown in Fig.6.

The program have been applied to make operation plan of the control rod patterns through reload cycles. Figure 7 shows a typical example of the calculated overall power peaking factor including engineering margin, on the beginning three days in one of reload cycles. The peaking factors are smaller than the restricted value.

4.CONCLUSIONS

To support operation in high flux research reactors, a practical core management program have been developed, which consist of a three-dimensional three-group diffusion calculation. A new xenon model is adopted in the program, which is based on the assumption that the spatial power distribution in the core does not change in a calculational time step for xenon concentration. The model also uses the analytical solution of the differential equation of xenon instead of numerical integration.

In the program, 44×40×36 meshes in X-Y-Z co-ordinates are used. The calculational result was compared with measured data of the upgraded JRR-3. The calculated effective neutron multiplication factor agrees with the measurement within ±0.4%Δk/k. The calculation time (CPU time) is 20 sec per burnup step using HITAC S-820 super computer (1.5GFLOPS). Approximately 25

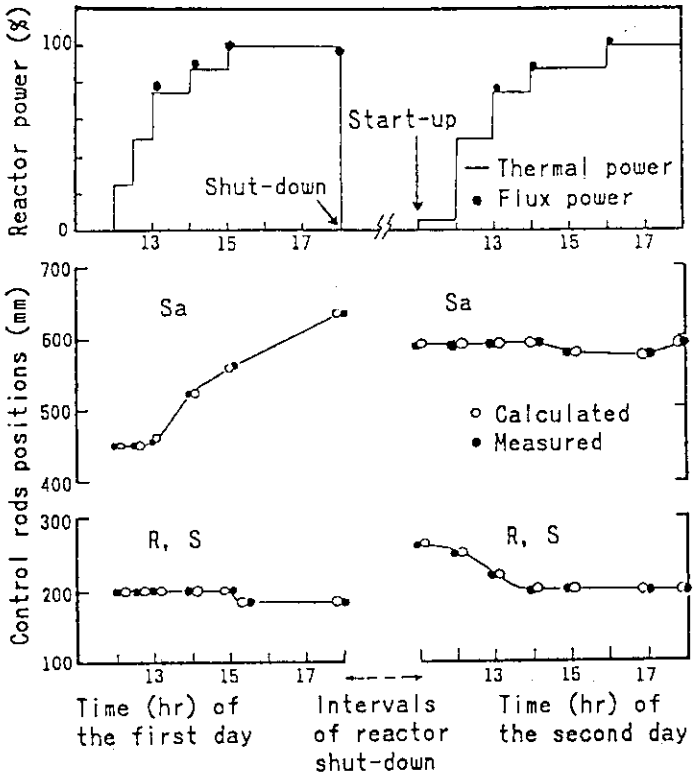

Fig.6 A typical example of the calculated and measured reactor powers and control rods positions in full power daily operation.

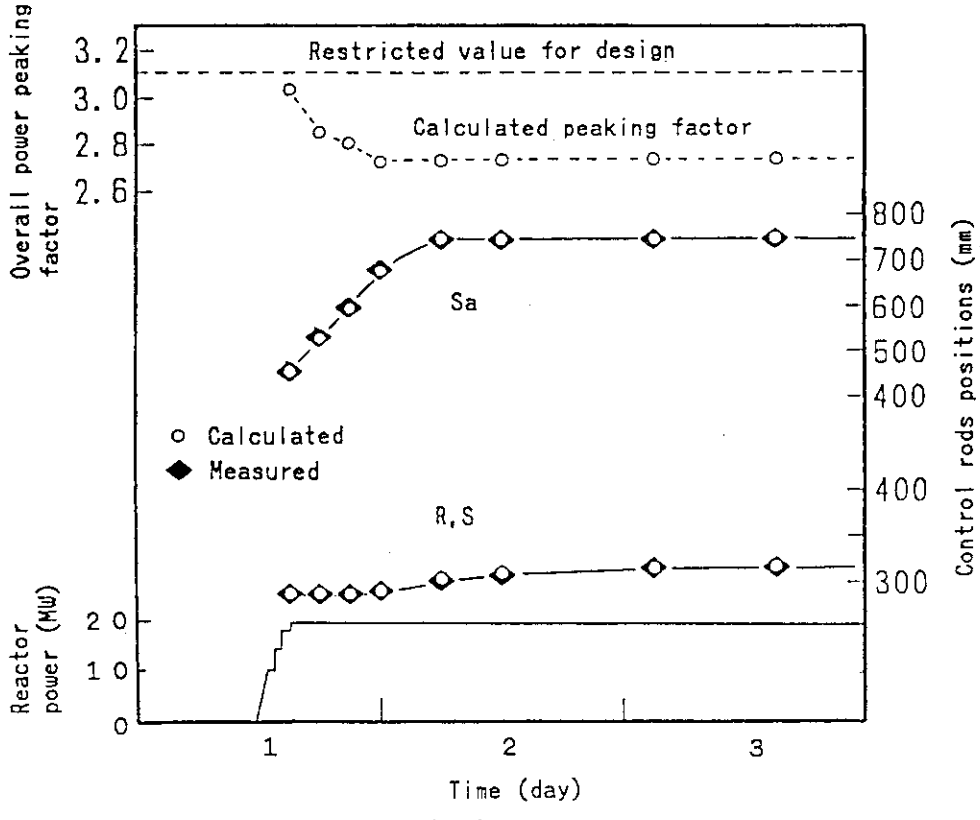

Fig.7 A typical example of the calculated overall power peaking factor and control rods positions on the beginning three days in one of reload cycles.

steps and 15 steps are usually enough for making a cycle operation and a re-start-up plan, respectively.

From these comparisons, the developed method is demonstrated to be practical in accuracy and calculation time.

ACKNOWLEDGMENTS

The authors are greatly indebted to N.Ohnishi and M.Issiki of Japan Atomic Energy Institute (JAERI) for continuous support necessary to this work. Thanks are also due T.Ohnishi and S.Izutsu of Hitachi,Ltd., A.Yamamoto of Hitachi Engineering Corporation (HEC),Ltd., M.Takami of CRC Research Institute, Inc., for the valuable advice given during the course of this work. Last but very important, thanks are expressed to the staff members of JAERI Tokai Establishment who engaged in the performance test and the operation of the upgraded JRR-3 .

REFERENCES

1. S.UCHIKAWA, Nucl. Technol., vol.33, 17 (1977).
2. T.KIGUCHI, K.DOI, T.FUKUZAKI, B.FROGNER, C.LIN and A.B.LONG, Nucl. Technol., vol.67, 38 (1984).
3. Y.BESSHO, H.MOTODA and M.WATANABE, Nucl. Technol., vol.58, 113 (1982).
4. N.YAMADA, T.KIGUCHI, Y.BESSHO, K.DOI and M.SAKURAI, Journal of the Atomic Energy Society of Japan, vol.23, 355 (1981).
5. H.TANAKA, H.KOJIMA, K.TAMURA, N.KITAMURA and Y.SUZAWA, 1991 Annual Meeting of the Atomic Energy Society of Japan, E23, 229 (1991).
6. A.NAKAJIMA, H.KATO, K.KATO, T.OHNISHI, A.TAGISHI and N.OHNISHI, 1991 Annual Meeting of the Atomic Energy Society of Japan, E24,230 (1991).
7. M.KAWASAKI, 1990 Fall Meeting of the Atomic Energy Society of Japan, "Outline of Design and Utilization on JRR-3".
8. N.OHNISHI, H.ICHIKAWA, M.TAKAYANAGI, M.WATANABE, H.KATO, A.TAGISHI and T.MIZUNO, 1990 Fall Meeting of the Atomic Energy Society of Japan, B31 89 (1990).
9. H.ICHIKAWA, N.OHNISHI, M.TAKAYANAGI, M.WATANABE, M.ISSIKI, H.KATO, A.TAGISHI and T.MIZUNO, 1991 Annual Meeting of the Atomic Energy Society of Japan, B1 57 (1991).
10. H.KATO, T.HAGA, S.OHTERU and H.KAMIKAWA, Nucl.Sci.Eng., vol.87, 361 (1984).
11. M.J. HALSALL, "LWR-WIMS, A Computor Code for Light Water Reactor Calculations", AEEW-R1498 (1982).
12. K.SOYAMA, H.ICHIKAWA, K.SHIMIZU, H.KATO, A.NAKAJIMA, A.TAGISHI, S.IZUTSU and T.MIZUNO, 1991 Annual Meeting of the Atomic Energy Society of Japan, B6, 62(1991).

1. Inherent Safety Features of the HTTR Revealed in the Accident Condition

K. KUNITOMI, M. SHINOZAKI, O. BABA, S.SAITO

Department of HTTR Project
Oarai Research Establishment, JAERI
Oarai-machi, Higashiibaraki-gun, Ibaraki-ken, 319-11, Japan

ABSTRACT

The High Temperature Engineering Test Reactor (HTTR) being constructed by JAERI (Japan Atomic Energy Research Institute) is a graphite-moderated and helium-cooled reactor with an outlet gas temperature of 950°C.

The inherent safety characteristics in the HTTR prevent temperature increase of reactor fuels and fission product release from the reactor core in postulated accident conditions. The reactor core can be cooled by a Vessel Cooling System (VCS) indirectly, even in the case that no forced cooling is expected during the accident such as primary pipe break. The VCS consists of independent water cooling loop and cooling panel around the reactor pressure vessel. The cooling panel whose temperature of 60-90°C cools the reactor pressure vessel by radiation and removes the decay heat from the core indirectly.

Furthermore, even if failure of VCS is assumed during this accident as a severe accident, the reactor core is remained safe despite the temperature increase of biological concrete shield around the reactor pressure vessel.

This paper describes the inherent safety features of the HTTR specially focused on the accident condition without forced cooling. The detailed analytical results of such an accident are described together with clarifying the role of the VCS.

INTRODUCTION

The HTTR[1] which is under construction at Oarai Research Establishment in JAERI will be utilized to establish and upgrade the technological basis and to conduct various modes of operation and test for the advanced HTGRs. A major design feature of the HTTR is, thus, that no forced cooling through the core is necessary for residual heat removal after the occurrence of an accident due to such inherent safety characteristics as large heat capacity and low power density of the core.

Various safety analyses have been carried out to confirm the validity of the safety provisions and features of the HTTR. Depressurization accidents, which are characterized by a primary pipe rupture, are one among the most important core heat up accidents. In the case of depressurization accidents, the fuel temperature and the reactor pressure vessel temperature are likely to increase due to the loss of integrity of forced cooling system. The danger is that fission product barriers may lose their function because the coated fuel particles fail under the higher temperature condition. However, the inherent safety feature of the HTTR prevents the immediate core heat up, and a direct core cooling system such as ECCS (Emergency Core Cooling System) of LWR (Light Water Reactor) is not necessary for the heat removal.

Safety evaluations on the depressurization accident were carried out in order to prove the above mentioned inherent safety characteristics and safety function of the VCS. The following cases are selected for the safety evaluations, one is the case that the VCS is normally operated during the

depressurization accident. The other is the case that the VCS is assumed to be failed after the depressurization accident occurs.

OUTLINE OF HTTR DESIGN

Hexagonal graphite block which hold fuel pins of coated particles are used in the reactor core. The fuel pins are cooled by helium gas which flows in the annular space between the fuel block and the fuel pins.

The HTTR reactor cooling system illustrated in Fig.1 consists of a main cooling system (MCS), a secondary helium cooling system, a pressurized water cooling system, an auxiliary cooling system (ACS), and the VCS. The ACS is in the stand-by condition during normal operation and is operated to remove residual heat from the core when there is a trouble in the MCS.

Fig.2 shows a flow sheet of the VCS. The VCS consists of an upper, lower and side cooling panel, heat removal adjustment panels around the reactor pressure vessel and a cooling water circulation system. The maximum temperature of the water inside the cooling panel is controlled less than 90°C. Cooling water flow rate in the heat adjustment panels is stopped by a shut valve so that the amount of the heat removal from the core during the normal operation is regulated in a design value.

Fig.3 shows a detailed structure of the cooling panel. The cooling panel which consists of fins and water cooling tubes is installed along the inner surface of the concrete biological shield, and the heat removal adjustment panels and thermally reflecting plates are located between the cooling panel and the reactor pressure vessel. The heat removal adjustment panel contains cooling water tubes. The amount of the heat removal is adjusted below 0.6 MW during the normal operation to accomplish the outlet gas temperature of 950°C and above 0.3 MW during the accident condition to cool the reactor pressure vessel.

SAFETY EVALUATION DURING THE DEPRESSURIZATION ACCIDENT

A. Accident Scenario

In the case of the primary pipe rupture, the primary coolant pressure decreases rapidly as the primary coolant leaks through the break. The reactor is scrammed by detecting the decrease of the differential pressure between the primary coolant and the pressurized water.

Forced cooling through the core is lost after the reactor scram. The depressurization accident is distinguished from a rupture of the heat tube in the pressurized water cooler by detecting increase of the pressure in the containment vessel. The ACS is not operated in this condition. The reason why the ACS is not operated during the depressurization accident is that the coolant circulation effective for core cooling can not be expected and the ACS operation is thought to cause rapid and local oxidation of graphite structure in the reactor pressure vessel. Operation of the VCS is continued as in the normal operational condition in order to cool the reactor pressure vessel and the core internal structure and to remove the decay heat.

A. Analytical Model

Temperature transients during the depressurization accident were analyzed with thermal-hydraulics codes TAC-NC[2]. Fig.4 shows an analytical model of TAC-NC during the depressurization accident. The concentric pipe is assumed to be completely broken beneath the reactor pressure vessel. The analytical model is an axisymmetric simulation of the reactor core, internal structure, reactor pressure vessel, VCS and concrete biological shield. Every flow path in the fuel columns is simulated by 6 equivalent flow paths in fuel columns of the analytical model. The equivalent flow paths have the shape similar to the real flow paths so that the same velocity, heat transfer coefficient and flow resistance can be obtained. The core decay heat is calculated according to Sure's formula including the decay heat of actinides in TAC-NC.

TAC-NC can calculate natural convection in the reactor pressure vessel during the accident condition. It is based on TAC-2D[3] which was developed by GA. The verification of TAC-NC was carried out by comparison of the experimental results obtained in a special test facility[4].

Natural convection in the reactor pressure vessel is calculated by a one-dimensional flow network model. The flow network consists of the flow paths in the reactor core and the flow path along the inner side of the reactor pressure vessel. The basic flow network equations to be solved are the steady-state, one-dimensional momentum equation for each flow path and the continuity equation, equation of state and energy equation for each plenum which connects each path.

The momentum equation for each flow path has the following forms;

$$\frac{Du_i}{Dt} = -\frac{1}{\rho_i}\left(\frac{\partial P}{\partial z}\right)_i - g - \left(\frac{\lambda_i}{d_i} + c_i\right)\frac{1}{2}|u_i|u_i$$

where

- c: inlet resistance coefficient in the flow path
- d: hydraulic diameter of the flow path
- g: gravity
- i: flow path number
- P: fluid pressure
- u: average flow velocity over the cross section
- z: coordinate of flow direction
- λ : friction factor
- ρ : fluid density

$$\frac{D}{Dt} = \frac{\partial}{\partial t} + u\frac{\partial}{\partial z}$$

The all analytical parameters such as thermal conductivity, emissivity, and heat transfer coefficient are considered to be conservative in order to obtain the maximum fuel temperature and pressure vessel temperature. The analyses also consider the magnitude of the fuel burn up when the accident happens since the properties of the graphite change gradually in high temperature and radiation exposure for a long time.

C. Analytical Results

Temperature transients during the depressurization accidents when the VCS is normally operated and when the VCS fails to operate were analyzed. Initial outlet gas temperature and outlet power before the accident for the analyses are 950°C and 30 MW, respectively.

Fig.5 shows the maximum fuel temperature, reactor pressure vessel temperature and concrete biological shield temperature during the accidents.

In both cases, the maximum fuel temperature decreases gradually after the reactor scram because the decay heat is smaller than the heat loss from the outer surface of the fuel pins to the fuel block by radiation. The maximum fuel temperature decreases until almost the same as that of the fuel block within 10 minutes and increases again. However it does not exceed the initial fuel temperature of 1495°C.

The peak vessel temperature appears at the side of the reactor pressure vessel and its temperature is 547°C at about 30 hours after the accident occurs when the VCS is normally operated. When the VCS fails to operate, it is slightly higher than that when the VCS is operated. Even if the VCS fails to operate, the concrete biological shield absorbs the core residual heat. Therefore, the maximum reactor pressure vessel temperature remains below the temperature limit of 550°C, assuring the integrity of the reactor pressure vessel.

The concrete biological shield temperature increases due to absorption of the decay heat in the

reactor core when the failure of the VCS operation is assumed.

Figs.6 and 7 show the radial temperature distribution of the reactor core during the depressurization accident when the VCS is normally operated and when the VCS fails to operate, respectively. The radial fuel temperature distributions of the reactor core in both cases within 100 hours are almost the same because the decay heat is removed from the reactor pressure vessel to the biological concrete or the VCS. However, temperature distributions of the reactor core at 500 hours are different because the inner surface temperature of the concrete biological shield increases gradually when the VCS fails to operate, and total amount of heat removal from the reactor core to the concrete biological shield from 100 to 500 hours is smaller than that from the rector core to the VCS when the VCS is normally operated.

The concrete biological shield temperatures in both cases are different. The average temperature of concrete biological shield when the VCS fails is approximately 70°C higher than when the VCS is normally operated. This is because the concrete biological shield absorbs the residual heat.

During the normal operation, the VCS cools not only the reactor pressure vessel operation in order to prevent creep damage of material of the reactor pressure vessel, but also the concrete biological shield.

In the case of the depressurization accident, the VCS cools the reactor pressure vessel and the concrete biological shield in order to maintain their structural integrity. However, even if the VCS fails, the core residual heat is transferred to the concrete biological shield, and the reactor core and the reactor pressure vessel remain safe. In this case, structural integrity of the concrete biological shield remains safe since the average temperature of the concrete biological shield does not exceed the temperature limit in spite of the local temperature rise of the concrete.

CONCLUSION

The maximum fuel temperature and reactor pressure vessel temperature are below the temperature limit, assuring the structural integrity during the depressurization both when the VCS is normally operated and when the VCS fails to operate. This is because most of the residual heat including the decay heat in the core is dispersed by the large thermal capacity of the core, and the residual heat is absorbed by the VCS or the concrete biological shield.

The VCS cools the reactor pressure vessel and the concrete biological shield during the normal operation and the accident conditions. However, even if the VCS were assumed to fail during no forced cooling accident such as depressurization accidents, the reactor core and the pressure vessel remain safe.

REFERENCE

(1) S.SAITO,"Present Status of HTGR Development Program in Japan", 11th International Conference on HTGR, Dimitrovgrad USSR, June 19-20, 1989.

(2) K.KUNITOMI et al, "Two-dimensional Thermal Analysis Code TAC-NC for High Temperature Engineering Test Reactor and its Verification", JAERI-M 89-001, 1989.

(3) S.S.Clerk and J.F.Peterson, "TAC-2D A General Purpose Two-dimensional Heat Transfer Computer Code", GA-9292, September 1969.

(4) M.Hishida et al, "Studies on the Primary Pipe Rupture Accident of a High Temperature Gas-cooled Reactor", NURETH-4, October 1989.

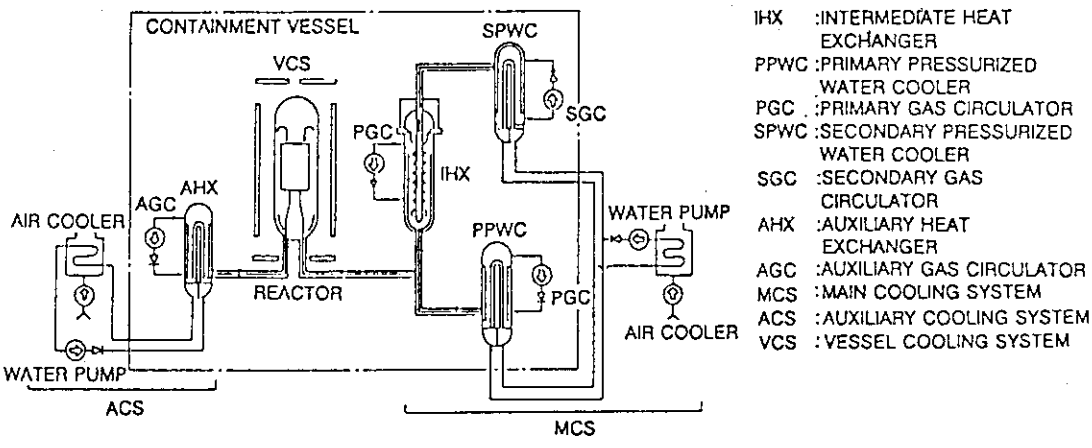

Fig.1 Flow sheet of the reactor cooling system

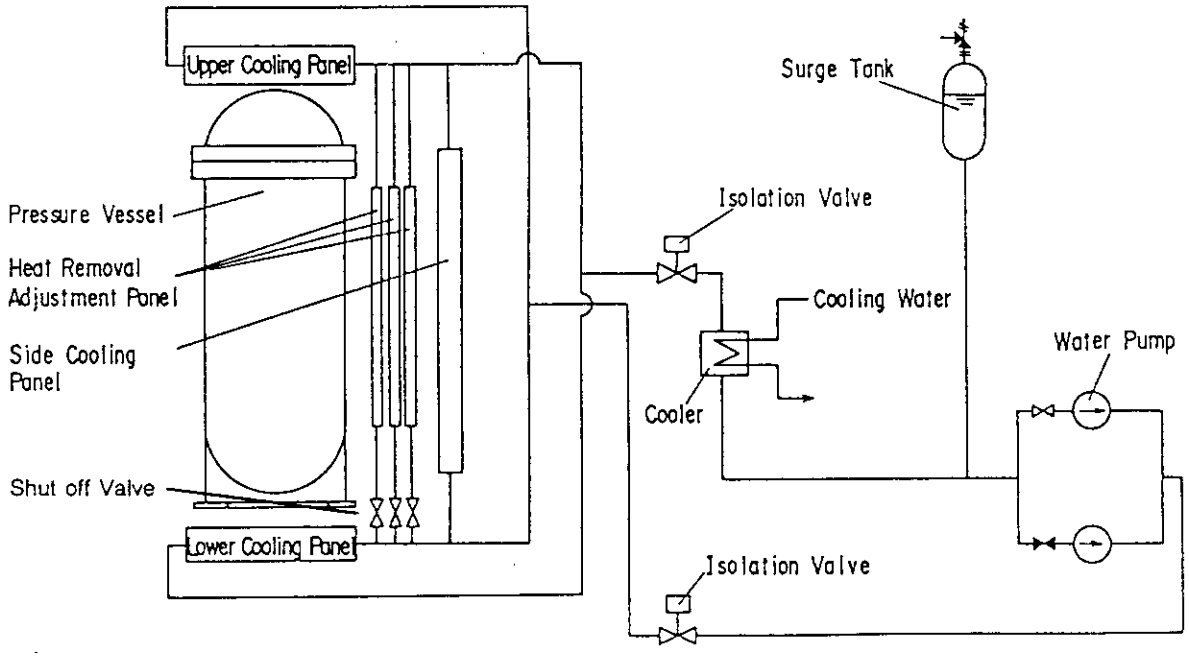

Fig.2 Flow sheet of the Vessel Cooling System (VCS)

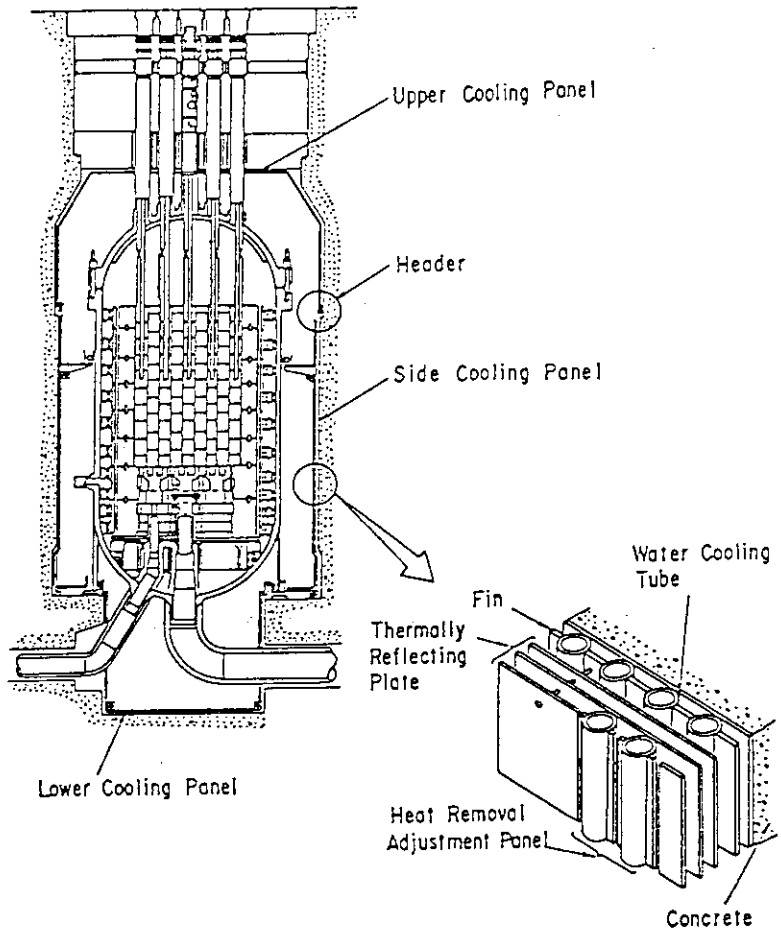

Fig.3 Location and detailed structure of the cooling panel

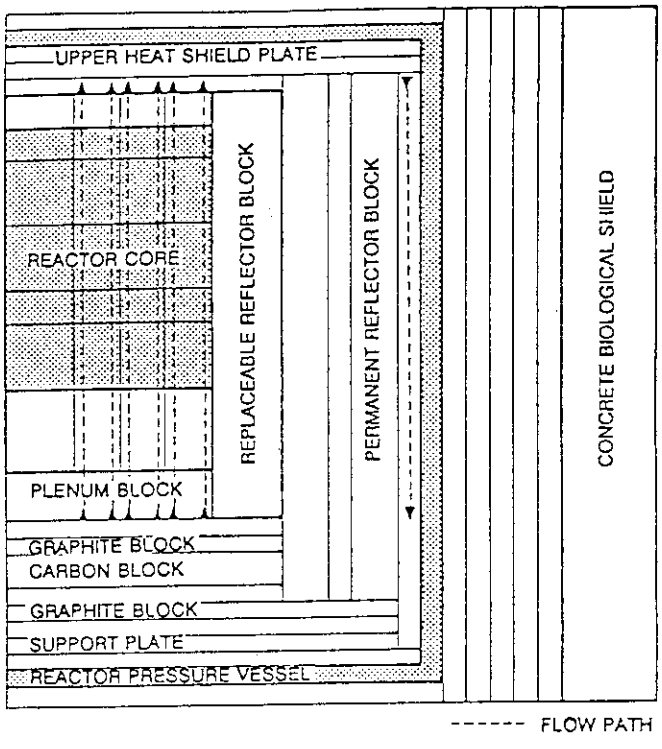

Fig.4 Analytical model of the reactor by TAC-NC

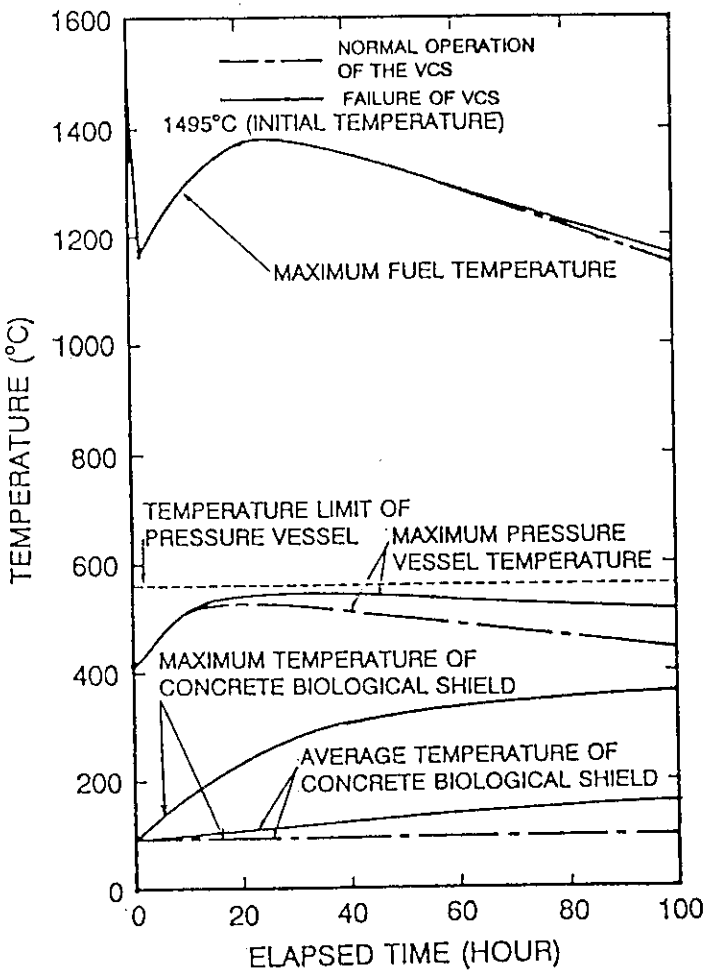

Fig.5 Analytical results during the depressurization accident

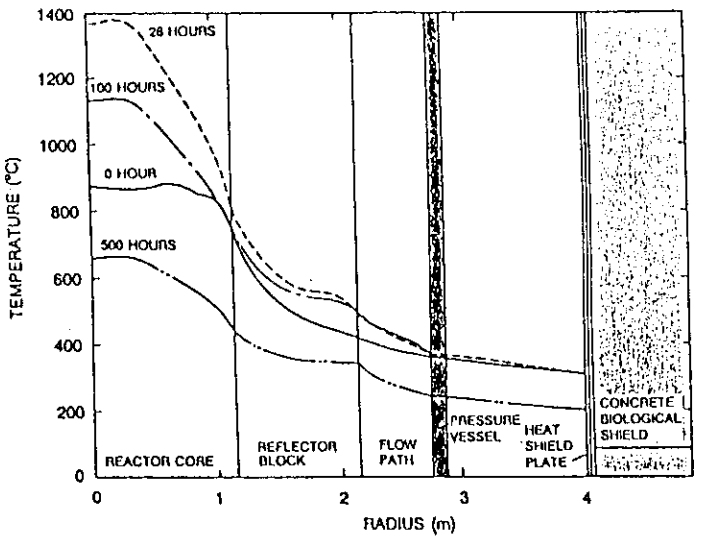

Fig.6 Radial temperature distribution of the HTTR during the depressurization accident when the VCS is normally operated

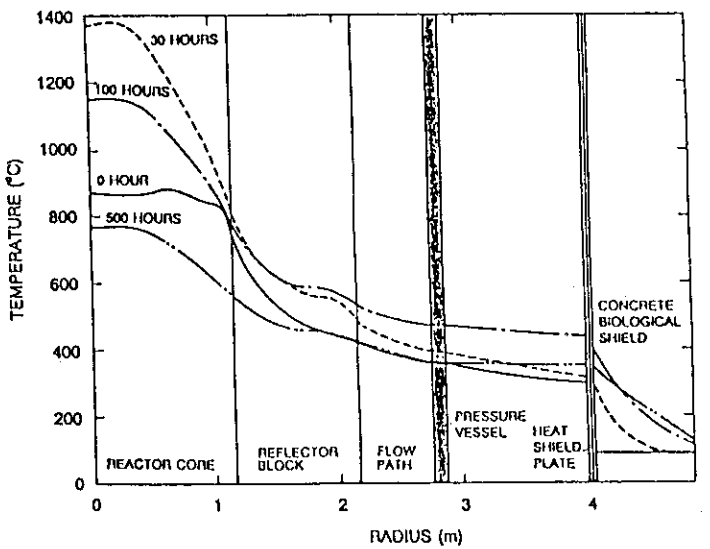

Fig.7 Radial temperature distribution of the HTTR during the depressurization accident when the VCS fails to operate

2. Safety Criterion for Burnout of the Plate-Type Fuel in Pressurized Conditions

Y. Komori, M. Kaminaga, F. Sakurai,
H. Ando, Y. Sudo, M.Saito and Y. Futamura

Oarai Research Establishment
Japan Atomic Energy Research Institute
Oarai-machi, Higashi-Ibaraki-gun, Ibaraki-ken, Japan

ABSTRACT

The reduced enrichment program for JMTR is now underway and the core conversion to LEU (Low Enrichment Uranium) is scheduled to be made in 1993. Consistent with the safety guide which have been recently developed for research and test reactors in Japan, the safety analysis for the JMTR LEU conversion was conducted. In the safety analysis, DNB (Departure from Nucleate Boiling) heat flux correlation for the JMTR downflow condition was reconsidered because recent studies on burnout show that DNB heat fluxes with thin rectangular channels under low flow rate and low pressure conditions are much lower than predicted values by conventional DNB correlations. Available DNB data, however, are very limited for the JMTR operation pressure range, so that DNB experiments were conducted simulating the JMTR fuel subchannel. Based mainly on the present experimental data, the DNB correlations scheme composed of three correlations was selected for the JMTR safety analysis. Errors of the correlations scheme with experimental data were evaluated in order to determine the allowable limit of the minimum DNB ratio for preventing fuel failure.

INTRODUCTION

In the safety analysis, the integrity of the fuel has to be ensured for anticipated operational transients of the reactor. Safety criteria for preventing fuel failure are as follows.

(1) Minimum DNB ratio (MDNBR) $\geqq$ 1.5
(2) No mechanical failure of the fuel
  1) The maximum temperature of the fuel meat $\leqq$ Blister threshold temperature
  2) Thermal stress of the fuel cladding $\leqq$ Proof stress
(3) Pressure of the Primary Cooling System $\leqq$ Maximum Operating Pressure

The MDNBR is specified as one of safety criteria for preventing the fuel failure due to burnout and it should not exceed 1.5 for the reactor anticipated operational transients as well as for the normal operation. Since MDNBR is calculated based on the DNB correlation , careful consideration should be taken for determination of the DNB correlation and allowable limit of MDNBR.

Recent studies by Mishima[1] and Sudo[2], however, pointed out that most of conventional DNB correlations might be applicable only to high flow rate conditions and positive subcooling at the burnout position. They also suggested that experimental DNB heat fluxes with thin rectangular channels under low flow rate and low pressure conditions are much lower than predicted by those correlations particularly for downward flow, due to the buoyancy effects.

Therefore, DNB experiments were conducted to provide DNB heat flux data for reconsidering DNB correlations applicable to JMTR thermohydraulic conditions, because available data are very scarce except for ones around atmospheric pressure.

DNB EXPERIMENT

OPERATING CONDITIONS OF JMTR

The fuel element of the JMTR has 19 flat fuel plates arranged in parallel, with 2.67 mm water gap. The core thermohydraulic design of the JMTR has been made for the normal operation condition at 50MWt, and primary coolant is pressurized at about 13 kg/cm^{2}abs (reactor core). Fuel plates are cooled by forced convection of downflow at the velocity of 10 m/s in order to avoid the nucleate boiling on the surface of fuel plates. Safety analysis for the normal operation, anticipated operational transients and postulated accidents are made in the pressure range of 1 ～13 kg/cm^{2}abs and the coolant velocity range of 0～10 m/s.

EXPERIMENTAL LOOP

The experimental loop consists of a test section, a pressurizer, a heat exchanger, a circulating pump, a resin tank, an electric heater, a flow control valve, stop valves and pipings connecting these components. A flow diagram of the experimental loop is shown in Figure 1. The flow orientation in the test section can be set either upward or downward with stop valves. Valves are placed in front of the loop for easiness of operation. Loop water can be pressurized up to 18 kg/cm^{2}abs by helium gas. The loop is filled with distilled water and the resin tank is installed to maintain water quality. The electric heater is employed to control the inlet water temperature.

The test section, which was designed simulating the JMTR fuel subchannel, consists of a pair of heating plates, alumina insulators, glass windows and frames as shown in Figure 2. Each heating plate, which is 760 mm long, is made of Inconel 600 and placed on the two opposite sides of the flow channel with a gap of 2.67 mm, simulating a rectangular subchannel of a fuel element. Besides heating plates of 61.6 mm wide which is equal to the real fuel plate, heating plates of 30.8 mm and 17.2 wide were also employed. Glass windows are attached on both sides of the flow channel especially for first few test sections in order to allow us to observe flow patterns.

To eliminate premature burnout by corner effect, edges of the flow channel are extended 5 mm beyond edges of heating plates. The test section is enclosed in a containment tube for protecting personnel from flashing steam when a test section is failed. The power to the test section was applied by a 80 V, 2600 A, ac power supply. The flow rate of coolant is measured with a turbine flowmeter and a mass flowmeter. The temperature and pressure of coolant are measured in the upper and lower plena. Sheathed Chromel-Almel thermocouples are spot-welded with thin strips of stainless steel on the back surface of each heating plate to detect DNB.

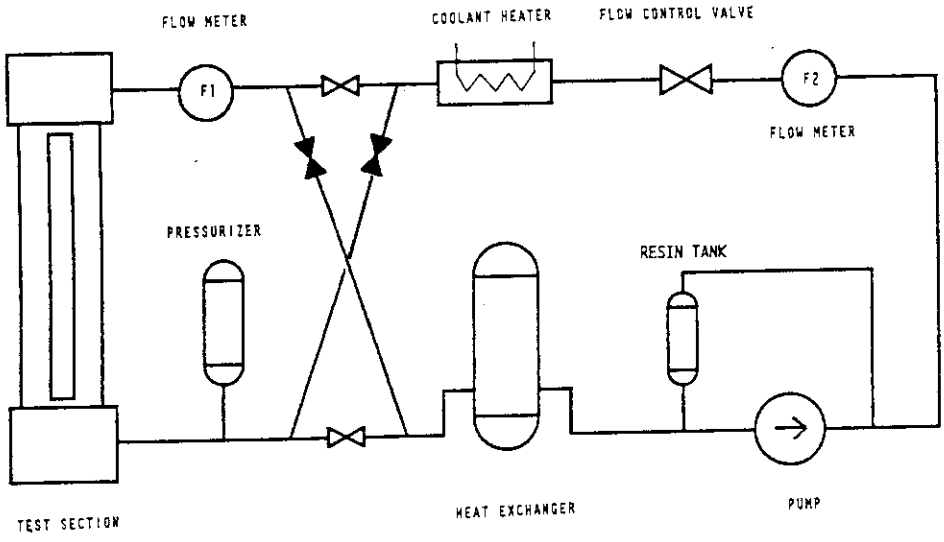

Figure 1 Flow Diagram of Experimental Loop

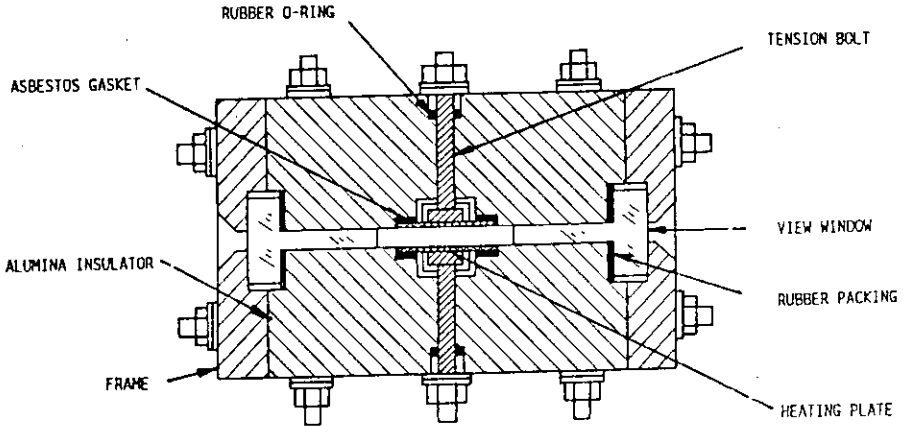

Figure 2 Schematic of Test Section

EXPERIMENTAL PROCEDURE AND CONDITIONS

The loop is evacuated by a vacuum pump, then filled with distilled water and the pump is operated for purification until electric conductivity reaches below 0.1 μS/cm. Then, coolant is heated up to about 80 ℃ with the electric heater and heating plates for deaeration. After deaeration, coolant velocity and pressure are adjusted to the determined values. The coolant inlet temperature is kept at 49 ℃ by feedback control. The electric power to heating plates is increased stepwise until burnout occurs. When burnout occurs and any of thermocouples attached on heating plates detects a steep rise of temperature beyond a preset value which is 400 ～ 450℃ in most cases, the power to heating plates is instantaneously cut off in order to prevent failure of heating plates. The ranges of variables covered in the present experiment are as follows.

(1) Flow direction ; Downward
(2) Pressure ; 1 ～ 13 kg/cm^{2}abs
(3) Flow rate ; 0 ～7000 kg/m^{2}s
(4) Coolant inlet temperature ; 49℃ (Inlet Subcooling ; 51～ 145℃)
(5) Equivalent diameter ; 5.4 ～ 5.6 mm
(6) Heat flux ; 30 ～ 1150 kcal/m^{2}s

EXPERIMENTAL RESULTS

Periodic flow instabilities of large amplitude, which resulted in premature burnout, were observed in initial few experiments. Flow rate and temperature of heating plates were oscillated with a period of few seconds. This flow instability was presumably thought to be a pressure-drop oscillation type. There possibly remained certain amount of gas in the upper plenum which served as an upstream compressibility in spite of the deaeration procedure. This was eliminated by connecting the inlet piping and the inlet of the flow channel directory with a guide tube to cancel the effect of the upper plenum. DNB behavior varied strongly depending on experimental conditions such as pressure and mass flow rate, and this suggests the difficulty in predicting DNB heat fluxes by a single correlation even for the JMTR operating range. Successful results could not obtained in experiments with heating plates of 61.6 mm wide, because heating plates failed around edges. This might be due to uneven flow distribution in lateral direction of heating plates, and the uneven flow causes abnormal local heating which resulted in the failure of heating plates far below DNB heat fluxes. No such troubles were experienced for heating plates of 30.8 mm and 17.2 mm wide.

COMPARISON OF EXPERIMENTAL DATA WITH EXISTED DNB CORRELATIONS

Existing DNB heat flux correlations were reviewed to consider applicability to the JMTR downflow condition. Since existing correlations are generally supported by many data in other studies, it is considered that selection of the existing correlation which satisfactorily represents experimental data would be more reliable than development of new correlations. Reviewed correlations are listed in Table 1. Five round tube correlations (Lowdermilk, Macbeth, Labuntsov, Thorgerson, Katto) and Mirshak correlation in Table 1 were reviewed by IAEA[3]. Bernath correlation[4] was applied to the JMTR original safety analysis which was revised in 1983. Zenkevich-Subbotin correlations were applied to the HFIR thermohydraulic design with an uncertainty factor of 1.3 based on comparison with DNB data by Gambill[4]. Sudo correlations scheme[2] was proposed in recent experimental study for the JRR-3 safety analysis. Considering ranges of thermohydraulic conditions for each correlation, Labuntsov, Mirshak, Bernath and Sudo correlations appear to be applicable to the JMTR safety analysis.

Table 1 Thermohydraulic Parameters' Ranges of DNB Heat Flux Correlations

		Pressure (kg/cm²abs.)	Velocity (m/s)	Subcooling (℃)	Steam quality
Lowdermilk		Atmospheric	0.03～30	～24 (inlet)	positive
Macbeth	low Velocity	1 ～138	14～841(kg/m²s)	65～1400(kJ/kg,inlet)	positive
	high Velocity	Atmospheric	14～5750(kg/m²s)		positive
Labuntsov		1 ～200	0.7 ～45	0 ～240 (burnout point)	negative-0
Thorgerson		1.7 ～13.3	3.05～18.3	>25 (burnout point)	negative
Katto		1 ～200			negative - positive
Mirshak		1.7 ～5.9	1.5 ～13.7	5 ～75 (burnout point)	negative
Bernath		1 ～210	0.1 ～47.6	0 ～182 (burnout point)	negative-0
Zenkevich		105 ～217	>270(kg/m²s)	>10 (burnout point)	negative
Sudo		Atmospheric	<3000(kg/m²s)		negative - positive

Experimental data at 1, 5, 13 kg/cm²abs are compared with these DNB correlations as shown in Figure 3 (a)～ (c). Non-dimensional heat flux : q^* is taken on the ordinate and non-dimensional mass velocity : G^* on the abscissa and the coolant inlet temperature is 49 ℃. Experimental data are in good agreement with Sudo correlations scheme which predicts the lowest DNB heat fluxes of four correlations. Similar results were obtained at other pressures of 1 ～13 kg/cm²abs. The correlations scheme agrees fairly well with experimental data especially at atmospheric pressure.

Sudo correlations scheme consists of three correlations as shown below.

$$q^* = 0.7(A/A_H)(W(\gamma_l/\sigma)^{1/2})^{1/2} / (1+(\gamma_g/\gamma_l)^{1/4})^2 \quad (1)$$

$$q^* = (A/A_H)(\Delta h_i/h_{fg})\, G^* \quad (2)$$

$$q^* = 0.005(G^*)^{0.611} \quad (3)$$

Correlation(1) means DNB heat flux for the counter-current two phase flow under the flooding phenomena[2], and correlation(2) is derived from the condition that the exit water temperature reaches saturation[ ]. Correlation(3), which was proposed by Sudo[2], is correspondent to 1.5 times of the lower limit of the experimental data for upflow. The correlation(3) is applied for downflow in the high flow region because the significant difference between upflow and downflow is not seen in the high flow rate region. For downflow, lower q^* of correlations(2) and (3) is selected. If the selected q^* is less than the q^* calculated by correlation(1), then the correlation(1) is applied. Therefore, correlations(1), (2), (3) are virtually applied to the low, intermediate and high flow rate region respectively.

For low flow rate region, correlation(1) seems to provide conservative prediction compared with present experimental data as shown in Figure 3(a)～3(c). Other experimental data by Mishima[1] and Sudo[2], however, are in good agreement with correlation(1), so that further data should be obtained in the low flow rate region.

For medium flow rate region, present experimental data well agree with correlation(2), though the correlations scheme slightly overpredict DNB heat fluxes just below the intersection of correlation(2) and correlation(3) at 5 kg/cm²abs as shown in Figure 3(b). Coolant outlet temperatures reached near saturation temperature in most cases, so that the thermohydraulic condition for correlation(2), in which exit quality is zero, was satisfied.

For high flow rate region, downflow DNB data with a rectangular subchannel by Gambill[4] and Mirshak[6] were compared with correlation(3) because the present experiments could not cover the region due to limitation on electric power capacity for heating plates. These data are larger than predicted values by correlation(3) and this difference might be due to effect of subcooling, because correlation(3) is experimentally determined without considering any effect of subcooling. Downflow DNB data in the high flow rate region by Gambill and Mirshak are well correlated empirically by modifying correlation(3) with a factor of subcooling as follows.

$$q^* = 0.005(G^*)^{0.611}(3.75\, C_p \Delta T_{SUB} / h_{fg} + 1) \quad (4)$$

DNB data are in good agreement with the correlation(4) as shown in Figure 4. Predicted DNB heat fluxes by the correlation(4) are close to predicted values by subcooled-boiling DNB correlations such as by Mirshak or Labuntsov.

Although Sudo correlations scheme has been supported by many round and rectangular channel DNB data around the atmospheric pressure, the extended applicability of the scheme to the pressurized condition was not verified. It became clear by the present study that the correlations scheme is in good agreement with experimental data for the pressure range of JMTR(1 ～13 kg/cm²abs).

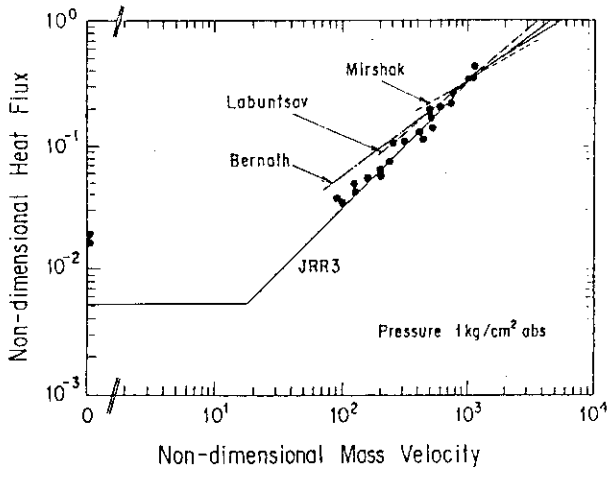

(a) Pressure : 1 kg/cm²abs

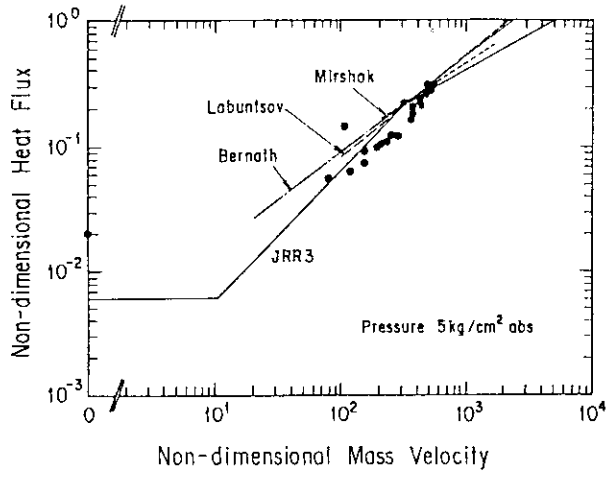

(b) Pressure : 5 kg/cm²abs

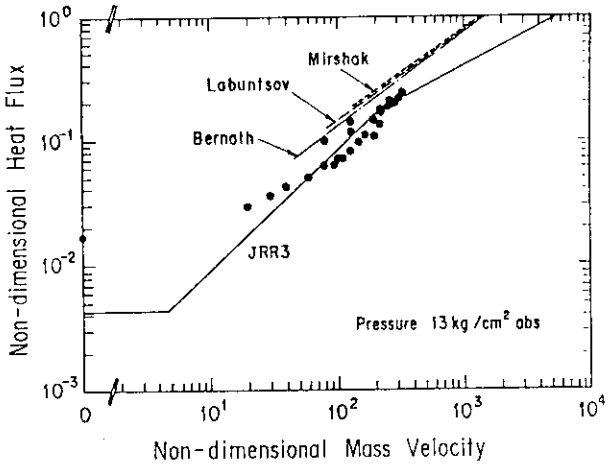

(c) Pressure : 13 kg/cm²abs

Figure 3 Comparison of Experimental DNB Data with DNB Correlations

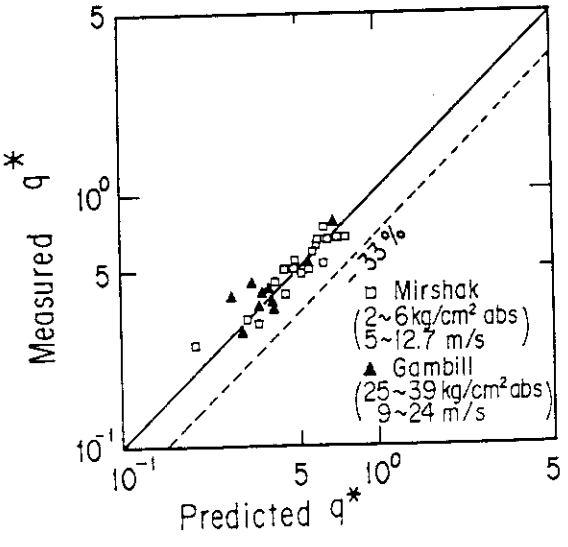

Figure 4 Comparison of Experimental DNB Data with Correlation(4) in the High Flow Rate Region

ALLOWABLE LIMIT OF MDNBR

DNB data in the present study and other studies are compared with Sudo correlations scheme to check the error of correlations for determination of allowable limit of MDNBR as shown in Figure 5. The dotted line is correspondent to 2/3 of the predicted DNB heat fluxes, and no experimental data fall below the dotted line. Therefore, it is concluded that Sudo correlations scheme with subcooling factor for the high flow rate region gives good predictions, allowing the error of 33% to the lower limit of the experimental data, so that minimum DNBR of 1.5 is considered to be conservative criterion for preventing fuel failure.

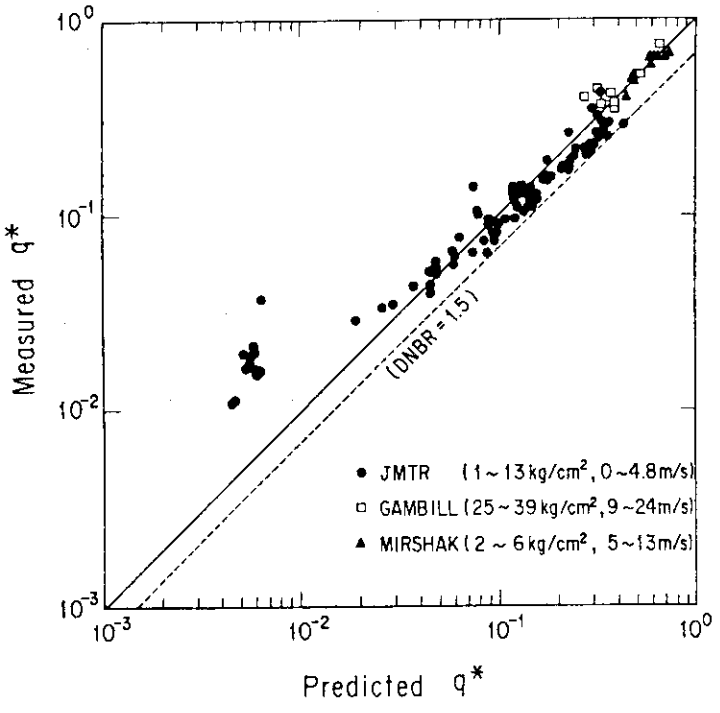

Figure 5 Comparison of Experimental DNB Data with the Correlations Scheme

CONSIDERATION ON EXPERIMENTAL CONDITIONS

Following parameters have to be carefully considered in designing DNB experiments from the viewpoint of similarity to the reactor fuel subchannel.

(a) Equivalent diameter and heated length
(b) Axial distribution of heat flux
(c) Quality, mass velocity and pressure of coolant

Parameters (a) and (c) in the present experiments are designed to be almost identical to a JMTR fuel subcahnnel except that mass velocity doesn't fully cover the JMTR operating range because of limited power capacity of the experimental loop. Experiments in other studies provides complementary data. Regarding (b), experiments were conducted with test specimens of uniform heat flux, whereas the heat flux of the reactor fuel is axially distributed in the shape of chopped cosine.

Kaminaga[7] et al experimentally investigated the effect of heat flux distribution on DNB heat flux in the JRR-3 flat plate fuel and showed that Sudo correlations scheme was applicable not only for uniform heat flux but for non-uniform heat flux.

Therefore, the difference in heat flux distribution is not thought to cause significant effect on DNB heat fluxes.

CONCLUSION

DNB experiments with the thin rectangular channel, simulated the JMTR fuel subchannel, were carried out to determine applicable DNB correlations to the JMTR safety analysis for conversion to LEU fuel. Comparison of experimental DNB data with DNB correlations shows that the Sudo correlations scheme with a subcooling factor for high flow rate region, which predicts the lowest DNB heat fluxes, is in good agreement with experimental data. MDNBR of 1.5 with the correlations scheme is considered to be conservative criterion for preventing fuel failure.

NOMENCLATURE

A ; Flow Area (m^2)
A_H ; Heated Area (m^2)
C_p ; Specific Heat (kcal/kg℃)
G ; Mass Velocity (kg/m^2s)
G^* ; Non-dimensional Mass Velocity $= G / [\lambda \gamma_g g(\gamma_l - \gamma_g)]^{1/2}$
h_{fg} ; Latent Heat of Evaporation (kcal/kg)
Δh_i ; Inlet Subcooled Enthalpy (kcal/kg)
q ; DNB Heat Flux ($kcal/m^2s$)
q^* ; Non-dimensional DNB Heat Flux $= q / h_{fg} [\lambda \gamma_g g(\gamma_l - \gamma_g)]^{1/2}$
ΔT_{SUB} ; Water Subcooling (℃)
W ; Width of Channel (m)
γ_g ; Specific Weight of Vapor (kg/m^3)
γ_l ; Specific Weight of Liquid (kg/m^3)
λ ; Characteristic Length (m) $= [\sigma/(\gamma_l - \gamma_g)]^{1/2}$
σ ; Surface Tension (kg/m)

ACKNOWLEDGEMENTS

The authors would like to express their hearty gratitude to Professor K. Mishima of Kyoto University for his suggestions and discussions.

REFERENCES

[1] K. Mishima, The Effect of Flow Direction and Magnitude on CHF for Low Pressure in Thin Rectangular Channels, Nucl.Eng.Design 86, pp.165-181,1985
[2] Y. Sudo, Experimental Study of Differences in DNB Heat Flux between Upflow and Downflow in Vertical Rectangular Channel, J.Nucl.Sci.Technol. Vol.22, No.8, pp.604-618, 1985
[3] Research Reactor Core Conversion from the Use of Highly Enriched Uranium to the Use of Low Enriched Uranium Fuels, IAEA-TECDOC-233, 1980
[4] W.R. Gambill, HFIR Heat Transfer Studies of Turbulent Water Flow in Thin Rectangular Channels, ORNL-3079, 1964
[5] L. Bernath, A Theory of Local Boiling Burnout and Its Application to Existing Data, Chem. Eng. Prog. Symp. Series 56, No.30, 95, 1960
[6] Samuel Mirshak, Heat Flux at Burnout, DP-355, 1959
[7] M. Kaminaga et al, Experimental Study of the Critical Heat Flux in a narrow Vertical Rectangular Channel, Heat Transfer, Vol.20, No.1, 1991

3. Neutronic Calculations for Modification of Kinki University Reactor from HEU to LEU Fuels

R. MIKI, T. ITOH

Atomic Energy Research Institute
Kinki University
Higashi-Osaka, Osaka 577, Japan
and
K. TSUCHIHASHI
Japan Atomic Energy Reesearch Institute
Tokai-mura, Ibaraki 319-11, Japan

ABSTRACT

The Kinki University Reactor (UTR-KINKI) is a modified Argonaut type, light water-moderated zero power reactor with highly enriched (90 wt.%), uranium-aluminum alloy flat MTR plate type fuel. Neutronic calculations was performed on UTR-KINKI to examine the feasibility of replacing the current HEU fuels with low enriched (19.75 wt.%) fuels without changing the main core dimensions and configurations other than the fuel element. The primary reason for studying the conversion is the concern with safeguard associated with the HEU plate fuel. The second reason for converting is related to a desire to introduce some spectrum modifying material around the experimental cavity at the center of the internal graphite reflector to establish a "modified spectrum neutron field" for radiation biological researches. The effect of reducing fuel enrichment on the nuclear characteristics including the neutron spectrum and the neutron flux distribution around the experimental cavity of UTR-KINKI are investigated. It is concluded from the present neutronic calculation that the LEU fuel is feasible for UTR-KINKI without any significant reduction or changes in the reactor performance.

INTRODUCTION

The Kinki University Reactor, UTR-KINKI[1], is a modified Argonaut type, light water-moderted and graphite-reflected, zero power (1W) reactor. The reactor is heterogeneous in design and consists of twelve fuel boxes in two slab arrangement separated by 46cm internal graphite reflector. The overall dimensions of the reactor core, placement of the fuel boxes relative to other regions, along with the experimental cavity in the internal graphite reflector are indicated on the horizontal cross-sectional view of the core of UTR-KINKI in Fig. 1.

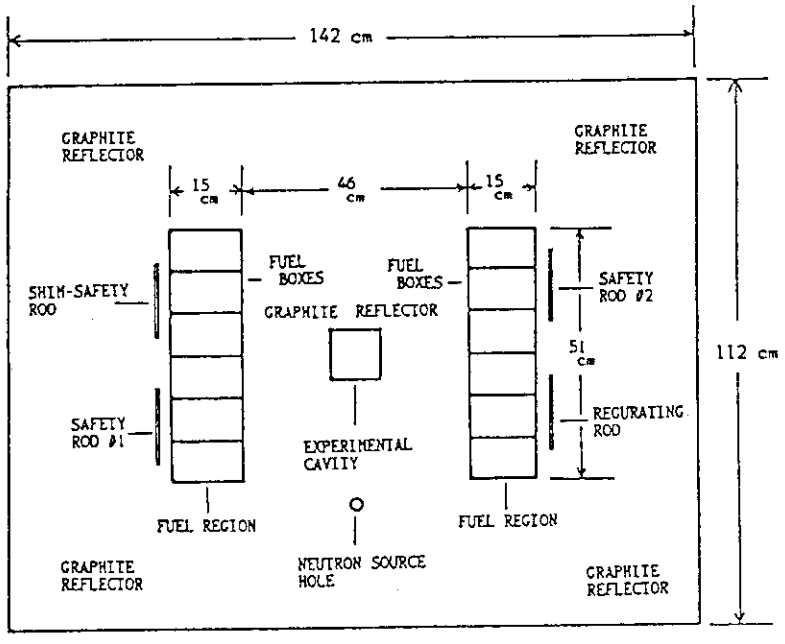

Fig. 1 Horizontal cross sectional view of UTR-KINKI core

The UTR-KINKI currently employs a highly-enriched (90 wt.%), uranium-aluminum alloy, flat MTR-type plate fuel. Investigation were performed to examine the feasibility of replacing the HEU fuel of current UTR-KINKI with low-enriched (nominal 20 wt.%) silicide or aluminide fuel without changing the main core configurations other than the fuel element. The primary reason for studying conversion of the UTR-KINKI to the LEU fuel is the concern with safeguards associated with the HEU plate fuel. A second reason for converting to the LEU fuel is related a desire to introduce some neutron spectrum modifying materials around the experimental cavity at the center of internal graphite reflector to establish a "modified spectrum neutron field" for radiation biological researches. Such a change would be difficult with the current HEU fuel because the introduction of substantial amount of spectrum modifying material into the core causes

the reactor subcritical and we have only limited amount of HEU fuel.

This paper represents the results of detailed neutronic investigations performed for UTR-KINKI conversion from HEU to LEU fuel. The study is concerned with the use of both LEU silicide (U_3Si_2-Al) and aluminide (UAl_x-Al) dispersion fuels from the point of view of the present commercial fuel fabrication bases. For uranium enrichment, 19.75% was selected and for uranium loading in the fuel matrix, 3.8g-U/cc for silicide and 2.0g-U/cc in the case of aluminide, were selected as conservative values, respectively.

The neutronic investigations was done under the following restrictions: (1) Main core dimensions and configuration including the size and thickness of each fuel plate of UTR-KINKI except the water gaps between the fuel plates, i.e. the number of fuel plates per element, must be exactly same as in the current HEU core. (2) The change of neutron spectrum around the experimental cavity in the center of the internal graphite reflector should be minimum.

METHOD OF CALCULATION

Neutronic calculation was performed using SRAC Code System[2]. The system, JEARI Thermal Reactor Standard Code System for Reactor Design and Analysis, was developed at Japan Atomic Energy Research Institute and its adaptability to complex core configuration has been demonstrated through many benchmark experiments. SRAC Code System consists of neutron cross section libraries and auxiliary processing codes, neutron spectrum routines, a variety of transport and diffusion routines, dynamic parameters and cell burn-up routines, etc.

The fundamental group constant library was produced mainly from ENDF/B-IV nuclear data file with the energy structure of 107-group (48-group for thermal and 74-group for fast energy ranges, respectively, with 15 overlapping groups). The transport cross-sections for the P_0 transport calculation were calculated by the B_1 approximation, and the diffusion coefficients were obtained assuming $D = 1/(\Sigma_{tr})$. The resonance absorption for heavy nuclides was calculated by a table look-up method for the neutron energy above 130.04 eV and a collision probability method using ultra-fine energy points of 4600 for neutron energy between 130.07 and 0.68256 eV. The user library was constructed with a energy group structure of 50 groups (23 fast groups and 27 thermal groups).

The unit cell calculation for multi-group constants was performed by collision probability method in 1-D slab

geometry for fuel meat region composed of fuel meat (U_3Si_2-Al for silicide dispersion fuel and UAl_x-Al for aluminide dispersion fuel), aluminum cladding and light-water. Multi-group (fast 31 and thermal 10 groups or fast 5 and thermal 5 groups) core calculation was performed by 2-D diffusion code (CITATION) in X-Y geometry and 2-D trnasport code (TWOTRAN) in R-Z geometry.

RESULTS OF NEUTRONIC CALCULATIONS

The results of preliminary calculations on the minimum critical masses of LEU with reducing water gaps between the fuel plates of each fuel element are shown on Table I. In general, the minimum critical masses of LEU are several per cent larger in the case of aluminide dispersion fuels than silicide fuels.

Table I. Minimum Critical Masses for LEU fuel cores

Water Gap	Critical Mass (LEU 19.75%)	
	Silicide (U_3Si_2-Al)	Aluminide (UAl_x-Al)
1.016cm (12 plates per element)	3,420g U-235 17,330g U	3,670g U-235 18,590g U
0.660cm (17 plates per element)	3,500g U-235 17,620g U	3,750g U-235 18,990g U
0.500cm (21 plates per element)	3,850g U-235 19,220g U	4,060g U-235 21,070g U

The effects of reducing fuel enrichment on the nuclear characteristics including neutron spectrum and thermal neutron flux distribution around the experimental cavity at the center of internal graphite reflector of UTR-KINKI were also investigated. The results show that there are no significant change in the neutron spectrum and the thermal neutron flux levels in the fueled region of LEU core are about 10% lower than that of current HEU core. However, they are much more flat in the internal graphite reflector region than that of HEU core. In the current HEU core, neutron spectrum in the experimental cavity at the center of internal graphite reflector has an excellent 1/E neutron spectrum over wide energy range. The calculated neutron spectra of this region are almost unchanged, both for silicide and aluminide LEU fuel core. Fig. 2 shows

the neutron spectrum of this region in the HEU core and Fig. 3 shows the neutron spectra in the LEU silicide core.

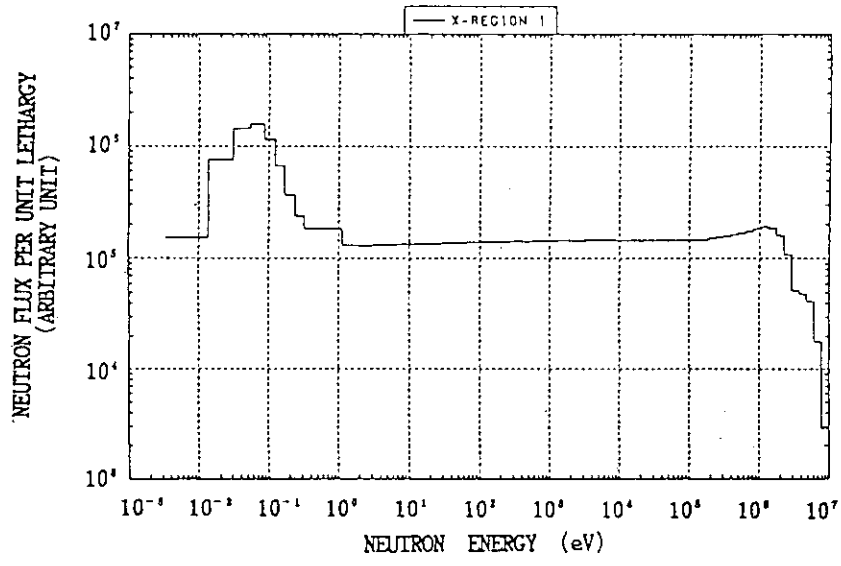

Fig. 2 Neutron spectrum in the experimental cavity of UTR-KINKI, HEU fueled core

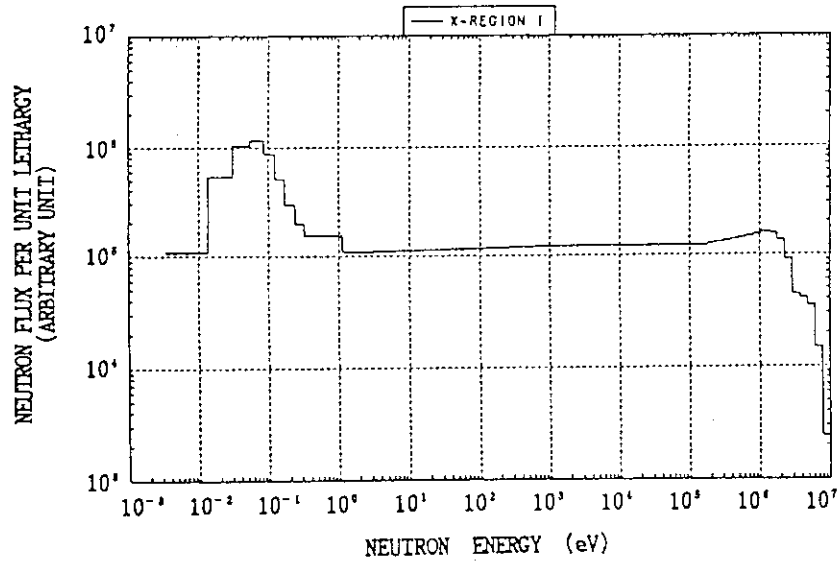

Fig. 3 Neutron spectrum in the experimental cavity of UTR-KINKI, LEU silicide fueled core

The modified neutron spectrum in the experimental cavity at the center of internal graphite reflector due to the introduction of spectrum modifying materials were

also investigated. By replacing part of the graphite reflector with some spectrum modifying materials, such as bismuth, aluminum, lead or stainless steel blocks, etc., significant modification of neutron spectrum can be attained. But these spectrum modifying materials have large negative reactivity vales, i.e. about -2.5% $\Delta k/k$ for 3.82cm thick stainless steel blocks and about -0.05% $\Delta k/k$ for bismuth blocks of same thickness. Nevertheless, by increasing the loading of fuel plates per element, these large negative reactivity can be compensated without serious troubles. Figs. 4 shows the "modified" neutron spectrum in the experimental cavity of UTR-KINKI when 3.82cm thick stainless steel blocks were inserted around the experimental cavity in center of the internal graphite reflector.

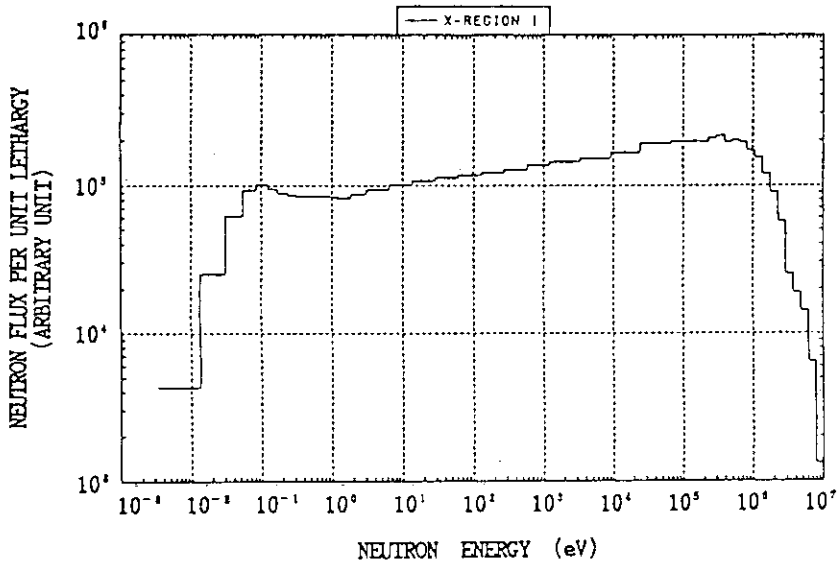

Fig. 4 Modified neutron spectrum in the experimental cavity with stainless steel modifier, LEU core

Some of the results of core calculations other than the results mentioned above are as follows: (1) The temperature effect of reactivity in the LEU core is more negative than that in HEU core, both for silicide and aluminide fuels. (2) The value of β/l in LEU core is approximately equivalent to that in HEU core.

CONCLUSION

The results of the present neutronic investigation show that the conversion of UTR-KINKI from HEU fuel to LEU fuel is quite feasible without changing any main core dimensions

or configurations except the number of fuel plates per element. The effects of reducing fuel enrichement on the main nuclear characteristics of UTR-KINKI including the neutron spectrum in the experimental cavity and neutron flux distribution in the internal graphite reflector are very small and provide no problem in the application of UTR-KINKI.

ACKNOWLEDGEMENT

The part of this study was carried out under the co-operative research program between Kinki University and Japan Atomic Energy Research Institute. The authers are grateful to Professor T.Shibata, the director of Kinki Univeristy Atomic Energy Research Institute, for his help in performing the calculation.

REFERENCES

1. Miki,R., Atomkern-energie Kerntechnik, Supplement 44 260 (1984).
2. Tsuchihashi,K. et al., SRAC; JAERI Thermal Reactor Standard Code System for Reactor Design and Analysis, JAERI 1285 (1983) and Revised SRAC Code System, JAERI 1302 (1986).

4. Fully Integrated Analysis of Reactor Kinetics, Thermalhydraulics and the Reactor Control System in the MAPLE-X10 Research Reactor

S.Y. Shim, P.A. Carlson and D.K. Baxter

AECL Research
Whiteshell Laboratories
Pinawa, Manitoba, Canada R0E 1L0
Telephone: (204)753-2311 Fax: (204)753-2455

ABSTRACT

A prototype research reactor, designated MAPLE-X10 (Multipurpose Applied Physics Lattice Experimental - X 10MW), is currently being built at AECL's Chalk River Laboratories. The CATHENA (Canadian Algorithm for Thermalhydraulic Network Analysis) two-fluid code was used in the safety analysis of the reactor to determine the adequacy of core cooling during postulated reactivity and loss-of-forced-flow transients. The system responses to a postulated transient are predicted including the feedback between reactor kinetics, thermalhydraulics and the reactor control system. This paper describes the MAPLE-X10 reactor and the modelling methodology used. Sample simulations of postulated loss-of-heat-sink and loss-of-regulation transients are presented.

INTRODUCTION

MAPLE is a new-generation research reactor developed by AECL Research [1]. Two reactors based on the MAPLE concept are currently being built, MAPLE-X10 (10 MW_{th}) at AECL's Chalk River Laboratories and the Korean Multipurpose Research Reactor (30 MW_{th}) in Korea. The MAPLE-X10 reactor will serve as a prototype of the MAPLE concept and as a dedicated isotope producer.

The MAPLE-X10 primary cooling system (PCS) together with the layout of the reactor core is shown schematically in Figure 1. It is a light-water-cooled research reactor with an open-chimney-in-pool arrangement. The core consists of 19 vertical flow channels, each containing a bundle of U_3SiAl or U_3Al finned fuel pins, shown in Figure 1. For normal operation, the fuel in the core is cooled by upward flow from the inlet plenum that enters the chimney from the bottom. Pool water also enters the chimney from the top. A pump draws the water from the chimney just above the core and delivers it to the heat exchanger. Most of the flow is then directed to the core through the inlet plenum to cool the fuel. The remainder, called bypass flow, returns to the top of the chimney through the pool and mixes with the core flow in the chimney.

The CATHENA two-fluid code has been used in the safety analysis of the MAPLE-X10 research reactor [2]. The code includes a point-reactor kinetics model, heat transfer relations appropriate to the finned fuel geometry of MAPLE-X10 and the ability to model the subcooled void generation required in the analysis. The reactor has been analyzed using CATHENA to determine the adequacy of core cooling during postulated reactivity and loss-of-forced-flow transients. The system responses to the postulated transients are predicted by considering the feedback between reactor kinetics, thermalhydraulics and the reactor control system.

This paper describes the MAPLE-X10 reactor and the modelling methodology used. Sample simulations of postulated loss-of-heat-sink and loss-of-regulation transients are presented to demonstrate the application of CATHENA to MAPLE-X10 conditions.

DESCRIPTION OF CATHENA

CATHENA [3,4] is a computer code which uses a one-dimensional, two-fluid thermalhydraulic model to describe the steam-water/noncondensable-gas flow in a pipe network. The code also includes a model for reactor kinetics and models to describe the thermalhydraulic behavior of the core, heat exchanger, tank, pump, valves, area changes and discharge through postulated breaks. CATHENA allows user-specified models to control the behaviour of reactor components such as valves and shutdown systems. Control devices and instrumentation-response delay times can also be modelled. As illustrated in Figure 2, the simulations include models of the reactor control system and reactor kinetics which feed back on the thermalhydraulic system variables. The code has been used for a wide range of applications for power and research reactor analyses, as well as design and analysis of experiments. CATHENA has been extensively validated using separate-effect, component and integral experiments [5].

The conservation equations for mass, momentum and energy for each phase (liquid and vapour) solved in CATHENA result in a six-equation model. An additional mass equation is solved for each noncondensable gas component modelled. The equation of state, which defines the phase densities of H_2O or D_2O as a function of phase pressure and enthalpy, provides mathematical closure of these equations. In addition, the thermodynamic and transport properties of noncondensable gas components (such as air, H_2 and N_2) are provided.

Constitutive relationships required in the conservation equations to specify the rates of phase change, interfacial and wall-to-fluid momentum transfer, and interfacial and wall-to-fluid heat transfer have been formulated from information obtained from the literature. These relationships depend on the flow regime, which is predicted using a flow-regime map. A heat conduction equation is solved for temperature distribution within a pipe wall or fuel rod (or simulator), and is coupled with the conservation equations at the wall-to-fluid interface. A full boiling curve is provided to model convective, boiling and condensation heat transfer processes at wall surfaces. More details on the constitutive relationships used may be found in [3].

The governing equations are represented by finite-difference equations written on a staggered mesh, where pressure, phase enthalpies, void fraction and noncondensable fractions are evaluated at mesh centres and phase velocities are evaluated at mesh boundaries. The numerical scheme is based on a one-step, semi-implicit method in which the solution is not transit-time-limited [4]. A time-step controller in CATHENA automatically selects the next time step based on accuracy considerations. Conservation of mass is achieved using a truncation-error correction technique.

Additional features of the CATHENA code used for the MAPLE-X10 analysis are highlighted below:

(1) the CATHENA point-reactor kinetics model is used to calculate asymmetric reactivity effects of the core. The reactivity feedback due to changes in fuel temperature, fluid temperature and void is accounted for based on the changes in each flow channel in the core. The total reactivity change for the entire core is calculated by the sum of these flux-squared weighted reactivity changes. Also, the xenon and iodine concentration equations are solved to account for the xenon effect on reactivity.
(2) all heat transfer relations used were developed for the finned fuel geometry and operating conditions of the MAPLE reactor. These include correlations for single-phase and two-phase heat transfer coefficients, and the onset-of-nucleate-boiling (ONB), onset-of-significant-void (OSV) and critical heat flux (CHF).
(3) CATHENA is capable of modelling the non-equilibrium effects of subcooled boiling. The CATHENA subcooled void generation model uses the MAPLE OSV heat flux relation to determine the wall-to-interface heat transfer rate. Wall void prior to reaching the OSV point is modelled and is used in calculating the reactivity feedback but not in calculating the pressure drop.

MODELLING OF MAPLE-X10

Figure 3 shows the idealization of the MAPLE-X10 cooling systems. The idealization includes the equipment room, pump, all piping, valves, the pool, and the primary and the secondary side of the heat exchanger. The figure also shows in more detail the representation of the MAPLE-X10 core used.

Reactor Core

The 19-site fresh core of MAPLE-X10 is divided into seven representative parallel channels to account for the different channel hydraulic resistances, reactivity worths and power distributions. The seven channels represent: the central 36-pin driver channel; three inner 36-pin driver channels; six outer 36-pin driver channels; three 18-pin control-rod channels; three 18-pin shutoff-rod channels; three aluminium dummy sites with the same geometry as the 12-pin molybdenum targets; and the water gaps between flow channels.

The pin-power distributions in each fuel bundle are nonuniform both radially and axially. To account for this nonuniformity, each bundle is

represented by a number of pin groups and divided into a number of axial segments having different heat generation rates. The outer 36-pin driver channel type is represented by four pin groups based on their individual pin powers. All other fuelled channel types are represented by three pin groups. One of the pin groups includes the hottest pin in each bundle. All pin groups in the same channel type are exposed to the same average hydraulic conditions at each axial node.

The flow resistance coefficients in the 36-pin and 18-pin driver channels, and molybdenum channels were derived from the pressure drop data measured using actual reactor components.

Reactivity Coefficients

Reactivity worths due to changes in fuel temperature, coolant temperature and void for the seven representative channels were produced using WIMS-AECL and 3DDT [6]. Reactivity feedback information is provided separately for every channel. This feature is required for the initial MAPLE-X10 core to account for the reactivity effects of nonfuelled sites and water in the gaps between flow channels.

Thermal Power Split

Thermal power calculated from the reactor kinetics model is assumed to be split between the fuel (95.7%), the coolant in the fuelled channels (2.7%), the interstitial water (1.4%) and the pool water (0.2%). This split was estimated from an analysis of gamma-heat deposition in the MAPLE-X10 core made using the MCNP code.

Reactor Trip

All reactor trip logic and associated instrumentation delays were simulated for the analysis. However, for the two sample simulations presented in this paper, the reactor was assumed not to shut down. Instead, all three control rods were assumed to stall and not to respond to the trip signal.

Process Water Flow Control

The process water control valve on the secondary side of the heat exchanger is modelled to control the core inlet temperature at 35°C. Details of the valve characteristics and the response time delay of associated instrumentation were modelled to simulate their effects on the PCS behaviour during the transient.

Heat Exchanger

The heat exchanger used for MAPLE-X10 is a countercurrent plate-type heat exchanger with 52 parallel passes. In the simulations, it was represented by 52 identical flow passes, each with the area and metal mass of a single plate in the MAPLE-X10 heat exchanger. Details of the flow area, and the manufacturer's heat removal data were included to simulate the proper heat transfer rate and thermalhydraulic response time. The initial flow in the secondary side of the heat exchanger was established to remove the 10-MW reactor power and the pump heat. The inlet temperature of the process water on the secondary side was assumed to remain at 20°C

during the sample transients.

Pump

The manufacturer's pump characteristic data (head vs flow and torque vs flow) and the pump degradation due to cavitation were included in the pump model. As well, the rundown of the MAPLE-X10 pump may be modelled using the pump inertia and frictional torque.

RESULTS AND DISCUSSION

CATHENA results for two postulated transients of (1) a loss of heat sink and (2) a loss of regulation are discussed. The initial and boundary conditions were the same for both cases.

Initial and Boundary Conditions

The initial conditions simulated are the full-power normal operating conditions given by:

- core power of 10 MW_{th};
- a core-inlet coolant temperature of 35°C; and
- a primary-side flow rate of 288.7 kg/s with a core flow of 259.3 kg/s and a bypass flow of 29.4 kg/s. This translates to flow velocities of 5.0 (for the 36-pin sites) and 8.6 m/s (for the 18-pin sites).

The boundary conditions were:

- a pressure of 100 kPa, temperature of 35°C, and void fraction of 1.0 for the air over the pool surface; and
- a secondary-side heat-exchanger inlet temperature of 20°C.

Loss-of-Heat-Sink Transient with No Reactor Trip

The transient was initiated by closing the secondary-side flow valve over 0.01 s at time 0 s. This valve then remained shut throughout the transient. No shutdown systems were assumed to be deployed during the transient and no xenon effects were included because a fresh core was analyzed.

Results of the loss-of-heat-sink transient are shown in Figures 4 to 6.

Figures 4 and 5 show the reactor power and reactivity transients. The power decreased to 1.9 MW after about 200 s because of the negative reactivity feedback that resulted mainly from the rising coolant temperatures (Figure 6). As the temperature of the coolant returning from the heat exchanger rises, the fuel temperature initially rises a few degrees peaking very early in the transient. Then, it decreases with time to below the initial values for the remainder of the transient.

No void was predicted in any of the fuel channels during the transient.

The pump suction temperature was predicted to remain below 62°C

throughout the transient. Thus, no pump degradation by cavitation at high pump-suction temperatures was predicted.

Loss-of-Regulation (LOR) Reactivity Transient with No Reactor Trip

This case assumes that all three control rods are withdrawn from the core to yield a reactivity insertion rate of 0.5 mk/s starting at 0 s. The control rods are assumed to stall when the trip signal on high power (120% power) or high log-power rate (12%/s) is detected. The system delay and instrumentation response times were simulated. No shutdown systems were assumed to be deployed during the transient and no xenon effects were included because a fresh core was analyzed.

Results of the LOR reactivity transient are shown in Figures 7 to 9. The sequence of events is:

Time, s	Events
0.0	• reactivity insertion starts at 0.5 mk/s
2.24	• 12 MW high-power trip signal is detected
2.89	• control rods are stalled • 1.440 mk excess reactivity is added
58.5	• secondary-side flow control valve opens nearly fully and the pump delivers 250 kg/s
200.0	• power levels off at 19.4 MW and remains quasi-steady.

Figures 7 and 8 show the reactor power and reactivity transients. The power rises and levels off at 19.0 MW around 100 s. The peak fuel centreline and sheath temperatures were predicted to be about 233 and 145°C, respectively (Figure 9). The minimum CHF ratio (CHF/actual heat flux) at the hottest point was predicted to be 1.9 during the transient.

The core power rise was halted through negative reactivity feedback of -0.57 mk from the rising fuel temperature and -0.84 mk from the rising coolant temperature. Near-full-capacity flow was supplied to the secondary side by 58.5 s into the transient as set by the reactor control system.

No void was predicted in any fuel channel.

The maximum pump suction temperature was predicted to remain below 55°C during the transient. Thus, no pump degradation by cavitation at high pump-suction temperatures was predicted.

CONCLUDING REMARKS

The CATHENA analysis presented demonstrates that a model suitable for reactor transient analysis has been developed for MAPLE-X10. The model accounts for the major effects of reactor kinetics, thermalhydraulics and the reactor control system.

ACKNOWLEDGEMENTS

The authors acknowledge many contributions made by their colleagues in the Code Development Section of the Thermalhydraulics Branch, especially B.N. Hanna, J.P. Mallory and P.J. Mills for their support of the CATHENA code.

REFERENCES

1. R.F. Lidstone and J.I. Saroudis, "MAPLE: A New Multipurpose Reactor for National Nuclear Development in the 1990s," Proceedings of an International Symposium on the Significance and Impact of Nuclear Research in Developing Countries, Athens, Greece, 1986 September 8-12, IAEA-SM-291/19.

2. S.Y. Shim, D.J. Richards and T.E. MacDonald, "A CATHENA Study of the Requirement for a Flap Valve in the MAPLE-X10 Research Reactor," Proceedings of the 10th Annual Conference of the Canadian Nuclear Society, Ottawa, 1989 June 4-7.

3. D.J. Richards, B.N. Hanna, N. Hobson and K.H. Ardron, "ATHENA: A Two-Fluid Code for CANDU LOCA Analysis," Proceedings of the Third International Topical Meeting on Reactor Thermalhydraulics, Newport, RI, 1985 October 15-18. *(the code has since been renamed CATHENA)*

4. B.N. Hanna, N. Hobson and D.J. Richards, "One-Step Semi-Implicit Method for Solving the Transient Two-Fluid Equations that is Non-Courant Limited," Proceedings of the 23rd ANS National Heat Transfer Conference, Denver, CO, 1985 August 4-7.

5. D.J. Richards, "Validation of the CATHENA Two-Fluid Code," Proceedings of the Third International Topical Meeting on Nuclear Power Plant Thermal Hydraulics and Operations, Seoul, Korea, 1988 November 14-17.

6. P.A. Carlson, W. Heeds, S.Y. Shim and S.G. King, "Analysis of Reactivity Effects of Void and Temperature in the MAPLE-X10 Reactor," to be presented at the ANS Topical Meeting on Advances in Reactor Physics, Charleston, SC, 1992 March 8-11.

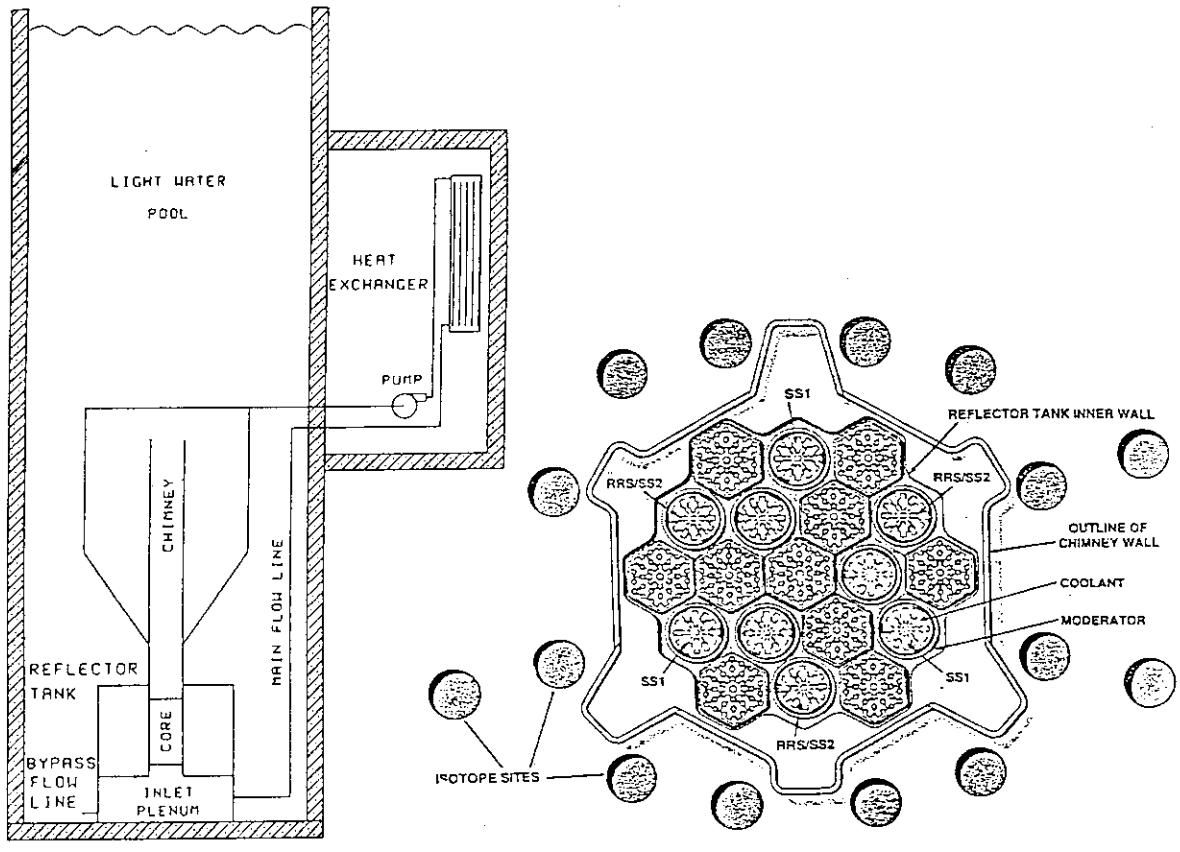

Figure 1: Schematic Diagram of the Primary Cooing System and the Core of MAPLE-X10

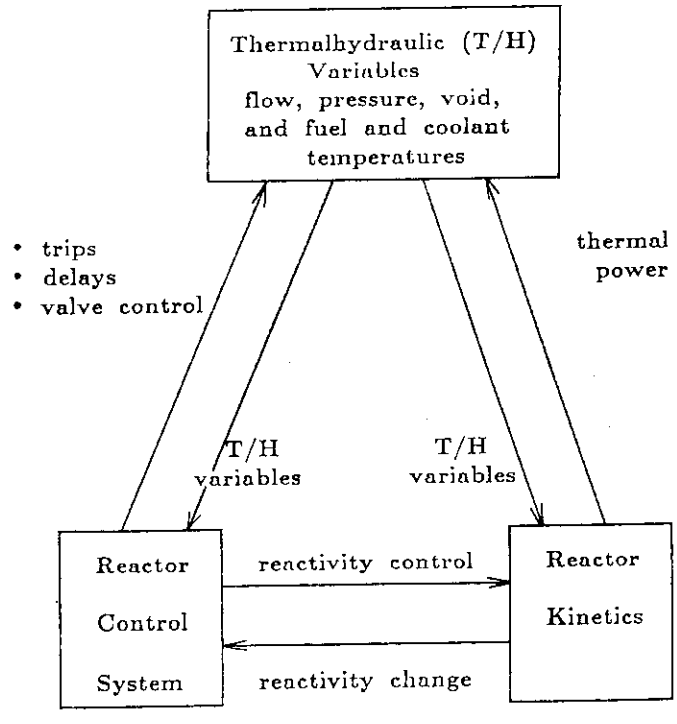

Figure 2: Fully Integrated Analysis of Thermalhydraulics, Reactor Kinetics and the Reactor Control System.

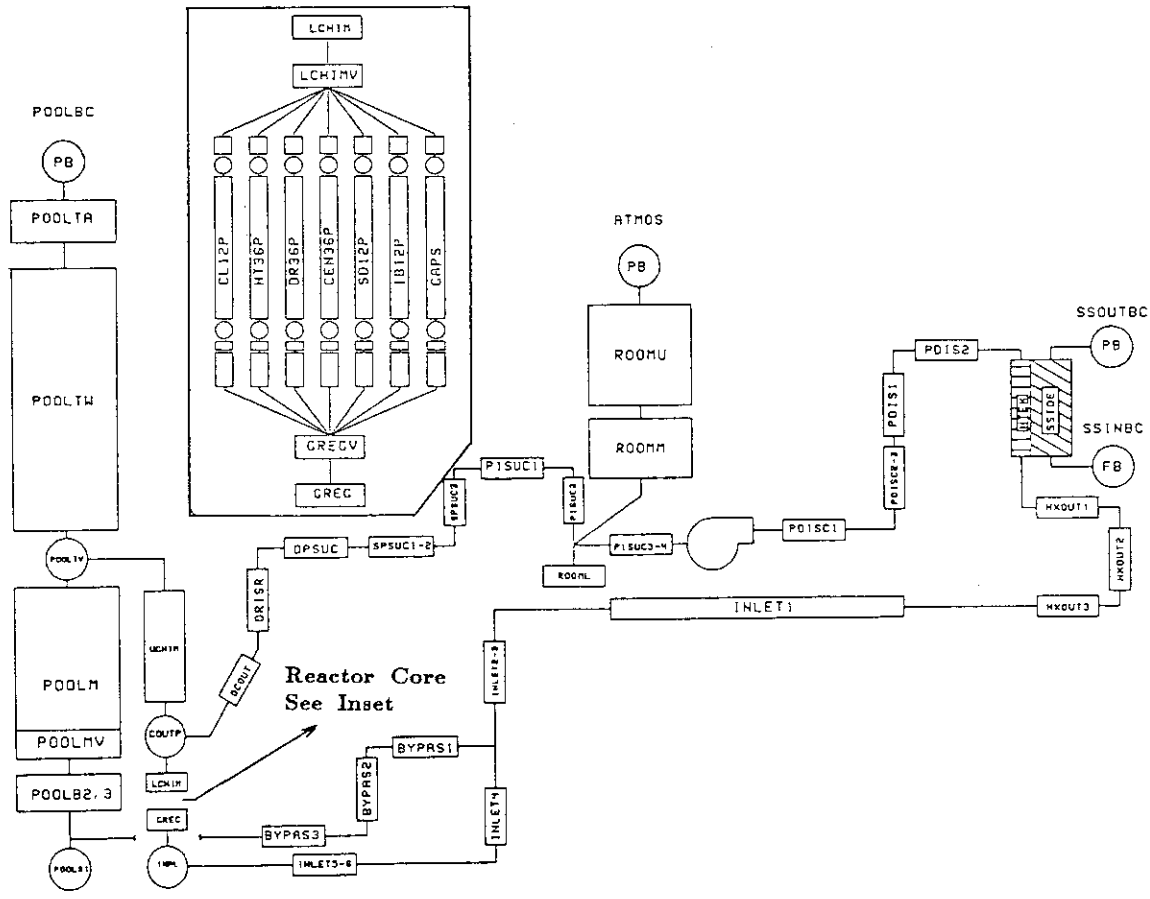

Figure 3: CATHENA Idealization of the Primary Cooling System and the Reactor Core of MAPLE-X10

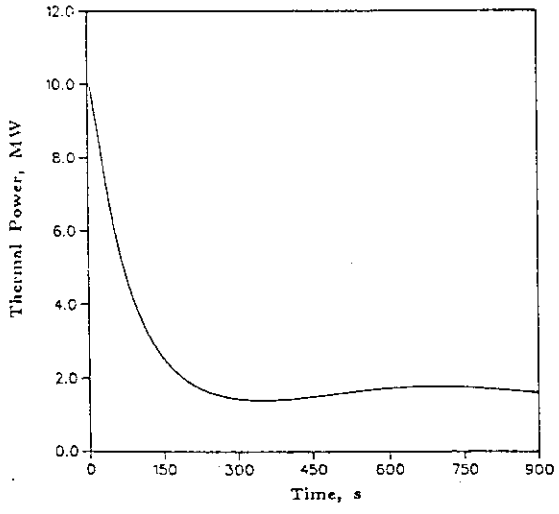

FIGURE 4: Power Transient during a Loss of Heat Sink with No Reactor Shutdown

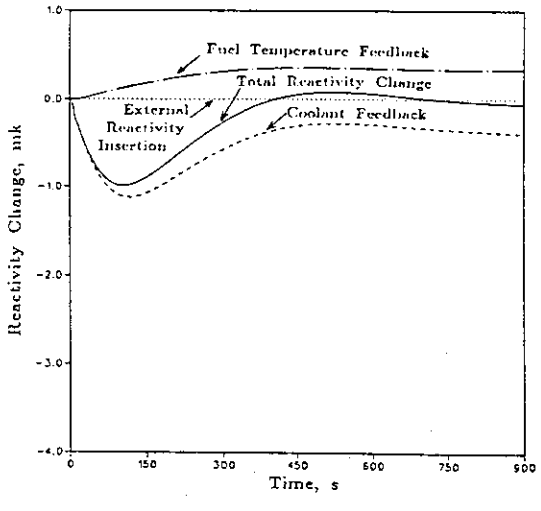

FIGURE 5: Reactivity Transient during a Loss of Heat Sink with No Reactor Shutdown

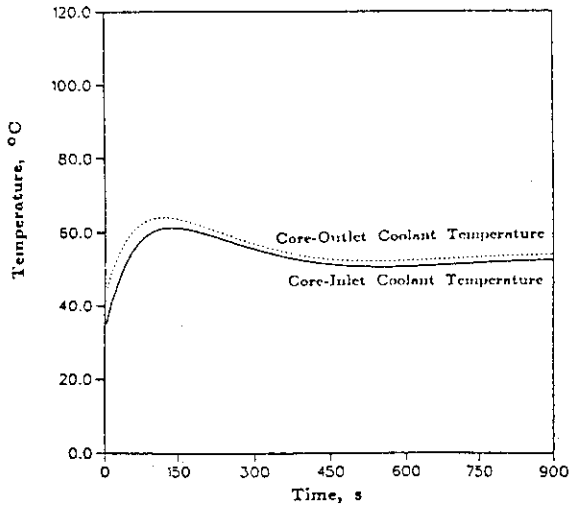

Figure 6: Coolant Temperature Transient in the Core during a Loss of Heat Sink with No Reactor Shutdown

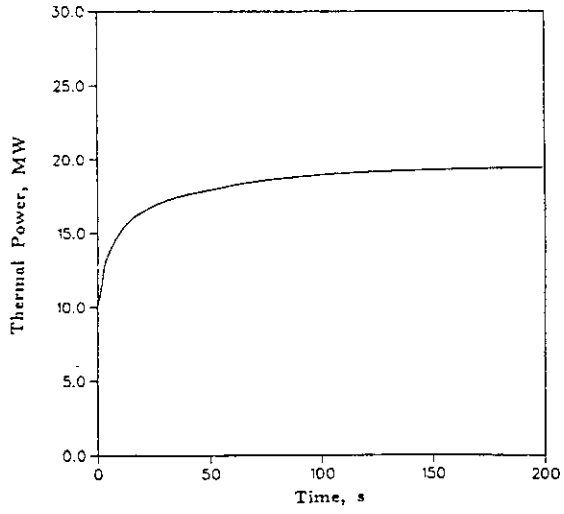

Figure 7: Power Transient during a Loss of Regulation with No Reactor Shutdown

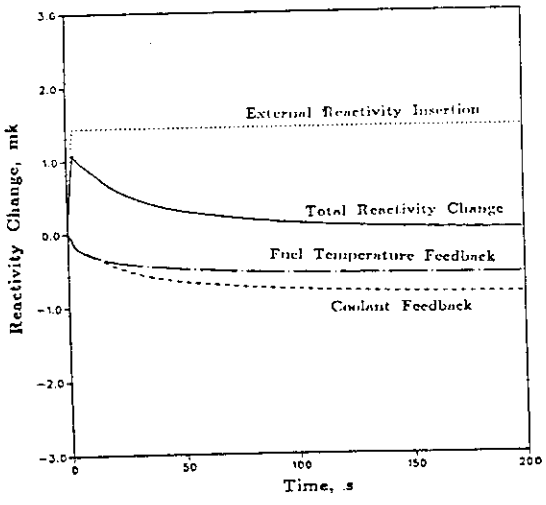

FIGURE 8: Reactivity Transient during a Loss of Regulation with No Reactor Shutdown

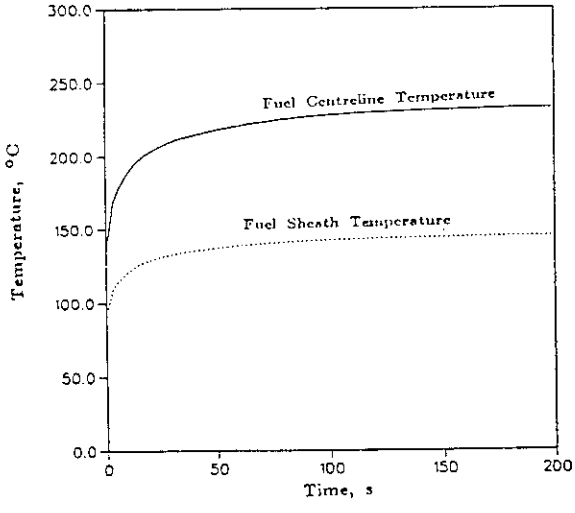

FIGURE 9: Peak Fuel Temperature Transient during a Loss of Regulation with No Reactor Shutdown

5. Design Study of a Medical Reactor for Boron Neuton Capture Therapy

M. SASAKI, J. HIROTA
Mitsubishi Atomic Power Industries, Inc.
4-1 Shibakouen 2-chome, Minato-ku, Tokyo 105
S. TAMAO
Mitsubishi Heavy Industries, Ltd.
4-1 Shibakouen 2-chome, Minato-ku, Tokyo 105
K. KANDA
Research Reactor Institute, Kyoto Univ.
Noda, Kumatori-cho, Sennan-gun, Osaka-Fu 590-04
Y. MISHIMA
Kobe Univ. School of Medicine
5-1 Kusunoki-cho 7-chome, Chuo-ku, Kobe 650, Japan

ABSTRACT

A new design study of a medical reactor for Boron Neutron Capture Therapy (BNCT) has been carried out. The reactor is to be used exclusively for the treatment of malignant melanoma and other cancers as well as for the further biomedical research. Main specifications of the reactor are as follows; thermal power of 2 MW, water cooling by natural convection, semitight core of triangular lattice, UO_2 fuel rod of 9.5 mm diameter and no refueling in the reactor-life. Three horizontal and one vertical neutron beam hole are to be provided to deliver thermal and epithermal neutrons. N-γ coupling Sn transport calculations indicate that the patient treatment period will be about 30 minutes with minimal fast neutron and gamma contaminants.

INTRODUCTION

A design study of a medical reactor has been carried on since July, 1988, in cooperation of Kobe Univ., Kyoto Univ., Mitsubishi Heavy Industries, Ltd. and Mitsubishi Atomic Power Industries, Inc.. It is intended in this study to survey and investigate the reactor concepts suitable for Boron Neutron Capture Therapy (BNCT) and to set up the main specifications of the reactor which is to be used exclusively for the treatment of malignant melanoma and other cancers as well as for the further biomedical research.

Melanoma treatment by BNCT using ^{10}B-chemicals which accumulate in melanoma tissue by specific cell metabolic activities has been developed by Y. Mishima and his collaborators. The continuous investigation in vitro and in vivo over ten years based on their unique idea led to the first successful cure of malignant melanoma in a human patient in 1987. In 1985, Japan-Australia Science and Culture Agreement was accomplished by the

requirement of Australia Goverment. An arrangement between the Japanese and Australian Research Groups on BNCT treatment in Japan for Australian melanoma patients was established at the 3rd Japan-Australia Workshop on BNCT for melanoma held in Sidney in Dec., 1988.

It is generally accepted that the optimum neutron source for BNCT is a small reactor. However, currently available research reactors are not constructed exclusively for medical use, but rather multi-purpose reactors. It is difficult to treat a patient with melanoma on his back in a certain reactor, since it is impossible to properly position the patient. Since the thermal neutron flux level at the patient is not so high, the treatment period is usually rather long. Further, as the research reactor is used for different purposes and the schedule is very tight, the time available for medical use is limited.

In Japan, about 120 patients have been treated by BNCT, including those from abroad. The most part of these treatments is the brain tumor treatment by Prof. H. Hatanaka of Teikyo Univ., using thermal neutrons from the Musashi reactor, KUR and JRR-2. For the brain tumor treatment at present, it is necessary to operate just before the neutron irradiation. If epithermal neutrons are available, it is possible to treat deep-seated various tumors including metastic melanoma in lymphnode and other organs without surgery.

More than ten years ago in the fiscal year 1978-79, the team (Chairman: Prof. S. An of Univ. of Tokyo) was given support by Japanese Goverment in their investigation into the design of a BNCT reactor[1]. In the study, the configuration of the neutron filter which delivers thermal or epithermal neutrons from a TRIGA reactor was mainly investigated. A neutronics design of a medical therapy reactor[2] was presented from INEL at the 1988 Int. Reactor Physics Conf.. The paper addresses the feasibility of utilizing existing reactor technologies to deliver therapeutic doses by epithermal neutrons. The two primary fuel candidates are a 10 wt% ^{235}U enriched UO_2 fuel and a 45 wt% U in UZrH, 20 wt% ^{235}U enriched hydride fuel.

CORE CONFIGURATION AND ANALYSIS

Principal requirements for the medical reactor aimed in this study are as follows:

(1) The reactor is to be used exclusively for medical purposes.
(2) 50,000 patients are to be treated or diagnosed in the reactor-life without refueling.
(3) The thermal power is less than 2 MW.
(4) The core is cooled by natural convection.
(5) Thermal and epithermal neutron beam holes are provided, separately.
(6) No heavy water is used in the core.
(7) Existing proven reactor technologies are to be utilized.

A survey of characteristics of research reactors and small reactors in the world was performed. In comparison of the reactor characteristics with the principal requirements, light water cooled and moderated PWR-type (oxide fueled) and TRIGA-type (hydride fueled) reactor were seemed suitable for the BNCT reactor. Analyses of the core characteristics of the oxide fueled and

hydride fueled reactor indicated that the oxide fueled core would be more feasible to the BNCT reactor because of the higher epithermal neutron flux level, the less excess reactivety requirement and no need of refueling. Since then, the design study has been concentrated on the oxide fueled reactor.

A harder neutron spectrum of the core is preferable in view of the availability of epithermal neutrons at the beam port. A too tight core, however, results in an excessive increase of the fuel enrichment and a decrease of the control rod worth. Therefore, a semitight core of triangular lattice is preferable. The permissible linear heat rate in the core was examined and the average linear heat rate was selected to be 20 w/m. The characteristics of the core were examined to optimize the core parameters such as the volume ratio of moderator to fuel pellet, ratio of core height to diameter and fuel enrichment.

The control rod worth was calculated and it was confirmed that seven control rods of cluster type would be able to shut down the reactor safely under the condition of one rod stuck. It was also confirmed that the local boiling would not occur in the core even if the reactor power was raised ramp-wise to the nominal power in about 5 minutes.

The main specifications of the core and fuel are given in Table 1 and the bird eye's view of the core is shown in Fig. 1.

Table 1 Main Specifications of Core and Fuel

thermal output	2 MWt
ave./max. L.H.R.	20/50 W/cm
active core hight	62 cm
equivalent radius	25.5 cm
Vm/Vp	1.0
fuel material	UO_2(~0.5 t)
^{235}U enrichment	4 wt%
cladding O. D.	9.5 mm
assembly pitch	112 mm
pin pitch	11.4 mm
lattice geometry	hexagonal
no. of fuel rods	91/ass'y
no. of fuel assemblies	19

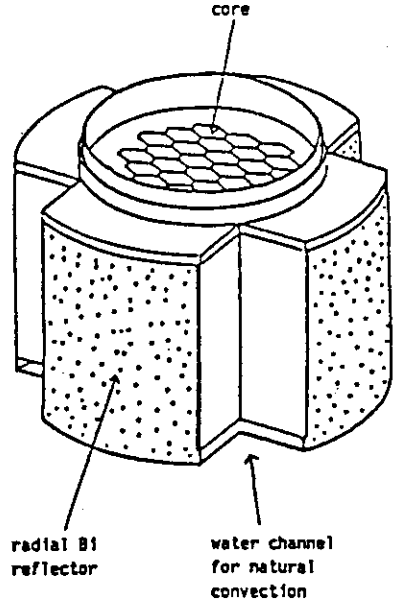

Fig. 1 Bird Eeye's View of Core

NEUTRON FILTER CONFIGURATION AND ANALYSIS

Three horizontal neutron beam ports are to be provided for simultaneous patient treatments and advanced research. Therapeutic doses of thermal and epithermal neutrons are also available at a vertical neutron beam port by using a rotating plug. In order to examine the neutron filter composition and to optimize the neutron filter configuration, 1-dim. n-γ coupling Sn transport calculations were carried out using JSSTDL-100N/40G-J3[3].

The neutron filter for epithermal neutrons which consists of aluminum and heavy water was first proposed by Y. Oka, et al[4]. The effect of (γ,n) reactions of heavy water on beam quality is taken into account by Aoki's method[5]. The fast neutron and gamma dose due to the fast neutron and gamma contaminant are calculated using the convertion coefficients[6,7]. In this study, the thermal, epithermal and fast neutrons are denoted as the neutrons less than 1 eV, between 1 eV and 1 KeV and more than 1 KeV, respectively.

The reference slab models of neutron beam holes are shown in Fig. 2. No. 1 and 7 are for the horizontal thermal and epithermal neutron beam hole. No. 14 and 19 are for the vertical thermal and epithermal neutron beam hole, respectively. Comparisons of calculated results of the neutron flux (n/cm²·s), neutron dose rate (Gy/h) and gamma dose rate (Sv/h) at the beam ports are given in Table 2. No. 1', 7', 8', 14' and 19' are the cases when the (γ,n) reactions of heavy water are neglected in No. 1, 7, 8, 14 and 19, respectively. It can be seen that the (γ,n) reactions of heavy water have large effects on the fast neutron dose rates, especially in case of the thermal neutron beam hole. No. 2 and 8 are the cases when the Rossi liquid located at the beam port for tissue simulation are removed from No. 1 and 7, respectively. It should be noticed that the gamma contaminants contribute to the gamma dose rates by only 10 %.

No. 3 and 10 are the cases when the reflector is changed from bismuth to stainless steel. No. 4 and 11 are the cases when the gamma shield is changed from to lead. No. 9 is the case when the thermal neutron shield is changed from LiF to cadmium. These results indicate that the reference cases, No. 1 and 7, are almost the best choice for the horizontal thermal and epithermal neutron beam hole, respectively.

No. 5, 6, 12 and 13 show the effectiveness of the beam shutter inserted in the place of the of the collimator. Enough attenuation of the neutron fluxes and dose rates is seen, in Table 2.

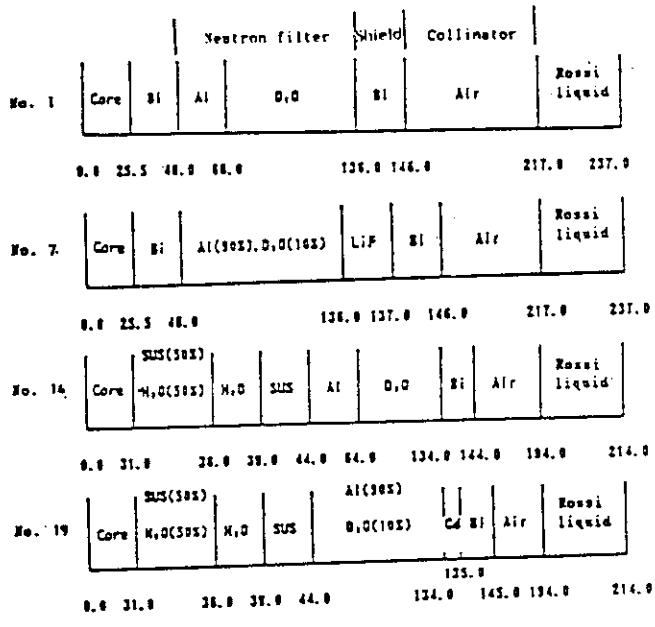

Fig. 2 Reference Slab Models of Neutron Beam Hole

As for the vertical neutron beam hole, the existence of the cooling water region tends to decrease the neutron flux level at the beam port. It can be seen in Table 2 that No.17 is promising for the vertical thermal neutron beam hole. The neutron filter of No.17 consists of the aluminum region of 25 cm in length and the heavy water region of 55 cm in length, and the collimator is 60 cm in length. Table 2 indicates that No.22 is promising for the vertical epithermal neutron beam hole, if the fast neutron dose rate is permissible. The neutron filter of No.22 consists of aluminum (95 %) and heavy water (5 %). The neutron filter and the collimator are 80 cm and 60 cm in length, respectively.

Table 2 Comparisons of Neutron Fluxes and Dose Rates at Beam Ports

No.	F. N. D. R.	E. N. D. R.	T. N. F.	γ D. R.
1	1.00 (6.99 + 0)	1.00 (1.83 - 2)	1.00 (7.44 + 10)	1.00 (2.23 + 2)
1'	5.8－2	7.2－2	0.88	1.00
2	1.05	0.71	0.68	0.10
3	0.64	0.63	0.58	0.61
4	0.93	0.91	0.70	0.91
5	3.2－5	5.1－6	1.4－8	1.5－6
6	1.8－5	2.1－6	6.1－9	1.3－4

a) Horizontal thermal neutron beam hole

No.	F. N. D. R.	E. N. F.	T. N. D. R.	γ D. R.
7	1.00 (1.16 + 2)	1.00 (1.50 + 11)	1.00 (2.31 + 2)	1.00 (7.02 + 2)
7'	0.47	0.87	0.88	0.88
8	1.67	0.89	4.8－2	7.3－2
8'	1.08	0.88	4.8－2	7.1－2
9	1.97	1.37	1.54	1.57
10	1.09	0.82	0.93	0.95
11	1.86	1.18	1.37	1.46
12	8.1－6	3.0－8	3.2－8	2.4－6
13	4.2－6	1.9－8	1.2－8	1.7－4

b) Horizontal epithermal neutron beam hole

No.	F. N. D. R.	E. N. D. R.	T. N. F.	γ D. R.
14	1.00 (5.47 + 0)	1.00 (1.76 - 2)	1.00 (2.46 + 10)	1.00 (9.06 +1)
14'	8.6－2	7.7－2	0.94	0.95
15	1.72	1.88	1.81	1.64
16	2.84	2.67	1.12	1.39
17	1.45	1.68	2.00	1.84
18	0.48	0.51	1.22	1.05

c) Vertical thermal neutron beam hole

No.	F. N. D. R.	E. N. F.	T. N. D. R	γ D. R.
19	1.00 (8.62 + 1)	1.00 (6.52 + 10)	1.00 (1.14 + 2)	1.00 (3.38 + 2)
19'	0.38	0.96	0.98	0.98
20	1.60	1.39	1.34	1.36
21	1.03	0.80	0.83	0.84
22	2.88	2.38	2.08	2.18
23	0.99	1.06	1.03	1.04

d) Vertical epithermal neutron beam hole

(Values given in parentheses are absolute ones)

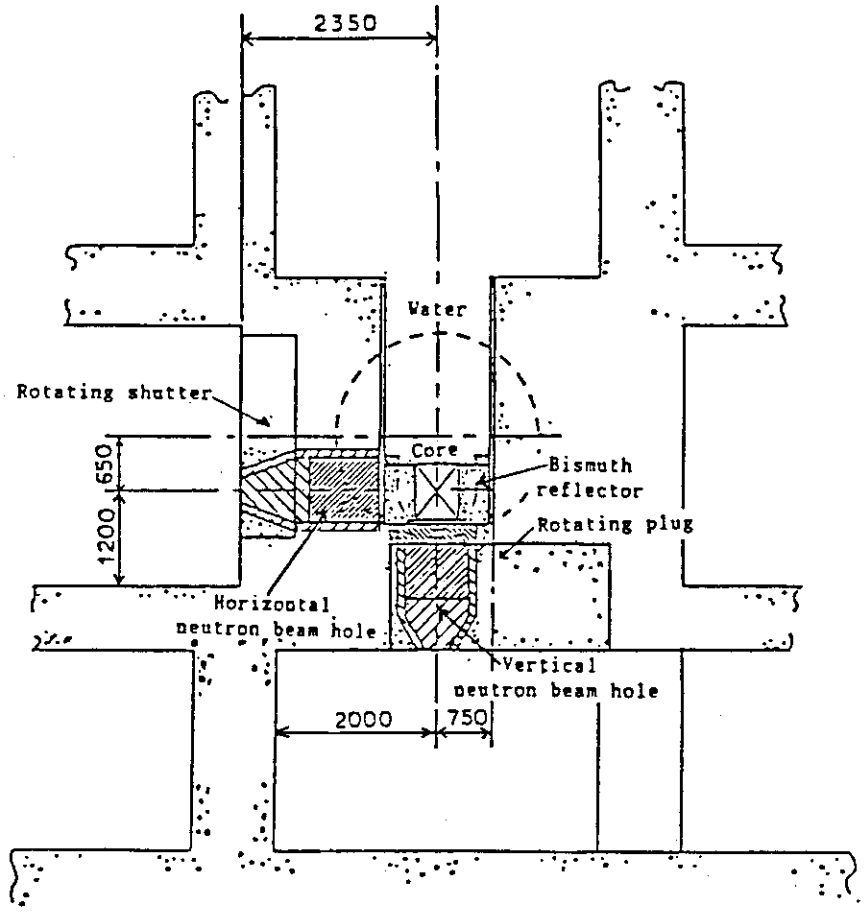

Fig. 3 Vertical Cross Section

STRUCTURES AND LAYOUT INSIDE OF REACTOR BUILDING

Three horizontal irradiation rooms (one for thermal neutrons, one for epithermal neutrons and one for epithermal neutrons to animal) and one vertical irradiation room are provided. One neutron guide tube room is also provided for in vivo measurement of ^{10}B concentrations in tumor cells. The vertical cross section around the core is shown in Fig. 3.

A rotating beam shutter is provided for each horizontal neutron beam hole to shut the neutron beam in emergency. The level of the center of the horizontal beam hole is 1,200 mm high above the floor and the center of the rotating shutter is higher by 650 mm than the center of the horizontal beam hole. The rotating plug provided for the vertical beam hole is able to deliver thermal or epithermal neutron beam and shut the neutron beam by it's rotation. The center of this rotating plug is eccentric by 750 mm not to interfere with the rotating shutter. Each irradiation room is 4,000 mm wide to facilitate the neutron irradiation of the patient. The outlet of the horizontal beam hole is apart from the core center by 2,350 mm as seen in Fig. 4.

Other rooms are needed for preparation, operation, measurement and etc., except for the rooms needed for operation and maintenance of the reactor. A patient on the bed is sent from the preparation room to the irradiation room. In the measurement room, measurements of gold foils and TLDs irradiated with the patient are carried out to monitor the neutron and gamma flux.

EVALUATION OF CHARACTERISTICS OF NEUTRON BEAM HOLE

The design objectives for the neutron beam hole are as follows:

(1) Thermal neutron flux; 1.2×10^{13} n/cm^2 in about 30 minutes.
(2) Epithermal neutron flux; 0.6×10^{13} n/cm^2 in about 30 minutes.
(3) Fast neutron dose during treatment period; less than 2 Gy.
(4) Gamma contaminant dose during treatment period; less than 1 Sv.

In order to evaluate the thermal and epithermal neutron flux, fast neutron and gamma dose rate at the horizontal thermal and epithermal neutron beam port, 2-dim. n-γ coupling Sn transport calculations have been carried out, neglecting the (γ,n) reactions of heavy water. The R-Z model of the epithermal neutron beam hole is shown in Fig. 4, including the beam shutter configuration. The contour map of the epithermal neutron flux is shown in Fig. 5.

The epithermal neutron flux available at the beam port is about 8×10^9 n/cm^2·s as seen in Fig. 5. Therefore, the patient treatment period is expected to be about 13 minutes. The contaminant doses during the treatment period are about 1.5 Gy due to fast neutrons and about 0.2 Sv due to gamma rays. It is not likely that the (γ,n) reactions of heavy water contribute so much to the fast neutron contaminant in case of the epithermal neutron beam hole. Therefore, it can be concluded that the design objectives will be achievable for the epithermal neutron beam hole.

As to the horizontal thermal neutron beam hole, the present calculation indicates that it is necessary to reexamine the R-Z model used in the calculation in order to improve the thermal neutron flux available at the beam port. The design objectives will be achievable also for the horizontal thermal neutron beam hole, since good results were obtained in the preliminary calculation[8]. As for the vertical neutron beam hole, R-Z models of the thermal and epithermal neutron beam hole are assumed and the n-γ coupling calculations are in progress.

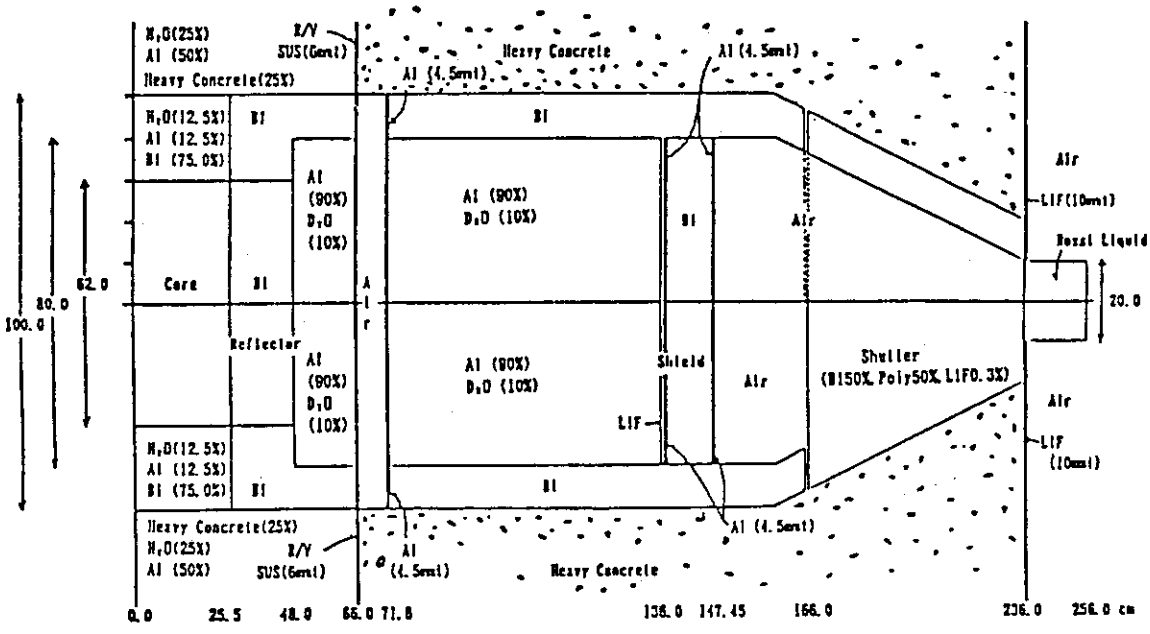

Fig. 4 2-Dim. Model of Horizontal Epithermal Neutron Beam Hole

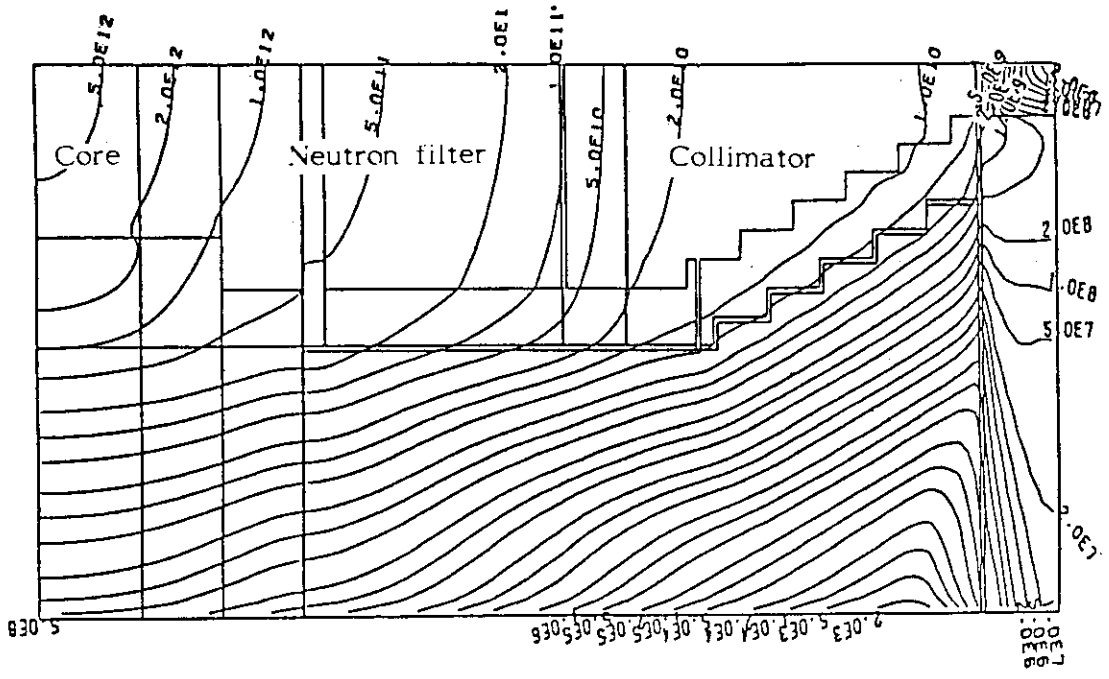

Fig. 5 Contour Map of Epithermal Neutron Flux in Horizontal Epithermal Neutron Beam Hole

CONCLUTIONS

The conceptual design of the medical reactor for BNCT has been completed. This cocept utilizes only existing proven reactor technologies. The low power, low temperature reactor will be inherently safe and the refueling will be unnecessary for the medical use of 30 years. The special features of this medical reactor is the availability of epithermal neutrons and the provision of vertical neutron beam hole. The reactor will be able to deliver the therapeutic dose in about 30 minutes with minimal fast neutron and gamma contaminants and the treatments of patients more than 1,000 per year will be possible. It is expected that this medical reactor, if constructed, will contribute greatly to the advancement of cancer treatment in the world.

ACKNOWLEDGEMENTS

This work is performed as the cooperative research under Grant-in-Aid of the Ministry of Education, Science and Culture, Japan in the fiscal year 1988-91.

REFERENCES

1. S. An, et al., Conceptual Design of a Medical Reactor, UTNL-R-0093, Grant-in-Aid for Scientific Research from the Ministry of Education, Science and Culture, Japan in the fiscal year 1978-79, No. 389001.
2. W. A. NEUMAN, et al., Neutronics Design of a Medical Therapy Reactor, Proceedings of the 1988 Int. Reactor Physics Conf., Sept. 18-22, Jackson Hole, Wyoming.
3. A. HASEGAWA, N-γ Library Based on JENDL-3, Private Communication, 1989.
4. Y. OKA, et al., Nucl. Tech., 55, 642-655(1981).
5. K. AOKI, Effect of (γ,n) Reactions of Heavy Water Moderator on Beam Quality in Biomedical Irradiation Facility, Kyoto Univ. Master Thesis (1989).
6. Protection against Neutron Radiation, Jan. 4, 1971, National Council on Radiation Protection and Measurement (NCRP), Report No. 38.
7. ICRP Publication-21, Table 4 (Old Edition).
8. M. SASAKI, et al., Design Study of a Reactor Facility for Boron Neutron Capture Therapy, 1990 Fall Meeting of the Atomic Energy Society of Japan, B 26 (in Japanese).

6. Evaluation of the WIMS(KAERI)-VENTURE Code System for Peak Power Prediction of KMRR Core Using MCNP

W. S. Park, K. M. Lee, C. S. Lee, J. T. Lee, and S. K. Oh

Department of Reactor Performance Test
KMRR Project, KAERI
P.O.Box 7, Daeduk-Danji
Taejeon, Korea

ABSTRACT

In this work, the validity and quantitative uncertainty of WIMS(KAERI)-VENTURE code system for the design and analysis of KMRR core was tried to be inferred using a well known benchmark code, MCNP. WIMS(KAERI) showed an excellent agreement with MCNP code. For three different control rod positions at a simulated core which has a quarter symmetry, total peaking factors and three sub-factors (radial, axial, and local) obtained from VENTURE were compared with those of MCNP. The comparison proved the validity of VENTURE and showed better agreement in the order of radial, axial, and local factors. The uncertainty of WIMS(KAERI)-VENTURE system was inferred using the 2σ band of total peaking obtained by MCNP. The uncertainty of WIMS(KAERI)-VENTURE system were found to be 18.5% for the operating condition.

I. INTRODUCTION

KMRR(Korea Multipurpose Research Reactor) project has been progressed since 1986. It was designed to output 30 Mw_{th} and to be loaded with two different types of fuel assemblies. Figures 1 and 2 show the cross sectional view of KMRR core and the fuel assembly types to be loaded.

WIMS(KAERI)-VENTURE code system was selected for the design and analysis of the KMRR core. It was very difficult to describe the KMRR core accurately using VENTURE mesh structure for the analysis because the core is shaped basically with hexagonal and circular structures while the rectangular mesh shape is the basic mesh shape of VENTURE code. Therefore, there was a natural demand to check the validity and the amount of uncertainty of WIMS(KAERI)-VENTURE system. MCNP(Monte Carlo Neutron Photon) code was adopted as a reference code to meet the demand. Table 1 shows the characteristics of MCNP and WIMS(KAERI)-VENTURE system. Because of the characteristics of MCNP and the storage limitation of the computer system used (Cyber 170-875), a clean core that has a quarter symmetry was constructed and all the calculations for this work were done on quarter core basis.

The validity of WIMS(KAERI) was checked by comparing a couple of nuclear parameters obtained from lattice calculation of 36-element driver assembly while that of VENTURE code was confirmed by comparing total peaking factors

and their three sub-factors(radial(F_R), axial(F_Z), local(F_L)) determined from core calculation. Finally the amount of the uncertainty in the calculation of the total peaking by WIMS(KAERI)-VENTURE system was tried to be inferred by the 2σ band of total peakings obtained by MCNP.

II. CALCULATIONAL MODEL AND PEAK POWER ANALYSIS METHOD

II.1 Lattice Calculation

The lower side of Figure 3 shows the calculational model of 36 element driver assembly in WIMS(KAERI). Because of the limited describable geometry of WIMS(KAERI), the original hexagonal array of fuel pins was transformed into a circular array based on equivalent volume concept. On the other hand, exact geometrical configuration was used in MCNP calculation. WIMS(KAERI) has no means to account for the axial leakage except axial buckling. As usual for lattice calculation, reflective boundary condition was imposed on the lattice surface in both of WIMS(KAERI) and MCNP calculation.

II.2 Core Calculation

In order to perform core analysis using MCNP, it is required to input atomic fractions for all nuclides comprising the core. Therefore a fresh clean core was selected in order to avoid such a complicated work. In addition, the clean core was tried to have exact quarter symmetry by repositioning the control rod sites because the computer storage limitation (Cyber 170-875) did not allow MCNP code to perform full core calculation. Figure 4 shows the core model of MCNP calculation.

Because of the reasons to be mentioned in Section II.3, 3-D and 2-D VENTURE models were employed for the core analysis. The mesh grid of 57 x 47 x 20 was adopted for the 3-D XYZ model in accordance with a cost-and-benefit analysis done in the early stage of KMRR design. A fuel assembly was represented by 4 x 4 x 8 meshes. The mesh size in reflector region was decided on the basis of material properties and the actual geometry of various kinds of experimental holes. On the other hand, the mesh grid of 2-D XY model was determined to be 148 x 117.

The control rod insertion was considered from the very top of the active core instead of the top of the core for both of MCNP and VENTURE calculation.

II.3 Peak Power Analysis Method

Total peaking factor at each assembly is defined as follows,

$$F_T(i) = \mathrm{Max}\ [\ F_R(i)*F_Z(i,j)*F_L(i,j)\ ],\ j=1,\ 2,\ \ldots,8 \qquad \text{----------(1)}$$

In above equation, indexes i, j represent the assembly, the axial plane of the assembly, respectively. In addition, F_R, F_Z, F_L are used to represent the radial, axial, local peaking factors of the assembly i, respectively. Radial peaking is defined as relative power sharing of the assembly i and axial peaking is the ratio of the power of plane j to the average plane power at the assembly i. Local peaking is obtained from the ratio of maximum to average rod power at the plane j of the assembly i.

In addition to the computer storage problem, it was not desirable to calculate the total peaking using Eq. (1) in terms of computer cost. Following approximated equation was used to determine total peak,

$$F_T(i) = F_R(i)*F_Z(i)*F_L(i), \qquad \text{----------(2)}$$

where axial peaking factor(F_Z) is the ratio of maximum to average plane power of assembly i and local peaking factor(F_L) is the ratio of maximum to average rod power in the assembly i. At all rod out condition, radial and axial peaking factors were calculated by 3-D VENTURE while local peaking factor was determined from 2-D VENTURE model. When there was partial or full insertion of rods, radial and axial peaking factors were obtained from 3-D calculation at that rod position while local peaking was from 2-D calculation at all rod-in condition.

III. RESULTS AND CONCLUSION

III.1 Lattice Calculation

The main difficulty in the use of Monte Carlo code for the criticality and power distribution calculation is, how fast to have the source distribution converged. For the effective running, 500 source locations per cycle were sampled for first 10 cycles and 3000 source locations per cycle for last 15 cycles. Table 2 shows the power sharing of each ring in driver assembly. Because of the difference in the treatment of axial boundary, it is meaningless to compare the K-effective values. The comparison of power sharing can prove the validity of WIMS(KAERI).

III.2 Core Calculation

In order to improve the calculational accuracy, 1000 source locations per cycle were sampled for first 15 cycles and 5000 location per cycle were selected randomly for last 20 cycles.

Table 3 shows the comparison of K-effective values at three different control rod positions. The comparison confirms that 3-D VENTURE has a good capability to predict the reactivity of KMRR core although there is slight overestimation that seems to come from the homogenization[3]. Tables 4 and 5 show the local peaking factors at ARO and ARI conditions, respectively. From these tables, it can be asserted that 2-D VENTURE predictions are in good agreement with the nominal value of MCNP within 10 % relative error. As expected, the insertion of control rods increases considerably the local peaking factors of assemblies surrounding control site while it causes negligible effects on the assemblies having no direct contact with control site. Tables 6 and 7 prove the validity of 3-D VENTURE model for the calculation of the axial peaking factors. Tables 8 and 9 show the radial power sharing at all rod out and half-in conditions, respectively. 3-D VENTURE seems to underestimate the power sharing slightly. It is believed that 3-D VENTURE has a good capability to predict the radial peaking factor for KMRR core analysis.

III.3 Total peaking and Uncertainty of WIMS(KAERI)-VENTURE System

Tables 10 and 11 show the total peaking factors at ARO and rod half-in conditions, respectively. Fractional standard deviation(f.s.d.) of total peaking was calculated based on the assumption that sub-factors are independent one another. In order to keep the consistency of the calculation, total peakings of MCNP were determined based on the same calculational method (Eq.(2)) mentioned in Section II.3. True total peaking for each assembly is not known. However, the true value can be assumed to be lower than upper top of 2σ band of MCNP with more than 97.7% confidence level. Table 12 shows the amount of the required fraction to lift up VENTURE value to the upper top of the MCNP band. Therefore, we have to consider about 18.5% uncertainty for the operating condition as long as there is no improvement on the peak power analysis method and WIMS(KAERI)-VENTURE model for KMRR analysis.

REFERENCES

1. Y. J. Kim, B. J. Kim, and H. R. Kim, "Physics Design Manual for KMRR", KM-031-400-01, KAERI, 1989.

2. J. F. Briesmeister, editor, "MCNP-A General Monte Carlo Code for Neutron and Photon Transport Version 3A," Los Alamos National Lab. Manual, LA-7396, Rev. 2, Sept. 1986.

3. J. R. Lamarsh, "Introduction to Nuclear Engineering," Addison-Wesley, 1975.

4. D. R. Vondy, et al.,"VENTURE : A Code Block for Solving Multigroup Neutronics Problems Applying the Finite-Difference Diffusion Theory Approximation to Neutron Transport", ORNL-5602, ORNL, 1975.

5. J. D. Kim, et al., "Nuclear Data Evaluation and Group Constant Generation for Reactor Analysis," RR-750, KAERI, 1988.

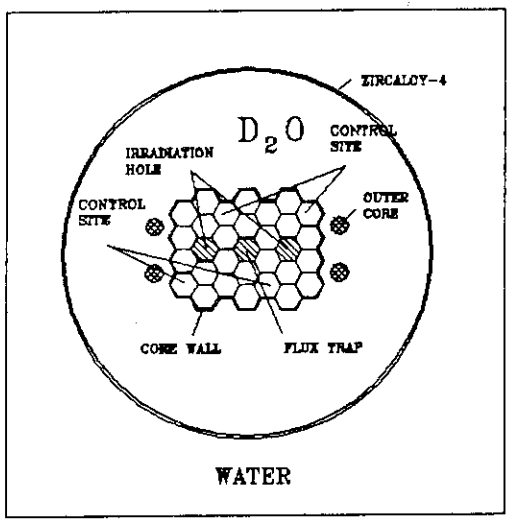

Fig. 1 Cross Sectional View of KMRR Core

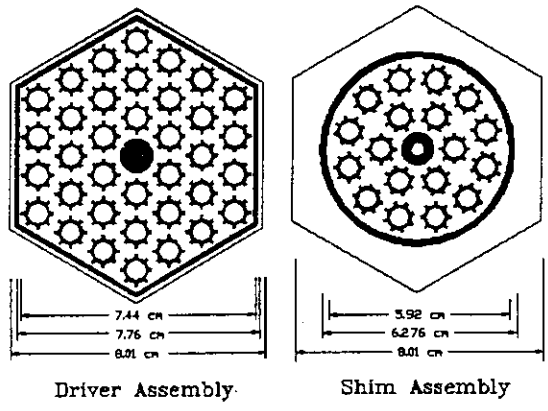

Fig. 2 Two Assembly Types

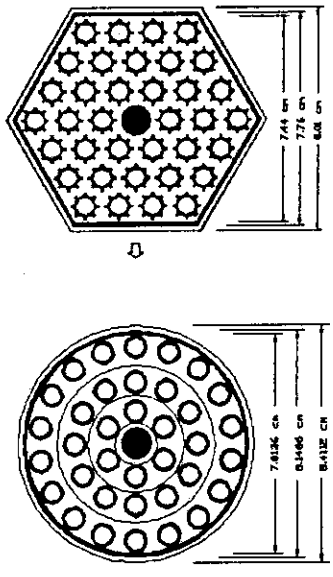

Fig. 3 Geometrical Transformation

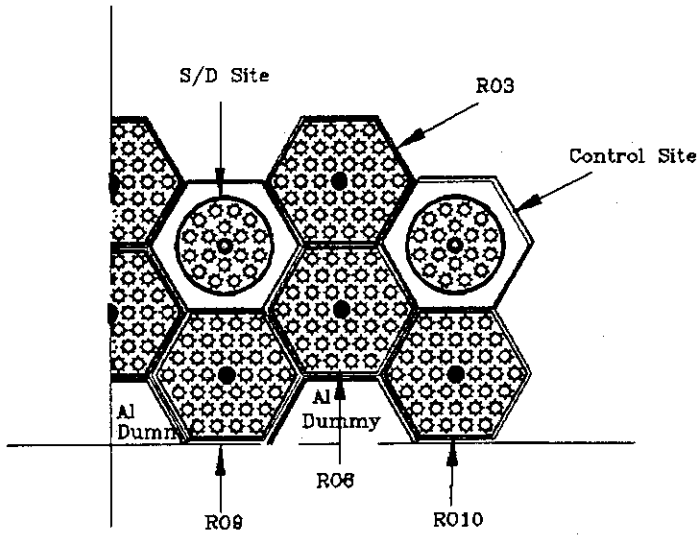

Fig. 4 Core Model of MCNP

Code / Items	MCNP	WIMS-VENTURE
Library	ENDL, ENDF/B-IV	ENDF/B-IV, V
Energy Group	Continuous	5 Group
System Equation	Integral Transport Equation	Multigroup Diffusion Equation
Geometry Description	Explicit	Approximation
Assembly Treatment	Purely Hetero.	Homogenize
Etc.	Stochastic Code (Monte Carlo)	Deterministic Code

Table 1 Characteristics of MCNP and WIMS(KAERI)-VENTURE

Item / Code	K-eff.	Inner Ring	Middle Ring	Outer Ring
MCNP	1.570091 ± 0.26%	0.1635	0.3177	0.5188
WIMS	N/A	0.1684	0.3219	0.5097
Ratio		0.97	0.99	1.02

* Ratio = MCNP / WIMS

Table 2 Ring Power Sharing of Driver Ass.

Tools / Rod Position	MCNP (f.s.d.)	VENTURE	Rel. Error
All Rod Out	1.303435 (0.22 %)	1.3228684	1.5 %
All Rod Half-In	1.245756 (0.20 %)	1.2676236	1.7 %
All Rod In	1.193370 (0.29 %)	1.206227	0.99 %

Table 3 K-effective Comparison

Code / Ass. Loc.	MCNP		VENTURE	Rel. Err.
	factor	f.s.d.		
R03	1.461	0.0648	1.437	-0.0167
R06	1.450	0.0454	1.375	-0.0545
R09	1.333	0.0438	1.385	0.0375
R010	1.291	0.0504	1.329	0.0286

Table 4 Local Factor Comparison at ARO Condition

Code / Ass. Loc.	MCNP		VENTURE	Rel. Err.
	factor	f.s.d.		
R03	1.649	0.0507	1.786	0.0767
R06	1.562	0.0561	1.509	−0.0351
R09	1.343	0.0494	1.341	−0.0015
R010	1.670	0.0592	1.770	0.0599

Table 5 Local Factors at All Rod In

Code / Ass. Loc.	MCNP		VENTURE	Rel. Err.
	factor	f.s.d.		
R03	1.247	0.0399	1.241	−0.0045
R06	1.299	0.0430	1.271	−0.0222
R09	1.328	0.0418	1.277	−0.0381
R010	1.277	0.0488	1.256	−0.0170

Table 6 Axial Factors at All Rod Out

Code / Ass. Loc.	MCNP		VENTURE	Rel. Err.
	factor	f.s.d.		
R03	1.347	0.0316	1.380	0.024
R06	1.424	0.0327	1.420	−0.003
R09	1.337	0.0299	1.340	0.002
R010	1.461	0.0338	1.461	0.000

Table 7 Axial Factors at All Rod Half-In

Code / Ass. Loc.	MCNP		VENTURE	Rel. Err.
	factor	f.s.d.		
R03	0.955	0.0129	0.965	0.0104
R06	0.895	0.0133	0.852	−0.0505
R09	1.016	0.0127	0.976	−0.0410
R010	0.902	0.0135	0.867	−0.0404

Table 8 Radial Factors at All Rod Out

Code / Ass. Loc.	MCNP		VENTURE	Rel. Err.
	factor	f.s.d.		
R03	0.904	0.0164	0.926	0.0237
R06	0.854	0.0131	0.847	−0.0083
R09	1.116	0.0131	1.073	−0.0401
R010	0.797	0.0152	0.793	−0.0050

Table 9 Radial Factors at All Rod Half-In

Code / Ass. Loc.	MCNP		VENTURE	Rel. Err.
	factor	f.s.d.		
R03	1.740	0.0772	1.721	−0.110
R06	1.686	0.0639	1.489	−0.132
R09	1.796	0.0617	1.726	−0.041
R010	1.487	0.0714	1.447	−0.028

Table 10 Total Factors at All Rod Out

Code / Ass. Loc.	MCNP		VENTURE	Rel. Err.
	factor	f.s.d.		
R03	2.008	0.0620	2.262	0.2101
R06	1.900	0.0662	1.815	−0.0468
R09	2.004	0.0592	1.928	−0.0394
R010	1.945	0.0698	2.051	0.0517

Table 11 Total Factors at All Rod Half-In

Rod Loc. / Ass. Loc.	All Rod Out	All Rod Half -In
R03	0.167	−0.011
R06	0.277	0.185
R09	0.169	0.162
R010	0.174	0.081

Table 12 Uncertainty Factors

7. Two-Dimensional Natural Convective Heat Transfer Analysis in an Open Cavity and Its Application to KMRR

H.T.CHAE, B.W.RHEE, B.S.SIM
Korea Atomic Energy Research Institute (KAERI)
PO Box 7,Daeduk-danji, Daejeon,Korea

S.H.CHANG, T.H.SONG
Korea Advanced Institute of Science and Technology (KAIST)
Daeduk-danji, Daejeon,Korea

ABSTRACT

Natural convection flow is established in KMRR (Korea Multi-Purpose Research Reactor) reflector tank at the loss of reflector circulation. To simulate the reflector tank natural convection flow with high temperatures at the inner shell and bottom plate due to nuclear heating, experimental and numerical studies in an open cavity with 'L' type heated wall made by the combination of a vertical and horizontal plate were performed.It was confirmed through these studies that the heat transfer rates were highest at the lower region of the vertical plate and the inlet region of horizontal plate and comparatively high at the middle portion of both plates. The heat transfer rate distribution of this trend shows a desirable trend for the effective natural convection cooling of KMRR reflector tank. It was also confirmed that the average Nusselts numbers at the 'L' type heated wall were lower than those obtained from the existing natural convection heat transfer correlations for the vertical and horizontal plates.

INTRODUCTION

A 30 MWth research reactor, the so-called KMRR,has been developed by the Korea Atomic Energy Research Institute. The KMRR is an upward-flowing, light-water-cooled and heavy-water-moderated research reactor with an open-chimney-in-pool arrangement. An ultimate heat transfer mode in KMRR is the pool natural circulation and natural convection flow is established in the reflector tank at the loss of reflector circulation [1].

KMRR reflector tank encompasses the reactor core cylindrically as shown in Fig.1. At some spots of the inner shell and bottom plate of the reflector tank,high temperature is maintained due to the nuclear heating inside the tank wall and it is a design concern to prevent any local boiling inside tank not only during steady state but also transient.

To simulate the natural convection flow and the associated heat transfer inside the reflector tank a laminar natural convective heat transfer test in an open cavity with 'L' type heated wall made by the combination of a vertical and bottom horizontal plate was performed using the Mach-Zehnder interferometer.

As a test result, the fluid temperature distribution in the test section and the local Nusselt number distribution at the heated wall were obtained

for various Rayleigh numbers. Also a numerical model which predicted the experimental results well was developed using SIMPLER algorithm. It was confirmed through the experimental results and the numerical analysis that the heat transfer rates were highest at the lower region of vertical plate and the inlet region of the horizontal plate and comparatively high at the middle portion of both plate. It is thought that this heat transfer rate distribution shows a desirable trend for the effective natural convection cooling of the KMRR reflector tank considering that the highest wall temperature occurs at the middle portion of the inner shell and bottom plate. It was also confirmed that the average Nusselt numbers at the 'L' type heated wall were lower than those obtained from the existing natural convection heat transfer correlations for the vertical and horizontal plate.

EXPERIMENTAL APPARATUS AND PROCEDURE

Test section shown schematically in Fig.2 consisted of a long square open cavity with height h= 7.0cm, width W= 7.0cm and length L= 30.0cm so that the aspect ratio A=h/W=1. The left vertical wall and bottom plate were isothermal at an elevated temperature Tw and constructed from a 2.0cm thick aluminum plate with immersed electric heater wires. The right wall and ceiling were made by plexiglas with 1.5cm thick as adiabatic walls maintaining room temperature T_∞. In the left upper corner and right lower corner, inlet and outlet slits for the gravity driven air flow are located. Four thermocouples were embedded in the 'L'type heated wall to monitor actual temperature of the plate. It was found that the heated wall could be maintained indefinitely to within ± 0.1 °C of the set temperature.

A Mach-Zehnder interferometer was used to evaluate the temperature distribution within the open cavity. The interferometer is ideally suited for the investigation of two dimensional temperature fields since it does not introduce disturbances into the gas layer,and the entire temperature field can be recorded instantaneously [2]. A 10mW He-Ne laser serves as a light source and the schematic diagram of Mach-Zehnder interferometer is shown in Fig.3. From the interferograms local Nusselt number may be evaluated by the following equation.

$$Nu_x = \left.\frac{\partial T}{\partial y}\right|_w \cdot \frac{h}{T_w - T_\infty} = \left.\frac{\partial \theta}{\partial Y}\right|_w \qquad (1)$$

where Nu_x = local Nusselt numbers for horizontal heated wall
h = width and height of heated wall
θ = dimensionless temperature
Y = dimensionless length.

Term of the right hand side of Eq.(1) was obtained by measuring the distances from heated wall to the first and second fringe shift and assuming the quadratic function of normal distance to the wall.

NUMERICAL ANALYSIS

The geometry of numerical model is illustrated in Fig.4. Numerical model was simulated such as the test section was located in a corner of large

square enclosure. The flow is laminar and two-dimensional. Fluid within model is assumed to have constant properties except insofar as the buoyancy is concerned,i.e, the Boussinesq approximation of linear temperature dependence of density is utilized. The governing equations may be written in non-dimensional form as :

$$\frac{\partial U}{\partial X} + \frac{\partial V}{\partial Y} = 0 \tag{2}$$

$$\frac{\partial (UU)}{\partial X} + \frac{\partial (UV)}{\partial Y} = -\frac{\partial P}{\partial X} + \left(\frac{\partial^2 U}{\partial X^2} + \frac{\partial^2 U}{\partial Y^2}\right) \tag{3}$$

$$\frac{\partial (UV)}{\partial X} + \frac{\partial (VV)}{\partial Y} = -\frac{\partial P}{\partial Y} + \left(\frac{\partial^2 V}{\partial X^2} + \frac{\partial^2 V}{\partial Y^2}\right) + \frac{Ra}{Pr} \cdot \theta \tag{4}$$

$$\frac{\partial (U\theta)}{\partial X} + \frac{\partial (V\theta)}{\partial Y} = \frac{1}{Pr}\left(\frac{\partial^2 \theta}{\partial X^2} + \frac{\partial^2 \theta}{\partial Y^2}\right) \tag{5}$$

where

$$p' = p + \rho_\infty \cdot g \cdot y, \quad X = \frac{x}{h}, \quad Y = \frac{y}{h}, \quad U = \frac{uh}{\nu}, \quad V = \frac{vh}{\nu} \tag{6}$$

$$P = \frac{h^2 p'}{\rho_\infty \cdot \nu^2}, \quad \theta = \frac{T - T_\infty}{T_w - T_\infty}, \quad Pr = \frac{\nu}{\alpha}, \quad Ra = \frac{g\beta\left(T_w - T_\infty\right) \cdot h^3}{\nu\alpha}$$

The boundary conditions are as follows :

$\theta = 0, U = 0, V = 0$ on the enclosure wall and the insulated wall of test section

$\theta = 1, U = 0, V = 0$ on the hot wall of test section.

The above governing differential equations were approximated by a finite difference method following the SIMPLER procedure that handles the velocity-pressure coupling through the pressure correction equation [3].

RESULTS AND DISCUSSION

Experimental Results

Typical interferograms from Mach-Zehnder interferometry are presented in Fig.5. Fringes shown in the interferograms represent isotherms.Since the temperature difference between isotherms is the same, the heat transfer rates increase as they become close near the heated wall.

An inspection of isotherms in Fig.5 clearly reveals that the highest heat transfer occurred at the inlet region of heated horizontal plate where the boundary layer is developed and at the lower region of heated vertical plate where the horizontal inlet flow direction is vertically changed. It can be seen that the lowest heat transfer, as expected, occurs at the corner of 'L' type heated wall due to the flow stagnation.

Comparison with Numerical Prediction

Experimental isotherms are compared with numerical prediction for $Ra=6.0\times10^5$ in Fig.6. Except for minor distortion at the outlet region there is an excellent agreement between the numerical and experimental isotherms.

Numerical and experimental local Nu distributions for $Ra=4.9\times10^5$ are presented in Fig.7. A good agreement also prevails except the inlet region of horizontal plate. It is judged that these differences are induced by the upstream boundary layer effect found near the edge [4]. Relative errors of numerical and experimental results for local Nu are about 12% for the horizontal wall and about 7% for the vertical wall.

Average Nusselt Number

Numerical analyses were performed within the laminar region as a function of Ra based on the above mentioned agreements between experimental and numerical results.

The average Nusselt numbers were obtained by integration of local Nu along the heated wall. The calculated average Nu in the range of $5\times10^4 \leq Ra \leq 5\times10^6$ are compared with the existing natural convection heat transfer correlations for the vertical and horizontal plate in Fig.8. The average heat transfer rates at the 'L' type heated wall were lower than those for both plates. It is speculated that this phenomenon comes from the reduction of heat transfer rate due to the flow stagnation at the corner of 'L' type heated wall while the highest heat transfer rates are generally found at the edge of plate due to the thermal boundary layer generation.

Application to KMRR

At the middle region of the inner shell and bottom plate of KMRR reflector tank high temperature is maintained due to the nuclear heating inside the tank wall. It can be seen in Fig.6 that the heat transfer rates are relatively high at those regions. It is judged that this heat transfer distribution makes the hot point cooling effective.

On the other hand at the transient analysis for the loss of reflector circulation the half value of natural convection correlation for plate was used for considering conservatism in a design [5]. To confirm the above assumption, the average Nu was compared with the transient analysis value in Fig.9. Though numerical analysis was performed in lower Ra range than KMRR reflector tank natural convection flow condition , Ra= about 10^{11} , it is considered that the above assumption for design conservatism is reasonable since the heat transfer rate of 'L' type heated wall becomes higher than those of transient analysis as Ra increases.

CONCLUSIONS

This paper has dealt with the prediction of natural convection in a square open cavity with the 'L' type heated wall. The important findings obtained from experiment and numerical analysis are as follows:

1) Experimental and numerical results for isotherms and local Nu distributions showed good agreement.
2) It was confirmed that the highest heat transfer rates in the test section occurred at the inlet region of horizontal plate and the lower region of vertical plate.
3) The average heat transfer rate for each plate of 'L' type heated wall was

lower than that of vertical or horizontal plate.

4) The local heat transfer rate distributions showed a desirable trend for the effective natural convection cooling of KMRR reflector tank.

REFERENCES

1) KMRR Safety Analysis Report, KAERI/TR-107/87, KAERI, 1987
2) Hauf,W.,Grigull,U., Optical Methods in Heat Transfer, Advances in Heat Transfer, Vol.6, Academic Press, New York, pp.133-366, 1970
3) S.V.Patankar, Numerical Heat Transfer and Fluid Flow, McGraw-Hill, 1980
4) S.M. Yang and F. Chen, Experimental Investigation of The Influence of Upstream Boundary Layer on Natural Convection Heat Transfer of a Heated Upward Facing Surface, Proceedings of the Ninth International Heat Transfer Conference, Jerusalem, Israel, pp.187-191, 1990
5) Technical Report, Analysis of T/H Behavior of Reflector System, KM-033-RT-K020, KAERI, 1990

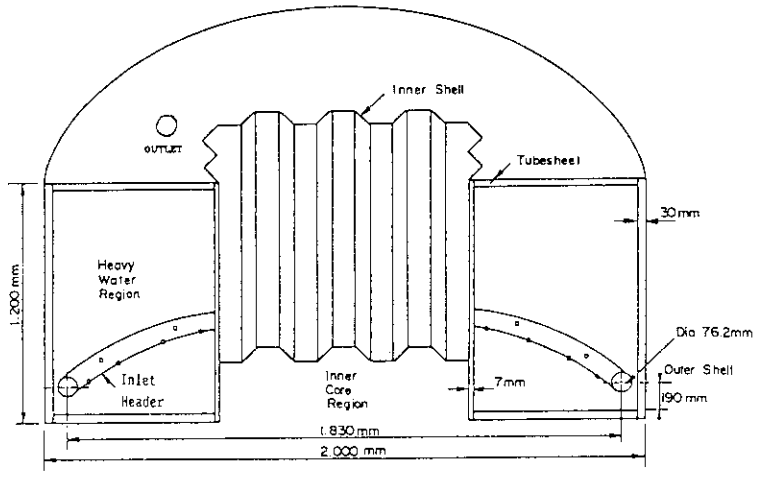

Fig.1. Schematic Diagram of KMRR Reflector Tank

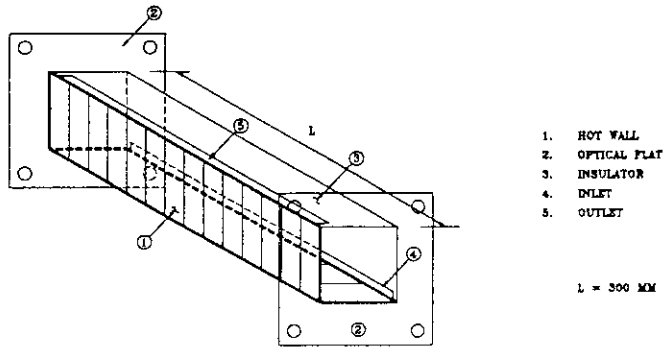

Fig.2. Sketch of Experimental Model

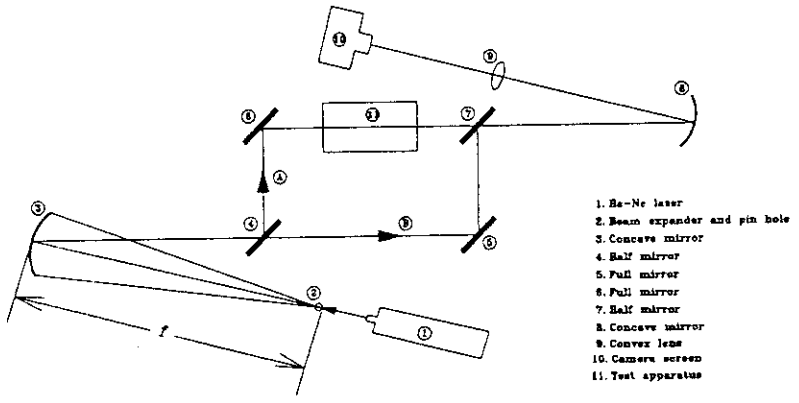

Fig.3. Schematic Diagram of Mach-Zehnder Interferometer

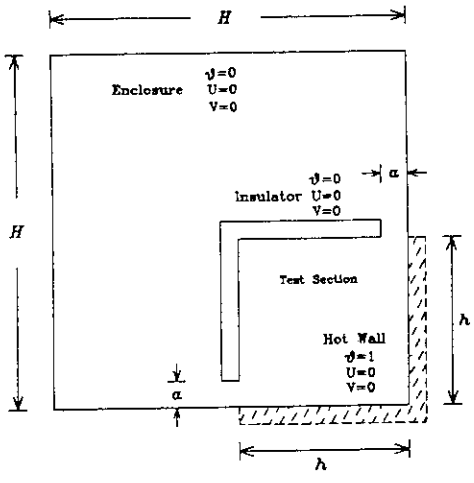

Fig.4. Numerical Model

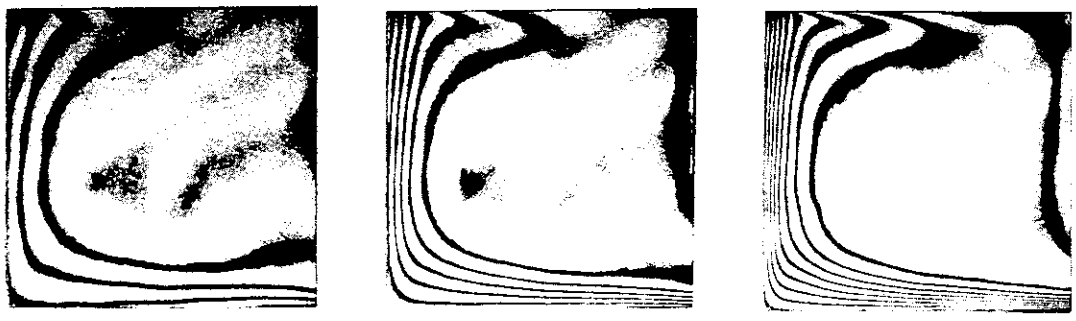

Ra = 2.296 x 10^5　　Ra = 4.641 x 10^5　　Ra = 7.070 x 10^5

Fig.5. Interferograms for Various Ra

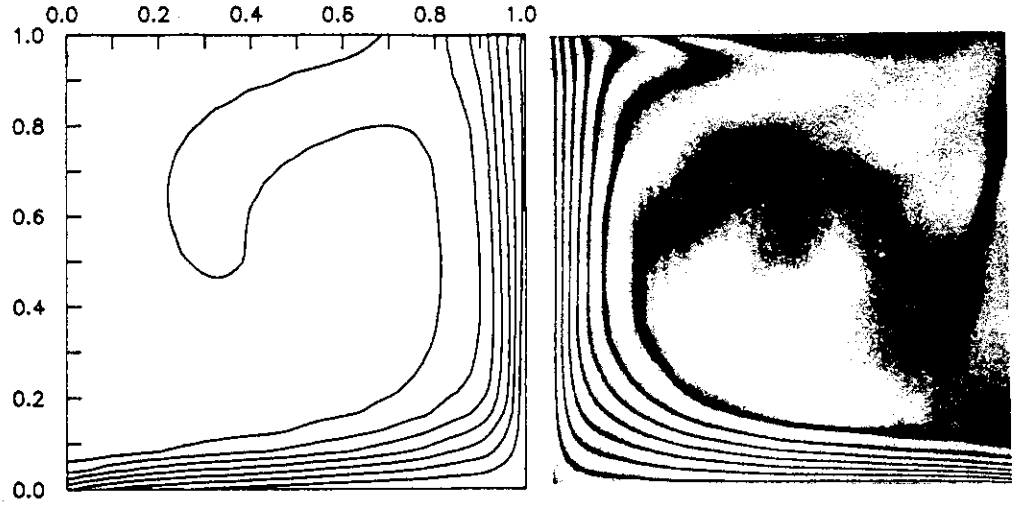

a) Numerical Prediction　　b) Experimental Result

Fig. 6. Comparison of Isotherm Distribution between Numerical and Experimental Result for Ra = 6.02 x 10^5

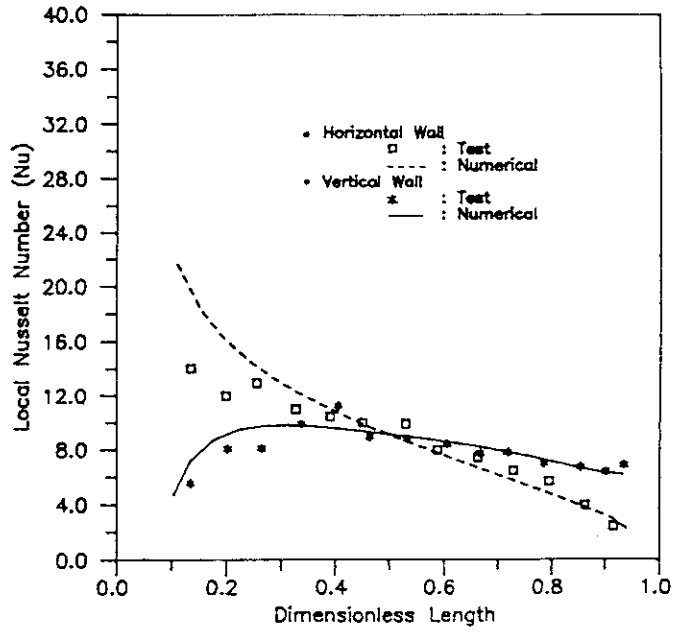

Fig. 7. Comparison of Local Nu Distribution between Numerical and Experimental Result for Ra = 4.9 x 10^5

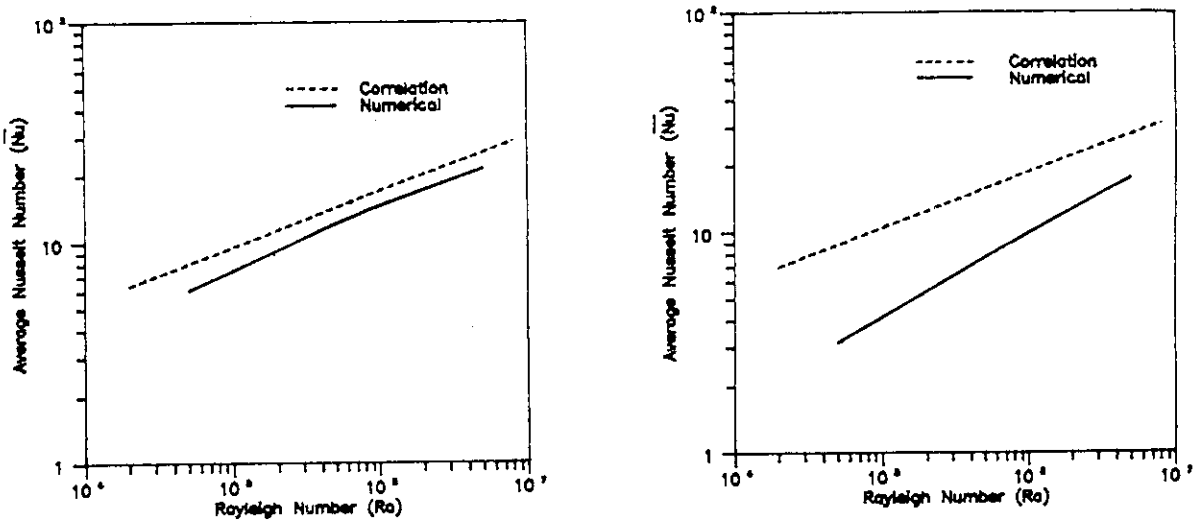

a) Horizontal Plate

b) Vertical Plate

Fig. 8. Comparison of Average Nu with Existing Correlation as a Function of Rayleigh Number

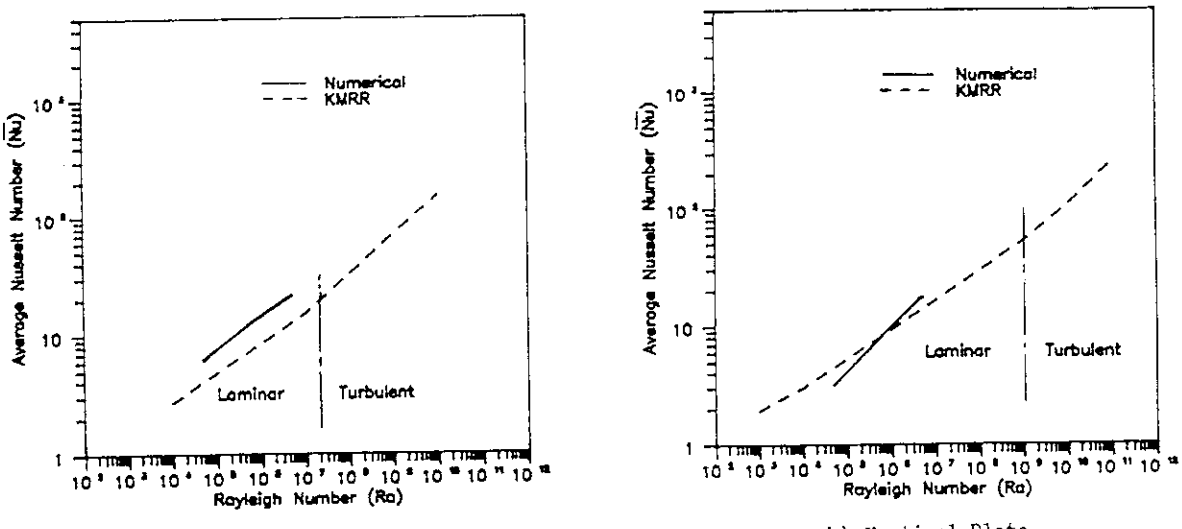

a) Horizontal Plate

b) Vertical Plate

Fig. 9. Comparison of Average Nu with Those Used in KMRR Reflector System Analysis

8. Three-Dimensional Core Physics Analyses for the Reactor of Nuclear Ship "MUTSU"

Masafumi ITAGAKI, Yoshinori MIYOSHI
Department of Nuclear Ship Engineering
Japan Atomic Energy Research Institute
Kita-Sekine, Mutsu-shi, Aomori-ken 035, Japan

Tomohiro SAKAI
The Japan Research Institute, Limited
Kamiohsaki, Shinagawa-ku, Tokyo 141, Japan

ABSTRACT

Three-dimensional (3-D) considerations are important in core physics calculations for ship reactors. This paper deals with some 3-D analyses for the N.S. Mutsu power-up test results: There were discrepancies between measured control-rod positions at criticality and 1-D diffusion calculation results, while our 3-D code STEADY-SHIP has given excellent agreements; The moderator temperature coefficients calculated by the code agree well with the measured ones for wide range of temperature when the actual control-rod patterns are taken into consideration; Significant control-rod interferences observed in our excess reactivity measurement are also well simulated by the 3-D diffusion analyses; The analyses based on the Crump-Lee method with calculated 3-D source distributions provide acceptable agreements between the calculated and the measured ex-core detector response caused by control-rod motion.

I . INTRODUCTION

Chemical shim control is not employed for ship reactors to prevent a reactivity increase due to an exchange between reactor water and sea water if the ship is sunk. The reactivity is controlled only by means of control-rods; some of the rods are partially inserted even in power operations. Hence a ship reactor has a 3-D distorted flux distribution in the core. Three-dimensional considerations are therefore important for precise analyses of ship reactor performances.

On March 29, 1990, Japan Atomic Energy Research Institute began low power reactor tests of the first Japanese nuclear ship "Mutsu" after a 16 year hiatus beginning in 1974 when the reactor was stopped due to unexpected radiation leakage. The tests up to about 20% of the reactor output were performed at the Sekinehama port and ended on April 28. The first high power operation on the Pacific ocean was conducted in July and the entire power-up test series were completed during the fourth ocean trial in December. A lot of reactor physics performances were measured during the tests through 1990 and systematic computer analyses have been carried out for these results.

Present paper describes some special topics among them, which are all related to the 3-D core characteristics peculiar to ship reactors.

II . DESCRIPTION OF THE N.S. MUTSU REACTOR CORE

The reactor of the Mutsu is a small two-loop type PWR rated at 36MW (thermal). The principal design parameters of the reactor are summarized in Table 1 and a geometrical cross section of the core is illustrated in Fig.1.

Table 1 Parameters of the Mutsu reactor core

Thermal output (MW)	36
Coolant pressure [MPa(gauge)]	11.15
Average coolant temperature (℃)	273.5
Effective core height (mm)	1040
Equivalent diameter (mm)	1146
Number of fuel assemblies	32
Assembly pitch (mm)	179.6
Fuel enrichment (w/o)	3.24/4.44
Fuel rod pitch (mm)	15.0
Fuel rod diameter (mm)	10.53
Fuel pellet diameter (mm)	9.6

The core is divided into two zones: twelve assemblies in the central region are of 3.24w/o enrichment and twenty ones in the outer region are of 4.44 w/o. Each fuel assembly has a square lattice arrangement of 112 fuel rods and 9 burnable poison rods. These rods are supported by grid spacers, which are welded to a outer can-box. Each fuel rod is composed of a cladding tube made of stainless-steel filled with UO_2 pellets. The reactivity is controlled by means of a total of twelve cruciform control-rods. The eight rods located in the peripheral zone are fully withdrawn under hot critical conditions. The reactivity during power operation is controlled solely by the four control-rods located in the center of the core: two of the four rods (G1 or G2 group) are moved as a pair, and the other group (G2 or G1) is fixed at a constant elevation. The reactor pressure vessel is surounded by an annular iron-water shield tank, in which ex-core neutron detectors are located in a circle with a radius of 140cm around the core center.

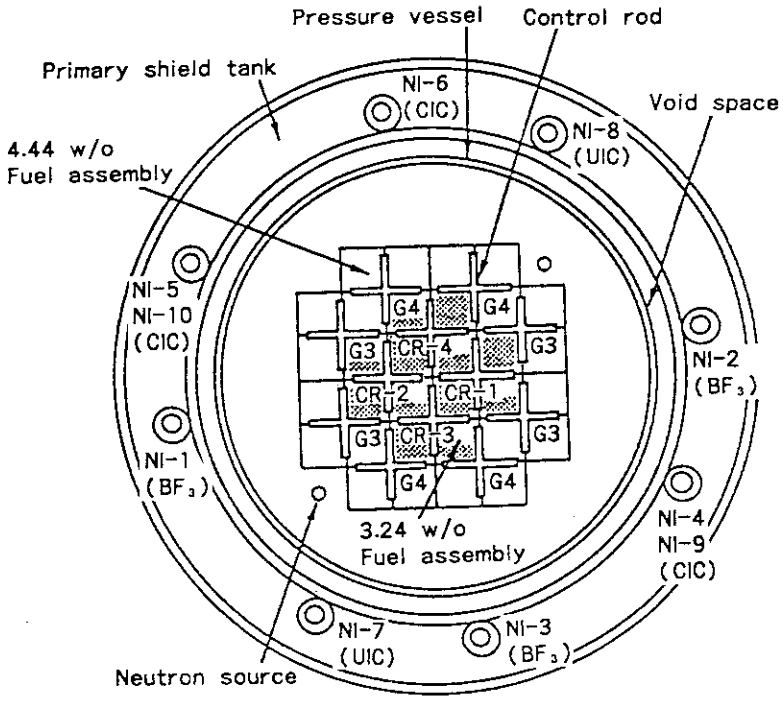

Fig.1 Core configuration of N.S. Mutsu reactor

Ⅲ. OUTLINE OF THE REACTOR PHYSICS CODES FOR THE N.S. MUTSU

A code STEADY-SHIP[1] has been developed to calculate reactivity and 3-D distributions of neutron flux, power and coolant temperature in the core of N.S. Mutsu. The code consists of two parts: a three-group 3-D neutron diffusion module and a thermal-hydraulic one. The required nuclear constants for the STEADY-SHIP are provided from a code ASSEMBLY-SHIP[2]. This code also consists of two parts; a module for generating burnup-dependent multi-energy group constants for a lattice-cell and a 2-D diffusion module for producing three-group constants for a fuel assembly. The former module is based on a GAM-type slowing-down program and a THERMOS-type thermalization transport program. In the STEADY-SHIP calculations, the control-rod effect is modelled by a ratio of the neutron current to the flux which can be generated by the 1-D transport code ANISN[3] and the ratio is assigned to the control-rod regions as internal boundary conditions.

The reactor power is monitored by means of the four ex-core neutron detectors (CIC and UIC). The detector signals depend on the local neutron flux at the detectors rather than the core-average power, with the result that the signals vary when a control-rod pattern changes even if the power level remains constant. A code EXCORE has been developed, based on the Crump-Lee method[4], to predict such detector responses. Weighting functions required for the prediction analyses are calculated using the ray-tracing technique with the Anderson-Shure point kernel.

Ⅳ. PREDICTION OF HOT CRITICAL ROD POSITIONS

Figure 2 illustrates combinations of G1 and G2 control-rod positions required to attain criticality at hot zero power conditions (273.5℃ and 11.15MPa). The symbol ○ shows the results measured on April 6, while the symbol ● represents the ones measured in 1974. The dotted line was obtained from 1-D diffusion calculations performed before 1974. The solid line is the newly calculated curve obtained using the code STEADY-SHIP. There is large discrepancies between the 1-D diffusion calculation results and the measured ones since this old 1-D model could not simulate well the complicated flux distributions in the core. While the present 3-D results agree quite well with the measured ones. The 1-D diffusion codes are still widely used for core design of land-based PWRs. The reason for this is that the flux shape in the core of such a reactor can be practically

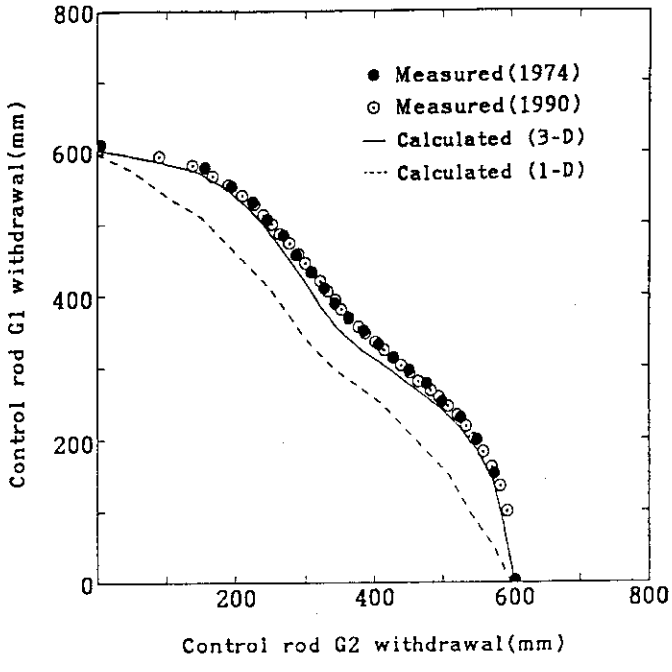

Fig.2 Critical rod positions of G1 and G2 at hot zero-power conditions

assumed to be separated into the axial and the horizontal components:

$$\Phi(x,y,z) \sim \phi(x,y)\cdot\Psi(z). \quad (1)$$

This is due to the fact that all control-rods are almost fully withdrawn during power operations of land-based PWRs since they use chemical shim control. In contrast, a ship reactor generally shows strong 3-D characteristics caused by partial insertion of control-rods even under full power conditions. Three-dimensional considerations are therefore important for precise analyses of neutronic performances of a ship reactor core.

V . MODERATOR TEMPERATURE COEFFICIENT

The moderator temperature coefficient is also affected by the 3-D effect, since the control-rod pattern changes with the temperature increase and then the 3-D neutron leakage distribution drastically changes.

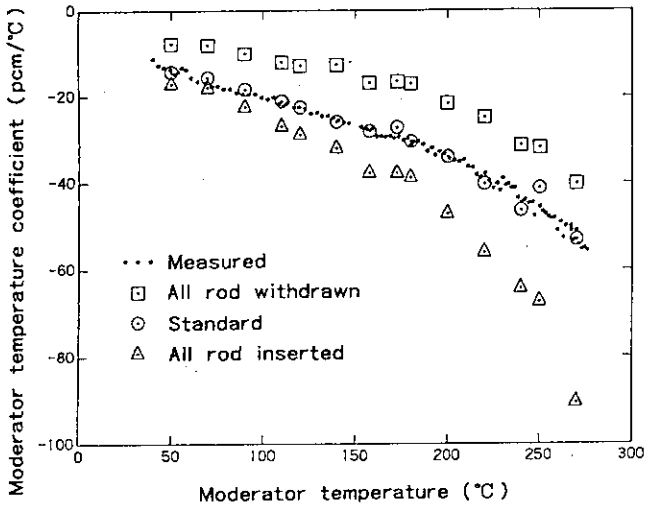

Fig.3 Variation in moderator temperature coefficients. The "standard" results were calculated assuming the actual rod pattern changes following the moderator temperature increase. The calculations performed under simple assumptions, "all rod fully withdrawn" and "all rod fully inserted", under-estimated and over-estimated the temperature coefficients, respectively.

Figure 4 shows the variation in moderator temperature coefficients. The reactivity unit "pcm" means $10^{-3}\%\,\Delta\rho$. The small symbol ● represents the results measured in the power-up tests. While the symbols ○, □ and △ show the values calculated by the STEADY-SHIP. The plots ○ were obtained from "standard" calculations performed assuming the actual control-rod pattern for each moderator temperature. These results agree well with the measured values for wide range of temperature, from 40 to 275℃. The other results (symbols □ and △) were obtained from hypothetical calculations performed under simple assumptions, i.e., all rods are fully withdrawn and fully inserted, respectively.

The moderator temperature coefficient α_T can be simply defined as follows and it can be divided into two parts, each of which is related to the infinite multiplication factor k_∞ and the non-leakage probability P:

$$\alpha_T \sim \frac{\partial}{\partial T}\ell n\, k_{eff} = \frac{\partial}{\partial T}\ell n\, k_\infty + \frac{\partial}{\partial T}\ell n\, P \ . \quad (2)$$

The quantity P is usually defined as a function of "buckling" B^2, e.g., as $P = 1/(M^2B^2)$ for the one-group approximation. In this case the second term in the right-hand side of Eq.(2) can be expressed in the form,

$$\frac{\partial}{\partial T}\ell n\, P = -\ell n\,(1+M^2B^2) \ . \quad (3)$$

Generally, the migration area M^2 has a large value with the temperature increase because the water density decreases. On the contrary, control-rods

are withdrawn following the temperature increase, so the effective core size becomes large and the buckling B^2 has a small value. The latter effect is essential in actual situations of ship reactors. Hence the absolute value of the quantity $(\partial/\partial T)\ell n P$ in Eq.(2) decreases as the temperature increases or as the control-rods are withdrawn. For precise predictions the non-leakage probability should be of course computed using the 3-D neutron leakage distribution obtained by a 3-D diffusion calculations instead of using the constant buckling B^2. Accurate results cannot be obtained unless the actual control-rod pattern as a function of moderator temperature is taken into account to estimate the moderator temperature coefficients. For this reason the above "all rod withdrawn" case and the "all rod inserted" case under-estimates and over-estimates the coefficients, respectively.

Ⅵ. CONTROL-ROD INTERFERENCES OBSERVED IN THE EXCESS REACTIVITY MEASUREMENT

The excess reactivity is defined as the reactivity when all control-rods are fully withdrawn under cold clean conditions. It is impossible to measure this quantity in a direct manner, so we adopted the following expedient method. We practically redefined the excess reactivity, ρ_{ex}, as

$$\rho_{ex} \sim \Delta\rho_1 + \Delta\rho_2 \times C . \qquad (4)$$

Here $\Delta\rho_1$ is the measured reactivity defect caused by the moderator temperature change from a cold state (40℃) to a hot state (273.5℃). The quantity $\Delta\rho_2$ is the integral worth of G1 and G2 control-rod groups measured at the hot zero-power state. The rods G1 and G2 had been partially and fully inserted, respectively at the beginning of the measurement. The quantity C is a correction factor expressing the rod interaction effects, as estimated using the 3-D diffusion code STEADY-SHIP.

On April 7, the measurement of $\Delta\rho_2$ started at the hot zero-power critical state with the control-rod group G1 withdrawn by approximately 600mm and the group G2 remained fully inserted. The groups of G3 and G4 had been fully withdrawn at that time. The rod worths of G1 and G2 were measured by withdrawing little by little these control-rods, watching a digital reactivity meter[5]. In this case, the outer rods G3 or G4 were gradually inserted so as to compensate for the positive reactivity due to the G1 or G2 withdrawal, as illustrated in Fig.4. The variation in integral worths during the measurement is also shown in Fig.4. The slope of G1 integral worth is gentle. But the G2 worth increases drastically after the G2 is withdrawn more than 200mm, and again the worth slope becomes gentle after beginning of G4 insertion. These phenomena suggest that the rod interaction mechanism is not uniform during the process. For further investigation, the measured differential worths of G1 and G2 are plotted in Fig.5. The solid lines show the calculated worths obtained by using the STEADY-SHIP. The dotted lines represent the results of hypothetical calculations performed assuming the halt of G3 and G4 insertion at the points Ⓐ, Ⓑ and Ⓒ; the chain line represents the results calculated assuming the full withdrawal of both G3 and G4. The following explanations can be given for these results:

i) With the G3 insertion, the G1 worth reduces but the G2 worth is magnified.

ii) The growing G2 worth reduces by the additional G4 insertion.

These phenomena can be described by investigating the control-rod arrangement shown in Fig.1. The flux near G1 is depressed by the presence of G3, and this effect is known as "shadowing." On the contrary, the flux near

G2 relatively swells due to the flux depression at the position of G3 which is located at a certain distance from G2. This effect is called "anti-shadowing". These rod patterns during this measurement are not encountered in normal operations. But the above-measured results are useful as benchmark data for developing a new model of control-rod effects.

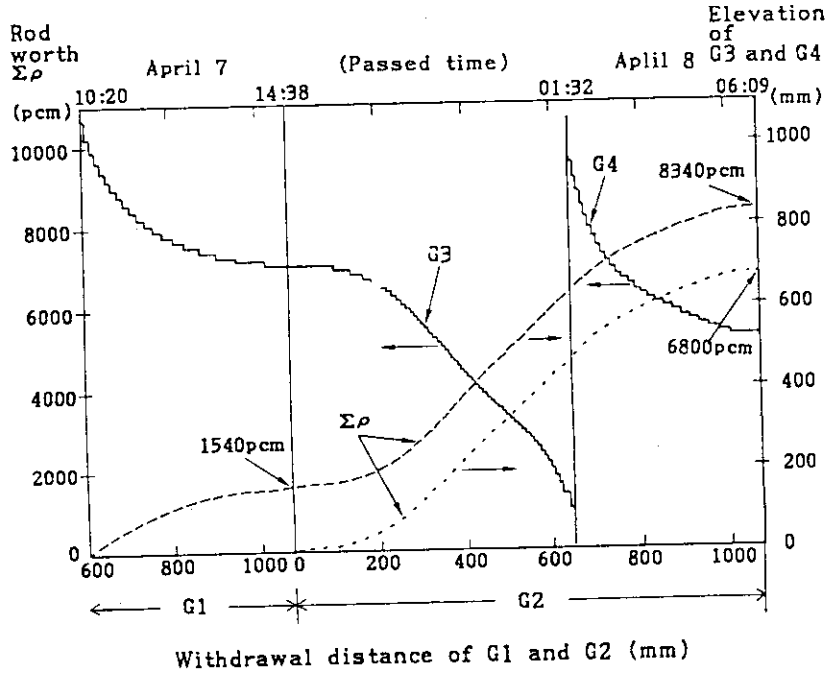

Fig.4 Control rod position and integrated worth in the excess reactivity measurement. The rods G3 or G4 were gradually inserted so as to compensate for the positive reactivity due to the withdrawal of G1 or G2. The integrated worths of G1 and G2 indicated 1540pcm and 6800pcm, respectively.

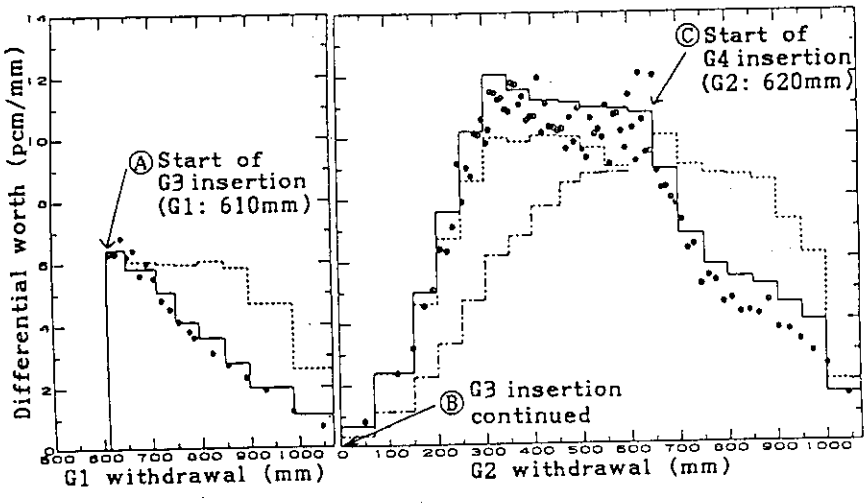

Fig.5 Differential rod worths of G1 and G2 groups in the excess reactivity measurement. The plots represent the measured values; the solid lines show results obtained from 3-D calculations assuming the actual rod patterns. The dotted lines and the chain line show the results of hypothetical calculations performed under the assumption of no insertion of G3 or G4 at positions Ⓐ, Ⓑ and Ⓒ.

Ⅶ. EX-CORE DETECTOR RESPONSE VARIATION CAUSED BY CONTROL-ROD MOTION

The reactor power is monitored by means of the four ex-core neutron detectors (CIC and UIC) as illustrated in Fig.1. The detector signals depend on the local neutron flux at the detectors rather than the core-average power, with the result that the signals vary when a control-rod pattern changes even if the power level remains constant.

The first systematic measurement of the detector response was carried out from October 2 through 5 during the second ocean trial. The reactor started under xenon-free condition and had been operated at approximately 90% output for 56 hours. The control-rods were withdrawn following the xenon accumulation in the core. The signals of four detectors (NI-7～NI-10) and the rod positions were continuously recorded and the thermal output of the reactor was measured every four hours.

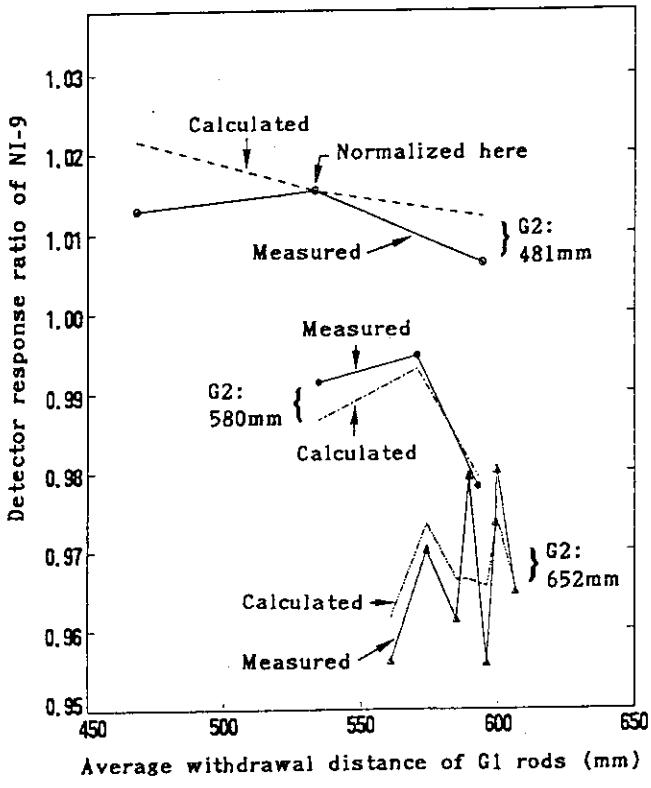

Fig.6 Response characteristics of ex-core neutron detector NI-9. The solid lines denote measured results, the other lines show calculated ones. The fixed elevation of G2 rod group was changed twice: 481mm→580mm and 580mm→652mm.

The "response ratio" of ex-core detector, R, is simply defined by

$$R \propto \frac{\text{Detector Signal}}{\text{Thermal Output}} \quad . \qquad (5)$$

Figure 6 shows the response ratio of NI-9 as a function of control-rod positions. The solid lines represent the measured results during the experiment while the other lines show the calculated results. The calculation procedure was based on the Crump-Lee method[4, 6]. In this technique, the response ratio is calculated as follows:

$$R = \sum_{j=1}^{N} S_j W_j \quad , \qquad (6)$$

where S_j is the fission source and W_j the spatial weighting function over a volume element ΔV_j in the core. The weighting function is calculated using the code EXCORE described in Sec.Ⅲ; the 3-D fission source distribution is produced using the 3-D diffusion code STEADY-SHIP for various control-rod patterns.

According to our previous analyses[6], the ex-core detector response tends to decrease with the withdrawal of the control-rods if there is no misalignment within a rod group. However Fig.6 does not always support this tendency. The reason for this is supposedly due to the within-group misalignment caused by a single rod motion corresponding to a small reactivity change during power operation. The calculated results in Fig.6 were provided from the response analyses with unsymmetric source distributions due to the rod misalignment.

Ⅷ. CONCLUSIONS

Three-dimensional (3-D) considerations are important in core physics calculations for ship reactors where the control-rods are partially inserted even in full power operations, as seen in the analyses for the N.S. Mutsu power-up tests. Conclusions about each topic are given as follows:

1. It is recommended from our excellent results that 3-D analyses should be adopted for precise prediction of criticality of ship reactors. The 1-D diffusion technique, which is widely used for land-based PWRs, could not simulate well the measured critical rod positions of the Mutsu reactor.
2. The moderator temperature coefficient is also affected by the 3-D effect, because the control-rod pattern changes with the increase in the temperature and then the 3-D neutron leakage distribution drastically changes. Excellent calculation results of the coefficients can be obtained for wide range of temperature, when one assumes the actual control-rod pattern for each moderator temperature in 3-D analyses.
3. Our 3-D calculation system has been proved to be a useful tool for analysing strong control-rod interference effects, such as "shadowing" and "antishadowing" encountered in our excess reactivity measurement.
4. The problem of the ex-core detector response due to rod motion will be important not only in ship reactors but in future LWRs designed for load following operations. The analyses based on the Crump-Lee technique with calculated 3-D source distributions provided acceptable agreement with the measured response characteristics.

REFERENCES

1. M. ITAGAKI, Y. NAITOH, Y. TOKUNO and Y. MATSUI, "STEADY-SHIP: A Computer Code for Three-Dimensional Nuclear and Thermal-Hydraulic Analyses of Marine Reactors," JAERI-1309, (1988) (in Japanese).
2. M. ITAGAKI, Y. NAITOH, K. IIJIMA and H. INOUE, "ASSEMBLY-SHIP: A Computer Code for Generating Few-Group Cross-Sections for Heterogeneous Fuel Assemblies of a Marine Reactor," JAERI-M 87-150, (1987) (in Japanese).
3. W.W. ENGLE, Jr., "A User's Manual for ANISN: A One Dimensional Discrete Ordinates Transport Code with Anisotropic Scattering," K-1693, (1967).
4. M.W. CRUMP and J.C. LEE, "Calculation of Spatial Weighting Functions for Ex-Core Neutron Detectors," Nucl. Technol., 58, 310 (1982).
5. Y. SHIMAZU, Y. NAKANO, Y. TAHARA and T. OKAYAMA, "Development of a Digital Reactivity Meter and a Reactor Physics Data Processor," Nucl. Technol., 77, 247 (1987).
6. M. ITAGAKI, J. ABE and K. KURIBAYASHI, "Analysis of Ex-Core Detector Response Measured During Nuclear Ship Mutsu Land-Loaded Core Critical Experiment," Nucl. Technol., 78, 140 (1987).

1. Irradiation Experiments of HTGR Fuel by an In-Pile Gas Loop, OGL-1

K. FUKUDA, K. HAYASHI and I. TANAKA

Department of Fuels and Materials Research
Tokai Research Establishment
Japan Atomic Energy Research Institute
Tokai−mura, Naka−gun, Ibaraki−ken, 319−11, Japan

Abstract

In the framework of the HTGR Development Program at JAERI, an in−pile gas loop, OGL−1, installed in JMTR has been used for irradiation experiments of the HTGR fuel. Capabilities of OGL−1 were such that maximum gas temperature was 1000 °C and a maximum gas pressure was 3.0 MPa. Characteristics and structure of OGL−1 were described in detail. The coated particles with 12 or 20% ^{235}U enrichment which had been consolidated in a shape of the annuler fuel compacts, were loaded in the OGL−1 fuel element. During an operation of OGL−1 various monitoring works were conducted. A measurement of a fission gas release from the fuel element was of importance for evaluation of the irradiation performance of the HTGR fuel tested in the loop. The post−irradiation examination on the OGL−1 fuel element was carried out.

INTRODUCTION

The Japan Atomic Energy Research Institute, JAERI, commenced the HTGR Development Program in 1969. The HTGR designed to date by JAERI is a reactor with a thermal out−put of 30 MW which is called the High Temperature Engineering Test Reactor,HTTR, and being constructed at the Oarai Research Establishment with a schedule of its criticality in 1996. In the framework of the program the coated particle fuel has been developed for utilization in the JAERI−designed HTGR since 1970. With purposes for technological developments in a hot gas circulation and HTGR fuel, JAERI constructed a in−pile gas loop called Oarai Gas Loop No. 1, OGL−1 in 1976[1] and put it in operation thereafter.

For the fuel development JAERI has conducted comprehensive works including manufacturing tests, fuel characterization and intensive irradiation tests using OGL−1, closed capsules and gas−swept capsules in the Japan Materials Testing Reactor, JMTR and the Japan Research Reactor−2, JRR−2. In the development of the HTGR fuel, OGL−1 has played important roles in the several fields[2]; testing a irradiation performance of the HTGR fuel assembly, studying a plate−out behavior of fission products in a gas circulating loop and a development of a fuel failure detection system(FFD). This paper is concerned in OGL−1 facility and its experiments with an emphasis on the fuel tests.

OGL-1 FACILITY

OGL-1 is a high temperature and high pressure gas loop installed in a reflector region of the JMTR core, of which major characteristics are summarized in Table 1[2]. Maximum helium(He) gas temperature is 1000°C, total content of the gas in a primary loop, 6800 g with a pressure of 3.0 Mpa, a maximum heat generation of the fuel element, 135 kW, and maximum fuel temperature, 1500°C.

The OGL-1 gas flow diagram is presented in Fig. 1[2]. OGL-1 consisted of an in-pile tube for loading the HTGR fuel element in its bottom region, and relevant out-of-pile facilities including heat exchangers, a cooler, a gas purification system, a gas circulator and a heater, all of which were connected as a primary loop. The gas in the out-of-pile tube was heated at about 650°C by both regenerative heat-exchangers and an electric heater, thereafter flowing into the in-pile tube, where gas temperature was furthermore elevated up to about 1000°C by fission heat of the fuel element. The out-flow gas from the in-pile tube was cooled down to about 700°C by a heat exchange with the in-flow gas in the in-pile tube, and to 150°C by the regenerative heat-exchanger and the cooler, then forced back toward the in-pile tube by the circulator. About 1 % of the circulating gas was branched off the main stream into the purification system to eliminate a content of gas impurities and fission gases released into the helium gas in the in-pile tube. The purification system consisted of a charcoal trap, a molecular sieve, a cold charcoal trap and a titanium trap. The system had a capability of a removal efficiency of 99 % for the fission gas and 60-85% for tritium. From a gas valve attached at an entrance of the purification system, the helium gas was sampled to measure a fission gas concentration in the circulating gas. In the in-pile tube with 7825 mm in length the fuel element was positioned at the bottom region which was connected with a long Hatelloy metal tube for hanging the element. The in-pile tube contained an inner tube to separate the in-flow and out-flow gases; the in-flow gas moved to a bottom end through the outer region of the tube, turning at the bottom end, sweeping on the inner- and outer-surfaces of the element in the inner region and being exhausted from the tube.

OGL-1 FUEL ELEMENT

The coated particles were micro-fuel spheres covered with fourfold coating layers which were generally embedded in the graphite matrix forming various shapes of the fuel compact. In the case of the HTTR fuel, the fuel compact having been tested in the development work was a hollow cylinder shape with 26-36mm in outer diameter, 8-18 mm in inner diameter and 36-39 mm in length, where about 10^4 in number of UO_2 coated particles were loaded. The fuel compacts were encased in a long graphite tube(graphite sleeve), forming a fuel rod, and the rods were furthermore loaded in vertical holes of a prismatic graphite block[3].

The OGL-1 fuel element consisted of a graphite cylinder with 800 mm in length and 80 mm in diameter, fuel rods and metal components[3], as depicted in Fig. 2. In the fuel design, safety assessments of the fuel element such as a stress analysis on the graphite block, a temperature estimation and so on, were performed to determine the fuel configuration. Due to a limitation of an outer diameter of the in-pile tube, two types of the fuel element which were loaded with one or three fuel rods were tested. For the sake of a relatively low thermal neutron flux at the OGL-1 position(see Table 1), ^{235}U enrichment of the fuel was either 12% or 19.5% to get a adequate burnup.

OGL-1 EXPERIMENT

In a series of the OGL-1 experiments as listed in Table 2, twelve times of the experiments were completed so far, the 13th experiment is ongoing, and two more experiments are projected. A procedure of the OGL-1 experiments is displayed in Fig. 3. During irradiation of the fuel element, temperature at various positions in the loop, gas flows, gas pressures, fission gas concentrations in the circulating gas and so on were monitored. Temperature of the fuel was controlled by changing a flow rate of the coolant gas. Measurements of temperature of the in-flow- and out-flow gas gave a thermal out-put of the fuel element, from which an average burnup of the fuel rod was estimated. Temperature distributions through the fuel rod, the graphite tube and the graphite block in an axial direction were computed using OGL-1 thermal evaluation code, STEPDSP, and a more detail and precise information on temperature in axial and radial directions of the fuel compacts was computed by a code system[4] including a three-dimension thermal analysis code, TRUMP[5].

A typical result of the temperature evaluation in an axial direction by TRUMP code is given in Fig. 4. A distribution of fuel burnup through the fuel rod was decided by both computation on base of the thermal out-put and a direct measurement in the post-irradiation examination. For the measurement of the fission gas concentration, a certain quantity of the He gas was sampled at the entrance of the purification system as above-mentioned, in which radioactivity of the fission gas was measured to determine the fission gas concentration. Also, were conducted the FFD experiment, where the activity of very short-lived fission gases was measured to establish the fuel failure detection system, and a measurement of the plated-out activities on the primary circuit. The fuel element after irradiation was transported from JMTR to the Tokai Hot Cells to carry out the post-irradiation examination.

IRRADIATION BEHAVIOR OF OGL-1 FUEL ELEMENT

The fission gas release from the fuel element, which was directly related to the failure fraction of the coated particles in the fuel compacts reflected an irradiation performance of the fuel. For the release evaluation, the concentration of the short-lived fission gas in the circulating gas was converted to a universal parameter for the fission gas release designated by R/B(Release rate / Birth rate)[3]. The typical results of R/B obtained recently in the 12th and 13th experiments are presented in Fig. 5, where variations of R/B are plotted against the irradiation time. As listed in Table 2, both the fuel elements contained a single fuel rod, thus showing the average R/B of the compacts included in each of the fuel rod. All of the release behaviors of the fuel elements tested so far, exhibited the initial decrease of R/B with burnup (or irradiation time), followed by an almost constant level of R/B. Also, the release behavior in a transient condition was investigated by changing the gas flow rate in the loop with a control of the fuel temperature from 1100°C to 1500°C at an axial center of the fuel rod. Figure 6 presents the results in the 6th and 10th experiments. Difference of R/B levels in both of the experiments was reflected by difference of the initial failure fractions of the coated fuel particles in the fuel elements.

A flow diagram of the post-irradiation examination(PIE) on the OGL-1 fuel elements is depicted in Fig. 7[6]. In the PIE procedure an optical surface inspection and X-ray radiography was carried out to check any deterioration before disassembling the fuel element, followed by testing individual elements such as a graphite block, graphite sleeves, the fuel compacts and the coated particles. The main tests for the block and the sleeve were on

bowing, dimension, weight and fission−product distribution. The measurement of the fission product distribution which had been released from the fuel compacts and absorbed in the graphite substances during high temperature irradiation, was aimed at getting information on release behavior of the individual metallic fission product. The typical results which was obtained for the graphite sleeve taken out from the 8th fuel element[8] is given in Fig. 8, where the fractional releases of the some metallic fission products are plotted in an axial direction of the sleeve. As indicated in the figure, this fuel rod contained a special fuel compact among the standard fuel compacts in which 1% of the coated particles(so called BISO particles) did not possess the SiC coating layer in order to simulate SiC defective particles. These results clarified that ^{155}Eu was strongly retained by the SiC coating layer , since this nuclide indicated a peak activity at a position of the sleeve neighboring the compact which included the BISO particles. Also clarified was that the other fission product, ^{134}Cs,^{137}Cs and ^{125}Sb, exhibited the peak activities at two positions of the sleeve adjoining the fuel compact, where a broken particle exposed just near the surface of the fuel compacts. It implied that the activity of the sleeve was strongly affected by the location of the broken particles in the compact.

The PIE on the fuel compacts and the coated particles was the most important to evaluate the fuel performance in irradiation. Due to a carbonaceous property of the fuel compact, dimensional change and stress cracking of the compacts by fast neutron irradiation was intensively measured. For the coated particles the failure fraction by irradiation was measured by an acid−leaching technique after an electrochemical disintegration of the irradiated fuel compact for separating the coated particles. The results indicated a remarkable increase of the failure by irradiation was not detected in all of the fuel elements tested so far.

SUMMARY

OGL−1 is the in−pile gas loop installed in JMTR, which has been used for the irradiation tests of the HTGR fuel in the framework of the HTTR development program by JAERI. It has been operated without any trouble since 1977. Twelve irradiation experiments were completed so far, 13th experiment is ongoing, and two more experiments are planned. During operation of OGL−1, comprehensive monitoring works were conducted. Particularly the measurement of the fission gas concentration in the primary loop was significantly important to evaluate an irradiation performance of the fuel. The OGL−1 fuel element was provided to the post−irradiation examination to investigate the irradiation behavior of the fuel.

REFERENCES

(1) S. Matsunaga, T. Tanaka et. al., J. Atom. Energy Soc. Japan, 21(1979) 245.
(2) H. Tanaka, T. Saruta, et al., JAERI−M 86−068(1986).
(3) K. Fukuda, T. Ogawa, et al., JAERI−M 89−007(1989).
(4) K. Fukuda, F. Kobayashi, et al., JAERI−M 84−183(1984).
(5) ORNL, SCALE−03(IBM−360 System Version, 1977).
(6) K. Fukuda, F. Kobayashi, et. al., J. Atom. Energy Soc. Japan, 26(1984)57.
(7) K. Hayashi and K. Fukuda, to be submitted to J. Nucl. Mater.

Table 1 Major characteristics of OGL-1

coolant	helium gas
operating pressure	max. 3.9MPa
gas temperature	max. 1000°C
gas flow rate	max. 100g/sec
gas content in the loop	6800g
^{235}U in the fuel element	150g
heat generation	max. 135kW
fuel temperature	1500°C
thermal neutron flux	5.9×10^{17} n/m^{2}sec
fast neutron flux(>1Mev)	1.3×10^{17} n/m^{2}sec

Table 2 OGL-1 experiment

Exp. No.	Purpose	No. fuel rod	Irrad. time (hrs)	Max. fuel burnup(%FIMA)	Max. fuel temperature(°C)
1	Test of the loop	3	930	0.5	1440
2	Fuel performance test(1)	3	1720	0.8	1470
3	Bowing test	1	975	0.5	1320
4	Fuel performance test(2)	3	1870	1.7	1350
5	High burnup test	3	3415	2.9	1360
6	Transient test(1)	1	525	0.4	1480
7	Graphite matrix test	3	1392	1.3	1380
8	Defective fuel test	1	1291	1.0	1390
9	Mass-produced fuel test	1	3492	2.7	1340
10	Transient test(2)	1	3125	2.8	1500
11	Fuel performance test(3)	1	1494	1.6	1350
12	Long term test	1	4680	3.9	1340
13	Modern fuel test(1)	1	(5900)	(4.9)	(1330)
14	Modern fuel test(2)	1	(2160)	(1.8)	(1500)
15	HTTR driver fuel test	1	(5160)	(4.3)	(1330)

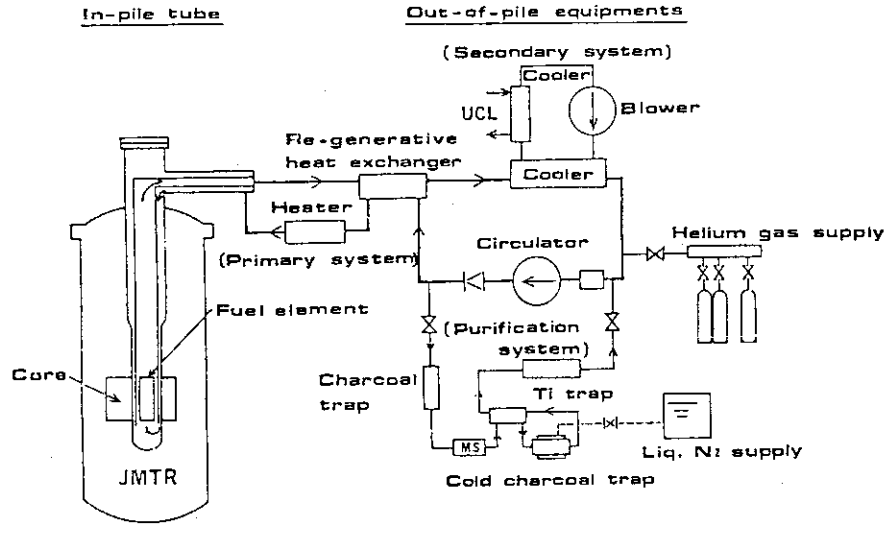

Fig. 1 Gas flow diagram of OGL-1.

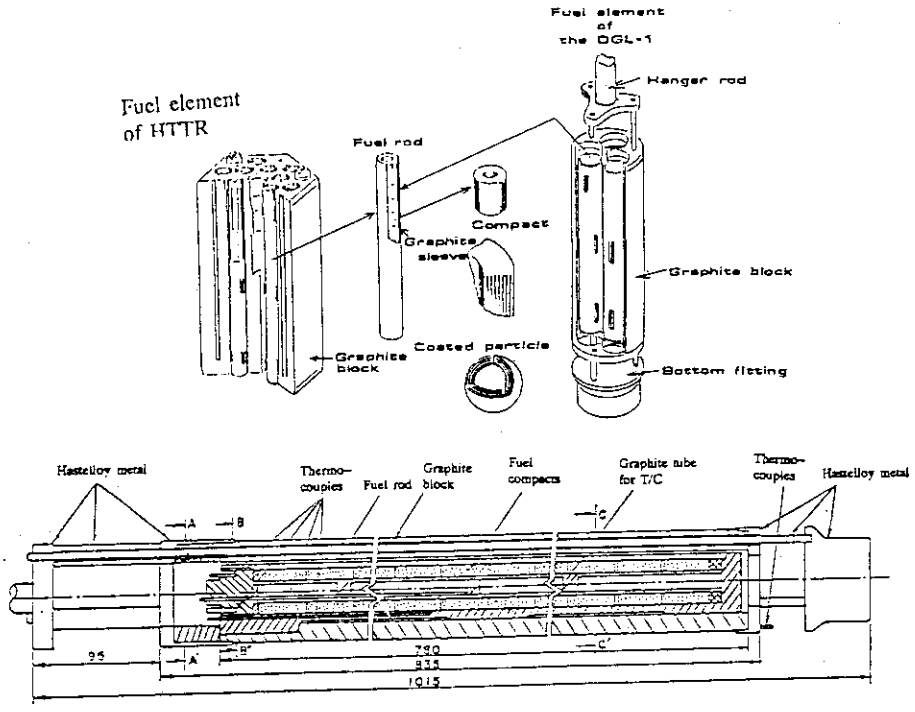

Fig. 2 Configuration of OGL–1 fuel element and HTTR fuel element.

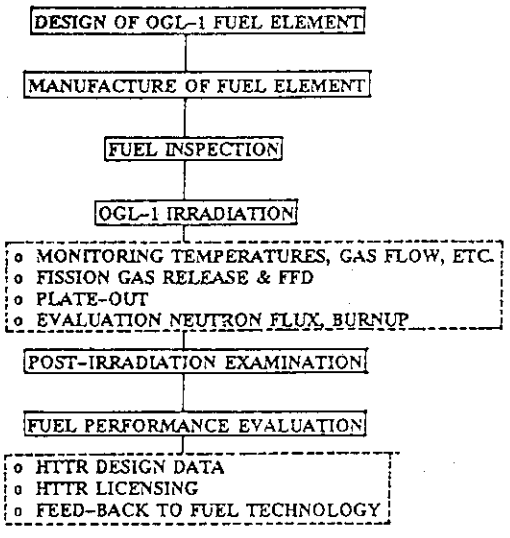

Fig. 3 Procedure of OGL–1 experiment.

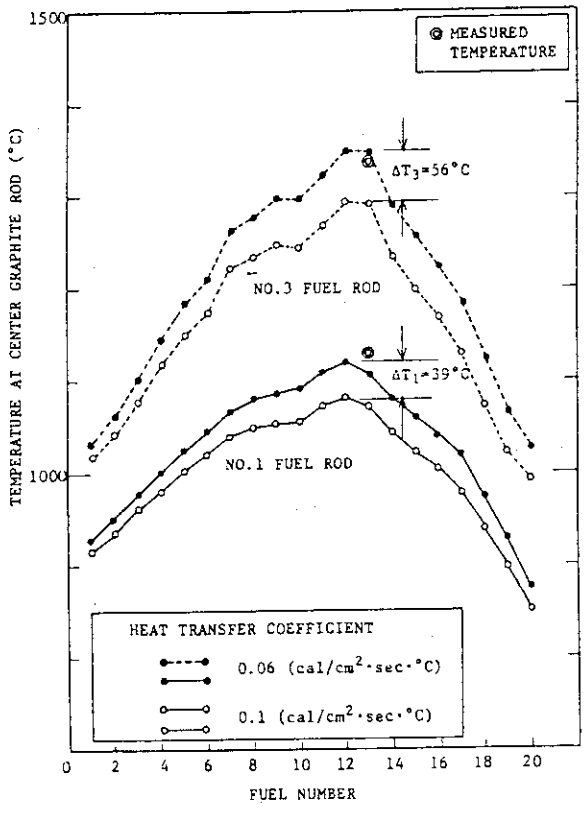

Fig. 4 Temperature distribution computed by TRUMP.

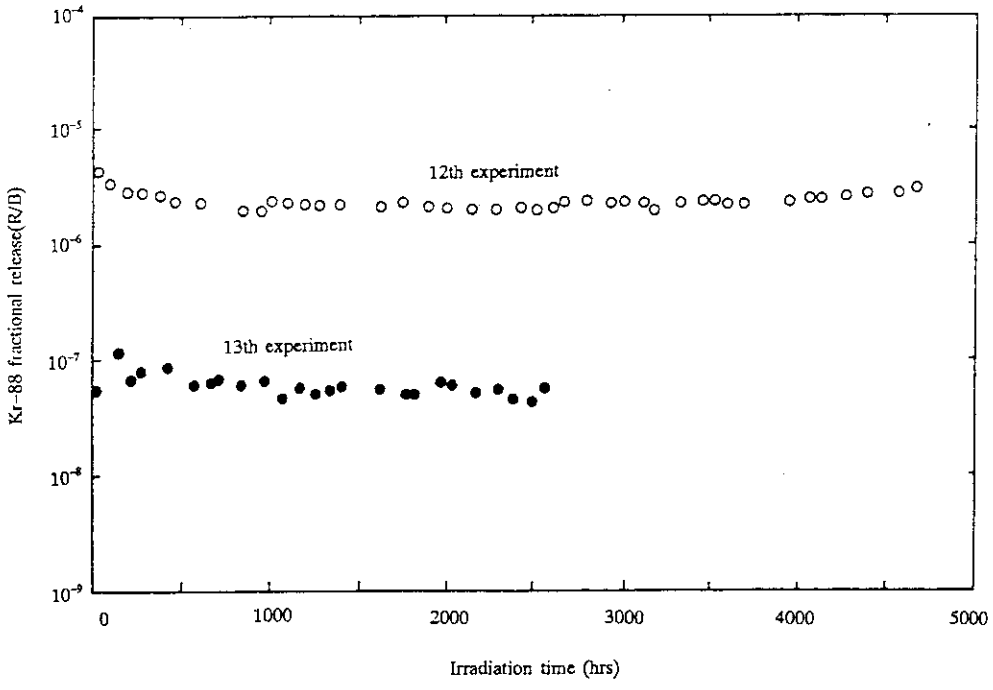

Fig. 5 Fission gas release measured in OGL-1 experiments.

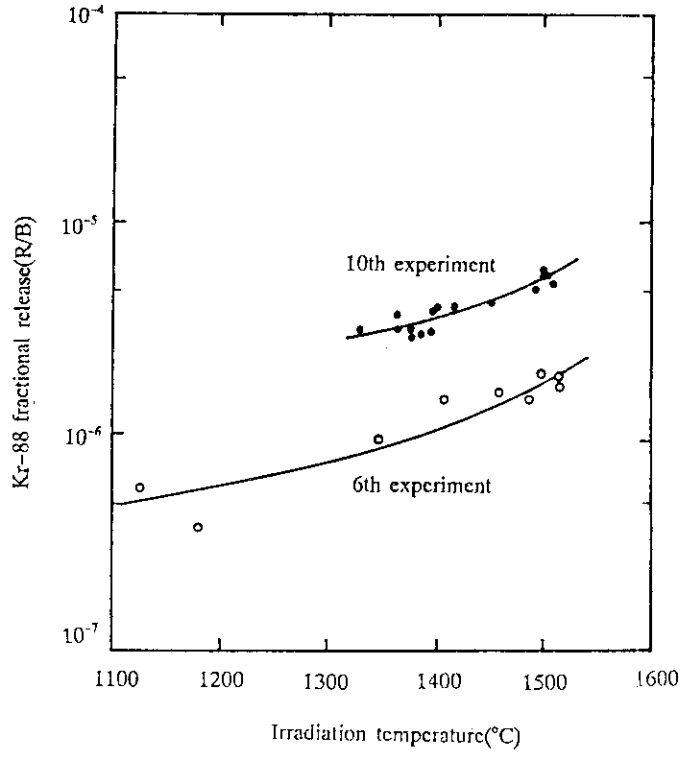

Fig. 6 Fission gas release behavior in transient conditions.

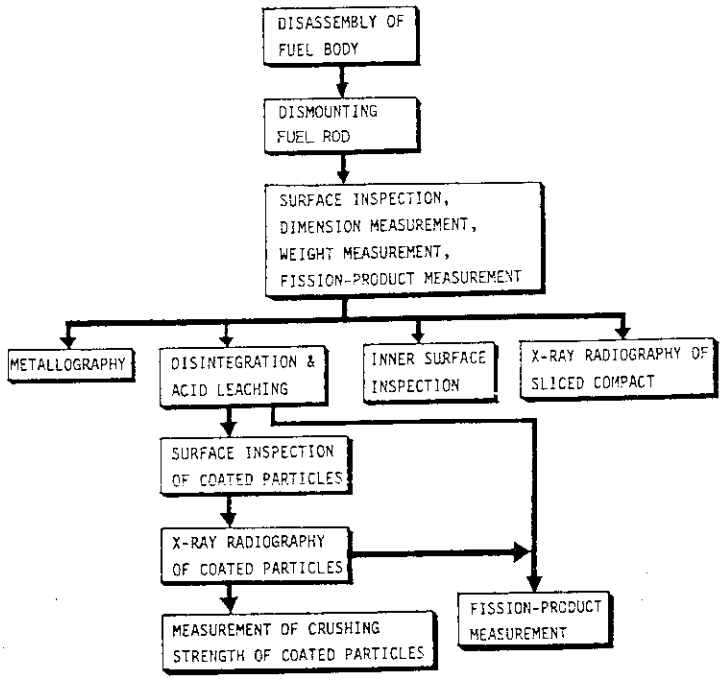

Fig. 7 Procedure of post-irradiation examination.

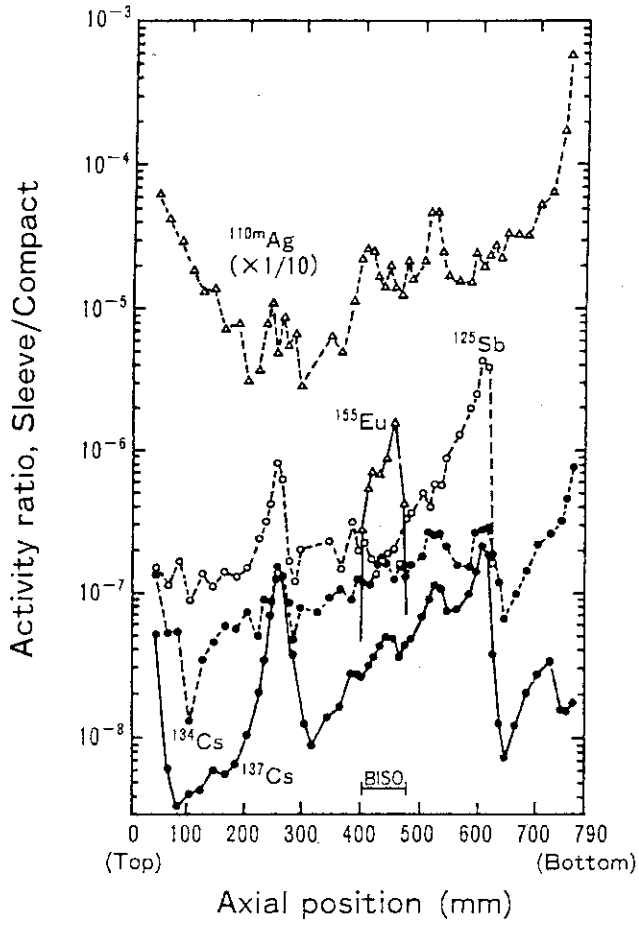

Fig. 8 Fractional release of metallic fission product in a graphite sleeve.

2. Irradiation Tests of Advanced Plutonium-Bearing Fuels

Atsushi MAEDA[1], Motoji NIIMI[2], Toshihiko OHMICHI[1]

[1]Department of Fuels and Materials Research
Tokai Research Establishment
Japan Atomic Energy Research Institute
Tokai-mura, Naka-gun, Ibaraki-ken 319-11, Japan

[2]Department of JMTR Project
Oarai Research Establishment
Japan Atomic Energy Research Institute
Oarai-machi, Higashiibaraki-gun, Ibaraki-ken 311-13, Japan

ABSTRACT

The capsule irradiation tests of uranium-plutonium mixed carbide and nitride fuels are under way in Japan Materials Testing Reactor (JMTR) for evaluating the fuel performance. The fuel pins containing these fuels, helium bonded to stainless steel cladding, have been irradiated in the NaK bonded capsules with a double metal containment in which thermocouples are installed. The present paper summarizes the results of the development in irradiation technology of these plutonium-bearing fuels utilizing JMTR.

1. INTRODUCTION

Uranium-plutonium mixed carbide and nitride fuels have been recognized as important alternatives to mixed oxide, which is currently used as a refernce fuel for the fast breeder reactors (FBRs). Since these advanced fuels have the advantage in their superior thermal conductivities and higher fissile atom densities, they offer an improved fuel system for FBRs with an economical fuel concept with large pin diameters[1].

In Japan the studies of mixed carbide and nitride fuels with regard to fabrication technology, characterization tests and fuel property measurements have been carried out mainly at Plutonium Fuel Research Facility (PFRF) in Oarai Research Establishment, JAERI since 1977[2]. In order to realize the practical use of these fuels, it is essential to investigate the irradiation behavior. The irradiation program of these fuels in research thermal reactors in JAERI was planned after the development of fuel pin fabrication technology. Preliminary capsule irradiation tests of carbide fuels with low burn-ups started in 1983 using Japan Research Reactor-2 (JRR-2). These irradiation tests were successfully performed without any pin failure. Thereafter five encapsulated mixed carbide fuel pins and four mixed nitride fuel pins have been subjected to irradiation in Japan Materials Testing Reactor (JMTR) to establish the

performance at higher burn-ups. This paper describes the results of technological development, mainly fuel pin fabrication and capsule construction, to perform the irradiation tests of these advanced plutonium-bearing fuels.

2. DESIGN OF FUEL PIN AND CAPSULE

Table 1 shows the present status of the irradiation tests of the advanced fuels at JAERI. Up to now the irradiation of four encapsulated carbide fuel pins in JMTR have been completed. At present the capsule irradiations of one carbide fuel pin and four nitride fuel pins are under way in JMTR aiming at a maximum burn-up of 6%FIMA.

Table 1 Present status of the irradiation tests of advanced fuels

Capsule	Fuel type	Number of pins	Reactor	Irradiation period	Linear power (kW/m)	Burnup (%FIMA)
ICF-37H	Carbide	2	JRR-2	1983 ～1984	42	1.2
ICF-47H	Carbide	2	JRR-2	1985 ～1986	64	1.6
84F-10A	Carbide	2	JMTR	1986 ～1989	59	3.0
84F-12A	Carbide	2	JMTR	1986 ～1990	62	4.6
87F-2A*	Carbide	1	JMTR	1988 ～1992	(66)	(6)
88F-5A*	Nitride	2	JMTR	1990 ～1992	(66)	(3.5)
89F-3A*	Nitride	2	JMTR	1991 ～1994	(66)	(6)

* Capsules 87F-2A, 88F-5A and 89F-3A are under irradiation and the values in parentheses show those of fuel pin design.

2.1 DESIGN OF FUEL PIN

Figure 1 shows a basic structure of fuel pin for irradiation tests in JMTR. Each fuel pin consists of a 100mm long stack of fuel pellets and insulater pellets of uranium carbide or nitride placed on both sides of the stack. Helium gas is used as the thermal bond between fuel and cladding. For irradiation tests, each capsule except 87F-2A capsule contains two fuel pins with different design. The fuel pins containing the carbide fuel pellets with different composition of $(U,Pu)C_{1.0}$ and $(U,Pu)C_{1.1}$ are loaded in the same capsule. For the capsules of nitride fuel, $(U,Pu)N_{1.0}$, the variation of the gap between pellets and cladding and the difference of cladding materials are selected as irradiation parameters. Plutonium of 20% enrichment and natural uranium are used as a composition of fuel materials, similar to that of an usual fuel design of FBRs. To accommodate fuel and clad mechanical intraction (FCMI), it is important to depress pellet densities relative low[3]. Geometrical pellet density is in the range 81-

86% of theoretical. Pellet diameter 8.23mm has been chosen in order to respect a smear density in the range 79-83% of thoretical and a gap of 0.15mm. One nitride fuel pin has a gap of 0.20mm using fuel pellets of 8.18mm in diameter. Cladding material is an austenitic type 316 stainless steel (9.40mm in outer diameter, 0.51mm of thickness) except one nitride fuel pin in which a ferritic stainless steel is used. Moreover in a case of one nitride fuel pin, a W5%Re-W26%Re thermocouple sheathed with Nb-1%Zr alloy is equipped to the center of mixed nitride fuel pellets through the lower end plug for measuring the temperature change during irradiation to obtain some information on gap conductance.

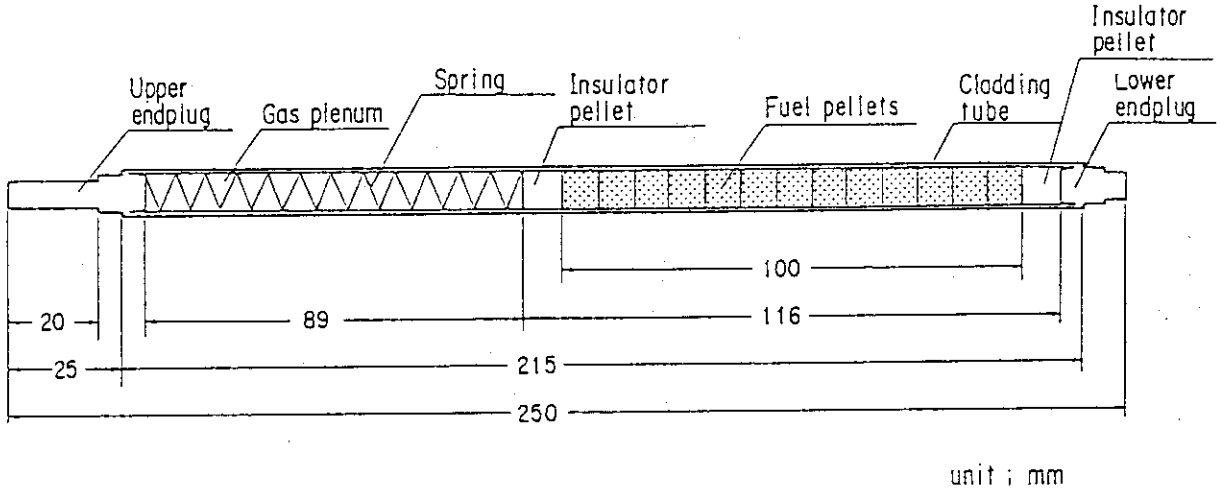

Fig. 1 Basic structure of fuel pin for irradiation tests in JMTR

2.2 DESIGN OF FUEL CAPSULE

A typical structure of capsule for irradiation tests in JMTR is shown in Fig. 2. Fuel pins containing plutonium-bearing fuels in each capsule are required to be sealed by two coaxial stainless steel tubes to provide the containment of the fuels. It can prevent FP and plutonium from releasing into reactor coolant, even if the cladding might be perforated under irradiation.

Carbide and nitride fuels are usually irradiated at relatively high linear heat rating of 60-80 kW/m to emphasize the merit of the fuels. NaK, which is used as thermal medium between fuel pins and an inner stainless steel tube, allows a high linear heat rating to be reached. NaK has a good thermal conduction and a high boiling point, so the removal of heat is possible to perform high power tests. A double metal containment is also used for the protection from the reaction of NaK with coolant water.

In each instrumented capsule several Chromel-Alumel (CA) thermocouples are installed at the fuel pin surface and the inner tube to measure temperatures accurately during irradiation. The estimation of linear heat rating is available by calculating on the basis of temperature readings. The temperature in the upper side of the inner tube filled with NaK is also measured as a monitor for pin failure. Neutron fluence monitors are also mounted in the capsule to obtain both radial and axial distributions of flux dose. The outer configuration is designed to be a conventional JMTR irradiation capsule.

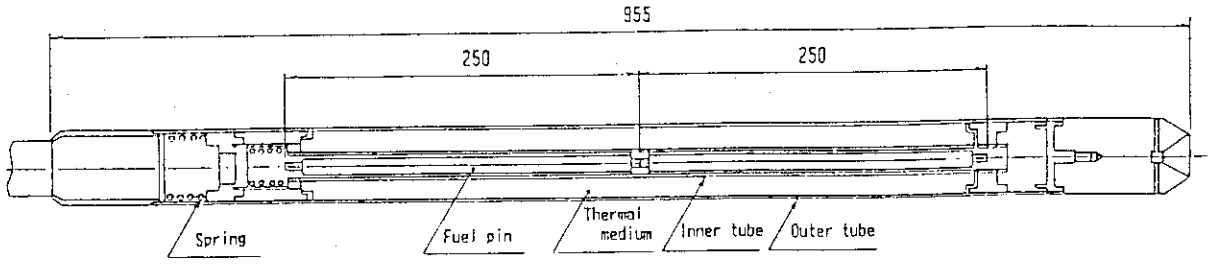

Fig. 2 Typical structure of capsule for irradiation tests in JMTR

3. FABRICATION OF FUEL PIN AND CONSTRUCTION INTO CAPSULE

3.1 FUEL FABRICATION

Uranium-plutonium mixed carbide is fabricated by carbothermic reduction of blended UO_2 and PuO_2 powders. The resulting carbide powder is pressed and sintered into dense pellets[4]. Mixed nitride fuel has been also fabricated by one-step carbothermic reduction in a stream of N_2-8%H_2 mixed gas[5]. The fabrication of the fuel pellets is carried out in glove boxes filled with high purity Ar gas to preclude the oxidation of these chemically reactive fuels especially in powder form[6]. The impurity levels of oxygen and moisture are kept less than 3 and 5 ppm, respectively, by circulating purified Ar. The pellet diameter is adjusted by centerless griding with a precision of $\pm$ 0.002mm. The procedures for the fuel characterization, such as chemical analysis, X-ray powder diffraction analysis and occluded gas measurement, have been also established[7,8].

3.2 FUEL PIN FABRICATION

A typical flowsheet of fabrication of fuel pins is shown in Fig. 3. Loading of fuel pellets to a stainless steel cladding tube and welding of an end plug to a cladding tube are carried out in glove boxes filled with pure He gas, which is used as thermal bonding and also used as an inert gas for TIG welding. Air in the glove boxes is first purged by Ar gas in order to decrease the oxygen and moisture. Then a fuel pin is fabricated in a flow of pure He gas. The change of gas concentrations in the glove boxes is shown in Fig. 4. The impurity levels about 10 ppm moisture and 3 ppm oxygen can be obtained and pure He gas is almost substituted for Ar.

It is most important that the plutonium contamination of the pin surface at welding is well below the permitted levels requiring only minor clean-off. The procedure of fuel pin fabrication without any plutonium contamination of outer surface and welded bead area of fuel pin has been established as follows. The glove box for loading fuel pellets to a cladding tube, whose schematic drawing is shown in Fig. 5, consists of two zone with different plutonium contamination level. Helium gas is introduced into the low contamination zone and flows forward the high contamination zone. A cladding tube with the lower end plug welded in place is put into the low contamination zone. The opening of the cladding is just faced in the high contamination zone through a hole on the partition wall between two zones. In the high contamination zone, fuel pellets of one stack length

are concurrently lined up on a V grooved bar. The lined pellets are then pushed into the opening of the cladding through a stainless steel protective tube between the bar and the opening. The role of the protective tube is to minimize a loose cotamination of the opening surface before welding. The cladding tube is also covered with a vinyl heat-shrink tube. After decontamination of the opening, an end plug is inserted into the opening and then the cladding tube is transferred to the adjacent glove box for welding filled with He gas. The welded fuel pins are submitted to inspections of helium leak test, X-ray radiography and dimensional check, which give results conforming to the specification for JMTR capsule irradiation.

The nitride fuel pin equipped with a W5%Re-W26%Re thermocouple sheathed with Nb-1%Zr alloy was fabricated. This sheathed thermocouple has been mostly applied to measure the high temperature of fuel pins during irradiation in JMTR. No reaction occurred during the compatibility examination of uranium nitride pellet with Nb-1%Zr alloy at 1900K, higher than irradiation temperature, for 25 hours in vacuum. Fuel pellets were bored in their center positions with an ultrasonic machining tool. Diameter of central holes was ajusted to about 0.5mm larger than that of thermocouple sheath (1.6mm) for obtaining a dimensional margin in loading the pellets into the cladding tube. Attaching the thermocouple sheath to a lower end plug was made by soldering.

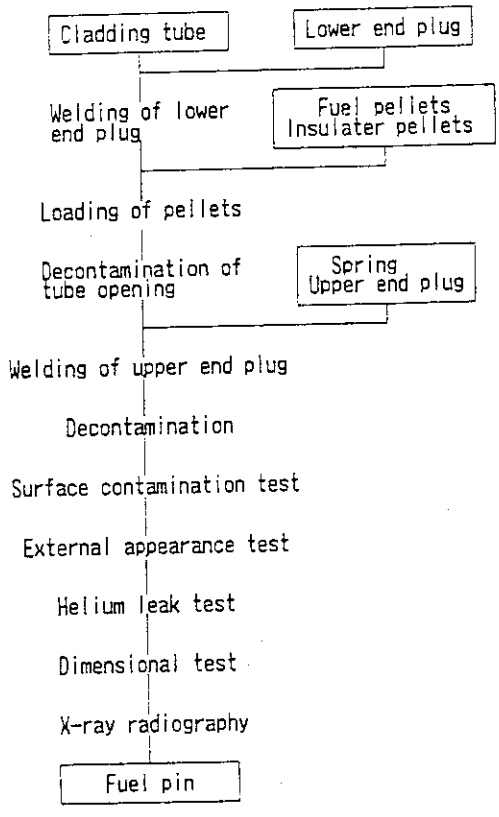

Fig. 3 Flowsheet of fabrication of fuel pins

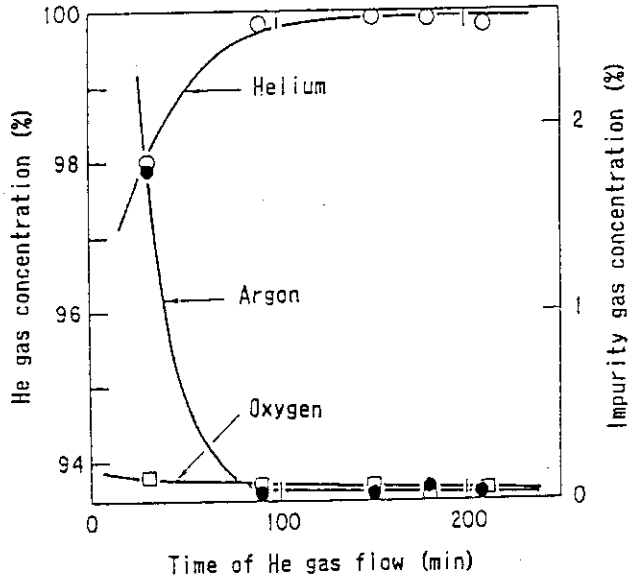

Fig. 4 Change of gas concentrations in glove box

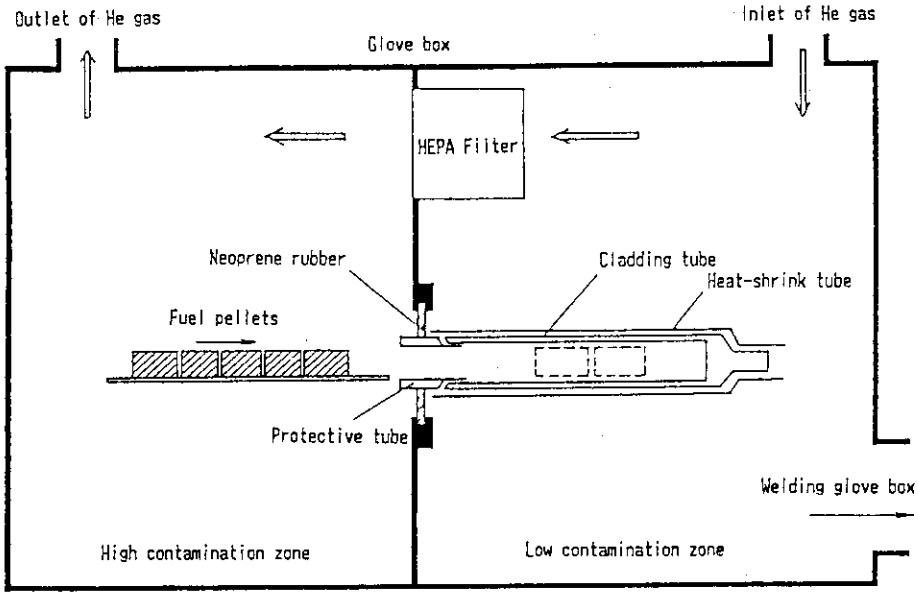

Fig. 5 Schematic drawing of glove box for loading fuel pellets

3.3 CAPSULE CONSTRUCTION

An equipment has been successfully developed for loading chemically reactive NaK into capsules. The general structure of the inner tube of capsule and the schematic diagram of NaK loading system are shown in Figs. 6 and 7, respectively.

The lines of NaK loading system are first evacuated in vacuum by rotary pumps and filled with pure He gas. NaK is extruded from a storage vessel to a measuring vessel and is loaded into the inner tube of capsule through an inlet tube. Then remaining NaK is transferred through a level tube to an accumlator. The NaK tubes are cut at the upper position of their valves followed by pressure-sealing hermetically. An upper end plug of the inner tube is inserted and welded. NaK level in the inner tube is checked by X-ray radiography. The inner tube with co-extruded aluminum thermal medium and associated hold-down fixtures are loaded into the outer tube of a type 304 stainless steel. The capsule components are prepared and examined non-destructively several times during loading process by radiographic, penetrant and helium leak tests. All components are also submitted to dimensional, weight and visual examinations.

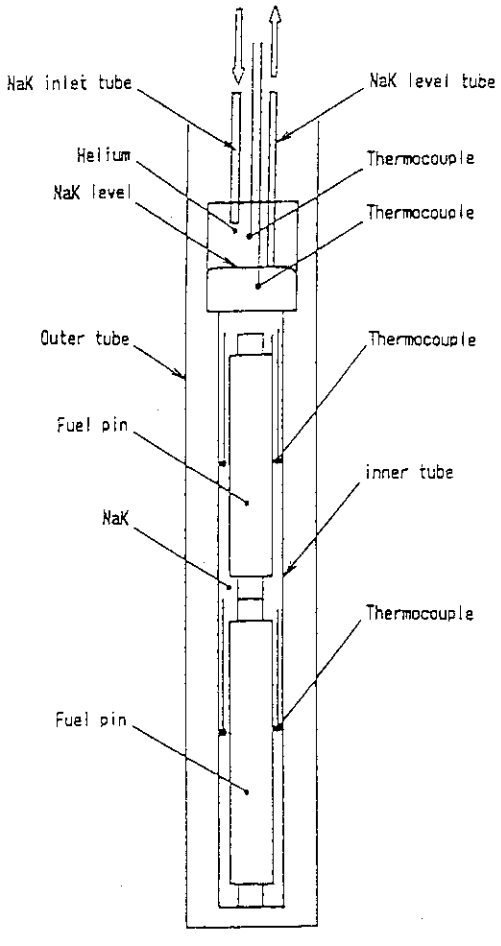

Fig. 6 General structure of inner tube of capsule

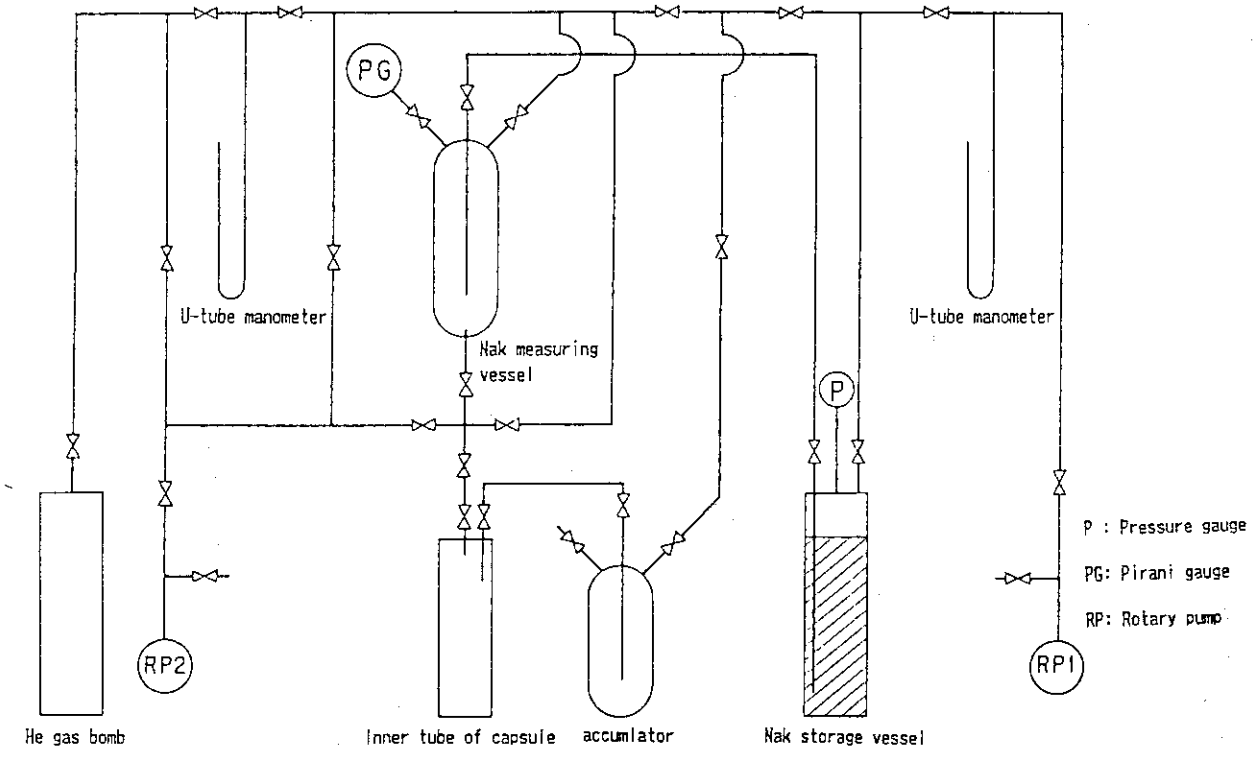

Fig. 7 Schematic diagram of NaK loading system

4. IRRADIATION IN JMTR AND PIE

The capsules of carbide and nitride fuels have been irradiated in holes in the outer aluminum reflector region of the reactor core, which is served mainly as a space for irradiation of fuel materials because of producing relatively constant and high thermal neutron flux. During irradiation, temperature indicated by each thermocouple in the instrumented capsule is recorded continuously by data acquisition system. The temperature changes of the fuel pellet center and fuel pin surface of the nitride fuel during irradiation are shown in Fig. 8. The central temperature of the pellet decreases gradually, which would correspond an overall contraction of the gap between pellet and cladding. The estimation of gap conductance would be available by evaluating this temperature profile.

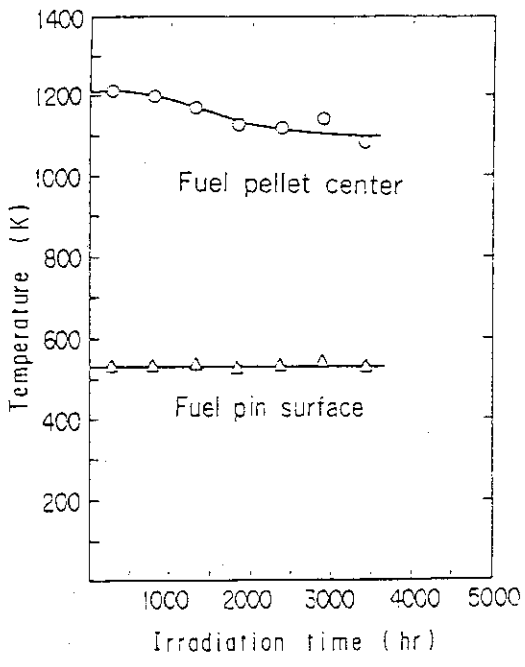

Fig. 8 Temperature change of the nitride fuel pin during irradiation

Post irradiation examinations (PIEs) of the carbide fuel pins irradiated in JRR-2 and JMTR have been performed in the hot cells of Reactor Fuel Examination Facility (RFEF) in Tokai Research Establishment, JAERI. Destructive examinations such as pellet density measurement, autoradiography, micro γ scanning and ceramography are performed in Ar gas atmosphere of the α-γ hot cells. Various data for investigating the fuel behavior such as restructuring, FP gas release and the redistribution of solid FPs have been obtained. The analysis of the PIE results of the carbide fuels shows a good performance up to 3%FIMA[9]. The carbide and nitride fuels under irradiation in JMTR will undergo PIEs in the near future.

5. CONCLUSION

The technology of fuel pin fabrication and capsule construction for the irradiation tests of the uranium-plutonium mixed carbide and nitride fuels has been developed and these fuels are under irradiation in JMTR to confirm the performance of these advanced FBR fuels. Based on these achievements, the irradiation tests of carbide and nitride fuels in the experimental fast reactor, JOYO, from 1993 are also planned in collaboration with Power Reactor and Nuclear Fuel Development Corporation (PNC)[9].

The authors wish to express their thanks to the staffs of Mechanical Engeering Division, JAERI, for the construction of the irradiation capsules and also to Drs. T. Kondo, Y. Futamura and M. Handa for their interests in this work.

REFERENCES

[1] Hj. Matzke, Science of Advanced LMFBR Fuels, North-hollands, Amsterdam (1986).
[2] Y. Suzuki, Y. Arai, M. Handa, K. Shiba, IAEA-TECDOC-577 (1990) P.73.
[3] K. H. Kummerer, J. Nucl. Mater., 124, 147 (1984).
[4] Y. Suzuki, T. Sasayama, Y. Arai, H. Watanabe, J. Nucl. Sci. Technol., 18, 61 (1981).
[5] Y. Arai, S. Fukushima, K. Shiozawa, M. Handa, J. Nucl. Mater., 168, 280 (1989).
[6] S. Nomura, J. Shimokawa, K. Uematsu, K. Noro, Proc. on Advanced LMFBR Fuels, Tucson, Oct. 10-13, 1977, p.61.
[7] A. Maeda, T. Iwai, T. Ohmichi, IAEA-TECDOC-466 (1988) P.35.
[8] M. Handa, K. Shiozawa, T. Iwai, Y. Arai, Anal. Chim. Acta, 239,107 (1990).
[9] Y. Arai, Y. Suzuki, T. Ohmichi, M. Handa, S. Shikakura, S. Nagai, N. Mizoo, Int. Conf. on Fast Reactors and Related Fuel Cycles (FR'91), Kyoto, Oct. 28～Nov. 1 (1991).

3. A Technique for In-situ Tritium Recovery Experiment of Breeder Material

H. WATANABE and T. KURASAWA

Department of Fuels and Materials Research
Tokai Research Establishment, JAERI
Tokai-mura, Naka-gun, Ibaraki-ken 319-11, Japan

ABSTRACT

In-situ tritium recovery experiments on several lithium ceramics (Li_2O, $LiAlO_2$, Li_4SiO_4, Li_2ZrO_3) have been conducted in the JRR-2 reactor since 1983, to evaluate tritium recovery characteristics and tritium inventory which are key issues for design of fusion reactor blanket.

The experimental apparatus consist of irradiation capsule, tritium measurement system and tritium cleanup system. A capsule was designed to separately accommodate a couple of candidate lithium ceramics. Premixed purge gases of helium and helium plus deuterium or hydrogen flowed down into the capsule contained lithium ceramics and then followed to the measurement system installed ionization chambers. An ceramic electrolyte cell was first used to directly reduce HTO into HT in an actual tritium recovery experiment. Tritium in the purge gas streams was oxidized and completely removed prior to being exhausted through a stack.

In the series of experiments, tritium recovery characteristics of candidate breeder materials have been clarified.

INTRODUCTION

In-situ tritium recovery experiments on several lithium ceramics (Li_2O, $LiAlO_2$, Li_4SiO_4, Li_2ZrO_3) have been conducted in the VT-10 vertical hole in the Japan Research Reactor (JRR-2) since 1983, to evaluate tritium recovery characteristics and tritium inventory which are key issues on design of fusion reactor blanket.

In-situ tritium recovery experiments similar to ours was done in the ORR and have been conducted in the SILOE, MELUSINE, HFR, NRU and FFTF. Those reactors except the FFTF have mainly thermal or mixed neutron spectra. The designs of the system and apparatus for these experiments in JAERI are distinguished as described below. The knowledge and technology for these experiments have been transferred to the design and fabrication of the IEA collaborative irradiation experiment by using the FFTF (Richland, USA), which is called Breeder Exchange Matrix-II (BEATRIX-II).

IN-SITU TRITIUM RECOVERY MEASUREMENT SYSTEM

In order to minimize a surface effect of piping on tritium recovery behavior, the tritium measurement apparatus were installed in the measurement hood on the deck of the JRR-2 in this system. The distance from the capsule to the measurement apparatus is about 8 meters and is shorter comparing to other experiments in the world.

A schematic representation of the purge gas steams in these experiments is shown in figure 1. Premixed purge gases of helium or helium plus hydrogen (10, 100, 1000, 10000 ppm) or helium plus deuterium flow down the inlet line into a couple of inner capsules and then back up to the measurement hood. For example, each lithium ceramic specimen was put in a cylindrical space (14 mm ID x 17 mm OD x 52 mm L) of each inner capsule. The purge gas from each inner capsule was split into two parts (50 cm^3/min) by mass flow controllers. One flow channel proceeded through a ceramic electrolyte cell where tritiated water from the purge gas was reduced to an elemental form for a subsequent measurement of the total tritium in the purge gas by an ionization chamber. The other flow channel proceeded through a molecular sieve bed where tritiated water was removed. Finally the gas streams were oxidized through a oxidation bed and then tritium was cleaned up by a molecular sieve bed prior to being exhausted from the measurement hood [1].

CHARACTERISTIC TRITIUM MEASUREMENT APPARATUS

1. Irradiation Rig

Capsules were designed to separately accommodate two lithium ceramic specimens, in order to simultaneously measure tritium recovery from individual specimen at same irradiation condition [2,3]. Temperatures were measured by the K-type thermocouple located in the center of each specimen canister. Temperature of capsule was controlled by electrical heating and changing Ne/He content ratio of gap gas. A self-powered neutron detector (SPND) in the capsule was monitored changing neutron flux during irradiation run.

A heat resistance alloy, Hastelloy X-R, was mainly used as a structural material of capsule. A thin platinum spacer was placed between a specimen and an inner capsule wall to prevent a reaction of specimen with Hastelloy X-R. One of typical capsules is shown in figure 2.

2. Ceramic Electrolyte Cell

A couple of ceramic electrolyte cells (CEC) were installed in each purge gas stream to reduce any moisture in purge gas into tritium/hydrogen and oxygen gases. This cell which was improved by Ohno and Konishi in JAERI, consists of an electrolyte of yittria-stabilized zirconia [4]. Moisture (HTO) was directly reduced to elemental form (HT) through the cell which operated at 600°C with a nominal voltage bias of 1.6 volts, as illustrated the mechanism in figure 3. Approximately 95 % efficiency was anticipated in converting a moisture to elemental gases.

This is the first attempt to apply CEC in the actual tritium recovery experiment [1].

In one of experiments, hydrogen isotopes in the purge gas stream were determined HT, DT, T_2 in turn by linking a gas chromatograph and an ionization chamber, after the purge gas passing through a separation column [5].

3. Ionization Chamber

An ionization chamber measuring *beta*-decay of tritium was designed to provide both rapid response for changes of tritium release rates and high accuracy for anticipated tritium concentrations in purge gas lines [1]. Several types of ionization chamber were utilized in these experiments. The response of ionization chambers of 30, 100, 1370 cm^3 internal volume after an instantaneous shutdown of the reactor are shown in figure 4. Although the tritium content in the gas stream was expected to immediately drop to zero, the large chamber required more than an hour to completely recover. The 100 cm^3 chamber took considerably less time and the 30 cm^3 chamber was very fast. An instrumentation time constant depends on gas mixing in a chamber, and an exponential adjustment for the response of transient data is needed. The smaller volume of chamber is better from the standpoint of gas mixing, but worse from the standpoint of contamination which raises a background.

Tritiated water tends to contaminate a surface of ionization chamber and results in recalibration. Accordingly it was intended to detect only tritium in an elemental form.

3. Oxidation Bed

In order to clean up tritium in the purge gas streams passing through ionization chambers, a oxidation bed was used [1]. Tritium and hydrogen gases reacted with oxygen at 200°C on a Pd-Al_2O_3 catalyzer packed in the bed and then were oxidized to moisture. A subsequent molecular sieve system cleaned up moisture from the purge gas streams, before being exhausted through a stack. Detritiation factor is approximately 10^4.

IRRADIATIONS AND RESULTS

For each specimen under individual irradiation condition as shown in table 1, in-situ tritium recovery measurements have been executed. A few of typical results are described below.

In figure 5 the tritium release rates from both Li_2O and $LiAlO_2$ are compared during a set of irradiation runs [1]. In figure 5(a) tritium was retained in the $LiAlO_2$ after reducing temperature to 851°C from 901°C and abruptly released by increment of temperature to recover to the steady state. On the contrary the tritium release rate of the Li_2O was unaffected by temperature changes and kept in the steady state. In figure 5(b) in the lower temperature regime a small transient release of tritium was observed in the Li_2O, but the tritium release ceased at 557°C in the $LiAlO_2$.

As a typical example, the effect of hydrogen content in the purge gas on the tritium release rate is shown in figure 6. In both cases of Li_2O single crystal and sintered pellet specimens the release rate increased with increasing hydrogen content. The lines in this figure represent a curve fitting from the theoretical model which was previously reported [6].

In these experiments, the following summary has been deduced:

(1) The rank of superior tritium recovery performance is ordered as $Li_2O > Li_4SiO_4 > LiAlO_2$.
(2) Tritium recovery rate strongly depends on hydrogen content of the sweep gas as well as specimen temperature and characteristics.
(3) Tritium recovery behavior is governed not only by diffusion but also

by surface adsorption/desorption mechanism.

Table 1 In Situ Tritium Recovery Experiments in JRR-2

EXPERIMENT	SPECIMEN	DENSITY (%T.D)	G.S. (μm)	WEIGHT (g)	IRRADIATION TEPERATURE (°C)	IRRADIATION TIME BURN-UP (% of total Li)	IRRADIATION TIME FPD (days)	PURGE GAS	IRRDIATION DATE (Y,M)
VOM-15H	Li_2O, pellet	86	5~10	6.4	480-760	0.24	44	He	1983,5~8
VOM-21H	Li_2O, pellet	90	25	2.0	480-900	0.85	111	He, ≤0.1%D_2	1984,6 ~1985,3
VOM-22H	Li_2O, pebble $LiAlO_2^*$, pebble	85 77	10 11	3.9 4.3	350-900 430-900	0.5 4.7	88	He, ≤1%H_2	1985,7 ~1986,3
VOM-23H (BEATRIX-I)	Li_4SiO_4, pebble $LiAlO_2$, pellet	88 77	14 0.5	17.9 34.9	500-850 500-850	0.21 0.40	55	He, ≤0.1%H_2	1986,6 ~1987,2
VOM-27H	Li_2O, pellet $LiAlO_2$, pebble	79 78	7 0.7	11.1 12.1	390-600 500-825	0.11 0.27	33	He, ≤0.1%H_2	1987,3~4
VOM-31	Li_2O, single crystal Li_2O, pebble	100 90	— 27	22.3 8.6	400-810 450-780	0.35 0.56	121	He, ≤1%H_2	1988,3 ~1989,2
VOM-32	Li_2ZrO_3, pellet Li_4SiO_4, pellet	79 76	5 8	19.9 17.1	470-700 470-700	0.22 0.29	55	He, ≤1%H_2	1989,5~11
VOM-34	Li_2O, pellet Li_2O, single crystal	91 100	12 —	4.3 1.6	300-700 350-700	0.19 0.28	66	He, ≤0.1%H_2	1990,5 ~1991,5

* $LiAlO_2$: 26% Li-6 ENRICHMENT

CONCLUSIONS

In-situ tritium recovery experiments of lithium ceramics as tritium breeding material have been carried out using the JRR-2 in order to clarify tritium recovery behavior in blanket and contribute to the design activity of a fusion reactor. In these irradiation experiments in-situ tritium measurement system was designed and several unique technique in ceramic electrolyte cell, ionization chamber, capsule and so on was utilized.

The design and technology produced in these experiments have been very useful for the design and fabrication of the IEA collaborative irradiation experiment, BEATRIX-II.

Acknowledgments

The authors are indebted to staffs of the Research Reactor Utilization Division of JAERI for assistance in these experiments. The authors also wish to express their thanks to Drs. T.Kondo, M.Hands and Y.Naruse for their encouragement and support of these activities.

References

[1] T.Kurasawa, H.Watanabe, G.W.Hollenberg, Y.Ishii, A.Nishimura, H.Yoshida, Y.Naruse, M.Aizawa, H.Ohno and S.Konishi, J. Nucl. Mater., 141-143 (1986) 265

[2] H.Watanabe, T.Kurasawa, E.Roth and D.Vollath, In Proc. Inter. Symp. on Fusion Reactor Blanket and Fusion Cycle Technology, pp 33-36, October 27 -29, 1986, Tokai, Ibaraki, Japan, University of Tokyo
[3] T.Kurasawa, H.Takeshita, H.Yoshida, M.Aizawa, H.Ohno, K.Mimura, H.Umei and H.Watanabe, JAERI-M 86-129 (1986) (in Japanese)
[4] H.Ohno, J. Nucl. Mater., 179-181 (1991) 60
[5] H.Takeshita, H.Yoshida,T.Kurasawa,T.Matsui and H.Watanabe, JAERI-M 86-136 (1986) (in Japanese)
[6] T.Kurasawa and H.Watanabe, J. Nucl. Mater., 179-181 (1991) 851

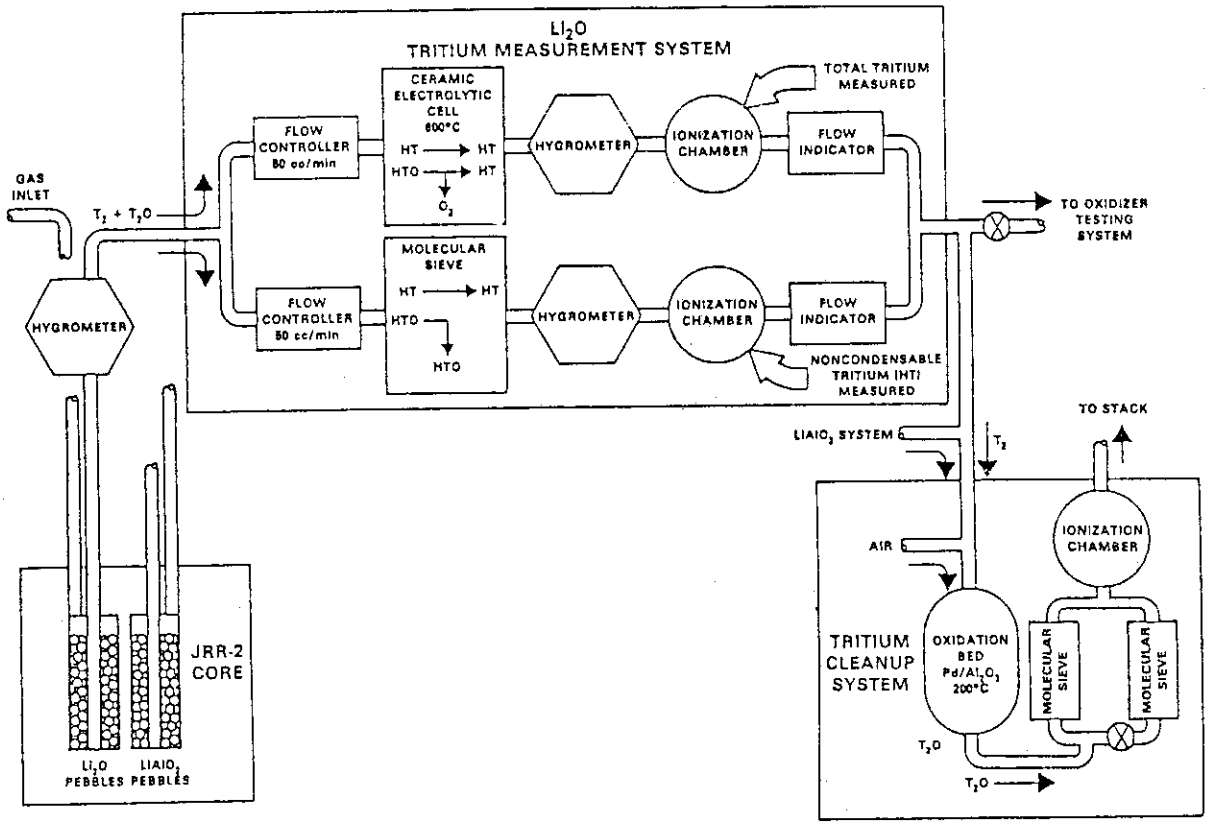

Fig.1. Schematic diagram of the purge gas flow in the in-situ tritium recovery measurement experiment.

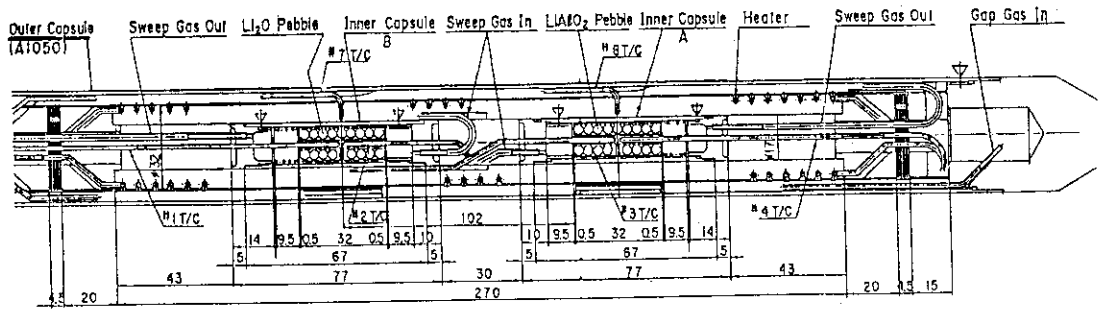

Fig.2. Structure of the capsule of VOM-22H experiment.

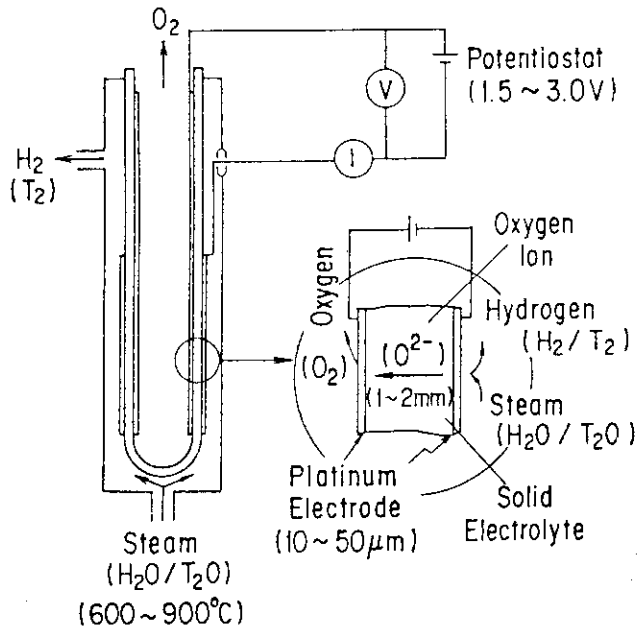

Fig.3. Reduction mechanism of tritiated water to gaseous form by using ceramic electrolyte cell.

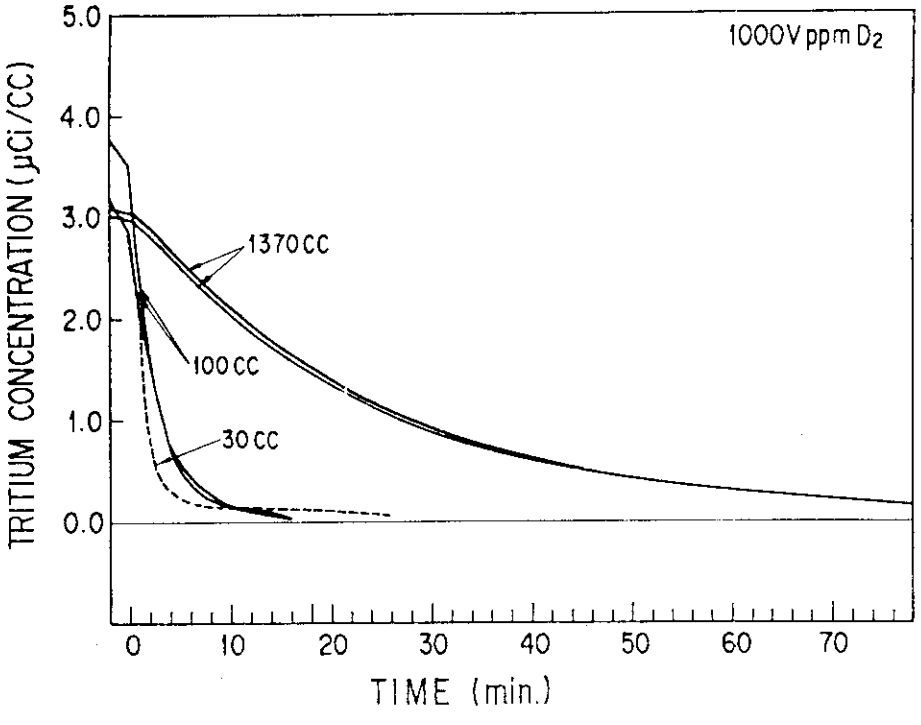

Fig.4. Effect of ionization chamber size on measuring the tritium concentration after reactor shutdown.

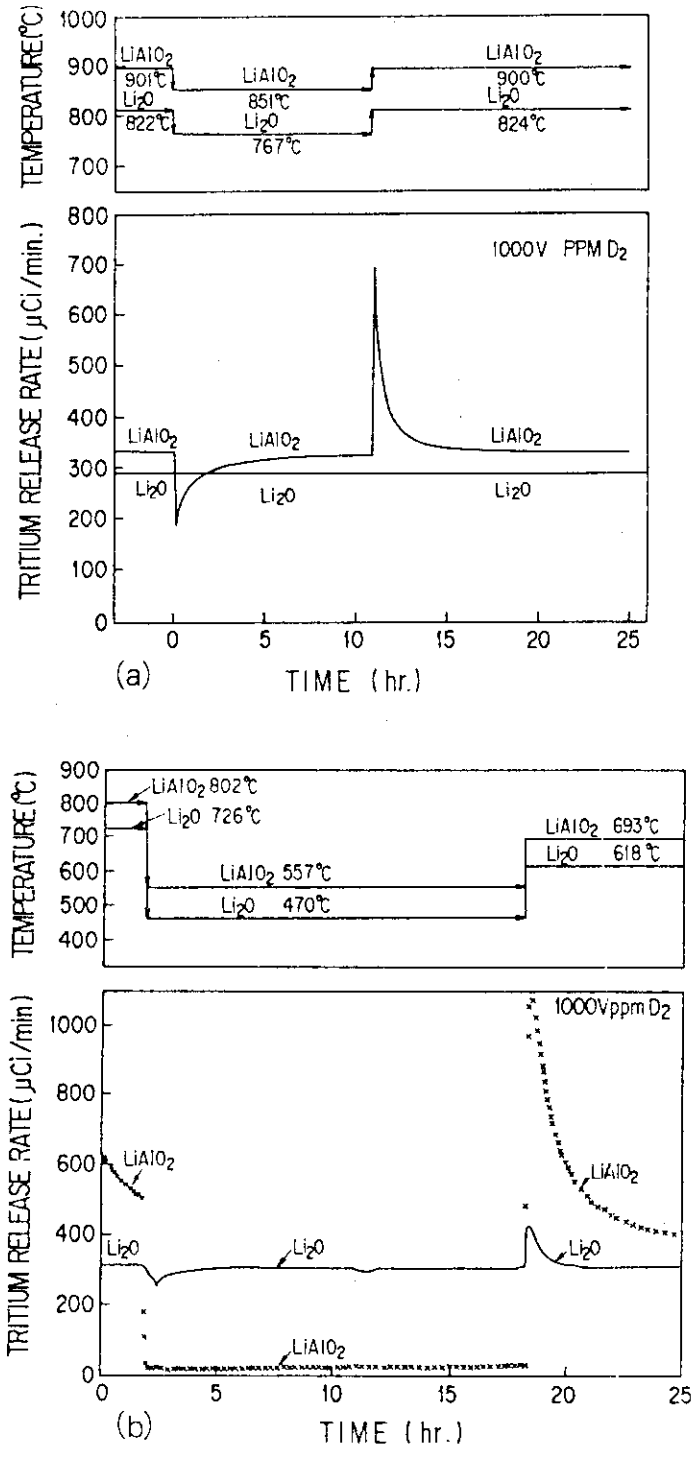

Fig.5. Comparison of the effect of an incremental temperature decrease and then increase on the tritium release rates of both Li2O and LiAlO2 spheres. (a) at higher temperature; (b) at lower temperature.

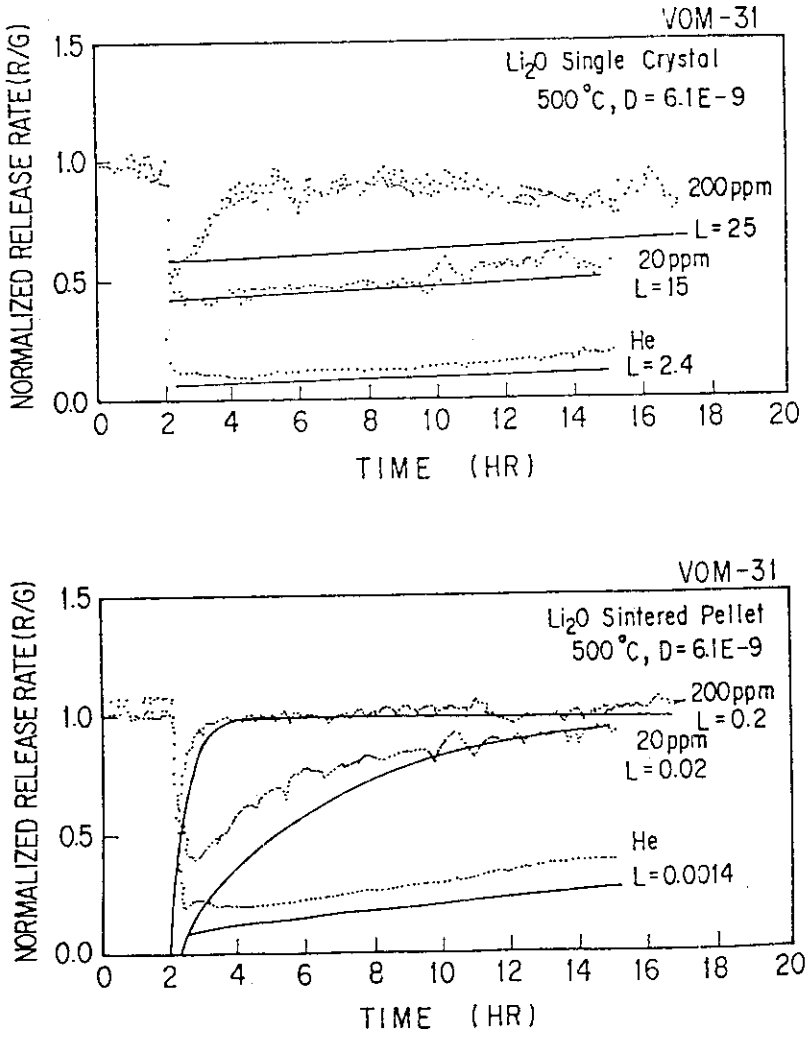

Fig.6. Time dependence of the normalized tritium release rate (R/G) on both Li2O single crystal and sintered pellet, after changing H_2 contents in the purge gas from 1000 vppm to the indicated content at 500°C. The lines represent curve fitting at the indicated values in this figure.

4. Irradiation Experiments of Nuclear Graphite at High Temperatures for HTTR

H. MATSUO, H. IMAI* and H. AMEZAWA**

Department of Fuels and Materials Research,
Tokai Research Establishment, JAERI
Tokai-mura, Naka-gun, Ibaraki-ken, 319-11 Japan
* Research Association for Nuclear Facilities Decommissioning,
Tokai-mura, Naka-gun, Ibaraki-ken, 319-11 Japan
** Department of JMTR Project,
Oarai Research Establishment, JAERI,
Oarai-machi, Higashiibaraki-gun, Ibaraki-ken, 311-13 Japan

ABSTRACT

A capsule for high temperature irradiation was developed and the irradiation technique has been established. Neutron irradiation experiments were carried out to accumulate data on dimensional changes, physical, chemical and mechanical properties of nuclear graphite for the design and safety analysis of the core material in the HTTR(High Temperature Engineering Test Reactor).

Neutron irradiation was carried out in the temperature range 600-1200°C to a maximum neutron fluence of about 3×10^{25} n/m^2 (E > 29fJ). Many capsules were employed for the irradiation, and data on the property changes of nuclear graphites have been accumulated.

INTRODUCTION

The effect of neutron irradiation at high temperatures on the properties of nuclear graphite has been extensively studied because of the development of graphite moderated reactors, since Wigner predicted property changes of nuclear graphite by neutron irradiation[1]. A lot of data have been published, and the property changes of nuclear graphite have been clarified to be dependent on irradiation conditions as well as kind of graphite materials. It is therefore necessary for designers to obtain the data on the irradiation behaviors of the nuclear graphite which is actually to be used in the reactors.

Two kinds of nuclear graphites for fuels assembly. replaceable reflector, permanent reflector and support post, and one nuclear carbon for thermal barrier are used in the HTTR (High Temperature Engineering Test Reactor). The nuclear graphite for use in the core of the reactor is exposed to high fluence by

neutron irradiation. Therefore much works have been done for obtaining irradiation data of the candidate materials for the reactor, because data published in the literatures can not be used for the design and safety analysis of the components in the HTTR from viewpoint of variation of irradiation effects on the kind of graphite.

The high temperature irradiation tests had been done for over 15 years in JAERI for the objectives of material selection for use in the HTTR and for obtaining sufficient data for the selected material by irradiation in the JMTR, JRR-2 and HFR. The present paper describes the neutron irradiation experiments techniques at high temperatures and some typical results on the effect of irradiation on the property changes for fine-grained isotropic graphite.

NEEDS OF IRRADIATION DATA FOR NUCLEAR GRAPHITE FOR USE IN THE HTTR

The outlet and inlet temperatures of coolant helium in the HTTR are 395°C and 950°C, respectively. And the temperatures of graphite sleeve are higher than 950°C, and neutron fluence is high for the graphite sleeve. For use of nuclear graphite in such reactor environment, data on property changes for irradiation temperature 400-1200°C, a maximum neutron fluence 1.5×10^{25} n/m^2 ($E > 29fJ$) were required to be at least necessary for design and safety analysis of graphite components.

IRRADIATION TECHNIQUES

1. Design of an irradiation capsule

(1) Samples and irradiation conditions

Materials to be irradiated were selected through a screening test for unirradiated materials, and based on the irradiation program for the candidate materials irradiation experiments were carried out.

Expected irradiation temperatures were chosen every 200°C from 400°C to 1200°C, and neutron fluence was selected to be much higher than the expected fluences, because scattering of data were expected to be large and data in the region of high neutron fluence is useful to obtain accurately design curve at lower fluence for new graphite materials.

As the samples can be irradiated in one condition for one irradiation capsule, the experiments in the region of high fluence at high temperatures were especially done, because we could not irradiate the samples again after the measurement of irradiated samples and the successive accumulation of irradiation data for the same samples at the similar temperatures was impossible. Therefore, it took much time to obtain data on neutron fluence dependence for new samples used for each irradiation experiment,

especially for irradiation in the region of high neutron fluence where property changes were expected to be seriously large.

(2) Arrangement of samples in the capsule

A capsule for irradiation in the JMTR is shown in Fig.1. The outer and inner tubes are made of SUS 316. Sample holders, spacers, rings for adjustment of heating and reflector tubes are loaded in the inner tube in addition to the samples to be irradiated. Eight thermocouples and four fluence monitor were loaded in the capsule as well in order to measure and control the irradiation temperatures and also to obtain neutron fluence of the samples exposed.

Every irradiation capsule was designed to include the samples to be measured for dimensional changes, thermal, physical, mechanical and chemical properties. Arrangement of the samples in the capsule was decided from considering the distribution of neutron fluence and irradiation temperature in order to obtain the data in different irradiation conditions as much as possible. Because distributions of temperature and neutron fluence existed, though the samples were aimed to be irradiated at uniform temperature in the capsule.

(3) Design of an irradiation capsule[2)]

Thermal and strength analysis were made in designing a capsule in order to achieve best irradiation conditions and to keep safety during irradiation at high temperatures.

In the case of thermal analysis assumption was made on that materials in the inner tube is packed in uniform condition,regardless of use of different kinds of samples, and the GENOA code was used to analyze temperature distribution in the capsule in order to obtain expected irradiation temperature by adjusting materials to be used for ring adjustment and gap between inner and outer tube. The value of 7.5 W/g was used for the rate of gamma heating in the analysis.

Strength, stress generated by inner pressure, and thermal stress of inner and outer tubes were estimated by analyzing the increase of pressure in an inner tube, which was caused by both helium and gas leased from samples, holders and so on. Based on the analysis described above the safety of the irradiation capsule was confirmed.

2. Control of irradiation temperature during reactor operation

(1) Flow diagram for control of irradiation temperatures

In Fig.2 a flow diagram for the control of irradiation temperature is shown. Helium gas is used to optimize the irradiation temperature by introducing into or evacuate from the gap between inner and outer tubes. For instance, when the temperature of samples become higher than the expected value, helium gas is introduced into the gap, and heat transfer from inner to outer tube was forced to become easier. This leads to decrease of irradiation temperature. The control system is automatically operated during reactor operation and irradiation temperature is kept continuously constant within ± 30°C at the controlling point.

(2) Examples of irradiation temperature history

In Fig.3 a typical example of irradiation temperature history is shown for one operation cycle in the JMTR. Irradiation temperature was controlled within the expected value. But it is necessary to recognize that this temperature control was done only on one point in the capsule. We have observed that temperature on the other locations showed variation with reactor operation time. So the scattering of irradiation temperature became larger at other locations in the capsule.

3. Neutron dosimetry[2)]

(1) Method

Pure iron contained in a quartz tube was installed on the four points in the capsule. After irradiation and dismantling the capsule the fluence monitors were measured with Ge detector and gamma-ray analysis was done to estimate ^{54}Mn which was produced by the following reaction, $^{54}Fe(n.p)^{54}Mn$, and the distribution of neutron fluence in the capsule was obtained in the range of neutron energy greater than 29fJ.

(2) Examples of estimation

Examples of the estimation of neutron fluence are shown in Fig.4. Circles are measured values and solid line is calculated one which is estimated by using the measured values.

4. Determination of irradiation temperature and neutron fluence of the irradiated samples

Distributions of irradiation temperature and neutron fluence in the capsule were decided by interpolating or extrapolating the measured values. As the precise position of each sample in the capsule is fixed, the irradiation conditions of each specimen were decided from the figure. It was assumed in this estimation that there were no distributions of neutron fluence and temperature in the radial direction of the capsule.

POST-IRRADIATION EXAMINATION

1. Measurement method of property changes

(1) Dimensional changes

A high accuracy comparator was used for the measurement of length changes at room temperature, where the precision of the measuring device was 0.03 %. Length was measured at multiple locations, and the average values were taken as the measured values.

(2) Thermal expansivity

A dilatometer was used for the measurement of thermal expansivity using a fused quartz as a standard sample, where the samples was heated at a rate of 5°C/min from room temperature to high temperature.

(3) Thermal conductivity

A laser pulse technique was applied to the measurement of thermal conductivity. Specimen size was 10 mm in diameter and about 1.5 mm in thickness. A ruby laser was used and the rear face temperature rise of the specimen was measured by a remote sensor, In-Sb detector. Thermal diffusivity was obtained from the following formula.

$$\alpha = 0.0388\, \ell / T_{1/2}$$

where α is thermal diffusivity(cm^2/s), ℓ specimen thickness(cm), $T_{1/2}$ half time to reach maximum temperature rise.

In order to resolve finite pulse-width effect some correction were given using the center of gravity of laser pulse[3]. Thermal conductivity was obtained from the measured thermal diffusivity, bulk density and specific heat capacity.

(4) Young's modulus and electrical resistivity

Young's modulus at room temperature was obtained by combining measurements of the transmission time of a 100 kHz ultrasonic wave propagated through the specimen with the data for bulk density. Electrical resistivity was measured at room temperature by a potential-drop method.

(5) Corrosion rate

Specimens were reacted with water-vapor of 0.65 % in the flowing helium gas of the temperatures 780-1000 °C in the environment of atmospheric pressure. The flow rate of helium gas was 650mℓ/min which corresponds to a linear rate of 5.7 cm/s over the specimen. The BET surface area and pore radius distribution were also measured to study the effect of irradiation on chemical reactivity.

2. Results of irradiation effects on property changes[4-6]

In Figs.5-10 typical results on dimensional changes, thermal expansivity, thermal conductivity, Young's modulus, electrical resistivity and corrosion rate for fine-grained isotropic graphite IG-110 are shown as a function of neutron fluence. In the figures the data[4] on the results obtained from irradiation in HFR are combined with the results of irradiation experiments in the JMTR.

Dimensional shrinkages were observed and almost all data at similar irradiation conditions for parallel and perpendicular to the orientation of crystallites agreed with each other within the spread of the measured values.

Thermal expansivity increased owing to irradiation in the initial small range of neutron fluence, followed by the decrease with increasing neutron fluence.

Thermal conductivity decreased by irradiation and its temperature dependence changed, showing shift of the peak position to higher temperature after irradiation.

Young' modulus and electrical resistivity showed rapid increase in the early stage of irradiation and leveled off at higher neutron fluence.

Corrosion rate showing increase with increasing burn-off decreased owing to irradiation and the unirradiated and irradiated specimens had a tendency to merge into the same value with increasing burn-off. Significant difference of corrosion rate before and after irradiation was not observed.

SUMMARY

An specially designed irradiation capsule has been developed and neutron irradiation technique at high temperatures has been established. A lot of irradiation data on dimensional changes, thermal expansivity, thermal conductivity, Young's modulus, electrical resistivity and corrosion rate for nuclear graphites have been accumulated for design and safety analysis of graphite components of the HTTR.

REFERENCES

1) E.P.Wigner, CP-387(1942).
2) JMTR IRRADIATION HANDBOOK JAERI-M 83-053(1983).
3) A.Azumi, Y.Takahashi, Rev. Sci. Instrum. 52, 1411(1981).
4) H.Matsuo, JAERI-M 87-207(1987).
5) H.Matsuo, Netsu-Sokutei 17, 2(1990) (In Japanese).
6) H.Matsuo, Tanso, to be published.

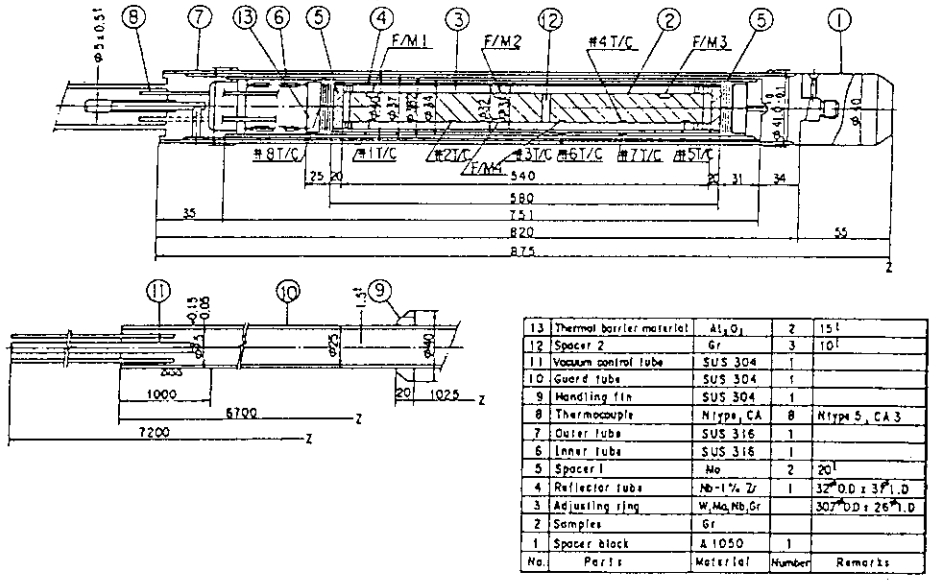

No.	Parts	Material	Number	Remarks
13	Thermal barrier material	Al_2O_3	2	15t
12	Spacer 2	Gr	3	10t
11	Vacuum control tube	SUS 304	1	
10	Guard tube	SUS 304	1	
9	Handling fin	SUS 304	1	
8	Thermocouple	N type, CA	8	N type 5, CA 3
7	Outer tube	SUS 316	1	
6	Inner tube	SUS 316	1	
5	Spacer 1	Mo	2	20t
4	Reflector tube	Nb-1% Zr	1	32mm O.D x 31mm I.D
3	Adjusting ring	W, Mo, Nb, Gr		307mm O.D x 265mm I.D
2	Samples	Gr		
1	Spacer block	A 1050	1	

Fig.1 A capsule for irradiation at high temperatures in the JMTR

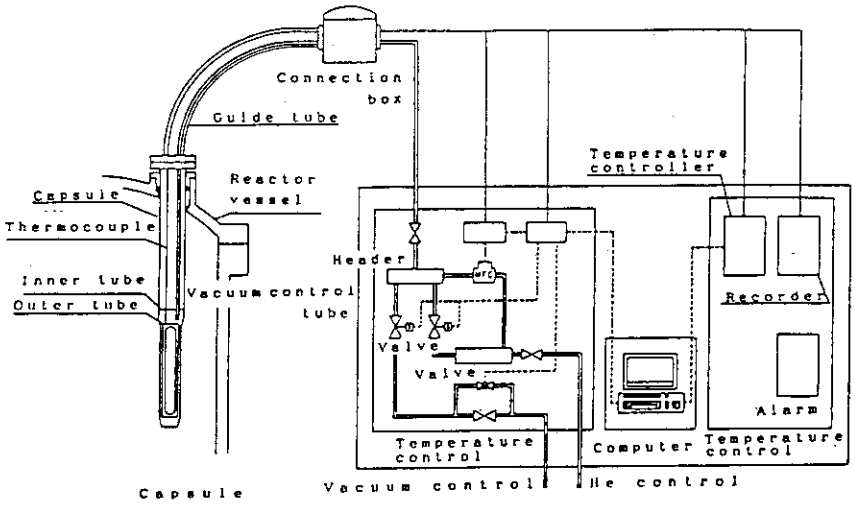

Fig.2 A flow diagram for control of irradiation temperatures

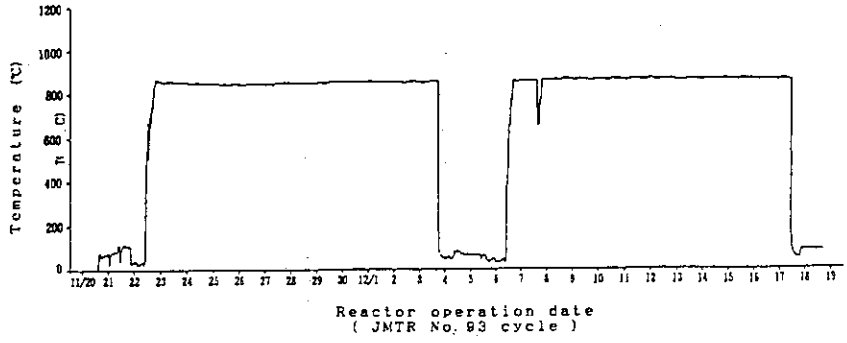

Fig.3 A typical example of irradiation temperature history

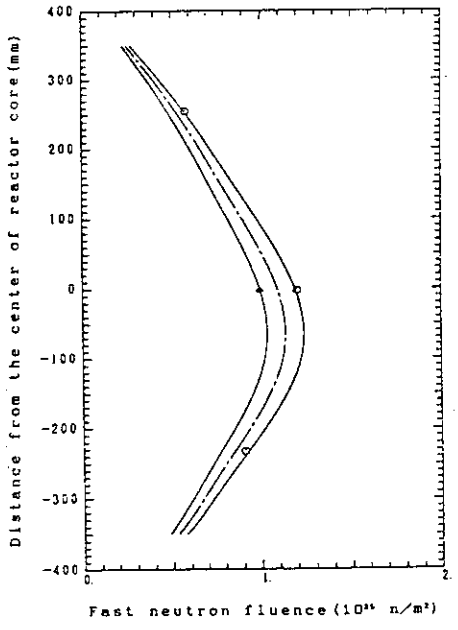

Fig.4 An example of the estimation of neutron fluence

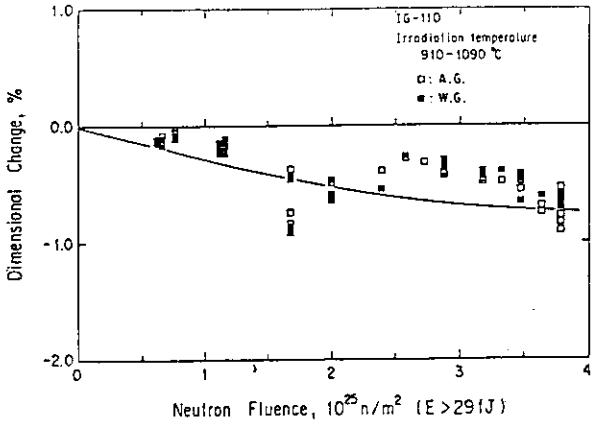

Fig.5 Dimensional changes

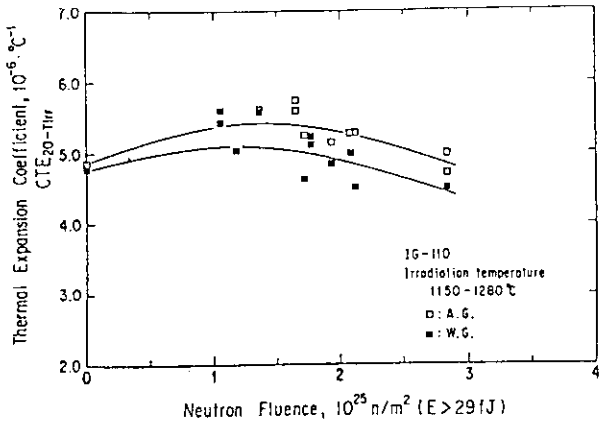

Fig.6 Change in thermal expansivity

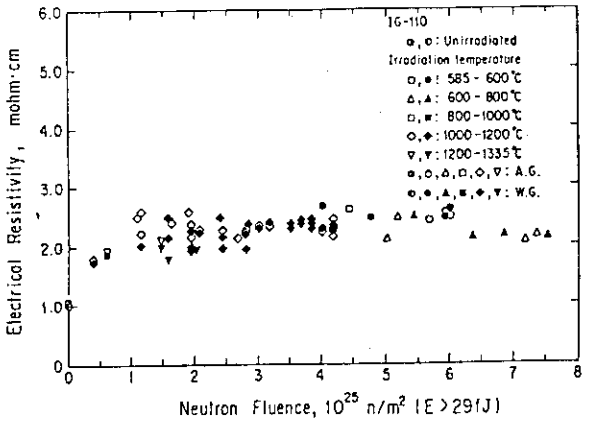

Fig.9 Change in electrical resistivity

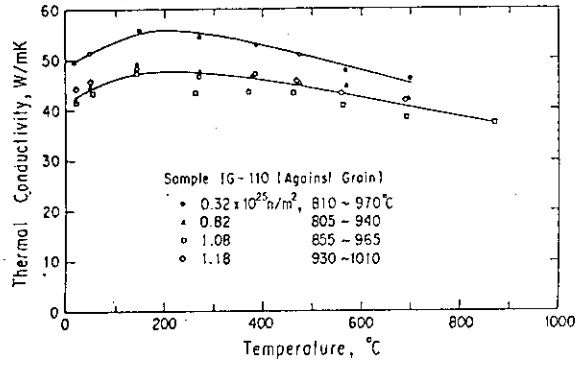

Fig.7 Change in thermal conductivity

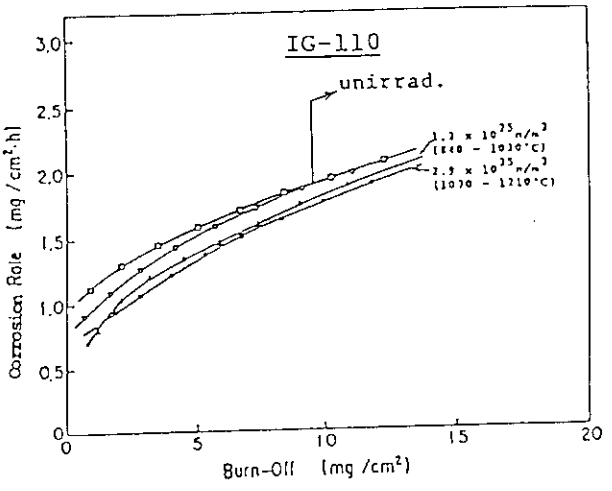

Fig.10 Change in corrosion rate

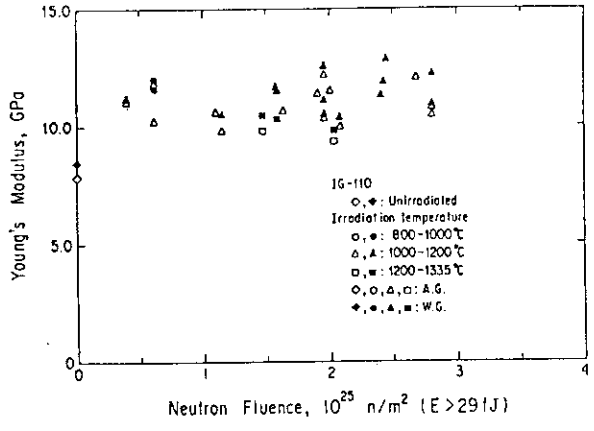

Fig.8 Change in Young's modulus

5. Development of Re-Instrumentation Techniques of FP Gas Pressure Gauge to the Irradiated LWR Fuel

H.Kawamura, K.Oshima, M.Shimizu, Y.Ichihashi and Y.Futamura

Department of JMTR Project
Oarai Research Establishment, JAERI
Oarai-machi, Higashiibaraki-gun, Ibaraki-ken 311-13, Japan

ABSTRACT

We have conducted the techniques for re-instrumentation of the FP gas pressure guage to the fuel rod irradiated to high burnup in order to clear the release behavior of FP gas from the high burnuped fuel pellet.

The items of developments of these techniques are mainly the development of devices for re-instrumentation of the FP gas pressure guage to the irradiated fuel rod and the development of remote re-intrumenting techniques at the hot laboratory.

From the results of out-of-pile test on re-instrumentation devices and in-pile assurance test using the re-instrumented fuel rod irradiated to about 25 GWd/t, the techniques for reinstrumenting the FP pressure guage to an irradiated fuel rod without leaking inner gas containing FP gas from the irradiated fuel rod were complete. Therefore, in future, the experiment for making clear the exact relation between the failure threshold of the high burnuped fuel rod and the mechanism of FP release in the high-burnuped fuel rods during power ramping by using BOCA capsule became possible.

INTRODUCTION

It is being desired to attain the high burnup of LWR fuel from a economical view point of fuel cycing[1]. Therefore, it is hurried up to clear the release behavior of FP gas from the fuel pellet in the high burnup level. In this context, the techniques for re-instrumentation of the FP gas pressure guage to the fuel rod irradiated to high burnup was developed, then the power ramping test using the re-instrumented fuel rod was performed.

The developments of these techniques are classified two items roughly.

The first one is the development of devices for re-instrumentation of the FP gas pressure guage to the irradiated fuel rod. The relevant re-instrumentation devices are panching device, FP gas pressure guage and conecting device. The punching device makes small hole on the end plug of fuel rod by the arc discharge, then lead the FP gas to pressure guage. The conecting device works to lead the electric signal of FP gas pressure guage to the irradiation capsule during the power ramping test.

The second is the development of remote operation techniques. The remote re-instrumenting techniques are separated two items roughly, i.e. welding technique of the fuel rod to above mentioned re-intrumentation devicesand inserting technique of re-instrumented fuel rod to the irradiation capsule.

In this paper, it is discussed about the results of out-of-pile test on re-instrumentation devices and in-pile demonstration test using the re-instrumented fuel rod irradiated to about 25GWd/t.

PROCEDURE OF RE-INSTRUMENTATION TO IRRADIATED LWR FUEL ROD

The re-instrumentation procedure was classified the four items as follows The outline of procedure is shown in Fig.1.

① machining the end plug of irradiated fuel rod,
② welding between the machined fuel rod and the re-instrumentation devices (FP gas pressure guage, panching device and connecting device are welded at the cold area outside the hot-laboratory) ,
③ punching the machined end plug of irradiated fuel rod by arc discharge
④ encapsuling (inserting the re-instrumented fuel rod into BOCA capsule)

DEVELOPMENT OF REINSTRUMENTATION DEVICES

The configuration of re-instrumentation devices, that is FP pressure guage, punching devise and connecting device, is shown in Fig.2.

As to FP gas pressure guage, differential transducer system was used for the miniaturization, welding bellows was used for measuring the high pressure in the fuel rod. The accuracy of pressure measuring was 1% (max.pressure ; 5MPa). The configuration of FP gas pressure guage and the results of out-of-pile of pressure calibration tests are shown in Fig.3 and Fig.4, respectively.

As the punching device, the punching system by arc discharge was used for

the miniaturization and no vibration on punching work. The configuration of the punching device and the results of out-of-pile of punching mockup tests are shown in Fig.5 and Fig.6, respectively.

As to the connecting device, the quick joint system with the metal O ring was used for easy inserting and removing work by remote operation. The configuration of the connecting device is shown in Fig.7.

DEVELOPMENT OF REMOTE REINSTRUMENTING TECHNIQUE

We used the torch-rotary typed and pulsed TIG welding machine, producted by Weldlogic INC., for welding the re-instrumentation devices and irradiated fuel rod. From the results of the welding mockup tests used this machine, the best suited welding conditions concerning welding current, welding speed, torch gap, shape of weldment, etc. were dicided. Then, using those welding conditions, we welded the irradiated fuel rod and the re-instrumentation device. However, because of the bends of the re-instrumented fuel rod both by the irradiation to the high burnup and by remote welding, the metal O ring of connecting device did not uniformly touch with the seal face, and re-instrumen ted fuel rod could not be securely inserted in the BOCA capsule. Therefore, the metal O ring could touch uniformly by correcting the bends by point-heating the parts of remote weldingand the re-instrumented fuel rod could insert in the BOCA capsule.

IN-PILE ASSURANCE TEST OF REINSTRUMENTATION TECHNIQUE

The in-pile assurance test of re-instrumentation technique were conducted in order to assure the function of all re-instrumentation devices installed to irradiated fuel rod which burnup is $\sim$ 25GWd/t by remote welding at hot-laboratory on basis of re-instrumentation procedure shown in Fig.1. The purposes of this test are to make clear the insulating performance of FP pressure guage, the conecting performance of signal line and the sealing performance of connecting devise. The test was conducted using the BOCA capsule in JMTR,

From the results of this test, it was obvious that the inductance does not decrease, the resistance between signal lines does not increase and the disconnection does not occur. Therefore, this re-instrumentation technique was assured that it have the excellent performance and durability against neut ron irradiation and BWR coolinng condition.

CONCLUSION

The techniques for reinstrumenting the FP pressure guage to an irradiated fuel rod without leaking inner gas containing FP gas from the irradiated fuel rod were complete. Therfore, the experiment for making clear the exact relation between the failure threshold of the high burnuped fuel rod and the mechanism of FP release in the high-burnuped fuel rods during power ramping by using BOCA capsule became possible.

ACKNOWLEDGMENT

We express our thanks to Mr.M.SAITO, Deputy Director of JMTR Project, H.ANDO H.ITO, H.SATO, T.ISHII, Y.TAYAMA of JMTR Project and T.NISHIGUCHI of Mechanical Engineering Dinision, JAERI who assisted us with this development.

REFFERENCES

[1] M.ICHIKAWA ; " High burnup of LWR fuel ", Nuclear engineering, 31 ,No.11, 43 (1985)

[2] Y.KOMORI, K.OHSHIMA, Y.SUZUKI, H.KAWAMURA, F.SAKURAI, K.OOKA and M.SAITO ; JAERI-M 88-156," Development of reinstrumenting technique of fuel rods with pressure guage " (1988)

[3] K.OHSHIMA, H.KAWAMURA, T.SUDO, Y.KOMORI, Y.SUZUKI and M.SAITO ; private communication (1987)

[4] H.KAWAMURA, K.OHSHIMA, Y.KOMORI, F.SAKURAI and R.OYAMADA ; JAERI-M 88-273, " The JMTR operation and technical development (No.2)/ (fiscal 1985) ", 92 (1989)

[5] H.KAWAMURA, K.OHSHIMA, Y.KOMORI, Y.SUZUKI and M.SAITO ; JAERI-M 89-160, " The JMTR operation and technical development (No.3)/ (fiscal 1986-1988)", 177 (1989)

[6] H.KAWAMURA, K.OHSHIMA and H.NAKATA ; JAERI-M 90-189, " The JMTR operation and technical development (No.4)/ (fiscal 1989)", 75 (1989)

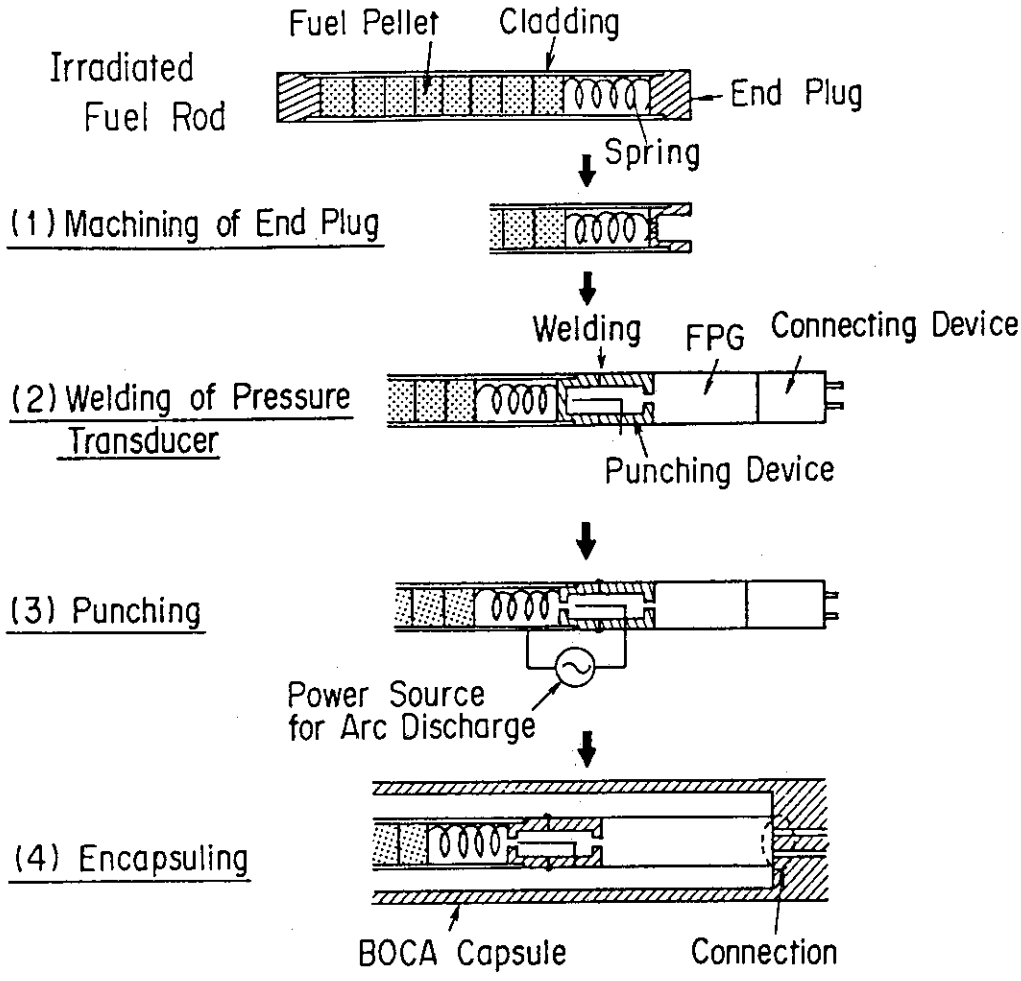

Fig. 1 Outline of re-instrumentation procedure

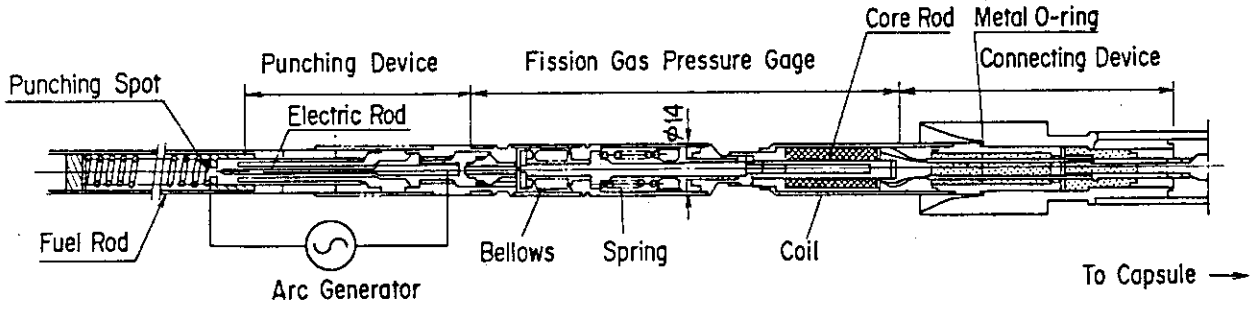

Fig. 2 Configuration of re-instrumentation devices

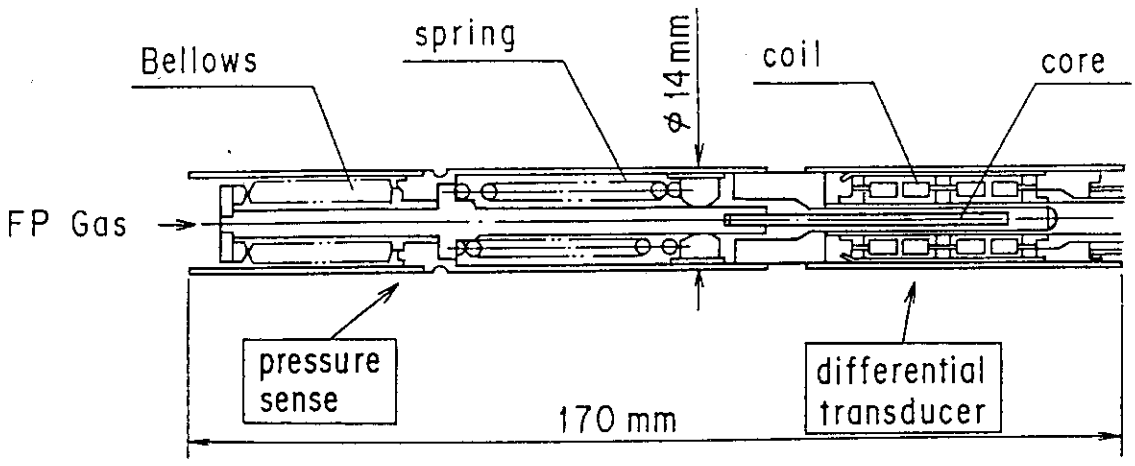

Fig. 3 Configuration of FP gas pressure guage

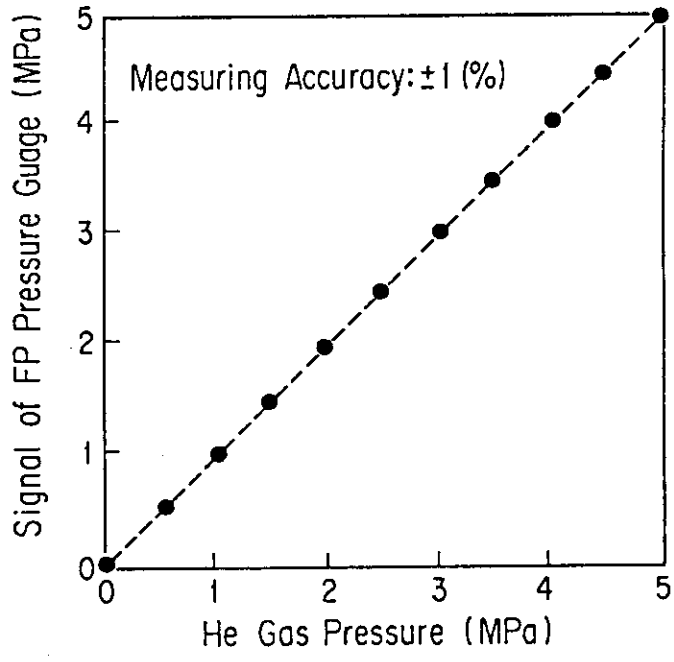

Fig. 4 Results of pressure calibration tests (out-of-pile)

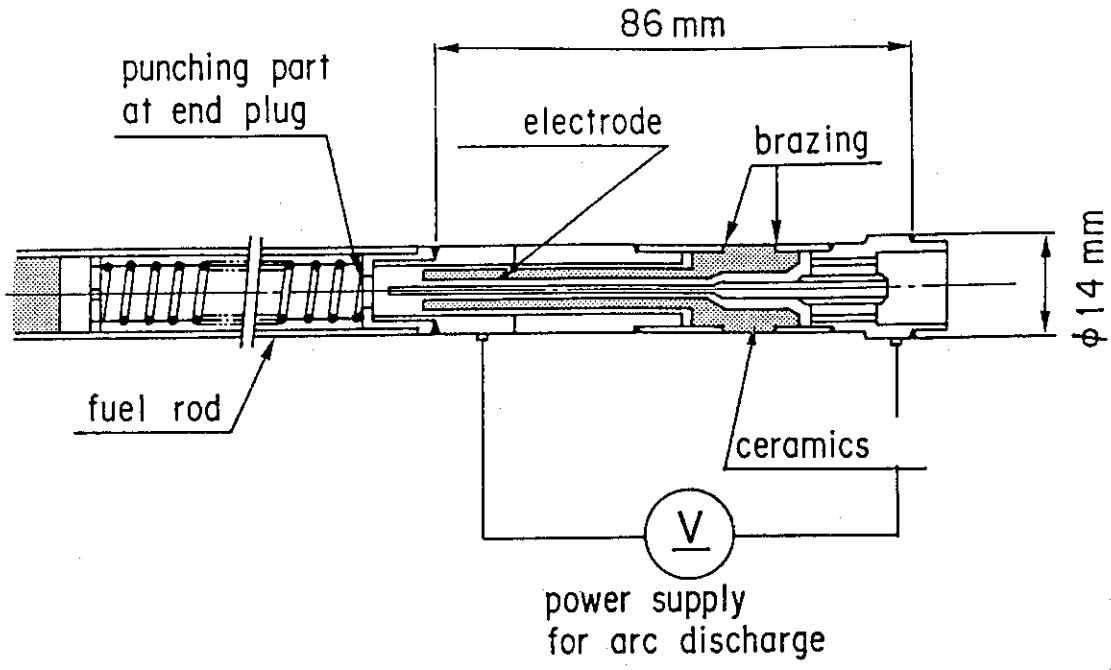

Fig. 5 Configuration of the punching device

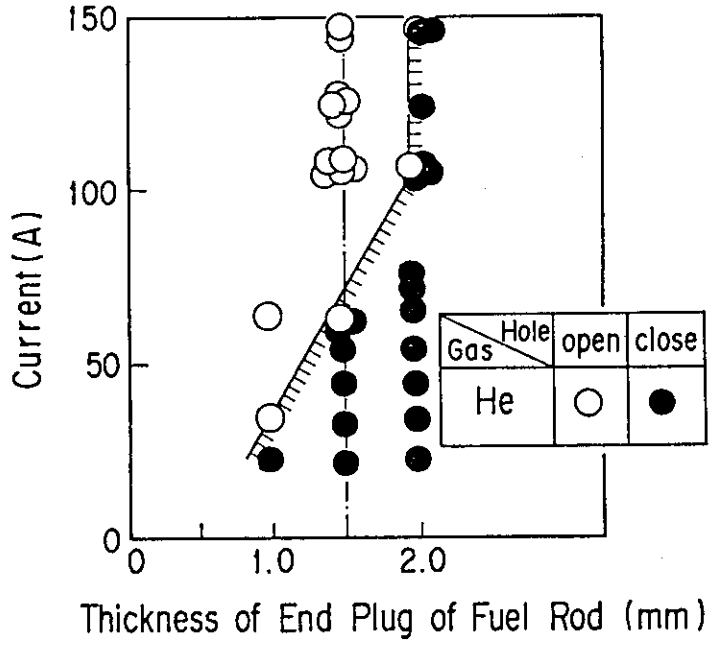

Fig. 6 Results of punching mockup tests (out-of-pile)

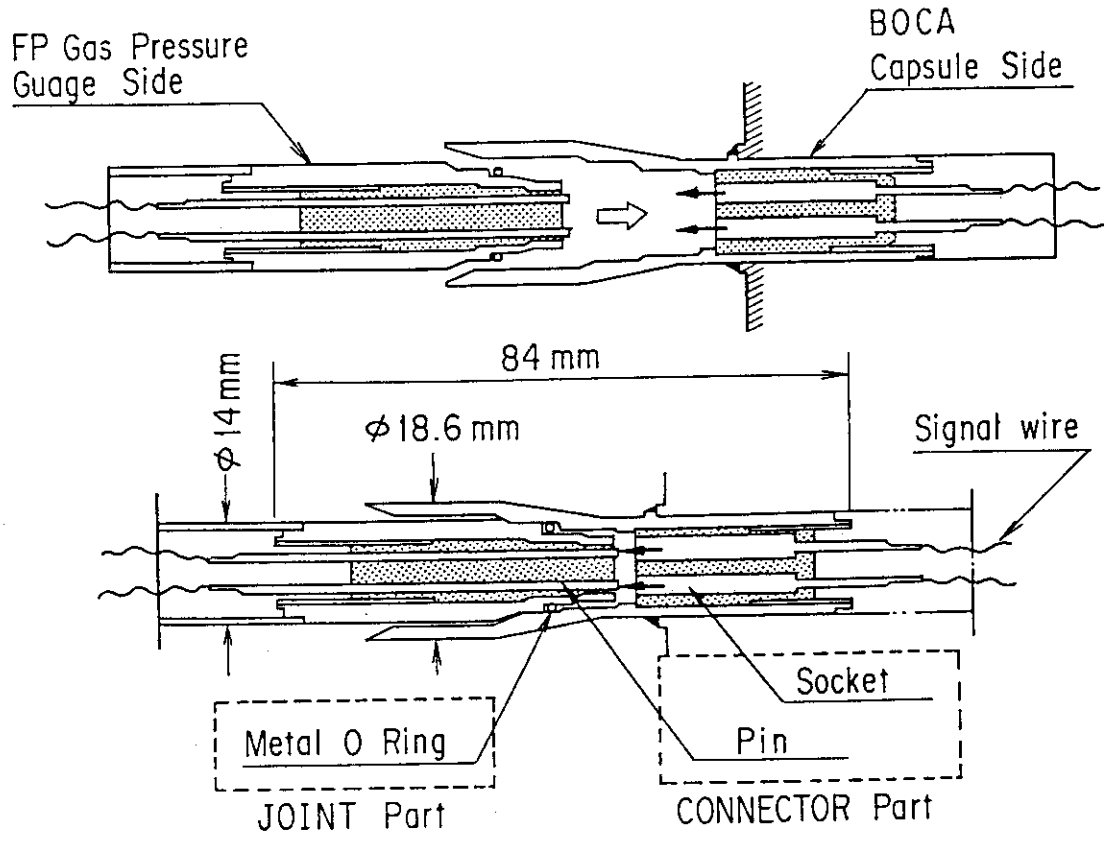

Fig. 7 Configuration of the connecting device

6. Irradiation Temperature Controlled by Nucleate Boiling of Pressurized Water

M. NIIMI, H. SOMEYA, Y. HARAYAMA, Y. ICHIHASHI,
Y. FUTAMURA and T. ONCHI*

Oarai Research Establishment, Japan Atomic Energy Research Institute (JAERI)
3607 Oarai-machi, Ibaraki-ken 311-13, Japan
* Central Research Institute of Electric Power Industry (CRIEPI)
2-11-1 Iwatokita, Komae-shi, Tokyo 201, Japan

ABSTRACT

Saturated Temperature Capsule (SATCAP) was designed and irradiated in order to study Irradiation Assisted Stress Corrosion Cracking (IASCC) in Japan Materials Testing Reactor (JMTR). The capsule is used boiling water for cooling of irradiation specimens. The water is supplied from outside of the capsule, and boiled at the specimen surface by γ heating of the specimens and the capsule structure. Water in general can be maintained a saturation temperature under some pressure. By pre-setting the water pressure, the specimen temperature is controlled at aimed temperature. The irradiation examination of the LWR core structural materials was carried out by using the SATCAP, in which an irradiation environment of the specimens simulates the BWR conditions.

The capsule design and the results of irradiation examination are described in this paper.

INTRODUCTION

In recent years, the life time estimation of nuclear power plants has become an important matter. The reactor core structure is one of critical components for the life time estimation of the plant, because it is difficult to replace with new one. And the reactor core structure is located in area of high neutron flux. In 40 years of operation period of a reactor, the neutron fluence of the core structure comes to $1\times10^{26}m^{-2}$ (E>1MeV). Therefore IASCC of the core structure is being investigated with interest.

Occurrence of IASCC depends on neutron fluence, and there is a threshold value $5\times10^{24}m^{-2}$ (E>1MeV) of neutron fluence[1]. When the neutron fluence is increased to more than the threshold value, the sensibility of the IASCC is more and more increasing. In order to make clear the cause and mechanism of the IASCC, JAERI and CRIEPI carry out the collaboration study for the irradiation examination by using the JMTR.

CONCEPTUAL DESIGN

In order to obtain neutron fluence of $1\times10^{26}m^{-2}$ (E>1MeV) for a short period, the irradiation examination must be carried out at area of high neutron flux in the JMTR. But this

area is of a high γ heat generation. When an irradiation examination is carried out at this area by using the conventional capsule in which the temperature of specimens are controlled by the electric heater, the irradiation temperatures of the specimens increase to more than 600°C. So that the use of conventional capsule does not meet the requirements in the temperature of the experiment for materials for LWRs. Therefore, a new type capsule need to be developed. In order to resolve the issue of irradiation temperature and to improve irradiation techniques, the new type capsule using boiling water for cooling of specimens is developed. In the capsule, water is supplied from outside of the capsule, and the water boils at surface of specimens. Cooling capability of water is the greatest when it boils.

Now, if a pressure of the supplied water into the capsule is constantly kept, the temperature of water come to a saturation temperature depending on pressure of water. This physical property can be used for the control of the specimen temperature. The heat generation of the specimen is mainly absorbed as the latent heat of the supplied water, then the specimen temperature is almost kept at constant.

SHAPE AND DIMENSIONS OF SPECIMENS

In the post-irradiation examinations, Slow Strain Rate Tensile Test (SSRT) and Uniaxial Constant Load Test (UCL) of the irradiated specimens are carried out in the hot laboratory .

The dimensions of specimens are shown in Fig.1. The shape of the specimen is the plate type for tensile tests. The total number of specimens in a capsule is 105 pieces.

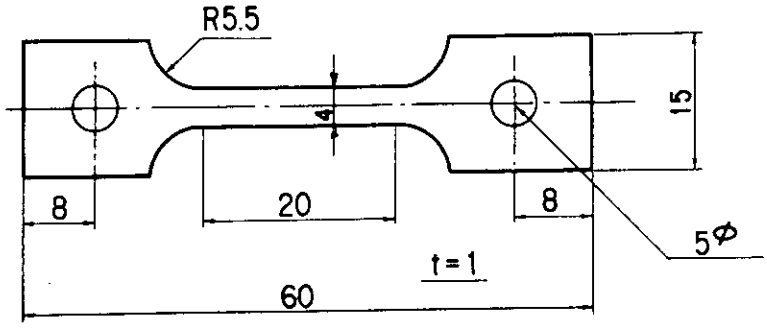

(mm)

Fig.1. Tensile/SCC specimen of plate type.

CAPSULE AND CONTROLLER

Outlines of the capsule and the controller are shown in Fig.2. The capsule and the controller have a simple mechanism. The capsule consists of double tubes. One tube is an outer-tube. The other tube is a baffle-tube. The specimens are loaded inside of the baffle-tube. The capsule is mainly made of stainless steel. The water supplied into the capsule is divided into double flows by the baffle-tube in the inside of the capsule. One flow is the down stream between the outer-tube and the baffle-tube, the other flow is the up stream between the specimens and the baffle-tube. In the baffle-tube, nuclear heat is generated by γ ray from the reactor core. The temperature of specimens are maintained by using the baffle-tube as the heat source.

The flow of the supplied water is once through, in order to prevent contamination from radioactive corrosion products in the equipment for feeding the water.

The dimensions of the outer-tube of the capsule are 60mmO.D., 3mm thickness. And the dimensions of the baffle-tube are 40mm, 4mm thickness. The capsule has a coil to cool the high temperature water. The coil is located above the capsule. There are 13 pieces of thermocouples in capsule. The 3 pieces of thermocouples are inserted in the position of specimens. The 10 pieces of thermocouples measure the water temperature in the inside of the capsule.

The controller mainly consists of a pump, an accumulator and a control valve for keeping the supplied water pressure. The pump supplies water at a constant flow rate. The accumulator is set up to prevent a pulsating pressure for the water system. The pressure control valve is a spring type. The water pressure is controlled by adjusting the strength of the spring of the valve. There are pressure gauges and a flow meter. The decay tank for ^{16}N is provided on the out-let side of the capsule.

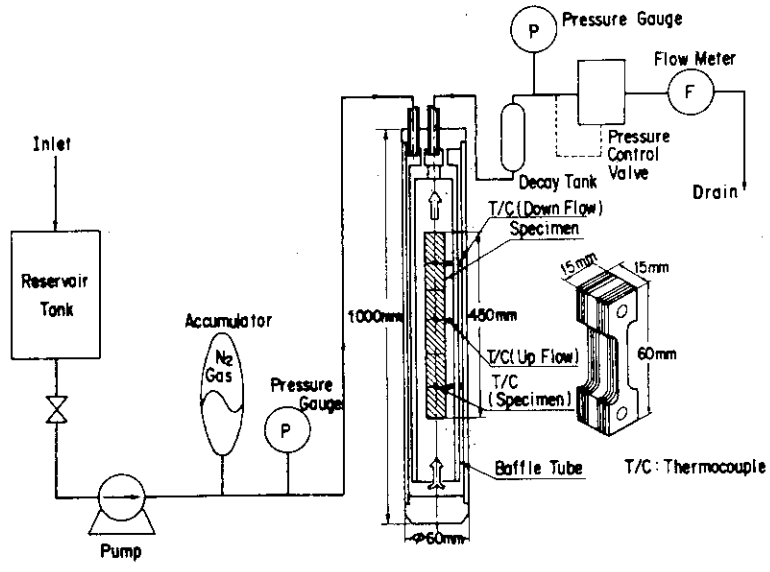

Fig.2. Flow diagram of equipment for the irradiation examination.

IRRADIATION CONDITIONS

In order to obtain a high fluence of neutron in a short irradiation period, the capsule is loaded at the area of high neutron flux in the JMTR.

The irradiation conditions are as follows:

thermal neutron	$2\times10^{18}m^{-2}s^{-1}$,
fast neutron (E>1MeV)	$2\times10^{18}m^{-2}s^{-1}$,
γ heat generation	10W/g (by stainless steel) [2],
temperature	290±30°C,
environment	pressurized water ($75kg/cm^2g$),
total length of specimens	450mm.

KEY POINT OF CAPSULE DESIGN

The γ heating distribution of the vertical direction in the irradiation field is formed a cosine curve, as shown in Fig.3. In the specimens too, there is a cosine distribution of the heat generation. If the heat removal capacity in the capsule is the same all along the whole specimens, the temperature distribution of the specimens takes a form of cosine curve due to the γ heating. In order to obtain a flattened distribution of the temperature along the axis of the specimens, boiling water is used in the capsule.

In this experiment, the specimens are the reactor core structural materials used in the LWR. When the pressure of water is kept at 75kg/cm^{2}g, the temperature of specimens increases to 300°C. From the view point of creating the same environment as the LWR, this capsule becomes a better equipment to irradiate reactor core structural materials .

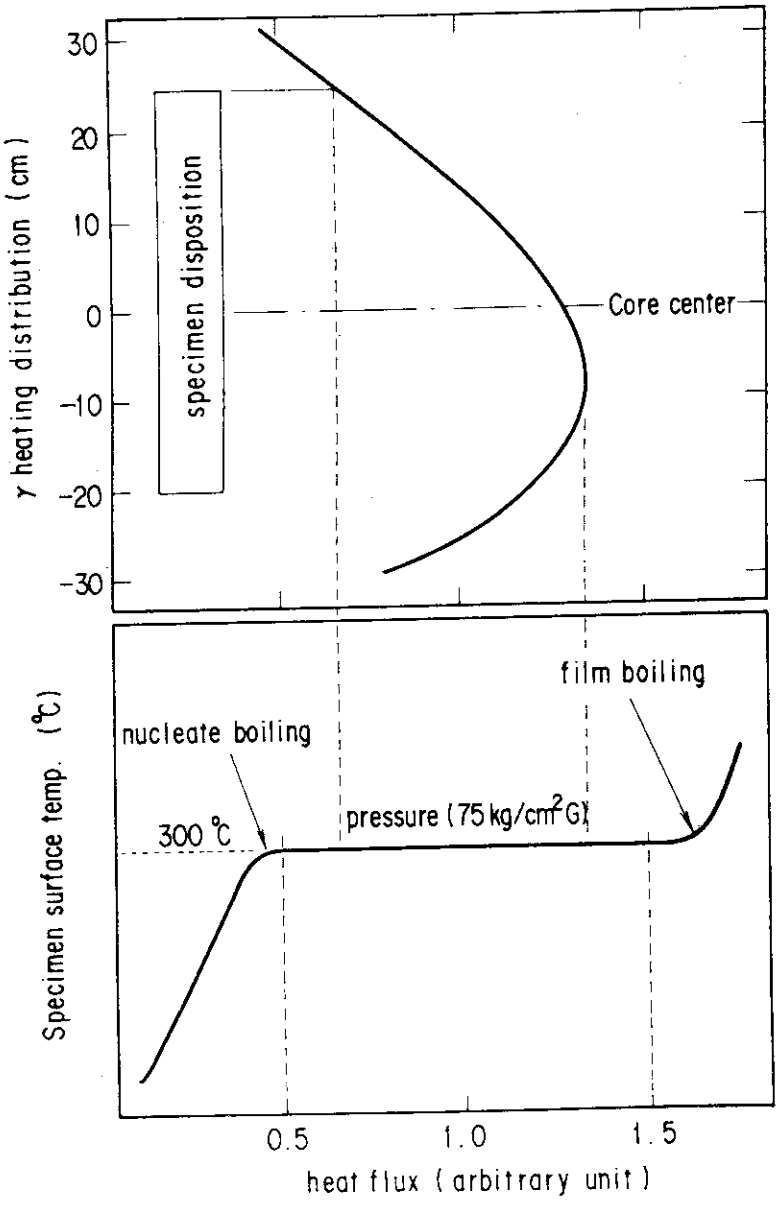

Fig.3. Distribution of γ heat generation in axial direction.

TEMPERATURE DISTRIBUTION IN THE CAPSULE

The flow of the water in the capsule is as follows. The water supplied from the outside of the capsule flows down between the outer-tube and the baffle-tube, and reverses its direction, upwards, at the bottom of the capsule. In this time, the water is warmed by γ heating of the capsule structural materials. And the water temperature increases to an optimum temperature at the surface of the specimens. The velocity of the water flow in the capsule is about 0.2m/s. As for the outside of the capsule, the velocity is about 5m/s.

Temperature distribution in the capsule is obtained by the following equations[3]. The outer-tube temperature T_1 is given by

$$T_1 = T_0 + \frac{\phi_1}{h_f}, \tag{1}$$

where T_0 is temperature of the reactor primary water, ϕ_1 is the heat flux of outer-tube, h_f is the heat transfer coefficient. ϕ_1 is given by

$$\phi_1 = \frac{q''' R_1}{2} - \frac{R_2}{R_1}\left(\frac{q''' R_2}{2} - \frac{Q}{2\pi R_2}\right), \tag{2}$$

where q''' is heat flux density at inner surface of the outer-tube, R_1 is the outer radius of the outer-tube, R_2 is the inner radius of the outer-tube , Q is the amount of heat flowing into the outer-tube. h_f is given by

$$h_f = \frac{Nu\,\lambda}{D}, \tag{3}$$

where Nu is the Nusselt number, λ is the thermal conductivity of water, D is the hydraulic diameter. Nu is given by

$$Nu = 0.023\, Re^{0.8} Pr^{0.4}, \tag{4}$$

where Re is the Reynolds number, Pr is the Prandtl number. Re is given by

$$Re = \frac{V D}{\nu}, \tag{5}$$

where V is the velocity of the reactor primary coolant, ν is the kinetic viscosity of the coolant.

The outer-tube inside surface temperature T_2 is obtained by

$$T_2 = T_1 + \frac{q'''}{4k}\left(R_1^2 - R_2^2\right) - \frac{R_2}{k}\left(\frac{q''' R_2}{2} - \frac{Q}{2\pi R_2}\right) ln\left(\frac{R_1}{R_2}\right), \tag{6}$$

where k is the thermal conductivity of the outer-tube.

Temperature difference ΔT in the baffle-tube is obtained by following equations.

$$\Delta T = \frac{\phi_2}{h_f}, \tag{7}$$

where ϕ_2 is heat flux in the baffle-tube. The ϕ_2 is given by

$$\phi_2 = \frac{q_b''' R_3}{2} - \frac{R_4}{R_3}\left(\frac{q_b''' R_4}{2} - \frac{Q'}{2\pi R_4}\right), \tag{8}$$

where q_b''' is heat flux density of the baffle-tube, R_3 is the baffle-tube outer radius, R_4 is the baffle-tube inner radius, Q' is the heat flowed into the baffle-tube, h_f is the heat transfer coefficient of the outer surface of the baffle-tube. The h_f' is given by

$$h_f' = \frac{Nu' \lambda'}{X}, \tag{9}$$

where Nu' is the Nusselt number, λ' is the thermal conductivity of the water, X is the length of boundary layer. Nu' is given by

$$Nu' = 0.0246\, Gr^{2/5} Pr^{7/5}\left(1 + 0.494\, Pr^{2/3}\right)^{-2/5}. \tag{10}$$

The Grashof number Gr is given by

$$Gr = \frac{g \beta \Delta T X^3}{\nu'^2}, \tag{11}$$

where g is the gravitational acceleration, β is the thermal expansion of water, ΔT is the temperature difference, Pr is the Prandtl number of water.

The temperature T_4 of the baffle-tube is obtained by

$$T_4 = T_3 + \frac{q_b'''}{4k}\left(R_3^2 - R_4^2\right) - \frac{R_4}{k}\left(\frac{q_b''' R_4}{2} - \frac{Q'}{2\pi R_4}\right) ln\left(\frac{R_3}{R_4}\right), \tag{12}$$

where T_3 is the temperature of the baffle-tube outer surface.

The temperature difference ΔT_{sat} between the specimen surface and the saturation temperature of bulk water is obtained by

$$\Delta T_{sat} = 0.82\, q_s'''^{1/4} e^{-P/63}, \tag{13}$$

where q_s''' is the heat flux of the specimen, P is the pressure of the specimen cooling water.

The specimen center temperature T_c is obtained by

$$T_c = T_s + \frac{q_s'''}{8k} t^2, \tag{14}$$

where T_s is the temperature at specimen surface, t is the thickness of specimens.

IRRADIATION EXAMINATION

Conditions of experiment

pressure	75kg/cm^{2}g,
flow rate	800g/min.

A result of the irradiation is shown in Fig.4. The irradiation temperature of specimen surface increased to 300°C and the water temperature become 285°C at a rated thermal power of 50MW in the JMTR and these temperature was constantly kept during irradiation.

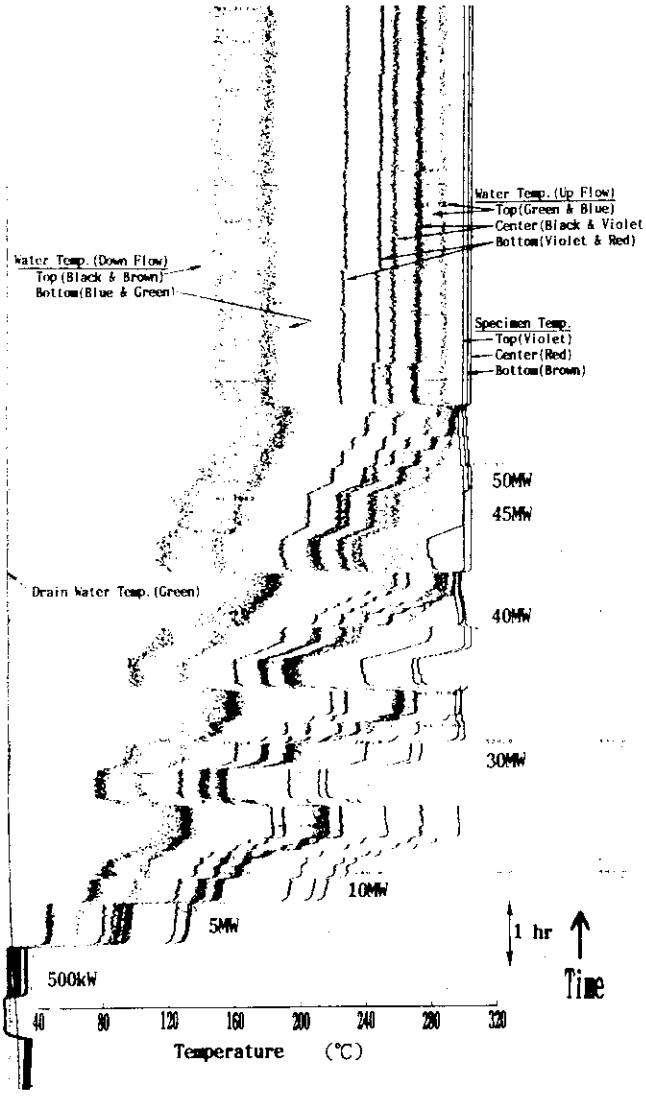

Fig.4. Results of irradiation on reactor start up and on changing flow rate of the water in the capsule.

Table 1. Temperature differences between experimental and calculated values.[4]

Distance from core center [mm]	Temperature differences, $T_{exp.} - T_{cal.}$ [°C]		
	Specimen surface	Up flow of water	Down flow of water
-130	1	11	- 4
0	4	7	———
180	0	0	11

By decreasing flow rate of the supplied water at low reactor power which corresponds to low γ heating in the JMTR, the specimen surface temperature became 300°C too.

The temperature differences between the experimental values and the calculated values are shown in Table 1. Regardless of distance from core center, the experimental values agree well with the calculated values.

CONCLUSIONS

The irradiation examination of reactor core structural materials of LWRs was carried out by using the capsule capable of controlling the saturation temperature of water. It is confirmed that this irradiation technique can simulate the LWR conditions as the high pressure and temperature water. And this technique can accelerate the study on IASCC in LWR conditions.

ACKNOWLEDGMENT

The authors wish to express their thanks to Mr. H. Itoh, Mr. M. Ouchi (JAERI) and Mr.K. Hide (CRIEPI) who participate in the discussion of this project. The authors are also grateful to the members of reactor division 1 operating the reactor and irradiation division 2 operating the irradiation facilities for cooperation in the study.

REFERENCES

[1] J. E. LE SURF, "Life Extension and Water Chemistry of LWRs," *Proc. JAIF Int. Conf. Water Chemistry in Nuclear Power Plants*, Tokyo, Japan, April 19-22, 1988, Vol. 2, p. 575, Japan Atomic Industrial Forum (1988).

[2] T. HAYASHI, H. ANDO, H. TAKAHASHI and K. ONODERA, "Measurement of Gamma-Heat in the JMTR," *J. Nucl. Sci. Technol.*, **9**, 1 (1972).

[3] Y. HARAYAMA, H. SOMEYA and M. NIIMI, "SATCAP-B ; A Program for Thermal-Hydraulic Design of Saturated Temperature Capsule," *JAERI-M 89-187*, Japan Atomic Energy Research Institute (1989).

[4] Y. HARAYAMA, H. SOMEYA, M. NIIMI, et al., private communication, 1989.

7. Programmed Temperature Control of Capsule in Irradiation Test with Personal Computer at JMTR

H. SAITO, T. URAMOTO, M. FUKUSHIMA, M. OBATA
S. SUZUKI, C. NAKAZAKI, and I. TANAKA

Department of JMTR Project
Oarai Research Establishment, JAERI
Oarai-machi, Higashiibaraki-gun, Ibaraki-ken 311-13, Japan

ABSTRACT

The capsule irradiation facility is one of various equipments employed at the Japan Materials Testing Reactor (JMTR). The capsule facility has been used in irradiation tests of both nuclear fuels and materials.

The capsule to be irradiated consists of the specimen, the outer tube and inner tube with a annular space between them. The temperature of the specimen is controlled by varying the degree of pressure (below the atmospheric pressure) of He gas in the annular space (vacuum-controlled). Beside this, in another system the temperature of the specimen is controlled with electric heaters mounted around the specimen (heater-controlled).

The use of personal computer in the capsule facility has led to the development of a versatile temperature control system at the JMTR. Features of this newly-developed temperature control system lie in the following: the temperature control mode for a operation period can be preset prior to the operation; and the vacuum-controlled irradiation facility can be used in cooperation with the heater-controlled.

The introduction of personal computer has brought in automatic heat-up and cool-down operations of the capsule, setting aside the hand-operated jobs which had been conducted by the operators. As a result of this, the various requirements seeking a higher accuracy and efficiency in the irradiation can be met by fully exploiting the capabilities incorporated into the facility which allow the cyclic or delicate changes in the temperature.

This paper deals with a capsule temperature control system with personal computer.

1. INTRODUCTION

The JMTR, a light water-moderated and cooled tank-type reactor, was built for the chief purposes of irradiating nuclear fuels and materials and for isotope production. Currently, the JMTR is operated at a rated thermal power of 50 MW for an operation period of 26 days with two-day long shutdown for refueling operation at the middle of the operation period. In the core where the irradiation holes are located, the thermal neutron flux ranges

from 0.1 x 10^{18} n/m^{2}s through 3 x 10^{18} n/m^{2}s and the fast neutron flux from 0.01 x 10^{18} n/m^{2}s to 2 x 10^{18} n/m^{2}s. The reactor core configuration is shown in Fig.1.

At the JMTR, a wide variety of irradiation facilities such as the loop irradiation facilities, hydraulic rabbit irradiation facilities, power ramping test facility and capsule irradiation facilities have been built to meet the diversified requirements for the irradiation from customers.

The capsule irradiation facility is so versatile that it can be used in various irradiation tests since the location of the irradiation hole into which a capsule goes can be determined according to the purpose of the irradiation test, taking into consideration the neutron flux, neutron energies and gamma heating.

A temperature at which a specimen is bombarded with neutrons is the most significant item among those subjected to the control in an irradiation test so that, at the JMTR, a lot of ways of capsule temperature control have been employed with a view to satisfying requirements set out for the irradiation.

At present, basically the two control methods of capsule temperature are in use at the JMTR. Firstly, the vacuum-controlled method, in which the thermal conductivity between the inner tube of a capsule and the outer tube, the outside of which is in contact with reactor primary coolant, is varied by changing the degree of vacuum in the annular thermal insulation space (gas gap space) formed between the inner tube and the outer one so as to control the temperature of the specimen being accommodated in the inner tube. Secondly, the heater-controlled method, in which more than one specimens loaded in one capsule, one over another, can be controlled in temperature individually with the electrical heater winded separately on each specimen by regulating electrical supply to each heater, thus enabling each specimen to be controlled over an extensive temperature range. In addition to these, the third capsule temperature control method is a combination of the two methods stated above.

2 CAPSULE TEMPERATURE CONTROL METHODS

2.1 VACUUM-CONTROLLED METHOD

The vacuum-controlled system has been used at the JMTR for about 20 years since it was developed at the time the JMTR came into operation. A vacuum-controlled capsule temperature control panel on the floor round the reactor varies the degree of pressure of the helium gas in the thin gas gap in a low pressure range of 1.4 x 10^5 Pa through 1.3 x 10^2 Pa.

While the reactor is in its power-up phase at the beginning of an operation period, the capsule temperature is kept low (in damp state) by filling the gas gap with helium gas at 1.4 x 10^5 Pa. After the rated power of the reactor is attained, the leak valve (motor-operated valve in Fig.3) is gradually opened with the flow control valve for feeding the helium gas opened to a slight degree, allowing the helium gas to flow at a rate of 5.5 x 10^{-5} g/s. The opening of the leak valve results in reducing the pressure in the gas gap down below the atmospheric pressure, causing the specimen temperature to rise. The heat-up operation continues until the desired temperature of the specimen is reached. The heat-up operation is followed by shifting the flow control valve to automatic control so as to maintain the specimen temperature at the desired temperature.

The cool-down operation at the end of the irradiation is carried out

before the reactor is shut down. The cool-down procedure begins with shifting the flow control valve from automatic control to manual one, followed by a gradual closing of the leak valve to close it completely, bringing the capsule into the damp state. Fig.2 shows data of the irradiation test in this method.

2.2 HEATER-CONTROLLED METHOD

In this system the temperature of a specimen is regulated by altering the amount of electricity fed into the heater winded on the specimen being controlled.

More than one specimens, up to 6, can be loaded one over another in a capsule, with heater mounted individually on each specimen, thus enabling each specimen to be separately controlled in its temperature at will. In the heat-up operation for the capsule, no electrical power is supplied to the heaters on the specimens before the rated power of the reactor, 50 MW, is attained. Once the rated power is reached, the specimen temperature are raised up to the desired value by means of adjusting the power supply to each heater. On attaining the steady state of the capsule, the temperature controller on the capsule control panel is shifted to automatic control from manual control.

The features of this control method lies in the fact that an even temperature distribution across each specimen can be achieved even though each specimen can be controlled at a temperature different from that of another. However the difficulty encountered in incorporating an electrical heater with a great power in the capsule due to limitation in size of the capsule does not allow the heater-controlled capsule to be controlled so wide temperature range as the vacuum-controlled capsule to be done, confining a temperature range for which the heater controlled method is applicable to a relatively low temperature region.

2.3 COMBINED CONTROL SYSTEM

The combined control system incorporates in one system the features of the two methods stated above. In this method, the temperature of the specimen is elevated up to that slightly below the desired one by adjusting the degree of vacuum in the gas gap with the flow controller on manual position for the helium gas being regulated, and further heating of the specimen up to the target temperature is carried out by means of the heater controller to adjust the amount of heat from the heater before the heater controller is shifted to automatic control.

The heat-up operation with the combined control system is performed after the rated thermal power of the reactor, 50 MW, is attained. The cool-down operation with the combined method is conducted before the reactor is shut down, by lowering the specimen temperature through the reduction of electrical power supply by means of the heater temperature controller and then by the vacuum control system to cool all the specimens down.

2.4 CAPSULE TEMPERATURE CONTROL WITH PERSONAL COMPUTER

2.4.1 THE BACKGROUND OF THE DEVELOPMENT

Requirements for the irradiation from customers have been so

diversified as to necessitate improvements in the irradiation techniques available at the JMTR in order to meet the demands which seek possibilities of altering the specimen temperature in a cyclical manner in a irradiation period, heating up and cooling down the specimen temperature in linear or step-wise fashion at a predetermined rate and of maintaining the specimen temperature constant even in a shut-down period as well as in power-up period of the reactor.

To satisfy these requirements through the use of conventional systems requires the preset values at which the temperature of a specimen is aimed to be changed by operators whenever need arise. Heat-up and cool-down of a capsule at a fixed rate are almost impossible to perform above all. For the purpose of satisfying these diversified requirements, a temperature control system with personal computer incorporated has been developed on the basis of knowledge gained through both the vacuum-controlled and heater-controlled capsule temperature control methods.

2.4.2 PERSONAL-COMPUTERIZED CAPSULE TEMPERATURE CONTROL SYSTEM

As a combination of both the vacuum-controlled capsule temperature control system and the heater-controlled capsule temperatere control system, a personal-computerized capsule temperature control system has been developed with the aim of controlling automatically the temperature of the specimen in a capsule in a irradiation period according to the information previously stored in the personal computer on the control circuit as the program of the operation. This system is composed of the vacuum control section for adjusting the degree of vacuum in the gas gap space, heater control section to control the heater temperature, temperature measurement section performing both the jobs of measuring and controlling the specimen temperature, and the personal computer section for sending signal to the control circuit on the basis of the programmed instruction, for gathering data on the specimen temperature and for observing the operational conditions of the capsule. This control panel is shown in Fig.3.

3. DATA GAINED THROUGH THE PERSONAL-COMPUTERIZED CAPSULE TEMPERATURE CONTROL SYSTEM

3.1 TEMPERATURE-VARIED IRRADIATION TEST

In capsule irradiation tests done up to now, the specimen temperature was kept constant when the reactor is operated at its rated output. Recently, however, endeavor to find the effect of variation of temperature on the brittlement induced in a material during the irradiation in view of its possible application in the fusion reactor under conditions where the temperature varies has required irradiation tests to be conducted with the temperature of the specimen varied. To comply with this requisition, irradiation tests conducted by employing the capsule temperature control system having personal computer to vary the specimen temperature repeatedly. The high temperature and low temperature at which the specimen is irradiated are given in the personal computer in advance as the operational direction together with the rates at which the temperature rises and lowers, in addition to the period for which the temperature is maintained and the number of the repeat of the temperature variation in a cyclic manner in order that the irradiation test is regulated by the signal from the stored

instructions. Fig.4 shows data of the irradiation test.

The capsule containing the four specimens, which were arranged one over another, was subjected to the irradiation test for the first half period of a JMTR operation period during which one specimen was maintained at a fixed temperature while the other three were changed in their temperature in a cyclical manner. In the second half operation period, a heater controlled system and a vacuum controlled system were brought into one system so as to conduct the irradiation test in which all the four specimens were subjected to the cyclical change in the temperature.

With the first half operation period, the range in which the temperature was varied was not so great as originally planned, however in the second half a temperature range, from 300 °C to 440 °C, was large enough to meet the predetermined temperature range.

3.2 IRRADIATION TEST AT A FIXED TEMPERATURE FOR THE WHOLE OPERATION PERIOD

A power-up operation of the JMTR lasts about 8 hours before attaining its rated power of 50 MW so as to prevent thermal stress from occurring in the irradiation facilities owing to a rapid rise in the temperature. During the power-up phase of the reactor, the specimen being irradiated is kept at a temperature below the desired temperature.

However, lately, it has been brought to light that the irradiation of materials at a lower temperature seemed to affect the specimen adversely from the point of view of metallurgy,thus requiring the material to be irradiated at a fixed temperature in the whole irradiation period.

To investigate into the effect of temperature change on the properties of the material, at the JMTR, irradiation test was performed with a capsule containing the four specimens through the use of the capsule temperature control system with personal computer installed. The temperature of the three specimens was elevated as high as the desired one prior to the start-up the reactor through the heater-controlled system and the control system was shifted to automatic control. As the output of the reactor went up, the output of the heater control system reduced automatically to maintain the specimen temperature at a constant value because the gamma heating of the specimens increase as reactor output goes up. On the other hand the other specimens was heated up to the desired temperature after the full power of the reactor was attained. Data on the capsule temperature in the phase of the reactor power-up is presented in Fig.5. With the specimen which was not controlled, the greatest change in the specimen temperature occurred at a rate of about 40°C/10 min when the power of the reactor was altered from 15 MW to 30 MW, while the corresponding change in the temperature took place in the specimens controlled was as small as about 5°C.

4. CONCLUSIONS

Conventional irradiation tests in which the specimen temperature is maintained constant have been conducted by using the personal-computerized capsule temperature control system. Although the newly developed irradiation tests in which the specimen temperature is varied in an cyclical fashion or is kept at a fixed value have been conducted with only several capsules through the use of the personal-computerized capsule temperature

system, the versatility of the system in irradiation tests was fully confirmed as stated above.

The diversified requirements in the irradiation test would lead to the improvement of associated technology in the future so that the importance of the personal-computerized capsule temperature control system should be magnified accordingly. To better the capability of the system, further improvements in the controllability of the system as well as the extension of the scope in which the control of the capsule based on the programmed instructions works have to be materialized for the purpose of meeting the demands put forth for the irradiation tests carried out at the JMTR.

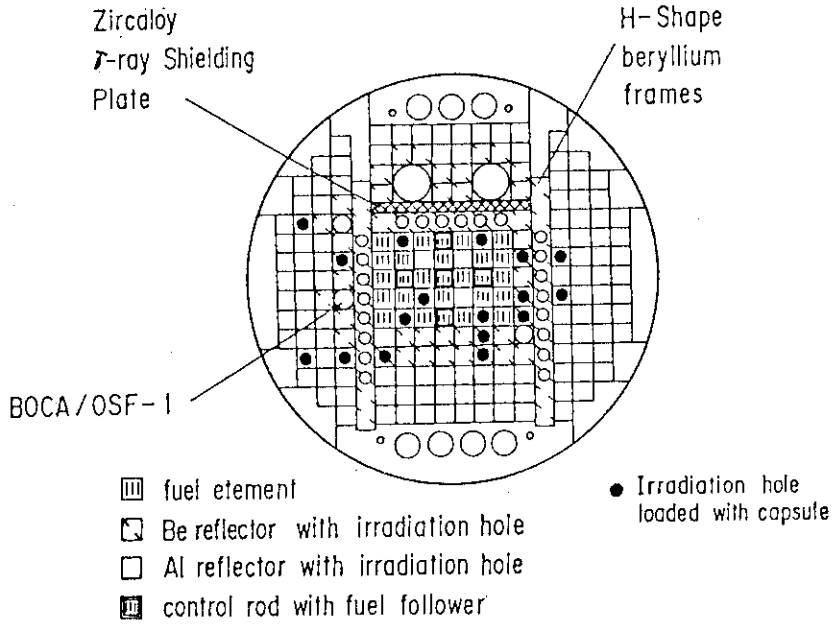

Fig.-1 Reactor Core Arrangement of the JMTR

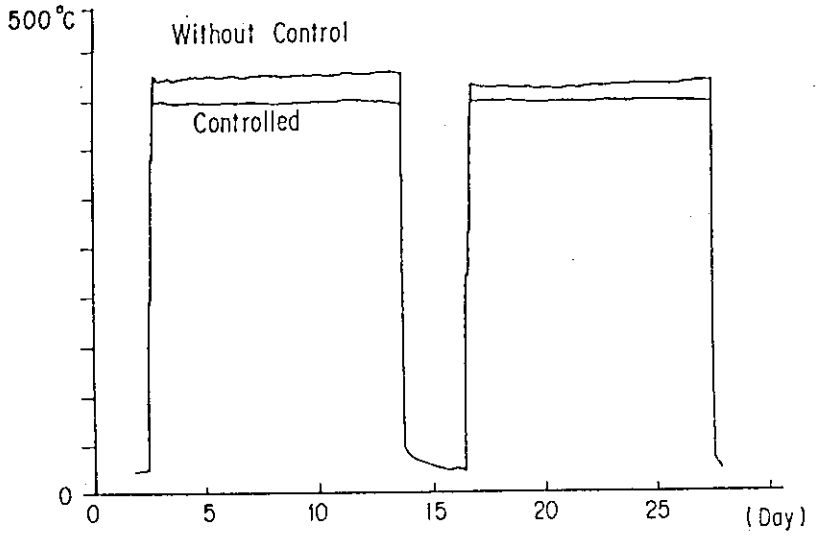

Fig.-2 Comparison Between Temperature Controlled And One Without Control

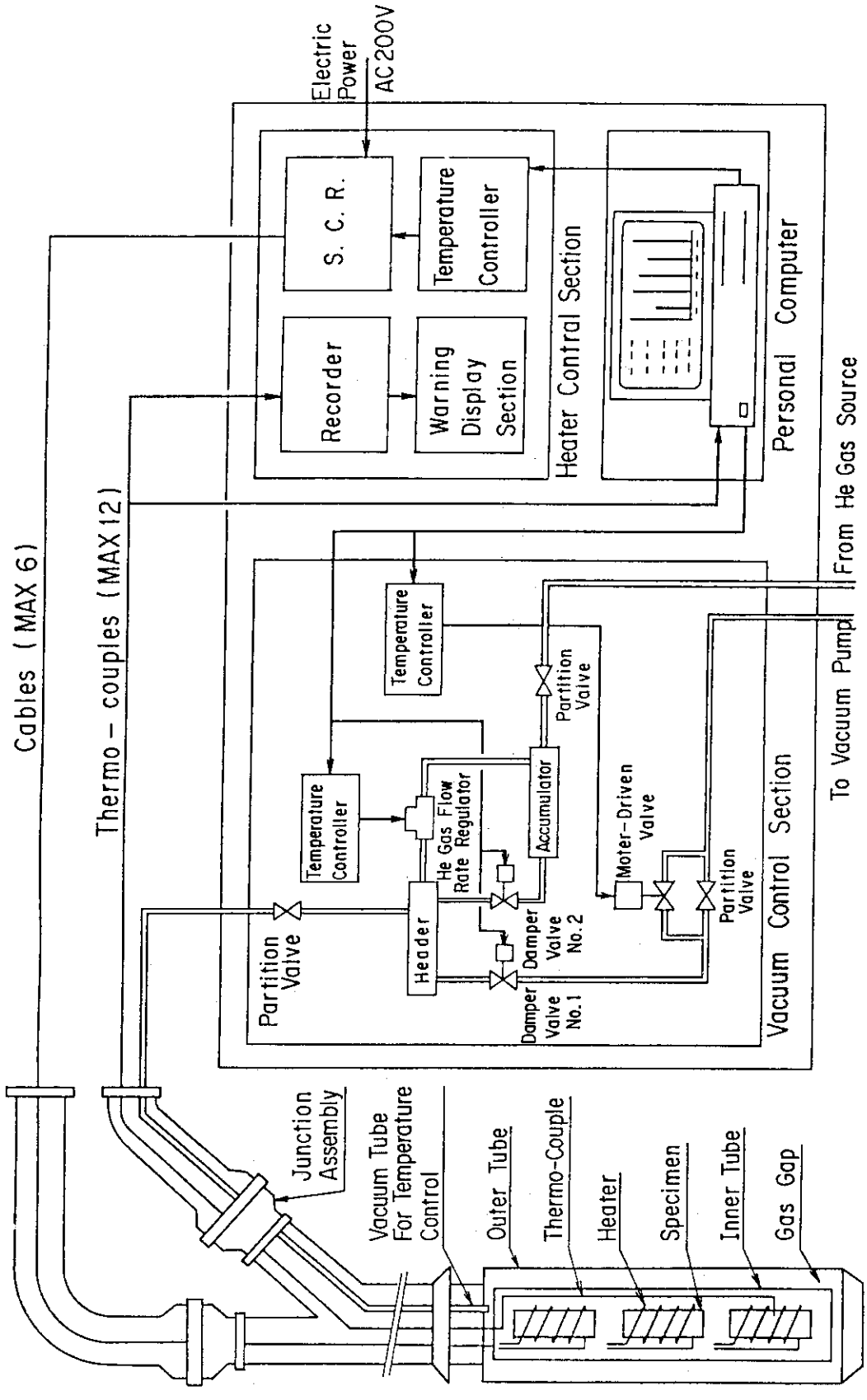

Fig.-3 Automated Capsule Control Panel

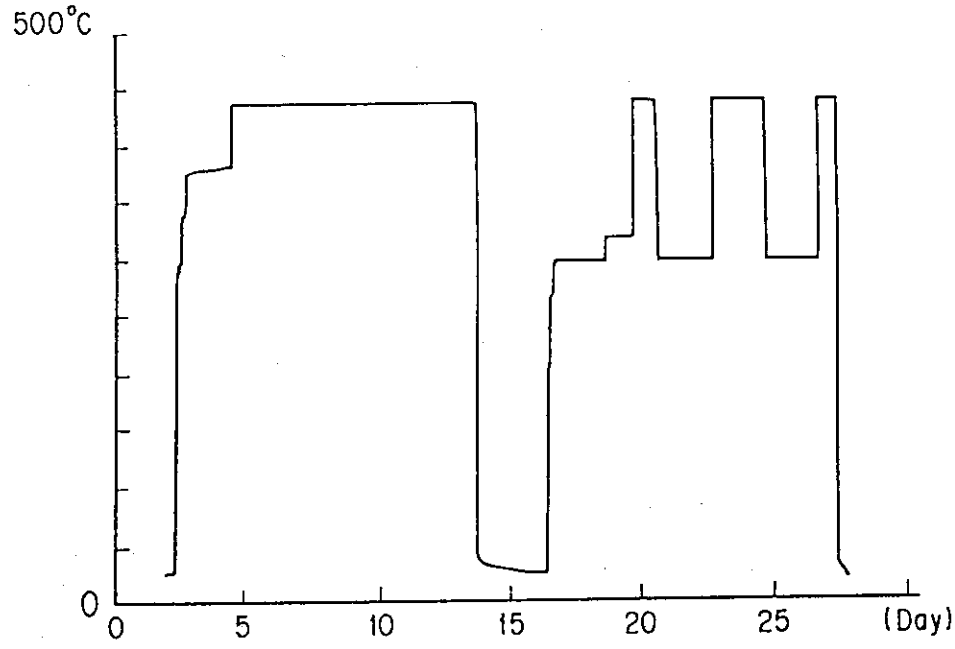

Fig.-4 Capsule Temperature Variation Produced By The Automated Controller With Personal Computer

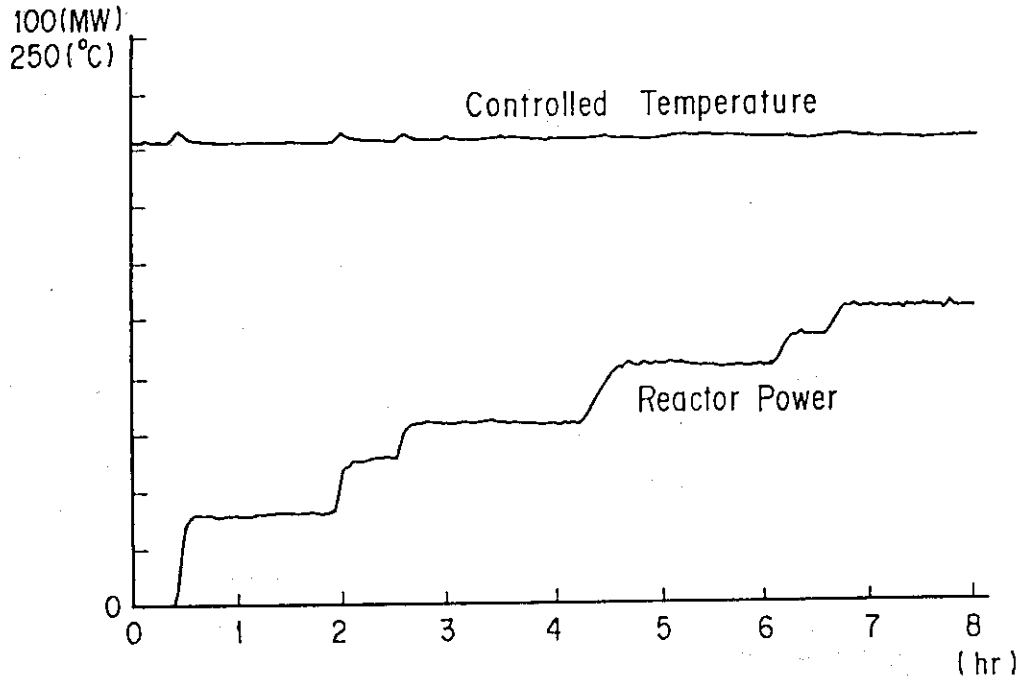

Fig.-5 Specimen Temperature Maintained Constant Against Step-Wise Increase In Reactor Power

8. Irradiation Facilities in JRR-3M

Akitoshi OHTOMO, Masamitsu SIGEMOTO, Hidetake TAKAHASHI

Department of Research Reactor
Tokai Research Establishment
Japan Atomic Energy Reseach Institute
Tokai-mura, Naka-gun, Ibaraki-ken, JAPAN

ABSTRACT

Irradiation facilities have been installed in the upgraded JRR-3(JRR-3M) in Japan Atomic Energy Research Institute(JAERI). There are hydraulic rabbit facilities(HR), pneumatic rabbit facilities(PN), neutron activation analysis facility(PN3), uniform irradiation facility(SI), rotating irradiation facility and capsule irradiation facilities to carry out the neutron irradiation in the JRR-3M. These facilities are operated using a process control computer system to centerize the process information.

Some of the characteristics for the facilities were satisfactorily measured at the same time of reactor performance test in 1990.

During reactor operation, some of the tests are continued to confirm the basic characteristics on facilities, for example, PN3 was confirmed to have enough performane for activation analysis. Measurement of neutron flux at all irradiation positions has been carried out for the equilibrium core.

1. INTRODUCTION

The old Japan Research Reactor NO.3(JRR-3) with the thermal power of 10MW was a tank type, heavy water moderated and cooled reactor, and it was the first domestically constructed reactor in Japan.

In recent years, high quality irradiation conditions including high neutron flux have been required for neutron irradiation and neutron beam experiments in research reactors. To fulfil these requirements, it was decided that JRR-3 should be reconstructed for upgrading.

The JRR-3 had been operated for 21 years and shut down in 1983. The construction of the upgraded JRR-3(JRR-3M) had started in 1985,and completed in 1990. The old reactor was removed from the reactor room, and the new reactor is reconstructed at the place where the old core was. JRR-3M is a pool type, 20MW(th), light water moderated and cooled, beryllium and heavy water reflected, and the fuel is 20% enriched UAlx-Al(LEU) plate type. Irradiation facilities are also installed in the JRR-3M.

The irradiation facilities consist of a short term irradiation facility where samples can be loaded/unloaded into the core during reactor operation, and a long term irradiation facility where samples are loaded into the core prior to reactor operation and unloaded after reactor shutdown. A short term irradiation facilities include two hydraulic rabbit facilities(HR), two pneumatic rabbit facilities(PN), an activation analysis facility(PN3) and an

uniform irradiation facility(SI). A long term irradiation facilities include a rotating irradiation facility(DR) and ten capsule irradiation facilities (RG, BR, VT, SH).

These facilities are operated and monitored using process control computer system. The computer is linked to a management computer system to manage the irradiation data and schedule.

Arrangement of the irradiation facilities in the JRR-3M are shown in Fig. 1. The outline of the irradiation facilities are given in Table 1.

2. Hydraulic rabbit facility(HR)

This facility consists of irradiation circuit and transfer circuit. In irradiation circuit, coolant water circulate through irradiation tube located in the core. In transfer circuit, a rabbit is loaded and transferred to irradiation circuit and unloaded from the irradiation circuit.

A rabbit is 32 mm of outer diameter, 150 mm of length, which is made of aluminum or stainless steel.

A feature of this facility is to have three circuits for unloading individually the three rabbits in the irradiation tube, independently for the better efficiency of the utilization facility. Several newly developed equipments such as individual irradiation tubes, 8-port ball valve type transferrer and a new control system are used for this facility.

Fig. 2 shows a schematic drawing of hydraulic rabbit facility.

3. Pneumatic rabbit facility(PN)

The configuration of this facility is essentially the same as that of the hydraulic rabbit facility. The coolant is nitrogen gas for the irradiation circuit and compressed air for the transfer circuit.

A rabbit for PN is 33 mm of outer diameter, 95 mm of length, which is made of polyethylene or polyimide(for several hours irradiation).

This facility allows to irradiate two rabbits at the time. In contrast to the hydraulic facility, individual transfer system is not provided because of the short irradiation time.

Fig. 3 shows a schematic drawing of pneumatic rabbit facility.

4. Activation analysis facility(PN3)

In this facility, a sample in a small rabbit is irradiated for activation analysis. Nitrogen gas is used as a transfer medium.

The analysis system is located close to the reactor to shorten the traveling time of the rabbit. It brings accurate analysis for short-lived nuclides(about 10 sec).

A rabbit for PN3 is about 17 mm of outer diameter, 30 mm of length, which is made of polyethylene. A rabbit can be held at both the bottom and upper positions in the irradiation tube for the two corresponding types of neutron flux.

The measurement of radioactivity and the analysis of nuclides are accomplished with a multi-channel analyzer and a mini-computer system.

Fig. 4 shows a schematic drawing of activation analysis facility.

5. Uniform irradiation facility(SI)

This facility is designed to uniformly irradiate large sized samples such as a single crystal of silicon. Samples up to about 130 mm of diameter and 300 mm of length can be used for SI.

The sample is rotated about 2 r.p.m. during irradiation, and its position in the reactor can be adjusted vertically corresponding to the shift of neutron flux distribution due to fuel consumption. By this method, the sample is irradiated to be radially and vertically uniform.

The neutron exposure is monitored by three SPNDs(self-powered neutron detector), and the sample is transferred from the reactor core to cooling bed when the exposure reached to the preset value.

Thermal neutron flux for SI has a good flatness for axial direction and a enough quality since the irradiation tube is located in heavy water tank. Sufficient uniformity of neutron exposure for the sample can be expected.

Figure 5 shows the arragement of the uniform irradiation facility in the reactor pool.

6. Rotating irradiation facility(DR)

In this facility, a capsule is inserted into the heavy water reflector region for long-term thermal neutron irradiation. This capsule can contain relatively large samples.

The capsule is rotated alternatively to have uniform irradiation, and the sample temperature can be monitored during irradiation to provide irradiation data.

7. Capsule irradiation facility(VT, RG, BR, SH)

This facility allows the insertion of fuel or material capsules into the fuel and beryllium reflector regions in the core for long-term, thermal and fast neutron irradiation.

The temperature of the sample can be continuously controlled during irradiation using a mixed gas control system, a vacuum control system or an electric heater control system. These are based on control of the thermal resistance of cooling from sample to coolant.

Figure 5 shows an arragement of the capsule irradiation facility in the reactor pool.

8. Instrumentation and Control system

Instrumentatin and control system of irradiation facility is distributed to close to the equipment in the reactor building and the experimental building.

It consists of process control computer, control stations and detector such as flowmeters or pressure gauges.

In the HR and PN, process of irradiation is carried out automatically by sequence of the computer using time schedule data prepared by JRR-3M management computer system.

PN3 has a control panel in the analysis room, and allows set parameters such as operation mode, irradiation position, irradiation time. Irradiation are carried out by sequence of the computer.

The temperature control system of the capsule irradiation facility is linked to process control computer, which is designed to control of capsule

temperature and make a report using mini-computer.

Since the information of the above mentioned facilities is centerized to the process control computer, operation and monitoring of the facilities are carried out using CRT of the computer at facility control room.

Hydraulic rabbit facility and pneumatic rabbit facility have a signal to stop the reactor operation when the flow rate of facilities decrease abnormaly.

Figure 6 shows an arragement of the capsule irradiation facility in the reactor pool.

9. Characteristic test

Performance test of irradiation facility had been carried out from April to October in 1990 after the reactor reached first critical. Characteristics of the irradiation port after the equilibrium core have measured at full power and low power condition of reactor since July to August of 1991. The thermal neutron fluxes at the irradiation position are 1×10^{14} n/cm²/sec for HR, 6×10^{13} n/cm²/sec for PN and 2×10^{13} n/cm²/sec for PN3. Table 2 shows a maximum neutron flux and Cd cut-off ratio of the irradiation facilities.

Fig.7 shows an activation analysis result for short-lived nuclide at PN-3 facility. The accuracy for quantitative analysis can be increased using a repeat irradiation method.

The performance of these facilities are evaluated to be satisfactory.

Table 1 Outline of irradiation facility

Irradiation facility	Region	Dimension of capsules(mm)	irradiation time	Irradiation Purpose
Hydraulic rabbit (HR-1, HR-2)	Heavy water tank	φ32xL150	20min -1cycle	Radioisotope production
Pneumatic rabbit (PN-1, PN-2)	Heavy water tank	φ33xL95	1-60min	Activation analysis Radioisotope production
Activation analysis (PN-3)	Heavy water tank	φ17xL30	5-120sec	Activation analysis
Uniform (SI)	Heavy water tank	φ130xL300	1-5hr	Si doping Material irradiation
Rotating (DR)	Heavy water tank	φ130xL1000	1-5cycle	Large volume sample irradiation
Capsule (VT, RG) (BR) (SH)	Fuel	φ55xL914	1-20cycle	Fuel/Material irradiation
	Be reflector	φ40xL914		Radioisotope production
	Heavy water tank	φ90xL914		

Table 2 Maximum neutron flux and Cd cut-off ratio

Facility	Thermal neutron flux(n/cm2/sec)	Fast neutron flux(n/cm2/sec)	Cd cut-off ratio	Note
HR－1	1×10^{14}	6×10^{11}	10	
HR－2	9×10^{13}	5×10^{11}	10	
PN－1	6×10^{13}	6×10^{10}	30	
PN－2	5×10^{13}	5×10^{10}	30	
PN－3	2×10^{13}	1×10^{9}	300	bottom
	1×10^{12}	5×10^{8}	900	upper
SI	2×10^{13}	—	70	
DR	3×10^{13}	—	50	
VT	3×10^{14}	2×10^{14}	3	
RG	2×10^{14}	1×10^{14}	4	
BR	2×10^{14}	1×10^{14}	4	
SH	4×10^{13}	—	50	

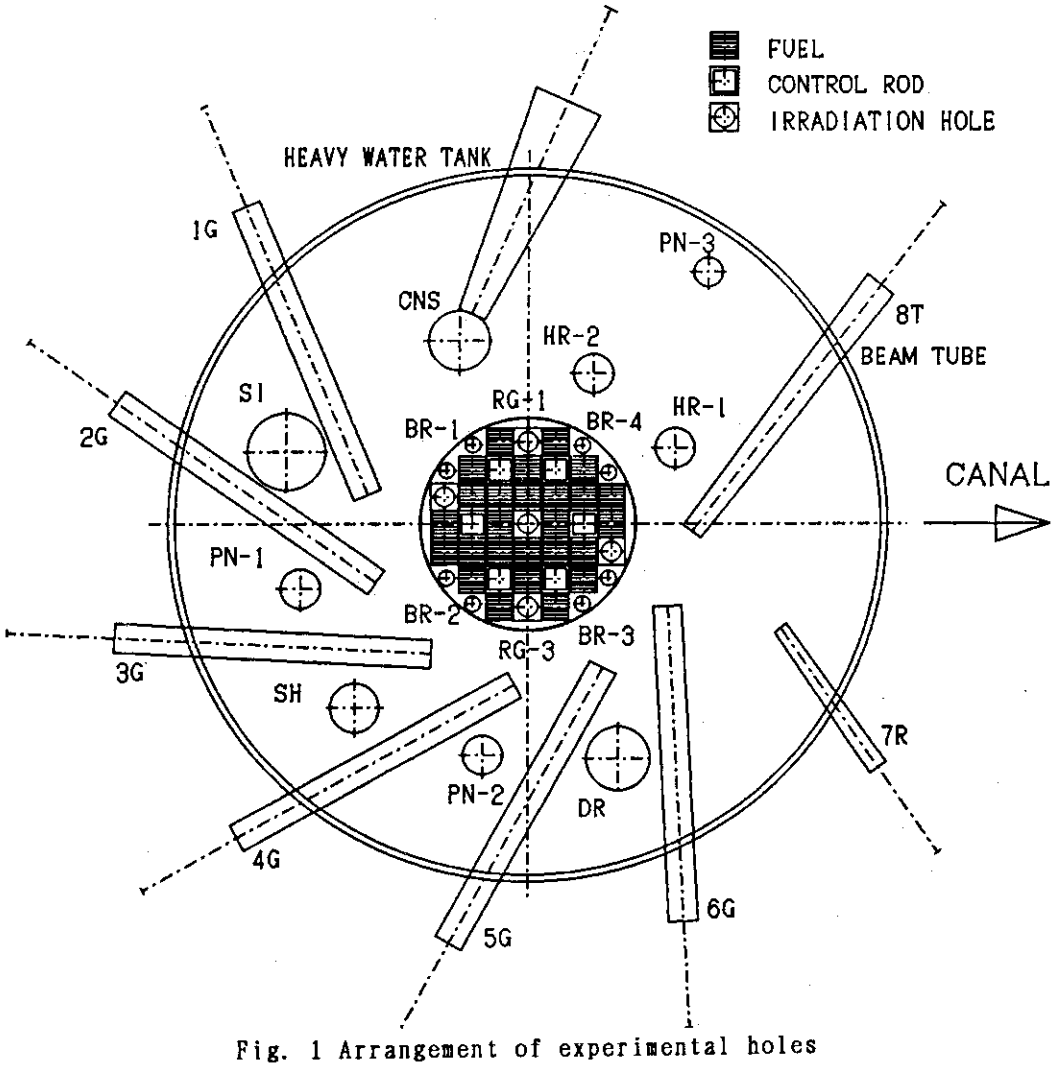

Fig. 1 Arrangement of experimental holes

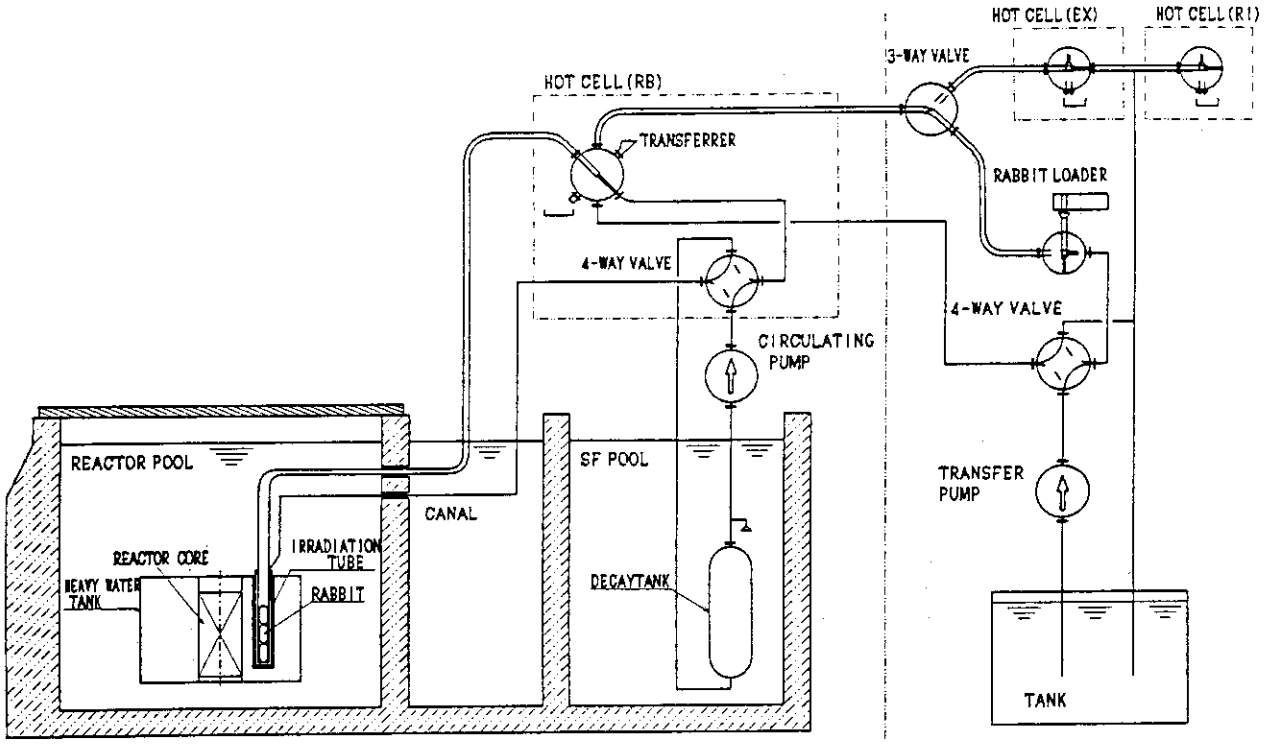

Fig. 2 Schematic drawing of hydraulic rabbit facility(HR)

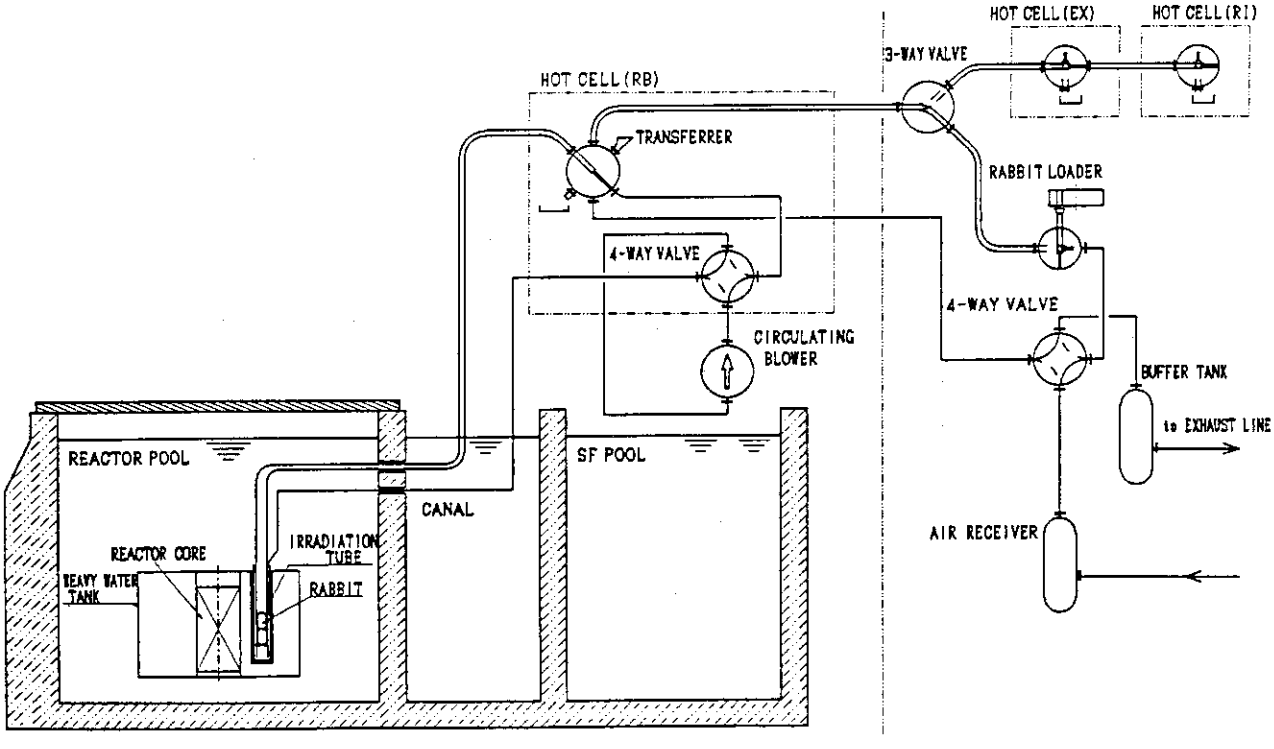

Fig. 3 Schematic drawing of pneumatic rabbit facility(PN)

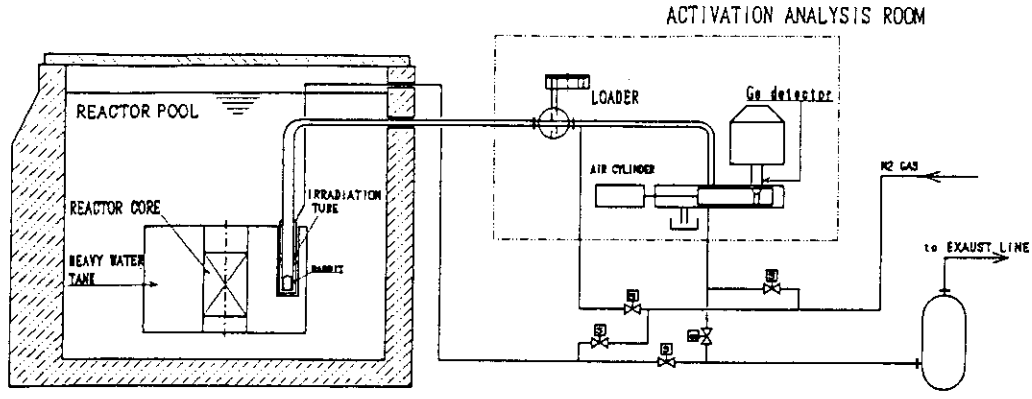

Fig. 4 Schematic drawing of activation analysis facility(PN3)

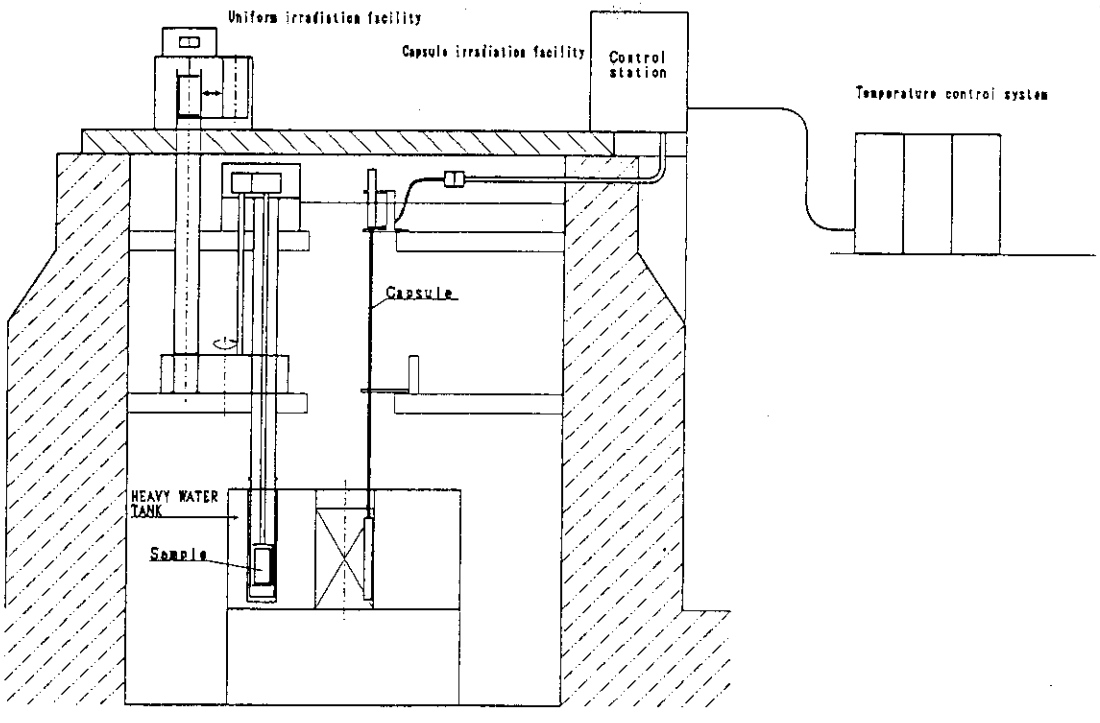

Fig. 5 Uniform irradiation facility(SI)
and capsule irradiation facility(VT, RG, BR, SH)

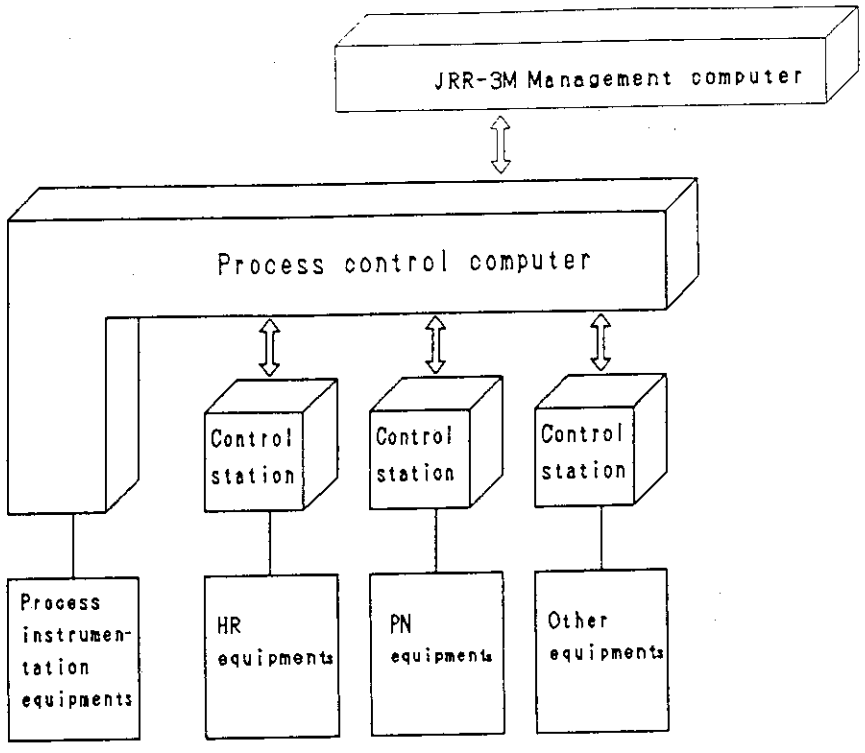

Fig. 6 Instrumentation and control system of irradiation facility

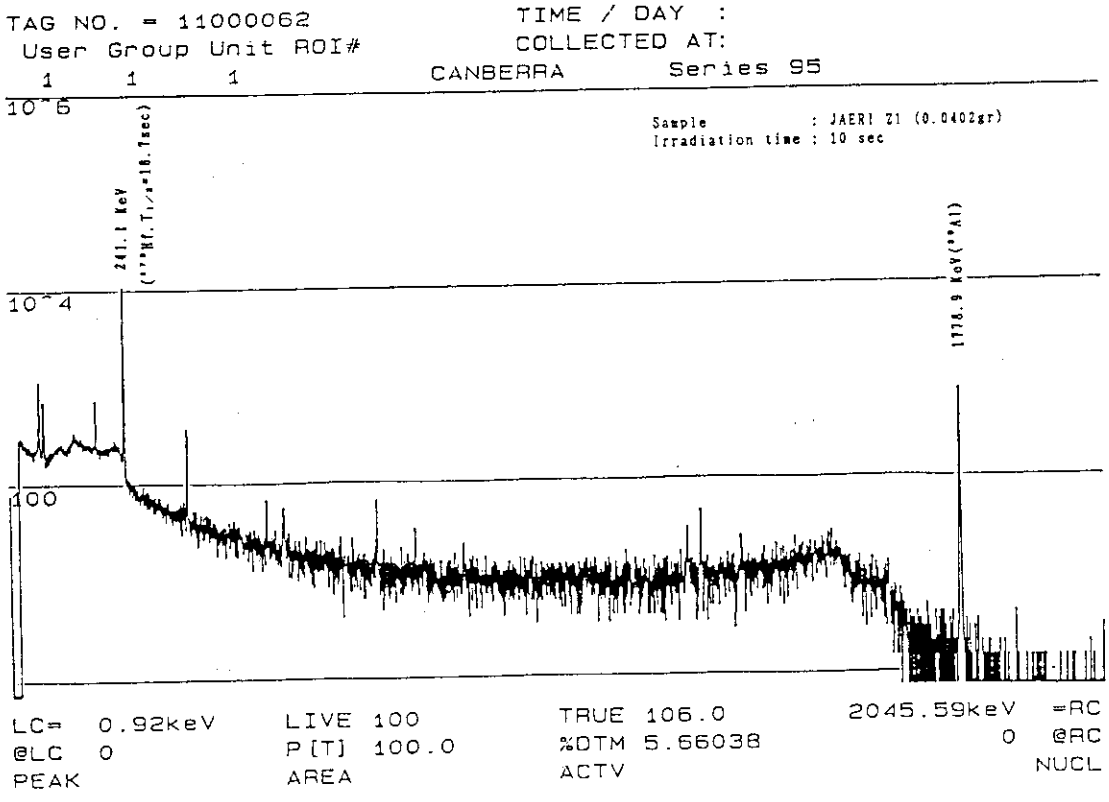

Fig. 7 Gamma spectrum of JAERI Z1 sample irradiated at PN3

1. Improvement of Neutron Irradiation Field of Research Reactors for BNCT

OTOHIKO AIZAWA

Atomic Energy Research Laboratory
Musashi Institute of Technology
Ozenji 971, Asao-ku, Kawasaki, 215 Japan

ABSTRACT

The modification of research reactors for an improvement of the irradiation field for BNCT has been investigated in comparison with the field characteristics of the "old" configuration at the Musashi reactor.

The new point of this study is that the evaluation has been done by using an arrangement including both the facility structure and a whole-body phantom, and also by considering the whole-body absorbed dose.

INTRODUCTION

In recent years, several research reactors in the world have been modified for Boron Neutron Capture Therapy(BNCT). The modification of the research reactor for BNCT is fairly old. The Musashi reactor was modified for BNCT in 1975, and ninety-nine patients with brain tumors and nine patients with melanoma were treated until 1989. After the suspension of the Musashi reactor for a tank leak problem, the improvement of the neutron irradiation field has been considered. Although the Musashi reactor is a TRIGA-type reactor, the results can also be applied for another type of reactors.

DEFINITION AND APPROXIMATION OF CALCULATIONS

Here we define the epithermal flux as the integrated flux from 0.1 eV to 3,350 eV, and we have the measured value of the epithermal flux without any phantom as 1.6×10^7 (n/cm^2sec) at the "old" irradiation port of the Musashi reactor. This value was used for the normalization of calculations. Also we define the faster-epithermal flux as the integrated flux from 3.35 keV to 821 keV, and the fast flux as the integrated flux from 821 keV to 17.3 MeV.

To make the explanation more convenient, we define the words, "spectrum shifter", "neutron filter", "gamma filter" and "neutron collimator" as shown in Fig. 1. The difference between the "spectrum shifter" and the "neutron filter" is the location against the core.

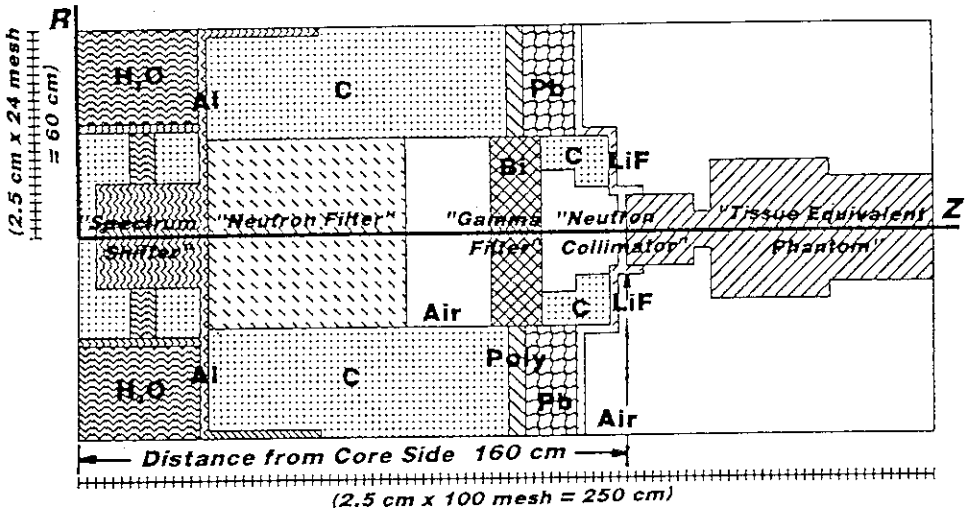

Fig. 1 Definition of "spectrum shifter" and "neutron filter" ("Spectrum shifter" is located inside of the reflector.)

A two-dimensional discrete ordinate transport code DOT3.5 was employed for the following calculations by adopting the S_{12} and P_3 approximations. The group constants used are the neutron and gamma coupled cross sections based on the BUGLE Library. The calculation was initiated from the "old" configuration at the Musashi reactor by using a shell source at the core side as shown in Fig. 2. The new point is that the calculation was done by the use of an arrangement including both the facility structure and a whole-body phantom as shown in the figure. The size of the mesh used for the calculations was 24 x 100 in R-Z geometry for 2.5 cm mesh-intervals.

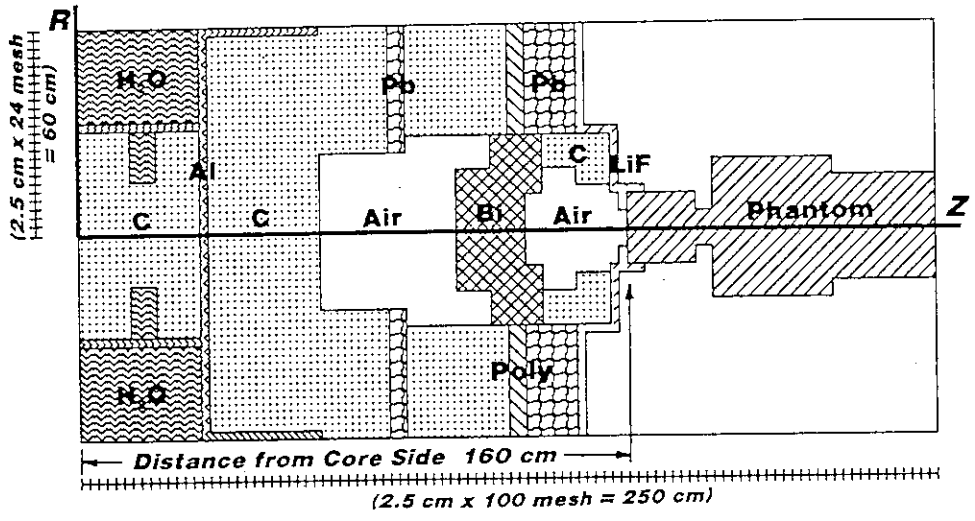

Fig. 2 "Old" configuration at the Musashi reactor

The dose rate distribution in a phantom was calculated assuming 30μg/g B-10 in tumor and 3μg/g B-10 in normal tissue by using 0.5cm mesh-intervals and using an arrangement shown in Fig. 5(a). The RBE dose was calculated using RBE values of 1.0 for all gamma rays, 1.6 for non-thermal neutrons and $^{14}N(n,p)$ protons, and 2.3 for $^{10}B(n,\alpha)Li$ reaction products. The maximum advantage depth(MAX AD) is defined here as the depth in a phantom where the total dose rate with 30μg/g B-10 equals the maximum total background dose rate. The advantage ratio is defined here as the quotient of the integral of the total dose with 30μg/g B-10 divided by the integral of the total background dose from 0 cm to the maximum advantage depth.

EFFECT OF NEUTRON COLLIMATOR FOR THERMAL BEAMS

In the "old" configuration of the Musashi reactor, the collimator diameter was changed from 5 cm to 20 cm. The results are shown in Table 1.

Table 1. Effect of "neutron collimator" for the "old" configuration at the Musashi reactor

"Old" Configuration of the Musashi Reactor at 100kW	Collimator Diameter (cm)			
	5	10	15	20
	Case-(01)	Case-(02)	Case-(03)	Case-(04)
Thermal Neutron Flux★ (n/cm²sec)	9.6E+8	1.7E+9	2.0E+9	2.0E+9
Epithermal Neutron★ Flux (n/cm²sec)	1.9E+7	2.2E+7	2.3E+7	2.3E+7
Faster-Epi Neutron★ Flux (n/cm²sec)	6.9E+6	6.6E+6	6.5E+6	6.3E+6
Fast Neutron Flux★ (n/cm²sec)	2.3E+6	2.2E+6	2.2E+6	2.2E+6
Gamma Dose Rate★ (cGy/hr)	68.9	175	246	276
Maximum Total Dose Rate with 30μg/g B-10 (RBE-cGy/hr)	2580	4890	5460	5550
Maximum Total Background Dose Rate (RBE-cGy/hr)	336	616	745	774
Irradiation Time★★ (Irr. Time) (hr)	7.45	4.06	3.36	3.23
Advantage Ratio with RBE	5.73	6.22	5.77	5.57
Maximum Advantage Depth (cm)	4.23	5.34	6.09	6.35
Eye Dose Rate (RBE-cGy/hr)	32.7	51.1	79.6	102
Eye Dose in Irr. Time (RBE-cGy)	244	207	268	331
Whole-Body Dose Rate (RBE-cGy/hr)	10.1	15.5	22.7	27.9
Whole-Body Dose in Irr. Time (RBE-cGy)	75.5	62.9	76.3	90.1
Whole-Body Dose Rate Except Head (RBE-cGy/hr)	5.16	5.82	6.83	7.63
Whole-Body Dose Except Head in Irr. Time (RBE-cGy)	38.4	23.6	23.0	24.6

★ flux values in front of a phantom ★★ time of irradiation in which the maximum total background dose becomes 2500 RBE-cGy.

In this table the neutron fluxes are the flux values in front of a phantom, and the irradiation time is defined here as the time of irradiation in which the maximum total background dose becomes 2,500 cGy. "Eye dose" is defined as the absorbed dose in the position of eye in a phantom. "Whole-body dose" is defined as the volume-averaged whole-body absorbed dose. "Whole-body dose except head" means the volume-averaged whole-body absorbed dose except the head portion, i.e., under the neck. It is clear from this table that "eye dose" was under 300 RBE-cGy, "whole-body dose" was under 100 RBE-cGy, and "except-head dose" was under 30 RBE-cGy in the usual treatment done in the Musashi reactor. It can also be seen that the maximum advantage depth is about 5∿6 cm in the "old" configuration.

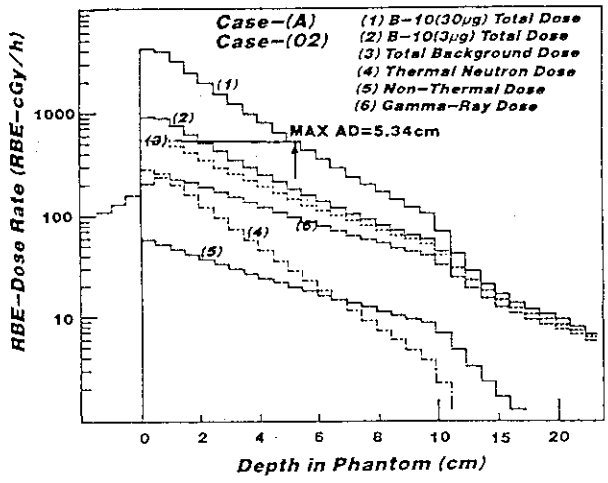

Fig. 3 RBE-dose rate distributions in a phantom for the "old" configuration at the Musashi reactor

The absorbed dose rate distribution in the phantom is shown in Fig. 3 in the case of the collimator diameter of 10 cm. The MAX AD is also shown in this figure. We can see that the absorbed dose rate of non-thermal neutrons is much lower than both the thermal neutron dose rate and the gamma dose rate in the "old" configuration.

SMALL MODIFICATION FOR THE "OLD" CONFIGURATION

Usually it is very difficult to change the structure of reflector in the reactor tank, but it is not difficult to modify the structure in the thermal column. Here we examined the small modification in the thermal column. The "gamma filter" of bismuth was fixed to 15 cm in thickness, and the collimator diameter was also fixed here to 15 cm in diameter. The configuration is shown in Fig. 4, in which the thickness X of carbon was changed from 32.5 cm to 42.5 cm. The results are shown in Table 2. We can see from this table that the irradiation time defined here is shortened under 3 hours. It is clear that the structure shown here is better than the "old" configuration at the Musashi reactor.

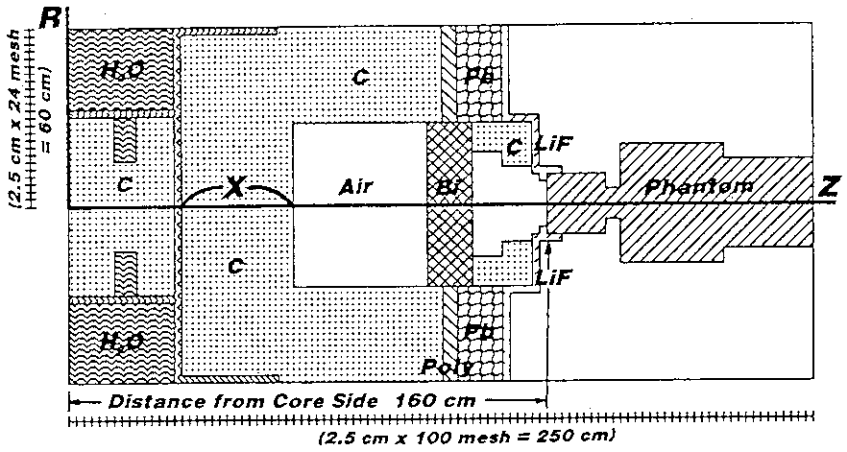

Fig. 4 Small modification for the "old" configuration

Table 2. Effect of carbon thickness as a "neutron filter"

"Small Modification" at 100kW Coll. Dia.=15cm Bismuth=15cm	Thickness of "Neutron Filter" of Carbon (cm)		
	32.5	37.5	42.5
	Case-(05)	Case-(06)	Case-(07)
Thermal Neutron Flux★ (n/cm²sec)	2.8E+9	2.4E+9	2.0E+9
Epithermal Neutron★ Flux (n/cm²sec)	3.2E+7	1.9E+7	1.1E+7
Faster-Epi Neutron★ Flux (n/cm²sec)	9.2E+6	5.3E+6	3.2E+6
Fast Neutron Flux★ (n/cm²sec)	3.4E+6	2.0E+6	1.2E+6
Gamma Dose Rate★ (cGy/hr)	356	297	245
Maximum Total Dose Rate with 30μg/g B-10 (RBE-cGy/hr)	7730	6470	5360
Maximum Total Background Dose Rate (RBE-cGy/hr)	1060	870	708
Irradiation Time★★ (Irr. Time) (hr)	2.35	2.87	3.53
Advantage Ratio with RBE	5.69	5.82	5.91
Maximum Advantage Depth (cm)	6.08	6.09	6.08
Eye Dose Rate (RBE-cGy/hr)	116	92.7	75.2
Eye Dose in Irr. Time (RBE-cGy)	274	266	266
Whole-Body Dose Rate (RBE-cGy/hr)	33.2	26.5	21.6
Whole-Body Dose in Irr. Time (RBE-cGy)	78.0	76.2	76.1
Whole-Body Dose Rate Except Head (RBE-cGy/hr)	10.6	8.33	6.68
Whole-Body Dose Except Head in Irr. Time (RBE-cGy)	24.9	23.9	23.6

★ flux values in front of a phantom
★★ time of irradiation in which the maximum total background dose becomes 2500 RBE-cGy.

EFFECT OF ALUMINUM AS SPECTRUM SHIFTER AND NEUTRON FILTER

Although the structure change of the reflector for the TRIGA reactor is usually difficult, there are some other reactors that the reflector elements can easily be replaced. As shown in Fig. 5, Case-(B) and (C) are the configurations that a part (30 cm in diameter and 30 cm in thickness) of the reflector is replaced to aluminum as a "spectrum shifter", and the "neutron filter" is also changed from carbon to aluminum in the case of Case-(C). The neutron energy spectra in front of the phantom are compared each other among Case-(A), (B) and (C) as shown in Fig. 6.

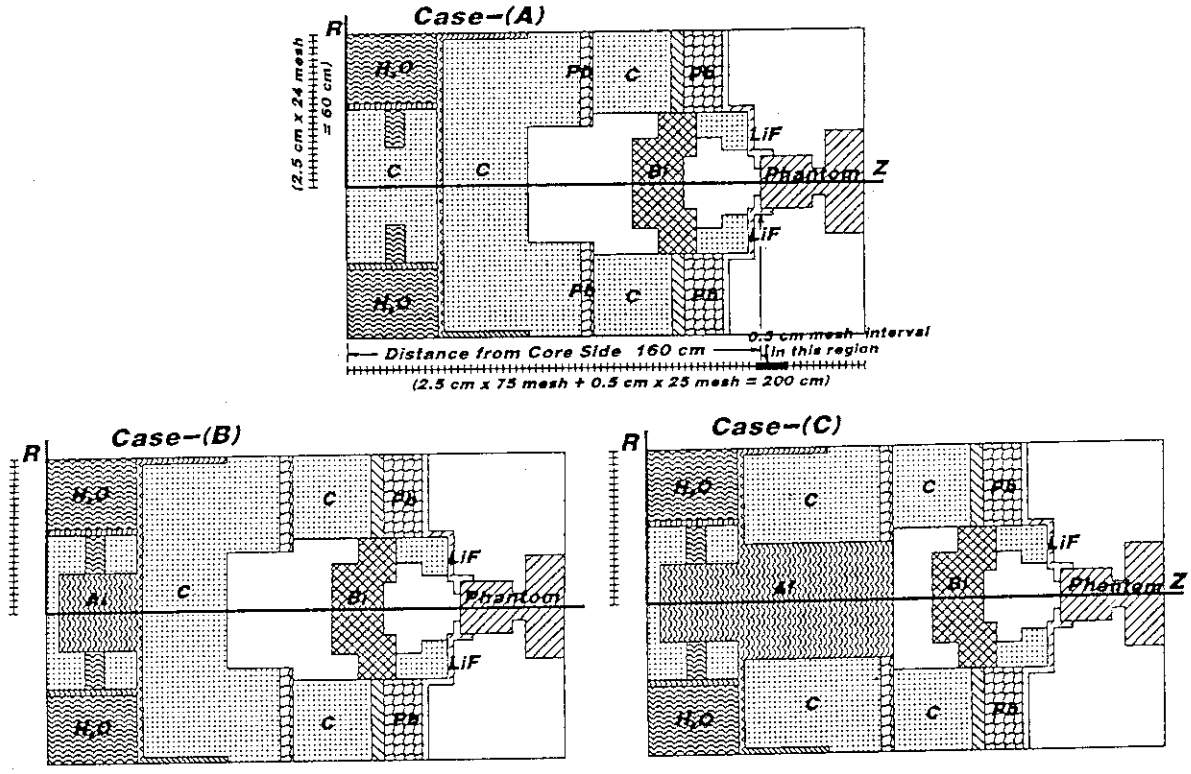

Fig. 5(a) "Old" configuration at the Musashi reactor
(b) Effect of aluminum as a "spectrum shifter"
(c) Effect of aluminum as "spectrum shifter" and "neutron filter"

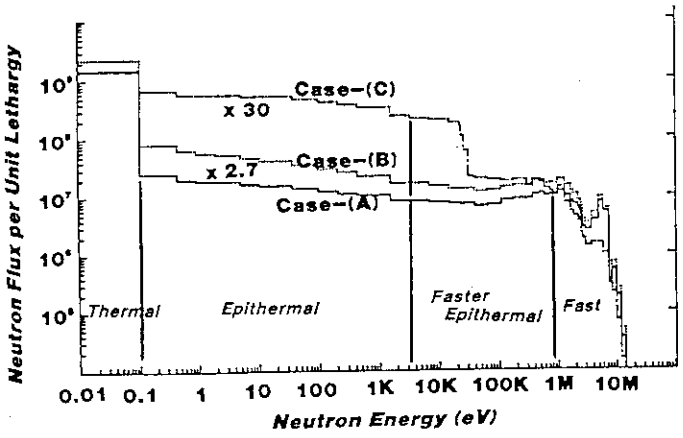

Fig. 6 Comparison of the energy spectra among Case-(A), (B) and (C)

The field characteristics are tabulated in Table 3. It can be seen that the thermal and epithermal fluxes of Case-(B) increase about 1.5 and 2.7 times, respectively, in comparison with Case-(A). The irradiation time defined here decreases about 67% as the results. It is clear that aluminum is better than carbon as a "spectrum shifter" for an increase of the neutron flux.

From the comparison of Case-(A) and (C), it is clear that the epithermal flux increases about 30 times as shown in Fig. 6, and the maximum advantage depth increases from 5.3 cm to 7.7 cm. We can see that aluminum is better than carbon for increasing the epithermal flux as the "neutron filter". However, the whole-body absorbed dose of Case-(C) increases about 30% in comparison with the Case-(A) for the irradiation time defined here.

Table 3. Effect of aluminum as a "spectrum shifter" and a "neutron filter"

Minor Change of the "Old" Configuration at 100kW Coll. Dia.=10cm Bismuth=unchanged	"Old" Configuration	"Spectrum Shifter" Changed to Aluminum	"Neutron Filter" and "Spectrum Shifter" Changed to Aluminum
	Case-(A)	Case-(B)	Case-(C)
Thermal Neutron Flux★ (n/cm²sec)	1.7E+9	2.5E+9	1.6E+9
Epithermal Neutron★ Flux (n/cm²sec)	2.2E+7	6.1E+7	6.8E+8
Faster-Epi Neutron★ Flux (n/cm²sec)	6.6E+6	1.2E+7	6.7E+7
Fast Neutron Flux★ (n/cm²sec)	2.2E+6	3.2E+6	1.6E+6
Gamma Dose Rate★ (cGy/hr)	175	261	250
Maximum Total Dose Rate with 30μg/g B-10 (RBE-cGy/hr)	4890	7240	5550
Maximum Total Background Dose Rate (RBE-cGy/hr)	616	917	847
Irradiation Time★★ (Irr. Time) (hr)	4.06	2.73	2.95
Advantage Ratio with RBE	6.22	6.23	5.68
Maximum Advantage Depth (cm)	5.34	5.44	7.69
Eye Dose Rate (RBE-cGy/hr)	51.1	76.1	92.9
Eye Dose in Irr. Time (RBE-cGy)	207	208	274
Whole-Body Dose Rate (RBE-cGy/hr)	15.5	23.2	27.7
Whole-Body Dose in Irr. Time (RBE-cGy)	62.9	63.2	81.8
Whole-Body Dose Rate Except Head (RBE-cGy/hr)	5.82	8.60	10.2
Whole-Body Dose Except Head in Irr. Time (RBE-cGy)	23.6	23.5	30.0

★ flux values in front of a phantom

★★ time of irradiation in which the maximum total background dose becomes 2500 RBE-cGy.

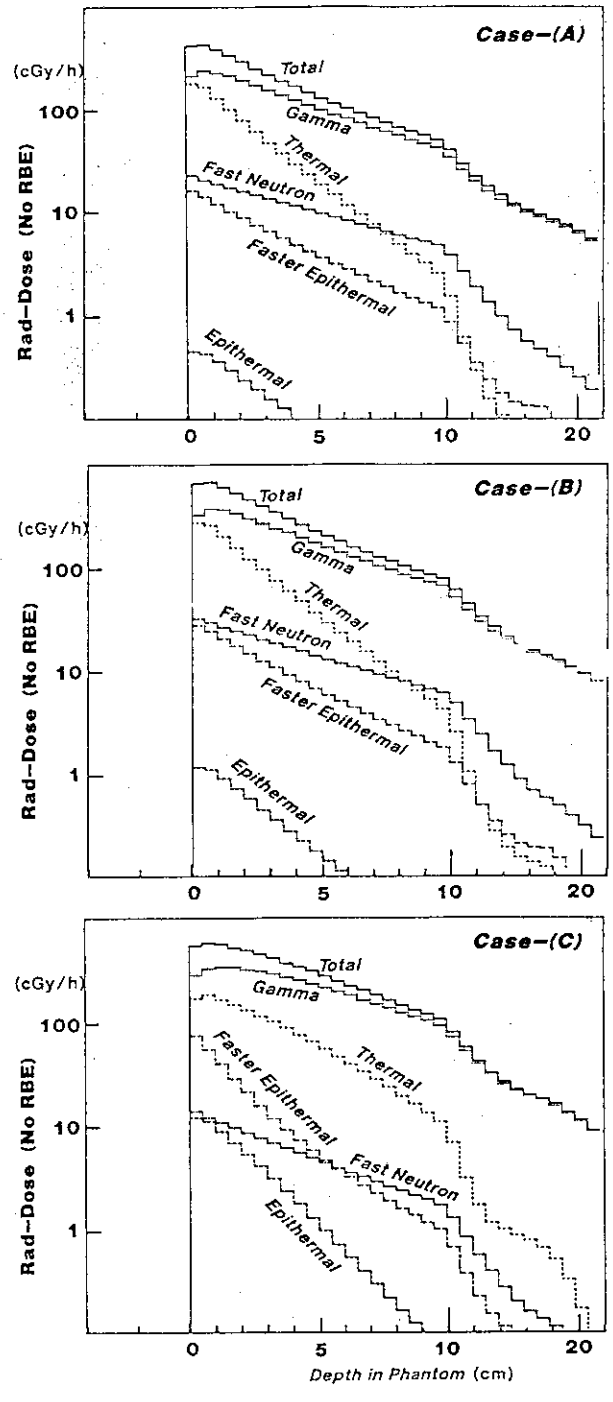

Fig. 7 Components of the total background dose rate in a phantom for Case-(A), (B) and (C)

Figure 7 shows the absorbed dose rate distribution in a phantom for each component of the total background dose. From this figure we can see that the epithermal dose gradually increases in the order of Case-(A), (B) and (C). It is also clear that the maximum absorbed dose in a phantom is due to gamma-rays that is caused from the thermal neutron capture.

In order to investigate the effect of aluminum as the "neutron filter", the thickness of aluminum was changed from 37.5 cm to 67.5 cm in the configuration as shown in Fig. 1. The results are shown in Table 4. It is clear from this table that the irradiation time can be shortened under 2 hours at 100 kW, and the maximum advantage depth becomes larger than the former cases, while the advantage ratio becomes smaller. This means that the epithermal and the faster epithermal components are effective to enlarge the maximum advantage depth, however, they also increase the whole-body absorbed dose.

Table 4. Effect of aluminum thickness as a "neutron filter"

"Large Modification" at 100kW "Spectrum Shifter": Changed to Aluminum Coll. Dia.=10cm	Thickness of "Neutron Filter" of Aluminum (cm)			
	37.5	47.5	57.5	67.5
	Case-(08)	Case-(09)	Case-(10)	Case-(11)
Thermal Neutron Flux* (n/cm²sec)	3.7E+9	2.7E+9	1.9E+9	1.4E+9
Epithermal Neutron* Flux (n/cm²sec)	1.6E+9	1.2E+9	9.9E+8	8.0E+8
Faster-Epi Neutron* Flux (n/cm²sec)	2.4E+8	1.7E+8	1.2E+8	8.3E+7
Fast Neutron Flux* (n/cm²sec)	1.3E+7	5.8E+6	2.6E+6	1.2E+6
Gamma Dose Rate* (cGy/hr)	591	437	326	245
Maximum Total Dose Rate with 30μg/g B-10 (RBE-cGy/hr)	12500	9550	6990	5150
Maximum Total Background Dose Rate (RBE-cGy/hr)	2320	1590	1130	817
Irradiation Time** (Irr. Time) (hr)	1.08	1.57	2.22	3.06
Advantage Ratio with RBE	5.13	5.35	5.53	5.59
Maximum Advantage Depth (cm)	7.47	7.72	7.92	8.12
Eye Dose Rate (RBE-cGy/hr)	259	181	131	98.2
Eye Dose in Irr. Time (RBE-cGy)	280	284	291	300
Whole-Body Dose Rate (RBE-cGy/hr)	78.4	54.4	39.2	29.1
Whole-Body Dose in Irr. Time (RBE-cGy)	84.5	85.3	86.9	89.2
Whole-Body Dose Rate Except Head (RBE-cGy/hr)	29.1	20.2	14.6	10.8
Whole-Body Dose Except Head in Irr. Time (RBE-cGy)	31.4	31.7	32.4	33.2

★ flux values in front of a phantom ★★ time of irradiation in which the maximum total background dose becomes 2500 RBE-cGy.

CONCLUSIONS

It is concluded that the "old" configuration of the Musashi reactor was good enough as the characteristics for thermal beams, if we could not touch the inner structure of the reflector. It is clear that the characteristics will be much improved if we can replace a part of the reflector to aluminum as a "spectrum shifter". Moreover, we can increase the epithermal component by using aluminum as a "neutron filter" instead of carbon. However, we must decide it after the careful consideration of the whole-body absorbed dose, because the whole-body absorbed dose increases as the increase of the epithermal component.

2. Installation of JRR-2 Medical Irradiation Facility

K. ARIGANE, T. YAMADA, D. NEMOTO,
M. BANBA, K. KAWARAI, H. TAKAHASHI

Department of Research Reactor
Tokai Research Establishment, JAERI
Tokai-mura, Naka-gun, Ibaraki-ken, 319-11

ABSTRACT

A medical irradiation facility for boron neutron capture therapy (BNCT) has been installed in Japan Research Reactor No.2 (JRR-2) of Japan Atomic Energy Research Institute (JAERI). The facility consists of a neutron beam tube and an irradiation room. The irradiation room is made of steel and paraffin, and its inside dimension is 2.3 m width x 2.6 m length x 2.2 m height. Single crystal bismuth of 20 cm thick, a polyethylene collimator and LiF tiles were applied to optimized the neutron beam condition, and the rubber contained B_4C was stretched on the inside surface of the room to suppress the secondary gamma ray from the construction materials. The thermal neutron flux and gamma ray dose rate at the irradiation position is $1x10^9$ n/cm^2/s and 0.48 Sv/h, respectively, at reactor thermal power of 10 MW. First medical irradiation of the patient with brain tumor was performed on August 10, 1990 and 6 patients had been irradiated until the end of July, 1991.

INTRODUCTION

BNCT in Japan was started in Hitachi Training Reactor (HTR) at 1968 and medical irradiations for 17 patients had been performed until 1975 when the HTR was stopped. After that, Musashi Institute of Technology Research Reactor (MITR) had been mainly used for it in Japan. More than 100 patients with malignant brain tumors were irradiated in Japan until the end of 1990[1] when MITR was halted in December 1990 by a trouble. JAERI decided to collaborate on BNCT at JRR-2 for the request from doctors, and the installation works of the facility were started immediately in order to execute it by the end of July. The facility completed in August, 1990 and the first BNCT at JRR-2 was performed satisfactory on 10th of August, 1990.

OUTLINE OF MEDICAL IRRADIATION FACILITY[2)3)]

Neutron Beam Tube

The neutron irradiation facility for BNCT is shown in Fig.1. The irradiation condition for BNCT requests more than $1x10^9 n/cm^2/s$ of thermal neutron flux, less than 1 Sv/h of gamma ray dose rate and neutron beam size of 200 mm x 200 mm. To satisfy these conditions, the neutron radiography facility and graphite blocks installed on the thermal column were removed, and inside of thermal column was modified for BNCT as shown in Fig. 2. Many kinds of shielding materials, for example, single crystal bismuth, polyethylene plate, lead block, LiF tiles and B_4C rubber were used to optimize the neutron beam condition, and the neutron beam tube of 200 mm x 200 mm of cross section was set. When the BNCT is performed, a ^6LiF collimator is attached at outlet of the beam tube to provide a irradiation position and avoid the unnecessary exposure to a patient. The thermal neutron flux and gamma ray dose rate at irradiation position are $1x10^9$ $n/cm^2/s$ and 0.48 Sv/h, respectively, and gamma ray contamination of neutron beam is 1.7% in dose equivalent.

Irradiation Room

The structural design conditions for the irradiation room are to have proper shielding ability and strength for earthquake. The clinical design condition for it is to have enough space in order to set a patient in all positions according to the diseased part and avoid the unnecessary exposure. From these requirements and the limited space for the irradiation room, the irradiation room was designed as the box type of 2.3 m width x 2.6 m length x 2.2 m height. Many braces were applied to enhance the seismic strength. The thickness of the room was decided to be 200 mm of steel for the side wall and celling, and 200 mm of paraffin between the two plates of 200 mm steel for the back side wall. This back side wall is used as the main door to enter the irradiation room. The irradiation room is also fixed to the floor by bolts not to effect to the reactor body even if the class A grade earthquake occurred. Inside of the irradiation room is covered with the B_4C rubber to prevent the leakage of thermal neutron and avoid the activation of the room. Transportation of a patient into the irradiation room is done by taking off the main door by crane. For the emergency condition, for example, electric power stop, earthquake, taking a reactor shut down for the worse of a patient, a manual small door was provided to bring out a patient from the irradiation room. As the other equipments, two TV camera, monitoring detectors for gamma ray and neutron, and a guide tube for taking out of Au wire from the diseased part of a patient are provided in the irradiation room. Narcosis and oxygen gas tubes and other cables for clinical equipments were taking out through the two curved ducts which are attached at left side wall. During BNCT operation, doctors watch the patient by TV monitor and other clinical equipments.

CHARACTERISTICS OF MEDICAL IRRADIATION FACILITY[2)3)]

Neutron Beam Tube

Distributions of thermal neutron flux, gamma ray dose rate and cadmium ratio in the neutron beam tube are shown in Fig.3. The reduction rate of thermal neutron flux from top of the neutron beam tube to the outlet of the polyethylene collimator is mitigated at the part of polyethylene collimator for the thermalization of neutron by polyethylene. It is clear from the fact that the cadmium ratio at this part is also raising. The same phenomenon is also observed at phantom head which is set at outlet of the beam tube. The gamma ray shielding effect of 20 cm thick single crystal bismuth only reduced gamma ray to 1/23 against about 1/1000 of expected value. This result was considered due to secondary gamma ray which occurred from the construction materials. This estimation was confirmed by a experiment that thermal neutrons were shielded by B_4C rubber in front of polyethylene collimator. The LiF tiles attached on the inside surface of outlet of the beam tube reduced gamma ray to 1/2 at phantom head. Raising gamma ray dose rate at phantom head is also due to secondary gamma ray from the acrylic resin of phantom material.

Irradiation Room

To avoid the unnecessary exposure, the ^{6}LiF collimator is set at outlet of neutron beam tube. The neutron and gamma ray at outlet of the collimator are well collimated as shown in Fig.4. The peak which occurred at 300mm from the center of the collimator is due to radiation leakage from the edge of the collimator. The dose rate distributions of thermal neutron and gamma ray in the irradiation room are shown in Fig.5 and Fig.6. High dose rate areas are spread forward of the beam tube. To avoid the unnecessary exposure, a patient should be set with some angles against the neutron and gamma beams.

MEDICAL IRRADIATION AT JRR-2

The first BNCT at JRR-2 was performed on August 10, 1990. The patient was 43 years old female. Irradiation time was 4.5 hours at 10 MW and thermal neutron fluence of diseased part was 1.8×10^{13} n/cm^2/s. Outline of 6 medical irradiations performed up to today is shown in Table 1.

CONCLUSION

By remodeling the thermal column, the medical irradiation facility

was installed in JRR-2. The irradiation conditions for BNCT were gotten by the following structural changes.

1) By removing all graphite blocks in the thermal column, required thermal neutron flux was gotten.
2) By setting the 20 cm thick single crystal bismuth at backward of neutron beam tube, direct gamma ray from the reactor was reduced.
3) By using the B_4C rubber and LiF tiles, secondary gamma rays from the construction materials and outlet of neutron beam tube were suppressed.
4) By setting the polyethylene collimator in the neutron beam tube, attenuation of the thermal neutron flux was mitigated

ACKNOWLEDGEMENT

This work was done under the cooperation and support of many persons, many organization. The authors express deeply our appreciation to Prof. O. Aizawa of Musashi Institute of Technology, H. Hatanaka of Teikyo university and Y. Itou of Tokyo University for their good support and suggestion, and Director E. Shirai of Research Reactor Department of JAERI, and all members concerning with this work in JAERI, STA, universities for their support, effective discussions and constant encouragements.

REFERENCE

1) H. Hatanaka, K. Seto,; " Cancer Therapy Manual", Nippon Rinsho, No.49, 1988.
2) E. Shirai, et al,; "Clinical Experiment of BNCT for Brain Tumors at JAERI", Fourth International Symposium on Neutron Capture Therapy, Dec. 4-7, Sydney Australia.
3) K. Arigane, et al,; "Installation JRR-2 Medical Irradiation Facility", JAERI M 91-139, Sep. 1991.

Table 1　Outline of BNCT at JRR-2

No.	Date	Patient	Irradiation Time (hr : min.)	Thermal Neutron Fluence (n/cm^2)
1	1990. 8. 10	female	4 : 30	1.8×10^{13}
2	1991. 3. 8	female	3 : 55	1.9×10^{13}
3	1991. 4. 19	male	4 : 32	2.0×10^{13}
4	1991. 5. 10	female	4 : 30	2.0×10^{13}
5	1991. 6. 14	male	2 : 12	1.3×10^{13}
6	1991. 7. 5	male	4 : 40	2.6×10^{13}

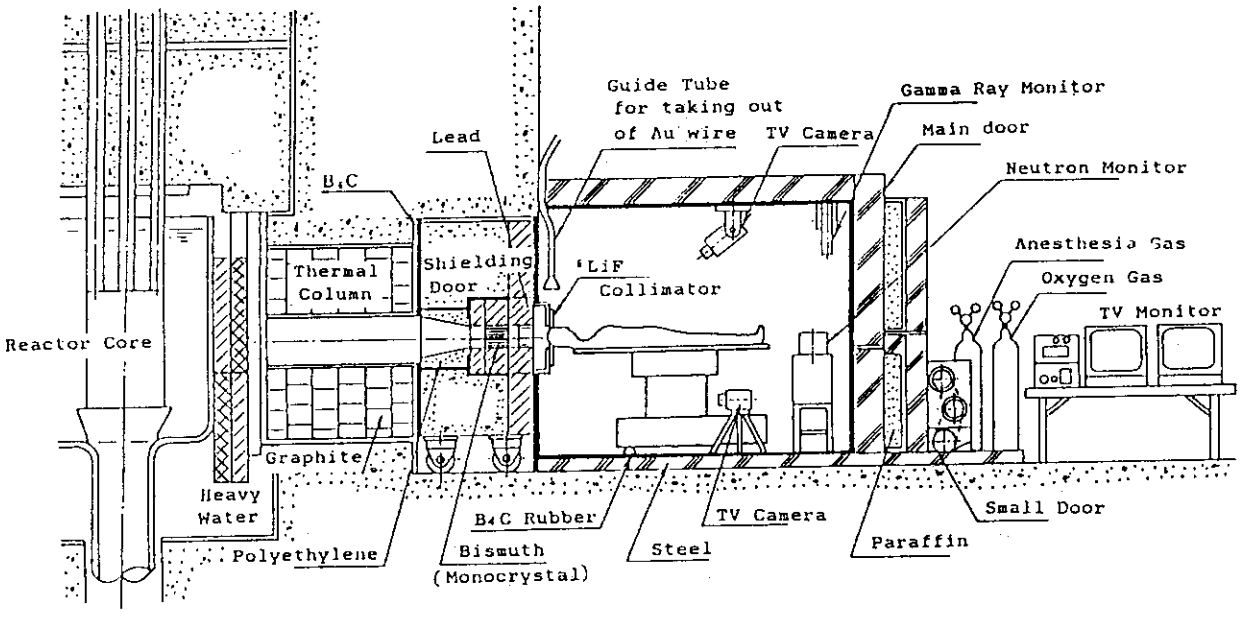

Fig.1　Medical irradiation Facility for BNCT in JRR-2

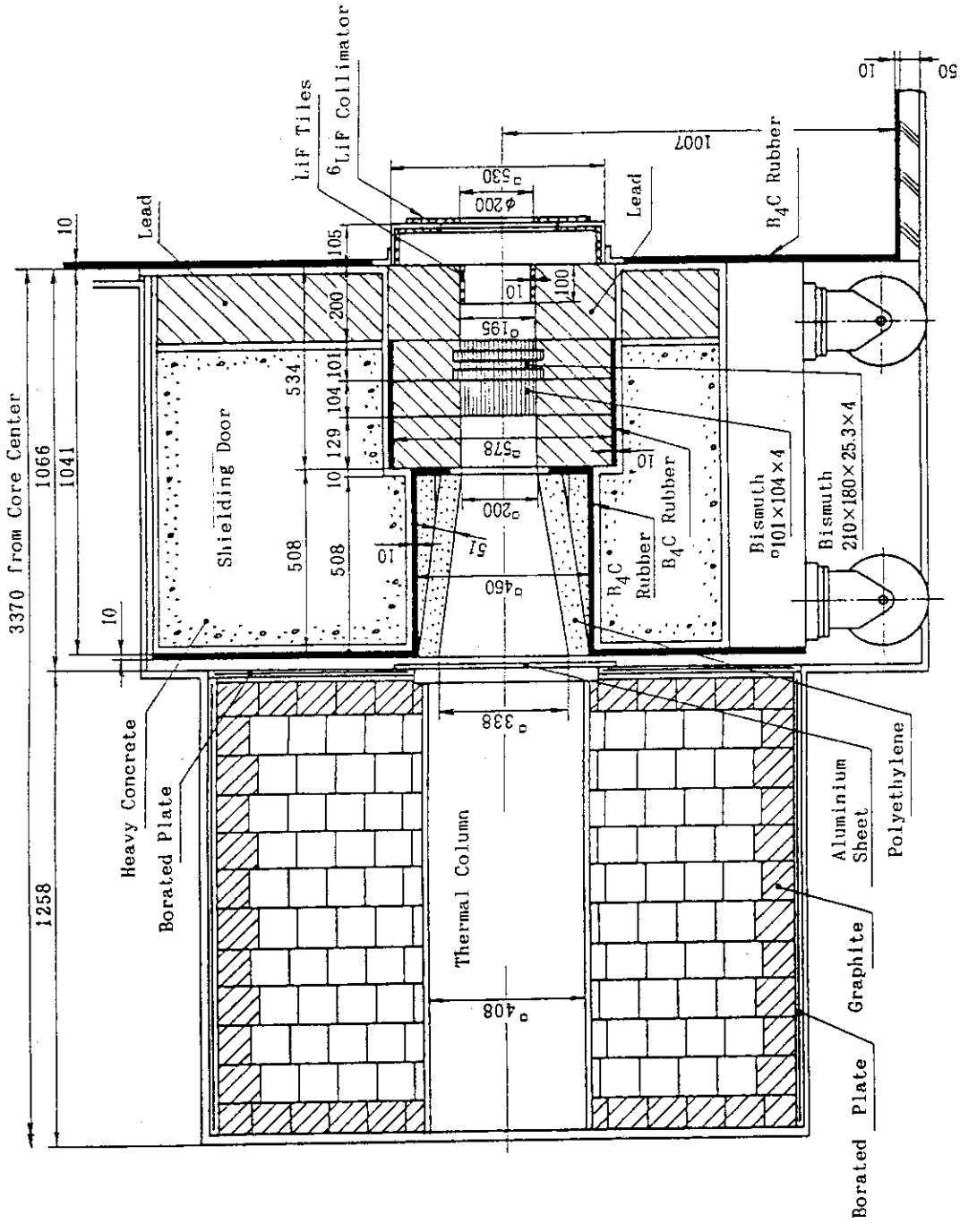

Fig.2 Neutron Beam Tube for BNCT

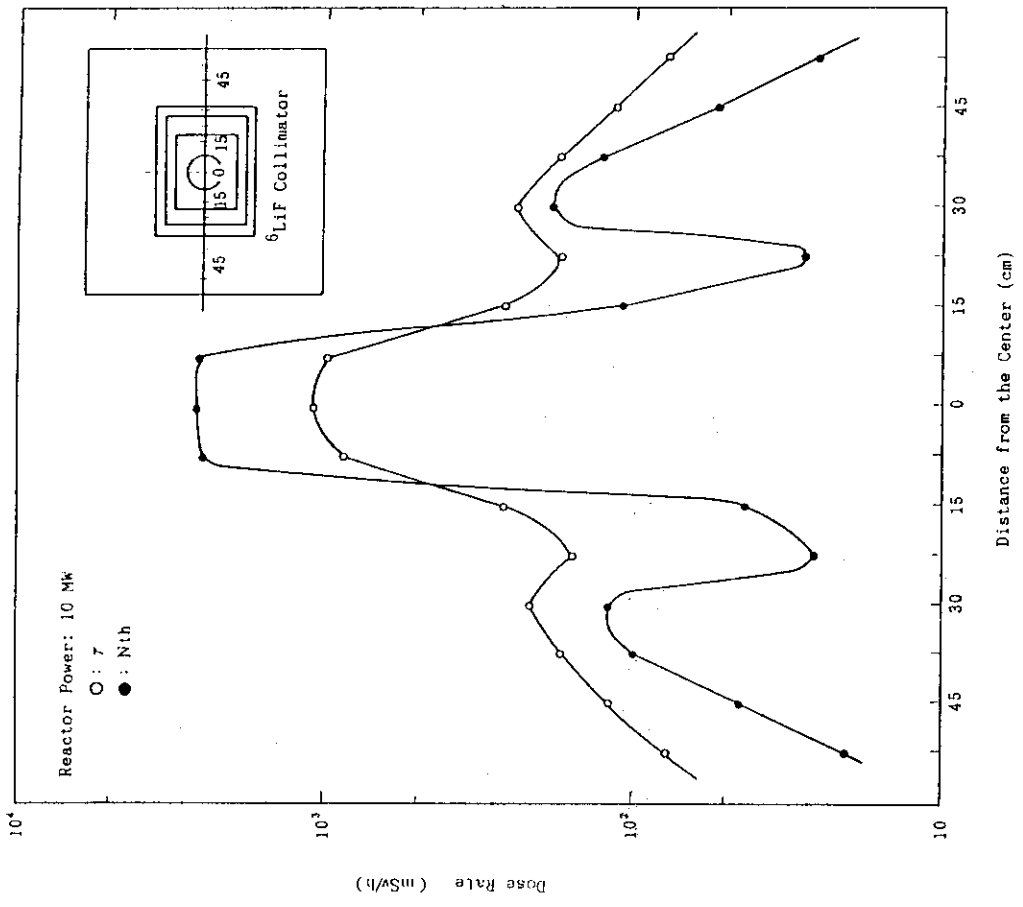

Fig.4 Distribution of Neutron and Gamma Ray Dose Rate at Outlet of 6LiF Collimator

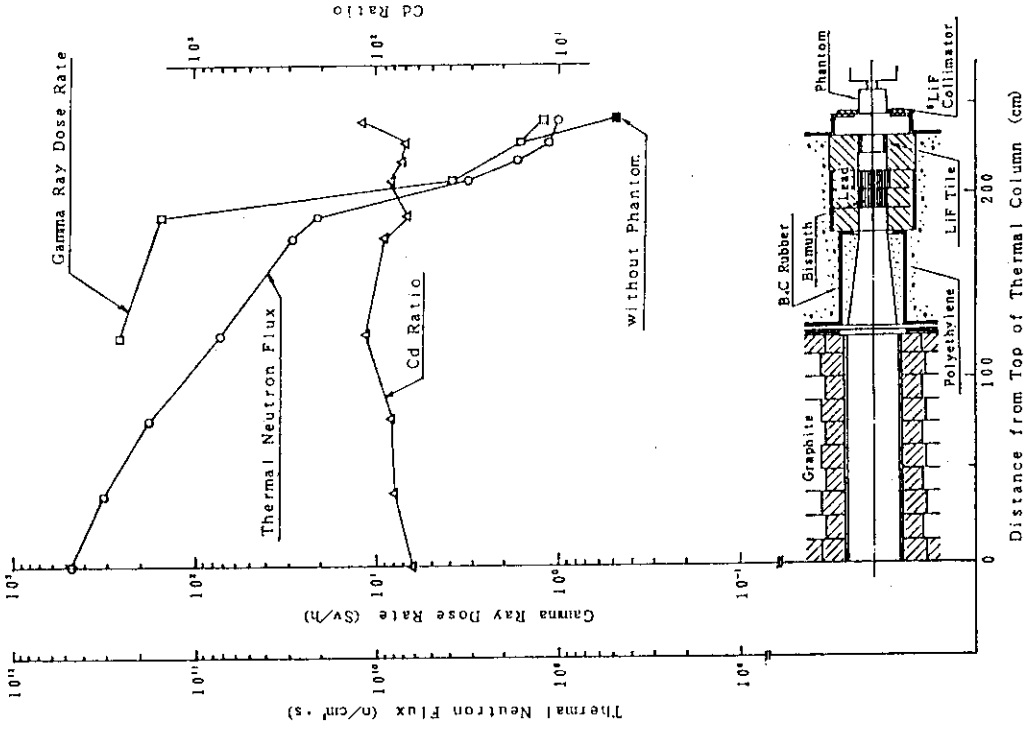

Fig.3 Distribution of Thermal Neutron, Gamma Ray and Cadmium Ratio in the Neutron Beam Tube

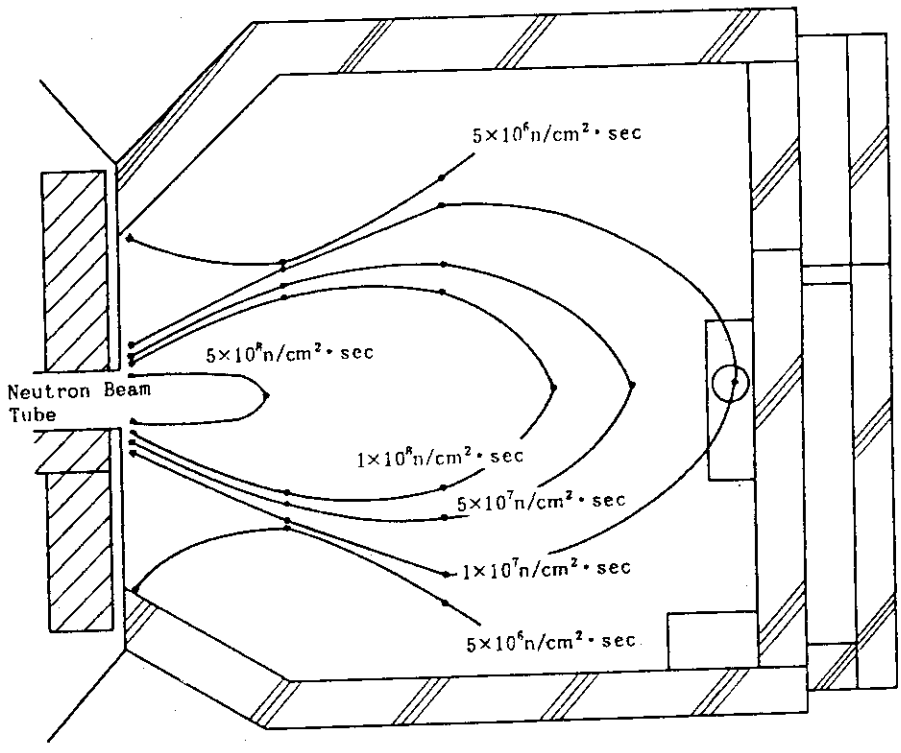

Fig.5 Distribution of Thermal Neutron Flux in the Irradiation Room

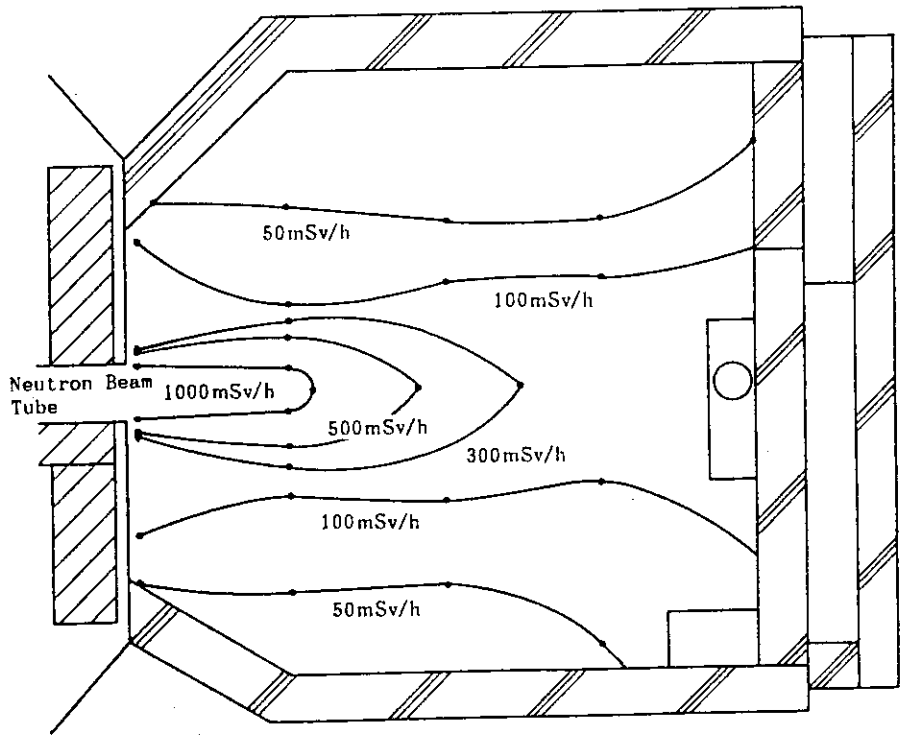

Fig.6 Distribution of Gamma Ray Dose Rate in the Irradiation Room

3. Somatic Reversion of a Xantha-like Gene in Soybean by Fission Neutrons and X-rays

Tetsuo ITOH and Sohei KONDO

Atomic Energy Research Institute, Kinki University,
Kowakae, Higashiosaka, Osaka 577

ABSTRACT

The variety T219 of Glycine max (soybean) has a wild-type chlorophyll development gene Y_{11} and its allele y_{11}. Seeds from autogamous T219 plants produce dark green ($Y_{11}Y_{11}$), light green ($Y_{11}y_{11}$) and yellow ($y_{11}y_{11}$) seedlings. Upon irradiation of dry seeds with X rays, the frequency of light-green mosaics on $y_{11}y_{11}$ simple leaves was about twice as high as that of dark-green mosaics on $Y_{11}y_{11}$ simple leaves. For the explanation of the two-fold difference in mutability, we propose that both the light-green and the dark-green mosaics are caused by reversion of y_{11} to Y_{11}, as the number of target gene y_{11} per cell in the $y_{11}y_{11}$ tissue is twice that in the $Y_{11}y_{11}$ tissue. Somatic reversion of the y_{11} gene was induced, in either $y_{11}y_{11}$ or $Y_{11}y_{11}$ plants by fission neutrons from Kinki nuclear reactor at a rate about 20 times higher than that by X rays, suggesting that the reversions result from deletion mutations. To explain the occurrence of the reversion by deletions, we assume that the y_{11} gene is a complex gene made of a transposable element inserted at the Y_{11} locus and that the reversion resulted from the deletion of the inserted transposon. The phenotype of the y_{11} gene shares many similarities with those of Xantha genes mapped at several loci in barley and tomato.

1. INTRODUCTION

Variety T219 of Glycine max (L.) Merrill (soybean) exhibits incomplete dominance of the chlorophyll development gene Y_{11} over its allele y_{11} so that $Y_{11}Y_{11}$ plants are dark green in color, $Y_{11}y_{11}$ plants are light green and $y_{11}y_{11}$ plants have golden yellow leaves; simple leaves of $Y_{11}y_{11}$ plants are frequently dotted with small spots that are either dark green (resembling leaves of $Y_{11}Y_{11}$), yellow (resembling leaves of $y_{11}y_{11}$) or twin (composed of a dark green area adjacent to a yellow area similar in size and shape) (Weber and Weiss, 1959; Vig and Paddock, 1968; Vig, 1973a). This strain has been used as a tester for environmental mutagens; $Y_{11}y_{11}$ seeds soaked in water containing mutagenic chemicals produced yellow, dark-green and/or twin spots at high frequencies on simple leaves (Vig, 1975; Fujii, 1981, 1982; Fujii et al., 1983). Mechanisms of twin spots have been extensively studied, leading to the conclusion that the twin spots are caused by somatic crossing over (Vig and Paddock, 1968; Vig, 1973a, 1973b, 1973c, 1974, 1978; Vig et al., 1976).

After exposure of $y_{11}y_{11}$ and $Y_{11}y_{11}$ seeds to gamma rays or ^{3}H beta rays, light-green spots were produced on simple leaves of $y_{11}y_{11}$ plants at frequencies as high as total frequencies of dark-green, yellow and twin spots on simple $Y_{11}y_{11}$ leaves (Vig, 1974). Vig (1974) and Vig et al. (1976) interpreted that the major cause of the occurrence of light-green spots on $y_{11}y_{11}$ leaves is point mutations. The present paper, however, deals with experimental results supporting the idea that light-green spots appearing on $y_{11}y_{11}$ leaves are caused by deletion of a cryptic transposable element inserted at the Y_{11} locus that partially suppresses the wild-type function of the Y_{11} gene, resulting in the formation of a Xantha-like y_{11} gene.

2. MATERIALS AND METHODS

Strain

The strain T219 of Glycine max used was obtained from the late Dr. T. Fujii, National Institute of Genetics; he obtained this strain from Prof. B. K. Vig, University of Nevada. The genotype of this strain is made of the wild-type gene Y_{11} and its allele y_{11}. $Y_{11}Y_{11}$ plants are dark green in color, $Y_{11}y_{11}$ plants are light green and $y_{11}y_{11}$ plants are golden yellow as if almost lacking chlorophyll (Vig, 1973a). Seeds were harvested from autogamous $Y_{11}y_{11}$ plants and stored at about 5°C in a refrigerator.

Irradiation and radiation dosimetry

X-irradiation was carried out with an X-ray generator (Rigaku Denki Co., Osaka) at Radiation Biology Research Center, Kyoto University; which was operated at 250 kVp and 15 mA with 1 mm Al filter. The dose rate used was 1.05 Gy/min as measured by a Victoreen chamber.

Irradiation of seeds with fission neutrons was made using a nuclear reactor in Kinki University. Dose rates of fission neutrons and gamma rays from the reactor were separately measured with a pair of a tissue-equivalent ion chamber and a graphite ion chamber; doses of neutrons and gamma rays given to seed samples were also monitored in situ by plastic-nuclear track detectors TS16N (Nagase-Landauer Co., Tokyo) and thermoluminescence dosimeters UD-170L (Matsushita Electric Industry Co., Osaka) attached to each of the sample containing dishes, as previously described (Yasubuchi et al., 1989).

Observation of somatic mutant mosaics

Within two hours after the completion of irradiation, seeds were sown on soil in nursery beds; they were kept in a greenhouse at 20-30°C for two to three weeks until simple and first compound leaves were formed. In $Y_{11}y_{11}$ seedlings, dark-green, yellow and twin mosaics were scored on simple leaves whereas in $y_{11}y_{11}$ seedlings, light-green mosaics were scored on simple leaves.

3. RESULTS AND DISCUSSION

Factors for conversion of neutron fluence and photon exposure to absorbed doses in tissue of dry soybean seeds

Table 1. Fluence-to-dose conversion factor k_{ST} and exposure-to-dose conversion factor f_{ST} for soybean dry seeds

Neutron energy (MeV)	k_{ST} (10^{-9} cGy/fluence)	k_{ST}/k_{HT}	Photon energy (MeV)	f_{ST}	f_{ST}/f_{HT}
14	5.70	0.88	1	0.886	0.92
1.3	2.04	0.81	0.3	0.886	0.92
1	1.91	0.78	0.15	0.874	0.91
0.8	1.63	0.82	0.1	0.837	0.88
0.3	1.00	0.81	0.08	0.792	0.84
0.1	0.518	0.81	0.06	0.694	0.74

$k_{ST} = N_A \Sigma (w_i[/g]/A_i) \sigma_i E_i$[MeV barns]/6.24 x 10^7 [MeV/g]. In this equation, N_A is Avogadro's number, w_i is the fraction of element i by weight in dry soybean seeds (7.9 ± 0.2 % H, 47.0 ± 0.1 % C, 7.0 ± 0.01 % N, 31.4 ± 0.2 % O, and 6.7 ± 0.3 % other elements; measured by Toray Research Center Inc., Siga), A_i is the mass number of element i, $\sigma_i E_i$ is the total kinetic energy transferred from reactions of neutrons with nuclei of element i, and the denominator is the (MeV/g)-to-cGy conversion factor. The $\sigma_i E_i$ values for 14 MeV neutrons were obtained from Randolph (1957), i.e., 4.86 for H, 2.99 for C, 3.42 for N, 3.73 for O. The k_{ST} values for neutrons with energies 0.1 to 1.3 MeV were calculated using Eq. (2) in the text with the values of kerma factors given in ICRU Report 13 (1969).
$f_{ST} = 0.877(\mu_{ST}/\mu_{AIR})$. In this equation, $\mu_{ST} = \Sigma \mu_i w_i$ (μ_i is energy absorption coefficient of element i per 1 g/cm^2 and w_i the fraction by weight of element i in tissue of dry soybean seeds) and μ_{AIR} is energy absorption coefficient of air per 1 g/cm^2. The μ_i and μ_{AIR} values for photons at various energies used were taken from ICRU Report 10b in 1962 (1964). The spectrum of X rays from the X-ray generator used at 250 kVp was assumed to be similar to that given in Fig. 3h of ICRU Report in 1956 (1957), which gives an average energy of about 100 keV.

Fluence of fast neutrons, F (neutrons/cm^2), and exposure of X or gamma rays, X, are related to absorbed dose D in the tissue of dry soybean seeds by

$$D = k_{ST}F; \quad D = f_{ST}X, \qquad (1)$$

where k_{ST} is the kerma factor, i.e., the fluence-to-dose conversion factor, for soybean cotyledon tissue and f_{ST} is the exposure-to-dose conversion factor for soybean cotyledon tissue. The k_{ST} and the f_{ST} values are calculated by

$$k_{ST} = k_i(E_N)w_i; \quad f_{ST} = f_i(E_G)w_i, \qquad (2)$$

where k_i is the kerma factor for neutrons for element i in energy E_N, w_i is the fraction by weight of element i in the tissue of dry soybean seeds and f_i is the R-to-Gy conversion factor for photons with energy E_G.

For dosimetry of fission neutrons from the nuclear reactor, k_{ST} values were calculated at discrete energies as given in Table 1; they vary greatly with changes in E_N but the ratio of k_{ST} to k_{HT} (k value for human tissue) remains almost constant for different E_N values. Dosimetry of the mixed radiation from the Kinki University Reactor was done with paired ion chambers; the dose rate was 0.20 and 0.22 (both in Gy in human tissue per hour) for neutrons and gamma rays, respectively. These numerical values become 0.16 and 0.19 (Gy in dry soybean cotyledon tissue per hour), respectively, when the k_{ST}/k_{HT} values and f_{ST}/f_{HT} values given in Table 1 are used.

Observed frequencies of somatic mosaics on $y_{11}y_{11}$ and $Y_{11}y_{11}$ leaves after irradiation

In Fig. 1, frequencies of light-green mosaics on yellow $\underline{y}_{11}\underline{y}_{11}$ simple leaves (Fig. 1A), and those of dark-green mosaics (Fig. 1B) and yellow ones on light green $\underline{Y}_{11}\underline{y}_{11}$ simple leaves (Fig. 1C) are plotted against doses of X rays and fission neutron-gamma mixed radiation given to dry soybean seeds.

Frequencies of twin mosaics did not increase appreciably above control levels after irradiation (data not shown).

Comparison of induction rates (/leaf/Gy) by X rays and fission neutrons for three types of somatic mutations

Observed frequency-versus-dose curves were approximately linear for the three types of somatic mutations (Fig. 1). Therefore, the data used for Fig. 1 were fitted by the least square method to a linear regression equation

$$\underline{Y} = \underline{a} + \underline{b}\underline{D}, \qquad (3)$$

where $\underline{Y}$ is frequency of mosaics per leaf after irradiation with dose $\underline{D}$ (Gy in dry soybean cotyledon tissue), $\underline{a}$ is spontaneous rate of mosaics and $\underline{b}$ is induced rate per Gy of mosaics.

The $\underline{b}$ value for induction by neutron-gamma mixed radiation, $\underline{b}_{n+g}$, may be approximated by

$$\underline{b}_{n+g} = (1-\underline{r})\underline{b}_g + \underline{r}\underline{b}_n, \qquad (4)$$

where $\underline{r}$ is a fraction of the total neutron-gamma dose contributed by neutrons, $\underline{b}_g$ is the induced rate per Gy by gamma rays and $\underline{b}_n$ is the induced rate per Gy by neutrons. Approximating the $\underline{b}_g$ values with observed $\underline{b}_X$ values, i.e., the induced rates by X rays given in Table 2, and using the experimental $\underline{r}$ values of 0.46 for the fission neutron-gamma mixed radiation, we can estimate the $\underline{b}_n$ values by Eq. (4) using the observed $\underline{b}_{n+g}$ values (Table 2). Ratios of the resultant $\underline{b}_n$ values to $\underline{b}_X$ values are the RBE (relative biological effectiveness) values of neutrons given in the last two columns of Table 2.

Table 2. Induced rates of three types of mosaics on simple leaves of soybeans by X rays and fission neutron-γ mixed radiation, and relative biological effectiveness (RBE) of fission neutrons for induction of the somatic mutations

Genotype of leaves studied	Type of induced mosaics	Induced rate $\underline{b}$ of mosaics/leaf/Gy by		Estimate for induced rate[a] of mosaics/leaf/Gy by	RBE for fast neutrons ($\underline{b}_n/\underline{b}_X$)
		X rays $\underline{b}_X$	Fission neutron-γ $\underline{b}_{n+g}$	Fission neutrons $\underline{b}_n$	Fission neutrons
$\underline{y}_{11}\underline{y}_{11}$	Light green	0.80 ± 0.09	9.3 ± 2.1	19 ± 4.5	24 ± 6.2
$\underline{Y}_{11}\underline{y}_{11}$	Dark green	0.43 ± 0.08	3.7 ± 1.1	7.5 ± 2.3	17 ± 6.2
$\underline{Y}_{11}\underline{y}_{11}$	Yellow	1.0 ± 0.16	12 ± 2.9	25 ± 6.7	25 ± 7.3

[a] Calculated from $\underline{b}_{n+g}$ and $\underline{b}_X$ values assuming that X and γ rays have an equal $\underline{b}$ value and using Equation 4 in text.

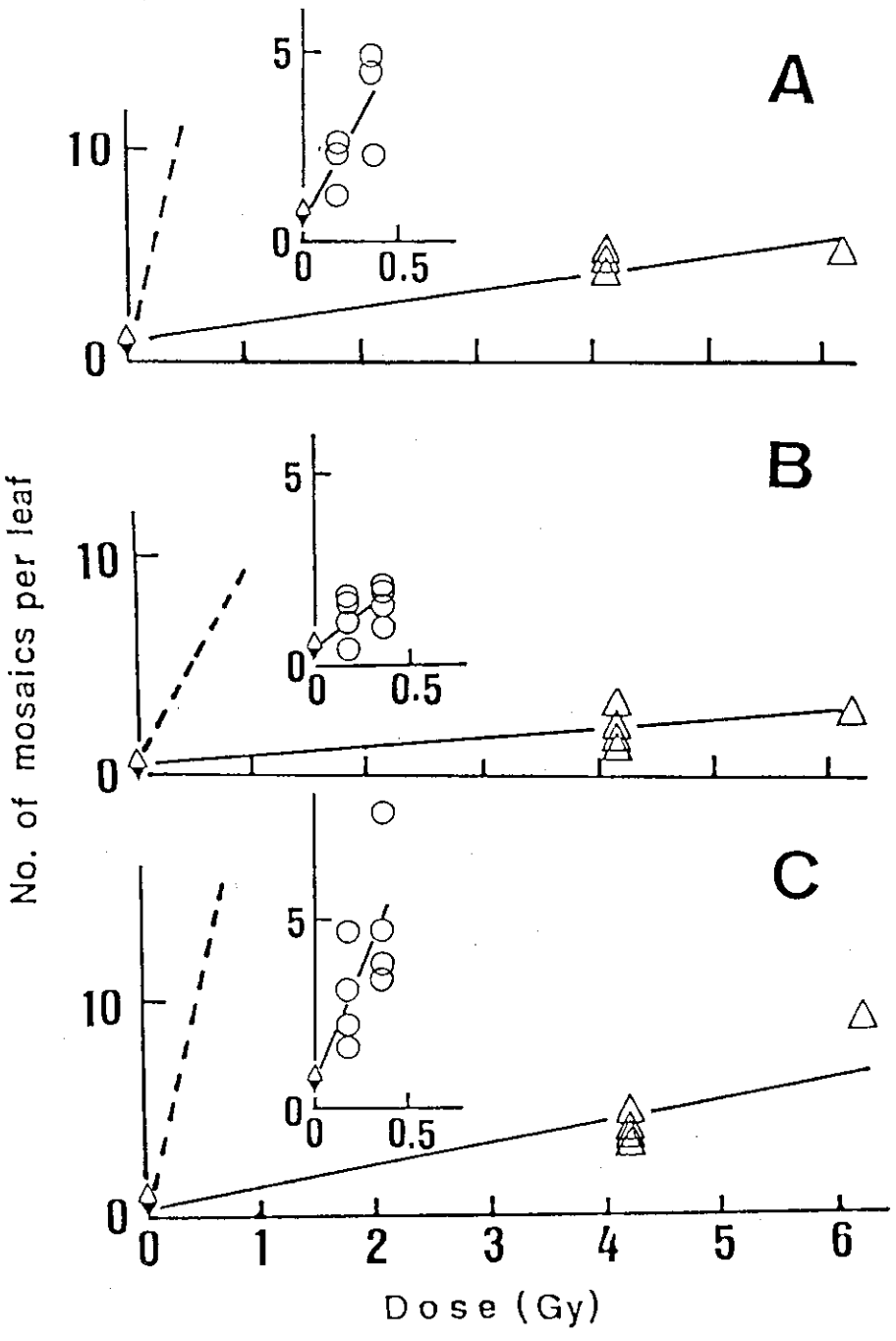

Fig. 1. Frequencies per leaf of three types of mosaics on simple leaves of soybeans plotted against absorbed doses in soybean seed tissue given by X rays (△) and fission neutron-gamma mixed radiation (◯). Symbol(◈) stands for spontaneous frequencies. A, Light-green mosaics on yellow ($\underline{y}_{11}\underline{y}_{11}$) leaves. The broken line represents a theoretical dose-response curve for fast neutrons; it was constructed using the average of the RBE values experimentally determined for fission neutrons given in Table 2. B, Dark-green mosaics on light-green ($\underline{Y}_{11}\underline{y}_{11}$) leaves. C, Yellow mosaics on light-green ($\underline{Y}_{11}\underline{y}_{11}$) leaves.

Similarity between dark-green mutatyions in $Y_{11}y_{11}$ plants and light-green mutations in $y_{11}y_{11}$ plants and dissimilarity between dark-green and yellow mutations

We conclude from Table 2 that X-ray induction of light- green mosaics in the $y_{11}y_{11}$ tissue occurred at a rate about twice as high as that of dark-green mosaics in the $Y_{11}y_{11}$ tissue. This result can be explained by the assumption that both the light-green and the dark-green mosaics result from reversion of the y_{11} gene to Y_{11} since the number of the target gene y_{11} in the $y_{11}y_{11}$ tissue is twice as many as that in the $Y_{11}y_{11}$ tissue. If this is the case, however, we must explain the reason why, in the $Y_{11}y_{11}$ tissue, X-ray induction of dark-green mosaics occurred at a rate about half as high as that of yellow mosaics (Table 2; Vig, 1974).

After treatment of $Y_{11}y_{11}$ seeds with Mitomycin C, i.e., a potent inducer of somatic crossing over, dark-green mosaics occurred more frequently than yellow mosaics whereas twin mosaics occurred far more frequently than dark-green mosaics (Vig and Paddock, 1968). Based on these and other results, Vig (1974) and Vig et al. (1976) proposed that yellow mosaics induced in $Y_{11}y_{11}$ plants resulted from the loss of the Y_{11} bearing chromosome fragments whereas light-green mosaics induced in $y_{11}y_{11}$ plants resulted from the point mutations. This proposal is compatible with the findings that in $Y_{11}y_{11}$ plants, yellow mosaics occurred more frequently than dark-green mosaics after X-irradiation, as we assume that dark-green mosaics are caused by the same reversion mutation that induces light-green mosaics in $y_{11}y_{11}$ plants, and as we know that deletion mutations are induced more frequently by X-irradiation than point mutations (Ishii and Kondo, 1975; Sankaranarayanan, 1982).

Hypothesis for the nature of the y_{11} gene

If X-ray induced yellow mosaics in $Y_{11}y_{11}$ plants result from the deletion mutations at the Y_{11} locus, fast neutrons must produce yellow mosaics at a rate much higher than the induced rate by X rays as previously reported for chlorophyll mutations in wheat and hairless somatic mutations in *Arabidopsis* (see Kondo, 1964, for review). This was actually the case; fission neutrons was 25 $\pm$ 7 times more effective for induction of yellow mosaics than X rays (see the numerical value of RBE for yellow mosaics in Table 2).

To our surprise, however, RBE value of neutrons for induction of dark-green mosaics in $Y_{11}y_{11}$ plants and that for induction of light-green mosaics in $y_{11}y_{11}$ plants were close to that for induction of yellow mosaics as seen from Table 2. Therefore, the high RBE values of neutrons strongly suggest that the y_{11} to Y_{11} reversion, which is assumed in this paper as the major cause of both the dark-green and the light-green mosaics, which are results from deletion mutations.

A simple model to explain these unexpected results is that the y_{11} gene is a complex of the Y_{11} gene with a transposon-like insert that partially suppresses the normal function of the Y_{11} gene. On this assumption, the inserted element is expected to be deleted --reversion process toward a wild-type gene-- at a high frequency when the inserted element and/or its neighboring DNA region are damaged by irradiation. Multiple DNA lesions are more frequently induced by fast neutrons than X rays (Leenthouts and Chadwick, 1978).

Our proposal is a working hypothesis for the future study of semi-dominant mutant genes called *Xantha* that partially suppress the chlorophyll development in plants. These dominant genes are named *Xa* for they produce xanthophyllic phenotypes; they are known at several loci in barley (Prina and Favret, 1988) and tomato (Young and MacArthur, 1947).

ACKNOWLEDGMENT

We thank the late Dr. T. Fujii for giving us the variety T219 of soybean, T. Yoshida for harvesting soybean, Dr. M. Ikenaga for the use of an X-ray generator, Dr. K. Fujikawa and H. Ryo for their suggestions during the preparation of the manuscript, Y. Aoki for operating the nuclear reactor of Kinki University.

REFERENCES

FUJII, T. (1981). Mutagenic effect of L-ethionine in soybean and maize. Environ. Expt. Bot. 21, 127-131.

FUJII, T. (1982). Mutagenicity testing of chemical mutagens in higher plants. In: Environmental Mutagens and Carcinogens, (eds.: T. Sugimura, S. Kondo and H. Takebe), pp. 399-410. University of Tokyo Press, Tokyo.

FUJII, T., SHIZAKI, M., FUJIKI, H. and SUGIMURA, T. (1983). Effect of TPA on the mutagenicity of caffeine in the soybean mutation test. Mutat. Res. 110, 263-269.

ICRU (1957). Report of the International Commission on Radiological Units and Measurements (ICRU) 1956, Natl/ Bureau of Standards Handbook 62. U.S. Department of Commerce, Washington, D.C.

ICRU (1964). Physical aspects of irradiation. Recommendations of the International Commission on Radiological Units and Measurements(ICRU), Report 10b 1962, Natl. Bureau of Standards Handbook 85, U.S. Department of Commerce, Washington, D.C.

ICRU (1969). Neutron fluence, neutron spectra and kerma. ICRU Report 13, International Commission on Radiation Units and Measurments, Washington, D.C.

ISHII, Y. and KONDO, S. (1975). Comparative analysis of deletion and base-change mutabilities of Escherichia coli B strains differing in DNA repair capacity (wild-type, uvrA⁻, polA⁻, recA⁻) by various mutagens. Mutat. Res. 27, 27-44.

KONDO, S. (1964). Variation in mutagenicity and radiation resistance with genome complexity and evolution. Jpn. J. Genet. 39, 176-198.

LEENTHOUTS, H. P. and CHADWICK, K. H. (1978). The crucial role of DNA double -strand breaks in cellular radiobiological effects. Adv. Radiat. Biol. 7, 55-101

PRINA, A. R. and FAVRET, E. A. (1988). Influence of marker genes on the expression of somatic mutations in barley. J. Heredity 79, 371-376.

RANDOLPH, M. L. (1957). Energy deposition in tissue and similar materials by 14.1-MeV neutrons. Radiat. Res. 7, 47-57.

SANKARANARAYANAN, K. (1982). Genetic effects of ionizing radiation in multicellular eukaryotes and the assessment of genetic radiation hazards in man. Elsevier, Amsterdam.

VIG, B. K. (1973a). Somatic crossing over in Glycine max (L.) Merrill: Effect of some inhibitors of DNA synthesis on the induction of somatic crossing over and point mutations. Genetics 73, 583-596.

VIG, B. K. (1973b). Somatic crossing over in Glycine max (L.) Merrill: Mutagenicity of sodium azide and lack of synergistic effect with caffeine and mitomycin C. Genetics 75, 265-277.

Vig, B. K. (1973c). Mitomycin C induced leaf mosaicism in Glycine max (L.) Merrill in relation to the post germination age of the seed. Theoret. Appl. Genet. 43, 27-30.

VIG, B. K. (1974). Somatic crossing-over in Glycine max (L.) Merrill: Differential response to ^{3}H-emitted β-particles and ^{60}Co emitted γ-rays. Radiat. Bot. 14, 127-137.

VIG, B. K. (1975). Soybean (Glycine max): A new test system for study of genetic parameters as affected by environmental mutagens. Mutat. Res. 31, 49-56.

VIG, B. K. (1978). Somatic mosaicism in plants with special reference to somatic crossing over. Environ. Health Perspect. 27, 27-36.

VIG, B. K., NILAN, R. A. and ARENAZ, P. (1976). Somatic crossing over in Glycine max (L.) Merrill: Induction of somatic crossing over and specific locus mutations by methyl methanesulfonate. Environ. Exp. Bot. 16, 223-234.

VIG, B. K. and PADDOCK, E. F. (1968). Alteration by mitomycin C of spot frequencies in soybean leaves. J. Heredity 59, 225-229.

YASUBUCHI, S., HOSHI, M., ITOH, T., HISANAGA, S., NIWA, T., MIKI, R. and KONDO, S. (1989). Dosimetry of fast neutrons in 1W nuclear reactor with plastic nuclear-track detectors. Radioisotopes 38, 359-365.

YOUNG, P. A. and MACARTHUR, J. W. (1947). Horticultural characters of tomatoes. Texas Agric. Expt. Sta. Bul. 698, 1-61.

WEBER, C. R. and WEISS, M. G. (1959). Chlorophyll mutant in soybeans provides teaching aid. J. Heredity 50, 53-54.

4. Characterization of Gamma-ray Fields in Research Reactors

Y. Sakurai*, I. Kimura*, S. Kanazawa*,
K. Kobayashi**, S. Shiroya**, K. Kanda**

* Department of Nuclear Engineering, Kyoto University,
Yoshida, Sakyo-ku, Kyoto 606-01, Japan
** Research Reactor Institute, Kyoto University,
Kumatori, Sennan-gun, Osaka 590-04, Japan

ABSTRACT

Neutron and gamma-ray flux distributions in a critical assembly (KUCA) were measured with gold wires and small thermoluminescence dosimeters (TLD) of magnesium orthosilicate, $Mg_2SiO_4(Tb)$ (MSO), respectively, and the results have been compared with those calculated by ANISN-JR with combined cross sections of neutrons and gamma-rays generated by RADHEAT-V3. For the comparison, we normalized the measured activity of the gold wire at the core center with the calculated one. Both the measured neutron flux distributions and the absorbed doses of MSO in the KUCA B-core with highly enriched uranium fuel and polyethylene moderator/reflector agree well with that calculated.

A similar comparison was carried out in four different irradiation fields (in void, and in three filter boxes) in an internal graphite reflector between two divided cores of a low power reactor (UTR-KINKI). Although the measured neutron flux distributions agree well with the calculated ones by DOT 3.5, the measured absorbed doses of MSO exceed considerably than those calculated.

INTRODUCTION

The importance of characterization of gamma-ray flux distribution in a reactor has risen recently, especially for the estimation of gamma-ray flux at experimental and therapeutic facilities in research and medical reactors. However there is hardly any established method to measure in-core gamma-flux distribution in a thermal reactor. Very recently, Abderrahim et al. had attempted to use three thermoluminescence dosimeters (TLD), namely ^7LiF, Al_2O_3 and BeO, for gamma-ray dosimetry in a reactor [1]. Integrated gamma dose in a power reactor had been measured with LiF dosimeters by King and Gilliam [2] recently. Hashizume et al. [3] showed the properties of magnesium orthosilicate activated with terbium, $Mg_2SiO_4(Tb)$ (MSO) as an excellent TLD and applied

it to wide range gamma-ray dosimetry. Sato and Ono [4] tried to use MSO for gamma-ray dosimetry in therapeutic and other experimental facilities of the Kyoto University Reactor, KUR. In this work we have adopted MSO to measure gamma-ray distribution in the Kyoto University Critical Assemblies, KUCA and the results have been compared with those calculated by ANISN-JR [5] with combined cross sections of neutrons and gamma-rays generated by RADHEAT-V3 [5].

A similar comparison was carried out for gamma-ray distributions in four different irradiation fields at the Kinki University Reactor, UTR-KINKI. In this case, the neutron and gamma-ray distributions were calculated by a two dimensional transport code DOT 3.5 [6].

EXPERIMENTAL PROCEDURES

MSO Detectors: The MSO powder of about 10 mg manufactured by Kasei Optonics Co. Ltd. was weighed and packed into aluminum tubes of 1 mm in inner diameter, 0.5 mm in thickness and 1 cm in length. The MSO detectors attached on an aluminum holder were irradiated in reactors. A few days after the irradiation for cooling, the MSO powder was taken out from its tube and was scattered on a sample plate of a TLD reader. An integral value of the thermoluminescence glow curve was digitally printed out for each MSO powder sample. The relation between this value and absorbed dose in Gy had been calibrated by using a ^{60}Co source. As an experimental error of absorbed dose determination, we took 10% from our preliminary experimental data.

The response of the MSO detector to slow neutrons were experimentally obtained using a supermirror neutron guide tube of the KUR. As a result, the obtained value is about 4.9×10^{-14} Gy·cm^2/n. Therefore, we can neglect the contribution of thermal neutrons.

Configuration of Reactors: We measured neutron and gamma-ray fluxes in the B-core of the KUCA and in four irradiation fields at the UTR-KINKI. The horizontal views of the KUCA B-core with highly enriched uranium fuel and polyethylene moderator/reflector is shown in Fig. 1, and the aspects of its fuel element is shown in Fig. 2. The gold wires of 0.5 mm in diameter and the MSO detectors were irradiated along the small vertical gap surrounded by four aluminum sheaths of fuel elements, of which position is shown in Fig. 1.

The UTR-KINKI has two divided cores with highly enriched uranium fuel and water moderator surrounded by a large graphite reflector. In the middle of the divided cores, a part of inner reflector (graphite blocks) can be withdrawn and one of three neutron filter boxes (Bi, Fe and polyethylene) can be inserted into this position to make irradiation fields for mainly biological samples. The horizontal view of UTR-KINKI is shown in Fig. 3 and the aspect of the irradiation field is shown in Fig.4.

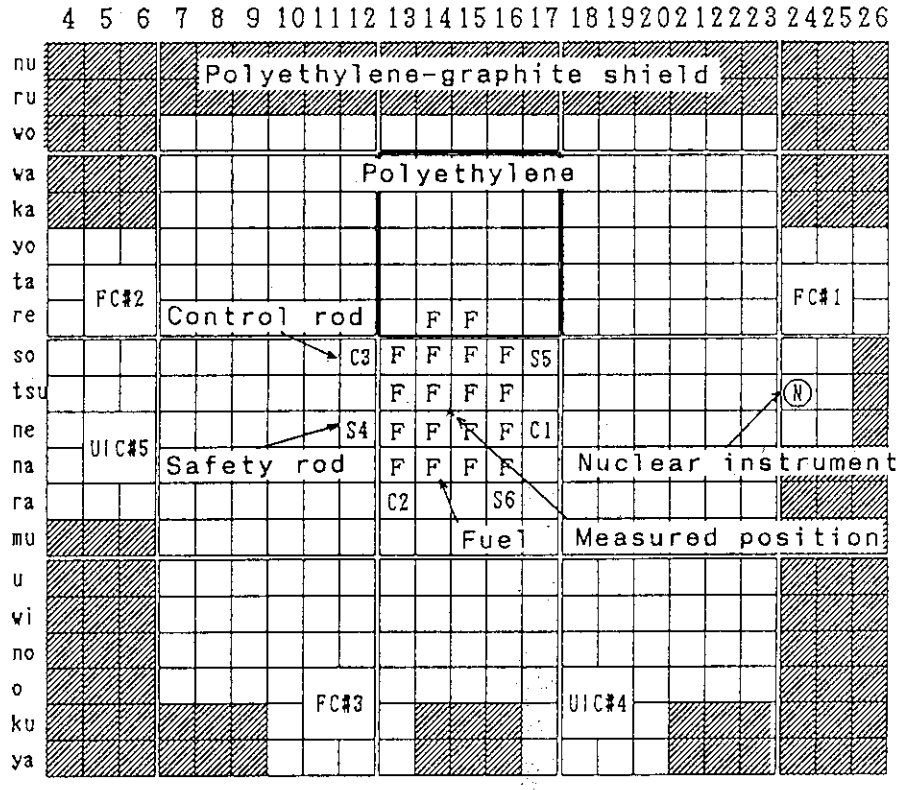

Fig. 1 Horizontal view of the KUCA B-core.

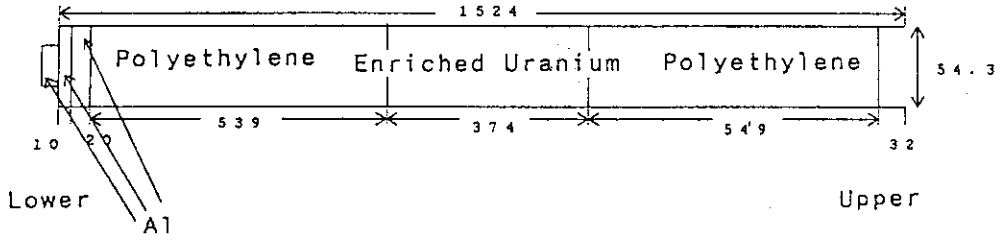

(Side view)

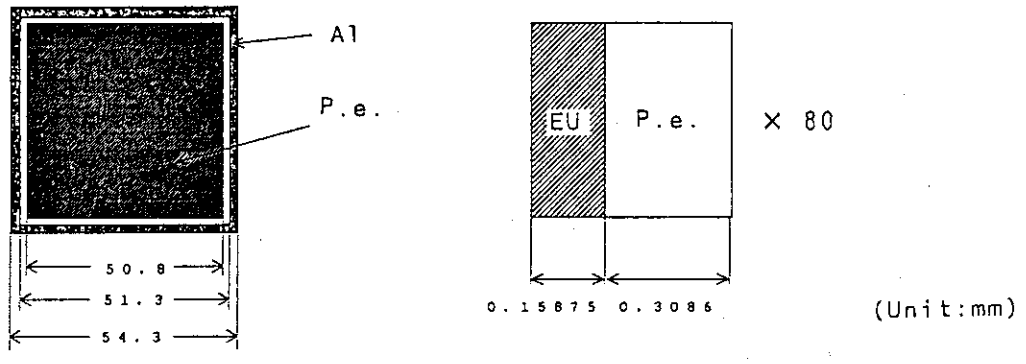

(Cross section) (Unit cell)

Fig. 2 Aspects of the KUCA fuel element.

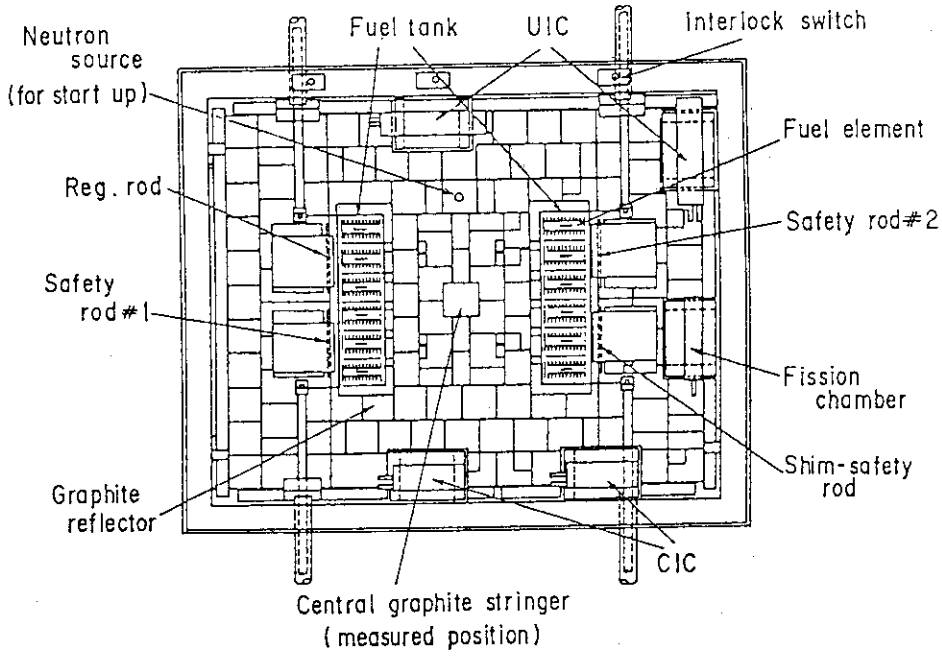

Fig. 3 Horizontal view of UTR-KINKI.

CALCULATION

For neutron-gamma coupled calculations, we assumed an infinite slab sandwiched by two polyethylene reflectors for the KUCA B-core and a finite cylinder for the UTR-KINKI. Neutron and gamma-ray combined cross sections for each region were generated by RADHEAT-V3 on the basis of the ENDF/B-IV and POPOP 4 libraries. As for neutron cross sections, JENDL-3[7] was also used. We took 100 and 18 groups for neutron and gamma-ray energies, respectively. For the transport calculation of neutrons and gamma-rays in the KUCA and the UTR-KINKI, we used ANISN-JR and DOT 3.5, respectively. For both cases, calculations

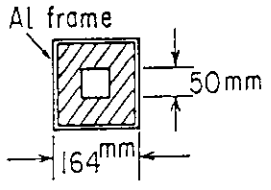

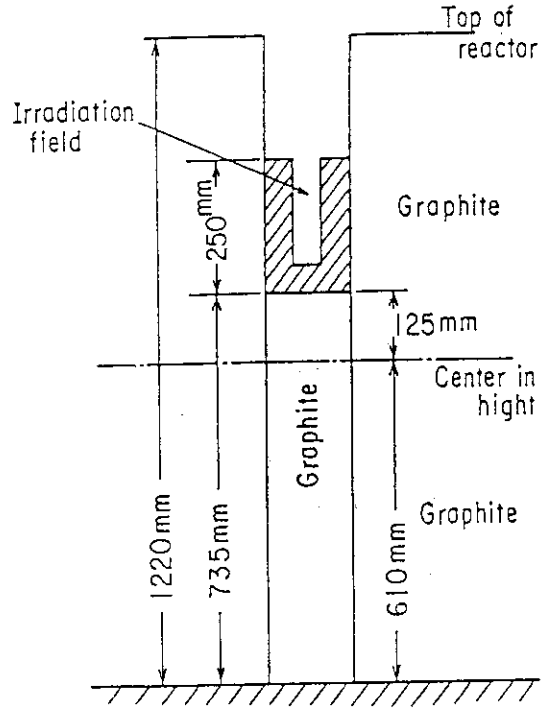

Fig. 4 Aspect of the irradiation field of UTR-KINKI.

were performed by P_3S_8 approximation.

Absorbed dose of gamma-rays was calculated from the obtained gamma-ray energy spectra and the mass absorption coefficients of MSO, and that of fast neutrons from the neutron spectra and kerma factors. The mass absorption coefficients and the kerma factors were taken from the references [8,9].

The contribution of delayed gamma-rays from fission products was estimated using the classical Way-Wigner's formula. We assumed that the delayed gamma-ray spectrum was similar to that of the fission gamma-rays. No cavity theory correction was considered, because the equivalent atomic number (11.1) of MSO is close to that of aluminum.

RESULTS AND DISCUSSION

The measured and calculated distributions of the neutron flux (gold wire activation) and those of absorbed dose of MSO in three KUCA cores are shown in Figs. 5 and 6. All data are normalized by the gold wire activation at the core center. The measured neutron flux distribution agrees very well with the calculated one. And then the absorbed doses of MSO in the core are slightly higher than the calculated values.

As seen in Figs. 7 and 8, all of the measured neutron flux distributions in the UTR-KINKI satisfactorily agree with the calculated ones, however the measured absorbed doses of MSO are considerably higher (about 20 - 50%) than the calculated ones for all cases under the similar normalization to the KUCA. In this case, the contribution of delayed gamma-rays was not taken into account for each irradiation field. Probably, this might cause the above discrepancy.

In the future, the calculations using JENDL-3 library [9] will be performed for both KUCA and UTR-KINKI, and then those results will be compared with those calculated using ENDF/B-IV library.

ACKNOWLEDGEMENT

The authors are deeply thankful to Mr. T. Sato for his guidance to use MSO detectors. The present work was achieved by the Cooperative Use Programs of both the KUCA of Kyoto University and the UTR-KINKI of Kinki University.

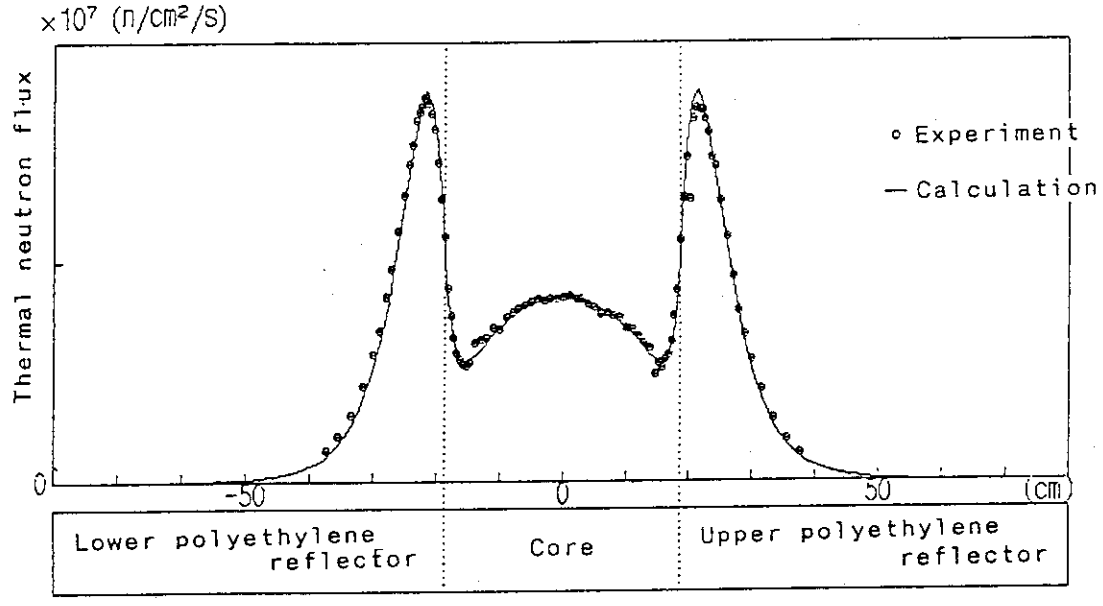

Fig. 5 Measured and calculated neutron flux distribution in the KUCA B-core.

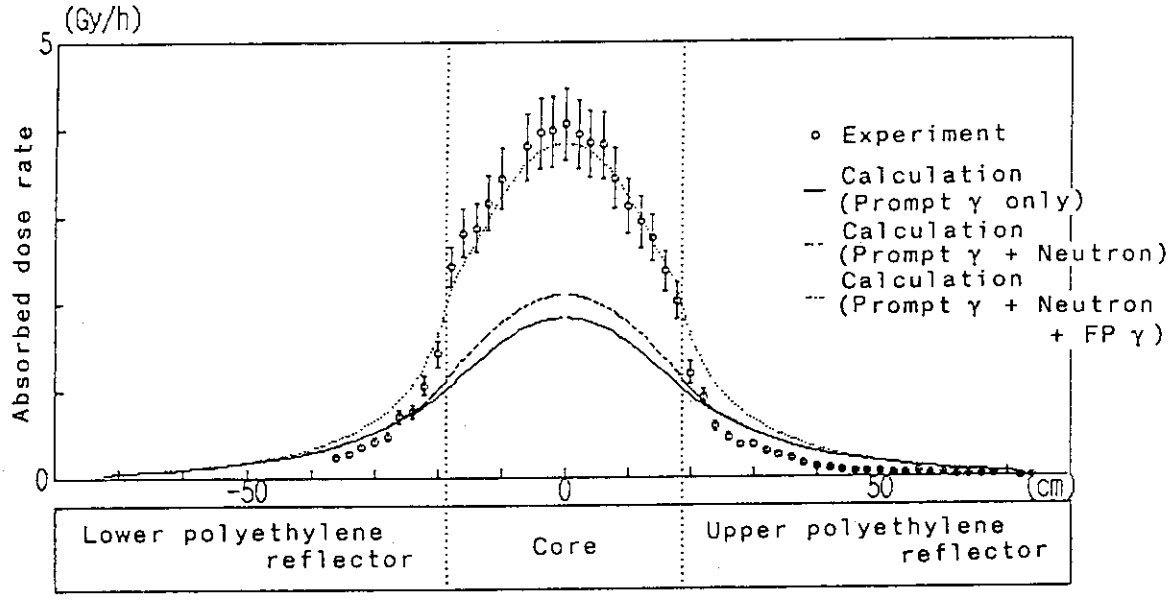

Fig. 6 Measured and calculated absorbed dose of MSO in the KUCA B-core.

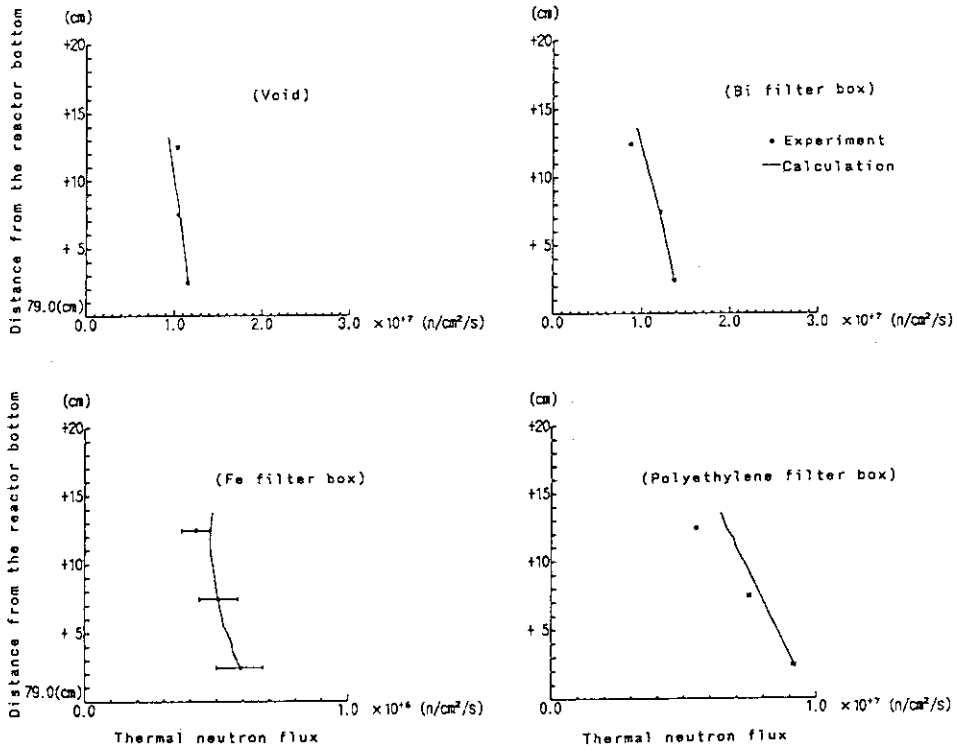

Fig. 7 Measured and calculated distributions of neutron fluxes for four cases of UTR-KINKI.

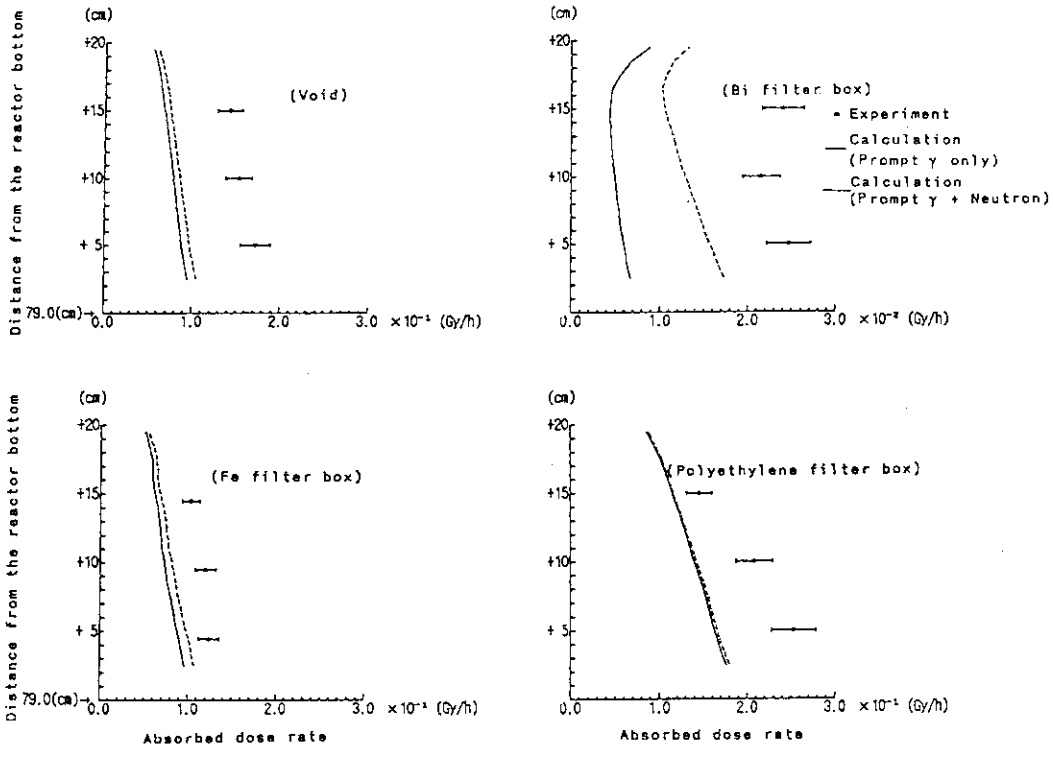

Fig. 8 Measured and calculated distributions of absorbed doses of MSO for four cases of UTR-KINKI.

References

1. H.A. Abderrahim, R. Menil and H. Geens : Proc. 7th ASTM/EURATOM Symp. on Reactor Dosimetry, Strasbourg, August, 1990, in press
2. S.Q. King and D.M.Gilliam : ibid.
3. T. Hashizume, Y. Kato, T. Nakajima, T. Toryu, H. Sakamoto, N. Kotera and S. Eguchi : Proc. IAEA Symp. on Advanced Radiation Detectors, SM-143/11, p. 91 (1971)
4. K. Sato and K. Ono : UNTL-R-0073, p. 46 (1979)
5. K. Koyama, K. Minami, Y. Taji and S. Miyasaka : JAERI-M 7155 (1977)
6. W. A. Rhoades and F. R. Mynatt, ORNL-TM-4280 (1973)
7. "JSSTDL-295/J3", A. Hasegawa, private communication (1989)
8. J.H. Hubbell : NSRDS-NBS 29 (1969)
9. ICRP Report 26 (1977)

1. Recent Studies on Short-Lived Fission-Product Nuclei Using the On-Line Isotope Separator KUR-ISOL

K. OKANO, Y. KAWASE, S. YAMADA, T. SHARSHAR
Research Reactor Institute, Kyoto University
Kumatori-cho, Sennan-gun, Osaka 590-04, JAPAN

T. KATOH, K. KAWADE, H. YAMAMOTO
Department of Nuclear Engineering, Faculty of Engineering
Nagoya University, Furo-cho, Chikusaku, Nagoya 464-01, JAPAN

K. AOKI
Himeji Institute of Technology, Shosha
Himeji, Hyogo-ken 671-22, JAPAN

and

J. Z. RUAN
Department of Physics, Rikkyo University
Nishiikebukuro, Toshima-ku, Tokyo 171, JAPAN

ABSTRACT

The He-jet fed isotope separator on-line facility(KUR-ISOL) attached to KUR(Kyoto University Reactor) has been used for the studies of neutron-rich nuclei in the rare-earth region. Recently two isotopes, ^{152}Ce($T_{1/2}$ = 1.4 ± 0.2 s) and ^{154}Pr($T_{1/2}$ = 2.3 ± 0.1 s), have been newly identified. From the γ-ray energies observed following the decay of ^{154}Pr, the excitation energy of the first excited state of ^{154}Nd was found to be 70.8 keV which indicates that the moment of inertia of this nucleus is the largest among those of known even-even nuclei in the rare-earth region. Nuclear spectroscopic studies on several short-lived nuclei around A = 150 have been performed and a lot of new results have been obtained. Ion implanted ^{140}Cs nuclei have been used for a solid-state physics research. Main results of these progresses will be described together with the recent developments on KUR-ISOL and on the high-efficiency, low-background detecting systems.

INTRODUCTION

In order to study systematically the Nuclei Far From Stability(NFFS) produced by fission, a He-jet fed isotope separator on-line has been constructed and installed at the KUR. Its basic layout and the identification of two new isotopes(^{155}Nd and ^{156}Pm) by using this facility have previously been described.[1] In addition to these two isotopes, two new isotopes (^{152}Ce and ^{154}Pr) have recently been identified. In order to search for new isotopes with lower fission yields, several developments are now tried to increase the beam intensity of KUR-ISOL.

Gamma-gamma angular correlation measurements have been performed on short-lived fission-product nuclei such as ^{146}La and ^{147}La using four HPGe multi-counter goniometer system recently developed. Precise determinations

of the decay schemes of a lot of short-lived fission-product nuclides around A = 150 have been performed including the measurements of Q_β-values and lifetimes of excited states. The detailed structures of these nuclei have been systematically studied. The mass-separated fission products have also been used as probe atoms for a microscopic study in solid-state physics. The time-differential perturbed angular correlation experiments with use of ^{140}Ba-^{140}La have been carried out to investigate the internal field at the Ba site in high-temperature superconducting YBaCuO compounds. Typical results of these studies will be presented together with recent developments around KUR-ISOL.

RECENT DEVELOPMENTS AT KUR-ISOL

1) N_2-jet transport system

In the actual design of He-jet coupled ISOL systems,[2,3] the exchange over time through the target chamber amounted to a few tens of second compared with the transit time through a capillary which was 1 s or shorter. As the range of fission products is much shorter in N_2 gas than in He gas, a smaller target chamber can be used for N_2 gas allowing much shorter exchange over time. The use of N_2 gas seems to have some advantage over He gas as both gases have almost the same transport time through a capillary.[4]

The yields of ionized activities from a surface-ionization type ion source of KUR-ISOL were measured as a function of the inlet gas pressure for both He and N_2 gases. Although the yields increased for N_2 gas, decreasing yields with pressure above $\sim$ 1.4 atm were observed and this was found to be quantitatively in agreement with the decrease of the first-skimmer efficiency originating from the increased opening angle of aerosol particles. The first-skimmer efficiencies were measured for the He- and N_2-jets by measuring the ratio of the transported activities of fission products and the results are listed in Table 1.[5] These test experiments were performed with a neutron flux of about 4×10^{11} n/cm^2•s or less. At the maximum neutron flux available($\sim 3 \times 10^{12}$ n/cm^2•s), these characteristics were found to be altered somewhat probably by the influence of strong radiations upon the characteristics of aerosol particles. Further investigations are now in progress.

Table 1. Opening angles and first-skimmer efficiencies of DOP aerosol particles in the case of a flat skimmer with a 1.5 mm dia. orifice, located at the distance of 5 mm from the end of a capillary of 1 mm inner dia.

Gas	Inlet pressure (atm)	Full opening angle[a] (degree)	50% opening angle[b] (degree)	First-skimmer efficiency[c] (%)
He	1.8		8.8	93
N_2	1.0	18	11.8	77
	1.4	25	14.5	62
	1.8	31	19.3	43
He(2)+N_2(1)	1.8		13.4	68

a) Measured full angle derived from the distribution of DOP aerosol particles collected on a Mylar film.
b) Full angle within which 50% intensity is included. This was calculated from the measured first-skimmer efficiency assuming a Gaussian distribution of aerosol particles at the skimmer orifice.
c) Measured efficiency using FP activities as mentioned in the text.

2) Ion source chemistry

In order to realize the efficient and selective ionization of Sr and Ba isotopes, a fluorination method has been investigated by the surface-ionization type ion source coupled with the double skimmer system. A small amount of CF_4 gas was introduced to a He-jet to generate molecular ions of the type MeF^+. The ionization characteristics have been studied as functions of the ionizer temperature and the CF_4 gas flow rate. [6] As illustrated in Fig. 1, it has been found that high ionization efficiencies for SrF and BaF can be achieved with relatively low ionizer temperature (1900°C) similarly to the oxidation method[7] for lanthanides. The elemental selection in the same mass chain can be done simultaneously by this method and pure Sr or Ba activities in fission products are available.

3) Four-Ge angular correlation apparatus

A high-efficiency γ-γ angular correlation apparatus using three 30% HPGe and one Ge(Li) detectors has been constructed for the measurements on short-lived nuclei. Commercially available four detectors are utilized as these can be used separately for other measurements. The front edge of each detector-cup was cut in a special shape so that the distance between the source and the detector can be as short as 5 cm in any actual configuration of the system.

Several kinds of multi-detector configurations for γ-γ angular correlation studies have been reported from various laboratories.[8-11] In the present experiment, measurements with the four Ge detectors are made twice at different fixed configurations. The differences in the coincidence efficiencies among the detector pairs can be eliminated by taking the ratio of the results of the two measurements.[12] The coincidence system employed in ref.[11] which gives different delays to each detector pulse and uses a single TAC unit is relatively simple. We have designed a special OR circuit which imposes a uniform delay time to all pairs, thereby decreasing accidental events.[12] Good results were obtained in spite of the large differences in the coincidence and detection efficiencies among the pairs. As an example, Fig. 2 shows a correlation pattern obtained for the 0-2-0 cascade in ^{146}Ce following the

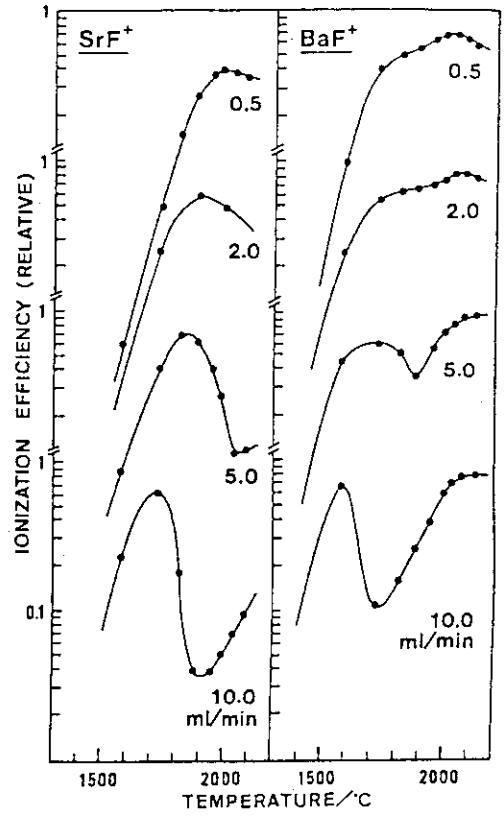

Fig. 1. Ionization characteristics of SrF and BaF. The CF_4 gas flow rate is changed from 0.5 to 10 mℓ/min while the He flow rate is fixed at 800 mℓ/min. Ionization efficiencies are given in relative values normalized to Cs(=100%).

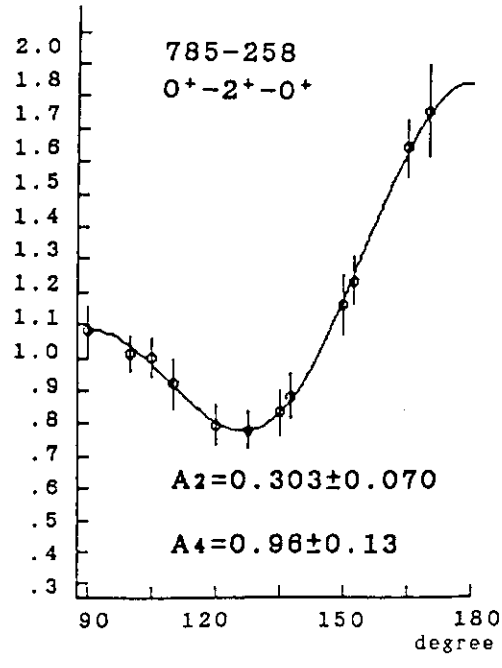

Fig. 2. The fitted result of γ-γ angular correlation measurements on the 0-2-0 cascade in ^{146}Ce following the decay of 6.3 s ^{146}La.

decay of 6.3 s ^{146}La.

4) $4\pi\beta$-γ detecting system

For the identification of new isotopes, β-X and β-γ coincidence measurements are usually essential to determine Z of the decaying nucleus, to discriminate against the possibility of an unknown isomer and to suppress room backgrounds. A $4\pi\beta$ counter with two 80 mm × 80 mm × 1 mm NE-102 plastic scintillator coupled to a low-noise RCA-8575 photomultiplier was used in conjunction with a CANBERRA 50% HPGe detector or with an ORTEC planar LEPS (Low-Energy Photon Spectrometer). The detecting efficiency of this system has been tested using several isotopes. In the case of off-line measurements, the detection efficiency almost equal to the solid angle(72%) was obtained for γ-rays from ^{42}K(E_γ = 1525 keV, Q_β = 3.53 MeV) as well as from ^{166}Ho(E_γ = 80.6 keV, Q_β = 1.85 MeV). In the case of on-line measurements, however, the efficiency was found to decrease on account of 0.3 mm thick Al windows. The efficiencies measured for prominent γ-rays and X-rays were 62% for ^{94}Rb(Q_β = 10.31 MeV) and 49% for ^{146}La(Q_β = 6.39 MeV). The thickness of the Al window is just enough to stop conversion electrons from an unknown isomer. The detailed characteristics of this system will be published later. [13]

RESEARCHES ON NFFS PRODUCED BY FISSION

I) Identification of new neutron-rich isotopes produced by fission

i) ^{154}Pr

The heaviest isotope of praseodymium, ^{154}Pr, was identified by γ-ray measurements of mass separated activities. Gamma-ray multi-spectrum scaling measurements were carried out with the LEPS for low-energy γ-rays and X-rays and with the 30% HPGe detector for high-energy γ-rays. From the half-life measurements on the observed γ-lines, 10 γ-rays and Nd X-rays were found to decay with a half-life of 2.3(1) s. The decay curves measured are shown in Fig. 3. It is then concluded that these short-lived components are generated by the β-decay of ^{154}Pr. The observed 70.8 and 162.4 keV γ-rays correspond to the 2^+-0^+ and 4^+-2^+ transitions in ^{154}Nd, respectively. The spin and parity of the ground state of ^{154}Pr are probably 3^+ because the log ft values to the 4^+ and 2^+ levels in ^{154}Nd are estimated to be about 5.4 and 4.8, respectively, and no β-feeding was observed to the 6^+ level in ^{154}Nd. [14]

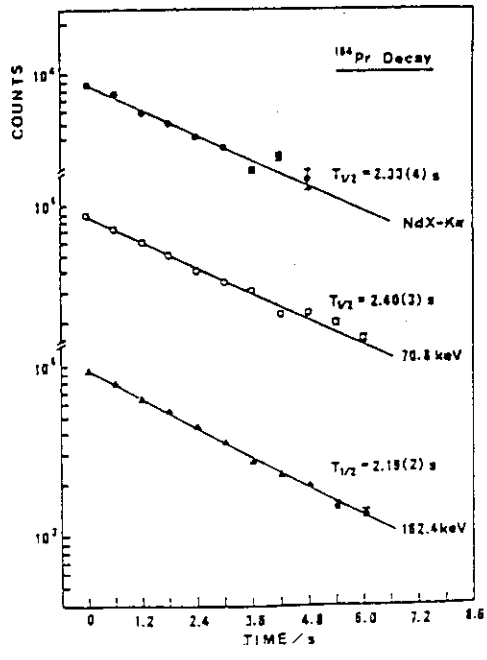

Fig. 3. Decay curves of γ- and X-rays assigned to the decay of ^{154}Pr.

ii) ^{152}Ce

Although the ^{152}Ce isotope was once reported as identified to decay with a half-life of 3.1(3) s,[15] the γ-γ coincidence experiments on ^{152}Pr showed that the 285 keV γ-ray, a single γ-ray line assigned to the ^{152}Ce decay, belongs to the decay of ^{152}Pr.[16] The search for ^{152}Ce has been carried out by means of γ-ray and X-ray decay measurements. The experimental procedure is almost the same as the ^{154}Pr case except that the optimum values of the collection and measuring times for ^{152}Ce were chosen.

Two γ-ray lines at 97.8 and 114.8 keV were found to have shorter half-lives than ^{152}Pr. The Pr X-K_α line was observed to decay with the same half-life. A β-γ coincidence measurement was also performed using a 1 mm thick Al absorber to suppress the contribution of internal-conversion electrons. The 97.8 keV transition was confirmed to be in full coincidence with the β-ray. The 114.8 keV transition, however, was found to be delayed about 1 μs.

It is then concluded that the two γ-rays and the Pr-K_α X-ray are generated by the β-decay of ^{152}Ce with a half-life of 1.4(2) s.[17]

iii) Moment of inertia and deformation

Neutron-rich isotopes with mass number 150 ≦ A ≦ 190 belong to the well-established deformed region of rare-earth nuclei. These nuclei show characteristic ground-state rotational band with the excitation energies $E_I = \hbar^2/2\mathcal{J}I(I+1)$ for rotational states with angular momentum I. The moment of inertia $\mathcal{J}$ at the ground state can be derived from the excitation energy of the first excited state, E_{2+}, as $3\hbar^2/E_{2+}$. The moments of inertia of nuclei for rotational motion thus derived for even-even nuclei in this mass region are plotted in Fig. 4, together with the rigid-body values. It can be seen that the newly found moment of inertia for ^{154}Nd shows the largest value among those of known even-even nuclei in this mass region.

As can be seen from Fig. 4, the maximum moment of inertia for each isotope seems to decrease with mass number in this mass region, in contrast to the general tendency hitherto reported.[18,19] This may indicate that the deformation increases towards the neutron-rich light rare-earth nuclei. The fact that the moments of inertia observed are appreciably smaller than rigid-body values has been attributed to the pairing correlations in the intrinsic nucleonic motion. For quantitative explanation of the tendency as described, precise estimates of deformation parameters and pairing-energy gap parameters are necessary for NFFS.

iv) Half-life of NFFS

The half-lives of unknown NFFS have first been predicted by Takahashi et al. by a gross theory of β-decay.[20] This theory has been modified recently and revised values of predicted half-lives have recently been published by Tachibana et al.[21,22] Klapdor et al. have also calculated beta-decay half-lives of neutron-rich NFFS by a microscopic theory using Tamm-Dancoff approximation.[23] This prediction was expected to improve the gross theory particularly in regions very far from stability. This microscopic approach has recently been revised to a second generation version using the proton-neutron quasiparticle random phase approximation with a schematic GT residual interaction.[24,25]

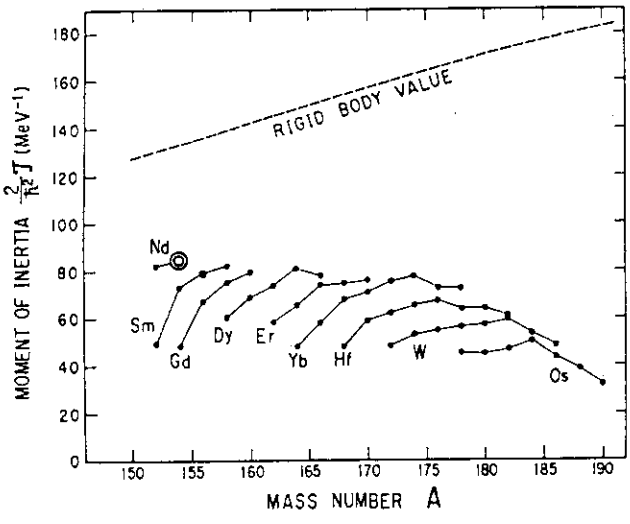

Fig. 4. Systematics of moments of inertia for even-even nuclei in the mass region 150 ≦ A ≦ 190. The mark ◎ indicates that the moment of inertia has been derived from the present measurement.

In Fig. 5, the half-lives of Ce isotopes so far experimentally determined are compared with these theoretical predictions. It can be seen that the theoretical predictions are always larger than experimental values for Ce isotopes, although the rate of decrease with mass number is well reproduced. It can also be noticed that the even-odd effect clearly observed experimentally is not well reproduced

in the case of the gross theory. Both theories predict that the half-life decreases mainly at even mass number for A ≧ 152, but this is in contradiction with the general tendency experimentally observed that the half-life decreases mainly at odd mass number for even Z nuclei. Whether the predicted tendency really exists or not at these neutron-rich isotopes is of interest.

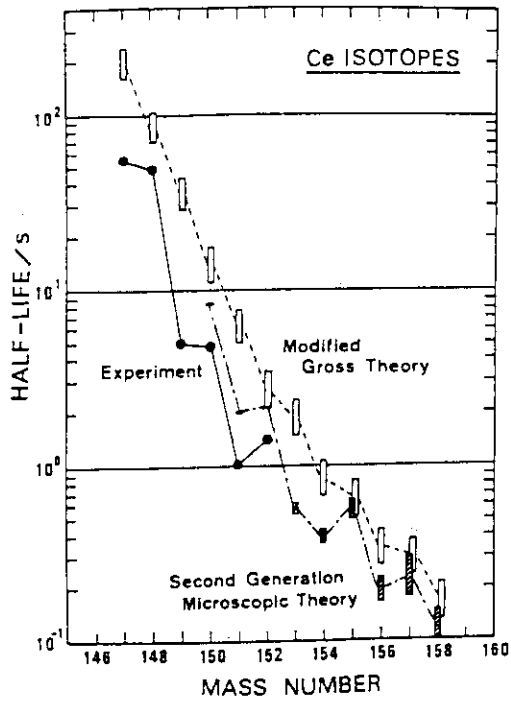

Fig. 5. Half-lives of Ce isotopes. The upper and lower limits of the bar shown for the modified gross theory[21,22] correspond to the predicted values in the cases of 2b and 1b, respectively, of ref.[22]. In the case of the second generation microscopic theory,[24,25] upper and lower limits shown for mass number between 153 and 158 correspond to the differences in predicted mass values.

II) Nuclear spectroscopic studies on NFFS

i) ^{146}La

The ^{146}Ce nucleus has N = 88 and is located at the onset of well-known deformed region. Although the decay scheme already reported[26] is rather complicated, coincidence measurements revealed fourteen new levels at 1551.2, 1627.3, 1711.9, 1736.7, 1769.4, 1810.7, 1875.8, 1891.9, 1916.2, 1956.7, 2139.7, 2177.7, 2257.0 and 2270.4 keV. The angular correlation coefficients obtained for the 1015.9-258.5 keV cascade using the four Ge system mentioned were $A_2 = -0.18 \pm 0.07$ and $A_4 = 0.35 \pm 0.14$. From these, the spin value of the level at 1274.3 keV could be uniquely decided as 2. The large E2 component ($\delta = 6.2 \pm \frac{9}{2}\frac{6}{8}$) obtained for the 1015.9 keV transition indicates the characteristic of the β-vibrational state for the 1274.3 keV level, which is consistent with the systematics observed in Ce isotopes.[27] More precise investigations on a lot of high-lying levels are continued.

ii) ^{147}La

Gamma-ray spectra following the decay of 4.1 s ^{147}La were measured using a 142 cc Ge(Li) detector and the 30% HPGe detector. The γ-rays originating from the decay of ^{147}La were identified by 1)comparing the spectra taken at different tape speeds, 2)spectrum-scaling measurements and 3)γ-γ coincidence measurements. A lot of doublet lines have been identified and about 60 new lines have been found. The analyses of γ-γ coincidence data of 2×10^7 events were carried out by setting the gates on almost all the γ-rays. The decay scheme of ^{147}La consisting only of the transitions confirmed by the coincidence measurements was newly established. 28 levels were newly identified in ^{147}Ce.[28]

The spins and parities of the low-lying levels in ^{147}Ce and the ground state of ^{147}La have been determined from the γ-γ angular correlation measurements as well as from the multipolarities of γ-rays determined by the internal-conversion electron measurements. Log ft values deduced from the β-branching ratios newly determined by a filiation measurement of main γ-rays were also utilized. Examples of the correlation patterns obtained are shown in Fig. 6. The spin sequence deduced indicates the similarity of the low-lying levels of $^{147}Ce^{89}$ to $^{149}Nd^{89}$ rather than to $^{145}Ba^{89}$, contrary to the tendency hitherto reported. The low-lying level structure observed in ^{147}Ce is in good agreement with the calculated one based on the rotation-vibration coupling model.

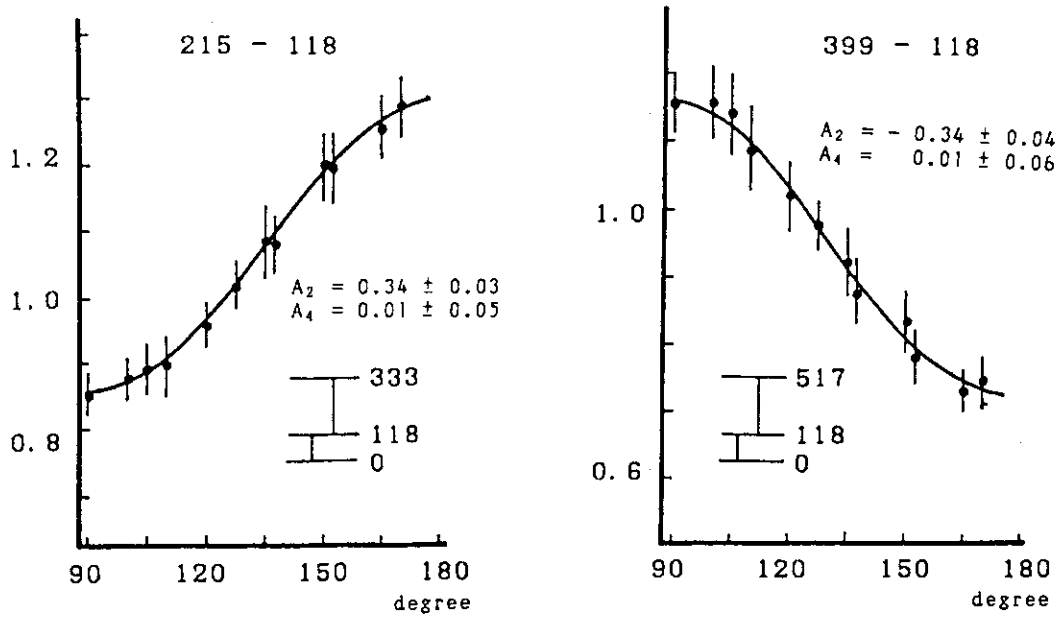

Fig. 6. Results of γ-γ angular correlation measurements on the cascades following the decay of 4.1 s ^{147}La.

ⅲ) ^{147}Pr, ^{151}Pr, ^{152}Nd, ^{152}Pm

The decay schemes of ^{147}Pr($T_{1/2}$ = 13.4 m),[29] ^{151}Pr($T_{1/2}$ = 4 s),[30] ^{152}Nd($T_{1/2}$ = 11.4 m)[31] and ^{152}Pm($T_{1/2}$ = 4.1 m)[31] have been precisely determined from the γ-ray singles, γ-γ coincidence, X-γ coincidence, β-ray singles, β-γ coincidence, β-γ delayed coincidence, internal-conversion electron and lifetime measurements.[32] In addition to the apparatus as mentioned above, another high-efficiency LEPS of Nagoya Univ. was utilized. A lot of new lines and levels in daughter nuclides have been identified. Precise Q_β values, mixing ratios of transitions and lifetimes of levels have been newly determined. As an example of the lifetime measurements, β-γ delayed coincidence curves measured are shown in Fig. 7. Spins, parities, log ft values and transition probabilities of the levels concerned have been deduced. The details of these precise experimental results and comparisons with theoretical predictions will soon be published.

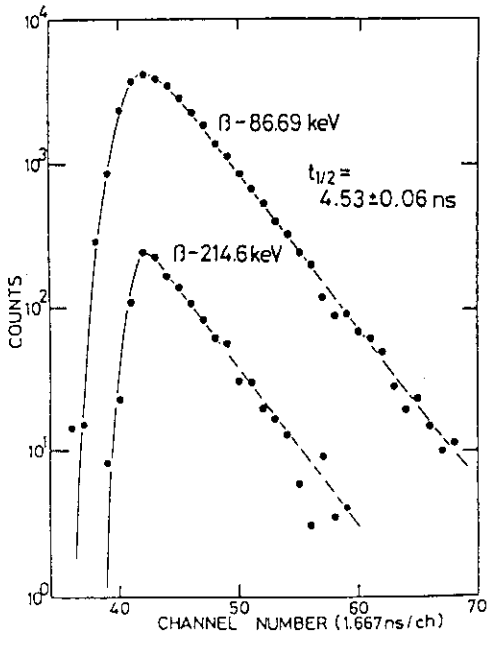

Fig. 7. Time distributions in the β-γ delayed coincidence measurements on ^{147}Pr.

Ⅲ) Solid-state physics research

^{140}Cs isotopes obtained by the ISOL were used as a tool to study on electromagnetic properties of YBaCuO superconducting compounds. ^{140}Cs atoms which decay to ^{140}Ba with a half-life of 63.7 s were implanted on a disk of $YBa_2Cu_3O_7$ or $YBa_2Cu_3O_6$. The time differential perturbed angular correlation experiments were carried out at 77 K and at room temperature.[33] The attenuation of the angular correlation was observed for the $YBa_2Cu_3O_6$ compound under a transverse magnetic field of 0.4 T. This result is consistent with the antiferromagnetic property of $YBa_2Cu_3O_6$ observed by the Mössbauer spectroscopy. [34]

ACKNOWLEDGEMENTS

The authors would like to express their sincere thanks to the reactor operating group of KURRI for their efforts. Thanks are also due to the members of our machine shop for their technical supports. The works on ^{147}Pr, ^{151}Pr, ^{152}Nd and ^{152}Pm were mainly performed by young researchers of Nagoya group as cited in refs.[29-32].

REFERENCES

1) K. Okano, Y. Kawase and K. Aoki, Proc. First Asian Symp. on Res. Reactors (1986, Tokyo) p.175.

2) R. A. Anderl, V. J. Novick and R. C. Greenwood, Nucl. Instr. and Meth. **186** (1981) 153.

3) M. Brügger, Doctorate Theses, University of Mainz(1983).

4) K. Kawade, H. Yamamoto, H. Amano, M. Hanada, T. Katoh, K. Okano, Y. Kawase and I. Fujiwara, Nucl. Instr. and Meth. **200** (1982) 417.

5) T. Sharshar, K. Okano and Y. Kawase, Proc. EMIS-12 Conf.(1991, Sendai), to be published in Nucl. Instr. and Meth. **B**.

6) Y. Kawase, K. Okano, M. Shibata and A. Taniguchi, Proc. EMIS-12 Conf. (1991, Sendai), to be published in Nucl. Instr. and Meth. **B**.

7) Y. Kawase and K. Okano, Nucl. Instr. and Meth. **B37/38** (1989) 116.

8) T. Hayashi, K. Okano, K. Yuasa, Y. Kawase and S. Uehara, Nucl. Instr. and Meth. **53** (1967) 123.

9) T. Hayashi, S. Uehara and T. Seo, Nucl. Instr. and Meth. **118** (1974) 541.

10) E. W. Schneider, M. D. Glascock and W. B. Walters, Phys. Rev. **C19** (1979) 1025.

11) A. Wolf et al., Nucl. Instr. and Meth. **206** (1983) 397.

12) S. Yamada, T. Sharshar, K. Aoki and K. Okano, to be published in Nucl. Instr. and Meth. **A**.

13) T. Sharshar and K. Okano, to be published.

14) Y. Kawase and K. Okano, Z. Phys. A-Atomic Nuclei, **330** (1988) 231.

15) J. C. Hill, H. Yamamoto and A. Wolf, Phys. Rev. **C27** (1983) 2857.

16) T. Karlewsky, N. Hildebrand, M. Brügger, N. Kaffrel, N. Trautmann and G. Herrmann, Z. Phys. A-Atomic Nuclei **330** (1988) 55.

17) I. Tago, Y. Kawase and K. Okano, Z. Phys. A-Atomic Nuclei **335** (1990) 477.

18) S. G. Nilsson and O. Prior, Mat. Fys. Medd. Dan. Vid. Selsk. **32** no.16 (1960).

19) A. Bohr and B. R. Mottelson, Nuclear Structure, vol.II, p.74, Benjamin, Massachusetts (1975).

20) K. Takahashi, M. Yamada and T. Kondoh, At. Data Nucl. Data Tables **12** (1973) 101.

21) T. Kondoh, T. Tachibana and M. Yamada, Prog. Theor. Phys. **74** (1985) 708.

22) T. Tachibana, M. Yamada and K. Nakata, Report of Sci. and Eng. Res. Lab. Waseda Univ. No. **88-4** (1988).

23) H. V. Klapdor, J. Metzinger and T. Oda, At. Data Nucl. Data Tables **31** (1984) 81.

24) A. Staudt, E. Bender, K. Muto and H. V. Klapdor, Z. Phys. A-Atomic Nuclei **334** (1989) 47.

25) A. Staudt, E. Bender, K. Muto and H. V. Klapdor, At. Data Nucl. Data Tables **44** (1990) 79.

26) L. K. Peker, Nucl. Data Sheets **60** (1990) 953.

27) S. Yamada, K. Aoki, T. Sharshar, Y. Kawase and K. Okano, Annu. Rep. Res. Reactor Inst. Kyoto Univ. **24**.

28) K. Aoki et al., to be published.

29) M. Shibata, H. Yamamoto, K. Kawade, T. Katoh, J. Z. Ruan, T. Tamai, Y. Kawase and K. Okano, to be published.

30) M. Shibata, A. Taniguchi, T. Ikuta, A. Osa, H. Yamamoto, K. Kawade, J. Z. Ruan, Y. Kawase and K. Okano, to be published.

31) M. Shibata et al., to be published.

32) M. Shibata, A. Taniguchi, T. Ikuta, H. Yamamoto, K. Kawade, T. Katoh, J. Z. Ruan, Y. Kawase and K. Okano, Kyoto Univ. Res. Reactor Inst. Technical Report KURRI-TR-348 (1991) p.83.

33) Y. Kawase, S. Uehara, S. Nasu and Y. Ueda, Proc. M^2S-HTSC Ⅲ Conf. (1991 Kanazawa), to be published in Physica C.

34) S. Nasu et al., Advances in Superconductivity Ⅱ, (1990) p.559.

2. Rapid Chemical Separation of Short-Lived Nuclides Formed by the Irradiation of Reactor Neutron

T.TAMAI, S.NISHIKAWA, J.TAKADA, R.MATSUSHITA, Y.TANAKA

Research Reactor Institute, Kyoto University,
Kumatori-cho, Sennan-gun, Osaka-fu 590-04, JAPAN

ABSTRACT

A brief review is presented on both a paper electrophoretic and radio ionchromatographic methods for the rapid chemical separation of short-lived nuclides formed by the irradiation of reactor neutron. A general consideration of separating the element of interest from the other fission products and the separation procedure with the specially designed migration apparatus are described. The isolation of Cs, Rb, Sr, Ba, rare earths, Se, Mo, and halogens are carried out only within 20 sec under the selected migration condition: the kind and the pH of supporting electrolyte solution, the addition of a stopping agent against the interfering ions. On the other hand, a new system of radio ionchromatography is also described in which radioactive ions are separated on a single ion exchange column of low capacity and are detected with both a conductivity detector and a NaI(Tl) detector. The elements in question are alkali metal ions, alkaline earths, rare earths, halogens, and selenium. Separation is generally achieved within 10 min.

These techniques provide a rapid and highly selective method for separating the chemical species of the radioactive ions under the state of carrier-free and determining the nuclear properties of short-lived nuclides in fission products and/or recoiled atoms formed by nuclear reaction.

INTRODUCTION

Up to today, many kinds of rapid chemical separation techniques have been employed in the study of short-lived nuclides irradiated by the reactor neutrons. An excellent review on rapid radiochemical separations of short-lived nuclides was published by Herrmann & Trautmann[1]. As a rapid chemical separation method for short-lived nuclides, we developed two rapid chromatographic techniques: one is a high voltage paper electrophoretic technique, and the other is a radio ionchromatographic technique.

As a simple separation technique, an usual paper electrophoretic method has been used for a long time in many fields such as medical, pharmacological, biological, chemical fields. However, the method is not rapid enough for the separation of short-lived nuclides which has to be done within a few min. In order to isolate these short-lived nuclides from the mixtures of many elements, development of a more simple and rapid technique is required. For the achievement of this goal, a migration apparatus was specially and produced.By using this apparatus, the short-lived nuclides

with half-lives less than one min have been successfully isolated for the determination of these nuclear properties.

On the other hand, the ionchromatograph with a conductivity detector was invented as a dual-column system for the rapid separation and determination of inorganic anions by Small et al.[2]. Gjerde et al.[3] developed a single-column method for a quantitative separation of several common anions and cations. Both apparatus have a separating column filled with an ion exchange resin of low exchange capacity and are employed with very dilute solutions. Although many conductivity detectors for the determination of the amount of ions in a solution have been greatly improved in recent years, these conductivity detectors could not be used for the detection of very low concentrations of the ions less than a ppb, such as short-lived fission products.

By combining a radiation detector with the usual conductivity detector, we have been able to develop a successful system for the separation and detection of very low concentration of radioactive ions. The separated radioactive ions are easily detected by the radiation detector placed immediately after the conductivity detector. The final goal of the present study was to develop a new ionchromatograph system that uses a NaI(Tl) detector and to apply it the isolation and detection of the short-lived nuclides in fission products resulting from reactor-neutron irradiation.

EXPERIMENTAL

Apparatus

In general, the migration distance of ion D is proportional to the mobility U. The given potential gradient E and the migration time t also relate each other as follows:

$$D = U \cdot E \cdot t$$

For the sake of rapid separation, the considerable migration distance over several centimeters and the narrow band of the migrated ions must be obtained by making the migration time as short as possible. For this migration condition, the potential gradient ought to be applied as high as possible. Under the high potential gradient, and the paper strip heats due to Joule's heat, and the migration bands are apt to broaden. To avoid such undesirable results, a forced removal of the Joule's heat is necessary to keep the temperature low enough and constant during the migration. A good reproducibility of the migration band is then obtained. For the sake of separation, the temperature should moderately be higher and constant. In this case the forced cooling method is also helpful.

With the object as stated above, an electrophoretic apparatus has been specially designed by Matsushita et al.[4] for separation of very short-lived fission products. The improved migration apparatus consists of three separated cells; a pair of electrode cells connected with platinum electrodes and a migration cell as shown in Fig. 1.

For releasing Joule's heat from electrophoretic paper strip, copper-fins attached to the supporting plate are constantly cooled with circulating water. The paper strip dipped with the supporting electrolyte solution is placed on the supporting plate and at both ends of the strip the electro-conductive pieces of double fold paper partly covered with cellophane sheet so as not to be ooze are mounted on. After setting the paper strip, a cover plate is placed by hand touching. On releasing the hand, the cover plate lifts up automatically. Both plates mentioned above are made of

copper. Using this apparatus, rapid separation of short-lived nuclides can be performed in 5 to 100 sec of migration time.

The basic liquid chromatographic system (HLC-847), which is marketed as a commercial instrument by Toso Co., was connected to a radio-ion chromatograph with a single separation column containing a gel-type resin and was used for the separation of fission products. The radio ion chromatographic system used, as shown in Fig. 2, consists of a pump system, three eluents tanks, a sample injection valve, a resin column, a conductivity detector, a radiation detector, a fraction collector, a two-pen recorder, and 16-bit microcomputer.

The radiation detector consisted of 2"x 2" NaI(Tl) detector with 200 µl loop for the detection of radioactive nuclides. For the injection of sample solution, a sample loop of 20 µl was used.

The column was packed with a gel-type resin of particle size 5-10 µm. The dimensions of the column were 50 mm in length by 4.6 mm in diameter. The cation exchange resin was sulfonated to give a low-exchange capacity of the order of micro equivalents per gram. The silica-base resin and a polymer-type resin were used for the separation of anions in the aqueous sample solution.

All eluents were prepared with double distilled deionized water and passed through a degasing apparatus just before pump. The pump serves to force the eluent from the eluent tanks to the fraction collector through the sample loop, column, and detector at a flow rate of 1.0-1.2 ml/min.

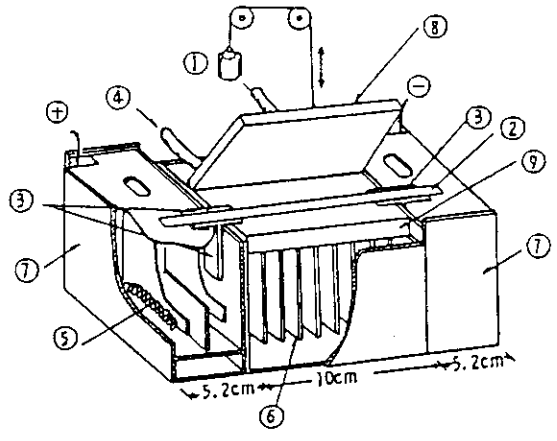

1: weight for lifting cover plate 8,
2: paper strip as a migration medium,
3: conductive guide of double folded filter paper convered with a cellophane sheet,
4: cooling water,
5: platinum electrode,
6: copper fins for cooling of copper plate with circulating coolig water,
7: electrode cell,
8: cover plate sealed with tephlon sheet,
9: copper plate sealed with tephlon sheet for supportig paper strip.

Fig.1 Migration apparatus.

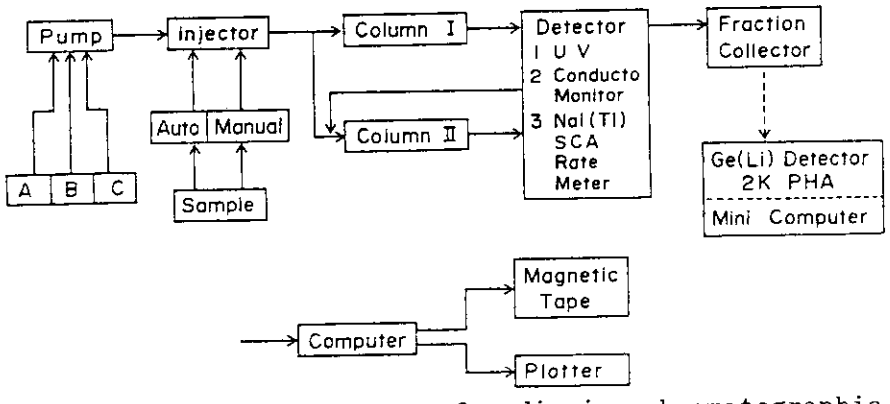

Fig.2 Schematic diagram of radio-ion chromatographic apparatus.

Procedure

For a typical electrophoretic separation, a small amount(5 μl) of 0.02 M enriched (90%) uranyl nitrate solution sealed in polyethylene capillary was irradiated for 10-100 sec at a thermal neutron flux of 2.35×10^{13} n/cm^2 sec at dry ice temperature in the pneumatic tube facility of the Kyoto University Reactor (KUR). The transport time of irradiated sample from the irradiation position in the reactor to a receiving station of radiochemical receiving laboratory near the separation apparatus was about 4 sec.

Before the start of sample irradiation, a paper strip(Toyo Roshi No. 50, 1 cm x 25 cm) was dipped uniformly with supporting electrolyte solution and removed the excess solution with another filter paper. Thus treated filter paper was set on the migration apparatus as seen in Fig. 1. After 10-20 sec of the setting, the irradiated sample was received and opened at the receiving station. The sample solution was spotted from the capillary on the penciled premarked line of the paper strip. After pressing softly the strip with a cover plate, the high voltage(500 V/cm) was applied for 10-60 sec. For the sake of quickness, without drying the migration paper, the located position of the desirable element on the strip was cut in the range of 5-10 mm in width.

To prepare the sample solution for injection into the radio ionchromatographic system, the irradiated sample solution (5 μl) was diluted immediately with distilled water to volume of 100 μl. The fraction of eluents corresponding to the peaks of the separation pattern were collected for gamma-ray measurements with a Ge(Li) detector. The spectral data were stored on magnetic tape. The energies and photopeak areas of the gamma-rays were determined with a minicomputer.The identification of the short-lived nuclides was done by those of comparison of the observed energies of gamma-rays and half-lives of the nuclides with those of the reference values.

RESULTS AND DISCUSSION

Most of the chemical species of the fission products are ionic in a common aqueous solution and the half of them are cations. The complete separation of a desired species of cation from many others is very difficult within short migration time. However, the oxidation numbers or the chemical forms of many cations are changeable as functions of the kind, the concentration and the pH value of the supporting electrolyte solution.

Cesium and rubidium are contained in fission products of binary fission of neutron captured uranium. Generally, these elements are unchangeable into anion by complex formation. These cations except alkali metal elements are able to change into citrate complex anions that electromigrate toward anode. When 0.01 M citric acid (pH 9.0) solution is chosen as supporting electrolyte solution, cesium and rubidium will be separated easily from other fission products .

If one would like to separate cesium from rubidium each other, the separation can be carried out using atomic exchange reaction. A small amounts of cesium silico-tungstate are spotted on a paper strip at the position where alkali metal ions will pass through, thereafter sample solution is spotted. And the potential is applied to make cesium and rubidium start to migrate toward cathode. When alkaline ions contact with the cesium silico-tungstate, cesium ions are trapped with the precipitate,

while rubidium ions continue to migrate toward cathode. Then separation of cesium and rubidium is achieved.

For separation of strontium and barium from rare earths and other cations in fission products, a nitrirotriacetic acid (NTA) is used as a complex agent[5],[6]. The NTA solution of 0.01 M concentration is optimum for the separation. A 0.01 M potassium chromate solution, containing 0.001 M NTA, is effectively used for the isolation of barium from strontium on a paper strip during migration. The potassium chromate solution is spotted at the cathodic side 10 mm apart from the original position where the sample solution will be spotted. A carrier solution of strontium and barium is previously prepared by mixing equal volumes of both 0.01 M barium chloride and strontium nitrate solution. The mixture is spotted at the original position before the sample solution is spotted.

On starting the electrophoretic separation, the chromate ions migrate toward the anode, while the strontium and barium ions migrate toward the cathode. Soon the alkaline earth ions come across the chromate ions. Barium ions react selectively with chromate ions to remain precipitated, separating from strontium which migrate farther. As the results, barium and strontium can be isolated each other. The other fission products like as rare earths migrate toward anode as NTA complex anions. The typical isolation patterns of barium and strontium from fission products are shown in Fig. 3.

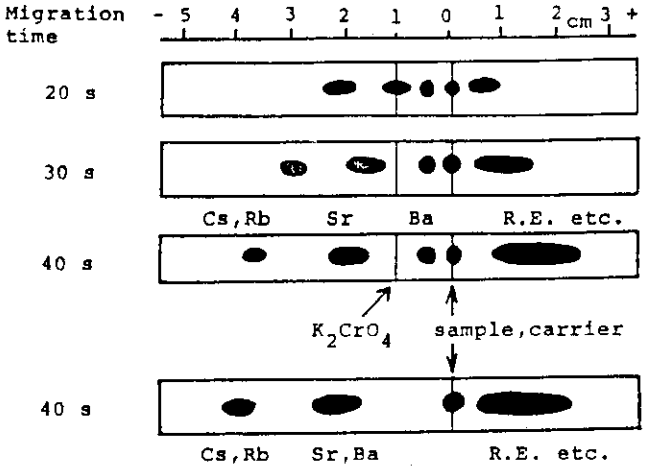

Fig. 3 Separated Pattern of Sr and Ba in Fission Products.
Experimental Condition :
Potential Gradient
5000 V/ 15 cm
Electrolyte Solution
0.01 M NTA (pH 4.1)

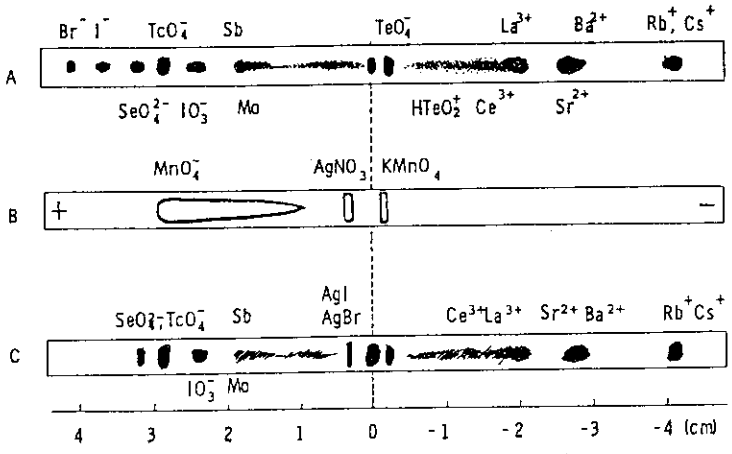

Fig. 4 Separation Patterns of Short Lived Fission Products.
Experimental Condition:
Potential Gradient
5000 V/ 10 cm
Electrolyte Solution
0.01 M Perchloric Acid (pH 2.2)
Migration Time
20 sec

It has been found that separation of rare earths from other fission products can be made by controlling the value of concentration of ligand ion. The zones separated were identified in their locations by color reactions with Arsenazo III.

The mobilities of anions such as oxyacids of arsenic, selenium, molybdenum, technetium, antimony and tellurium can not be estimated completely because there are few informations of dissociation constant or experimental results. Also, chemical behaviors in carrier-free state is not always same as in ordinary concentration of solution. The location of migration band of a desirable element had to be decided by a side experiment of carrier-free ions.

The identification of the separated elements on the electrophoretic paper is conveniently carried out by gamma-ray spectroscopy especially using Ge(Li) detector. For the sake of rapid detection of the location of a desirable element on the paper strip, visible migration front of a colored ion is helpful as a maker. Using by 0.01 M perchrolic acid (pH 2.2), the typical separation pattern of selenium using was shown in Fig. 4[7].

Halogens in fission products of binary fission of uranium are bromine and iodine. Bromide and iodide ions existed in all halogens ions have the highest mobilities among anions . A 0.01 M sulphurous acid (pH 1.9) is used as a supporting electrolyte solution for bromine separation. The solution is also useful for reducing bromate to bromide and selenate to selenite during the electrophoresis on a paper strip.

The migration distance of bromide and bromate ions are almost same as that of the selenate and iodide ions. However, it has been found that little amount of iodide ion exists in the supporting electrolyte solution below pH 2.8 according to a side experiment of relatively long-lived iodine nuclides (for instance,I-134) in fission products and/or beta-decay products of neutron irradiated tellurium. In the case of pH 1.9, the minute contamination of iodine nuclides is apt to be in gamma-ray spectrum.

On the other hand, it has become clear that the selenate ion can hardly be produced in uranyl nitrate solution. These experimental results are further described later. Rapid separation of bromine from fission products is achieved by cutting out quickly the migrated portion from the paper strip. The location of bromide and bromate ions on the strip have previously been estimated using known sample. For this purpose, autoradiography is helpful using Br-83 formed by beta-decay of Se-83.

For the separation of iodine from fission products, a 0.01 M perchloric acid solution (pH 2.1) is used as a supporting electrolyte solution. A 0.1 M potassium permanganate solution is used as an oxidizing agent to oxidize iodide to iodate and as a marker for the location of the migration position of iodate ion. A 0.01 M silver nitrate solution is also used a stopping agent of bromide and iodide ions. At the location of iodate ions, traces of technetium and bromine are apt to be contained, and no other elements can be found in gamma-ray spectrum. Selenium in fission products is isolated by using a 0.01 M perchloric acid (pH 2.2) as a supporting electrolyte solution. A small amounts (2μl) of 0.1 M solution of potassium selenite is spotted at the cathode side of the paper strip before irradiated uranium sample solution is spotted. Since most of radioactive selenium yielded in fission is selenite ion in uranyl nitrate solution, the selenite added above plays the role of carrier and is oxidized to selenate altogether to make broad selenate band.

Moreover, the carrier enhances the oxidation rate. A 0.1 M potassium permanganate solution is used as an oxidizing agent to oxidize selenite to selenate. At the same time technetium is also oxidized and distinct zone of pertechnetate is formed. A visible migration front of the permanganate ion

is also effective as a marker for the location of the migrated position of pertechnetate and selenate ions.

A 0.01 M silver nitrate solution is used as a stopping agent of bromide and iodide ions whose mobilities are large than those of selenate ions. If the stopping solution is not spotted on the paper strip, the migration band of selenate ion will suffer an inevitable contamination during the migration with the daughters produced from very short-lived parent nuclides migrated farther than selenate ions. The separated fraction of selenate ions is usually slightly contaminated with technetium. The electrophoretic separation of molybdenum is done using a 0.01 M perchloric acid solution adjusted to pH=12 with sodium hydroxide. A 0.01 M silver nitrate and 0.01 M ammonium bromide are successively added and freshly prepared to use as stopping agent of radioactive bromide and iodide during the electrophoresis. The migrated positions of molybdenum and technetium ions are indicated by the pattern of migrated permanganate ions. Molybdenum locates at 5-7 mm farther site than the front of the permanganate band, while technetium locates just at the front. The separation behavior of fission products is observed by autoradiography in a side experiment using relatively long-lived fission products along with by gamma-ray spectrometry.

Although eluents containing nitric acid are ineffective for the separation of divalent and trivalent metal ions, such as alkaline earth and rare earth ions, these eluents are suitable for the separation of the alkali metal ions. Rubidium and cesium ions in the aqueous solution of fission products could be separated very easily within 15 min with 2 mM nitric acid. The separation pattern obtained by the conductivity detector (CM-8) shows the total amount of sodium, ammonium and potassium ions that were present in the sample solution as a monitor. On the other hand, the pattern obtained by the NaI(Tl) radiation detector indicates only the amounts of the radioactive rubidium and cesium nuclides from fission products. This pattern was independent of the eluent temperature and the pressure of the pump flowing the eluent, and the pattern was also not affected by the water dip that appears in the usual pattern observed with conductivity detector.

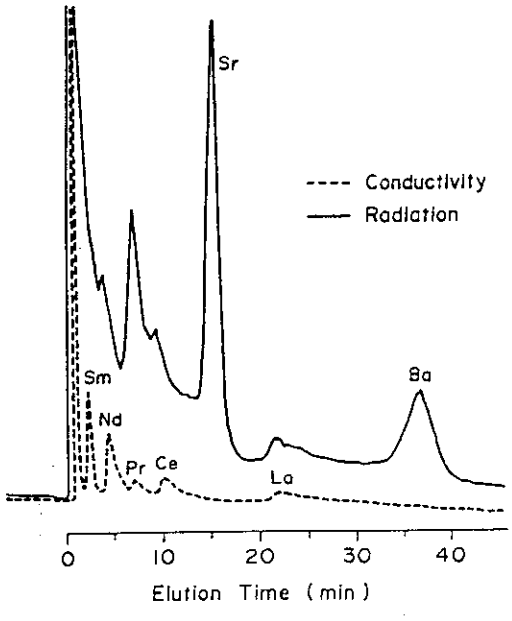

Fig. 5 Radio-ionchromatogram of Cations in Fission Products.

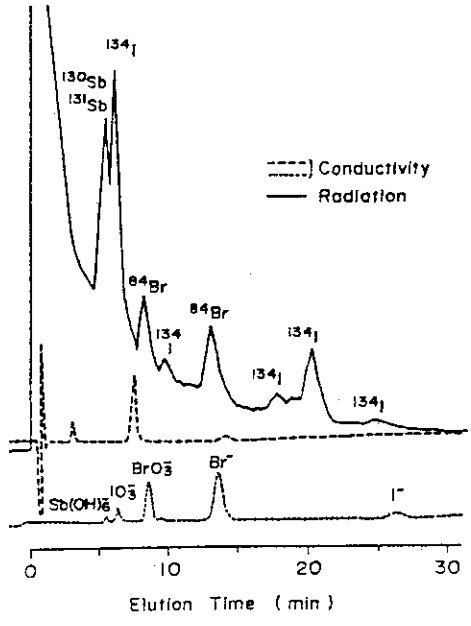

Fig. 6 Separation Pattern of Anions in Fission Products.

The nuclides found in the rubidium fraction were Rb-88, Rb-89, Rb-90, and Rb-90m. The nuclides detected were Cs-138, Cs-138m, and Cs-139.

The separation of alkaline earth ions from fission products by means of the eluent 1 mM ethylendiamine was achieved within 10 min. The nuclides observed in the separated strontium and barium fractions, identified by counting their gamma-rays with the Ge(Li) detector, were Sr-91, Sr-92, Sr-93 in the strontium fraction and Ba-139, Ba-141, Ba-142 in the barium fraction, respectively.[8]

The separation pattern of fission product rare earth elements obtained with the eluent 7.5 mM alpha-hydroxy isobutyric acid solution (pH 4.6) is shown in Fig. 5. The flow rate of the eluent was 1.0 ml/min. The dashed line shows the ion chromatogram of 20 ppm concentration of samarium, neodymium, praseodymium, cerium, and lanthanum. The fraction of eluent corresponding to each peak was collected for the gamma-ray measurement by the Ge(Li) detector.

The typical separation pattern of anionic species from a carrier-free solution of fission products is shown in Fig. 6. The nuclides detected were the short-lived iodine isotopes, I-134 and I-135. In the carrier-free experiment, a few peaks of unidentified chemical species existed in fraction No. 5, 8, and 9 of the separation pattern. The nuclides in these peaks were I-131, I-134, and I-135. These unidentified species were at a position lying between iodate and iodide ions on the chromatogram. In order to examine the species, iodate and iodide carriers were added to the carrier-free solution, and the effect of carrier on the separation pattern was observed. These unidentified peaks disappeared with the addition of the carrier solution. We think that these chemical species of iodine might be hypoiodite and iodite ions.

ACKNOWLEDGMENTS

The authors ,would like to express their greatest appreciation to Professor S. Iwata of Ottemon University who has guided authors to the present study and has been giving the continuous interest and encouragement. In addition, the authors are deeply indebted to Professors Y. Kiso and H. Takemi of Hiroshima University for their kind encouragement and many helpful discussions and suggestions, without which this work could never has been accomplished.

REFERENCES

[1] Herrmann G. and Trautmann N. : Ann. Rev. Nucl. Particle Sci., 32, 1 (1982).
[2] Small H., Stevens T.S. and Bauman W.C. : Anal. Chem., 47, 1801 (1975).
[3] Gjerde D.T., Fritz J.S. and Schmackler G.J. : J. Chromatog.,186, 509 (1979).
[4] Tamai T. et al. : J. Nucl. Sci. Technol., 13 219 (1976).
[5] idem : Inorg. Nucl. Chem. Lett., 9, 245 (1973).
[6] idem : ibid., 9, 973 (1973).
[7] idem : ibid., 9. 1145 (1973).
[8] Tamai T., Nishikawa S., Tanaka Y. and Takemi H. : " Research on Thorium Fuel" SPEY 21, 29 (1987).

3. Development of Radioisotope Production in JAERI

H. YAMABAYASHI, H. KATO, H. UMEZAWA

Department of Radioisotopes
Tokai Research Establishment, JAERI
Tokai-mura, Naka-gun, Ibaraki-ken 319-11, Japan

ABSTRACT

Since 1962, we have been developing methods and technology for producing a wide variety of processed radioisotopes and sealed radiation sources by using the JAERI's reactors, JRR-2, JRR-3, JRR-4 and JMTR, and providing the products to domestic users. At present, 29 nuclides and 31 products are on our list of processed radioisotopes. Some of those isotopes such as P-32, S-35, Cr-51 and short-lived nuclides are being produced regularly for distribution, but most of the rest are produced upon request. The radiation sources of Co-60 needles and Ir-192 pellets for industrial use and Gd-153 pellet, 7 kinds of Ir-192 and Au-198 grain for medical applications are produced and distributed routinely.

1. INTRODUCTION

When the Japan Atomic Energy Research Institute (JAERI) was established in 1956, a number of radioisotopes had been produced and used in the USA and other developed countries, so that priority was given to the production of short-lived nuclides, which were difficult to import, such as Na-24, K-42, and Mn-56, and some nuclides of a large demand, such as P-32, S-35, I-131, Au-198.
After 5 years preparation, production of 32 kinds of radioisotope products was started with the uses of research reactors JRR-1, -2 and -3 in 1962. The scale of production was increased afterward, as the irradiation service with JRR-4 and JMTR became available.

The Szilard-Chalmer's effect in nuclear reactions was applied for producing some nuclides in high specific activity.

Mercury-197 had been produced and supplid for the inventry measurement of mercury in electrolytic cells of caustic soda factories.

Small radiation sources of Co-60 have been produced for medical and industrial instruments. Iridium-192 was developed to produce gamma radiation sources for brachy therapy of cancer and industrial nondestructive tests of steel weldings and jet engine inspections.

Twelve cycles irradiation with JMTR could produce C-14 in the form of barium carbonate. That enabled us to supply a variety of C-14 labelled compounds.

The production of Mo-99 was developed on the (n, f) and (n, γ) reactions. Gold-198 grains were developed for brachy therapy. Gadolinium-153 was prepared as a dual photon source for a born mineral analyzer.

New radiation souces of Ir-192 for remote after loading systems(RALS) for cancer therapy and of Yb-169 for industrial nondestructive tests of thin steel pipings are under development. Labelled compounds of Y-90 and P-32 are studied for applications as well.

Nuclear reactors available for the radioisotope production in JAERI are listed in Table 1.

Table 1 Reactors for Radioisotope Production

Reactors	Irradiation hole	Neutron flux ($m^{-2}s^{-1}$), ():Fast	Irradiation time	RI products []:Radiation source
JRR－2 (10MW)	・Pneumatic tube	6×10^{17}	～25 min.	^{24}Na, ^{42}K, ^{64}Cu, ^{56}Mn etc.
	・Vertical hole VT-4	2×10^{17} (2×10^{15})	1～280 hrs.	[^{192}Ir], [^{198}Au], ^{198}Au, ^{197}Hg, ^{82}Br etc.
	VT-8	3×10^{17}		^{35}S
	VT-1	1×10^{18}	1 cycle(280hrs) ～	^{51}Cr, ^{192}Ir, ^{99}Mo, ^{63}Ni etc.
	・In-core 3A	9×10^{17} (6×10^{17})		^{32}P, [^{153}Gd], ^{99}Mo
JRR－3 (20MW)	・Pneumatic tube	5×10^{17} (1×10^{15})	～20 min.	^{24}Na, ^{42}K, ^{64}Cu, ^{56}Mn etc.
	・Hydraulic rabbit	9×10^{17} (1×10^{16})	10min.～1cycle (1cycle=26days)	[^{192}Ir], [^{198}Au], ^{198}Au, ^{82}Br ^{99}Mo etc.
	・Vertical hole VT-1	1×10^{18}	1cycle ～	^{35}S, [^{153}Gd]
	RG 1-4	2×10^{18} (2×10^{16})	1cycle ～	^{32}P, [^{169}Yb]
	BR 1-4	2×10^{18} (9×10^{17})	1cycle ～	^{51}Cr, [^{192}Ir], [^{169}Yb]
JRR－4 (3.5MW)	・Pneumatic tube	4×10^{17}	～20 min.	
	・Vertical hole T,S (pipe)	6×10^{17}	1min.～6 hrs.	^{24}Na, ^{42}K, ^{64}Cu, [^{198}Au] [^{192}Ir] etc.
JMTR (50MW)	・Hydraulic rabbit (No.2)	1×10^{18}	1～7 days	^{99}Mo, ^{197}Hg, ^{198}Au, [^{60}Co] [^{192}Ir], [^{198}Au]
	・Fuel region	1×10^{18} (2×10^{16})	1cycle ～ (1cycle=21days)	^{32}P, [^{169}Yb], ^{14}C
	・Reflector region	2×10^{18}	1cycle ～	^{51}Cr, ^{35}S, [^{192}Ir], [^{153}Gd]

2. PRODUCTION OF PROCESSED RADIOISOTOPES

The products of processed radioisotopes of JAERI are shown in Table 2. P-32, S-35, and Cr-51 are being produced regulary and shipped in accordance with annual schedule, and the others are produced upon request. In addition, we cope with requests of special radioisotope productions on a technical assistance or cooperative work basis.

The Szilard-Chalmer's process was applied to produce Cr-51 and Cu-64 of high specific activity. In the case of Cr-51, it was made but hardly applied for routine production because of unstable yields, and our products of Cr-51 are produced from enriched Cr-50 targets. On the other hand, it was done successfully for Cu-64 by using Cu phthalocyanine as target material. A specific activity more than 2 TBq/g-Cu can be easily performed in routine productions: an enrichment more than 1,000 times is made. One may obtain 20 TBq/g-Cu under well prepared conditions.

For the production of P-32, neutron irradiated elementary sulphur target is distilled in a quartz vessel under a reduced pressure. P-32 remained in vessel as residue is refluxed with 0.1 N HCl followed by a cation exchange, and is finally obtained in the form of $H_3{}^{32}PO_4$. The production batch of 5 TBq is made 8 times a year.

Table 2 The products of processed radioisotopes of JAERI

Nuclide (Half life)	Product code	Chemical form	Specific activity (GBq/g. ele.)	Activity conc. (MBq/ml)
^{110m}Ag (249.8 d)	Ag-110m-1	$AgNO_3$ in 1 N HNO_3	> 3.7	> 37
^{76}As (1.10 d)	As-76-1	$HAsO_2$ in 1 N HCl	> 37	> 37
^{198}Au (2.6937 d)	Au-198-1	$HAuCl_4$ in 1 N HCl	> 18.5	> 37
^{82}Br (1.47 d)	Br-82-2	NaBr in H_2O	> 11.1	> 37
^{14}C (5730 y)	C-14	$BaCO_3$ Powder	> 1.11 GBq/mol	—
^{45}Ca (163 d)	Ca-45-1	$CaCl_2$ in 1 N HCl	> 0.185	> 18.5
^{60}Co (5.269 y)	Co-60-1	$CoCl_2$ in 1 N HCl	> 0.0185	> 37
^{51}Cr (27.70 d)	Cr-51-2E	Na_2CrO_4, pH7～9 0.9% NaCl soln.	> 555	> 185
^{134}Cs (2.0658 y)	Cs-134-1	CsCl in 1 N HCl	> 18.5	> 185
^{64}Cu (12.70 h)	Cu-64-2R	$Cu(CH_3COO)_2$ in acetic acid (pH2 ～4)	>2,220	> 37
〃	Cu-64-1	$CuCl_2$ in 1 N HCl	> 3.7	> 37
^{72}Ga (14.1 h)	Ga-72-1	$GaCl_3$ in 1 N HCl	> 2.22	> 37
^{197}Hg (2.67 d)	Hg-197-1	$Hg(NO_3)_2$ in 1 N HNO_3	> 3.7	> 37
^{42}K (12.36 h)	K-42-2N	KCl, pH7.0～8.5 in neutral soln.	> 5.55	> 37
〃	K-42-2	〃	> 0.222	> 37
^{140}La (1.68 d)	La-140-1	$LaCl_3$ in 1 N HCl	> 3.7	> 37
^{177}Lu (6.71 d)	Lu-177-1	$LuCl_3$ in 1 N HCl	>1,850	> 370

Nuclide (Half life)	Product code	Chemical form	Specific activity (GBq/g.ele.)	Activity conc. (MBq/ml)
^{56}Mn (2.579 h)	Mn-56-1	$MnCl_2$ in 1 N HCl	> 74	> 185
^{99}Mo (2.75 d)	Mo-99-2	Na_2MoO_4, pH>7 in NaOH soln.	> 0.185	> 37
^{24}Na (14.959 h)	Na-24-2	NaCl, pH7.0～8.5 in neutral soln.	> 2.22	> 37
^{32}P (14.26 d)	P-32-1	H_3PO_4 in 0.1 N HCl	Carrier-free	> 370
^{86}Rb (18.66 d)	Rb-86-1	RbCl in 0.1 N HCl	> 18.5	> 37
^{35}S (87.5 d)	S-35-1	H_2SO_4 in 0.1 N HCl	Carrier-free	> 370
^{124}Sb (60.2 d)	Sb-124-1	$SbCl_3$ in 5N HCl, HNO_3 mix. soln.	> 7.4	> 37
^{75}Se (119.78 d)	Se-75-2	Na_2SeO_3 in H_2O	> 1.85	> 37
^{153}Sm (1.95 d)	Sm-153-1	$SmCl_3$ in 0.1 N HCl	> 18.5	> 74
^{204}Tl (3.78 y)	Tl-204-1	$Tl(NO_3)_3$ 3 N HNO_3	> 0.74	> 37
^{170}Tm (128.6 d)	Tm-170-1	$TmCl_3$ in 1 N HCl	> 370	> 185
^{185}W (75.1 d)	W-185-1	Na_2WO_4 1 N NaOH soln.	> 1.85	> 37
^{90}Y (2.67 d)	Y-90-1	YCl_3 in 1 N HCl	> 7.4	> 37
^{65}Zn (244.0 d)	Zn-65-1	$ZnCl_2$ in 1 N HCl	> 0.74	> 37

S-35 is produced from KCl targets. An irradiated target is dissolved in distilled water, and S-35 is purified from K, Cl and byproduct ^{32}P by cation exchange and distillation. The chemical form of product is $H_2{}^{35}SO_4$ in 0.1 N HCl. Production of 50 GBq batch is done 2 or 3 times a year.

Production of I-131 from irradiated TeO_2 had been done to deliver 750 GBq/week from 1968 to 1972.

Carrier-free Mo-99 was produced dy irradiating a 2.6 % enriched UO_2 target of 340 g in JRR-2, -3, and JMTR for 4-7 days. It was extracted with D2EHPA and purified with an alumina column. We had been producing 740 GBq/week.

Later, Mo-99 was produced from (n, γ) reaction on molybdenum targets to reduce radiowaste generation. The production of 7 TBq/batch is feasible with shielded cells of Pb 10-15 cm thick. With well selected irradiations in our reactors, a specific activity of 74 GBq/g-Mo was obtained.

Production of P-33, Re-186 and W-188/Re-188 is being studied for further development, as well as developing more sophisticated products of radioisotopes, for instance ^{32}P labelled DNA probes and ^{90}Y immobilized polymers.

3. PRODUCTION OF RADIATION SOURCES

Our products of radiation sources are given in Table 3, which are widely used in the fields of medicine, science, engineering, and agriculture.

Table 3 The products of radiation sources of JAERI

Nuclide (Half life)	Product code	Shape	Dimension (mm)	Activity (MBq/piece)
^{60}Co (5.269 y) for industrial instruments	CNB-1	Needle	0.46ϕ×10	37
	CNB-2	Needle	0.91ϕ×15	185
	CNB-3	Needle	0.91ϕ×15	370
	CNB-4	Needle	0.91ϕ×15	740
^{192}Ir (73.83 d) for industrial nondestructive tests	IPB-1	Pellet	2.0 ϕ×2.0	370,000
^{192}Ir (73.83 d) for brachy cancer therapy	IHS-1	Hairpin	0.65ϕ×93	740
	ISS-1	Single-pin	0.65ϕ×47.6	370
	ISDS-1	Seed	0.5 ϕ×3.0	37
	ISDS-3	Seed assembly	1.0 ϕ×93(Max.)	37/seed
	ITS-1	Thin wire	0.3 ϕ×20	148
	ITS-2	Thin wire	0.3 ϕ×30	222
	ITS-3	Thin wire	0.3 ϕ×50	370
^{198}Au (2.697 d)	AGS-1	Grain	0.8 ϕ×2.5	185
^{153}Gd (241.6 d) for bone mineral analyzer	GPS-1E	Pellet in Al & Ti capusule	7 ϕ×10	1,850
	GPS-3E	〃	7 ϕ×10	3,700

Radiation sources are produced by irradiating targets of a definite shape and size. It is needed to give an adequate and definite radioactivity to every piece of target. This requires to make well characterized neutron irradiations for the production of radiation sources. On-line neutron dose monitoring and various in-line measurements on the production process are very important for quality assurance of products accordingly. For those purposes we have been developing and applying various instruments and techniques in accordance with our process and facilities.

Needles of Co-60 are produced: 37, 185, 370 and 740 GBq/piece. About two hundred needles are delivered mainly for industrial instruments every year. Irradiation capacity of research reactors is not enough to do a large scale production of Co-60 to be supplied to gamma irradiation facilities.

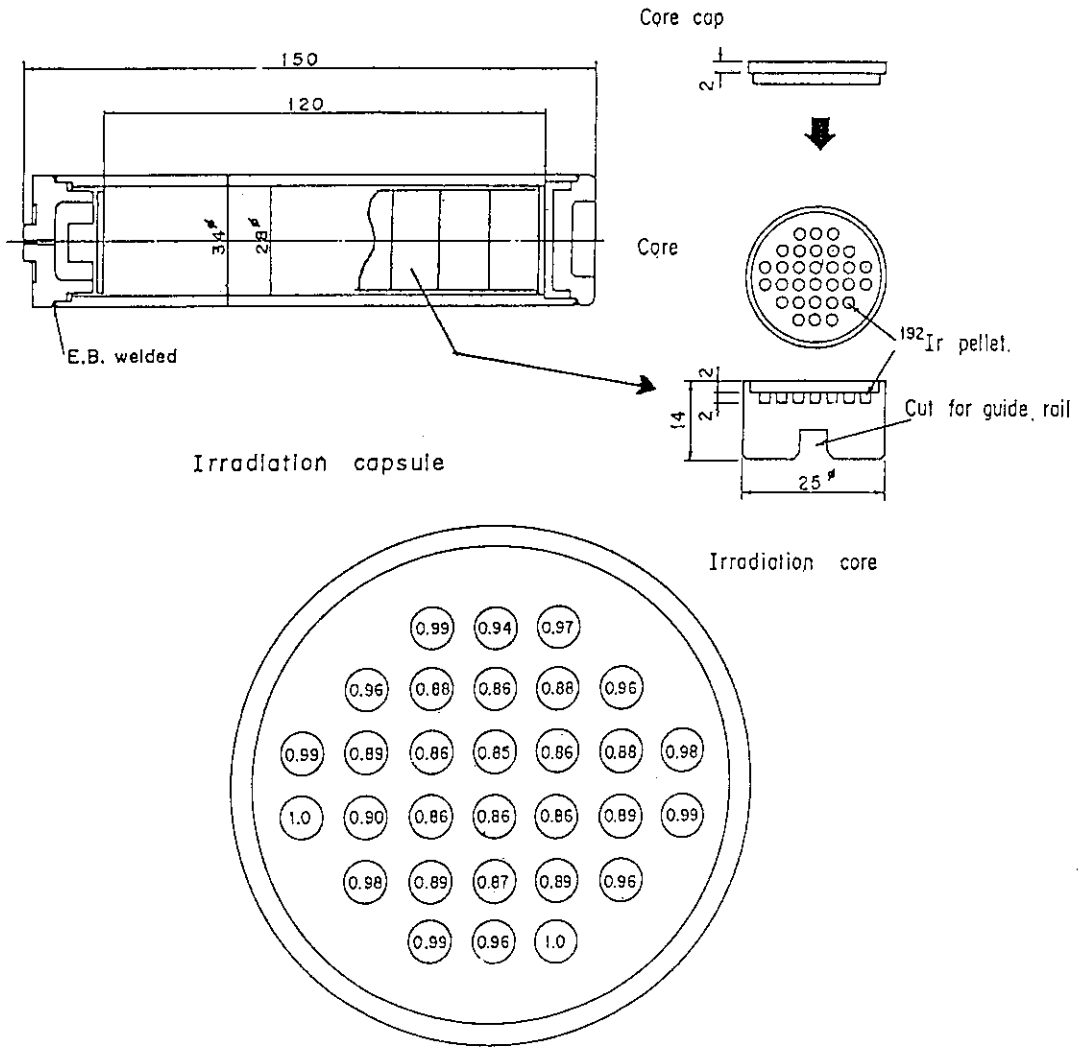

The max. activity is normalized to 1.0

Fig. 1 An example of radioactivity distribution of Ir-192 in the irradiation core

For the production of Ir-192 sources for industrial nondestructive tests, iridium pellets of 2 mm $\phi \times$ 2 mm are irradiated to 2×10^{15} n/m^2. Figure 1 shows an arrangement of the pellets in an irradiation capsule, as well as radioactivity distribution given to the pellets. Radioactivity of the pellets is measured one by one with a calibrated ion chamber and selected with its intensity. Each of the pellets is encapsulated and loaded to an irradiator for nondestructive tests. Nominal gamma intensity of the source is 370 GBq, so that it is generally 15% up at the shipment. This gamma source is produced five times a year, and anuual shipment is 1,500.

With uses of wafer-type targets of 3 mm$\phi \times$ 0.4 mm, Ir-192 sources of 3.7 TBq each could be made of 8 to 10 wafer stacked. This source was developed to use for the inspection of jet engines of airliners, and had been shipped for use from 1976 to 1984.

With regard to radiation sources for the remort after loading system(RALS) we are developing 300 GBq Ir-192 source of 1.1 mm $\phi \times$ 1.2 mm. It will contribute to extend applicability of radiation therapy to lung cancer and so on.

In order to produce Ir-192 sources for brachy therapy, iridium-platinum alloy has been used to give enough flexibility as it is applied to patients. Pellets and needles made of Ir-Pt alloy are prepared in a wide variety of shape, and are coated with pure platinum. The platinum coating is little activated with neutrons and work to seal Ir-192 from the source surface. The targets are placed in capsules with spacers made of aluminum to minimize activity deviations, and are irradiated with JRR-2, -3 and -4 for 1 to 40 hours in accordance with the product specifications. In JRR-2 and -4 a self-powered neutron detector (SPND) facilitates controlling irradiation period by monitoring neutron dose on line. Gamma intensities are 740 MBq for hairpins, 370 MBq for single-pins, 37 MBq for seeds, 370 MBq seed-assemblies, and 145, 222, 370 MBq for thin-wires.

For replacing Rn-222 seeds, that were used world wide in the begining, Au-198 grains were developed since 1974: pollution problems associated with Rn-222 were recognized. Gold pellets of 0.5 mm $\phi \times$ 2.5 mm sealed in platinum sheath are irradiated for 2.5 hours to give the radioactivity of 185 GBq of Au-198 at the time to be used. We have been shipping the Au-198 grains every week through the year. Annual shipment is 2,000.

Gadolinium-153 sources are produced for a born mineral analizer. Gadolinium oxide enriched in Gd-152 30-40% is prepared in a sintered oxide pellet of 3 mm$\phi \times$ 2 mm and is contained with a high purity aluminum capsule. Irradiation is done in the fuel region of JRR-2 or JMTR for 260-530 hours. After irradiation it is encapsulated in an outer capsule made of titanium by plasma arc welding in argon atomosphare. The Gd-153 sources of 1.85 GBq and 3.75 GBq are being supplied.

Another method of producing Gd-153 from irradiated europium was also studied, but it has not been used yet.

Recently a Yb-169 source has been developed for industrial uses, that is 1.0 mm$\phi \times$ 1.2 mm and 200 GBq. being encapsulated with titanium. This is very promising to apply for nondestructive tests of weldings of thin steel pipings and plates, that will become more important in chemical plant constructions.

4. Production of Carbon-14 and Preparation of Some Key Precursors for Labeling Organic Molecules

T. MORIYA AND S. MOTOISHI

Department of Radioisotopes
Tokai Research Establishment, JAERI
Tokai-mura, Naka-gun, Ibaraki-ken 319-11, Japan

ABSTRACT

Production of carbon-14 on 50 GBq scale has been performed by neutron irradiation of aluminium nitride target in the JMTR. This nuclide is separated in carbon dioxide form by combustion of the irradiated target at 1100°C with oxygen. The [^{14}C] carbon dioxide liberated thus is trapped in caustic solution and finally recovered as [^{14}C] barium carbonate.

Some precursors useful for incorporating carbon-14 into a given organic molecule have been prepared. Precursors such as [1-^{14}C] sodium acetate, [^{14}C] methanol and [^{14}C] potassium cyanide are prepared by rather conventional methods involving carbonation of methyl magnesium iodide, reduction of carbon dioxide with lithium aluminium hydride and reduction of carbonate with metallic potassium in the presence of ammonium salt, respectively. A catalytic polymerization of acetylene is used to prepare benzene.

INTRODCUTION

Carbon-14 ($t_{1/2}$; 5730y) is an important radionuclide for the preparation of a veriety of labeled organic molecules. They are widely used as a tracer in biological and pharmacological studies due to the favourable properties of emitting only low energy beta particles, which are adequate for radioactivity measurement and autoradiography.

Carbon-14 is produced by the nuclear reaction of ^{14}N (n,p)^{14}C in a reactor. We started production on 50 GBq scale in 1970 when a long term irradiation became available in the JMTR. Target materials which were being used at that time were beryllium nitride and aluminium nitride. From the irradiated beryllium nitride, carbon-14 is separated as carbon dioxide by dissolving the irradiated target in sulfuric acid, followed by treatment of an oxidizing agent (1). Carbon-14 produced in the irradiated aluminium nitride, on the other hand, is extracted as carbon dioxide by dry oxydation procedure (2). The latter method was chosen because it can be performed with simple apparatus (3). As target material, sintered tablet of aluminium nitride was found to be preferable to powdery one from the viewpoint of easy remote handling due to its increased hardness. In addition, it is advantageous feature that the content of natural carbon decreases after sintered at high temperature. Consequently, reduction of specific activity of the carbon-14 product can be minimized.

Preparation of ^{14}C-labeled compounds is in most cases different from that of ordinary organic compounds. Preparation has to be carried out with

[^{14}C] carbon dioxide, the only starting material for labeling, at early stage of reactions. It is well-known that carbon dioxide undergoes some useful reactions to provide various key compounds such as [1-^{14}C] sodium acetate, [^{14}C] methanol, [^{14}C] potassium cyanide and [U-^{14}C] benzene by way of [1,2-^{14}C] acetylene. Many carboxylic acids including acetic acid are prepared by carboxylation of Grignard reagents or organo-metallic compounds with carbon dioxide (4). Some procedures for preparing methanol and potassium cyanide by reduction of carbon dioxide or carbonate have been reported (4). Reduction of carbonate to carbide is often used to prepare, from which labeled benzene can be prepared by catalytic polymerization (5)-(8). We have been prepared these key compounds according to the published methods with some modification.

The present paper describes the production procedures of carbon-14 and four kinds of ^{14}C-labeled key compounds in detail. Short discussion on technical problems is also presented.

PRODUCTION OF CARBON-14

Powdery AlN purchased from Nippon Denko Co. Ltd. was used as a target material after sintering as described below. It is desirable that the target material has high nitrogen content and low carbon content to obtain high specific activity ^{14}C product. The contents of nitrogen and carbon in the AlN were in the range of 30 to 34 % and 0.027 to 0.053 %, respectively. The powdery AlN is molded into tablets under a pressure of 0.9 ton·cm^{-2} and sintered at 1000°C for 1 hour under He atmosphere. Table 1 shows the difference in contents of nitrogen and carbon in sintered and not-sintered AlN.

Table 1 Content of nitrogen and carbon in AlN before and after sintering at 1000°C

AlN	Content (%) Nitrogen	Carbon-12
before sintering	33.4 (100)	0.037 (100)
after sintering	32.0 (96)	0.023 (62)

As is seen in the table, the content of carbon decreases considerably after sintering, whereas that of nitrogen does slightly.

Four sintered tablets, each of which weighs 8 g, are packed in an aluminium capsule and the capsule is welded hermetically. Five capsules together with spacers are packed in a capsule holder and welded hermetically. The airtightness of the capsules and the holder is confirmed by He leak test. Totally 160 g of the AlN in a capsule holder are irradiated in a beryllium reflector region in the JMTR for 12 to 14 cycles. The JMTR is normally operated at 50 MW for about 110 days in 5 cycles per year. The operation period of each cycle is 12 days. Thermal and fast neutron fluxes are approximately 2 x 10^{14} cm^{-2}·s^{-1} and 0.5 x 10^{14} cm^{-2}·s^{-1}, respectively.

The irradiated target is transfered to a vessel in an apparatus for separation of carbon-14 as shown in Fig. 1. The irradiated AlN tablets are placed in a porcelain crucble (A) and heated in an electric furnace (B) at 1100 °C in a stream of O_2. A quartz tube filled with wiry CuO (C) is connected to the end of the furnace to oxidize any ^{14}C compounds into $^{14}CO_2$. The $^{14}CO_2$ is absorbed in a carbon-free NaOH solution (D) under O_2 flow and $Na_2{}^{14}CO_3$ formed is then converted to $Ba^{14}CO_3$ by addition of $BaCl_2$ solution.

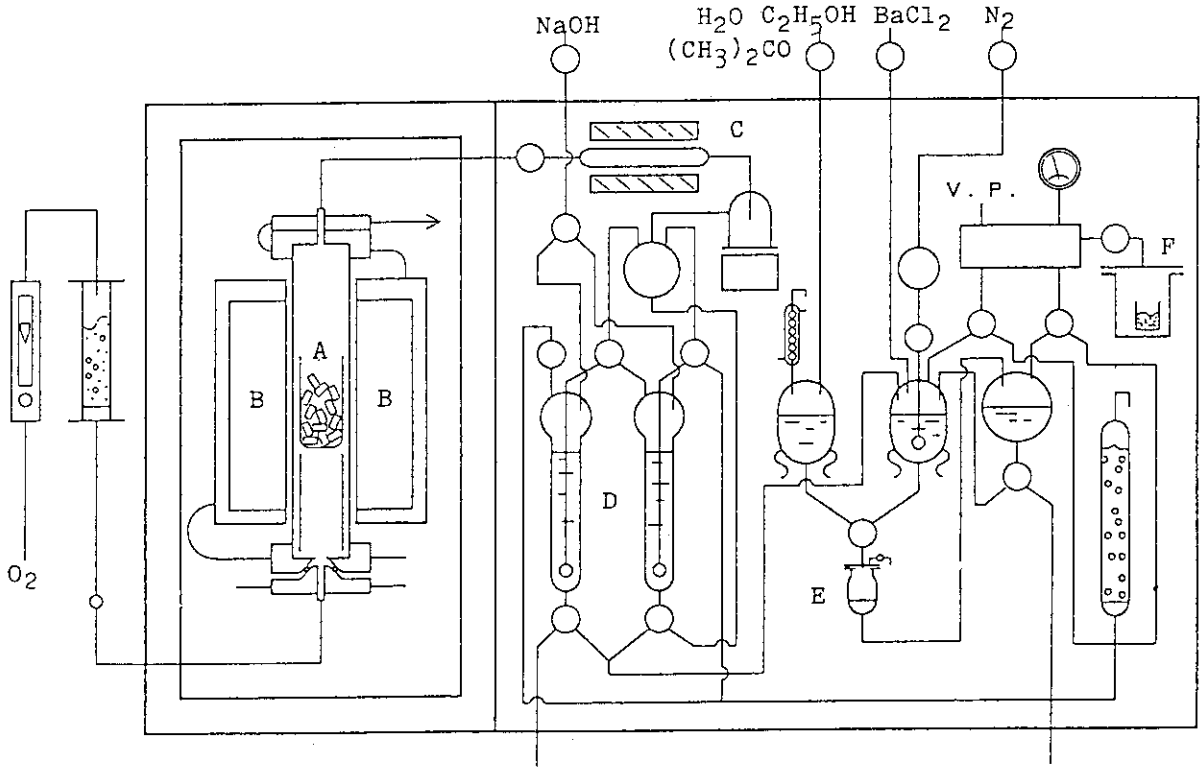

Fig. 1 Apparatus for separation of ^{14}C from the irradiated target

The precipitate of $Ba^{14}CO_3$ is collected by filtration on a filter (E), washed with distillated water, ethanol and acetone. It is dried in a vessel (F) under vacuum. Typical results of productions are shown in Table 2.

Table 2 Production of carbon-14 by neutron irradiation in the JMTR

Target		Irradiation			Yield		
Sample No.	AlN (g)	Irradiation Position	Irradiation Time (h) (cycle)	Particle fluence($\times 10^{21}$)	$Ba^{14}CO_3$ (g)	Specificactivity (GBq·m mol^{-1})	Total activity (GBq)
1	160.7	E-8	6179(14)	5.96	4.92	2.11	52.6
2	164.3	J-5	6103(14)	5.42	4.63	2.04	47.8
3	163.6	E-7	5768(12)	5.81	5.81	1.81	53.4
4	163.3	E-8	5792(12)	6.01	6.01	1.92	58.6
5	167.7	E-6	6234(14)	6.03	6.03	1.92	58.8

Carbon-12 content in the sintered target material
1.2 : 0.014 % 3.5 : 0.013 % 4 : 0.026 %

Specific activity of the products ranging from 1.81 to 2.11 GBq·m mol^{-1} is equivalent to approximately 77 to 90 % abundance of ^{14}C. Dilution with natural carbon is mainly due to the original content in the target materials used. Yields are close to the expected values estimated from extrapolation in smaller scale experiments.

Decomposition of the target materials during irradiation was obserbed by radio-gaschromatographic analysis of the gases produced in the capsule. Presence of N_2, O_2 and He was confirmed. Both N_2 and O_2 are likely to be

decomposition gases, while He is a fraction of replacing gas used in the process of welding the capsule. However, any possible ^{14}C compounds reported in the literature such as $^{14}CH_4$, $(NH_2)_2{}^{14}C{=}NH$, $^{14}CO_2$ etc. (4) were not detected. Maximum quantity of decomposition gas was 112.5 cm^3 when a target was irradiated to 7.3×10^{21} cm^{-2}. Inner pressure of the capsule was estimated to be 15.6 $kg \cdot cm^{-2}$ which was lower than burst pressure of the aluminium capsules.

PREPARATION OF KEY PRECURSORS

[1-^{14}C] SODIUM ACETATE

[1-^{14}C] sodium acetate has been prepared by the Grignard reaction. The Grignard reagent, CH_3MgI, is prepared by dropwise addition of CH_3I in dry ether to magnesium ribbon in dry ether with stirring under dry N_2 atmosphere. An excess CH_3MgI in ether is frozen with liquid N_2 in a flask on a Grignard carbonation apparatus. After evacuation of the flask, $^{14}CO_2$ produced from $Ba^{14}CO_3$ with concentrated H_2SO_4 is introduced into the flask. The reaction flask is isolated from the vacuum line and the mixture is stirred at -20 °C with Dry Ice-aceton for 20 minutes. The stirred mixture is treated with water while cold to destroy the excess of CH_3MgI and then with NaOH solution. The mixture is transferred into a distillation flask containing $AgNO_3$ to remove free iodine and acidified with 50 % H_2SO_4. The product, [1-^{14}C] acetic acid, is steam-distilled in a receiver. The distillate is titrated with standard NaOH solution. The chemical yields of 1 to 3 m mol scale preparations are higher than 95 %. The solution is evaporated to dryness under reduced pressure. The residue is dissolved in warm 90 % methanol and [1-^{14}C] sodium acetate is recrystallized by cooling the solution. The radiochemical purity determined by radio-paper chromatography is higher than 99 %.

The use of higher concentration and too much excess of the Grignard reagent causes the formation of by-products. The Grignard reagent of 0.2 to 0.4 m $mol \cdot ml^{-1}$ and 4 times the number of millimoles of $^{14}CO_2$ have been used for the carbonation reaction.

[^{14}C] METHANOL

[^{14}C] Methanol has been prepared by the reduction of $^{14}CO_2$ with $LiAlH_4$, followed by alcoholysis. The reaction sequence is as follows.

$$4\,{}^{*}CO_2 + 3\,LiAlH_4 \xrightarrow{(C_2H_5OCH_2CH_2)_2O} LiAl(O{}^{*}CH_3)_4 + 2\,LiAlO_2$$

$$(LiAlH_4 + 4\,ROH \longrightarrow LiAl(OR)_4 + 4\,H_2)$$

$$LiAl(O{}^{*}CH_3)_4 + 4\,ROH \longrightarrow LiAl(OR)_4 + 4\,{}^{*}CH_3OH$$

$$R = \text{C}_4\text{H}_3\text{O}-CH_2-$$

Lithium aluminium hydride is dissolved in bis-(2-ethoxyethyl) ether which is previously purified by fractional distillation under reduced pressure. A supernant solution containing $LiAlH_4$ is placed in a flask equipped with a magnetic stirrer, a reflux condenser, a pressure equalizing dropping funnel containing tetrahydrofurfuryl alcohol and two receivers connected in series to an attachment to vacuum manifold. The flask is evacuated and closed off from the manifold. Dry $^{14}CO_2$ is vacuum-distilled into the flask and the mixture is stirred at 0 °C for 1 hour. After the reduction is

complete, tetrahydrofurfuryl alcohol is added dropwise to the mixture with stirring. Nitrogen is admitted to the system, and the mixture is refluxed for 1 hour with stirring. The product together with some solvents is distilled under reduced pressure into the receiver cooled with liquid N_2. Radio-gaschromatographic analysis of the product showed the presence of impurities consisting of $H^{14}CHO$, C_2H_5OH and water. The gaschromatographic set-up consists of a thermal conductivity detector (TCD) and a stainless steel column packed with 15 % PEG-1000 on Uniport B as a stationary phase. The radioactivity of organic samples leaving the TCD cell is oxidized to $^{14}CO_2$ and detected with a GM detector.

For purification of the crude product, a simple preparative gas chromatographic set-up as shown in Fig. 2 is used.

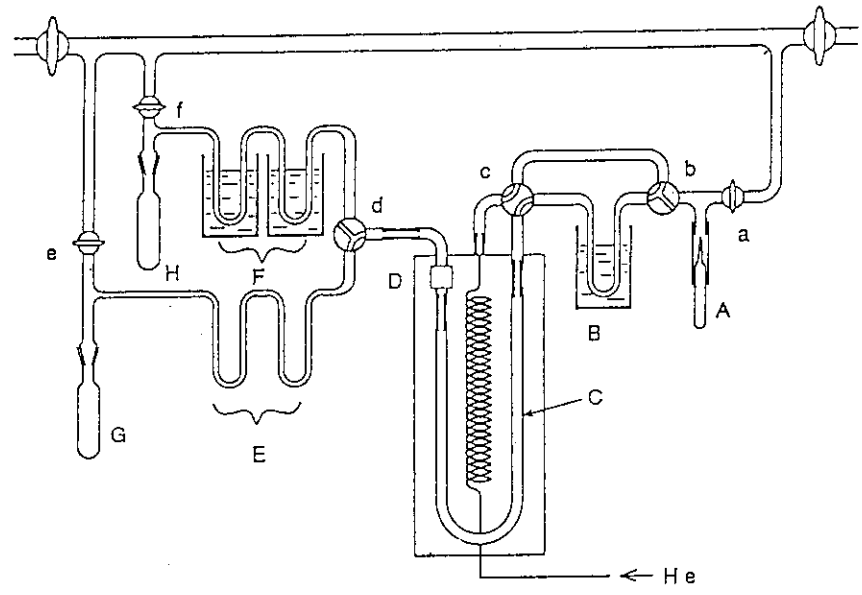

Fig. 2 Preparative gaschromatograph for the purification of crude [^{14}C] methanol
A; Ampoule containing sample, B; Injection part,
C; Colomn, 20mmx2m, packed with PEG-20m, D; TCD,
E,F; Cold traps, G,H; Collector, a-f; Glass cocks.

The set-up consists of a specially designed injection device (B), a stainless steel column of 10 mm x 2 m packed with PEG-20m (C), a TCD cell (D) an oven and cold traps (E,F). The crude product collected in an ampoule (A) is vacuum-distilled into the injection device and is vaporized by heating. The product is then introduced into the column under He flow. The purification is achieved at 30 °C under He flow of 70 ml·min^{-1}. Figure 3 shows an example of separation of a crude product. As is seen on the gaschromatogram methanol can be separated well from the impurities.

[^{14}C] POTASSIUM CYANIDE

The preparation of [^{14}C] potassium cyanide has been carried out by heating the mixture of K, $Ba^{14}CO_3$ and NH_4Cl in a sealed tube. A quartz tube, one end of which is adaptable to a glass cock, is used for the reaction. To a mixture of $Ba^{14}CO_3$ and NH_4Cl (molar ratio of 1 : 2) in the tube, is added excess K, which has previously been cleaned by filtering the melted K on a glass fiber. The tube is evacuated and closed. The K is melted by heating and the contents are mixed well by shaking. The tube is placed in an electric furnace kept at 630 °C and heated for 1 hour. The tube

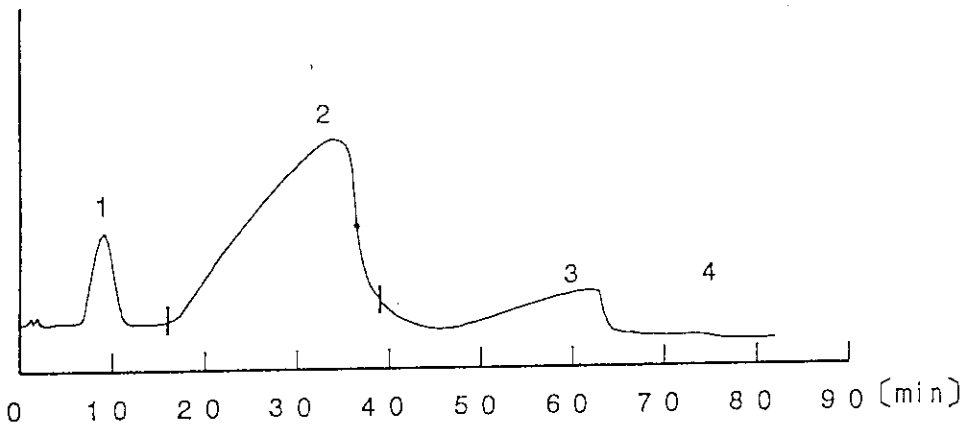

Fig.3 Gaschromatogram of crude (^{14}C)methanol on PEG20m column (10mmφ×2m)

1; Formaldehyde, 2; Methanol 3; Ethanol, 4; Water

is cooled and opened. The excess K is destroyed by careful addition of methanol through the hole of glass cock. The mixture is transfered into a distillation flask and acidified with H_2SO_4. The product, $H^{14}CN$, is distilled into a receiver containing excess NaOH solution. The chemical yield determined by titration with $AgNO_2$ is 90 to 95 %.

The solution is condensed to small quantity by distillation. The solution is acidified with H_2SO_4 and $H^{14}CN$ is distilled into two receivers which are connected in series, the first receiver containing equimolar KOH to $H^{14}CN$ and the second one containing additional KOH to recover $H^{14}CN$ completely. The solution in the receivers is evaporated to dryness under vacuum. The chemical purity of $K^{14}CN$ obtained from the first vessel is about 90 %. It is very difficult to obtain dehydrated cyanide without containing excess KOH, because evaporation under vacuum cannot be achieved without loss of $H^{14}CN$. Purification by extraction of crude $K^{14}CN$ from liquid NH_3 has been achieved where necessary. Radio-paper chromatographic analysis shows only one peak on the Rf value corresponding to that of KCN.

[U-^{14}C] BENZENE

[U-^{14}C] Benzene has been prepared by combination of the reactions as shown below, consisting of reduction of carbonate to carbide, formation of acetylene and polymerization of acetylene with catalyst.

$$Ba^*CO_3 \xrightarrow{Ba,\ \Delta} Ba^*C_2 \xrightarrow{H_2O} {}^*CH\equiv{}^*CH$$

$$^*CH\equiv{}^*CH \xrightarrow{\text{"Perikatalysator Neu"}} \text{benzene-}^*C_6$$

[^{14}C] Barium carbide is prepared by heating $Ba^{14}CO_3$ with Ba metal in a Pyrex glass tube under He atmosphere. [^{14}C] Barium carbonate and finely divided Ba are heated in a tube with a flame and the mixture ignites soon. The tube is cooled and placed in a flask equipped with a dropping funnel containing water, N_2 gas inlet, two cold traps connected in series for collecting $^{14}CH\equiv{}^{14}CH$. Water is added dropwise to the carbide and $^{14}CH\equiv{}^{14}CH$

formed is trapped in the vessels cooled with liquid N_2 in a stream of N_2. The reaction mixture is refluxed for 1 hour to recover $^{14}CH{\equiv}^{14}CH$ completely. The acetylene is then dried over P_2O_5.

For catalytic polymerization of $^{14}CH{\equiv}^{14}CH$, the method using catalyst "Perlkatalysator Neu" (Kali-Chemie AG) has been applied. The apparatus is shown in Fig. 4.

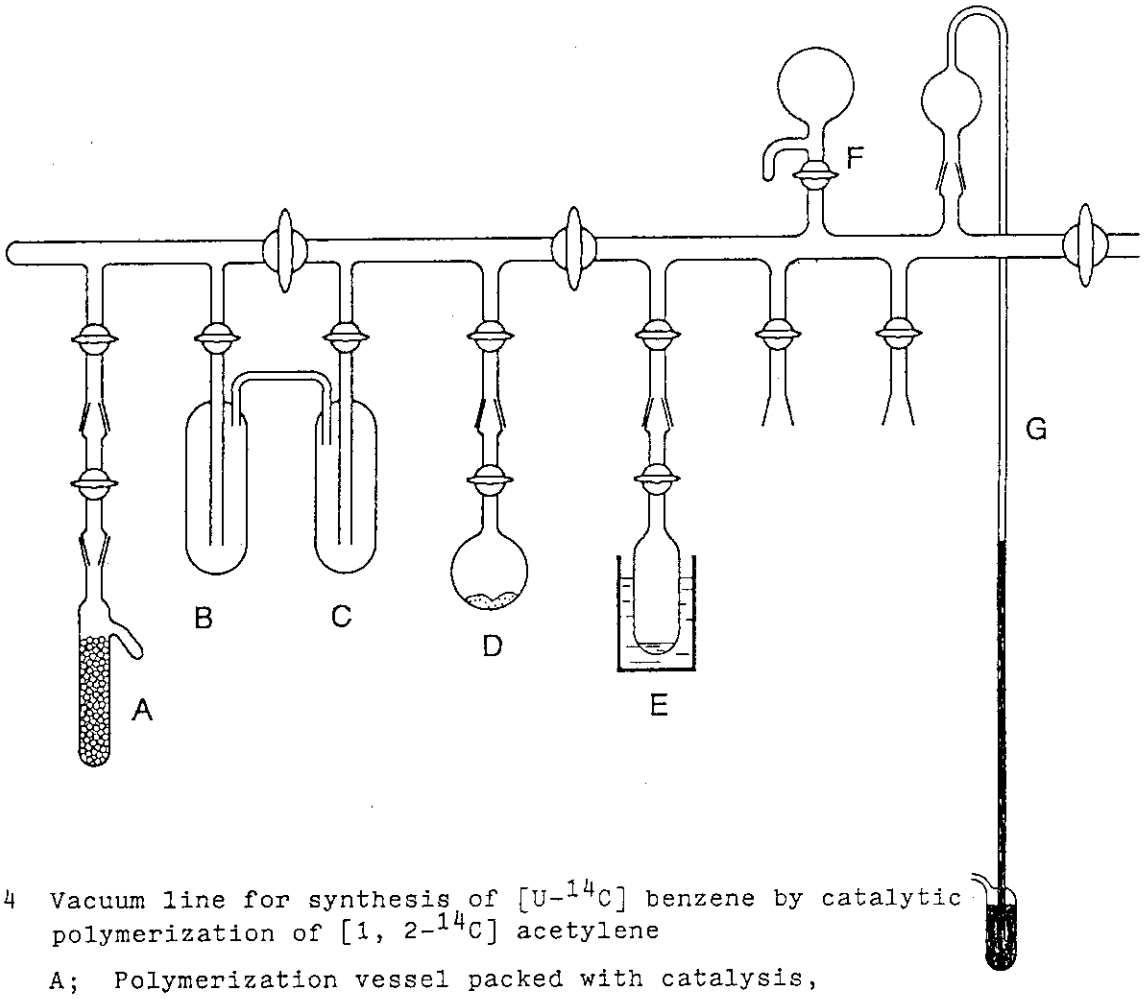

Fig. 4 Vacuum line for synthesis of [U-^{14}C] benzene by catalytic polymerization of [1, 2-^{14}C] acetylene

A; Polymerization vessel packed with catalysis, B and C; Liquid nitrogen trap, D; Dehydration flask containing P_2O_5, E; Flask for collection of [U-^{14}C] benzene, F; Gas strage and aliquoting bulb, G; Manometer.

The catalyst is placed in a polymerization vessel (A) and activated by heating overnight at 300 °C under vacuum. Acetylene is introduced into the vessel by vacuum-transfer and absorbed on the catalyst in a short time. The vessel is heated overnight at 50 °C. [U-^{14}C] Benzene produced on the catalyst is released by heating at 200 °C and transferred into the traps (B, C) cooled with liquid N_2 under vacuum. [U-^{14}C] Benzene is dried over P_2O_5 (D) and collected in a vessel (E). Radiochemical yields of typical preparations on 37 GBq scale were 72 to 86 % based on $Ba^{14}CO_3$. Radiogaschromatographic analysis showed that the product was pure enough not to need further purification.

This method enables us to prepare benzene with specific activity six times that of $Ba^{14}CO_3$. We have been successfully prepared benzen with the specific activity of about 2 GBq m·mol^{-1} by using 1 g of the catalyst to every 1 m mole of acetylene. Polymerization of $^{14}CH{\equiv}^{14}CH$ and subsequent procedures can conveniently be carried out in a vacuum-manifold.

ACKNOWLEDGEMENTS

The authors are indebted to Mr. H. Yamabayashi and Mr. K. Onoma for valuable discussion on production of carbon-14. We also wish to thank Mr. T. Moki and Mr. H. Matsuoka for skillful work on quality control of labeled precursors.

REFERANCES

(1) ORNL Radioisotopes procedures manual, ORNL 3633 p.41 (1964)
(2) British Patent 784125 (1955)
(3) K. Hata, E. Shikata and H. Amano; J. of Nuclear Science and Technology 10[2]89 (1973)
(4) For synthetic procedures of [1-^{14}C] sodium acetate, [^{14}C] methanol and [^{14}C] potassium cyanide, see: A. Murray and D.L. Williams; "Organic syntheses with Isotopes" Part I (1958) and H.R. Schütte; Radioactive Isotope in der Organischen und Biochemie, Veb Deutscher Verlag der Wissenschaften, (1966)
(5) K. Schmid, H. Furer and G. Dändliker; Proc. of 10th Symposium on Advances in Tracer Methodology, March 25-26, 1965 p.37
(6) L. Pichat and C. Baret; Tetrahedron, 1957, 1, 269
(7) S. Ikeda and A. Tamaki; Radioisotopes (Tokyo) 12[4]368 (1963)
(8) J.P. Noel and L. Pichat; J. of Labelled Compounds and Radiopharmaceuticals 13, 87 (1977)

5. Radionuclide Metrology for the Quality Assurance of Radioisotope Products

T. GENKA, N. TAKEUCHI, S. IWAMOTO AND K. KOBAYASHI

Department of Radioisotopes
Tokai Research Establishment, JAERI
Tokai-mura, Naka-gun, Ibaraki-ken 319-11, Japan

ABSTRACT

In order to control the production process and quality of radioisotope products, various methods and systems have been developed since shortly after the foundation of JAERI in 1956. A brief history of radionuclide metrology for this purpose till seventies is introduced and more detailed discussion on topics after the decade is given in the text. They are categorized into a gamma-ray spectrometry, a radiocalorimetry, a high efficiency counting for gamma-ray emitters of complex decay mode and an ionisation current measurement with a stable ionisation chamber system. Examples of some peculiar applications in the process control of radioisotope production are briefly described. Collaborational works with the medical and life sciences groups currently going on are also outlined.

INTRODUCTION

At present about 40 kinds of radioisotopes are being produced using reactors JRR-2,3 and 4 as well as JMTR in Japan Atomic Energy Research Institute (JAERI). In order to control the production process and quality of radioisotopes, various techniques and instruments for radionuclide metrology have been developed. For research and developmental work on radionuclide metrology, various fields such as radiochemistry (preparation of samples), nuclear spectrometry (radionuclidic impurity testing) and activity measurements (direct and relative measuring methods, designing of measuring apparatus, intercomparisons) have to be adequately combined.

Production and distribution of radioisotopes such as ^{24}Na, ^{32}P and ^{198}Au etc. started in 1962. Prior to this, development of techniques of absolute measurements, that were $4\pi\beta$ counting and $4\pi\beta$-γ coincidence counting method, have already been going

on since 1958. An efficiency tracing method for pure beta emitting nuclides [1] and an X, gamma-ray coincidence counting method for electron capture nuclides [2] have also been successively developed since 1962. Furthermore, the methods of absolute measurement of ^{197}Hg and ^{99}Mo-^{99m}Tc in equilibrium state were established by 1970. These techniques played important roles in the both projects of establishing an accurate mercury inventory in coustic soda industries since 1972 and a large scale production of ^{99}Mo in expectation of commencing distribution from 1976. Gratified results were obtained in the intercomparisons of ^{60}Co and other nuclides with Electrotechnical Laboratory and Nagoya University in 1975. In following 1976, standardisation of ^{64}Cu was successfully carried out [3]. As to the assay of ^{14}C, a liquid scintillation counting method in that aqueous sodium hydroxide was used instead of organic base chemicals as an absorber for $^{14}CO_2$ was developed [4]. In this method, organic liquid waste of which treatment is very difficult does not arise.

Developmental work on the technique of tritium measurement started in the latter half of 1980. At the early stage of this decade, a long-path proportional counter was developed to use for the standardisation of low-level gaseous tritium samples avoiding "end-effect"[5].

This paper discusses our recent accomplishments in the field of radioactivity measurements in detail.

RADIOACTIVITY MEASURING SYSTEMS AND METHODS

Gamma-ray spectrometry

Multi-gamma sources for the calibration of gamma-ray spectrometers such as ^{152}Eu (in 1978) and ^{166m}Ho (in 1983) as well as a combination source by which any combinations of spectra could be arbitrarily synthesized [6] were developed . Gamma-ray spectrometer equipped with full automatic sample changing system was designed by JAERI and constructed in 1985. Up to 24 samples of various types can be loaded unless their dimensions exceed 50 x 60 x 100 mm and placed at any distances within the accuracy of 0.01 mm at every 1 mm step ranging from 25 to 520 mm. Construction of this system and assembly of sample holder, which are now commercially available, are illustrated in Fig. 1. This system showed usefulness for the preparation of relatively large number of calibration sources, for instance, 13 sources of ^{24}Na and 17 sources of ^{166m}Ho. The former was distributed to the laboratories to make extension of energy range for efficiency calibration of their gamma-ray spectrometers even though the laboratories were limited whithin the site of JAERI because of shortness of its half-life. The latter was sent to the Australian Safeguards Office for the sake of IAEA resional training course of accountancy and control for nuclear materials.

Participation to the international intercomparison related

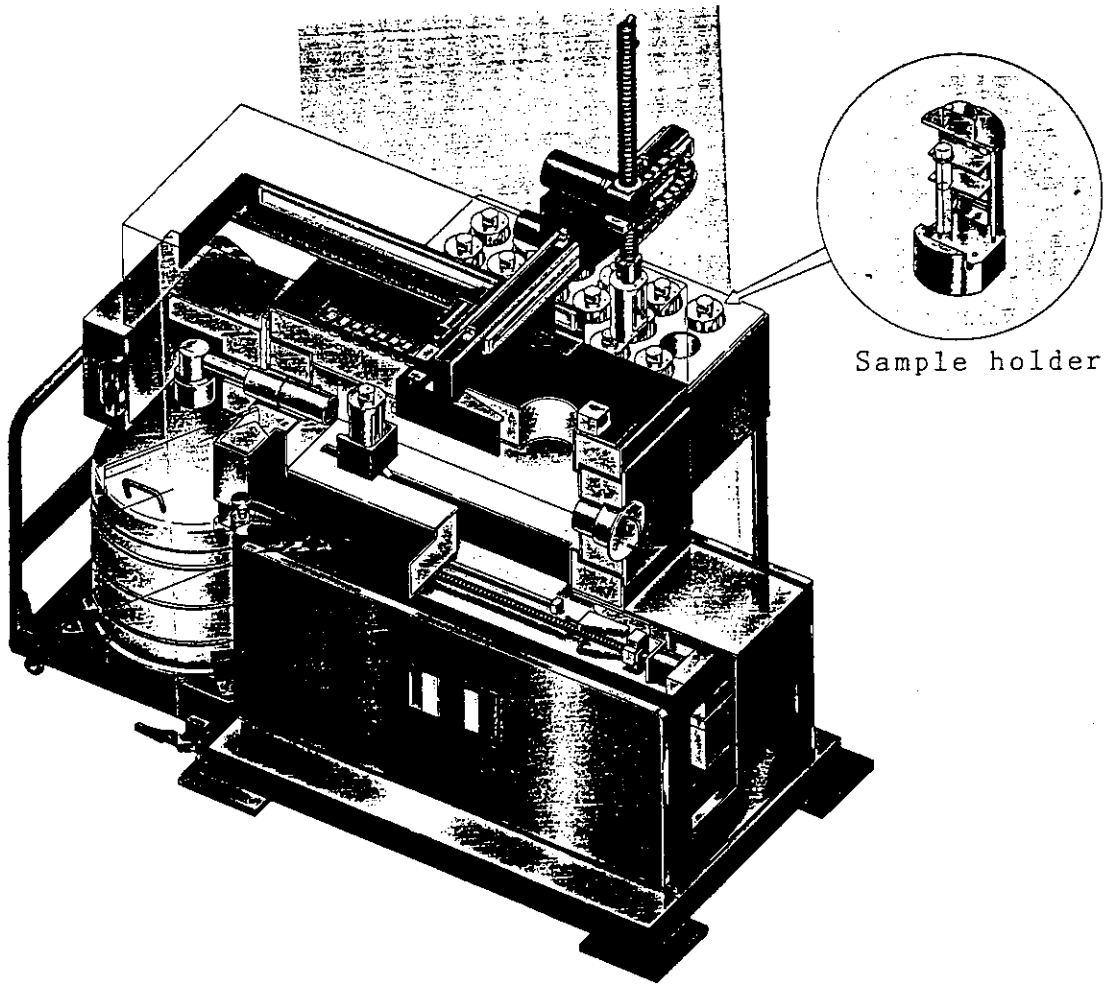

Fig. 1 A full automatic gamma-ray spectrum analyser.

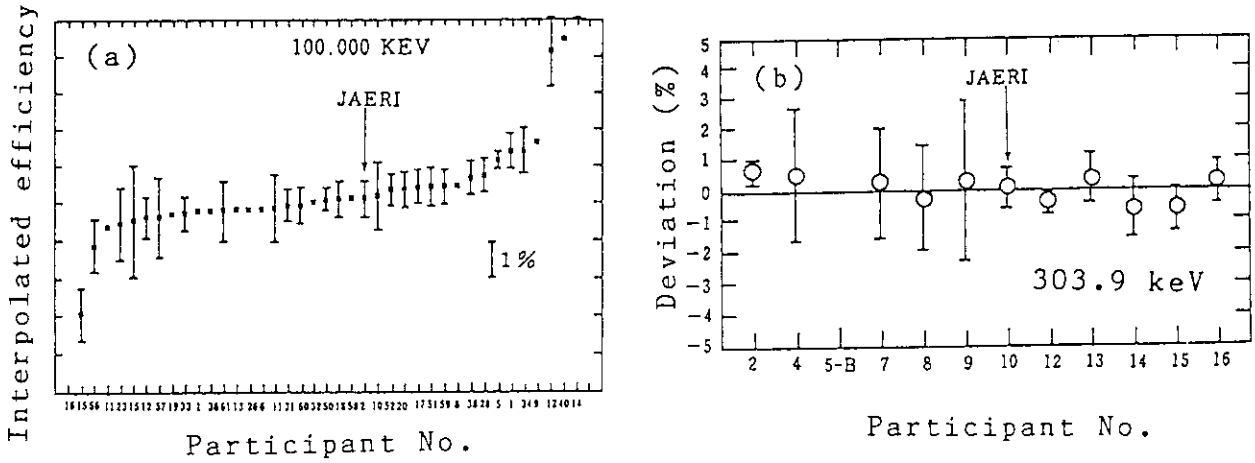

Fig. 2 Examples of the results of international intercomparison organised by International Committee for Radionuclide Metrology (ICRM).
(a) Interporated efficiencies of 100 keV gamma-ray against the code number of participant (1983).
(b) Deviations from the weighted mean of relative gamma-ray emission probabilities of ^{75}Se (1987).

to the gamma-ray spectrometry among overseas laboratories also brought the satisfactory results. They were intercomparisons related to gamma-ray spectroscopic analysis [7] in 1983 and relative gamma-ray emission probabilities of ^{75}Se [8] in 1987 both coordinated by the International Committee for Radionuclide Metrology (ICRM). A couple of examples of our results is demonstrated in Fig. 2. Presently, we are also participating in another ICRM project which is regarding computer calculation of detector efficiencies for volume sources.

Radiometric calorimetry

In a calorimetric measurement of beta-emitters, problems of self absorption, counting loss, dilution error and energy dependence of detection efficiency do not exist. An absolute measurement is possible if an average energy per disintegration is accurately known. Examples of recent data of average energies [9] and calculated thermal powers as μW per 37 MBq (1 mCi) are summarised in Table 1. Calorimetric methods for determining radioactivities of relatively high level tritium was introduced in 1983 and theoretical and experimental works on a twin-cup heat-flow microcalorimeter have been done [10]. Development of technique for measuring tritium produced in neutron irradiated ^{6}Li-Al alloy targets whithin an error of 1.5% was an example. This microcalorimeter was also applied for the radioactivity measurements of beta emitting nuclides such as ^{14}C, ^{32}P and ^{35}S etc. to prove its usefulness [11,12]. Schematic diagram of the microcalorimeter and a cross section of its main part are shown in Fig. 3.

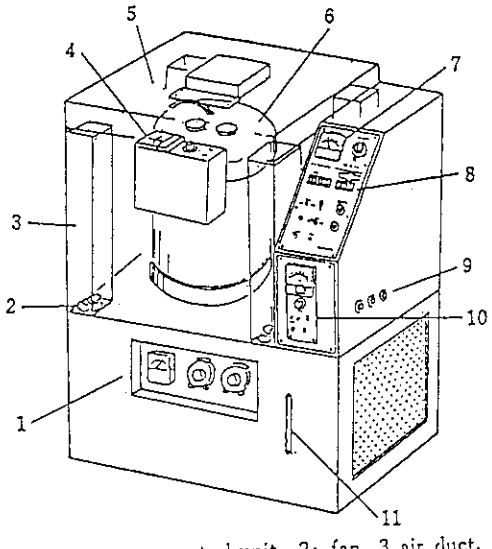

1: temperature control unit, 2: fan, 3 air duct, 4: amplifier (1 μV full scale), 5: thermostated air bath, 6: calorimetric body, 7: thermometer, 8: joule power supply, 9: output connectors, 10: amplifier (10 μV full scale) 11: coolant level indicator.

(a)

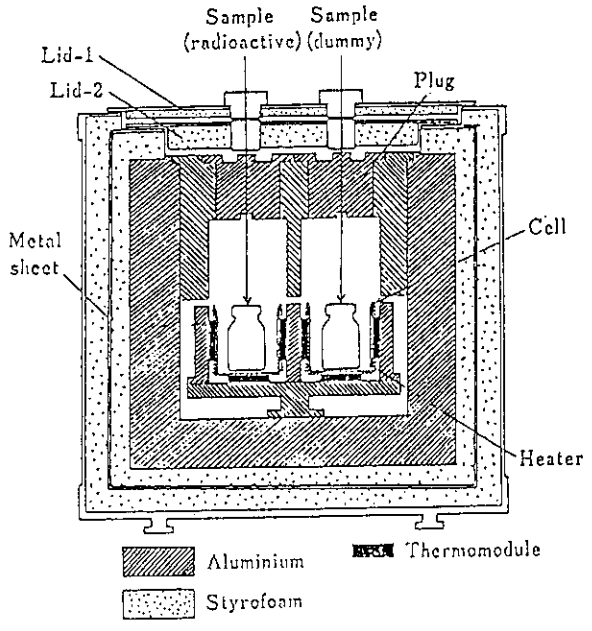

(b)

Fig. 3 Illustration of twin-type heat-flow microcalorimeter.
(a) Diagram of the calorimeter
(b) Simplified cross section of the calorimetric body

Table 1. Average energies of beta-rays and internal bremsstrahlung per disintegration and calculrated thermal powers of some pure beta-emitters.

Nuclide	Half-life	Beta-rays (keV)	Internal brem. (keV)	Thermal power (μW/37MBq)
^{3}H	12.33 y	5.7	0.000112	0.034
^{14}C	5730 y	49.5	0.0084	0.293
^{32}P	14.282 d	695	1.18	4.13
^{33}P	25.34 d	76	0.020	0.45
^{35}S	87.51 d	48.6	0.0086	0.288
^{90}Y	2.671 d	934	2.20	5.55

In 1987, the application of radiocalorimetry was extended to low energy X-ray or gamma-ray emitters. The radioactivity of sealed ^{153}Gd pellet sources which were used in bone density analysers in the medical field was determined using photon absorber made of copper [13]. Nuclear data of average energies per disintegration for photons, atomic electrons, continuous radiation (beta-ray) as well as internal bremsstrahlung were used to calculate thermal powers (Table 2).

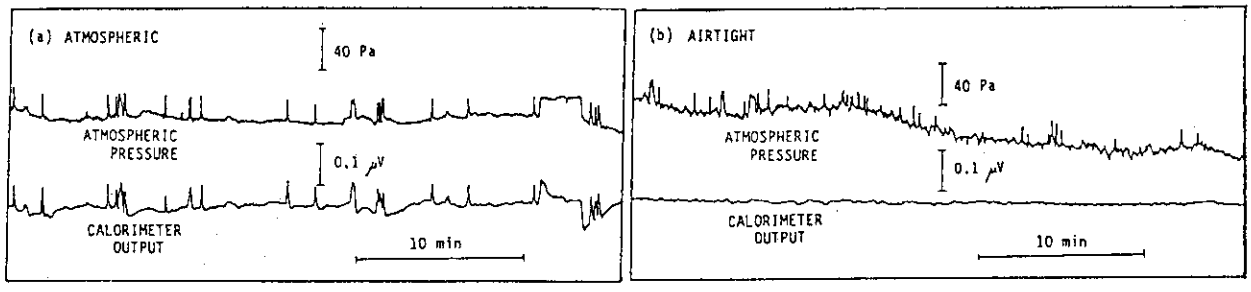

Fig. 4 Atmospheric pressure change and output of a calorimeter in (a) "atmospheric" and (b) "airtight" conditions.

Table 2. Average energies and calculated thermal powers of some soft X/gamma-ray emitters.

Nuclide	Decay mode	Photons (keV)	Atom.elect. (keV)	Cont.rad. (keV)	Int.brem. (keV)	Therm.pow. (μW/37MBq)
^{153}Gd	EC	101.5	39.9	-	0.155	0.839
^{169}Yb	EC	312.1	111.7	-	0.25	2.514
^{192}Ir	beta-,EC	813	45.2	171	0.123	6.10

For the measurements of more penetrative radiation emitters such as ^{32}P or photon emitters, appropriate radiation absorbers made of lead, copper or tungsten etc. were tested to get satisfactory results [12,13].

In the process of developing the calorimetry, fluctuation in the output signals from microcalorimeters were found to be correlated with temperature variations resulting from adiabatic expansion and compression of the air with atmospheric pressure changes [14]. This finding gave impact on designing calorimeters. Fig. 4 demonstrates the effect of isolation of the calorimetric cells from surrounding air.

High efficiency gamma-ray detection

A high efficiency gamma-ray detection system containing large NaI(Tl) detector (13cmϕ x 13cm) was developed in 1989. The purpose of introducing this system was determining radioactivities of gamma-ray emitting nuclides having very complex decay scheme. Generally in this system a nuclide of the more complicated decay mode takes advantage of the higher detection efficiency, sometimes almost unity. Examples of the total detection efficiencies for various nuclides are shown in Table 3.

Table 3. Examples of total efficiency

Nuclide	Half-life	Decay mode	Total efficiency
^{137}Cs	30.0 y	beta-	69.0%
^{54}Mn	312.20 d	EC	70.8%
^{60}Co	5.271 y	beta-	84.2%
^{152}Eu	13.33 y	beta-,EC	93.8%
^{22}Na	2.602 y	beta+,EC	94.9%
^{57}Co	271.77 d	EC	95.0%
^{133}Ba	10.54 y	EC	96.4%
^{166m}Ho	1200 y	beta-	98.6%

Dimensions of X-tal; 127mmϕ x 127mm, well; 27mmϕ x 65mm
Geometrical efficiency; 98.92%

As can be seen in the table, the more complex decay nuclides show the higher efficiencies as a general rule. However, ^{57}Co and ^{22}Na whose decay schemes are not complex give rather higher efficiencies. It seems due to that energies of dominant gamm-rays of the ^{57}Co are in the region of nearly 100% efficiency of the NaI detector and that anihillation radiations are emitted from the ^{22}Na at probability of 180% per decay.

Stable and precise ionisation current measurements

A system of pressurised 4πγ ionisation chamber filled with nitrogen gas at a pressure of 2 MPa, with which the current was determined from a time to charge up a suitable capacitor repeating in semi-automatic manner, was designed and constructed in 1987 as a secondary standard instrument for gamma-ray emitting nuclides. Setup of the system is shown in Fig. 5. The long-term stability and linearity are 0.05%/year and 0.1% respectively. This system, an ability of which was comparable to a system used in the Bureau International des Poids et Mesures (BIPM), was proven to be well suited for quality control of calibration sources by measuring relative ratio of ionisation current of each source. The ratio of the current and determined activity should agree with the ratio of the current and dispensed mass of each source if the preparation procedure is reasonably controlled. An example of quality control of ^{166m}Ho calibration sources is shown in Fig. 6. It suggested that activity determination of No.8 source might have some problem.

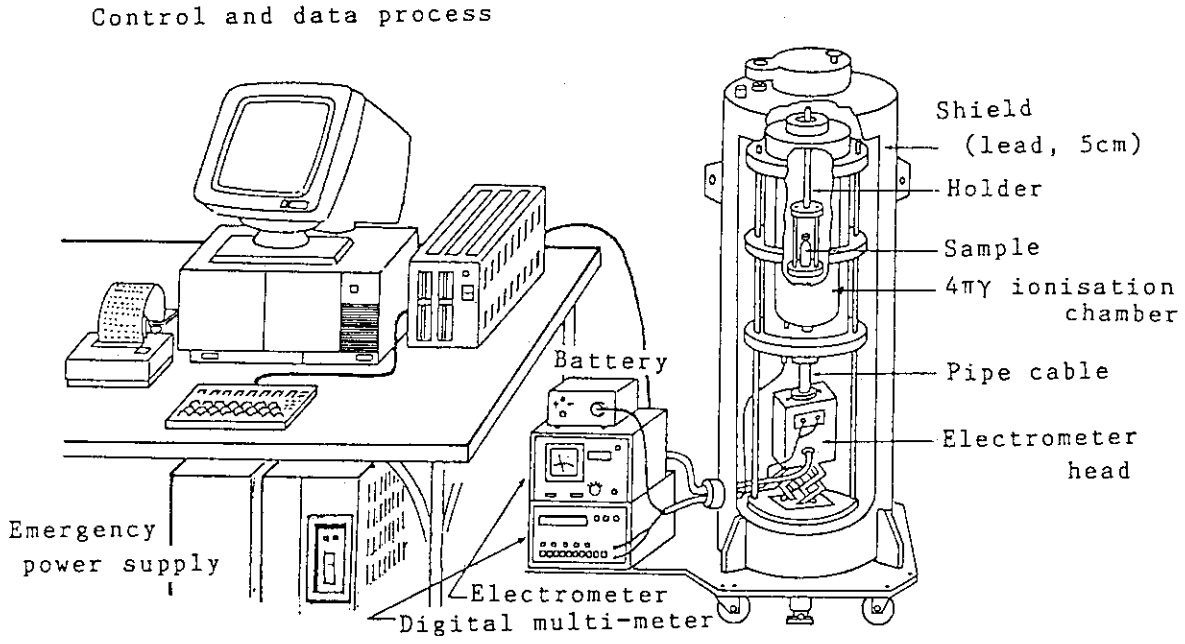

Fig. 5 Setup of the 4πγ ionisation chamber system.

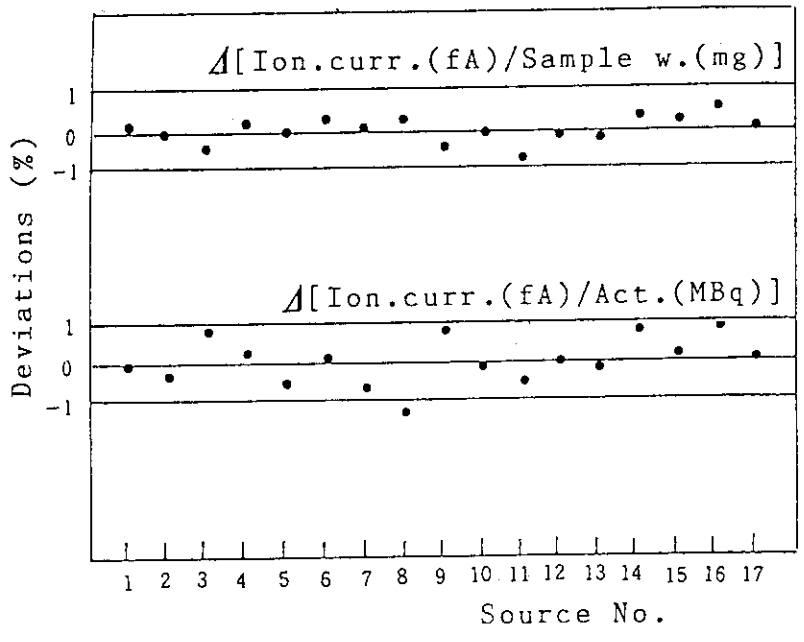

Fig. 6 A graph for quality control of 17 pieces of ^{166m}Ho calibration sources.

APPLICATION FOR PROCESS CONTROL IN RADIOISOTOPE PRODUCTION

Some application techniques for process control were derived from the results of development of measurements. Estimation methods applicable for production of radioisotopes will be discussed here. It is very useful to know activity of produced radioisotopes beforehand starting processing. In addition to the calorimetric nondestructive method for determining the amount of tritium in the metallic targets prior to melting process, a method of very accurate estimation of process yield of ^{32}P was investigated. For this purpose, an ionisation chamber installed in the process line of ^{32}P was calibrated for ^{32}P with the calorimeter as it was in a capsule to quantify produced ^{32}P in prior to cutting the capsule. Another pre-estimation method of applicable for production control of radiation sources of industrial use was also developed. Dose of radiation from irradiated cartridge containing up to 30 pellets (each 2mmϕ x 2mm) of ^{192}Ir was measured with an ionisation chamber and frequency of sources in this lot in terms of activity could be estimated by applying proper coefficients in accordance with position of each pellet in the cartridge. Correlation between the coefficients and the positions were determined experimentally. Thus estimated values of a range of activity and its average agreed well within 5% with the values obtained by complete measurement.

CONTRIBUTIONS TO THE MEDICAL AND LIFE SCIENCE FIELDS

Recently collaborational work in the medical and life science fields has become important. Contribution to Boron Neutron Capture Therapy (BNCT) of tumour in brain was highly appreciated when it was carried out using neutron flux of the JRR-2 in 1990. Quick determination of ^{198}Au in gold wire monitors for estimation of density and distribution of neutron flux were our responsibilities. Cooperation with the National Cancer Centre of Japan in calculational estimation of dose in tissues at the instant of $^{157}Gd(n,\gamma)^{158}Gd$ reaction has just started. This is also related to a neutron capture therapy. Calibration by standardised ^{32}P for a new instrument used in the process of ^{32}P labelled DNA was done. Necessity of establishing traceability of dose measurement in brachytherapy ^{192}Ir sources is realised by particularly medical doctors and physicists. In response to this circumstances, calibration sources of various types such as "hairpin", "single pin", "thin wire" and "seed" are under developing. Nominal activities of these sources have been so far specified by "apparent" activity because of difficulty to determine "absolute" activity directly by conventional means. Europian countries are also facing with such problems and trying to solve it in the frame of an international project (EUROMET Project No.219) of establishing traceability of the ^{192}Ir brachytherapy sources. We were exceptionally invited to participate in it from the Asian

community with an expectation of contribution by a calorimetric method in which a problem of self absorption effect did not exist. Results of the measurements of four wires (each 0.3mm ϕ x 10mm) of ^{192}Ir sent from NPL (National Physical Laboratory, U.K.) were summarised in Table 4 and they were reported to the coordinator of the project.

Table 4. Results of the EUROMET Project submitted by JAERI.

Wire	Mass (mg)	Abs. act. (MBq)	Appar. act. (MBq)	Ion. curr. (pA)	Abs./Appar.
C5	15.2	156.7	144.3	585.19	1.086
C7	15.1	153.8	141.3	572.01	1.088
C8	15.2	149.8	136.3	553.03	1.099
C9	15.0	148.4	136.0	549.82	1.091

The ratio Abs./Appar. in the above table suggests that the self absorption (attenuation within the wires) coefficient lies betwen 8.6 and 9.9%. All measurements have been corrected to the reference date, 1st April 1991.

SUMMARY

In the present paper, we tried to outline the activity of the Department of Radioisotope Production, JAERI in the field of radionuclide metrology, relying mainly on description of our recent and present work.

We like to stress on the use of calorimetric methods for measuring radioactivities of beta-emitting and soft X or/and gamma-emitting radioisotopes. The calorimetry has a potential of being most accurate and precise nondestructive technique available for assay of radioisotopes. In addition, it has many advantages in terms of economy, personnel safety and environmental safety. In the economical point of view, the sample solutions are not consumed at all so that the solution can be used, stored and even sold after measurement. Accordingly, the calorimetric method is particularly suitable in the facilities of radioisotope producers and radiopharmaceutical manufacturers as well as wholesale dealers, where relatively large amount of radioisotopes is handled.

Collaborational work with the fields of medical and life sciences is an important subject of recent years and being expected to be prosperous.

Acknowledgements

The authors gratefully acknowledge the valuable discussions throughout our activities with Professor emeritus, T. Watanabe and Professor C. Mori of Nagoya University. Thanks are also expressed to Dr. H. Umezawa for his support and helpful suggestions in metrology of radioisotopes for the medical use and other applications.

REFERENCES

[1] Watanabe, T., Absolute measurement of sulfur-35. J. Atomic Energy Soc. Japan, Vol.4, No.7, pp.435-439 1962
[2] Watanabe, T. and Takeuchi N., Absolute measurement of disintegration rate of radioisotope sources by X-gamma ray coincidece counting method. Oyo Buturi (Applied Physics) Vol.33, No.5, pp.322-327, 1964
[3] Kobayashi, K. and Ishikawa, I., Absolute measurement of ^{64}Cu. JAERI-M 7402 1977
[4] Kobayashi, K., Radioactivity measurement of barium carbonate [^{14}C] by liquid scintillation counting. JAERI-M 85-042, 1985
[5] Kushita, K., Takeuchi, N. and Hoizumi, K., Preparation of tritium standard gas by the use of tritiated methane. Radioisotopes, Vol.34, No.1, pp.1-6, 1985
[6] Genka, T. and Ishikawa, I., Combination source for gamma-ray spectrometry. Int. J. Appl. Radiat. Isot. Vol.34. No.8, pp.1067-1072, 1983
[7] Zijp, W.L. et al., International Intercomparison of Interpolation Procedures for the Efficiency of Germanium Gamma-Ray Spectrometers (GAM83 Exercise). ECN-181/ICRM-S-13, January 1985
[8] Jedlovszky, R., Intercomparison of the measurements of gamma-ray emission probabilities of ^{75}Se. Report of the Gamma and Beta-Ray Spectrometry Working Group of the International Committee for Radionuclide Metrology, Report OMH-8901/ICRM-S-14, May 1989
[9] Browne, E. and Firestone, R.B., Table of Radioactive Isotopes (Wiley, New York) 1986
[10] Genka, T., Kobayashi, K., Takeuchi, N., Ishikawa, I. and Hoizumi, K., A twin type heat flow microcalorimeter for radioactivity measurements. Radioisotopes, Vol.37, No.3, pp.155-158, 1988
[11] Genka, T., Kobayashi, K. and Hagiwara, S., A calorimeter for the measurement of the activity of tritium and other pure beta emitters. Appl. Radiat. Isot. Vol.38, No.10, pp.845-850, Int. J. Radiat. Appl. Instrum. Part A, 1987
[12] Genka, T. and Nataredja I. K., Radioactivity measurements of ^{32}P solutions by calorimetric methods. 1991 (in this proceedings)
[13] Genka, T. and Imahashi, T., Radioactivity measurements of ^{153}Gd pellet sources by calorimetric methods. Nucl. Instr. and Methods, 1991 (in press).
[14] Genka, T. and Iwamoto, S., Effect of atmospheric pressure variations on thermal power measurements with radiometric microcalorimeters. Nucl. Instr. and Methods A286 pp.395-397, 1990

6. Radioactivity Measurements of ^{32}P Solutions by Calorimetric Methods

T. GENKA AND I.K. NATAREDJA*

Department of Radioisotopes
Tokai Research Establishment, JAERI
Tokai-mura, Naka-gun, Ibaraki-ken, 319-11
Japan

*Radioisotopes Production Centre
National Atomic Energy Agency
PUSPIPTEK Serpong, Tanggerang, Jakarta
Indonesia

ABSTRAC

Radioactivity of ^{32}P solution is measured with a twin-cup heat-flow microcalorimeter. In order to convert whole decay energy evolved from the ^{32}P solution in a glass vial into thermal power, 5mm-thick lead container was used as a radiation absorber. Corrections for heat loss due to thermal radiation and bremsstrahlung escape as well as an effect of impurity (^{33}P) are conducted. The overall uncertainty of the nondestructive measurement as a sample is in a container is estimated to be ±1.5%. Discussion about estimates of uncertainties is also given in detail.

INTRODUCTION

In Japan Atomic Energy Research Institute (JAERI), annually about 6 TBq of ^{32}P solution is being produced and distributed. Neutron irradiation for $^{32}S(n,p)^{32}P$ reaction is performed in the research reactors JRR-2 and JMTR. For routine assays of radioactive concentration of the solutions, we adopt a method of bremsstrahlung radiation measurement with a well type ionisation chamber calibrated by a solution which has been standardised by a radiocalorimetric method. In the calorimetric method, an absolute measurement of beta-emitters is possible when an average energy per disintegration is accurately known. In this method, problems of self absorption, counting loss, dilution error and energy dependence of detection efficiency

do not exist. The calorimetry has the potential of being most accurate and precise nondestructive technique available for measurements of radioisotopes [1].

As to the applications of the radiometric calorimetry for determinig radioactivity of ^{32}P, Zumwalt et al. used a liquid nitrogen calorimeter in which the rate of evaporation of nitrogen at constant pressure was measured in 1948 [2]. Bayly also determined the disintegration rate of some 400 MBq (11 mCi) of ^{32}P with a twin, differential calorimeter in 1950 [3]. Highly accurate results of the experiments in early days suggest that the most exact method for determining radioactivity may be to measure the rate of heat evolution because it involves few of the uncertainties of the counting method. Apart from the radioactivity determinations, Shimanskaia has worked on the calorimetric determination of the average energy of the beta-spectrum of ^{32}P with an absolute activity determined by counting method in 1956 [4]. Since then no work in relevant to the calorimetric experiments on ^{32}P isotopes seems to have appeared in literatures.

In the present work, we demonstrate the procedures to suite the absolute measurement of ^{32}P solutions by nondestructive way using a microcalorimeter [5,6] characterised by being equipped with cell (measuring cup) of enough size for practical sample such as a penicillin vial as it is even in a lead container without sacrificing accuracy.

MEASURING PRINCIPLE

According to recently evaluated data [7], ^{32}P decays to stable ^{32}S in pure beta-minus mode with a half-life of 14.282 ± 0.005 day and the average energy of beta-spectrum is 695 keV. In addition to this, the energy of average 1.18 keV per disintegration is emitted as an internal bremsstrahlung. Accordingly, the average dissipation energy per disintegration is 696.18 keV. The beta particle having kinetic energy of maximum 1.7 MeV can easily penetrate through the wall of glass vial. Then the vial has to be put into a lead container of enough thickness to convert the kinetic energy of beta particles into the thermal energy. The calorimeter used is a twin-cup heat-flow differential type microcalorimeter in which thermal energy evolved from the sample flows into the aluminium mantle of "infinite" heat capacity through a sensor (thermomodule) which also acts as a thermal conductor.

The radioactivity A can be calculated from the thermal power P knowing average energy E_{av} of beta-ray spectrum by

$$A=P/E_{av} . \qquad (1)$$

The thermal power evolved from 37 MBq (1 mCi) of ^{32}P can be easily calculated as P = 4.127 μW.

Assuming the Newton's law of cooling, the following

equation applies to heat-flow calorimetry [8].

$$T_c - T_e = (P/k)(1 - e^{-kt/C}) \qquad (2)$$

where, T_c ; Temperature of a calorimetric body
T_e ; Temperature of environment (aluminium mantle)
k ; Heat transfer coefficient of the thermomodule
P ; Power dissipated in the cell
C ; Total heat capacity (sample and cell)

As can be seen from the equation (2), the right hand second term approaches zero when t elapses a sufficient time so that

$$P = k(T_c - T_e). \qquad (3)$$

Thus, one can measure the thermal power independent to the heat capacity once the equilibrium state has been established. Accordingly, any kind of material with large heat capacity such as even a lead container including sample in it is acceptable in principle.

MATERIALS

The sample solution of ^{32}P (H_3PO_4 in HCl solution) was obtained in the procedure described below [9].

Target material of sulphur was purified by sublimating the crystalline sulphur for four times prior to be irradiated in the JMTR (Japan Materials Testing Reactor). Irradiation was performed at thermal neutron flux of 2.1×10^{14} n/cm^2/s and fast neutron flux of 1.0×10^{14} n/cm^2/s for 1 cycle (21 days). The production is relied on the reaction $^{32}S(n,p)^{32}P$ in the fast neutron flux region (60 mb).

The solution was prepared in the procedures of sublimation (3 mmHg, 500 °C, 70 min.) of the irradiated target, addition of HCl (0.1 N, 70 ml) to heat (100 °C, 60 min.), second addition of HCl (0.1 N, 70 ml) to heat (100 °C, 30 min.) and purification by ion exchange column after cooling. Then the material was evaporated, followed by addition of HCl (0.1 N, 10 ml) and adjustment of acidity.

A sample solution was prepared dispensing 0.3048g in penicilline vial from the master solution. The thickness of the glass vial is typically 1 mm which is not thick enough to absorb the beta-rays of maximum energy as high as 1.7 MeV. A 5mm-thick lead container having outer diameter of 36mm and height of 64mm was used as a radiation absorber in the present experiment. Figure 1 shows the sample solution in the glass vial contained in the lead container which is placed in the calorimeter cell. Another container of the same shape, same material with distilled water of the same volume substituting for the radioactive solution in a vial was prepared to balance the heat capacity of the twin calorimeter.

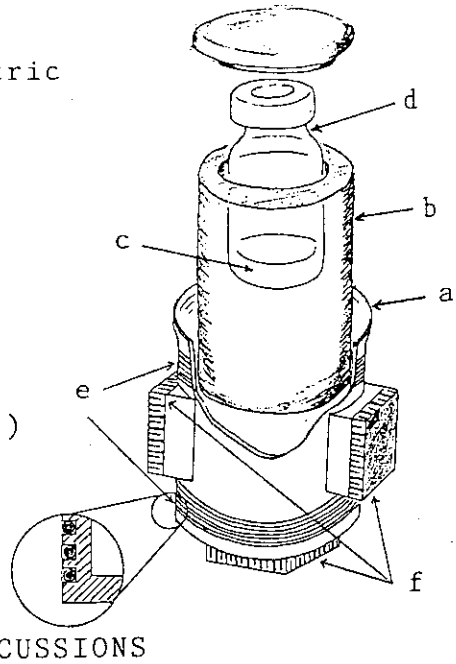

Fig. 1 Cut-away view of a calorimetric measurering cell(a) with a 5mm-thick lead container(b) in which a ^{32}P sample solution(c) in a glass vial(d) is contained. Calibration heaters(e) are embedded in the cell made of aluminium. Sensors(f) contact a common heat sink (aluminium mantle, not shown) to make heat flow paths.

RESULTS AND DISCUSSIONS

Thermal power produced by ^{32}P

A thermal power dissipating from the sample solution was compared with an accurately known power source through the heater coil. Sensitivity of thermomodules fixed on a measuring cell was measured by applying electricity on the manganin heater coil embedded in the groove cut in the wall of each cell. The sensitivity is found to be 0.144 μV/μW or inversely 6.96 μW/μV. The results of radioactivity measurement of ^{32}P solutions are summarised in Table 1.

Table 1 The results of microcalorimetric measurement. Reference time: 12:00, March 31, 1989

Run	Date [m/d/yr]	Time [h:min]	Output [μV]	Thermal power [μW]* at reference time
1	3/18/89	03:37	54.0	201.0
2	3/19/89	00:24	51.8	201.1
3	3/19/89	05:24	51.3	201.2
4	3/21/89	03:30	46.6	200.4
5	3/30/89	06:00	29.9	199.9
6	3/30/89	21:40	28.9	199.7
7	3/31/89	06:00	28.5	200.3
Average value:				200.5 ± 0.6**

* Corrected for heat loss, bremsstrahlung escape and radionuclidic impurity.
** Corresponds to an equivalent estimated one standard deviation.

Corrections for thermal power measurements

Heat loss due to thermal radiation

Heat loss from the surface of lead container due to thermal radiation has to be estimated and corrected. The estimation was done experimentally as firstly a thermal power was applied on the cell through the heater coil. In this time the cell must be empty. Then, the lead container with non-active solution (water) was set in the cell to be applied exactly the same thermal power as applied for the empty cell before. Output voltage in the latter case should be less than that of the former because some fraction of thermal power escapes from the surface of the container. The amount of heat loss thus obtained was found to be 2.2%. The same amount of power as expected to dissipate from the sample solution should be used in this experiment.

Bremsstrahlung escape

The amount of energy lost by bremsstrahlung escape from the sample is small, because the greater part of the photons due to external bremsstrahlung were dissipated in the materials of glass (1mm-thick) and lead (5mm-thick). The effect of "internal" bremsstrahlung was accounted in the average energy of 696.18 keV as described above. Ramthun [10] proposed the approximation which gave the thermal energy lost by escaping by external bremsstrahlung P_b as

$$P_b = 11.2 \times 10^{-3} \times r^2 \times X \quad \text{Watt},$$

where r was the distance from the surface of calorimeter cell in metre and X was measured exposure rate in R/h at r. The exposure rate at 30 cm from the sample was 0.4 mR/h at the measured time, 10:00, March 17, 1989. The loss of thermal power thus computed was 0.2 μW at the reference time. It is relatively very small in comparison with more than 200 μW of power generation by the sample solution.

Radionuclidic impurity

It is unavoidable to be contaminated by ^{33}P ($T_{\frac{1}{2}}$ 25.34d) as a side reaction $^{33}S(n,p)^{33}P$ due to fast neutron (65 mb) and thermal neutron (2.3 mb). Estimation of ^{33}P contamination by calculation gives approximately 0.6% at the end of irradiation. This calculation extends it to 1% at the measurement time. Contribution to the thermal power measurement of ^{32}P by 1% of ^{33}P impurity is as small as 0.1% because the thermal power evolved by disintegration of ^{33}P is about one tenth of that of ^{32}P. The corrections for bremsstrahlung and radionuclidic impurity may cancel out each other.

Estimates of uncertainties

In activity determination by the calorimetric method, an accuracy of the average energy of beta-ray spectrum is

essential. We adopted the value of 695 keV from the data table [7], but an estimated error of this value was not given in it. In the NCRP Report [11] the value 694.8±0.3 keV is given. It suggests the quality of recent data of the average energy, resulting in deriving an uncertainty to be ±0.13% correspond to an equivalent 3 sigma. Uncertainty of the half-life value is estimated as ±0.005 day against 14.282 day in the table [7] so that ±0.11% may be justified to use. Base-line drift of the calorimeter system was claimed to be ±0.05 μV/5°C/24h which reflects on the random uncertainty of thermal power measurement, but we found it rather worse in such a condition

Table 2. Corrections and estimates of uncertainties in ^{32}P activity determination

	Correction [%]
Heat loss due to thermal radiation	+2.2
Bremsstrahlung escape	+0.1
Radionuclidic impurity	-0.1
	Uncertainty[%]
Random(99.7%CL):	
Thermal power measurement reproducibility	±0.90
Estimated systematic:	
Average energy of beta spectrum	±0.13
Uncertainty in half-life	±0.11
Calibration of the calorimeter	±0.50
Correction for heat loss	±0.30
Correction for bremsstrahlung escape	±0.05
Correction for radionuclidic impurity	±0.02
Overall*	±1.51

*Overall uncertainty is expressed by cmbining thr random uncertainty and the quadratic sum of systematic uncertainties.

under a turbulence of ventillation operation in a "hot" zone laboratory. Estimated amount of 0.50% for calibration of the calorimeter comes from the drift of base-line and uncertainty of electrical power measurement. Stability of the electric source is 3×10^{-5} and temperature coefficient is 30 ppm/°C. An electric resistance of the heater coil is adjusted to realise 100 ± 0.1 ohm.

Reproducibility of the results for 5 runs of heat loss measurements was ±0.30% at an equivarent 3 sigma. For the correction of bremstrahlung escape, we assumed the uncertainty at most ±50%, so that ±0.05% was taken into account in error estimation for this correction. About ±20% of uncertainty

was assumed for the correction factor of 0.1% due to radionuclidic impurity ^{33}P, giving only 0.02% to the final thermal power determination.

CONCLUSIONS

Calorimetric method of measuring radioactivity of energetic beta-ray emitter was established using a lead container having enough thickness to absorb the beta-rays to convert them into thermal energy.

The final result of the calorimetric measurements showed that the sample solution was producing 200.5 μW ± 0.9% at 99.7% confidence level at 12:00, March 31, 1989. The disintegration rate at 12:00, March 31, 1989 was 1.798×10^9 disintegrations per second with the overall uncertainty ±1.5%.

The calorimetric method is intrinsically accurate, but requires a larger sample activity than does the counting method. Accordingly, it is a useful procedure where activity levels of the order of MBq and GBq are to be measured.

Acknowledgement

The authors wish to thank Professor C. Mori of the Nagoya University for valuable discussions. We are indebted to Mr. M. Izumo for preparing and providing the ^{32}P solutions.

REFERENCES

[1] Genka, T., Takeuchi, N., Iwamoto, S. and Kobayashi, K., Radionuclide metrology for the quality assurance of radioisotope products, 1991 (in this proceedings)

[2] Zumwalt, L.R., Cannon, C.V., Jenks, G.H., Peacock, W.C., and Gunning, L.M., Comparison of the determination of the disintegration rate of radiophosphorus by absolute beta counting and calorimetric measurement. Science, Vol.107, p.47, 1948.

[3] Bayly, J.G., A calorimetric measurement of the disintegration rate of a ^{32}P source. Canadian Journal of Research, Vol. 28, SEC. A, pp.520-529, 1950.

[4] Shimanskaia, N.S., A calorimetric determination of the mean energy of the beta-spectra of ^{32}P, ^{35}S, ^{64}Cu, ^{185}W and ^{198}Au. J. Exptl. Theoret. Phys. (U.S.S.R.) Vol.31, pp.393-396, 1956 English translation, Soviet Physics JETP, Vol.4, No.3, pp.355-358, 1957

[5] Genka, T., Kobayashi, K. and Hagiwara, S., A calorimeter for the measurement of activity of tritium and other pure beta emitters. Appl, Radiat. Isot. Vol. 38, No. 10, pp.845-850, Int. J. Radiat. Appl. Instrum. Part A, 1987.

[6] Genka, T., Kobayashi, K., Takeuchi, N., Ishikawa, I. and Hoizumi, K., A twin type heat flow microcalorimeter for radioactivity measurements. Radioisotopes, Vol.37, No.3, pp.155-158, 1988 (in Japanese)
[7] Browne, E. and Firestone, R.B., Table of Radioactive Isotopes, Ed. Shirley, V.S., John Wiley & Sons 1986.
[8] Gunn, S.R., Radiometric calorimetry, Nucl. Instr. Meth., Vol. 29, pp.1-24, 1964.
[9] Izumo, M., Private communication
[10] Ramthun, H., Microcalorimetry determination of the beta-energy of ^{90}Sr-^{90}Y. Proc. Symp. Standardization of radionuclides. IAEA, Vienna, pp.589-599, 1967.
[11] NCRP, A handbook of radioactivity measurements procedures, Report No. 58, 2nd edition, 1985

1. Basic Research on High-Uranium Density Fuels for Research and Test Reactors

M. UGAJIN, A. ITOH, M. AKABORI

Department of Fuels and Materials Research
Tokai Research Establishment, JAERI
Tokai-mura, Naka-gun, Ibaraki-ken 319-11, Japan

ABSTRACT

High-uranium density fuels, uranium silicides (U_3Si_2, U_3Si) and U_6Me-type uranium alloys (Me=Fe,Mn, Ni), were prepared and examined metallurgically as low-enriched uranium (LEU) fuels for research and test reactors. Miniature aluminum-dispersion plate-type fuel (miniplate) and aluminum-clad disk-type fuel specimens were fabricated and subjected to the neutron irradiation in JMTR (Japan Materials Testing Reactor).
Fuel-aluminum compatibility tests were conducted to elucidate the extent of reaction and to identify reaction products. The relative stability of the fuels in an aluminum matrix was established at 350°C or above. Experiments were also performed to predict the chemical form of the solid fission-products in the uranium silicide (U_3Si_2) simulating a high burnup anticipated for reactor service.

1. INTRODUCTION

The Fuel Processing and Qualification Laboratory of the Department implemented a new program of exploring the next generation fuel for use in research and test reactors in April 1988. Uranium silicides U_3Si_2, U_3Si and U_6Me-type uranium alloys (Me = Fe,Mn,Ni) have been chosen as target fuel materials for R & D because of their high-uranium densities: 11.3, 14.9 and 17.0 gU/cm^3, respectively.

The installation of equipment necessary for the preparation of miniature Al-dispersion plate-type fuel was completed at the end of March 1989. The first irradiation capsule (designated 88F-2A) containing uranium silicides was produced in November 1989 [1]; the neutron irradiation in JMTR started in May 1990 and terminated in May 1991. Postirradiation examinations of the 88F-2A capsule commenced at the beginning of October 1991.

The second irradiation capsule (designated 89F-1A) containing uranium silicides and U_6Me-type fuels was made in July 1990. The neutron irradiation was started also in JMTR in November 1990 and will continue to the end of November 1992, aiming at a burnup level higher than that achievable in the 88F-2A capsule.

This paper will deal with the experimental results so far obtained for uranium silicides and U_6Me-type fuels with emphasis on: (1) fuel preparation, (2) fuel-aluminum compatibility and (3) high-burnup simulation.

2. FUEL PREPARATION

2.1 MINIATURE PLATE-TYPE FUEL

Experiments were carried out to prepare miniature aluminum-dispersion plate-type fuel (miniplate); the process used is based on the conventional picture-frame method. Fuel materials produced were U_3Si_2, U_3Si, $U_3(Si,Ge)$, USi and U_6Me (Me=Fe,Mn, Ni). A total of 14 miniplates with uranium densities from 4.0 to 6.3 gU/cm^3 were fabricated and subjected to the neutron irradiation in JMTR as described in the preceding section.

Miniplates were fabricated according to the following steps:

(1) argon arc-melting of together charges of U metal and silicon tips
(2) annealing of arc-melted button at 850 °C for 72 h
(3) crushing and powdering of arc-melted and annealed button
(4) sieving fuel powders to 4 classes of particle sizes (≦150 μm)
(5) weighing and blending fuel powders and aluminum powders
(6) cold pressing of mixed powders to form fuel compact
(7) assembling fuel compact, frame and cover made with 6061 Al alloy
(8) peripheral welding of assembly
(9) 500°C hot-rolling and cold rolling
(10) mechanical bond test: bending (delamination) test of a sample trimmed from rolled plate-end
(11) sizing (partial shearing and polishing) to finished miniplate: 20mm x 30mm x 1.3～1.4mm thick
(12) X-ray radiographic inspection to check fuel meat homogeneity and fuel-frame bond
(13) immersion density measurement

Steps (3)-(6) were processed in argon-circulated glove boxes in which oxygen and moisture concentrations were controlled to less than ～30 and ～50 ppm, respectively.

U_6Mn and $U_6(Fe_{0.6}Mn_{0.4})$ are friable materials; powders can easily be produced from the alloy castings by the use of jaw crusher and agate mortar/pestle. This is the greater advantage of U_6Me-type fuels to the U_3Si that is too ductile to be comminuted.

Table 1. lists important parameters of miniplates fabricated. The fuel compositions of each plate are as follows:

88F2A-01, 89F1A-01 = 100 wt% U_3Si_2
88F2A-02, 89F1A-02 = 80 wt% U_3Si_2 + 20 wt% USi
88F2A-03, 89F1A-03 = 99.5 wt% U_3Si_2 + 0.5 wt% Mo
88F2A-04, 89F1A-04 = 80 wt% U_3Si_2 + 20 wt% U_3Si
89F1A-05 = 100 wt% U_6Mn, 89F1A-06 = 100 wt% $U_6(Fe_{0.6}Mn_{0.4})$

The following miniplates are also included in the 89F-1A series capsule now under irradiation: $U_3(Si_{0.8}Ge_{0.2})$, $U_3(Si_{0.6}Ge_{0.4})$, $U_6(Fe_{0.4}Ni_{0.6})$ and U_6Ni.

Fig.1 shows a typical example[1,2] of a metallographic cross-section of a 1.4-mm-thick miniplate; the fuel meat consists of U_3Si_2-Al with uranium density of 4.69 gU/cm^3 and void volume fraction of 13 %. Weight fractions of each U_3Si_2 particle-size (ps) range adopted for manufacturing the fuel compact are: 19% for ps≦45, 20% for 45＜ps≦75, 21% for 75＜ps≦106 and 40% for 106＜ps≦150 μm.

2.2 ALUMINUM-CLAD DISK-TYPE FUEL

U_3Si, $U_3Si + U_3Si_2$, U_3Si_2 and $U_3Si_2 + USi$ were arc-melted and heat-treated at 850°C for 72 h. The annealed silicide buttons were cut into a thin-plate form; each plate was then clad with two aluminum disks by hot-pressing at about 25 MPa and at 400-450 °C for 30 min in vacuum. Fig.2 shows a typical cross section of the aluminum-clad disk-type silicide fuel. The 28 disks fabricated were irradiated in the capsules 88F-2A and 89F-1A.

3. FUEL - ALUMINUM COMPATIBILITY

Fuel-aluminum compatibility is a matter of concern not only in the irradiation performance but also in the fabrication of fuels involving elevated temperatures[3,4]. Tests were conducted to elucidate the extent of the reaction and to identify reaction products by EPMA and X-ray diffraction analysis as well as metallographic examination. The results showed that U_3Si_2 exhibits greater stability than U_3Si in contact with aluminum at temperatures $\geqq$ 350°C. Ge-added U_3Si showed essentially no improvement in the compatibility with aluminum. The rates of reaction at temperatures $<$ ~300°C have been demonstrated to be very low.

Fig.3 shows volume increases of fuel-aluminum dispersion compacts as a function of temperature and time of heating for uranium silicides and U_6Mn.

The relative stability of the fuels was thus established for aluminum at temperatures $\geqq$ 350°C as follows:

$$U_3Si \sim U_3(Si,Ge) < U_6Mn << U_3Si_2 \sim USi$$

As seen from the 450°C data points in Fig.3, U_6Mn is marginally more stable than U_3Si despite its lower peritectic temperature 726°C, compared with the peritectoid temperature of 925°C for U_3Si.
This may be due to the differences between U_3Si and U_6Mn in the reaction kinetics for aluminum; in the former, path for the preferential diffusion of aluminum is formed along the U_3Si grain boundaries.

As the reaction products, the compounds $U(Al,Si)_3$ and $(U,Me)Al_3$ were identified respectively, for uranium silicides and for U_6Me-type fuels. Fig.4 illustrates an EPMA image of reacted $U_6(Fe_{0.6}Mn_{0.4})$ particles in a miniplate shown next. Fig.5 shows a metallographic cross-section (perpendicular to the rolling direction) of an initially 1.38-mm $U_6(Fe_{0.6}Mn_{0.4})$-dispersion miniplate heated at 450°C for 120 h; a plate-thickness increase of about 30% is noted at the fuel-aluminum interaction zone.

The observed volume and thickness increases are considered to be attributed to the void formation due to the reaction and to the formation of less-dense $U(Al,Si)_3$ and $(U,Mn)Al_3$ (U/Mn atom ratio ~6). These compounds have a lower density of ~6.7 g/cm^3, compared with the respective theoretical density of 12.2 and 17.8 g/cm^3 for U_3Si_2 and U_6Mn.

To improve the compatibility of U_3Si and aluminum, the U_3Si-Al matrix interface was stabilized by the slight oxidation of the surface of U_3Si. The validity of this method was examined employing the disk-type fuel. The surface oxidation of the thin U_3Si plate was performed at 500-800 °C under a low oxygen partial pressure in a vacuum < 0.1 Pa. This treatment yielded the dense thin layer of UO_{2+X} on the surface of the U_3Si plate. The compatibility test was carried out at 500°C for 20 h using a disk-type specimen in which the U_3Si plate had the oxide layer on one side only. As evident in Fig.6, no reaction was observed at the interface between the surface-oxidized U_3Si and the Al-cladding while the reaction zone of ~50 μm was observed on the other side of the U_3Si plate.

4. HIGH-BURNUP SIMULATION EXPERIMENT

The chemical form of solid fission-products is of particular importance since it may affect the fission product release under a hypothetical accidental condition and the fuel-aluminum reaction during irradiation especially at abnormally high temperatures. However, essentially no information was previously available for the silicide fuel.

The uranium silicide (U_3Si_2) with 19.7% ^{235}U was assumed here to have

been irradiated under the likely operating conditions of research reactor: thermal neutron flux = 1.0×10^{15} n/cm^2 · sec, irradiation time = 75 EFPD. Inventories of actinide and fission products were calculated using the ORIGEN code with input parameters THERM=0.7989, RES=0.18388 and FAST=1.5305. The burnup value, ~98% of ^{235}U, is considerably high and may be the maximum anticipated for this type of fuel in reactor service.

Three simulated fuel samples were prepared by arc melting the together charges of elements according to the calculated inventories, and were heat-treated at 900-1100°C for 4-7 days. The following 13 elements were simulated in this work:

U, Si, Mo, Ru, Rh, Pd, Nd, Ce, La, Pr, Y, Zr, Sr.

Other rare earth, alkaline earth and actinide elements were taken into consideration by adding their equivalent quantities to the charges using the elements listed above. Phases present in the samples were identified by EPMA and X-ray diffractometer.

On the basis of the present investigation, the chemical form of the solid fission-products can tentatively be classified into the following four categories:

(A) Matrix phase U_3Si_2:

The major constituents of the matrix phase are uranium and silicon; it consists of tetragonal U_3Si_2. The solubility limits of other elements were found to be very small to the U_3Si_2 phase; e.g., the Mo solubility is less than ~0.05 wt%.

(B) U_5MoSi_4-type precipitate:

Mo, Ru and Rh form a solid solution based on this new compound; its crystal structure has not yet been defined but found very close to that of U_3Si_2. It should be noted that palladium added as one of the platinum group elements does not coexist with Ru and Rh.

(C) RESi-type (RE=rare-earth elements) precipitate:

Rare-earth elements (Nd, Ce, La, Pr and Y) form this type of silicide. Palladium and part of the uranium enter into the lattice to form the solid solution (RE,Pd,U)Si.

Fig.7 shows EPMA data indicating the existence of the RESi-type precipitates in the matrix phase of U_3Si_2.

(D) Free metal

Strontium and barium appear to remain as metallic state without forming silicide or uranium compound. Attempts using $SrSi_2$ instead of strontium metal as starting material failed to form any type of strontium silicide.

Table 1. List of miniplates fabricated for the capsule irradiation in JMTR

MINIPLATE	PLATE WT. (g)	PLATE VOL. (cm^3)	TOTAL U WT. (g)	U DENSITY (gU/cm^3)	VOID (%)	FUEL VOL. (%)
88F2A-01	2.2508	0.7907	0.1348	4.38	5.94	38.76
88F2A-02	2.2748	0.8023	0.1247	4.37	5.28	39.83
88F2A-03	2.2447	0.7941	0.1125	4.66	2.82	41.67
88F2A-04	2.2669	0.7989	0.1279	4.66	7.78	39.25
89F1A-01	2.2204	0.7808	0.1408	4.07	14.37	36.00
89F1A-02	2.2518	0.7917	0.1389	4.03	11.03	36.79
89F1A-03	2.2223	0.7789	0.1454	4.15	11.42	37.17
89F1A-04	2.2641	0.7930	0.1515	4.39	13.26	37.03
89F1A-05	2.2784	0.7767	0.2105	6.31	12.84	36.79
89F1A-06	2.3152	0.7929	0.2057	5.98	15.59	34.88

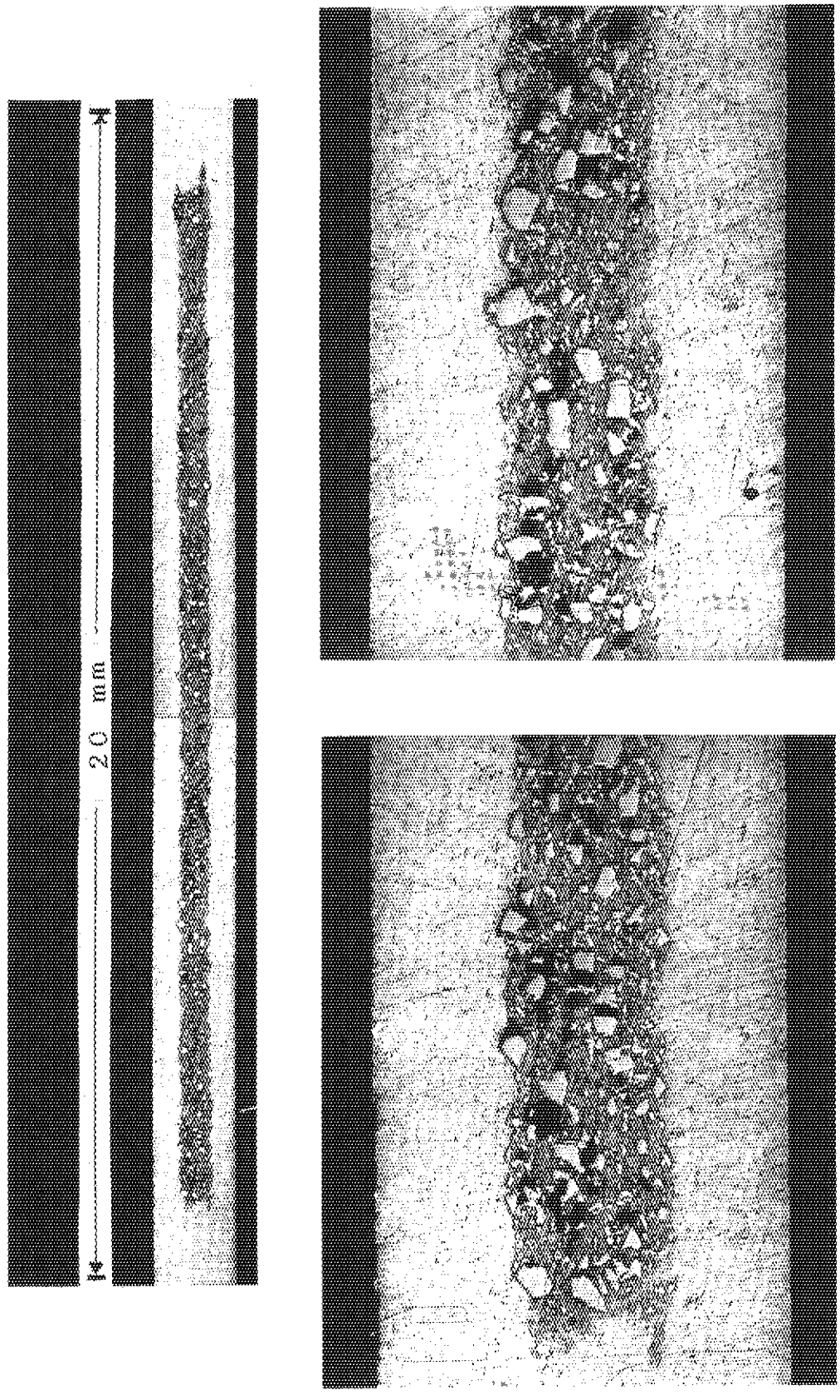

Fig.1 Cross-section of 1.40-mm-thick miniplate with fuel meat of U_3Si_2 and Al, clad with 6061Al alloy (Bottom:Partly enlarged of the top)

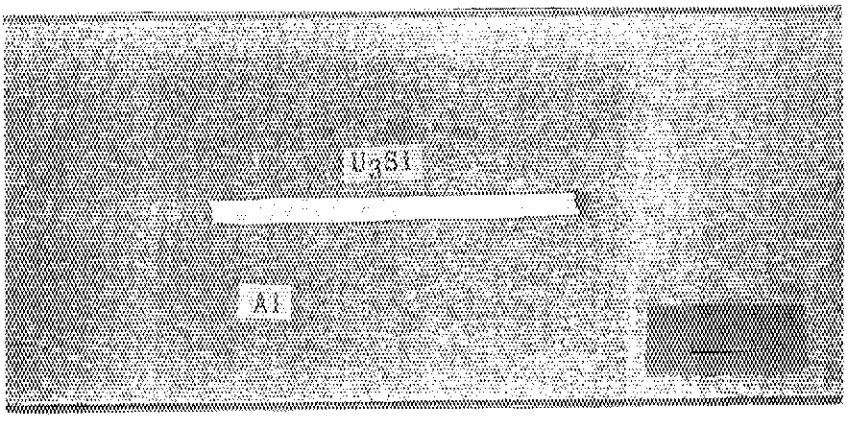

Fig.2 Cross section of aluminum-clad disk-type silicide fuel

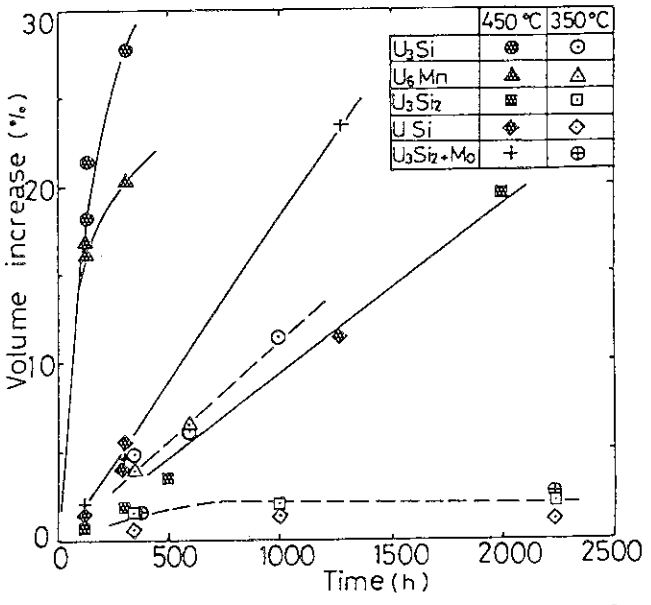

Fig.3 Volume increases of fuel compacts comprising aluminum and uranium silicides or U_6Mn due to their reaction at 350° and 450°C

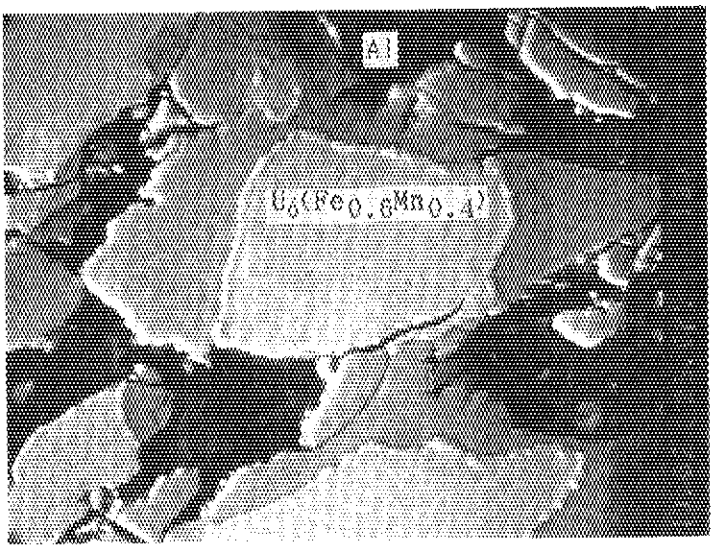

Fig.4 EPMA backscatter image of $U_6(Fe_{0.6}Mn_{0.4})$ particles reacted with aluminum in a miniplate same as in Fig.5

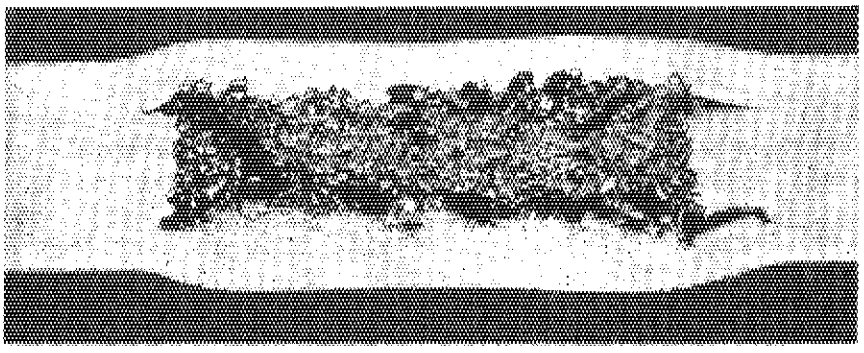

Fig.5 Cross-section of initially 1.38-mm-thick miniplate with fuel meat $U_6(Fe_{0.6}Mn_{0.4})$-Al after heating at 450°C for 120 h (see also Fig.4)

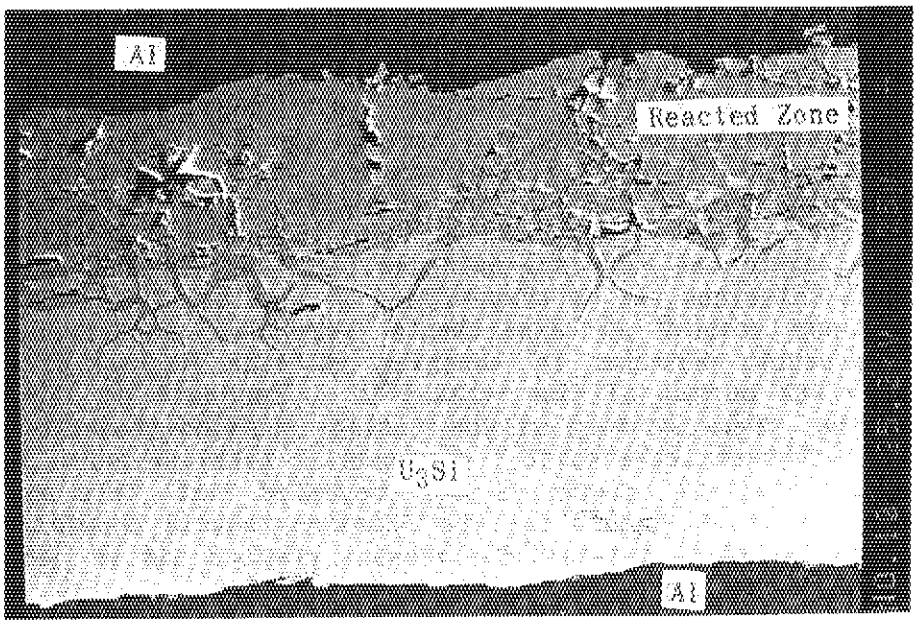

Fig.6 Cross section of aluminum-clad disk-type U_3Si (Lower side: surface-oxidized) after heating at 500°C for 20 h (EPMA backscatter image)

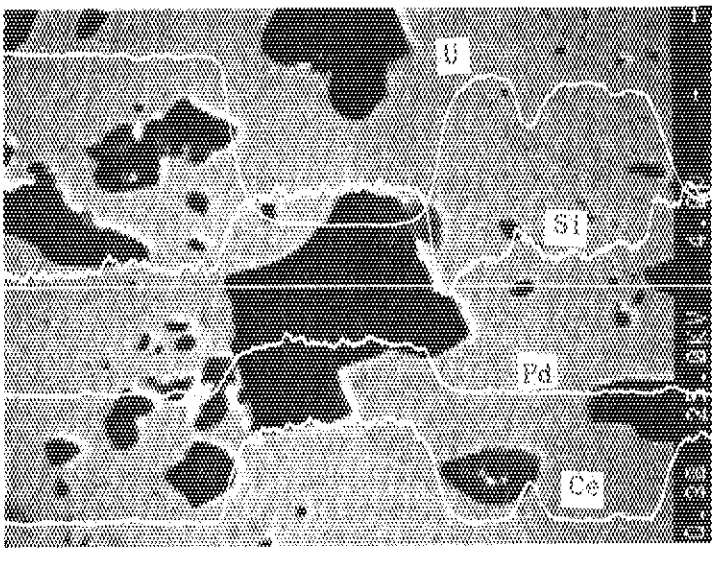

Fig.7 EPMA backscatter image and line-scan analysis showing the existence of the (RE,Pd,U)Si phase (RE=Ce,La,Nd,Y) in the matrix of U_3Si_2

5. SUMMARY AND CONCLUSIONS

Preparation experiments were carried out to fabricate miniature aluminum-dispersion plate-type fuel and aluminum-clad disk-type fuel by using the conventional picture-frame method and hot-pressing technique, respectively. Fuel materials produced were U_3Si_2, U_3Si, USi and U_6Me (Me=Fe,Mn, Ni). Totally 14 miniplates with uranium densities from 4.0 to 6.3 gU/cm^3 and 28 disk-type fuel specimens containing structurally-modified U_3Si were prepared and subjected to the neutron irradiation in JMTR. Postirradiation examinations just started for the first domestic fuel specimens will provide a basis for better understanding of the behavior of high-uranium density fuels.

Fuel-aluminum compatibility tests demonstrated that U_3Si_2 exhibits greater stability than U_3Si in contact with aluminum at or above 350°C. It was also shown that the rates of reaction at temperatures less than ~300°C are very low. U_6Mn is marginally more stable than U_3Si in the aluminum matrix. $U(Al,Si)_3$ and $(U,Me)Al_3$ were identified as the reaction products, respectively, for uranium silicides and for U_6Me-type fuels. The observed volume and thickness increases are considered to be attributed to the void formation due to the reaction and to the formation of these less-dense compounds. Ge-added U_3Si indicated no improvement in compatibility, while the surface-oxidized U_3Si showed no evidence of the reaction with aluminum at a temperature as high as 500°C.

High-burnup simulation experiments were also performed to predict the fission-products behavior in uranium silicide (U_3Si_2) irradiated to approximately 98% burnup of the ~20% ^{235}U. Emphasis of the study was placed on the chemical form of the solid fission-products comprising zirconium, molybdenum, rare-earth elements, alkaline-earth metals and elements of the platinum group. It was revealed that this new type of fuel shows the unique nature in the fission-products chemistry. Further study will be needed to confirm the present results and to obtain more detailed information on this multicomponent system.

ACKNOWLEDGEMENTS

The present authors are grateful to Dr. T. Kondo and Dr. M. Handa, respectively, Director and Deputy Director of the Department of Fuels and Materials Research for their encouragement.

REFERENCES

(1) M.Ugajin, A. Itoh, M. Akabori, K.Ikawa,"Preparation of silicide fuel for capsule irradiation" : presented at the 1989 fall meeting of the Atomic Energy Society of Japan, Oct.17-19, 1989 (Tokai-mura, Japan) Abstract No. K57 (in Japanese)

(2) M.Ugajin, "Basic program to compute uranium density and void volume fraction in laboratory-scale uranium silicide aluminum dispersion plate-type fuel", JAERI-M 91-069 (May, 1991)

(3) N.Ooka, K.Kanaya, Y.Etou, H.Yamashita, "Experiments on compatibility of U_3Si_2 and Aluminum at high temperature in out-pile", Keikinzoku yousetsu 339,28(1990)8 (in Japanese)

(4) T.C.Wiencek,R.F.Domagala and H.R. Thresh, "Thermal compatibility studies of unirradiated uranium silicide dispersed in aluminum", Nucl. Technol. 71(1985)608

2. Studies of Transient Behavior of Low Enriched Silicide Fuel Plates by Pulse-Irradiation in the NSRR

K. Yanagisawa*, T. Fujishiro*, S. Kobayashi*, O. Horiki*
K. Soyama**, H. Ichikawa**, T. Kodaira** and T. Yamahara***

* Department of Fuel Safety Research
** Department of Research Reactor
*** Department of Hot Laboratories
Tokai Research Establishment, JAERI
Naka-gun, Ibaraki-ken, 319-11 Japan

ABSTRACT

Since the utilization of high-density silicide fuels are now being expanded in research reactors, the behavior of these fuels under transient and accidental conditions are of big concern. The transient behavior of the low-enriched uranium (19.89 w/o) silicide miniature fuel plates have been studied by the irradiation in the Nuclear Safety Research Reactor (NSRR) in the Japan Atomic Energy Research Institute. The energy of 154 cal at maximum was deposited per unit gram of the silicide fuel quite promptly by pulse-irradiating in the NSRR, and realized the transient temperature increase up to 970° C. Major results obtained from experiment are: (1) At fuel temperatures below 400° C, the silicide fuel plates kept a good dimensional stability and intactness. Fuel deformation started beyond 400° C, and beyond the melting temperature of Al-3%Mg alloy cladding, 640° C, fuel plates were largely damaged showing a bowing up to 7mm. (2) Despite the large degradation of the fuel at cladding temperatures around 970° C, no fuel fragmentation nor mechanical energy generation was observed.

INTRODUCTION

With respect to the fuel behavior of the silicide plate-type fuels under transient/accident conditions, no experimental studies have been conducted, to date. The experiments performed so far were only addressed to aluminide related fuels[1−6].

To establish a data base necessary to define the licensing criteria for the silicide plate-type fuels under transient/accident conditions, the experiments were conducted using the NSRR at JAERI. Emphasis was made to understanding the dimensional stability and the failure threshold under power transient conditions.

EXPERIMENT

1. Test fuel plate

The test fuel plates used in these experiments, shown in **Fig. 1**, were designed by JAERI and fabricated by Cerca at Romans, France. Fabrication process of fuel plate is described elsewhere[6]. This is a typical low enriched uranium (19.89w/o U-235) silicide-aluminum dispersion plate-type fuel (hereinafter abbreviated the silicide plate-type fuel). As shown in **Table 1**, the fuel plate consisted of fuel core (25mm width x 70mm length x 0.51mm thickness) sandwiched by Al-3w/o Mg alloy cladding (35mm width x 130mm length x 0.38mm thickness).

2. Instrumentations and irradiation capsule

In-core instrumentation attached to the silicide fuel plate was five Pt/Pt-13%Rh thermocouples (hereinafter abbreviated T/C's), of which melting point was 1780° C. T/C's were spot welded directly to the front surface of the plate fuel at five different locations, as shown in **Fig. 1**. After assembling to the supporting jig with electric cables, the fuel plate was loaded into the irradiation capsule. The capsule assembly was then installed to the test cavity of the NSRR for subsequent pulse irradiation. All the tests were conducted in stagnant water at room temperature (about 20° C) and 1 atmosphic pressure inside the irradiation capsule[7].

3. Pulse history

The half-width of power of NSRR pulse irradiation is a minimum of about 4.4ms at a maximum integral power of 110MWs. The value of this width varies from 4.4 to 20ms depending on the magnitude of inserted reactively.

The integral value of the reactor power P (MW·s) measured by micro fission chambers was used to estimate deposited energy Eg (cal/g·fuel) in each test fuel plate by Eg= kg x P, where the power conversion ratio kg (cal/g fuel per MWs), is the ratio of fuel plate power to reactor power. This ratio was determined through fuel burn-up analysis[6] taking the radial and axial power skew into consideration.

The power profile across the fuel plate was relatively flat, although locally sharp peaks of about 15% ～ 28% higher than the average were revealed at both ends of the fuel plate.

RESULTS AND DISCUSSION

1. Transient temperature and failure threshold

In experiment 508-4, all T/C's were exceeded the melting point (m.p.), i.e., 640° C of Al-3%Mg alloy cladding (hereinafter abbreviated Al cladding). **Figure 2** shows transient temperature at interval of 0.05s around melting point. It can be revealed from this that measured solidus-liquidus temperatures are between 531° C and 612° C. On the other hand, physical solidus-liquidus ones according to the phase diagram are between 573° C and 640° C. Hence, a maximum temperature error band between the two was approximately 40° C.

Figure 3 summarizes the relation between the measured fuel plate temperature and the given deposited energy. At temperature below 400° C, the silicide plate fuels are intact. Maximum estimated temperatures both for steady-state and unusual transient conditions of research reactors are well below the threshold temperature of 400° C. Hence, there is enough safety margins in research reactors. However, once exceeding the temperature of 400° C, the silicide plate fuel was defective due mainly to the occurrence of intergranular crackings. Consequently, it is reasonable from safety point of view to set the temperature of 400° C as the failure threshold of the silicide fuel plate.

2. Dimensional stability

In **Fig. 4**, a maximum bowing of the fuel plate is shown. As the fuel plate temperature was below 400° C, the bowing was negligible. When the temperature exceeded 400° C, however, the bowing became evident. The bowing was enhanced significantly by necking, that is, a significant thinning of plate wall thickness at end peak locations where melting of Al cladding and fuel separation occurred simultaneously.

It is worthy mentioning that the maximum channel flow width in research reactors is to be designed from 2.7 to 3mm. So, care must be taken not to increase the fuel plate temperature above 400° C so as not to cause the channel closure.

3. Microstructure of fuel core

One specimen of Ex. 508-4 (154 cal/g·fuel) was cut from the location of T/C #5 (peak temperature 957° C) and the other specimen of 508-1 (62 cal/g·fuel) was cut from the location of T/C #1 (estimated peak temperature <200° C). Then, the two were provided for microstructural study.

Results is shown in **Photo. 1**. At temperature below 400° C, there is no trace of metal to metal reaction between Al matrix and silicide particles. However, as shown in (a), at temperature around 925° C, there is a trace of reaction between Al matrix and silicide particles resulting in the formation of two additional phases at outermost of the silicide particles. The outermost (first) phase consisted of Al riched U (Al, Si) compounds with thickness of about 4 μ m. The subsequent (second) phase consisted of Si riched (U, Si) compounds with thickness of about 1 μ m. The last largest phase consisted of the original U riched (U_3Si_2+USi) compounds, respectively. It should be mentioned that thickness of additional two phases is reached of order of 1/3 of the original silicide particles diameter.

CONCLUSIONS

The conclusions reached in the present experiments are summarized as follows:

(1) Neither failure nor degradation of dimensional stability of the silicide

plate fuel occurred in the temperature below 400° C. At temperatures beyond 400° C, the dimensional stability was gradually degraded with temperature.

(2) Despite the large degradation of the fuel at cladding temperatures around 970° C, no fuel fragmentation nor mechanical energy generation was observed.

(3) At higher temperature around 925° C, there occurred reaction between molten Al (Al or Al-3%Mg) and fuel meat (U_3Si_2+USi). Total thicknesses of the additional phases were of the order of 1/3 at the original silicide particle diameter. Reacted phases were estimated to be Al riched U(Al, Si) and Si riched (U, Si) from outermost of the fuel silicide particles.

ACKNOWLEDGMENTS

Appreciation is expressed to Dr. K. Shiba, Head, Dep. Fuel Safety Res. and Mr. M. Kawasaki, Head, Dep. Res. Reactor and Mr. N. Ohnishi, Office of Planning at JAERI for thier encouragement and promotion of this work.

REFERENCES

(1) MILLER, R. W.: IDO-16883 (1984)

(2) USAEC: IDO-19311 (1962)

(3) WRIGHT, R. W.: STL 372-30 (1965)

(4) ISHIKAWA, M.: JAERI-memo 3057 (published) (1968)

(5) BEESTON, J. M., HOBBINS, R. R., GIBSON, G. W., FRANCIS, W. C.: Nucl. Technol. 49, 136 (1980)

(6) Japan Metal Society: "Metal data handbook", Maruzen (1974)

(7) YANAGISAWA, K.: J. Nucl. Sci. Technol. 28, [5], 459 (1991)

(8) ASTM-E 321-79, (1985)

Table 1 Characteristics of the low enriched uranium silicide plate-type miniature fuel used in NSRR transient experiment and those of JMTR full-scale plate

ITEMS	NSRR MINIATURE PLATE	JMTR FULL-SCALE PLATE
(1) CORE MATERIAL	U_3Si_2-Al	U_3Si_2 -Al
ENRICHMENT (w/o)	ca. 19.89	ca. 20
THICKNESS (mm)	0.51	0.51
WIDTH (mm)	25	62
LENGTH (mm)	70	760
URANIUM DENSITY (g/c.c.)	4.8	4.8
(2) CLADDING MATERIAL	Al-3w/o Mg (AG3NE*)	JIS A6061 or AG3NE*
THICKNESS (mm)	0.380	0.380
(3) PLATE		
THICKNESS (mm)	1.27	1.27
WIDTH (mm)	35	71
LENGTH (mm)	130	780

NOTE: * Industrial Standard of France

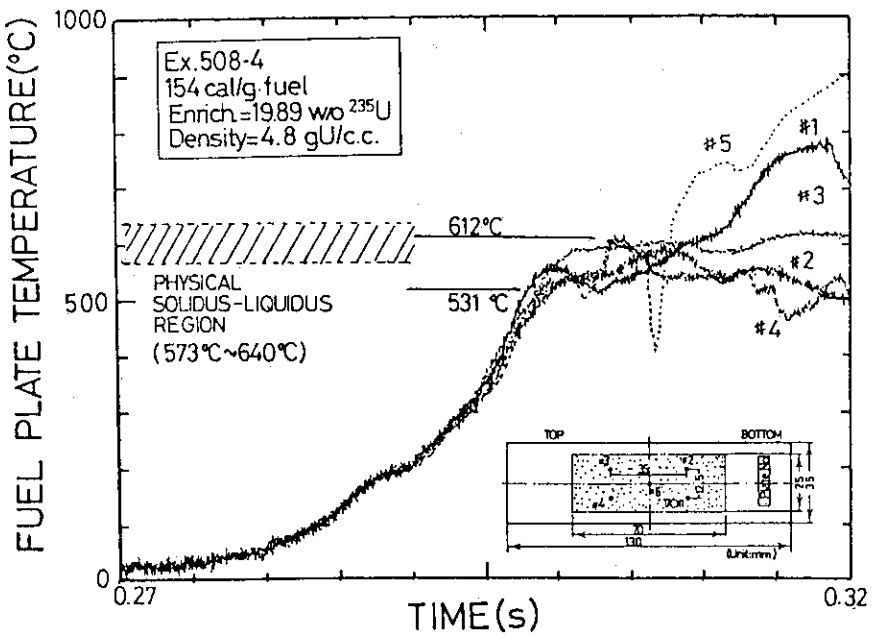

Fig. 2 Solidus-liquidus transformation temperatures of Al-3%Mg alloy (AG3NE) observed by experiment and those (hatched area) referred to phase diagram in Al-Mg binary alloy

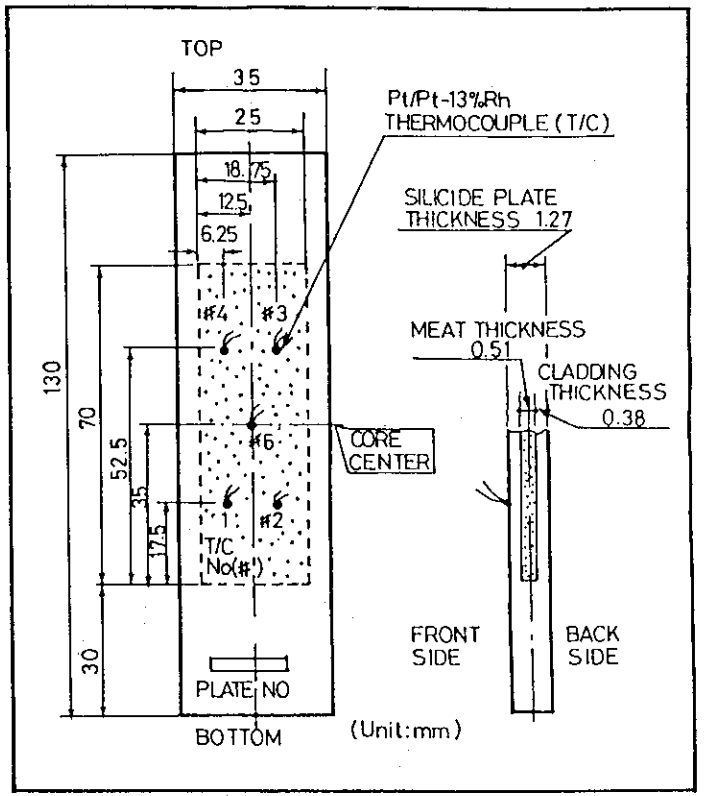

Fig. 1 A schematic representation of the tested silicide plate-type miniature fuel, having the enrichment by 19.89w/o ^{235}U and the density by 4.8 gU/cm^3

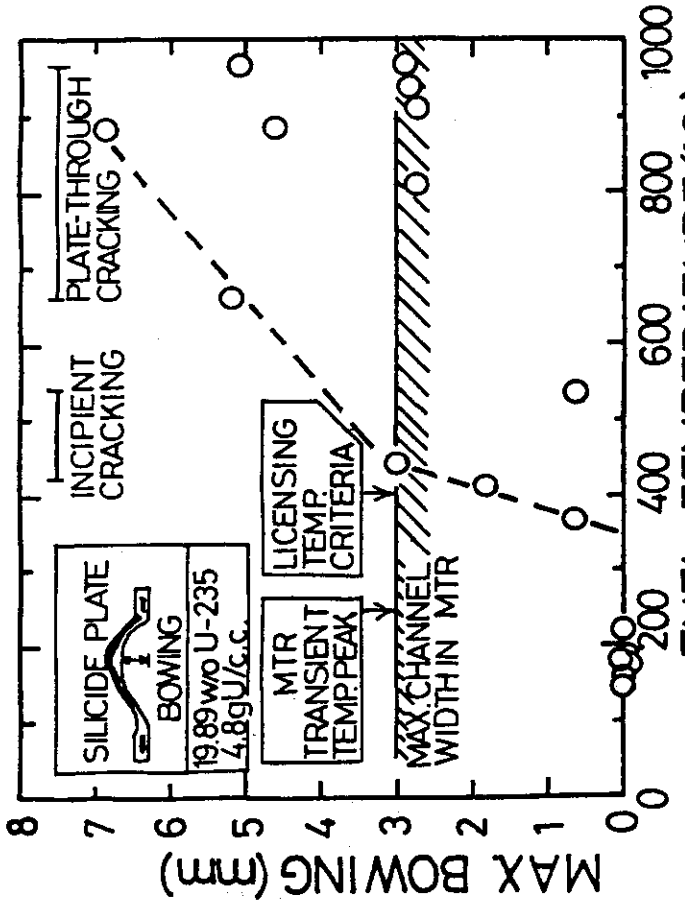

Fig. 4 Observed maximum bowing of the silicide plate-type fuel from post- pulse irradiation examination

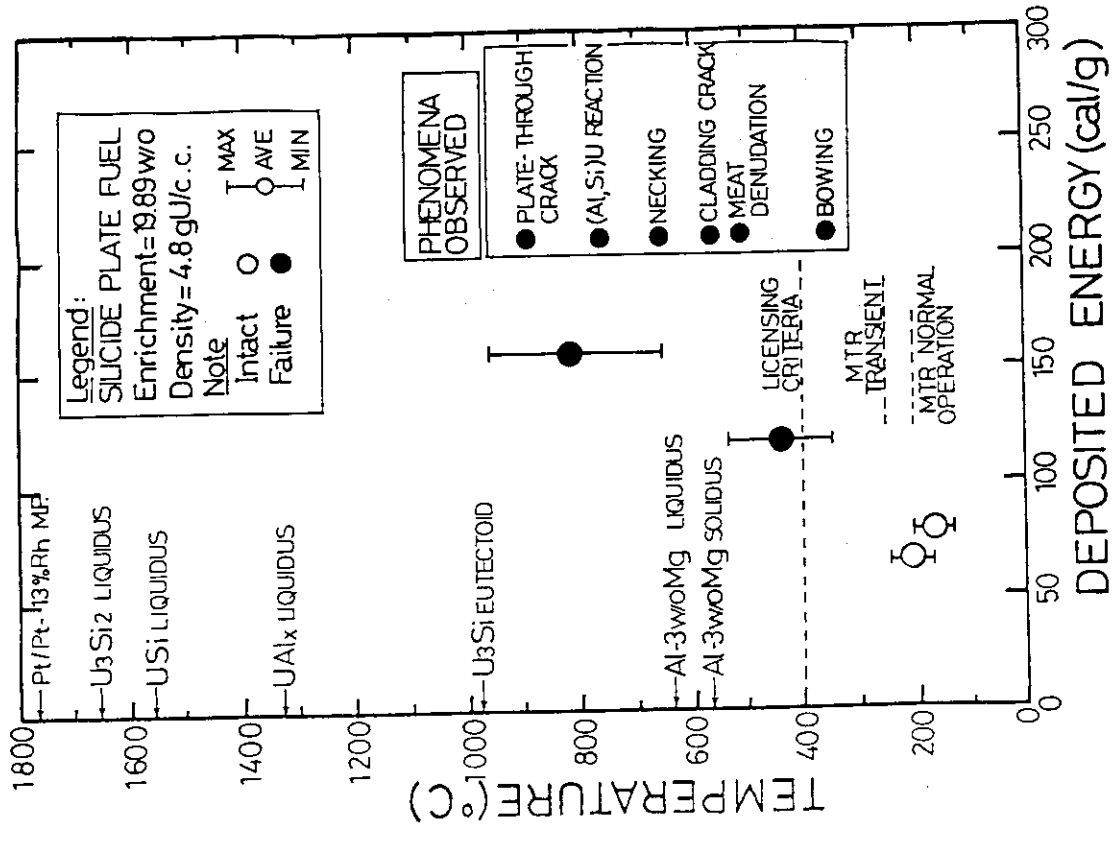

Fig. 3 Measured temperatures of the silicide plate-type fuel as a function of deposited energy

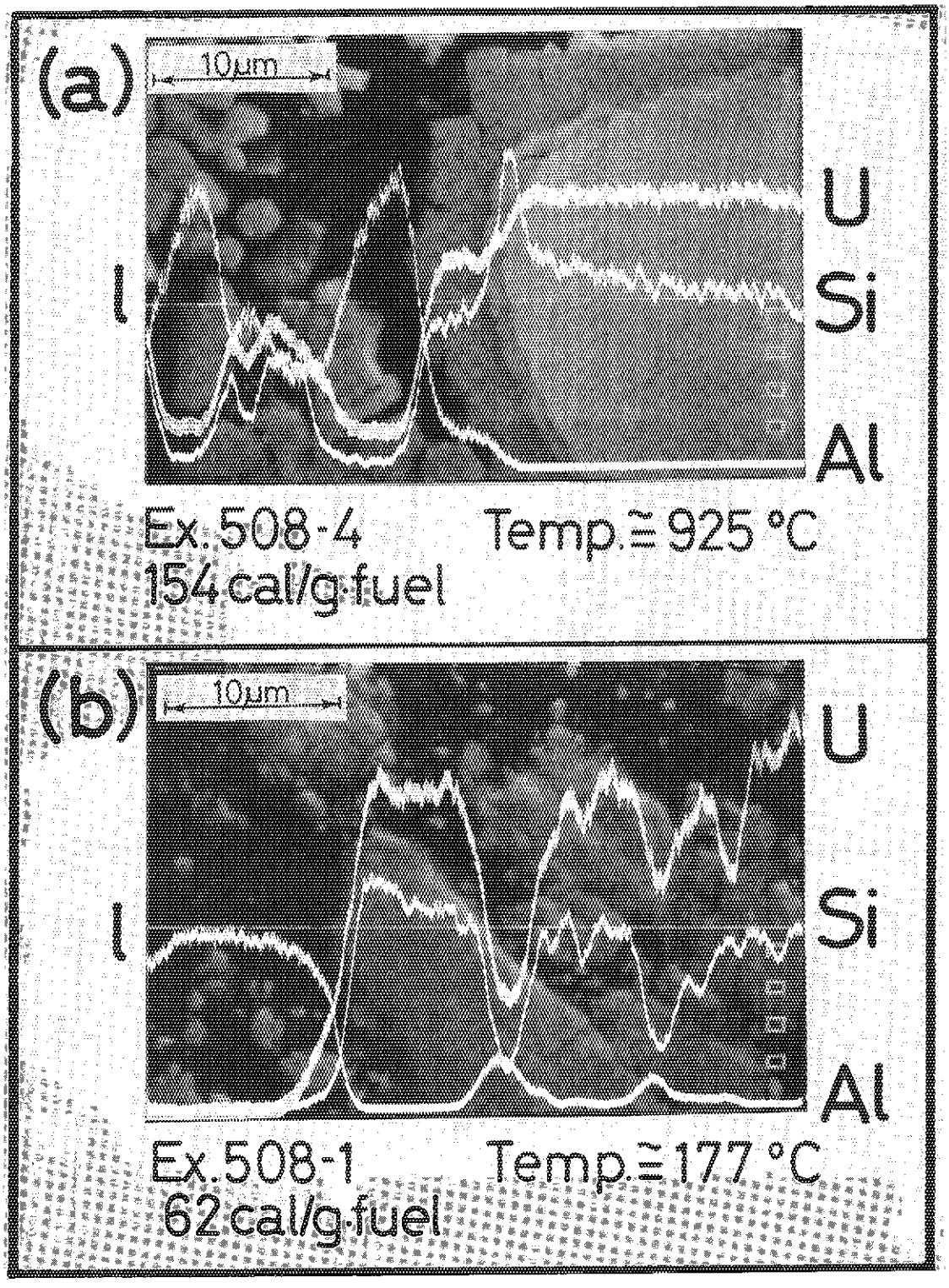

Photo. 1 Results of the SEM/XMA analysis made on (a) the silicide plate-type diffective fuel at 154 cal/g·fuel and (b) the silicide plate-type intact fuel at 62 cal/g·fuel. Elements U, Si, and Al were measured along line ℓ of which background level was set to the bottom of the pictures

3. MTR Fuel Inspection at CERCA

Y. FANJAS

C E R C A
Les Bérauds - B.P. 1114
26104 ROMANS SUR ISERE - FRANCE

ABSTRACT

The stringent specifications for MTR fuel plates and fuel elements require various sophisticated inspection techniques. In particular, the development of low enriched silicide fuels made it necessary to adapt these techniques to high density plates. This paper presents the status of inspection technology at CERCA.

INTRODUCTION

Our presentations at the various meetings about MTR fuel have been mainly focused on the development work carried out in the field of fuel fabrication. In parallel to this work, an intensive program for improvement of inspection methods was also conducted over the past years. This program aimed at four goals :

- adapt the methods to LEU, high density fuel plates by designing new equipments.
- improve the quality of inspection by modernization of tools and machines.
- increase the efficiency and reliability of inspection by computerization of equipments.
- bring inspection closer to fabrication by "on line" inspection whenever possible.

The purpose of this paper is to present the to-day status of inspection techniques at CERCA. We shall successively examine how the four above mentioned goals have been reached.

1- ADAPTATION OF INSPECTION METHODS TO LEU FUELS :

High density, low enriched fuel plates contain five times as much uranium as the high enriched ones.

Slide 1 shows the main fields where inspection techniques had to get adapted to this increase in uranium loading.

1.1 Computerized weighing system

The five fold increase in the uranium density made the classical gamma counting method for U-235 content determination in fuel cores inappropriate any more mainly due to the higher self shielding effect in the high density cores.

A fully computerized weighing system was developed (1). The computer network controls the weighing operations and records the weights of the powders fractions which are mixed before compaction of fuel cores. The dimensions and weights of pressed cores are also recorded and checked. This allows the calculation of the total U and U_{235} contents for each core. This prevents from any weighing mistake : data cannot be put into the computer if the weights do not meet the customer's requirements.

This system has been operating since 1988. It was recently connected to the main plant computer so that the data it generates are automatically taken into account by uranium accountancy.

1.2 Specially designed UT machine

Increasing the core density also resulted in the appearance of false defects called the "core edge effect" (1) during ultrasonic inspection. UT machines are used to screen each fuel plate to reveal and to point out any decohesion between the cladding and the core of the fuel plate.

The difference of densities between the core and the aluminium edge of the plate led the previous UT machine to image the core edge as a decohesion defect. CERCA designed a unique UT testing equipment which takes into account this phenomenon.

Only real defects, if any, are detected, located and measured. This equipement has been routinely used for silicide fuels since 1988.

1.3 Fuel plates enrichment checking equipment

Finally, when developing the manufacture of low enriched fuel in the same facility as for high enriched fuel, CERCA took into account the risk of mistakenly mixing fuel cores of different enrichments despite a full identification and

traceability program was applied. In order to make sure that no mistake had occured at any step of the fabrication process, it was decided to carry out an enrichment inspection on the finished fuel plates.

An equipment based upon gamma ray spectrometry was designed and operated since 1984 (1). No customer's specifications ask for this inspection. It is carried out as part of our internal checks.

2- IMPROVEMENT OF THE QUALITY OF INSPECTION.

In addition to designing new equipments adapted to LEU fuels, CERCA improved the quality of its inspection by standardization and modernization of its equipments.

A few examples of modernization can be mentioned :

2.1 Surface defects inspection

. In order to detect tiny defects on the surface of fuel plates, operators must work in good lighting conditions. Therefore, illumination of the inspection room was carefully studied in terms of light spectrum and quantity of light to be used. An artificial daylight spectrum was selected which presents two advantages : a good visual comfort for operators which minimizes eyestrain and constant lighting conditions independent from the variations due to the weather or the time of the day encountered with natural daylight.
Other important details such as the choice of colours were also of importance and treated accordingly.

. The measurement of surface defects depth used to be carried out by light section microscope. New microscopes equiped with TV camera and using a different measurement principle were installed which allow to have a much easier and more accurate depth measurement.

2.2 Micrographic inspection

. The optical microscopes have been equiped with video systems delivering instant, high accuracy pictures and tapes.

. The cladding thickness measuring device was equiped with TV camera and semi automatic measuring system.

3- ON LINE INSPECTION.

It is generally desirable that inspection take place simultaneously or immediately after the fabrication operation. By such "on line" inspection, the operator is kept informed of the result of his work and can bring the necessary corrections in case of need.

Whenever possible, we are applying this principle to our production line. One good example of such an application is the computer assisted weighing system previously described.

Another application is the on line dimensional inspection of flat fuel plates as well as curvature inspection of bent fuel plates.

The corresponding equipments have been specifically designed and manufactured by CERCA. Our permanent development effort is materialized by the fact that the present devices already correspond to the second generation which present significant improvements with respect to the first previously developed generation.

4- COMPUTERIZATION OF EQUIPEMENTS.

Computerization of CERCA inspection equipements is part of the general computerization system which involves in particular workshop management, fabrication, quality and uranium accountancy. Slides 2 and 3 show the schematic organization of CERCA computer system. As far as inspection equipments are concerned, their computerization allows to improve the efficiency and reliability of inspection. It also makes the equipments more flexible and easy to adjust from one type of product to another (in our facility more than 100 different types of plates and 70 different types of fuel elements are manufactured, most of them simultaneously. Therefore quick adjustment of equipments is an important factor). Finally, computerization also allows automatic printing of results which improves presentation and reliability of documents.

As of today, the following inspection equipments are computerized :

- weighing network and gamma counting device
- UT machine
- homogeneity scanning machines
- dimensional inspection equipments (for flat and curved plates)
- surface contamination inspection equipment
- cladding thickness measurement equipments
- isotopic analysis
- impurity analysis in fuel powder
- surface image analysis

- water channel inspection machines
- fuel element dimension inspection devices

5- FURTHER DEVELOPEMENT

Brand new equipments have been installed in the past months (second generation of plate curvature inspection equipment, second water channel inspection machine, surface contamination inspection equipment). To-day, all the inspection equipements of the facility have been either replaced or significantly up-dated.

As far as the availability of these equipments is concerned, we have applied the same philosophy as for fabrication equipments: for each type of inspection, we have installed at least two devices, so that, in case one of them is out of order, another one is able to continue the work.

We consider this is a very important factor to guarantee a safe supply of fuel to our customers. It also allows to work on different products simultaneously.

CERCA continues its development effort to further improve the quality of its products and its service to customers. New inspection techniques are under development and will be reported next year. However, we can mention that, among others, we are developing a new technique for determination of the relative amounts of various phases in aluminide and silicide materials.

CONCLUSION

Since it started MTR fuel production in 1960, CERCA has permanently improved its fabrication and inspection technology. The research effort was intensified when the program for development of reduced enrichment fuel started in 1978. It lead to the successful development of LEU silicide fuels which are now routinely produced on industrial level in our facility.

The sharp increase in our market shares and correspondingly our production output over the past three years has allowed us to significantly increase our investments in production and inspection equipments.

New sophisticated techniques have been introduced. Further development is going on in the frame of our very active research program for offering better and better products to our customers and keeping our advance in this field.

References :

(1) "ADAPTATION OF INSPECTION METHODS TO LOW ENRICHED URANIUM FUEL" J.F. POUPARD - CERCA - Proceedings of the RERTR Meeting in SAN DIEGO;CA - 1988

CERCA

INSPECTION METHODS FOR MTR FUEL

METHODS USED FOR HEU	ADAPTATION TO LEU
URANIUM ANALYSIS	UNCHANGED
UAlx ANALYSIS	ADAPTATION TO SILICIDES
GRAIN SIZE MEASUREMENT	UNCHANGED
U235 CONTENT OF FUEL CORES BY GAMMA COUNTING	**U235 CONTENT OF FUEL CORES BY WEIGHING METHOD**
DIMENSIONAL INSPECTION OF FUEL CORES	UNCHANGED
No inspection performed when only one enrichment	**ENRICHMENT CONTROL OF FUEL PLATES**
ULTRASONIC INSPECTION OF FUEL PLATES	**NEW EQUIPMENT FOR CORE EDGE EFFECT**
X-RAY INSPECTION OF FUEL PLATES	UNCHANGED
VISUAL INSPECTION OF FUEL PLATES	UNCHANGED
CLADDING THICKNESS INSPECTION	UNCHANGED
DIMENSIONAL INSPECTION OF FUEL PLATES	UNCHANGED
SURFACE CONTAMINATION OF FUEL PLATES	UNCHANGED
FUEL ELEMENTS INSPECTION	UNCHANGED

CERCA

COMPUTER ASSISTED PRODUCTION MANAGEMENT

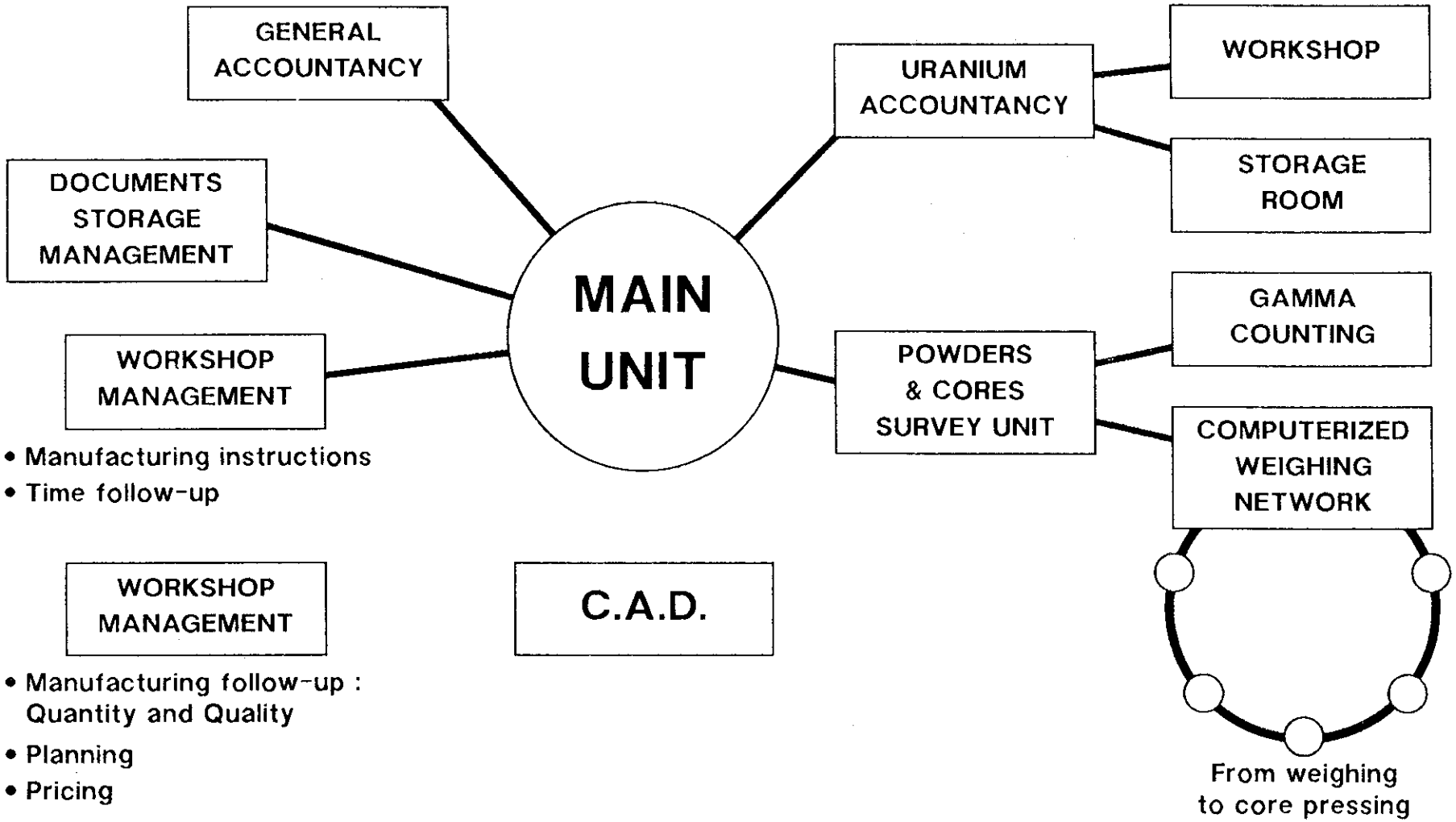

JAERI—M 92—028

CERCA

COMPUTER ASSISTED COMPLIANCE TREATMENT

COMPUTERIZED
CONTROL EQUIPMENTS

- UT
- U HOMOGENEITY
- FLAT PLATE DIMENSIONS
- CURVED PLATE DIMENSIONS
- FUEL ELEMENT DIMENSIONS
- WATER CHANNELS
- CLADDING THICKNESS
- ⋮
- ISOTOPIC ANALYSIS

QC REPORT
COMPLIANCE TREATMENT

EQUIPMENTS
CALIBRATION
FOLLOW-UP

4. Development of Shipping Cask for JMTR Fresh Fuels

M. MIYAZAWA, K. TUBOI, K. AKASHI, M. SATO, T. KOGANEZAWA and K. FUTAMURA
Department of JMTR Project
Oarai Research Establishment, JAERI
Oarai-machi, Higashiibaraki-gun, Ibaraki-ken 311-13, Japan

ABSTRACT

The fresh fuel elements used in the JMTR are now being transported from France. Since the relevant regulations in Japan and the countries through which the casks are to be transported are revised in accordance with the IAEA regulation of the Safe Transport of the Radioactive Material 1985 edition (hereafter referred to as 'the IAEA regulations'), the casks currently in use for the JMTR fuel transportation will be no longer used, because they do not meet the revised regulations. In the revised regulations, it is provided that the integrity of the casks conducted mechanical tests shall be evaluated in consideration of an ambient temperature range from - 40℃ to 38℃.

Considering the circumstances mentioned above, new type cask was developed according to the IAEA regulations. In the process of the development, two full scale casks (hereafter referred to as 'specimen') were fabricated. One specimen was carried out a series of tests consisting of mechanical tests under an environmental condition of room temperature, a fire test and so forth provided in the IAEA regulations. The other one cooled to - 40 ℃ was carreid out the mechanical tests which were a nine-meter-height-drop-test and a one-meter-height-drop-test onto a solid mild steel bar. The integrity of these casks were enough under the test conditions described above.

The detail of the latter tests which are no precedent in Japan as well as in the world is presented.

INTRODUCTION

According to the IAEA regulations, nuclear fuel casks are classified into four types --- Type L, Type A, Type B, and Type IP or fissile package, depending upon the quantity and nature of the radioactive material to be transported in the the cask. The new type cask for JMTR fresh fuel elements, classified as type B, shall be designed an ambient temperature range from -40℃ to 38℃. Then test performance requirements must be met under specified test environments for normal transport and accident conditions as shown in Figure 1.

Performance of the cask must be evaluated by tests or analyses for a test sequence of a free drop of 9 m, a free drop 1 m onto a puncture bar, a fire test with flame temperature of 800 ℃ for a period of 30 minutes, and water immersion test under a head of water for a period of 8 hours.

The safety analyses of the new type cask were mainly analysed using computer codes. Drop tests at room temperature and a fire test were carried out on the specimen to verifiy the validity of the safety analyses. Drop tests were carried out on the specimen cooled to -40 ℃ to demonstrate the ability to maintain its structural integrity at this low temperature. The 9 m free drop test of the specimen kept at - 40 ℃ is described in the following section.

GENERAL DESCRIPTION OF CASK

The newly developed cask is shown in Figure 2. The cask has dimensions of 840mm OD and 1800mm length, being composed of a stainless steel inner shell(10 mm thickness), and an outer shell (3 mm thickness). It weighs about 860kg. Balsa and hard polyurethane foam are filled between the inner and outer shell for a shock absorber and a thermal insulator. A inner lid made of stainless steel has double silicone rubber O-rings for sealing on the parts to be coupled with the inner shell onto which the lid is bolted. Containment system consists of the inner shell, the inner lid and a silicone rubber O-ring. Two kinds of baskets made of stainless steel are designed to contain 10 fresh fuel elements of JMTR or fuel elements for other research reactors in JAERI.

MECHANICAL TESTS AT LOW TEMPERATURE

SPECIMEN

The specimen is a full scale cask having the same material as an actual cask. The specimen was instrumented with 2 accelerometers and 15 strain gauges to measure decelerations and strains, and 9 thermocouples to measure temperatures at selected positions during the tests. The specimen was loaded with dummy fuel elements during the tests.

TEST EQUIPMENT

The test equipment consists of a drop test target, a separating system, a gantry crane and a cooling system as shown in Figure 3. The drop test target which met the IAEA criteria for an unyield surface is 50 mm steel plate on top of the 100 ton concrete foundation. The cooling system consists of a liquid nitrogen feeder unit, an insulated box with pipings, and nozzles. The specimen is cooled by intermittent spraying of liquid nitrogen in the insulated box.

TEST CONDITIONS AND PROCEDURE

Temperature condition

As there is no large indoor space capable of making an indoor environment to required low temperature and dropping the specimen from a height of 9 m, it was decided to cool the specimen to below -40 ℃ and to carry out the drop test in the open air. When the specimen was kept the temperature between -45 ℃ and -40℃, the drop test was started. This temperature range was selected to compensate for the rise in the temperature of the specimen during the period required for its transportation to the drop test target, implementing leaktightness checks immediately before and after the drop test, hoisting it to a height of 9 m, and adjusting the orientation of its fall. If the specimen was to be cooled to significantly below -45 ℃, the silicone rubber used sealing would lose its retraction and leaktightness. This account for the selection of -45 ℃ as the lowest temperature at which the drop test may be started.

As shown in Figure 4, this temperature range can be obtained by intermittently spraying liquid nitrogen onto the specimen for 8 to 10 hours and taking it out from the cooling system when the outer shell had reached the temperature of -80℃ and the inner shell -45℃. This cooling operation was repeated several times because the results depended on the outside air temperature, sunlight conditions, and the velocity of the wind.

Drop orientation

For free drop tests, either the vertical, the horizontal or the corner drop condition has been considered to cause the maximum damage. The vertical drop was chosen, because the preliminary analyses showed that the most severe shock occurs in this orientation from the viewpoint of acceleration.

Test procedure

The free drop tests were conducted at a test field of Mitsubishi Heavy Industries Ltd., as shown in Figure 5.

TEST RESULTS

Photograph 1 and 2 show the moments at which the drop has just started and at which the specimen has crashed onto the drop test target. The leakage tests carried out immediately before and after drop tests at a temperature below -40℃ so that leaktightness at low temperature was maintained throughout the test and after it. According to the visual inspection after the drop tests, no cracks were observed in the outer surface of the specimen, nor was any deformation found except at the lid side which was made to undergo direct shock. Neither the inner inspection nor the dismantling inspection which was conducted on the cut specimen revealed any deformation to be affected the integrity of the cask. Figure 6 shows the measurement of the acceleration, deformation and leakage rate of the specimen. Analyses are totally conservative comparing with test results.

CONCLUSION

A specimen temperature for drop test must be set at a temperature below - 40 ℃. It was very difficult to keep such a very low temperature during drop test owing to mild climate in Japan.

However, we could obtain satisfactory results on the newly developed cask at the drop tests. The structure of cask, such as containment system, welded portions and so on, showed enough integrity under the above-mentioned drop tests .

In addition, the cask was also proved enough strength under other test conditions, i.e. drop tests at room temperature and a fire test.

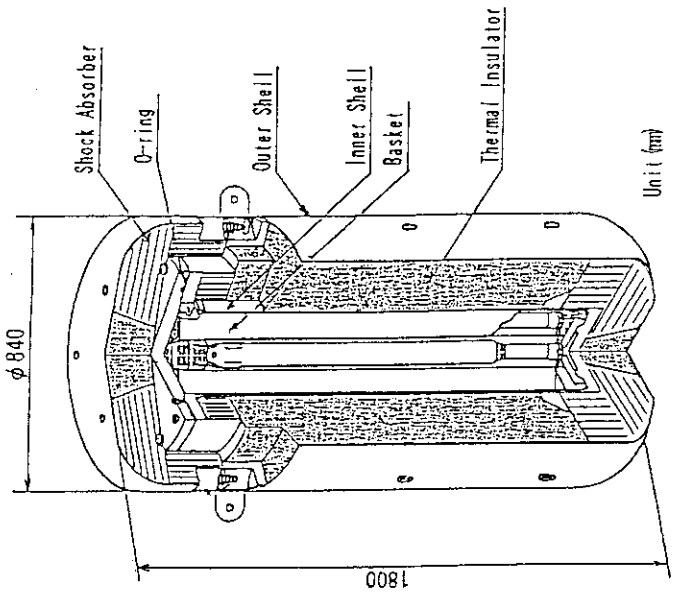

Figure 2. General View of the Newly Developed Cask for JMTR Fresh Fuel Elements

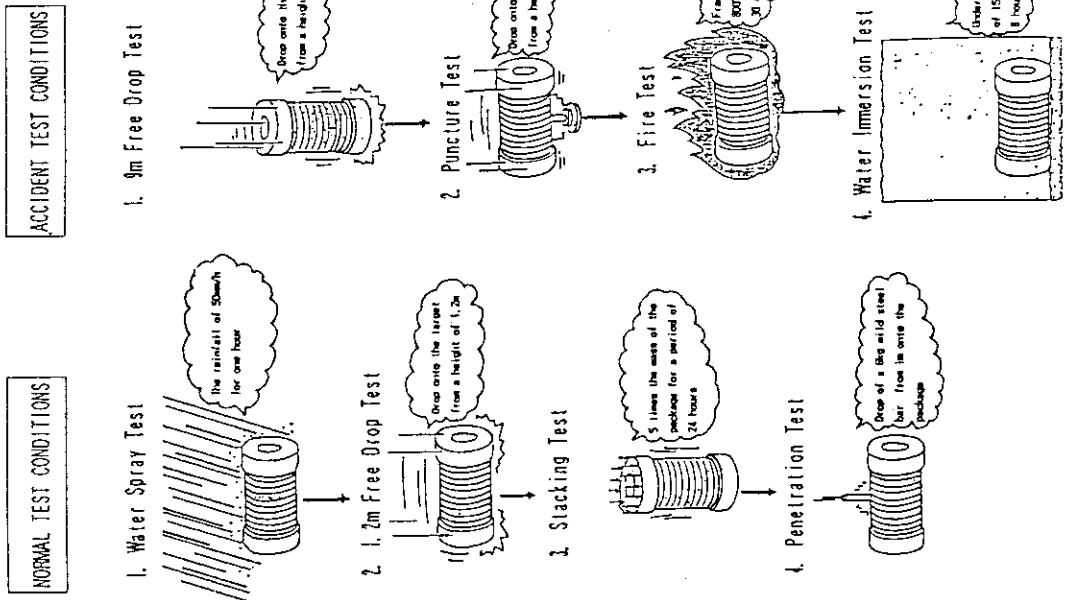

Figure 1. Test Conditions for Type B Nuclear Fuel Cask

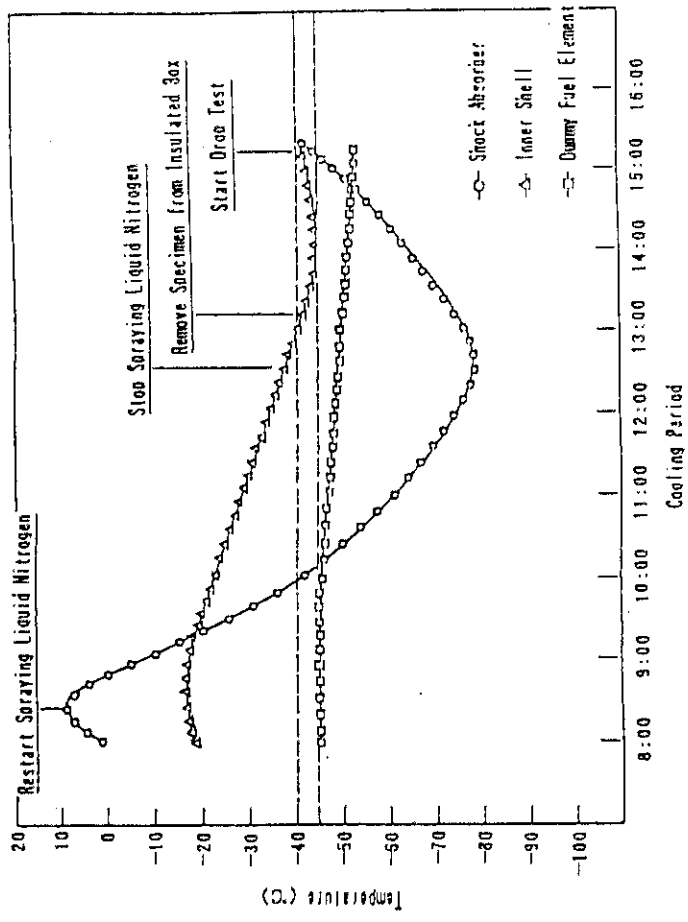

Figure 1. Temperature Profile of Specimen Being Cooled

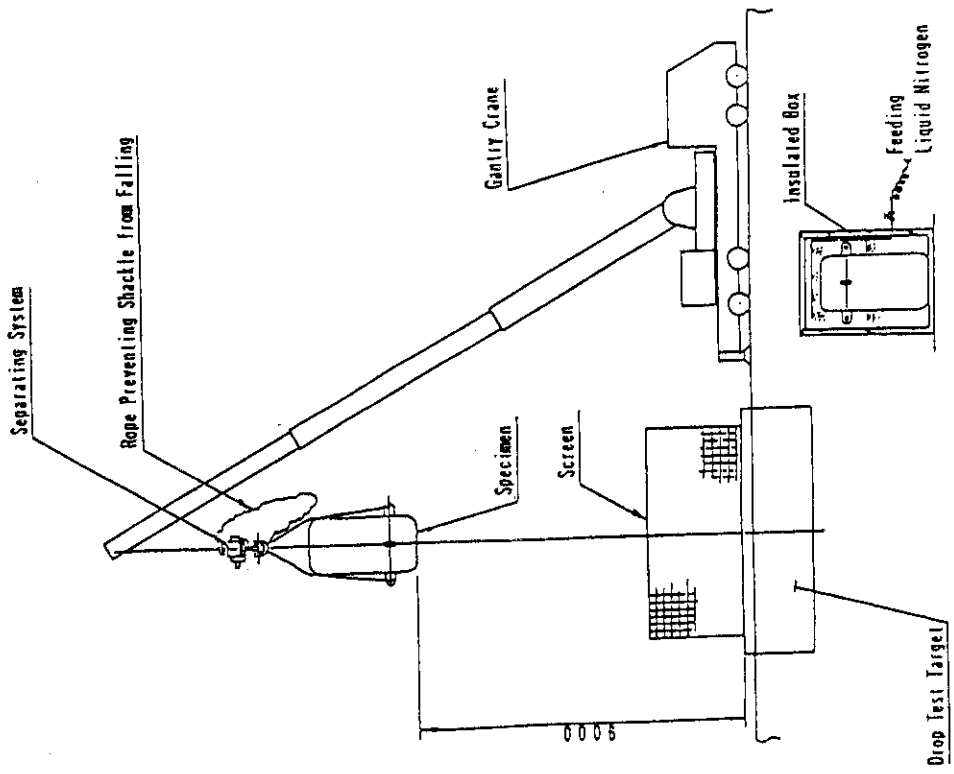

Figure 2. Drop Test Equipment

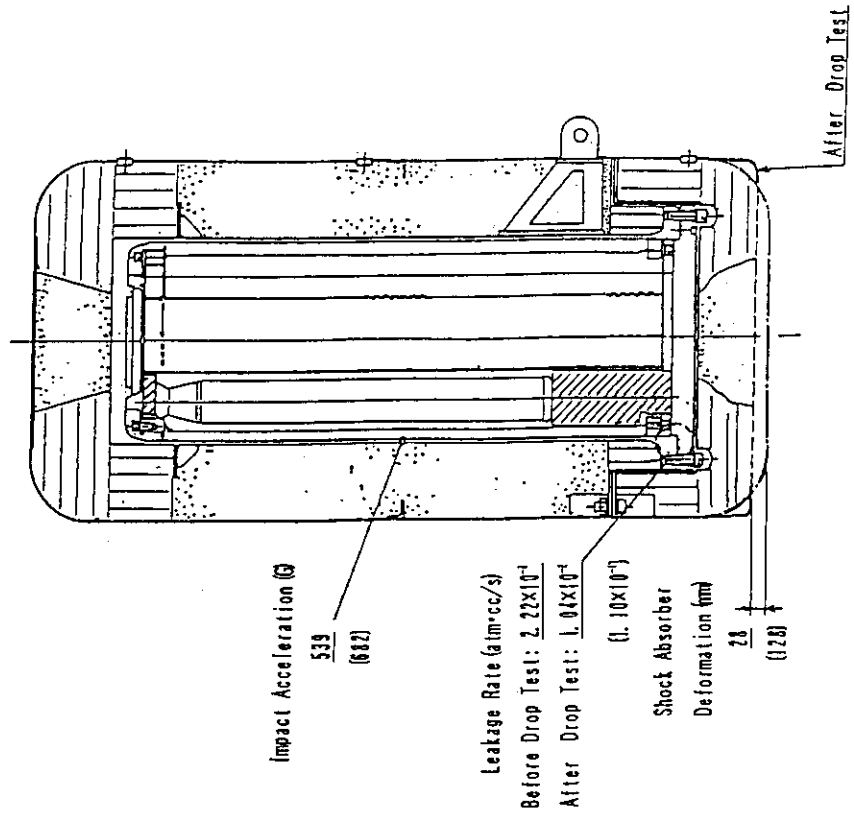

Figure 6. Comparison of Test Results with Calculations

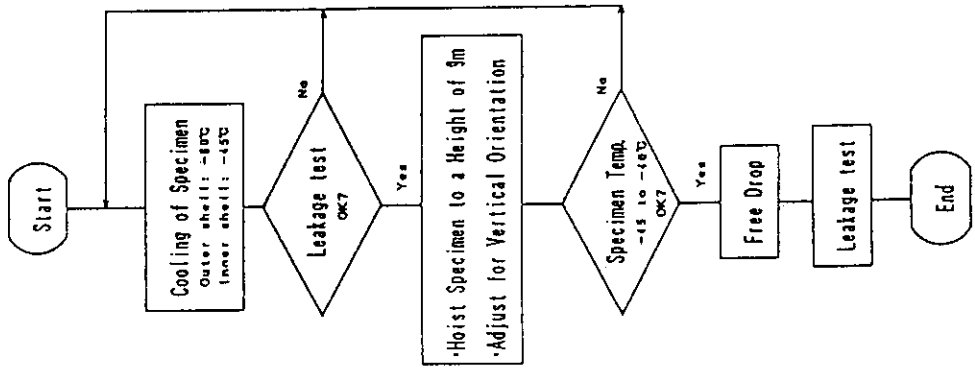

Figure 5. Test Procedure

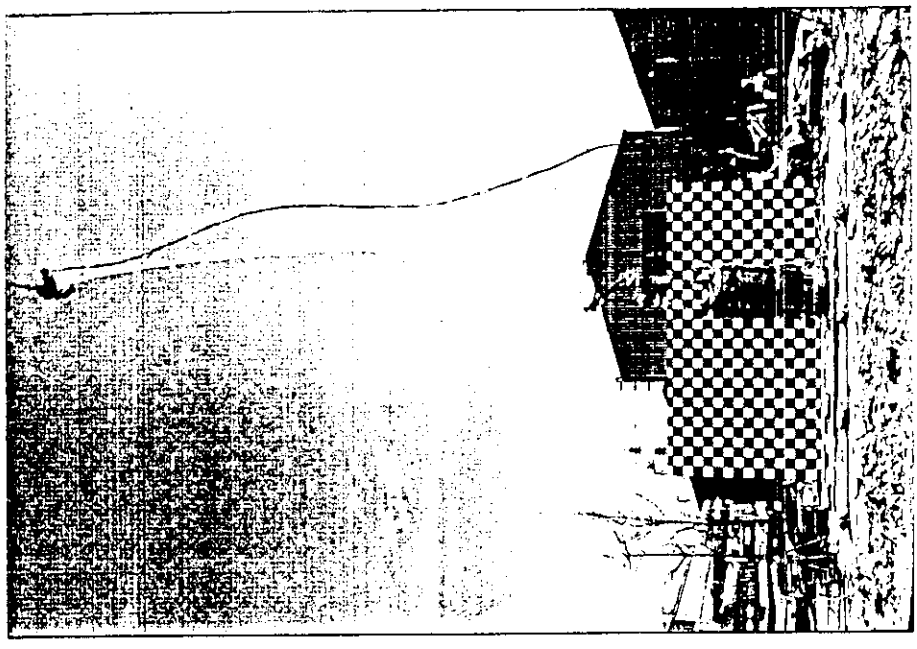

Photograph 2. Moments at which Specimen Crashed onto Drop Test Target

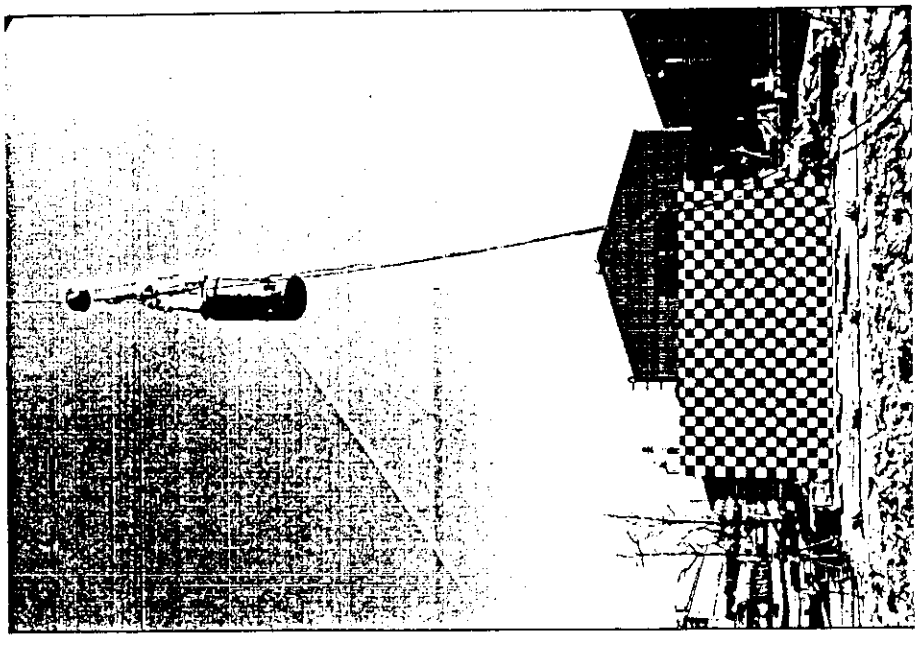

Photograph 1. Moments at which Specimen dropped from a height of 9 m

1. The Development of ZPRL Digital Control System

Jin-Den Hsu, Sheau-Yieh Yang, Der-Jhy Shieh

ABSTRACT

Zero Power Reactor at Lung-Tan (ZPRL) is a small open-pool type research reactor located at Lung-Tan, Taiwan. The reactor achieved its first criticality in 1971. An analog control system has been used for almost over 20 years and the power regulating function is found gradually out of order. Therefore, we decided to develop a digital control system to replace the existing analog one. A prototype system has been developed and under on-line test now.

The proposed ZPRL digital control system consists of three personal computers. These computers are used as (1) operator console, (2)data acquisition and control system, and(3)auxiliary and backup system. The operator console contains all the man-machine interface functions in the form of graphic display. The data acquisition and control system converts the analog signals into digital ones and feeds to the other two computers. The auxiliary and backup system normally emulates a strip chart recorder for the linear and logrithmic neutron powers and also acts as a transient recorder to keep the trace of the operating conditions on demand or when the reactor scrams.

On-line test shows that the system does assure a satisfactory performance. It is not only as good as the analog system but also has the advantages of flexibility, testibility, and a user friendly man-machine interface.

1. INTRODUCTION

Power maneuver at ZPRL is achieved manually with shim rods and a regulating rod. The rods are at first adjusted manually. After the reactor attains its target power, an automatic power regulating system is used to maintain the reactor in steady operation. This analog control mechanism has been used for almost over 20 years and the power regulating function is out of order now Therefore, we decide to develop a digital control system to replace the existing analog one.

In order to design a digital controller of ZPRL, the hardware -in-the-loop simulation [1] and regulating rod dynamic test [2] are conducted to establish the configuration of digital control system. It consists of operator console, data acquisition and control system, auxiliary and backup system, and simulator. The following sections present the ZPRL digital control system, the control algorithm, and on-line test result.

2. SYSTEM DESCRIPTION

The function diagram of the control system [3] is shown in Fig.1 .

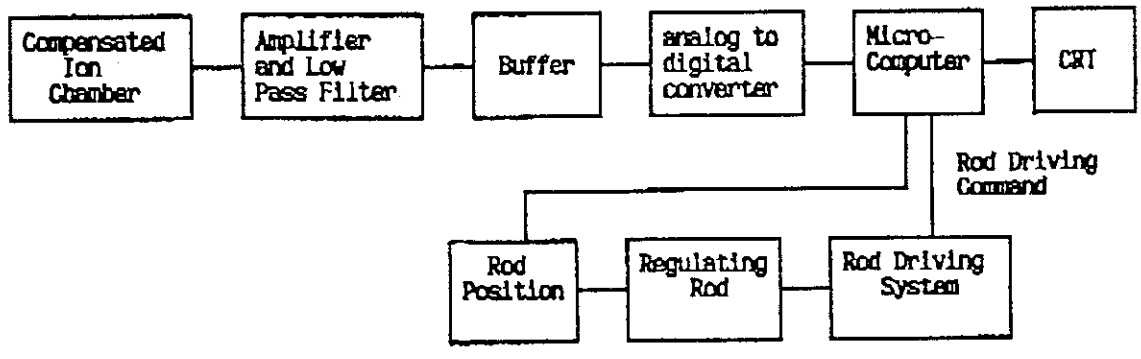

Figure 1. Block diagram of control system

This digital control system consists of three PC-based micro-computers, which are used as (1) operator console,(2) data acquisition and control system, and (3) auxiliary and backup system as shown in Fig.2 .

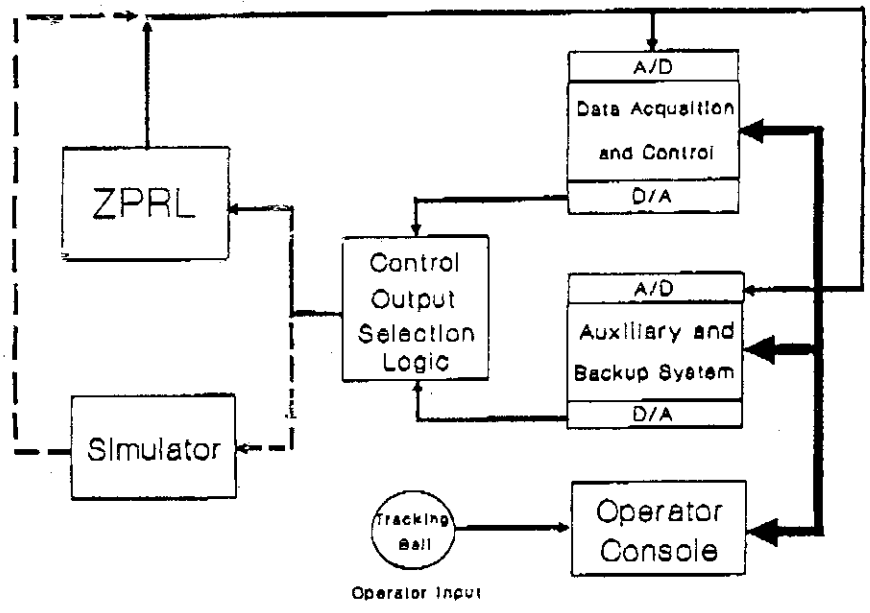

Figure 2. ZPRL Digital Control System

The operator console contains all the man-machine interface functions in the form of graphic display.The data acquisition and control system converts the analog signals which are extracted from a compensated ion chamber into digits and then feeds to the other two computers through IEEE-488. Meanwhile an array of control parameters is calculated and sent to the control rod drivers through D/A converters. By incorporating certain rules of inference, the system is able to adapt to the operating conditions, so that the digital controller can raise the power of the reactor from subcriticality to full power automatically.

The auxiliary and backup system normally emulates a strip chart recorder for the linear and logrithmic neutron powers and also acts as a transient recorder to keep the trace of the operating conditions on demand or when the reactor scrams. In

addition, it works as a backup computer for the operator console. If ever the operator console computer comes out of order, this auxiliary and backup system will suspend its normal function and works as a console instead.

3. CONTROL STRATEGY

Several control algorithms have been studied such as the conventional PID type control, the LQG optimal control and the fussy control. The result shows that the conventional PID type control is still the simplest and the most practical control algorithm in this application. With the flexibility of digital controller, the PID algorithm could have additional adaptive ability to cope with the reactor status. The control algorithm is shown in Fig.3 . Basically, it is a two-loop control system.

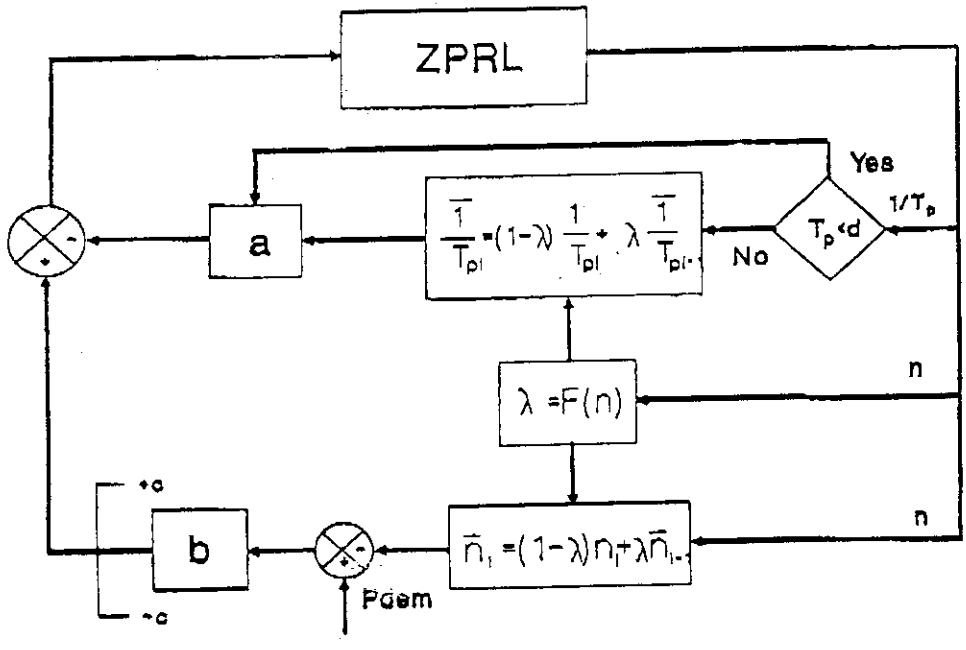

Figure 3. ZPRL Control Alogrithm

The inner loop uses the inverse of period as the variable of measure. Because the inverse of period is equivalent to the differentiation of the logrithm neutron power, the inner loop essentially is the D part of a PID controller. The outer loop uses the neutron power as the variable of measure. It is the P part of a PID controller. The basic calculations of the controller are quite simple and yet reliable. It contains only two multiplications, two additions and one limitation judgement. Simple low-pass filters, which are adaptive to the neutron power, are used when the neutron power is low and the noise is extraordinarily high. Because the low-pass filters slow down the response of the control system, an immediate-action bypass channel is provided to take care of the case while the period is too short. The stability of the control system has been examined with the control system design tool, MATLAB. In addition,a hardware-in-the-loop test using a PC based simulator has been performed prior to the on-line test.

4. ON-LINE TEST

After having conducted the hardware-in-the-loop simulation and system analysis [4], the digital controller is ready for on-line test. The digital controller raises the power of the reactor from subcriticality to criticality automatically as shown in Fig. 4. Fig.5 compares the automatic and manual control performance of power regulating and power maneuvering. The result of on-line test shows that the system does assure a satisfactory performance. It is not only as good as the analog system but also has the advantages of flexibility, testibility, and a user friendly man-machine interface.

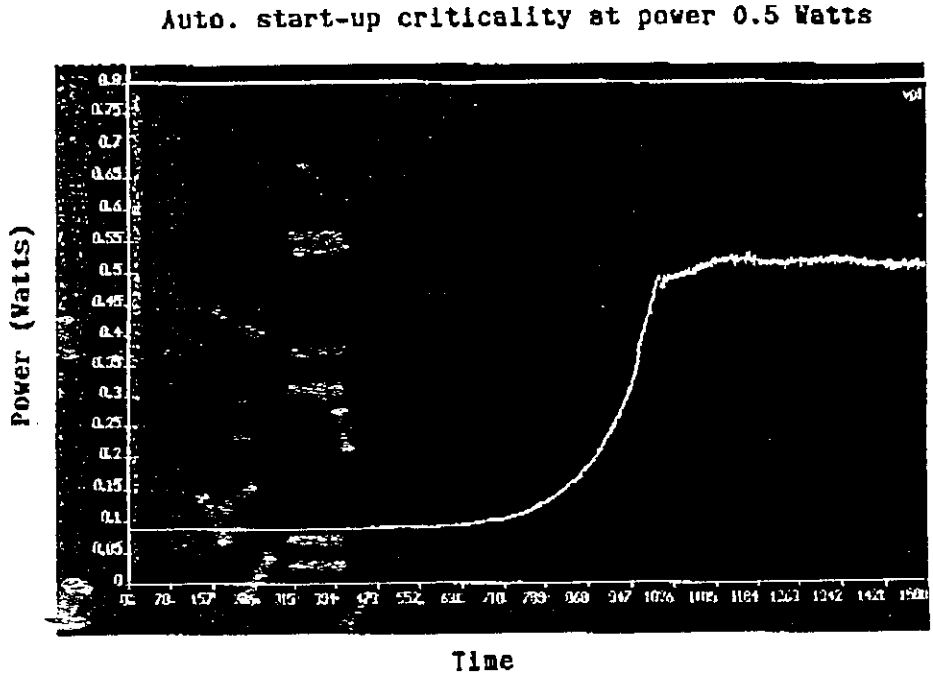

Figure 4. Power curva with ZPRL automatic start-up system

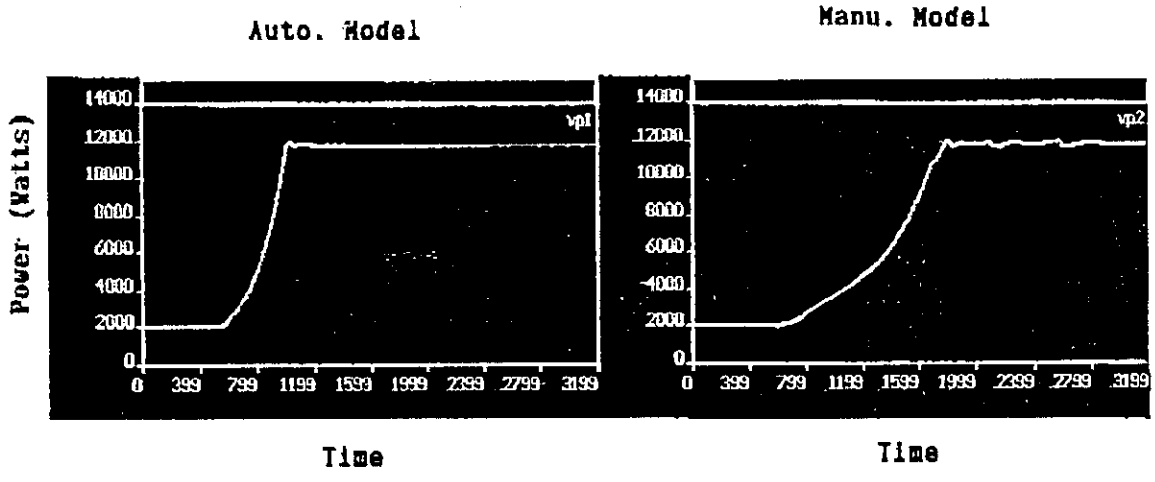

Figure 5. Power curve of AUTO. and MANUAL model control
(Power Demand from 2KW to 12KW)

5. CONCLUSION

Our digital control system has exhibited a satisfactory on-line test performance. However with the flexibility of the digital system , it seems that further improvements are still possible. For instance, the surveillence and monitoring functions could be integrated into the system. The following items are planned to be implemented in the near future.

1. Establishing a software configuration control procedure to assure the reliability and maintainability of the digital system.
2. Replacing the IEEE-488 with computer network for inter-computer data communication.
3. Developing a protection system that can be integrated with the digital control system.

6. REFERENCES

[1] " ZPRL Digital Control System Development and Simulation ", INER-T1358, Institute of Nuclear Energy Research (April 1990).

[2] " ZPRL Regulating Rod Performance Test " , INER-T1370, Institute of Nuclear Energy Research (May 1990).

[3] " Reactor Description and Safety Analysis of ZPRL " INER-NR-0101, Institute of Nuclear Energy Research (June 1970).

[4] " Design of ZPRL Power Regulating Digital Controller ", INER-T1429, Institute of Nuclear Energy Research (September 1990).

2. Control Rod Calibration by Means of Inverse Kinetics Method

Seiji Tamura
Hitachi Engineering & Service Co., Ltd.

Sadayuki Izutsu
Hitachi Ltd.

Hiroki Ichikawa
Japan Atomic Energy Research Institute

Abstract

In order to increase testing efficiency for reactivity measurement, an inverse kinetics method (IKM) was applied during performance test for the up-graded core of JRR-3. The IKM is one of the means to measure reactivity, continuously and real-time. Through the simulation test, conducted before its application, significance of the IKM was proved in accuracy and response time with comparing the positive period method (PPM). The application of the IKM for the control rod calibration is one of the best cases among its utilization. In the beginning of the calibration, one control rod is in the position withdrawn and the other is in the position inserted. After repeating of withdrawal and insertion of respective rod until either rod reaches its end to move, reactivity of each control rod is obtained with less than .1% error.

1. Introduction

Most of the test items during the low power test period are reactivity measurement. For these tests, the basic tool of reactivity measurement is calibration curves of the control rods. Although popular and simple method of reactivity measurement is PPM, it is applicable for only positive reactivity measurement and it takes a time to obtain accurate data. A tiresome procedure in the PPM is that you have to make criticality in each step of measurement. When a real-time and continuous reactivity measurement means is applied to the control rod calibration, critical operation in the reactivity measurement would be put away.

2. Inverse Kinetics Method

The IKM is one of the means of real-time and continuous reactivity measurement, and which is derived from the reactor kinetics. The reactor kinetics is expressed by following equations.

$$\frac{dn(t)}{dt} = \frac{\rho-\beta}{\ell} n(t) + \sum_{i=1}^{6} \lambda_i C_i(t) \tag{2.1}$$

$$\frac{dC_i(t)}{dt} = \frac{\beta_i}{\ell} n(t) - \lambda_i C_i(t) \tag{2.2}$$

Hence, $n(t)$: neutron density
ρ : reactivity
ℓ : neutron lifetime
β_i : fraction of ith group delayed neutron
λ_i : decay constant of ith group precursor
$C_i(t)$: ith group precursor nuclei

The reactivity is derived from equation (2.1) as follows.

$$\rho = \beta + \frac{\ell}{n(t)} \frac{dn(t)}{dt} - \frac{1}{n(t)} \sum_{i=1}^{6} \lambda_i C_i(t) \tag{2.3}$$

The precursor in the second term of equation (2.1) is obtained by integrating equation (2.2) as follows.

$$C_i(t) = C_i(0) e^{-\lambda_i t} + \frac{\beta_i}{\ell} \int_0^t n(\tau) \cdot e^{-\lambda_i (t-\tau)} d\tau \tag{2.4}$$

Supposed that the measurement is proceeded on discrete data of neutron density at sampling interval Δt, the neutron density is denoted n_j at the time j, and n_{j+1} at the time $j+\Delta t$. To integrate the second term of equation (2.4), assumption that the neutron density changes exponentially for the interval of Δt is introduced. Applying the assumption and combining equations (2.3) and (2.4), the equations to measure reactivity are derived and given as equations (2.5), (2.6) and (2.7).

$$\rho_j = \beta + \ell \mu_j - \frac{1}{n_j} \sum_{i=1}^{6} \beta_i (n_0 e^{-\lambda_i t} + \lambda_i A_{i,j}) \tag{2.5}$$

$$\mu_j = \frac{\ln(n_j / n_{j-1})}{\Delta t} \tag{2.6}$$

$$A_{i,j} = A_{i,j-1} e^{-\lambda_i \Delta t} + \frac{1}{\mu_j + \lambda_i} (n_j - n_{j-1}) e^{-\lambda_i \Delta t} \tag{2.7}$$

As initial conditions, the measurement is to be started at the condition that the reactor is critical at n_0, then $\rho_0=0$、$\mu_0=0$ and $A_{i,0}=n_0/\lambda_i$.

3. Simulation test

In order to prove feasibility of IKM in application to control rod calibration, authors conducted simulation test. The neutron response is calculated by solving the reactor kinetics on the simulated control rod movement at around critical condition. For this response data of neutron, the reactivity was calculated by the IKM and PPM. Then the calculated reactivity was compared with the given reactivity that was applied to obtain the response data of neutron density, to measure their accuracy.

Figure (3.1) shows the test result by the PPM and IKM. In this case, the given reactivity is 0.1%dk/k of a ramp function. The calculated reactivity by the IKM is tracing well against the given reactivity. That by the PPM, however, provides the correct reactivity after about 50 seconds elapsed. This result shows that the IKM responds sufficiently well. On this test, the sampling time of 0.2 Sec was taken and reactivity by PPM was calculated by solving the in-hour equation using two adjacent data.

The accuracy test result for the IKM is shown in figure (3.2). To measure sampling time dependency, test was proceeded for 0.1S, 0.2S, 0.5S, and 1.0S of sampling time. The trend curve on the top is the flux response that is simulating a repetition of rod withdrawal and insertion, where + and −0.15%dk/k are provided. For different sampling time, trends of calculated reactivity and its error are shown. The error is obtained simply by taking difference of given reactivity and measured reactivity.

The accuracy tends to be poor on the reactivity transient. This tendency is due to that neutron change may not be expressed by a single exponential function for a transient condition of reactivity. The IKM, however, is based on the assumption explained in the previous chapter. The error on the transient depends on the length of sampling time. Yet, the error at the reactivity transient is within approximately 2% of the given reactivity for 1.0 Sec sampling time, and the error for a stationary reactivity condition is small enough. These characteristics are nothing wrong for the measurement of control rod reactivity, since we need to know how much reactivity is given to the reactor only after control rod movement finished.

As the consequence of the simulation test, the IKM is preferable to the control rod calibration.

4. Method of Control Rod Calibration

To measure total worth of control rod and to obtain calibration curve, it is necessary to measure a step reactivity of about 0.15%dk/k that corresponds to about 30 sec of period, for about 50 steps, in case

of the JRR-3 core.

A schematic procedure of control rod calibration by the IKM is shown in figure 4.1. At the very beginning of calibration, the reactor is of critical state, under a condition where one rod, named A, is placed at the bottom and the other, named B, is withdrawn all the way, where these two control rods are to be calibrated. To establish this state, the third control rod is used for the criticality.

To begin with the measurement, the rod A at the bottom is withdrawn by a certain amount, then during neutron level increasing, its step reactivity is measured. When the neutron level reaches an upper return level, an operator should insert the rod B to provide a necessary amount of reactivity to decrease the neutron level. Then its step reactivity is measured. Further, when the neutron level reaches the lower return level, the operator withdraws the rod A. The same procedure continues until either rod reaches its end to move.

The step reactivity used for the calibration is a mean of data within a certain range, A, as shown in the figure. The range begins after the control rod movement finished, and ends right before either return level. This consideration is to prevent from effect of reactivity transient error and an effect of flux fluctuation during the measurement.

Before the test, the operator should be notified that both two upper and lower return levels, and approximate amount of reactivity to be given to the reactor at each step. During the test, to follow the procedure the operator may monitor current reactivity on a recorder, to which the calculated reactivity on a computer is fed. So, the operator may easily realize when to stop control rod movement. Important notification to the operator is not to move either control rod after rod operation finished until the neutron level reaches its return level, even if given reactivity is different from the amount expected. If moved, the error of step reactivity increases.

Since the control rod calibration by the IKM is not required to have critical condition to measure the step reactivity, reduction of test time and avoidance of error due to critical operation are accomplished. Once the test started, the control rod operation should continue till either control rod reaches its end to move. For the case of JRR-3, it took about 2 and half hours to finish calibration for two control rods. However, should the PPM be used, it provably takes five times more of this.

5. System Configuration and Outputs

The system mainly composed of a personal computer, A-D converter, D-A converter, plotter, and CRT display. The block diagram of the system is shown in figure 5.1. The D-A converter is for reactivity output to the recorder for operators.

During a test, the CRT displays reactivity and neutron level trend. Figure 5.2 shows an example of on-line display graph while in testing of the JRR-3. While the test continues, each step reactivity is stored on a

table in the computer. When the test operation is finished, the control rod positions at each step should be provided to the table for the differential reactivity. The control rod position data should be taken each control rod movement during the test. The control rod positions are not fed into the computer for the sake of resolution of the A-D converter. The required resolution is at least 0.1mm over the stroke range of 800mm.

When the differential reactivity is obtained in the computer, the differential and integrated calibration curves are displayed on the CRT and plotted out. The integrated calibration curves are also expressed by a polynomial function fitted by the least square process. Some example of curves is shown in the figure 5.3.

6. Conclusion

That application of IKM to the control rod calibration provides the test efficiency and avoidance of error is proved through the JRR-3 commissioning tests. This is simply due to that you do not have to make critical condition that is necessary for the case when the PPM used.

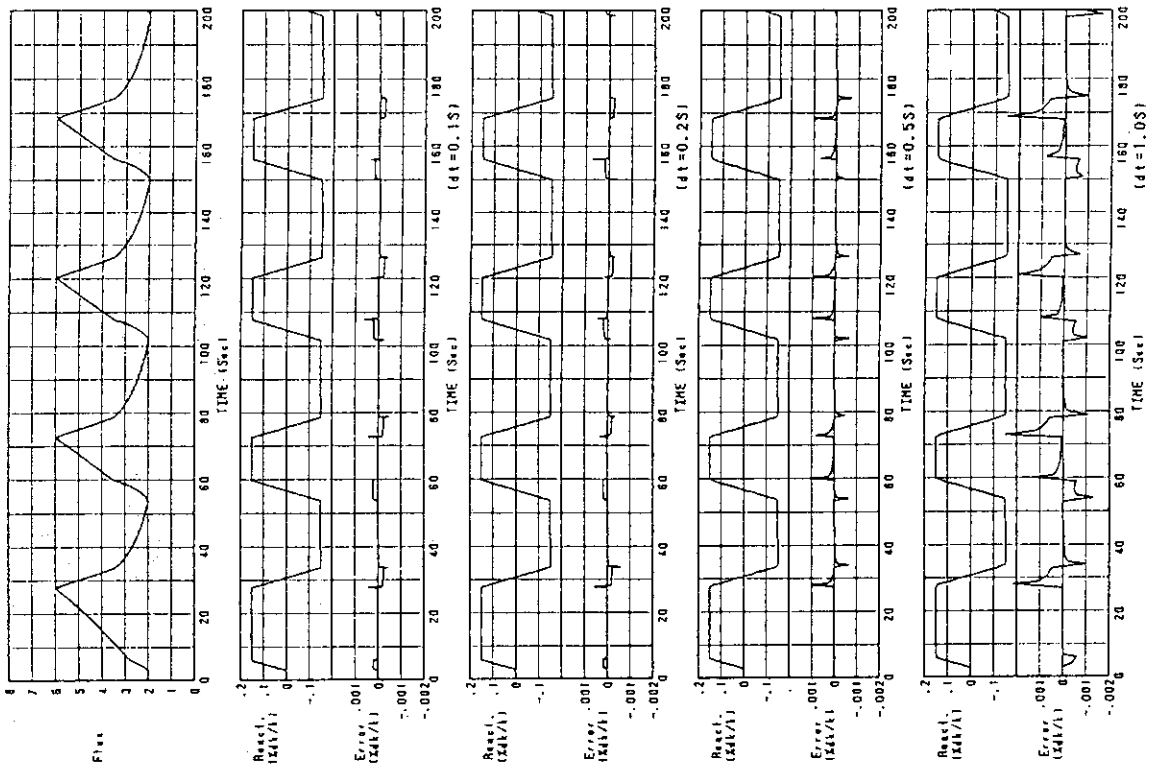

Fig. (3.2) Accuracy test by simulation (dt dependency)

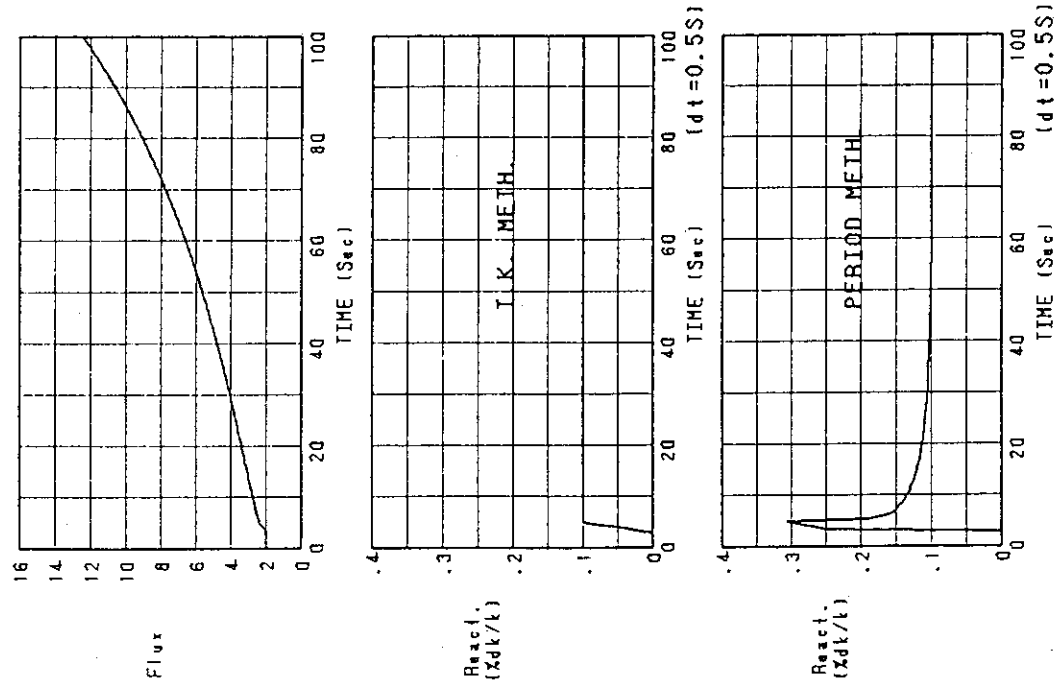

Fig. (3.1) Comparison of measurements by IKM and PPM

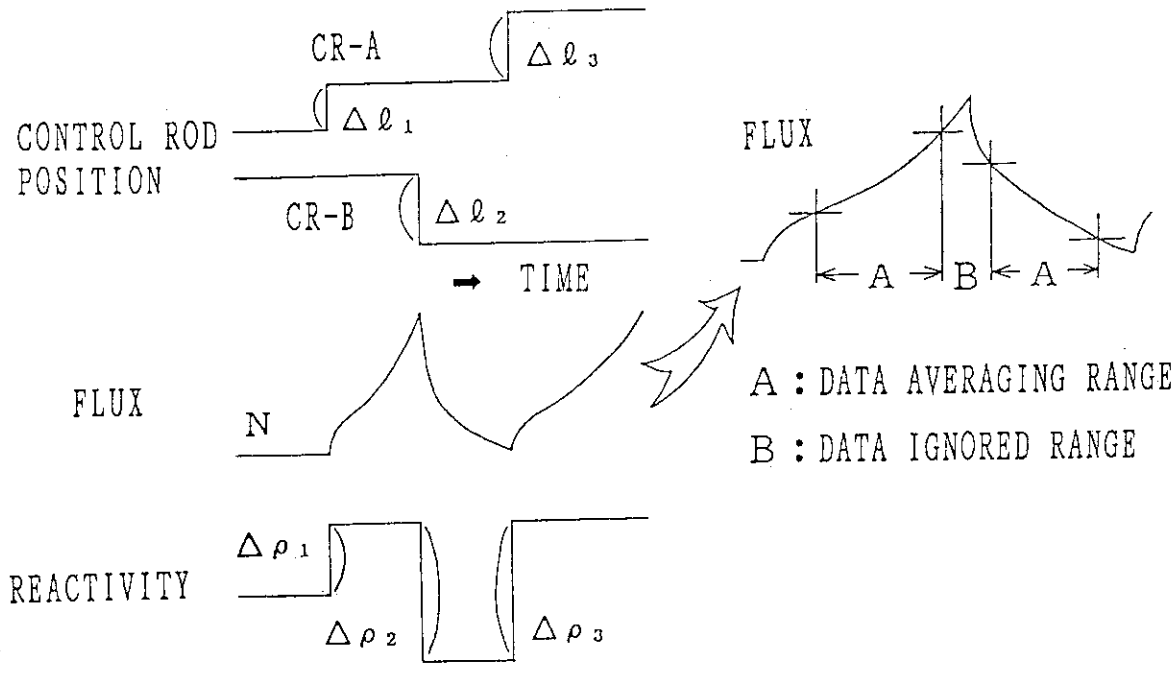

Fig. (4.1) Procedure of control rod calibration

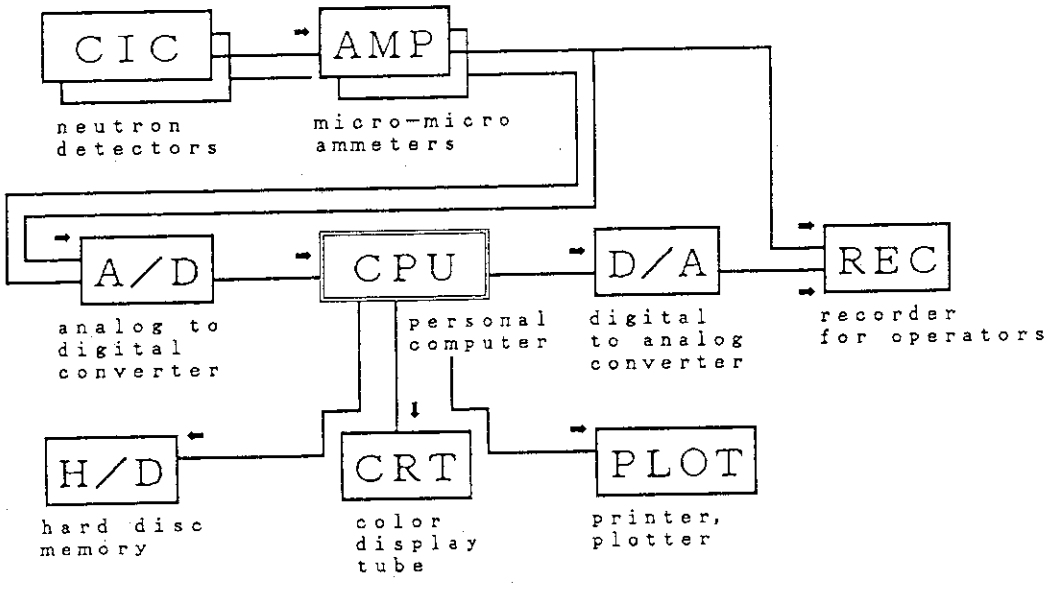

Fig. (5.1) Schimatic diagram of the system

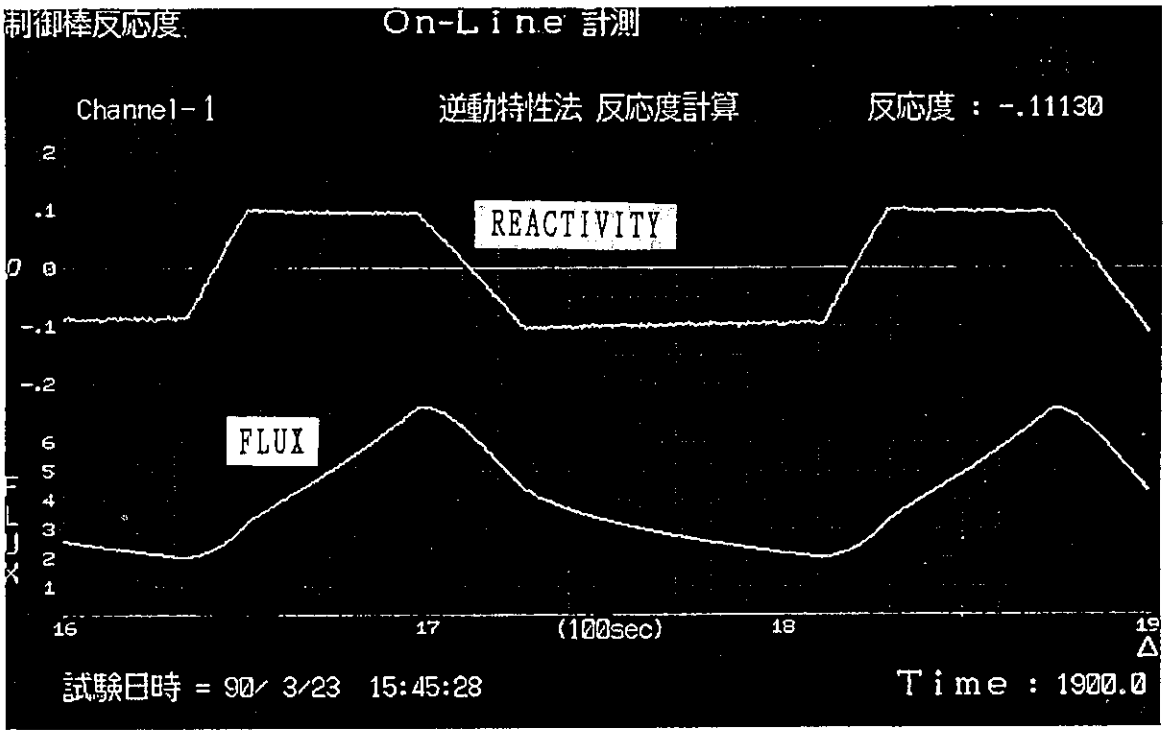

Fig. (5.2) Display graph during test

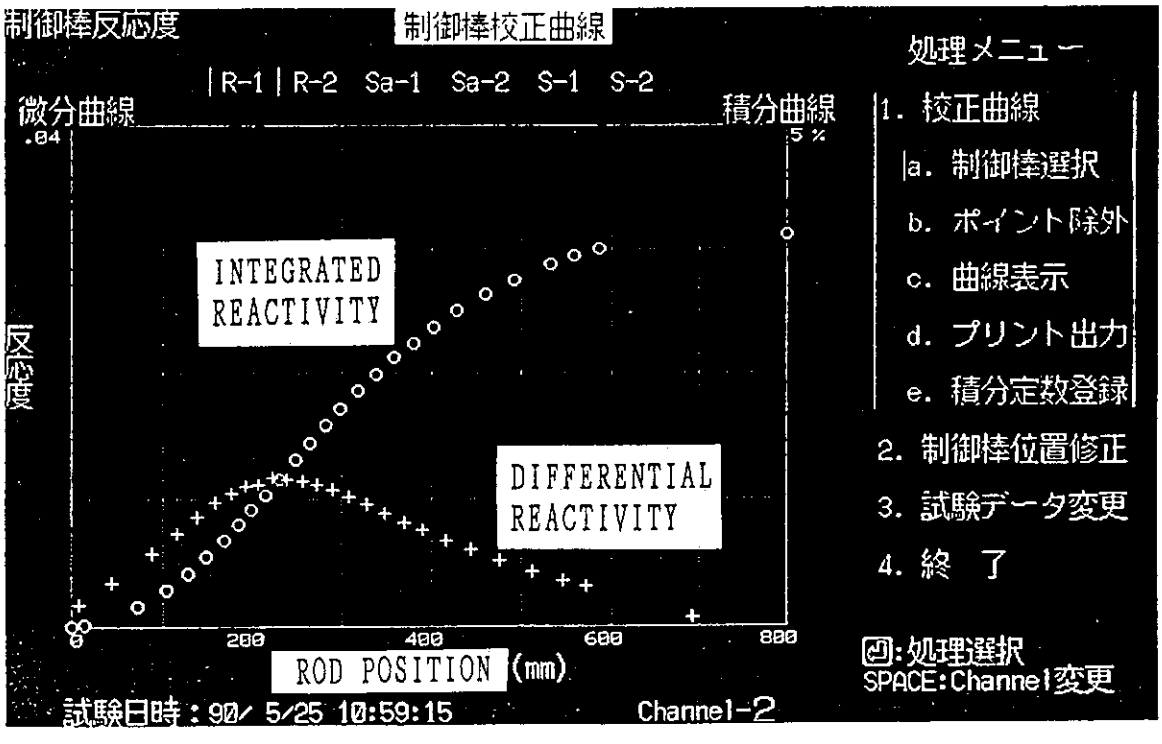

Fig. (5.3) Differential and integrated reactivity (off-line process)

3. Use of PC-Counter for the Research Reactor Parameter Measurement

Byung Jin JUN, Sang Jun PARK, Kwang Pyo HONG, Doo Hwan SUH

Reactor Operations Department, Seoul Office,
Korea Atomic Energy Research Institute,
Cheong Ryang P.O.Box 7, Seoul 130-650, Korea

ABSTRACT

A PC equipped with a counter board which can accept up to nine pulse channels, has been applied to the research reactor parameter measurement. It has been applied as a multi-counter, multi-input multi-channel scaler and pulse input reactivity computer.

The PC multi-counter replaces up to eight conventional counters granting advantages as conveniency in data handling. The multi-scaler which can accept up to four detector signals simultaneously, is to generate neutron pulse sequence data for the random neutron process analysis. It can scale as fast as 80 μ seconds for four detectors. The reactivity computer can accept up to nine channels, calculates and displays data once every second, and saves data for the revival of experiment. As the dead time effect is corrected by software, accurate reactivity can be obtained at very high count rate.

INTRODUCTION

The recent rapid development of personal computer (PC), has been encouraging research reactor operation staffs to utilize it for their reactor analysis and experiments. International Atomic Energy Agency also recognized that the PC can be a good tool for the research reactor and a Coordinated Research Project on the use of PC to enhance research reactor operation and management, is under progress among Asian countries. This report summarizes an intrim progress made in Korean TRIGA reactors on the use of PC for the research reactor parameter measurement accomplished as a part of above mentioned research project.

So far, the effort has been concentrated on the use of PC counter because its application is not so popular compared to the use of analog to digital converter (ADC) but it shares one of the very important parts in the reactor experiments especially for a new reactor commissioning.

As an ADC interfaces between analog instruments and the computer, a counter/timer makes the computer to count pulses. There have been many kinds of conventional instruments dealing with pulse signals but they are gradually changing to the computerized system, especially in the spectroscopy field. For the case of research reactor experiments, however, it is not so active so far, since its demand is very limited and most of reactor

operators are not specialists in the computer. From this point of view, it is considered that establishing a reactor parameter measuring system based on the PC-counter is worthwhile.

This report demonstrates that the PC-counter can be successfully utilized as a multi-counter, multi-scaler and reactivity computer. A less expensive counter board can replace several conventional counters for the startup operation or criticality approach, can replace one or more multi-channel scaler (MCS) or other sophisticated instruments for the random neutron process analysis in the thermal reactor, and can also be utilized for the real time reactivity measurement at very low power level where current detectors cannot generate dependable signal. As its data treatment is computerized, bulky data are easily manipulated granting much more precise experimental results.

MULTI-COUNTER

The PC multi-counter is to replace up to eight conventional counter modules. Therefore, when eight detector signals are fed to this system it is just like the case as if eight conventional counters are working. In addition, it has several advantages compared to counter modules - there is no dwell time between each counting step, several past records are displayed on the CRT screen as well as the flying current data, the dead time effect is corrected by the software, and requested data are saved for the further analysis. Thus, it is a convenient and cost-effective tool for the criticality approach of any reactor and can be utilized for other counting works as well.

Fig. 1 shows a sample CRT screen while multi-counter is working. Current counting line is updated at every 1/50 second, and it is not interrupted by key input requests such as counting time change, *i.e.*, counters are flying while the user is typing in. There are four functions of counting time set, reset, data save and end of work. Counting time can be set by 1/50 second precision. Data can be saved continuously or selectively. including each counted time interval and time from the start of the experiment. Data saved or to be saved, are displayed by the reverse mode for its easy identification. The data screen scrolls upward when it reaches the bottom.

The basic working concept of PC multi-counter is shown in Fig. 2. The timer interrupt reguest is generated at every 1/50 second. Its interrupt source which can be used for this function, is a timer of the PC system itself, one on the counter board, or regular external triggering pulses. Should the time be kept very precisely, higher priority interrupt source should be used. For the case of IBM PC clone, the system timer interrupt (IRQ0) has the highest priority available to the user. Therefore, the PC system timer interrupt is utilzed in this program.

The interrupt service routine whose functioning is synchronized with the interrupt request, latches all working counters at the same time, reads counter register values, and stores them in the circulating buffer memory. This function is common to other programs utilizing PC counter except the sampling frequency and number of bits assigned to a count value. For the case of this multi-counter, full 16-bits are used for one count value, and the maximum count rate that can be measured is $2^{16} \times 50$/second ~ 3 Mcps.

The host program checks and reads buffer memory, calculates counts, corrects dead time effect, displays counted data, and responds to the aforementioned user requests comming through the keyboard.

MULTI-SCALER

It is to use a PC for the random neutron process measurement covering up to four neutron counters. There are various methods for the random neutron process measurement such as correlation, variance to mean ratio, count probability, dead time methods, etc. Each method measures neutron pulse sequence information and obtains reactor dynamic parameters, but the instrumentation or analysis method of each case is different.

The success of these techniques is dependent on the time resolution of individual count(s) and amount of data. The time resolution should be comparable to the prompt neutron life time (~ μ second in a fast reactor and ~ 100 μ seconds in a thermal reactor), and the data amount should be sufficient enough to ensure statistical reliability. There have been several experimental techniques to satisfy aforementioned requirements depending on the instrumentation and reactor type. However, if the count sequence can be measured and saved in the mass storage then numerical simulations for most techniques are possible. The conventional method of this approach is utilizing a sufficiently long record of detector signal on the magnetic tape, which is to be analysed by the computer.

Nowadays a PC is equipped with enough mass storage and speed for the neutron pulse sequence measurement. The feasibility of PC counter application to the above mentioned approach, was tested at the Korean TRIGA Mk-II reactor using single detector, and its results were analysed by several different methods[1,2]. This test encourages that a PC counter can be a good tool for the pulse sequence measurement in the thermal reactor. For the fast reactor application, however, a special I/O board should be designed for very fast scaling.

The system is now upgraded to accommodate up to four detector signals simultaneously. Its scaling speed is dependent on the number of counters and PC speed, but it can be as fast as 80 μ seconds when an IBM-AT is used, which is fast enough to determine the prompt neutron decay constant of usual thermal reactor. It also has automatic switching feature from the fast to slow scaling for the delayed neutron effect measurement. For the case of fast scaling, the number of bits to save each count value is minimized to relax huge memory requirement since the count probability during one very short time is very low. Current program can scale up to 192 K channels if one or two detectors are used and up to 96 K for three or four detectors. For the case of slow scaling, data are stored in the 16-bit array and channel size is 72 K/(number of counters). As the dwell time between each scaling is only for the data saving to the hard disk, data loss is minimized.

Fig. 3 shows a result obtained by the variance to mean ratio (VTMR) analysis for the scaled data at Korean TRIGA Mk-II reactor with two neutron counters. Counter-1 in the figure is a fission chamber located at the upper part of the core in the central irradiation hole, and counter-2 is also a fission chamber but located near the outer surface of graphite reflector and used as the start- up power monitoring channel. The fast scaling was by about 215 μ seconds of Δ for about 1,000 seconds and slow scaling was by about 27.6 milli-seconds for about 4,000 seconds. VTMRs were calculated for all possible grouping of nΔ, *i.e.*, (1, 2, .., n)Δ, (2, 3, ..., n+1)Δ, ... groups but not for the simple (1, 2, ..., n)Δ, (n+1, n+2, ..., 2n)Δ, ... ones, so as to enhance data precision. While it generates very precise VTMRs its computing time is too long. For the case of

an IBM-AT, it takes several nights for one experi- mental data analysis.

Dot lines in the figure represents fitted results only for the fast scaled data assuming all delayed neutron terms are linear function of T. Solid lines are fitted for all data to the exact VTMR equation including all delayed neutron terms, and for all variables related with VTMRs - counting efficiency (counts/fission), reactivity, Pu-239 fission portion (assuming fissions are occured only by U-235 and Pu-239), neutron generation time and effective delayed neutron fraction.

It shows something like discontinuity between the fast and slow scaled data which is caused by the different time band of measurement. This trend is amplified if the measuring time is shortened or VTMRs are the smaller by the lower counting efficiency or the higher subcriticality. For the case this experiment, The counting efficiency of each detector is rather low (less than 3×10^{-5}/fission), but the reactivity (~ -0.1 $) is rather close to the critical status.

As it can scale multiple detector signals simultaneously it will be a very useful tool for the analyses of cross-correlation and cross power spectral density (CPSD) as well.

REAL TIME REACTIVITY MEASUREMENT

The usual real time reactivity measurement by inverse point kinetics utilizes current detector signal fed through the ADC. The counter signal can also be used by similar manner if the square pulse train coming from the discriminator is converted to DC signal by count rate to voltage converter (CRVC), but has limitation by response time and dead time effect. In order to get stable DC signal with fast response time (short integration time) from the CRVC, the count rate should be high enough but it causes larger dead time effect. The dead time effect can be relaxed by adding dead time correction circuit and utilizing faster response components but there is still limitation. Actual counting system has at least four or five parts directly connected - detector itself, preamplifier, amplifier, discriminator and counter(or CRVC) - and each has different dead time and characteristics (extendable or non-extendable). Thus it is almost impossible to make a fixed relationship which will be used for the design of an accurate dead time correction circuit, between the count rate and reaction rate. Furthermore, the dead time can vary with the change of discriminator level setting.

When the PC counts pulses directly, aforementioned difficulties still remains unresolved but it does not need CRVC, and dead time effect can be corrected by software if it is measured. The experimentally measured dead time can be fitted to proper form such as polynomial, and it can be easily reflected to the software dead time correction. Its feasibility was tested by single detector[3] at very high count rate. It was successful but its results was rather sensitive to the dead time, which requires very accute dead time information.

If the counting interval can be longer, the count rate during the reactivity measurement can be lowered to relax dead time effect, but it might cause other problems by the enlongated time interval itself in solving difference equations and the integrated power representation during that interval.

The concept of neutron density (or fission power) variation measured by the count rate is slightly different from that sampled by an AD conversion of current detector signal. For the latter case, the current is based

on sufficient reaction rates in the detector, and the sampled data can be successfully assumed to represent the power at that time. However, the count rate measurement needs at least a certain time interval to count pulses, and its result represents the time integrated power (or averaged power) during that interval but not the spot value. The usual power monitoring by the neutron counter is based on the assumption that this interval is short enough compared to the power variation, but it can be a source of error in the real time reactivity measurement.

The use of counter imposes strong possibility that the experiment is to be accomplished at the neutron source range (or startup range) where the neutron source is effective. Its effect is stronger when the count rate is lower but it can be neglected at the power range where current detectors can be used for the power monitoring.

In order to verify these effects - rather long sampling interval, integrated power during the sampling interval in lieu of spot value and source effect - to the reactivity calculation, a series of numerical simulation was carried out for various forms of finite difference approximation of reactivity equations to search an optimum one.

Reactivity is expressed as Eq.1 from point kinetic equation.

$$\rho = \beta + \Lambda \frac{d\ln(n)}{dt} - \frac{\Lambda}{n} \Sigma \lambda_i C_i - \frac{\Lambda S}{n} \quad \text{---- (1)}$$

And delayed neutron precursor concentraion is,

$$\frac{dC_i}{dt} = \frac{\beta_i}{\Lambda} n - \lambda_i C_i \quad \text{---------- (2)}$$

As the PC measures n(t), Eq.1 can be explicitly solved if $C_i(t)$ - the delayed neutron precursor concentration - is known. The usual inverse point kinetics modifies Eq.2 to the following form to calculate precursor concentration.

$$C_i(t+\Delta) = C_i(t)\, exp(-\lambda_i \Delta) + \frac{\beta_i}{\Lambda} exp[-\lambda_i(t+\Delta)] \int_t^{t+\Delta} n\, exp(\lambda_i t')\, dt' \quad \text{-- (3)}$$

If the integration term of the above equation is approximated by the trapezoidal method, $C_i(t+\Delta)$ can be solved explicitly.

However, Eq.2 can be solved by direct trapezoidal integration of the whole equation itself from t to t+Δ as well.

$$C_i(t+\Delta) - C_i(t) = \{ \frac{\beta_i}{\Lambda} [n(t+\Delta) + n(t)] - \lambda_i [C_i(t+\Delta) + C_i(t)] \} \frac{\Delta}{2} \quad \text{-- (4)}$$

This equation can also be solved explicitly.

Both of above equations were tested by simulating aforementioned conditions. And it was confirmed that Eq.4 results correct reactivity if $\Delta < 10$ seconds, while Eq.3 results the same accuracy when $\Delta < 0.1$ second. Therefore, instead of the well known inverse point kinetic equations (Eqs. 1 and 3), Eqs. 1 and 4 are used for the real time reactivity measurement. Should the sampling interval be more than 0.1 second, the superiority of latter equations is also apparent when current detectors are used.

Fig. 4 is an example of reactivity measuring experiment using two fission counters. It can treat up to nine counter signals. Reactivity calculation and data display take place once every second, but the actual count rate values used for reactivity calculations, are averaged ones of adjacent two seconds. Lower part curves in the figure drawn by log scale, represent count rate variation, and upper two curves(they looks like as if one line because they are too close) depict reactivity variation. If it reaches the right end of the screen, the screen is swapped half. Thus, the

screen always displays at least about 300 seconds' data except when it is just beginning of the experiment.

Time averaged reactivity value while it is in steady state, can be read in digital form by very simple key board manipulation. Those values displayed at the left-bottom corner of the screen are recently averaged reactivity values (unit: $) of each counting channel and the average of all channels(last one). Thicker parts of lines in the figure indicate that the averaging process is(was) occured at that time period. All the data related to the experiment are saved in the hard disk, and the experiment can be revived if data checking is needed.

CONCLUSION

Major important reactor experiments based on the neutron counters have been successfully accomplished by a PC-counter. A low cost counter board is effectively used for the criticality approach instead of conventional counter modules, multiple neutron pulse channels are scaled at the same time providing much easier data treatment than using conventional instrumentations for various kinds of random neutron process analysis, and real time reactivty measurement using startup channels or detectors for the criticality approach is accomplished at the very low fission power where current detectors cannot generate dependable signals.

The PC multi-scaler can be effectively used especially for the cross-correlation and cross power spectral density analysis since multiple detector signals can be easily scaled simultaneously.

Those problems which can be arisen because counters in lieu of current detectors are used for the real time reactivity measurement, are fully tested and a proper form of finite difference approximation for the delayed neutron precursor equation is searched. This equation can be effectively used for both of point kinetics and point reactivity calculation. Thanks of this equation, it is possible to measure very accurate and statistically reliable reactivity by one second sampling interval at the count rate range of 10^3 to 10^6 cps where the dead time can be assumed to be constant.

This system will be expanded to accommodate analog signals as well in order to cover all power range and to apply to many other experiments which should be accomplished by analog ones.

REFERENCES

1) B.J. Jun, *et al.*, "PC-Based Random Neutron Process Measurement in a Thermal Reactor," *J. Korean Nucl. Soc.*, Vol.22, No.1, pp. 58-65, March 1990.
2) S.J. Park, *et al.*, "Random Neutron Process Analysis by Counting Probability Method," *Proc. Korean Nucl. Soc.*, Autumn Meeting, Oct. 27, 1989, Seoul, pp. 15-26.
3) B.J. Jun, *et al.*, "Real Time Reactivity Measurement Using Neutron Pulse Counter," *Proc. Korean Nucl. Soc.* Spring Meeting, May 27, 1989, Soo Won, pp. 1-10.

F1(ctrl-T) F4(ctrl-R) F5(ctrl-S) F8(ctrl-E)
Set Time:100 Reset Save data Exit:

T(sec)	Counter1	Counter2	F.C-1	F.C-2	BF3-1	BF3-2	BF3-3	BF3-4
10.00	1000	1000	1000	1000	1000	1000	1222	551
cps	100.01	100.01	100.01	100.01	100.00	100.00	122.20	55.10
100.00	10000	10000	10000	10000	10000	10000	12015	5689
cps	100.01	100.01	100.01	100.01	100.00	100.00	122.02	56.89
100.00	10000	10000	10000	10000	10000	10000	12103	5674
cps	100.01	100.01	100.01	100.01	100.00	100.00	121.03	56.74
100.00	10000	10000	10000	10000	10000	10000	12050	5666
cps	100.01	100.01	100.01	100.01	100.00	100.00	120.50	56.66
100.00	10000	10000	10000	10000	10000	10000	12129	5598
cps	100.01	100.01	100.01	100.01	100.00	100.00	121.29	55.98
100.00	10000	10000	10000	10000	10000	10000	12142	5657
cps	100.01	100.01	100.01	100.01	100.00	100.00	121.42	56.57
100.00	10000	10000	10000	10000	10000	10000	12093	5631
cps	100.01	100.01	100.01	100.01	100.00	100.00	120.93	56.31
32.68	3268	3268	3268	3268	3268	3268	3943	1834

Fig. 1. A Sample of CRT Display While Multi-Counter is Working

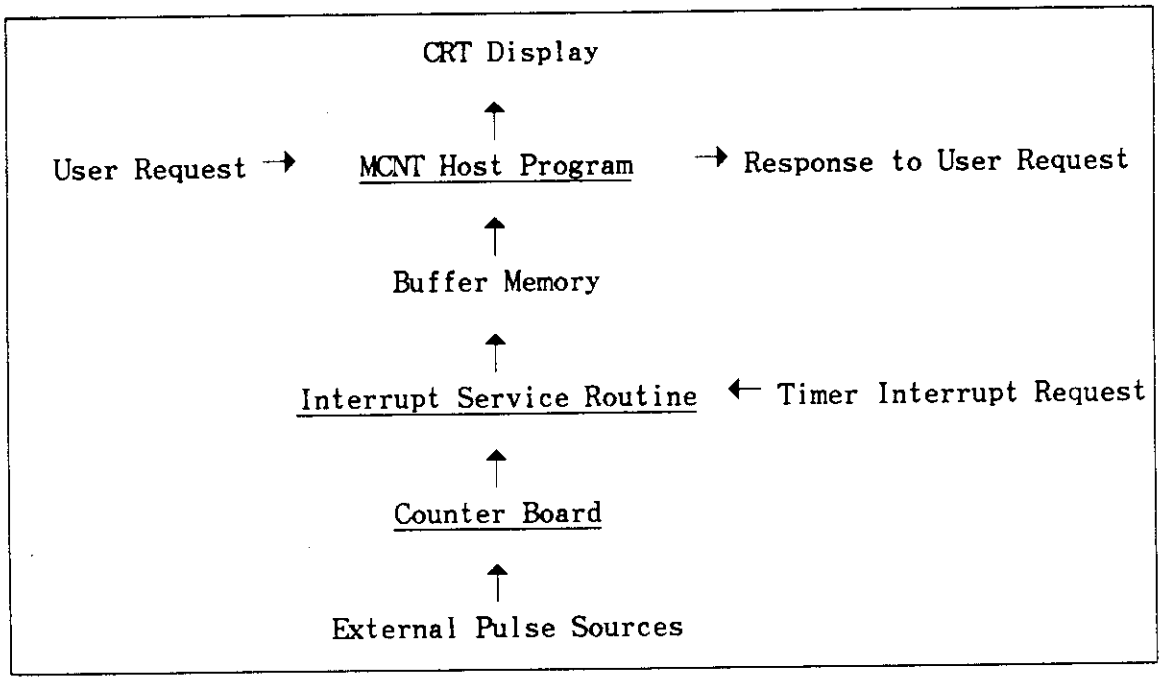

Fig. 2. The Working Concept of PC Multi-Counter

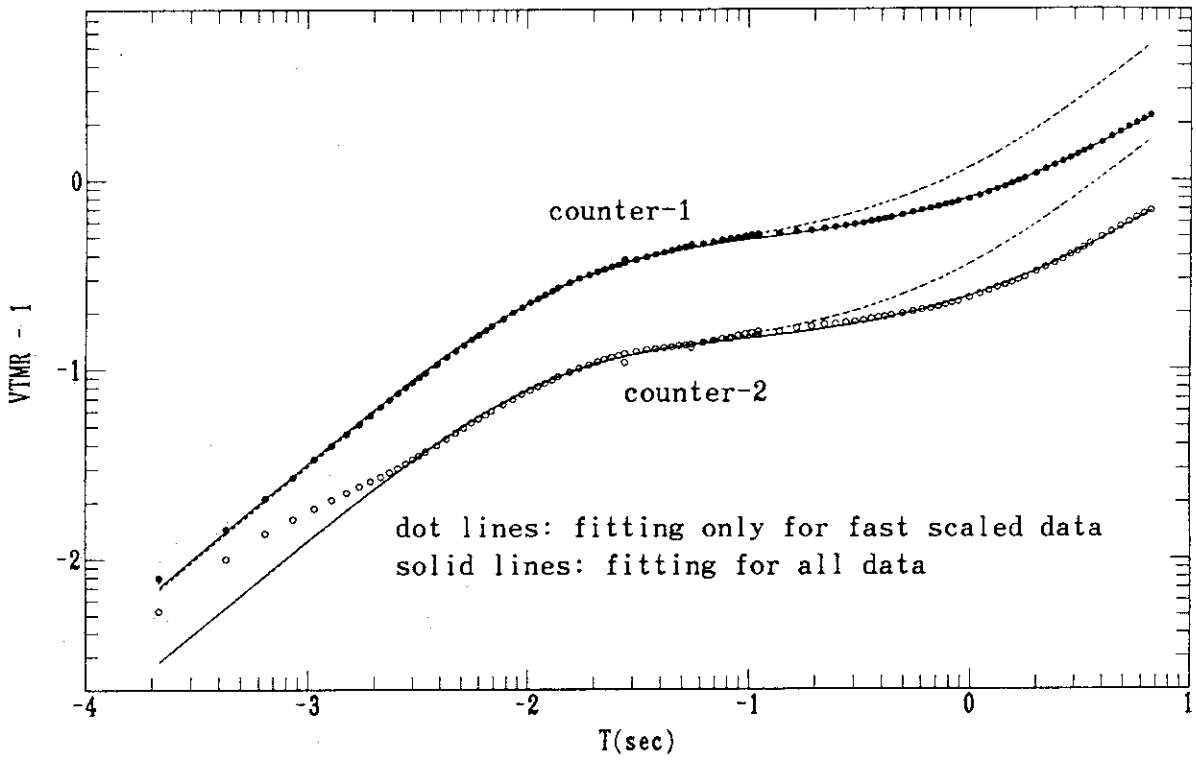

Fig. 3. An Example of VTMR Analysis for the Data Measured by the PC Multi-Scaler

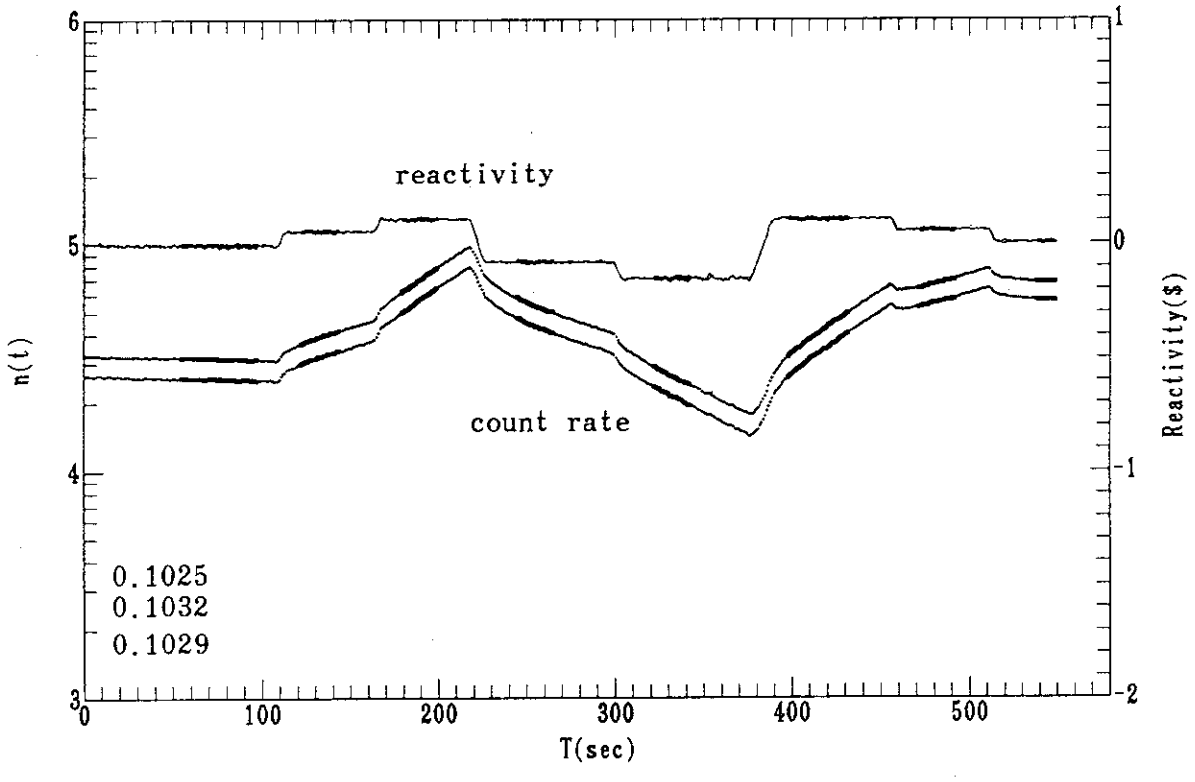

Fig. 4. An Example of Real Time Reactivity Measurement Using PC-Counter

4. Reactor Kinetics Measurements on Fast Breeder Test Reactor

OM PAL SINGH, G.S.SRINIVASAN, B.SHARADA, V.SATHIAMDORTHY, C.P.REDDY, S.M.LEE AND R.SHANKAR SINGH

Reactor Physics Division
Indira Gandhi Centre for Atomic Research
Kalpakkam 603 102, Tamil Nadu, INDIA

ABSTRACT

Fast Breeder Test Reactor (FBTR) is a carbide fueled, liquid sodium cooled fast reactor. The paper provides the results of kinetics measurments performed on the reactor for the mean delayed neutron life time, period reactivity relationship, zero power frequency response function, reactivity transients initiated by withdrawal and lowering of rods at different powers and during critical and subcritical state of the reactor. The constraints and other problems faced during the experiment are also discussed.

INTRODUCTION

The Fast Breeder Test Reactor (FBTR) is a carbide fueled liquid sodium cooled fast reactor. The present core contains 23 fuel subassemblies and could operate at a nominal power of 10 MWt with a maximum linear power rating of 250 W/cm, The subsequent cores would contain 65 fuel subassemblies and could provide a maximum power of 40 MWt. The reactor achieved its first criticality in 1985 and subsequently a number of physics tests have been performed on the reactor. The reactor kinetics measurements are a few of them. In this paper, the results of the measurements like determination of mean delayed neutron life time, inhour equation, zero power frequency response function, reactivity transients initiated by withdrawal and lowering of control rods at different power levels and state of the reactor, are reported. The measurements were basically aimed to verify the delayed neutron parameters of the reactor and to validate the point kinetics computer codes, POKIN/1/ and CRT/2/. In the code POKIN, the point kinetics equations are solved without taking any reactivity feedback into account. The code CRT, in addition accounts for reactivity feedback by solving the heat transfer equations applicable to the reactor core cooling channels. The reactivity feedback components accounted in the code are : Doppler, fuel and clad axial expansion, coolant expansion, core boundary movement in the upper axial blanket and radial blanket, differential control rod expansion, flowering of the core radially due to spacer pad heating and grid plate expansion. The feedback effects are calculated by considering detailed spatial dependence of power and temperature in the reactor.

DELAYED NEUTRON PARAMETER MEASUREMENTS

The delayed neutron parameters are measured indirectly by validating the theoretical period-reactivity relationship and comparing the theoretical and experimental zero power frequency response function of

the reactor by analysing the data of rod drop test.

A. Test Constraints

Certain constraints faced in carrying out the test are:

(i) Scram Reactivity Resulting from the Rod Drop

Prompt drop characteristics of the reactor and the background neutron noise level, demand that the scram reactivity resulting from the rod drop should be low enough so that prompt drop in power level following rod drop is perceptible and power profile is dependent on delayed neutrons for a sufficiently long time before coming to the background neutron noise level. Scram reactivity of 0.5$ was adjudged suitable for this purpose.

(ii) Neutron Source

For accurate measurements, the reactor should be operated in neutron source free state before the rod drop and following the rod drop, the power must not fall soon to the power level influenced by neutron source. It is estimated/3/ that reactor power level upto 100 watt is influenced by neutron source. Therefore, to have at least one decade of power profile free from neutron source influence, it was decided to perform the test at power level of more than 1.5 kWt.

(iii) Reactivity Feedback

Static power coefficient of reactivity for FBTR is estimated/4/ to be 40 pcm/MWt. Therefore, for performing the experiment in reactivity feedback free reactor state, the reactor power level before rod drop should be below 25 kWt. Therefore, it was decided to perform the test at a power level of 2 kWt. A power level of 200 kWt was also chosen for rod drop test so that the results of the two tests can be compared and the effects of neutron source and reactivity feedback can be discerned.

(iv) Data Recording Time Interval

Since the delayed neutron effect in zero power frequency response function is reflected upto 1 to 10 HZ frequency, it was decided to have the data recording at a time interval of 20 to 50 ms. Smaller data recording time intervals lead to larger statistical fluctuations in counts soon after the first decade of power decay after rod drop.

B. Data Analysis

The test 1 was conducted at a reactor power of 2 kWt and data recording was done at a time interval of 20 ms. A total of 4000 data points were recorded. Subsequently it has been realised that a choice of 20 ms data recording interval is not appropriate due to large statistical fluctuations in the counts and hence larger error in the analysis. A choice of 4000 data points provide data over a time of 80 s only. So the results of test 1 are not so accurate and complete.

For test 2 power level is 200 kWt, data recording time interval is 50 ms and 4000 total data points are recorded.

(i) Mean Delayed Neutron Life Time

Mean delayed neutron life time is given by,

$$\bar{\tau} = \frac{1}{\beta} \sum_j \frac{\beta_j}{\lambda_j} \quad ----(1)$$

Experimentally, $\bar{\tau}$ can be calculated using the formula,

$$\bar{\tau} = \frac{P_0 - P_1}{P_0 P_1} \cdot \int_0^\infty P(t')\,dt' \quad ---(2)$$

where Po is initial power level and P1 and P(t) are the prompt drop power +level and power profile following rod drop. (Po - P1)/ P1 is determined as 0.52 $. Measured value of $\bar{\tau}$ is found to be 13.04 s. These compare well with the theoretical value of 13.83 s from test 2 and from test 1, we get $\bar{\tau}$ = 13.83 s.

(ii) Inhour Equation

Theoretical inhour equation is given by,

$$\rho_0 = \frac{\Lambda}{\beta T} + \sum_j \frac{\beta_j / \beta}{1 + \lambda_j T} \quad ---(3)$$

where T is the reactor period for a step change in reactivity, ρ_0 is the reactivity in dollars. β_j and λ_j are the jth group delayed neutron fraction and decay constant respectively.

Experimentally, inhour equation results can be obtained from the rod drop test data using the formula/5/,

$$\rho_0 = \frac{P_0 - P_1}{P_1} \cdot \frac{sP(s)}{P_0 - sP(s)} \quad ----(4)$$

where

$$P(s) = \int_0^\infty P(t) e^{-st}\,dt \quad ---(5)$$

P(t) being the power profile following the rod drop and s the Laplace transform variable. 1/s represents the reactor period.

The experimental and theoretical values of reactivity for different reactor period are plotted in Fig.1. It can be seen that for a reactor period in the range 0.1 s to 3600 s, the theoretical value is more than experimental value by a maximum of 6.4%. This deviation is almost same as we observed for $\bar{\tau}$.

(iii) Zero Power Transfer Function

Theoretical expression for zero power transfer function is,

$$Z(i\omega) = (i\omega \Lambda/\beta + \sum_j (i\omega \beta_j/\beta/(\lambda_j + i\omega)) \quad ---(6)$$

where w is the frequency in radians per sec. Experimentally, Z(iw) is determined from the rod drop test parameters as/3/,

$$Z(iw) = \frac{P_1}{P_0 - P_1} \cdot \frac{P_0 - iw\,P(iw)}{iw\,P(iw)} \quad - - - (7)$$

where

$$P(iw) = \int_0^\infty P(t)\, e^{iwt}\, dt \quad - - - (8)$$

the Fourier transform of P(t).

The theoretical and test 2 experimental values of Z(iw) are plotted in Fig.2 and Fig.3 and covers the frequency range of 0.3×10^{-3} rps to 20 rps. Amplitude of theoretical Z(iw) differs from the experimental value by a maximum amount of 9.6%. Deviation in the phase factor increases as the frequency increases. This is because as the frequency increases, Fourier transform demands rod drop test data at a finer interval of time.

REACTIVITY TRANSIENTS

A. Test Constraints

For code validation, ideally one would like to initiate a power transient by moving a control rod in or out with the maximum permissible speed for about 10 s. But in FBTR, continuous outward control rod movement near or at criticality is possible for a maximum time of 3 s only. Hence the code validation is possible for power increasing transients initiated by reactivity variation for a maximum time of 3 s.

B. Test Details

For reactivity ramp rates, the data is recorded as follows:

Initial Power	Rod movement			Data	Record
	Rod	mm to mm	Net reactivity (pcm)	Δt (s)	Points (K)
99.5 kW	A	267.6 to 270.6	+ 10.22	0·10	8
390.6 kW	F	271.6 to 264.0	- 25.72	0·05	8
6.20 kW	F	266.8 to 268.1	+ 4.50	0·05	8
Subcritical	A	262.4 to 265.7	+ 11.43	0·10	8
471.0 W	A	267.7 to 264.1	- 12.47	0·10	8

C. Results

The five reactivity transients mentioned above were analysed using the code POKIN and CRT. The comparison of the experimental results with the calculated one is discussed below.

(i) Positive Reactivity Ramp at 99.5 kWt Power

For the transient, the experimental power profile is shown in Fig.4. Actual power profiles recorded during the experiment show large statistical fluctuations. Therefore, the data have been smoothened for the clarity of theoretical points. The incident has been analysed by the codes CRT and POKIN. The calculations indicated that the incident can not be analysed for 3 mm movement of the rod by either codes. However, when the rod movement was simulated in the codes for only 2.25 mm, the results of the CRT code were found close to the experimental results (see solid dots in Fig.4). The corresponding results obtained with the code POKIN are also recorded in Fig.5 as cross. POKIN results are not close to experimental results. This indicates the effect of reactivity feedback at this power level. It is observed that while the control rod movement of 2.25 s gives 7.665 pcm of reactivity, a power rise by a factor of 2.5 gives 5.984 pcm calculated negative feedback reactivity. Since there is uncertainty of 1 mm in recording the control rod position, the comparison of CRT code predictions with the experimental results for control rod movement of 2.25 mm can be considered fairly good.

(ii) Negative Reactivity Ramp at 390.6 kWt Power

For this transient, the experimental power profile is plotted in Fig.5. The results of the code CRT are also plotted in the figure and marked as solid dots. The corresponding results of the code POKIN are marked as cross. The theoretical results of the code CRT appear to agree well with the experimental results in the beginning of the transient but falls below experimental curve for the longer times. The results of the code POKIN do not agree with the experimental results. This indicates the significance of the reactivity feedback effects. It is observed that while lowering of the rod by 7.6 mm gives 25.72 pcm negative reactivity, power reduction from 391.0 kWt to 328.0 kWt in the transient, gives 13.16 pcm calculated positive feedback reactivity.

(iii) Positive Reactivity Ramp at 6.2 kWt Power

For this transient, the experimental power profile is shown in fig.6. The corresponding theoretical results, marked as solid dots and generated by the code POKIN by simulating the rod movement of 2.00 mm (instead of 1.3 mm), are also shown in the figure. Here we find that the experimental power profile is well predicted for initial 150 s. However as the power transient becomes longer and longer, the code appears to overpredict the results. It may be due to small reactivity feedbacks effects that are not accounted in code POKIN.

(iv) Positive Reactivity Ramp in Subcritical State of the Reactor

For this transient, the experimental power profile is shown in Fig.7. The corresponding theoretical points generated by the code POKIN

taking rod movement for 2.5 mm are shown as crosses. Theoretical predictions fall within the statistical fluctuations of the experimental data.

(v) Negative Reactivity Ramp at 471.0 W Power Level

For this transient, experimental power profile is shown in Fig.8. Theoretical values calculated using the code POKIN are marked again as crosses in the graph. The theoretical prediction is within the statistical variations of the experimental points.

CONCLUSIONS

(i) The rod drop test results show the agreement between theoretical and experiment values of mean delayed neutron life time, period reactivity relationship and zero power frequency response function within 6 to 9%. The difference could be due to some reactivity feedback present at 200 kWt power level test and neutron source influence in the tail part of the power profile following rod drop. Rod drop test at power levels of 2 and 3 kW power levels are planned to be done with suitable data length and data recording time interval.

(ii) Keeping in view that the uncertainty in recording control rod position is of the order of 1 mm, all the reactivity initiated power transients are well explained by the codes POKIN and CRT. The reactivity initiated transient tests are to be done in future at higher power levels. This will further test the code CRT when relatively large reactivity feedbacks exist in the reactor.

Acknowledgements

The authors are thankful to Mr. P.Swaminathan and his staff for making available the data acquisition system. The authors are also thankful to FBTR operation crew for their excellent co-operation.

References

1. Om Pal Singh and R.C.Malik, "POKIN - A Point Kinetics Code with Space Dependent-Independent Reactivity Feedback" FRG/01140/80/RP192 (1980).

2. M.V.Parikh, S.Ponpandi and Om Pal Singh, "CRT : A Computer Code for Analysing Controlled Reactivity Transients in LMFBRs", REDG/01149/RP-279 (1985).

3. M.V.Parikh and Om Pal Singh, "Implications of Neutron Source Strength on the Calibration of Control Rods by Period Measurements in FBTR at Low Power" REDG/01140/RP-281 (1985).

4. S.Panpandi and Om Pal Singh, "Static Power Coefficient Calculations for FBTR Carbide 10 (L.P. 250 W/cm) and 16 MW (L.P. = 400 W/cm) Cores" RG/RPD/270 (Addendum) Oct. 1986.

5. G.R.Keepin, "Physics of Nuclear Kinetics" Addison Wesley pub. Co. Inc. (1965).

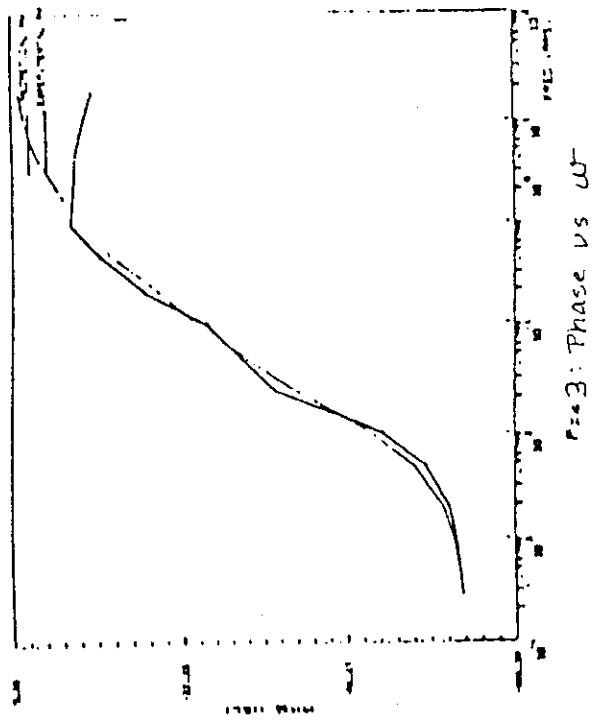

Fig 3: Phase vs ω

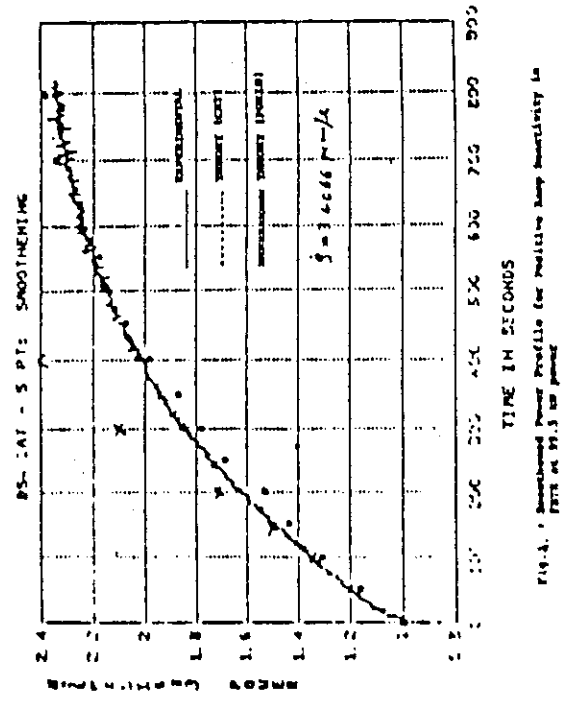

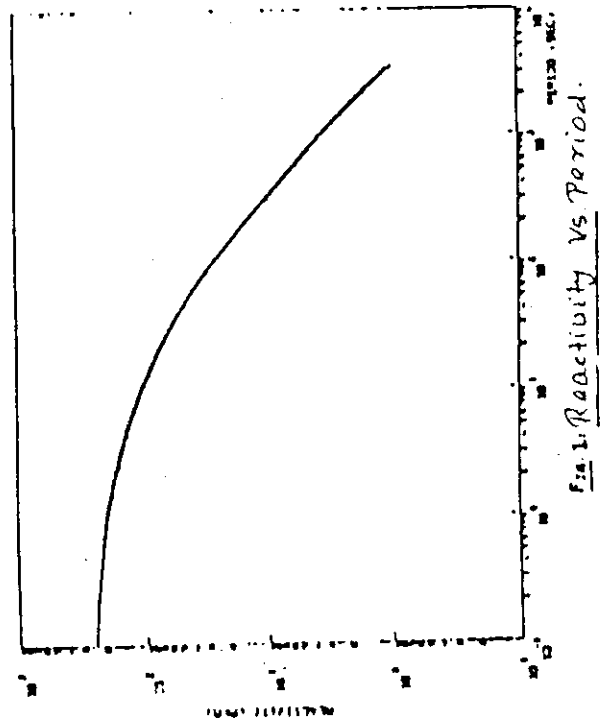

Fig 1: Reactivity Vs Period.

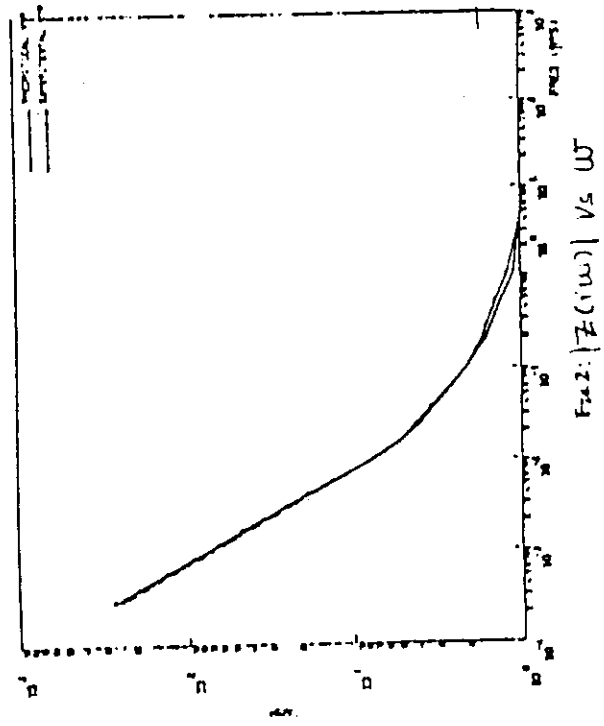

Fig 2: |Z(iω)| Vs ω

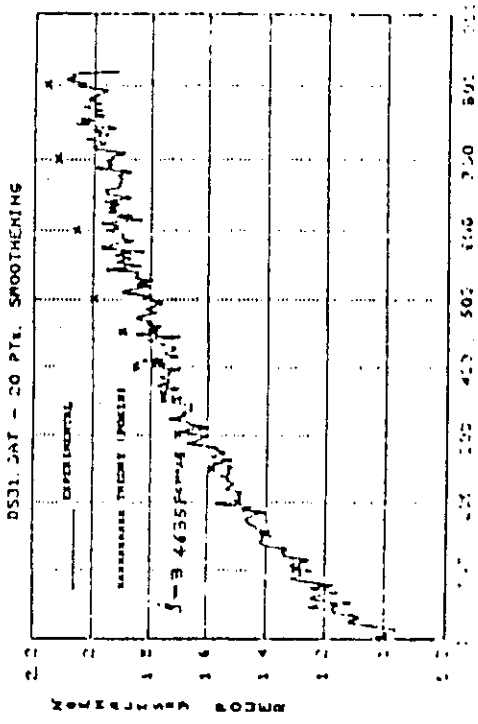

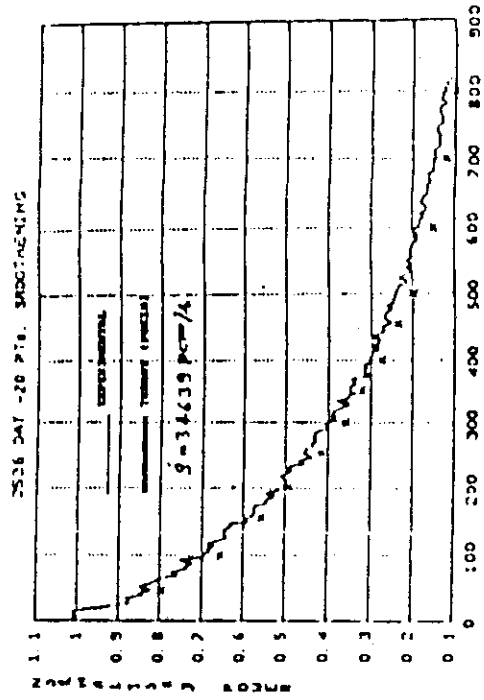

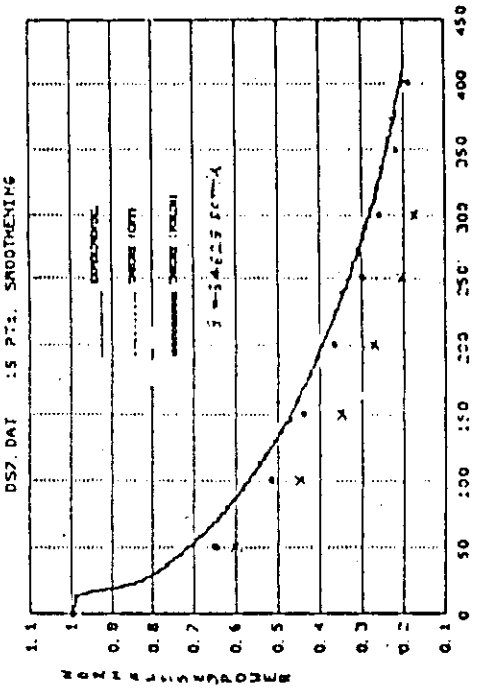

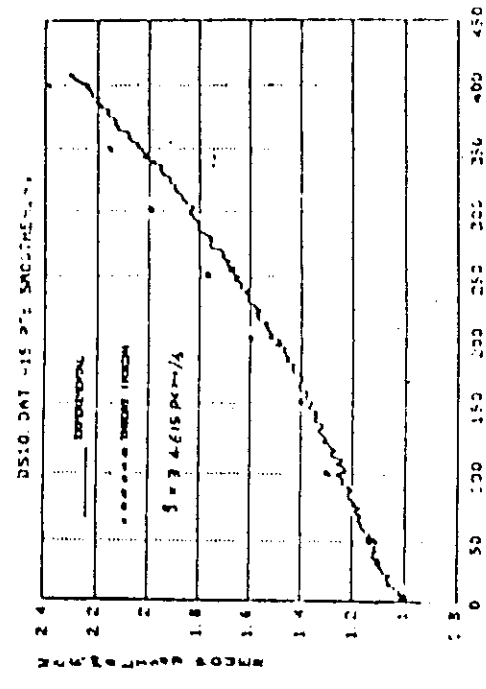

1. Detection of Radioactive Products in the Cooling System of the Bangladesh Research Reactor

A. S. MOLLAH

Institute of Nuclear Science and Technology
Atomic Energy Research Establishment
GPO Box 3787, Dhaka-1000
Bangladesh

ABSTRACT

The radionuclides containing in primary cooling system in the 3MW TRIGA Mark-II research reactor (pool type) have been measured using a high resolution HPGe detector in conjunction with a 4096 channel analyzer. A total of 10 radionuclides (such as Na-24, Mg-27, Ar-41, Cr-51, Mn-54, Mn-56, Cu-64, Co-60, Zn-65 and Ag-110m) have been found in gamma ray spectra of primary cooling water, ion exchange resins and filter cartige as activation products. The radionuclides which were detected are either in the water as a result of corrosion of material in the pool or in water soluble compounds of elements from material in the pool. No fission product radionuclides could be detected in the primary cooling system during the course of this experiment. This study will be useful not only from the point of view of radioactive waste management and radiation protection but also for safe operation of the reactor.

INTRODUCTION

At the Atomic Energy Research Establishment (AERE), a 3MW TRIGA Mark-II research reactor (pool type) has been in operation since October 1986. AERE is located at Ganakbari, Savar, 40 km from the capital city of Dhaka, Bangladesh. This is the first nuclear reactor in the country. The reactor is cooled by demineralized water which flows down the core to a hold up tank and is circulated by a pump (primary pump) through the heat exchange back to pool. In the heat exchanger the primary cooling water loses its heat to the secondary cooling system. In the hold up tank the primary water is retained for sometime to allow short lived activities (e.g. N-16, N-17 and O-18) to decay [1]. A part of the primary water is also routed through a filter cartige and mixed bed ion-exchange resins in the deminaralizer plant (containing cationic and anionic resins) before pumping it back to the reactor pool. The filter cartige and ion-exchange resins in the deminaralizer plant separates the radioactivity from the

pool water in addition to maintaining its quality [1].

Various radionuclides are formed during normal operation of a nuclear reactor by the fission of U-235 and the neutron activation of the surrounding material which includes the fuel element cladding, structural material of the reactor and impurities in the pool water, etc. [2-5]. The fission products remain within the cladding of the fuel and rarely released except in the event of rupture of the cladding material. The radioactive products generally found in the circulating coolant water are therefore neutron activation products [6]. The very shortlived nuclides due to N-16, N-17 and O-18 completely decay in the hold up tank [1]. The longer lived radionuclides, however, remain circulating in the primary cooling system. As the coolant passes through the demineralizer, these radionuclides are retained in the filter cartige and ion-exchange resins where their concentration goes on increasing depending on their half lives and the rate of operation of the reactor. In order to maintain the quality of the pool water, the deminaralizer is periodically regenerated.This operation washes away the radionuclides absorbed in the dimineralizer and gives rise to the liquid radioactive waste. The mixed bed ion-exchange resins are changed regularly and gives rise to the solid radioactive wastes. The measurement of radioactivity in these wastes and in the primary coolant water is an important exercise which is useful not only from the point of view of radioactive waste management but also for safe operation of the reactor. During the operation of a pool type reactor, it is necessary to control the activity concentration of the pool water for fuel element failure detection and for determination of contamination. This experiment has been undertaken to study the radionuclide contamination in primary cooling system such as, pool water , mixed bed ion-exchange resins and filter cartige. The nuclear reactions by which activation products have been formed are studied thoroughly.

EXPERIMENTAL METHODS

Analysis of the pool water and the radioactive waste effluent is aimed at identifying and measuring the radionuclides. This analysis is carried out by means of a gamma spectrometer consisting of a high resolution HPGe detector (volume: 84 cc) in conjunction with a 4096 channel analyzer. The efficiency of the HPGe detector was 18% relative to a 7.5 cm x 7.5 cm NaI(Tl) detector at 25 cm and 1.332 MeV. The resolution of the detector was 2.1 keV at 1.332 MeV. Approximately 1 litre of water was taken from the reactor pool in a Marinelli beaker. The water sample was collected while the reactor was operating at 3 MW. In order to detect any possible fission products from fuel defects, the resins and filter cartige from the water purifier system (demineralizer plant) were collected and measured with the gamma spectrometer for radioactivity measurements. About 100 ml of ion-exchange resins and the whole filter cartige were used for radioactivity measurements. Spectra were recorded at various

times after the samples had been collected. The efficiency calibration of two different counting geometries, such as, 1-litre Marinelli beaker and 100 ml petridish, was performed using known amounts of Co-57, Ce-139, Hg-203, Sn-113, Sr-85, Cs-137, Y-88 and Co-60. Photopeak detection efficiencies were determined for each of these radionuclides. The results of photopeak efficiencies are shown in Fig. 1. The concentration of the radionuclides in the sample is determined based on the measured photopeak efficiency and net area under the photopeak of the radionuclides.

RESULTS AND DISCUSSION

Figures 2-4 show a gamma-ray spectra of pool water, filter cartige and ion-exchange resins obtained in this work. Counting details are contained in the legends of Figs. 2-4. A total of 10 photopeaks were observed in the spectra during the course of the experiment. Two prominant peaks with energies of 111.62 keV and 1356.70 keV have not been assigned to any radionuclides. In addition, there were several weak peaks for which no assignment was made. In the pool water, Na-24, Ar-41, Cu-64, Mn-56 and Mg-27 were found in the gamma spectrum (Fig. 2). The radionuclides, such as,Zn-65, Co-60, Mn-54, Cr-51 and Ag-110m were observed in both the gamma spectra of filter cartige and ion-exchange resins (Figs.3 and 4). During reactor operation the radioactivity of pool water increases, mostly due to formation of Na-24 by the (n, gamma) reaction of the aluminium and Ar-41 by the (n, gamma) reaction of the argon dissolved in the pool water. The remaining radionuclides having significantly smaller activities are produced by activation of the impurities in the aluminium and in the metal components of the stainless steel of the fuel cans, screws and ball bearings. The radionuclides detected in pool water, ion-exchange resins and filter cartige have been studied thoroughly. Table 1 contains a list of the radionuclides detected and their modes of production [7]. These results are in good agreement with previous ones [2-5]. The data supporting our identifications of radionuclides consists of measured gamm ray energies and , in some cases, half-life measurements [7]. The specific activities of Na-24, Mg-27, Ar-41, Cu-64 and Mn-56 in pool water (collected on 26.5.1990) were found to be 10.12 kBq/l, 5.18 kBq/l, 38.59 kBq/l, 9.62 kBq/l and 4.92 kBq/l respectively. The specific radioactivities of the detected radionuclides differed from those reported previously and these were attributed to differences in the operating programmes of the reactor [6]. The most important contaminants from the point of view of radiation hazard are Co-60 and Zn-65 due to their long half-lives. The activities in the ion-exchange resins are Co-60 with a maximum of 10 MBq, Mn-56 with a maximum of about 2.5 MBq and Cr-51, Zn-65 and Ag-110m with less than 0.5 MBq. The results of the radionuclide concentration in the filter cartige are not presented here because at the time of experiment, the efficiency of the detector for the counting geometry for filter cartige was

not performed. All the radionuclides were detected as corrosion products or accidental water contaminants as observed by other workers [2,8]. No fission product radionuclides could be detected in the cooling system during the course of this experiment. This study will be useful not only from the point of view of radioactive waste management and radiation protection but also for safe operation of the reactor.

REFERENCES

[1] Safety Analysis Report for the 3 Mw Forced-flow TRIGA Mark-II Reactor, General Atomic Technologies Inc., E-117-990 (1981).

[2] T. Nozaki and M. Okamotu, Radioactivity in cooling water of Musashi reactor TRIGA-II, J. At. Energy Soc. Japan, Vol.25(10), 816-821 (1983).

[3] R.V. Mansevso and J.A. Ulinski, Identification of radioactive isotopes in reactor pool water, Am. J. Phys. 41, 405-409 (1973).

[4] H.A. Kostalas and J. Armiriotis, The determination of the radio-contamination in the pool-water of a reactor, Health Phys. 15, 84-87 (1986).

[5] R.C. Teitalbaum, J.M. Anderson, R.V. Mancuso and R. Palmer, Quantitative determination of radioactive isotopes in reactor pool water, Health Phys. 28, 301 (1975).

[6] A. S. Mollah and M. Hossain, Measurement of radioactivity in the pool water of 3 MW TRIGA Mark-II research reactor in Bangladesh, Nucl. Sci. Journal (in press).

[7] E. Browne and R. B. Firestone, Table of isotopes, 7th Edition, John Wiley and Sons, Inc., New York (1986).

[8] M. Alamgir, A. K. M. Sharif, A. S. Mollah and N. Nahar, Total analysis of water in the 3 MW TRIGA Mark-II research reactor, Proc. of the 2nd Seminar on Operation and Utilization of the 3MW TRIGA Research Reactor at AERE, Savar, p.68 (1989).

Table 1. Radionuclides detected in primary cooling system.

Isotopes	Half-life	Type of reaction	Prominent gamma energy (keV)	Intensity (%)
^{24}Na	14.65 h	$^{27}Al(n, \alpha)$	1368.5	100
^{27}Mg	9.46 min	$^{26}Mg(n, \gamma)$	843.7	73
			1014.4	29
		$^{27}Al(n, p)$		
^{41}Ar	1.82 h	$^{40}Ar(n, \gamma)$	1293.2	99
^{51}Cr	27 days	$^{50}Cr(n, \gamma)$	320.1	98
^{54}Mn	312.2 days	$^{54}Fe(n, p)$	834.8	100
^{56}Mn	2.57 h	$^{55}Mn(n, \gamma)$	846.8	99
^{60}Co	5.27 y	$^{59}Co(n, \gamma)$	1173.2	100
			1332.2	100
^{64}Cu	12.7 h	$^{63}Cu(n, \gamma)$		
^{65}Zn	244.1 days	$^{64}Zn(n, \gamma)$	1115.5	51
^{110m}Ag	249.8 days	$^{109}Ag(n, \gamma)$	657.8	95
			884.7	73
			937.5	35
			1384.3	24

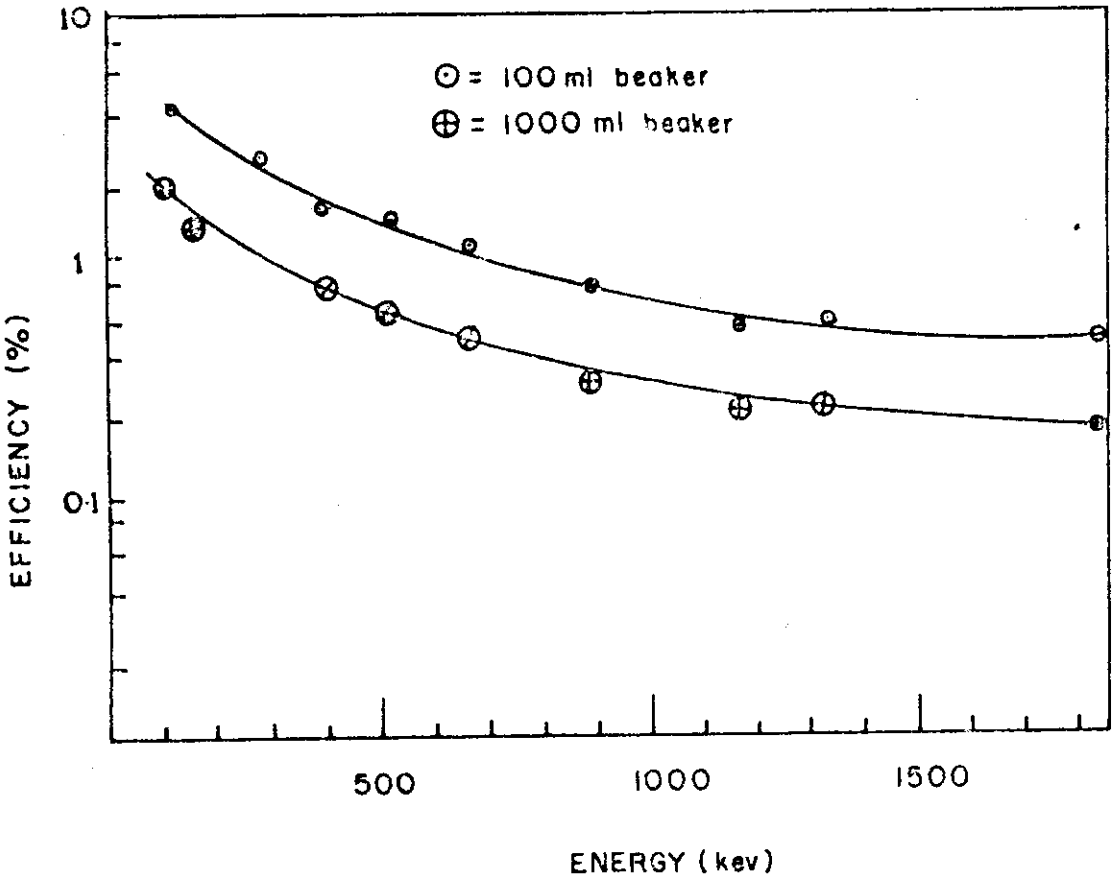

FIG. 1. EFFICIENCY CURVES OF HPGe DETECTOR.

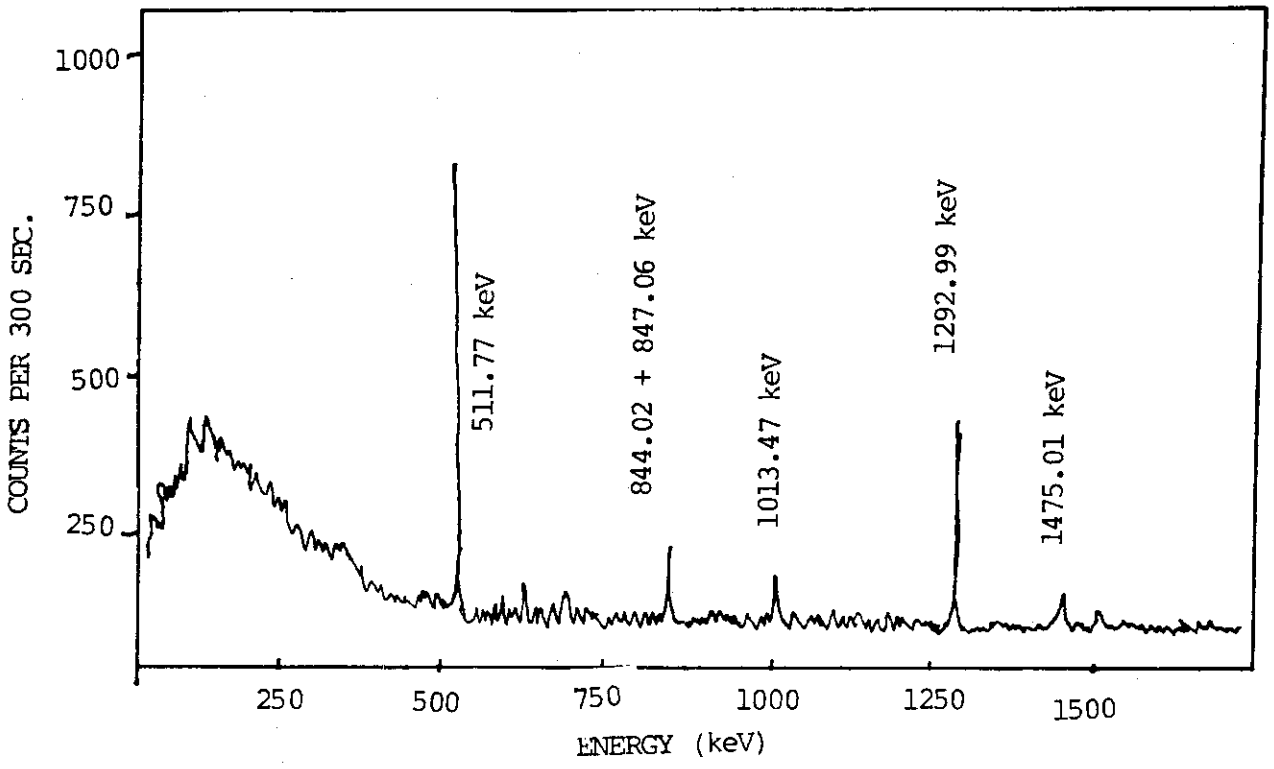

Fig. 2. Gamma energy spectrum of reactor pool water collected after 3 hr operation of the reactor at 3 MW on 26.5.90.

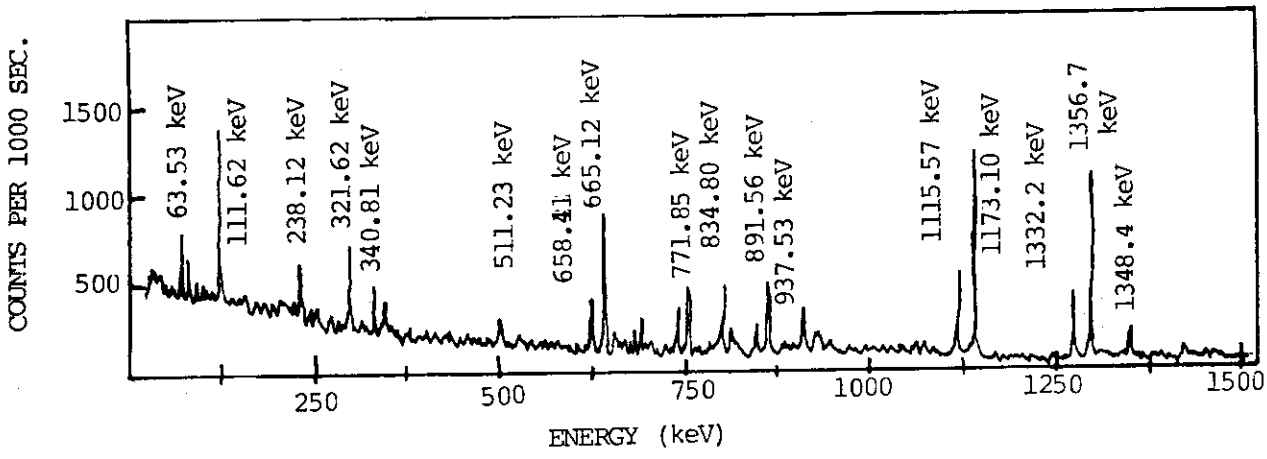

Fig. 3. Gamma energy spectrum of filter cartige collected from on-line purification system on 31.7.91.

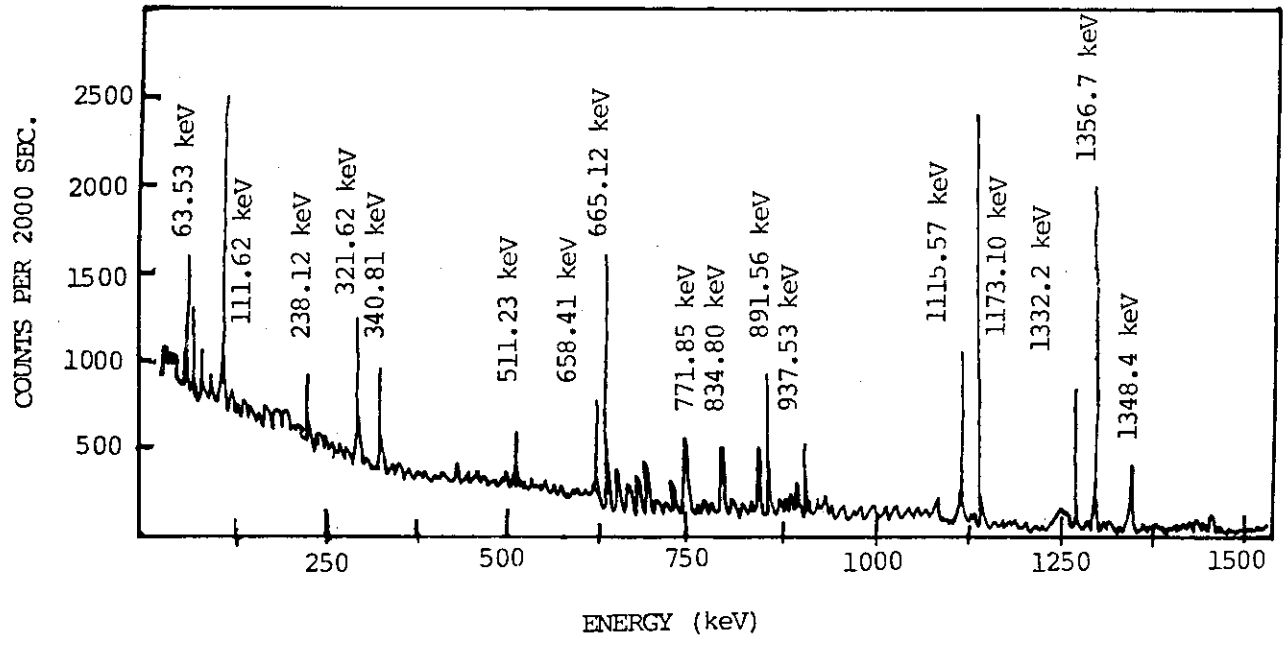

Fig. 4. Gamma energy spectrum of ion-exchange resins collected from on-line purification system on 26.7.91.

2. Measurement and Evaluation of Radioactive Corrosion Product Behaviour in Primary Sodium Circuits of JOYO

K. ITO, K. IIZAWA, K. TAKAHASHI*
M. A. ZULQUARNAIN**, S. SUZUKI and K. KINJO

O-arai Engineering Center
Power Reactor and Nuclear Fuel Development Corporation
4002 Narita, Oarai-machi, Ibaraki-ken, 311-13 JAPAN

ABSTRACT

In the experimental fast reactor JOYO, the radioactive corrosion product (CP) measurement has been conducted in the primary sodium circuits during each annual inspection. The measured data has been analyzed by the computer code "PSYCHE", which has been developed by PNC. Main results obtained from the measurements and/or calculations are as follows;

(1) The dominant CP nuclide is ^{54}Mn followed by ^{60}Co and ^{58}Co.
(2) Average surface gamma dose rate around the primary piping system at the 8th annual inspection is 0.96 mSv/h. The increasing rate of this value is 0.25 (mSv/h)/EFPY.
(3) The calculated deposition densities of ^{54}Mn and ^{60}Co agree with measured ones within a factor of 0.7 ~ 1.7.

INTRODUCTION

Radiation exposure of plant personnel during maintenance and repair works in an LMFBR plant mostly comes from the radionuclides of the radioactive corrosion product(CP) deposited on the inner surfaces of primary piping and components after sodium drain. Radioactive CPs are produced, transported and deposited in the primary sodium components and piping of an LMFBR plant as shown schematically in Fig.1. These radionuclides are produced in a fast reactor core mostly by (n,G) and (n,p) reactions on the constituent elements and impurities present in the stainless steel of fuel cladding, wrapper tube and other supporting structure of the core. These CP radionuclides are released into the circulating sodium either by bulk corrosion (i.e., surface loss) of the activated core materials or by diffusion of the radionuclides from the interior of steel. The released CP radionuclides are transported by the sodium coolant and then deposited on walls of primary piping, components and also the core subassemblies.

Therefore, dose rate from the radioactive CP deposited in the primary sodium circuits of JOYO has been measured. The computer code PSYCHE[2] developed

*On leave from Energy Research Laboratory, Hitachi,LTD.
**On leave from Reactor Operation and Maintenance Unit of Bangladesh Atomic Energy Commission

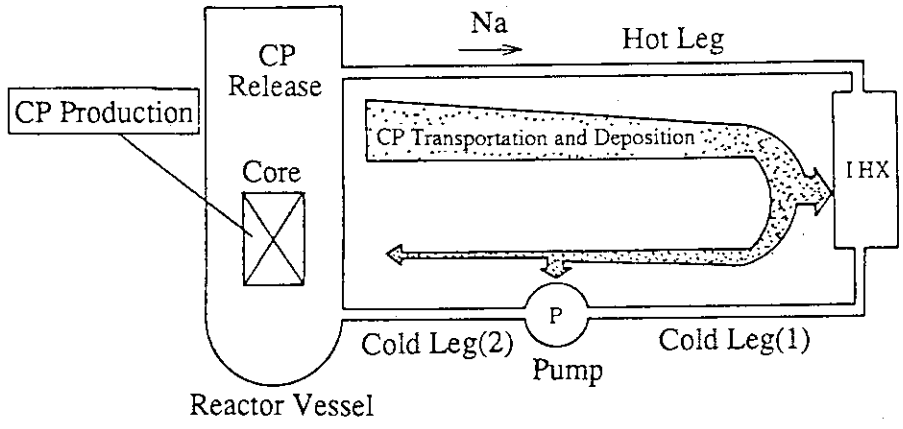

Fig.1 Schematic Diagram of CP Production, Transport and Deposition in an LMFBR Primary System

by PNC to evaluate CP behaviour in an LMFBR is validated with these measurement data.

Measurements were conducted by using both a pure germanium detector and calcium sulfate ($CaSO_4$(Tm)) thermo-luminescence dosimeters (TLDs) for CP deposition and surface dose rate in the primary sodium piping and components, after the sodium had been drained from the primary piping and components into the dump tank, except the reactor vessel.

This report presents the CP measurement and evaluation in the primary cooling system of JOYO.

DESCRIPTION OF JOYO

JOYO is a liquid sodium-cooled fast reactor of loop type with the power output of 100 MWt. JOYO achieved the first criticality in April, 1977. From the first criticality through the 23rd duty cycle, the accumulated reactor output reached 150 GWd.

JOYO consists of primary and secondary systems. Each system has two main cooling

Table 1 Specifications of Pure Ge Solid State Detector (SSD)

Item	Specifications
Detector Type	Coaxial Type of Pure Ge
Energy Resolution	1.75keV FWHM at 1332 keV of ^{60}Co G-ray
Photo peack to Compton Ratio	Peack/Compton=47.8
Detection Efficiency	13.7%

Table 2 Specifications of Themoluminescence Dosimeter (TLD)

Item	Specifications
TLD Type	UD-200S; $CaSO_4$(Tm)
Energy Response	±40% (> 30 keV)
Useful Range	0.1mR ~ 20 R

Table 3 Average Values of Deposition Densities within Different Regions (μCi/cm²)

	Hot Leg	Cold Leg(1)	Cold Leg(2)
^{54}Mn	0.89	2.18	4.46
^{60}Co	0.24	0.08	0.17
^{58}Co	0.07	0.04	0.06

Hot Leg : from the outlet of the reactor vessel to the inlet of IHX
Cold Leg(1) : from the outlet of IHX to the inlet of main pump
Cold Leg(2) : from the outlet of the main pump to the inlet of the reactor vessel

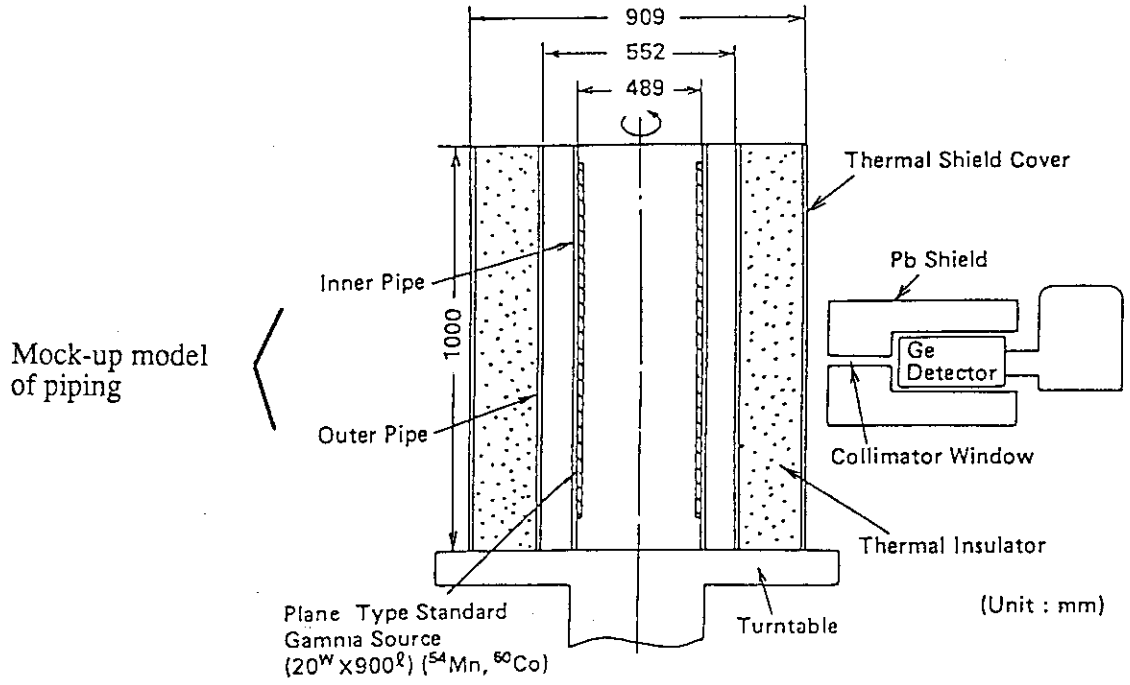

Fig.2 Calibration Arrangement for Ge-SSD System

loops (A and B), and one loop for auxiliary cooling of core and sodium purification with cold trap, respectively. The secondary sodium coolant is separated from the highly activated primary sodium coolant via intermediate heat exchangers (IHXs). Components in each main primary circuit are an IHX, a main pump, piping, the reactor tank itself and so on. Here the primary sodium enters the reactor vessel at temperature of 370 °C and flow rate of 1260 m^3/h/loop and comes out at 500 °C through the double-tubed piping. In order to facilitate the identification of different regions of primary piping, they have been designated as follows; Hot Leg is located from the outlet of the reactor vessel to the inlet of IHX, Cold Leg(1) from the outlet of IHX to the inlet of the primary pump and Cold Leg(2) from the outlet of the primary pump to the inlet of the reactor vessel. These piping designations are used to identify piping regions in this report. The sodium temperatures are 500 °C, 370 °C and 370 °C for Hot Leg, Cold Leg(1) and Cold Leg(2) regions, respectively. The sodium velocities are 1.9m/s, 2.3m/s and 4.8m/s along nominal inner diameter of piping of 20^B, 18^B and 12^B for Hot Leg, Cold Leg(1) and Cold Leg(2) regions, respectively.

MEASUREMENT METHODS

To ascertain the radioactive CP behaviour in JOYO two types of measurements have been made; gamma-ray spectroscopy from deposited CP radionuclides and the resulting dose rate measurement. Some additional measurements were made to calibrate TLDs and determine the effective decay constants for dose rate at some measurement points.

(1) Measurement of CP deposition density

Gamma spectra were measured at 16 locations to identify the deposited CP radionuclides and their deposition densities at the inner surfaces of the piping. A

pure Ge solid state detector (SSD) system and a suitable collimator assembly were used for this spectrum measurement. Table 1 indicates the specifications of the detector.

The CPS(counts per second) reading at each measurement point was converted into corresponding deposition density ($\mu Ci/cm^2$). The conversion factors ($\mu Ci/cm^2/CPS$) were determined earlier by the piping mock-up arrangements with plane type standard sources of ^{54}Mn and ^{60}Co in a way as shown in Fig.2 [1].

(2) Measurement of surface gamma dose rate

For determination of spatial dose rate distributions along the main primary piping, 93 locations have been marked and numbered in each loop at one meter intervals. At each location four TLDs were placed around the thermal insulator cover of the piping at 90 deg. intervals. TLDs were also placed around the IHXs, main primary pumps and over flow columns at different points in heights and angles in order to determine the gamma dose rate distribution at the surfaces of these components. The specifications of the TLD used in this measurement are given in Table 2. The effective decay constants of radioactive CP deposits were evaluated from two measurements of dose rates with time intervals.

RESULTS AND DISCUSSION

Results obtained from the measurement of radioactive CP deposit and gamma dose rate distribution during the 8th annual inspection are as follows;

(1) Deposition densities of CP radionuclides

In Fig.3 deposition densities of the CP radionuclides for Loop-A have been plotted v.s. distances along the piping measured from the outlet of the reactor vessel. From this figure it can be seen that ^{54}Mn is the most dominant CP radionuclide followed by ^{60}Co and ^{58}Co.

The average values for the deposition densities of these CP radionuclides within different regions of the primary circuit piping are given in Table 3. It may be shown from the above result that about 75% of the total accumulation of CPs in the Hot Leg region is rated for ^{54}Mn, 19% for ^{60}Co and the rest 6% for ^{58}Co. In the Cold Leg(1) region these percentages for ^{54}Mn, ^{60}Co and ^{58}Co depositions are rated about 95%, 3% and 2% and in the Cold Leg(2) region about 95%, 4% and 1%, respectively. From this table it can be seen that ^{54}Mn was found to be transferred and deposited dominantly in the Cold Leg regions, particularly in the Cold Leg(2). On the other hand, ^{60}Co and ^{58}Co are transferred and deposited dominantly in the Hot Leg region and also in the Cold Leg(2). It can be seen that these enhancements of CP deposition rates in the Cold Leg(2) are resulted from the sodium flow rate within its region being about two times as large as that within the Cold Leg(1). Deposition rates of CPs are enhanced as increasing sodium flow rate in the main piping.

(2) Gamma dose rate distributions along the main primary piping

In Fig.4 gamma dose rate distributions along the main primary sodium piping have been plotted v.s. distances measured from the outlet of the reactor vessel. This figure shows that the dose rate distribution patterns have that the patterns obtained from the previous measurements, except with some little deviations. In these distributions the peaks at the inlet and the outlet of the reactor vessel come from streaming gamma-rays from the core. Those around the piping near components come from radioactive CP deposits in the components of correspondence. The surface gamma dose rate averaged over the cold and the hot

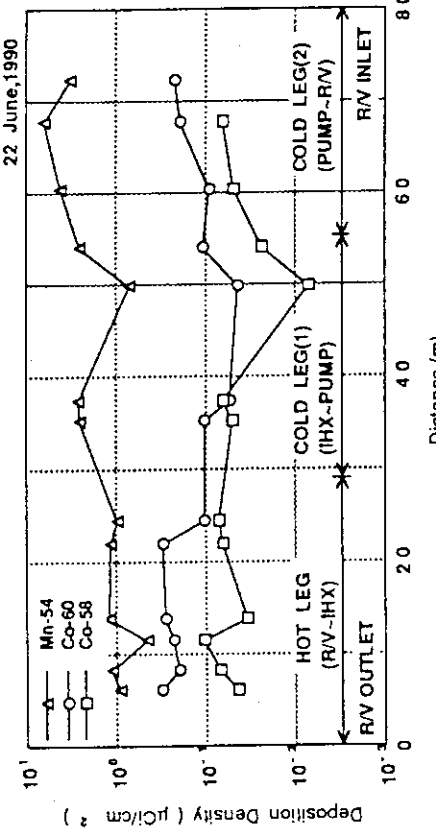

Fig. 3 Deposition of Corrosion Products Along the Main Primary Piping (Loop-A) Just after Reactor Shutdown of MK-II 20th Duty cycle operation (Cumulative Reactor Output: 131GWd)

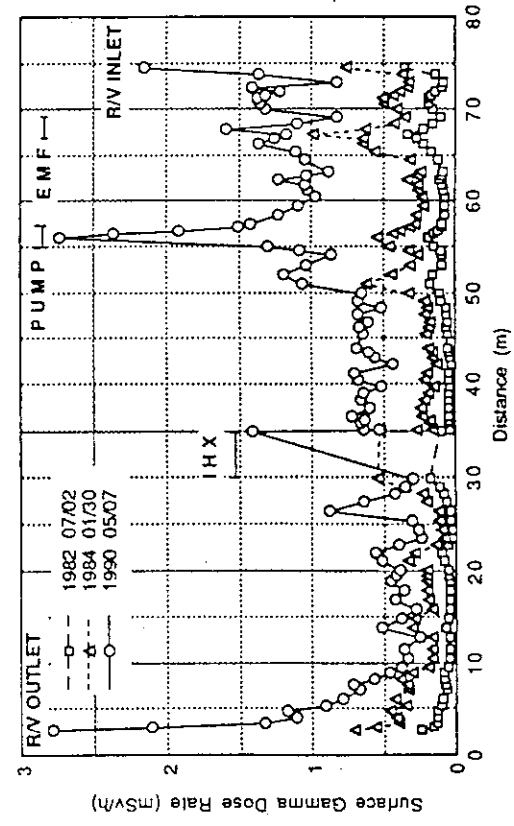

Fig. 4 Surface Gamma Dose Rate Distribution along Main Primary Piping (Loop-A) during Annual Inspections

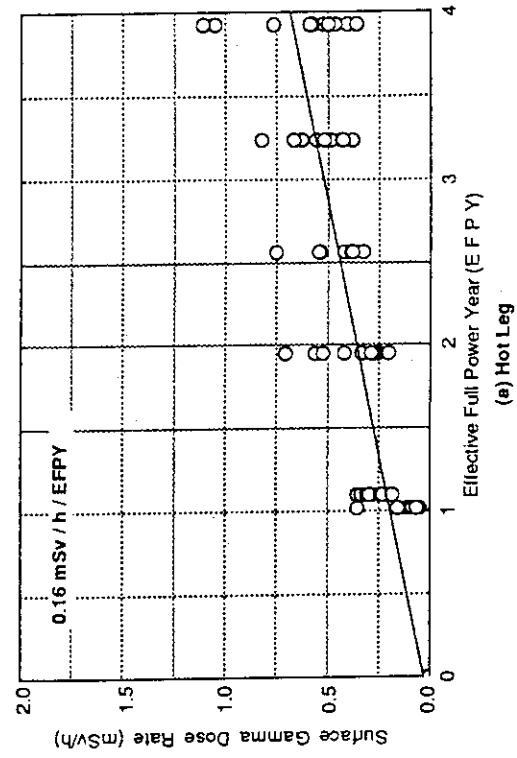

Fig.5 Increasing Rate of Surface Dose Rate at Main Primary Piping (Loop A and B Combined) with EFPY

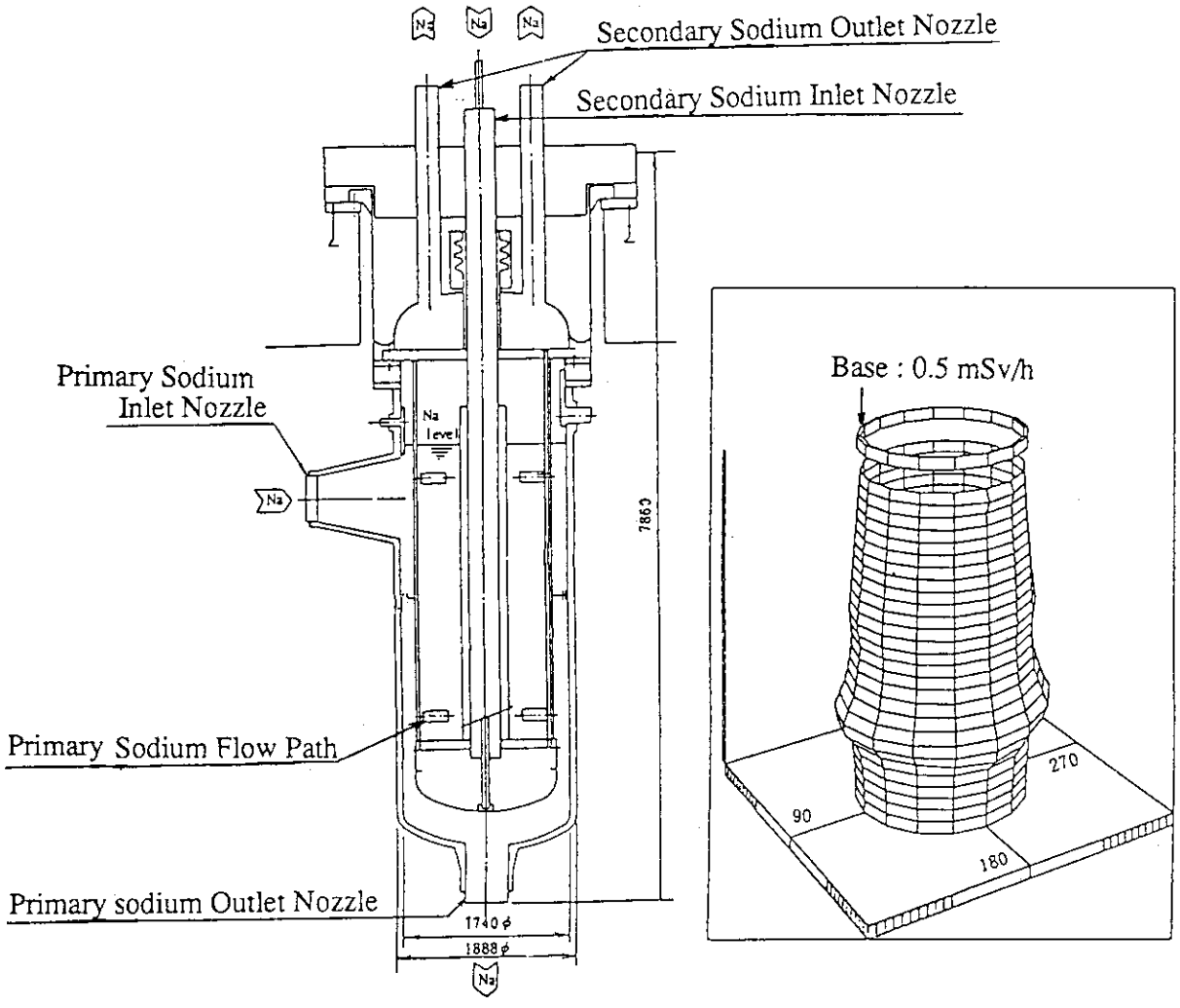

Fig.6 Surface Gamma Dose Rate Distribution around IHX(A)

legs of the primary cooling loops of A and B are 1.1 and 0.73 mSv/h, respectively, while that over the entire length (combined all cold and hot legs of both the loops) is 0.96 mSv/h.

The increasing rates of the averaged surface gamma dose rates for different regions of main primary piping, Hot Leg and Cold Leg(2), are shown in Fig.5 as a function of effective full power years (EFPY). Applying the least square curve fitting technique, increasing rates of dose rates per EFPY are obtained. These values are 0.16 (mSv/h)/EFPY and 0.33 (mSv/h)/EFPY for Hot Leg and Cold Leg, respectively. It means that the rate of build-up of gamma dose rate within the Cold Leg region is about twice as much as that within the Hot Leg region. These dose rates distribution and build-up are corresponding to ^{54}Mn deposition behaviour.

(3) Gamma dose rate distribution at the surfaces of primary components

The surface dose rate distribution around components during the 8th annual inspection has been measured. Figure 6 shows the dose rate distribution for IHX-A. From this figure it can be seen that maximum dose rate is found near the flow path of exit. This distribution is compared with the previous and found to be of similar nature.

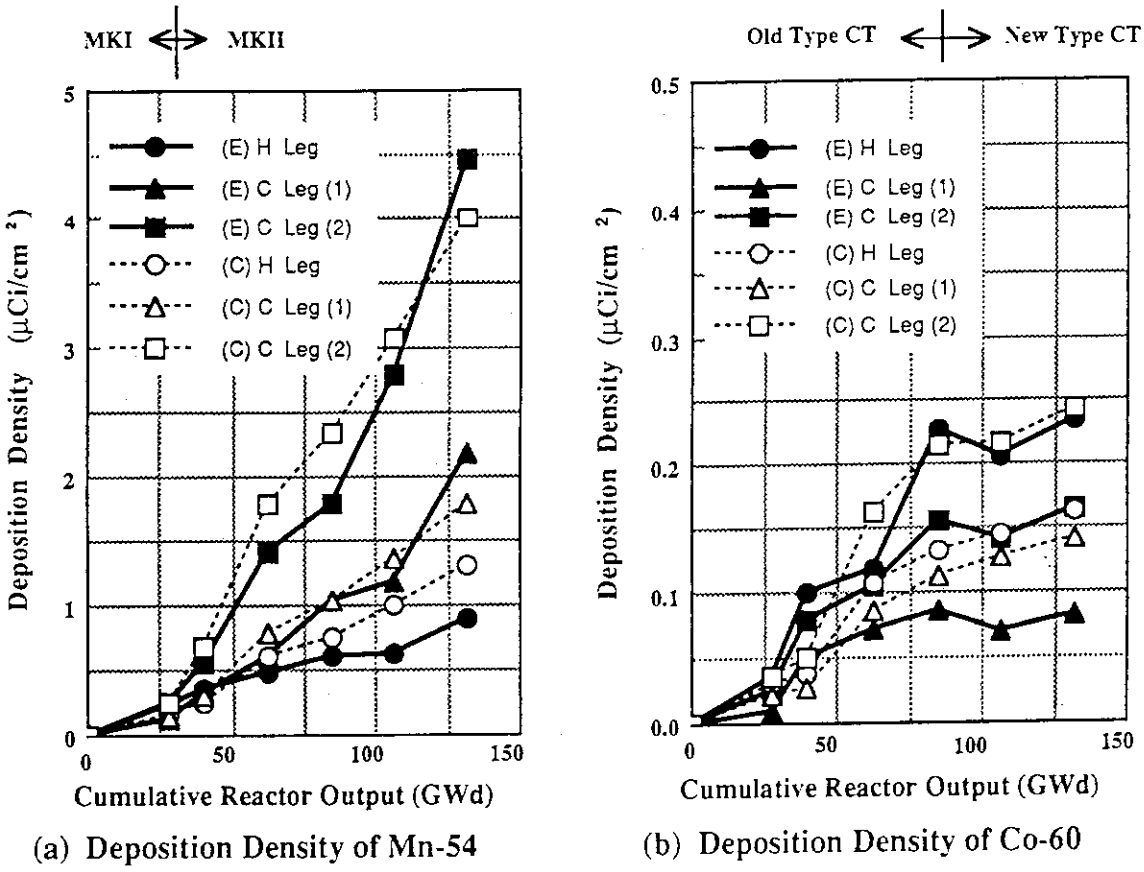

Fig.7 Comparison of Measured (E) and Calculated (C) Values of CP Buildup in Main Primary Loop Piping (A)

(4) Comparison of measured and calculated values of CP radionuclides behaviour

Deposition densities of ^{54}Mn and ^{60}Co measured within different piping regions of Loop-A are compared with the calculational results, using PSYCHE, which predicts build-up and distributions of CP radionuclides, and associated gamma dose rate distribution in LMFBR primary circuits. The calculated value (C) for deposition density of ^{54}Mn was found to agree very well with the measured value(E) for Cold Leg(2) of the piping. Here the C/E ratio is 0.9. For Cold Leg(1) this ratio is 0.8, while for Hot Leg it is 1.5. For ^{60}Co the C/E ratio is 0.7 for Hot Leg, while for Cold Leg(1) and Cold Leg(2) these are 1.7 and 1.6, respec

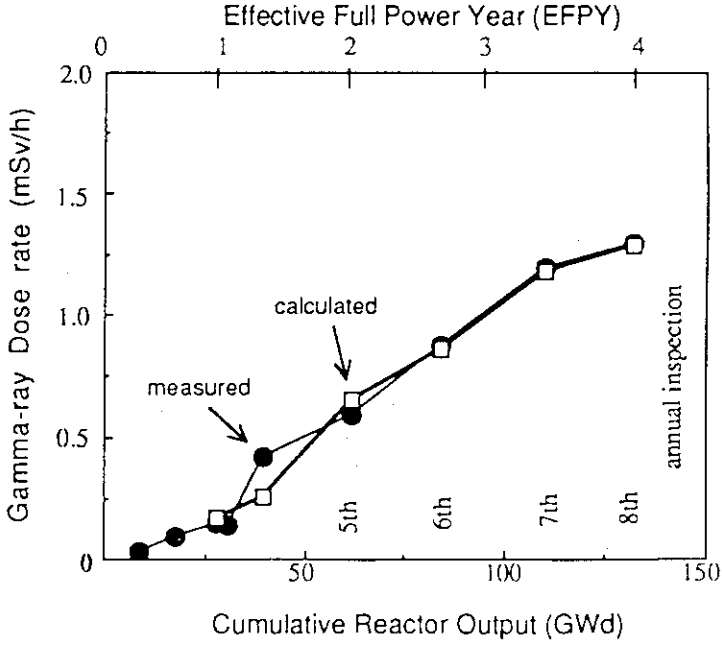

Fig.8 Comparison of Measured (E) and Calculated (C) Values of Surface Gamma-ray Dose Rate Build-up within Cold Leg(2) During Annual Inspections

tively. The above results show graphically in Fig.7.

In Fig.8 the calculated result for the surface gamma dose rate at the Cold Leg(2) of Loop-A is also compared with the corresponding measured result. The C/E ratio is 1.1.

CONCLUSION

- The dominant CP radionuclide is ^{54}Mn followed by ^{60}Co and ^{58}Co. ^{54}Mn deposits mostly in the Cold Leg region, particularly in the Cold Leg(2) region. On the other hand, ^{60}Co and ^{58}Co deposit preferentially in the Hot Leg region and Cold Leg(2) region. These CP deposition rates are enhanced by increasing the sodium flow rate.

- The surface gamma dose rates averaged over the primary loops are 1.1 mSv/h for the Cold Leg region and 0.73 mSv/h for the Hot Leg region , while that over the entire length (all cold and hot legs of both the loops combined) is 0.96 mSv/h.

  The increasing rate of surface gamma dose rate for Cold Leg region is 0.33 (mSv/h)/EFPY. The rate of build-up of gamma dose rate in the Cold Leg region is about twice as high as that in the Hot Leg region.

  The surface gamma dose rate distribution in IHX-A shows the maximum value near the flow path of exit and its patterns follows the previous measurement works.

- The calculated deposition densities agree with measured ones within a factor of 0.8 ~ 1.5 for ^{54}Mn and with in a factor of 0.7 ~ 1.7 for ^{60}Co. On the other hand, the calculated surface gamma dose rate at the primary piping agrees with measured one within a factor of 1.1.

REFERENCES

(1) K. Ito et al., "Radioactive Corrosion Product Behaviour in LMFBR(1) - Measure ments Results of CP Behaviour in Primary Circuits of JOYO" in Japanese, 1991 Annual Meeting of the Atomic Energy Society of Japan (Proceeding), p.297. (1991)

(2) K. Iizawa et al., "Radioactive Corrosion Product Behaviour in LMFBR(2) - Calculation and Evaluation for CP Behaviour in JOYO", ibid.,p.298. (1991)

3. Design of Fuel Failure Detection System for Multipurpose Reactor GA. SIWABESSY

Saiful SUJALMO, Iman KUNTORO

Badan Tenaga Atom Nasional. Jl. K.H. Abdul Rochim,
Kuningan Barat, Mampang Prapatan. PO.BOX 85 KBY.
Jakarta 12710, Indonesia.

Mitsugu SATO, Masahiko ISSHIKI

Department of Research Reactor
Tokai Research Establishment, JAERI
Tokaimura, Naka-gun, Ibaraki-ken 319-11, Japan

ABSTRACT

A fuel failure detection system (FFDS) has been designed for the Reactor GA. Siwabessy. The FFDS is aimed to detect fuel failure by observing delayed neutron released by fission products such as N-17, I-137, Br-87 and Br-88 in the primary cooling system. The delayed neutrons will be detected by using four neutron detectors, type BF-3, which are located inside a Sampling Tank. The detector location has been determined and the location is associated with the transit time from the reactor core outlet to the Sampling Tank, which is approximately 60 seconds. The neutron detection efficiency was calculated by using a computer code named MORSE. The FFDS has the capability to detect as quickly as possible, even a small failure of a fuel element occuring in the reactor core. Therefore the presence of FFDS in a reactor must be considered, in order to prevent further progress if the fuel failure occurs.

INTRODUCTION

The multipurpose reactor GA. Siwabessy is the newest research reactor in Indonesia. (1) The designed thermal power is 30 MW, with the neutron flux approximately 2.5 x 10^{14} n/cm^2.sec. in the centre irradiation position of the core.

The MTR type fuel elements with < 20 % enriched Uranium are used and recently 40 standard fuel elements and 8 control elements are loaded in the reactor core.

The reactor core is located at the bottom of the reactor pool. The reactor pool is a swimming pool type with diameter 5 m, and depth 13 m. The heat generated in the reactor core is removed by two primary pumps. The primary coolant flows downwards through the core and reflector to a delay chamber, valve chamber, heat exchangers and returns to the reactor pool.

For continuous operation of the reactor in a safe manner, it is necessary to monitor the fuel integrity during reactor operation. In case of fuel failure, it is necessary to detect at the most early stage. As the reactor GA Siwabessy is a pool type reactor, delayed neutron detection method is an easy and simply way for detection of fuel failure.

Determination of detector location, which is associated with transit time between the reactor core outlet and the detector location, evaluation of the back ground of neutron density, neutron detection efficiency and other general problems associated with the basic design of FFDS will be discussed briefly on this paper.

DETECTION METHOD

The integrity of the fuel element in the reactor core must be maintained during reactor operation, and fission products are kept in its fuel matrix.

When a fuel failure occurs, the primary coolant which is passing through the reactor core catches the released fission products. And after a few second, the fission product will decay and emit some neutrons until the fission product reaches its equilibrium concentration. During the decay, the emitted neutrons will be detected by the installed neutron detectors on the suction pipe of the primary cooling system. When the detection count rates increase a few times higher than the back ground value, [2] it indicates the fuel failure in the reactor core. Figure 1 shows the circuit diagram of the FFDS which will be installed in the reactor GA. Siwabessy.

DETECTOR LOCATION

The transit time between reactor core outlet and the detector location has been calculated. The detector location must be located approximately 60 seconds away from the reactor core outlet. At this time the fission product such as Br-87 reaches its decay time. For other fission products like N-17, I-137, and Br-88, their contribution on this measurement is relatively small, but must be taken into account.

The transit time depends on the primary coolant flow rates. Table 1 below gives the transit time from the reactor core outlet to the primary pumps at which the branch pipe to the FFDS is located.

The transit time from the pump to the detector location (t_4) can be ajusted by the installed regulating valve. Therefore the total transit time from the reactor core outlet to the detector location inside the sampling tank can be achieved.

Figure 2 shows the primary coolant flow scheme [1] and the transit time from the reactor core outlet to the sampling tank. The sampling tank configuration contains the neutron detectors, as shown in Figure 3 .

Table 1. The Transit Time From The Reactor Core to the FFDS Sampling Tank.

Flow rates (M3/H)	t1 (sec)	t2 (sec)	t3 (sec)
3000	3.13	47.09	7.33
3050	3.09	46.33	7.21
3100	3.04	45.58	7.09
3150	2.99	44.86	6.98
3200	2.94	44.16	6.87
3250	2.85	43.48	6.76
3300	2.81	42.82	6.66
3350	2.77	42.18	6.56

Notes :
t1 : transit time from core outlet to delay chamber
t2 : transit time in the delay chamber
t3 : transit time from delay chamber to the pumps

INSTRUMENTATION

The fuel failure detection system instrumentation consist of [2] :

1. BF-3, Counter	4 units	5. Lin. amplifier	1 unit
2. Pre Amplifier	4 units	6. Discriminator	1 unit
3. HV Power Supply	4 units	7. C R M	1 unit
4. Sum amplifier / mixer	1 unit	8. Recoder	1 unit

The arrangement of the neutron detection system is shown in Figure 4, and the BF3 counter specification which was taken into detection efficiency calculation are as follows [3] :

1. Manufacturer : Fuji Electric Company
2. Type : NBB 52151
3. Neutron sensetivity : 094 (cps/u/cm2/sec)
4. Measuring range : 10^{-1} - 10^{5}(n/cm^2.sec)
5. Plato range : 150 volt
6. Plato slope : 3 % /100 volt
7. Resistant : 10^{10} ohm
8. Cathode : OFC (Oxigen Free Cupper)
9. Anode / diameter : Tungtens Wire / 0,05 mm
10. Gas : BF3 (96% 10B)
11. Gas Pressure : 15 cm Hg
12. Voltage : 1650 Volt
13. Temperature : -5°C - 50°C
14. Lifetime : 10^{10} counts
15. Diameter : 2.5 cm
16. Length : 26.6 cm
17. Sentivity length : 12.0 cm

Other instrumentation listed above will not be described on this paper. And as shown in Figure 1, detectors, HV power supplies and the pre ampli-

fiers are located in the primary cell. Other instrumentation like mixer, amplifier, discrimanator, CRM, and recoder will be located the main control room.

EVALUATION OF BACK GROUND DELAYED NEUTRON DENSITY

Detectable nuclide of the FFDS in the main coolant is N-17 or Br-87, Br-88 and I-137 as fission products released from the fuel failure or only from the fuel element surface contamination.

Delayed neutron emitted from N-17 is pure back ground value of the light water coolant and another delayed neutron arising from the surface contamination as the fission products of U-235. If the fuel element has a surface contamination value of 5/ug/100 cm^2, it can be calculated that the back ground of delayed neutron density emitted from N-17, Br-87, Br-88 and I-137 is obtained from the following formulas (2) :

$$I_{Br87} = 1/2W \cdot Y_{Br87/100} \cdot \sigma f \cdot N \cdot \phi th \cdot (\lambda Se87 \cdot \lambda Br87)/(\lambda Se87 - \lambda Br87)(e^{-\lambda Br87.t} - e^{-\lambda Se87.t})$$

$$I_{Br88} = 1/2W \cdot Y_{Br88/100} \cdot \sigma f \cdot N \cdot \phi th \cdot \lambda Br88 \cdot e^{-\lambda Br88.t}$$

$$I_{I137} = 1/2W \cdot Y_{I137/100} \cdot \sigma f \cdot N \cdot \phi th \cdot \lambda I137 \cdot e^{-\lambda I137.t}$$

$$I_{N17} = \Sigma_{O17} \cdot \phi f \cdot (1 - e^{-\lambda N17.t1}) \; e^{-\lambda N17.t}$$

In the above formulas N is total surface contamination value of all loaded fuel elements in the core. The value N is given by,

$$N = 1/235.\ 6{,}02.10^{23}.f_u.S_f$$

Other parameters are as follows :

I_{Br87} : Br-87 neutron density ($n.cm^{-3}.sec^{-1}$)
I_{Br88} : Br-88 neutron density ($n.cm^{-3}.sec^{-1}$)
I_{I137} : I-137 neutron density ($n.cm^{-3}.sec^{-1}$)
I_{N17} : N-17 neutron density ($n.cm^{-3}.sec^{-1}$)
ϕf : Neutron flux over the energy 8.5 Mev at max. power
ϕth : Av. thermal neutron flux at max. power
W : Flow rate of the primary coolant
t1 : Transit time of the primary coolant in the fuel meat zone
t : Transit time from the core to detector
Σ_{O17} : Macroscopic cross section
λx : Decay constant
Y_x : Yield
σf : Microscopic cross section
fu : Total surface area of all looded fuel element plates
Sf : Surface contamination density of the fuel element

The calculation result given on the following Table 2 can be used as an initial (back ground) count rates value for FFDS in the research reactor GA. Siwabessy.

Table 2. Calculation Results of the Back Ground Count Rates of Delayed Neutron Density

Detectable nuclides	Half life time (sec)	Neutron density (n/cm3.sec)
N-17	4.14	1.99
Br-87	55.60	3.71
Br-88	16.60	4.37
I-137	24.50	10.86
Total	-------	20.93

CALCULATION OF NEUTRON DETECTION EFFICIENCY

The neutron detection effeciency was calculated using a Monte Carlo multi group neutron and gamma ray transport code with combinatorial geometry named MORSE [4]. The calculation was done with a given detection geometry as shown in Figure 4.

A standard neutron source Cf-252 with the activity of about 2/uCi was used in the calculation. This standard neutron source has the similar characteristics with the delayed neutron emitted from fission products released during fuel failure [5].

The macrospic cross section data of 26 energy groups for each material in the FFDS Sampling Tank has been calculated using a program named MACRO.

The calculation results are shown in Table 3, which gives different values of neutron detection efficiency between point neutron source and homogeneous source, including the reaction rates density, the fractional standard deviation (FSD), and the detector active volume.

Figure 5 shows the sampling tank geometry using the point source and Figure 6 for the homogeneous source.

Table 3. Neutron Detection Effeciency using the MORSE Code

Geometry	Source Form	Reaction Rates Density (R/Cm3)	Counting Efficiency %	FSD %	Detector Act.Vol. (Cm3)
Figure.5	Point	6.980×10^{-5}	0.287	2.5	42.778
Figure.6	Homogen	1.601×10^{-5}	0.047	2.6	

CONCLUSION

The most suitable method for the FFDS which will be installed in the reactor GA Siwabessy is the delayed neutron measurement system. The neutron detector are submerged in a sampling tank (Figure.3)

The FFDS will be installed using 4 BF_3 counters located in the suction line of the primary cooling system between the primary pumps and the header in the primary cell.

From the neutron detection efficiency calculation, the BF_3 counter has a small detection efficiency but have the following advantages :

a. Available in the world market;

b. Standardized Operational experience of the reactor;

c. Long lifetime, about 10^{10} Counts;

d. Gas pressure is low; the adaptation to severe environmental conditions, for example high temperature;

f. Gamma ray discrimination capability is high (+ 12 - 1000 R/h).

REFERENCES

1. Safety Analysis Report MPR-30 GA. Siwabessy. Vol 3, Rev.7 BATAN, INDONESIA, September, 1989.

2. Mitsugo Sato, et al., "a Study on the FFD System for RSG-GA. Siwabessy, January, 1991.

3. Saiful Sujalmo, "Training Activities Report", Department of Research Reactor, Tokai Research Establishment, JAERI, August, 1991.

4. J.Briesmeister, "MCNP-A General Monte Carlo Code for Neutron and Photon Transport, versin 3A, "LA-7396-M, Rev 2,Sep 1986.

5. Personal Communication with Mr. Mitsuo HARUYAMA et al, Reactor Instrumentation Laboratory, Reactor Engineering Division, JAERI, July 1991.

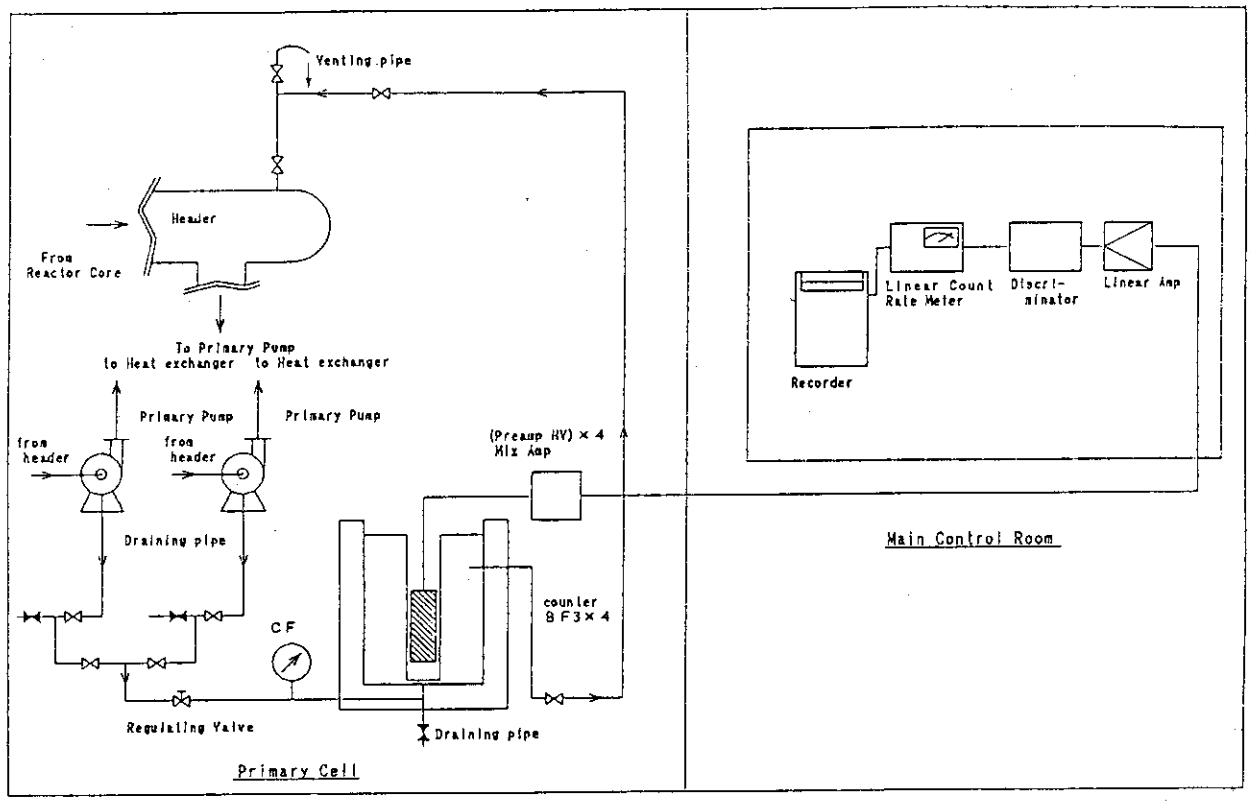

Fig －1－ FFDS Circuit Diagram

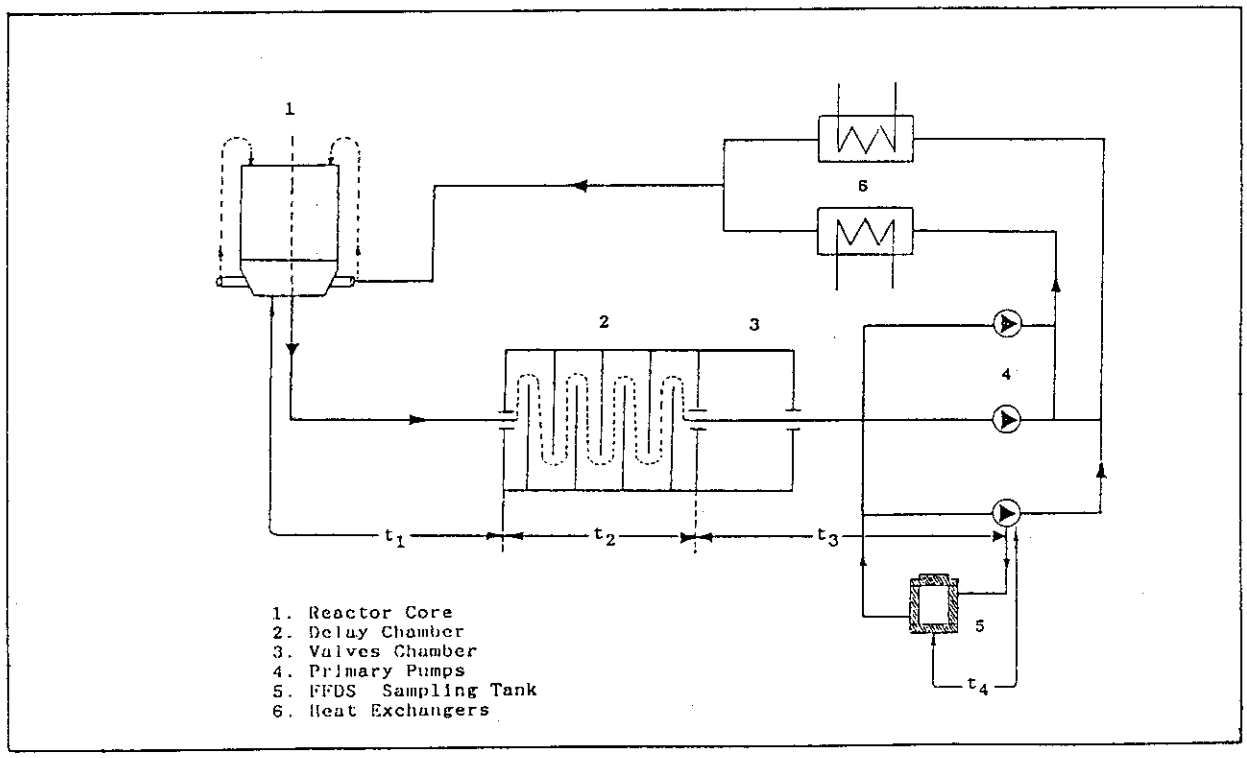

Fig －2－ The primary coolant flowscheme and transit time from reactor core to the sampling tank

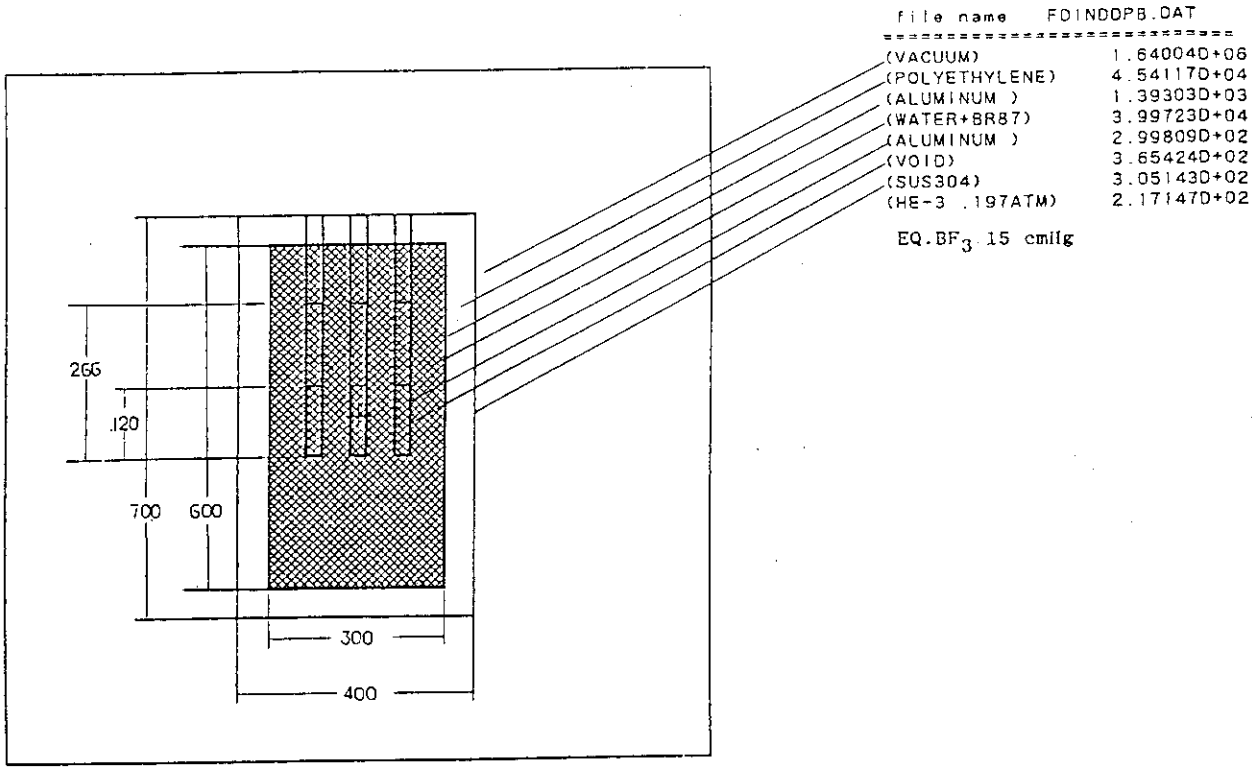

Fig -3- FFDS Sampling Tank

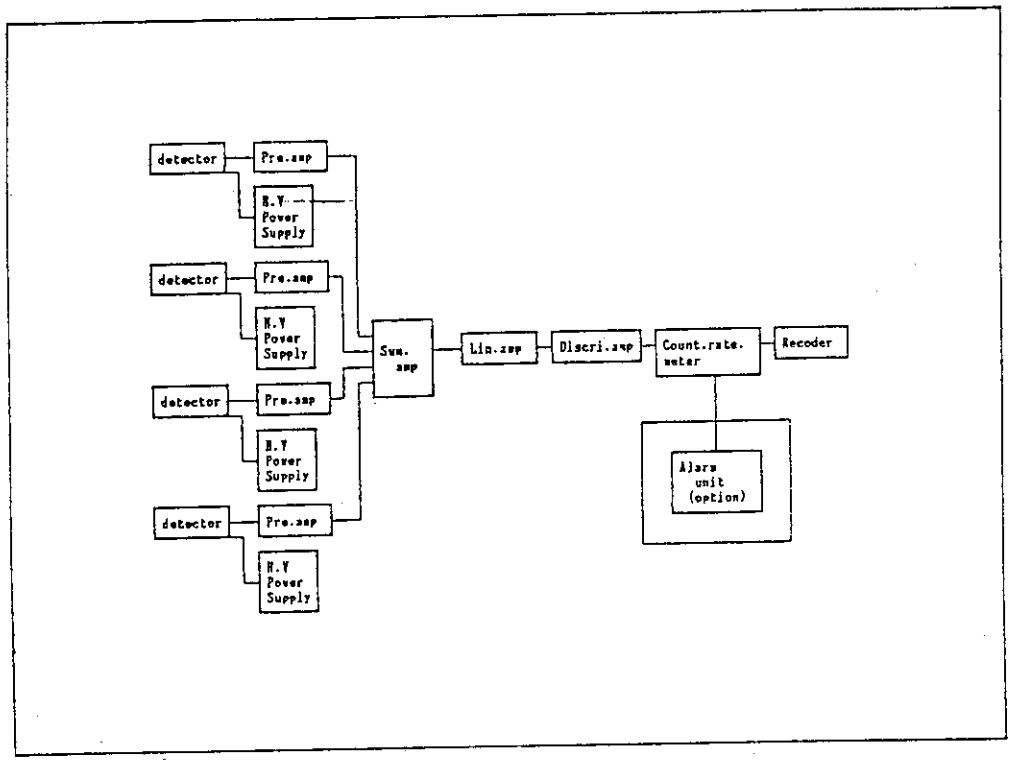

Fig -4- The Arrangement of Neutron Detection System

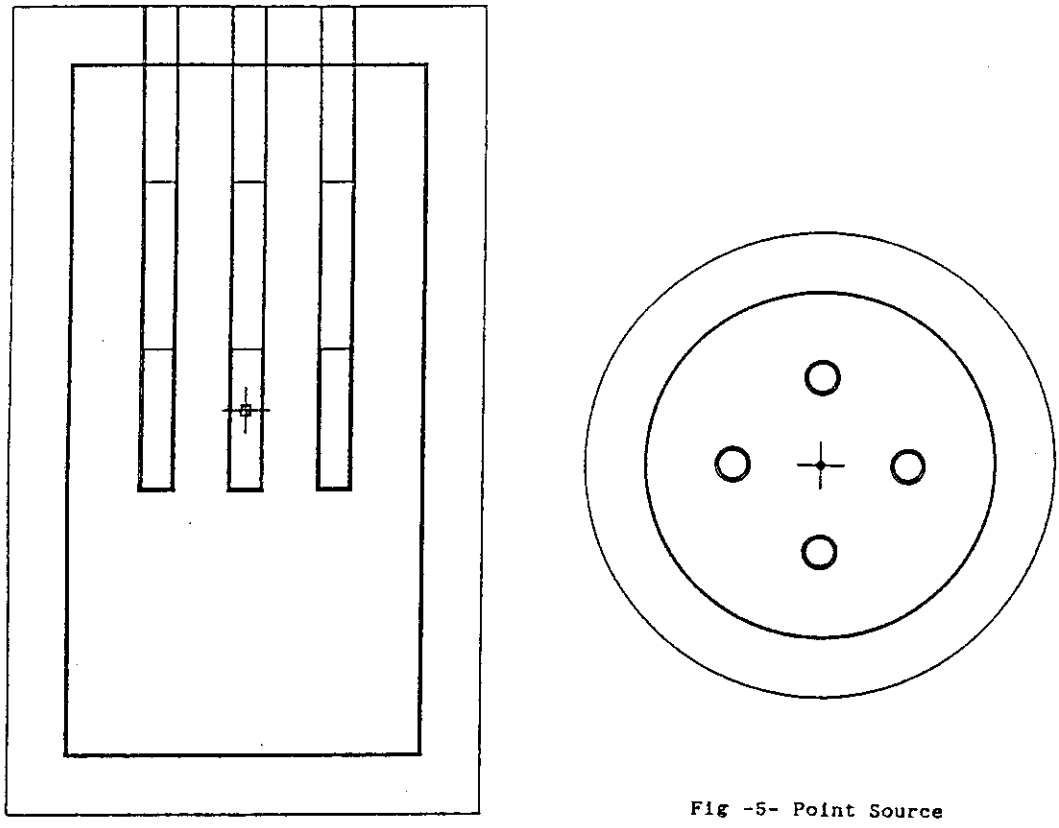

Fig -5- Point Source

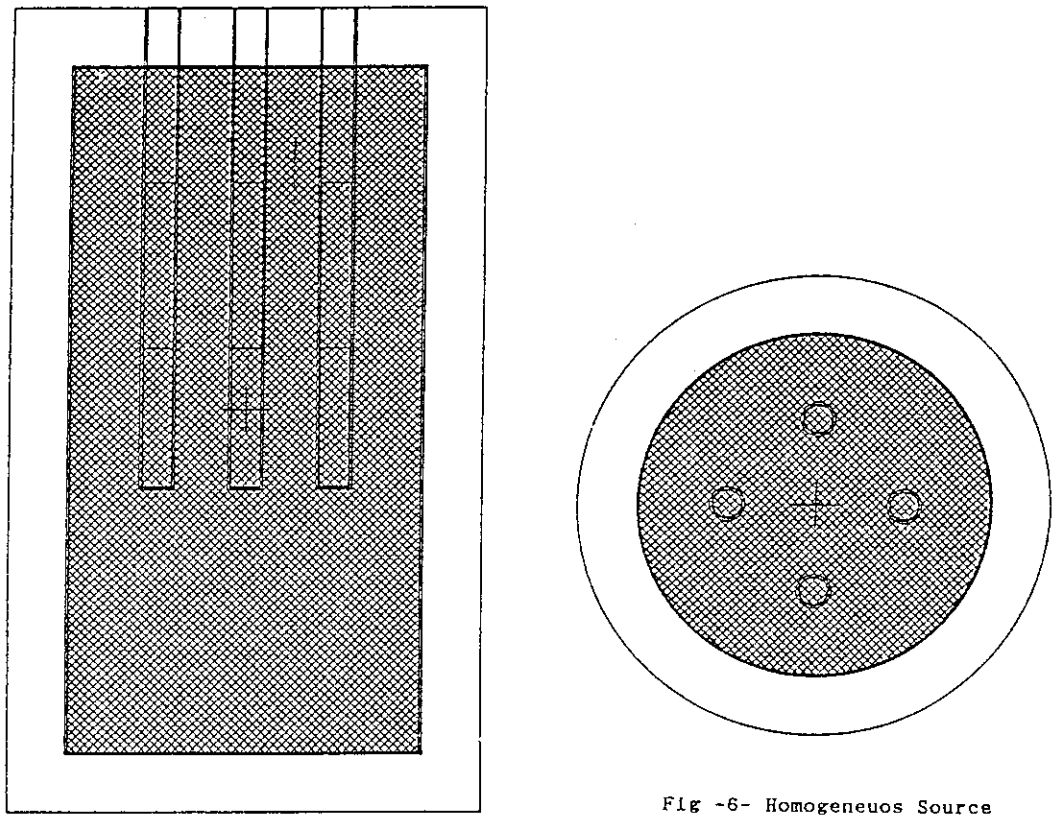

Fig -6- Homogeneuos Source

4. Studies on Fuel Failure Detection in Rikkyo Research Reactor

T. MATSUURA, Shu H. HAYASHI, S. HARASAWA, K. TOMURA

Institute for Atomic Energy, Rikkyo University,
2-5-1, Nagasaka, Yokosuka, 240-01 Japan

ABSTRACT

Studies on fuel failure detection have been made since 1986 in Rikkyo Research Reactor. One of the methods is the monitoring of the trace concentration of fission products appearing in the air on the surface of the water tank of the reactor. The interested radionuclides here are ^{89}Rb and ^{138}Cs, which are the daughter nuclides of the FP rare gas nuclides, ^{89}Kr and ^{138}Xe, respectively and have the half lives of 15.2 min and 32.2 min respectively. They are detected on a filter paper attached on a conventional dust sampler, by sucking the air of the surface of the water for 15 ～30 min during reactor operation (100 kW). In this presentation are reported the results of an attempt to increase the sensitivity of detecting these nuclides by introducing nitrogen gas bubbles into the water. The bubbling of the gas increased the sensitivity as much as several times compared with the case without bubbling. These measurements are giving us the "backgound" concentration, the order of which is almost unchanged for these several years,--in 10 $^{-6}$ Bq/cm^3. The origin of these nuclides is considered to be not from the fuel but from the uranium contained as an impurity in the reactor material in the core.

INTRODUCTION

Studies on fuel failure detection have been made since 1986 in Rikkyo Research Reactor (TRIGA, 100kW) in four approaches: 1) monitoring of fission products (FP) in the air covering the reactor cooling water, (2) monitoring of FP in the water, (3) the development of a "sniffer" device for detecting the location of failure fuel element when some anomaly is found in routine monitoring, and (4) the development of "sipping" inspection method of the fuel element.[1, 2]

In the first method, the fission-originating two radionulides, ^{89}Rb, and ^{138}Cs, contained as an aerosol in the air covering the water in the reactor tank, are caught on a filter paper through which the air is sucked for sampling. These are the daughters of the rare gas fission products, ^{89}Kr ($T_{1/2}$=3.18 min) and ^{138}Xe ($T_{1/2}$ =14.1 min) respectively, which are produced somewhere in the reactor core and dissolved into the water. This method has been regarded to be the most sensitive for the routine monitoring of the fuel elements in several TRIGA facilities.[3, 4]

We have recently attempted to improve the detection efficiency in this method, by introducing nitrogen gas into the reactor water to purge the fission rare gases dissolved in the water. By employing this "bubbling method", the sensitivity of

detection increased as much as several times, compared with the cases without bubbling of the gas. The results obtained up to present is reported in this paper.

EXPERIMENTAL

Fig. 1 shows the schematic setup of the system. During reactor irradiation (100kW), nitrogen gas was introduced into the reactor water through a porous exit in various flow rate (from ~0.2 to ~10 liter/min). The depth of the nitrogen gas exit in the reactor tank was varied also (from~430 to ~100 cm, from the top of the water surface). During introducing nitrogen gas, the air which covers the primary cooling water was sucked by a conventional dust sampler equipped with a filter paper by the flow rate of ~500 liter/min. After sampling the air for 15 or 30 min, the radioactivity of the filter paper was measured with a Ge-Li detector with MCA, by counting the photo-peaks of 1032 and 1434 keV due to ^{89}Rb and ^{138}Cs, respectively. The data were normalized to the time of the end of sampling, using the half lives of these nuclides, i.e. 15.2 min and 32.2 min respectively. The experiment without bubbling was also made, and the results were compared.

RESULTS

Preliminary experiments

Table 1 shows the data in the experiments done in fiscal 1990. From these data the followings were observed:
(1) The concentration of ^{138}Cs is almost always higher than that of ^{89}Rb.
(2) The bubbling of nitrogen gas clearly increased the detecting sensitivity of these nuclides, as shown in the ratio of the activities when bubbled to those without bubbling. The ratio, which is shown in the parentheses in the table, increased about three times compared with the case of no bubbling on the average.

Dependence on the position of the exit and flow rate of introducing gas

The dependence on the position of the exit of the introducing gas and on the flow rate was explored in the experiments done on June 14 and July 26, 1991. The data are shown in Figs. (a) and (b). The experiments were done at three different depths, 427cm, 214cm, and 105cm from the top of water level. The flow rate was varied from~0.5 to ~5 l/min. What were observed are:
(1) By the bubbling, the detection sensitivity increased as much as 4 or 5 times compared with the case of no bubbling.
(2) As the depth of exit of the bubbling gas increases, the ratio increased.
(3) The effect of radial direction at the same depth of the exit in the water seems to be unimportant. Also, the effect of on-or-off of the cooling pump did not change the efficiency of collecting the radioactivity.

We are attempting to continue the study on these effects more extensively.

Annual change of the FP concentration

In Fig. 3 is plotted the average concentration of these two radionuclides

Table 1. Radioactivity in the air and the effect of bubbling

Date determined	^{89}Rb (cpm)*	^{138}Cs (cpm)*	Condition of bubbling	
			Depth(m)	Flow rate(l/min)
April 16, 1990	11.0	12.5	(no Bubbling)	
Dec. 5, 1990	3.0	5.9	(no Bubbling)	
	20.8 (6.3)	17.0 (2.8)	4.5	~0.2
Dec. 13, 1990	8.0	10.1	(no Bubbling)	
	22.0 (2.7)	40.7 (4.1)	1.8	~5
Jan. 23, 1991	11.5	6.8	(no Bubbling)	
	23.7 (2.1)	25.8 (3.8)	1.8	~10
Feb. 6, 1991	5.9	6.5	(no Bubbling)	
	13.9 (2.4)	19.6 (3.0)	1.8	~2
Average	7.9	8.4	(no Bubbling)	
	20.1	25.5		

*The number shows the activities (normalized to the value just after the end of sampling) of the radionuclides collected on a filter paper, through which the air was sampled for 30 minutes by a dust sampler in the flow rate of 500 ml/min. The underlined value is for the case of nitrogen bubbling into the water. The value in the parentheses is the ratio compared with the case of no bubbling.

detected for the case of no bubbling as a function of calendar year, since 1986. It can be seen that the concentration detected in the air is almost constant in the order, 10^{-7} 10^{-6} Bq/cc.

OTHER INFORMATION AND CONSIDERATION

As to the origin of the FP found in the reactor coolant

It is important to investigate where is the origin of these fission products. What seems to be plausible at present is that these fission products come from the uranium which is contained as an impurity in the constructing materials in the core such as aluminum, not from the fuel. There are several reasons:
(1) Some FP, such as ^{131}I, are found in the cooling water of our reactor[1,2] and in Musashi Reactor,[5] which is the same type as ours. It is to be noted that in the latter reactor, where all the aluminum-clad fuel elements were replaced by stainless steel-clad ones, the FP can still be detected.[6]
(2) In JMTR Tokai, the FP (^{131}I) found in the primary cooling system was identified as from the uranium contained in the amount of as much as 42 ppm as an impurity in the beryllium reflector.[7]
(3) It has been reported that the "reactor grade" aluminum manufactured about thirty five years ago contains 1.7 ppm uranium as an impurity.[8]

Cases of fuel failure in TRIGA

Table 2 shows the cases of fuel failure which were reported in the literature.

This shows that most cases of the fuel failure occurred in the "pulsed" reactors. (These data have already been reported on the occasion of ref. 2.)

CONCLUDING REMARKS

To be sure its saftey, most research reactor facilities have the monitoring system for observing the state of the fuel elements, called CAM (continuous air monitor). The present study will be a useful information for constructing such a system, which has an improved efficiency in detecting FP. We hope to develop such a system, in which the routine monitoring for fuel element will be performed semi-automatically with high sensitivity.

From another point of view, as an active source term of the short lived fission products easily available during reactor operation, the present study may afford an interesting example to be performed in relation to the reactor safety, such as on the behavior of short lived FP in the water.

Acknowledgements

The experiments in Dec. 1990 were performed as a joint research between the staff of NSRR Operation Division, Nuclear Safety Research Center of JAERI (Chief: Dr. O. Horiki) and the authors. Some of the data in 1988 were obtained by the cooperation of Mr. B. Harutomo of Indonesia. The authors wish to thank Prof. Y. Takami, Chief of the Reactor Operating Staff, for his support and advice for this study. They also wish to thank Dr. R. H. Chesworth of GA Technologies for his kind check of the cases listed in Table 2.

REFERENCES

1. T. Matsuura, T. Nagahara, M. Hattori, K. Kawaguchi, "Plan of Studies on Fuel Failure Detection in Rikkyo Research Reactor": Proc. First Asian Symp. on Research Reactors, Tokyo, Nov. 18--21, 1986, p. 259.
2. T. Matsuura, "Studies on Fuel Failure Detection in Rikkyo Research Reactor": Proc. Japan-China Symp. on Research and Test Reactors, Tokai, Feb.-Mar., 1988, JAERI M 83-220 (1988), p. 220.
3. J. Kuusi, S. Salmenhaara, "Experiences on the Fuel Management during the Twenty Years of Operation of the Finnish TRIGA Reactor": TOC-15, 8-21 (1982).
4. B. Dodd, A. G. Johnson, "Searching for a Possible Fuel Element Leak": TOC-18, 3-5 (1986).
5. T. Nozaki, M. Okamoto, "Radioactivity in Coolinbg Water of Musashi Reactor": J. At. Energy Soc. Jpn., 25, 816 (1983).
6. T. Nozaki, T. Honda, N. Horiuchi, O. Aizawa, T. Sato, "Fuel Element Replacement and Cooling Water Activity at the Musashi Reactor": TOC-21, 3-39 (1988).
7. K. Yamamoto, I. Yokouchi, I. Hisa, C. Yonezawa, F. Nakayama: "Source of Radio-iodine in Rrimary Cooking Water of Japan Materials Testing Reactor": J. At. Energy Soc. Jpn., 29, 717 (1987).
8. R. E. Jervis, W. D. Macintosh: "Activation Analyses of Interest to Atomic Energy Programs": A. Conf., 28, 470 (1958).

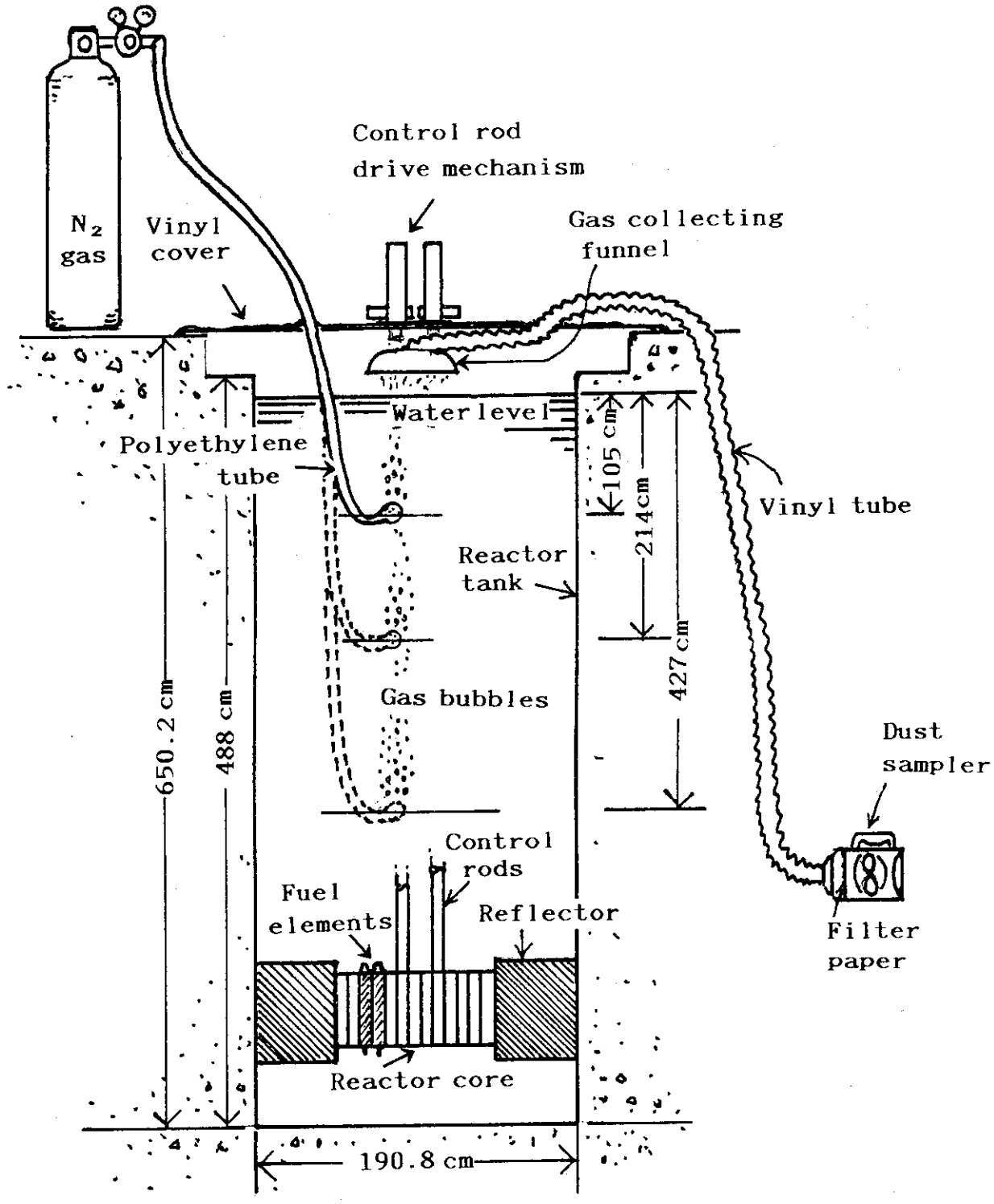

Fig.1 Schematic setup of dust sampling bubbled with N_2 gas.
(Bubbling method)

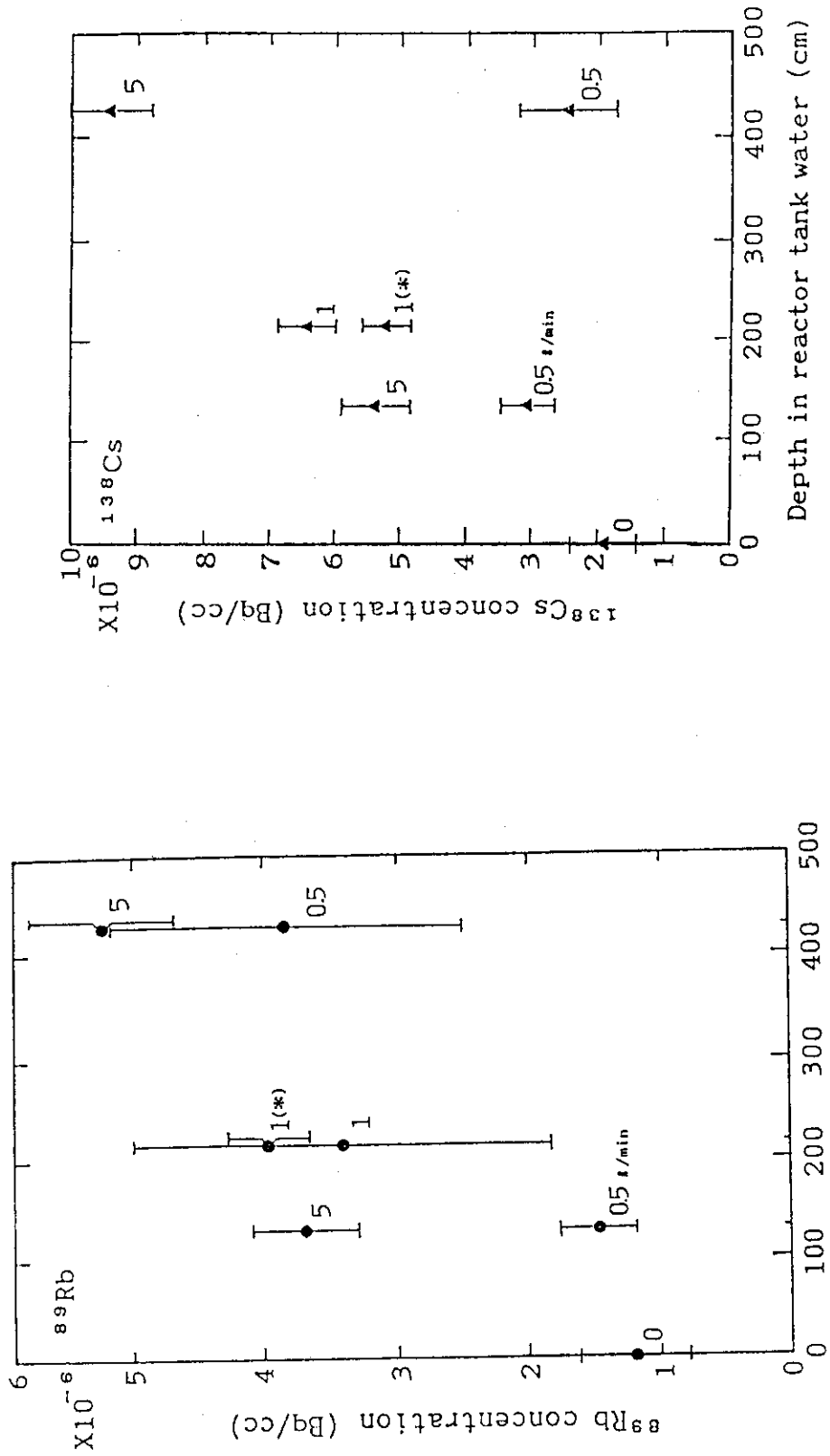

Fig. 2. Radioactive concentration in the air on the water surface of the reactor tank with and without N_2 gas bubbling. (Number shows a flow rate of the gas.)
(a) ^{89}Rb, (b) ^{138}Cs.

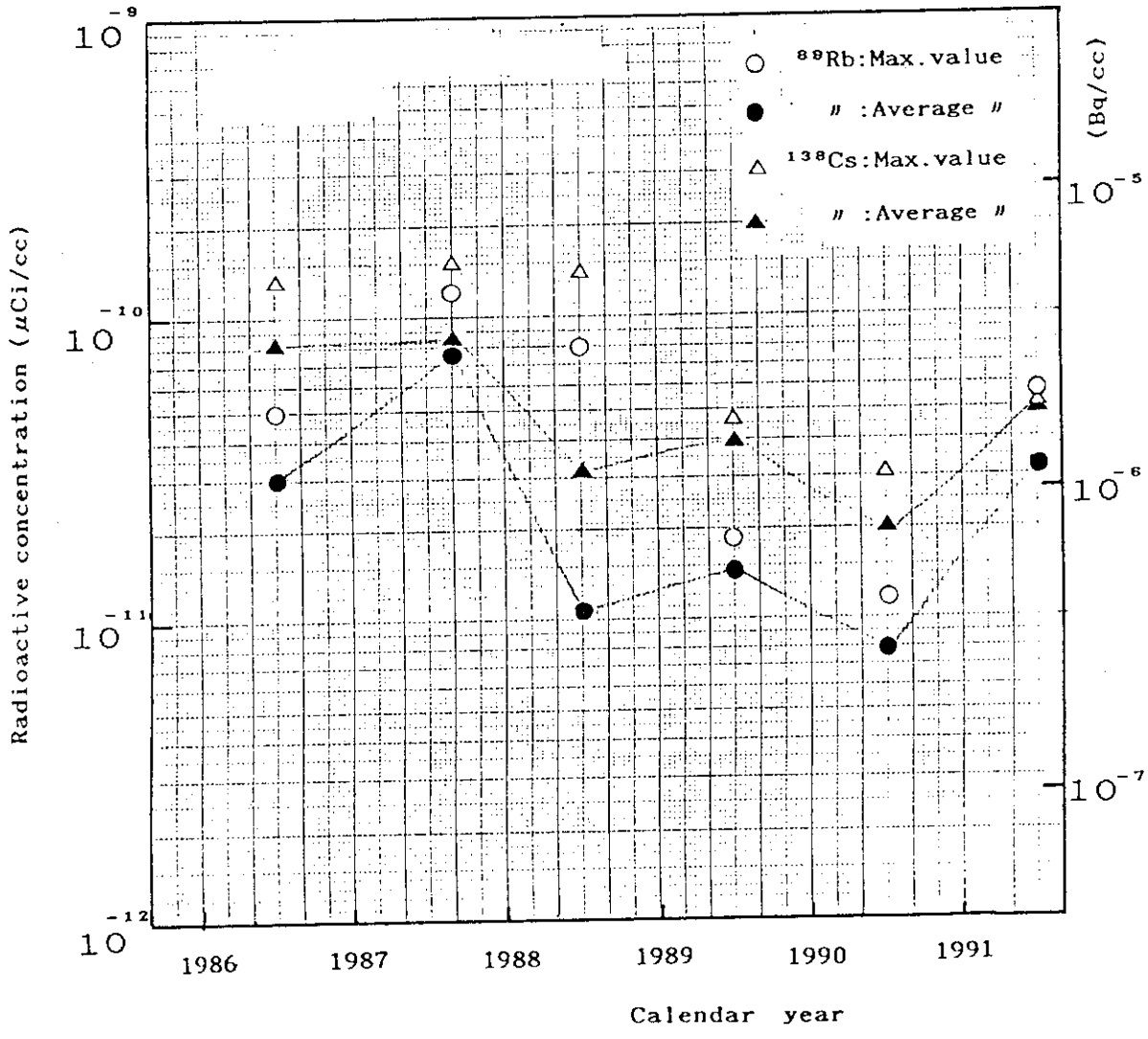

Fig. 3. Radioactive concentration of ^{89}Rb and ^{138}Cs in the air on the water surface of the reactor tank as a function of calendar year.

Table 2. Cases of fuel failure in TRIGA

	Location (Country) Type or Power (Date of Criticality)		Pulse (Peak Power)	Cladding	Date in Use	clad. (failed)	Discovery & Status	Date occurred	Ref.
1	Mainz(FRG) 250kW(1965-)		pulse	Al		Al	2 elongations 2 leak gas buble 2 swelling	1970	T- 721 (1970)
2	Pavia(Italy) 250kW(1965-)		pulse (250MW)	Al		Al	8 elongations/ 5 years (2 removed from core)	1970*	T- 721
3	Ljubliana(Yugoslavia)		steady	Al		Al	5 elongations (more than 2 cm)	1973*	TOC- 6 (1974)
4	München(FRG) 1 MW(1972-)		pulse	SS		SS	1 swelling (3cm) +Release of FP	1977	TOC-11 (1978)
5	Texas A & M (USA)		pulse	SS		SS	4 deformations	1982*	TOC-15 (1982)
6	Helsinki(Finland) 250kW(1967-)		pulse	Al		SS	1 crack+FP detected	1981	TOC-15
7	GA San Diego (USA)	250kW Mark I (1958-)	steady	23 SS 48 Al	1958-	SS	7 bent >1.6 mm	1982*	TOC-15
						Al	1 leaker 2 grew >1.8 cm 3 bent >1.6 mm		
		1.5MW Mark F (1960-)	pulse	100 Al 70-100 SS 65-100 FLIP	1960-1962 1962-1973 1973-	SS	54 bent >1.6 mm 1)		
						Al	35 bent 2) (including 1 leaker)		
		2 MW Mark III (1960-1973)	"	100 SS 100 FLIP	1960-1971 1971-1973	SS	1 leaker		
8	Vienna(Austria)		pulse	Al			1 swelling + gas bubling + FP detection 5 elongations or bents	Dec.1981	TOC-15
9	GA-ORR Oak-Ridge(USA) (Fuel test 1979-)		steady	SS (Incoloy 800)		SS (FLIP)	1 pin hole (/ 45 elements /4 year	1983	TOC-17 (1984)
10	Berkeley 1 MW(1966-1986)		pulse (2800MW)	SS		SS	1 FP detected (removed from core)	Oct.1986	TOC-18 (1986)

* reported date
1) Nearly all resulting from high power pulse development tests (up to $ 5.00)
2) Nearly all resulting from pulse development tests

5. Centralized Radiation Monitoring System for the JRR-3M

Y. SASAKI, T. FURUTA, H. KATAGIRI
Department of Health Physics,
Tokai Research Establishment, JAERI
Totai-mura, Naka-gun, Ibaraki-ken 319-11, Japan

ABSTRACT

This paper describes on the outline of centralized radiation monitoring system for the JRR-3M and its functions such as the acquisition, the monitoring, the filing, the display and the statistical analysis of the data measured and the diagnostic program for the projection of the phenomena of the events to offer the measures needed.

1. INTRODUCTION

The JRR-3M achieved initial criticality on March 22, 1990. Radiation monitoring in the workplace is performed to keep the radiation safety for workers and the public. For this purpose, radiation monitoring for the personnel, the workplace, the gaseous and liquid waste released from the facilities and the articles carried out from the radiation controlled area are planned and executed based on the radiation monitoring program.

Centralized radiation monitoring system for the JRR-3M was constructed by integrating the information of radiation measurement,of operational status (breakdown etc.) of instrument used in the system and of reactor operation to achieve more reliable, accurate, effective and quick radiation monitoring.

This paper describe on the outline of centralized radiation monitoring system for the JRR-3M and its functions such as the acquisition, the monitoring, the filing, the display and the statistical analysis of the data measured and the diagnostic program for the projection of abnormal situation and so on. For the diagnosis of abnormalities, 1,200 radiation related information and 3,300 reactor operational information previously installed in the host computer are used relationally according to the fault tree composed by reflecting the experience of the experts of radiation monitoring. The system also installs the wide range gamma area and gas monitors which cover 10^3Sv/h and 10^7Bq/cm^3, respectively for provision against emergency. [1,2]

2. GENERAL ASPECTS OF THE JRR-3M

High quality irradiation conditions and high neutron flux

conditions have been required in recent years for neutron irradiation and neutron beam experiments in the research reactors. To fulfil these requirements, the Japan research reactor No.3 (JRR-3) was reconstructed to be upgraded. The new JRR-3 (JRR-3M) achieved initial criticality on March 22, 1990.

The JRR-3M is equipped with various kinds of experimental facilities for irradiation and beam experiments including a cold neutron source. The maximum thermal neutron flux is about 2×10^{14} n/cm^2.s at the thermal power level of 20MW, which is one order higher than that of the old reactor. Table 1 shows major specifications of the JRR-3M.

Table 1 Major specifications of the JRR-3 M

Reactor Type	Low Enriched Uranium, Light Water Cooled and Moderated, Swimming Pool Type.
Rated Power	20 MW
Size of Core	Approx.60cm dia. and 75cm high (with Beryllium Reflector).
Fuel	UAlx-Al Dispersed, MTR Plate Type 20 % Enriched Fuel. 26 Standard Fuel Elements and 6 Follower Fuel Elements.
Control Rod	6 Control Rods, Box Type Absorber, Followed with Follower Fuel Element.
Reactor Pool	Swimming Pool Type 4.5 m dia. 8.5 m deep
Experimental Facilities	9 Horizontal Beam Tubes, 17 Vertical Irradiation Hole, and 1 Cold Neutron Source

3. RADIATION MONITORING SYSTEM

3.1 Design of Radiation Monitoring System

The radiation monitoring system for the JRR-3M is designed by reflecting "Guide for Measurement of the Radioactive Released from Light Water Nuclear Power Reactor Facilities (Sep・29,1978) " and " Guide for Radiation Measurement during Accident in Light Water Nuclear Facilities (July 23,1981) " issued by Japan Nuclear Safety Commission.

The radiation monitoring system was designed also to meet the following objectives based on experiences of radiation monitoring system and radiation monitoring experts.

(1) To centralized the information for the comprehensive radiation monitoring

Centralize and monitor the radiation monitoring data and the status of instrument installed in reactor building, experimental beam facility and irradiation facility etc. and the status of reactor itself using the computer system for the quick and effective response in case of abnormal situation and for the labor saving in the routine monitoring.

(2) To provide the radiation related information to the workers

Install the local indicators, which can be visible from as far as 10m, and cathode ray tube (CRT) at the workplace or the entrance of workplace to issue alarm and to show the real time levels of area monitor and air monitor to prevent undue exposure by carelessness and lack of information.

(3) To provide the information for supporting the decision making case of alarm situation

Prepare abnormality diagnosis program composed of fault tree analysis program triggered by the alarm of radiation monitors for assisting the radiation control officers and reactor operator by offering the highly accurate information concerning the abnormal situation quickly.

(4) To install the emergency radiation monitor

Install emergency gamma area monitors and a emergency gas monitor to estimate the amount of radioactivities released to confirm the soundness of barriers and to know the radiation level in the workplace.

(5) To prevent the lack of radiation monitoring during the malfunction and the repair of computer system

Equip the radiation measurement part with radiation indicator, visual and sound alarm annunciator and status lamp to maintain radiation monitoring during the suspension of computer system.

3.2 Composition of Radiation Monitoring System

The JRR-3M facility consists of reactor building, reactor control building and experimental building. Monitors are distributed throughout these building.

Figure 1 shows a diagram of the centralized radiation monitoring system. The system is composed of radiation measurement part and the computer system.

The centralized radiation monitoring system (including the computer system) is provided with the plant emergency power supply system.

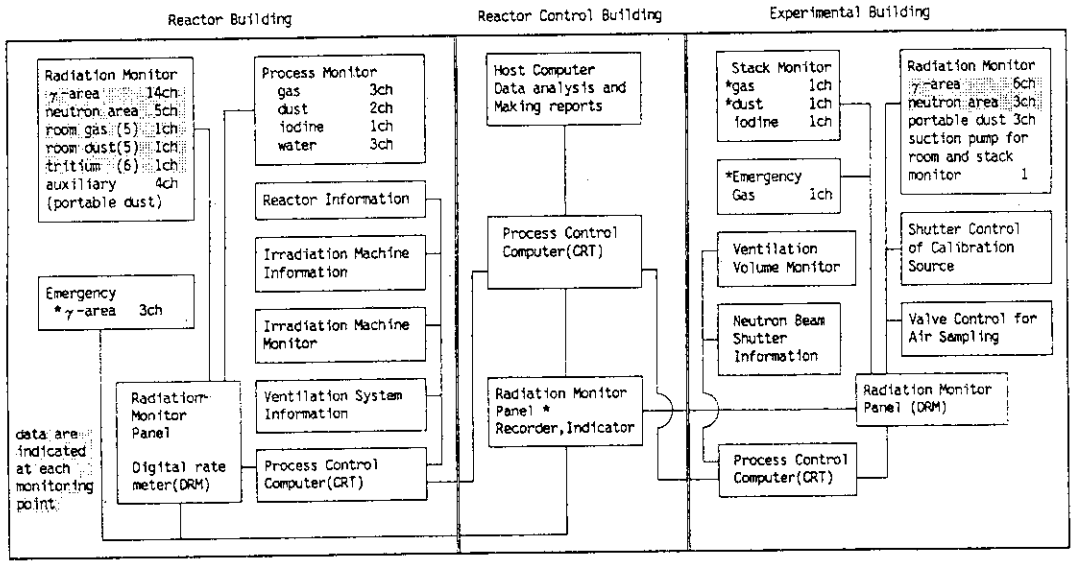

Fig. 1 Centralized radiation monitoring system for the JRR-3 M

(1) Radiation measurement part

There are 20 channels of gamma area monitors, 8 channels of neutron area monitors, 6 channels of continuous air monitors, 3 channels of emergency gamma area monitors and 1 channel of emergency gas monitor in the radiation measurement part (see Fig.1). The signals from the detectors of these monitors are centralized to the radiation monitor panels of reactor building, reactor control building and experimental building. The process control computer integrate the information from these panel.

The output of stack gas monitor (1ch), stack dust monitor (1ch), gamma area monitors (2ch), emergency gamma area monitors (3ch) and emergency gas monitor (1ch) are continuously recorded on multipoint recorders, too.

The detectors used for emergency gamma area monitors, which can

cover 10^3Sv/h, are stably operate up to 100% relative humidity, while the other detectors are stably operate up to 90% relative humidity.

a) Gamma and neutron area monitor

Table 2 shows the specification of gamma and neutron area monitor.

To cover the wide range of gamma radiation dose rate, two types of silicon semiconductor detector are used. Detector for lower range covers 10^{-1} to 10^4 μSv/h and one for higher range covers 10^1 to 10^6 μSv/h.

BF_3 neutron area monitor with moderator can measure radiation level from 10^{-1} to 10^4 μSv/h.

Table 2 Radiation area monitor at JRR-3M

Monitor	Objective		Detector	Measurable range	Number of location
γ-Area Low	Working area	γ	Si SSD	10^{-1}～10^4 μSv/h	17
High		γ	Si SSD	10 ～10^6 μSv/h	3
n-Area	Working area	n	BF_3, Moderator	10^{-1}～10^4 μSv/h	8
Emergency Low γ-Area	Reactor room working area	γ	Ionization Chamber	10^0 ～10^4 mSv/h	1
High		γ	Ionization Chamber	10 ～10^6 mSv/h	2

b) Air monitor

To measure the airborne radioactivities in the workplace and in the gaseous waste flowing out from stack continuously, dust monitors, gas monitors, an iodine monitor and a tritium monitor shown in Table 3 are installed.

Table 3 Gas and dust monitor at JRR-3M

Monitor	Objective		Detector	Measurable range	Detection Limit (3σ) Bq/cm^3
Gas	Noble gas Stack Room	γ	NaI(TL) Scinti. (2″ ϕ×2″ t) Sampler vol. 11.7 ℓ	10^{-4}～10^3 Bq/cm^3	Stack 1.6 ×10^{-3} Room 1.4 ×10^{-3}
Dust	Particulate Stack Room	$\beta\gamma$	GM-tube (50ϕ) Filter paper(HE-40T) Sampling rate100 ℓ/m	10^{-1}～10^5 cps	Stack 1.1 ×10^{-7} Room 3.0 ×10^{-8}
Iodine	Volatile gas Stack	$\beta\gamma$	GM-tube (50ϕ) ACF filter Sampling rate 50 ℓ/m	10^{-1}～10^5 cps	1.9 ×10^{-7}
Emergency gas (2)	Noble gas Stack	γ	Tow ionization chambers(Ar and Xe are filled respectively) Sampling chamber95 ℓ	Q*10^9～10^{15} Bq/h C*10 ～10^7 Bq/cm E*10^{-2}～10^1 MeV	C 2.4 ×10^0
Tritium	Tritium Stack Room	$\beta\gamma$	Flow-type Ionization chamber Sampler vol. 18 ℓ	10^{-2}～10^4 Bq/cm^3	2.2 ×10^{-2}

* Q: release rate, C: concentration, E: Effective energy of released gas

Each monitor routinely collects air from different area (place) through sampling pipes to one sampling media (filter paper, activated carbon fiber filter (ACF)) with a detector and/or a ionization chamber for the direct measurement of noble gases and tritium. But when the

radioactivity concentration exceeds alarm level previously defined, the air from the abnormal point (area) is selectively sampled through computer controlled sampling valve.

A GM detector, a NaI(Tl)scintillation detector and an ionization chamber are used for the dust monitors, the gas monitor and the tritium monitor, respectively. To sample the particulate radioactivities (dust) , filter papers made of glass and asbestos fiber (HE-40T) are used and to sample iodine, activated carbon fiber filter (ACF) is used.

The emergency gas monitor equipped with a ionization chamber as a detector can measure the the radioactivity concentration from 10^{1} to 10^{7} Bq/cm^{3}.

(2) Computer system

The computer system is compose of 3 groups of process control computers. Host and process computers are independently installed to keep reliability by sharing the roles of monitoring program shown in chapter 4. Fig.2 shows the computer system.

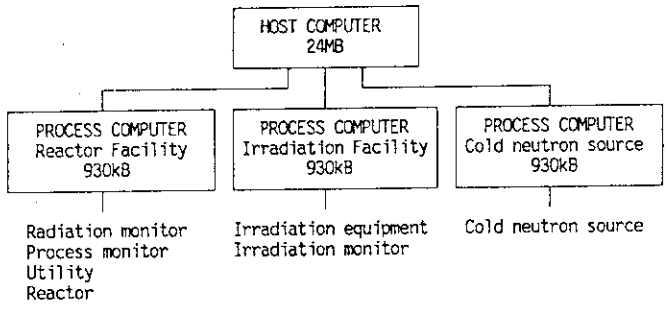

Fig.2 Computer system for JRR-3 M facilities.

There are seven CRT and one graphic display (GD) in the reactor control room, one GD in the radiation control officers room,two CRT in the reactor building, one GD in the computer room and one GD in the experimental building.

4. MONITORING PROGRAM

The monitoring program was designed to correspond quickly to the radiological abnormal situation by refferring the data such as radiation related and operational status of the JRR-3M reactor comprehensively and to file every monitoring data obtained for the future statistical analysis.

Monitoring items and status (shown in Table 4) are collected and monitored every 1 sec according to the radiation monitoring program shown in the flow-chart of Fig.3. The process control computer (930kB, hard disk 18.8MB) and the host computer (24MB, hard disk 1,200MB) share their functions as follow.

(1) Process control computer

a) Process control

Stop and/or start the installation and instrument incorporated in the system automatically or manually according to the sequence previously defined.

b) Display

Status (operation, stop, abnormal etc.) of installation and instrument and the monitoring data is renewed and displayed every 1 sec on the CRT with color.

c) Trend graph display

Two kind of linear trend display options which can display every 1

sec, 1 min and 10 min data are prepared. One can display 6 channels in one view and another can display 6 groups having 6 channels in each group in one view.

Table 4 The function of process control computer and host computer

Process control computer		Host computer	
Process control	• Stop and/or start the instillation and instrument • Sampling valve control • Sample changer control • Preoperational check • Calculation of airborn RI	Data control	• Monitoring data & status (operation, stop, abnormal etc.) every 1 min
		Display	• Monitoring data & status every 1 min
Display	• Monitoring data & status (operation, stop, abnormal etc.) every 1 sec.	Trend graph display	• Log. trend display every 1 min, mean value of 10 min, 1 hour and 1 day • 6 channel in one view
Trend graph display	• Linear trend display every 1 sec, 1 min, 10 min • 6 channel in one view • 6 groups having 6 channel in each group in one view	Message	• Display on CRT Sound buzzer • Alarm, status
		Reports	• Monitoring data (Hourly, Daily, Monthly) • Preoperational check list
Message	• Display on CRT & Sound buzzer • Print out • Alarm & status	Data save	• Data are saved to magnetic tape every 5 weeks
		Diagnosis of abnormality	• Fault tree analysis Display of results • Ar gas release projection (Quarterly,annualy) • Tritium dose projection • Guide for the evacuation from reactor facility

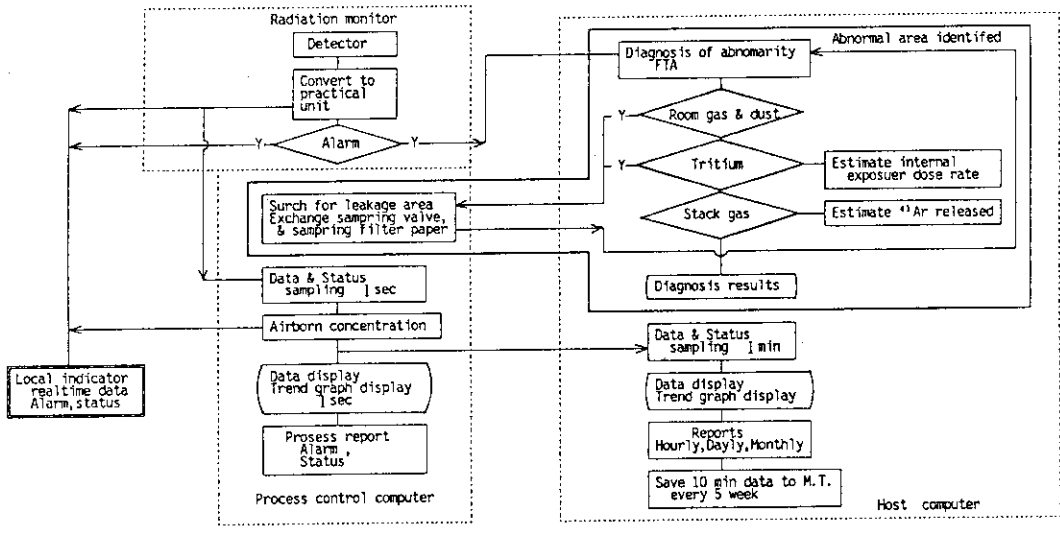

Fig.3 Diagnosis of abnomality in case of alarm.

d) Message

Display messages on CRT and sound alarms on annunciator when some abnormal status are found on the installation and instrument and also those abnormal status is printed out on printer.

(2) Host computer

a) Data control

Data and status are collected from the process control computers every 1min.

b) Display

Same as that of the process control computer only the exception of

min display interval.

c) Trend graph display

Almost same as those of the process control computer except that the logarithm output of trend and the output of the momentary value of 1min, mean value of 10 min, 1 hr and 1 day are available. Past 10weeks data are displayed from the hard disk of host computer directory and the data beyond the above term have to be transfered from magnetic tape to hard disk to display.

d) Data save to magnetic tape

Because the hard disk memory of host computer is limited and to protect the data from the break down of computer system, data in the hard disk are saved to magnetic tape every 5weeks.

e) Reports

Hourly, daily and monthly reports of monitoring data and those of statistically analyzed are printed out automatically.

f) Diagnosis of abnormality

To assist the radiation control officers and the reactor operators for their decision making in case of abnormal situation with rapid, precise and comprehensive information, this abnormality diagnosis program was developed by utilizing the operational experiences such as abnormal situation and accidental events of the research reactor and by considering the possibility of abnormal sequence in JRR-3M. Abnormality diagnosis program is consisted of fault tree analysis (FTA), release and dose projection program and the guide for the evacuation from the reactor room.

〔FTA〕

About 4,500 items including 1,200 radiation related information are monitored by the system. All these monitored values are classified and correlated considering the logical sequences of each accidental phenomena.

The abnormality diagnosis program is triggered by the alarm signal of radiation monitor and display the results of diagnosis on the GD with hard copy.

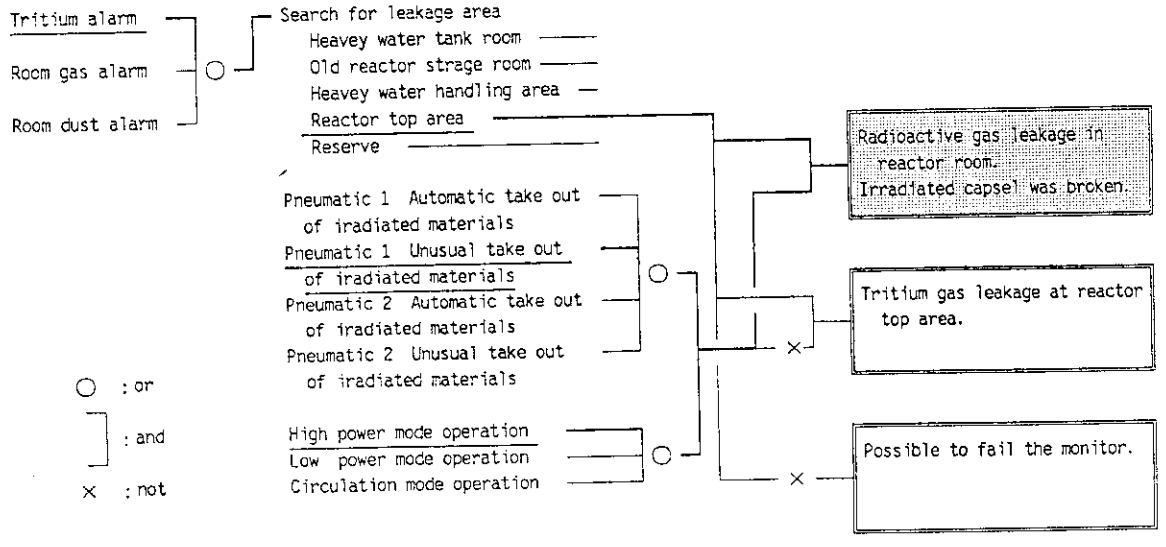

Fig. 4 An example of diagnosis of abnomality by fault tree analysis.

For example, if alarm is issued from the room gas monitor, the room dust monitor or the room tritium monitor, which centralized air from

different area (place) and/or ventilation air to one sampling medium (HE-40T, ACF and ionization chamber) or monitoring section, firstly the program order the process control computer to identify the abnormal point (area) by changing the sampling valves or by changing the filter papers of the dust monitor, then FTA begins to operate. FTA when the airborne contamination is detected at the reactor top area is shown in Fig.4. 70 diagnosis results for radiation monitoring are prepared.

〔Release and dose projection program〕

a) Release projection

Total amount of ^{41}Ar (energy equivalent release) released is estimated during the abnormal situation, a quarter and annual term including the abnormal release to compare the amount of abnormal release with the release objective value derived from dose objective value from the regal point.

b) Dose projection

Internal exposure by tritium due to the leakage of heavy water is estimated assuming one hour inhalation in the contaminated room.

〔Guide for the evacuation from the reactor and experimental room〕

This guide is prepared to indicate the direction (way) of evacuation for the workers in the reactor room, when area monitors issued the alarm at one time. The radiation dose rate at various points are arranged in descendent order from the highest point to help the radiation control officers for their judgement of the optimized evacuation way. With the aid of this information, radiation control officers can indicate the appropriate evacuation way to the workers in the reactor and experimental room.

5. CONCLUSIONS

By centralizing the radiation related data and the status of instrument and reactor comprehensively by using the computer, the accurate, rapid, effective and labor saving radiation monitoring was attained, and is now successfully operated.

Using the insitu radiation indication board, actions (confirmation of radiation level and temporal evacuation) should be taken by workers are informed.

To assist the reactor operator and the radiation control officer, reliable and rapid information obtained by the abnormality diagnosis program is available.

REFERENCES

1. Furuta, T., Nomura, T., Matsushita, K., Sasaki, Y.,etc. :Radiation Monitoring System in JRR-3M, In Proceedings of the 24th Annual Meeting of the Japan Health Physics Society, A39 (1989). (in japanese)

2. Minami, K., Murakami, H., and Yoshida, Y. : A New Type of Stack Gas Monitor Directly Indicating Exposure in Environment, Journal of the Atomic Energy Society of Japan, Vol.29, No.7, 656-663 (1987).

6. An Integrated Monitoring and Control System for THOR

H. P. Chou, T. H. Chou and T. L. Chen

ABSTRACT

The paper presents a computerized monitoring and control system for the THOR. The system is used to assist reactor operation and to facilitate data acquisition and teaching for reactor experimental laboratory courses. The design applies digital data processing for neutron detector and area monitor measurements. Signal validation is used to improve signal reliability. Color pictures in the forms of analog meters, strip charts, and bar graphs are displayed for the control room and for off-site as well. Power control is based on the "reactivity constraint" approach for wide range adjustment and on-off logics for narrow range regulation. Algorithms are coded in C language and implemented into a 32-bit microcomputer. Evaluations have shown satisfactory results for operation and teaching needs.

INTRODUCTION

The Tsing Hua Open-pool Reactor (THOR) was built near 1960 and has played an important role in the university's teaching and research activities since then. A THOR improvement program began several years ago; the reactor core was converted from the MTR plate-type fuel into the TRIGA rod-type fuel to upgrade its power level. The neutron detection system was upgraded with wide range fission chambers and modern integrated circuits to improve its sensitivity and reliability. Power maneuver at the THOR is performed using three safety control blades and one regulating blade. The original vacuum tube type power servo system was also replaced with integrated circuit devices.[1] The instrument display panels and the power control scheme, however, remain to be the original analog setup.

Recently, digital signal processing techniques and computer control strategies have a great advance and have successfully applied in many industries; examples can also be found for nuclear research reactors.[2-5] At the mean time, digital data analysis using microcomputers has become a common practice in many laboratory courses. Data acquisition from the conventional analog display panels are often troublesome for students during reactor experiments. The conventional power servo system using the DC differential level comparison technique was designed for narrow range power regulation and was found inconvenient for frequent power maneuvers during the student laboratory practices. Therefore, there is an interest in the development of a computerized monitoring and control system to assist the THOR operation as well as to meet the teaching needs.

Under the limited budget and time constraints, we have proposed to develop a microcomputer based system and concentrate the effort on the display and

control schemes while leave the reactor protection system, transducer systems, and mechanical setups untouched. To minimize hardware change and operation interference, we have the system attached in parallel with the existing ones. For the reactor experiment laboratory course, we would also like the system to run an off–line test mode to provide simulations of power maneuvers and to illustrate the basic reactor operating principles. Following sections present the system architecture, monitoring and control schemes, and performance demonstration.

SYSTEM ARCHITECTURE

Figure 1 illustrates the overall hardware arrangement. A 32–bit microcomputer acts as the control center for data acquisition and distribution. The VGA color monitor and the remote panels are for information display; the hard disk is used for data logging and storage. The electronic circuits are a relatively low–cost board level design using entirely off–the–shelf components. A modular approach is taken to reduce the maintenance effort. The system is designed to interface with the existing reactor power detection system, area radiation system, and control blade moving assemblies. Interfacing with the process signals, such as temperature and flow rate, is not considered for the time being.

The reactor power detection system consists of two wide range fission chambers and associate amplifier modules. Each detector channel provides a linear power signal and a log power signal. The area radiation monitor system has eight monitors distributed in the reactor building for radiation safety. Signal processor are designed to accept these output and feed into an analog digital (A/D) converter. Each signal processor consists of an isolation amplifier and a low pass filter. The low pass filter is a third order Butterworth circuit with the 3 dB frequency at 2 Hz. The A/D converter is a commercial product designed to use with personal computers; there are 16 channels with a 13–bit resolution. The A/D converter circuit board also contains 64 k–byte buffer memory and a co–processor for digital data preprocessing. The position signal of the control blades is generated from an electrical brush coding system. The position reading is a four–digit number with the voltage level of 25 volts and has the least significant number to be 0.01 inch. The position signal processor module contains a decoder circuit and converts the position signals to meet the TTL standards. The TTL digital readings are then feed to the computer through a parallel input/output interface board and to seven–segment LED displays on the THOR control panel.

The motor driver circuit is designed using digital IC components and solid state relays. A zero–voltage turn–on/turn–off circuit, interlocks with limit switches, and detection logics for contradictory commands are used for motor protection. In case of power failures, the relay is open and the control function can be override manually from the control panel.

Information for the remote display panel are transmitted using the RS–422 standards. Four display panels are installed in the remote experimental area and the emergency control center. Each panel is equipped with a single chip microprocessor for signal flow control and can perform self tests. Alarms are provided during high radiation level and over power transients.

MONITORING AND CONTROL SCHEMES

The monitoring and control schemes perform the following tasks:

1. validation of power, radiation, and control blade position measurements;
2. estimation of dynamic period and core reactivity;
3. reactor power control and regulation;
4. information display and man–machine interface.

Figure 2a illustrates the flow chart of the execution sequence. The schemes are coded in Turbo C language and are designed for both on–line and off–line operation.

During on–line operation, reactor power signals are sampled with 100 Hz frequency and the area monitors and control blade positions are scanned every second. Blade control commands are formatted in a 1 Hz square wave with a 50% duty cycle. During off–line operation, the core reactivity is generated from the pre–calibrated control blade worth data. The power and the blade positions are calculated according the point kinetics equations and the average blade traveling speed respectively. Data logging using disk storage and/or printing is user–defined with selectable frequency.

For parameter estimation, the sampled power signal are averaged every 0.5 s to smooth the high frequency quantization error. The smoothed linear power readings are then checked against a predicted value that is exponentially extrapolated from the previous readings. If the difference is beyond a certain amount, say ± 50%, the reading is replaced with the predicted one. The validated linear power readings are then combined with the integer part of the logarithmic power readings to indicate the power level.

The area monitoring readings are checked using the standard deviation of the data in the previous time interval of 100 s. Warnings are issued, if the disagreement lasts for a certain time steps. The control blade position readings are checked for jump failures according to the maximum available motor speed; the faulty reading is replaced with the previous one and a warning is issued.

Estimation of the dynamic period and the core reactivity is based on the smoothed and validated power readings.. The inverse of the dynamic period, defined as the slope of the logarithmic power, is calculated and smoothed by taking the moving average value every four time steps. The core reactivity is calculated according to the inverse point kinetics equation with six delayed neutron groups. In general, the value of the core reactivity is much less than the delayed neutron fraction β. Thus, the prompt jump approximation is considered a reasonable assumption and the reactivity ρ can be expressed as:

$$\frac{\rho(t)}{\beta} = 1 - \frac{S_d}{\beta\ p(t)} \qquad (1)$$

where p(t) is the power reading and S_d is the delayed neutron source. The delayed neutron source can be obtained by integrating the precursor balance equation with the power reading as the known input. Numerically, an integration time interval corresponding to five time constants of each precursor group, $5/\lambda_k$, is taken. The delayed neutron from the shortest half–life group is assumed to be generated promptly and a lead time of approximately 400 s is needed to estimate the population of the longest delayed neutron group.

The power control and regulation scheme determines the control blade motion. The "reactivity constraint" approach [7] is employed for coarse power level adjustment. Basically, the approach compares the time duration expected for the power changing from the current level to the target level with the time duration expected for the reactivity adjusted from the current value to a threshold value. The expected time duration for the power adjustment, T_a, is estimated by linearly extrapolating the logarithmic power based on the current dynamic period τ; i.e.,

$$T_a(t) = \tau(t)\ ln\ \frac{p^f}{p(t)} \qquad (2)$$

where p^f is the target power level. The expected time duration for the reactivity adjustment T_r is estimated by linearly extrapolating the reactivity:

$$T_r(t) = (\ |\rho(t)| - \rho^\Upsilon \ ) \ / \ \rho_s(t) \qquad (3)$$

where ρ^Υ is the threshold reactivity and ρ_s is the slope of the reactivity. The threshold reactivity represents the maximum amount of reactivity that can be left in the core so that the neutron power can be reversed by reversing the control blade motion. According to the point kinetics equation with the prompt jump approximation, the threshold reactivity would meet the following constraint:

$$\rho_{sm} \geq | \ \rho_{sf} + \lambda_e \rho^\Upsilon + \sum_k \beta_k \ (\lambda_k - \lambda_e)| \qquad (4)$$

where λ_e is an effective one group delayed neutron decay constant defined by:

$$\lambda_e = \frac{\sum_k \lambda_k^2 \ \xi_k}{S_d}; \quad \xi_k \text{ stands for the kth group precursor;} \qquad (5)$$

ρ_{sm} denotes the maximum allowable slope of reactivity that can be obtained from control blade motion. The ρ_{sf} denotes the reactivity slope due to temperature feedback effects. In practice, ρ_{sm} is set to according to the calibrated worth curve and the term ρ_{sm} is neglected for staying on the conservative side.

Although the reactivity constraint approach has been demonstrated to be an effective method for power maneuver, the simple on–off control is sufficient for narrow range power regulation from the past experience [1]. Therefore, we modified the existing on–off control circuit with a software and applied when the reactor power falls within 5% of the target value. To avoid excessive control blade motions, we reduce the control frequency to half. Considering the magnitude of the measurement fluctuations, a 2% power dead band is applied. Figure 2b shows the overall flow chart of the control scheme.

DEMONSTRATION

Figure 3 demonstrates the three picture frames designed for the display of the operating conditions. Figure 3a is a duplicate of the remote display panel which shows the operating power and the area radiation levels. Alarms are provided if limits are exceeded and can be acknowledged using a function key. Figure 3b is a condensed display of the main control panel. The picture shows the reactor linear power, logarithmic power and the dynamic period in a form identical to the panel analog meters. The demand power is also marked with a red line in the linear power meter for reference. Control blades are illustrated dynamically in bar graphs. In case that the faulty position readings are detected, the display blinks to warn the operator. Figure 3c is designed to assist the operator for power maneuvering. The history of power, period, and reactivity in the past 200 s is presented to indicate the trend. A demand power is shown on the upper left corner and can be on–line adjusted in units of 10% or 1% of the current power scale using a control (hot) keypads. Function keys are used to switch between the picture frames and the ESC key is used to manual override the build–in control schemes.

The period estimation scheme is on–line tested using transients with the period ranged from 30s to 100s and found to have a mean square error of ± 3%. The reactivity estimation scheme is off–line tested with a given reactivity ranged from 0 to 10 cents and an assumed of power fluctuation of 2%; The results

indicate an error around ± 0.5 cents.

Off–line tests of the control scheme with assumed power fluctuations show overshoots and steady state errors less than 1%. On–line steady state regulation for xenon compensation indicated a steady state error comparable to the power fluctuations ± 1%. Figures 4a and 4b are on–line disturbance tests by suddenly withdrawing and inserting of one main control blade from a critical state. The overshoot is approximately 2% and the steady state error is less than 1%. Figures 5a and 5b illustrates the on–line power adjustment for a factor of three. The result indicates an overshoot less than 2% and a steady state error of 1%.

SUMMARY

A computerized monitoring and control system has been developed for the THOR to assist the operation and to facilitate data acquisition and teaching of laboratory courses. The design considers digital data processing and signal validation to improve signal reliability. Displays are provided for the control room and for off–site information well. The simulated panel meters and operating trend are provided to strengthen the man–machine interface. Evaluations of the control scheme have shown satisfactory results for power regulation, disturbance rejection, and power maneuvering.

ACKNOWLEDGEMENT

The work is under the auspices of the National Science Council of Taiwan, China with contracts NSC78–0413–E007–11 and NSC77–0413–E007–05. The technical support from the technicians of the Reactor Division and the Instrumentation Division, Nuclear Science & Technology Development Center, National Tsing Hua University is gratefully acknowledged.

REFERENCE

[1] Yu Bin, "THOR Automatic Regulating Rod Control System," THOR Internal Report (1984).

[2] H. A. Larson, WW. F. Booty, D. R. Chick, L. J. Christensen, R. J. Forrester, and J. W. Sielinsky, "Installation of Automatic Control at Experimental Breeder Reactor II," **Nucl. Technol., 70,** 167 (1985).

[3] W. P. McDowell, "The TREAT Upgrade Manual Reactor Control System and Its Interface with the Automatic Reactor Control System and the Plant Protection System," **IEEE Tran. Nucl. Sci., 33,** 703 (1986).

[4] J. A. Bernard and D. D. Lanning, "Issues in the Closed–Loop Digital Control of Reactor Power: The MIT Experience," **IEEE Tran. Nucl. Sci., 33,** 992 (1986).

[5] S. E. Binney and A. J.M. Bakir, "Design and Development of A Personal–Computer–Based Reactivity Meter for a Research Reactor," **Nucl. Technol., 85,** 12 (1989).

[6] J. A. Bernard, A. F. Henry, and D. D. Lanning, "Application of the Reactivity Constraint Approach to Automatic Reactor Control", **Nucl. Sci. Eng., 98,** 87 (1988).

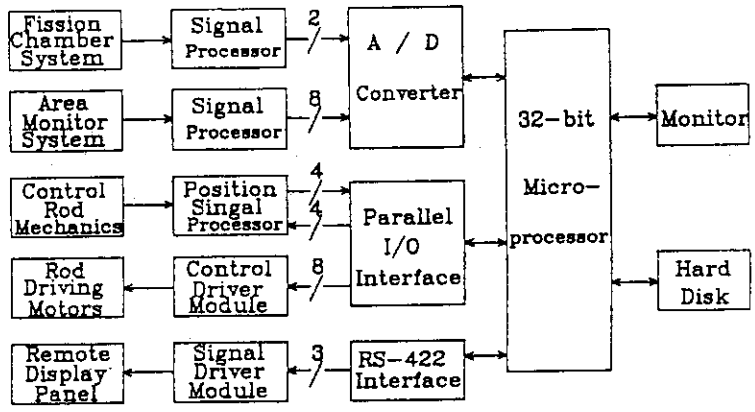

Figure 1 Block diagram of the monitoring and control system.

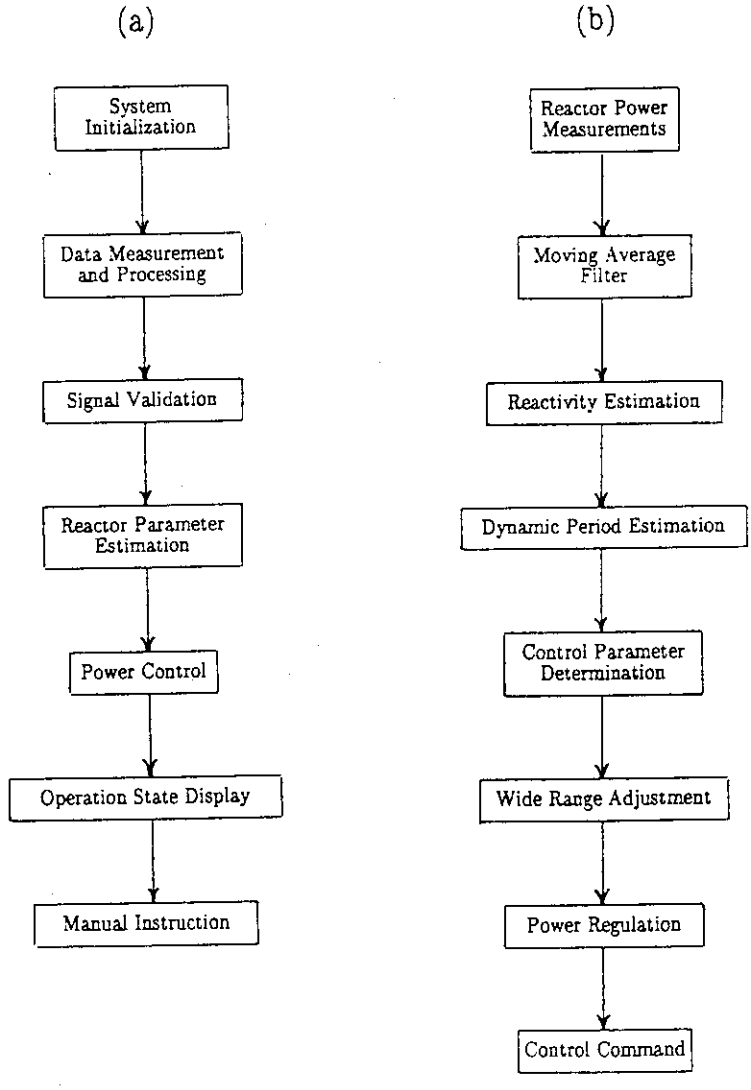

Figure 2 (a) Flow chart of the monitoring and control system;
(b) Flow chart of the power control scheme.

(a)

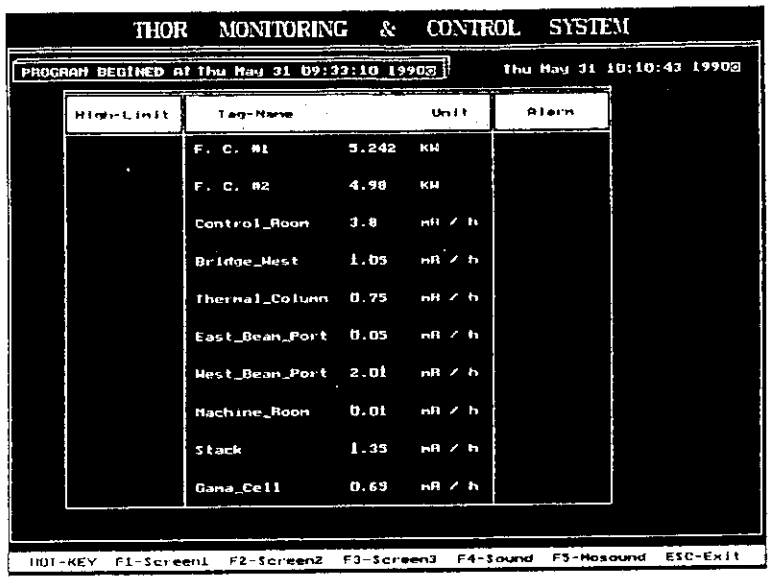

(b)

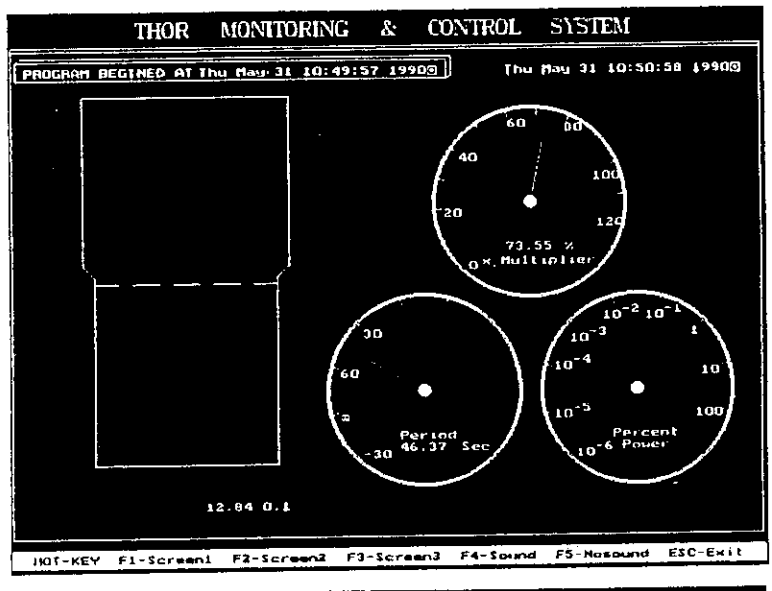

(c)

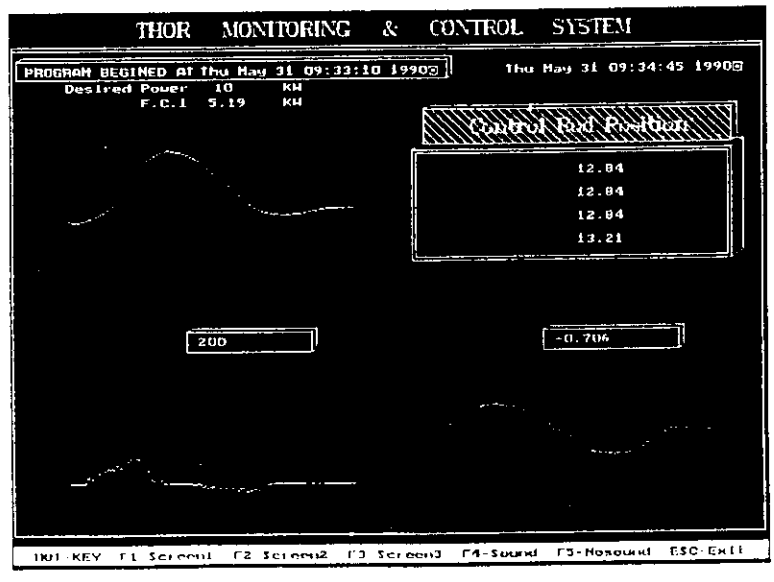

Figure 3 (a) Power and radiation level display; (b) Display of a simplified instrumentation panel; (c) Diplay of history of parameters.

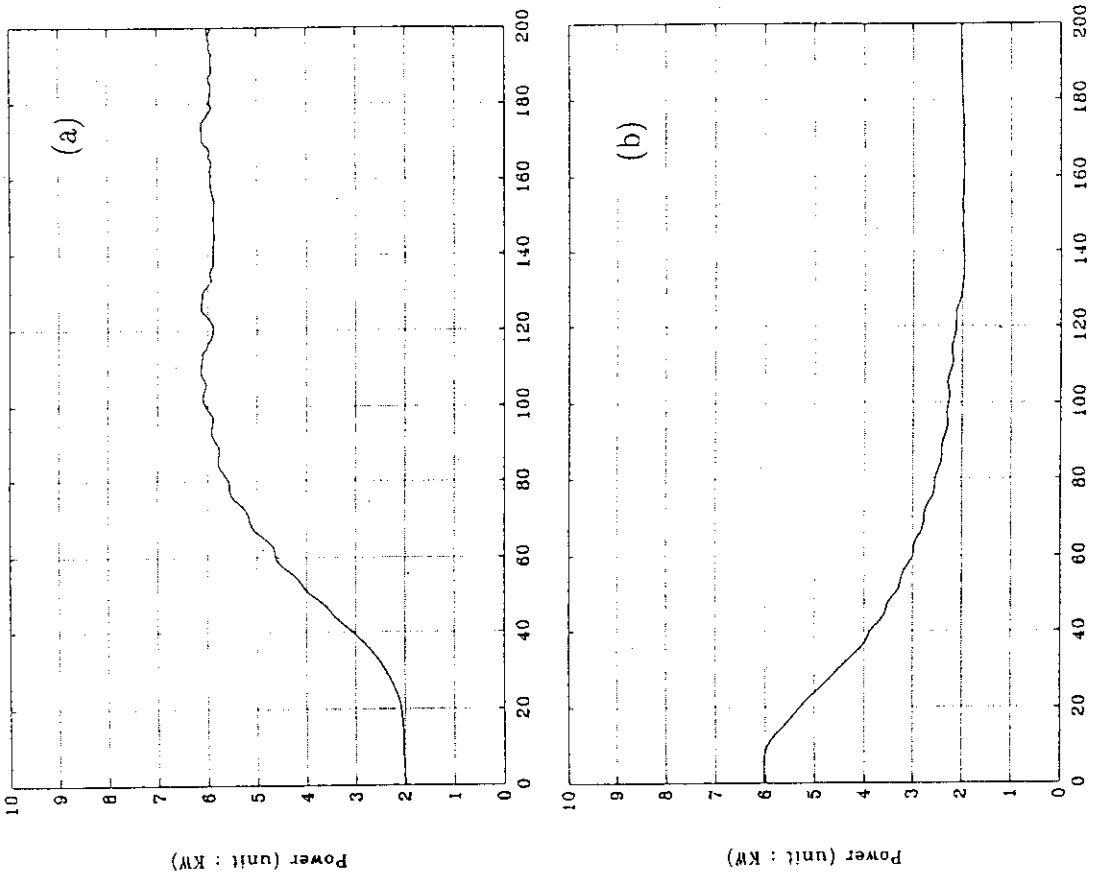

Figure 5 Power adujustment via automatic control
(a) power increment and (b) power reduction.

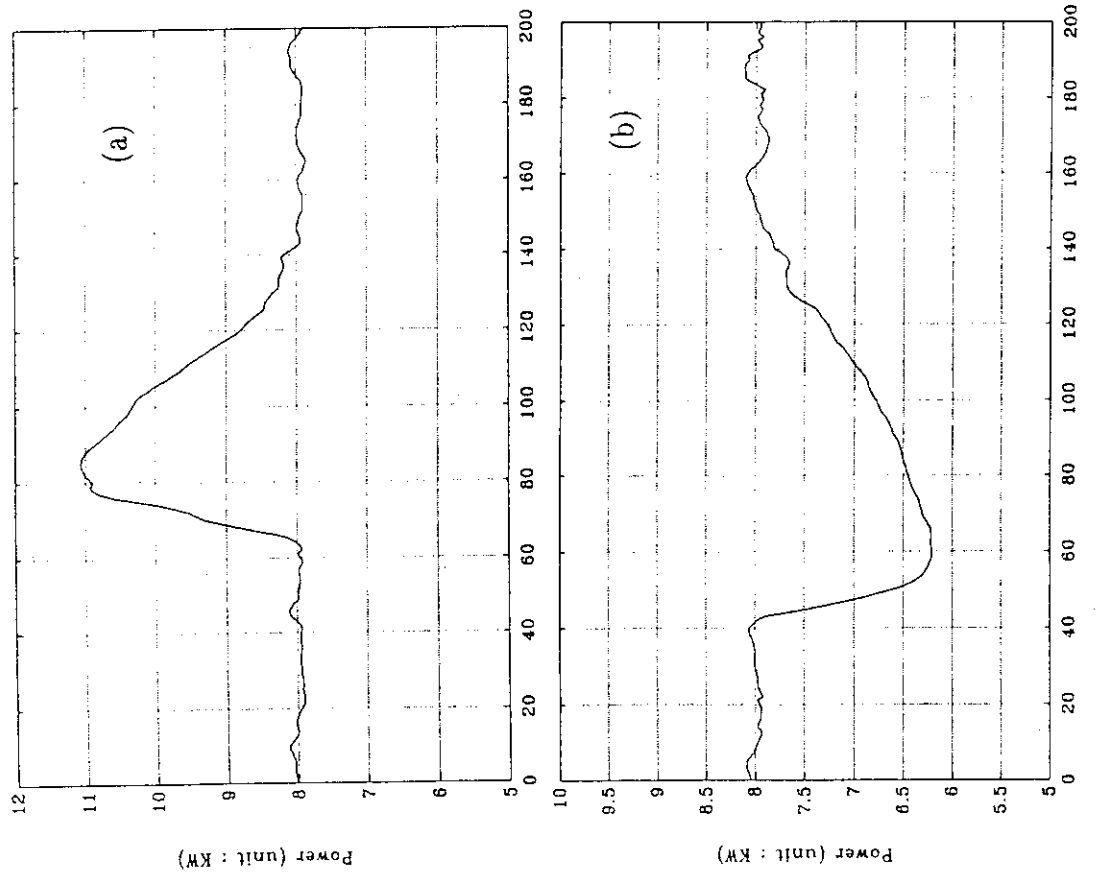

Figure 4 Disturbance rejection tests with a control blade
(a) suddenly withdrawl and (b) suddenly insertion.

7. Electrolytic Technique for the Chemical Decontamination Process with Sulfuric Acid-Cerium(IV) for Decommissioning

Tsong-Yang Wei*, Jung-Chun Hsieh

ABSTRACT

An electrolyzer with an ion-exchange membrane as the separator has been used to study the electrolytic redox reaction of Ce^{4+}/Ce^{3+} in sulfuric acid solution, which is a reagent for predismantling system decontamination.

Influencing factors such as current density, cerium concentration, acidity, electrolyte flow rate, membrane type and electrode material were studied experimentally. The results indicate that the redox can be achieved with high conversion even as the cerium concentration is below 0.005 M. However, the current efficiency strongly depends on the cerium concentration. In addition, the acid content and the electrolyte flow rate show little influence on the redox reaction. Both cation and anion membrane are feasible for this process. Therefore, the operation conditions are widely applicable. Moreover, two different electrode materials, platinized titanium meshes and graphite, were used. The results show that the platinized titanium meshes is preferable to the graphite for higher current efficiency.

1. INTRODUCTION

A chemical decontamination process with a high decontamination factor(DF) is requested for decommissioning. Usually, the process should be qualified with the characteristics such as the feasibility of treating large or complicated form waste, the secondary waste should be minimized[1]. The conventional chemical decontamination method using acid or alkaline can clean large or complicated equipment but the decontamination rate and DF are small. Therefore, a powerful technique of redox decontamination has been developed[2-5] and the Ce^{4+}/Ce^{3+} system is a common choice. A H_2SO_4 -Ce^{4+} solution was developed and applied to the primary system of JPDR in 1987[6]. There are many chemical methods, such as adding H_2O_2 or Fe^{2+} can fulfill the redox of Ce^{4+}/Ce^{3+}. Nevertheless, the redox proceeded with electrolytic method is the most convenient way. And the redox decontamination process needs an electrolytic unit to regenerate the Ce^{4+} solution. Suwa et al.[2] reported that the DF was ca. 33 at 90°

* To whom correspondences should be addressed

C for 24 h with 0.25 M H_2SO_4-5x10^{-3} Ce^{4+} but under electrolytic regeneration of Ce^{4+} from Ce^{3+} during the decontamination, the DF was raised to 460 even at 80° C for 24 h with 0.25 M H_2SO_4-1.3x10^{-3} M Ce^{4+}. Moreover, after the decontamination step the Ce^{4+} must be reduced to Ce^{3+} for the convenience of the subsequent liquid waste treatment. Fujita et al.[4] reported that the Ce^{4+} ions remaining in the spent redox solution were effectively reduced to Ce^{3+} ions by electrolysis. Therefore, the electrolytic technique is very important for the redox decontamination process. However, the electrolyer design is not much concerned, it is worthy to have further investigation.

The objectives of this study are to develop the technique of using an ion exchange membrane as cell separator and to find its optimum operation conditions.

2.EXPERIMENTAL

The cell depicted in Fig.1 is rectangular in cross section in two halves, and made of plexiglass. The internal dimension of each half was 21x13x1 cm^3. The anode and cathode compartment were separated by an ion exchange membrane(Ionac MA-3475 or MC-3470). The two halves of the cell were bolted together using neoprene gasket with two pieces of baskelite plate in the dimension of 30.5x21x0.8 cm^3. There was a piece of propylene screen in each compartment to enhance the mixing of electrolyte. The electrolyte was pumped into the compartment chamber with a diaphragm metering pump from the reservoir. The outlet electrolyte can be totally recirculated or stored in other reservoir without recycle depending on the selected operation method. Platinized titanium meshes with the dimension 21x13 cm^2 and rhombic type hole were used as the electrodes. Graphite plate was also used as cathode. The electrode was bolted on the plexiglass with a titanium rod, and this titanium rod was extended to the outside of the compartment, which was used as the port of current feeder. A 10A-30V DC power supply was used in all runs. Constant current was operated to measure the current efficiency.

The solutions were prepared using deionized water and reagent grade chemicals. In each run the volume of catholyte and anolyte was 2 liters respectively. Al samples, each of 3 cm^3, were taken periodically for analysis. The total cerium concentration was measured with indutive couple plasma(Kontron S35), and the Ce^{4+} concentration was determined by the titroprocessor(Metrohm 682). The current efficiency was back calculated from the Ce^{4+} concentration change in the electrolyte.

3.RESULTS AND DISCUSSION

3-1. Effect of current density

The electrochemical reaction rate depends on the applied current. However, as the applied current reaches a value, limiting current, the current efficiency will be drastically decreased if the applied current increases further. The applied current will electrolyze water rather than the cerium species in this case.

Fig.2 shows the effect of applied current on the Ce^{3+} oxidation. It indicates that during the same electrolysis cycle

the oxidation percentage increases when the applied current increases from 2 to 5 A. However, when the applied current is over 6 A, the oxidation percentage does not increase further. Fig.3 shows the effect of applied current on the reduction percentage. It can be seen that 4 A is the best, the Ce^{4+} (0.05 M) are totally reduced to Ce^{3+} within 10 electrolysis cycle. Comparing Fig.2 and Fig.3, it appears that the electrolytic reduction of Ce^{3+} from Ce^{4+} is more effecvtive than that of the electrolytic oxidation of Ce^{4+} from Ce^{3+}.

3-2. Effect of electrolyte acidity

The acidity of electrolyte will affect the degree of conductivity. The lower acidity is the lower conductivity of the electrolyte. However, the high acidity will induce the evolution of hydrogen at cathode, which would decrease the current efficiency. In addition, the stability of Ce^{4+} and Ce^{3+} depends on the acidity too. Therefore, there is a suitable range of acidity for redox decontamination process. The sulfuric acid concentration of sulfuric acid-cerium(IV) solution used in JPDR decontamination experiment was in the range of 0.5-1.0 N[6]. Fujita et al.[4] developed the redox decontamination system with HNO_3-Ce^{4+} solution and found that 2.0 N HNO_3 was suitable. Therefore, the acidity of Ce^{4+} solution used in decontamination process is about 0.5-2.0 N.

Fig.4 is the experimental results of the influence of acidity on the electrolytic oxidation of Ce^{4+} from Ce^{3+}. It is obvious that the acidity of the electrolyte does not affect the oxidation percentage when the acidity is in the range of 0.5 N to 6.0 N. This result shows that the electrolytic regeneration of Ce^{4+} is feasible in this acidity range when an ion exchange membrane is used as cell separator. Meanwhile, the electrolytic reduction of Ce^{3+} from Ce^{4+} is feasible too in this acidity range, the experimental results are shown in Fig.5. However, it should be noted that the current efficiency will decrease gently due to the problem of H_2 evolution when the acidity is over 8 N. Fortunately, the redox decontamination process is not necessary to use so high acidity.

3-3. Effect of electrolyte flow rate

The mixing of electrolyte results from the turbulance of flow for a flow-type electrolyzer. The higher flow rate is the better of mixing. However, the residence time of electrolyte passing through the compartment decreases with increasing flow rate. In addition, high flow rate is energy consumptive.

Fig.6 is the experimental results of the effect of electrolyte flow rate on the Ce^{3+} oxidation. It indicates that the reaction rate increases with increasing flow rate from 50 to 75 $ml.min^{-1}$ only. The further increasing flow rate does not increase oxidation rate. Therefore, it can be seen that the electrolyte oxidation rate is not limited by the flow rate. Fig.7 shows the experimental results of the influence of flow rate on the Ce^{4+} reduction. It appears that the reduction percentage are all the same when the flow rates are in the range of 50 to 200 $ml.min^{-1}$. From Fig.6 and 7, it is clear that the mixing of electrolyte is easy to achieve in this flow-type electrolyzer, the available flow rate is versatile for the demand of whole

decontamination process.

3-4. Electrode materials

The redox decontamination technique is one of the oxidative dissolution decontamination methods, so the used electrode materials should be corrosion resistive. Fujita et al.[4] measured the corrosion rate for platium, gold, titanium, niobium, Hastelloy-C and Zircaloy-2 in the Ce^{4+}-HNO_3 solutions and found that the platium, gold and titanium were not corroded. In this study, we choose platinized titanium meshes as anode , and platinized titanium meshes or graphite plate as cathode.

Fig.8 is the electrolytic reduction rate comparison between platinized titanium meshes and graphite plate which are used as cathode. The result shown in Fig.8 demonstrates that reduction rate is faster using platinized titanium meshes than that of using graphite plate. Furthermore, the cell voltage of using platinized titanium meshes is lower than that of using graphite. From other investigators' experiences and our own experimental results, it is obvious that the platinized titanium material is a good choice as electrode for Ce^{4+}/Ce^{3+} redox reaction.

3-5. Type of ion exchange membrane

Using ion exchange membrane as cell separator has many advantages such as prevention of reverse reaction of redox, free choice of the ions transferred across the membrane. Generally, there are two types of ion exchange membrane, which are anion and cation membrane. After the pretreatment with sulfuric acid solution, the anion membrane can transfer SO_4^{2-} ions and the cation membrane can transfer H^+ ions. Therefore, during the electrolysis with cation membrane the H^+ ions are transferred from anode compartment to cathode compartment due to the electric field. On the other hand, the SO_4^{2-} ions are transferred from cathode compartment to anode compartment if the anion membrane is used as cell separator.

Fig.9 is the results of using different membranes in electrolytic reduction of Ce^{4+} from Ce^{3+}. Both anion and cation membrane as separator can achieve 100% reduction, but it seems that the anion membrane is better than cation membrane in this operation condition. In the beforementioned discussion, we know that electrolyte acidity does not drastically affect the redox performance using anion membrane as cell separator. However, the acidity of electrolyte will affect the transfer of H^+ across the membrane when the cation membrane is used. Fig.10 shows that the average current efficiency of Ce^{4+} reduction increases with increasing electrolyte acidity, but the average current efficiency markedly decreases when the acidity is over 5 N. The phenomenon shown in Fig.10 can be explained as follows. In the beginning, since the electrolyte conductivity and H^+ ions transfer rate depend on the $[H^+]$, the average current efficiency of Ce^{4+} reduction increases as the acidity of electrolyte is from 0.25 to 3 N. However, the increasing $[H^+]$ both from the initial addition and transferred from anode compartment will enhance the opportunity of evolution of H_2, so the current efficiency decreases when the acidity is over 5 N. In the meantime, since the acidity does not affect the evolution of O_2 at anode, the acidity of electrolyte would have less influence on oxidation.

3-6. Effect of cerium concentration

Although different concentration of cerium solutions all can obtain high conversion in redox reaction, the current efficiency drastically depends on the cerium concentration.

Fig.11 shows that the average current efficiency of Ce^{3+} oxidation increases linearly with increasing Ce^{3+} concentration. Fig.12 indicates the same tendency for the Ce^{4+} reduction. Since we have shown in above that the electrolyte flow rate does not affect the redox rate when the flow rate is over 70 $ml.min^{-1}$, it seems that redox rate is controlled by the Ce^{4+} or Ce^{3+} diffusion rate from the diffusion layer to electrode surface.

3-7. Feasibility of simultaneous redox in the same electrolyzer

In the common redox decontamination process, the regeneration of Ce^{4+} from Ce^{3+} needs an electrolyzer in which the working electrode is anode. Moreover, the electrolytic reduction of Ce^{3+} from Ce^{4+} for the purpose of subsequent wastewater treatment needs another electrolyzer in which the working electrode is cathode. If these two separated steps can be combined into one step, Ce^{4+} reduction happens in cathode compartment and the Ce^{3+} oxidation occurs in anode compartment at the same time, then the redox decontamination process can be improved. The electrolyzer using ion exchange membrane as cell separator is suitable for this requirement.

Fig.13 is the performance of simultaneous Ce^{4+}/Ce^{3+} redox reaction in the same electrolyzer but different compartment with anion membrane as cell separator. It appears that both reduction and oxidation can achieve near 100% conversion in 2 h electrolysis. Experimental result also shows good performance when using cation membrane as cell separator. Therefore, it can conclude that the simultaneous redox of Ce^{4+}/Ce^{3+} in the same electrolyzer is feasible. This result is encouraging for the improvement of redox decontamination process.

4. CONCLUSIONS

An electrolyzer separated with ion exchange membrane is suitable for the redox decontamination process. The experimental results show its widely applicable operation conditions. The available acidity and electrolyte flow rate are versatile for the choice to fit the process requirement. In addition, both anion and cation membrane can be used in Ce^{4+}/Ce^{3+} redox reaction. The platinized titanium meshes is good material as anode and cathode. Although the current efficiency drastically depends on the cerium concentration, even very diluted cerium solution can achieve high redox conversion within limited electrolysis time. Finally, the most important result is that the simultaneous Ce^{4+}/Ce^{3+} redox with the same electrolyzer in different compartment can proceed with good performance. And this advantage can be used to improve the redox decontamination process.

5. REFERENCES

1. Ishibe T., Fujita R., Enda M. and Morisue T., "Redox decontamination technique development using sulfuric acid", Proceedings of the 1989 joint international

waste manegement conference, Japan ,October 22-
Vol.1, 421-436(1989).

2. Suwa T., Kuribayashi N. and Tachikawa E., "Development of chemical decontamination process with sulfuric acid-cerium(IV) for decommissioning: Single step process to dissolve chromium-rich oxides", J. Nucl. Sci. Technol., 23, 7,622-632(1986).

3. Suwa T., Kuribayashi N. and Tachikawa E., "Development of chemical decontamination process with sulfuric acid-cerium(IV) for decommissioning: System decontamination process with electrolytic regeneration of Ce^{4+} from Ce^{3+}", J. Nucl. Sci. Technol., 25, 7, 574-585(1988).

4. Fujita R., Enda M. and Morisue T., "Redox decontamination technique development, (I) Selection for disolutive and regenerative conditions", J. Nucl. Sci. Technol., 26, 3, 339-349(1989).

5. Fujita R., Enda M. and Morisue T., "Redox decontamination technique development, (II) Redox decontamination system using pilot plant", J. Nucl. Sci. Technol., 26, 4, 449-458(1989).

6. Kuroiwa K. et al.(Editors), "Progress of JPDR decommissioning program, second progress report (August,1987- March, 1988)", Department of JPDR, Japan Atomic Energy Research Institute, 20-24(1988).

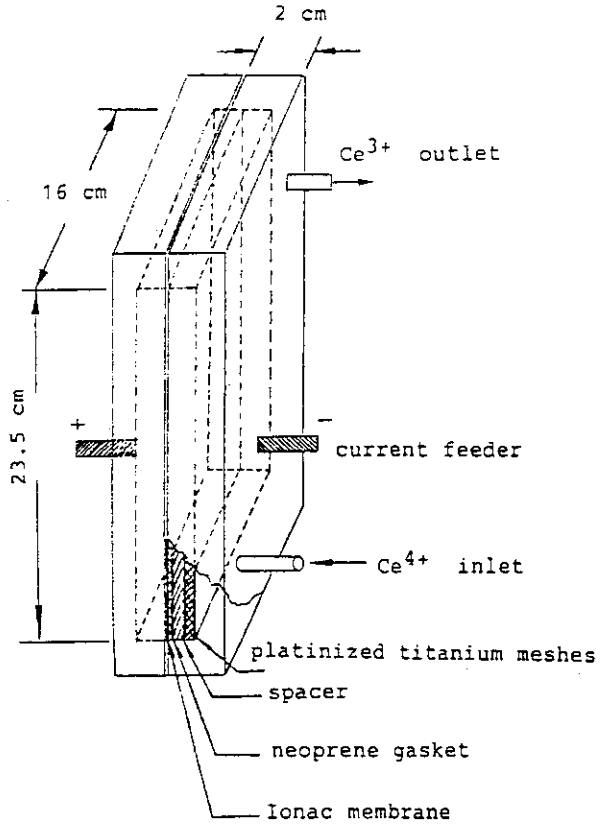

Figure 1. Schematic diagram of electrolyzer used in this experiment.

Figure 2.

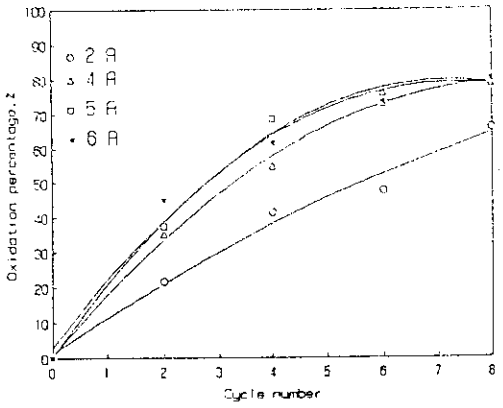

Effect of operation current on the oxidation percentage (initial $[Ce^{3+}]$=0.05 M; $[H^+]$=1 N; 1 N H_2SO_4 solution as catholyte)

Figure 3.

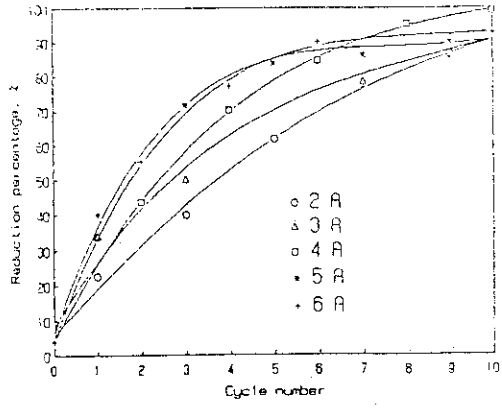

Effect of operation current on the reduction percentage (initial $[Ce^{4+}]$=0.05 M; $[H^+]$=1 N; 1 N H_2SO_4 solution as anolyte)

Figure 4.

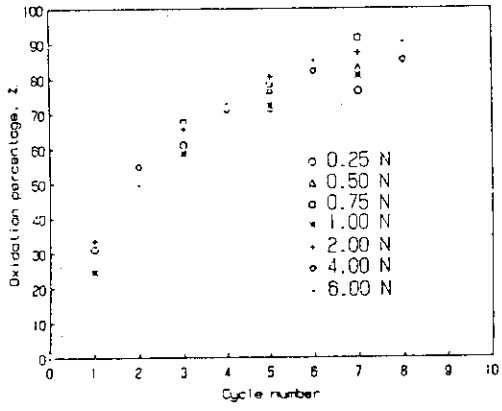

Effect of anolyte acidity on Ce^{3+} oxidation with platinized titanium meshes anode and anion membrane as cell separator($[Ce^{3+}]$=0.0025 M)

Figure 5.

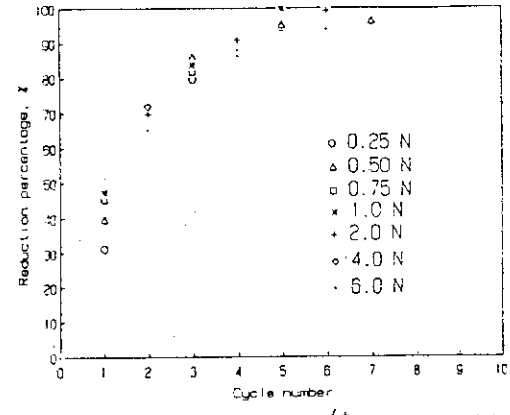

Effect of catholyte acidity on Ce^{4+} reduction with platinized titanium meshes cathode and anion membrane as cell separator(initial $[Ce^{4+}]$=0.0025 M)

Figure 6.

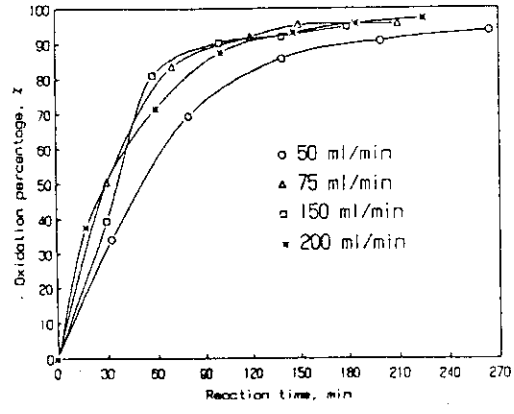

Effect of electrolyte flow rate on Ce^{3+} oxidation (operation current=4 A; initial $[Ce^{4+}]$=0.05 M)

Figure 7.

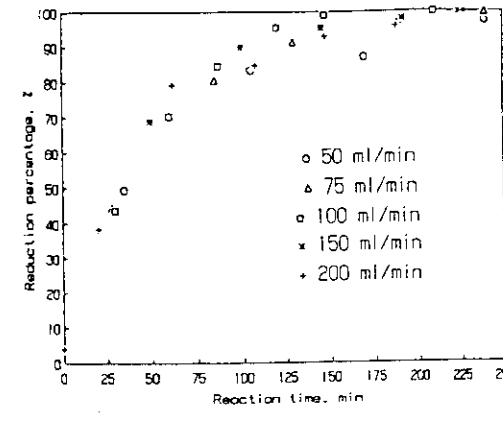

Effect of electrolyte flow rate on Ce_{4+} reduction (operation current=4 A; initial $[Ce^{4+}]$=0.05 M)

Figure 8.

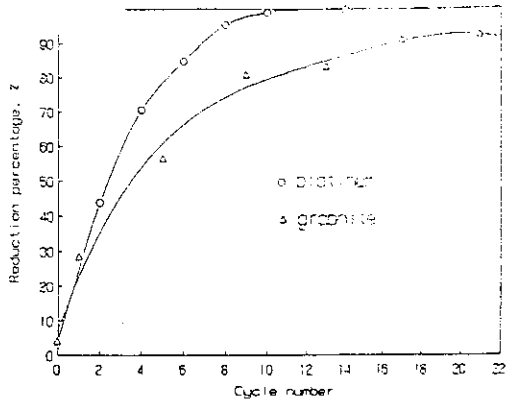

Comparing the reduction performance between the platinized titanium meshes and graphite as cathode (operation current=4 A; initial $[Ce^{4+}]$=0.05 M)

Figure 9.

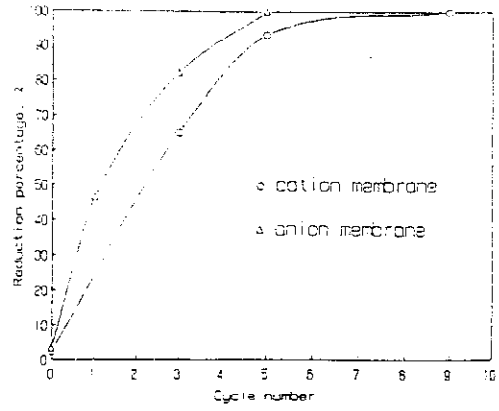

Comparison of Ce^{4+} reduction percentage between the different type of membrane used as cell separator (initial $[Ce^{4+}]$=0.05 M; $[H^+]$=1 N)

Figure 10.

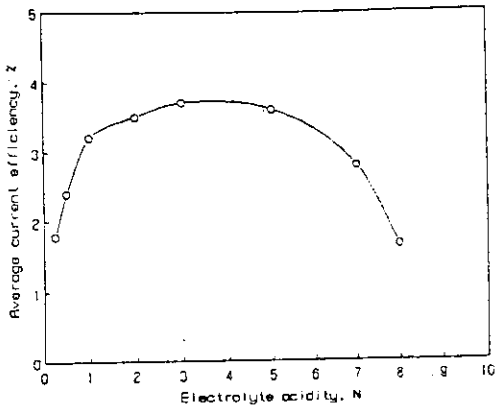

Effect of catholyte acidity on the average Ce^{4+} reduction current efficiency with platinized titanium meshes cathode and cation membrane as cell separator (operation current=4 A; initial $[Ce^{4+}]$=0.005 M)

Figure 11.

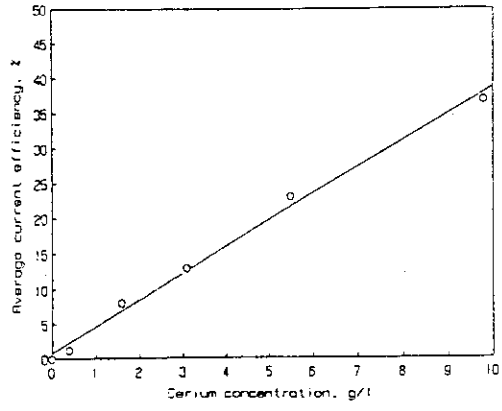

Effect of Ce^{3+} concentration on the average oxidation current efficiency calculated on the basis of 85% conversion (operation current=4 A; $[H^+]$=1 N)

Figure 12.

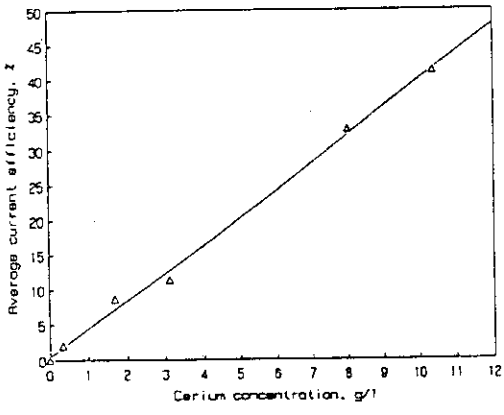

Effect of Ce^{4+} concentration on the average reduction current efficiency calculated on the basis of 90% conversion (operation current=4 A; $[H^+]$=1 N)

Figure 13.

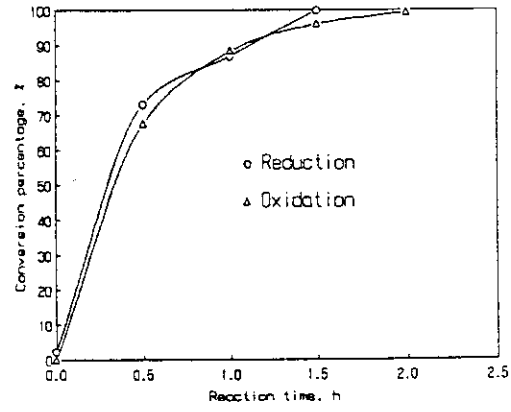

Performance of simultaneous Ce^{4+}/Ce^{3+} redox reaction in the same electrolyzer but different compartment with anion membrane as cell separator (operation current=6 A; initial $[Ce^{4+}]$=0.015 M; initial $[Ce^{3+}]$=0.015 M; $[H^+]$=6 N)

8. Support Method for Solving an Optimal Xenon Shutdown Problem

LE CHI DUNG

Vietnam National Atomic Energy Commission
59 Ly Thuong Kiet, Hanoi
Telex: 411518 VAEC.VT

ABSTRACT

Since the discovering of the maximum principle by Pontriagin in 1956, methods for solving optimal control problems have been developed fast. There are the efforts to solve an optimal problem of transient process in a nuclear reactor using its ideas. However, the classical maximum principle does not show how to construct an optimal control or suboptimal control with a given exactness.

We exploit mainly in the present work the ideas of the support method proposed by Gabasov and Kirillova for linear systems, in order to solve an optimal control problem for non-linear systems. The constructive maximum principle for non-linear dynamic systems with controllable structure received by us in this paper is new result.The ε - maximum principle is used for receiving an 7-phase ε-optimal control of optimal xenon shutdown problem.

1. OPTIMAL CONTROL PROBLEM.

We consider an optimal control problem of the following form:

$$J(u) = \phi(x(t^*)) \rightarrow min \tag{1}$$

$$\dot{x} = f_1(x) + f_2(x)u,\ x(0) = x_0 \tag{2}$$

$$|u(t)| \leq 1,\quad t \in T = [0,t^*] \tag{3}$$

$$d(x(t)) \leq 0,\ t \in T,\ g(x(t^*)) = 0 \tag{4}$$

Here $x(t) \in R^n$, the given n-functions $f_1(.), f_2(.)$, m-function $g(.)$ and scalar functions $d(.), \phi(.)$ are supposed to be continuous and to have continuous derivatives up to the second order; x_0 is a given vector of R^n; $u(t)$ is a scalar function; the final moment 0 can be replaced by any finite moment $t^* < t^*$ and (3) can be replaced by the constraint $u^* \le u(t) \le u^*, t \in T$. An admissible control $u(.)$, an optimal control $u^0(.)$ and a suboptimal (ε-optimal) control $u^\varepsilon(.)$ are defined as usual.

Suppose that we have already got an admissible control $u(.)$. To have a control variation $\Delta u(.)$ with the property that a control $u(t) = u(t) + \Delta u(t)$, $t \in T$, is admissible, we construct a support, which guarantees the constraints (4) in computing process.

We use the following symbols:

$$A(t) = \frac{\partial f'_1(x(t))}{\partial x} + \frac{\partial f'_2(x(t))}{\partial x} u(t)$$

$$b(t) = f_2(x(t)), \quad D(t) = \frac{\partial d(x(t))}{\partial x}, \ t \in T$$

$$c(t^*) = \frac{\partial \phi(x(t^*))}{\partial x}, \quad G(t^*) = \frac{\partial g'(x(t^*))}{\partial x}$$

(the superscript ' denotes transposition of vector or matrix)

In general, let us introduce a set

$$T_x = \{T_i = [\tau_i, \tau^i] \subset T, \tau_i \le \tau^i < \tau_{i+1}, i \in N = \{1,2, \ldots ,p\}\}.$$

Denote by $N^* = \{i \in N : t_i < t^i\}$, $N_0 = N \setminus N^*$, $T^*_x = \bigcup_{i \in N^*} T_i$, $T_{nx} = T \setminus T^*_x$

Suppose that rank $G(t^*) = m < n$ and $\Phi(t,\tau)$ is a fundamental matrix of the solutions of homogeneous system:

$$\dot{z}(t) = \overline{A}(t)\, z(t), \ z(0) = 0$$

where

$$\overline{A}(t) = A(t), \quad t \in T_{nx}$$

$$\overline{A}(t) = \left[E - \frac{b(t)D(t)}{D(t)b(t)} \right] A(t) - \frac{b(t)D(t)}{D(t)b(t)}, \ t \in T^*_x$$

E is the unit diagonal ($n \times n$)-matrix.

Suppose that there is a set $t_x = \{t_j, j \in J^*\}$, $t_j \in T^0_{nx} = T \setminus \bigcup_{i \in N} T_i$ so that

$|N| + m = |J^*|$, $det\, P_X \neq 0$, $J_i = \{j \in J^* : t_j \leq \tau_j\}$.

$$P_X = \begin{Bmatrix} G(t^*)\,\Phi(t^*,t_j)\,b(t_j),\ j \in J^* \\ D(\tau_i)\,\Phi(\tau_i,t_j)\,b(t_j),\ j \in J_i\ ;\ 0,\ j \in J^* \setminus J_i \\ i \in N \end{Bmatrix}$$

DEFINITION. The set $S_X = \{T_X, t_X\}$ is called a (local) support of the constraints of the problem (1) - (4), if $det\, P_X \neq 0$. The pair $\{u(.), S_X\}$, where $u(.)$ is an admissible control, S_X is a support, is called a support control. We say that a support control $\{u(.), S_X\}$ is optimal, if $u(.)$ is optimal, and it is non-singular if

a) $|u(t_j + 0) + u(t_j - 0)| / 2 < 1,\ j \in J^*$

b) $d(x(t)) < 0, t \in T \setminus T_X$

c) Equality $|u(t)| = 1$ can be true at a finite number of isolate points of T_X only. Moreover, if $|u(\tau_i)| = 1\ (|u(\tau^i)| = 1)$ there is a natural number $p_i > 1$ $(p^i > 1)$ such that $d^{P_i}u(\tau_i) / dt^{P_i} = 0$ $(d^{p^i}u(\tau^i) / dt^{p^i} = 0)$.

We can show that a support has a direct connection with a controllable essence of the system (1) - (4) on T_X.

Let $\{u(.), S_X\}$ be a support control. Then we calculate $(y, \bar{v}_i, i \in N) = (c'(t^*)\,\Phi(t^*,t_j)\,b(t_j), j \in J^*)'\ P_X^{-1}$ and solve the following system:

$$\dot{\Psi}_* = -\overline{A}'(t)\Psi_*\ ,\ \Psi_*(t^*) = G'(t^*)y - c(t^*)$$

$$\Psi_*(\tau_i - 0) = \Psi_*(\tau_i) - d(\tau_i)\bar{v}_i,\ i \in N$$

Choose now

$$\Psi(t) = \Psi_*(t),\ t \in [\tau^i, \tau_{i+1}]$$

$$\Psi'(t) = \Psi'_*(\tau)\left[E - \frac{b(t)D(t)}{D(t)b(t)}\right], t \in [\tau_i, \tau^i], i = \overline{0,p}$$

$$v_i = \bar{v}_i - \Psi'_*(\tau_i + 0)\,b(\tau_i) / D(\tau_i)\,b(\tau_i)$$

$$v^i = \Psi'_*(\tau^i + 0)\,b(\tau^i) / D(\tau^i)\,b\tau^i),\ i \in N \qquad (5)$$

$$\xi(t) = \frac{-\Psi'(t)\,(A(t)b(t) - b(t))}{D(t)b(t)}\ ,\ t \in T_i,\ i \in N_*$$

$$\xi(t) = 0,\ t \in T_{nx} \qquad (6)$$

Then $\Psi(t)$, $t \in T$, is a solution of a conjugate system

$$\dot{\Psi}(t) = -A'(t)\Psi(t) - D'(t)\xi(t)$$

$$\Psi(t^*) = G'(t^*)y - c(t^*) \tag{7}$$

$$\Psi(t^i) = \Psi(t^i + 0) - D'(\tau^i)\nu^i$$

$$\Psi(\tau_i - 0) = \Psi(\tau_i) - D'(\tau_i)\nu_i, \quad i \in N \tag{8}$$

We have the following constructive analogy of the Pontriagin maximum principle:

THEOREM 1. Suppose that $\{u(.), S_X\}$ is a non-singular optimal support control, x(.) is a corresponding trajectory of the system (2), $\Psi(.)$ is a solution of the system (7) - (8) with the parameters of the form (5) - (6). Then the following condition holds

$$H(x(t), \Psi(t), u(t)) = \max_{|u| \le 1} H(x(t), \Psi(t), u), \quad t \in T$$

where

$$H(x, \Psi, u) = \Psi'(f_1(x) + f_2(x)u)$$

ALGORITHM. Using the above result, we can realize an algorithm for the problem (1) - (4) in three stages (as seen in reference[2]):

a) Formulating a support (linear) problem: Instead of the non-linear problem we formulate its approximation, which is easier to solve.

b) Solving the support problem and analysing its solution.

We use first two stages as iterative steps to get a support control, which is near enough to the solution of the given problem to pass to the next stage.

c) Improving a support control : We formulate a system of equations, its solution is a solution of the given problem.That system of equations could be solved via Newton method, which is the fastest method to solve nonlinear problems.

We illustrate first two stages of an algorithm for the following practical example.

2.OPTIMAL XENON SHUT-DOWN PROBLEM.

We consider the single-point model of a reactor operating at a neutron flux N. The instantaneous state equations relating the concentrations of I-135 and Xe-135 are [3] :

$$\dot{I} = \gamma_1 \Sigma N - \lambda_1 I$$

$$\dot{X} = \gamma_2 \Sigma N + \lambda_1 I - \lambda_2 X - \sigma_2 X N \qquad (9)$$

where γ and λ = yield and decay constants of the particular isotop, respectively;
Σ = macroscopic fission cross section of the fuel;
σ_2 = microscopic cross section of xenon.

Suppose that in a transient process the concentration of Xe-135 is not greater than X_{max}

$$X(t) \leq X_{max} \qquad (10)$$

We choose R^2 as the phase space with the components $x_1(t) = I(t)/\Sigma N_{max}$, $x_2(t) = X(t)/\Sigma N_{max}$, where N_{max} is the maximal neutron flux of the reactor.

Let us use the notations $\sigma = \sigma_2 N_{max}$, $u(t) = N(t)/N_{max}$, $R = X_{max}/N_{max}$. The system (9) (10) has the following form

$$\dot{x}_1 = -\lambda_1 x_1 + \gamma_1 u \qquad (11)$$

$$\dot{x}_2 = \lambda_1 x_1 - \lambda_2 x_2 + (\gamma_2 - \sigma x_2)\, u$$

$$x_2(t) \leq R \qquad (12)$$

Naturally, we have a constraint $0 \leq u(t) \leq 1$ in the transient process $t \in T = [0, t^*]$ and a condition at the beginning

$$x_1(0) = \gamma_1 / \lambda_1,\ x_2(0) = (\gamma_1 + \gamma_2)/(\lambda_2 + \sigma) \qquad (13)$$

The problem is to control a phase trajectory of the system (11)-(13) to the post-shutdown trajectory, which has the following equation

$$x_2 = \left[R \left(\frac{x_1}{R\delta} \right)^{\delta} - x_1 \right] \frac{1}{1-\delta}, \quad \delta = \lambda_2 / \lambda_1$$

We have the different optimal control problems by choosing the different control critetions :

1) If $J(u) = t^* \rightarrow \min$, we have the time-optimal shutdown problem;

2) If $J(u) = \int_T u(t) x_2(t)\, dt$, we have the problem of minimization of an energy in the transient process;

3) If $J(u) = \int_T u(t)x2(t)dt$, we have the problem of minimization of the number of neutrons, which are captured by xenon.

Suppose that $\gamma 1 = 0.061$; $\gamma 2 = 0.003$; $\lambda_1 = 2.8525 \times 10^{-5}$/sec; $\lambda_2 = 2.1088 \times 10^{-5}$/sec; $\sigma_2 = 2.7 \times 10^{-18}$ barn; $N = 10^{14}$ neutrons/(cm^2. sec); $X_{max} = 6 \times 10^{16}$ /cm^2.

The 3-phase control $u(t)$, $t \in T = [0, t^*]$, and its corresponding phase trajectory $x(t)$, $t \in T$, (see Figure 1), satisfy the maximum principle. Here, we have $\tau 1 = 8400$ sec, $\tau^1 = 33960$ sec, $t^* = 37140$ sec.

As it is showed in reference[1] the time-optimal shutdown problem can be reduced to an optimal control problem, which is stated in the following form

$$J(u) = \frac{(1-\delta)\, x_2(t^*) + x_{1(t^*)}}{x_1^{\delta}(t^*)} \rightarrow min \qquad (14)$$

where $x_1(t)$, $x_2(t)$, $t \in T$, are phase components of the system (11) - (13).

Choose $t_1 = 8000$ sec. We have $P_x = D(\tau 1)\, \Phi(\tau 1, t1) b(t1) \neq 0$. So we can see $S_x = \{[\tau 1, \tau^1], t1\}$ as a local support of the problem (11) - (14). We formulate its support (linear) problem as a particular case of the problem

$$\begin{aligned} &J(v) = c'(t^*)z(t^*) \rightarrow min \\ &\dot{z}(t) = A(t)z(t) + b(t)v(t),\ z(0) = 0 \\ &d_*(t) \leq d'z(t) \leq d^*(t),\ v_*(t) \leq v(t) \leq v^*(t),\ t \in T \end{aligned} \qquad (15)$$

In general, given matrix- and vector-functions $A(.)$, $b(.)$, $c(.)$, $d_*(.)$, $d^*(.)$, $v_*(.)$, $v^*(.)$ are supposed piecewise smooth, d is a given vector. In our case,

$$A(t) = \begin{bmatrix} -\lambda 1 & 0 \\ \lambda 1 & -\lambda 2 \end{bmatrix} + \begin{bmatrix} 0 & 0 \\ 0 & -\sigma \end{bmatrix} u(t)$$

$$b'(t) = (\gamma 1,\ \gamma 2 - \sigma x_2(t)),\quad c'(t) = \left(1 - \delta \frac{x_2(t^*)}{x_1(t^*)} -,\ 1\right) \frac{1-\delta}{x_1^{\delta}(t^*)},$$

$$d' = (0, 1),\ d_*(t) = -x_2(t),\ d^*(t) = R - x_2(t),\ v_*(t) = -u(t),\ v^*(t) = 1 - u(t),\ t \in T$$

To get $\Psi(t)$, $\xi(t)$, $t \in T$, v_i, v^i, $i \in N$, as they are defined in section 1, we have the following result for suboptimality of an admissible control

v(t), t ∈T,of the problem (15).

THEOREM 2. For any $\varepsilon \geq 0$, an admissible $v(t), t \in T$, is suboptimal (ε - optimal) iff there is a support S_z so that the phase trajectories $z(t)$, $\Psi(t)$, $t \in T$, corresponding to the support control $\{ v(.), S_z \}$, satisfy the following conditions

$$\Psi'(t)\, b(t)\, v(t) = \max_{v_*(t) \leq v \leq v^*(t)} \Psi'(t)\, b(t)\, v - \varepsilon_v(t), \quad t \in T$$

$$\xi(t)\, d'z(t) = \min_{d_*(t) \leq \gamma \leq d^*(t)} \xi(t)\, \gamma + \varepsilon_z(t), \quad t \in T$$

$$v_i\, d'z(\tau_i) = \max_{d_*(\tau_i) \leq \gamma \leq d^*(\tau_i)} v_i \gamma - \varepsilon_i, \quad i \in N$$

$$v^i\, d'z(\tau^i) = \max_{d_*(\tau^i) \leq \gamma \leq d^*(\tau^i)} v^i \gamma - \varepsilon^i, \quad i \in N$$

$$\int_T (\varepsilon_v(t) + \varepsilon_z(t))\, dt + \sum_{i \in N} (\varepsilon_i + \varepsilon^i) \leq \varepsilon$$

Choose a parameter $h > 0$. We can construct an h-approximation of the problem (15) as the following

$$\begin{aligned}
&c'(t^*)z(t^*) \to \min \\
&\dot{z} = A(t)z + b(t)v, \; z(0) = 0, \qquad (16) \\
&d_*(\tau_{(k)}) \leq d'z(\tau_{(k)}) \leq d^*(\tau_{(k)}), \; k = \overline{1, n^* + 1} \\
&v(t) = v_k, \; t \in T_{(k)}, \; v_{*k} \leq v_k \leq v^*_k, \; k = \overline{0, n^*} \text{ where } \tau_{(k)} = hk, \; k = \overline{0, n^*}, \; n^* = [t^*/h], \\
&\tau_{(n+1)} = t^*, \; T_{(k)} = [\tau_{(k)}, \tau_{(k+1)}], \; k = \overline{0, n^*}
\end{aligned}$$

Suppose that $F(t,\tau)$, $t \geq \tau$, is a fundamental matrix of the solutions of homogeneous system $\dot{z} = A(t)z$, and $B(k) = F(\tau_{(k+1)}, \tau_{(k)})$, $b(k) = \int_{\tau(k)}^{\tau(k+1)} F(\tau_{(k+1)}, \tau)\, b(\tau)\, d\tau$

$z(k) = z(\tau_{(k)})$, $v(k) = v_k$, we rewrite the problem (16) in the equivalent form :

$$\begin{aligned}
&c'z(n^* + 1) \to \min \\
&z(t+1) = B(t)z(t) + b(t)v(t), \; t = \overline{0, n^*}, \; z(0) = 0 \qquad (17) \\
&d_*(t) \leq (t)\; d'z(t) \leq d^*(t), \; t = \overline{1, n^* + 1} \\
&v_*(t) \leq v(t) \leq v^*(t), \quad t = \overline{0, n^*}
\end{aligned}$$

To solve the problem (17) using well-known procedures, we get an h-approximation of real solution of our problem.And then we can use a procedure as shown in reference[2] for improvement stage.

For the case if the change velocity of N is restricted, for example between -3 and 3 , an ε - optimal 7-phase optimal control is showed on the Figure 2. It takes 10.57 hours to reach the post-shutdown trajectory.

ACKNOWLEDGEMENT

I would like to thank Prof. Rafail Gabasov, consults with him are very useful for this work.

REFERENCES

[1] **R.Gabasov, F.M.Kirillova,** *The Maximum Principle in Theory of Optimal Control,* Minsk (1974). *In Russian.*

[2] **R.Gabasov, F.M.Kirillova, et al.,** *Constructive Methods for Optimization,* Vol.5 - *Nonlinear Problems,* Minsk (1991). *In Russian.*

[3] **A.Gerasimov, A.P.Rudik,** *A Xenon-135 Poison of Reactor,* Moscow (1982). *In Russian.*

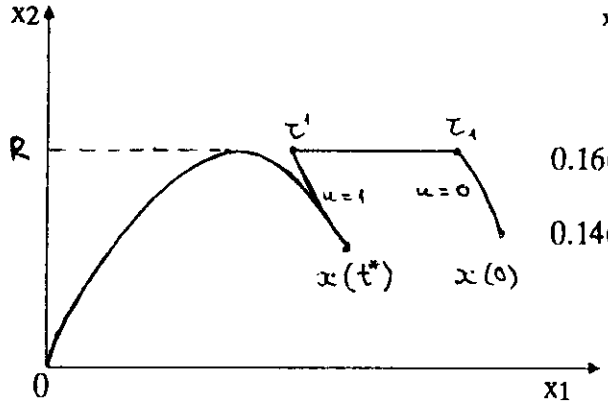

Figure 1. 3-phase trajectory .

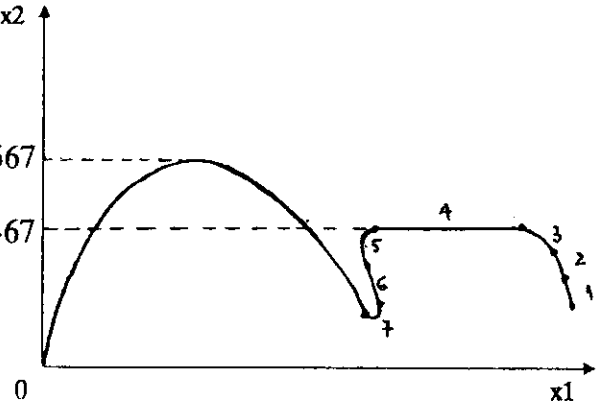

Figure 2. 7-phase trajectory .

1. Some Unique Activities of the Smallest Reactor: UTR-KINKI

TOSHIKAZU SHIBATA

Atomic Energy Research Institute, Kinki University

ABSTRACT

In the UTR-KINKI, school teachers trainings are being done, besides utilizations for research and student experiments. In this paper, some details of the school teachers training course are presented. 267 teachers have attended the training since 1987, the beginning of the program. Drastic impacts by the training were recognized in impressions of the attended teachers about nuclear energy.

INTRODUCTION

The UTR-KINKI was built initially at the Exposition which was held in Tokyo. The Kinki University bought the reactor, and transported to the university campus near Osaka City in 1961.

The nominal power was 0.1 watt for the first 12 years, and then increased to 1 watt. Because the power is very small, radio-activities of the core elements including fuel elements are very weak. The core elements can easily be handled by hands just after the shutdown of reactor. And the irradiation of samples can be set up by manually with sufficient accuracy. Also the induced activity of the irradiated sample is so small, that precise treatments of the sample are possible.

Various experiments are being done using the UTR-KINKI. Typical annual record of the reactor utilization is shown in Table 1. Each utilization has unique feature in order to compensate the lack of the reactor power. In this paper, school teacher's training program, which is one of the significant utilizations of the UTR-KINKI, shall be explained.

SCHOOL TEACHER'S TRAINING PROGRAM

OBJECTIVES

In Japan, many debates about the nuclear energy issues are being done. But some of them are not based on scientific basis. Sometimes, only emotional opinions overwhelm cool and scientific discussions. At the present proper considerations and decisions have to be required for energy problems at the global level. And, public acceptance is the most important condition for realizing the decisions.

High school teachers are supposed as very influential for young people

who will make future public opinions. And if teachers had sufficient training and experience about nuclear energy, their influences will be increased in proper directions.

The training program started with the above considerations.

Table.1 UTR-KINKI Typical Annual Working Records

Subjects		Operating Days
Reactor Physics and Reactor Applications		37
Biological Effects of Radiations		31
Reactor Chemistry, Radio Chemistry		19
Neutron Radiography		10
Student Experiments	Kinki Univ.	22
	Other Univ.	11
School Teacher's Training		21
Annual Official Examinations		10
Overhauls, Preparations		6
Tatal		221

CURRICULUM

The main parts of the training are reactor experiments and free discussions on not only nuclear energy but general educational problems. The contents of the experiments in the training course are ; 1) critical experiment, 2) control rod worth measurement, 3) neutron flux distribution and power evaluation, 4) activation analysis, 5) measurements of radiations, and so on.

These contents are very similar to the student experiments in the university curriculum, but descriptions of the experiments are so contrived that is quite easy to understand even for teachers of non scientific fields.

TRAININGS

The training program started in 1987 and courses have been done 18 times. Affiliations of the attended teachers in the past are listed in Table 2. Some photographs of practical scenes are shown for better understandings.

Table. 2
Affiliations of Attendants to School Teacher's Training Course

Year	No. of courses	Affiliations					Total
		University	senior High	Junior high	Education center, Comm.	Graduate Student	
1987	1		8		5		13
1988	4	15	16		16	1	48
1989	4	6	36	3	16	2	63
1990	4	1	42	1	10	4	58
1991	5	1	52	26	3	3	85
Total		23	154	30	50	10	267

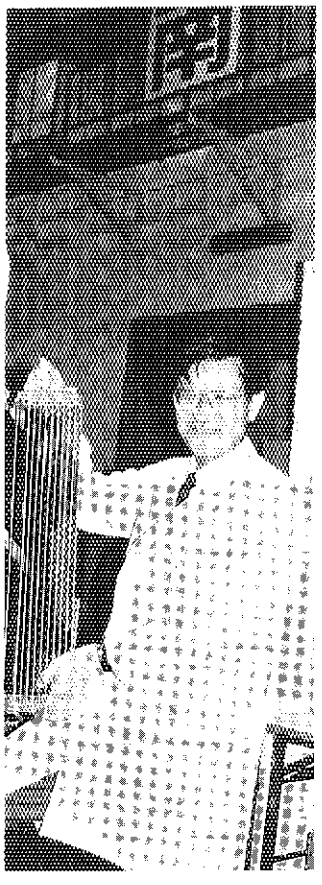

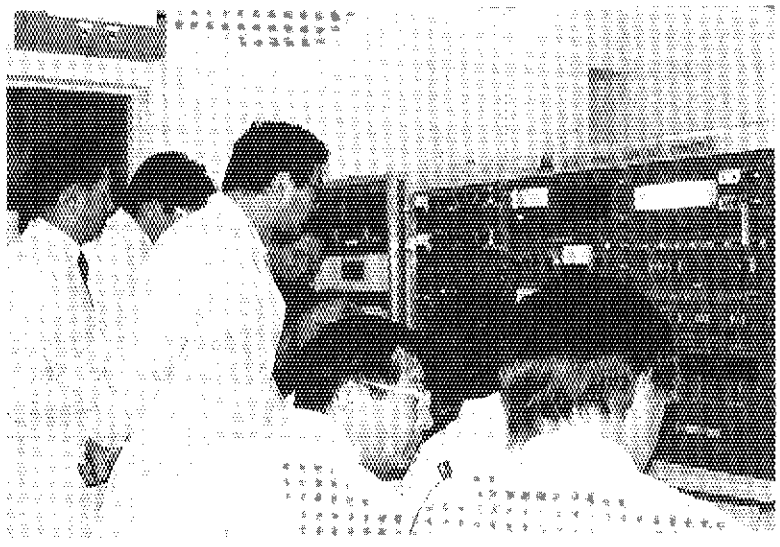

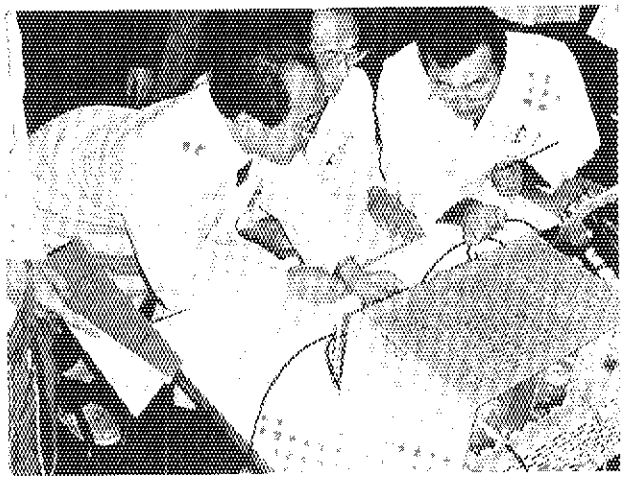

IMPACTS TO THE ATTENDANTS

Some quetionaire were requested to the attended teachers at the recent two courses for investigating the impacts of the training. The results of questionarie are listed in Table 3 and 4. The changes in impressions and self-confidence in teaching on nuclear energy are quite obvious.

Table.3 Changes in Impressions as to Nuclear Energy (Results of quessionare, secret ballots by attendee)

Feeling about nuclear Energy (Reactor, Radiations etc)	1 st		2 nd	
	before training	after training	before training	after training
1, Very terrible still very terrible	6	0	4	0
2, Considerably terrible still considerably terrible	4	5	6	5
3, Neutral	3	8	3	4
4, Almost not terrible	2	3	2	6
5, Not terrible at all	1	0	0	0

Table.4 Changes in Self Confidence in Teaching Nuclear Energy (Result of quessionaire, secret ballots by attendee)

Self confidence in teaching nuclear energy	1 st		2 nd	
	before training	after training	before training	after training
1, Not confident at all	4	1	1	0
2, Not confident almost	3	2	3	3
3, Neutral	8	5	7	2
4, Confident considerably	1	8	3	9
5, Confident absolutely	0	0	1	1

FREE DISCUSSIONS

The free discussions are held in every evening until midnight. Almost of the attendant were sutisfied for the contents. Some of the attending teachers are "against nuclear." In general, they stated, however, that learning and experience on real reactors and facilities are important for sufficient considerations and correct decisions.

CONCLUSION

It is supposed that real results of educational efforts will appear after many years. Therefore the efforts should be continued for long period.

2. Semiconductor Research with Reactor Neutrons

ITSURO KIMURA

Department of Nuclear Engineering
Kyoto University, Yoshida
Sakyo-ku, Kyoto 606-01, Japan

ABSTRACT

Reactor neutrons play an important role for characterization of semiconductor materials as same as other advanced materials. On the other hand reactor neutrons bring about not only malignant irradiation effects called radiation damage, but also useful effects such as neutron transmutation doping and defect formation for opto-electronics. Research works on semiconductor materials with the reactor neutrons of the Kyoto University Reactor (KUR) are briefly reviewed. In this review, a stress is laid on the present author's works.

INTRODUCTION

Atomic and mesoscopic structures of semiconductor crystals can be analyzed by neutron diffraction (ND) and neutron small angle scattering (NSAS), respectively. For instance, A. Okazaki et al. found an abnormal crystal structure of silicon with a neutron diffractometer of KUR [1]. An oxygen precipitate process in Czochralski-grown silicon crystal was studied with a NSAS spectrometer at KUR by T. Takeda et al. [2]. Frequency distribution of phonons or phonon spectrum of semiconductor crystals can be obtained by neutron inelastic scattering (NIS), but more intense neutron beam may be desirable for NIS spectrometry than that of KUR.

Characteristics of semiconductor materials are strongly governed by very small amount of impurity elements and lattice defects. Reactor neutrons are of great use to measure some of these quantities. Because of its excellent sensitivity, neutron activation analysis (NAA) is widely applied to analyze not only impurity elements in a matrix of semiconductor materials, but also impurity distributions close to their surface. By making use of a radioactive isotope with considerably short half life as a tracer, dynamic behaviour of impurity distributions in semiconductor materials can be also observed, and these radioactive isotopes are mainly produced by reactor neutron irradiation. A few examples are shown later. Profiles of boron distribution close to a surface of semiconductor materials can be also obtained by neutron depth profiling (NDP), however none of NDP work has been attempted in KUR so far. We may apply prompt gamma-ray analysis (PGA) using neutron capture reactions to impurity analysis of semiconductor materials, but none has tried this technique at KUR yet.

When we irradiate a semiconductor material with neutrons especially with fast ones, atoms in a crystal lattice are knocked on and there arise lattice defects which are often called radiation damage. On the other hand, when a constituent nucleus in a semiconductor material captures a thermal neutron and then its residual nucleus converts to a new element by beta decay, this newly produced nucleus often acts as a new dopant in the original matrix. The most typical example is the $^{30}Si\ (n,\gamma)\ ^{31}Si$ reaction and $^{31}Si \rightarrow {}^{31}P + \beta^- + \bar{\nu}$, by which phospher is doped in the silicon matrix. This technique is called neutron transmutation doping (NTD). The NTD for silicon has been developed and is now already in practical use. In Japan silicon of about 110 tons (estimated value in 1990) is processed by NTD and the NTD silicon is widely used for manufacturing power electronic elements. When we irradiate a semiconductor material with reactor neutrons, radiation damages take place together with NTD. These damages are often annealed by heating a specimen, but all of the behaviours about the radiation damages for semiconductor materials have not been elucidated yet. Using KUR, a large number of research works on radiation damage of semiconductor materials have been carried out so far. The present author is now trying to compare the radiation damage of silicon caused by the KUR neutrons with those by other reactor and accelerator neutrons. A part of newly obtained data is shown later.

IMPURITY ANALYSIS

Trace elements in an intrinsic semiconductor material can be analyzed by NAA, one of which is instrumental neutron activation analysis (INAA) and the other radiochemical NAA (RNAA). T. Takeuchi et al. obtained many impurity elements in silicon with KUR by INAA [3]. Their detection limit and an example of their results are cited in Figs. 1 and 2, respectively.

More than 20 years ago staff from Osaka University and the present author jointly started to study spatial distribution of impurity elements close to their surface. For example [4], the distributions of antimony atoms which were ion-implanted into silicon wafers at elevated temperatures is shown in Fig. 3. From this data, we found an enhanced diffusion effect of the antimony atoms in silicon.

K. Yokota et al. of Kansai University joined this group later and we tried to develop a technique of radioactive ion implantation. A radioactive isotope such as ^{76}As and ^{115}Cd was produced at a hydraulic conveyor of KUR and was loaded in an ion source of a small accelerator, with which these radioactive ions were accelerated about 45kV and were implanted into semiconductor wafers [5]. In order to investigate stability of a compound semiconductor namely GaAs during thermal processes, ^{76}As ions were implanted into GaAs wafers. The surface of the GaAs wafers was covered by SiO_2 or by Si_3N_4. Finally, we found that the surface GaAs layer covered by SiO_2 decomposed but that covered by Si_3N_4 didn't as shown in Fig. 4 [6]. A large number of similar works have been carried out by this group so far.

I. Ohdomari et al. of Waseda University and the present author attempted to study redistribution of implanted arsenic atoms in silicon wafers during metallic silicide formation [7]. After arsenic atoms were implanted into a silicon wafer, paradium was vacuum-evaporated on it and this wafer was heated at 250℃ to form a $PdSi_2$ layer. During this paradium

silicide formation, the redistribution profiles of arsenic atoms were observed by INAA using KUR. As shown in Fig. 5, we found an extraordinary rise at the front boundary of silicon and named this "snowplow effect" of impurity atoms in silicon during silicide formation. However we also found that there is no snowplow effect in the case of molybdenum silicide formation [8].

IRRADIATION EFFECTS

Research on radiation damage of semiconductor materials has a long history and a huge number of works on this subject have been carried out using reactor neutrons together with other various radiations. This subject is decribed and discussed in many textbooks and review papers, but it is pointed out that further more study is still required to elucidate radiation damage model from its primary process to its final stage. A more quantitative evaluation of radiation damage of semiconductor materials by reactor neutrons should be investigated, in which the approach to use so-called damage function may be recommendable.

At KUR several groups have irradiated semiconductor materials not only in common irradiation facilities such as pneumatic tubes but also in a low temperature irradiation loop (LTL). Very recently N. Fukuoka et al. of Naruto University of Education irradiated a germanium crystal at the temperature of 25K in LTL of KUR and found two levels below its conduction band [9]. They also studied the nature of oxygen donors and radiation defects in oxygen-doped silicon recently [10]. In this work, the neutron irradiation was made in the pneumatic tube of KUR.

K. Kuriyama et al. of Hosei University and the present author began NTD study of compound semiconductors, mainly GaAs, several years ago. When GaAs is irradiated by reactor neutrons, germanium (^{70}Ge and ^{72}Ge) and selenium (^{76}Se) atoms are produced from gallium atoms (^{69}Ga and ^{71}Ga) and arsenic atoms (^{75}As), respectively, and both germanium and arsenic atoms are expected to act as donors in the GaAs matrix. However these NTD atoms are usually not in the original positions but are displaced into interstitial ones. In addition, the defects induced by fast neutron irradiation disturb the electrical activation of NTD impurities. We irradiated GaAs wafers in three different positions of KUR, namely an in-core plug (P-1), a hydraulic conveyor (P-2) and a graphite thermal column (P-3). Figure 6 shows the electric resistivity as a function of annealing temperature [11]. There is a remarkable difference in the recovery process between the samples irradiated at P-1 (or P-2) and P-3. The abrupt change or decrease in electric resistivity of P-1 or P-2 around 400℃ is assumed to be based on the hopping conduction. The increase in that around 500℃ is associated with the disappearance of the hopping conduction. This assumption of the hopping conduction was proven by photoconductance measurements. Recently M. Satoh and K. Kuriyama have actively performed more works related to the NTD GaAs crystals [12]. Two coworkers of this group, T. Kawakubo and M. Okada of Research Reactor Institute, Kyoto University tried to measure electron spin resonance (ESR) spectra and Fourier transformed infrared (FTIR) absorption spectra of both GaAs and GaP after irradiation of reactor neutrons [13]. Their results together with other earlier data are comprehensively reviewed in a recently published paper by T. Kawakubo[14].

Y. Nishida et al. of Osaka University irradiated several types of diamonds with the neutrons of KUR and observed color centers by means of optical and ESR measurements [15]. They are aiming at searching for the possibility of opto-electronics applications of the color centers in these diamonds. Although diamond is not a semiconductor but an insulating material, the objectives of this work is so interesting and creative that I introduce it here.

Very recently we started to study irradiation effects of silicon by reactor neutrons with several different spectra, 14MeV neutrons from the D-T reaction with a low energy accelerator and charged particles with medium energy accelerators. Results are compared with each other and with the calculated ones. The electrical resistivities of four type silicon wafers with different oxygen contents were measured after the neutron irradiations at the Glory Hole in the Fast Source Reactor of the University of Tokyo, YAYOI and at three positions in KUR. An example of these measurements is shown in Fig. 7 [16]. It can be seen that the electrical resistivity of all silicon wafers increases with fast neutron fluence. This increment of the electrical resistivity is due to the trap of carriers by some defects which are created by the neutron irradiation. We are going to measure deep level defects with a deep level transient spectrometer (DLTS) and to observe lattice disorders by Rutherford backscattering (RBS) very soon.

CONCLUSION

Making use of the neutrons of KUR, a large number of research works about semiconductor materials have been carried out by many groups for about 27 years. Their results have markedly contributed the progress in semiconductor science and technology. A research reactor has been and will be really a powerful and useful tool not only to characterize semiconductor materials, but also to reform significantly their characteristics. More semiconductor research with research reactors is expected and to be enhanced in future.

REFERENCES

[1] A. Okazaki, "Abnormal crystal structure of silicon", in "Semiconductor Research with Research Reactors" (eds. T. Kawakubo and I. Kimura) KURRI-TR-289 (1987).

[2] T. Takeda et al., Japan. J. Appl. Phys., 26 (1987) 106.

[3] T. Takeuchi et al., Annu. Rep. Res. Reactor Inst., Kyoto Univ., 21 (1988) 69.

[4] K. Gamo et al.*, Japan. J. Appl. Phys., 9 (1970) 333 and ibid. 12 (1973) 735.

[5] M. Iwaki et al.*, Nucl. Instr. Meth., 127 (1975) 93.

[6] K. Yokota et al.*, Japan. J. Appl. Phys., 17 (1978) 1881 and Appl. Surface Sci., 41/42 (1989) 411.

[7] I. Ohdomari et al.*, Appl. Phys. Lett., 38 (1981) 1015.

[8] I. Ohdomari et al.*, J. Appl. Phys., 59 (1986) 3073.

[9] N. Fukuoka et al., Japan. J. Appl. Phys., 30 (1991) 784.

[10] N. Fukuoka et al., Defect Control in Semiconductors (K. Sumino (ed.)), p. 547, Elsevier Science Publishers B. V. (1990).

[11] M. Satoh et al.*, J. Appl. Phys., 50 (1987) 580.

[12] M. Satoh et al., Phys. Rev., B 40 (1989) 3473, J. Appl. Phys., 65 (1989) 2248 and J. Appl. Phys., 67 (1990) 3542.

[13] T. Kawakubo and M. Okada, J. Appl. Phys., 67 (1990) 3111.

[14] T. Kawakubo, Annu. Rep. Res. Reactor Inst., Kyoto Univ., 23 (1990) 97.

[15] Y. Nisida et al., Material Sci. Forum 38-41 (1989) 561.

[16] I. Kimura et al.*, "Irradiation effects of silicon by neutrons with different spectra ····· Variation of electrical resistivity", to be presented at the Fall Meeting of Atomic Energy Society of Japan (1991).

---

* : The present author is one of the coauthors of these papers.

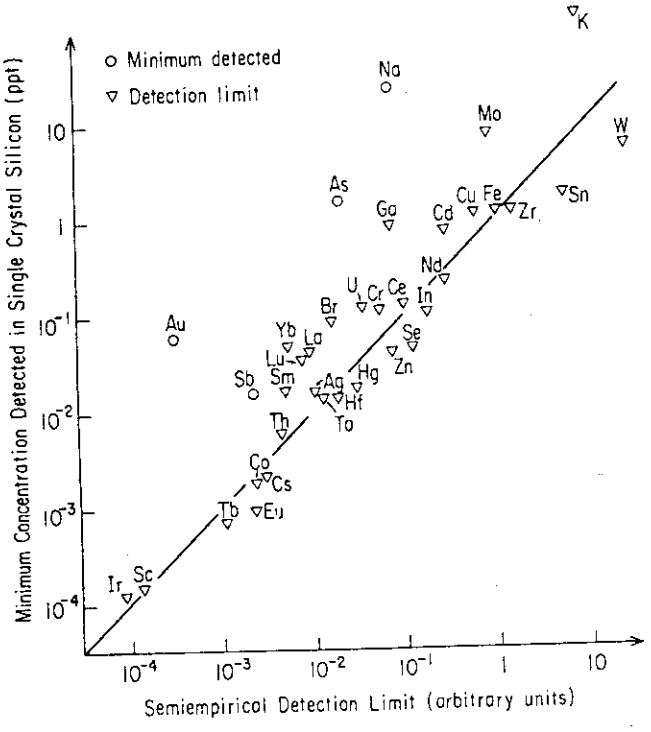

Fig. 1 Minimum concentration detected in a silicon crystal versus a semiempirical detection limit
(T. Takeuchi et al. [3])

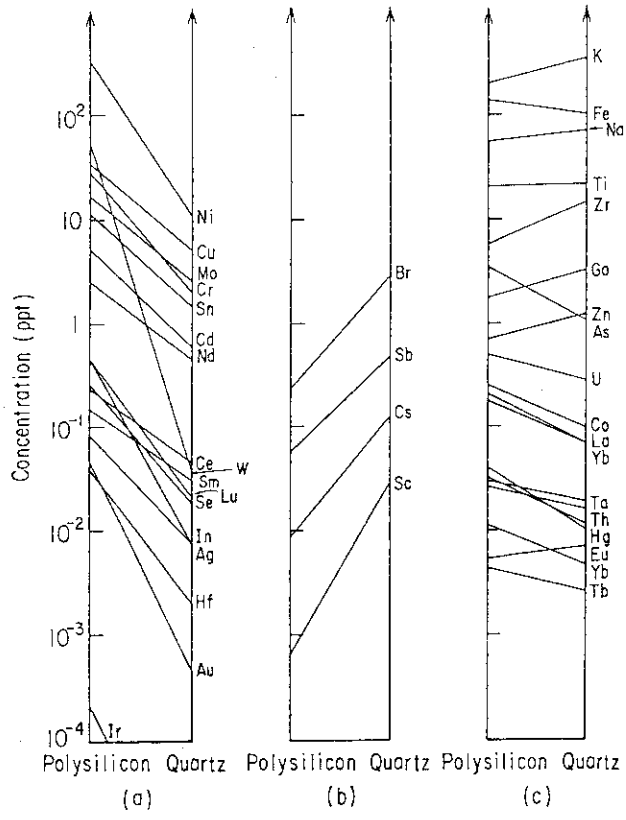

Fig. 2 Comparison of impurity consentrations in polysilicon and quartz ($\times 10^{-3}$) measured by INAA (T. Takeuchi et al. [3])

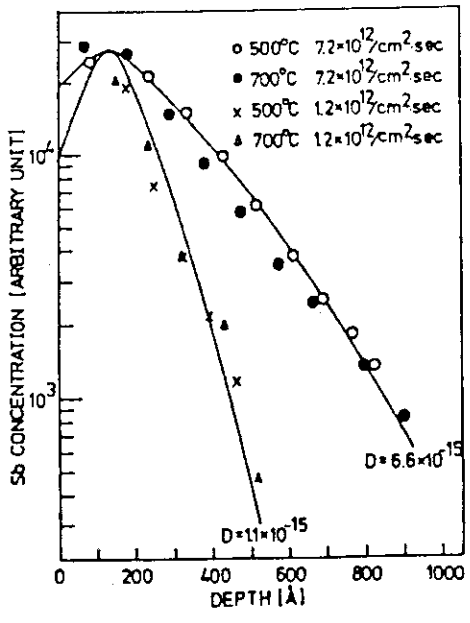

Fig. 3 Spatial distributions of ion-implanted antimony atoms in silicon measured by INAA (K. Gamo et al. [4])

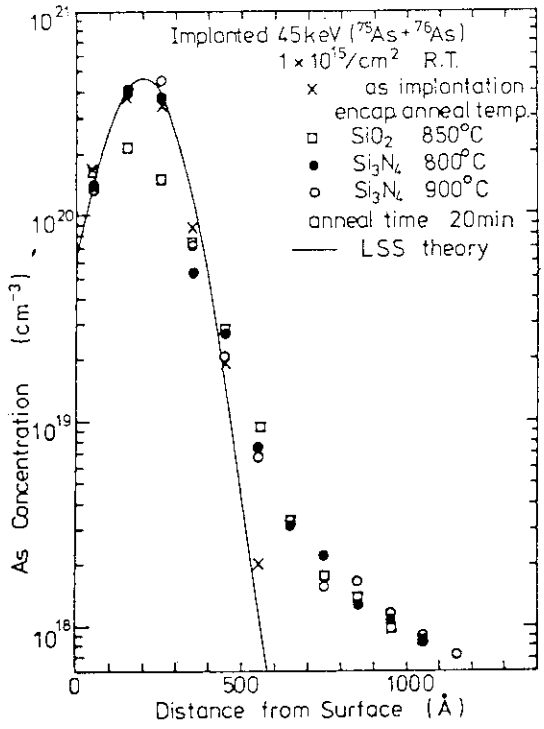

Fig. 4 Spatial distributions of radioactive-ion-implanted arsenic atoms in GaAs encapulated by SiO_2 and Si_3N_4 (K. Yokota et al. [6])

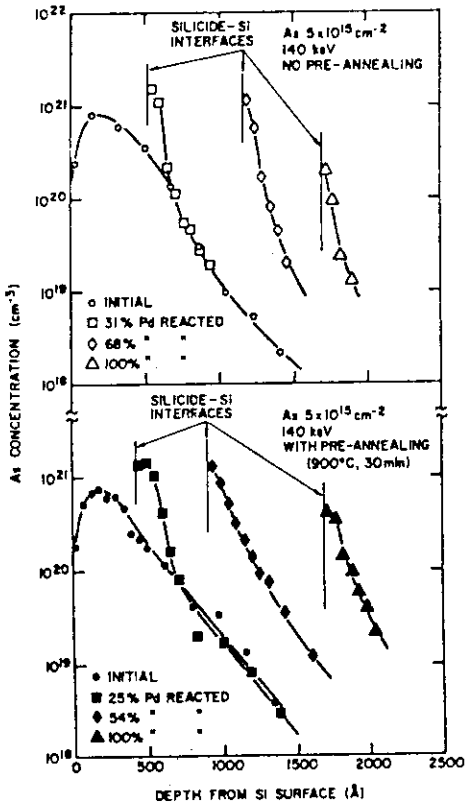

Fig. 5 Variation of spatial distributions of ion-implanted arsenic atoms in silicon during Pd_2Si formation measured by INAA (I. Ohdomari et al. [7])

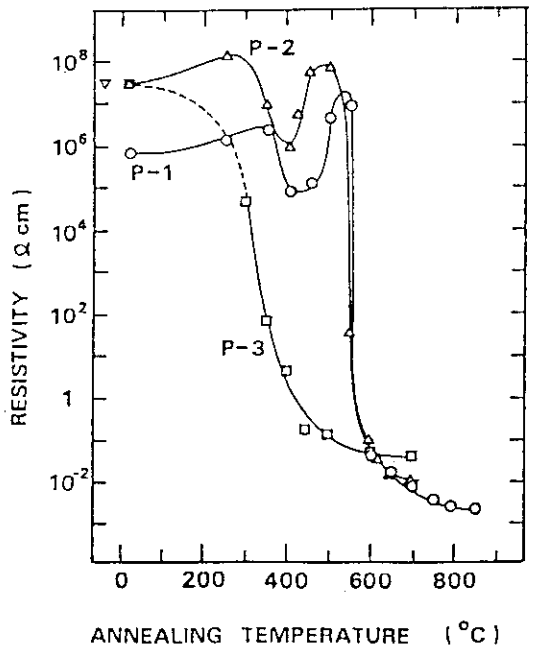

Fig. 6 Electrical resistivity of reactor neutron irradiated GaAs versus annealing temperature. P-1, P-2 and P-3 show the positions in KUR and are described in text. (M. Satoh et al. [11])

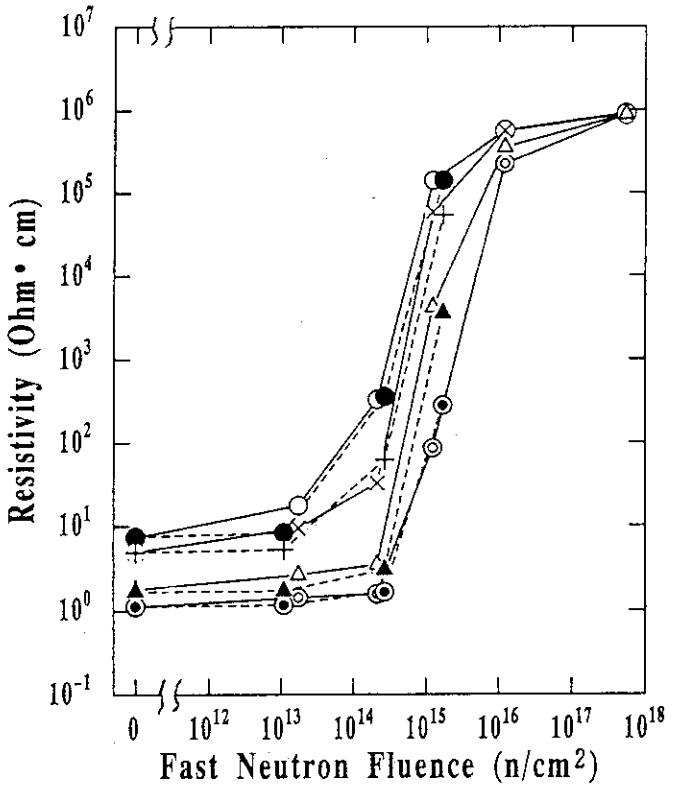

Fig. 7 Electrical resistivity of four type silicon wafers with different oxygen contents versus fast neutron fluence [16].

3. Neutron Spectra Adjusted with Multi-Foil Activation Data in Research Reactors

KATSUHEI KOBAYASHI
Research Reactor Institute, Kyoto University
Kumatori-cho, Sennan-gun, Osaka 590-04 Japan

ITSURO KIMURA
Department of Nuclear Engineering, Kyoto University
Yoshidahonmachi, Sakyo-ku, Kyoto 606 Japan

LI ZHAOHUAN, WANG YONGQING
Institute of Atomic Energy, P. O. Box 275(54)
Beijing, People's Republic of China

RYOTA MIKI
Kinki University Atomic Energy Research Institute
3-4-1, Kowakae, Higashiosaka-shi, Osaka 577 Japan

ABSTRACT

Using the NEUPAC and NEUSPEC(SAND-II type) codes, neutron spectra have been experimentally obtained by adjusting with multi-foil activation data at (1) the Kyoto University Reactor, KUR of Research Reactor Institute, Kyoto University, KURRI, (2) the Swimming Pool Reactor, SPR of Institute of Atomic Energy, China, IAE and (3) the University Training and Research Reactor, UTR-KINKI of Kinki University Atomic Energy Research Institute. The Kyoto University group made 11 kinds of activation measurements at KUR and analyzed the data with the NEUPAC code. The IAE group selected 26 kinds of activation reactions for SPR and obtained neutron spectrum using the NEUSPEC code. Both groups exchanged the multi-foil activation data and each group obtained other group's reactor spectrum with its own adjusting code. The results obtained by both groups were compared with each other and were in general agreement for both cases. The flux spectrum of neutrons at the central graphite cavity of the UTR-KINKI was measured with 9 kinds of reaction data and with 4 kinds of sandwiched resonance foils. The spectral results showed a good 1/E standard neutron field in the energy region from about 1 eV to a few hundreds keV.

INTRODUCTION

An accurate description of the neutron spectrum is of great importance for understanding the reactor characteristics and evaluating the quantity of radiation effect with neutrons in a research reactor. Recently, much interest has been taken in the neutron spectrum for the quantitative comparison with the radiation effects caused by 14 MeV neutrons[1-3].

The multi-foil activation method is one of candidate spectrometries to experimentally characterize the neutron spectrum in and around a reactor. Two of the present authors (KK and IK) who belong to the Kyoto University (KU group) obtained the neutron spectrum at the Hyd facility[4] of the Kyoto University Reactor (KUR) by the multi-foil activation method using the adjust-

ment code NEUPAC[5]. On the other hand, other two (LZ and WY) of the present authors who belong to the Institute of Atomic Energy (IAE group) obtained the neutron spectra at the core and the reflector regions of the Swimming Pool Reactor (SPR) of IAE by the multi-foil activation method using the NEUSPEC code[6] which had been developed by adding a subroutine to the SAND-II code[7] to generate uncertainty in the obtained flux spectrum using the Monte Carlo method. Both KU and IAE groups exchanged their activation data and adjusted the neutron spectrum of the other group with their own code and cross section libraries. Intercomparison of the neutron spectrum adjustment has been made. The present author (RM) of the Kinki University Atomic Energy Research Institute and the KU group obtained the neutron spectrum at the central graphite cavity between the two divided cores of the Kinki University Reactor (UTR-KINKI) by using the NEUPAC code. Flux measurements with sandwiched resonance foils of In, Au, W and Mn have been also made.

EXPERIMENTAL

1) Facilities

The KUR at the Research Reactor Institute, Kyoto University KURRI, is a light water-moderated research reactor, whose nominal power is 5 MW. The fuel element, 8.1 x 7.7 cm square and 72 cm long, is of MTR-type, made of 93 % enriched uranium and aluminum. A typical core configuration is illustrated in Fig. 1. Neutron fluxes and/or neutron spectra at main experimental facilities have been measured by the KU group using the activation techniques[4]. At the core center of the KUR, where one can obtain the highest neutron flux, there is a hydraulic conveyor facility Hyd for high fluence irradiation. An aluminum capsule can be conveyed in the Hyd facility even during reactor operation.

The SPR of the Institute of Atomic Energy, IAE is also a light water-moderated research reactor of 3.5 MW designed for multi-purpose uses[8]. A fuel pin, 10 mm in diameter and 50 cm in active length, is made of 10 % enriched uranium-dispersed oxide in magnesium base and covered with 1.5 mm thick aluminum cladding. Each fuel assembly consists of 16 fuel pins. The reactor is normally loaded by 42 fuel assemblies about 25 % burn-up on average. A typical core loading is shown in Fig. 2. The neutron spectra were measured

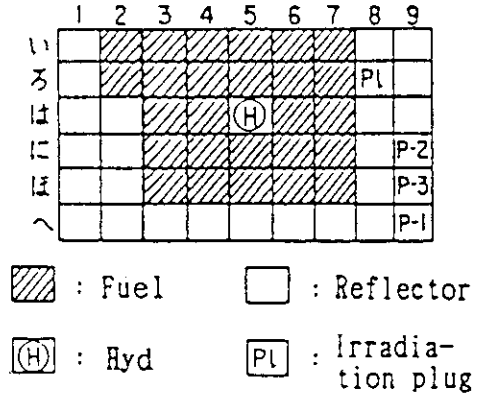

Fig. 1 A typical core configuration of KUR in Japan.

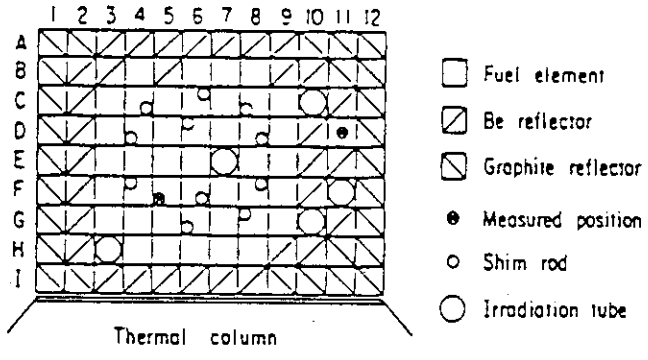

Fig. 2 A typical core loading at SPR in China.

at the F-5 and D-11 positions of the fuel and reflector regions, respectively. The reactor core is made of aluminum lattice frame which supports the fuel assemblies, reflectors and irradiation tubes. The inner and outer reflectors are made of beryllium and graphite, respectively.

The UTR-KINKI is a light water-moderated and graphite-reflected research reactor[9], which has the 46 cm separate cores. It has twelve fuel elements and each of them contains twelve aluminum clad, flat ETR-type fuel plates whose enrichment is 90 %. The nominal output power is 1 W. At the center of the internal graphite reflector between the two divided cores as shown in Fig. 3, a graphite stringer of 9.6 x 9.6 cm square and 122 cm long can be withdrawn to make a void region or a central cavity for sample irradiation[10]. An aluminum sample holder of 66 cm length with activation foils was set at the center of the core height and sandwiched by two 28 cm graphite stringers up and down.

2) Reaction Rate Measurement

Eleven kinds of activation reactions were measured at the Hyd facility of KUR. After the foil irradiation was performed for 30 minutes, gamma-rays from the induced activities were measured with Ge(Li) and/or HPGe detector, whose detection efficiency had been calibrated with a standard source with mixed radioactive nuclei. The reaction rates measured at KUR are summarized in Table 1, where the errors in percent are due to the statistical ones, detection efficiency and so on, as treated before[11].

At the central graphite cavity of the UTR-KINKI, 9 kinds of activation reactions as seen in Table 1 and (n, γ) reactions for the sandwiched foils of In, Au, W and Mn were measured[10]. The activation foils were attached on an aluminum holder and irradiated for 2-3 hours with the nominal power of 1 W. The Cd ratio there was also measured with gold foils. Measurements of the induced activities were almost similar to those mentioned above.

For the measurement of neutron spectrum at SPR, 26 kinds of activation

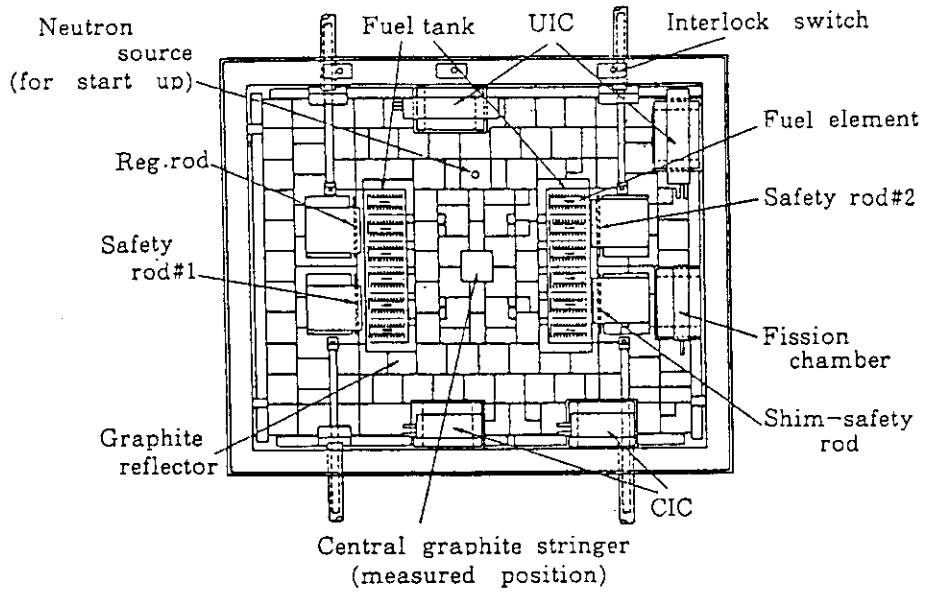

Fig. 3 Cross sectional view of UTR-KINKI.

reactions were selected. Several sets of the activation foils were separately irradiated to get appropriate induced activities with different reactor power and operating time. Most of the induced activities were measured by a $4\pi\beta\gamma$ coincidence counter and/or a Ge(Li) detector. The reaction rates and their uncertainties are tabulated in Table 2, where the positions F-5 and D-11 are in the fuel and reflector regions at SPR, respectively.

SPECTRUM MEASUREMENT

The KU group has successfully obtained neutron spectra[4,10,12,13] by adjusting multi-foil activation data using the NEUPAC code, which was developed by Nakazawa et al.[5]. The principle of this code is due to the J-1 type unfolding method[5,14,15] which gives an approximate solution based on the Bayes' theorem.

The NEUPAC code contains energy dependent group cross section libraries including the error matrices for main important neutron dosimetry reactions in ENDF/B-V. These constants with 144 groups were processed by the N-JOY code[16] in the energy range from 0.01 eV to 16.4 MeV. In the NEUPAC calculation, variance-covariance errors for every input data and initial neutron spectrum are required. The output gives not only neutron spectrum with its covariance errors but also relating integral quantities and their uncertainties. The chi-squares test in the calculation can be performed to check a physical validity of the resultant spectrum.

The SAND-II code[7] has been widely applied to the spectrum derivation using multi-foil activation techniques in a wide energy range from 0.1 meV to 20 MeV. The code named NEUSPEC was developed by the IAE group who revised

Table 1 Reaction rate data used for the spectrum adjustment at KUR and UTR-KINKI.

Reaction	Reaction rate & error (%) for Hyd of KUR	KUR data used for adjustment by KU	IAE group	Reaction rate & error(%) for UTR-KINKI
$^{197}Au(n,\gamma)^{198}Au$	*1.611E-08 3.73	o	o	2.513E-15 4.74
$^{58}Fe(n,\gamma)^{59}Fe$	1.293E-10 3.38	o		
$^{59}Co(n,\gamma)^{60}Co$	4.087E-09 3.40	o	o	4.533E-16 3.95
$^{115}In(n,\gamma)^{116m}In$				5.025E-15 5.44
$^{23}Na(n,\gamma)^{24}Na$				6.010E-18 4.67
$^{63}Cu(n,\gamma)^{64}Cu$				4.746E-17 9.22
$^{115}In(n,n')^{115m}In$				3.290E-19 5.35
$^{27}Al(n,p)^{27}Mg$				4.525E-21 11.6
$^{27}Al(n,\alpha)^{24}Na$	2.699E-14 2.84	o	o	1.478E-21 10.2
$^{46}Ti(n,p)^{46}Sc$	4.175E-13 3.12	o	o	
$^{47}Ti(n,p)^{47}Sc$	6.704E-13 3.36	o	o	
$^{48}Ti(n,p)^{48}Sc$	1.132E-14 2.94	o	o	
$^{54}Fe(n,p)^{54}Mn$	3.139E-12 3.02	o	o	
$^{58}Ni(n,p)^{58}Co$	3.887E-12 3.02	o	o	1.2189-19 4.86
$^{90}Zr(n,2n)^{89}Zr$	4.361E-15 3.55	o		
$^{93}Nb(n,2n)^{92m}Nb$	1.774E-14 3.14	o		

* Read as 1.611×10^{-8}.

the original SAND-II code to deduce the analytical uncertainties using the Monte Carlo method[6]. The group cross sections of 641 energy bins for the NEUSPEC code have been produced from either ENDF/B-V or the data which the IAE group evaluated by themselves[8]. In addition, 427 group constants of scattering and total cross sections have been prepared for the self-shielding correction in the foil[17].

RESULTS AND DISCUSSION

1) KUR Spectrum

The neutron spectra at the Hyd facility of KUR obtained with the NEUPAC and NEUSPEC codes are shown in Fig. 4, where the spectrum calculated by the ANISN code[4] is also given. The initial spectrum for NEUPAC was referred to the ANISN calculation, while that for NEUSPEC was taken from the Maxwellian and 1/E spectrum below 50 keV and the NEUPAC calculation above the energy.

Table 2 Reaction rate data used for the spectrum adjustment at SPR.

Reaction	Reaction rate and error (%)				Data used for adjustment by	
	at F-5 position		at D-11 position		KU (NEUPAC)	IAE group (NEUSPEC)
$^{55}Mn(n,\gamma)^{54}Mn$	*1.336E-14	2.16	6.454E-15	2.16		o
$^{164}Dy(n,\gamma)^{165}Dy$	2.476E-12	2.65	1.210E-12	2.61		o
$^{176}Lu(n,\gamma)^{177}lu$	4.169E-12	2.76	1.828E-12	2.76		o
$^{151}Eu(n,\gamma)^{152}Eu$	2.660E-12	3.17	1.252E-12	3.12		o
$^{191}Ir(n,\gamma)^{192}Ir$	9.003E-13	2.55	3.868E-13	2.50		o
$^{115}In(n,\gamma)^{116m}In$	2.695E-13	1.31	8.866E-14	1.31	o	o
$^{197}Au(n,\gamma)^{198}Au$	2.003E-13	1.82	5.635E-14	1.82	o	o
$^{98}Mo(n,\gamma)^{99}Mo$	7.151E-16	2.68	1.062E-16	2.76		o
$^{186}W(n,\gamma)^{187}W$	4.899E-14	2.94	1.843E-14	2.79		o
$^{59}Co(n,\gamma)^{60}Co$	3.655E-14	2.30	1.677E-14	2.30	o	o
$^{63}Cu(n,\gamma)^{64}Cu$	4.276E-15	2.48	1.967E-15	2.72	o	o
$^{23}Na(n,\gamma)^{24}Na$	5.139E-16	2.30	2.419E-16	1.71	o	o
$^{235}U(n,f)$	5.199E-13	2.44	2.381E-13	3.01		o
$^{238}U(n,f)$	5.598E-15	3.41	1.115E-15	3.82		o
$^{47}Ti(n,p)^{47}Sc$	1.920E-17	4.63	7.425E-19	4.77	o	o
$^{115}In(n,n')^{115m}In$	1.916E-16	2.22	6.876E-18	2.25	o	o
$^{54}Fe(n,p)^{54}Mn$	9.014E-17	2.43	3.451E-18	3.67	o	o
$^{58}Ni(n,p)^{58}Co$	1.151E-16	2.83	4.157E-18	2.46	o	o
$^{64}Zn(n,p)^{64}Cu$	3.551E-17	4.68	1.363E-18	4.38	o	o
$^{32}S(n,p)^{32}P$	6.970E-17	2.25	2.572E-18	2.30		o
$^{46}Ti(n,p)^{46}Sc$	1.322E-17	2.45	5.041E-19	2.63	o	o
$^{56}Fe(n,p)^{56}Mn$	1.392E-18	3.69	- - -	- -	o	o
$^{48}Ti(n,p)^{48}Sc$	2.988E-19	2.34	1.291E-20	2.60	o	o
$^{24}Mg(n,p)^{24}Na$	1.690E-18	1.78	7.592E-20	1.78	o	o
$^{27}Al(n,\alpha)^{24}Na$	7.885E-19	1.76	3.380E-20	1.75	o	o
$^{63}Cu(n,\alpha)^{60}Co$	4.574E-19	2.34	1.893E-20	2.83	o	o

* Read as 1.336×10^{-14}.

General agreement can be seen between the NEUPAC and NEUSPEC spectra below 10 keV. In the higher energy region, however, the NEUSPEC spectrum is lower at energies between 20 keV and 3 MeV and higher between 3 and 7 MeV than the NEUPAC spectrum. The discrepancy may be due to the difference of the initial spectrum used in the NEUPAC and NEUSPEC codes. Considering the uncertainties of several percent in the neutron spectra by the NEUSPEC and NEUPAC codes, both results in the higher energy region seem to be close to each other in their error range.

2) SPR Spectrum

The neutron spectra in the fuel region F-5 and the reflector region D-11 at SPR were obtained by the NEUSPEC code using 26 kinds of activation data. In the NEUPAC cross section libraries, 16 data of the above 26 kinds of activation data were applicable to the spectrum adjustment. The results by the NEUSPEC and the NEUPAC codes are illustrated in Fig. 5. The initial spectrum for the NEUSPEC was deduced from Maxwellian, 1/E and fission neutron spectra[8], in principle, and the NEUSPEC result was used as an initial spectrum for the NEUPAC calculation. It is realized that the flux spectrum in the reflector region is softer than that in the fuel region. The analytical errors are 5-9 % in both calculations. Very good agreement can be seen between the NEUSPEC and the NEUPAC calculations in the whole energy region.

3) UTR-KINKI Spectrum

The neutron spectra at the central graphite cavity of UTR-KINKI have been obtained by the calculation using the SRAC code system[9] and by the adjustment of the 9 kinds of activation data using the NEUPAC code. The results are shown in Figs. 6(a) and 6(b). The initial spectrum for the NEUPAC code was taken from the calculation. Neutron flux spectrum measured with the sandwiched foil method is plotted in Fig. 6(b) and the results are in good agreement with the adjusted and the calculated ones. The thermal neutron flux and the Cd ratios measured in the central cavity were about 1.8×10^7 $n/cm^2/sec$ and about 4.4, respectively. From the present results obtained, it was found that the spatial distributions of thermal neutrons and Cd ratios

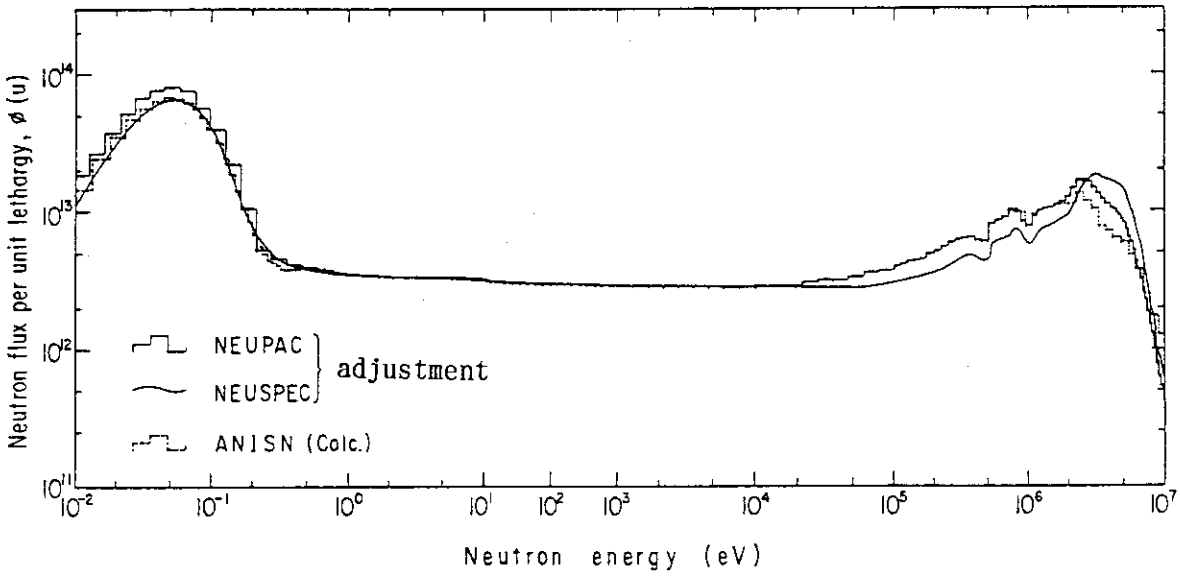

Fig. 4 Neutron spectrum at Hyd facility of KUR in Japan.

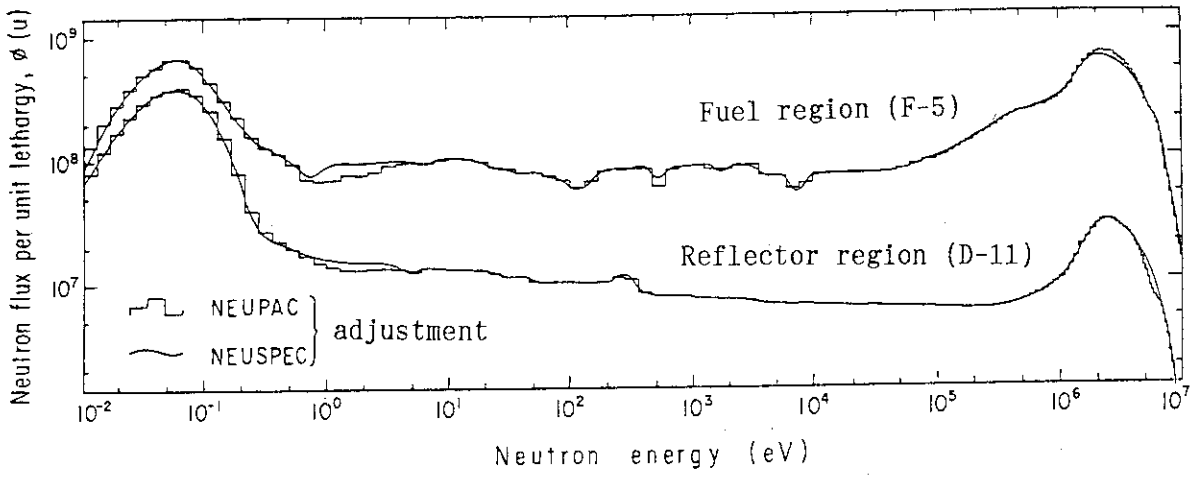

Fig. 5 Neutron spectrum at SPR in China.

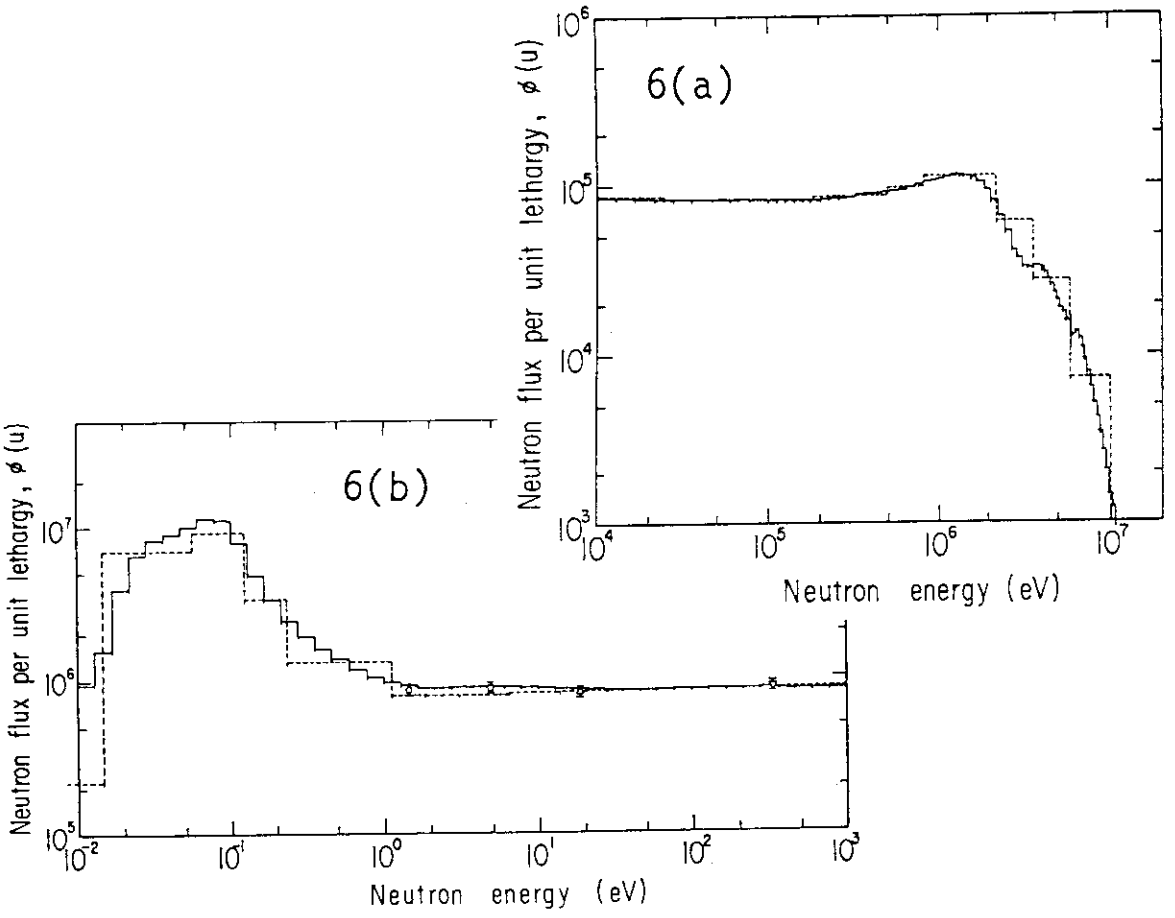

Fig. 6 Neutron spectrum at the central graphite cavity of UTR-KINKI.
○□△▽ sandwiched foil method by In, Au, W and Mn, respectively,
------- calculation by the SRAC code system[9],
——— adjusted spectrum with NEUPAC.

were uniform and flat in the central graphite region and showed a very good 1/E standard neutron field from about 1 eV to a few hundreds keV.

CONCLUSION

The neutron spectrum adjustment codes of NEUPAC and NEUSPEC were employed and successfully applied to the spectrum measurement by unfolding the multi-foil activation data obtained at the Hyd facility of KUR, in the core and the reflector regions of SPR and at the central graphite cavity of UTR-KINKI. The KU group and the IAE group exchanged their activation foil data and made an intercomparison of the analyzed neutron spectrum using their own cross section libraries and codes. Both spectra obtained by the former group using the NEUPAC code and by the latter group using the NEUSPEC code have been in general agreement with each other. The neutron spectrum adjusted with the activation data measured at the UTR-KINKI showed a good agreement with the calculations and with the neutron fluxes at the main resonances using the In, Au, W and Mn sandwiched foils.

ACKNOWLEDGEMENT

The authors would like to express their sincere thanks to Prof. M. Nakazawa of University of Tokyo for his useful discussion and suggestion on the NEUPAC calculation and the sandwiched foil method.

REFERENCES

1. G. R. Odtte and D. R. Doiron, Nucl. Technol., 29, 346 (1976).
2. M. A. Kirl and L. R. Greenwood, J. Nucl. Materials, 80, 159 (1979).
3. T. Okada, et al., J. Nucl. Materials, 133 & 134, 791 (1985).
4. K. Kobayashi, et al., Annu. Rep. Res. Reactor Inst. Kyoto Univ., Vol.20, 1 (1987).
5. M. Nakazawa and A. Sekiguchi, Proc. 2nd ASTM-Euratom Symp. on Reactor Dosimetry, NEUREG/CP-0004, Vol.3, p.1423 (1977).
6. Li Zhaohuan, et al., "An Improving Method for Monitoring Neutron Dose on PWR Vessel Steel by Flux Spectrum Measurement with a Few Nonfissionable Foils", The 7-th ASTM-Euratom Symp. on Reactor Dosimetry, held on Aug. 27-31, 1990, at Strasbourg, France.
7. S. Iijima, et al., "JENDL Dosimetry File", in print as JAERI-M report.
8. Li Zhaohuan, et al., "Measurements of Neutron Flux Spectra in SPR", Japan-China Symp. on Research and Test Reactors, held on Feb.29 - Mar.2, 1988, JAERI, UT-01 (1988).
9. R. Miki, et al., Annu. Rep. Kinki Univ. Atomic Res. Inst., 23, 33 (1986), and ibid., 24, 39 (1987).
10. K. Kobayashi, et al., Annu. Rep. Kinki Univ. Atomic Energy Res. Inst., Vol.25, 21 (1988).
11. K. Kobayashi, et al., J. Nucl. Sci. Technol., 19, 341 (1982).
12. I. Kimura and K. Kobayashi, Nucl. Sci. Eng., 106, 332 (1990).
13. K. Kobayashi, et al., "The U-235 Fission Neutron Spectrum Adjusted with Multi-Foil Activation Data", The 7-th ASTM-Euratom Symp. on Reactor Dosimetry, held on Aug. 27-31, 1990, at Strasbourg, France.
14. T. Taniguchi, et al., NEUT Res. Rep. 83-10 (1983).
15. M. Nakazawa, et al., J. Fac. Eng., Univ. Tokyo, A-22, 44 (1984).
16. R. E. MacFarlane, et al., LA-9303 M (1982).
17. Argonne National Laboratory, ANL-5800, 2nd Ed., p.667 (1963).

4. Effective Cross Sections of U-235 and Au in a TRIGA-Type Reactor Core

S. Harasawa and Gui Ah Auu *

Institute for Atomic Energy, Rikkyo University

2-5-1, Nagasaka, Yokosuka, 240-01 Japan

* Kansas State University, U.S.A.

ABSTRACT

The dependence of effective cross sections of gold and uranium for neutron spectrum in Rikkyo University Reactor (TRIGA Mark- Ⅱ, RUR) fuel cell was studied using computer calculations. The dependence of thermal neutron spectrum with temperature was also investigated. The effective cross section of gold in water of the fuel cell at 32 ℃ was 90.3 barn and the fission cross section of U-235, 483 barn. These two values are similar to the cross sections for neutron energy of 0.034 eV.

INTRODUCTION

The TRIGA fuel of RUR consists of a homogeneous mixture of uranium and zirconium hydride. The atomic ratio of zirconium to hydrogen in the zirconium hydride is 1 to 1.6. The hydrogen atoms in the meat are the main neutron moderator and is quite strongly bound in the zirconium hydride lattice. The movement of the hydrogen atoms in the zirconium hydride lattice can be described by the broaden Einstein oscillator model [1] . According to this model, the oscillation of hydrogen atoms can be described by a combination of the standard Einstein (optical) mode and the acoustic mode.

Binding of the hydrogen atoms has given rise to a unique moderating properties as

followings :

(1) Under the optical vibration mode, the hydrogen atoms can only occupy certain discrete energy levels of (n + 1/2) $h\omega$. Since the product $h\omega$ (n is a positive integer, h is Plank's constant and ω the lowest frequency of the vibration model) is about 0.14 eV, the hydrogen atoms in zirconium hydride can slow down neutrons in the steps of 0.14 eV but can not slow down neutrons having energy lower than 0.14 eV.

(2) On the other hand, neutrons with energy lower than 0.14 eV can receive energy after colliding with hydrogen atoms, resulting in up-scattering of thermal neutrons. Up-scattering of thermal neutrons in TRIGA reactor is greater than light water moderated reactor, because the hydrogen atoms in water are only weakly bound and able to slow down neutrons to the energy lower than 0.14 eV.

(3) In the acoustic vibration mode, the collective motion of hydrogen and zirconium atoms can be represented by a nuclide having a heavy effective mass. This provides the zirconium hydride lattice behaves in a less effective way in slowing down the neutrons to the energies below 0.14 eV .

Based on the above characteristics, the LIBP and THERMOS computer code[2)3)] were used to calculate the thermal neutron spectrum in a TRIGA fuel cell. Thermal neutrons were divided into 30 groups. Thermal neutron energy structure in THERMOS is shown in Table 1.

The moderating properties affects the thermal neutron spectrum in the reactor core. The main objective of the present study is to investigate the effect of thermal neutron spectrum to obtain effective cross sections in the reactor core of RUR.

RUR FUEL CELL

RUR reactor uses aluminium cladded fuel rods containing 8.5 w/o (weight percent) uranium and with a fuel section length of 34.56 cm (14 inch). The dimension and composition of the fuel cell of RUR are shown in Table 2.

	Upper boundary		Mid point		Mesh width	Group
	Energy(eV)	Velocity	Energy(eV)	Velocity	Velocity	
1	0.00057	0.15	0.00023	0.1	0.1	
2	0.00158	0.25	0.00101	0.2	0.1	
3	0.00310	0.35	0.00228	0.3	0.1	
4	0.00512	0.45	0.00405	0.4	0.1	
5	0.00765	0.55	0.00632	0.5	0.1	
6	0.01069	0.65	0.00911	0.6	0.1	1
7	0.01423	0.75	0.01240	0.7	0.1	
8	0.01828	0.85	0.01619	0.8	0.1	
9	0.02283	0.95	0.02049	0.9	0.1	
10	0.02789	1.05	0.02530	1.0	0.1	
11	0.03346	1.15	0.03061	1.1	0.1	
12	0.03953	1.25	0.03643	1.2	0.1	
13	0.04611	1.35	0.04276	1.3	0.1	
14	0.05319	1.45	0.04959	1.4	0.1	
15	0.06078	1.55	0.05692	1.5	0.1	
16	0.07384	1.7084	0.06699	1.6273	0.15835	2
17	0.08970	1.8829	0.08138	1.7935	0.17453	
18	0.10896	2.0752	0.09886	1.9767	0.19236	
19	0.13236	2.2873	0.12009	2.1787	0.21201	
20	0.16078	2.5209	0.14688	2.4013	0.23367	
21	0.19531	2.7785	0.17721	2.6466	0.25754	
22	0.23726	3.0623	0.21527	2.9169	0.28386	3
23	0.28821	3.3752	0.26150	3.2150	0.31285	
24	0.35011	3.7252	0.31776	3.5434	0.34482	
25	0.42530	4.1000	0.38588	3.9054	0.38004	
26	0.51664	4.5189	0.46875	4.3044	0.41887	
27	0.62759	4.9806	0.56942	4.7441	0.46166	
28	0.76238	5.4894	0.69171	5.2288	0.50883	4
29	0.92611	6.0502	0.84026	5.7630	0.56081	
30	1.12500	6.6683	1.02070	6.3517	0.61810	

Table 1. Neutron Energy Structure in THERMOS

Region	Radius (cm)	Volume fraction	Nuclide	Atomic density ($x10^{24}$atoms/cm^3)
Fuel meet	1.7985	0.6082	U-235 U-238 Zr H(ZrH)	2.5665×10^{-4} 1.0258×10^{-3} 3.7171×10^{-2} 5.9474×10^{-2}
Clad	1.8745	0.0525	Al	6.0200×10^{-2}
Water	2.3062	0.3393	H O	6.7000×10^{-2} 3.3500×10^{-2}

Table 2. RUR Fuel Cell

RESULTS AND DISCUSSION

Figure 1 shows the thermal neutron flux distributions of four energy groups in the fuel cell. In the table, 30 thermal neutron groups were put into four broad groups. The four groups were :

Group 1 : 0.0006 eV ～ 0.046 eV
Group 2 : 0.046 eV ～ 0.132 eV
Group 3 : 0.132 eV ～ 0.425 eV
Group 4 : 0.425 eV ～ 1.125 eV

The thermal neutron flux distributions in the TRIGA fuel cell vary sensitively with temperature. Neutron distribution with respect to temperature is also shown in Figure 1.

The neutron spectra at three positions in the fuel cell are shown in Figure 2, and compared with a Maxwell distribution with the peak energy of 0.025 eV. The three positions were :

1 : Center of the fuel cell r=0.00 cm
2 : mid point of the clad r=1.8365m
3 : mid point of the water r=2.0903m

The neutron spectrum in a TRIGA fuel cell differs from the one in a reactor core which gives the neutron flux of the Maxwell distribution. The peak energy of the neutron spectrum shifts towards higher energy and the neutron flux of very low energy is more intense than the Maxwell distribution.

The effective cross sections of gold and uranium in a RUR fuel cell were calculated using the obtained neutron spectrum. The results are shown in Table 3.

irradiation point	center in the meet	in the clad	water	Maxwell distribut.
total cross section gold, (barn)	72.5	84.0	90.3	105
fission cross section, U-235,(barn)	366	442	505	700
energy corresponding cross section (eV)	0.055	0.040	0.032	0.025

Table 3. Effective Cross Section of gold and Uranium

REFERENCES

1) G. W. Carriveau, Single Differential Cross Section of Zirconium Hydride, GA-8345, 1967

2) A Thermalization Transport Theory Code for Reactor Lattice Calculations, BNL-5826.

3) T. Ise, Y. Nakahara, M. Akimoto, JAERI-M 5730, 1974

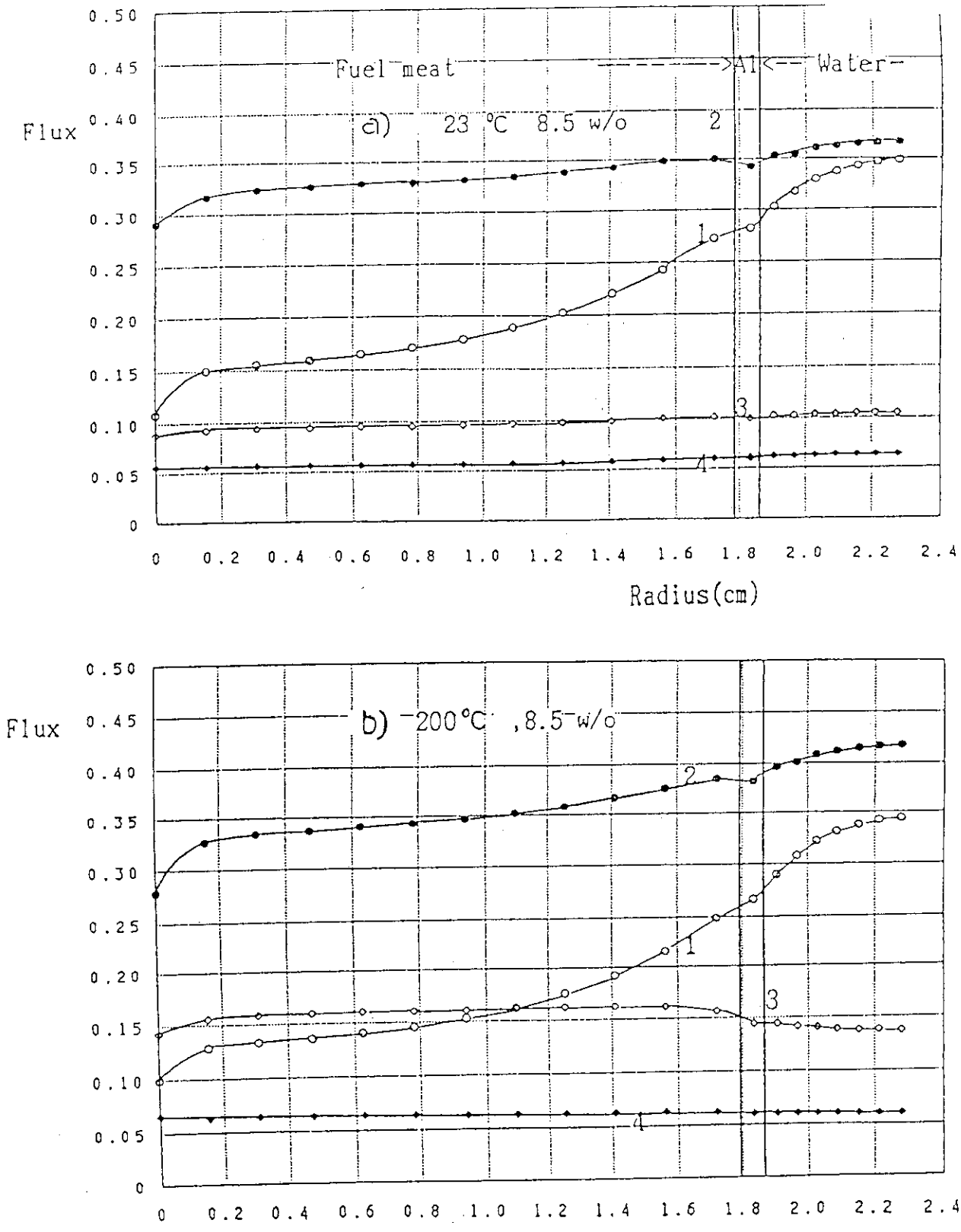

Figure 1. Neutron distribution in the fuel cell at various fuel meat temperatures. The numbers on the graphs correspond to the neutron groups.

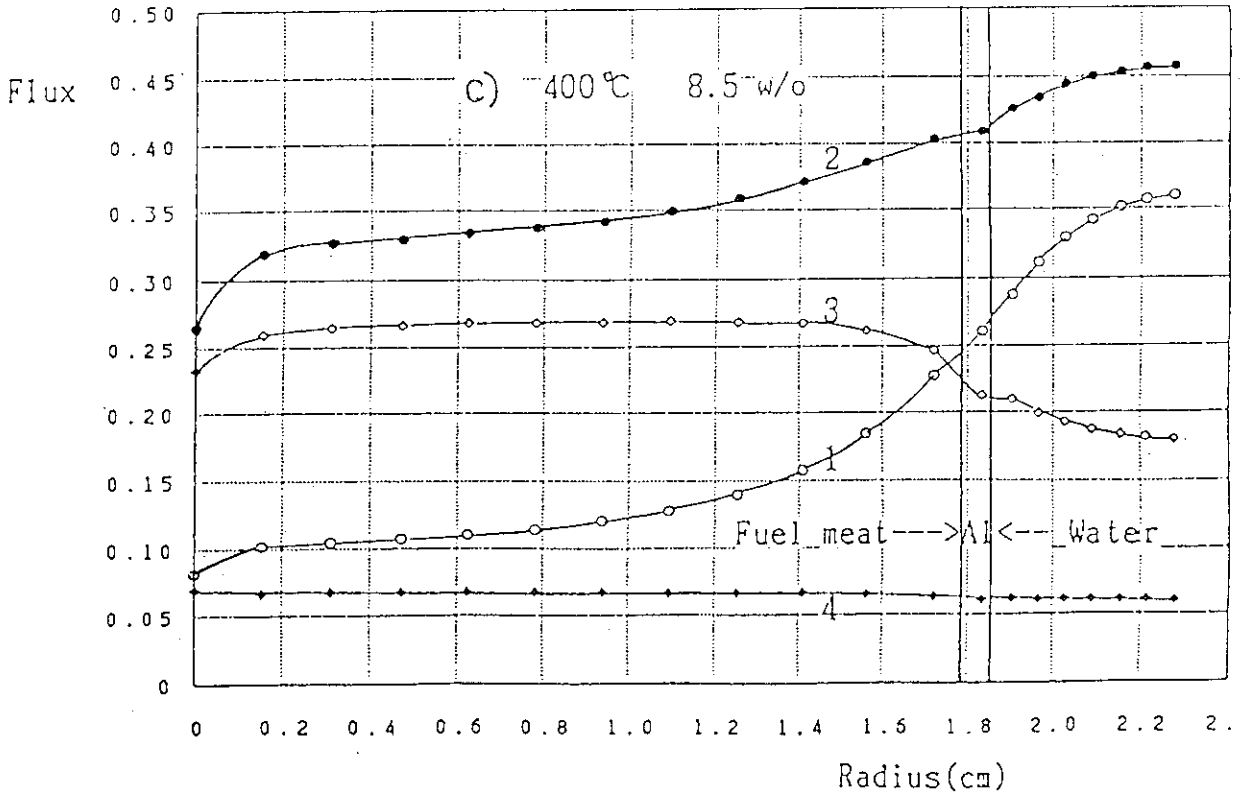

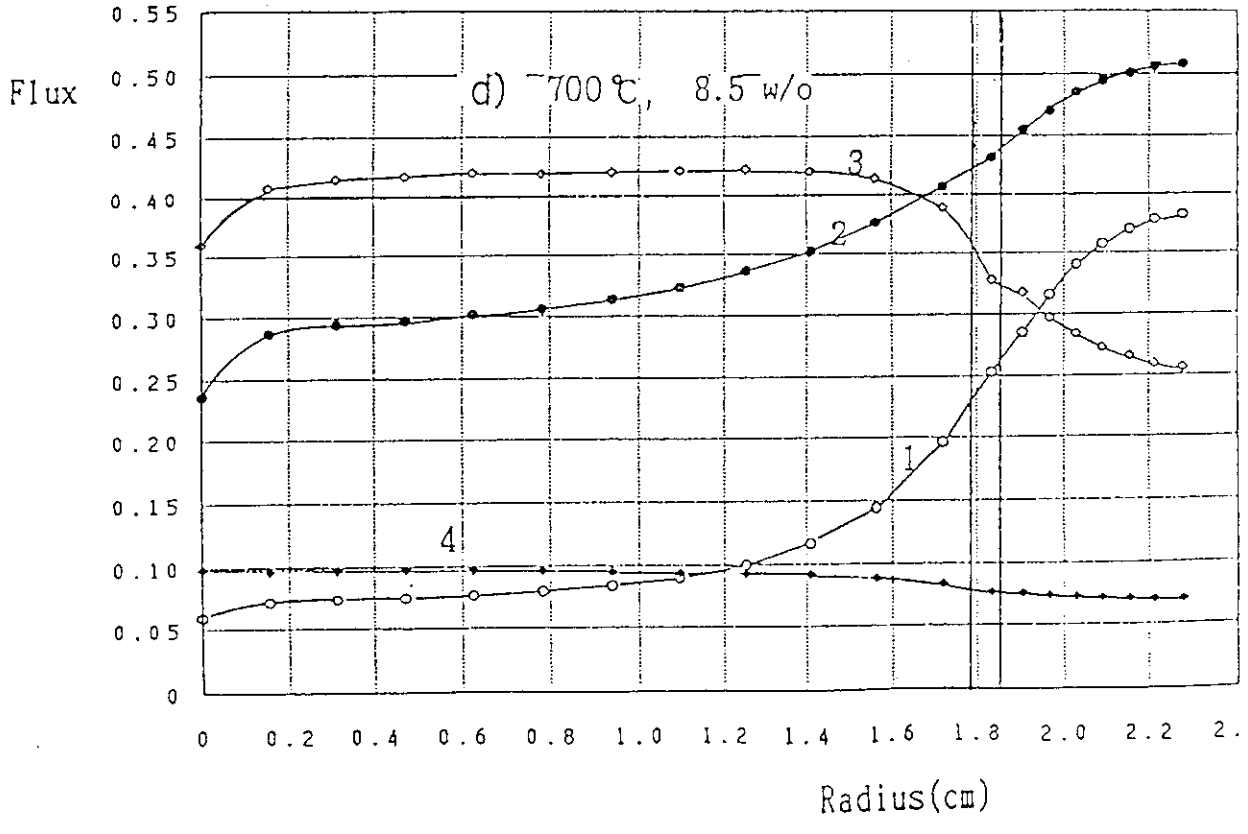

Figure 1 Continued

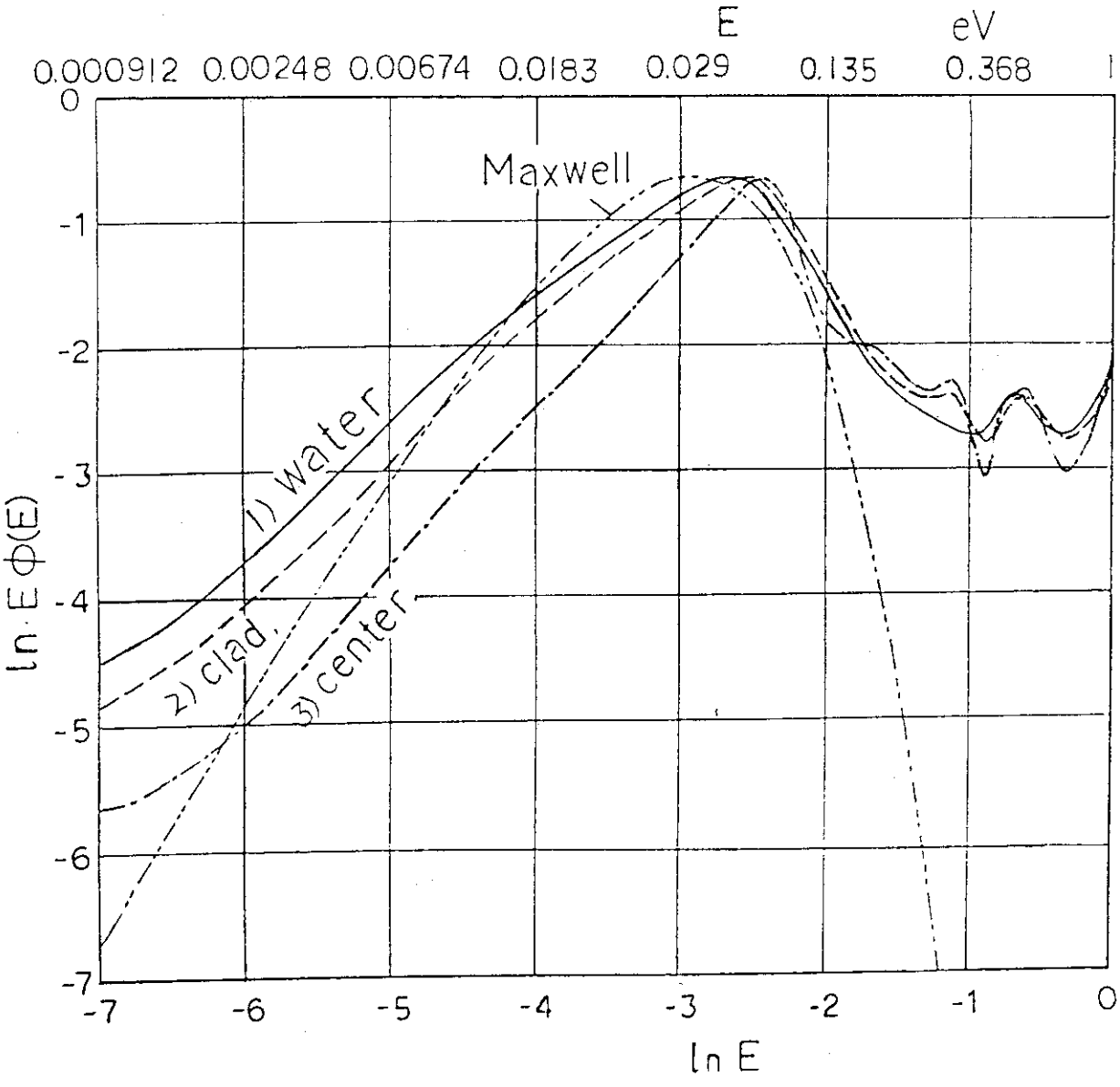

Figure 2. Neutron spectra at three positions in the fuel cell and the Maxwell distribution

1. Neutron Scattering Research at JAERI Reactors - Past, Present and Future -

Satoru Funahashi, Yukio Morii and Nobuaki Minakawa

Department of Physics
Tokai Research Establishment, JAERI
Toaki-mura, Naka-gun, Ibaraki-ken 319-11, Japan

Abstract

It was in 1961 that the first neutron scattering experiment was performed in Japan at JRR-2. The start of JRR-3 in 1964 accelerated the neutron scattering activities in Japan. The research in this field in Japan grew up by using these two research reactors. Among them JRR-2 has played an important role because its neutron flux was about seven times higher than that of the old JRR-3. The completion of the new JRR-3M in 1990 made an epoch to the neutron scattering activities in Japan. The long-waited JRR-3M came up to the expectations of the scientists of Japan. It is a realization of the ideal reactor with tangential beam holes, cold source and neutron guides in a large guide hall. The flux at the neutron scattering instruments is about five times higher than that of JRR-2. Utilization of JRR-3M has just started. Twelve neutron scattering machines are running there. The number will increase up to close twenty in a couple of years.

INTRODUCTION

The completion of JRR-3M in 1990 made a great epoch to the neutron scattering research in Japan. Great expectation is held by scientists who are interested in neutron scattering experiments.

When the first neutron diffraction experiment was performed at JRR-2 about thirty years preceding the JRR-3M, only two horizontal beam holes were used for neutron scattering facilities. The number of instruments, however, had been increased year by year until when the old JRR-3 was closed in 1983 for the upgrading. Four neutron spectrometers had been installed at JRR-3 and eight instruments had been installed at JRR-2 by that time. Most of them have been repeatedly improved and upgraded to keep up with the very rapid progress of the neutron scattering technology. Out of them, three instruments have been moved to JRR-3M, but six of them are still being used at JRR-2.

The design, construction of those instruments and research activities utilizing them had been done by the great effort of the solid state physicists who were interested in neutron scattering especially in relation with magnetism, ferroelectricity and metallurgy. From the beginning up to now about one third of the beam ports for the neutron scattering have been used

by the Department of Physics of JAERI and the rest two thirds by universities represented by the Institute for Solid State Physics(ISSP) of the University of Tokyo, the Faculty of Science of Tohoku University and the Institute for Materials Research(IMR) of Tohoku University. In this paper, the short history of the neutron scattering activities performed at JAERI reactors, the present status of the neutron scattering facilities there and the future instrumentation plan at JRR-3M are reported.

DAWNING

Neutron scattering experiment in Japan was started as soon as JRR-2 started to operate at low power. That experiment was performed by the solid state physics scientist of JAERI who had been longing for their own thermal neutron beam for a long time. The first experiment done in 1961 was the magnetic structure study of UFe_2 using a polycrystalline sample. It is worth pointing out here that the measurement was made not only at room temperature but also at liquid nitrogen temperature and under applied external magnetic field. The result was reported at the International Conference on Magnetism held in Kyoto in 1961[1]. Two other papers[2,3] were presented there by JAERI and ISSP to report their respective diffractometers built at JRR-2. Therefore the start of the neutron scattering experiment in Japan was about fifteen years after the first substantial neutron diffraction experiment performed at the graphite reactor in Oak Ridge USA.

Prior to this, when it was decided to construct the JRR-2 reactor, a committee was organized in JAERI to study the basic plan of the neutron scattering instrumentation. There it had been decided to construct a double-axis diffractometer in JRR-2. At the almost same time, university scientists started similar committee and it had been decided that ISSP to construct another diffractometer to JRR-2. The Electrical Communication Laboratory of Nippon Telegraph and Telephone Public Corporation also decided to construct another diffractometer. The latter two diffractometers shared one beam because only two horizontal beams were available in total for neutron scattering at that time. In Japan, they had to wait until 1964 to have the 10MW full power operation of JRR-2.

Among the many fields for which neutron scattering is utilized, magnetic problem is always one of the central issues because neutron scattering is almost the only source of the microscopic structural information from magnetic materials. At both JRR-2 and JRR-3 magnetic problems were taken up at first and since then many experiments have been done up to now. Another central issue is the structural research of the systems in which the heavy atoms and light ones coexist for which X-ray cannot give accurate information of the light atoms.

The experiments reported by JAERI at the International Symposium of Neutron Scattering held at Grenoble in 1963 typically reflected the above distinctive feature of the neutron scattering. Namely, magnetic structure of MnTe[4], Mn-Cr alloy, crystal structure of UF_4, frequency distribution in Ti-H[5] were reported there.

In those days, machines were not automatically operated as they are now done by computers. Scientists had to sit up at the machine side not to waste any neutrons while the reactor was running.

EARLY DAYS

The research activity was accelerated by the completion of JRR-3 in 1964. Both JRR-2 and JRR-3 had been used by the scientists of JAERI and universities. In 1965, JRR-3 became operational at full power. A TOF spectrometer of JAERI and a double-axis diffractometer shared by the Research Institute for Iron Steel and Other Metals of Tohoku University, Faculty of Science of Osaka University and JAERI were built there. Another diffractometer with polarized neutron capability was built there by ISSP.

When the starting period had passed and the initial constructions had settled down in JRR-2 it was well confirmed that the elastic scattering experiments can be performed steadily. Then there sprang up the next trial to challenge more difficult problems to measure inelastic scattering. As is well known, the cross section of the inelastic scattering caused by the excitations in solids like phonons or magnons is about three orders of magnitude smaller than that of elastic scattering but those information of lattice dynamics or spin dynamics are the really central problem of neutrons because X-ray cannot give rise to those information. All scientists were not necessarily confident that the flux at JRR-2 was high enough to measure inelastic scattering. Some people were feeling too pessimistic for the feasibility of phonon or magnon measurement at JRR-2. In 1965, however, the double-axis diffractometer of JAERI was changed into a triple-axis spectrometer of which type is now one of the most common neutron spectrometer to utilize the reactor neutrons. Then it was shown by the first successful measurement of inelastic scattering of the phonon dispersion relations of Cu-Ni alloy in Japan[6] that the flux at JRR-2 is high enough. Based on that experience phonons of CaF_2 was investigated there by measuring not only the dispersion relation but also the intensity of the scattering and a new way of analysis of lattice dynamics was developed[7]. The first measurement of spin-waves in Japan was also performed with that spectrometer on MnTe[8] of which magnetic structure had been analyzed at JRR-2 long before that time[4]. This triple-axis spectrometer has been used as one of the main instruments of neutron scattering of JAERI group. Many experiments including phonon measurements of alloys related with martensitic transformations, measurements of magnons related with ferro-antiferromagnetic transitions, measurement of early stage of precipitation in alloys were performed with that instrument. Beam plug, monochromator shielding, operating system and many other part of this machine have been changed by now but it is still running at JRR-2.

At the university spectrometers in JRR-2 and JRR-3, studies of ferroelectricity, ionic crystals, magnetic problems of chromium, other metals and alloys were performed energetically.

In 1964 a time-of-flight spectrometer equipped with three-disc phased chopper was installed to HT-14 beam hole in JRR-2. This machine was used to measure paramagnetic scattering of MnO_2[9] and $KMnF_3$[10] and frequency distribution of metal hydrides. It is not easy, however, to maintain the high speed mechanical chopper in good condition to keep the phase precisely for a long operation time continuously. This machine was stopped years ago.

It was not until in 1971 that computers came to be used to operate the neutron spectrometers. The 8K word HITAC-10 computer was introduced by JAERI to operate both the triple-axis spectrometer and the chopper TOF machine with CAMAC simultaneously. Another HITAC-10 was introduced by Tohoku University to operate the triple-axis spectrometer. Computers were really expensive in those days.

THE PRIME OF JRR-2

As it turned out that JRR-2 is very powerful and the reactor operation became more stable, more and more experiments came to be performed there. It was unfortunate that the Electrical Communication Laboratory of Nippon Telegraph and Telephone Public Corporation stopped their neutron scattering activities early 60's though some structural studies of magnetic materials like MnAs etc. were performed in the very early days. This, however, gave the ISSP machine which used to share the beam hole more free utilization of the beam. The ISSP spectrometer was changed into a triple-axis spectrometer which has double monochromator for the first time in Japan. The spectrometer has been used by many university users for the studies of ferroelectricity, ionic crystals, superionic conductors, phase transition of low-dimensional magnetic materials, mixed magnetic materials with different anisotropy axis etc. The spectrometer is still now running at JRR-2.

In 1970, after ten years since the first spectrometer was installed in JRR-2 another conventional triple-axis spectrometer was installed in JRR-2 by the Faculty of Science of Tohoku University. Studies of magnetic excitations in metals and alloys in which magnetic electrons have strongly localized character to those with quite itinerant ones were performed intensively. In 1971, JAERI added a neutron topography machine in JRR-2. Studies of imperfections reflecting crystal growth, fundamental studies of neutron interferometry etc. were performed there. In 1975 JAERI added another triple-axis spectrometer with double monochromator in JRR-2. It was operated on the granite air-cushion floor for the first time in Japan. Studies of lattice dynamics of intercalated graphite, phase transition of alloys etc. were carried out with this machine. This machine is now moved to the end of T2 thermal guide of JRR-3M. In 1976, ISSP added a polarized neutron spectrometer. This machine was used not only for the standard measurement of magnetic studies but also as the prototype of the sophisticated Neutron Spectral Modulation(NSM) spectrometer proposed by Y.Ito. The last neutron scattering instrument installed to JRR-2 was the diffractometer with polarized neutrons which was installed by IMR of Tohoku University. Magnetic structure studies of uranium compounds, structure studies of metal hydrides were carried out with this diffractometer. It is now moved to T1 thermal guide in the guide hall of the JRR-3M reactor.

As described above, four triple-axis spectrometers, two polarized spectrometers, one TOF machine and one topography machine were once installed in JRR-2. Two spectrometers among them have been moved to the guide hall of JRR-3M. The rest six machines are still running at JRR-2.

JRR-3 IN THE PAST

In the early days of JRR-3, three spectrometers were installed in JRR-3 as described before. Later on a polarized neutron spectrometer was added by IMR of Tohoku University. This is the only machine which was once in old JRR-3 and again used in the JRR-3M. It is installed to the T1 thermal guide in the guide hall.

Since the flux of JRR-3 was not high enough to measure inelastic scattering, all of them have been used for elastic scattering. Studies of crystal structure of U_4O_9, magnetic structure of alpha-Mn, spin density in magnetic materials, measurement of magnetic form factor etc. were carried

out by making use of the old JRR-3 reactor. One of the unique experiments which were carried out there was an experiment to test feasibility of proton polarized filter as the neutron polarizer. To provide polarized neutrons, usually magnetic diffraction is used. In that case, however, the neutrons are monochromatized at the same time. Supermirror is another way to get polarized neutrons. It is very efficient for longer wavelength neutrons. On the other hand for rather short wavelength white beam as in the case of pulsed neutrons, the polarized proton filter is a good polarizer. The experiment was carried out by the collaboration of JAERI, IMR and High Energy Physics Institute(KEK). With the dynamic polarization of ethylene glycol, a satisfactory result that 80% polarization of neutrons was obtained[11].

PRESENT STATUS

The start of JRR-3M is a great epoch to the neutron scattering research in Japan. All the six horizontal beam holes in the reactor room are already being used. Four of them are used for the triple-axis spectrometers. Rest two are used for the high-resolution powder diffractometer and the neutron topography/optics machine. In the guide hall, six neutron scattering instruments have been installed up to now. They consists of two small-angle scattering machines, one triple-axis spectrometer, one neutron camera machine and two double-axis diffractometers.

Since the triple-axis spectrometers(TAS) have the most universal capability of thermal neutron scattering, it is quite natural that most of the beam holes with high intensity are occupied with them. Some of these triple-axis spectrometers are equipped with polarizer and polarization analyzer.

The high-resolution powder diffractometer(HRPD) equipped with sixty-four ^{3}He detectors in front of each of which are installed 6' fine collimators is the machine which is very powerful for the structural analysis especially for cases where the magnetic diffraction exists.

The neutron topography/optics machine is equipped with very delicate parts to control the goniometer angle with 0.01" increments. The whole apparatus is arranged on a vibration-free table enclosed in a double chamber which not only shields the background from the outside but also isolates the spectrometer from the reactor room environment to stabilize the temperature within less than 0.01 degree drift.

The two small-angle neutron scattering(SANS) machines in the guide hall are the first ones with large-scale two-dimensional position sensitive detectors installed in Japan. Among them, the one installed by JAERI at the end of 0.6nm guide is equipped with a 10m collimation guide and a 10m flight tube. The incoming neutron spectrum is chosen by the velocity selector made by KFKI Hungary which is installed between the end of the cold guide and the collimation guide. The 64x64cm^{2} ^{3}He position sensitive detector made by Riso Denmark can be moved inside the flight tube from 2 to 10m position from the sample. The flight tube can be turned on the air-cushion up to 15 degrees away from the direct beam axis. Another one built by ISSP at 0.4nm guide has 16m collimator and 16m fixed flight tube. It is equipped with Dornier velocity selector made in Germany and ORDELA two-dimensional detector made in USA.

The triple-axis spectrometer installed at the end of 0.2nm guide is the one moved from JRR-2 as described in the preceding section. Because it is installed at the end port it has great advantages that the scattering angle

can go up to very high, the monochromator can collect the beam from the total height of the guide and it can use rather short wavelength with low monochromator angle where no half-wavelength contaminatation comes. One of the two diffractometers installed by IMR at 0.2nm guide is also the one moved from JRR-2. This machine will be used mainly for single crystal samples. It will be added capabilities for triple-axis and four-circle functions in future. Another one is the diffractometer which used to be used at the old JRR-3 as the polarized neutron diffractometer. It will be used mainly for polycrystalline samples at the guide. It will be added the high-resolution powder diffractometer function in the future.

The neutron diffraction camera machine installed on the 0.2nm guide supplies monochromatic beam on the sample table on the air-cushion. This machine can be used not only as the camera but also for various purposes. Since the start of the JRR-3M in 1990, data are coming out of the machines already. The triple-axis spectrometers and the high-resolution powder diffractometer are running producing plenty of new results.

FUTURE

The neutron scattering instruments installed or to be installed at JRR-3M are summarized in Table 1 below. Twelve instruments have been installed up to now as described above. They are rather standard machines which are to be used on the well established way. Two double-axis diffractometers in the table will be modified in the future as described above.

Table 1 Neutron Scattering Instruments at JRR-3M

Instrument	Number		Location	Status	
Triple-axis spectrometers	8	4	Reactor room	4	running
		2	Thermal guide	1	running
		2	Cold guide		
High-resolution powder diffractometers	1	1	Reactor room	1	running
Double-axis diffractometers	2	2	Thermal guide	2	running
Small-angle scattering instruments	2	2	Cold guide	2	running
Topography, camera interferometry etc.	3	1	Reactor room	1	running
		2	Thermal guide	1	running
Special polarized neutron instruments(NSM,NSE)	2	2	Cold guide		
Other special neutron scattering instruments(TFS etc.)	2	1	Thermal guide		
		1	Cold guide		
Total	20			12	

In the coming few years, triple-axis spectrometers at thermal and cold guides, and other more challenging and sophisticated machines like neutron spectral modulation(NSM) machine, neutron spin-echo(NSE) machine, time focusing neutron spectrometer(NSF) and so on are planned in the guide hall.

In total, over twenty neutron scattering machines will be installed in JRR-3M[12], eight among which will be the triple-axis spectrometers and two are the small-angle scattering machines.

SUMMARY

Since the time when the first instrument was installed at JRR-2 the number of neutron scattering instruments increased gradually as shown in Fig.1 below. Most of them were triple-axis spectrometers in the past. It took nearly thirty years to have new JRR-3M in Japan. The circumstances of the neutron scattering research have been changed during these years. The rapid development of pulsed neutron sources affected the neutron scattering field greatly.

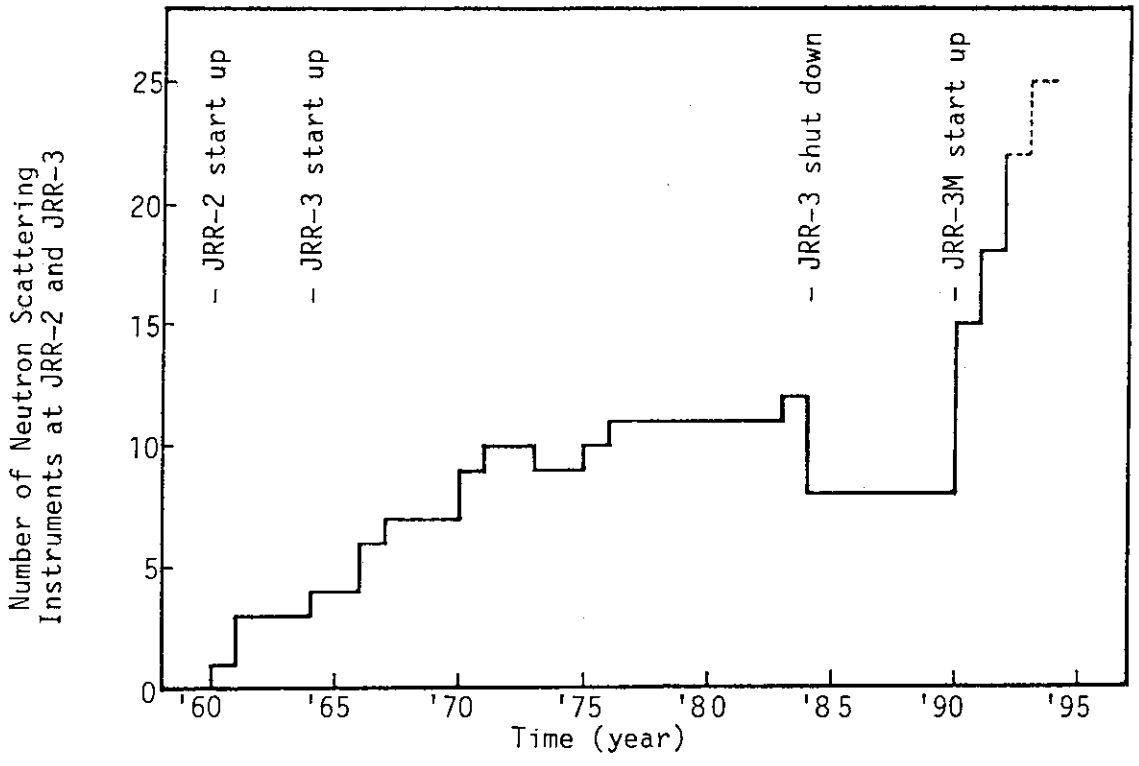

Fig.1 Time evolution of neutron scattering instruments at JRR-2 and JRR-3.

During these years, the field of the research to be studied with neutrons widened. In the early days, it was limited almost within magnetism, metallurgy and crystallography. Recently polymer became one of the most important fields of the neutron scattering research. Industrial application has just started.

The development is so quick recently. The pulsed neutrons are powerful for some problems. At the same time it is deeply recognized that the reactor neutrons are coming more and more indispensable.

References

[1] Y.Hamaguchi, S.Komura, N.Kunitomi and M.Sakamoto; J. Phys. Soc. Jpn.17, Supplement B-III,(1962)46.
[2] N.Kunitomi, Y.Hamaguchi, M.Sakamoto and S.Komura; J. Phys. Soc. Jpn.17, Supplement B-II,(1962)354.
[3] S.Miyake, S.Hoshino, K.Suzuki, H.Katsuragi, S.Hagiwara, T.Yoshie and K.Miyashita; J.Phys. Soc. Jpn. 17, Supplement B-II,(1962)9.
[4] N.Kunitomi, Y.Hamaguchi and S.Anzai; J. de Phys. 25(1964)568.
[5] N.Kunitomi, Y.Hamaguchi, M.Sakamoto, K.Doi and S.Komura; J. de Phys. 25 (1964)462.
[6] M.Sakamoto and Y.Hamaguchi; Proceedings of 4th IAEA Symposium on Neutron Inelasic Scattering, Vienna 1968, vol.1, p.181.
[7] M.Iizumi; J. Phys. Soc. Jpn. 33(1972)647.
[8] S.Funahashi and Y.Hamaguchi; Proceedings of the International Conference of Magnetism, Moscow 1973, vol.5, p. 571.
[9] N.Ohama and Y.Hamaguchi; J. Phys. Soc. Jpn. 30(1971)1311.
[10] H.Betsuyaku, Y.Hamaguchi and S.Funahashi; Proceedings of the International Conference of Magnetism, Moscow 1973, vol.5, p.595.
[11] S.Hiramatsu, S.Isagawa, S.Ishimoto, A.Masaike, K.Morimoto, S.Funahashi, Y.Hamaguchi, N.Minakawa, Y.Yamaguchi; J. Phys. Soc. Jpn. 45(1978)949.
[12] S.Funahashi; Physica B 174(1991)470.

2. The Cold Neutron Facility of the JRR-3M

T. KUMAI, M. SUZUKI and K. KAKEFUDA

Department of Research Reactor
Tokai Research Establishment
Japan Atomic Energy Research Institute
Tokai-mura, Naka-gun, Ibaraki-ken

ABSTRACT

A description is given of a cold neutron source and neutron guide tubes of the JRR-3M.

The installation of the cold neutron source (CNS) together with the neutron guide system is one of the principal objectives of the remodeling project of the JRR-3 and this CNS is the first one that was installed in the high neutron flux reactors of 14 orders of magnitude in Japan.

The CNS is a liquid hydrogen moderator and vertical thermosyphon type. It mainly consists of a hydrogen plant for liquid hydrogen and hleium refrigerator plant for cold helium gas.

Five neutron guide tubes are installed to get thermal and cold neutron beams in the beam hall.

The CNS and the guide tubes have been operated very well since August 1990.

I. INTRODUCTION

The cold neutron source (CNS) together with the neutron guide system in the JRR-3M is one of the most important experimental facilities because it is first one to be installed in a high power research reactor in Japan.

Primary goal for construction and operation of the CNS was to design, construct and operate an efficient system which can be operated safely and increase the cold neutrons significantly for neutron beam experiments. The project to develop a CNS and guide tubes for the JRR-3M started in 1979. Since then feasibility studies, coceptual design, detailed design, assembly and mockup tests, licensing review, fabrication, construction and several kinds of functional tests had been carried out together with the reactor itself, and the CNS and the guide tubes have been working very well since August 1990.

The CNS uses liquid hydrogen as cold moderator for cold neutrons which is circulated vertically by thermosyphone and cooled by cold helium gas from gas to liquid. The strength of cold neutron flux is about 2×10^{8} $n/cm^2\cdot s/20MW$ at the end of the longest cold neutron guide tube C2. The cold neutron source gain for neutron wavelength of 4Å becomes about 10.

II. LAYOUT OF THE COLD NEUTRON FACILITY

Fig. 1 shows the whole diagram of the cold neutron facility. This consists of a cold neutron source and neutron guide tubes.

The cold neutron source mainly consists of a hydrogen plant, in the reactor building and a helium refrigerator plant, in the compressor building. furthermore, the hydrogen containment of the hydrogen plant is set in the reactor pool and the sub pool.

Five neutron guide tubes are stretched from the reactor to the beam hall through the guide tunnel and the guide tube room.

The compressor building is located about 50m apart from the beam hall and about 100m apart from the reactor building, in order to provide wider space for the beam hall and the reactor room.

III. COLD NEUTRON SOURCE

A. HYDROGEN PLANT AND REFRIGERATOR PLANT

The main part of hydrogen plant is a cryostat, which consists of moderator cell, cold transfer line and condenser, and contains about 1.4ℓ of liquid hydrogen at approximately 20K at 1.2 ata as cold moderator.[1] The moderator cell located in the maximum thermal neutron flux area where is about 50cm far from the reactor core is an flask shape vessel, 20cm high, 13cm wide, 5cm thick and 0.8ℓ in volume, and made of 0.8mm thick stainless steel. The cold transfer line is a three walled piping structure, 4m long in horizontal 3.5m long in vertical. Liquid hydrogen flows down from the condenser to the moderator cell through the inner pipe and gas hydrogen flows back to the condenser through the inner annulus. Thus, the cold hydrogen, mixture of liquid and gas, circulates by means of thermosyphon through condenser, cold transfer line and moderator cell removing about 300W of the nuclear heat and about 150W of the thermal radiation heat from the moderator cell to the condenser.

Other systems of the hydrogen plant are helium dump system, hydrogen and nitrogen gas supply system, vacuum system and gas analyzer. The helium dump system enables the reactor to be operated in the event that the helium refrigerator plant stops accidentally. Namely, the helium dump system fills both the vacuum space and the hydrogen space with helium gas in order to prevent the temperature of the moderator cell from exceeding more 400°C.

A Brayton cycle type helium refrigerator plant consists of a cold box, a control heater, two oil screw compressors, two staticgas bearing turbo expanders, refrigerant transfer lines, a cooling water system and a helium tank. One pair of a compressor and a turbo expander is for standby duty. This plant is capable of supplying the coolant of about 1360W at 14.5K to condenser and control heater including the heat loss of the 160m long refrigerant transfer lines themselves.

Cold helium gas is obtained by reducing pressure of the helium gas from about 19 bar to 2 bar through a turbo expander, and the gas is previously compressed to standard temperature at 19 bar using a compressor.

B. SAFETY ASPECTS WITH HYDROGEN

Safety aspects with hydrogen are based on a double containment structure for hydrogen with a vacuum blanket and complete immersion of the hydrogen container both in the reactor pool and the sub pool.

These aspects are focussed on preventing a contact between hydrogen and air in case of an accidental loss of leaktightness. The whole outer containment of hydrogen is strong enough to withstand the pressure of detonation that is the severest phonomenom of oxygen/hydrogen reaction, that was verified by qualification tests performed on the full-scaled models.[2]

The 3.3m deep sub pool is completely separated from the reactor pool so that independent maintenance works for the CNS from the reactor pool can be carried out.

C. OPERATION AND CONTROL

The CNS used to start its operation one day before the reactor operation and stop its operation one hour after the reactor shut down. It takes about 24 hours to get steady operational state and about 20 hours to become complete stop. During a steady operation cycle of four weeks, it is no need to control the CNS manually even at the time of the reactor start up and shut down because the CNS is fully automatic.

Fig. 2 shows the control system of the CNS. The control loop 1 and 4 work to keep helium pressure at the delivery and the suction point of the compressor constantly to 18.6 and 1.6 bar respectively. The control loop 2 keeps temperature, pressure and flow rate of cold helium gas constant at the delivery side of the turbo expander by regulating the by-pass valve. Then the effective power output of the refrigerator is always kept to 1200W consequently. The control loop 3 works to keep the hydrogen pressure in the buffer tank within 1.2±0.1 ata by the control heater compensating the heat load variations in the cryostat.

IV. NEUTRON GUIDE TUBE

Fig. 3 shows the layout of the neutron guide tubes. Five neutron guide tubes, T1 and T2 for thermal neutrons and C1, C2 and C3 for cold neutrons, are installed efficently to extract neutron beams from the heavy water reflector and the liquid hydrogen moderator in the D_2O tank through the horizontal beam hole 8T and 9C respectively to the beam hall.

16 neutron beam ports of which 8 are set on the thermal neutron guide tubes and another 8 on the cold neutron guide tubes, are available in the beam hall, 30m wide × 50m long, which is located next to the reactor building.

Each of the guide tubes consists of three sections. The first straight section is inbedded inside the reactor biological shield plugs. The curved section has a radius of curvature correspond to the critical neutron wavelength of the guide tubes and installed in the guide tunnel and the guide tube room. The second straight section is installed in the beam hall.

The curved section permits very efficiently to separate thermal and cold neutron beams from fast neutron beams and γ rays, and the second straight section works to make good cross-sectional homogeneity of neutron flux at the beam ports.

Each of the neutron guide tubes is a line-up of the neutron guide elements and each of the elements has rectangular cross-section, $20\times200mm^2$ for thermal neutrons and $20\times120mm^2$ for cold neutrons, and 850mm long for both one. The walls of the elements are made of borosilicate glass plates polished opticaly and coated in pure natural nickel of 2000Å thick. The glass plates are 19mm thick and themselves make up the vacuum enclosure to reduce neutron losses due to air scattering.

T1 and T2 are for the critical neutron wavelength of 2Å with the radius of curvature of 3340m and have the overall length of about 60m. C1 and C2 are for 4Å with the radius of 834m and have the length of about 41m and 51m respectively. C3 is for 6Å with the radius of 370m and has 31m long.

Autocollimator enabled to install the neutron guide elements with tolerance of ±0.01mm and within 1".

V. CHARACTERISTICS

The neutron fluxes and their distributions were measured by gold foil activation method at the beam port C2-3, during the reactor commissioning test period in 1990.

Mean neutron fluxes are $1.9\times10^8 n/cm^2\cdot sec$ in case of liquid hydrogen and $1.9\times10^7 n/cm^2\cdot sec$ in case of no liquid hydrogen. Neutron flux deviations over the cross section of the neutron guide tube are about 10% in both cases.

Fig. 4 shows two neutron spectra measured by means of time-of-flight method at the beam port C2-3 at the same time when the neutron fluxes and distributions were measured. The top one is obtained in the case of liquid hydrogen, and the bottom one is no liquid hydrogen. These spectra indicate the effectivness of the existence of the liquid hydrogen because the counts with liquid hydrogen is larger than those without liquid hydrogen on the longer neutron wavelength than 2Å.

A cold neutron source gain curve for various wavelength is obtained as the ratio of neutrons, top one divided by bottom one, and the results plotted on Fig. 5. The cold neutron source gain at wavelength of 5Å and 10Å are 15 and 28 respectively. These gains are large enough to satisfy the primary goal for the construction and the operation of the CNS.

REFERENCES

1. Kumai T., Kudo M. et al. "Fundamental Experiment on Closed Circuit Type Thermosyphon with Concentric Tubes for the JRR-3M Cold Neutron Source (II)," JAERI-M 89-114 (1989)
2. Hibi T., Takahashi H., Kumai T. et al. "JRR-3 Cold Neutron Source Facility H_2-O_2 Explosion Safety Proof Testing," IAEA-SM-310 (1989)

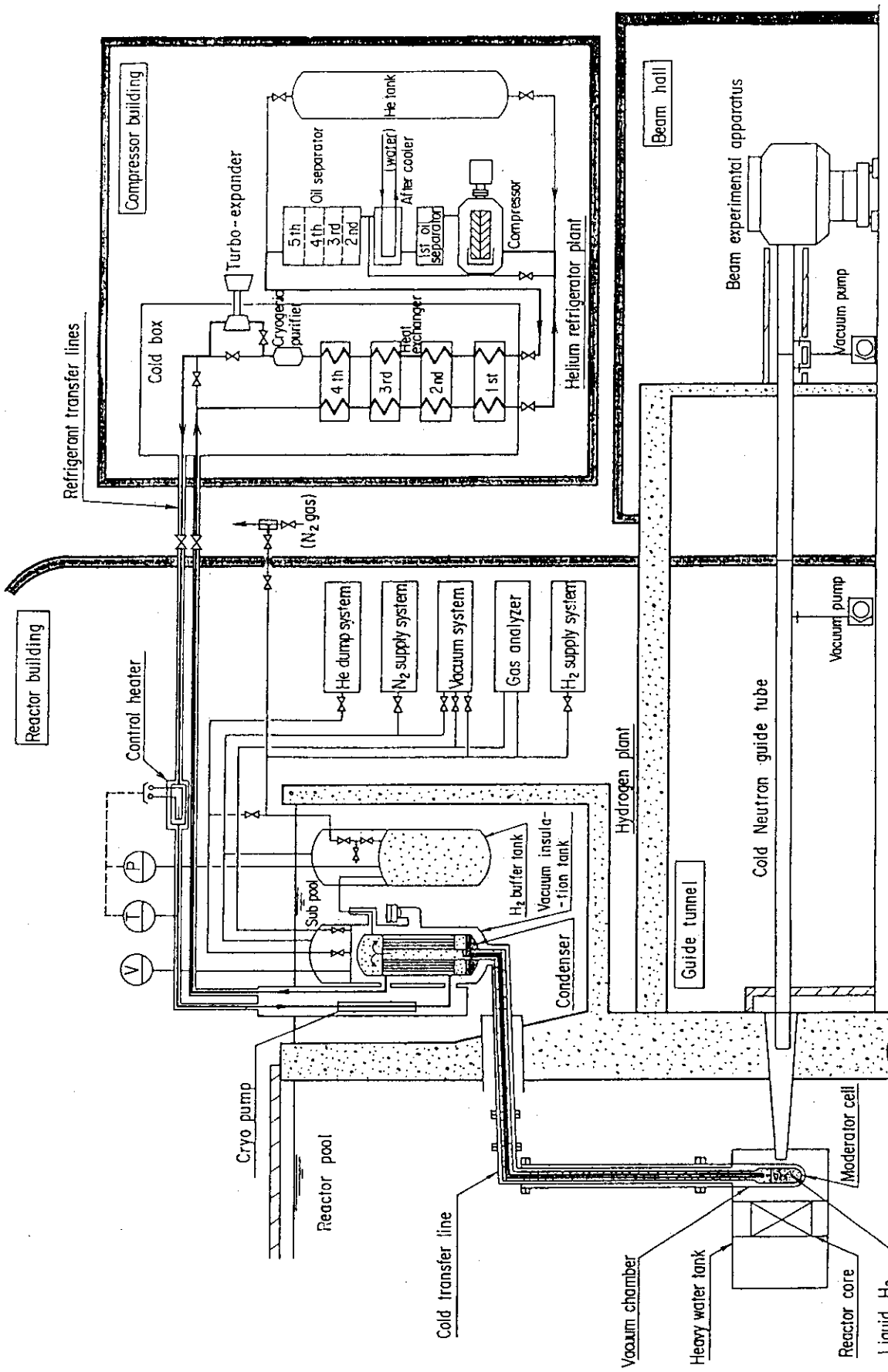

Fig.1 Whole diagram of the cold neutron facility

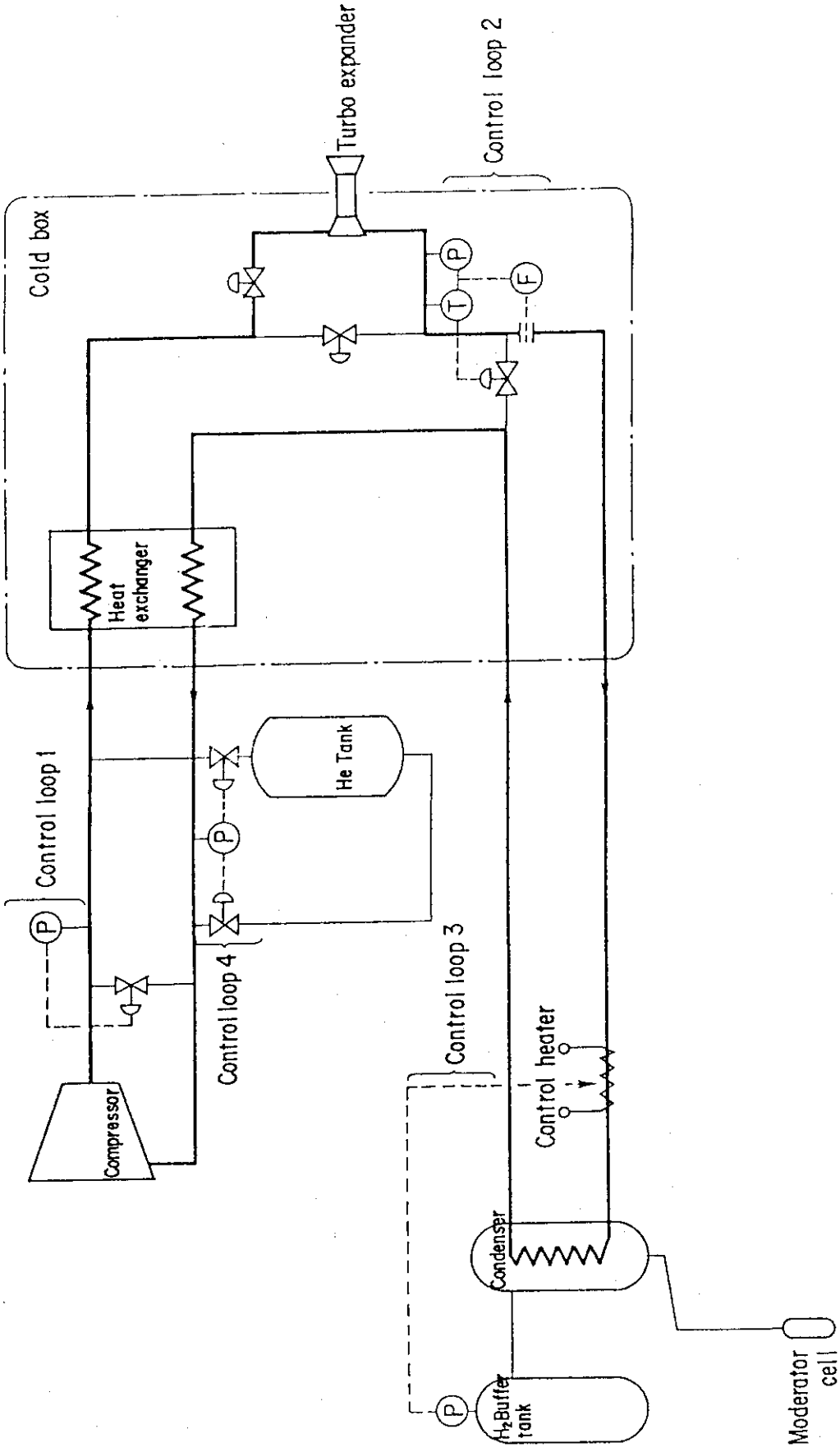

Fig. 2 Control system

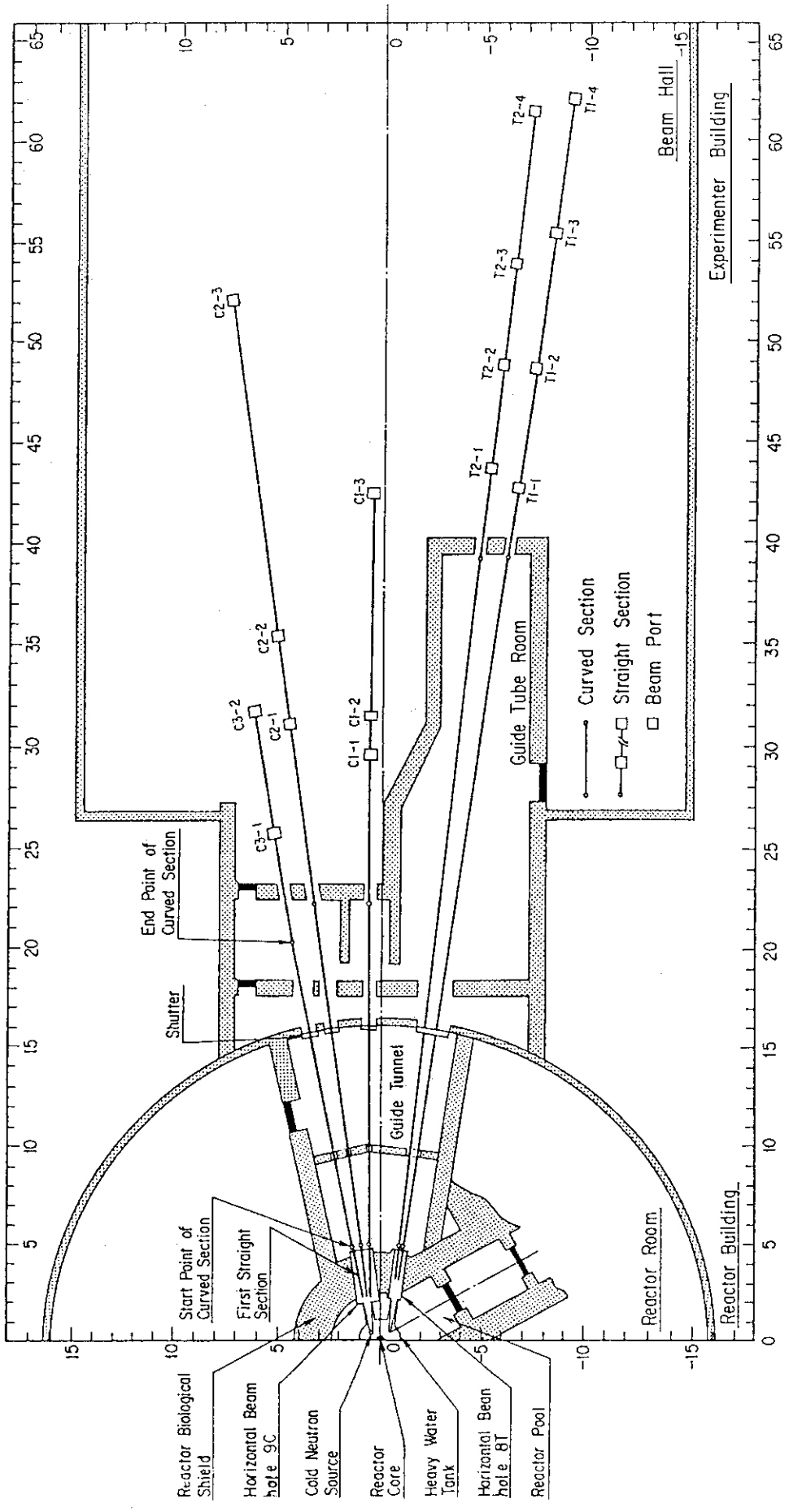

Fig. 3 Layout of the neutron guide tubes for the JRR-3M

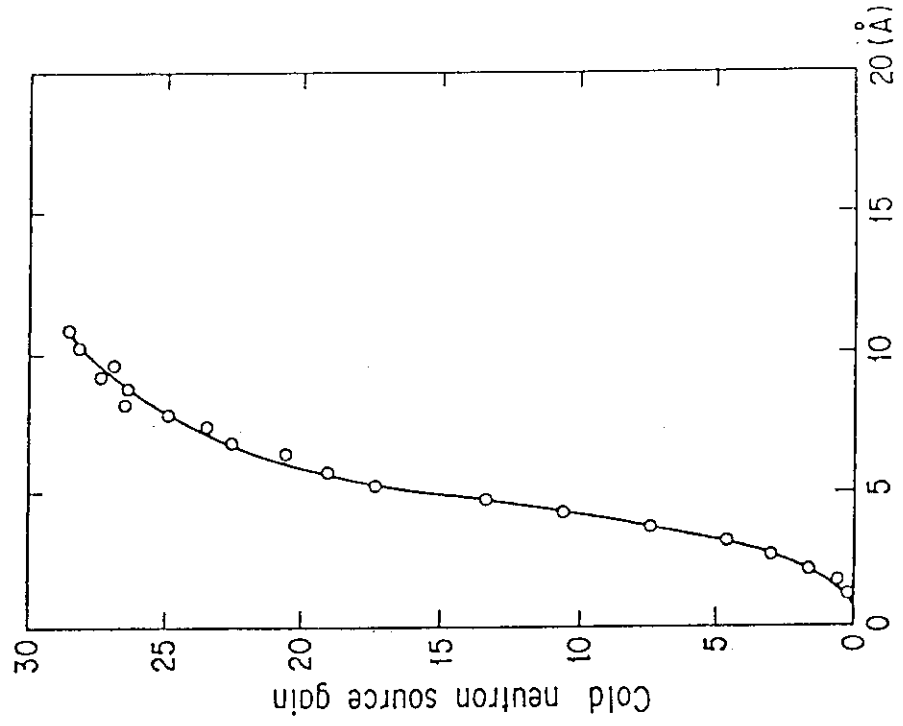

Fig. 5 Cold neutron source gain

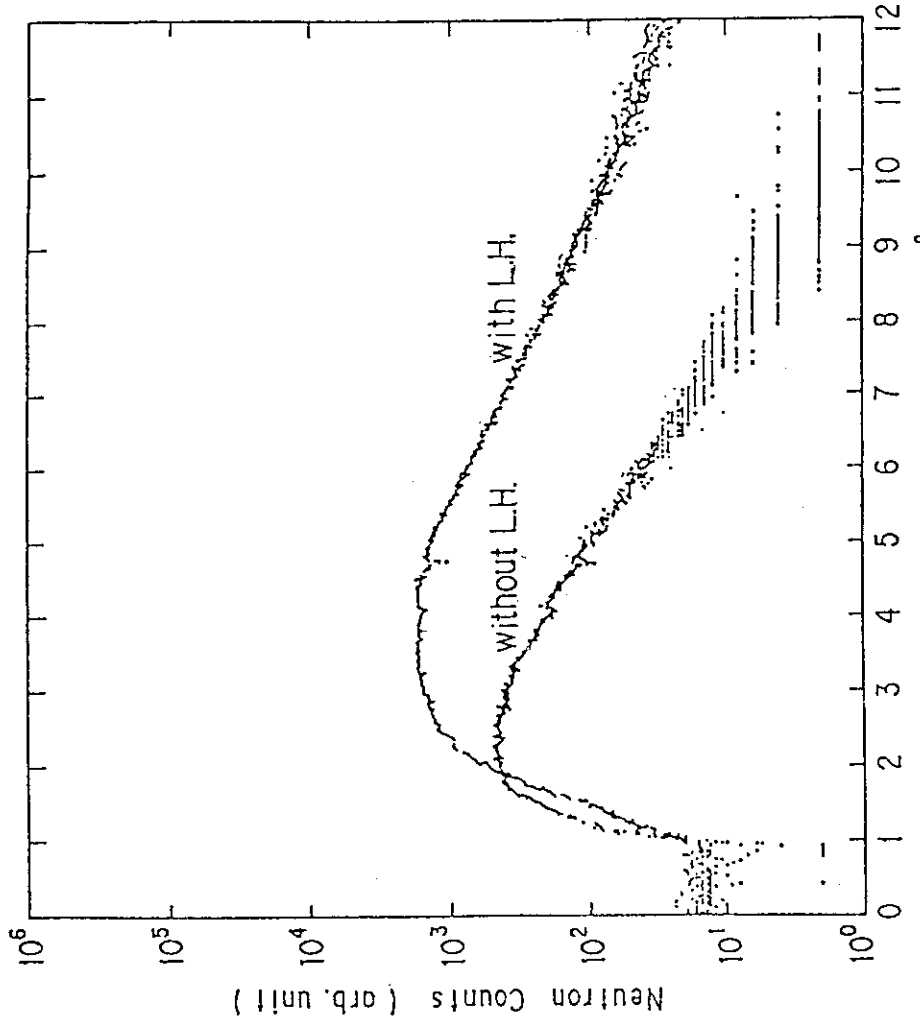

Fig.4 Neutron spectrum

3. Ultracold and Very Cold Neutron Facility in KUR

Yuji KAWABATA and Masahiko UTSURO

Research Reactor Institute, Kyoto University,
Kumatori-cho, Sennan-gun, Osaka 590-04, Japan

ABSTRACT

The present status of the ultracold and very cold neutron facility installed in the Kyoto University Reactor (KUR) is described in this presentation. It consists of a VCN (very cold neutrons) guide tube, a VCN bender and a supermirror neutron turbine. The guide tube extracts VCN from a liquid deuterium cold neutron source in a graphite thermal column and the neutron turbine converts VCN to UCN (ultracold neutrons). As for the utilization of the present facitily, VCN radiography and an UCN gravity spectrometer are shown for the practical examples of the research with VCN and UCN.

INTRODUCTION

Kyoto University Reactor (KUR) is a 5MW pool type light water moderated and cooled research reactor. A preliminary stage of a VCN guide tube installed into the graphite thermal column was already reported earlier,[1] and also a description of a supermirror neutron turbine combined to the preliminary VCN guide tube was given.[2] Recently, a cold neutron source has been installed in the graphite thermal column.[3] The moderator of the cold neutron source is liquid deuterium. With this modernization of our neutron facility, the VCN and UCN intensities are much more improved and they are reported in the followings.

The ultracold and very cold neutron facility connected to the cold neutron source provides very low energy neutrons. It consists of a VCN guide tube,[4] a VCN bender and a supermirror neutron turbine.[5] The guide tube extracts VCN from a cold neutron source and the neutron turbine converts VCN to UCN.

The research field of UCN and VCN is a new front of the lowest energy in the scientific field. One of the most noticeable fields of the UCN utilization is the fundamental physics. As UCN can be contained in a

material bottle for a long time, the precision of measuring basic properties of a neutron, like the life time,[6] the electric dipole moment,[7] etc., have been improved by the use of UCN.

A whole description of the UCN-VCN facility, the research proposals for using VCN and UCN in KUR and some trials in the new fields are presented in this paper.

VERY COLD NEUTRON GUIDE TUBE

General layout of the cold neutron source and the UCN-VCN facility is shown in Fig.1.

Very cold neutrons are extracted from a cold neutron source through a VCN guide tube. The characteristic wavelength of this guide tube is 23.5Å. The beam width is 45mm and the height is 90mm. The radius of curvature is 54.8m for the curved part and the total length of the VCN guide tube is 7.0m.

The innermost portion of this guide tube is inserted deeply into the VCN beam hole of the thermal column to extract VCN effectively. The guide tube units of the portion inserted in the thermal column were prepared specially to withstand the nuclear irradiations and heating. They were made of nickel mirrors evaporated on aluminum plates which were polished by the diamond cutting method. The thickness of the Ni layer is about 2000 Å. The total length of this in-pile portion is 2m.

The out-of-pile portion consists of a 4.5m long curved part and a 0.5m long straight part. The neutron mirrors for these parts were made of nikel evaporated float glasses. All of this out-of-pile portion guide tube consist of straight units which are 50cm long.

The time-of-flight (TOF) spectrum of VCN outlet of this VCN guide tube measured is shown in Fig.2. When the spectrum was measured, a 1.0m long straight part was further added at the exit and thus the tolal length of the VCN guide tube was 8m. The neutron pulse width was 0.40msec and the flight length was 1.3m for the TOF measurement. The spectrum shows that this VCN guide tube gives good VCN beam. The last 2 units of this guide tube was now removed to set the VCN bender.

VERY COLD NEUTRON BENDER

The VCN beam from the VCN guide tube is curved upward sharply by the vertical VCN bender in order to fit it to the VCN inlet port of the supermirror neutron turbine. This VCN bender bends the VCN beam from the VCN

guide tube vertically with the radius of curvature 5.24m. Its characteristic wavelength is designed to be 48Å.

The vertical view of the VCN bender is shown in Fig.3 and the beam cross section is shown in Fig.4. The VCN bender is also made of 180mm long straight units. The beam width is 30mm and the height is 90mm. The neutron beam in the bender is divided into 5 sections by the nickel evaporated silicon wafer mirrors, as shown in Fig.4. Nickel layers were evaporated on both sides of these dividing walls.

SUPERMIRROR NEUTRON TURBINE

The purpose of the neuton turbine is to convert VCN to UCN. The turbine has moving neutron mirrors which goes to the same direction with neutrons to reflect and to decelerate neutrons.

The first neutron turbine in the world was developed in Munich[8] and the improved version is installed in ILL.[9] The present supermirror turbine[2] has an essentially similar structure to them, except using sets of flat three supermirrors[10] for the blades.

The structure of the present supermirror turbine is shown in Fig.5. The diameter of the turbine wheel is 1m and it rotates with the blade speed of about 25m/s. VCN are fed with a small angle to the moving direction of blades. VCN with the velocity of about 50m/s have the relative velocity of about 25m/s to the blades. When they are reflected on the blade, they are deceleated to near to 0m/s. In the present design of the turbine, only the velocity component which is parallel to the moving direction of the blades decelerates, and the velocity component perpendicular to it does not change. Therefore, incident VCN do not stop and the final neutron velocity of our design becomes about 5m/s.

When the blades are made by supermirror, the number of blades can be significantly lessened. This is because the supermirror has a much larger critical angle of the total reflection than that of a metallic mirror.

GRAVITY SPECTROMETER USING ULTRACOLD NEUTRONS

One of the proposed experiments using UCN is the gravity spectrometry. The use of UCN is expected to provide the highest resolutions both for energy and for momentum transfers on neutron scattering experiments, because UCN have a very small energy as well as a very small momentum.

The first gravity spectrometer in the world with UCN was constructed and installed in ILL and it gives very good resolutions.[11] The working principle in this first gravity spectrometer named NESSIE is "reach-foccusing" and it measures the reaching distance of the scattered neutron with the scattering angle of about 45° to the horizontal plane.

We are developing another type of UCN gravity spectrometer with a "fall-focussing principle".[12,13] An ellipsoidal mirror can concentrate light emitted from one focus to another, but neutrons cannot follow the same trajectries becauses of the gravity. Qualitatively speaking, a slower neutron goes to a lower point. When we use one ellipsoidal mirror, the incident angle of a neutron to the mirror surface is complicatedly changed according to the reflection height. Therefore, we already proposed an appropriate arrangement of ellipsoidal mirror elements on a modified surface in order to compensate for the undesirable divergence of trajectries due to various reflection height.

Fig.6 shows the schematic arrangement of the reflecting surfaces, deviding into three regions. The first foci of all mirror elements are located on the sample point, and the distance between the first and second foci varies according to the regional grouping of the changes in the scattering angle. Thus, the neutrons scattered in different group of the polar angles with a certain scattered energy are focussed to different points below the different second foci with a fall distance corresponding to their energy. Consequently, the energy and momentum analyses can be performed by the vertical and horizontal positions of the neutron detection, respectively.

The horizontal view of the gravity spectrometer we are developing now is shown in Fig.7. The scattering angle is devided into 5 regions. The 2nd and 4th regions with totally 108 mirror elements have been manufactured. The mirror elements are spherically curved, and every elements have different shapes, sizes, radii and setting positions. We decided them from numerical analyses and manufactured them according to the calculated results. Supermirrors were evaporated on all mirror elements to expand the measuring energy window.

VERY COLD NEUTRON RADIOGRAPHY

Neutron radiography with thermal neutrons or cold neutrons has been developed in many institutes,[14] but study with VCN or UCN was not reported except a preliminary trial.[15] In order to show the possibility of VCN radiography with our facility, some trials have been

made.

Photo 1 shows the measured neutron beam distribution of the VCN guide tube when the cold neutron source was not operated. The exposure time was 10 minutes. It shows the flux distributions. The difference of darkness between right side and left results from the curved geometry of the guide tube. The outer side of the curvature has much neutron flux because of the contribution due to the garland reflections.

Photo 2 shows a figure of a cigarette lighter as an example of the VCN radiography. The exposure time was 6 minutes when the cold neutron source was operated. We can notice that the contrast of this figure is much better than that of thermal neutron radiography.

CONCLUDING REMARKS

There are a few ultracold and very cold neutron source in the world and the importance of researches with sub-cold neutrons is growing greater. It can be said that the continuous neutron source is more suitable for the neutron source of the lower energy than the pulsed neutron source because of the longer slowing down time from the high energy to the lowest energy and also longer flight time of the low energy neutrons. From such points of view, research reactors are most advantageous as the sources for the ultracold and very cold neutrons.

REFERENCES

1) M.Utsuro et al., Annu.Rep.Res.Reactor Inst.Kyoto Univ. 13, 161 (1980).
2) M.Utsuro et al., Nucl.Instr. and Meth. in Phys. Res. A270, 456 (1988).
3) M.Utsuro et al., Physica 156&157B, 540 (1989).
4) M.Utsuro et al., Physica 156&157B, 537 (1989).
5) M.Utsuro et al., Proc. Int.Conf. on Thin Film Neutron Optical Devices, San Diego, SPIE - The Int. Soc. for Optical Eng., Vol.983, 114 (1988).
6) W.Mampe et al., Phys.Rev.Lett. 63, 593(1989).
7) N.F.Ramsey et al., Phys.Lett. 234B, 191(1990).
8) A.Steyerl et al., Nucl.Instr. and Meth.125,461(1972).
9) A.Steyerl et al., Phys. Lett. 116A, 347(1986).
10) T.Ebisawa et al., J.Nucl.Sci.Technol., 16, 647(1979).
11) A.Steyerl et al., Z. Phys. 50B, 281(1983).
12) M.Utsuro, Nucl.Instr. and Meth. 213, 557(1983).
13) Y.Kawabata et al., Nucl.Instr. and Meth. A245, 106 (1986).
14) for example, S.Matsubayashi et al., presented in these proceedings.
15) J.C.Bates, Phys. Lett. 83A,29(1981).

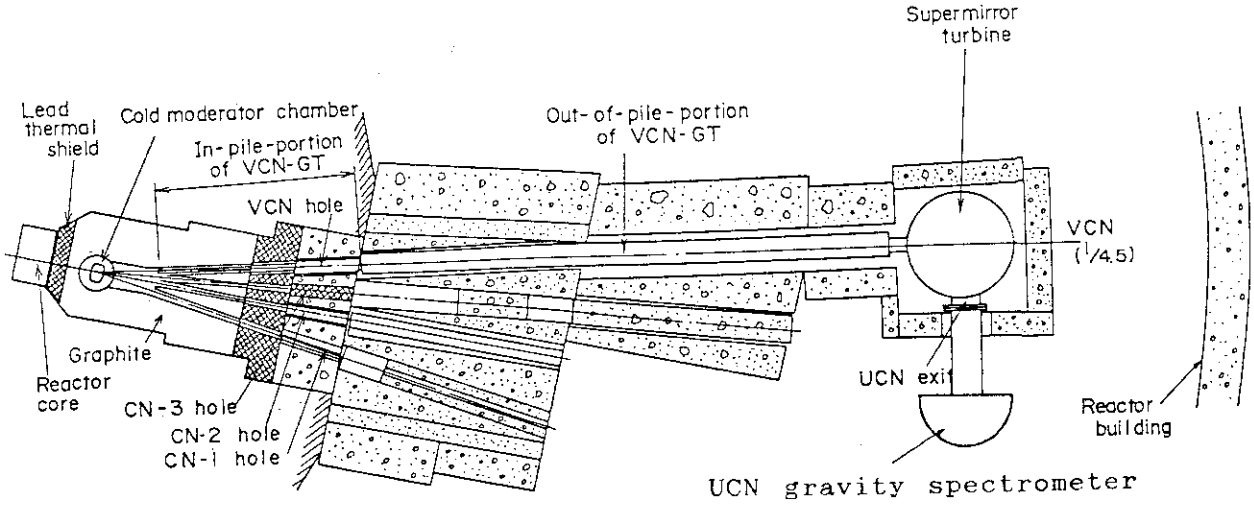

Fig.1 Overall layout of the UCN-VCN facility in KUR

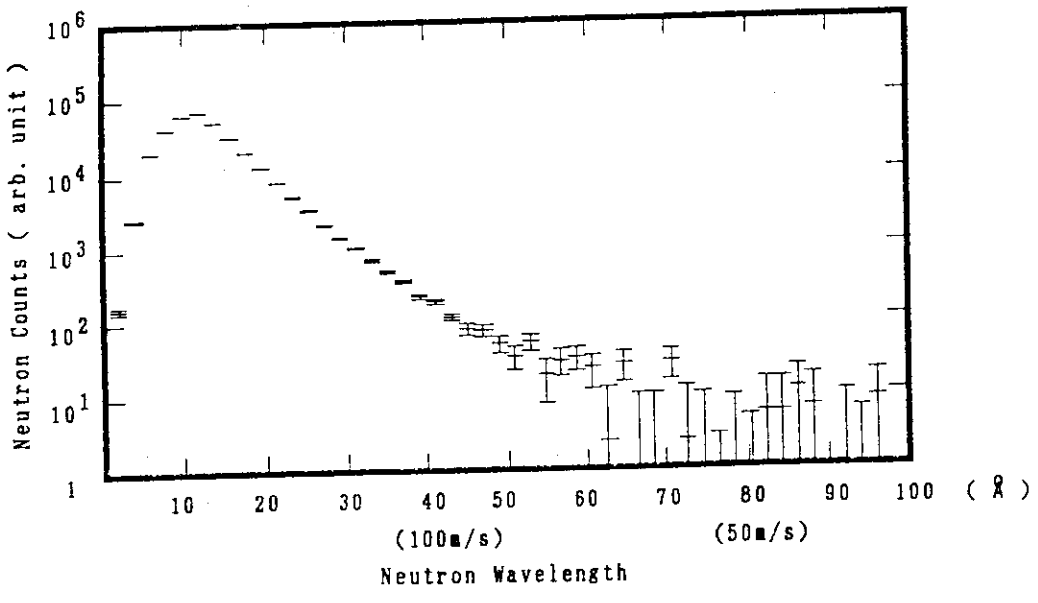

Fig.2 Time-of-flight spectrum of the VCN outlet from the center of the guide tube

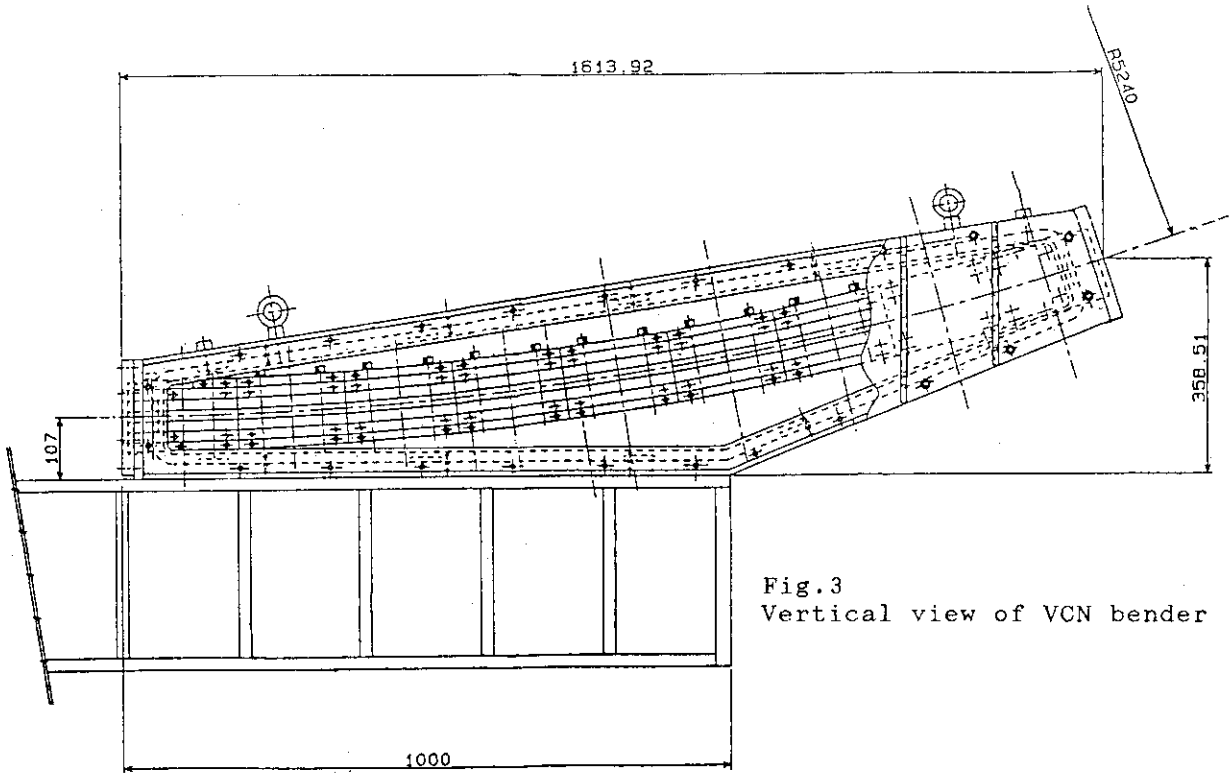

Fig.3
Vertical view of VCN bender

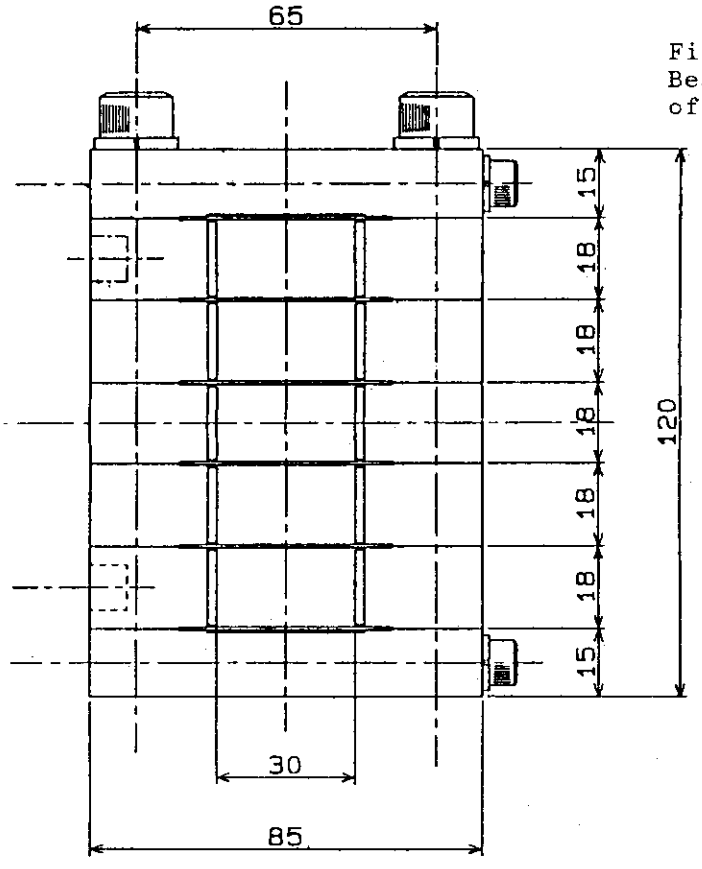

Fig.4
Beam cross section
of the VCN vender unit

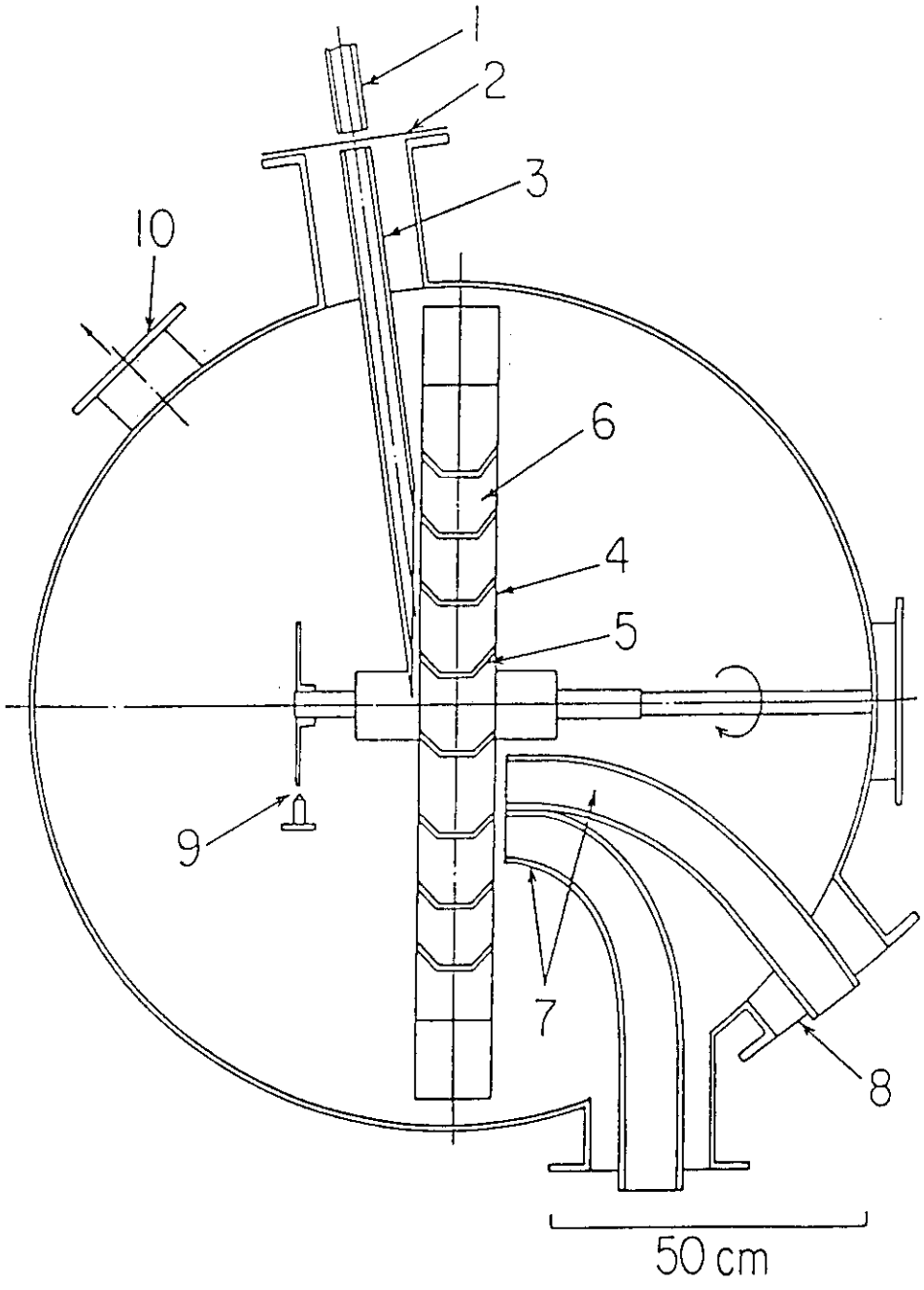

Fig.5 Structure of supermirror UCN turbine

1;Neutron feeding guide tube, 2;Al window,
3;Connecting guide tube, 4;Turbine wheel,
5;Reflecting blades of supermirrors,
6;Lower reflector mirror, 7;UCN extraction guide tube,
8;Connecting flange, 9;Rotation pick-up device,
10;Evacuation port.

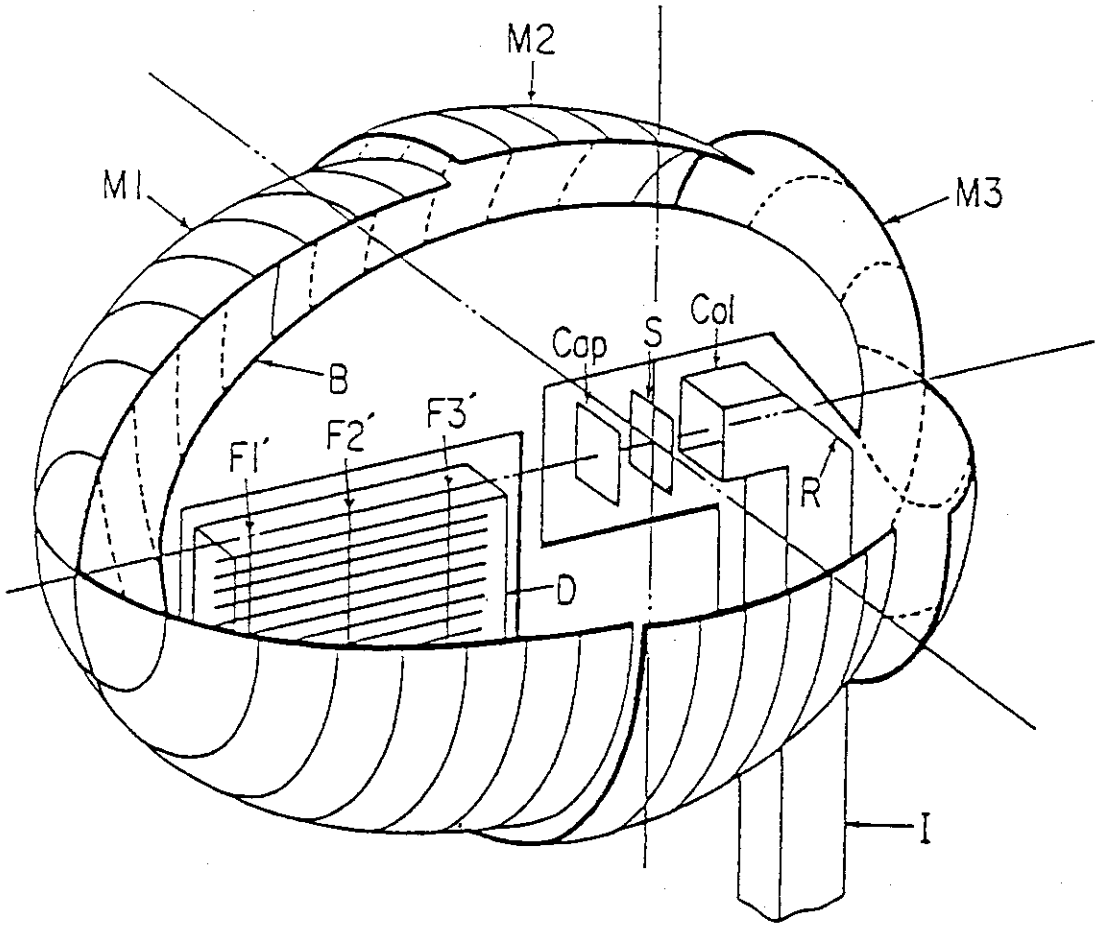

Fig.6 Schematic structure of the fall focussing gravity spectrometer

M1,M2,M3;Fall focussing mirrors,
F1',F2',F3';Second foci of the mirrors,
D;Position sensitive UCN detector, S;Scattering sample,
I;UCN feeding guide tube, B;Neutron capture board,
R;Reflector, Col;UCN collimator,
Cap;Beam cature for the transmitted UCN.

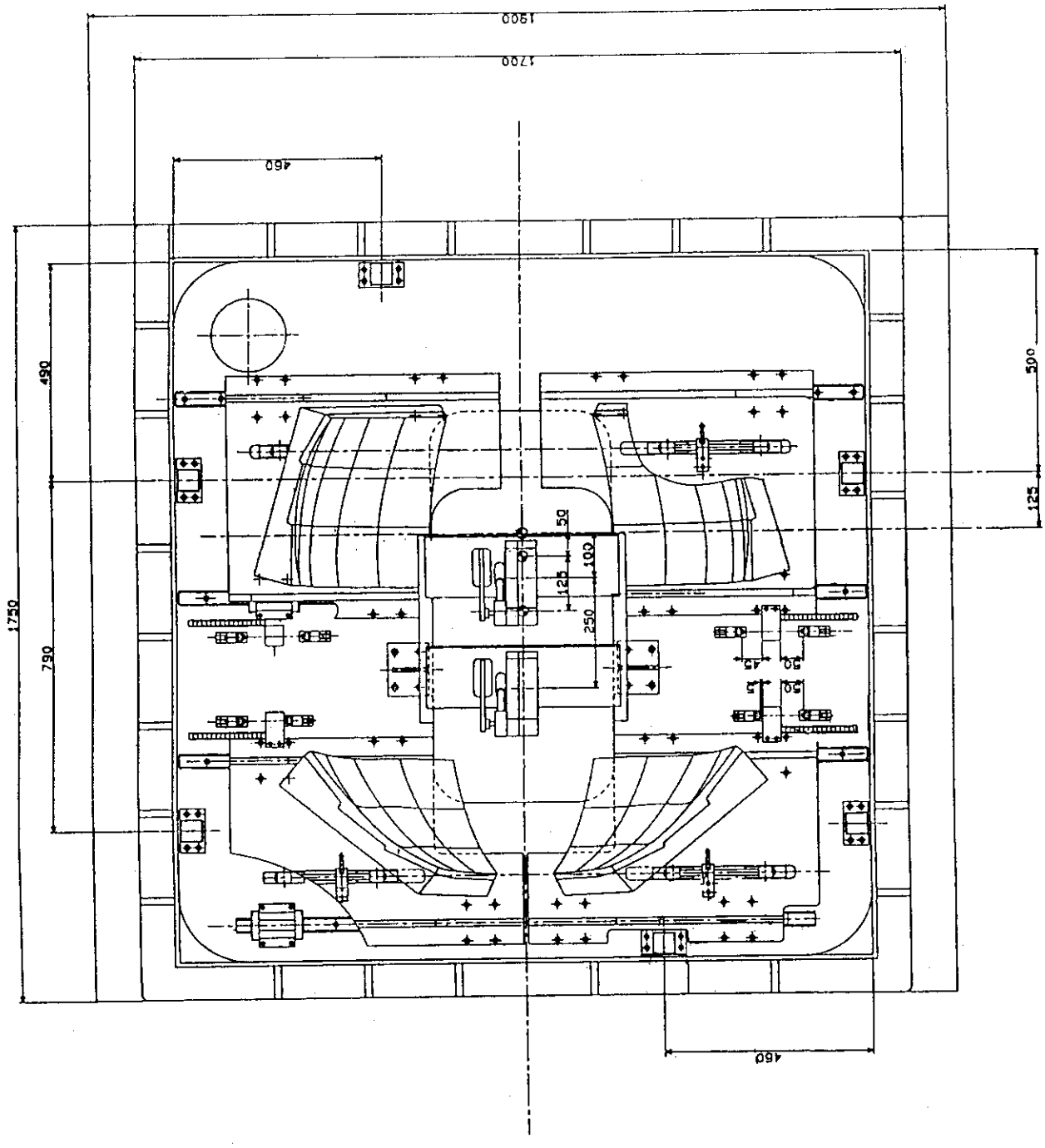

Fig.7 Horizotal view of the gravity spectrometer

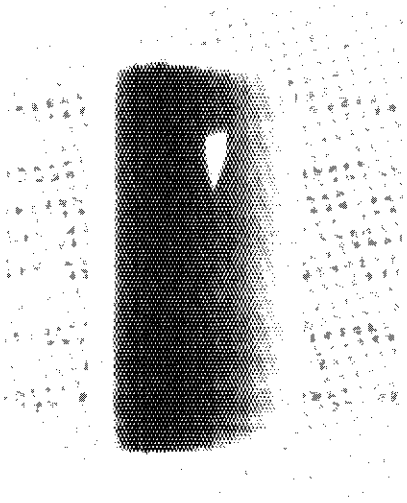

Photo 1
Neutron beam distribution
of VCN bender outlet

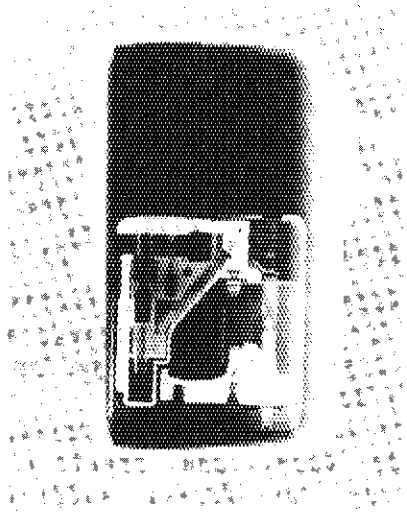

Photo 2
VCN radiography of
a cigarette lighter

4. Design of Neutron Bender Using Supermirrors

Kazuhiko SOYAMA* and Yuji KAWABATA**

*Department of Research Reactor
Tokai Research Establishment,
Japan Atomic Energy Research Institute
Tokai-mura, Naka-gun, Ibaraki-ken 319-11, JAPAN

**Research Reactor Institute,
Kyoto University
Kumatori-cho, Sennan-gun, Osaka 590-04, JAPAN

ABSTRACT

A neutron bender using supermirrors has been designed. In this paper we will describe the fabrication of Ni-Ti supermirror and the characterization concerning the neutron reflectivity and the layers structure. After that, a design of a supermirror neutron bender is described.

INTRODUCTION

Neutron guide tubes using nickel mirrors or supermirrors, can provide slow neutrons to experimental facilities with low backgrounds of fast neutrons and gamma-rays in research reactors. Neutron mirror reflection is based on the phenomenon of total reflection. The critical reflection angle of natural nickel is 1.7 mrad/Å and that of ^{58}Ni is 2.0 mrad/Å. Supermirror which was proposed by F.Mezei[1], extend effectively the critical angle of total reflection up to $2 \sim 3$ times as large as that of natural nickel, because a multilayer with a gradually changing lattice spacing reflects the higher energy neutrons with Bragg reflections.

Neutron bender which is a kind of guide tubes, can branch off a neutron beam from the main guide tube, and create a new beam port for various beam experiments. In order to obtain sufficient area for installing instrument, it is needed to separate additional beam line from the main guide tube. A neutron bender using supermirrors makes radius of curvature to be smaller and makes it much easier to separate the neutron beam from the main guide tube.

In this paper we will describe the fabrication of Ni-Ti supermirror and the characterization concerning the neutron reflectivity and the layer structure. After that, a design of a supermirror neutron bender will be described.

SUPERMIRROR

(1) Fabrication

A supermirror consisits of the 62 bilayers, each consisting of Ni and Ti with thickness between 716 Å and 149 Å. Ni-Ti supermirrors are fabricated by a vacuum evapolation system with an electron gun. The vacuum chamber has a large volume of 80 cm diameter and 100 cm height. Multylayers are deposited by automatic control system according to the signal from a thickness monitor with quartz crystal oscillator. It is evaporated in a high vacuum chamber (1×10^{-6}Torr). Vapour pressure is 7×10^{-6}Torr. Temperature of the substrate is less than 40 C. Deposition rate of layers is 0.5 Å/sec. The substrates used for these supermirrors are float glasses of surface area of 150 mm by 300 mm, thickness of 5.0 mm. Average surface roughness (Ra) of the glass substrate is 4 Å measured by Talystep which is a stylus instrument. These substrates are cleaned in cleaning solution of ethanol and methanol (8:2).

The distribution of layer thickness is same as the supermirror which was made by T.Ebisawa et. al.[2] The calculation method are based on the theory of conventional optics on reflectivity. This theory was apllied to the case of neutron optics by replacing the role of electromagnetic waves of light with the plane waves of neutrons.[3]

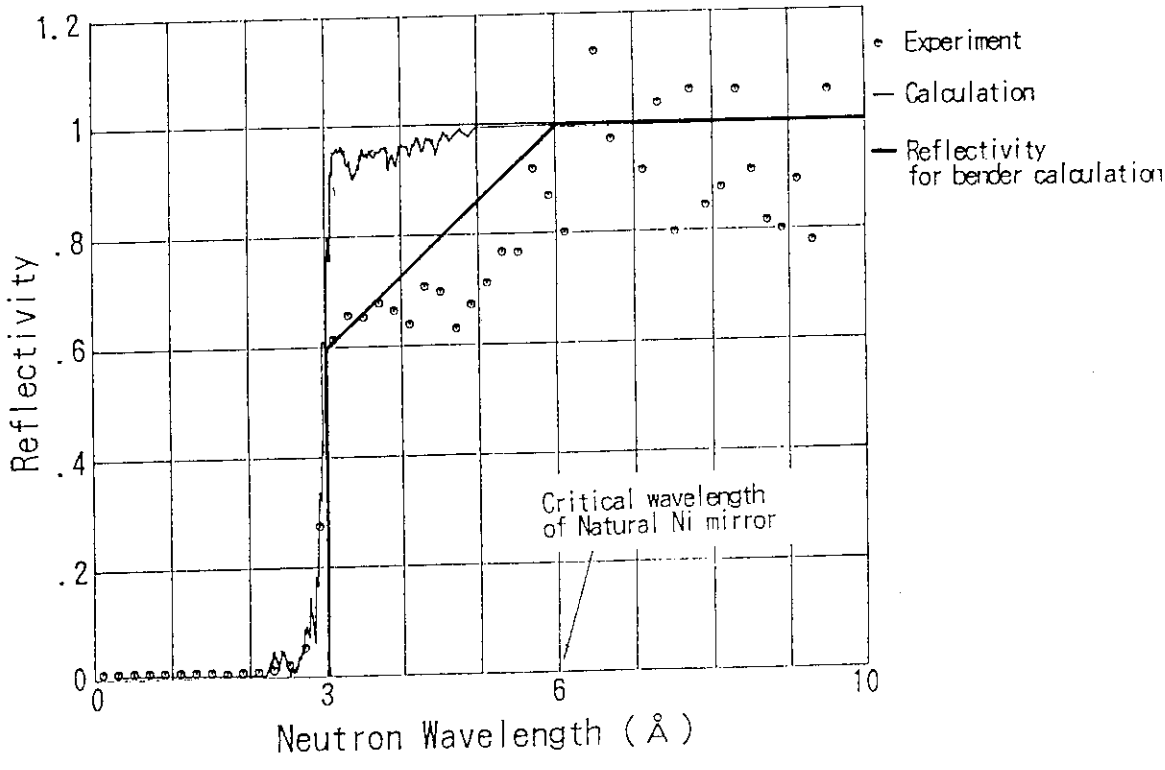

Fig.1 Measured and calculated reflectivities of Ni-Ti supermirror (62 bilayers)

(2) Characterization

The total film thickness measured by Talystep which is 1.30 μm, and it shows good agreement with design value of 1.27 μm. Neutron reflectivity of the supermirrors is measured by time-of-flight method in JRR-3M (the upgraded Japan Research Reactor No.3). The beam is collimated with two cadmium slits whose each size is 0.5 mm by 2.0 mm. Figure 1 shows the results of reflectivity measurement and theoretical calculation about supermirror with 62 bilayers compared to the reflectivity from natural nickel. The reflectivity increases rapidly to 0.6 at wavelength (λ / θ) of 300 Å. It becomes higher with increasing neutron wavelength up to nealy unity for wavelength longer than about 500 Å. It has a critical wavelength of reflection half smaller than a natural nickel mirror. It means that critical reflection angle of this supermirror is same as twice of a natural nickel mirror. The measured reflectivity is lower than the calculated one.

In order to understand the reason why the measured reflectivity is differnt from the theoretical one, microscopic observations by transmission electron microscope (TEM) were performed. This high resolution TEM provides a point resolution better than 2 Å. The cross-section samples were prepared by the method of Ion milling. In Figure 2, a TEM photomicrograph (magnification:50,000) shows the layers of supermirror with 62 bilayers (Ti layers are light and Ni layers are dark). In Figure 3, a TEM photomicrograph (magnification:400,000) shows the undulation due to the growth of crystallities and interdifusion between Ni and Ti layers. This explains the lower reflectivity of measured one.

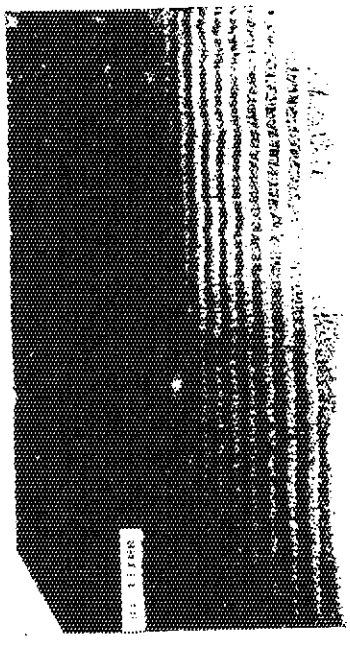

Fig.2 Cross-sectional TEM images of Ni-Ti supermirror (magnification : 50,000)

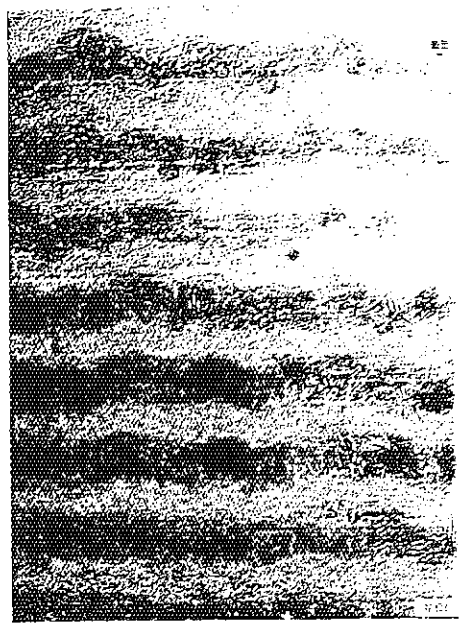

Fig.3 Cross-sectional TEM images of Ni-Ti supermirror (magnification : 400,000)

DESIGN OF A SUPERMIRROR NEUTRON BENDER

Figure 4 shows the scheme of the supermirror neutron bender. It will be set at the end of cold neutron guide tube[4][5] (C2-3) whose characteristic wavelength is 4 Å. The bender has a beam cross-section of 150 mm height by 20 mm width and its length is 2 m. The bender has nine channels of 2.0 mm width which are divided by glass plates of 0.5 mm thickness. Ni-Ti supermirrors are coated on both sides of these glass plates. A neutron bender is evaluated by the NEUGT program.[6] The NEUGT program can calculate a neutron transmission and spectra, assuming the maxwellian spectra at the entrance of a guide tube. The reflectivity of supermirrors is assumed to be equal to that measured in the former section. Figure 5 shows the spectra at the exit of cold neutron guide, this supermirror bender and natural nickel bender. The characteristic wavelength is 8 Å and the radius of curvature is 7 m. The total length of this bender is 2 m, but the end is 28 cm distant from main guide tube.

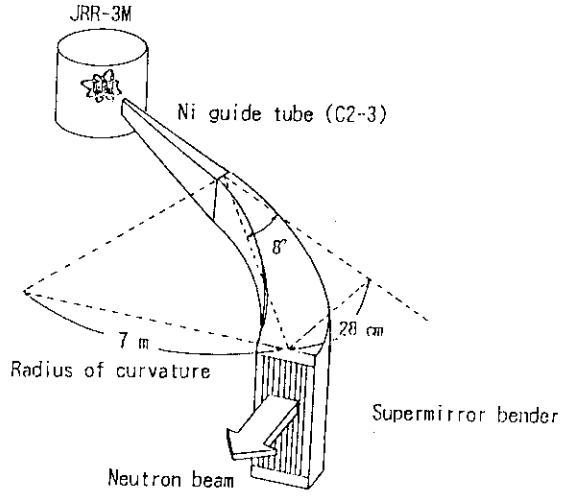

Fig.4 Schematic view of supermirror neutron bender in the JRR-3M

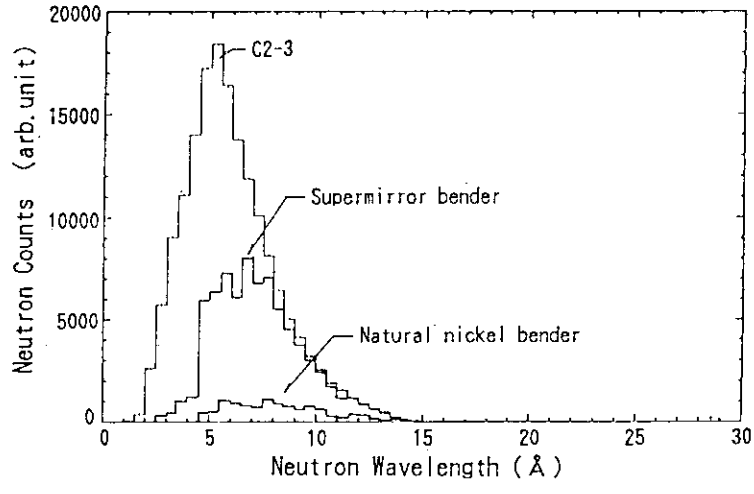

Fig.5 Neutron spectrum in the bender

CONCLUDING REMARKS

Ni-Ti supermirrors with 62 bilayers have been made by vacuum evapolation system. We can get the supermirror which has a critical wavelength of total reflection half smaller than a natural nickel mirror. TEM observations were performed to understand the reason why the measured reflectivity is lower than the theoretical one. The undulation due to the growth of crystallities and interdifusion between Ni and Ti layers explains the lower reflectivity of measured one.

A neutron bender using these supermirrors has been designed. This bender has a very small radius of curvature (7 m), so we can get sufficient beam separation from the main guide tube. This neutron bender has a characteristic wavelength of 8 Å at the exit of this bender, while it is 4 Å at the exit of the cold neutron guide tube. This bender will be set at the end of cold neutron guide tube (C2-3) in JRR-3M for Neutron radiography.

ACKNOWLEGEMENT

The authers would like to thank Drs.T.Ebisawa, S.Tasaki for useful discussions about making supermirrors and to M.Suzuki for reflectivity measurement. The supermirrors were fabricated by Nikon Cop.

REFERENCE

(1)Mezei,F.: Communications on Physics 1 81-85 (1976)
(2)Yamada,S., Ebisawa,T., Achiwa,N., Akiyoshi,T., Okamoto,S.: Annu. Rep. Res. Reactor Inst. Kyoto Univ. 8-27 Vol.11 (1978)
(3)Ebisawa,T., Akiyoshi,T., Tasaki,S., Kawai,T., Achiwa,N., Utsuro,M.: SPIE Vol.983, Thin-Film Neutron Optical Devices, 54 (1988)
(4)Kawabata,Y., et. al, J. Nucl. Sci. Technol., 1138-1146 27(12) (1990)
(5)Kawabata,Y., Suzuki,M., Tsuruno,A., Onishi,N., Kikuchi,H., Sano,M., Physica B (1991) in print.
(6)Harami,T., Uemura,M., Ebisawa,T.: JAERI-M 85-092 (1985)

5. Construction of Reactor Neutron Induced Prompt Gamma-Ray Analyzing System at the Neutron Beam Guide of JRR-3M

Chushiro YONEZAWA, Michio HOSHI, Yasuo ITO* and Enzo TACHIKAWA

Department of Chemistry, Japan Atomic Energy Research Institute,
*Research Center for Nuclear Science and Technology, The University of Tokyo

ABSTRACT

A reactor neutron induced prompt gamma-ray analyzing system is being constructed at the cold and the thermal neutron beam guides of JRR-3M. The system consists of neutron beam shutter, sample box with shielding, neutron stopper and a multi-mode gamma-ray spectrometer. The neutron intensity at the sample position is 2.0×10^8 and 1.2×10^8 n cm^{-2} s^{-1} for cold and thermal neutrons, respectively. In order to reduce gamma-ray background, LiF tiles, made either of natural isotopic or of ^6Li enriched compositions, are used for neutron shielding, and the sample box can be filled with He gas. The multi-mode gamma-ray spectrometer consists of a Ge detector surrounded by BGO (bismuth germanate, $Bi_4Ge_3O_{12}$) scintillation detectors and high counting rate electronics, all being controlled by a computer analyzer system. Owing to the high purity of the slow neutron beams, the detectors can be placed near the sample without intolerable background, so that the detection efficiency of prompt gamma-rays is largely improved compared to the case in usual systems. The system will be used for basic studies of elemental and isotopic analysis and then applied to various fields as, environmental science, material science, geology, archeology, biology, and so on.

INTRODUCTION

A reactor neutron induced prompt gamma-ray analysis (PGA) is an elemental and isotopic analytical technique by measuring prompt gamma-rays emitted within ca. 10^{-14} sec after neutron capture reaction. Although its analytical technique is similar to the conventional neutron activation analysis (NAA), PGA is characterized by non-destructive multi-element analysis including elements that cannot be determined by NAA. According to a calculation[1] the analytical sensitivity of PGA is higher than NAA toward some elements under the same condition of neutron flux and gamma-ray measurement. Usually PGA has been carried out by using, 1) an internal type analyzing system[2),3)] in which the sample was placed in a reactor and the gamma-rays are measured outside the reactor, and 2) a beam type analyzing system[4)-6)] in which the sample is irradiated with neutron beam from horizontal or vertical experimental hole of the reactor and the gamma-rays are measured by a detector placed near the sample. Since the efficiency and the S/N ratio of these conventional methods have been low, their applicabil-

ity has been limited to small number of elements in practice and PGA has been regarded no more than a complementary method to NAA.

Cold and thermal neutron beams guided by Ni coated glass mirror tube from reactor core to outside the reactor room are virtually free of gamma-rays and epithermal and fast neutrons. If the low energy neutron guide beam is used for the PGA as neutron source, the following advantages will be obtained, 1) the shift to lower neutron energy increases the effective cross sections, and 2) the absence of fast neutrons and gamma-rays permits detectors to be placed near the sample without intolerable background, and thus 3) the efficiency of counting prompt gamma-rays can become higher than the usual systems. From the above advantages, PGA that uses low energy guide beam[7)-10)] has gained serious improvement of analytical sensitivity. A comparison of reported analytical sensitivity between the beam type and the guide beam type analyzing systems is shown in Table 1. The thermal neutron guide beam analyzing system of the ILL has much higher sensitivity than the beam type systems. The JRR-3M of Japan Atomic Energy Research Institute (JAERI) has the cold and thermal neutron beams through the guide tubes with fluxes larger than 10^8 n cm^{-2} s^{-1}. By using these beams the so far serious disadvantage of low analytical sensitivity will be overcome. The present PGA system is constructed as a permanent and stand-alone instrumentation while most of the conventional PGA systems have been used only temporarily or as a supplement to other methods.

Table 1 A comparison of analytical sensitivity between the beam type and the guide beam type analyzing systems

Element	Gamma-ray energy keV	Sensitivity (cps/mg) of analyzing systems			
		Univ.Md-NBS[a]	Univ.Missouri[b]	JAERI[c]	ILL[d]
H	2223	0.86	1.23		
B	478	530	759	122	2700
Cl	1165	1.0	1.45	0.24	
Cr	835	0.11	0.176	0.029	
Ni	465	0.12	0.167	0.027	
Cd	558	170	247	35	
Sm	334	640	740		3700
Gd	182	680	956	147	6900
Flux, n cm^{-2} s^{-1}		2 x 10^8	5 x 10^8	8.0 x 10^7	1.3 x 10^8

a: Beam type Ref.4), b: Beam type Ref. 5), c: Beam type Ref. 6),
d: Thermal neutron guide beam type Ref. 9)

SPECIFICATION OF THE ANALYZING SYSTEM

Neutron beam

The analyzing system can be set at the cold neutron beam port (C2-3-1) or the thermal neutron beam port (T1-4-1) of JRR-3M[11),12)]. The neutron

intensity and the beam size are 2.0×10^8 n $cm^{-2}s^{-1}$, 20 x 50 mm for cold neutron beam (C2-3-2) and 1.2×10^8 n cm^{-2} s^{-1}, 20 x 91 mm for thermal neutron beam (T1-4-1). Because of its high neutron intensity and low energy, the cold neutron beam is more suitable for high sensitive analysis than the thermal neutron beam.

Shielding and sample positioning

The primary criteria for designing the analyzing system are to achieve a low radiation field to meet safety limitations, to reduce gamma-ray background counts, and to reduce neutron damage to the detector. The setup at the thermal neutron beam port (T1-4-1) is illustrated in Fig. 1. The system consists of beam guide tube, neutron beam shutter, neutron beam collimator, sample box , neutron stopper, shielding, and a multi-mode gamma-ray spectrometer.

The neutron beam is guided to the sample position through the neutron collimator (hole size 2 x 2 cm) made with LiF tile and an evacuated guide tube. The guide tube can be filled with He gas. The window materials of the inlet and the outlet of the guide tube are 1 mm thick of Al and 0.5 mm thick Teflon film. The neutron beam is stopped by the beam shutter and the beam stopper. The neutron can be absorbed by 10 mm of sintered B_4C and the emitted prompt gamma-rays (478 keV) are absorbed by Pb in the shutter and the stopper. Both automatic and manual operations are possible for the beam shutter. The neutron beam is collimated to 1 x 1 or 2 x 2 cm by LiF collimator made with LiF tile placed at the entrance position of the guide tube and at the side of the beam shutter. A Teflon sample box is placed behind the beam collimator. The sample is placed and irradiated in the sample box. The sample box can be filled with He to reduce loss of beam intensity by neutron absorption in air and to reduce capture gamma-rays from nitrogen in air. The windows of the sample box, at the inlet and the outlet of the beam and at both sides of the box, are made of Teflon film (0.5 mm thick) to avoid reduction of neutron intensity and background capture gamma-rays. The emitted prompt gamma-rays are detected through the window of the sample box and thorough ^{6}LiF tile. In order to reduce the gamma-ray background, scattered neutrons and prompt gamma-rays from the sample and surrounding materials of the sample are shielded with 2 and 3 cm of natural isotopic composition of LiF tile and 5 and 10 cm of Pb. Neutron and gamma-ray shielding around the beam stopper and the beam collimator is carried out with 1 cm of rubber containing 20 % B_4C, 5 , 8 cm of Fe, and 3, 5 cm of Pb. The whole set of the analyzing system except for the guide tube is transferred to the cold neutron beam port (C2-3-2) for the cold neutron beam experiments. Three detector windows are prepared for multi mode detecting of the gamma-rays.

Gamma-ray spectrometer

The multi mode gamma-ray spectrometer consists of a closed end coaxial type high purity Ge detector, a nose corn type BGO (bismuth germanate, $Bi_4Ge_3O_{12}$) scintillation detector, catcher BGO detectors, and a pulse height analyzer (PHA) system controlled by a personal computer. Three modes of prompt gamma-ray measurements; single mode, two Compton suppression modes, and pair spectrum mode can be performed simultaneously.

Cross sectional view of the detector systems is shown in Fig. 2. The Ge detector (ORTEC GMX-2019-Plus-S) has an energy resolution (FWHM) of 1.80

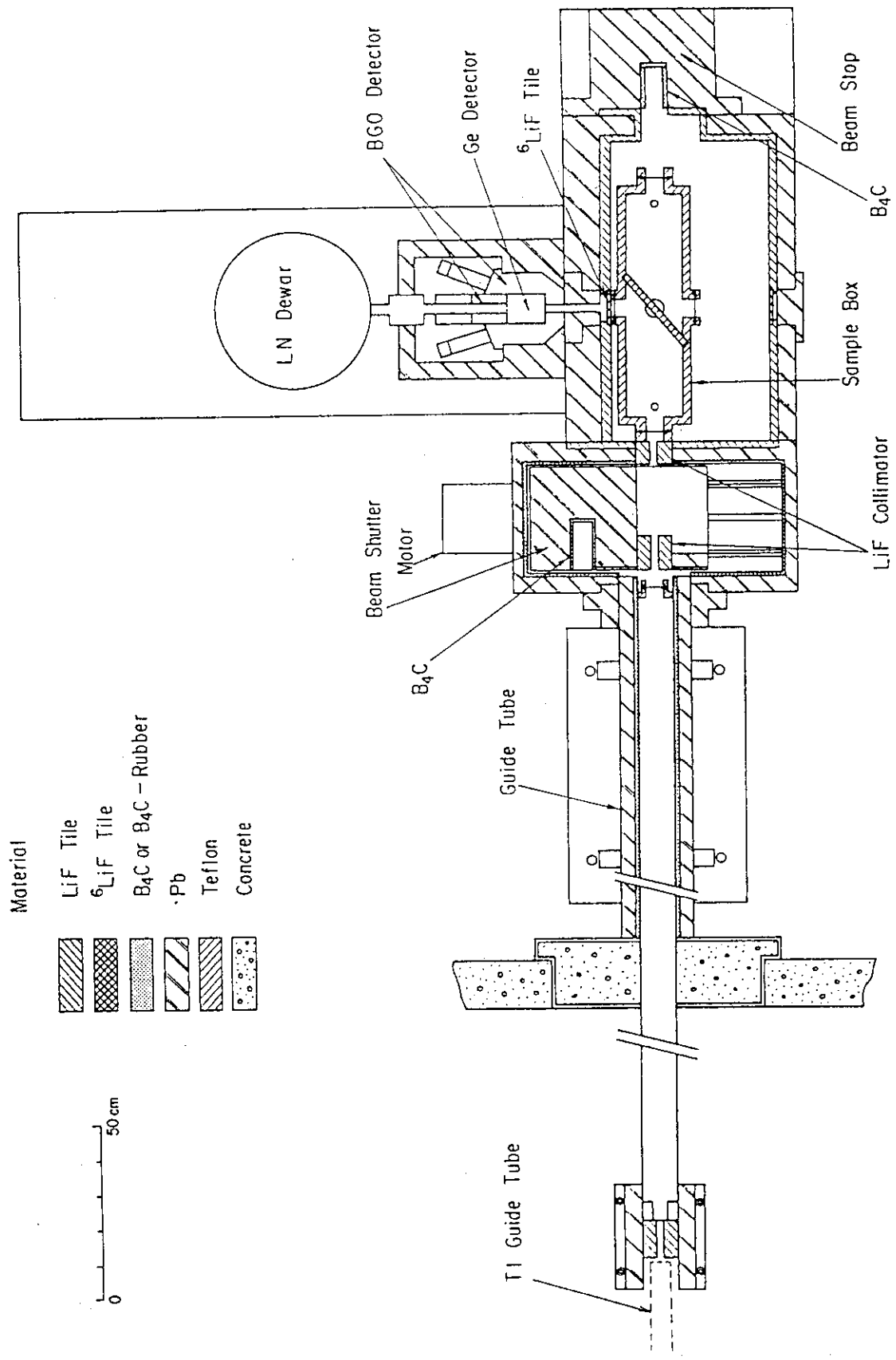

Fig. 1 Layout of JRR-3M neutron induced prompt gamma-ray analyzing system at the thermal neutron guide beam port (T1-4-1)

keV for the 1332 keV gamma-ray from ^{60}Co , a peak-to-Compton ratio of 54.5 and an efficiency of 23.5 % relative to a 7.6 x 7.6 cm^2 NaI(Tl) detector. The Ge detector has a horizontal cryostat with a 57 cm extended endcap mounted in 30 liter side looking type Dewar. The Ge detector is set with its axis perpendicular to the neutron beam at a distance 29.5 cm from the sample position. The distance from the sample to the detector can be decreased to 16 cm by moving the Ge detector. A transistor reset charge-sensitive preamplifier is used in connection with an ORTEC 673 main amplifier and gated integrator to allow good throughput at high count rate. The BGO detectors, nose corn type main BGO (BICRON, 171 mm ϕ x 206.5 mm) and catcher BGOs (BICRON 63.6 mm ϕ x 133.3 mm), are used as guard detector. The main BGO is optically separated to eight parts and the scintillation photons are collected by eight photomultiplier tubes (PMT). The catcher BGOs are separated to two parts and the photons are collected by four PMTs.

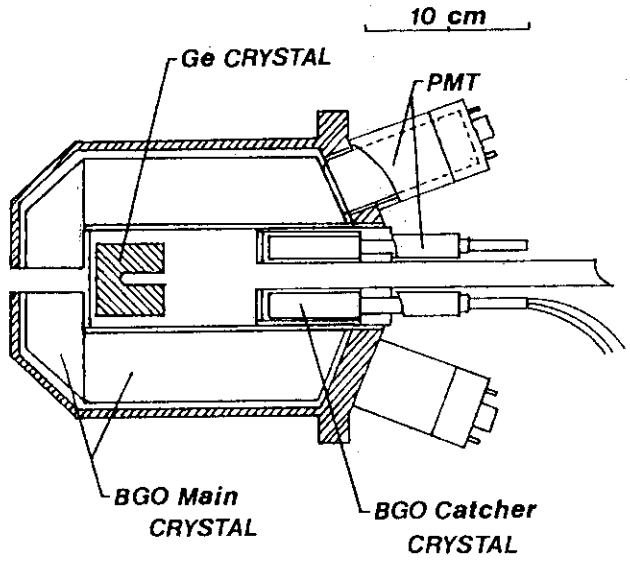

Fig. 2 Cross sectional view of the Ge-BGO detector system

The detector system is surrounded by a 10 cm Pb shielding. The prompt gamma-rays from the irradiated sample must pass through a removable 2.0 or 1.0 cm diameter collimator of length 10 cm. ^{6}Li 95.4 % enriched LiF tiles (5 mm thick) are set up to the entrance of the Pb collimator to decrease the background and to avoid damage by neutrons scattered from the sample irradiation.

A block diagram of the electronics used in the multi-mode gamma-ray spectrometer is illustrated in Fig. 3. Single mode, two Compton suppression modes, and pair mode of the prompt gamma-ray spectra are measured simultaneously. Each of these four signals is fed thorough an 8192-channel analog to digital converter (ADC). In the single mode, all signals in the Ge detector are recorded, i.e., photopeaks, escape peaks, and Compton events. In the Compton suppression mode only those signals in the Ge detector which do not have a coincident signal in the BGO detectors are recorded. The Compton continuum of ^{60}Co in this spectrum was reduced to about 17 % relative to the single. In addition, the single- and double-escape peaks are reduced. In the pair spectrum mode, the events recorded are those which have a corresponding event in the BGOs with an energy of 1022 keV. For the pair spec-

trum, triple coincidence between the Ge detector and two halves of the main BGO crystals are required to accept a Ge pulse at the ADC.

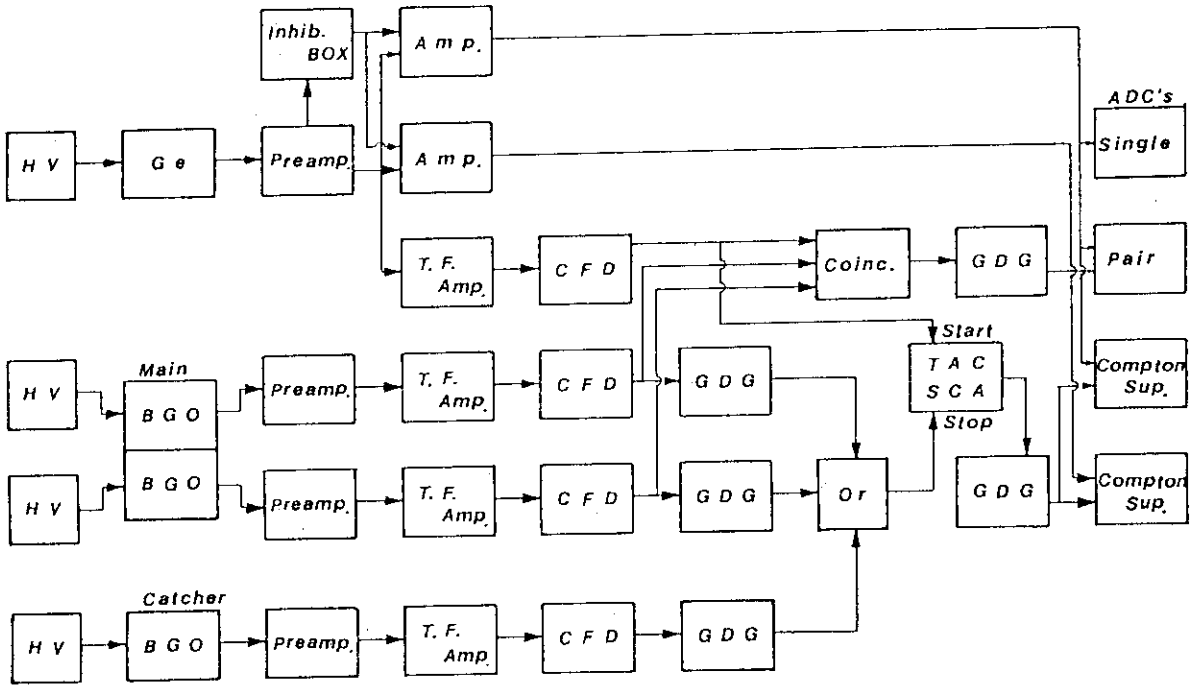

Fig. 3 Block diagram of the electronics for the multi-mode gamma-ray spectrometer
HV: high voltage supply, T.F.Amp.: timing filter amplifier, CFD: constant fraction discriminator, GDG: gate and delay generator, TACSCA: time to amplitude converter and single channel analyzer

RESEARCH PROGRAM

Construction of the analyzing system has been finished, and the experiment will be started on the end of October 1991. At first, characteristics of the system, i.e., neutron flux and homogeneity of the neutron beam at the sample position, characterization of multi mode gamma-ray spectrometer, measurement of analytical sensitivity and detection limit of typical elements will be determined. After finishing the characteristic measurements, basic studies of PGA such as, calibration for element and isotope determination, isotope analysis, isotope dilution analysis, study of prompt gamma-ray measurement, measurement of nuclear data and so on, will be performed. After establishing the elemental and isotopic analytical methods, the PGA will be applied to the following various fields: environmental science, material science, geology, archeology, biology, and so on. PGA will also be useful for the following analysis: depth profiling analysis, short lived nuclide activation analysis, and charged particle measurement analysis, and

so on. The PGA analyzing system is also useful for studying the following nuclear chemistry and hot atom chemistry: measurement of excited levels of nuclides, perturbed angular correlation, elucidation of emission phenomenon on nuclear reactions, chemical reaction of recoiled tritium in the pure neutron fields, and so on.

ACKNOWLEDGEMENT

The authors wish to acknowledge T.Matsumoto, Y.Minai, N.Nakahara, R.Seki, F.Shiraishi, K.Sueki, A.Yokoyama, M.Kawasaki, H.Takahashi, T.Tojyo, E.Shirai, and N.Wada for their useful discussions and support of this program.

REFERENCES

1) T.L.Isenhour, G.H.Morrison: Anal. Chem., 38, 162 (1966).
2) E.T.Jurney, H.T.Motz, S.H.Vegors Jr.: Nucl. Phys. A94, 351(1967).
3) M.Spychala, W.Michaelis, H.-U.Fanger: J. Radioanal. Nucl. Chem., 112, 331 (1987).
4) D.L.Anderson, M.P.Failey, W.H.Zoller, W.B.Walters, G.E.Gordon, R.M.Lindstrom: J. Radioanal. Chem., 63, 97 (1981).
5) A.G.Hanna, R.M.Brugger, M.D.Glascock: Nucl. Instrm. Methods, 188, 619 (1981).
6) T.Tojyo, C.Yonezawa, S.Koura, S.Arai, T.Komori: JAERI-M 8791 (1980).
7) R.Henkelmann, H.-J.Born: J. Radioanal. Chem. 16, 473 (1973).
8) R.M.Lindstrom, R.Zeisler, M.Rossbach: J. Radioanal. Nucl. Chem., 112 321 (1987).
9) S.A.Kerr, R.A.Oliver, P.Vittoz, G.Vivier, F.Hoyler, T.D. MacMahon, N.I.Ward: J. Radioanal. Nucl. Chem., 113, 249 (1987).
10) T.Kobayashi, K.Kanda: Nucl. Instrm. Methods, 204, 525 (1983).
11) N.Onishi, H.Takahashi, M.Takayanagi, H.Ichikawa, M.Kawasaki: J. Atom. Energy Soc. Jpn., 32, 962 (1990).
12) Y.Kawabata, M.Suzuki, H.Takahashi, N.Onishi, A.Shimanuki, Y.Sugawa, N.Niino, T.Kasai, K.Funasho, K.Okuhata: J. Nucl. Sci. Technol., 27, 1138 (1990).

6. Utilizations of Filtered Neutron Beams at DALAT Nuclear Research Reactor

Pham Duy Hien, Luong Ngoc Chau,
Vuong Huu Tan, Nguyen Trong Hiep,
Le Ba Phuong.

Dalat Institute for Nuclear Research
Dalat, Vietnam.

ABSTRACT

Neutron beam utilizations in basic and applied researches have been important activities at the Dalat nuclear reactor. The neutron filters with single crystal of silicon are used to produce thermal neutrons at the tangential horizontal channel and quasi-monoenergetic 144 KeV and 54 KeV neutrons at the piercing beam tube. The paper presents some relevant characteristics of the filtered neutron beams at the two horizontal channels. Applications of neutron beams in prompt gamma-ray activation analysis and in nuclear data measurements are briefly described.

I. INTRODUCTION

The exploitation of the Dalat nuclear research reactor began in early 1984 with main activities in neutron activation analysis (NAA) and radioisotope production. The space around the horizontal beam ports had been empty until 1987, when a pneumatic transfer system was installed near the thermal column for rapid NAA and delayed neutron counting analysis. These instrumental analytical techniques, together with the development of radiochemical methods have substantially strengthened our capability in analytical services. However, there was a number of elements, for which the neutron activation method is not suitable, or cannot be applied at all. Thus, prompt gamma-ray activation analysis (PGAA) has been developed, and to some extent, the new non-destructive analytical technique enabled us to overcome the above mentioned difficulty. From 1989, thermal neutrons from the tangential horizontal channel No 3 have been used for PGAA. The insertion in this channel of a neutron filter assembly with single crystal of silicon has significantly enhanced the thermal-to-fast fluxes ratio and the collimation of the extracted neutron beam. The beam port facilities and arrangements were designed not only for PGAA, but also for neutron radiography and thermal neutron transmission experiments. Encouraged by the success of using neutron filters in channel No 3 for producing the thermal neutron beam, efforts have been made in the last years in extracting and using quasi-monoenergetic intermediate neutrons at the piercing horizontal channel No 4. Single crystal silicon filter in combination with additional neutron absorbers, such as B, S, Ti provides quasi-monoenergetic neutron beams of 144 KeV and 54 KeV. The neutron beam intensities are high enough for a number of applied and basic researches.

II. THERMAL NEUTRON BEAM AT TANGENTIAL CHANNEL (CHANNEL NO.3)

II.1. Experimental set-up and neutron beam characteristics.

In order to improve the thermal-to-fast fluxes ratio and to decrease gamma background as much as possible, different combinations of neutron filters consisting of graphite, lead, single crystal of silicon etc. were tested (Fig. 1). The main characteristics of the thermal neutron beam with some filter assemblies are shown in Table I.

Table I : Main characteristics of the filtered thermal neutron beam.

Composition of the filter assemblies	F(th) (n/cm2/s)	F(f>1MeV) (n/cm2/s)	R(Cd/Au)	I(gamma) (R/h)
No filter	5.8 E7	4.5 E5	5	4
80mmC + 50mmPb	1.7 E7	3.5 E4	12	1.8
80mmC +100mmPb	5.5 E6	1.2 E4	19.5	0.8
comp. No2 + 366 mm Si	3.5 E6	n E1	77.5	0.22

The variation of the neutron beam parameters with the thickness of the silicon filter was also investigated and shown in Fig 2.

The single crystal silicon filter improved significantly the collimation and the sharpness of the neutron beam as shown in Fig. 3, where the resolution ratio L/D determined by taking the radiographs of the cadmium foil with holes of different diameters is plotted versus the thickness of the filter [1,2]

From the above mentioned experimental results it is obvious that the use of single crystal silicon filter with optimum thickness would considerably improve the relevant characteristics of the thermal neutron beam. In fact, such improvement has been observed through the increase in the precision and sensitivity of PGAA due to the reduction of the background under peaks in the prompt gamma ray spectra. As an example, in Fig. 4 and Fig. 5 are shown two prompt gamma spectra of the same sample obtained without and with the neutron filter, where the peaks of interest at low energy range (for instance 182 KeV peak of Gd) appear only in the latter case.

II.2. Applications

The thermal neutron beam has been utilized in PGAA [3], neutron radiography [4] and measurements of the macro neutron cross-sections of geological samples [5]. Some applications

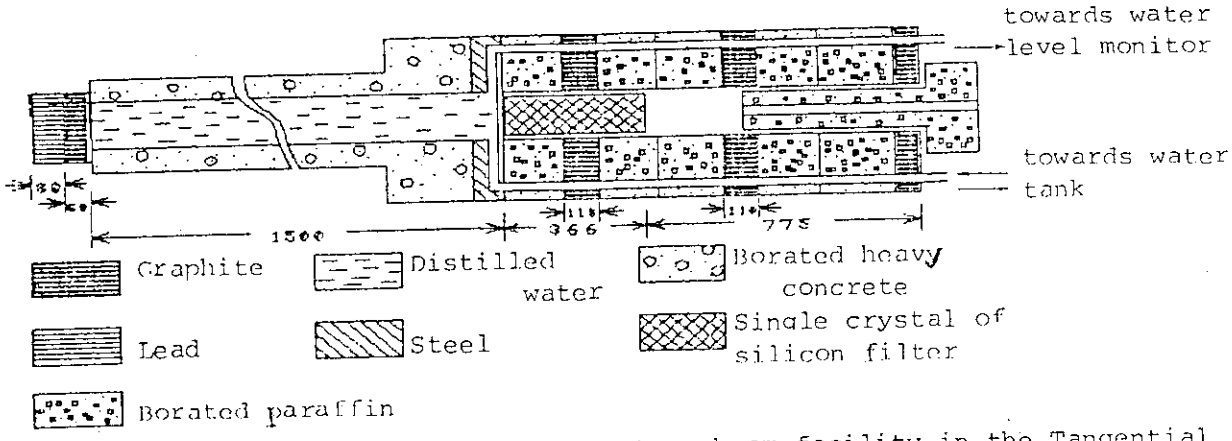

Fig. 1 : Sectional view of the neutron beam facility in the Tangential channel (No 3).

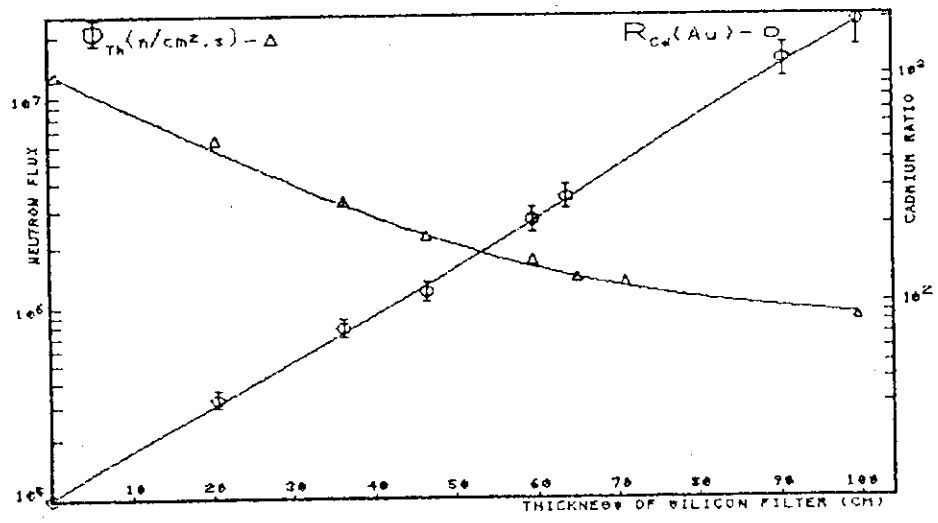

Fig. 2 : Variation of the thermal neutron flux and cadmium ratio (Au) with thickness of the silicon filter

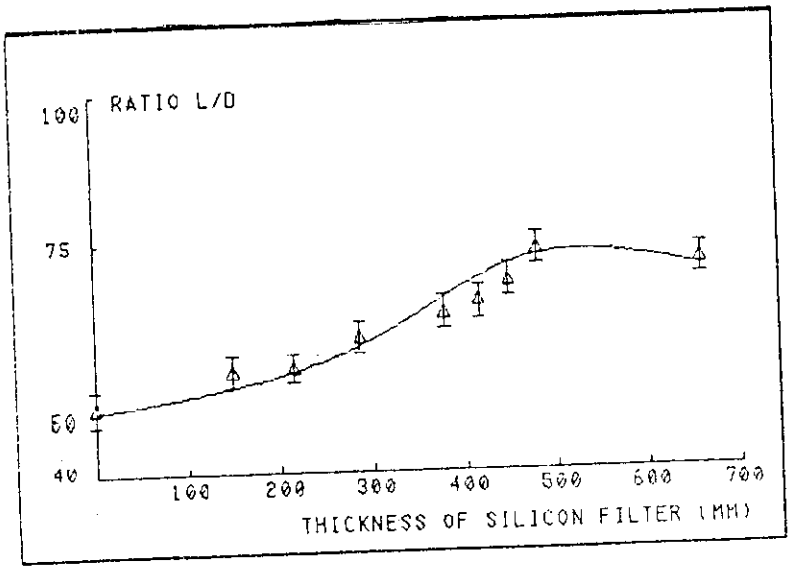

Fig. 3 : Variation of the L/D resolution ratio versus thickness of the silicon filter.

of PGAA in elemental analysis will be presented below.

In the experiments, prompt gamma spectra were measured by the coaxial HP-Ge detector with FWHM of 2 KeV at 1332 KeV. The data-handling system is an 8K channels ADC/MCD combination interfaced with a fast computer IBM/PC-AT of 26 MHz. The elemental concentrations were determined by the relative method with the use of certified reference materials such as NBS-1573, IAEA-SL-1, IAEA-A-11, NBS-1632A, NBS-1571, NBS-Bowen's Kale etc.. Besides, the internal standard method has also been used in cases where matrices of analysed samples and standards are not similar. Table II shows the estimation of the analytical sensitivity of elements based upon 1 gram sample for 1 hour irradiation.

Table II : Sensitivity for PGAA measurements at Dalat Reactor (estimate is based on 1g sample in 1h irradiation)

Elements	Sensitivity (%)
B,Gd,Sm	0.0001 - 0.0005
Cd(*),Hg,Dy	0.001 - 0.002
Cl,Mn,Nd	0.01 - 0.04
K,Na,V,Ti	0.02 - 0.5
Si,Al,Ca,Fe,Ni,H	0.4 - 2.0
N,C	5.0 - 10.0

Among the elements listed in Table II, B,N,H,C cannot be determined by conventional NAA while PGAA is an unique non-destructive method of analysis based on the reactor facility. From routine determinations of boron concentration in biological, geological and environmental samples, several interesting practical uses of the PGAA method can be mentioned as following :

- Comparison of the boron concentrations in natural gingsengs and in callus ginsengs obtained by the plant tissue culture technique would permit to choose the suitable culture medium , the quantity of boron needed to add into that medium as well as to apply some relevant procedures of tissue culture process.
- Investigation of the correlation between boron and tin concentrations in geological samples serves as the geo-chemical indication in exploration and assessment of natural mineral resources.
- Analysis of boron in sediment and sand samples has been carried out because boron could be chosen as a relevant candidate for labelling sand in harbours.
- Determination of the C/H ratios in crude oil.
- Determination of the nitrogen concentration in various categories of animal foods using a (5 x 5) inches NaI(Tl) detector helps farmers to regulate rational food portions to domestic animals during different growth periods.

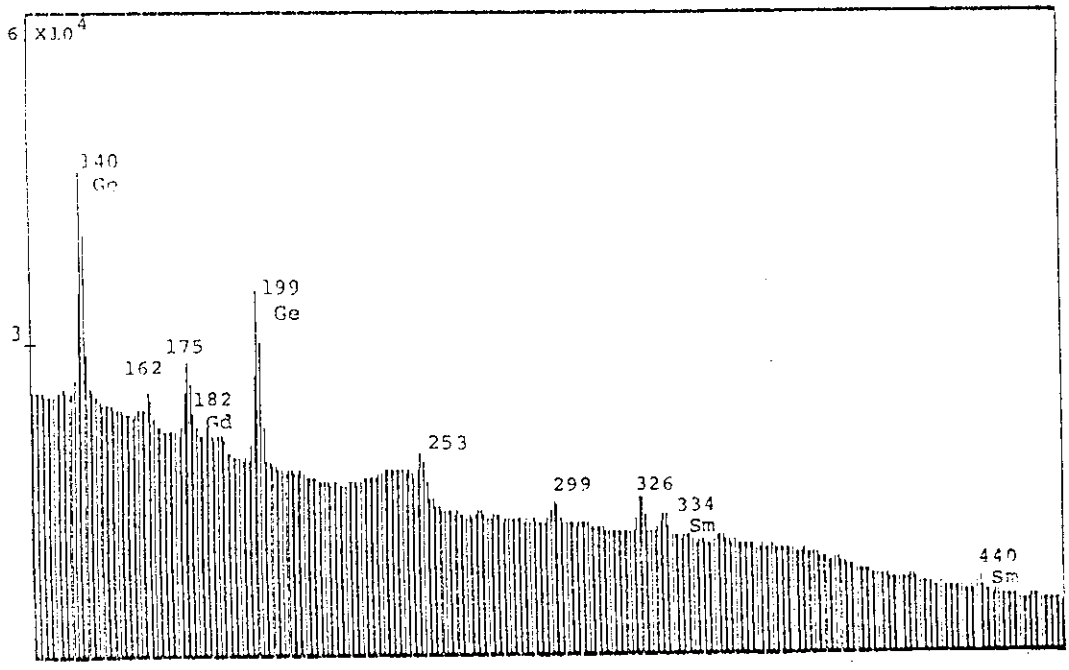

Fig. 4 : A portion of the prompt gamma spectrum of a rare earth sample irradiated by the neutron beam without the silicon filter.

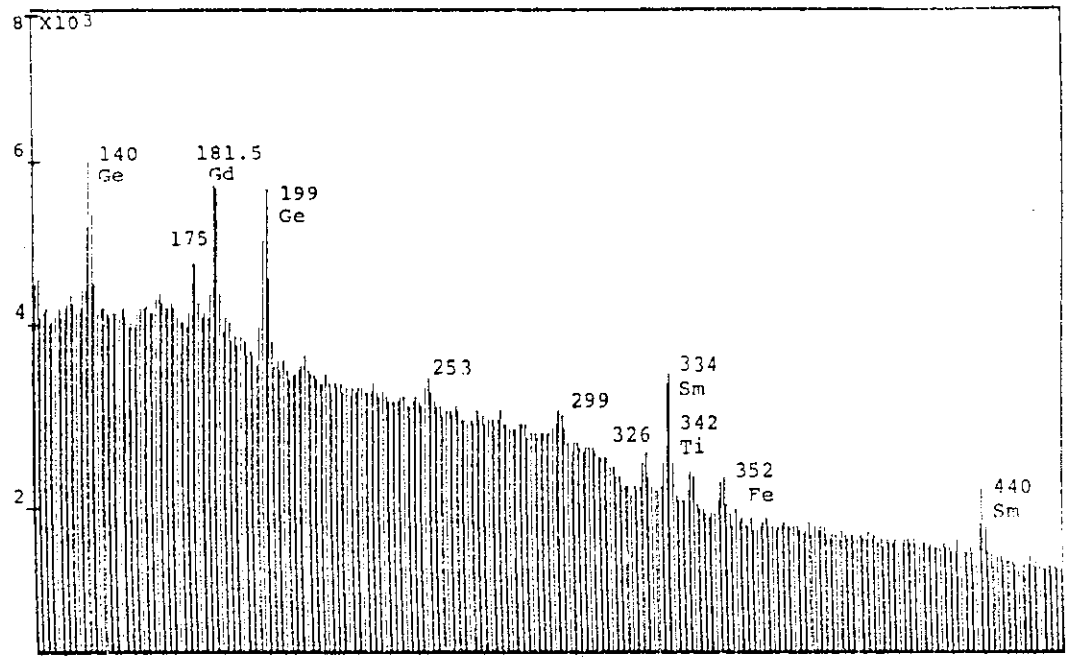

Fig. 5 : The corresponding spectrum portion of the same sample irradiated by the neutron beam with the single crystal silicon filter of 366 mm thickness.

- The PGAA technique is also used in analysis of Gd,Sm,Nd in products derived from separation and extraction process of rare earth ores. The prominent advantage of gadolinium analysis with trace concentrations in other rare earth matrices by PGAA comparing with INAA and even RNAA is proved.
- Advantage of PGAA in analysis of macro-constituents in various materials as cement, steel etc. is exploited in the estimation of the quality of some industrial products.

III. FILTERED NEUTRON BEAMS AT PIERCING HORIZONTAL CHANNEL No 4

III.1. Filtered neutron beams characteristics.

Due to the abundance of fast and epithermal neutrons, the piercing horizontal channel is most suitable for producing quasi-monoenergetic neutrons in the intermediate - energy region by using neutron filters. A 98 cm long single crystal of silicon filter has been installed in the channel (Fig. 6), enabling us to produce well collimated beam of thermal neutrons, as well as neutrons with energy 144 KeV and 54 KeV. Fig. 7 shows the pulse-height distribution of recoil protons measured with a cylindrical proton proportional counter type SNM-38. A 764 KeV peak corresponding to the total energy of (n,p) reaction with thermal neutrons on He-3 serves as reference energy. The energetic spectrum of the filtered neutron beam was obtained by differentiating the recoil proton energy distribution of Fig. 7 . The FWHM of the 144 KeV and 54 KeV lines are 22 KeV and 8 KeV respectively. To obtain single line spectra, additional selective neutron absorbers were used (Fig. 8, 9). The fluxes of quasi-monoenergetic neutrons measured at 25 cm from the beam port outlet by activation of Au-foils are as following :

F(th) = 1.8E7 n/cm2/s
F(54 KeV) = 4.0E6 n/cm2/s
F(144 KeV) = 1.2E7 n/cm2/s

III.2. Utilization of filtered neutron beams in nuclear data measurements. Present status and future prospects.

The intensities of the neutron fluxes and the quality of quasi-monoenergetic neutron beams as shown in Fig. 8,9 are generally adequate for a number of nuclear data measurements, enabling the Dalat nuclear research center, with very limited resources, to approach to some up-to-date fundamental and applied research directions in nuclear physics. The filtered neutron beams provide an efficient tool for measuring the average nuclear resonance parameters in unresolved region. We have started recently the measurements of total neutron cross-sections with 144 KeV neutrons. The experiments were intended basically for checking our neutron transmission technique using literature data as reference. U-238 and C-12

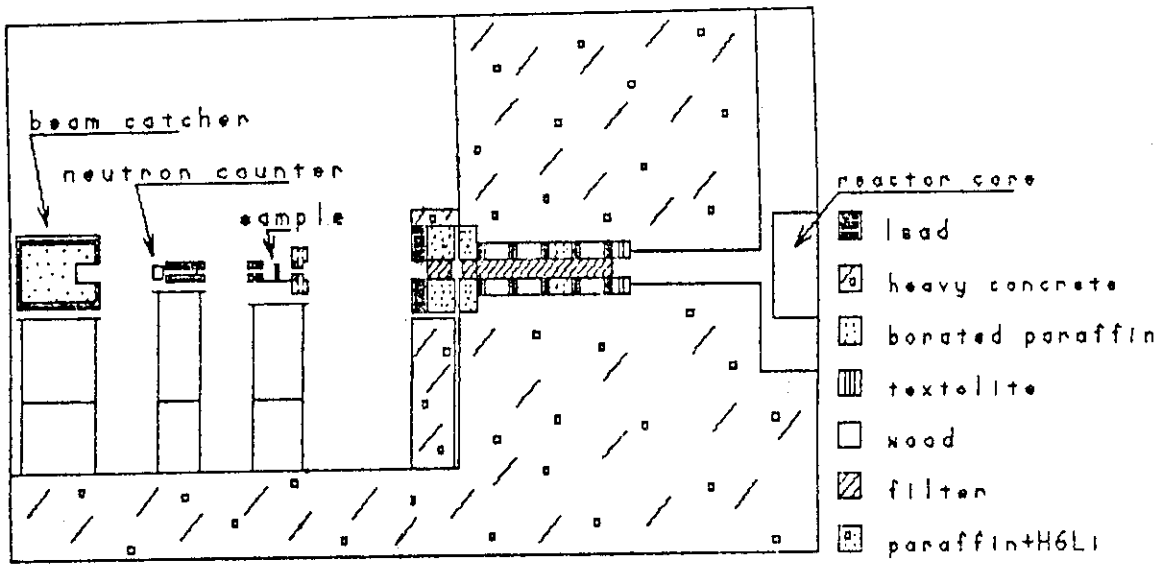

Fig.6: Experimental set-up at the piercing beam port of Dalat nuclear reactor

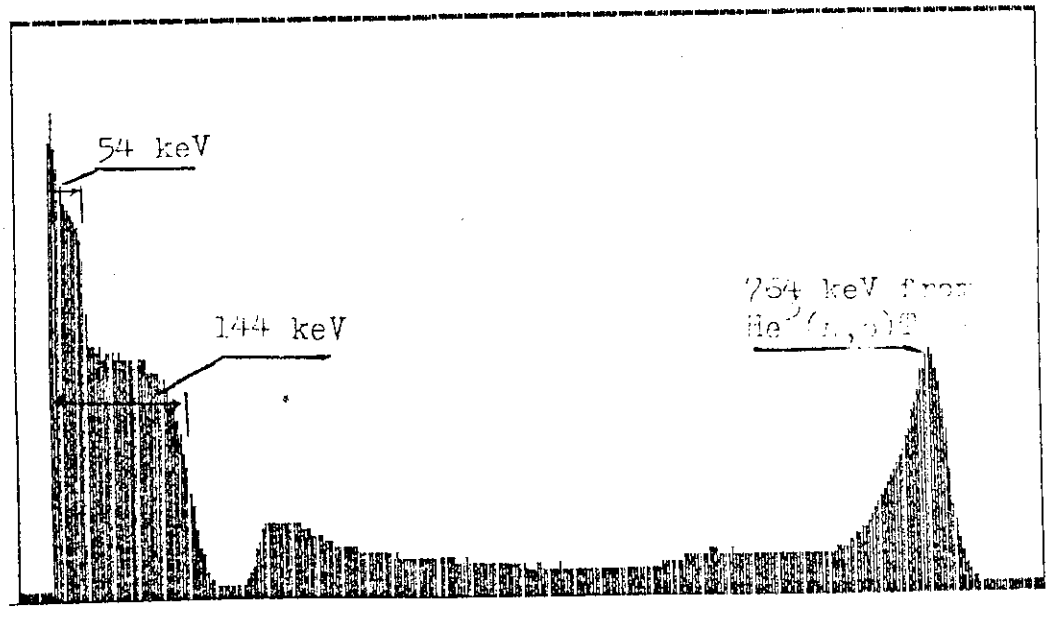

Fig.7: Recoil proton energy distribution obtained with hydrogen proportional counter (4 atm) SNM-38 (98 cm single crystal of silicon neutron filter)

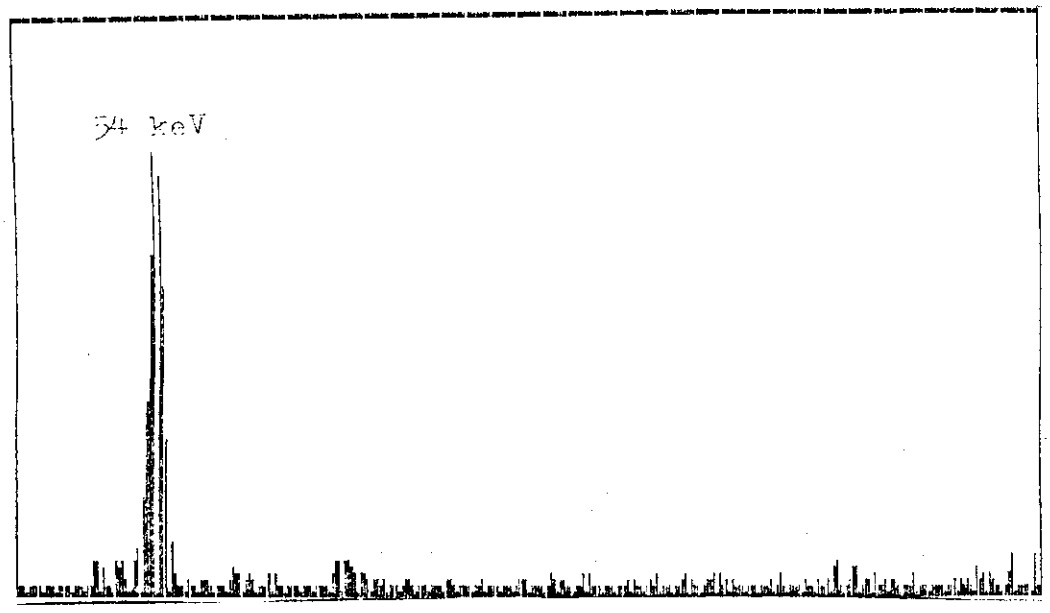

Fig.8: 54 keV differential energy spectrum
(98 cm Si +50 g/cm^2 S +0.4 cm B_4C)

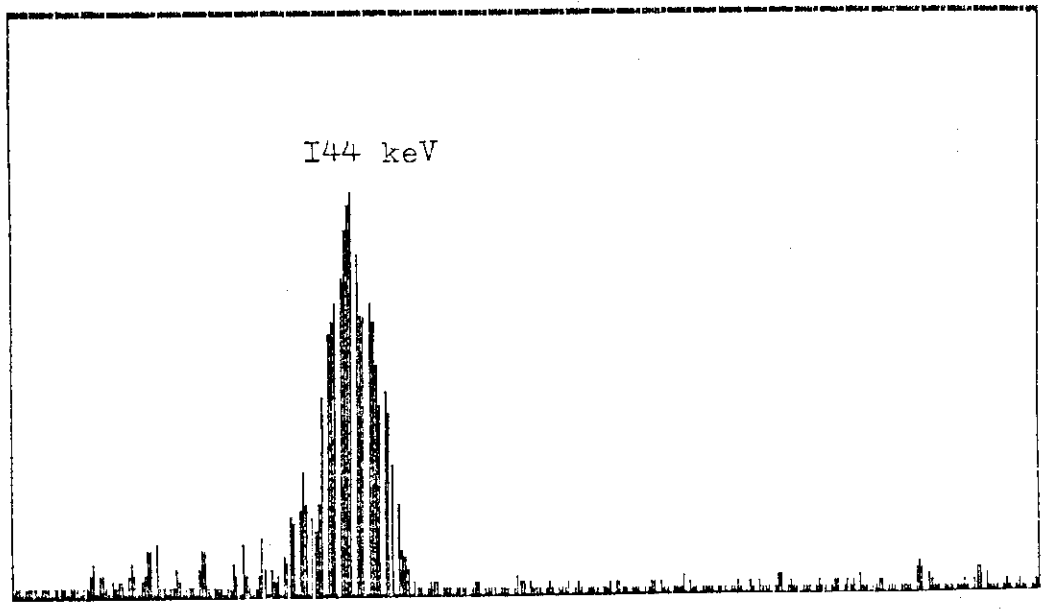

Fig.9: 144 keV differential energy spectrum
(98 cm Si +10 cm Ti +0.4 cm B_4C)

were chosen as targets in such experiments due to the high accurracy of the literature data. Metallic depleted uranium and nuclear-grade graphite have been used for target preparation. The isotopic abundance of U-235 in the uranium target was 0.2 % as determined by gamma spectrometry method. In Table III are shown the "observed" total neutron cross-sections (σ_t^{obs}) of U-238 defined as

$$\langle \sigma_t^{obs} \rangle = \mathrm{Ln}\ (T/n)$$

where T is the neutron transmission and n is the sample thickness given in nuclei/barn. The average total neutron cross-section $\langle \sigma_t \rangle$ can be obtained by extrapolating the "observed" values to zero sample thickness.

Table III: Observed 144 KeV neutron total cross-section of U-238 with different thicknesses of the sample.

No	Thickness (nuclei/barn)	Transmission	$\langle \sigma_t^{obs} \rangle$ (barn)
1	0.048	0.5706 +- 0.0100	11.68 +- 0.36
2	0.094	0.3437 +- 0.0084	11.31 +- 0.26
3	0.159	0.1659 +- 0.0077	11.33 +- 0.29
4	0.172	0.1454 +- 0.0077	11.29 +- 0.32
5	0.207	0.1003 +- 0.0074	11.13 +- 0.36

The fitting procedure yielded the results : $\langle \sigma_t \rangle$ = 11.66 +- 0.14 barns for U-238 which is in good agreement with the literature data (for example $\langle \sigma_t \rangle$ = 11.5 +- 0.2 in [6]). The corresponding values for C-12 are $\langle \sigma_t \rangle$ = 4.24 +- 0.12 and $\langle \sigma_t \rangle$ = 4.28 +- 0.06 [7]. The accuracy of the experimental results was due almost to the neutron counting errors, which could be reduced by increasing the number of measuring cycles. Thus the results obtained in the control experiments proved the ability of our experimental conditions for the measurements of neutron cross-sections in the unresolved region. At present, measurements of total neutron cross-sections and isomeric ratios at neutron energies of 144 KeV and 54 KeV are underway. The obtained data are compared to those with thermal neutrons in order to evaluate the s and p-neutron strength functions [8], and to reveal the neutron energy dependence of the contributions of p,d ... neutrons in the formation cross-sections of compound nuclei.

The authors are very thankful to Dr. Murzin A.V. (Kiev Nuclear Research Institute) for his valuable constribution to the successful utilizations of neutron filters at Dalat nuclear research reactor.

IV. REFERENCES

[1] R. M. Brugger, Nucl. Instr. and Meth., 135 (1976) 289
[2] ASTM, E 803-81, "Standard method for determining the L/D ratio of neutron radiography beams"
[3] Chau L.N. et al., " Prompt Gamma Activation Analysis at Dalat Reactor", Report to MARC - II, 23-26 April 1991, Hawai,USA
[4] Chau L.N. et al., "Neutron Radiography at Dalat reactor", in publication
[5] Bang V.D. et al., " Measurement of the thermal neutron absorption cross-section for small samples by poisoning method",Report to the RCM symposium, April 1991,Debrecen, Hungary.
[6] Vertebnji V.P. et al., Neutron Physics, Proc. of the 1987 Kiev Conf. on Neutron Physics, Vol. 2,p. 175
[7] Litvinsky L.L. et al., Preprint of KNRI, Kiev,40(1985)
[8] Zaretsky D.F., Urin M.G., Neutron Physics, Proc. of the 1977 Kiev Conf. on Neutron Physics, Vol. 1, p.1

7. JRR-3 Neutron Radiography Facility

M. Matsubayashi, A. Tsuruno and Y. Horiguchi

Department of Research Reactor
Tokai Research Esatblishment
Japan Atomic Energy Research Institute
Tokai-mura, Naka-gun, Ibaraki-ken 319-11, Japan

ABSTRACT

This year, a new neutron radiography facility was completed in the upgraded JRR-3. This facility consists of the thermal neutron radiography facility and the cold neutron radiography facility. It came into operation this March, and its characteristics have subsequently been measured. And its high performance was confirmed. In this paper, outline and characteristics of the facility, examples of utilization and techniques are described.

INTRODUCTION

Neutron radiography at Department of Research Reactor, Tokai Research Establishment, JAERI has always used reactors as the neutron source, since the first such radiographs were made by Tsuruno on JRR-2. Many neutron radiographs had been taken on JRR-2, JRR-3 and JRR-4.

After twenty-one year operation, the JRR-3 was shutdown for upgrading. And a renewal of the JRR-3 neutron radiography facility followed the reconstruction of JRR-3. Advantages of the JRR-3 neutron radiography facility are multiple usage, high resolution, non-destructive examination on mid-irradiation, real-time non-destructive inspection, image processing and ability of choosing neutron energy.

REACTOR AS A NEUTRON SOURCE

The upgraded JRR-3 (JRR-3M) is a low enriched-uranium, light water moderated/cooled and beryllium reflected, 20MW thermal reactor.[1] It has a cylindrical core surrounded by a double cylindrical heavy water tank. It has nine horizontal beam tubes (1G～6G,7R,8T,9C). All horizontal beam tubes are arranged in the heavy water tank. In addition the cold neutron source (CNS) is also installed in the heavy water tank. 9C of these beam tubes is for CNS. Figure 1 shows a horizontal section of the JRR-3M.

The JRR-3M is operated on four-week cycle with one-week scheduled shutdown per cycle for refueling, irradiation sample handling and

maintenance.

THERMAL NEUTRON BEAM

Thermal neutron beam is taken from a 30 mm x 30 mm square aperture of the horizontal beam tube (7R) in the heavy water tank. The maximum thermal neutron flux in the tank is about 2 x 10^{14} n/ cm^2 • s. The beam tube is arranged tangentially to the core to reduce γ rays and fast neutrons. This beam is collimated by a Boron Nitride lined divergent aluminium followed by a beam shutter. This thermal neutron collimator supplies the thermal neutron radiography facility (TNRF) with more than 10^8 n/cm^2 • s thermal neutron beam. The collimator ratio (L/D) is expected to be about 200. The cross section of the collimator is shown in Fig. 2.

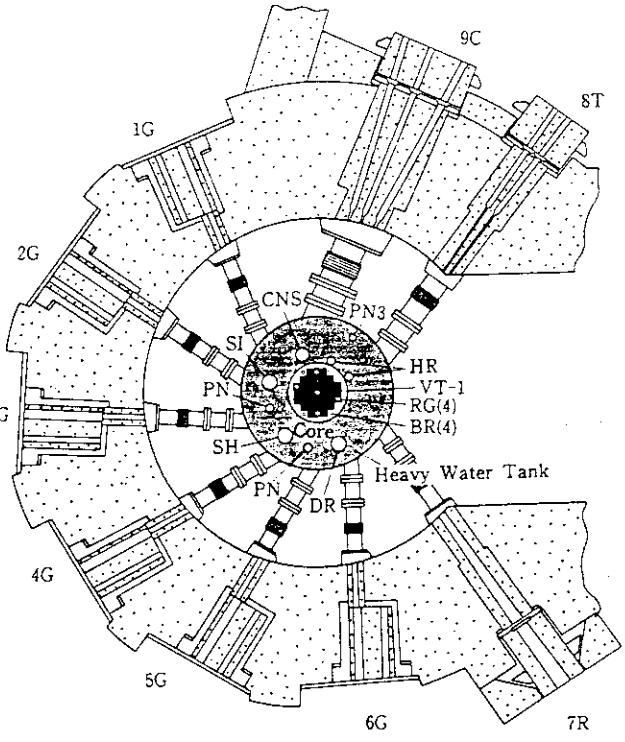

Figure 1 Horizontal section of the JRR-3M

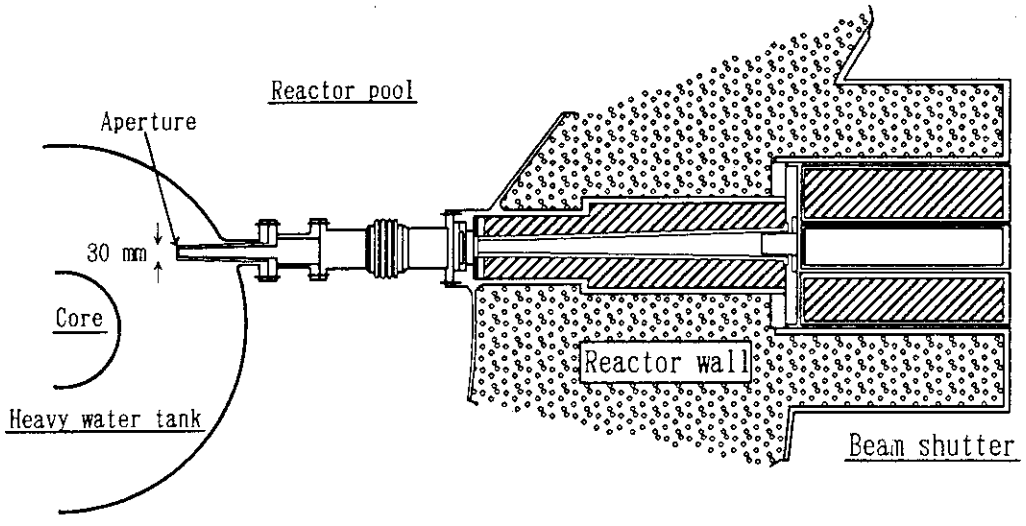

Figure 2 Thermal Neutron Collimator

COLD NEUTRON BEAM

Cold neutron beam is taken from CNS. CNS converts thermal neutrons into cold neutrons with liquid H_2 at 20 K. The cold neutron beam is led to the cold neutron radiography facility (CNRF) through the neutron guide tube (C2-3). These guide tubes supply CNRF with more than 10^8 n/cm^2•s parallel and low γ ray contained cold neutron beam but narrow neutron beam. And its characteristic wave length is 4 Å.[2] The beam size (section size of the inner guide tube) is 20 mm x 50 mm.

FACILITY DESCRIPTION

A general layout of the JRR-3 neutron radiography facility is shown in Fig. 3. This facility consists of TNRF and CNRF.[3] TNRF is installed at the horizontal beam tube, 7R, in the JRR-3M Reactor Hall. CNRF is installed at the cold neutron guide tube, C2-3, in the Beam Hall adjacent to the reactor building.

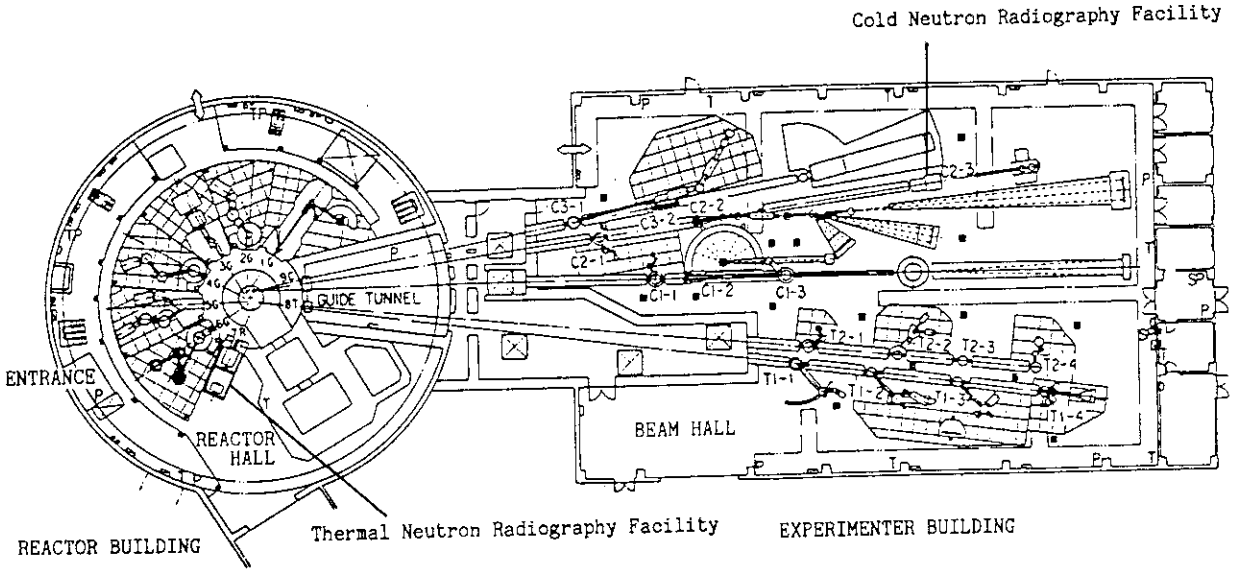

Figure 3 Layout of the JRR-3 Neutron Radiography Facility

THERMAL NEUTRON RADIOGRAPHY FACILITY(TNRF)

TNRF has two radiographing rooms. One (TNRF-1) is for examination of irradiated materials. The other (TNRF-2) is for conventional non-destructive inspections. TNRF-2 is set behind TNRF-1. Although they share the 7R thermal neutron beam as the neutron source, they cannot be used at the same time. Each radiographing room can be used by switching the collimator. A cross-sectional view of TNRF is shown in Fig. 4.

TNRF-1

TNRF-1 is depicted on the left of Fig. 4. This room is typically used for post- and mid-irradiation examination. The inner room size is 900 mm wide, 1,400 mm long and 1,850 mm high. The capacity of sample

radioactivity is 370 TBq, which is estimated as a spent nuclear fuel. The room is enclosed with shielding walls. They are composed of 400 mm thick steel and 150 mm thick boron mixed polyethlene. Highly activated samples, such as spent nuclear fuels and irradiated samples are put into the room through its roof port by the transfer cask. A spent nuclear fuel element of maximum 140 mmϕ and 1,100 mm long is acceptable. The transfer method or tracketch method is used to take radiographs of samples which contain high γ ray source or are highly activated. The transfer foils or tracketch films are inserted into the room and are close contact with the samples by the cassette handling device. This room is equipped with a collimator switching mechanism, a sample holder and a cassette handling device.

TNRF-2

TNRF-2 is depicted on the right of Fig. 4. The inner room size is 800 mm wide, 2,000 mm long and 1,850 mm high. This room has an entrance with a shielding door and a 1 m x 1 m hatch. Experimenters can enter the room through the entrance and set samples by hand. Samples also can be inserted into the room through the hatch using the roof crane. Thermal neutrons come from the behind wall of TNRF-1. This room is equipped with a beam shutter followed by collimator, a sample table, a boron nitride shutter and a neutron television camera (NTV). NTV is composed of a fluorescent screen, a mirror, a high sensitive television camera and a dark box. NTV makes real-time non-destructive inspection available in this room. NTV is connected to a personal computer (PC) via an image processor (IP). Neutron computed tomography (NCT) is also available.

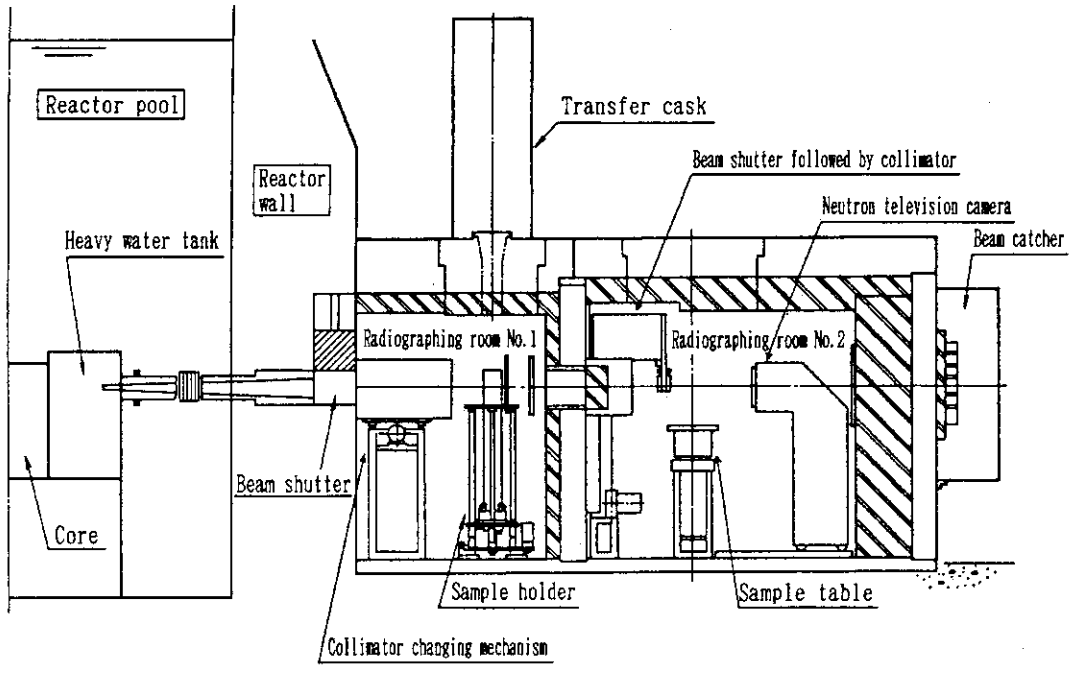

Figure 4 Thermal Neutron Radiography Facility

COLD NEUTRON RADIOGRAPHY FACILITY(CNRF)

A cross-sectional view of CNRF is shown in Fig. 5. The inner room size is 900 mm wide, 1,400 mm long and 1,600 mm high. This facility is equiped with a beam shutter, a sample table and an NTV. This NTV ,as well as NTV in TNRF-2, makes real-time non-destructive inspection available, however, the beam size is too narrow (20 mm x 50 mm) to observe larger samples on real-time. Dynamic Image Integration using the IP which is usually set at TNRF makes the observation of wider samples than beam size available. The utility time at C2-3 ,where CNRF is installed, is shared with four experimenter groups. Therefore CNRF is a movable box type apparatus.

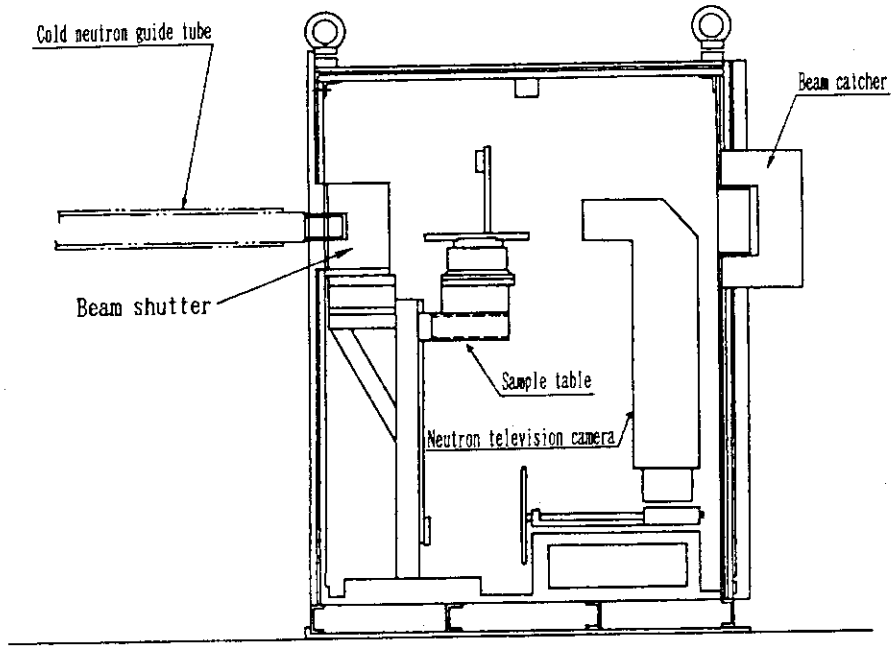

Figure 5 Cold Neutron Radiography Facility

NEUTRON RADIOGRAPHY TECHNIQUES

Many neutron radiography techniques are used in the JRR-3 neutron radiography facility.[4]

DYNAMIC RADIOGRAPHY

A particular advantage of TNRF is the availability of 255 mm x 305 mm beam with high neutron flux. It makes dynamic radiographing of relatively large samples possible. An example is the radiography of two-phase flow which will be carried out in conjunction with Heat Transfer and Fluid Flow Laboratory in the next year.

For the dynamic radiography a gadolinium fluorescent converter is used coupled to a Silicon Intensifier Target tube. This is viewed by a scan TV system to give a frame repetition rate of 30 frame/minute and a

video tape is recorded.

STATIC RADIOGRAPHY

The two prime methods employed are the direct exposure method using a gadolinium vapor deposited screen in a vacuum cassette and the transfer method using a dysprosium foil and a pressure cassette. The gadolinium screens are used in TNRF-2 and CNRF. The dysprosium foils are available in TNRF-1, TNRF-2 and CNRF. They are primarily used in TNRF-1 when neutron radiographing highly radioactive samples.

COMPUTED TOMOGRAPHY

TNRF-2 has the function of NCT. PC controls the turn table, on which the sample is set, and takes projection data of the sample from some angles. After taking projection data, PC calculates these data for reconstruction of the image using transputer. And the tompgraphic image is displayed on the TV by 512 x 512 pixels.

IMAGE INTEGRATION

The image from NTV is converted to the digital data and added by the A/D converter. The integrated images are accumulated to the frame memory. The image data on the frame memory are converted to the video signals by the D/A converter and displyed on the monitor TV.

DYNAMIC IMAGE INTEGRATION

The sample images which shift horizontally through the slit-type narrow beam, are integrated in the frame memory according to the sample locations. This function enable to generate the over all sample image from the partial images under the slit-beam. Consequently, the image of the sample, crossing through the slit-beam, appears at the left side on the monitor and shift to the right side as the sample moves.

CHARACTERISTICS OF THE JRR-3 NEUTRON RADIOGRAPHY FACILITY

The characteristics of the JRR-3 neutron radiography facility are shown in Table 1. Gold foils were used for the measurment of the neutron flux, and 0.5 mm thick cadmium (Cd) plate for the measurment of Cd ratio. Thermo luminescence detectors (TLDs) were used with fluoride lithium (LiF) capsules, which eliminate the effect of neutrons, for the measurment of γ ray.[5]

As a result, neutron fluxes are about 10^8 n/cm^2•s in both TNRF and CNRF. This value is ten times higher than the neutron flux in the old facility. This improves the quality of moving samples' radiography on real-time. The Cd ratio, measured in TNRF-1 and TNRF-2, were 81 and 130 respectively. The γ ray was measured only in TNRF-2. The γ ray dose equivalent rate was 2.16 Sv/h. When radiographing by a gadolinium screen and SR film, this means that n/γ is 62.5. In this condition, the best exposure time is about 20 s.

The collimator ratio, measured in TNRF-2, was 176 in the vertical direction and 153 in the horizontal direction. This guarantees the high

resolution of radiographs.

Table 1 Characteristics of JRR-3 Neutron Radiography Facility

Item / Facility	Neutron flux $n/cm^2 \cdot s$	Cd Ratio	n/γ $n/cm^2 - \mu Sv$ (Sv/h)	Collimator ratio L/D *2 L mm D mm	Radiographic Field size W × H mm	Sample size W×H×t mm kg
TNRF1	2.6×10^8	81	———	(5,638) (178) (30)	115 × 432	960 × φ130 50
TNRF2	1.5×10^8	130	62.5 *1 (2.16)	H 7,277 176 41 V 7,352 153 48 (7,138) (238) (30)	255 × 305	400 × 400 × 500 50
CNRF	2.3×10^8	—	———	—	20 × 50	400 × 400 × 600 30

* 1 Combination of Gd screen and SR film *2 Kobayshi's method[6]

4×10^3 $n/cm^2 - \mu Sv=1$ ( ): Designed value

CONCLUDING REMARKS

Based on the results of the characteristics measurement, it was confirmed that the performance of JRR-3 neutron radiography facility is higher than that we expected.

ACKNOWLEDGEMENT

The authors would like to thank N. Aoyagi, T. Tabata, H. Suzuki and T. Kodaira.

REFFERENCES

[1] N. ONISHI, et al., "Reconstruction Program of Japan Research Reactor-3 (JRR-3)," International Symposium on the Utilization of Mult-Purpose Research Reactors and Related International Cooperation, IAEA-SM-300/002

[2] Y. KAWABATA, et al., "Neutron Fluxes and Spectra of the Neutron Guide Tubes in the Upgraded JRR-3." International Cnference on

Neutron Scattering, Oxford, 1991, to be published
[3] A. TSURUNO, et al., "Description of JRR-3 Neutron Radiography Facility Plan," Proceedings of the Third World Conference on Neutron Radiography, Osaka, 1989
[4] A. TSURUNO, et al., "Design and Develpment on JRR-3 Neutron Radiography System," Proceedings of the Third World Conference on Neutron Radiography, Osaka, 1989
[5] M. MATSUBAYASHI, et al., "JRR-3 Neutron Radiography Facility," Preprint 1991 Spring Meeting of Atomic Energy Society Japan, B11.
[6] H. Kobayashi, et al., "Accurate Measurement of L, D, and L/D for Divergent Collimators," Proceedings of the Third World Conference on Neutron Radiography, Osaka, 1989

8. Preliminary Study for Cold Neutron Radiography

Hisao KOBAYASHI

Institute for Atomic Energy, Rikkyo University,
Nagasaka, Yokosuka, 240-01, JAPAN.

ABSTRACT

What is a value and a merit to use a cold neutron beam instead of a thermal neutron beam in neutron radiography? What are leading parameters to make a plan for detailed study in the field of cold neutron radiography? A beam quality and an effective macroscopic cross section as well as an intensity are required as an essential parameters to answer those questions. Firstly, beam qualities were analyzed by use of beryllium filter for the output of the guide tube CN-2 in KUR and the C2-1 in JRR-3. Secondly, transmission characteristics were measured for some materials.

INTRODUCTION

Neutron radiography (NR) is a powerful tool for nondestructive inspection of industrial materials as a complemental technique of X-ray radiography. Thermal neutron radiography (TNR) is used generally in this field, because thermal neutron (TN) beam can be easily obtained by a nuclear reactor and other facilities.

It is expected that a contrast of a cold neutron radiography (CNR) image increases usually with decreasing neutron energy than those given by the TNR. Then, the image quality should be fairly improved in the CNR images. An integrated macroscopic cross section for a given neutron spectrum is a leading parameter of a material to define transmittance for given thickness. Macroscopic cross sections as a function of neutron energy in the cold neutron (CN) region have been measured for only a few elements in detail and for several elements in briefly. Then, an accumulation of those data is essential to analyze the image and to estimate quantitatively thickness changes and defect sizes.

Recently, cold neutron sources (CNS) and guide tubes were installed on the two research reactors in Japan. One is the Kyoto University Reactor (KUR, 5 MW) in Research Reactor Institute, Kyoto University and another is the Japan Research Reactor No.3 (JRR-3, 20 MW) in Japan Atomic Energy Research Institute. Several research works have been started using the CNR facility on KUR at Oct. 1989,[1-3] and on JRR-3 at Feb. 1991.[4]

In this study, first, neutron spectra were computed after transmitted beryllium filters for incident neutrons with Maxwell distributions at 20°K and 293°K, and integral intensities of transmitted neutrons were analyzed for both temperatures. Secondly,

effective neutron energy or neutron *coldness* for two CNR facilities were measured using Be filters with various thickness. Finally, transmittances were measured for some materials as a basic data for the CNR study itself, after scattering components were estimated and subtracted from observed neutron intensities at behind of slabs. Effective macroscopic cross sections for given CN beams were compared with that for the TN.

COLD NEUTRON NR FACILITIES

The CN guide tube named CN-2 in KUR has been opened to CNR researchers since 1989.[1] The bottle of the CNS is installed in the graphite thermal column and cooled by liquid deuterium. The guide tube consists of twelve units of Ni mirrors with 90 cm in length and resulted total length of 10.8 meters. In the mirror unit, a pair of plane surface Ni mirrors are combined face to face each other in parallel with separation of 1 cm. The upper side and the lower side of the mirror units are covered with other Ni mirrors with 1 cm in width. The twelve mirror units are connected each other and are slightly bent along a circular arc with a radius of 995 meters. Corresponding characteristic wavelength is estimated to be 2.6 Å (~12 meV) from this curvature. Intensity of the neutron beam was measured by the gold foil activation method and found to be 1.34×10^7 n/cm^2/s as a thermal neutron equivalent value at the exit of the guide tube and at the center of the beam section which is 7.5 cm in vertical length and 1 cm in horizontal width.[1,2]

Three CN guide tubes and two TN guide tubes were constructed in JRR-3 at 1990 and one of CN guide tube named as C2-1 is opened to CNR study projects (fig.1).[4] The CNS in JRR-3 is cooled by liquid hydrogen. A mirror unit of the C2-1 is also made of a combination of plane surface Ni mirrors of 85 cm in length. The C2-1 consists of two parts: One is the curved guide of 17.2 meters in length with the radius of 834 meters and another is the straight one of 27.0 meters. The characteristic

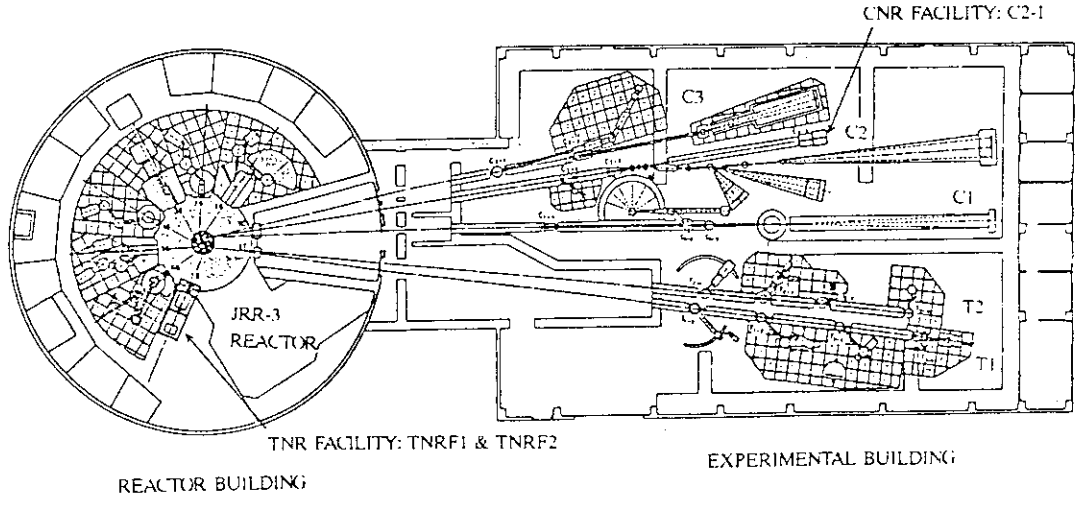

Fig.1 Plan view of cold and thermal neutron radiography facilities, C2-1, TNRF1 and TNRF2 in the JRR-3.

wavelength of the guide tube is 4 Å (~5 meV). The beam has a section of 5 cm by 2 cm and its cold neutron equivalent intensity was measured to be 2.3×10^8 n/cm^2/s.

In addition to the CNR facility, two serially connected TNR facilities have been constructed along one of beam port in JRR-3 and named as TNRF1 and TNRF2 (fig.1). The TNRF1 facility is designed use for an NR inspection of spent nuclear fuel elements. The TNRF2 is utilized for regular TNR research works and has a L/D value of 250 (designed value), an intensity of 1.5×10^8 n/cm^2/s, and a cadmium ratio of 130.

ESTIMATIONS OF BEAM QUALITY

Neutron spectrum $\phi(E)$ is one of important parameters to define the performance of the NR system. However, detailed spectrum does not necessarily required in the NR study, because an integral value of transmitted spectrum $\int\phi(E,t)dE$ is related to a signal intensity or to an optical density from an imaging device. Where $\phi(E,t)$ is a spectrum after passing through an object of thickness t. The equation is approximated to be $\phi(E)\mu(E)\exp[-\Sigma(E)t]$. Where build up phenomena of scattered neutrons are neglected in our experiments. Because narrow neutron beams were used for CNR and because scattering component were subtracted experimentally for CNR and TNR as shown later. In this equation, $\mu(E)$ is a detection efficiency of the imaging device at energy E, and is approximated to be independent on E for sufficiently thick converter. The notation $\Sigma(E)$ is a macroscopic cross section of the object at E.

For the TN beam generated from a nuclear reactor, Maxwell distribution is frequently assumed for NR studies. In this case, mean energy $<E>$ instead of 25.3 meV (2200 m/s) and $\Sigma(<E>)$ are useful parameter to rough analyses of transmission phenomena. However, in the CN region, beam spectrum ejected through a guide tube has more complicated feature, and $\Sigma(E)$ of some materials have more complex energy

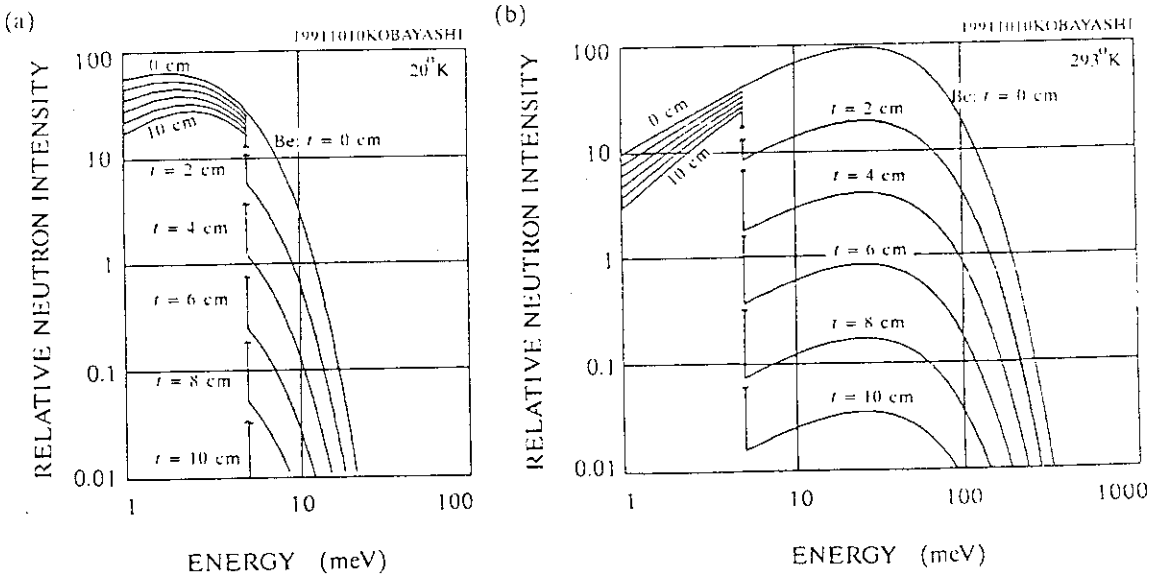

Fig.2 Computed spectra after passing through Be filters for various thicknesses. Temperature of incident spectra are assumed to be (a) 20°K and (b) 293°K.

dependence due to Bragg cut off characteristics. Furthermore, values of $\Sigma(E)$ are not completely known for all elements.

Beryllium is one of useful material to characterize a beam quality in the CN region. The polycrystalline Be has a sharp and deep Bragg cut off in neutron cross section at 5 meV. The value of cross section is approximately 0.4 barn at 5 meV at 300°K[5] in the energy range lower than 5 meV. The value depends on velocity with the $1/v$ law and on bulk temperature. In the region above 5 meV, the cross section become independent on v and is approximately 6 barn.[5,6] We can use the cut off characteristics to rough estimation of the beam quality in the CN region.

Figures 2(a) and (b) show computed spectra $\phi(E,t)$ filtered by various t of Be for incident beams of 20°K and 293° K Maxwell distributions, respectively. In figures 2(a) and (b), macroscopic cross sections $\Sigma(E)$ in the two regions $E<5$ meV and $E>5$ meV were assumed to be $0.43\times(5/E)^{1/2}$ barn and an energy independent value of 6.4 barn, respectively. In fig.2(a), analyzed spectra in the energy region higher than 12 meV is less accurate at the output of the CN-2 because of the cut off character of the transmission rate through the guide tube. However, the spectrum distortion give negligible effects for the CN-2 beam. For the C2-1, the spectrum distortions from fig.2(a) should be more greater in the region 5>meV than the CN-2 case, because of the longer characteristic wavelength (equivalent to ~5 meV) of the guide tube.

Two sets of integral intensities, $I_{low}(t)=\int_0^{5meV}\phi(E,t)dE$ and $I_{hi}(t)=\int_{5meV}^{\infty}\phi(E,t)dE$, after transmitted through Be as a function of thickness t are computed for two separate energy regions divided by 5 meV. Results are shown for 20°K Maxwell distribution and for 293°K in figs.3(a) and (b), respectively. The figure 3(a) corresponds to a simulation for the CN-2 beam experiment. In the C2-1 experiment, however, $I_{hi}(t)$ should be

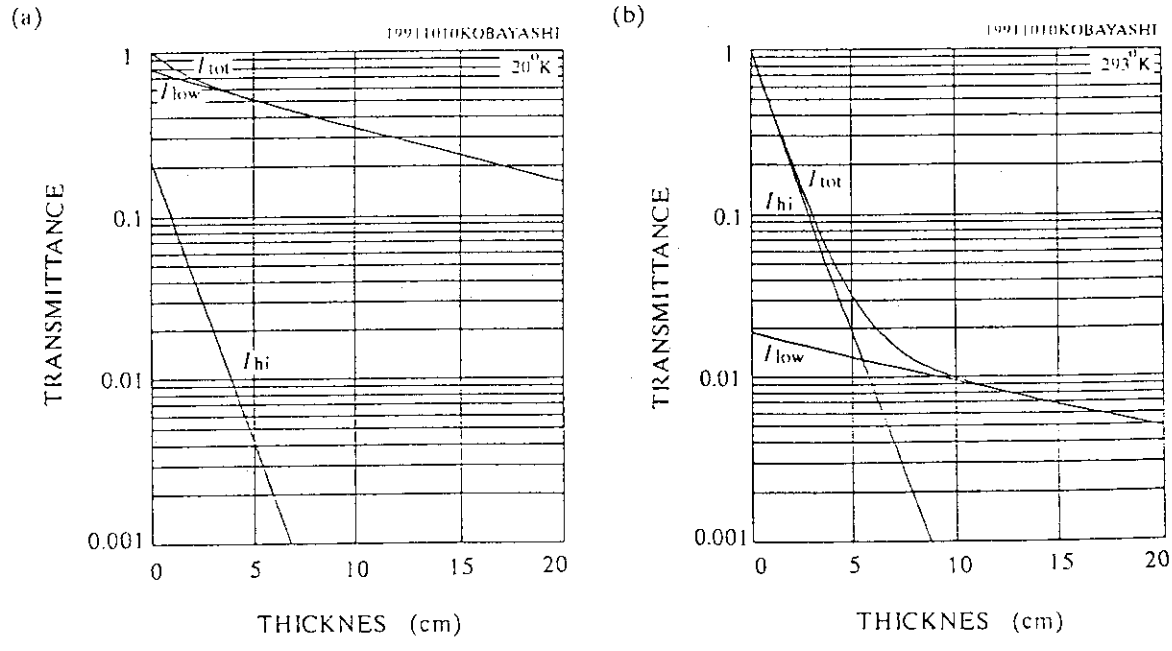

Fig.3 Computed transmission curves for Be filter as a function of thickness. Incident spectra are assumed as (a) the Maxwell distribution at 20°K and (b) at 293°K.

expected to be more lower value than fig.3(a).

A beam *hardening effect* is found to be negligible for both energy regions as discussed later in this section. This result leads to use analytical deconvolution from measured transmission data with use of the Be filter. And the two intensities can be expressed as two effective macroscopic cross sections $<\Sigma_{low}>$ and $<\Sigma_{hi}>$, respectively. Thus, we can estimate analytically $I_{low}(0)$ and $I_{hi}(0)$ as well as $<\Sigma_{low}>$ and $<\Sigma_{hi}>$ from measured total intensities $I(t)$ at least four different t values corresponding to four unknown parameters.

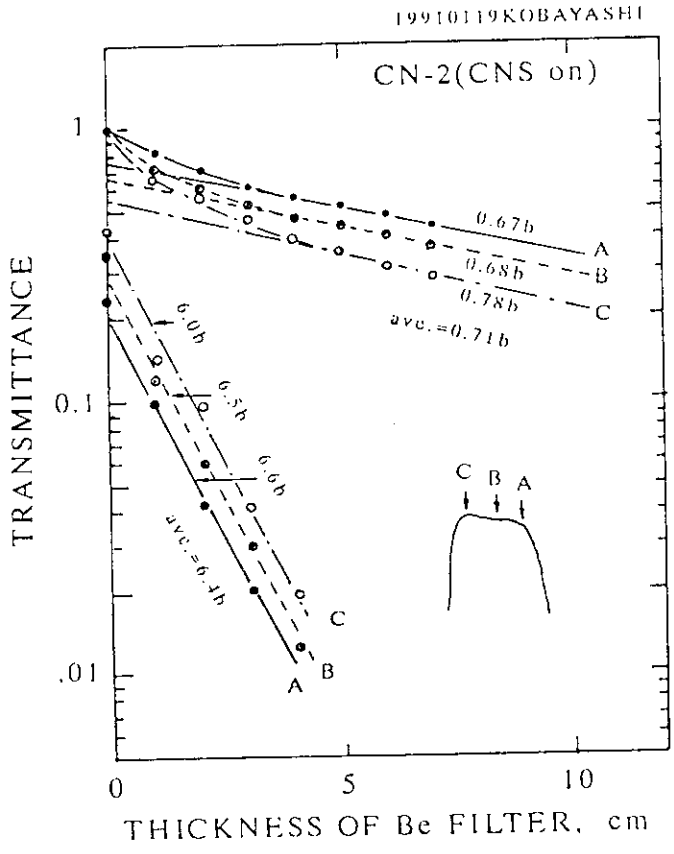

Fig.4 Transmission curves measured for Be at three positions in the beam section of the CN-2 in the KUR.

Kobayashi *et al.*[3] have been measured $I(t)$ and analyzed $I_{low}(t)$ and $I_{hi}(t)$ as a function of t of Be filter from 0 to 7 cm at three different positions in a CN-2 beam section. Results are shown in fig.4. The notation A shown in fig.4 indicates the position of the shoulder near the inner mirror side in shape of horizontal section of beam profile. The notation B is the middle point of the two mirrors, and C is the peak point of the profile near the outer mirror side. The data were measured at the CN-2 guide tube in KUR by a conventional Gd-KODAK film system. Differences between curves A, B and C can be understood as spectrum difference due to difference of transmission characteristics depending on the beam position. Initial integral intensities $I_{low}(0)$ and $I_{hi}(0)$ can be obtained by extrapolation of fig.4 to t=0.

Effective macroscopic cross sections $<\Sigma_{low}>$ and $<\Sigma_{hi}>$ were estimated from calculated transmittances averaging from t=0 to 20 cm (fig.3), and corresponding energy $<E_{low}>$ and $<E_{hi}>$ at t=0 from fig.2(a). Results are summarized in table I. Measured results for the CN-2 (fig.4) are shown for reference in this table. Mean energy $<E_{low}>$ increases slightly with increasing the thickness of Be filter t by the hardening effect. Furthermore, the hardening effect is shown in the CN region as a peak shift in fig.2(a). However, it is shown that the hardening effect is not important for the transmission characteristics of the cut off component of Be at least t<20 cm.

If an element, which have not a cut off character, is interested to analyze an image, mean energy for whole spectrum $<E_{tot}>$ become more useful and is shown for reference in table I.

Table I. Effective macroscopic cross sections $<\Sigma_{low}>$ and $<\Sigma_{hi}>$, and effective energy $<E_{low}>$, $<E_{hi}>$ and $<E_{tot}>$.

Beam Temp. (°K)		$<\Sigma_{low}>$ (cm^{-1})	$<E_{low}>$ (meV)	$<\Sigma_{hi}>$ (cm^{-1})	$<E_{hi}>$ (meV)	$<E_{tot}>$ (meV)
20	calc.	$0.080^{4}\pm0.000^{8}$	2.44	$0.787^{8}\pm0.000^{1}$	7.17	3.46
	exper.	0.087±0.005	---	0.79 ±0.03	---	---
293	calc.	$0.067^{7}\pm0.000^{4}$	3.28	$0.787^{8}\pm0.000^{2}$	43.0	42.3

Experimental results of the relative intensity of cut off component $I_{low}(0)/I(0)$ are summarized for the CN-2 in KUR,[3] for the C2-1 and the TNRF2 in JRR-3 together with calculations and are shown in table II. Notation CNS-on means that the bottle of the CNS is cooled by liquid deuterium for the CN-1 or by liquid hydrogen for the C2-1, and CNS-off means using the same CNS and guide tube but not cooled by the liquid. Position dependent $I_{low}(0)/I(0)$ values are observed for the CN-2 and should result from different spectrum shape depending on position in the beam section. On the contrary, the ratio did not depend on position for the C2-1 in JRR-3. The different characteristics of two beams should arise from the different guide tube configurations: Only the C2-1 has a long straight guide tube. The measured ratios $I_{low}(0)/I(0)$ are agreed well with calculated values.

The table II should suggest a rough guide for the *coldness* of the beam quality and should give a parameter to estimate an effective macroscopic cross sections $<\Sigma_{low}>$, which is one of basic parameters for analyses of CNR images.

Table II. Ratios of the cut off cold neutron component below 5 meV to total incident neutron intensity for KUR CN-2, JRR-3 C2-1 and TNRF2.

Facility		Measured positions in the beam	$I_{low}(0)/I(0)$		
			CNS-on	CNS-off	calc.
KUR CN-2		A: Near inside mirror	79.4 %	64.4 %	78.4 %
		B: Center	70.5	44.8	
		C: Near outside mirror	64.7	28.1	
JRR-3	C2-1	Center	85.4	---	---
	TNRF2	Center	2.9		1.9

TRANSMISSION MEASUREMENTS FOR VARIOUS MATERIALS

Usefulness of the CNR technique has been anticipated for various inhomogeneous materials more than that of usual TNR technique because of a characteristics of increasing contrast. That is, some elements, which dominate the scattering process, become more transparent for the CN beam, and thicker materials can be expected to inspect than that for the TN beam. On the contrary, a macroscopic cross section of capture dominant elements increases with decreasing velocity of neutron based on the $1/v$ law. Then, that materials become more neutron opaque as decreasing velocity and more thinner materials become more distinguishable embedded in a base material.

When effective values $<\Sigma>$ without including buildup effects are required to know at a given neutron spectrum, scattering neutron background must be corrected from measured intensities. A model has been analyzed on behavior of thermal neutrons in a slab taking into consideration of scattering component.[7,8] The model have discussed the way of reliable estimation for neutron transmittances from NR images and was applied for the CN experiments.

Figure 5 shows measured transmission curves of step like samples of C, Be, Al, Pb, Ti, Fe, Ni, and H_2O after subtracted scattering components. Where the H_2O step was realized by fill up the water into an aluminum vessel hollowed out with step like in shape. Dashed curves and solid curves correspond to results of the CN beam from the C2-1 and of the TN beam from the TNRF2, respectively.

This figure clearly indicates a possibility of contrast enhancement in CNR for capture dominant materials. That is, Ti, Fe, Ni and H_2O have usually large macroscopic cross sections in the TN region. The values are much more increased in the CN region.

On the contrary, scattering dominant materials, C, Al, Be and Pb, are rather transparent in the TN region and become much more transparent in the CN region.

Therefore, if first group materials are embedded in one of second group material, the combination should expect to enhance the contrast most effectively in the CNR.

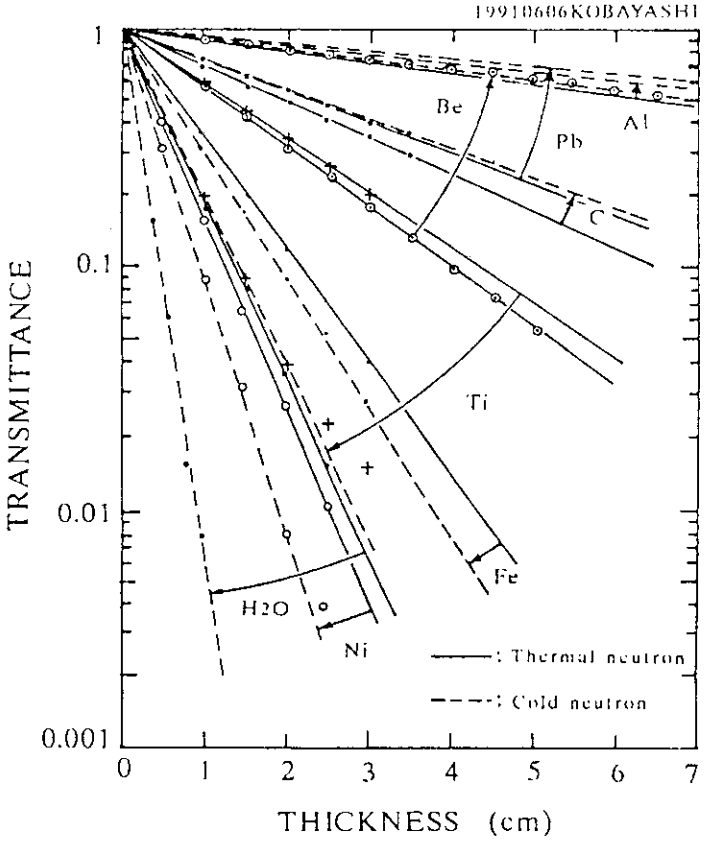

Fig.5 Transmission curves for various materials using the CN beam from JRR-3 C2-1 (dashed curves) and the TN beam from TNRF2 (solid curves).

CONCLUSION

Transmitted neutron spectra were computed after passing through various thickness of Be filters in the no build up condition for two incident neutrons with 20°K and 293°K Maxwell distributions. Integral intensities I_{low} and I_{hi} were analyzed for two energy regions separated by the cut off energy of 5 meV. Negligible hardening effects of I_{low} and I_{hi} were shown from the calculations. In spite of rough estimations, results were well agreed with following experiments.

Transmittances of Be filter were measured for two different CN beams from the CN-2 and the C2-1 guide tube. Observed intensities were analyzed under the two component assumption and initial intensities I_{low} and I_{hi} were estimated from the measured intensities I. The results were compared with calculated values. An appreciable difference of initial intensities I_{low} is observed between the two CN facilities and can be explained from the difference of the characteristic wavelength of the guide tube.

Transmission curves were measured for various materials by CNR. Results are compared with that measured by TNR. The results should give useful data in the field of material evaluations, agriculture, biological and medical science as well as in the field of nondestructive testing. The effort will be continuously extended for other materials including alloys and chemical compounds.

REFERENCES

[1] K. Yoneda, T. Kawai, S. Fujine, M. Utsuro, M. M. Panitra, Y. Ikeda, M. Yokoi, and H. Kobayashi, *"Cold Neutron Beam Hole in KUR and its Radiography Test"* , First Int. Topical Meeting on Neutron Radiography System Design and Characterization, (Pembroke, Aug.28-30, 1990) paper No.7.

[2] K. Yoneda, T. Kawai, S. Fujine, Y. Ikeda, M. Yokoi, and H. Kobayashi, *"Radiographic Measurements of Cold Neutron Guide Output from KUR-CNS"*, Ann. Rep. Res. Reactor, Kyoto Univ., Vol.23 (1990) 37.

[3] H. Kobayashi, Y. Ikeda, K. Ohokubo, M. Yokoi, K. Yoneda, S. Fujine, K. Okamoto, T. Kawai, M. Utsuro, *"Experimental Results of Cold Neutron Radiography - Measurements of the CN-2 Characteristics (II)"*, Workshop on Developments and Applications of Cold and Ultra-Cold Neutrons, (KUR, Jan. 1991) p.98, [in Japanese].

[4] A. Tsuruno, Y. Horiguchi, N. Aoyagi, and E. Shirai, *"Description of JRR-3 Neutron Radiography Facility Plan"*, *Neutron Radiography (3)* (Reidel Publ.1990) p.81.

[5] D. I. Garber and D. D. Kinsey, *"Neutron Cross Sections, II, Curves"*, BNL-325 3rd ed., (Brookhaven National Lab., New York, Jan. 1976).

[6] S. F. Mughabghab and D. I. Garber, *"Neutron Cross Sections, I, Resonance Parameters"*, BNL-325 3rd ed., (Brookhaven National Lab., New York, June, 1973).

[7] H. Kobayashi, Y. Ikeda, K. Ohkubo, and H. Wakao, *"An Evaluation of Detection Limit for Defects in Materials"*, *Neutron Radiography (3)* (Reidel Publ.1990)p.885.

[8] H. Kobayashi, *"Studies of Neutron Transmittance Measurements using Cooled CCD Camera"*, Proc. 1st Intern. Topical Meeting on Neutron Radiography System Design and Characterization, (Pembroke, Canada, Aug. 28-30, 1990) paper No.14.

9. Study on Two-Phase Flow in a Coolant Channel of a Plate-Type Fuel with Use of Neutron Radiography Technique

K. MISHIMA, T. HIBIKI, H. NISHIHARA

Research Reactor Institute, Kyoto University
Kumatori-cho, Sennan-gun, Osaka 590-04, Japan

ABSTRACT

Two-phase flow in a narrow rectangular duct is important related to abnormal cooling conditions of a MTR type research reactor. In view of this, flow regime, void fraction, slug bubble velocity and pressure loss were measured for rectangular ducts with a narrow gap. The neutron radiography technique was used to visualize the flow and the void fraction was obtained by image processing. The void fraction was correlated well by the drift flux model with existing correlation for the distribution parameter which was about 1.35. Similar results were obtained for slug bubble velocity, however the distribution parameter was in the range from 1.0 to 1.2. The frictional pressure loss was correlated well by the Chisholm-Laird correlation. In collaboration with previously obtained data, it was found that the Chisholm's parameter C, however, changed from 21 to zero as the gap decreased.

INTRODUCTION

A coolant channel of a MTR-type fuel element has a rectangular cross-sectional shape with a very narrow gap and a large aspect ratio. It is anticipated that the characteristics of two-phase flow in such a narrow duct differ from those in other channel geometries, because of its significant restriction to the bubble motion, which may deterioarate, as a consequence, boiling heat transfer under abnormal operating conditions. Although much work has been performed on gas-liquid two-phase flows in round tubes, only a little is found for test sections with a narrow gap or a non-circular cross-sectional shape[1-5]. In view of this, the flow regime, void fraction, pressure loss and the mean velocity of slug bubbles have been investigated for two-phase flow in rectangular ducts with a narrow gap ranging from 1.0 mm to 5.0 mm.

EXPERIMENTAL

1. Test Rig

The same test loop was used as described previously.[5] Air was supplied by a compressor and introduced into a mixing chamber through an

injection nozzle which is consisted of ten capillary tubes mounted in a line to fit the flow channel. The air and the purified water were mixed in the mixing chamber and the mixture flowed upward through the test section. After the test section, the air was released into the atmosphere through a separator, while the water was circulated by a centrifugal pump. The flow rates of the air and the water were measured with a float-type flowmeter and a turbine flow meter, respectively.

The test sections used in the present experiment were rectangular ducts made of transparent acrylic resin. In the measurement of void fraction, however, the test sections were made of aluminum so that the neutron radiography technique could be applied[5]. Three test sections were fabricated: the gaps were 1.0, 2.4 and 5.0 mm. The width and the length of those test sections were 40 mm and 1400 mm, respectively.

2. Measurement

(1) Flow Regimes

The bubble behavior and the overall pattern of flow were observed by a high-speed video camera at a speed of 200 or 1000 frames per second and the images were played back at slow motion for detail observation.

(2) Void fraction

The void fraction was measured with use of the neutron radiography and image processing techniques. The flow in the test section made of aluminum was visualized by the neutron television system and the images were processed to calculate the channel-average void fraction. The methods have been described previously.[5]

(3) Slug Bubble Velocity

The average velocity of slug bubbles were measured from the intervals for bubbles to rise a given distance in the slow motion picture. The velocity of small bubbles was not taken into account in this measurement.

(4) Pressure Loss

Two pressure taps were located at 50 cm and 150 cm from the entrance of the test section. The pressure difference between the taps was measured with a differential pressure transducer.

RESULTS

1. Flow Regimes

Four flow regimes were specified, i.e. bubbly, slug, churn and annular flows. Since the gap of the channel was so narrow, small bubbles, cap bubbles and slug bubbles looked as if they were crushed between the two walls. Thus, the flow regime was determined based upon the pattern of the bubbles observed through the wider wall. The discrimination between the slug and churn flows was rather subjective, however the flow was called churn flow when the round nose of large bubbles became unstable and lost its identity.

Figures 1 and 2 show flow regime maps for the test sections with 1.0 and 2.4 mm gaps, respectively. The map for 5.0 mm gap was similar to that for 2.4 mm gap. The broken lines denote approximate locations of the boundaries between flow regimes while the solid one denotes the boundary between the slug and annular flows predicted by the Jones-Zuber equation[1]. It can be seen that the Jones-Zuber equation reproduces the boundary for slug and annular flows. It is also noted that, according to the present

definition, the churn flow was not observed when the gap is 1.0 mm.

2. Void Fraction

The void fraction was correlated in view of the drift flux model[1]:

$$V_g = j_g/\alpha = C_0 j + (0.23+0.13s/w)\sqrt{\Delta\rho g w/\rho_\ell} \quad (1)$$

where j_g:superficial gas velocity, α:channel-average void fraction, C_0:distribution parameter, j:mixture volumetric flux ($=j_g+j_\ell$), ρ_ℓ:liquid density, $\Delta\rho$:difference of the densities between two phases, s:gap of the flow channel, w:width of the flow channel. The second term on the right hand side of Eq.(1) expresses the drift velocity for bubbles in a rectangular duct obtained by Griffith[6]. The distribution parameter C_0 is 1.2 according to Jones-Zuber[1], while Ishii[7] proposed the following equation for the distribution parameter for rectangular ducts:

$$C_0 = 1.35 - 0.35\sqrt{\rho_g/\rho_\ell} \quad (2)$$

The experimental results are shown in Figs.3 and 4 for the gap 1.0 and 2.4 mm, respectively. It is seen from the figures that the void fraction can be correlated well by the drift flux model with the distribution parameter given by Eq.(2).

On the other hand, Moriyama et al.[8] reported recently larger values of distribution parameter C_0 for extremely narrow gaps. Figure 5 shows the comparison of the distribution parameter between existing data[1-3,5,8]. There is observed a tendency that the distribution parameter becomes large when the gap is very small, otherwise it is predicted by Eq.(2). When the gap is larger than 5.0 mm, the distribution parameter appears to be 1.2. On the contrary, the database for the Ishii correlation, Eq.(2), includes data for the gap 11 mm. Therefore, it is suggested that the distribution parameter be a function of the aspect ratio. More data are needed on this point.

3. Bubble Velocity

The average velocity of slug bubbles was correlated by the drift flux model. The results indicated that the drift velocity appears to be constant for all the gaps, which value agrees well with the Griffith correlation[6]. The distribution patameter, however, was in the range between 1.0 and 1.2, which is smaller than that for the void correlation.

4. Pressure Loss

(1) Single-phase pressure loss

Since the friction factor of a single-phase flow in a narrow rectangular duct is different from that in a round tube, pressure loss for single-phase flow was measured as the reference.

For the friction factor of a single-phase flow in a noncircular tube, Sadatomi et al.[3] took account of the effect of channel geometry and proposed the following correlation:

$$\lambda = C_L Re^{-1} \quad \text{for laminar flow} \quad (3)$$

$$\lambda = C_T Re^{-0.25} \quad \text{for turbulent flow} \quad (4)$$

where λ:friction factor, Re:Reynolds number.

The relationship between the coefficients C_L and C_T is given by the following equation:

$$C_T = C_{TO}(0.0154\ C_L/C_{LO}-0.012)^{1/3}+ 0.85 \quad (5)$$

where C_{LO}= 64 and C_{TO}= 0.3164. Since C_L is given by the theoretical solution for a laminar flow in a rectangular duct, C_T is obtained from Eq.(5).

Measured friction factors for single-phase flows were compared with the theoretical solution for laminar flow and Eq.(5) for turbulent flow, and good agreements were obtained within the measurement error.

(2) Two-phase pressure loss

Two-phase frictional pressure loss was correlated by the Lockhart-Martinelli method[9], i.e. the data were plotted in terms of the two-phase multiplier ϕ_ℓ vs. the Lockhart-Martinelli parameter X. Measured values were used for the reference single-phase friction factor.

Some of the results are shown in Figs.6, 7 and 8 for 1.0, 2.4 and 5.0 mm gaps, respectively. The solid lines in the figures denote the prediction by the Chisholm-Laird correlation[10]:

$$\phi_\ell^2 = 1 + C/X + 1/X^2 \quad (6)$$

The relation between the classification of flow in the Lockhart-Martinelli correlation[9] and Chisholm's parameter C is given.[10]

Sadatomi et al.[3] reported that the frictional pressure loss was correlated by Eq.(6) with C=21. On the other hand, Moriyama et al.[8] obtained C=0 with some modification for Eq.(6) for extremely narrow gaps. Those data for parameter C are plotted together with the present results as a function of the gap in Fig.9. In the present results, the value of C changes depending upon the classification of flow, therefore the range of the value of C is shown with a bar. From Fig.9 it can be seen that the parameter C changes its value from 21 to zero as the gap decreases in the range about 5 mm to 0.1 mm.

SUMMARY

Experimental data on flow regime, void fraction, slug bubble velocity and pressure loss were obtained for narrow rectangular ducts, and the results were compared with existing results. The following characteristics has been found for narrow rectangular ducts:

a. The shape and the motion of bubbles in a narrow duct are strongly restricted by the proximity of the walls. The churn flow was not observed when the gap is 1.0 mm.
b. The void fraction was well correlated by the drift flux model. In collaboration with existing data, there was found a tendency that the distribution parameter becomes large when the gap is smaller than 0.1 mm, otherwise it is predicted by the Ishii correlation[7].
c. The average velocity of slug bubbles was correlated by the drift flux model. The drift velocity was the same as that for the void correlation, however, the distribution parameter was found to be in the range between 1.0 and 1.2 which value is smaller than that for the void correlation.
d. The frictional pressure loss was found to be correlated well by the Chisholm-Laird correlation. Chisholm's parameter C, however, decreases from about 20 to zero as the gap decreases from 5 mm to 0.1 mm.

ACKNOWLEDGMENTS

Part of this work was supported by the Grant-in-Aid for Scientific Research from the Ministry of Education, Science and Culture (No.01420046 and No.63580178). The authors wish to express their gratitude to Dr. Shigenori Fujine and Mr. Kenji Yoneda, Research Reactor Institute, Kyoto University (KURRI), for their assistance and suggestions in performing neutron radiography experiment. They are also indebted to Prof. Keiji Kanda of KURRI for his support in this work.

REFERENCES

1) Jones, Jr., O.C. and Zuber N.:Two-Phase Momentum, Heat and Mass Transfer in Chemical, Process and Energy Engineering Systems, ed. Durst, Tsiklauri and Afgan, Hemisphere, Washington, pp.345-355 (1979).
2) Iida, Y. and Takahashi, K.:Kagaku Kogaku Ronbunshu 2, pp.228-234 (1976) in Japanese.
3) Sadatomi, Y., Sato, Y. and Saruwatari, S.: Int. J. Multiphase Flow 8, pp.641- (1982).
4) Troniewski, L. and Ulbrich, R.:Chem. Eng. Sci. 39, pp.751-765 (1984).
5) Mishima, K. et al.:Proc. Japan-U.S. Seminar on Two-Phase Flow Dynamics, Ohtsu, Japan (1988).
6) Griffith, P.:ASME Preprint 63-HT-20 (1963).
7) Ishii, M.:ANL-77-47 (1977).
8) Moriyama, k. and Inoue, A.:Proc. 28th National Heat Transfer Symp. of Japan, Fukuoka, p.763 (1991) in Japanese.
9) Lockhart, R.W. and Martinelli, R.C.:Chem. Eng. Prog. 45, p.34 (1949).
10) Chisholm, D. and Laird, A.D.K.:Trans. ASME 80, p.276 (1958).

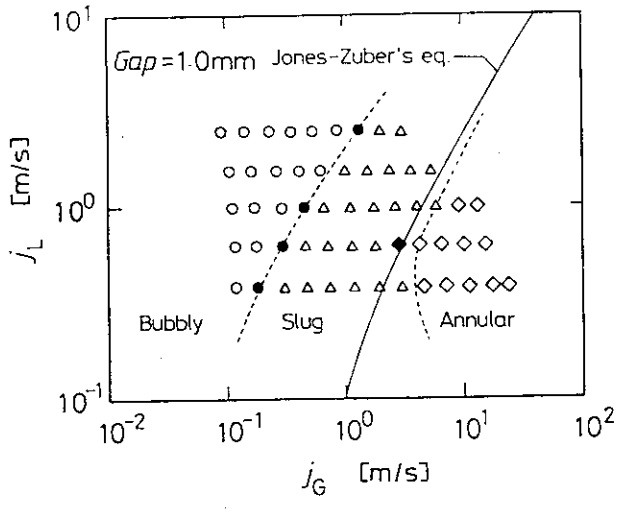

Fig. 1 Flow regime map for 1.0 mm gap.

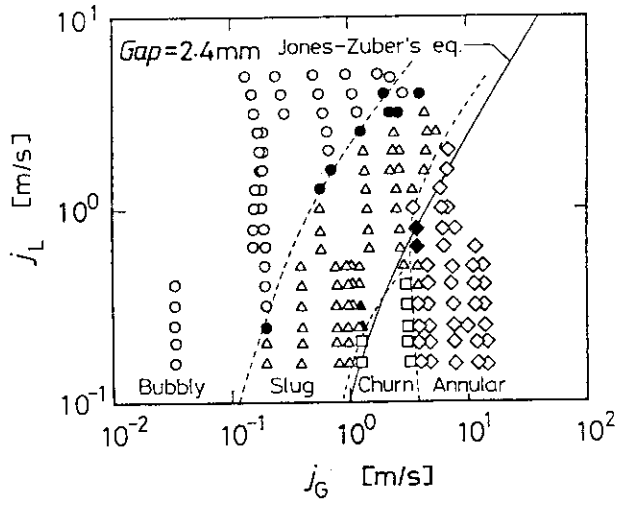

Fig. 2 Flow regime map for 2.4 mm gap.

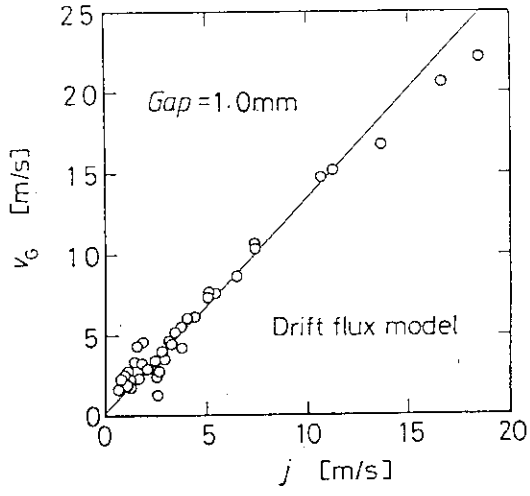

Fig. 3 Void fraction correlation for 1.0 mm gap.

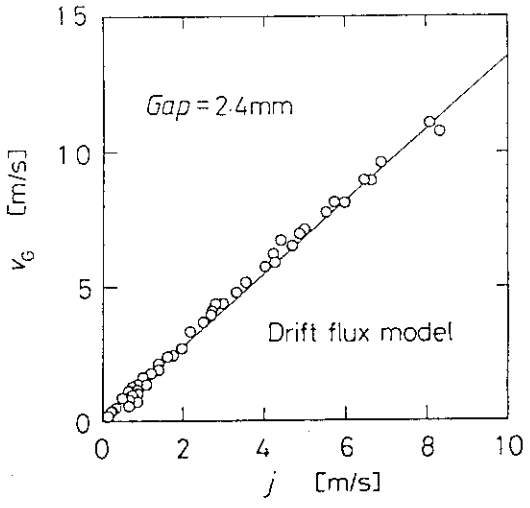

Fig. 4 Void fraction correlation for 2.4 mm gap.

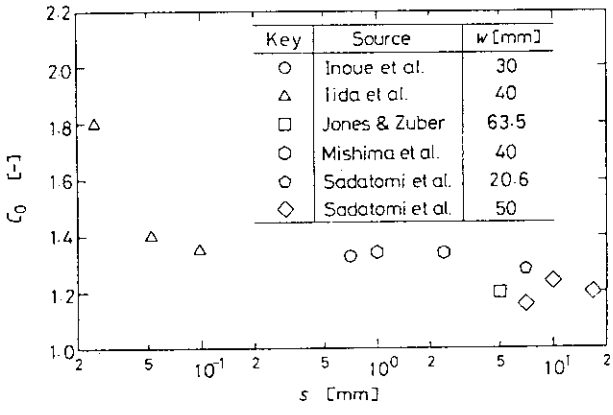

Fig. 5 Distribution parameter as a function of the gap of rectangular ducts.

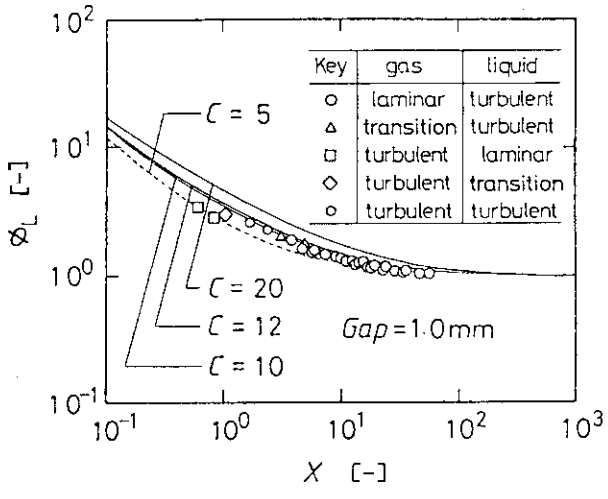

Fig. 6 L-M correlation for 1.0 mm gap.

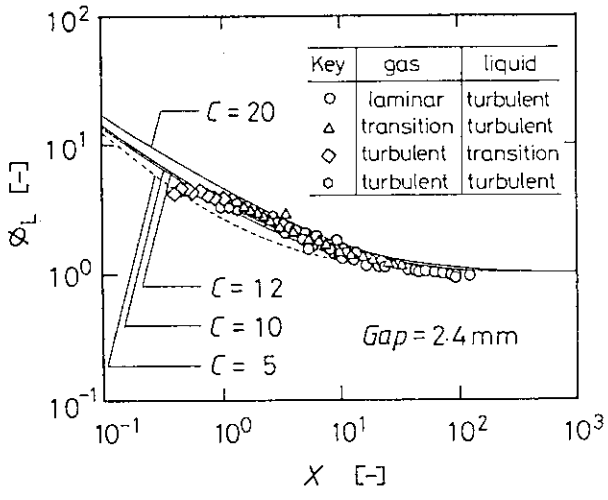

Fig. 7 L-M correlation for 2.4 mm gap.

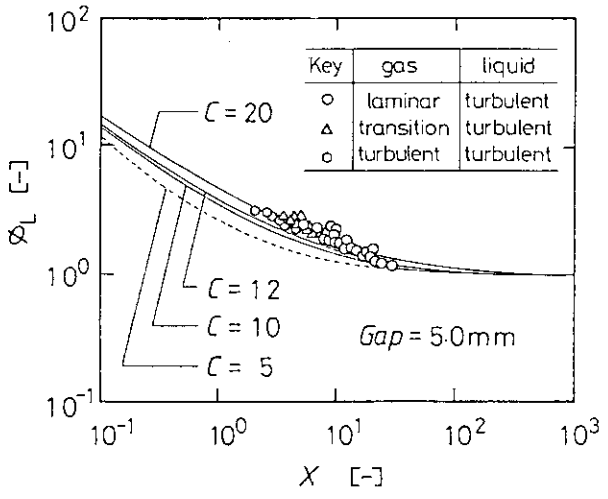

Fig. 8 L-M correlation for 5.0 mm gap.

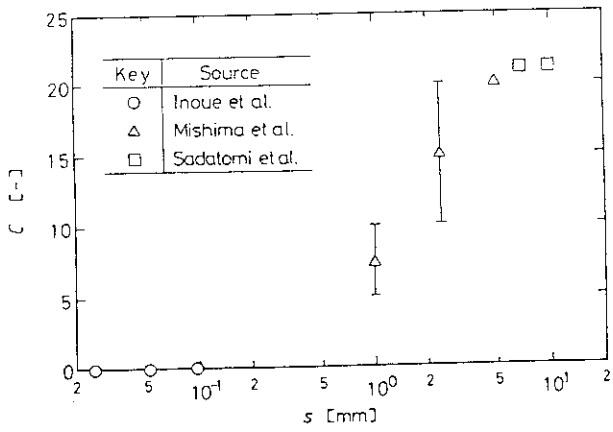

Fig. 9 Parameter C as a function of the gap.

1. Current Status of JAERI Tokai Hot Cell Facilities

Hiroharu ITAMI, Minoru MOROZUMI and Takeshi YAMAHARA

Department of Hot Laboratories
Tokai Research Establishment, JAERI
Tokai-mura, Naka-gun, Ibaraki-ken 319-11, Japan

ABSTRACT

JAERI has 4 hot cell facilities in order to examine high radioactive materials. Three of them, the Research Hot Laboratory, the Reactor Fuel Examination Faciliy and the Waste Safety Testing Facility are located in the JAERI Tokai site, and the rest is the JMTR Hot Laboratory in the Oarai site.

The Research Hot Laboratory(RHL) was constructed for post-irradiation examination (PIE), especially nuclear related basic research experiment, such as metallurgical, chemical and mechanical examination on fuels and materials irradiated in research and test reactors. This facility has 10 large dimension concrete and 38 lead cells. At present the RHL is used for various kinds of examinations of high radioactive samples such as fuels of research and test reactors, power reactors and high temperature testing reactor(HTTR), and structural materials.

The Reactor Fuel Examination Facility (RFEF) was designed and constructed for carrying out PIE of irradiated full-size fuel assemblies of lihgt water reactors(LWRs). This facility has a storage pool, 8 concrete and 5 lead cells. They are currently used for safety evaluation on high burnup and advanced LWR fuels as part of the national program.

The Waste Safety Testing Facility (WASTEF) was designed and constructed for safety research on long-term storage and disposal of high level rdioactive wastes, generated by fuel reprocessing. The WASTEF has 5 concrete cells and 1 lead cell. Examinations on the behavior of various long-lived fission products in a glass form and in a canister and, releasing behavior of them out of a canister are carrying out under the condition at storage.

INTRODUCTION

It is well known that post-irradiation tests on nuclear materials is of prime importance as well as irradiation tests in the development of nuclear energy. In the early stage of nuclear research and development at the JAERI, radioactive samples irradiated in the small research reactor Japan Research Reactor-1 (JRR-1) had not so high radioactivity. Therefore a small hot cell was installed in the reactor building, mainly to separate irradiated specimens from capsules.

Following the construction of large scale research reactor JRR-2, the RHL capable for PIEs for very high radioactive materials irradiated in the JRR-2 was constructed in conjunction with the JRR-2, and has been operated since 1961. Increaseing wide variety of PIE items for nuclear fuel and structural materials irradiated in JRR-2, -3, Japan Material Test Reactor (JMTR) and the commercial gas cooled power reactor of Japan Atomic Power Co.(JAPCO), required numerous modification and additions of hot cells . Under these circumstances, extension of the facility and installation of the new PIE apparatus were carried out in 1965.

Since LWRs were introduced in Japan, new important needs required the construction of additional facilities; one is for PIE of full-size fuel assembly to verify the good performance of fuel assembly throughout its life in reactor core, and the other for examination of high level waste disposal. The facility for the former is the RFEF, and for the latter is the WASTEF. These facilities were established in late 1970's. The operation of these hot cell facilities have been continued by the already existing organizations separately untill last March. In 1991, their management structure was reorganized to a new Department of Hot Laboratories to capitalize on existing facilities and expertise for PIE works in efficiency one another.

THE RESEARCH HOT LABORATORY [1] [2]

The Research Hot Laboratory(RHL) was built to examine nuclear fuels and materials irradiated in research or test reactors, and started operation in November 1961. Initial design of the RHL was as follows;

- 4 concrete caves for metallurgical and mechanical examination
- 2 concrete caves for chemical treatment
- 14 lead cells for radiochemical analysis
- 3 semi-hot cells for radiochemical experiment on small samples

Main PIEs in the early stage were mechanical and metallurgical examination on reactor fuels and reactor structural materials irradiated in JRR-2 or foreign country reactors.

To monitor fuels and moderator graphite samples, and to survey reactor vessel steel samples of Tokai Power Station of JAPCO, the extension of the facility was started in 1963, and completed the work in 1965. The monitoring tests on these materials have been carried out as one of the main PIEs at the RHL.

After that, further improvement makes the RHL a versatile beta-gamma hot cell facility. The latest floor layout of the facility is shown in Fig.1. Main specifications of these cells, and available techniques and equipments to the PIE in each cell are shown in Table 1 and Table 2, respectively. Figure 2 shows the relative use of the hot cells by JAERI and external organizations in Japan. The utilization for LWRs' safety-related tests including both of fuels and pressure vessel materials accounted for 45.7%, and for the high temperature gas cooled test reactor(HTTR) program for 30%. The results of PIE on these program were reported elsewhere .

Because new research and technology needs to the hot cell facility are increasing, to satisfy these needs, re-extension and upgrade of the facility have being considered presently.

THE REACTOR FUEL EXAMINATION FACILITY (RFEF) [3] [4] [5]

When LWRs were introduced in Japan, it was a matter of concern that the integrity of the fuel assembly throughout its whole life shall be verified by PIE. However, the RHL has not capability to treat full-size commercial LWR fuel assembly, construction of another hot cell facility at JAERI Tokai was decided in 1974, and the new facility RFEF started its operation in 1979.

Layout of the RFEF is shown in Fig.3. A storage pool, 6 beta-gamma concrete cells with 3 lead cells, 2 alpha-gamma concrete cells with 2 lead cells are located at the first floor. Main specifications and functions of these cells are shown in Table 3. Major advantages of the beta-gamma cells are capability to receive, store, handle, disassemble and re-assemble full-length of LWR fuel assembly and to carry out non-destructive examination for full-length fuel rods with vertical location. And also, the RFEF has JAERI's first alpha-gamma concrete cells for the PIE of advanced fast breeder reactor (FBR) fuel under development.

Fuel assemblies irradiated in power reactors are shipped to the RFEF using a special transfer cask for PIE. The fuel assembly is first inspected in the pool and cell No.1, then disassembled in the cell No.3. After fuel rod cutting, detailed destructive examinations such as metallurgical, mechanical and analytical PIE for pellets and cladding tube specimens are carried out. These PIE flow is shown in Fig.4. Following the PIEs, fuel rods are re-assembled and sent to a reprocessing plant at Power Reactor and Nuclear Fuel Development Corporation (PNC) in Tokai-mura.

So far, PIEs of 2 BWR, 6 PWR and 2 Fugen(ATR) fuel assemblies, and some gadolinia bearing and high burnup of 48 GWd/t fuel rods have been performed successfully as shown in Table 4.

THE WASTE SAFETY TESTING FACILITY (WASTEF) [6]

The safety on the long-term storage and disposal of high level waste is one of the most important part in nuclear safety. It has decided that high level waste(HLW) from fuel reprocessing plant is vitrified to solid waste, and will be storaged in deep underground in Japan. Behavior of radioactive substances released from the solid wastes in long-term storage and disposal condition is most important parameter on safety evaluation to this method, and it has to be estimate accurately. Construction of the WASTEF focusing on these experimental items was satrted in 1978. The facility is composed of 3 beta-gamma concrete cells for solidification and sampling, and 2 alpha-gamma concrete cells, 1 lead cell and 4 glove boxes for experiment and analyses. Layout of the facility is shown in Fig.5.

Main items of the examination are vitrification,radioactivity balance, homogenity, alpha radioactivity stability, volatility, leachability and devitrification tests. These tests have been carried out since 1982.

To date, more than 40 HLW vitrified samples have been produced. Following the vitrification test, samples were provided for testing on characterization of HLW glass forms, and release behavior of radioactive substances under storage and disposal conditions. In addition, an accelerated alpha radiation stability test continues in connection with characterization of returnable forms from oversea reprocessing.

Figure 6 shows a typical test result on release behavior of ^{134}Cs into the plenum of a canister from a vitrified glass for evaluation of safety in a storage condition.

SUMMARY

Hot Laboratories in JAERI Tokai are outlined their specifications, functions and their current activities. The sphere of PIE activities in these facilities will be continued extending to R & D on LWR, HTTR, fusion reactor and high level waste management. As a versatile PIE facility, the RHL will continue PIE on variety of very high radioactive samples such as fuels and materials for research and test reactors, LWR, HTTR, and fusion reactor materials. The RFEF will be used for PIE works on the high burnup and advanced fuel performance for LWRs in Japan. The WASTEF will be also available for safety research on long-term storage and disposal of high level waste.

REFERENCES

(1)S.Honma et al., Present Status of Post-irradiation Examination Facility of Japan Atomic Energy Research Institute, Proceedings of the 18th Conference on Remote Systems Technology, ANS, 1970
(2)Y.Ishida et al., PIE of HTGR Fuels and Materials -Dimension Measuring of OGL-1 Irradiated Fuels-, Proceedings of the 30th Conference on Remote Systems Technology, ANS, 1982
(3)A.Sakakura et al., Post-irradiation Examination Facility of JAERI for Power Reactor Fuels, Proceedings of the 30th Conference on Remote Systems Technology, ANS, 1982
(4)K.Iwamoto, Post-irradiation examination of power reactor fuels at the Reactor Fuel Examination Facility in JAERI Tokai, IAEA Specialists' Meeting on Examination of Fuel Assembly for Water Cooled Power Reactor, Tokyo Japan, November 9-13, 1981
(5)Y.Mishima et al., Monitoring Program for LWR Fuel Assembly Performance, ibid.
(6)S.Tashiro et al., Safety Examination of HLW Solidification Products at WASTEF, High Level Radioactive Waste and Spent Fuel Management, 1989, ANS

Table 1 Specification of hot cells in the RHL

Name of Cells	Inside Dimension W×D×H(m)	Number of Windows ※1	Gamma-Shielding ※2	Gamma-Capacity (TBq)
Clean	10 ×2.6 ×4.2	3	magnetite concrete density 3.5g/cc thickness 100cm	3.700
Dirty	12 ×2.6 ×4.2	4		3.700
Storage	4.4 ×2.6 ×4.2	2		3.700
Maintenance	3.0 ×2.6 ×4.2	1		3.700
Metallurgy A,B,C	2.4 ×2.4 ×4.1 3 cells	3	magnetite concrete density 3.5g/cc thickness 100cm	1.100
Metallurgy D	4.0 ×2.4 ×4.4	2		1.850
Chemistry	2.4 ×2.0 ×3.8 2 cells	2		370
U/M No.1～12	(1～1.6)×1.1 ×1.1 12 cells	12	Lead No.1～4 : 25cm No.5～12 : 17cm	370 18.5
Steel No.1～6	1.5 ×1.3 ×2.3	6	Lead 10cm	0.185
Junior	1.1 ×1.0 ×1.0 14 cells	14	Lead 15cm	18.5
Semi-hot	(1.0～1.2)×0.8 ×(1.0～1.2)	4	Lead 10cm	0.185
SE	2.1 ×1.3 ×1.2	2	Lead 15cm	18.5

※1. Window means working position for P I E.
※2. All of cells are non-gas tight ($\beta-\gamma$ cells).

Table 2 Available PIE items in the RHL

Name of Cells	Items of Post-Irradiation Examination
Storage	Loading, Unloading, Storage
Clean	NDE ; Visual Inspection, Dimension measurement, X-ray radiography
Dirty	Dismantling (fuel elements, Capsules) Waste disposal; Cutting, Compressing, Packaging
Maintenance	Decontamination and repair of equipment
Metallurgy	Cell A Dismantling, Storage Cell B・C Tensile test (Max. 1500 ℃), Cell D Gamma-scanning, Visual Inspection Creep test (max. 900℃) Weighing
Chemistry	・Fission gas collection (Puncture) ・Electrolytic deconsolidation and acid leaching ・Dissolution of fuel for burn-up determination
U/M No.1～12	Metallography and its preparation work ; Sampling, Mounting, Polishing, Etching, Optical micrography, Autoradiography, Hardness test, etc.
Steel No.1～6	Tensile and Compressive test, Instrumented impact test, Fracture toughness test
SE	SEM Observation, X-ray microanalysis
Junior and Semi-hot	Visual Inspection, X-ray microradiography X-ray diffraction, Compression test and Very high temperature heating of coated particle fuel

Table 3 Specification and function of hot cells in the RFEF

Cell or Pool		Inside Dimension(m)	Shielding Wall (cm)	No. of Window	Max. Activity (TBq)	Function
Pool		10x6 x15.5 (Depth)	———	———	3.6×10^{3}	Loading, Storage, Carry out Assy. or fuel rod to / from Cell No. 1 via. canal. Visual Inspection, Radiation Measurement
βγ Cell Line	No. 1	W x D x H 8.5x 3 x 12.6	120 (High Density Concrete)	8	3.0×10^{3}	Assy: Visual Inspn. & Photo., Metrology, Temp. Measurement, De-cruding Rod: Visual Inspn. & Photo., Profilometory Gamma Scanning, PCG Measurement
	No. 2	6 x 3 x 7	120	3	3.0×10^{3}	Rod: X-ray Radiography, Puncture & Gas Sampling, Eddy-current Test, Oxide Thickness Measurement
	No. 3	10 x 3x 7	120	5	3.0×10^{3}	Assy: Disassembly & Rod Extraction, Reassembly Rod: Cutting, De-fueling, Re-fabrication for Irradiation Test, SCC Test (Cladding Sample)
	No. 4	4 x 3x 4.5	100	2	3.3×10^{3}	Tensile/Compression Test, Expansion Mandrel Test
	No. 5	2.5x 3 x 4.5	100	1	3.3×10^{3}	Precise Cutting & Mounting, Micro Sampling, Higt Temp. Released FP Gas Analysis
	No. 6	6 x 3 x 4.5	100	3	3.3×10^{3}	Polishing, Etching, Macro-Photo.,
βγ Lead Cell	No. 1	1.2x 1 x 2	17.7(Lead)	1	3.7	Optical Microscopy
	No. 2	1.7x 1 x 2	17.7	2	3.7	Optical Microscopy, Micro Hardness Test
	No. 3	2 x 1 x 2	17.7	2	3.7	Micro-γ Scan, X-ray Diffraction, Ultra Micro Hardness Test, Autoradiography
αγ Cell Line	No. 1	4 x 3 x 4.5	100	2	3.3×10^{3}	Visual Inspn. & Photo., Profilometory, Gamma Scanning, Puncture & Gas Collection, Density Measurement
	No. 2	6 x 3 x 4.5	100	3	3.3×10^{3}	Sectioning & Mounting, Polishing, Etching, Macro-Photo.
αγ Lead Cell	No. 1	1.5 x1.8 x 2	17.7	1	3.7	SEM, Mosaic Photo.
	No. 2	1.3 x1.8 x 2	17.7	1	3.7	Optical Maicroscopy

Table 4 PIE schedule of WR fuels in the RFEF

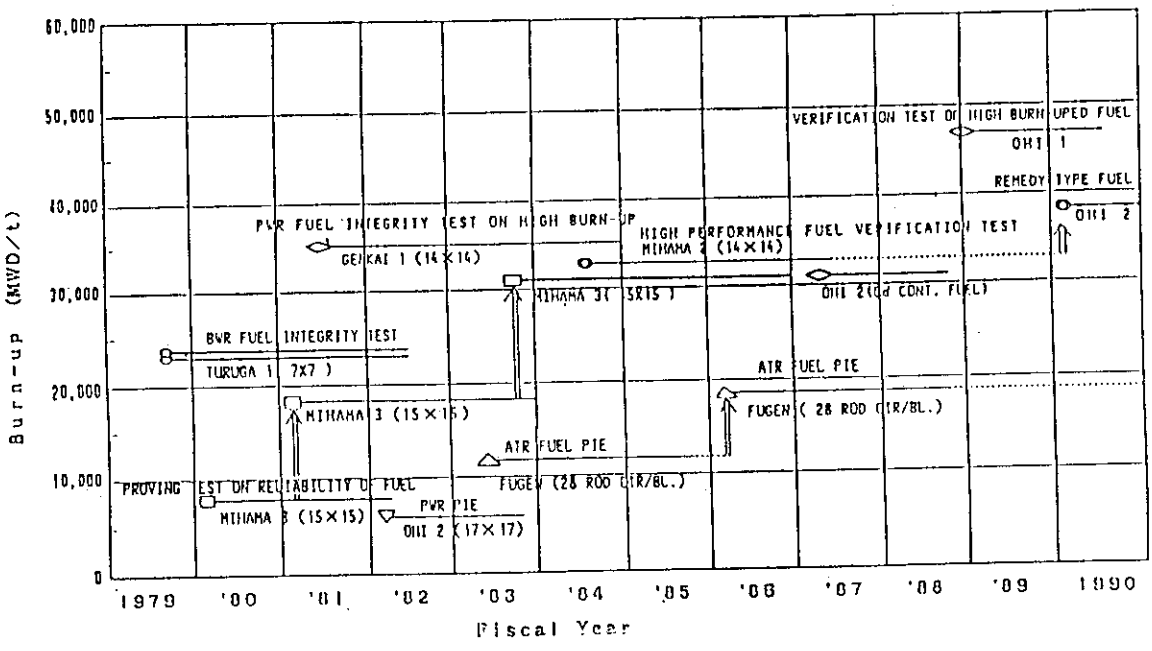

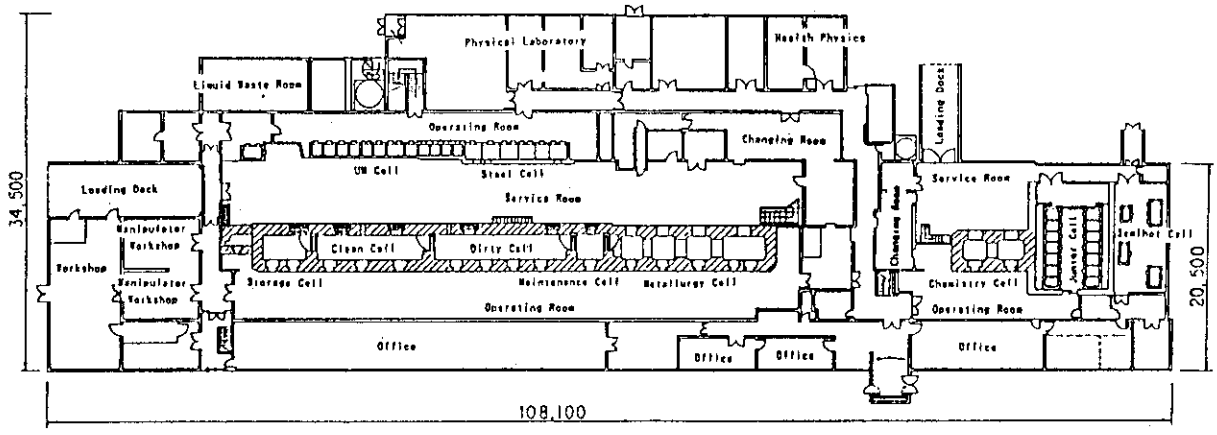

Fig. 1 Floor layout of the RHL

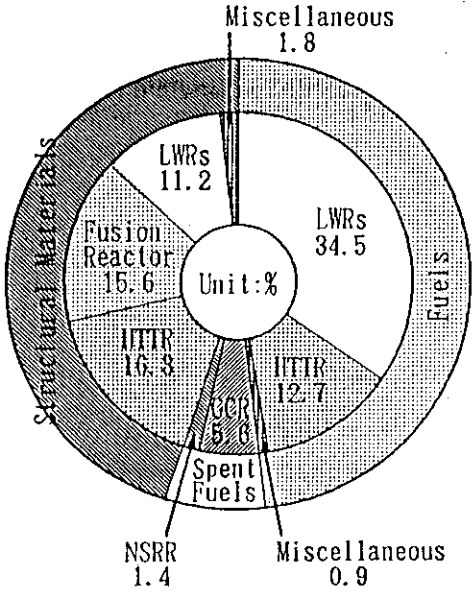

Fig. 2
Utilization of the RHL in 1990

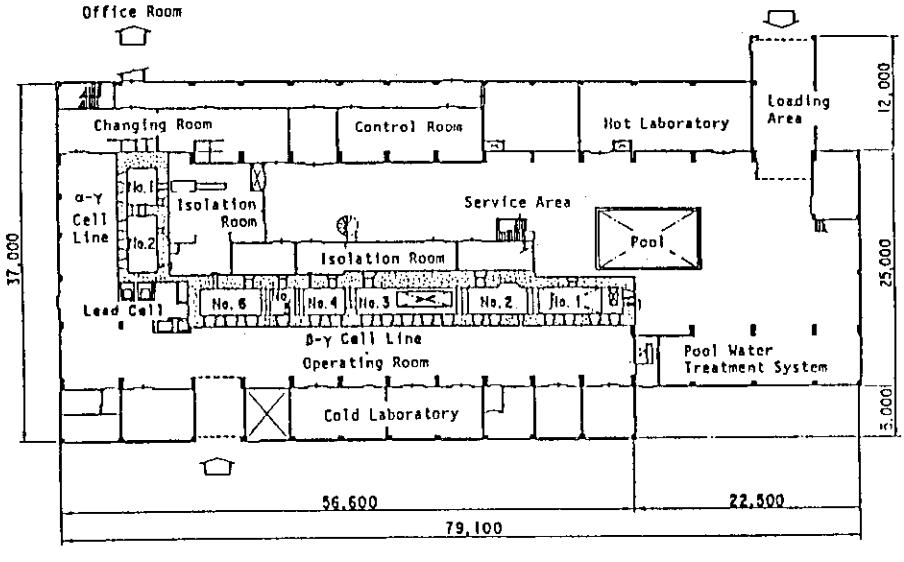

Fig. 3 Floor layout of the RFEF

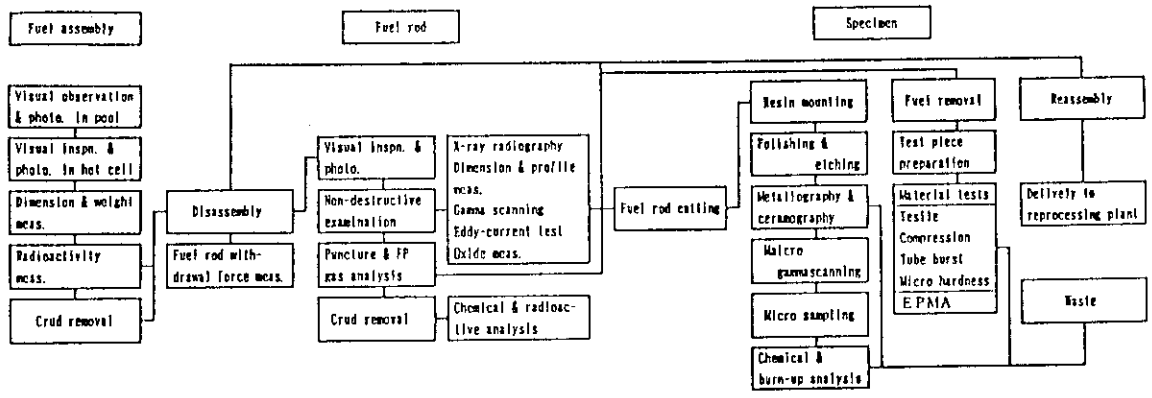

Fig. 4 Flow of Examination in the RFEF

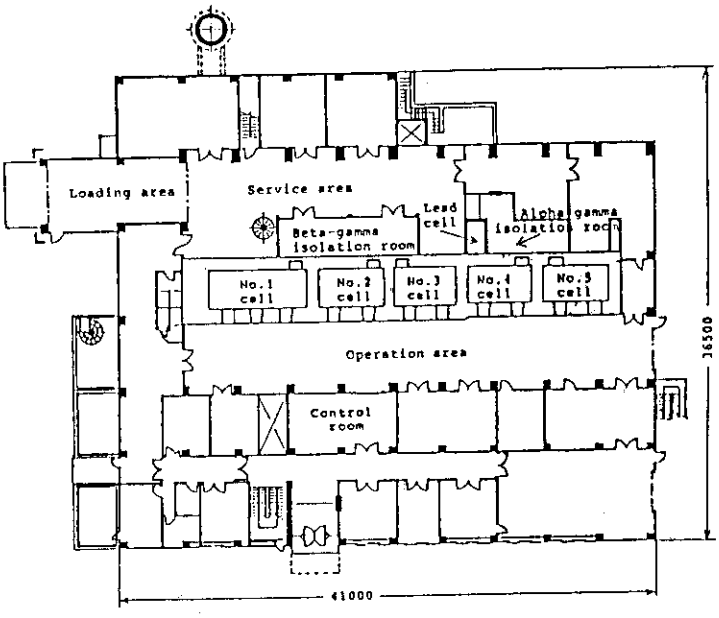

Fig. 5 Floor layout of the WASTEF

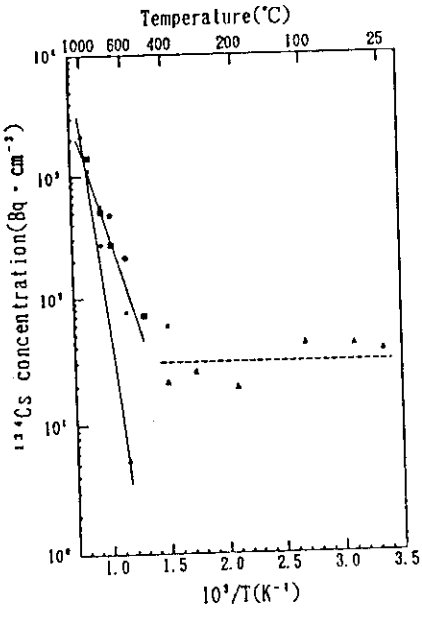

Fig. 6
Release behavior of ^{134}Cs in a canister contained vitrified glass.

2. Development Status of Post Irradiation Examination Techniques at the JMTR Hot Laboratory

M. Ohmi, K. Ohsawa, T. Nakagawa, A. Umino, M. Shimizu
H. Satoh and R. Oyamada

Department of JMTR Project
Oarai Research Establishment, JAERI
Oarai-machi Higashi-Ibaraki-gun Ibaraki-ken Japan

ABSTRACT

Hot laboratory at Oarai Research Establishment was founded to examine the objects mainly irradiated at JMTR(Japan Materials Testing Reactor) and has been operated since 1971. A wide variety of post-irradiation examinations(PIE) is available using the hot laboratory. Continuous efforts are made to develop new PIE techniques to accommodate the user's requirements.

The following are main techniques recently developed in the hot laboratory;

1. Remote capsule assembly including remote weld of irradiated objects for reirradiation in JMTR.
2. Fracture toughness tests of reactor component materials.
3. Creep tests of heat resistance alloys in high temperature conditions.
4. Tests of irradiation assisted stress corrosion cracking(IASCC).
5. Examination techniques of miniaturized test specimens.

This report describes an outline of the hot laboratory with main emphasis on the new PIE techniques.

INTRODUCTION

The hot laboratory is mainly used for examinations of nuclear fuel and materials irradiated in JMTR for light water reactors(LWR), high temperature gas reactors, fast breeder reactors(FBR), etc..

New PIE techniques are necessary to accommodate the user's requirements which reflect the theme of the time in nuclear field. The current main requirements are concerning assembly of capsule for power ramp tests of LWR fuel in JMTR. Fracture toughness tests of material, SCC tests, high temperature tests for high temperature gas reactor, miniaturized test specimens, etc..

This report describes an outline of hot laboratory with main emphasis on the new PIE techniques developed in the hot laboratory.

1. Outline of Hot Laboratory

The hot laboratory is situated adjacent to the JMTR with a canal connecting them. The canal permits the high radioactive irradiated specimens removed from the JMTR to be transferred to the hot laboratory without employing any shielding

devices, leading to a safe and efficient PIE to be performed at the hot laboratory.

The hot laboratory has three hot cell lines; a concrete cell line with lead microscope cells, a lead cell and a steel cell line. The concrete cell line is mainly used for dismantling irradiated capsules and examination of fuels. The lead line and steel line are used for mechanical property tests of irradiated materials.(1), (2), (3) Figures 1.1 and 1.2 show the hot cell arrangement and flow diagram of PIE, respectively.

2. Main newly developed PIE techniques

2.1 Remote welding machine for reirradiation in JMTR

Load following of LWR is to be necessary when fraction of its electric power to total electric power becomes high for some extent, which leads nuclear fuel in severe conditions due to pellet/clad interaction, etc..

Extensive power ramping tests of LWR fuels to investigate fuel behavior under the load following are under way using BOCA(Boiling Capsule) facility installed in JMTR. Fuel specimens irradiated in LWR are assembled into capsule in the hot laboratory for the power ramping tests in JMTR. In some case fission product(FP) gas pressure gauge is attached to end plug of fuel pin by means of welding in order to measure its pressure during the power ramping tests. The end plug is perforated by electric arc to lead FP gas pressure of fuel pin to the pressure gauge without gas release.

Remotely operated welding is a key technique in assembly of capsule for reirradiation. Specifications of welding machine are shown in a part of Table 1.

2.2 Fracture toughness tests of reactor component materials

To evaluate the integrity of reactor component materials in terms of brittle fracture, obtaining data for fracture toughness is necessary.

In nuclear field, fracture toughness tests is generally carried out using fatigue testing machine or impact testing machine, with small-sized specimens such as impact specimen and compact specimen,etc. to prevent a size effect.

Fracture toughness testing device with unloading compliance method for J_{Ic} and instrumented impact testing machine for K_{Id} (dynamic fracture toughness) were installed in the hot laboratory at the present. An outline of these is explained bellow.

2.2.1 Fracture toughness testing device with unloading compliance method

The fracture toughness testing device using hydraulic servo control type fatigue testing machine provides test temperature controlled bath and crack opening displacement measurement device , e.g. clip gauge, and laser-micro gauge, etc.. Specifications of fracture toughness testing machine are shown in a part of Table 1.

2.2.2 Instrumented impact testing machine for dynamic fracture toughness test

The impact testing machine with instrumentation to measure impact load and deflection during hammering provides an automatic specimens setting system with a robotic mechanism, which enables to hold the specimen temperature within ±2 ℃ in temperature range between around -120℃ and 200℃. In addition, instrumented edge can be exchangeable.

Specifications of impact testing machine are shown in a part of Table 1.

2.3 Remotely operated creep testing machine for heat resistance alloy

Four creep testing machines are provided in the hot laboratory in order to obtain the creep property of heat resistance alloys such as control rod cladding material(Incolly 800H), to be used in High Temperature Engineering Testing Reactor (HTTR) which is now under construction at Oarai Research Establishment.

In respect of the structural materials of HTTR, Incolloy 800H is to be used and necessitates the creep property data under high temperature inert gas atmosphere up to around 900℃ with some safety margin.

Up to present, the creep tests of irradiated heat resistance alloy were performed under only atmospheric condition for easy implementation. Therefore, the tests in inert gas condition as is the actual environment is strongly requested. In such back ground, this creep testing machine was developed at the hot laboratory.

Specifications of each testing machine are shown in Table 2.

2.4 Irradiation assisted stress corrosion cracking testing facility

Stress corrosion cracking (SCC) of LWR core structural materials is one of big problems in terms of LWR integrity. Therefore, a lot of studies on SCC were so far done. Recently affections of neutron and gamma rays on SCC are taken up. (4) To study the affections, a testing facility for irradiation assisted stress corrosion cracking (IASCC) is recently provided in the hot laboratory.

The purposes of the testing facility of IASCC are to study the initiation mechanism of IASCC and growth mechanism on stainless steel at high temperature and in highly pressurized water of which quality is electro-chemically controlled, and is to define the sensibility on the SCC of irradiated materials.

The testing facility consists of slow strain rate tensile(SSRT) testing machine with a single axis type and an autoclave to provide corrosive water environment with high temperature and highly pressurized water which were installed in inside the hot cell, and water purification/circulation system to control the water quality, instruments and control panels for test operation, data processor, etc. which were set up in outside the hot cell, i.e. operation room.

Those apparatuses were designed and manufactured in such that the autoclave was remotely sealed up with manipulators by means of adoption of hanging type specimen clamp method and O-ring seal system with clutch mechanism. Furthermore, this testing facility has adopted many ideas e.g. double filters system set up in the test loop so as to prevent the inflow of the radio-active fragments from the specimen, and automatic conductivity measurement system of corrosive water (inlet and outlet), etc..

Specifications of SSRT testing machine and facility are shown in a part of Table 1.

2.5 Examination techniques of miniaturized test specimens

The use of miniaturized test specimens is indispensable for evaluating mechanical property in particular in the research and development of materials for the fusion reactors due to small space available for irradiation in accelerators where neutron energy as high as fission neutron energy is available. (5) The hot laboratory has performed technical development of the tests in cooperation with material researchers at JAERI, since 1987.

As test methods for evaluating mechanical properties of miniaturized specimens, small punch testing method, desk bend testing method, uni-axial micro -tensile testing method, micro-hardness testing method and high speed punch testing method are planned. In implementation of these methods, handling technology(i.e. identification, separation and storage technology) and fabrication technology as well as accurate displacement measurement technology are necessary to be developed.

Small punch testing device and electric discharge fabricating machine has been installed in the hot laboratory at the present. An outline of these is explained bellow.

2.5.1 Small punch testing machine

The small punch testing device provides an automatic specimens exchanger

with a turntable which can perform the test of 12 specimens in a batch in vacuum condition and in temperature range from around -120 ℃ to around 800℃.
Specifications of SP testing machine are shown in a part of Table 1.

2.5.2 Electric discharge fabricating machine
This machine is used to fabricate micro-tensile specimen and micro-fatigue specimens from irradiated TEM(Transmission electron microscope) with $\phi 3 \times 0.25$ mm and small punch specimen fabricated from charpy impact specimen of which test is finished, and consists of electrode mechanism with X, Y and Z axises-numerical control, fabricating stage and liquid tank, fabricating liquid circulation pump, filter and controller. Specifications of electric discharge fabricating machine are shown in a part of Table 1.

3. Conclusions
New PIE techniques are continuously developed in the hot laboratory associated to JMTR in order to accommodate the user's requirements. Prior to appling the new techniques, the functions including remote manipulation ability are carefully confirmed.
PIE techniques presently strongly required to be developed are to obtain accurate displacement measurement of specimens at high temperature, to perform tests with miniturized test specimens and to prepare specimen from irradiated materials. In addition, further reinstrumentation techniques on BOCA capsules for center temperature measurement, etc. are also urgent development works. Therefore the hot laboratory's works are mainly focussing on them at the present.
The hot laboratory is making a great endeavor to develop new PIE techniques to accommodate the user's requirements in parallel to the routine works.

4. Acknowledgements
We gratefully acknowledge Dr. Y. Futamura, the director and Mr. M. Saito, the deputy director of Department of JMTR Project for encouragement. They also acknowledge staff members of the hot laboratory by describing that PIE techniques presented here are the results of their efforts with strong cooperation.

References
(1) A. Sakakura et al.; Post Irradiation Examination of Status (1), (2). Nuclear Industry Vol. 34, No. 5 ~Vol. 34, No. 7 (1988).

(2) Dep. of JMTR Project.: JMTR Operation and Technical Development-No. 4, JAERI-M-90-189(1990).

(3) N. Tsuyuzaki et al.: General Description of Irradiation and Post Irradiation Examination in JMTR, JAERI-M-86-164(1986).

(4) W. R. Clarke et al.: Dynamic Straining Stress Corrosion Test for Predicting Boiling Water Reactor Materials Performance. ASTM STP 665, pp. 149-169 (1979)

(5) W. R. Corwin et al.: The Use of Small-Scale Specimens for Testing Irradiated Materials. A symposium sponsored by ASTM Committee E-10 on Nuclear Technology and Applications Albuquerque N. M., 23 Sept. 1983.

Table 1　Specification of each testing machine

testing machine	Item and specification
Welding machine	①Type of welding machine ;Tungsten inert gas(TIG) method ②Environment of welding ;Inert gas(He) ③Output voltage ;20V ④Output current ;75A ⑤Size of tube ;ϕ 3～ϕ50 (Diamater of tube) 0.13～3.2mm(Thickness of tube)
Fatigue testing machine	①Type of machine ; Hydraulic servo control type ②Capacity ; 1×10^5 N ③Test temperature ; -150 ℃～500 ℃ ④Test method ; Unloading compliance method
Impact testing machine	①Type of machine ; Charpy type ②Capacity ; 3 $\times10^2$J ③Test temperature ; -120 ℃～200 ℃ ④Setting of specimen ; Automatic robot system ⑤Form of specimen ; $10^{W}\times10^{H}\times55^{L}$mm or $10^{W}\times5^{H}\times55^{L}$mm
SSRT (slow strain rate test) testing machine	(1) SSRT testing machine ①Max. load ; 2.9× 10^4 N ②Tensile speed ; 1.0～ 1×10^{-5} mm/min (2) Autoclave ①Volumetric capacity ; 1.9 ℓ ②Max. test temperature ; 300 ℃ ③Max. test pressure ; 9.8 MPa (3) Displacement measurement device ①Type ; Strain meter type ②Detection method ; Pull rod displacement (4) Instrument, etc. ①Desolved Oxygen meter, ②Liquid electric conductivity meter ③pH meter
SP(small punch) testing machine	①Max. load ;5 $\times10^3$ N ②Test speed ;0.01mm～ 1mm ③Punch stroke ;10 mm ④Test temperature ;-120℃～ 800℃ ⑤Specimen set quantity ;12 test specimens ⑥Test environment ;Vacuum ⑦Extensionmeter ;Digital gauge (2μm)
Electric discharge fabricating machine	①Electrode ;Cu-Cr ②Controller ;X,Y,Z automatic control ③Processing voltage ;3 V ～125V ④Processing stage ;$200^{W}\times125^{D}\times50^{H}$mm

Table 2 Specification of each creep testing machine

Machine No. / Items	1	2	3	4
①Type of lever	Single		Same as left	
②Load capacity	1 $\times 10^4$N		5 $\times 10^3$N	Same as left
③Temperature	Max. 1000℃		Same as left	
④Size of specimen	ϕ 4, ϕ6		ϕ 4	Same as left
⑤Environment	Vacuum or inert gas		Same as left	
⑥Weight unit for loading	hand-operated		Automatic	Same as left
⑦Displacement measurement	Digital gauge Diale gauge		Same as left	Laser-micro gauge Digital gauge

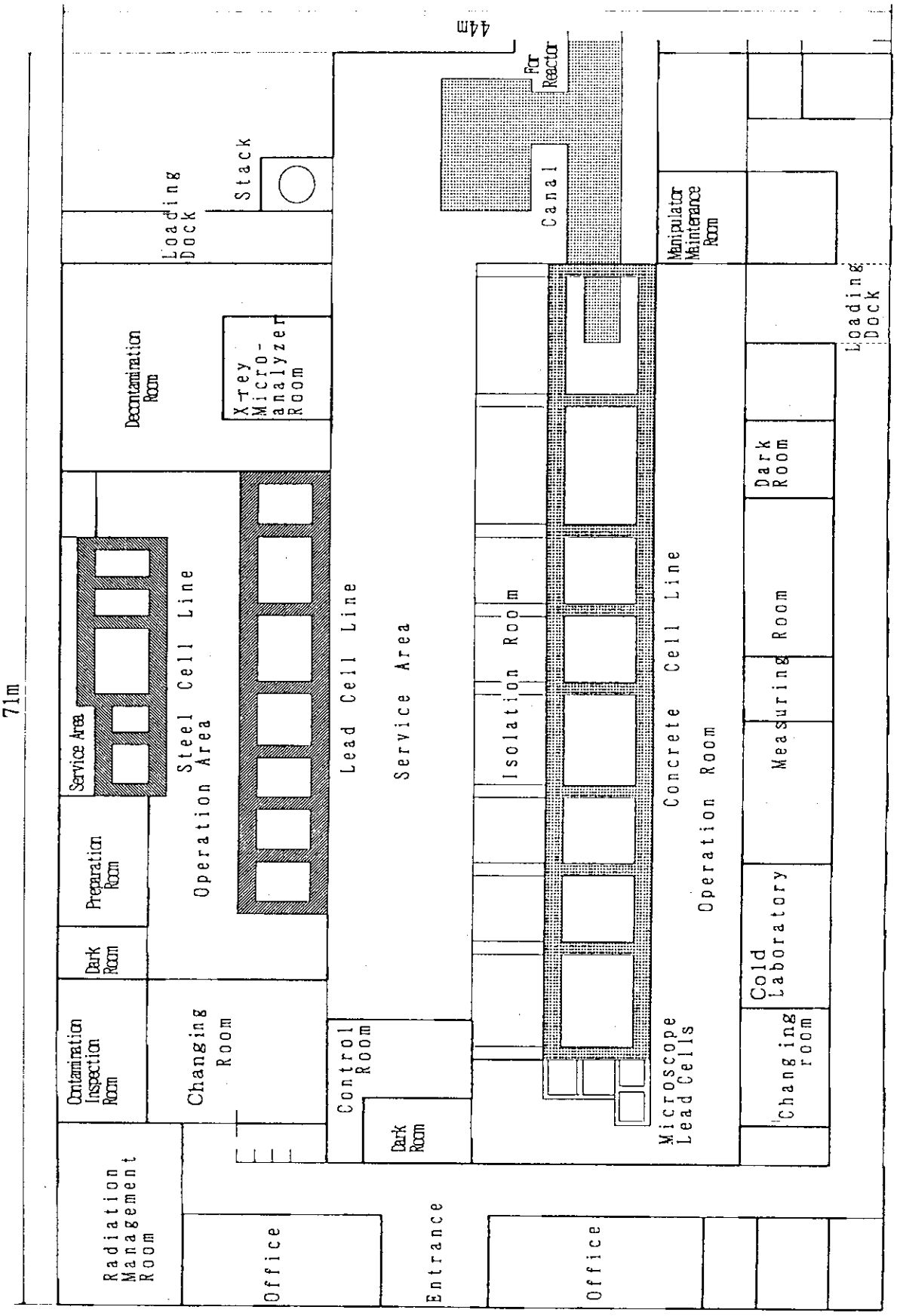

Fig. 1.1 Arrangement of the Hot Laboratory

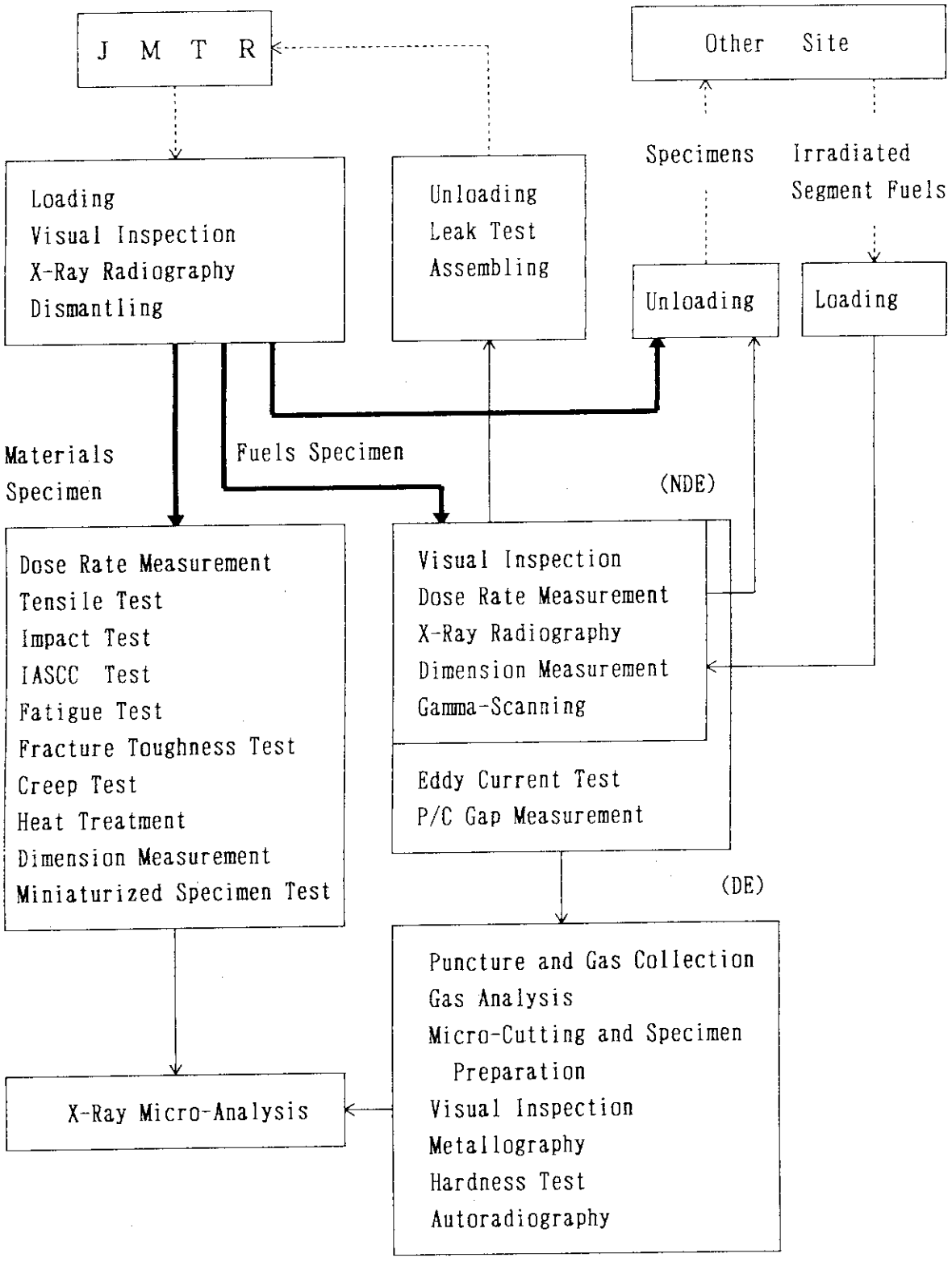

Fig. 1.2 Flow diagram of PIE

3. Post Irradiation Test Facilities for Irradiation Assisted Stress Corrosion Cracking Research

T. TSUKADA[1], K. SHIBA[1], M. OHMI[2], M. KIZAKI[3], H. MATSUSHIMA[3], AND H. NAKAJIMA[1]

[1]Department of Fuels and Materials Research
[2]Department of JMTR Project
[3]Department of Hot Laboratories
[1,3]Tokai Research Establishment, JAERI
Tokai-mura, Naka-gun, Ibaraki-ken 319-11
[2]Oarai Research Establishment, JAERI
Oarai-machi, Higashi-Ibaraki-gun, Ibaraki-ken 311-13
Japan

ABSTRACT

Irradiation Assisted Stress Corrosion Cracking is a common environmental degradation phenomenon of structural materials in nuclear reactor cores. It has been recently considered as a life/function-limiting phenomenon not only for core internals in light water reactors but also for plasma facing water-cooled structures in proposed fusion reactor designs. At JAERI IASCC research program has been performed since 1988, which includes the development of post irradiation test facilities for stress corrosion cracking testing in high temperature water and electrochemical corrosion testing by remote operations.

INTRODUCTION

The structural materials of core internal components (e.g. top grid, core shroud in LWR) have been suffered from environmental degradation caused by the synergistic effect of neutron/gamma radiations and aqueous environment. In the materials radiation accumulates various kinds of effects. Neutron irradiation, for instance, induces lattice defects formation, H and He generations, and enhanced/induced change of metallurgical microstructures. Radiations affect also both thin oxide film formed the alloy surface and aqueous chemical environment. Radiolysis of water and formation of radical species in the core are considered to be accelerating factor for corrosion processes through increasing electrochemical potential of the alloys.

As a consequence of such synergistic effects intergranular crackings of solution annealed austenitic stainless steels served in reactor cores have been experienced and it has been termed "Irradiation Assisted Stress Corrosion Cracking (IASCC)"(1). IASCC has been, in recent years, given

intensive attentions as a common environmental degradation phenomenon of core internal structures specifically from a viewpoint of life extension of LWR power plants. JAERI had initiated the study of IASCC in 1988 which involved developments of post irradiation test facilities for this purpose.

IASCC is relating to various physical and chemical processes, therefore, to clarify the mechanism of this phenomenon an effective combination of experimental techniques is necessary. Susceptibility of stress corrosion cracking in aqueous environment has to be evaluated by post irradiation experiments. To interpret SCC behavior, information of corrosion characteristics of irradiated alloys is one of important items.

At JAERI for IASCC research Slow Strain Rate Technique (SSRT) and electrochemical measurement technique have been applied to materials irradiated in reactors. In order to perform the tests on the heavily irradiated specimens the facilities were designed to be compact and suitable to remote and safe operations of specimens and equipments in the hot cells. In the following parts the constructions and specifications of these facilities and typical test results are described.

SSRT TEST FACILITY

SSRT is widely adopted for SCC testing that can produce quantitative data in short testing time to evaluate SCC susceptibility of alloys. Concept of SSRT is a tensile test at very slow and constant strain rate (e.g. 10^{-7} sec^{-1}) in corrosive environment(2).

The post irradiation SSRT test facility at JAERI consists of SSRT test machine, recirculating water loop system and electric control panels. SSRT test machine was installed in lead hot cell at Oarai hot laboratory in 1990 which was arranged for material testings. Handling capacity of active materials in the cell is 37 GBq (equivalent ^{60}Co). Fig.1 shows a simplified flow diagram. Dissolved oxygen (DO) concentration can be controlled in the system. On Table 1 key specifications of the facility are summarized. The system has been operated without trouble more than 2000 h so far.

WATER LOOP SYSTEM

This system consists of three subsystems located outside hot cell and coupled to test section of SSRT test machine as shown in Fig.1. In the water makeup system DO level is controlled in treatment tank by bubbling of argon gas or argon/oxygen mixture gas. During tests of heavily irradiated specimens radioactive crud, i.e. corrosion products, might be released from the specimen and transferred into water loop system. Contamination of piping system will be a possible future problem of the facility maintenance, therefore at the outlet position from the hot cell high pressure filters are equipped doubly. Those are sintered stainless steel filters of 10 μm and 40 μm mesh respectively. Water chemistry is monitored in this system and monitored parameters are DO level, electric conductivity and pH level. Monitoring data are recorded by computer system together with data of test temperature and pressure. Before water is sent back to water makeup system, it is fully deionized by a ion exchanger. To cope with a case of water leakage, the system parts except heat exchanger and preheater on top of the hot cell are placed in a house made of acrylic panels and stainless steel frame.

SSRT TEST SECTION

Construction of test section is shown in Fig.2. Handling of irradiated specimen and sealing of autoclave are performed by two manipulators. In order to fix autoclave cover to autoclave body a clutch sealing mechanism was developed. Fig.3 explains schematically this mechanism. Bottom of autoclave cover has ridges and this part is moved down into clutch. Then the handle equipped on the clutch is rotated by manipulator and the cover is pressed and fixed on the body.

Monitoring of electrochemical potential of specimen during SSRT test offers an important information about cracking process. On the bottom of autoclave an Ag/AgCl type external reference electrode is equipped for potential measurement.

Load applied on specimen is monitored with load cell equipped outside autoclave. To minimize the friction a diameter of pull rod made of Hastelloy C-276 was reduced to required minimum size. Internal pressure compensator is also equipped to improve an accuracy of load measurement. A program controller monitors output of extensometer and controls cross head speed. Computer system inputs actuation data into program controller. Conditions of load and extension are recorded by computer.

Fig.4 shows a specimen gripping system which is designed for flat specimen. Thickness of the specimen is 0.8 mm, total length is 45 mm and width of gage section is 2 mm. To fix it on gripping system by manipulators simple mechanism was developed. Pins standing on the chucks align the specimen and filed grip plates lock up it by tightening a bolt. Gripping system set up a specimen is mounted in the autoclave as shown in Fig.5.

SSRT TEST OF IRRADIATED SPECIMEN

SSRT test was performed on the specimen which had been irradiated up to 2×10^{26} n/m^2(>0.1MeV) and 97 appmHe at 400°C under spectrally-tailored condition in Oak Ridge Research Reactor. Specimen material is solution annealed type 316 stainless steel. The test was carried out at a extension rate of 1.8×10^{-4} mm/min, temperature of 300°C, pressure of 9.5 MPa and DO level of 32 ppm. Fig.6 shows intergranular fracture surface observed after test by scanning electron microscope. IGSCC fracture of this specimen originally confirms that alloy irradiated under simulated fusion device condition has a susceptibility of IASCC in high temperature pure water(3).

ELECTROCHEMICAL MEASUREMENT FACILITY

Electrochemical measurement technique has advantages to apply for post irradiation test by reasons of continuous and remote monitoring of data, moderate test solutions compared with chemical corrosion tests, and relatively short test time. Electrochemical Potentiokinetic Reactivation (EPR) test is a promising technique to adopt electrochemical technique to irradiated materials. It was developed to investigate the thermally induced sensitization of austenitic stainless steels(4). Applicability of this test to detect irradiation induced sensitization has been explored at some hot laboratories(5) as well as at JAERI's present facility which was installed in lead hot cell at Tokai hot laboratory in 1989.

Fig.7 shows an arrangement of the facility. For handling of irradiated specimens, constructions of specimen holder and electrochemical cell

were designed simply. Fig.8 shows a schematic view of three electrodes immersed in test solution in electrochemical cell. Irradiated specimen in size of 10x10x2 mm is mounted in epoxy resin with lead metal bar (dia. 6 mm). Mounting in resin makes it easy to polish specimen surface before test and metallurgical examination after measurement.

After polishing specimen surface it is set into the specimen holder and the electrochemical cell made of acrylic resin. From outside cell test solution is filled in the electrochemical cell and nitrogen gas is bubbling to purge dissolved oxygen in solution. Measurements are performed automatically by computer software (EG&G PARC Model 273) installed in IBM PS/2 computer system. Test solution is contaminated by measurements and drained to tank in isolation room.

EPR TEST OF IRRADIATED MATERIAL

EPR tests were performed on irradiated specimens(6). Specimen material is 10% cold worked type 316 stainless steel irradiated in the experimental fast breeder reactor "JOYO" at 400°C as a wrapper tube of fuel assembly. Neutron fluence is $4x10^{26}$ n/m^2(>0.1 MeV). Test solution is 0.5M H_2SO_4+0.01M KSCN controlled at 30°C. Fig.9 shows a result of single loop EPR measurement. As shown in Fig.9 on irradiated specimen a reactivation peak of current density curve was observed. It means some parts of surface passive film were not sound and reactivated on the specimen. Thermally sensitized stainless steel shows similar reactivation peak caused by Cr depleted zone formed along grain boundaries. Optical microscopy, however, showed that on the irradiated specimen grain faces were etched rather than grain boundaries. Therefore it is considered that neuron irradiation accumulates damages in matrix of the alloy and degrades corrosion resistance of grain faces. It might affect the stress corrosion cracking behavior.

CONCLUDING REMARKS

Two types of post irradiation test facilities had been developed at JAERI hot laboratories for Irradiation Assisted Stress Corrosion Cracking (IASCC) research. SSRT test facility was designed to investigate SCC susceptibility of irradiated specimens in high temperature pure water. Electrochemical measurement facility is utilized to study corrosion behavior of irradiated materials. These facilities have already produced informative data from stainless steel specimens irradiated in reactors. Details of the results will be reported and discussed in separate papers(3,6).

REFERENCES

(1) P.L.Andresen et al, Proc. Environmental Degradation of Materials in Nuclear Power Plant Systems - Water Reactors, NACE, 1990, pp.83-120.
(2) ASTM STP 665, edited by G.M.Ugiansky and J.H.Payer, ASTM, 1979.
(3) T.Tsukada et al, to be presented in CORROSION/92, NACE, 1992.
(4) W.L.Clarke, NUREG/CR-1095, 1980.
(5) T.Inazumi et al, Corrosion 46(10), 1990, pp.786-792.
(6) T.Tsukada et al, Proc. Fushoku-Boshoku'90, JSCE, 1990, pp.83-86(Jap.).

Table 1 Specification of SSRT test facility

Load capacity	30 kN	Flow rate (fixed)	5 litter / h
Cross head speed	$1x10^{-5}$～1mm/min	Dissolved oxygen(DO)	0.01～32 ppm
Test temperature	Max. 300 ℃	Monitoring capacity	DO,CON,ECP,pH
Test pressure	Max. 10 MPa	Autoclave volume	1.7 litter

(Note) CON : Conductivity, ECP : Electrochemical potential

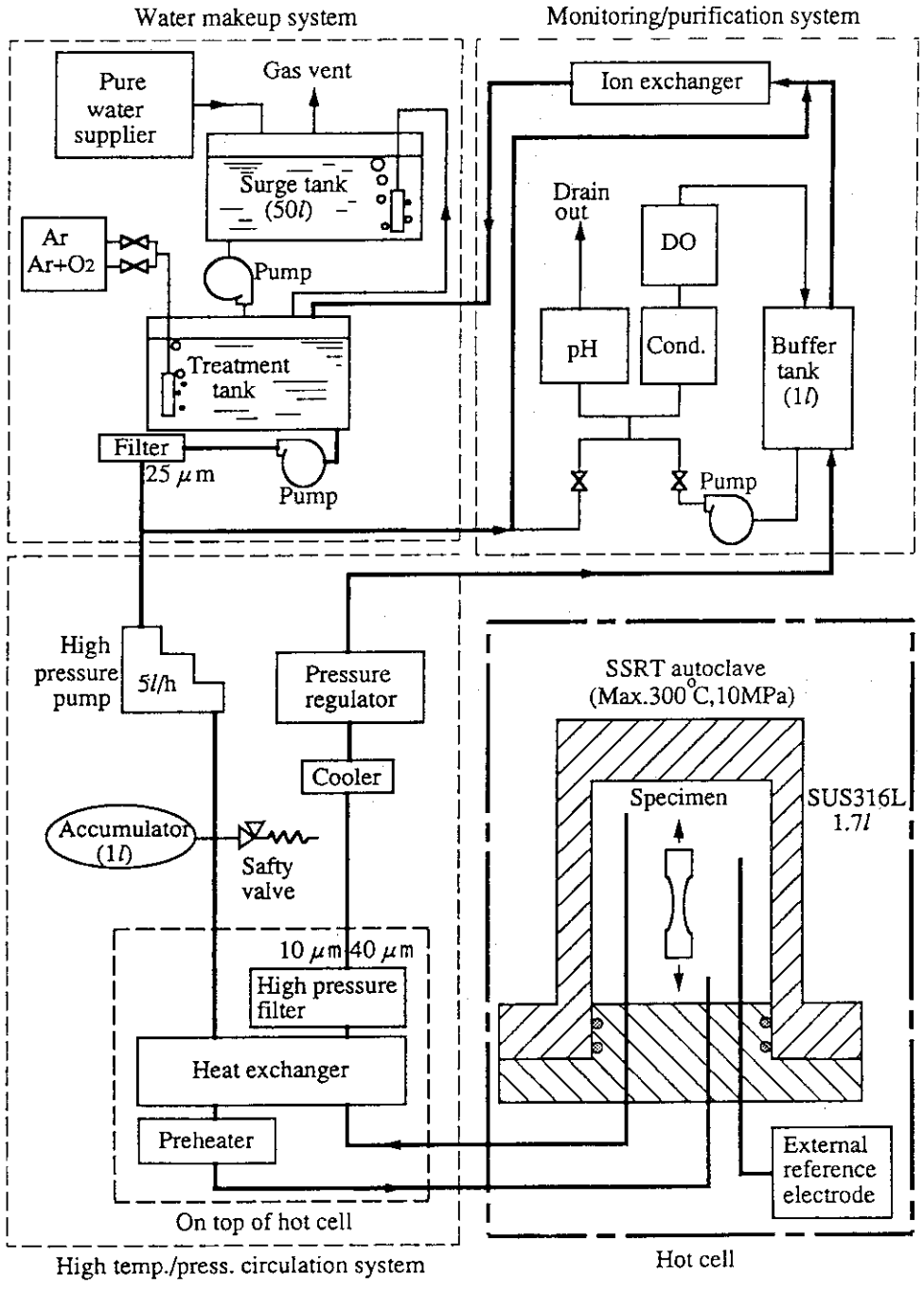

Fig.1 Flow diagram of SSRT test facility

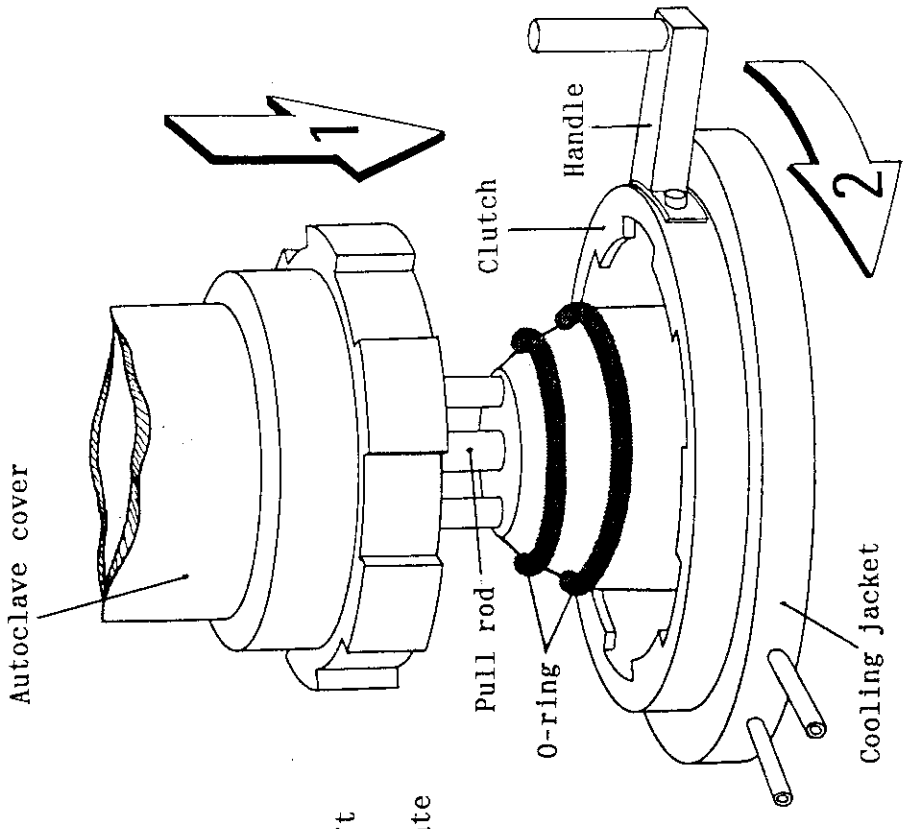

Fig.3 Schematic of clutch sealing mechanism of autoclave

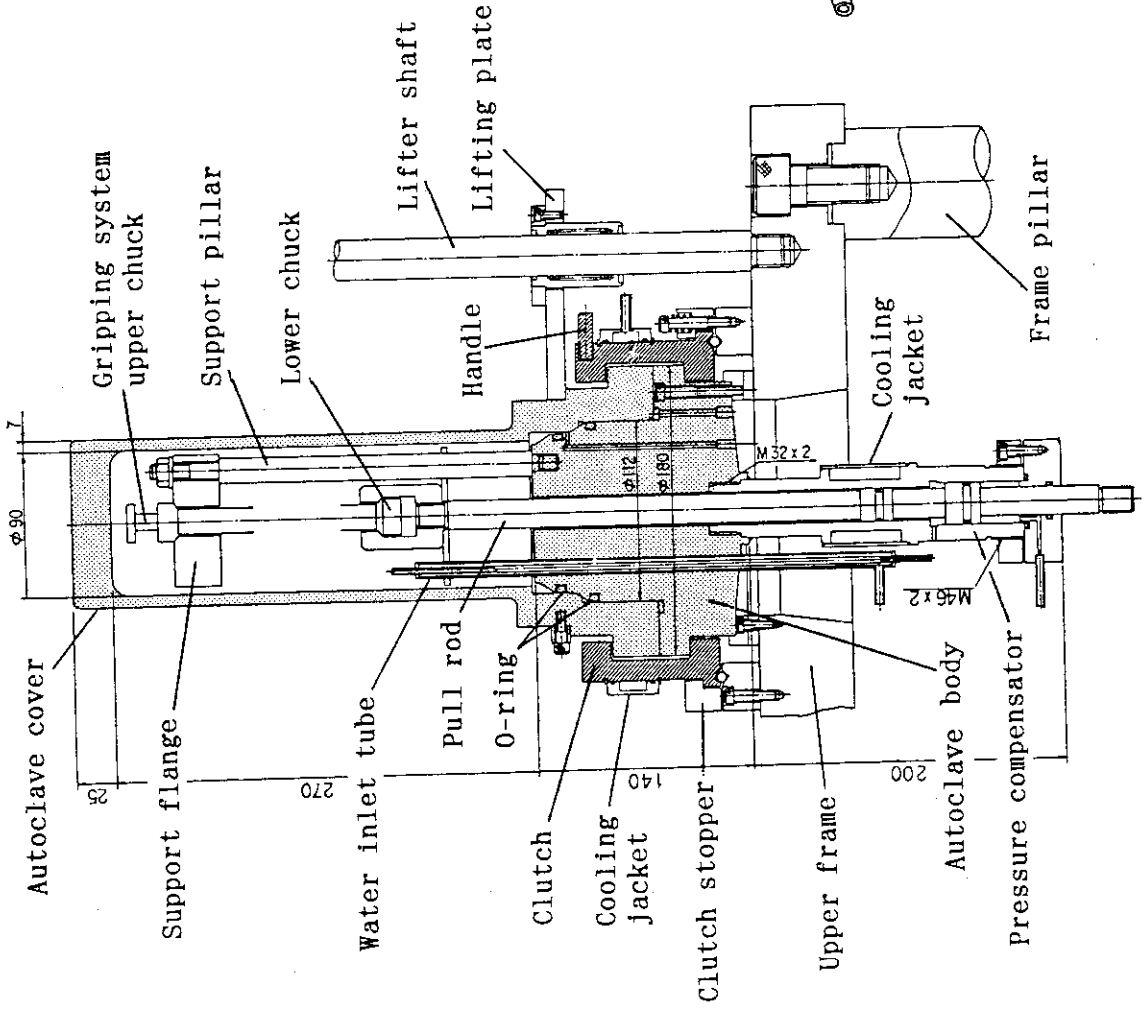

Fig.2 Test section of SSRT test machine

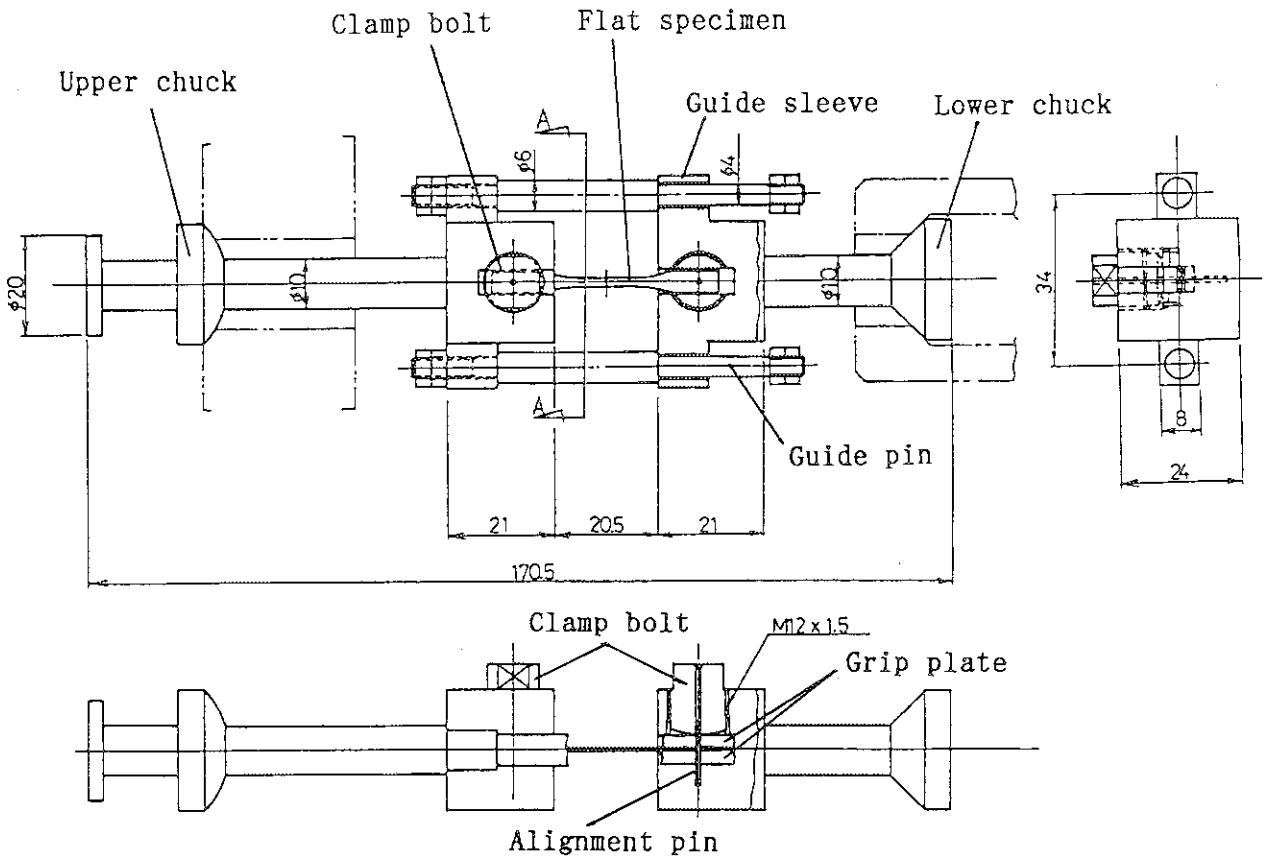

Fig.4 Gripping system for flat type specimen

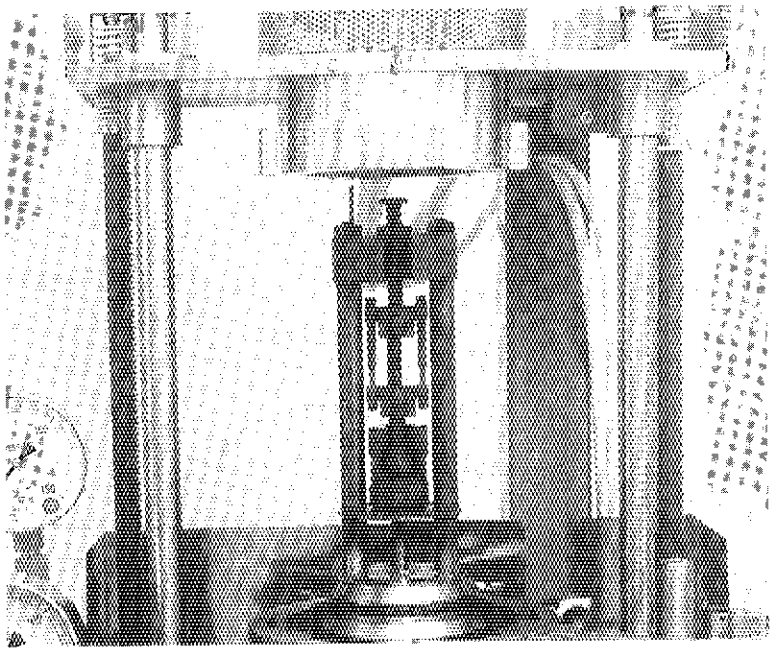

Fig.5 Gripping system mounted in autoclave

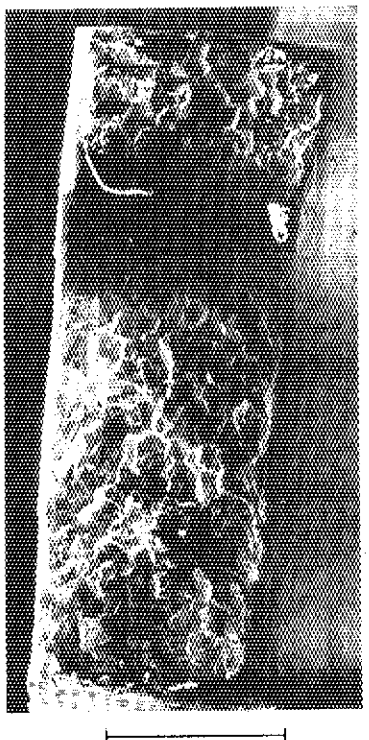

Fig.6 IGSCC fracture of irradiated type 316 stainless steel

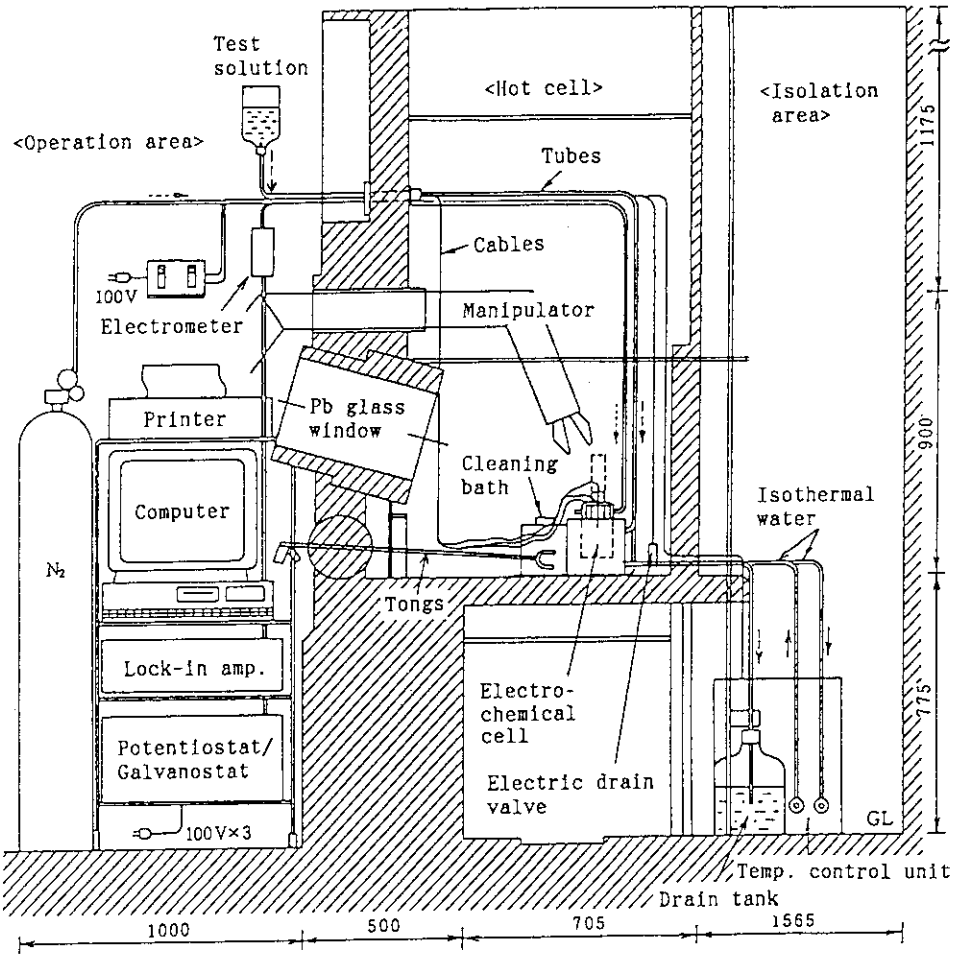

Fig.7 Electrochemical measurement facility

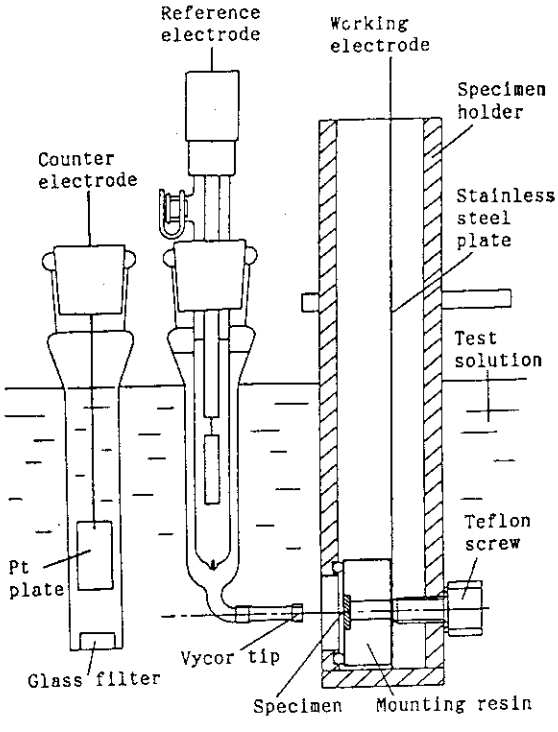

Fig.8 Electrodes set up in electrochemical cell

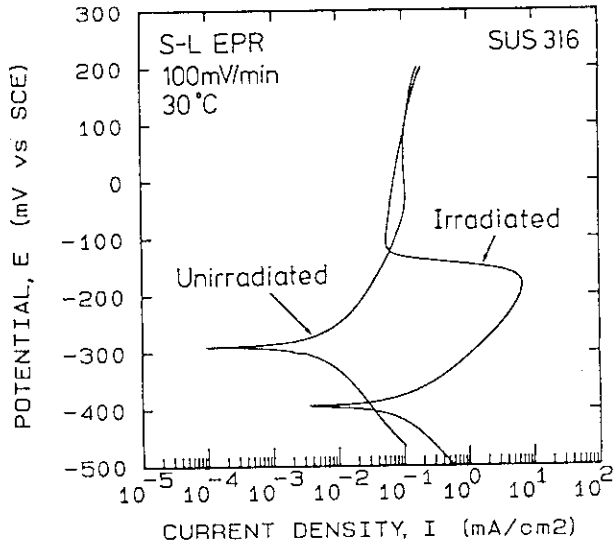

Fig.9 Result of EPR measurement on irradiated type 316 stainless steel

Closing Remarks

Eiji SHIRAI

Excutive Secretary

Director, Department of Research Reactor
Tokai Research Establishment
Japan Atomic Rnergy Research Institute

Ladies and Gentlemen;

On behalf of the Japan Atomic Energy Research Institute, I am honored to address this closing remarks of the Third Asian Symposium on Research Reactor. I heartily appreciate your participation and contribution to this symposium.

During this Symposium, we could have 301 participants including 62 participants from overseas. Finally, 77 of highly technical and very interesting oral presentations have been contributed in this Symposium.

For instance, the special talk on the latest ANS project presented by Dr. Colin D. West is very impressive for us who have been engaged in the field of fission reactors. It is expected to contribute for technical development in various fields.

And introduction of the examination and evaluation guide of water-cooled research reactors established in Japan, which is presented by Dr. Fujio Yoshino of STA, is expected to give us a useful guidance.

We also have had various significate information from the other presentations. We feel that this symposium encouraged us for future research reactor activities.

We, herewith, would highly appreciate the contributors and participants again. We would like to express our appreciation to the Science and Technology Agency, the Atomic Energy Society of Japan and the Japan Atomic Industrial Forum for their collaboration.
Thanks are also due to the members of the symposium secretariat for their sincere contribution to this symposium.

The efforts to organize the next symposium have been continued in our committee. We expect many countries will offer to hold the next symposium.

Thank you for your cooperation, and see you again at the next symposium.

LIST OF PARTICIPANTS

ADIWIJAYA, Yunus Hasan	Badan Tenaga Atom National, Indonesia
ANTHONY, Simanjuntak	Badan Tenaga Atom National, Indonesia
BAKRI, Arbie	Badan Tenaga Atom National, Indonesia
BUSAMONGKOL, Yuthapong	Office of Atomic Energy for Peace, Thailand
CHAO, Guo-Gin	Nuclear Power Institute of China, People's Republic of China
CHOU, Hwai-Pwu	Taiwan
DERA ROSA, Alumanda M.	Philippine Nuclear Research Institute, Philippines
DEWI, Usmiyanti	Indonesia (Presentry, staying at Tokai University, Japan.)
DEWITA, Erlan	Indonesia (Presentry, staying at Tokai University, Japan.)
FAN, Xuegang	Beijing Institute of Nuclear Engineering, People's Republic of China
FANJAS, Yves	CERCA, France
GANLEY, John T.	General Atomics, USA
GITAWATI, Iswani	Badan Tenaga Atom National, Indonesia
HAMZAH, Amir	Badan Tenaga Atom National, Indonesia
HSU, Jin Den	Taiwan
HUBIES, Hisyam	Badan Tenaga Atom National, Indonesia
JUN, Byung Jin	Korea Atomic Energy Research Institute, Korea
KABIR, Enamul	Bangladesh Atomic Energy Commission, Bangladesh
KASSIM, Mohammad S.	Ministry of Science, Technology & Environment, Malaysia
KIM, Kwang-Rag	Korea Atomic Energy Research Institute, Korea
KITVITAYASAK, Sureerat	Ministry of Public Health, Thailand
KUNTORO, Iman	Badan Tenaga Atom National, Indonesia
LEE, Albert G.	Atomic Energy of Canada Ltd., Canada
LEE, Hoo-Kun	Korea Atomic Energy Research Institute, Korea
LUONG, Dang Thang	Vietnam National Atomic Energy Commission, Vietnam
MANNAN, Muhammad A.	Bangladesh Atomic Energy Commission, Bangladesh
MARDHA, Amil	Indonesia (Presentry, staying at Tokai University, Japan.)

McCORMIK, Gerry	Babcock & Wilcox, USA
MIN, Duck-Kee	Korea Atomic Energy Research Institute, Korea
MOHAMED, Abdul Aziz	Ministry of Science, Technology & Environment, Malaysia
MONGKULMANN, Chothip	Office of Atomic Energy for Peace, Thailand
NACCACHE, Samir J. P.	CERCA, France
PARK, Won Seok	Korea Atomic Energy Research Institute, Korea
PREBLE, Harry	Babcock & Wilcox, USA
RHEE, Chang-Kyu	Korea Atomic Energy Research Institute, Korea
SALIMIN, Zainus	Badan Tenaga Atom National, Indonesia
SANGUENSAT, Attakovit	Depertmant of Medical Sciences, Thailand
SARWANI	Badan Tenaga Atom National, Indonesia
SARYATI	Badan Tenaga Atom National, Indonesia
SHIM, Sang Yong	Atomic Energy of Canada Ltd., Canada
SOENARJO, Sunarhadijoso	Badan Tenaga Atom National, Indonesia
SRI WARDANI	Indonesia (Presentry, staying at Rikkyo University, Japan.)
SUFI, Mohammad A. B.	Ministry of Science, Technology & Environment, Malaysia
SUGIYANTO, Muhammad	Indonesia (Presentry, staying at Tokai University, Japan.)
SUYITNO	Badan Tenaga Atom National, Indonesia
SYARBAINI	Badan Tenaga Atom National, Indonesia
UDI, Achidiat	Badan Tenaga Atom National, Indonesia
VERA, Cecilia	Philippine Nuclear Research Institute, Philippines
WAN ABDULLAH, Wan Saffiry	Ministry of Science, Technology & Environment, Malaysia
WAN, Mingzhi	China Institute of Atomic Energy, People's Republic of China
WANG, Rengtao	Beijing Institute of Nuclear Engineering, People's Republic of China
WANG, Zhi-Yong	Shanghai Nuclear Engineering Research and Design Institute, People's Republic of China
WEI, Tsong-Yang	Taiwan
WEST, Colin D.	Oak Ridge National Laboratory, USA
WHITTEMORE, William L.	General Atomics, USA

WURYANTO	Badan Tenaga Atom National, Indonesia
ZHAO, Peng Ji	South-West Institute of Nuclear Physics and Chemistry, People's Republic of China
ZUHAIR	Indonesia (Presentry, staying at Rikkyo University, Japan.)
AIZAWA, Otohiko	Musashi Institute of Technology , Japan
AOYAMA, Takafumi	Power Reactor and Nuclear Fuel Development Corp., Japan
FUJINE, Shigenori	Kyoto University, Japan
HARASAWA, Susumu	Rikkyo University, Japan
HAYASHI, Shuhei	Rikkyo University, Japan
HIBIKI, Takashi	Kyoto University, Japan
HIRAMATSU, Ichiro	Pechiney Japon, Japan
HIROTA, Jitsuya	Mitsubishi Atomoic Power Industries Inc., Japan
ITO, Kazuhiko	Power Reactor and Nuclear Fuel Development Corp., Japan
ITOH, Tetsuo	Kinki University, Japan
KAGEYAMA, Teruhisa	Mitsubishi Heavy Industries Ltd., Japan
KANEKO, Mitsunobu	Nuclear Fuel Industries Ltd., Japan
KATO, Hidemasa	Hitachi Ltd., Japan
KATO, Kanji	Hitachi Ltd., Japan
KAWABATA, Yuji	Kyoto University, Japan
KIMURA, Itsuro	Kyoto University, Japan
KOBAYASHI, Hisao	Rikkyo University, Japan
KOBAYASHI, Katsuhei	Kyoto University, Japan
KOSHIZUKA, Seiichi	Univ.of Tokyo, Japan
KOMORI, Takuji	Radiation Application Development Association, Japan
MATSUURA, Tetsuo	Rikkyo University, Japan
MIKI, Ryota	Kinki University, Japan
MISHIMA, Kaichiro	Kyoto University, Japan
MIYAJI, Maki	Nissho Iwai Corp., Japan
MIZOO, Nobutatsu	Power Reactor and Nuclear Fuel Development Corp., Japan

NAKAI, Masaru	Toshiba Corp., Japan
NAKAJIMA, Akinobu	Hitachi Ltd., Japan
NISHIHARA, Hideaki	Kyoto University, Japan
OKANO, Kotoyuki	Kyoto University, Japan
SAKAI, Tomohiro	Japan Research Institute, Japan
SAKURAI, Yoshinori	Kyoto University, Japan
SATOH, Tadashi	Musashi Institute of Technology, Japan
SHIBATA, Toshikazu	Kinki University, Japan
SUZUKI, Soujuu	Power Reactor and Nuclear Fuel Development Corp., Japan
TAGAWA, Seiichi	University of Tokyo, Japan
TAMAI, Tadaharu	Kyoto University, Japan
TAMURA, Seiji	Hitachi Engineering & Service Co.Ltd., Japan
TOMURA, Kinji	Rikkyo University, Japan
TSUNODA, Junsaku	Radiation Application Development Association, Japan
UEDE, Toshio	Fuji Electric Co.Ltd., Japan
UTSURO, Masahiko	Kyoto University, Japan
YAMAGUCHI, Hiroshi	NKK, Japan
YAMANAKA, Kazuo	NKK, Japan
YOSHIDA, Akihiro	Power Reactor and Nuclear Fuel Development Corp., Japan
YOSHINO, Fujio	Science and Technology Agency, Japan

AKASHI, Kazutomo	Japan Atomic Energy Research Institute, Japan
AMEZAWA, Hiroo	Japan Atomic Energy Research Institute, Japan
ANDOH, Hiroe	Japan Atomic Energy Research Institute, Japan
AOYAGI, Naganori	Japan Atomic Energy Research Institute, Japan
ARAI, Nobuyoshi	Japan Atomic Energy Research Institute, Japan
ARIGANE, Kenji	Japan Atomic Energy Research Institute, Japan
ASAOKA, Takumi	Japan Atomic Energy Research Institute, Japan
BABA, Osamu	Japan Atomic Energy Research Institute, Japan
BANBA, Masao	Japan Atomic Energy Research Institute, Japan

FUJISHIRO, Toshio	Japan Atomic Energy Research Institute, Japan
FUKETA, Toyojiro	Japan Atomic Energy Research Institute, Japan
FUKUDA, Kosaku	Japan Atomic Energy Research Institute, Japan
FUNAHASHI, Satoru	Japan Atomic Energy Research Institute, Japan
FURUTA, Toshiki	Japan Atomic Energy Research Institute, Japan
FUTAMURA, Yoshiaki	Japan Atomic Energy Research Institute, Japan
GENKA, Tsuguo	Japan Atomic Energy Research Institute, Japan
GOTOH, Ichiro	Japan Atomic Energy Research Institute, Japan
HANAWA, Hiroshi	Japan Atomic Energy Research Institute, Japan
HARA, Kunio	Japan Atomic Energy Research Institute, Japan
HARAYAMA, Yasuo	Japan Atomic Energy Research Institute, Japan
HIGASHIYAMA, Yutaka	Japan Atomic Energy Research Institute, Japan
HIRABAYASHI, Takakuni	Japan Atomic Energy Research Institute, Japan
HIRAOKA, Toru	Japan Atomic Energy Research Institute, Japan
HIROSE, Akira	Japan Atomic Energy Research Institute, Japan
HORI, Naohiko	Japan Atomic Energy Research Institute, Japan
HORIGUCHI, Yoji	Japan Atomic Energy Research Institute, Japan
HORIKI, Ohichiro	Japan Atomic Energy Research Institute, Japan
HOSHINO, Osamu	Japan Atomic Energy Research Institute, Japan
ICHIHASHI, Yoshinori	Japan Atomic Energy Research Institute, Japan
ICHIKAWA, Hiroki	Japan Atomic Energy Research Institute, Japan
IGUCHI, Akira	Japan Atomic Energy Research Institute, Japan
IIDA, Kenichi	Japan Atomic Energy Research Institute, Japan
IIZUMI, Masashi	Japan Atomic Energy Research Institute, Japan
IKEDA, Yoshikazu	Japan Atomic Energy Research Institute, Japan
INOUE, Takeshi	Japan Atomic Energy Research Institute, Japan
ISE, Takeharu	Japan Atomic Energy Research Institute, Japan
ISHIDA, Yoshimi	Japan Atomic Energy Research Institute, Japan
ISHII, Toshio	Japan Atomic Energy Research Institute, Japan
ISHIJIMA, Kiyomi	Japan Atomic Energy Research Institute, Japan

ISHIMOTO, Kiyoshi	Japan Atomic Energy Research Institute, Japan
ISSHIKI, Masahiko	Japan Atomic Energy Research Institute, Japan
ITAGAKI, Masafumi	Japan Atomic Energy Research Institute, Japan
ITAMI, Hiroharu	Japan Atomic Energy Research Institute, Japan
ITOH, Haruhiko	Japan Atomic Energy Research Institute, Japan
IZUMI, Yoshinori	Japan Atomic Energy Research Institute, Japan
KAIEDA, Keisuke	Japan Atomic Energy Research Institute, Japan
KAKEFUDA, Kazuhiko	Japan Atomic Energy Research Institute, Japan
KAMATA, Takashi	Japan Atomic Energy Research Institute, Japan
KAMATA, Yutaka	Japan Atomic Energy Research Institute, Japan
KAMEYAMA, Iwao	Japan Atomic Energy Research Institute, Japan
KAMINAGA, Masanori	Japan Atomic Energy Research Institute, Japan
KANAZAWA, Hiroyuki	Japan Atomic Energy Research Institute, Japan
KANEDA, Yoshiro	Japan Atomic Energy Research Institute, Japan
KANO, Koji	Japan Atomic Energy Research Institute, Japan
KATAGIRI, Hiroshi	Japan Atomic Energy Research Institute, Japan
KATANISHI, Shoji	Japan Atomic Energy Research Institute, Japan
KATOH, Hisashi	Japan Atomic Energy Research Institute, Japan
KATOH, Mineo	Japan Atomic Energy Research Institute, Japan
KAWAMURA, Hiroshi	Japan Atomic Energy Research Institute, Japan
KAWASAKI, Minoru	Japan Atomic Energy Research Institute, Japan
KIKUCHI, Masaru	Japan Atomic Energy Research Institute, Japan
KIKUCHI, Nobuyoshi	Japan Atomic Energy Research Institute, Japan
KIKUCHI, Teruo	Japan Atomic Energy Research Institute, Japan
KIKUCHI, Yasuyuki	Japan Atomic Energy Research Institute, Japan
KINASE, Masami	Japan Atomic Energy Research Institute, Japan
KINASE, Sakae	Japan Atomic Energy Research Institute, Japan
KISHI, Toshiaki	Japan Atomic Energy Research Institute, Japan
KIZAKI, Minoru	Japan Atomic Energy Research Institute, Japan
KOBAYASHI, Iwao	Japan Atomic Energy Research Institute, Japan

KODAIRA, Tsuneo	Japan Atomic Energy Research Institute, Japan
KOGANEZAWA, Takashi	Japan Atomic Energy Research Institute, Japan
KOHSAKA, Atsuo	Japan Atomic Energy Research Institute, Japan
KOJIMA, Kiyoe	Japan Atomic Energy Research Institute, Japan
KOMORI, Yoshihiro	Japan Atomic Energy Research Institute, Japan
KOSUGE, Masao	Japan Atomic Energy Research Institute, Japan
KOYAMA, Yoshimi	Japan Atomic Energy Research Institute, Japan
KUDOH, Hiroshi	Japan Atomic Energy Research Institute, Japan
KUMAI, Toshio	Japan Atomic Energy Research Institute, Japan
KUNITAMA, Takehiko	Japan Atomic Energy Research Institute, Japan
KUNITOMI, Kazuhiko	Japan Atomic Energy Research Institute, Japan
KUROSAWA, Kazuo	Japan Atomic Energy Research Institute, Japan
KUROSAWA, Masayoshi	Japan Atomic Energy Research Institute, Japan
MAEDA, Atsushi	Japan Atomic Energy Research Institute, Japan
MARUO, Takeshi	Japan Atomic Energy Research Institute, Japan
MATSUBAYASHI, Masahito	Japan Atomic Energy Research Institute, Japan
MATSUMOTO, Hiroyuki	Japan Atomic Energy Research Institute, Japan
MATSUO, Hideto	Japan Atomic Energy Research Institute, Japan
MATSUSHIMA, Hideo	Japan Atomic Energy Research Institute, Japan
MATSUURA, Shojiro	Japan Atomic Energy Research Institute, Japan
MINAGAWA, Nobuaki	Japan Atomic Energy Research Institute, Japan
MIYAMOTO, Toshihiro	Japan Atomic Energy Research Institute, Japan
MIYAZAWA, Masataka	Japan Atomic Energy Research Institute, Japan
MOGI, Terutomi	Japan Atomic Energy Research Institute, Japan
MORIYA, Takashi	Japan Atomic Energy Research Institute, Japan
MOTOISHI, Shoji	Japan Atomic Energy Research Institute, Japan
MURAYAMA, Youji	Japan Atomic Energy Research Institute, Japan
NAGAHORI, Kazuhisa	Japan Atomic Energy Research Institute, Japan
NAGAOKA, Yoshiharu	Japan Atomic Energy Research Institute, Japan
NAKAGAWA, Shigeaki	Japan Atomic Energy Research Institute, Japan

NAKAGAWA, Tetsuya	Japan Atomic Energy Research Institute, Japan
NAKAJIMA, Hajime	Japan Atomic Energy Research Institute, Japan
NAKAJIMA, Teruo	Japan Atomic Energy Research Institute, Japan
NAKAKURA, Yuichi	Japan Atomic Energy Research Institute, Japan
NAKAMURA, Chikara	Japan Atomic Energy Research Institute, Japan
NAKAMURA, Kiyoshi	Japan Atomic Energy Research Institute, Japan
NAKAMURA, Takehiko	Japan Atomic Energy Research Institute, Japan
NAKANO, Akira	Japan Atomic Energy Research Institute, Japan
NAKANO, Makiro	Japan Atomic Energy Research Institute, Japan
NAKANO, Masahiro	Japan Atomic Energy Research Institute, Japan
NAKANO, Yoshihiro	Japan Atomic Energy Research Institute, Japan
NAKATA, Hirokatsu	Japan Atomic Energy Research Institute, Japan
NAKAYAMA, Fusao	Japan Atomic Energy Research Institute, Japan
NAKAYAMA, Soukichi	Japan Atomic Energy Research Institute, Japan
NEMOTO, Denjiro	Japan Atomic Energy Research Institute, Japan
NEMOTO, Takumi	Japan Atomic Energy Research Institute, Japan
NIHO, Toshisada	Japan Atomic Energy Research Institute, Japan
NIIMI, Motoji	Japan Atomic Energy Research Institute, Japan
OBATA, Kazuichi	Japan Atomic Energy Research Institute, Japan
OGAWA, Kazuhiko	Japan Atomic Energy Research Institute, Japan
OGINO, Nobuaki	Japan Atomic Energy Research Institute, Japan
OHMI, Masao	Japan Atomic Energy Research Institute, Japan
OHMICHI, Toshihiko	Japan Atomic Energy Research Institute, Japan
OHMORI, Kazuyuki	Japan Atomic Energy Research Institute, Japan
OHTOMO, Akitoshi	Japan Atomic Energy Research Institute, Japan
OKASHITA, Hiroshi	Japan Atomic Energy Research Institute, Japan
OKUMURA, Keisuke	Japan Atomic Energy Research Institute, Japan
OKUMURA, Kimie	Japan Atomic Energy Research Institute, Japan
ONODERA, Junichi	Japan Atomic Energy Research Institute, Japan
ONODERA, Tetsuya	Japan Atomic Energy Research Institute, Japan

ONOMA, Katsuyuki	Japan Atomic Energy Research Institute, Japan
OOKUBO, Masatake	Japan Atomic Energy Research Institute, Japan
OOTAKE, Masao	Japan Atomic Energy Research Institute, Japan
OOTAKE, Naomi	Japan Atomic Energy Research Institute, Japan
OYAMADA, Rokuro	Japan Atomic Energy Research Institute, Japan
SAITO, Haruo	Japan Atomic Energy Research Institute, Japan
SAITOH, Minoru	Japan Atomic Energy Research Institute, Japan
SAITOH, Shinzou	Japan Atomic Energy Research Institute, Japan
SAKANO, Kazuo	Japan Atomic Energy Research Institute, Japan
SAKUTA, Takashi	Japan Atomic Energy Research Institute, Japan
SASA, Yoichi	Japan Atomic Energy Research Institute, Japan
SASAKI, Yukio	Japan Atomic Energy Research Institute, Japan
SATOH, Hitoshi	Japan Atomic Energy Research Institute, Japan
SATOH, Kenji	Japan Atomic Energy Research Institute, Japan
SATOH, Masashi	Japan Atomic Energy Research Institute, Japan
SATOH, Mitsugu	Japan Atomic Energy Research Institute, Japan
SATOH, Sadayuki	Japan Atomic Energy Research Institute, Japan
SHIBA, Koreyuki	Japan Atomic Energy Research Institute, Japan
SHIBATA, Katsuyuki	Japan Atomic Energy Research Institute, Japan
SHIMAKAWA, Satoshi	Japan Atomic Energy Research Institute, Japan
SHIMIZU, Kenichi	Japan Atomic Energy Research Institute, Japan
SHIMIZU, Yoshihiro	Japan Atomic Energy Research Institute, Japan
SHIRAI, Eiji	Japan Atomic Energy Research Institute, Japan
SHIRAISHI, Tadao	Japan Atomic Energy Research Institute, Japan
SHITOMI, Hajimu	Japan Atomic Energy Research Institute, Japan
SOBAJIMA, Makoto	Japan Atomic Energy Research Institute, Japan
SOMEYA, Hiroyuki	Japan Atomic Energy Research Institute, Japan
SOYAMA, Kazuhiko	Japan Atomic Energy Research Institute, Japan
SUDO, Yukio	Japan Atomic Energy Research Institute, Japan
SUDOH, Kenji	Japan Atomic Energy Research Institute, Japan

SUZUKI, Junichi	Japan Atomic Energy Research Institute, Japan
SUZUKI, Shinobu	Japan Atomic Energy Research Institute, Japan
TACHIKAWA, Enzo	Japan Atomic Energy Research Institute, Japan
TAKAHASHI, Hidetake	Japan Atomic Energy Research Institute, Japan
TAKAYANAGI, Masaji	Japan Atomic Energy Research Institute, Japan
TAKESHITA, Isao	Japan Atomic Energy Research Institute, Japan
TAKEUCHI, Mitsuo	Japan Atomic Energy Research Institute, Japan
TAMAI, Kazuo	Japan Atomic Energy Research Institute, Japan
TANAKA, Isao	Japan Atomic Energy Research Institute, Japan
TANASE, Masakazu	Japan Atomic Energy Research Institute, Japan
TANI, Masanori	Japan Atomic Energy Research Institute, Japan
TANIFUJI, Takaaki	Japan Atomic Energy Research Institute, Japan
TERUNUMA, Kusuo	Japan Atomic Energy Research Institute, Japan
TSUBOI, Kazuaki	Japan Atomic Energy Research Institute, Japan
UGAJIN, Mitsuhiro	Japan Atomic Energy Research Institute, Japan
UMEZAWA, Kouichi	Japan Atomic Energy Research Institute, Japan
UMINO, Akira	Japan Atomic Energy Research Institute, Japan
WADA, Shigeru	Japan Atomic Energy Research Institute, Japan
WATANABE, Hitoshi	Japan Atomic Energy Research Institute, Japan
WATANABE, Shukichi	Japan Atomic Energy Research Institute, Japan
YAMABAYASHI, Hisamichi	Japan Atomic Energy Research Institute, Japan
YAMAGUCHI, Shin	Japan Atomic Energy Research Institute, Japan
YAMAHARA, Takeshi	Japan Atomic Energy Research Institute, Japan
YAMAMOTO, Kazuyoshi	Japan Atomic Energy Research Institute, Japan
YANAGISAWA, Kazuaki	Japan Atomic Energy Research Institute, Japan
YANAGISAWA, Kouji	Japan Atomic Energy Research Institute, Japan
YOKOBORI, Tan	Japan Atomic Energy Research Institute, Japan
YOKOO, Kenji	Japan Atomic Energy Research Institute, Japan
YONEZAWA, Chushiro	Japan Atomic Energy Research Institute, Japan